HANDBOOK OF THERMAL ANALYSIS AND CALORIMETRY

SERIES EDITOR: PATRICK K. GALLAGHER

VOLUME

FROM MACROMOLECULES TO MAN

EDITOR

R.B. KEMP

ELSEVIER

HANDBOOK OF THERMAL ANALYSIS AND CALORIMETRY

VOLUME 4

FROM MACROMOLECULES TO MAN

EDITED BY

R.B. KEMP

INSTITUTE OF BIOLOGICAL SCIENCES
UNIVERSITY OF WALES
EDWARD LLWYD BUILDING
ABERYSTWYTH
SY 23 3DA
WALES, UK

1999

ELSEVIER

AMSTERDAM - LAUSANNE - NEW YORK - OXFORD - SHANNON - SINGAPORE - TOKYO

This Page Intentionally Left Blank

FROM MACROMOLECULES TO MAN

ELSEVIER SCIENCE B.V.
Sara Burgerhartstraat 25
P.O. Box 211, 1000 AE Amsterdam, The Netherlands

First edition 1999

Library of Congress Cataloging in Publication Data
A catalog record from the Library of Congress has been applied for.

ISBN: 0-444-82088-4

⊗ The paper used in this publication meets the requirements of ANSI/NISO Z39.48-1992 (Permanence of Paper).
Printed in The Netherlands.

FOREWORD

The applications and interest in thermal analysis and calorimetry have grown enormously during the last half of the 20th century. The renaissance in these methods has been fueled by several influences. Certainly the revolution in instrumentation brought on by the computer and automation has been a key factor. Our imaginations and outlooks have also expanded to recognize the tremendous versatility of these techniques. They have long been used to characterize materials, decompositions, and transitions. We now appreciate the fact that these techniques have greatly expanded their utility to studying many processes such as catalysis, hazards evaluation, etc. or to measuring important physical properties quickly, conveniently, and with markedly improved accuracy over that in the past.

Consequently, thermal analysis and calorimetry have grown in stature and more scientists and engineers have become, at least part time, practitioners. It is very desirable that these people new to the field can have a source of information describing the basic principles and current state of the art. Examples of the current applications of these methods are also essential to spur recognition of the potential for future uses. The application of these methods is highly interdisciplinary and any adequate description must encompass a range of topics well beyond the interests and capabilities of any single investigator. To this end, we have produced a convenient four volume compendium of such information (a handbook) prepared by recognized experts in various aspects of the topic.

Volume 1 describes the basic background information common to the broad subject in general. Thermodynamic and kinetic principles are discussed along with the instrumentation and methodology associated with thermoanalytical and calorimetric techniques. The purpose is to collect the discussion of these general principles and minimize redundancies in the subsequent volumes that are concerned with the applications of these principles and methods. More unique methods which pertain to specific processes or materials are covered in later volumes.

The three subsequent volumes primarily describe applications and are divided based on general categories of materials. Volume 2 concerns the wide range of inorganic materials, e.g., chemicals, ceramics, metals, etc. It covers the synthesis, characterization, and reactivity of such materials. Similarly, Volume 3 pertains to polymers and describes applications to these materials in an appropriate manner. Lastly the many important biological applications are described in Volume 4.

Each of these four volumes has an Editor, who has been active in the field for many years and is an established expert in the material covered by that specific volume. This team of Editors has chosen authors with great care in an effort to produce a readable informative handbook on this broad topic. The chapters are not intended to be a comprehensive review of the specific subject. The intent is that they enable the reader to glean the essence of the subject and form the basis for further critical reading or actual involvement in the topic. Our goal is to spur your imaginations to recognize the potential application of these methods to your specific goals and efforts. In addition we hope to anticipate and answer your questions, to guide you in the selection of appropriate techniques, and to help you to perform them in a proper and meaningful manner.

P.K. GALLAGHER
Series Editor

PREFACE TO VOLUME 4

This volume contains 17 chapters on many aspects of biological thermal analysis and calorimetry. I wish I could have written the words "all aspects" but it proved impossible to cover every ground. This is because some potential authors for Volume 4 either were not prepared to commit themselves to a spot of work that does not bring high impact brownie points or they fell by the wayside owing to the increasing pressure on academe as we hit the next millennium! After all, a Handbook is not intended as a flagship for disseminating the latest research results, though it is easy to be tempted down this path, but rather "how and what to do and when to do it".

So, what started 5 years ago as a Thessalonian labour of love has, in some ways, become "emprisoned in black, purgatorial rails" (Keats)! I received the first chapter three, long years ago and some of the excellent chapters have been with me for two years or more. These authors have only made (to me!) the very occasional complaint (while probably inwardly fuming!) but my increasingly urgent nightmare has been of them bearing down on me all at once – as Mike Jagger sang "Ev'rywhere I hear the sound of marching, charging feet, boy"! I do apologise to all of them but I did what I could and it is in deference to these justifiably "charging boys" that I have called "stumps" (an end to it), inevitably leaving some holes. There would have been more but for some colleagues coming in late to replace those that failed to stay the course – each one is "like a diamond in the sky"!

Talking of precious jewels, I must make mention of Ms Swan Go of Elsevier. Without her, I would have cracked up long ago! Not only was she there for every technical problem, there are many in camera ready work, but she would act as the proverbial shoulder in one's darkest hours, help to find alternatives, ring the recalcitrant and sooth the sibilant! *Mirabile dictu*!

I would also like to salute the Editor of Volume 1, Mike Brown, as a fellow trooper! In cricketing terms, we had a long batting partnership against some devilish spin bowling that turned in every direction and, in the end, we won the match! *Palma non sine pulvere*!

Finally, I am pleased to express my gratitude to all the contributors, fast and slow, to the Series Editor, Pat Gallagher and to the long suffering guys ("groupies") in my laboratory ("group", we have to call it in these post-Beatles days) for enabling this Volume to appear at all!

I learned a great deal from reading all the chapters but sometimes felt that in my work I am playing the triangle rather than the tympani. I trust that the book will prove valuable in assisting more scientists to realise the potential of heat

measurements in their research while showing those already in the business what is done in other areas in the name of heat! After all, the use of the technique in biology is two hundred and twenty years old enough to be of a mature vintage!

RICHARD B. KEMP
Volume Editor

CONTENTS

Foreward – P.K. Gallagher v
Preface – R.B. Kemp vii
Contributors xxvi

CHAPTER 1. ENERGETICS THAT CONTROL THE STABILITY AND DYNAMICS OF SECONDARY AND TERTIARY STRUCTURE OF NUCLEIC ACIDS
(H.H. Klump)

1. **Introduction: Current Advances in the Studies of DNA and RNA Structures** 1

2. **The DNA World** 2
2.1 Thermodynamics of DNA-helix formation: Correlation between enthalpy and entropy changes 2
2.2 Forces that control triple helix stability 5
2.3 Investigation of sequence specificity of DNA triplex formation using isothermal calorimetry 8
2.4 Determinants of oligosaccharide triple-helix stability and specificity 11
2.5 Variation in DNA-helix stability and health: Triple repeat expansion diseases 21
2.6 DNA analogues with nonphosphodiester backbones: The peptide nucleic acids (PNAs) 24
2.7 Multistem DNA structures 27
2.7 Competitive equilibria between DNA triplex and quadruplex: The role of the G-quartets 31

3. **The RNA World** 34
3.1 Origin of the different stability of DNA and RNA helices 34
3.2 The discovery of the RNA world 38
3.3 Principles governing RNA folding 41
3.4 Superstable hairpin structures in large RNAs 48

References 54–61

CHAPTER 2. THEORY AND PRACTICE OF DSC MEASUREMENTS ON PROTEINS
(J. Rösgen and H.-J. Hinz)

1. **Introduction** 63

2. **The DSC-experiment** 63
2.1 Sample preparation 63
2.2 Measurement and data treatment 64

3. **Thermodynamic analysis of heat capacity curves** 65
3.1 The shape of heat capacity curves 65

3.2 Protein stability 66
3.3 The heat capacity peak 70
3.4 Cold denaturation 72
3.5 The temperature dependence of $\Delta^{D}{}_{N}C_{p}(T)$ 74

4. **Predicting the *Cp* value of the denatured state on the basis of model compounds** 76
4.1 Oligopeptide-based model compounds 78

5. **Analysis of heat capacity curves by statistical physics** 81
5.1 General considerations 81
5.2 Definition of relative partition functions 82
5.3 Calculation of the partition function by integrating heat capacity curves 84
5.4 Fitting of heat capacity curves 86
5.4.1 Two-state model, 1:1 stoichiometry 87
5.4.2 Three-state model, 1:1:1 stoichiometry 88
5.4.3 Two-state model, 1:2 stoichiometry 88
5.4.4 Three-state model, 1:2:2 stoichiometry 90
5.4.4 Three-state model, 1:1:2 stoichiometry 91
5.5 Fit strategy 92

6. Treatment of irreversible transitions 94
6.1 First order kinetics 94
6.2 Aggregation process 97

7. **Response of the calorimeter** 98

8. **DSC calorimeter types, practical hints** 100
8.1 The influence of differences in the shape of calorimeter cells 100
8.2 Calibration 101

9. **Fit Macros** 101
9.1 Macros for the denaturation of a monomeric protein 102
9.1.1 Macro using Gnuplot 102
9.1.2 Macro using Sigmaplot 103
9.2 Macros for the denaturation of a dimeric protein 104
9.2.1 Macro using Gnuplot 104
9.2.2 Macro using Sigmaplot 105

References 106–108

CHAPTER 3. LIPID MODEL MEMBRANES AND BIOMEMBRANES (A. Blume and P. Garidel)

1. **Introduction** 109
1.1 Lipids as model membranes 109

1.2 Chemical structure of lipids 111
1.3 Thermotropic and lyotropic phase behavior of lipids 113

2. **Differential scanning calorimetry of membranes** 118
2.1 Thermotropic phase transitions of pure lipids in excess water 118
2.1.1 Influence of headgroup structure and hydrocarbon chain length 121
2.1.1 influence of pH and ion binding 123
2.2 Phase transitions of lipid mixtures 129
2.2.1 Lipid-cholesterol mixtures 130
2.2.2 Binary phospholipid mixtures 133
2.2.3 Lipid-protein interactions 143
2.2.4 Lipid-surfactant mixtures 144

3. **Isothermal titration calorimetry (ITC)** 146
3.1 Isothermal phase transitions 147
3.2 Heats of ion binding 150
3.3 Heats of incorporation of hydrophobic molecules 152
3.4 Lipid-surfactant interactions 154
3.4.1 Demicellization of surfactants 154
3.4.2 Partitioning of surfactants into bilayers 157
3.4.3 Solubilization of membranes by surfactants 161
3.5 Lipid-protein and lipid-peptide interactions 164

4. **Conclusions** 167

References 168–173

CHAPTER 4. COMBUSTION CALORIMETRY
(I. Lamprecht)

1. **Introduction** 175
1.1 Historical aspects 175
1.2 Instrumentation 175
1.3 Chemical and thermodynamical aspects 177
1.4 Biological aspects 180

2. **Sample preparation** 182
2.1 General sample preparation 182
2.2 Drying of samples 183
2.3 Determination of the ash content 184
2.4 Acid corrections 185
2.5 Application of filters 186

3. **Combustion of microbial samples** 186

4. **Combustion of plant material** 188

5. **Combustion of animal material** 193
5.1 Terrestrial animals 194
5.1.1 Vertebrates 194
5.1.2 Invertebrates 196
5.2 Aquatic animals 197

6. **Combustion of ecological material** 201
6.1 General aspects 201
6.2 Applications 204
6.3 Fuel alternatives 207

7. **Conclusions** 211

References 212–218

CHAPTER 5. THE THERMODYNAMICS OF MICROBIAL GROWTH (E. H. Battley)

1. **Introduction** 219

2. **Material growth process systems** 220
2.1 The initial state of a growth process system 221
2.2 The final state of a growth process system 222
2.3 A cautionary note 222
2.4 Growth process equations 223
2.4.1 Harvesting the cells 223
2.4.2 Determining cellular composition 224
2.4.3 Constructing growth-process equations representing the system 228
2.4.4 Representing anabolism and catabolism 228
2.4.5 Available electrons and equivalents 230
2.4.6 Representing anabolism 231
2.4.7 Representing organic product formation 232
2.4.8 Another way of representing anabolism 233
2.4.9 Representing catabolism 234
2.4.10 Representing metabolism 234
2.1.11 Points to consider 234
2.1.12 Examples 235

3. **The thermodynamics of growth process systems** 238
3.1 The Gibbs free energy equation 238
3.2 Thermodynamic properties for substances participating in growth processes 239
3.2.1 Values for the enthalpy, free energy, and entropy of formation in aqueous solution of substances utilized or produced during growth, excluding cells 240
3.2.2 Values for cellular enthalpy, entropy, and free energy of formation 242
3.2.3 Examples of thermodynamic changes accompanying growth processes 246
3.3 Alternate ways of representing cellular substance 247

3.3.1 Values for the enthalpy, entropy and free energy of formation of cells from which the ions have been theoretically removed 247
3.3.2 Values for the enthalpy, entropy and free energy of formation of cells, assuming that all ions can be represented by potassium ion 248
3.3.3 Comparative values for $\Delta_p G'_{met}$ and $\Delta_p H'_{met}$ using different representations of the unit carbon formula 249
3.4 Other methods of calculating thermodynamic changes accompanying growth 249
3.4.1 Thornton's Rule 250
3.4.2 Using Thornton's Rule to calculate $\Delta_f H_{cells}$ 251
3.4.3 Another way to calculste $\Delta_p H'_{met}$ 251
3.4.4 Calculating the values for $\Delta_f G_{cells}$, $\Delta_p G'_{an}$ and $\Delta_p G'_{met}$ 252
3.5 The efficiency of growth 253
3.5.1 Calculating electron conservation efficiencies for aerobic growth processes 254
2.5.2 Calculating free energy conservation efficiencies for aerobic growth processes 255
3.5.3. Calculation of the enthalpy conservation efficiencies for aerobic growth processes 257
3.5.4 Calculating electron conservation efficiencies for anaerobic growth processes 258
3.5.5 Calculating free energy conservation efficiencies for anaerobic growth processes 259
3.5.6 Calculating enthalpy conservation efficiencies for anaerobic growth processes 260
3.5.7 Why calculate efficiencies? 261
3.6 A comment on entropy 261

References 264–266

CHAPTER 6. QUANTITATIVE CALORIMETRY AND BIOCHEMICAL ENGINEERING
(P. Duboc, I. Marison and U. von Stockar)

1. **Introduction: Applications of calorimetry in biochemical engineering** 267
1.1 Cooling requirements 267
1.2 Data consistency 268
1.3 On-line monitoring and control of bioreactors 268
1.4 Thermodynamics of living systems: What is measureable? 268

2. **Heat flow rate measurement** 269
2.1 Heat conduction calorimeters 269
2.2 Heat accumulation calorimeters 270
2.3 Heat compensation calorimeters 270
2.4 Dynamic response of the calorimetric measurements 272
2.4.1 Comparison of the dynamic response of various on-line measurements 272
2.4.2 Time constant of heat transfer 274
2.4.3 Time constant of temperature control 275

3. **Mole and enthalpy balances in open systems** 278
3.1 System boundary 278
3.2 Molar balance 280
3.3 Enthalpy balance 281
3.4 Growth reaction stoichiometry 283
3.5 Cumulated quantities 285

4. **Elemental composition** 287
4.1 Sample preparation, humidity and ash determination 287
4.2 CHN measurement 288
4.3 Elemental formula and molar mass 288
4.4 Dry weight or ash-free biomass 289
4.5 Sulfur, phosphorus and ions content of biomass 289
4.6 Integration of S and P into the elemental composition 291
4.7 Composition of bacterial strains, algae, filamentous fungi and yeast 293
4.8 Statistical comparison of the composition of bacteria, algae, filamentous fungi and yeast 297
4.9 Influence of growth conditions 301

5. **Enthalpy of combustion of biomass** 304
5.1 Sample preparation, and the principle of measurement 304
5.2 Modified enthalpy of combustion 305
5.3 Enthalpies of combustion of bacteria, algae, filamentous fungi and yeast 306

6. **Detection and correction of measurement errors** 306
6.1 Constraints on rates or cumulated quantities 306
6.2 Statistical test 309
6.3 Example of calculation of the test function 310
6.4 Example of balance calculation during dynamic experiment 311
6.4.1 Concentrations and cumulated quantities profiles 311
6.4.2 Atom balance 312
6.4.3 Balance profiles 314
6.4.4 Energy balance 314
6.5 Data reconciliation 315
6.6 Indirect balancing 316

7. **Energetics of microorganisms** 319
7.1 Driving force of biochemical reactions 320
7.2 ATP production and utilization 322
7.2.1 ATP requirements for biosynthesis 324
7.2.2 ATP production by reductive metabolism 325
7.2.3 ATP production by aerobic catabolism 326
7.3 Enthalpy and Gibbs energy dissipation 327
7.4 Thermodynamic constraints on biomass and product yields 330

8. **Calorimetric investigation of multiple limited growth** 333

8.1 Glucose and oxygen limitation 334
8.2 Glucose and ammonium limitation 336

9. **Monitoring of aerobic bioprocesses by calorimetry** 339
9.1 Aerobic batch culture on glucose 339
9.2 Glucose pulse 341
9.3 Shift-up in dilution rate in aerobic continuous culture 341
9.4 Cell cycle oscillations of *Saccharomyces cerevisiae* 343

10. **Monitoring of anaerobic bioprocesses by calorimetry** 344
10.1 Anaerobic batch of *S. cerevisiae* 344
10.2 Methanogens 344

11. **Control of bioprocesses based on calorimetric measurements** 347
11.1 Fed batch of *S. cerevisiae* 347
11.1.1 Estimation of the respiratory quotient 347
11.1.2 Controlled glucose pulses 349
11.1.3 Control based on RQ and heat flow rate measurements 350
11.2 Fed-batch culture for heat flow rate measurements 351
11.3 Control of dilution rate increase in continuous culture 357

12 **Conclusions** 361

References 362–365

CHAPTER 7. CALORIMETRY OF MICROBIAL PROCESSES
(B. Larsson and L. Gustafsson)

1. **Background** 367
2. **The origin of heat production in metabolism** 371
2.1 Anabolism versus catabolism 371
2.2 Coupled versus uncouples metabolism 374
2.2.1 Heat yield determinations 375

3. **Future areas of applied calorimetry** 378
3.1 Continuous registration and control of fermentations 378
3.2 Analysis of metabolic fluxes in non-growing/starved cells 380
3.2.1 Catabolic flux distribution 380
3.2.2 The control of catabolic flux 382
3.2.3 Heat flux and metabolic dynamics 383
3.2.4 Mechanisms of ageing 385
3.2.5 Maintenance energy flux 386
3.3 Bioadhesion 387
3.4 Ecosystem studies 390
3.4.1 Sample handling 391
3.4.2 Mixed metabolisms on organism and population level 393

3.4.3 Final thermodynamic remark 399

4. **Conclusions** 399

References 400–404

CHAPTER 8. CALORIMETRY OF SMALL ANIMALS
(I. Lamprecht and E. Schmolz)

1. **Introduction** 405
1.1 General aspects 405
1.2 Time constant 408
1.3 Remarks on calorimetric nomenclature 409

2. **Direct and indirect calorimetry** 410
2.1 Determination of gas metabolism 412
2.2 Metabolic investigations by tracer techniques 413
2.3 Heart rate and metabolism 414

3. **Additional equipment** 415
3.1 Optical monitoring 415
3.2 Acoustic monitoring 417
3.3 Gas monitoring 418
3.3.1 Gas sensors 418
3.3.2 Pressure monitoring 420
3.4 Electrical stimulation 420
3.5 Poor man's calorimeter PMC 421

4. **Amphibia and reptilia** 423

5. **Insects** 426
5.1 Insects in general 426
5.2 Calorimetric investigations on special insects 428
5.3 Flight calorimeter for small insects 434
5.4 Insect development 434
5.5 Social insects 436
5.5.1 Some general features 436
5.5.2 Honeybees 437
5.5.3 Bumblebees 439
5.5.4 Hornets 440
5.5.5 Wood ants 442

6. **Protozoa** 444

7. **Aquatic animals** 445
7.1 General considerations 445

7.2 Fish 446
7.3 Aquatic invertebrates 448

8. **Ecology** 454

9. **Conclusions and perspectives** 457

References 459–467

CHAPTER 9. CALORIMETRIC APPROACHES TO ANIMAL PHYSIOLOGY AND BIOENERGETICS
(S.C. Hand)

1. **Introduction** 469

2. **Metabolic status and the CR ratio** 470

3. **Heat flux and oxygen limitation** 476
3.1 Molluscs 476
3.2 Exothermic gap under anoxia 478
3.3 Arthropods 479
3.4 Vertebrates 480
3.5 Isolated tissues and organelles 481

4. **Developmental physiology** 485
4.1 Invertebrate larvae 485
4.2 Vertebrate embryos and larvae 488

5. **Quiescence and diapause** 490
5.1 Anaerobic quiescence in brine shrimp embryos 490
5.2 Anhydrobiosis in brine shrimp embryos 493
5.3 Estivation in land snails 495
5.4 Diapause in sponge gemmules 497

6. **Nitrate respiration in a clam-bacterium symbiosis** 500

7. **Conclusions and future directions** 503

References 504–510

CHAPTER 10. WHOLE BODY CALORIMETRY
(U. Frenz)

1. **Introduction** 511

2. **Basics** 513

3. **Methods and equipment** 514
3.1 Direct calorimetry 515
3.1.1 Principles of measurement 517
3.1.2 Equipment 517
3.2 Indirect calorimetry 520
3.2.1 Theoretical basis 520
3.2.2 Principles 522
3.2.3 Equipment 524
3.2.4 Timing problems 527
3.3. Applications 528
3.3.1 Experimental scheduling 528
3.3.2 Investigating metabolism 529
3.4 Comparisons 532
3.5 Locomotor activity 533
3.6 Other methods to assess EE 536

4. **Whole body calorimetry in biological and nutritional research** 539
4.1 Energy balance and components 540
4.1.1 Energy sinks and energy intake 540
4.1.2 Calorimetric results – extrapolation to free living conditions 541
4.1.3 Substrate balance 542
4.2 Methods to assess energy balance components 543
4.2.1 Long-term balancing 543
4.2.2 Calorimetric detection of BMR and ppTh 543
4.2.3 Detection of LA 544
4.3 Energy utilisation 545
4.4 Other applications of whole body calorimetery 547
4.4.1 Gut fermentation 548
4.4.2 Thermoregulation 549
4.4.3 Behavioural research 550
4.4.4 Pharmacological research 550

5. **Conclusions** 553

References 553–555

CHAPTER 11. MICROCALORIMETRIC STUDIES OF ANIMAL TISSUES AND THEIR ISOLATED CELLS
(R.B. Kemp and Y.H. Guan)

1. **Introduction** 557

2. **Thermodynamics** 558

3. **Reasons for systematic errors in calorimetry** 562
3.1 Physical environment 562

3.1.1 Conditions that cause tissue/cell damage 562
3.1.2 Inaccurate/non-existent electrical and chemical calibration 566
3.2 Physiological environment 567
3.2.1 Oxygen tension 567
3.2.2 pH 567
3.2.3 Temperature 568
3.2.4 Osmotic pressure 569
3.2.5 Substrates 570
3.2.6 Waste products 571
3.2.7 Size 572
3.2.8 Metabolism 575
3.2.9 Growth 576

4. **Tissues/Organs** 577
4.1 Muscle 577
4.1.1 Striated muscle 577
4.1.2 Smooth muscle 581
4.1.3 Cardiac muscle 582
4.2 Nerve 584
4.3 Diseased and damaged human tissues 588

5. **Cells** 591
5.1 Cell types and their differing adhesion 591
5.2 Heat flow rate as a variable in animal cell bioreactors 593
5.2.1 The bioreactor as a calorimeter 594
5.2.2 Combination of bioreactor with flow microcalorimeter 594
5.2.3 Heat flux and the growth reaction 600
5.2.4 The growth reaction and the enthalpy balance method 603
5.2.5 The application of the growth reaction to medium design 605
5.2.6 The role of the heat flux biosensor in fed-batch culture 607
5.3 Metabolic studies to identify and quantify pathways in cells 612
5.4 Pharmacological studies 623
5.4.1 Cancer drugs 624
5.4.2 Clinical studies 631
5.4.3 Cell signalling 633
5.5 The calorimetric-respirometric ratio 635

6. **Conclusions** 649

References 650–656

CHAPTER 12. CALORIMETRIC STUDIES IN MEDICINE (M. Monti)

1. **Hematology** 657
1.1 Anaemia, obesity 657

1.2 Trace elements, drugs 662

2. **Malignancy** 666
2.1 Lymphoma, cancer 666
2.2 Leukaemia 669

3. **Immunology** 671
3.1 Lymphocytes 671
3.2 Macrophages 672
3.3 Immune complexes 674

4. **Endocrinology** 676
4.1 Hyperthyroidism, hypothyroidism 676
4.2 Acromegaly 680

5. **Cardiovascular system** 681
5.1 Cardiovascular drugs and cell metabolism 681
5.2 Arterial insufficiency 685
5.3 Prosthetic heart valves 686
5.4 Myocardial metabolism, cardiomyopathy, myocardial infarction 687
5.5 Hybernation and myocardial metabolism 689

6. **Nutritional and metabolic disorders** 690
6.1 Obesity 690
6.2 Adiposis dolorosa 694
6.3 Anorexia nervosa 695
6.4 Malignant hyperpyrexia 696
6.5 Liver 696

7. **Kidney** 698
7.1 Renal insufficiency 698
7.2 Biocompatibility 702
7.3 Uremic plasma 704

References 705–710

CHAPTER 13. CALORIMERIC METHODS FOR ANALYSIS OF PLANT METABOISM
(R.S. Criddle and L.D. Hansen)

1. **Background and general methods** 711
1.1 Introduction 711
1.2 Quantities measured during plant calorimetry 713
1.3 Tissues used for calorimetry studies 714
1.4 Amounts of tissue required 714
1.5 Tissue preparation 716

1.6 Plant sources ... 717
1.7 Calorimeter requirements ... 718
1.8 Isothermal calorimetry methods ... 721
1.8.1 Isothermal heat rate measurements ... 721
1.8.2 Isothermal measurements of time dependent activity loss ... 721
1.8.3 Temperature cycling ... 722
1.8.4 Calorespirometry ... 723
Batch studies ... 723
Flow and perfusion studies ... 725
1.8.5 Batch studies of samples requiring contact with liquid media ... 725
1.8.6 Studies above ambient pressure ... 726
1.9 Temperature scans of plant metabolic rates ... 726
1.9.1 Heat rate measurements by temperature scanning calorimetry ... 726
1.9.2 Temperature scanning methods ... 727
1.9.3 interpretation of scanning thermograms ... 728
1.9.4 Results obtained from scanning studies ... 730
1.10 Limitations in plant calorimetry measurements and interpretations ... 732

2. **Plant growth model** ... 733
2.1 Introduction ... 733
2.2 Development of plant growth model ... 735
2.3 Test of temperature dependence predictions ... 737

3. **Applications** ... 739
3.1 Introduction ... 739
3.2 Growth rates and production ... 740
3.3 Taxonomy ... 740
3.4 Dormant or near dormant tissues, germination, and vernalization ... 742
3.5 Temperature dependence of plant growth ... 743
3.6 Low and high temperature hardiness ... 745
3.7 Stresses other than temperature ... 746
3.7.1 Salt ... 746
3.7.2 Methanol ... 747
3.8 Nutrient limitations ... 747
3.9 Herbicide effects on plant metabolic properties ... 748
3.10 Pathogens on plants ... 748
3.11 Forestry applications ... 748
3.11.1 Larch ... 749
3.11.2 Redwood ... 749
3.11.3 Eucalyptus ... 752
3.11.4 Other trees ... 753
Poplars ... 753
Pines ... 754
3.12 Annual crops ... 754
3.13 Ecology and climate change ... 755
3.14 Molecular biology ... 757

References 757–763

CHAPTER 14. WOOD
(H.G. Wiedemann and I. Lamprecht)

1. **Introduction** 765
2. **Characteristics of Wood** 766
3. **Investigations on wood** 767
4. **Pyrolysis of wood** 768
5. **Pyrolysis of wood components** 770
6. **Wood and fire retardants** 773
7. **Wood and synthetic polymers** 776
8. **Wood and water** 777
9. **Energy content of wood** 779
10. **Aging and fossilization of wood** 786
11. **Wood for musical instruments** 788
12. **Wood and paper** 791
13. **Wood and wasp nests** 797
14. **Microbial degradation of wood** 798
15. **Other observations on wood** 802
16. **Conclusion** 803

References 803–809

CHAPTER 15. DYNAMIC MECHANICAL ANALYSIS OF ELASTOMERS
(C.M. Roland)

1. **Introduction** 811
1.1 Modes of motion in polymers 811
1.2 Time dependence of relaxation 813

2. **Temperature dependence of relaxation** 814
2.1 Thermorheological simplicity and complexity 818

3. **Compounding variables** 821
3.1 Crosslink density 821
3.2 Diluent and blending 822
3.3 Filler reinforcement (carbon black) 824

References 826–828

CHAPTER 16. THERMAL ANALYSES IN FOODS AND FOOD PROCESSES (A. Schiraldi, L. Piazza, D. Fessas and M. Riva)

1. **Introduction** 829

2. **Phase diagrams** 836

3. **Cereal Products** 839
3.1 Starch 839
3.2 Doughs 844
3.3 Viscoelastic properties of doughs 849
3.3.1 Testing conditions 849
Strain amplitude 849
Oscillation frequency 850
Rest time before test 852
Heating rate 852
3.4 Baked and cooked products 852
3.4.1 TA investigations 852
3.4.2 Thermomechanical analysis of baked products 859

4. **Proteins** 863
4.1 Thermodynamic approach to protein denaturation 865
4.2 pH effects 872
4.3 Effect of ligands and other protein modifiers 873
4.4 Protein aggregation 877
4.5 Effects of salts and sugars 879
4.6 Protein gels 880
4.7 Cereal proteins 882
4.7.1 State diagrams of cereal proteins 882
4.7.2 Gluten thermoset and gluten-starch interactions 887
4.7.3 Thermomechanical evaluation of starch 892

Appendix 896
A1 Treatment of DSC signals 896
A1.1 Thermodynamic approach 896
A1.2 Kinetic approach 896

A2 Treatment of TGA signals 898
A3 Elements of thermomechanical analysis in polymer science 899
A4 Proteins 903
A4.1 Two-state equilibrium transition 903
A4.2 The effect of pH and other co-solutes on thermal stability of globular Proteins: the preferential binding model 905
A4.3 Dissociation and aggregation 909

References 911–921

CHAPTER 17. THERMAL ANALYSIS AND CALORIMETRY OF PHARMACEUTICALS
(J.L. Ford and R. Willson)

1. **Introduction** 923

2. **Characterisation of pharmaceutical solids** 924
2.1 Morphological stability 927
2.1.1 Polymorphism 928
2.1.2 Solvates and hydrates 933
Adsorption isotherms 939
2.1.3 Hygroscopicity 940
2.1.4 Amorphousness and the glassy state 942
Solution calorimetry 946
2.1.5 Purity 948

3. **Chemical stability studies** 951
3.1 Chemical stability studies of solutions 951
3.1.1 Simple observation of the calorimetric signal 954
3.1.2 The determination of reaction extent using fractions 955
3.1.3 The calculation of the kinetic and thermodynamic parameters that specifically describe the reaction 956
3.1.4 Calculation of the reaction order 957
3.1.5 The calculation of the enthalpy change and rate constant 957
3.2 Chemical stability study of the solid state 963
3.3 Compatibility studies 966
3.3.1 Compatibility studies using thermal analytical techniques 967
3.3.2 Compatibility studies using isothermal calorimetry 969
3.4 Bomb calorimetry 971
3.5 Heat capacity 972
3.6 Biological stability studies 973
3.7 Photo-stability 975

4. **Miscellaneous uses** 976
4.1 Phase diagrams 976
4.2 Polymers of pharmaceutical interest 979

4.2.1 Polyethylene glycols 980
4.2.2 Poly-lactic acids 981
4.2.3 Cellulose ethers 984
4.3 Polymer-hydration 986
4.4 Liposomes 988
4.5 Thermal analysis and industrial processes 990
4.5.1 Spray-dried products 990
4.5.2 Freeze drying (lyophilisation) 994
4.5.3 Polymeric films and film coating 1000
4.6 Thermal analysis of transdermals and semi-solids 1002
4.7 Transdermal delivery of drugs 1006

References 1009–1015

INDEX 1017–1032

CONTRIBUTORS

Battley, E.H. Department of Ecology and Evolution, State University of New York at Stony Brook, Stony Brook, NY 11794-5245, USA.

Blume, A. Martin-Luther-University Halle-Wittenberg, Institute of Physical Chemistry, Muehlpforte 1, D-06108 Halle, Germany.

Criddle, R.S. Section of Molecular and Cellular Biology, University of California, Davis, CA 95616, USA.

Duboc, P. Center for Process Biotechnology, Denmark Technical University, DK2800 Lyngby, Denmark.

Fessas, D. Dipartimento Scienze e Tecnologie Alimentari e Microbiologiche, University of Milan, via Celoria 2, 20133 Milano, Italy.

Ford, J.L. School of Pharmacy and Chemistry, Liverpool John Moores University, Byrom Street, Liverpool, L3 3AF, United Kingdom

Frenz, U. Department of Biochemistry and Physiology of Nutrition, German Institute of Human Nutrition, Arthur-Scheunert-Allee 114-155, 14558 BergholzRehbrücke, Germany.

Garidel, P. Martin-Luther-University Halle-Wittenberg, Institute of Physical Chemistry, Muehlpforte 1, D-06108 Halle, Germany.

Guan, Y.H. Institute of Biological Sciences, University of Wales, Aberystwyth, SY23 3DA, Wales, UK.

Gustafsson, L. General and Marine Microbiology, Lundberg Laboratory, Göteborg University, Medicinaregatan 9C, 5-41390 Göteborg, Sweden.

Hand, S.C. Department of Environmental, Population and Organismic Biology, University of Colorado, Boulder, Colorado 80309-0334 USA.

Hansen, L.D. Department of Chemistry and Biochemistry, Brigham Young University, Provo, UT 84602, USA.

Hinz, H.-J. Institute für Physikalische Chemie, Westfälische Wilhelms Universität Münster, Schossplatz 7, 48149 Münster, Germany.

Kemp, R.B. Institute of Biological Sciences, University of Wales, Aberystwyth, SY23 3DA, Wales, UK.

Klump, H.H. Department of Biochemistry, University of Cape Town, Republic of South Africa.

Lamprecht, I. Institut für Biophysik, Freie Universitat Berlin, Thielallee 63, D-14195 Berlin, Germany

Larsson, C. General and Marine Microbiology, Lundberg Laboratory, Göteborg University, Medicinaregatan 9C, 5-41390 Göteborg, Sweden.

Marison, I. Institute of Chemical Engineering and Bioengineering, Swiss Federal Institute of Technology, CH-1015 Lausanne, Switzerland.

Monti, M. Department of Cell Biology 1, University Hospital of Lund, 221 85 Lund, Sweden.

Piazza, L. Dipartimento Scienze e Tecnologie Alimentari e Microbiologiche, University of Milan, via Celoria 2, 20133 Milano, Italy.

Riva, M. Dipartimento Scienze e Tecnologie Alimentari e Microbiologiche, University of Milan, via Celoria 2, 20133 Milano, Italy.

Roland, C.M. Naval Research Laboratory, Chemistry Division, Code

6120, Washington, DC 20375-5342, USA.

Rösgen, J. Institute für Physikalische Chemie, Westfälische Wilhelms Universität Münster, Schossplatz 7, 48149 Münster, Germany.

Schiraldi, A. Dipartimento Scienze e Tecnologie Alimentari e Microbiologiche, University of Milan, via Celoria 2, 20133 Milano, Italy.

Schmolz, E. Institut für Biophysik, Freie Universität Berlin, Thielallee 63, D-14195 Berlin, Germany.

Stockar, U. von Institute of Chemical Engineering and Bioengineering, Swiss Federal Institute of Technology, CH-1015 Lausanne, Switzerland.

Wiedemann, H.G. Mettler-Toledo GmbH, Sonnenbergstrasse 74, CH-8603 Schwerzenbach, Switzerland.

Willson, R. SmithKline Beecham Pharmaceuticals, New Frontiers Science Park (South), Third Avenue, Harlow, Essex,CM19 5AW, United Kingdom

Handbook of Thermal Analysis and Calorimetry. Vol. 4: From Macromolecules to Man.
R.B. Kemp, editor.

Chapter 1

ENERGETICS THAT CONTROL THE STABILITY AND DYNAMICS OF SECONDARY AND TERTIARY STRUCTURE OF NUCLEIC ACIDS.

H.H. Klump

Department of Biochemistry, University of Cape Town, Republic of South Africa.

1. INTRODUCTION: CURRENT ADVANCES IN THE STUDIES OF DNA AND RNA STRUCTURES.

The concurrent advances in the preparation of significant quantities of nucleic acids, both RNAs and DNAs, coupled with the development of sensitive calorimetric instrumentation, has resulted in a substantial increase in the thermodynamic characterization of biologically important systems. In this chapter I will describe some of the recent applications of calorimetry for exploring the origins of nucleic acid stability, the mechanisms of secondary and tertiary structure folding and unfolding, as studied through the use of model compounds, and the prospect of nanostructures based on nucleic acids. Certainly, many additional investigations will be required to understand the macroscopic and microscopic origin of the intra and inter-molecular recognition events that are at the roots of biologically significant processes.
There have been several reviews on the thermodynamics of DNA unfolding [1, 2,3] so that the overall stability and the melting behaviour of any given B-DNA duplex structure can be predicted from its known primary sequence [4]. In this overview I will rather concentrate on non-inear nucleic acids/structures. Several non-linear, but nevertheless highly helical structures have been found. In these cases apparently random sequences find complementary sequences with which they pair generally in the standard Watson-Crick base pairing mode. There have been cases of local three-strandedness, and even G-quartet structures have been reported. The best known and most widely studied non-linear structures are the transfer RNAs (tRNAs). Here a two-dimensional set of stem-loop structures are arranged in a clover-leaf in the absence of Mg^{2+}, which folds into a three-dimensional structure in the presence of Mg^{2+}. Other naturally occurring RNAs

rarely show the strict complementarity known from DNA double helices. Researchers therefore concentrate on the information available on the structure and stability of hairpin loops, internal loops and bulges. While true knots are almost certainly rare, pseudoknots were suggested to exist at the 3'-end of some plant viruses. In a pseudoknot the stems of the two separate double helices can stack on each other coaxially, separated by two loops, which cross in the major and minor groove, respectively, of the composite helix. These structures have been studied by NMR and more recently by calorimetry. By no means can this compilation be regarded as exhaustive, it should rather serve as an indication of new and exciting developments in a field of which, according to Francis Crick, "you can hardly know too much about."

2. THE DNA WORLD

2.1 Thermodynamics of DNA-helix formation: Correlation between enthalpy and entropy changes

The focal point of this section pertains to the strong correlation between enthalpy and entropy changes observed for the dissociation/association of DNA base pairs and their next nearest neighbours' impact on a particular base pair. In short this is called enthalpy-entropy compensation in DNA melting thermodynamics.

The formula developed to describe the melting temperature T_m of a DNA double helix in terms of nearest-neighbour doublets (parametrization of DNA melting) takes for granted that the entropy change upon melting is the same for all doublets and is only a representation of the gain in conformational entropy per segment along the backbone (ΔS = 100 J/mol K) [5]. If ΔS is constant then the enthalpy for the denaturation of a given doublet is proportional to the transition temperature ($T_m = \Delta H/\Delta S$) [6]. For each doublet there is a characteristic enthalpy change upon melting (ΔH_{xy}) that originates from base pairing and from the stacking interaction between nearest neighbours x and y [7]. The average enthalpy change per mole of doublet is given as

$$\Delta H = \sum \Delta H_{xy} f_{xy} \tag{1}$$

where $f$xy is the mole fraction of doublet xy and $\sum$ is the sum for all xy doublets in the helix of length n (number of base pairs) which has n-1 stacked base pairs (bp) contributing to helix stability [8]. The term xy means that the base sequence 5′-xy-3′ on one strand pairs with the complementary base sequence 3′-xy-5′ on the opposite strand. This takes into account that the two strands are antiparallel

[9]. So there are 10 distinguishable xy pairs arising from the 16 possible nearest neighbour base sequences in a canonical DNA. The average entropy change per mole of doublet is $\Delta S = \Delta H/T_m$. If we consider ΔS_{xy} = C (constant) then $\Delta H_{xy}/T_{mxy}$ must be constant and accordingly the T_m of a particular sequence must be the sum of the individual xy base pair contributions [10].

$$T_m = \sum T_{xy} f_{xy} \tag{2}$$

The validity of this equation is limited to long DNA sequences where end effects and strand concentration do not play any role. For shorter sequences corrections have to be introduced to account for end effects and for the dependence of T_m on strand concentration. It has to be kept in mind that T_m is strongly dependent on the ionic strength of the solution [11], so to make these experiments viable the ionic strength (μ = 20 mM or 75 mM) must be low enough to allow even the most stable base pairs to melt below the normal boiling temperature of water. In salt solutions of 1 M or even higher, T_m for most long DNA sequences exceeds the boiling point of water and cannot be measured directly unless precautions have been taken [12]. But short duplexes of 10 bp can be carefully investigated over a wide range of total oligomer concentration [13]. Tinoco and co-workers have developed an empirical equation which gives the relation between the equilibrium constant for the duplex dissociation at T_m and the corresponding free energy change under standard conditions,

$$\Delta G^\circ = -RT \ln \mu K = R T_m \ln (4/C_t) = \Delta H^\circ - T_m \Delta S^\circ \tag{3}$$

Accordingly ΔS° and ΔH° can be extracted from a van't Hoff plot of $R \ln (4/C_t)$ versus $1/T_m$. The data extracted from a set of optical melting curves has been confirmed by Breslauer and co-workers [14] using calorimetry (Table I). The data are extracted from a set of short helices where one base pair was replaced at a time by another. As duplexes are made longer, their enthalpy and entropy changes increase with the number of base pairs and the contribution from C_t becomes less significant. When n = 100 then total strand concentration drops to 10^{-5} M and the term reflecting the strand concentration becomes negligently small. A plot of ΔS° versus ΔH° fits a rectangular hyperbola showing the enthalpy-entropy compensation clearly [15]. A satisfactory fit of the data is obtained by using an analytical expression for the hyperbolic curve according to equation 4 where:
$T_m = T_o + (\Delta H^\circ/\alpha)$, T_o = 273 K and α = 334 J/mol K.

$$\Delta S^\circ = \frac{\alpha \Delta H^\circ}{\alpha T_o + \Delta H^\circ} \qquad (4)$$

This expression for ΔS° versus ΔH° has the form of a rectangular hyperbola passing through the origin. Near the origin, where ΔH° is much less than αT_o, ΔS° is close to $\Delta H^\circ / T_m$. If ΔH° increases the slope decreases continuously as ΔS° approaches α. Taken together the melting temperature for a particular doublet relates in the following way to the standard melting enthalpy of this doublet,

$$T_m = T_o + \frac{\Delta H^\circ}{\alpha} = \sum T_{xy} f_{xy} \qquad (5)$$

where $T_{xy} = T_o + (\Delta H^\circ_{xy}/\alpha)$. The constant T_o may reflect the influence of solvent on DNA melting, α is assumed to reflect the combined entropy change due to rotational freedom along the backbone single bonds after the inplane H-bonds have been abolished and due to the solvent entropy change. T_o is within experimental error the same as the melting temperature of ice. This is the result for canonical DNA doublets in 1M NaCl, where T_o becomes 273 ± 15 K and α is about 334 ± 42 J/mol K. It can be assumed that the same constant values hold at lower salt concentration (Table I).

In summary it can be stated that the analysis of thermal melting and calorimetric data has established the following points:

(i) ΔS° is not a constant for DNA doublets but varies according the enthalpy-entropy compensation needs;

(ii) the variation of ΔS° with ΔH° follows a rectangular hyperbola, characterised by two constants, T_o and α;

(iii) the constant α is much larger than ΔS° and is interpreted as the combined DNA plus solvent entropy change during the DNA melting;

(iv) the constant T_o is close to the melting temperature of solid H_2O. The large value of α (334 J/mol K) indicates that the calculated solvent enthalpy change, αT_o = 92 kJ/mol, is considerably larger than any ΔH° value found experimentally for any base doublet. The implication is that the solvent related enthalpy and entropy changes exceed the corresponding parameters for DNA upon melting. From the magnitude of αT_o one can conclude that at least 4 H-bonds within the water structure are broken. The number could be larger depending on the strength of H-bonding between H_2O and the dissociated Watson and Crick base of a denatured base pair.

Table I
Experimental $\Delta H°$ and $\Delta S°$ values for melting of normal DNA doublets in 1M NaCl, pH 7.0 and corresponding calculated values of T_m.[a]

Doublet XY/X'Y'	ΔH^{ob} kJ/mol	ΔS^{ob} J/mol K	T_m °C
AA/TT	38.0	100.3	113±1
AT/TA	35.9	100.0	105±3
TA/AT	25.1	70.6	76±2
GT/CA	27.2	72.3	85±4
	(36.8)	(101.2)	(108±3)
TG/AC	24.2	53.9	94±21
	(33.9)	(82.8)	(107±6)
GA/CT	23.4	57.7	85±15
	(57.7)	(81.1)	(87±5)
AG/TC	32.6	86.9	99±1
	(36.4)	(111.6)	(105±4)
GG/CC	46.0	111.2	138±1
GC/CG	46.4	111.6	139±1
CG/GC	49.7	116.2	149±1

[a] Adapted from Reference [14].

2.2 Forces that control triple helix stability

Felsenfeld et al. were the first to combine long monotonous polyribonucleotides to form triple helices [16]. More than ten years later (1968) Riley et al. [17] and Morgan and Wells [18] obtained triplexes from polydeoxynucleotides and from hybrid sequences. These structures either originate by a disproportionation reaction of two identical polypurine polypyrimidine complexes which at moderate to high ionic strength and elevated temperature rearrange to a triple helix consisting of two pyrimidine strands and a purine strand, and a partly stacked, single stranded polypurine strand, or by mixing matching polypurine and polypyrimidine strands at high temperature and high ionic strength in a ratio of 1-2 [2]. The purine strand forms an antiparallel Watson-Crick double helix with a pyrimidine strand while the second pyrimidine stand binds via Hoogsteen hydrogen bonds to the major groove parallel to the purine strand, forming T-A*T and C-G*C^+ triplets (Table II) [19]. The cytosine of the third strand has to be

protonated at the N3 position in order to establish a CG*C^+ base triplet. Since the pKa of the amino group of cytosine is well below 7, the formation of the C^+ containing triplexes is pH-dependent. Replacing cytosine by 5′ methyl-cytosine abolishes the pH-dependency. There is an alternative to this first motif. The second motif involves 2 polypurine strands and one polypyrimidine strand. T or A in the third strand will bind to the Hoogsteen site of A in the duplex, leaving the Watson-Crick hydrogen bonds intact [20].

Correspondingly G in the third strand binds to G in the duplex [21,22,23]. The second motif often requires high divalent cation concentrations, and the third strand being G-rich, is prone to form self-associated structures involving G-quartets [24]. This is particularly pronounced when the third strand is a triplex-forming oligonucleotide (TFO) [25,26]. Another competing structure, a G-A parallel duplex, can also interfere with triplex formation [27].

Table II
The Third-Strand Binding Code.

	Third Strand Residue				
Watson-Crick Core	A	T/U	I	G	C
A T/U	+	+	+	-	-
G C	-	-	+	+	+

The possibility of undesired competition from self-association of the pyrimidine third strand in triplexes which form in the first motif has been generally neglected except in a few cases [23,28]. At slightly acidic or even neutral pH, oligodeoxyribonucleotides which include stretches of cytidines form a tetrameric structure involving C-C^+ base pairs in a so called i-motif [29]. Formation of this motif, whether intramolecular or intermolecular, was demonstrated to act as an undesired, competing structure for triplex formation. The so-called i-motif is a tetramer of equivalent strands, which present the novel feature of intercalated C-C^+ base pairs of two parallel-stranded duplexes, which are only topologically linked. The individual parallel-stranded duplexes are underwound and right-handed. The two duplexes are "zipped together" in an antiparallel fashion. Recently, the structure and stoichiometry of the complexes formed by short, cytosine rich oligonucleotides has been solved by NMR [29] and by x-ray crystallography [30,31]. Because of the undesired side reactions much effort has been centred on intramolecular triple helices (Figures 1 & 2) [32,33]. In these conditions, intramolecular folding based on cytosine self-pairing is limited.

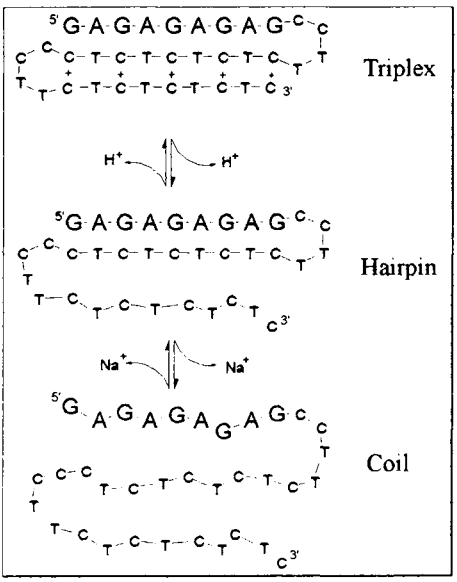

Figure 1. Unfolding pathway of an intramolecular triple-helix forming oligomer. Adapted from Reference [39].

There are several factors that could affect the balance between self-association and triplex formation. Triplexes are particularly stabilised with an RNA third strand binding to a DNA double helix [34,35,36,37]. In general, these triplexes are more stable than the corresponding triplexes with a DNA third strand. 2'0-methyl oligonucleotides will introduce a further gain in stability [34, 38]. There is a limited tendency to form undesired structures in these modified sequences. The first motif with its Hoogsteen code (T recognising TA base pairs, C^+ recognising CG base pairs) can be expanded when one uses inosine with its ability to bind indiscriminately to both AT and GC base pairs [38]. One or more inosines can be incorporated into the Hoogsteen strand in place of T and/or C. The influence of inosine on the triplex-duplex equilibrium can be assessed through the melting temperature of the triplex [39]. In all cases inosine replacement lowers the stability of the complex. This is due to a combination of distinguishable influences of third-strand inosines which affect binding, namely backbone distortion due to a bulkier purine residue and/or loss of intramolecular ion pairs between charged cytosines and phosphate residues when inosine replaces cytosine-cations. Replacing more than two thymines and/or cytosines, respectively, eliminates the binding of the Hoogsteen strand at room temperature altogether. Under no circumstances does inosine stabilise the triple helix: it is a

poor substitute and its value as a "wild-card" or an extension of the "Hoogsteen code" is very limited. There is a severe penalty for promiscuity [39].

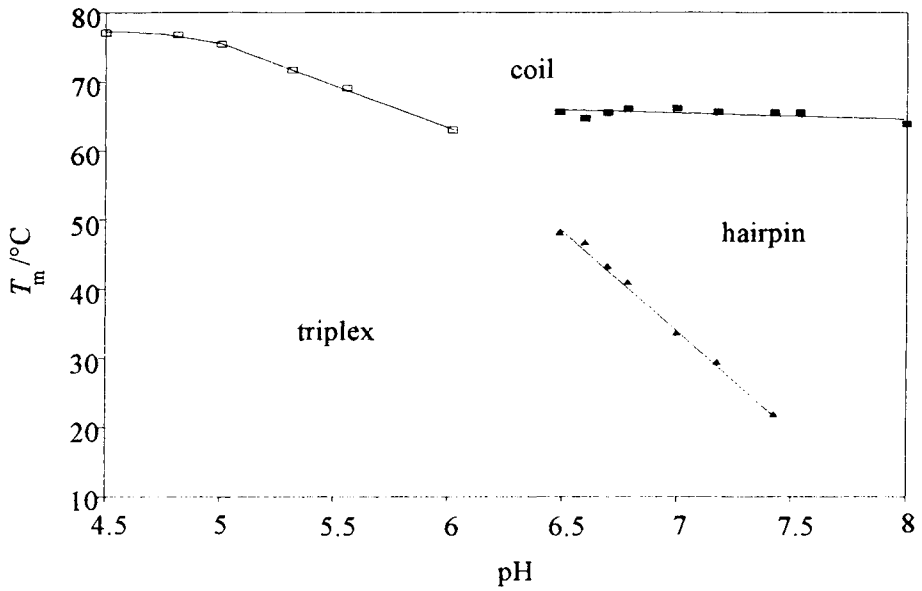

Figure 2. Phase diagram (T_m vs. pH) of an intramolecular triplex in 100 mM [Na^+] Adapted from Reference [39].

2.3 Investigation of sequence specificity of DNA triplex formation using isothermal calorimetry

DNA triplex formation has developed into a versatile tool for modification and gene control [21]. It has been applied to specific cleavage of DNA [40], repression of gene expression [41], and genome screening. Triplexes can form between a double-stranded homopurine-homopyrimidine (Watson-Crick) and a single stranded homopyrimidine tract (Hoogsteen) or more recently a homopurine tract [22]. The main differences between binding of the homopyrimidine vs homopurine tract is a pH-requirement for homopyrimidines (pH 5) if there are cytosines within the Hoogsteen-strand while purine-oligonucleotides do not require and are not sensitive to pH shifts [42]. In any case the strand binds to the major groove of the double-stranded W-C complex homopolypyrimidine strands bind in parallel to the purine strand while the complementary polypurine strands binds in the antiparallel orientation with respect to the Watson-Crick purine strand.

Besides the canonical triplexes formed, for example, between thymine and the adenine-thymine base pair and cytosine and the guanine-cytosine base pair other combinations have been suggested to form stable triplexes, e.g. G-TA, G-GC and T-GC [43]. The stability of triplexes depends on pH, ionic strength, temperature, and, in cases where the Watson-Crick duplex is part of a plasmid DNA, it depends on supercoil density [44].

In order to understand the mechanism of triplex formation and to assess the effects of sequence and environment on specificity and stability, it is necessary to obtain detailed thermodynamic and kinetic data for the binding processes. The dissociation process has been widely investigated using UV-melting [35], CD melting and differential scanning calorimetry (DSC) [45]. The association process of triple formation has drawn much less attention and its mechanism has not been as well understood as the denaturation [46]. There are several pieces of evidence indicating that triplex formation is not compatible with the assumption of a simple two-state reaction. Thus it is important to investigate the formation of triplexes, and to acquire the data set which describes the complex formation by means of isothermal titration calorimetry (ITC). Titration calorimetry will give the complete set of thermodynamic data describing triplex formation such as enthalpy, heat capacity changes, binding free energy and entropy change (see Figure 3).

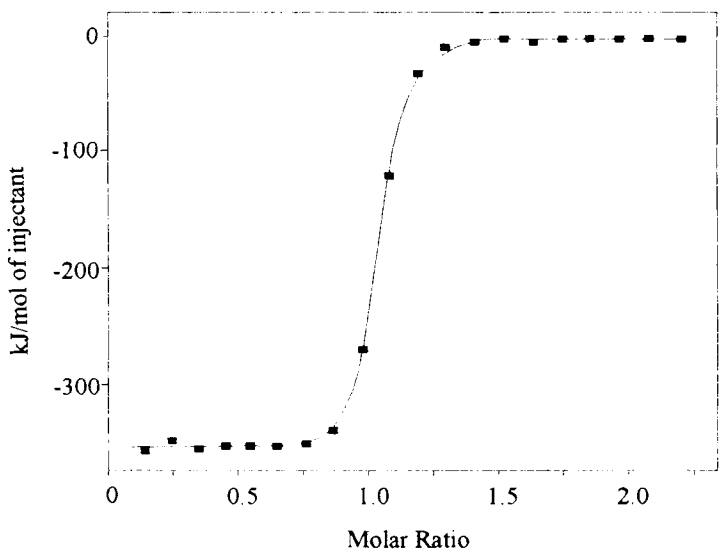

Figure 3. An isothermal titration calorimetry (ITC) curve of a 15mer triple helix. Adapted from Reference [46].

Kamiya et al. [46] mixed a double stranded homopurine - homopyrimidine complex with a single-stranded homopyrimidine oligonucleotide containing both T-AT and C^+-GC triads at pH 4.8. Based on their results one can discuss the mechanism of triplex formation and suggest possible means for enhancing sequence specificity. At 25 °C and pH 4.8, 200 mM Na^+ and 20 mM Mg^{2+} in 10 mM acetate buffer the single-stranded 15mer oligopyrimidine was added to a double-stranded 23mer oligopurine oligopyrimidine. The resulting reaction enthalpy amounts to 351 kJ/mol and the association constant K to 9×10^{-7} M^{-1}. The triplex formation is driven by a large negative enthalpy change. From the association constant the value for the binding free energy ΔG, is calculated to be -189 kJ/mol. Thus the entropy change ΔS, for triplex formation amounts to -1024 (J/mol K). To evaluate the heat capacity change (ΔC_p) the enthalpy change associated with the triplex formation has to be determined at different temperatures [46]. ΔH increases with increasing temperature from 305 kJ/mol at 15 °C to 380 kJ/mol at 35 °C. The estimated value of ΔC_p is -3820 (J/mol K). Since the magnitude of ΔC_p is much larger than that of ΔS, $-T\bullet\Delta S$ has a similar temperature dependency as ΔH. There is a pronounced energy-enthalpy compensation resulting in a marginal ΔG vs T slope (Figure 4).

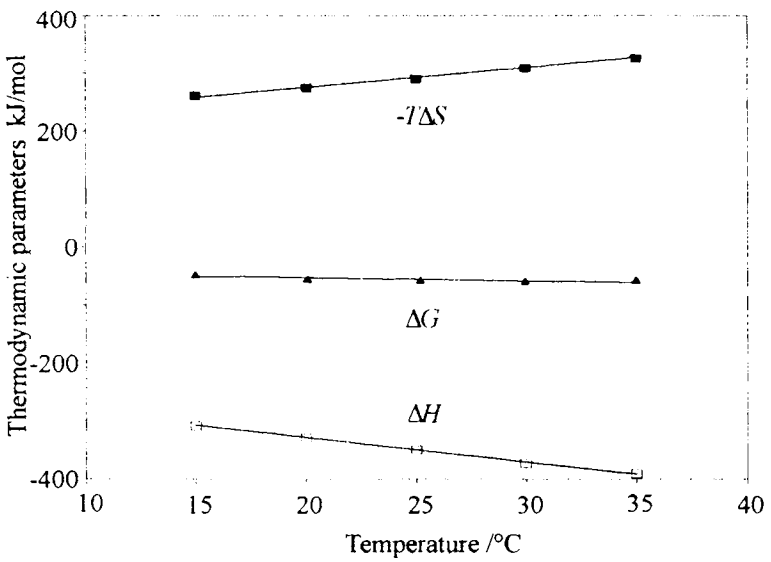

Figure 4. Thermodynamic parameters for the formation of a 15mer oligopyrimidine triple helix (10mM Na Acetate, 10 mM Na Cacodylate, 0.2 M NaCl, 20 mM $MgCl_2$ & pH 4.8). Adapted from Reference [46].

Concurrent CD measurements support the assumption that the enthalpy change observed is actually due to triplex formation. The magnitude of the enthalpy change due to triplex formation is sensitive to a number of influences, such as pH, ionic strength and sequence composition. Sequences containing cytosine, which have to be protonated to be included in the triple helix exhibit a pH dependent association enthalpy since upon binding cytosines have to be protonated on expense of the buffer. At pH 4.8 approximately 33% of cytosines will be protonated in solution (p*K*a of cytosine is 4.5). Accordingly the experimentally obtained ΔH value has to be corrected for the deprotonation enthalpy of buffer and protonation enthalpy of cytosine. The present results also suggest that the conformational states of the single-stranded oligopyrimidine in solution play an important role in the thermodynamics of triplex formation. It is also noted that the conformational stability of these sequences is strongly sequence dependent. In fact the conformational equilibrium of disordered single strands is coupled to the triplex formation in such a way that a well protonated single strand with prestacked nucleotides will yield a lowered association enthalpy on binding than a slinky sequence which requires extensive protonation. Any change in sequence which lower the conformational entropy of the single strands will lead to a preferred binding. This should be one of the features to take into account when designing modified oligonucleotides which should show enhanced sequence specificity as antisense drugs [47].

2.4 Determinants of oligonucleotide triple-helix stability and specificity

To assess the current state of the thermodynamic database for triplex helix formation from three complementary sequences which are either linked within one molecule or spread over two or more molecules one has to critically assess the methods applied to obtain the relevant data [48]. As a great many published papers reveal, the thermodynamic stability has to be discussed in terms of its dependence on a set of parameters, most important the temperature, the pH, sequence composition and lesser important the length, cation concentration, base and backbone modification, and ligand binding [32]. Understanding the fundamental principles underlying the specificity and energetics of the molecular interaction of one nucleic acid molecule with one or more other nucleic acids is a key to specific therapeutics, diagnostics or tools in biotechnology [49]. The parameters referring to the Watson-Crick DNA duplex, which is part of triple helix formation, have been extensively reviewed in the literature. The focus here is on non-Watson-Crick base-base interactions via hydrogen bonds and intrastrand interactions via base stacking. Since initially reported in 1957 [16] there was a long period of very limited interest in triplexes. Renewed interest has

sprung up recently mainly due to two factors. First came the discovery of an intramolecular triplex in supercoiled plasmids (H-DNA) which may play an important role in mediating gene activity in living cells [50]. A much higher degree of excitement was created by the proposal to use sequence-specific recognition of double stranded DNA by oligonucleotides to develop an antigene technology [40].

The elucidation of the cellular role of oligonucleotides as well as the rational design of them for the control of biological activities will require a basic understanding of how the solution conditions and the sequence will influence the stability of triple helices in vitro and in vivo. Characterising the linkage between thermodynamic parameters and solution conditions represents an essential first step towards such an understanding. Great care must be taken to define the states in any thermodynamic system, since meaningful comparisons can only be drawn if either the initial state of the final one of the two systems being compared are identical [51]. Great care must be taken to choose environmental conditions which suppress secondary equilibria that may compete with the desired triplex formation. One of the preconditions, usually taken for granted, is that the isolated single strands are present as random coils. At low pH and/or temperature this may not be the case. Only recently it has been discovered that C-rich single strands at low pH can form duplexes which combine through topological links to quadruplexes (i-motif) [29]. Similarly, oligopurines with continued runs of guanines in the presence of potassium can self-associate to form quadruplexes (G-quartets) [24]. Each of these self-association events will compete with duplex formation and even with triplex formation and influence the thermodynamic behaviour of the system. Another prerequisite which has to be met is that the system has to be at equilibrium. It has been observed that triplex formation proceeds at a slower rate compared with duplex formation, so sufficient time is required for the system to equilibrate [27]. Several model systems have been reported for the study of oligonucleotide based triple helices. An important difference between the model systems is the molecularity of the complex which in turn makes the system either concentration dependent or independent [52]. The choice of an intrastrand triplex formation seems to be the most straight forward approach yet the presence of the loops that connect the paired region in some of these model systems may not be as benign as anticipated. Nuclease digestion experiments show that the third stand binding of the 3′ end of the sequence into the groove of the 5 Watson Crick hairpin results in distortion of the loop that joins the Watson-Crick hairpin helix [53]. This observation is in line with the perturbation, relative to standard B-form DNA, as shown by Radhakrishnan & Patel [53]. In general there is always a possibility for at least

transient interactions between single stranded loop sequences and other single stranded extensions of hairpin helixes. An approach is made to minimise such complications by choosing non-nucleotide linkers [54].

Appropriate choice of solution conditions and careful design of helical and intervening sequences can enable triplexes to undergo two distinct order-disorder transitions. The triplex-to-duplex transition can be decoupled from the canonical duplex-to-coil transition [55]. The intramolecular triplex provides significant advantage when one considers stoichiometry of the different helical segment, and the orientation of the third strand with respect to the orientation of the Watson-Crick purine strand. They are also extremely useful for the systematic evaluations of basic triple defects, unusual bases, or internal bulge loops in the third strand. When considering the effects of small perturbations (mismatches, bulges, etc.) well removed form the ends, the analysis most suitable to use is based in differences ($\Delta\Delta H$, $\Delta\Delta G$, etc.) [56]. Anomalies which come from unavoidable end effects are treated independently from changes in the central region, and since they are identical in the reference system and the perturbed system, they can be subtracted out. Although the primary thermodynamic data will be to some extent compromised by the end effect, the change created by the perturbation will be readily reflected in the change of the thermodynamic parameters. Intramolecular triplex formation has been reported for a great number of pyr.pur.pur. and a few pyr.pur.pur. triplex motifs. The three dimensional structure of these folding motifs has been elucidated by NMR. As stated above, the main advantage of the molecularity of one for these transitions is that the thermodynamic parameters are by definition concentration independent. Thus influx of pH and/or ionic strength on the triplex-duplex transition are more clearly discernible [56]. In fact, the decoupling of concentration effects by studies on intramolecular triplexes has allowed construction of detailed phase diagrams and the development of a semi-empirical model for triplex-duplex and duplex-to-coil phase behaviour [48].

Coupled equilibria play a large role in the overall thermodynamic behaviour of oligonucleotide triple-helix systems. As one can clearly see there is a mutual effect of sequence composition on salt and pH dependence of the melting temperature. The most difficult assessment to date is the estimate of the uptake or release of potentially associated water molecules upon the conformational change. Drug binding also can couple to third-strand binding equilibria to either stabilise the triplex and shift the equilibria away from the Watson-Crick double helix stability or vice versa [57]. Any protonation reaction, necessary for third strand binding through cytosines which require a charge uptake, is linked to pH changes in the buffer solution present. So buffers with a large heat of protonation such as Tris (Tris-hydroxymethyl-amino-methane) will exhibit a temperature

dependent shift in pH and should be avoided. Finally one has to bear in mind that the pKa value of hydrogen-ion buffers depends on the concentration of the supporting electrolyte in solution.

All of the noncalorimetric methods for the determination of the change in Gibbs free energy accompanying the complex formation of oligonucleotides depend on the well known van't Hoff equation [8]. A complete description of this equilibrium requires the knowledge of the number of each chemical-distinctive species, including protons, cations, anions, and water, i.e. any change will influence the equilibrium. When comparing the equilibrium constants for different processes one must be sure that K is defined properly. In the simplest case K for a hybridisation process which leads to triplex formation is a function of the relative concentration of the contributing oligonucleotide species. The methods for the exact determination of the amount of free and bound oligonucleotide are usually based on one of the three physical principles: electrophoresis which leads to a physical separation of the species, spectroscopic estimation through selection of characteristic wave length for each component, or selecting a temperature (T_m) at which relative concentrations of components are equal [23].

The most straight forward approach to discriminate between the constituents and the complex at least for the qualitative description of the system is by gel electrophoresis, because the electrophoretic mobility of the larger complexes differs considerably from the single stranded oligonucleotides. This approach requires only very little material, and leads to rapid results but it requires that the complex is stable under the running conditions, i.e. temperature, buffer, and electric field strength. When single strands are radiolabelled the isolated bonds can be quantified and the equilibrium constant evaluated. Two dimensional gel electrophoresis can be used to elucidate the unfolding of the complex when the second dimension is a temperature gradient [33]. This method requires that the complex can be isolated and used as the starting material. Frequently one only is interested in the difference in free energy changes ($\Delta\Delta G$) associated with a mismatched complex as compared to a perfect one. Conditions can be found where both complexes are stable and can be separated by gel electrophoresis. Quantification of the bands allows the direct determination of the relative equilibrium constants and thus $\Delta\Delta G$. These techniques are relatively easy to execute when dealing with an intramolecular triplex, because only different conformations compete but no new molecular species are created. In all the cases where the molecularity is not one, more complex analytical methods are required which are beyond the scope of this chapter. A note of caution is necessary at this point. It has become common practice to measure T_m and T_m differences (ΔT_m)

between two processes, i.e. the melting of a perfectly matched complex and a mismatched complex, and to interpret the ΔT_m value as a true reflection of the difference in Gibbs free energy changes at some temperature well below T_m. This approach contains some pitfalls, i.e. it ignores any differences in the temperature dependence of ΔG; it does not account for the enthalpy change for the two processes which is usually not the same. Shifts in T_m with changes in the concentration of an effector (pH, peptide) can be interpreted as an indication of the affinity of the effector for the initial (T_m increases) or the final state (T_m decreases) of the nucleic acid complex. If no change in T_m is observed as a function of effector concentration, then there is either no binding to any of the molecular species present or equal binding to all of them [35].

The knowledge of the free energy change which goes with the triplex formation is useful, but it only applies to the conditions under which the measurement is made. The temperature dependence of the free energy change of a process is reflected in the enthalpy term (ΔH). Enthalpy changes are measured directly using sophisticated calorimetric techniques [58]. Isothermal mixing calorimeters have been employed to measure the binding of a single strand to hairpin helixes in order to form a triplex [59]. Differential scanning calorimetry (DSC) differs from other calorimetric techniques in its model free, direct measurement of the transition temperature, T_{max}, and the change in enthalpy, ΔH, heat capacity, ΔCp, entropy ΔS, and less directly, free energy ΔG, accompanying the temperature induced transition from an ordered state like the triplex, to a less ordered state, a hairpin helix with a dangling end, and finally to a randomly coiled state [60]. It should be noted that the results from mixing experiments (mostly at room temperature) are not identical to the results at the transition temperature T_m of canonical triplexes (ca. 50 °C) measured by DSC because the conformational state of single strands at room temperature is different from the conformational state of the same single strand when released from a hairpin helix at elevated temperature [47]. If direct calorimetric methods are not applicable for lack of material, model-dependent van't Hoff enthalpies can be obtained by measuring the temperature dependence of some equilibrium property such as the extinction coefficient (260nm). It has to be kept in mind that this approach is only valid for a two-state process and/or if the whole molecule can be viewed as the co-operative unit. Van't Hoff enthalpic techniques include optical spectroscopies in the ultraviolet range (UV), circular dichroism (CD), and nuclear magnetic resonance (NMR). The most widely used techniques among the three is temperature dependent UV absorbance spectroscopy [61]. The resulting absorbance vs. temperature curve can be analysed in several ways to derive the

necessary data (T_m, ΔH, ΔS, ΔCp, and ΔG). Since these are not direct measurements of the heat of the process certain assumptions about the nature of the reaction under study have to enter into the evaluation of data. How good is the quality of the data extracted? This depends profoundly on the appropriateness of the particular assumptions. In principle, the free energy ΔG can be extracted from the van't Hoff analysis as well as K, in addition to the enthalpy. However, the statistical coupling of the parameters and the propagation of error made this method less reliable than the determination of ΔG measured by equilibrium constant determination. The computation of ΔG based on data obtained by differential scanning calorimetry is hampered for the same reasons [62].

On planning experiments where an oligonucleotide is targeted to bind to one particular sequence within a large megabase DNA it has to be borne in mind that there are sequences along this DNA which bind with one, two, three or more mismatches. Under these circumstances, given the correct sequence is synthesised, the target complex and the thermodynamic stability depends on the chain length. For the *E.coli* genome every possible 12mer sequence can statistically be present only once. So, to choose a 15mer or even an 18mer will suffice to outscore all competing sequences [63]. Using a number of techniques, several groups have studied the influence of defects such as base triple mismatches or looped-out third strand bases on the triplex stability. They found that not only the number of mismatches but also their position is important [52]. Central mismatches have a more disabling effect as compared to mismatches positioned towards the ends. The free energy penalty for a single bulge or misspairing base amounts to 12.5 kJ/mol [35]. Interestingly, the enthalpic penalty is apparently small. To this aim several attempts have been made to improve stringency. One of the attempts is to use a different, non-ionic backbone (see section 2.6 on PNA). More advanced approaches try to use circular oligonucleotides which bind to the Watson-strand and probe the Hoogsteen strand, but eliminate the Crick strand, which results in an enthalpy penalty but an entropy gain [64]. The most recent approaches rely on a minor groove binder (not a nucleic acid) tethered to a major groove binder to create maximal specificity.

It is important to find ways and means to enhance specificity by chemical modification and/or changing the conformational entropy (circular structure) and/or linking the binding to the major groove to the binding to the minor groove (drug, peptide). In vitro pH, salt concentrations or temperature can be changed deliberately to increase specificity, but there is no such choice in vivo [65].

As discussed above, the free energy change accompanying the unfolding of the triplex, depends strongly on the solution conditions. This dependence is primarily

entropic in origin, due to the release of ions and exchange of water between the oligomer strands and the solution [66]. There is no detectable sequence dependency of the entropy change per triplet. To detect differences in stability between different triple helices under a given set of solvent conditions, one has to focus on the differences in enthalpies of unfolding. From early DSC experiments it was clear that the binding of the third strand is less tight than binding between the Watson and the Crick strand [67]. Only quite recently have oligonucleotides been used to systematically study the energetics of triple helix formation. Unfortunately the comparison of the available enthalpy data is complicated by different approaches the various research groups opted for in their quest to acquire triplex data. There is a variation in sequence, in base composition, in molecularity, and in the applied techniques. Despite these problems, inspection of the published enthalpy data reveals some regularities that may prove to be meaningful. Mixing calorimetry and DSC, at and near pH 7, yield enthalpy values of 8.4 - 17.6 kJ for the Hoogsteen bond forming nucleotides. It is surprising to note that the model-independent results are systematically lower in comparison to the van't Hoff enthalpies under identical conditions, which range from 8.4 - 29.3 kJ/mol nucleotide, but most of the values cluster in the range of 21 - 29 kJ/mol [35]. Only at lower pH is the apparent disparity between the two sets of data insignificant. Several explanations for the discrepancy are put forward. They centre on aggregation, slow rate of reaction or heats of protonation. No evidence of aggregation has been found, however, so this can be ruled out. Measuring protein unfolding of certain globular proteins by DSC and by spectroscopic methods one has observed a similar discrepancy in all cases where an unusual intermediate state (molten globular state) is present [68]. Variation in the scan rate is employed to test for the claim that equilibrium state has been reached and the scan rate of the instrument did not outrun the slow kinetic response of the system under investigation. So failure to reach equilibrium is not a good explanation either. It has to be stated that the true origin of the disparity in the calorimetric and van't Hoff enthalpy data remains unclear.

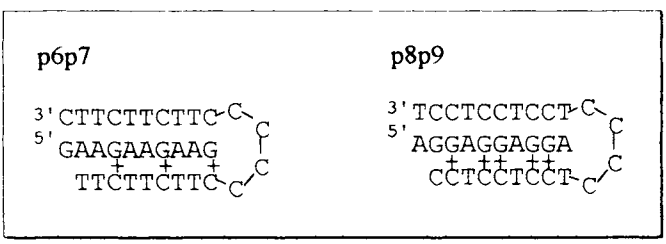

Figure 5. Purine oligomers p6 & p8 combine with pyrimidine oligomers p7 & p9 to form triple helices p6p7 & p8p9. Adapted from Reference [56].

Table III
Thermodynamic Parameters for the Unfolding of Triple Helices p6p7 and p8p9 and the Number of Protonated Hoogsteen Sites [a].

Triplex	ΔH kJ/mol	ΔS J/mol K	T_m °C	$\frac{\partial(1/T_m)}{\partial pH} 10^{-5}$	Integer Predicted n value	Number of value for n	Hoogsteen cytosines
p6p7[b]	-538.0±24.2	-2913±54	58.2	9.71±0.5	2.7±0.14	3	3
p8p9[c]	-568.1±24.7	-1596±100	60.0	16.3 ±1.0	4.8±0.30	5	6

Note: Buffer: 20 mM Na_2HPO_4, 1M NaCl. Thermodynamic parameters for the unfolding of triple helices p6p7 and p8p9 were obtained by differential scanning calorimetry and the number of protonated Hoogsteen sites (n) was deduced from the slope $\partial(1/T_m)/\partial pH$.

[a] Adapted from Reference [56].

[b] pH 6.0

[c] pH 5.3

Recently Singleton and Dervan proposed a direct application of the van't Hoff equation to determine the binding constant as a function of temperature [69]. In their approach they introduce an affinity cleavage titration method. The van't Hoff enthalpy of 8.4 kJ/mol triple base binding corresponds well to the DSC result of 8.4 kJ obtained for the identical triplet. This agreement between the van't Hoff data and the corresponding DSC data is gratifying and reflects a yet-to-be-understood advantage of the new cleavage-titration method. Taken together, the above observations suggest that a van't Hoff analysis is only meaningful for short oligonucleotide complexes, for which the all-or-none nature of the order-disorder transition can readily be assumed.

Because the C^+-containing triplexes have a reduced charge density relative to T-rich triple helices, the ionic strength dependence of the thermal stability (ΔT_m /$\Delta \ln[Na^+]$) of these triplexes can be positive, approximately zero, or even negative depending on the (C^+-GC) content [32]. In any case the counterion release upon dissociation is greater for T-rich triplexes than for duplexes. C^+ containing Hoogsteen strands exhibit an intrastrand charge compensation between the protons binding to cytosines and phosphate groups in the backbone, lowering the overall surface charge density of cytosine rich triplexes. Solutions containing not only a single cationic species, but for instance Mg^{2+} and either of the two alkali ions Na^+ or K^+ are difficult to assess in their impact on triplex stability. Clearly, an understanding of the details of such combined cation effects requires further studies.

To predict pH dependence of third strand binding one has to look at next nearest neighbour frequencies of protonated cytosines (see Figure 5). For isolated C^+ residues, T_m vs pH is linearly dependent on the fraction of cytosines in the third strand (Table III). It becomes more complex when cytosines are clustered because experimentally it was found that the number of released protons is smaller than the number of cytosines in putative C^+-GC triplets. The explanation put forward for this observation is that there is only partial protonation of the cytosines in the resultant single strands, a plausible explanation at low pH [33]. It is conceivable that there is an equilibrium between protonated and nonprotonated sites that will result in partial protonation. Since the interior of cells is strictly regulated it is obvious that for in vivo studies only triple helix formers can be applied which bind at pH 7. This requires modifications of the oligonucleotide sequence and the introduction of methylated cytosine residues, to allow for a pH-independent recognition of GC base pairs. Indeed, substitution of 5-methylcytosine for cytosine increases the stability of polymeric and oligomeric triplexes. The alternative approach requires a triplex formed by the association of a purine-rich oligonucleotide to a double helical target in a pH-independent

manor. Methylation of third strand cytosine results in an increase in triplex T_m. However, the methylation-induced enhancement of triplex stability is not accompanied by a change in enthalpy. Consequently, methylation seems to cause a favourable entropic contribution to the triplex Gibbs free energy. It is the increased hydrophobicity imparted by methylation which is reflected in the observed favourable entropy of triplex formation. This is in line with the postulated hydrophobic origin of the effect on triplex stability. There are particularly long-lived hydration sites in the major groove into which the 5 methyl group projects. Other substituents, however, do not seem to have the same effect although they are hydrophobic [45].

Some effort has gone into the study of the relative stability of triplexes composed of various combinations of DNA and RNA strands [36]. The qualitative agreement between data obtained from very different systems is gratifying. Quantitative differences in relative Gibbs energy changes are reported. This does not come as a surprise if one considers the variation in solution conditions, sequences, molecularity of the triplex forming reaction, and experimental methodology. One of the many surprises in these studies was the observation that, when the duplex purine strand is RNA and the Hoogsteen pyrimidine strand is DNA, no triplex is formed independent from the character of the duplex pyrimidine strand. Coupling triplex formation of mixed-backbone oligonucleotides with minor groove binding of a drug for example can improve triplex stability to such an extent that the complex is stable at room temperature [70]. Chemical modified backbones have been introduced with minor or major effects on the triplex stability. The most drastic modification such as in PNA and its impact on secondary formation between short strands is described elsewhere [71]. Great effort has gone into the investigations on the effect of ligand binding on the stability of triple helical complexes. Two different approaches have been favoured, either probing the influence of intercalators, which insert between consecutive base pairs/triplets, or looking at the effect of minor-groove-binding ligands. A striking example of a ligand binding effect on hybridisation of a third strand to its duplex target is the demonstration, that binding of berenil, 4^1-6^1-diamidino-2-phenylindole (DAPI) ethidium bromide, or netropsin all induce the formation of the $(dT)_n$, $(rA)_n$ $(dT)_n$ and/or $(rA)_n$ $(rA)_n$ $(dT)_n$ hybrid of these ligands. Again multivariant effects make it impossible to formulate a simple rule, from which it can be deduced whether the third strand will bind preferentially or whether its binding efficiency is reduced [72]. Efforts have been made to expand the lexicon of base pair recognition by a third strand to overcome the current rigid sequence requirements.

2.5 Variation in DNA-helix stability and health: triple repeat expansion diseases

Expansion of a $d(CGG)_n$ run within the 5'-untranslated region of the X-chromosome linked human gene, named FMR1, blocks eventually the transcription of this gene, delays its replication and by doing so constitutes the fragile X syndrome [73]. This is an inherited, X-linked dominant mental retardation disorder, affecting at the average one in two thousand adults, men more frequently than women [74]. The affected gene, FMR1, houses the Xq27.3 breakpoint sequence [75]. Whereas normal individuals have 2-50 copies of the d(CGG) sequence, the trinucleotide is amplified in affected subjects to >200-2000 copies [76]. Nadel et al. [77] have shown previously that $d(CGG)_n$ tracts have the potential to aggregate into inter-strung tetra helical complexes [78]. Expansion of the $d(CGG)_n$ repeat is accompanied by methylation of (CG) neighbour pairs within the FMR1 promoter as well as the amplified trinucleotide tract [79]. As a consequence of the methylation which again is a consequence of the triplet repeat expansion the FMR1 gene is transcriptionally silenced, and the replication of a chromosomal segment spanning >150 kb 5' and >34 kb 3' from the $d(CGG)_n$ stretch is delayed [80]. More recently it was shown that under physiological conditions, pH 7 and 200 mM NaCl, the stretches can form intramolecular hairpin helices in vitro [77]. The compact $d(CGG)_n$ structures form intramolecularly (unimolecular reactions) as suggested by their zero-order kinetics of formation. This finding is supported by a series of investigations by Gacy et al. [81] and Chen et al. [30] which showed not only the hairpin formation of $d(CGG)_n$ but also of other trinucleotide repeats, which are linked to other mental retardations. It is suggested that the folding of exposed (within a chromosomal loop of actively transcribed genes) expanded single strand runs of $d(CGG)_n$ during the replication of FMR1 could entail slippage and give rise to further trinucleotide expansion, which in turn worsens the defect.

The in vitro studies reported so far are based on kinetic measurements, NMR, UV-melting and mobility shifts as a function of temperature in a non-denaturing observation gel, and on chemical footprinting as well as on methylation protection analysis. The shortest oligonucleotide, an 8-mer, contains two $d(CGG)_n$ repeats while the largest oligonucleotide, a 33-mer, contains ten triplet repeats. Their electrophoretic migration slows down when they become thermally denatured. The heat-denatured $d(CGG)_n$ oligomers migrate in a non-denaturing gel at rates inversely proportional to their length. Their relative mobility becomes anomalously accelerated under annealing conditions.

Taken as evidence for the folding of triplet repeats into more compact forms, this observation is strengthened by the demonstration of UV hyperchomicity of

thermally denaturing $d(CGG)_n$ stretches. Similar hyperchromicity is displayed by unfolding of telomeric DNA sequences [82] (Figure 6).

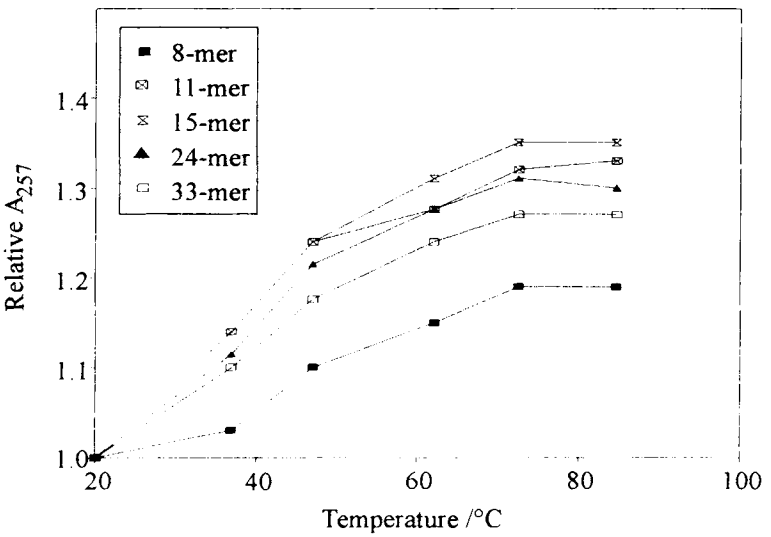

Figure 6. UV hyperchomicity of thermally denaturing $d(CGG)_n$ oligomers in TE buffer (100mM KCL, pH 8.0). Adapted from Reference [77].

The weight of the evidence provided here points to a similar structure of telomeric DNA sequences and the $d(CGG)_n$ tracts [83]. Both are capable of forming back-folded hairpin structures at a physiological range of salt concentrations, temperatures and pH values [84]. Calculations indicate that the stability of the $d(CGG)_n$ hairpin increases linearly with length and that it surpasses a threshold related to expanded $d(CGG)_n$ sequences observed in individuals suffering from Fragile X Syndrome. The proposed structure for the 33-mer has the following features: the sequence folds back with a nearly perfect symmetry to form a hairpin that is stabilised by four guanine-guanine Hoogsteen base pairs and/or ten guanine-cytosine Watson-Crick pairs (Figure 7). Molecular mechanics calculations based on NMR analysis implicates that in the Watson-Crick pairs both nucleotides assume the anti-conformation while in the Hoogsteen pair one guanine is anti, the other one is in the syn conformation. To determine the transition temperature of the hairpins either temperature gradient electrophoresis or electrophoretic mobility melting profiles can be used. Both allow an estimation of the midpoint temperature of its electrophoretic phase transition. T_m for a sequence of $d(CGG)_{15}$ was determined to be approximately

75 °C higher than the T_m of $d(CTG)_{15}$. The difference indicates that GG Hoogsteen base pairs contribute a significant amount to the stability to the hairpin structure of $d(CGG)_{15}$ [77].

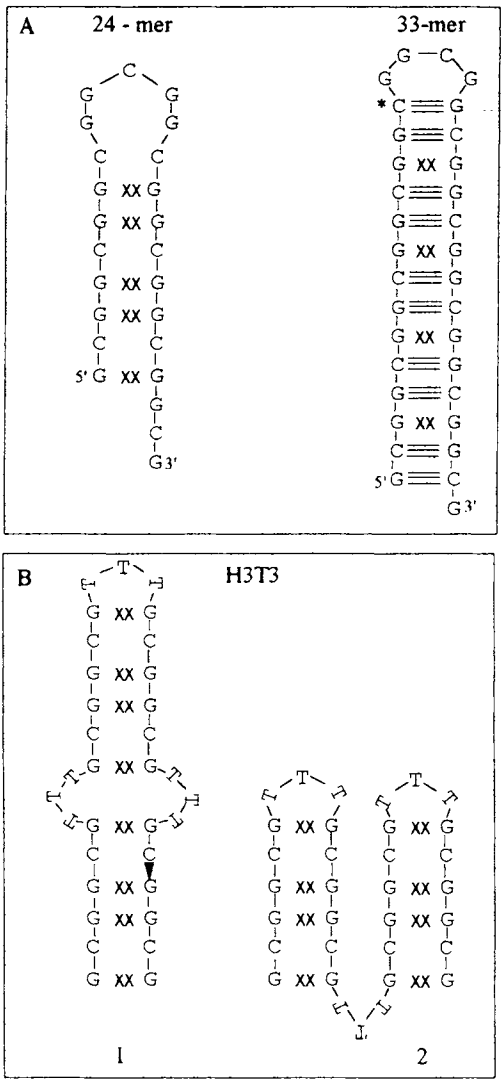

Figure 7. Models of hairpins (A) and alternative folded forms (B) of $d(CGG)_n$ oligomers formed with GG Hoogsteen base pairs (××). Adapted from Reference [77].

2.6. DNA analogues with nonphospodiester backbones: the peptide nucleic acids (PNAs)

Two successful attempts have been reported to replace the entire deoxyribose phosphate backbone on one side and still preserve the features of the DNA structure especially in view of antisense and antigene potential on the other side [85,86,87,88,89,90]. One is the morpholino derivative and the other one the peptide nucleic acids (PNA) which contains an N-(2-aminoethyl) glycine-based pseudopeptide backbone (Figure 8) [71]. It is obvious from the way PNA can mimic DNA that the deoxyribose backbone is not essential for the function of a helical duplex structure.

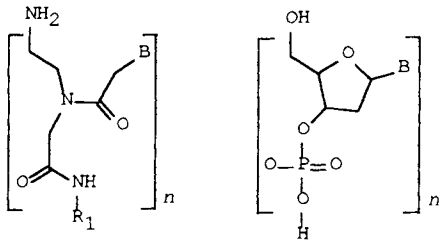

PNA DNA

Figure 8. The chemical structure of PNA and DNA.

The key parameters to judge the modified sequences to be considered are: geometry, flexibility, and hydrophobicity to increase base-pairing and stacking and to increase cellular uptake. The right geometry is the predominant criterion to achieve the helical parameters of the base pairs in the duplex that are determined by the type of double helix envisioned, A-DNA, B-DNA or any other type similar to the two families. The second criterion is flexibility. Only a backbone which is flexible enough will eventually adopt the right conformation. However, a linkage which is too flexible will raise the entropy cost of freezing out the particular conformation required for hybridisation. One of the tricks introduced is the use of a 2′, 3′-cyclic riboacetal linkage to impose restricted conformational flexibility on the backbone. But part of the improved binding to the major groove of double helix by these components is due to the concomitant reduction of negative charges. Finally a more hydrophobic backbone, although it may facilitate passage through cell membranes, may prove disadvantageous, because in the helical complex the backbone is the part of the structure that is exposed to the aqueous environment. The most radical design published so far shows no trace of the canonical deoxyribosephosphate backbone but retains just the nucleobases, it is the PNA sequence (Table IV) [91]. The peptide nucleic

acid (PNA) has an achiral, noncharged backbone, composed of N-(2-aminoethyl) glycine units as attachment for the nucleobases. Hybrids between PNA's and complementary oligonucleotides, either of RNA or DNA units show an improved thermal stability, as compared to DNA-DNA duplexes at physiological ionic strength, predominantly due to the decrease in interstrand electrostatic repulsion (Figure 9).

Table IV
Thermodynamic parameters for the formation of PNA-DNA, PNA-RNA, DNA-RNA and DNA-DNA duplexes with the sequence TGTACGTCACAACTA present in the PNA strand.

	DNA:RNA	PNA:RNA	DNA:DNA	PNA:DNA
$\Delta H°$ kJ/mol *	-538.8	-537.1	-440.2	-445.6
$\Delta S°$ J/mol *	-1558.3	-1445.9	-1238.1	-1194.6
$\Delta G°_{37}$ kJ/mol*	-55.6	-88.6	-56.0	-75.2
T_m °C, 8 μM *	50.1	72.2	53.5	68.8

Measured in 100 mM NaCl, 10 mM Na phosphate, 0.1 mM EDTA, pH 7.0.
* Obtained from linear plots of $1/T_m$ versus log (concentration). Adapted from Reference [91].

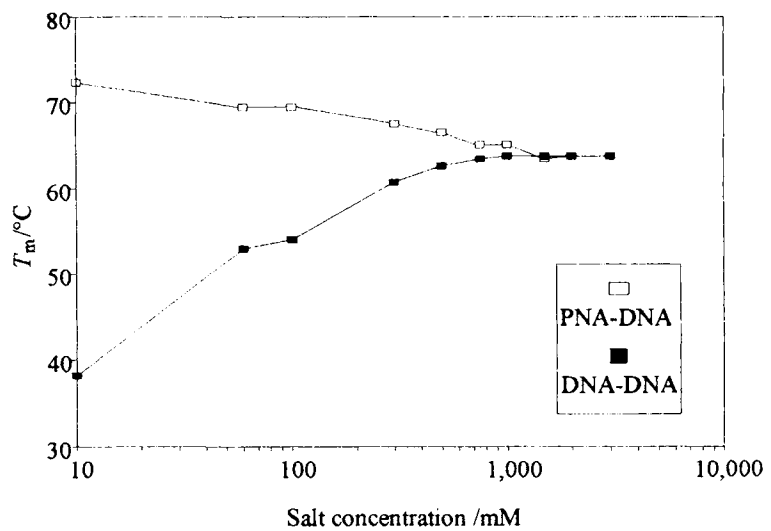

Figure 9. Ionic strength dependence of a PNA-DNA hyrid. Adapted from Reference [91].

PNA's can respond to base pair mismatches as well as or even better than natural DNA sequences [91] (Figure 10).

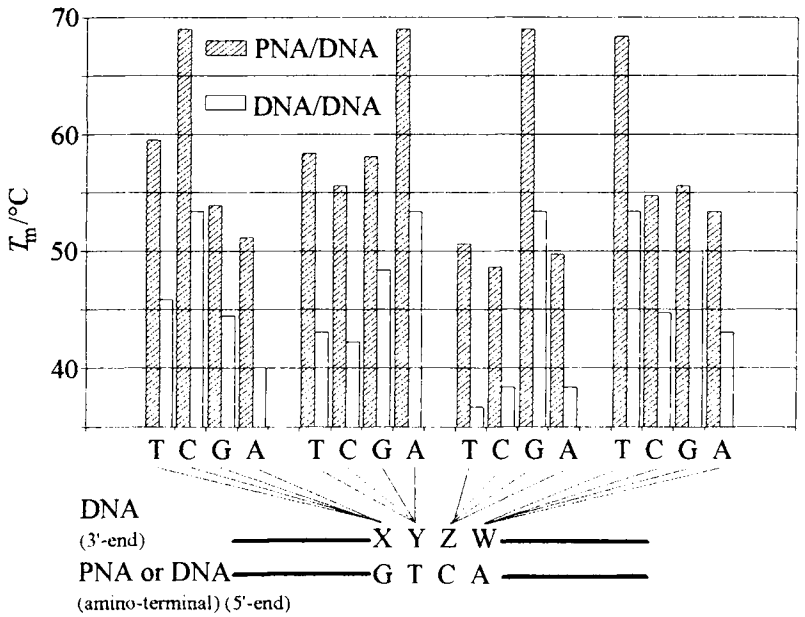

Figure 10. The response of a PNA-DNA hydrid to base pair mismatches. Adapted from Reference [91].

Surprisingly, the binding of PNA to double helical DNA does not take place via Hoogsteen base pairing in the major groove but by strand replacement invasion, leading to a P-loop complex with unique biological properties [92]. Subsequently, experiments revealed that strand invasion is favoured because of the formation of extremely stable PNA_2-DNA triplexes involving both Watson-Crick and Hoogsteen hydrogen bonding [93]. Triplex formation involving PNA is subject to the same constraints imposed by the sequence requirements of the Hoogsteen strand, they have to orient the sequence in parallel to the purine Watson-Crick strand and need to be at least pyrimidine rich to stabilise the complex sufficiently. Details of the strand invasion mechanism have not yet been solved. But available evidence supports a model involving an unstable duplex-invasion complex, initiated by the "breathing" of the DNA double helix. This metastable complex is further stabilised by the binding of the second PNA strand. With increasing ionic strength the stability of the DNA-DNA duplex is increased making the invasion reaction more and more difficult. Double helical complexes

involving two complementary PNA strands are inaccessible due to the lack of chirality. A recent study has demonstrated that "seeding" of left or right-handedness into a $(PNA)_2$ duplex can only be accomplished via one covalently attached chiral amino acid [94].

2.7. Multistem DNA structures

Multistem nucleic acid structures [95], overlooked for a long time, are part of a great number of conserved biological nucleic acid sequences such as rRNAs. Three way junctions [33] are the simplest of all possible multistem nucleic acid structures. Model structures can be obtained when one mixes three mutually complementary nucleic acid single strands that form three double helical arms which meet at a common branch point (Figure 11, Table V).

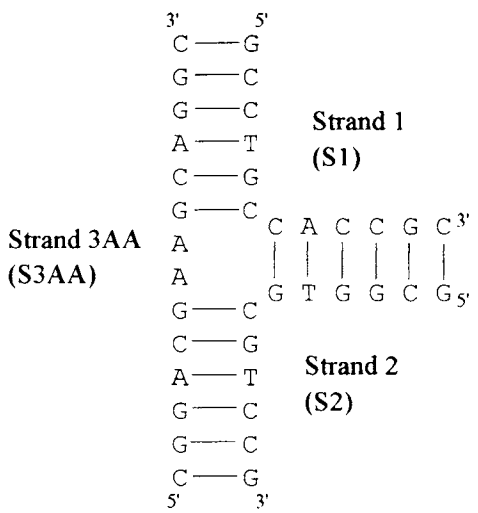

$$S1 + S2 \rightleftharpoons S2{:}S1 + S3AA \qquad \Delta G = -29.64 \text{ kJ/mol} \qquad \Delta G = -38.79$$

$$S1 + S3AA \rightleftharpoons S3AA{:}S1 + S2 \rightleftharpoons TWJ \qquad \Delta G = -33.89 \qquad \Delta G = -37.91$$

$$S3AA + S2 \rightleftharpoons S2{:}S3AA + S1 \qquad \Delta G = -33.73 \qquad \Delta G = -38.75$$

Figure 11. A double-helical, DNA three-way junction (TWJ) with the Gibbs free energy of formation of the individual arms and the complete complex. Adapted from Reference [95].

Table V
ΔC_p data for the formation of two-strand and three-way junction (TWJ) DNA complexes [a]

Reaction	ΔC_p kJ/mol
S2 + S1 = S2:S1	-2.30±0.50
S3AA + S2:S1 = S2:S1:S3AA	-4.47±0.84
sum ΔC_p for TWJ	-6.77
ΔC_p obtained fromΔH_{1+2}	-6.65±0.63
S3AA + S2 + S2:S3AA	-2.55±0.04
S1 + S2:S3AA = S2:S3AA:S1	-3.76±1.42
sum ΔC_p for TWJ	-6.31
ΔC_p obtained from ΔH_{1+2}	-6.52±0.71
S1 + S3AA = S3AA:S1	-2.26±0.54
S2 + S3AA:S1 = S3AA:S1:S2	-6.10±0.63
sum ΔC_p for TWJ	-6.65
ΔC_p obtained from ΔH_{1+2}	-6.98±0.63
Average ΔC_p for TWJ Assembly:	
from sum of ΔC_p	-6.56
from ΔH_{1+2}	-6.73

[a] ΔC_p was calculated for the formation of the two-strand complexes S2:S1, S2:S3AA, and S3AA:S1 by linear least-squares fitting of the ΔH vs. temperature. ΔC_p was calculated for the reactions of the two-strand complexes with the respective third strand to form the TWJ, S1:S1:S3AA, by linear least squares fitting of the ΔH vs. temperature. The overall value of ΔC_p for the formation of S1:S2:S3AA was calculated for each permutation of strand addition in two ways, by simply summing ΔC_p for each reaction and by linear least-squares fitting of the ΔH_{1+2} vs temperature data. Adapted from Reference [95].

Besides an intrinsic interest in three-way junctions as part of much larger structures [96], TWJs can give insight into other multistrand structures such as the four-way junctions reviewed by Lilley and Clegg [97]. Although DNA and RNA sequences have been published recently in ever growing numbers, progress in accurately predicting functional structures around multibranched loops have been hampered by the paucity of thermodynamic data on higher order structures, even on the most simple ones like three-way junctions. It is obvious that the progress in predicting the stability of elements of secondary structure can only

come from an extended data set derived from thermodynamic measurements of junction formation and/or denaturation. Three way junctions not only occur frequently in the ribosomal RNAs or in hammerhead ribozymes [98] but also as structural elements in single-stranded DNA molecules, such as in the genome of certain viruses. Three way junctions can be designed with triple-helical arms linked by either Watson-Crick or Hoogsteen hydrogen bonding (Figure 12).

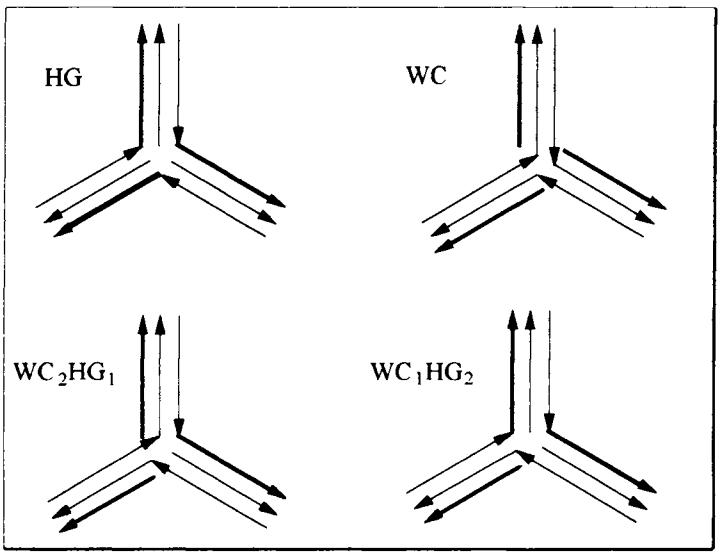

Figure 12. Three-way junctions with triple helical arms linked by either Watson-Crick (WC) or Hoogsteen (HG) hydrogen bonding. Adapted from Reference [33]

Ladbury et al. [95] investigated the thermodynamics of formation of a three-strand, DNA three-way junction.They studied a three-way junction which varied only by two unpaired nucleotides at the branch site from a three-way junction investigated by NMR by Letontis et al. [99]. The NMR spectra recorded as a function of temperature showed that each arm was stable and fully base-paired, forming canonical B-type right-handed helices. Ladbury's sequences were likely to combine into an even more stable complex since they could form one extra G-C base pair in each arm. For their investigation they were the first to use a highly sensitive isothermal titration calorimeter, OMEGA (MicroCal Inc., Northampton, MA). Figure 13 is an example of deconvoluted calorimetric profiles for the melting of a TWJ with triple helical arms.

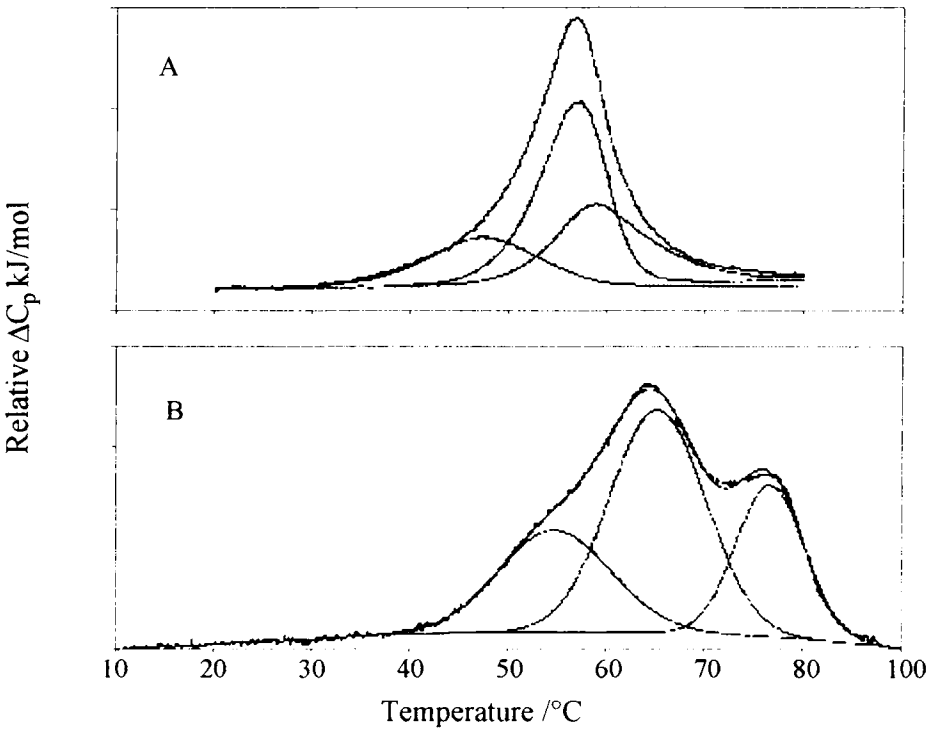

Figure 13. Excess heat capacity (ΔC_p) vs temperature curves for the denaturation of a DNA three-way junction and the deconvoluted enthalpy contributions of the three arms at (A) pH 5 and (B) pH 4.5 (1 M NaCl, 20 mM Na_3PO_4). Adapted from Reference [33].

Data was analysed using the ORIGIN software provided by the manufacturer. Initially, pairs of strands were titrated in the buffer solution used throughout the experiments, to form short (6 bp) helical duplexes, comprising one of the arms of the junction, with six to eight nucleotide extensions. It was made sure that the ratio of the two mixed strands was 1:1. The two-strand complexes were returned to the calorimeter cell after concentration determination and titrated by the addition of the appropriate third strand to form the three-way junction. Heats of dilution for each oligonucleotide solution injected into buffer and buffer into the oligonucleotide(s) in the cell were measured separately. These heats of dilution were used to correct the data. The titration curves, after correction for the dilution effects, were fitted to obtain the binding constant K_β, the stoichiometry

and the molar enthalpy of formation of the particular helical complex ΔH. From these quantities, the molar free energy of formation $\Delta G°$, and the entropy $\Delta S°$ may be calculated using van't Hoff equation and Gibbs-Helmholz equation. Each set of data was obtained at a pre-set temperature. Performing a series of titrations at different temperatures allows the determination of the change in heat capacity, ΔC_p [100]. The effect on ΔC_p of changing the order of strand addition was also tested. But it soon became obvious that this had no detectable effect on the measured heat. The base sequences were designed to form a three-way junction in which each arm contains five G-C base pairs and one A-T base pair. Unexpectedly, the formation constant, the enthalpy, entropy, and change in heat capacity are distinctly different for each of the pairs. There is no apparent reason for the observed discrepancies, so it is likely that it results from several contributing factors. The order and position of the A-T base pair between the G-C base pairs is obviously important. Another source for differences may be some initial secondary structure formed within strands of one kind, which have to be broken before complexes can be formed with a second strand. Native gel electrophoresis and UV melting experiments indicate that strand S2 may exist as a dimer. But at this time no single source for additional or missing formation enthalpy can be named. The formation of the three way junction from every possible combination of pre-annealed two strand and addition of the complementary third strand results in the same set of thermodynamic parameters. This result is actually very much in line with what one would expect for a complex which is formed from three suitable sequences which can only form one final complex, the double helical three-way junction [101]. Independent of the order of addition of the contributing strands the final data are all identical. The large negative ΔC_p obtained for the formation of three way junction is characteristic for biomolecular binding interactions [102]. Large negative ΔC_p values have been reported for protein-DNA interactions and appear to correlate with the removal of hydrophobic binding surface area from solvent exposure. NMR studies have demonstrated that the insertion of two impaired bases at the branch point facilitates stacking of two of the three helices and extra helical conformations for the unpaired bases [103].

2.8 Competitive equilibria between DNA triplex and quadruplex: the role of the G-quartets

Triplex formation, which involves site-specific recognition of duplex DNA by hydrogen bonding between oligonucleotide bases in the 3′ end extension and purine bases in the major groove, can occur in two distinct patterns termed the pyrimidine motif and the purine motif [22,40]. In the former motif, pyrimidine

rich sequence binds parallel to the purine strand of the double helix by Hoogsteen hydrogen bonding, while in the latter motif, the other purine rich sequence binds antiparallel to the purine strand of the duplex by reversed Hoogsteen bonding [22]. The purine motif has an advantage over the pyrimidine motif under physiological conditions in the way that it does not need protonation of one of the side chains (cytosine) [21]. There is, however an unexpected drawback in the purine-motif, because certain monovalent cations at physiological concentration inhibit this triplex formation [26]. The cation most effective in inhibition is potassium, the mechanism of the inhibition remains unclear [104]. It has been shown before that K^+ can stabilise intermolecular structures in G rich sequences [24]. It has been suggested, from the model, that K^+ co-ordinates guanines in stacked quartets because they are found in guanosine monomer gels as well as in poly G-structures [105]. Physiological concentrations of Na^+ and K^+ inhibit the formation of purine motif triplexes. Inhibition is related to the concentration and/or ionic radius, which in turn is correlated to its tendency to stabilise guanine quartet structures [106]. The quartets, once formed, cannot be destabilised by addition of physiological concentrations of polyamines spermidine 3^+ or spermine 4^+. The results presented in the literature favour quartet-mediated aggregation as the most plausible explanation for inhibition of purine motif triplet formation by M^+ (particularly K^+) [107]. These results have some implication for proposed in vivo therapeutic application of guanine-rich oligonucleotide sequences in anti-gene therapy [108]. Current designs for oligonucleotide drugs intended to recognise duplex DNA using a purine-rich sequence appear unlikely to permit triple helix formation with suitable chromosomal DNA under the ionic conditions of a living cell, where, as frequently overlooked, potassium is the most important cation [109].

Besides the competitive quartet/triplet equilibria four-stranded DNA structures have attracted interest in their own rights [110]. As early as 1960 and 1970's unusual conformations originating from guanosine-containing polymers and monomers have been proposed [31]. More recently the interest has been stimulated by the finding that oxytrichia telomers sequences [111] can form higher order structures, and the corresponding telometric sequences of tetrahymena form an unusual conformation in vitro. Telomers may play an important role to "orderly end" the DNA at the ends of chromosomes. Oligoguanine repeats have been found at a number of functionally important locations including elements that mediate immunoglobulin class switches and other recombination events. Structural studies in vitro have demonstrated that repetitive guanine-rich sequences have the capacity to form several non-

canonical structures, involving parallel-stranded tetraplex-structures with an unusual hydrogen-bonding pattern [110].

Sequences with a propensity for the formation of G-quartets have been found to occur in a number of genes, including the retinoblastoma tumour suppresser gene, the insulin gene, and others. At least two major classes of unusual conformations are formed by guanine-rich DNA sequences. At least two major classes of unusual conformations are formed by guanine-rich DNA sequences. Both are based on G-quartet formation. One class of structures comes about by the folding back of a repetitive sequence, or the formation of a hairpin dimer, resulting in anti-parallel strands and the alternation of anti and syn glucosidic angles for the guanine nucleotides within a strand [110]. The alternative class of structure is based on the association of four independent parallel strands [31] (Figure 14).

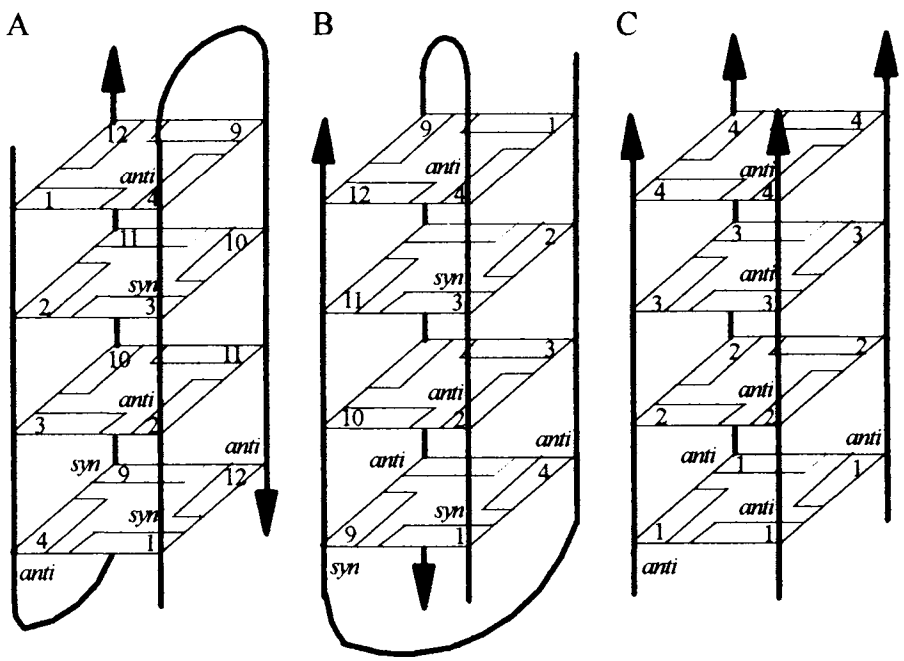

Figure 14. Classes of structures formed by G-quartets in G-rich DNA sequences. Adapted from Reference [52].

As stated above the preference for one of these structures depends on the presence of alkali metal ions, most notably on the presence of sodium or potassium ions. Sen & Gilbert [24] have proposed a sodium-potassium conformational switch to explain their results of differential stabilisation of guanine-rich quartet structures by the two ions. More detailed studies revealed that certain ions and specific base sequences, among other factors, can influence the equilibrium between these structures. Thermodynamic properties have been probed through the use of optical and calorimetric methods.

3.0. THE RNA WORLD

3.1. Origin of the different stability of DNA and RNA helices

It has long been known that there are large differences between the stability of DNA and RNA helical complexes even if the nucleotides present correspond to each other [112]. The variations have been attributed to differences in the sugar-phosphate backbone. A more careful consideration may lead to the conclusion that there are in fact two structural features which distinguish DNA from RNA (the 2′-hydroxyl and C-5 methyl groups) and that the differences arise from either or both of these factors [113]. From the standpoint of reactivity, RNA, with its additional 2′-OH group, is hydrolytically much less stable than DNA. On the other hand, the C-5 methyl group, which is only present in DNA by marking the thymine, is a useful chemical marker in distinguishing it from deaminated cytosine, thus allowing accurate enzymatic repair of a mutation. In terms of thermodynamic stability of the helical complexes, it was observed earlier that RNA-RNA duplexes are more stable than DNA-DNA duplexes with identical sequence, with DNA-RNA hybrid duplexes being the weakest of the three [2]. One still has to differentiate between the case where in a homopolymer duplex, the pyrimidine strand has an RNA backbone (least stable) and the purine strand has a DNA backbone. From the hybrid helix studies it is clear that the difference in stability is not explained from the backbone features alone. To fine-tune the research into the origin of difference in stability between DNA and RNA sequences a study is obviously needed of sequence-defined oligonucleotides [114], which can be systematically modified in all the important features controling stability of the helical duplex structures [36]. It has to be kept in mind that the replacement of one natural strand type for another involves inevitably two structural changes at a time. The more appropriate approach will independently measure the effects of these two groups in separate experiments. It does not come as a surprise that both the methyl and hydroxyl groups have substantial, and sometimes opposing effects on helix stability [37].

The thermal denaturation experiments were carried out at pH 7.0 with combinations of two complementary strands forming a pyrimidine-purine 12 bp duplex. The combinations were as follows: the purine target strand was either of the RNA-type (with hydroxyl) or of the DNA-type (without hydroxyl), the pyrimidine strands which all had the same sequence, were either void of methyl [113], void of methyl but containing hydroxyl [114] or the strand contained hydroxyl and methyl. The melting temperatures (T_m) and Gibbs free energy changes ($-\Delta G°$) for duplexes of all possible combinations of 2'- hydroxyl and C-5 methyl groups are given in the following table (Table VI).

Table VI
Melting temperatures (T_m /°C) and free energies ($-\Delta G°_{37}$ /kJ) for duplexes with all possible combinations of 2'-hydroxyl and C-5 methyl groups.

	purine strand			
	d(AAGAAAGAAAAG)		r(AAGAAAGAAAAG)	
pyrimidine strand	T_m' [a,b] °C	$-\Delta G_{37}$ [b] kJ	T_m' [a,b] °C	$-\Delta G_{37}$ [b] kJ
3'-d(UUCUUUCUUUUC)	32.4	31.8±3.3	37.1	36.4±3.8
3'-d(TTCTTTCTTTTC)	38.8	38.5±3.8	42.2	42.6±4.2
3'-r(UUCUUUCUUUUC)	19.9	20.5±2.1	46.5	47.7±4.6
3'-r(TTCTTTCTTTTC)	31.4	30.5±2.9	55.4	58.1±5.9

[a] Conditions: 3.0 μM total strand concentration, 100 mM NaCl, 10 mM $MgCl_2$, 10mM Na PIPES, pH 7.0.

[b] Error limits for individual measurements are estimated at ± 0.5 °C in T_m and ±10 % in Gibbs free energy. Adapted from Reference [37].

The melting temperature varies from 55°C to 19 °C and the standard free energy change, calculated for 37 °C drops from 58.1 kJ/mol to 20.5 kJ/mol respectively. The most stable duplex results from the interaction of the (unnatural) two methylated RNA strands. The weakest complex is the RNA-DNA hybrid, where the pyrimidine RNA strand contains the naturally present uridine residues. This finding sheds some light on the mRNA-DNA hybrid complex during transcription. The reannealing of the DNA double strand may be one of the driving forces to push the RNA-polymerase forward and to push the

single-stranded RNA out after completion of transcription. There is a good linear relationship between free energy changes and T_m values for all combinations, so stability's could either be compared on the basis of the free energy changes or on the T_m (Figure 15).

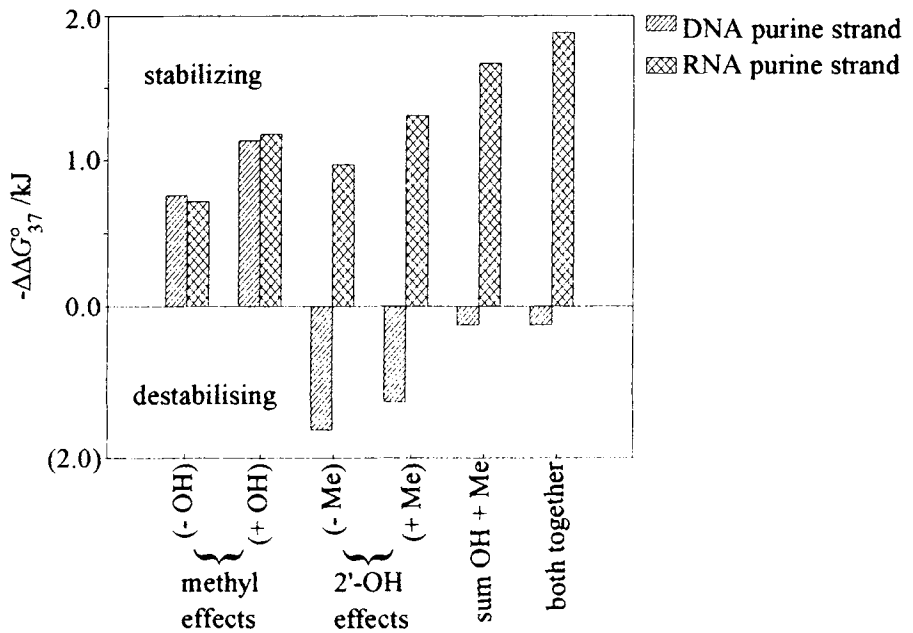

Figure 15. Comparing the methyl and the hydroxyl effects within DNA and RNA. Adapted from Reference [27].

Without going into any details it is obvious that methyl groups always stabilise the helix. A similar comparison made for the effects of hydroxyl is much more difficult to interpret. Hydroxyls can be stabilising, neutral, or destabilising, depending on the actual context. In general there is a preference of an RNA-type strand to bind to another RNA-type strand, as observed before [115]. The determining factor for this preferential pairing is the sugar pucker, which in turn is dominated by the absence or presence of the 2'-hydroxyl groups. The mutual preference of the hydroxylated backbones is independent of the methyl effect [34]. In hybrid sequences such as the deoxyribo-oligopyrimidine/ribo-oligopurine combination this combination is more stable than the inverse pair. The explanation for the difference is as follows: the methyl effect favours pyrimidine DNA strands, the hydroxyl effect favours purine RNA strands. Duplexes of two

ribostrands are more stable than duplexes of two deoxyribo-strands because the preference of a hydroxylated strand for another hydroxylated strand out-competes the lack of methyl-groups in the 5′ position of the pyrimidine residues. One can also draw some conclusions on the origin of the methyl effect. The present data can be interpreted in favour of an increased stacking due to the methyl groups present, and the increased van der Waals interactions based on induced dipole-induced dipole attraction. More studies with mixed sequences are required to settle the question once and for all [116]. These trends can be observed in triple-helices (Figure 16, Table 7).

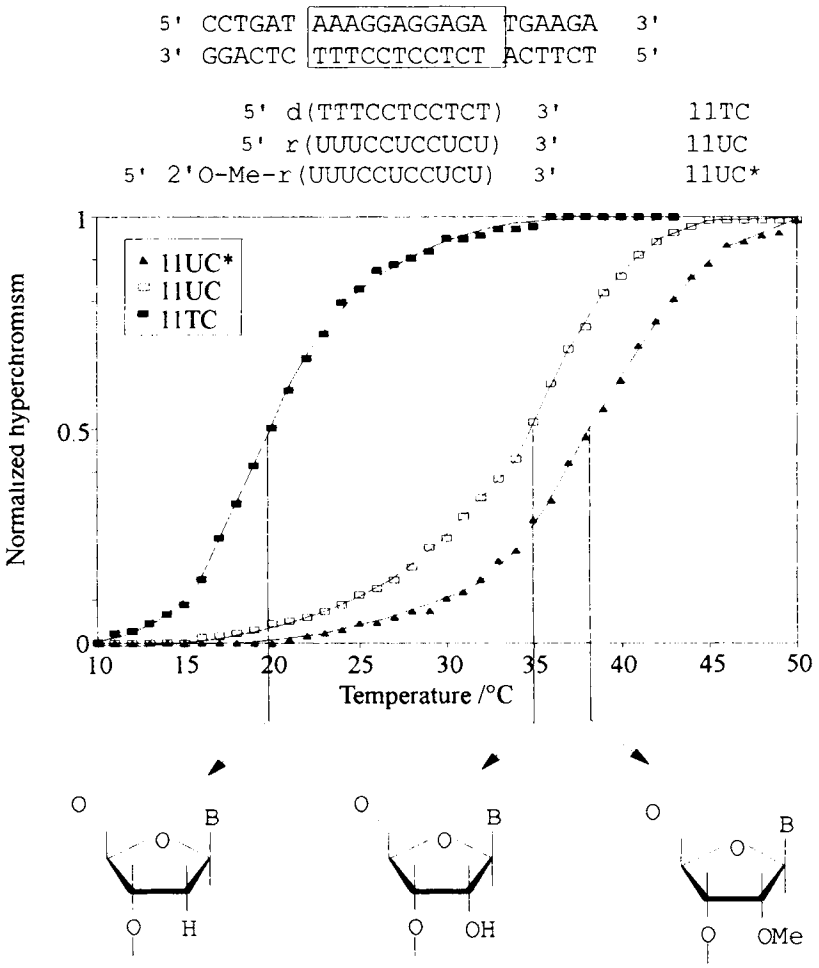

Figure 16. The hydroxyl- and methyl effects in an oligopyrimidine triple-helix. Adapted from Reference [27].

Table VII
Melting temperatures (T_m/°C) and free energies (-$\Delta G°_{37}$ /kJ) for third-strand binding to an unmodified DNA duplex at pH 5.5 [a].

	pyr-pur duplex		5′-d(AAGAAAGAAAAG) 3′-d(TTCTTTCTTTTC)	
Pyr third strand	T_m °C [b,c]	-$\Delta G°_{37}$ kJ [c]	methyl effect	2′-OH effect
5′-d(UUCUUUCUUUUC)	18.5	11.3	- 8.9°C	-
5′-d(TTCTTTCTTTTC)	27.4	18.8	-7.5±2.5 kJ	-
5′-r(UUCUUUCUUUUC)	38.3[d]	-[d]	-	19.8°C
5′-r(TTCTTTCTTTTC)	45.7[d]	-[d]	7.4°C	18.3°C

[a] The melting temperature and free energy differences are also separated into methyl and 2′-OH effects. [b] Conditions: 4.5 μM NaCl, 10 mM $MgCl_2$, 10 mM Na PIPES, pH 5.5. [c] Error limits for individual measurements are estimated at ±0.5 °C in T_m and ±10 % in free energy. [d] Third-strand transition coincides with duplex transition. Adapted from Reference [27].

3.2. The discovery of the RNA world

The term "RNA world" originally coined by Gilbert [117] referred initially to a hypothetical time in the evolution of earthly life when protein synthesis, as we know it today, was not developed [118]. Later it was discovered that besides m-RNA, besides t-RNA, and ribosomal RNA, there is a richness in versatile small RNAs including SnRNPs and ribozymes. New techniques are now being used to explore the vast "space" of small RNAs, which, because they can form relatively rigid structures more easily than can polypeptides of equal length, may have interesting properties such as the strong binding of a specific substrate or a particular type of catalytic activity [119].

The RNA world means different things to different authors. All hypotheses on this topic include three basic assumptions: (i) Genetic continuity was initially assured by the replication of RNA before a co-operation of RNA, DNA and proteins took over [120], (ii) Watson-Crick base pairing was at all times the key to replication [121], (iii) there was no nucleic acid based protein synthesis, and

proteins were not involved in RNA synthesis as catalysts [122], The study of the structure and stability of RNA has become a main focus in physical biochemistry with the aim of parameterization and incrimentation of the physical forces which contribute to a particular RNA structure [123]. With the development of reliable databases, it will be possible to predict from the primary sequence the thermodynamic behaviour of RNA duplexes, duplexes with modified or damaged sites, or higher-order nucleic acid structures [124].

A good case can be made that small-length RNAs can form relatively rigid structures more easily than can small proteins of equal or similar lengths [125]. Beyond what nature has provided there is a vast conformational space for small RNA molecules which gives rise to interesting properties. To explore the conformational space successfully, molecular biologists can rely on sophisticated tools, sharpened through billions of years of natural evolution among them replicases and restriction enzymes, proteins which act on nucleic acids. In an ingenious combination of biochemical processes, related to nucleic acid replication, the RNA "space" can be explored much more rapidly, comparable to massive parallel processing. It is reasonable to assume that "true" evolution as much as test tube evolution started with rather short molecules, and that oligonucleotides represent reasonable model systems for the study of intermolecular and intramolecular interactions. These interactions are the basis for organising RNAs into functional structures, essential for information transfer and catalysis. The thermodynamic measure of the strength of a particular interaction or the extent of organisation is given by the change in Gibbs free energy. As a rule of thumb the decrease of 5.9 kJ/mol in Gibbs free energy at 37 °C resulting in a tenfold increase in the equilibrium constant for an association or` folding reaction. Individual stacking and hydrogen bonding interactions can produce changes of this magnitude [126]. A particularly interesting example is the addition of an impaired nucleotide added to the 3' end of an RNA duplex, especially if it is a purine residue. These residues can make a substantial contribution to stability without any requirements for complementarity across the duplex. It may not be by chance that a 3' dangling purine typically follows the anticodon in tRNA. 5′ dangling ends in RNAs add little to the overall stability of the secondary structure, possibly due to the geometry of A-form RNA helix, which places a 5′ dangling end away form the opposite strand [127]. The end effects are very sequence-dependent. The contribution of H-bonding interactions have been discussed in the literature, but the conclusions were quite controversial. It has to be kept in mind that the formation of a H-bond within the structure during binding or folding must be accompanied by breakage of hydrogen bonds to water. What has to be considered is the net contribution of a

H-bond. A refined estimate for the enthalpy change attributed to a hydrogen-bond which includes the correction for conformational entropy effects gives a value of 6.7 kJ/mol hydrogen bond [128]. Other studies involving substitutions of single functional groups give values per hydrogen bond which range from 0 to 6.7 kJ/mol. This is obviously due to different contexts for the hydrogen bonds [129]. One has to take into account also other hydrogen-bonds but those between bases. Binding of substrates to group 1 ribozymes is partially dependent on particular 2'-OH groups. At 15°C the contribution of 2'-OH groups can be as large as 4.2 kJ/mol to the binding free energy [130]. From studies of the reactivity of ribozymes it is clear that a 2'-OH group can enhance binding in both ground state and transition state. Finally, studies on the structural domains of tRNAs have shown that hydrogen bonds to phosphate groups are also important for RNA binding and folding [131]. Different from amino acids a single nucleotide has more than one contact point that can either accept or donate a hydrogen bond and thus can provide specific contributions to structure formation.

The high density of negative charges along the single strands/double helices requires locally a high concentration of neutralising counterions. This high local concentration is independent of the cation concentration in the bulk solution [66], but is entropically unfavourable. Once the cation concentration in the bulk solution increases the entropic penalty decreases. A consequence of this is that the melting temperature T_m linearly dependent on log $[Na^+]$. Multivalent cations are much more effective in condensing onto the double helix than monovalent cations. Thus the vicinity of the double helix is enriched in multivalent cations. The most striking example is the "condensation" of the DNA double helix onto the histone octamer forming the nucleosome.

As for single stranded RNA structures, which contribute the overwhelming fraction of all naturally occurring functional nucleic acids, it is important to consider the stem-loop structure elements and the factors which influence their thermodynamic stability. It was shown that individual stacking and hydrogen bonding interactions can each contribute substantially to the binding free energy at body temperature, which will be even more favourable at 0°C. Mismatches with reduced stacking and/or hydrogen bonding capacity will consequently decrease helix stability. The only known exception is the insertion of a single or double GU mismatch into a helix [132]. Obviously some mismatches are less destabilising than others. Thermodynamic considerations also favour placing mismatches between helices instead of at the ends, as they exhibit less conformational freedom (entropy) than mismatches at the end of helices. Cation condensation should also be more pronounced in the middle than at the end of a helix. Hairpin helices have a smaller free-energy penalty than helices initiated

from two separate strands since loops, especially loops of four are less destabilising than any other helix initiation with penalties of less than 4.2 kJ/mol [133].

Finally, the intramolecular hairpin helix formation is concentration independent, a great advantage in a pre-biotic situation. There was an obvious 4.2 kJ/mol advantage in selecting hairpins at an early stage in evolution. The combination of several hairpin helices in a single molecule leads to more complicated structures. The same stacking and hydrogen bonding interactions drive the assembly of motifs as seen as part of 16S RNAs. For example crystal structures of tRNA have shown that these interactions are crucial for the fixation of the helix-loops relative to each other. One tertiary interaction unique to RNA is hydrogen bonding to the 2'-OH group as mentioned above. Whether new kinds of interactions for assembly of helices might occur, which for example could lower the dielectric constant locally and reduce water activity, has to be shown. Indication of such a structural arrangement comes form the proposed three-dimensional model of groups I introns [134]. Mapping experiments with hydroxyl radicals provide some evidence that, after folding is induced by Mg^{2+}, substantial regions of the ribozyme becomes inaccessible to solvent [135].

3.3. Principles governing RNA folding

Much like proteins, RNA is recognised to fold into specific shapes capable of ligand recognition and catalysis [136]. The thermodynamic analysis of the unfolding of several different RNAs has been employed to unravel the underlying principles of folding strategies [137]. At least three strategies have been identified that RNA might use to achieve a very stable and compact folded structure: hydrogen bonding between sequence segments through space (as in t-RNA tertiary structure); monovalent and even more divalent ions bound to specific sites, as found in t-RNA and fragments of a ribosomal RNA, and pseudoknot folds, exemplified by a messenger RNA fragment (Figures 17 & 19)[123].

A surprise of the past decade is the discovery that RNA readily adopts specific structures that are adapted, in their irregular complementary surface for molecular recognition and catalysis [138]. Random RNA sequence generation techniques shaped after in vitro genetics have been employed to create random sequence pools from which fairly short RNA can be selected with high affinity to small molecules such as organic dyes, other nucleotides or amino acids [139]. These selective binding properties imply that RNA's fold into 3D structures with unique and irregular shapes. It is obvious it does not require a vast number of different side chains to fulfil this task, but that side chains need to be available

for through-space hydrogen bonding, and that the regular and stable secondary structures from canonical base pairing is not sufficient for these particular binding properties. They rather form part of the three-dimensional scaffold to bring the reactive groups close together in space. Transfer RNA with its familiar tertiary structure which is based on the three modes of interaction listed above, is currently the only tertiary fold of any RNA which is understood in detail both with respect of spatial resolution and energetics of interactions [140]. Going from there it is obvious to ask, whether other RNA structures are a mere expansion of the tRNA structure. To answer this question, secondary structures can be determined by phylogenetic comparisons and by site-directed mutations. Any difference between actually determined folding energies and the expected stability must arise from additional interactions or missing ones [141]. Three model systems have been developed to study the different means by which stable tertiary folds could be achieved, namely t-RNA's and their tertiary structure, ribosomal RNA's and the ions which help them to fold properly, and the folding of m-RNA pseudoknots [142].

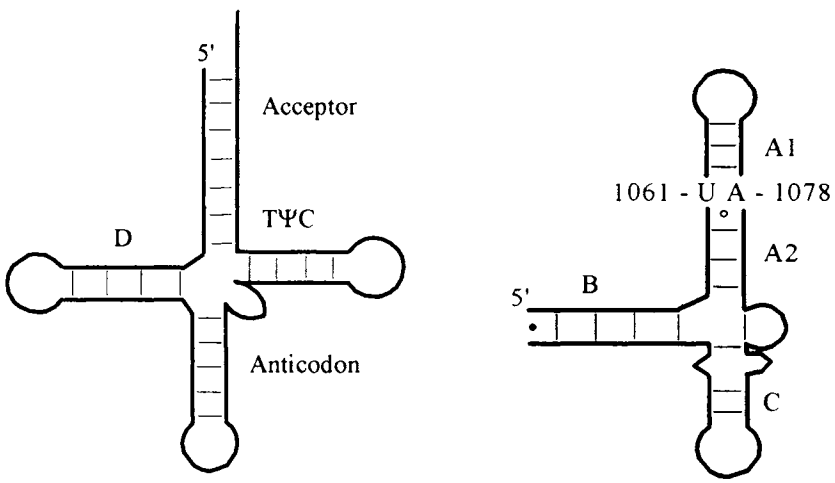

Figure 17. A 2D representation of the tRNA clover-leaf structure, and residues 1051-1108 from the large subunit of *E. coli* wild type ribosomal RNA. Reprinted with permission [123].

It was established in the 1970's that certain t-RNA can unfold in a highly co-operative manner, allowing only for a few stable intermediate steps as the temperature is raised and that the tertiary interactions are the first to be disrupted (see Figure 18) [140].

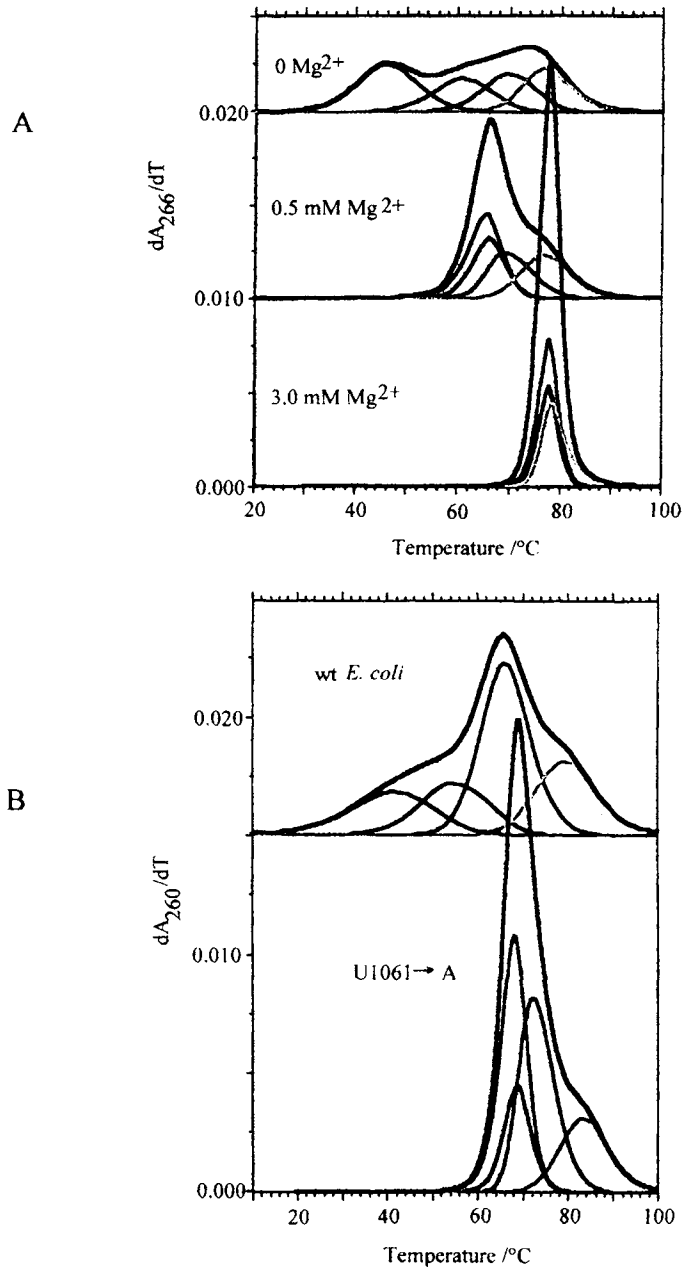

Figure 18. Thermal unfolding of A, tRNA (0.15 M NaCl) and B, an rRNA fragment (0.1 M NH_4Cl, 3 mM Mg^{2+}). Reprinted with permission [123].

A well known cloverleaf secondary structure consecutively unfolds in a series of additional steps. A total of four discreet unfolding transitions were distinguished in $tRNA^{MET}$ [143]. The major stabilising force is base stacking, which is associated with a large positive enthalpy. Accordingly, following the heat capacity change over the temperature interval of unfolding allows measurement of the contributions of the tertiary and the secondary structure to the overall stabilising contribution of the t-RNA. As in the case of $t\text{-}RNA^{MET}$, the unfolding of one of the stem-loop structures (D^{stem}) coincides with the decrease of tertiary structure. The combined enthalpy of unfolding is 217 kJ/mol of which about 125 kJ/mol is attributed to tertiary structure itself. The total amount due to the complete unfolding is over 836 kJ/mol. As stated above, besides hydrogen bonding and stacking interactions, preferential stabilisation of the highly folded structure is helped by divalent cations. At 150 mM Na^+ tRNA's are completely folded. So extra counterions will not improve on the stability of the stem-loop structure. However, the tertiary structure stability is grossly enhanced by adding Mg^{2+} [144].

The consequence of adding Mg^{2+} is in fact that the tertiary structure T_m shifts upwards to such an extent that it eventually will surpass the T_m of the individual stem-loop structures which constitute the cloverleaf [145]. Because the secondary structure elements cannot unfold without disrupting the tertiary structure first or concurrent with the secondary structure, the hairpin T_m is effectively merges with the unfolding of the tertiary structure at higher temperatures [123]. At 3 mM Mg^{2+} the entire molecule unfolds in a single highly co-operative transition. Folding a highly charged molecule like single stranded RNA into a compact structure such as the well known 3D-structure of t-RNA, is loaded with a high energy penalty, which is eased when polycations are present. The loop regions form a kind of binding pocket, where Mg^{2+} can specifically bind. This is not the place to define the term tertiary structure for RNA in great detail but reserve it for structures which originate from "crosslinking" individual secondary elements through space. Draper et al have investigated tertiary structures in a ribosomal RNA fragment and the influence of Mg^{2+} concentration on the stability of the folded state [123]. From initial studies it was suggested that all helical segments in this RNA fragment (residue 1051-1108 from the large subunit ribosomal RNA of *E. coli* wild type) melt at an elevated temperature (Figure 17). The lowest detectable transition cannot be detected by traditional means since it does not exhibit any hyperchromicity at 280 nm. Therefore it is concluded that it is not associated with any secondary structure unfolding the transition. This is in line with the other observation that it is more affected by the presence of Mg^{2+} than by other divalent cations, reminiscent of t-RNA, although

the specificity of tRNA folding is not affected by NH_4^+ ions. Furthermore, it was found that a particular mutation U1061→A increases the first transition's T_m by 24 °C [146].

The consequence of the T_m shift of the tertiary structure is an upward shift in all T_m and an increase in cooperativity due to the fact that the stem-loop structures in this RNA fragment have to "wait" with their unfolding until the tertiary structure (with the lowest T_m) is abolished. Support for this model comes from binding studies. The particularly stable folded structure in the presence of 3 mM Mg^{2+}, 100 mM NH_4 Cl recognises the ribosomal protein L11, its native ligand, and the antibiotic thiostrepton [147]. The drastic effect of the mutation transversion (U→A) at position 1061 can be understood on the assumption of a competition between two alternative foldings. This is not an uncommon behaviour of RNA structures. Unfolding of t-RNA^{GLY} (as observed by NMR) is accompanied by the formation of a new set of hydrogen bonds, so is the unfolding of viroids [138]. An intriguing observation is that A1061 is found naturally in several archeal thermophiles, suggesting that the mutation is selected for by the higher growth temperature which is dependent on a more stable tertiary structure. As can be shown by microcalorimetry, a large fraction of the 1051-1108 RNA unfolding enthalpy comes from tertiary structure unfolding. Prerequisite for the proper folding is the presence of either Mg^{2+} or NH_4^+ in their specific binding pocket. The ion selectivity implies that RNA extensively co-ordinates the two ions and is so rigid in its structure that it can distinguish between different size ions.

Finally, tertiary structure stability is shown to play a role in the function of mRNA. The tertiary structure element involved is a nested pseudoknot. A pseudoknot is a structure in which nucleotides located in a loop bind via Watson-Crick pairs to a single stranded segment within the same molecule. The mRNA fragment serves as the target or a translational repressor of the ribosomal protein S4. The four helical secondary-structure elements which contribute to the unusual structure frame work have been deduced from experiments with compensatory base replacements and their effect on S4 binding [140]. The unfolding pathway for this RNA was deduced from the same experimental approach, compensating mutation in the isolated secondary structure segments. The unfolding thermodynamics shows that there must be several sets of interactions that stabilise the RNA much more than expected from the known secondary structure. The unfolding starts at the tertiary structure level, is dependent on Mg^{2+} and does not show hyperchromicity, i.e. all helical segments shown stay intact. It is assumed that it reflects a tRNA like tertiary structure. In the next step a small helix, Helix IV, unfolds but the unfolding enthalpy is bigger than the unfolding of four base pairs. The two helical segments II and III melt as

a single co-operative unit. The enthalpy of unfolding obtained for this step is close to the predicted value for the melting of eight base pairs. What makes them melt co-operatively is not known. Nested pseudoknots have been identified in a group of RNA's with ligase activity. The catalytic site of group I introns is part of a double pseudoknot, and pseudoknots have been selected by in vitro genetics as high affinity binders of several different proteins and vitamin B12 [148].

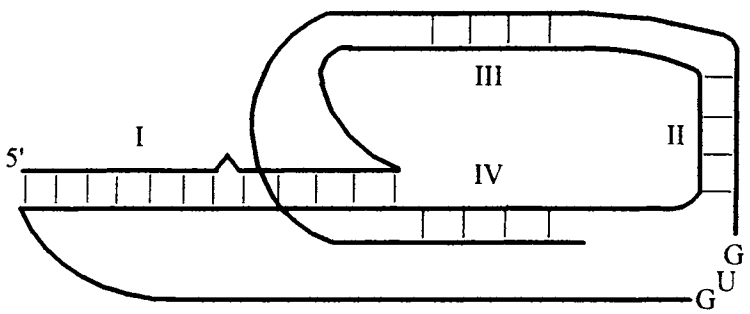

Figure 19. A nested α mRNA pseudoknot. Reprinted with permission [123].

Looking at these three examples, a tRNA, a defined sequence of the rRNA, and a nested mRNA pseudoknot, it can readily be seen that a set of rules are being developed for the formation of the secondary and tertiary structure of RNA species. By definition, secondary structure elements are double helices and single strands with pronounced stacking. Tertiary structure elements include through-space interactions of single stranded segments such as loops, with either loops or double helices or other non-canonical interactions. The biological function performed by these RNA's depends on the proper three-dimensional folding which allows specific motifs to be properly oriented in space. To fine-tune the through-space interactions, modified nucleotides and divalent cations, preferably Mg^{2+}, have to be envisaged as important modifiers. There are ten discernible physical contributions of modified nucleosides to tertiary structure stability, most of them related to the structure/function of t-RNA. The ten physicochemical contributions are: 1) introduction of transient charges dependent on protonation; 2) introduction of positive or/and negative charges; 3) alterations and restrictions of nucleotide conformation; 4) inhibition of noncanonical base-pairing; 5) disruption of canonical base-pairing; 6) enhancement of base stacking interactions; 7) reordering of water; 8) facilitation of, or direct co-ordination with, metal ions; 9) restriction of phosphodiester bond conformation (sugar

pucker); and 10) interaction between modifications of modified nucleosides. Determination of the contribution of these features to the tertiary structure stability has remained a challenge to conventional approaches. Eventually with new techniques we will gain insight into the "RNA World" and hopefully apply the knowledge to the design of nucleic acids with new and/or modified functions.

The secondary structure and its prediction is in reach, and attempts to predict it from sequence data started as early as 1960 [149]. The question addressed was how to determine a folding that provides the largest number of complementary base pairs. The most successful approach centres on the search of the lowest energy secondary structures with the use of thermodynamic parameters, and it is equally important to know both, the parameters of the helices and the parameters of loops of any kind. The respective contributions of helices and loops to secondary structure stability are opposed, as the stacking and hydrogen bonding lowers the free energy, while the closing of loops, owing to entropy losses, usually increases the free energy. The overall stability depends on the balance between these two opposing factors. Helix stability has to be evaluated based on a nearest-neighbour model, as a sum of the energy contributions of all next nearest neighbour base pairs within a helix [10].

Traditionally the thermodynamic data were derived from melting experiments of self-complementary short synthetic oligonucleotides of varying composition. Calorimetric and spectroscopic methods have been used [4]. The thermodynamic data are derived from the UV-melting curves by using a two state model, i.e. only the initial state and final state are highly populated, and intermediate states can be ignored. Under this assumption, data derived from optical melting must be equal to the data obtained by calorimetry or the two state model cannot be applied. Reference [14] contains the commonly used compilation of the sequence dependent melting enthalpy and entropy. Loop parameters are considerably less studied than those of helices. Little is known of the effect of the nucleotide sequence within the loop on the unfolding energy. Estimates are based on averaged data not dependent on nucleotide context. The only exemptions are data on so called tetraloops, Table VIII in section 3.4. The GNRA tetraloop motif plays an important role in group I intron tertiary interactions; there are two instances in which GNRA bases hydrogen-bond to helical bases elsewhere in the molecule [150].

It is worthwhile to contemplate the similarities of RNA and protein folding at this point. In both cases it is tempting to assume that a linear sequence of residues holds the key for three-dimensional structures, creating specific molecular shapes, capable of ligand recognition and catalysis. But there are fundamental differences in RNA and protein folding. Turner & Bevilaqua have

pointed out that a single nucleotide has the potential for a far stronger interaction than a single amino acid [151]. The addition of an extra base pair to the end of an existing helix adds 4-13 kJ/mol in Gibbs free energy to the structure and a simple hairpin of 7 base pairs can add as much as 42 kJ/mol in ΔG . Protein α-helices and β sheets are usually unstable in the absence of a bulk protein, and the complete molecule will only require a change in free energy of 42 kJ/mol for its complete unfolding. The second most important difference is the requirement of complementarity of interactions in the case of RNA's-hydrogen-bond acceptors, and donors have to be placed and spaced accordingly to make a stable folding. Protein secondary structure relies on the proper alignment of peptide-bonds of the backbone, giving rise to α-helices and β-sheets, but complementarity hardly extends to tertiary structure interactions [152]; disulphide bonds and salt bridges require complementarity but the interactions within the hydrophobic core does not relay on it. Coordination of distant motifs through a divalent or multivalent cation is used in tRNA's as well as Zn finger motifs in a protein, which is too small to be stabilised through an extended hydrophobic core. The contrast between strong and complementary interactions in RNA vs weak and non-complementary interactions in proteins has consequences for the general stability of an RNA motif vs a correspondent protein motif. Most globular proteins show two-state melting behaviour. RNA's with more stable secondary structure elements tend to unfold in a series of discrete steps. As a consequence of that even isolated motifs, which are normally part of a larger structure, can be isolated in their native conformation, as shown by NMR and studied separately from the complete RNA. Another consequence of this is the parametrization of RNA secondary structure components and the predictive power for new structures, based solely on sequence information. From the strong side chain interactions in RNA it follows that there is a notable sensitivity of the structural stability to base mutation. Proteins can vary to a large extent in their primary structure as long as the very few invariant residues are in place [153]. Hence, phylogenetic conservation of RNA is far more impressive [154]. The intricate balance between many weak interactions made prediction on protein folding and function very difficult although there is a rich body of structure information gathered from x-ray analysis of protein crystals. The strong and complementary interactions in RNA favour rapid progress in the prediction of RNA folding based on structural information and thermodynamic measurements.

3.4. Superstable hairpin structures in large RNAs

Any secondary structure which originates from folding of a single-stranded RNA is by definition dominated by hairpins [155]. The folding into hairpins

provides nucleation sites for tertiary interactions in RNA enzymes, provide for binding sites by RNA-binding proteins [156] and protect RNA's from degradation. So it is not unexpected that certain sequences are found with exceptional frequency [157] and are characterised by high thermodynamic stability. This originates from a network of stabilising interactions within the hairpin loop: non-Watson-Crick base pairs and base-phosphate and base-sugar contacts. The biological importance of DNA hairpins is less obvious [158]. It has long been suspected that palindromic DNA sequences form hairpin structures at replication origins or operator sequences, which are involved in the regulation of gene expression [159]. The presence of hairpin structures can be demonstrated in vitro and in vivo by the enhanced chemical and enzymatic reactivity within the single stranded section. The number and sequence of impaired nucleotides in hairpin loops vary, but certain sizes and sequences are found with a disproportionally high frequency. Among the tetraloops, which as a class are quite common, the two sequences UUCG and GCAA are especially favoured (Figure 20) [155,160].

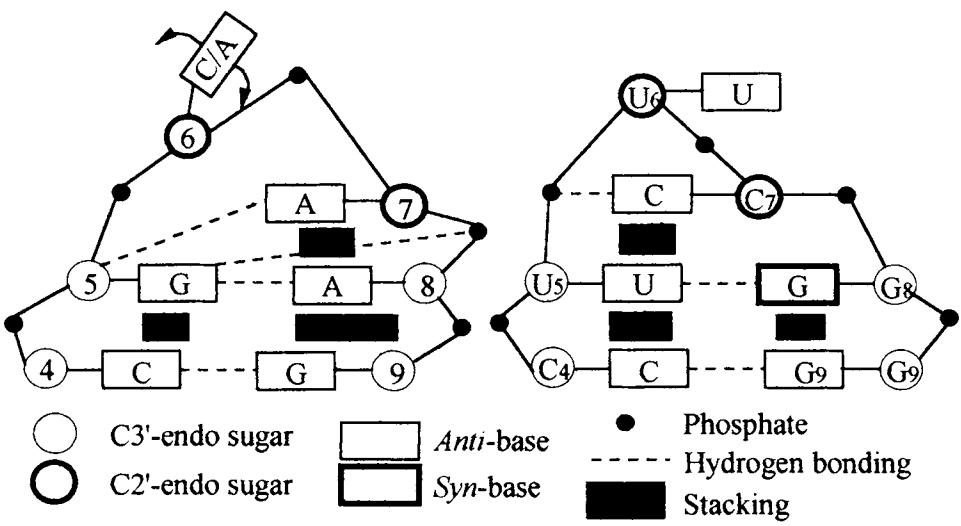

Figure 20. Schematic representation of the UUCG and GCAA tetraloops. Adapted from Reference [155].

The preference has both thermodynamic and structural reasons. Initially the sequence dependence of the hairpin-loop thermodynamic stability was attributed

only to the stem [161]. The single-stranded intervening sequence (loop) is assumed to contribute only to the destabilising entropy change upon folding (decrease in conformational entropy) by an amount depending only on the length of the intervening sequence [162]. DNA-hairpin loops of four to five nucleotides were shown to have higher stability than smaller or larger loops. There is a simple structure principle to be considered. The hairpin loop has to cover the gap between the opposite sides of the stem. The cross-strand phosphate-phosphate distance is ca. 18 Å for any double stranded nucleic acid and only determined by the width of a Watson-Crick base pair [163].

If, however, the unpaired nucleotides are stacked on top of the stem's base pair, shorter phosphate-phosphate distances are permitted across either the major or the minor groove. As a consequence of this, loops of four to five nucleotides in DNA could maximise stacking interactions while satisfying steric constraints [164]. The optimal loop size in RNA is six to seven nucleotides as one frequently observes in t-RNA's [165]. But in ribosomal RNA, loops are smaller usually consisting of four to five nucleotides. Increasing loop size has two adverse consequences. While the enthalpy of hairpin formation goes down with loop size increase and approaches a minimum for loops of five to seven nucleotides the entropy increase on loop size increase leads to a decrease in the melting temperature with increasing loop size [166]. Stacking of single stranded residues results in an enthalpy change which turns out to be 21 - 42 kJ/mol greater than expected from the contribution of the stem only.

For homonucleotide loops, sequence effects on loop stability are much smaller than length effects. The observed differences in stability between loops of different sequence are entirely enthalpic in origin. The order of stability observed in free energy follows the same trend as the calorimetrically determined enthalpies of hairpin formation [167]. More interesting than homonucleotide loops are obvious loop sequences which are often found in 16S RNA e.g., namely UNGC, GNRA, and CUUG, where N is any of the four nucleotides and R is any purine. The unusual thermodynamic properties of these sequences were first observed by Tuerk et al. [168]. In 16S RNA sequences the UUCG loop is predominantly closed by a CG base pair. It is reasonable to include the closing base pair in the discussion on the contribution of individual nucleotides to the thermodynamic stability of UNGC and GNRA loops. It has been observed that C(UUCG)G (with a stem of three additional base pairs) exhibits a denaturation temperature which is 20 °C higher than the corresponding homonucleotide loop C(UUUU)G. The DNA sequence analogue d C(TTCG)G has the expected thermal stability, while sequences such as r(GAAA) and d(GAAA) are both

unusually stable. Structural studies on the RNA loop UUCG reveal its very compact and hence very stable (Table VIII) [169].

Table VIII
Melting temperatures and free energies of hairpin formation for members of the UUCG family of stable RNA hairpins [a].

RNA loop sequence	T_m °C	$\Delta G°_{37}$ kJ/mol
C(UUCG)G	71.7	-23.8
C(UACG)G	69.3	-21.7
C(UUUG)G	64.0	-15.9
C(UUUU)G	60.4	-12.5
G(CUUG)C	62.4	-15.0
C(GCUU)G	62.2	-15.0
G(GCUU)C	52.3	-7.1
C(GAAA)G	65.9	-17.6

[a] Adapted from Reference [155]. Underlined letters denote mutations from the wild-type sequence.

The corresponding DNA structure exhibits considerable flexibility and lacks the well-defined interactions within the loop. Both RNA and DNA GNRA sequences result in exceptionally stable loops. There are various attempts to quantify the added stability. One approach is to compare the T_m of hairpin helices with identical stems and variable loop sequences. The more quantitative estimate is based on subtraction of the contribution of the stem region using nearest-neighbour parameters from the thermodynamic database for RNA secondary structure prediction [129]. It has to be kept in mind that even though these extra-stable sequences have a destabilising effect on RNA secondary structure, it is less pronounced (by 8.4 kJ/mol). The destabilising free energy change associated with the hairpin loops is entirely entropic and is only partially compensated by the favourable enthalpic contribution. Only for C_n loops are $\Delta H°$ and $\Delta S°$ both positive. As the contribution from tetraloops to RNA folding enthalpy is more favourable than from other hairpins one has to look out for the extra contribution. NMR analysis reveals that tetraloops have more hydrogen bonding and/or stacking interactions than the other loops. As stated above, the loop closing base pairs is part of the stabilising set of interactions. Other base pairs further along the stem have no noticeable influence on the stability of the loop. This result is

consistent with the finding that there is no preference in ribosomal RNA sequences for any base pair besides the conserved loop-closing base pairs. Within the UNCG-loops the second nucleotide can be replaced by any of the four nucleotides without reducing the hairpin stability. Mutations of the third loop nucleotide away from the canonical C or replacement of the fourth nucleotide G comes with a hefty penalty of $\Delta\Delta G$ of 6.3 kJ/mol in free energy [170]. The loss of 2′ hydroxyl on replacing the ribo-sequence by a deoxyribosequence has a large effect (ΔT_m = 8 °C) on the hairpin stability but almost no effect when it occurs in the stem. Variations in the sequence of an all-deoxy-ribonucleotide loop have no effect on the thermodynamic stability. A brief survey on the thermal stability of the GNRA loop shows that basically the same consideration hold for this sequence. The additional stability $\Delta G°$ = 4.2 kJ/mol is only marginally above the stability of the corresponding homopyrimidine loops [161]. Functional reasons such as the involvement in tertiary interactions rather than thermodynamics considerations have dominated the selective advantage, which may explain why these loops are so common in RNA. All possible nucleotide combinations were tested with sometimes dramatic consequences, such as drops in T_m by 30-40 °C for TTTT, GCCC, or GTTT loops. The stem sequence again does not influence the loop stability. The most dramatic effects are observed for the first G nucleotide. Substitution by A led to a ΔT_m of over 50 °C. Each functional group seems to contribute only modestly to the hairpin stability, the largest effect is observed on replacing G by I (removal of the exocyclic amino from the first G). The NMR determined structure shows that each of the functional groups is involved either in a direct or a water-mediated hydrogen bond. Single hydrogen bonds contribute very little to the overall stability. Substitution of functional groups may not only alter the hydrogen-bonding pattern, but may also change stacking efficiency. In a few cases it was shown that stacking effects can partially offset loss of hydrogen-bonding ability [171].

The structural features of the GAAA DNA loop are qualitatively consistent with the structure determined for its RNA analogue. This loop is found in phage ∅X174 at the origin of replication and herpes simplex virus, in the promoter region of an *E.coli* heat shock gene, and at virion RNA polymersase promoters. [172] The first and the last nucleotide can form an anti-anti GA base pair. Involvement of the N7 position of the adenine from the GA pair can be demonstrated. A loss of stability of the structure (ΔT_m = 12 °C) can be observed on replacing A by a 7-deaza substituent. NMR and molecular mechanics simulation suggest that base pair formation is possible in other hairpin loops as

well [173]. The additional base pair adds thermodynamic stability to the structure Sequences which allow the formation of an intrastrand hairpin were approximately 7-10 °C more stable than sequences which lack this potential, largely because of a more favourable enthalpy. There have been considerable evolutionary pressure for the selection of tetra loop hairpins especially in 16S rRNA. As the observed length and sequence vary it can be concluded that protein interactions are either absent or sequence independent, and any preference for a particular sequence should not reflect protein-binding requirements [174]. The stem loops can be viewed as nucleation sites for folding of RNA as it is transcribed. In rRNA's and even more in self splicing RNA's the tetraloops are involved in tertiary interactions. The conserved stem loop P5b in group I self-splicing introns interacts with a helical region within the P6 subdomain. This tertiary interaction requires a conserved sequence match rather than grossly elevated thermodynamic stability (Table IX) [175].

Table IX
Melting temperatures for members of the GNRA family of stable DNA hairpins[a]

DNA stem-loop sequence	T_m °C
GC(GAAA)GC	76.5
I	59-62
A T	<30
T	55-58
C	60-63
A	<30
T	71.5
C	72.0
G	71.0
T	71.0
C	72.0
G	71.5
T	70.0
C	67.0
G	70.5
TT	69.5
TTTT	33.0
CCC	41-44

[a] Adapted from Reference [155]. Only mutations from the wild-type sequence are explicitly indicated.

Of biological significance is the stabilisation of plant mRNA's against degradation by exonucleases through tetra-loop hairpin formation. Plant plastid mRNA's contain several inverted repeats in their 3′ end that can form stable hairpins to protect it against 3′-5′ exonucleases. Different mRNA's can despite an identical constitutive level of transcription accumulate in different amounts offering a mechanism by which transcriptional efficiency can be regulated. Artificial insertion of a tetraloop near the 3′ end of spinach chloroplast mRNA leads to an enhanced mRNA retention. Besides the thermodynamic stability of the hairpin special structural features are responsible for the resistance against nucleases. The resistance against nucleases of stable short RNA or DNA is required if they shall be utilised as antisense sequences [176]. This degradation occurs predominantly by 3′-5′ exonuclease activity. DNA hairpins with GAAA loops are resistant to nuclease digestion because of their rigid structure. The sugars in hairpin loops are almost always in the extended 2′-endo conformation rather than the 3′-endo geometry of A-form RNA helices, to lengthen the distance that can be spanned by each individual nucleotide. There is an intricate interplay between backbone structural rearrangements and stabilising interactions to allow nucleic acids to adjust steer local conformation to energetic needs by optimising stacking and base-pairing interactions [177]. In helical regions the hydrophilic character of the backbone dominates, but the balance of hydrophobic bases and hydrophilic sugar-phosphate surfaces may guide protein binding to loops. More will be undoubtedly found out about the role of hairpin structures and will guide us in designing stable sequences for a variety of applications.

REFERENCES

1. H. Hinz, in: M. Jones (Ed.), Biochemical Thermodynamics, Elsevier, Oxford U.K., 1979.
2. H. Klump, in: M. Jones (Ed.), Biochemical Thermodynamics, 2nd edition, Elsevier, Oxford U.K., 1988, p. 100.
3. K. Breslauer, in: H. Hinz (Ed.), Chemical Thermodynamics Data for the Biol. Sciences, Elsevier, Oxford U.K., 1986.
4. L. Marky, K. Breslauer, Biopolymers, 21 (1982) 2509.
5. O. Gotoh, Y. Tagashira, Biopolymers, 20 (1981) 1033.
6. S. Delcourt, R. Blake, J.Biol.Chem., 266 (1991) 15160.
7. H. Klump, in: M. Jones (Ed.), Biochemical Thermodynamics, Elsevier, N.Y., 1988, p.100.
8. L. Marky, K. Breslauer, Biopolymers, 26 (1987) 1601.
9. J. Watson, F. Crick, Nature, 171 (1953) 737.

10. H. Klump, in: W. Saenger (Ed.), Nucleic Acids, Landold Börnstein, Springer Ver., N.Y., 1990, p. 241.
11. J. Petruska, M. Goodman, J.Biol.Chem., 270 (1995) 746.
12. J. Marmur, P. Doty, J.Mol.Biol., 5 (1962) 107.
13. I. Tinoco, F. Aboul-ela, D. Kok, F. Martin, Nucl.Acid Res., 13 (1985) 4811.
14. K. Breslauer, R. Frank, H. Blocker, L. Marky, Proc.Natl.Acad.Sci. U.S.A., 83 (1986) 3746.
15. R. Lumry, S. Rajender, Biopolymers, 9 (1970) 1125.
16. G. Felsenfeld, D. Davies, A. Rich, J.Am.Chem.Soc., 79 (1957) 2023.
17. M. Riley, B. Maling, M. Chamberlin, J.Mol.Biol., 20 (1966) 359.
18. A. Morgan, R. Wells, J.Mol.Biol., 37 (1968) 63.
19. K. Hoogsteen, Acta Cryst., 12 (1959) 822.
20. Y. Cheng, B. Pettitt, Prog.Biophys.Mol.Biol., 58 (1992) 225.
21. M. Cooney, G. Czernuszewicz, E.H. Postel, S.J. Flint, M.E. Hogan, Science, 241 (1988) 456.
22. P.A. Beal, P.B. Dervan, Science, 251 (1991), 1360.
23. D. Pilch, R. Brousseau, R. Shafer, Nucl.Acids Res., 18 (1990) 5743.
24. D. Sen, W. Gilbert, Nature, 344 (1990) 410.
25. A.J. Cheng, M.W. Van Dyke, Nucl.Acids Research, 22 (1994) 4742.
26. W.M. Olivas, J.L. Maher III, Biochemistry, 34 (1995) 278.
27. J. Fossella, Y. Kim, G. Richards, J. Fresco, Nucl. Acids Res., 21 (1993) 4511.
28. D. Pilch, R. Shafer, J.Am.Chem.Soc., 115 (1993) 2565.
29. K. Gehring, J. Leroy, M. Gueron, Nature, 363 (1993) 561.
30. X. Chen, S. Mariappan, P. Catasi, E.M. Bradbury, G. Gupta, Proc.Natl.Acad.Sci.U.S.A., 92 (1995) 5199.
31. C.H. Kang, X. Zhang, R. Ratclif, R. Moyzis, A. Rich, Nature, 356 (1992) 126.
32. J. Völker, D. Botes, G. Lindsey, H. Klump, J.Mol.Biol., 230 (1993) 1278.
33. P.L. Hüsler, H.H. Klump, Arch.BioChem.Biophys., 313 (1994), 29.
34. C. Escude, J. Francois, J. Sun, G. Ott, M. Sprinel, T. Garestier, C. Hélène, Nucl.Acids Res., 21 (1993) 5547.
35. R. Roberts, D. Crothers, Proc.Natl.Acad.Sci.U.S.A., 88 (1991) 9397.
36. H. Han, P. Dervan, Proc.Natl.Acad.Sci. U.S.A., 90 (1993) 3806.
37. S. Wang, E. Kool, Biochemistry, 34 (1995) 4125.
38. S. Broitmann, J. Fresco, Proc.Natl.Acad.Sci.U.S.A., 84 (1987) 5120.

39. M. Mills, J. Völker, H. Klump, Biochemistry, 35 (1996) 13338.
40. H.E. Moser, P.B. Dervan, Science, 238 (1987) 645.
41. L. Maher, P. Dervan, P. Wold, Biochemistry, 13 (1992) 70.
42. R. Wells, D. Collier, J. Hanvey, M. Shimizu, F. Wohlrab, FASEB J., 2 (1988) 2939.
43. L.C. Griffin, P.B. Dervan, Science, 245 (1989) 967.
44. J. Sun, C. Hélène, Curr. Opin. Struct. Biol., 2 (1993) 345.
45. G.E. Plum, Y.W. Park, S.F. Singleton, P.B. Dervan, K.J. Breslauer, Proc. Natl. Acad. Sci. U.S.A., 87 (1990) 9436.
46. M. Kamiya, H. Torigoe, H. Shindo, A. Sarai, J.Am.Chem.Soc., 118 (1996) 4532.
47. G. Vesnaver, K. Breslauer, Proc. Natl. Acad. Sci. U.S.A., 88 (1991) 3569.
48. G. Plum, K. Breslauer, J.Mol.Biol., 248 (1995) 679.
49. C. Hélène, Eur.J.Cancer, 27 (1991) 1466.
50. S. Mirkin, V. Lyamichev, S. Filipoo, M. Frank-Kamenetskii, Nature, 330 (1987) 495.
51. E. Plum, D. Pilch, S. Singleton and K. Breslauer, Ann.Rev.Biophys.Biomol. Struct., 24 (1995) 319.
52. V. Sklénar, J. Feigon, Nature, 345 (1990) 836.
53. I. Radhakrishnan, D. Patel, Biochemistry, 33 (1994) 11405.
54. H. Htun, J. Dahlberg, Science, 243 (1989) 1571.
55. R. Häner, P. Dervan, Biochemistry, 29 (1990) 9761.
56. P. Hüsler, H.H. Klump, Arch.Biochem.Biophys., 317 (1995) 46.
57. C. Hélène, T. Garestier, T. Saison, M. Tagasugi, J. Toulme, Biochimie, 67 (1985) 777.
58. K. Breslauer, E. Friere, M. Strausse, Methods in Enzymology, 221 (1992) 533.
59. T. Wiseman, S. Wiliston, J. Brandts, L. Lin, Anal.Biochem., 179 (1989) 113.
60. P. Privalov, S. Petekhin, Meth. Enzymol., 131 (1986) 4.
61. V. Bloomfield, D. Crothers, I. Tinoco, Physical Chemistry of Nucleic Acids, Harper and Row, N.Y., 1974.
62. K. Breslauer, in: S. Agraval (Ed.), Methods in Mol.Biol., Vol. 26, Humana, New Jersey, 1994.
63. J. McGhee, Biopolymers, 15 (1976) 1345.
64. E.T. Kool, J.Am.Chem.Soc., 113 (1991) 6265.
65. M. Distefano, P.Dervan, J.Am.Chem.Soc., 114 (1992) 11006.
66. G. Manning, Q.Rev.Biophys., 11 (1978) 179.

67. M. Rawitscher, J. Sturtevant, J.Am.Chem.Soc., 82 (1960) 3739.
68. D. Xie, V. Bhakemi, E. Freire, Biochemistry, 31 (1991) 10673.
69. S. Singleton, P. Dervan, Biochemistry, 31 (1992) 10995.
70. M. Durand, T. Nguyen, J. Maurizot, J.Biol.Chem., 267 (1992) 24394.
71. P. Nielsen, M. Egholm, R. Berg, Science, 254 (1991) 1497.
72. M. Warring, Biochem.J., 143 (1974) 483.
73. T. Webb, in: K. Davies (Ed.), The Fragile X Syndrome, Oxford University Press, N.Y., 1989, p. 50.
74. R. Richard, G. Sutherland, Trends Genet., 8 (1992) 249.
75. A.J. Verkerk, Cell, 65 (1991) 905.
76. F. Fu, D. Kuhl, A. Pizzuti, Cell, 67 (1991) 1047.
77. Y. Nadel, P. Weisman-Shomer, M. Fry, J.Biol.Chem., 270 (1995) 28970.
78. M. Fry, L. Loeb, Proc.Natl.Acad.Sci.U.S.A., 91 (1994) 4950.
79. A. Vincent, D. Heitz, C. Petit, C. Kretz, I. Overle, J. Mandel, Nature, 369 (1991) 624.
80. R. Hansen, S. Gartler, S. Scott, C. Laird, Hum.Mol.Genet., 1 (1993) 571.
81. A. Gacy, G. Goellner, N. Juranic, S. Macura, C. McMurray, Cell, 81 (1995) 533.
82. P.Scaria, S. Shir, R. Shafer, Proc.Natl.Acad.Sci.U.S.A., 89 (1992) 10336.
83. W. Sundquist, A. Klug, Nature, 342 (1989) 825.
84. A. Zahler, R. Williamson, T. Cech, D. Prescott, Nature, 350 (1991) 718.
85. E. Ullmann, A. Peyman, Chem.Rev., 90 (1990) 543.
86. J. Clarenc, G. Degols, J. Leonetti, P. Milhaud, B. Lebleu, Anti-Cancer Drug Design, 8 (1993) 81.
87. C. Stein, Y. Cheng, Science, 261 (1993) 1004.
88. R. Wagner, Nature, 372 (1994) 333.
89. S. Agrawal, P. Iyer, Curr.Opin.Biotechnol., 6 (1995) 12.
90. H. Knudsen, P. Nielsen Nucl.Acids Res., 24 (1996) 494.
91. M. Egholm, O. Buchard, L. Christensen, C. Behrens, S.M. Freier, D.A. Driver, R.H. Berg, S. Kim, B. Norden, P. Nielsen, Nature, 365 (1993) 566.
92. M. Egholm, O. Buchardt, P. Nielsen, R. Berg, J.Am.Chem.Soc., 114 (1992) 1895.

93. M. Egholm, O. Buchardt, P. Nielsen, R. Berg, J.Am.Chem.Soc., 114 (1992) 9677.
94. M. Lyon, A. Graslund, P. Nielsen, O. Burchardt, B. Norden, S. Kristensen, M. Eriksson, Biochemistry, 33 (1994) 9820.
95. J. Ladbury, J. Sturtevant, N. Leontis, Biochemistry, 33 (1994) 6828.
96. H. Noller, Ann.Rev.Biochem., 53 (1984) 119.
97. D. Lilley, R. Clegg, Annu.Rev.Biophys.Biomol.Struct., 22 (1993) 299.
98. C. Hutchins, P. Rathjen, A. Forster, R. Symons, Nucl.Acids Res., 14 (1986) 3627.
99. N. Leontis, W. Kwok, J. Newman, Nucl.Acids Res., 19 (1991) 759.
100. J-H. Ha, R. Spolar, T. Record, J.Mol.Biol., 209 (1989) 801.
101. S. Delcourt, R. Blake, J.Biol.Chem., 266 (1991) 15160.
102. R. Spolar, T. Record, Science, 263 (1994) 777.
103. M. Rosen, D. Patel, Biochemistry, 32 (1993) 6563.
104. A. Cheng, M. van Dyke, Nucl.Acids Res., 21 (1993) 5630.
105. D. Sen, W. Gilbert, Biochemistry, 31 (1992) 65.
106. W. Guschlbauer, J. Chantot, D. Thiele, J.Biomol.Struct.Dyn., 8, (1990) 491.
107. J. Williamson, M. Raghuraman, T. Cech, Cell, 59 (1989) 871.
108. E. Postel, S. Flint, D. Kessler, M. Hogan, Proc.Natl.Acad.Sci. U.S.A., 88 (1991) 8227.
109. J. Milligan, S. Krawszyk, S. Wadwany, M. Matteucci, Nucl.Acids.Res., 21 (1993) 327.
110. F.W. Smith, J. Feigon, Nature, 356 (1992) 164.
111. W. Sundquist, Nucleic Acid Mol. Biol., 5 (1991) 1.
112. M. Chamberlin, P. Berg, J.Mol.Biol., 8 (1964) 297.
113. F. Martin and I. Tinoco, Nucl.Acids.Res., 8 (1980) 2295.
114. H. Moser, P. Dervan, Am.Chem.Soc., 111 (1990) 3059.
115. R. Roberts, D. Crothers, Science, 258 (1992) 1463.
116. L. Sowers, B. Shaw and W. Sedwick, Biochem.Biophys.Res.Commun., 148 (1987) 790.
117. W. Gilbert, Nature, 319 (1986) 618
118. C. Woese, in: The Genetic Code, Harper and Row, N.Y., 1967, p. 179.
119. T. Cech, Proc.Natl.Acad.Sci.USA., 83 (1986) 4360.
120. F. Crick, J.Mol.Biol., 38 (1968) 367.
121. M. Eigen, Naturwissenschaffen, 58 (1971) 465.
122. M. Been, T. Cech, Science, 239 (1988) 1412.
123. D. Draper, TIBS., 21 (1996) 145.

124. R. Gutell, N. Larsen, C. Woese, in: R.A. Zimmerman, A. Dahlberg (Eds.), Ribosomal RNA, Structure, Evolution, Gene expression and Function in Protein Synthesis, Telford Press, Caldwell, N.J., 1993.
125. L. Gold, P. Allen, J. Binkley, Brown, D.Schmeider, S. Eddy, in: R. Gesteland, J. Atkins (Eds.), The RNA World, Cold Spring Harbor Labs. Press., 1993, p. 497.
126. D. Turner, N. Sugeimoto, S. Frier, Ann.Rev.Biophys.Chem., 17 (1988) 167.
127. S. Frier, D. Alkema, A. Sinclair, T. Neilson, D. Turner, Biochemistry, 24 (1985) 4533.
128. S. Frier, N. Sugeimoto, D. Alkema, A. Sinclair, T. Neilson, R. Kierzek, M. Caruthers, D. Turner, Biochemistry, 24 (1986) 4533.
129. J. Santa Lucia, R. Kierzek, D. Turner, Science, 256 (1992) 217.
130. P. Bevilaqua, D. Turner, Biochemistry, 30 (1991) 106032.
131. G. Quigle, A. Rich, Science, 194 (1976) 796.
132. L. He, R. Kierzek, J. Santa Lucia, A. Walter, D. Turner, Biochemistry, 30 (1991) 11124.
133. V. Antao, I. Tinoco, Nucl. Acids Res., 20 (1992) 819.
134. F. Michel, E. Weshof, J.Mol.Biol., 216 (1990) 585.
135. D. Celander, T. Cech, Science, 251 (1991) 401.
136. L. Gold, B. Politsky, O. Uhlenbeck, M.Yarus, Ann.Rev.Biochem. 64, (1995) 73.
137. D. Crothers, P. Cole, P. Hilbers, R.Schulman, J.Mol.Biol., 87 (1974) 63.
138. C. Hilbers, Biochemistry, 15 (1976) 1784.
139. J. Szostak, A. Ellington, in: R. Gesteland, J. Atkuis (Eds.), The RNA World, Cold Spring Harbor Lab. Press, N.Y., 1993, p. 511.
140. P. Cole, S. Yang, D. Crothers, Biochemistry, 11 (1972) 4358.
141. D. Drape, T. Gluick, Meth.Enzymol., 250 (1995) 281.
142. C. Tang, D. Draper, Cell, 57 (1989) 531.
143. A. Stein, D. Crothers, Biochemistry, 15 (1976) 157.
144. D. Draper, Biophys. Chem., 21 (1985), 91.
145. L. Laing, D. Draper, J.Mol.Biol., 237 (1994) 560.
146. M. Lu, D. Draper, J.Mol.Biol., 244 (1994) 572.
147. M. Lu, D. Draper, Nucl.Acids Res., 23 (1995) 3426.
148. J. Lorsch, J. Szostak, Biochemistry, 33 (1994) 973.
149. W. Saenger, Physical Chemistry of Nucleic Acid Structures, Harper and Row, N.Y., 1974.

150. L. Jaeger, F. Michel, E. Westhof, J.Mol.Biol., 216 (1990) 55.
151. D. Turner and P. Bevilaqua, in: R. Gesteland, J. Atkins (Eds.) The RNA World, Cold Spring Harbor Lab. Press N.Y., 1993, p. 447
152. G. Rose, R. Wolfenden, Annu.Rev.Biophys.Biomol.Struct., 22 (1993) 381.
153. D. Bashford, C. Clothia, A. Lesk, J.Mol.Biol., 196 (1987) 199.
154. H. Grosjean, R. Cedergreen, W. McKay, Biochimie, 64 (1982) 387.
155. G. Varani, Ann.Rev.Biophys.Biomol.Struct., 24 (1995) 379.
156. I. Tinoco, J. Puglis, J. Wyatt, Nucl.Acids.Res., 4 (1990) 206.
157. C. Woese, S. Wurker, R. Guttel, Proc.Natl.Acad.Sci.USA., 87 (1990) 8467.
158. C. Haasnoot, S. De Brui, R. Berebolsen, J.Biomol.Struct.Dyn., 1 (1983) 115.
159. A. Van Belkum, M. Blommer, H. van der Elst, J. van Boom, C. Hillbers, Nucl.Acids.Res., 18 (1990) 4703.
160. O. Uhlenbeck, Nature, 346 (1990) 613.
161. V. Antao, S. Lai, I. Tinoco, Nucl.Acids.Res., 19 (1991) 5901.
162. J. Gralla, D. Crothers, J.Mol.Biol., 73 (1973) 497.
163. W. Cruse, P. Saludijan, E. Biala, P. Strazewski, T. Prauge, O. Kennard, Proc.Natl.Acad.Sci.USA., 91 (1994) 4160.
164. D. Erie, A. Suri, K. Breslauer, R. Jones, W. Olson, Biochemistry, 32 (1993) 436.
165. W. Saenger, in: Principles of Nucleic Acid Structure, Springer Verl. N.Y., 1984
166. O. Uhlenbeck, P. Borer, B. Dengler, I. Tinoco, J.Mol.Biol., 73 (1973) 483.
167. M. Senior, R. Jones, K. Breslauer, Proc.Natl.Acad.Sci.USA., 85 (1988) 6242.
168. C. Tuerk, P. Grauss, C. Thermes, D. Groebe, M. Gayles, Proc.Natl.Acad.Sci.USA., 85 (1988) 1364.
169. J. Wolters, Nucl.Acids.Res., 20 (1992) 1843.
170. H. Sakata, Y. Oda, T. Tanaka,. M. Ikehara S. Uesugi, Nucl. Acids. Res., 18 (1990) 3831.
171. I. Hiroa, Y. Nishimura, Y. Tagawa, K. Watanabe, K. Miura, Nucl.Acids.Res., 20 (1992) 3891.
172. L. Rothman-Denes, Sem. Virol., 40 (1995) 237.
173. I. Hirao, G. Kawai, S. Yosluizawa, Y. Nishimwa, Y. Ishido, Nucl.Acids.Res., 22 (1994) 576.

174. C. Zwieb, Nucl.Acids.Res., 20 (1992) 4397.
175. F. Murphy, T. Cech, J.Mol.Biol., 236 (1994) 49.
176. J. Khan, J. Coulson, Nucl.Acids.Res., 21 (1993) 2957,
177. J. Jaeger, D. Turner, M. Zuker, Proc.Natl.Acad.Sci.USA. 86, (1889) 7706.

This Page Intentionally Left Blank

Handbook of Thermal Analysis and Calorimetry. Vol. 4: From Macromolecules to Man.
R.B. Kemp, editor.

Chapter 2

THEORY AND PRACTICE OF DSC MEASUREMENTS ON PROTEINS

Jörg Rösgen & Hans-Jürgen Hinz

Institut für Physikalische Chemie, Westfälische Wilhelms Universität Münster, Schloßplatz 7, 48149 Münster, Germany

1. INTRODUCTION

Proteins are fascinating biological and physical objects. The investigation of protein energetics is not only important for the understanding of their biological function, such studies have also an intrinsic heuristic value for the rationalisation of some unique physical properties of proteins that result from the small size of these macromolecules compared to the magnitude of standard classical thermodynamic systems [1]. The understanding of the physical properties of proteins will also enhance the understanding of their biological reactions.

Experimental access to the energetic properties of proteins can be obtained by several methods. However, none of these methods provide such a direct and powerful approach as differential scanning calorimetry. DSC monitors the response function "heat capacity" which is directly related to the partition function of the system. Knowledge of the partition function is sufficient to derive all the thermodynamic information on the system.

2. THE DSC-EXPERIMENT

2.1 Sample preparation

An important starting point for a successful DSC experiment is the careful preparation of all solutions. Generally the buffer should be filtered and degassed. The sample solution should be essentially free of oxygen, especially if there are free cysteines in the protein [2]. If ligands are involved,

their concentrations have to be adjusted with great care. This is also true of H^+ ions as ligands. For example, in some cases pH-shifts of a few tenth of a pH unit can result in remarkable shifts in the unfolding temperature of a protein [3].

The protein must be dialysed exhaustively against buffer before the measurement. Typical protein concentrations that can be measured accurately by present day DSC instrumentation are in the range of 0.1 mg/ml to 10 mg/ml. High concentrations yield a favourable signal to noise ratio, but they may favour unspecific irreversible aggregation of the samples.

2.2 Measurement and data treatment

DSC monitors the energy needed to raise the temperature of the sample. Heating rates between 0.1 and 2 K/min are routinely employed with protein solutions. The temperature scans must be done with both the sample and the equilibrium dialysis buffer solution. The difference in heat capacity between these solutions – the so-called apparent heat capacity $\Delta C_{p,\mathrm{app}}$ – is the basis for all C_p calculations.

This difference originates from the replacement of buffer solution by proteins. The corresponding equation is:

$$\Delta C_{p,\mathrm{app}} = c_{p,\mathrm{buffer}} \cdot m_{\mathrm{buffer}} - c_{p,\mathrm{protein}} \cdot m_{\mathrm{protein}}, \tag{1}$$

where m_{buffer} and m_{protein} are, respectively, the mass of the replaced buffer and the protein. Introducing the specific volume $v = V/m$ and solving for the heat capacity of the protein one obtains the equation

$$C_{p,\mathrm{protein}} = C_{p,\mathrm{buffer}} \cdot \frac{v_{\mathrm{protein}}}{v_{\mathrm{buffer}}} - \frac{\Delta C_{p,\mathrm{app}}}{m_{\mathrm{protein}}}. \tag{2}$$

At low buffer concentration the heat capacity of the buffer is not very different from the heat capacity of water. Therefore often the heat capacity of water at room temperature (1 cal/gK = 4.184 J/gK) is used as an approximate value for the specific heat capacity of the buffer $c_{p,\mathrm{buffer}}$. However, if accurate data are needed, a third measurement of water against buffer must be performed, which yields the difference in heat capacity between buffer and water. Since the heat capacity of water is known accurately and can be expressed by the following polynomial equation based on the data of Stimson [4]

$$\begin{aligned} c_{p,\mathrm{water}}[\mathrm{J/gK}] &= 4.2174 - 3.176894 \cdot 10^{-3}\, T \\ &+ 8.574342 \cdot 10^{-5}\, T^2 - 9.3402 \cdot 10^{-7}\, T^3 \\ &+ 3.94926 \cdot 10^{-9}\, T^4 \end{aligned} \tag{3}$$

(fitted to a fourth order polynomial in temperature [°C]), $c_{p,\text{buffer}}$ can be determined properly, if necessary. As long as no absolute values of heat capacity are required, but only transition parameters such as enthalpies or entropies are of interest, approximate values for the specific volumes may be employed. Frequently mean values of $v_{\text{protein}} = 0.74$ ml/g and $v_{\text{buffer}} \approx 1$ ml/g have been used. However, in general it is preferable to determine experimentally the variation with temperature of both specific volumes directly [5,6] or take the individual values from data collections [7]. The specific volume of water is given by the following expression [8]

$$\begin{aligned} v_{\text{water}}[\text{ml/g}] &= (1 + 16.87985 \cdot 10^{-3}\, T)/ \\ &\quad (0.9998395 + 16.945176 \cdot 10^{-3}\, T \\ &\quad -7.9870401 \cdot 10^{-6}\, T^2 - 46.170461 \cdot 10^{-9}\, T^3 \\ &\quad +105.56302 \cdot 10^{-12}\, T^4 - 280.54253 \cdot 10^{-15}\, T^5). \end{aligned} \tag{4}$$

3. THERMODYNAMIC ANALYSIS OF HEAT CAPACITY CURVES

In this section heat capacity is interpreted in a classical thermodynamical way. A more general statistical thermodynamical analysis in a later section will show some differences in interpretation, which renders the DSC method an even more powerful tool in the investigation of protein folding.

3.1 The shape of heat capacity curves

In the simplest case a heat capacity curve of a protein consists of three parts. There are two regions showing roughly a linear temperature dependence of C_p separated by a peak (Figure 1). This peak reflects a first order transition between the two common states of proteins, the so-called native and the denatured state. The native state is the biologically functional state which is populated at physiological conditions. It is also characterised by a well defined three-dimensional structure. In contrast the denatured state has no defined single structure and lacks biological function. The transition region is marked by a heat absorption peak. Its stepwise integrated area has been assumed traditionally to be proportional to the fraction of denatured molecules or equivalently to the population shift. The midpoint temperature of the transition is called $T_{1/2}$ and has been traditionally defined as the temperature at which 50% of the molecules have been denatured.

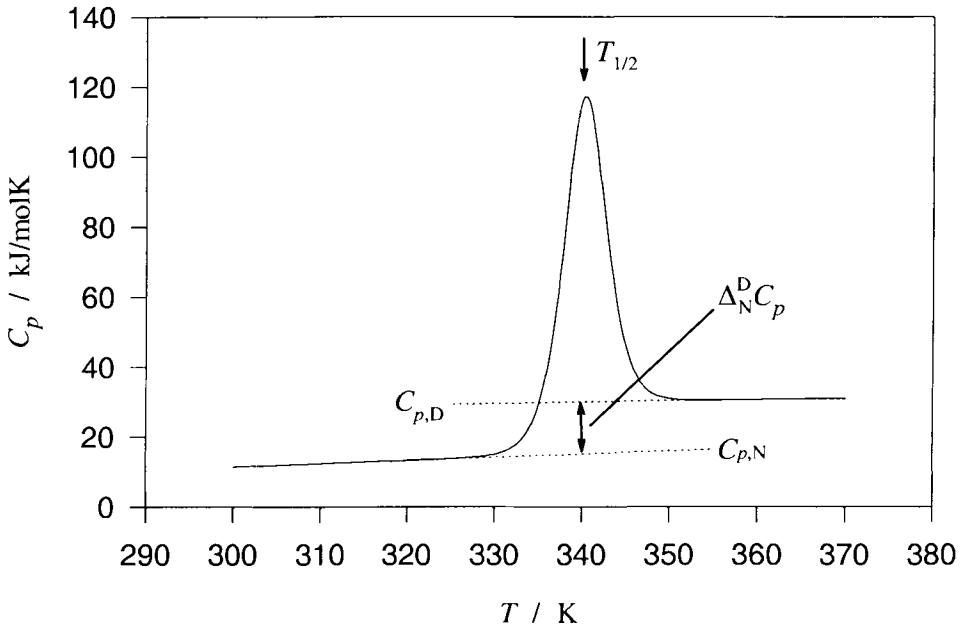

Figure 1: Simulated heat capacity curve of a protein. In the transition region around $T_{1/2}$ a characteristic peak occurs. The extrapolated heat capacities of pure native and pure denatured state $C_{p,N}$ and $C_{p,D}$ are indicated by the dotted lines. The parameters used in the calculation of the transition curve according to equation 44 are: $\Delta H^0 = 600$ kJ/mol, $T_{1/2} = 340$ K, $C_{p,N} = 15$ kJ/molK, $\partial_T C_{p,N} = 90$ J/molK^2, $C_{p,D} = 30$ kJ/molK, $\partial_T C_{p,D} = 40$ J/molK^2 and $\partial_T^2 C_{p,D} = -0.5$ J/molK^3

3.2 Protein stability

In the present survey protein stability will be defined thermodynamically [9]. Alternatively for other purposes it may be useful to characterise protein stability by the time during which a protein population shows biological activity. Such a criterion is not based on thermodynamic grounds but is rather a question of irreversible kinetics. Therefore we shall refer in this discussion to protein stability in the strict thermodynamic manner by using the standard Gibbs energy change of unfolding $\Delta_N^D G^0(T)$ as a quantitative measure of protein stability.

The use of $\Delta_N^D G^0(T)$ as a quantitative measure of stability implies reversible experimental conditions. Therefore measurements have to be optimised to exclude the occurrence of irreversibility. Two mayor causes of irreversibility can be distinguished. First, for the establishment of equilibrium conditions the scan rate must be slow compared to the folding kinetics [10,11]. Otherwise the $C_p(T)$-curve will become distorted. Second, reversible unfolding may be perturbed by an irreversible step following unfolding, if the heating rate is too slow compared with the rate of the irreversible reaction. Interference by such a process can be avoided, if the measurement is completed before a significant amount of the irreversibly misfolded state has accumulated [12-14]. The proper choice of the scan rate is therefore dictated by the intrinsic folding properties of the protein but also by the response time of the DSC instrument [15]. These constraints may lead to both an upper and lower limit of the heating rate.

The quantitative description of the transition curve shown in Figure 1 can be accomplished in the following manner. The overall excess heat contribution $\Delta_N^D H^0(T_{1/2})$ of the unfolding transition is represented by the area of the peak, since thermodynamically the heat capacity at constant pressure is defined by the equation

$$C_p = \left(\frac{\partial H}{\partial T}\right)_p . \tag{5}$$

Furthermore this means that the heat capacity difference between two states N and D, given by equation 6

$$\begin{aligned} \Delta_N^D C_p &= C_{p,D} - C_{p,N} \\ &= \left(\frac{\partial H_D}{\partial T}\right)_p - \left(\frac{\partial H_N}{\partial T}\right)_p = \left(\frac{\partial \Delta_N^D H^0(T)}{\partial T}\right)_p \end{aligned} \tag{6}$$

determines the temperature dependence of the enthalpy difference between the two states, $\Delta_N^D H^0(T)$. In Figure 1 $\Delta_N^D C_p$ is indicated at the midpoint temperature $T_{1/2}$. Integration of eq. 6 yields

$$\Delta_N^D H^0(T) = \Delta_N^D H^0(T_{1/2}) + \Delta_N^D C_p (T - T_{1/2}) \tag{7}$$

provided $\Delta_N^D C_p$ is assumed to be temperature independent. The more complicated case of a temperature dependent $\Delta_N^D C_p$ will be considered later. For the standard entropy difference between the native and the denatured states of the protein, the following relations hold

$$\frac{\Delta_N^D C_p}{T} = \left(\frac{\partial \Delta_N^D S^0(T)}{\partial T}\right)_p \tag{8}$$

$$\Delta_{\mathrm{N}}^{\mathrm{D}} S^0(T) = \Delta_{\mathrm{N}}^{\mathrm{D}} S^0(T_{1/2}) + \Delta_{\mathrm{N}}^{\mathrm{D}} C_p \ln \frac{T}{T_{1/2}}. \tag{9}$$

These parameters permit calculation of the standard Gibbs energy difference between the states of the protein. For a simple two-state transition of the type

$$\mathrm{N} \rightleftharpoons \mathrm{D} \qquad\qquad K = \frac{[\mathrm{D}]}{[\mathrm{N}]} \tag{10}$$

where K is the equilibrium constant, the value of K at the transition temperature $T_{1/2}$ is $K(T_{1/2}) = 1$. Therefore one obtains for the standard Gibbs energy change the relation

$$\begin{aligned} \Delta_{\mathrm{N}}^{\mathrm{D}} H^0(T_{1/2}) - T_{1/2} \cdot \Delta_{\mathrm{N}}^{\mathrm{D}} S^0(T_{1/2}) &= \Delta_{\mathrm{N}}^{\mathrm{D}} G^0(T_{1/2}) \\ &= -RT_{1/2} \ln[K(T_{1/2})] = 0 \end{aligned} \tag{11}$$

and thus

$$\Delta_{\mathrm{N}}^{\mathrm{D}} S^0(T_{1/2}) = \frac{\Delta_{\mathrm{N}}^{\mathrm{D}} H^0(T_{1/2})}{T_{1/2}}. \tag{12}$$

Using these relations the variation with temperature of the standard Gibbs energy change can be expressed in the following form

$$\begin{aligned} \Delta_{\mathrm{N}}^{\mathrm{D}} G^0(T) &= \Delta_{\mathrm{N}}^{\mathrm{D}} H^0(T) - T \cdot \Delta_{\mathrm{N}}^{\mathrm{D}} S^0(T) \\ &= \Delta_{\mathrm{N}}^{\mathrm{D}} H^0(T_{1/2}) + \Delta_{\mathrm{N}}^{\mathrm{D}} C_p (T - T_{1/2}) \\ &\quad -T \cdot \left[\frac{\Delta_{\mathrm{N}}^{\mathrm{D}} H^0(T_{1/2})}{T_{1/2}} + \Delta_{\mathrm{N}}^{\mathrm{D}} C_p \ln \frac{T}{T_{1/2}} \right]. \end{aligned} \tag{13}$$

This property is defined as the "stability of the protein". The function described by eq. 13 is the so-called "stability curve". By recalling the relation between the equilibrium constant $K(T)$ and the standard Gibbs energy change

$$K(T) = \exp\left(-\frac{\Delta_{\mathrm{N}}^{\mathrm{D}} G^0(T)}{RT} \right) \tag{14}$$

it is easy to see that for each temperature the fractions of both populations, N and D, are given by the expressions

$$\alpha_{\mathrm{N}}(T) = \frac{[\mathrm{N}](T)}{[\mathrm{N}](T) + [\mathrm{D}](T)} = \frac{1}{1+K} \tag{15}$$

and

$$\alpha_{\mathrm{D}}(T) = \frac{[\mathrm{D}](T)}{[\mathrm{N}](T) + [\mathrm{D}](T)} = \frac{K}{1+K}. \tag{16}$$

A typical stability curve and the fractional population sizes are shown in Figure 2. It is worth noting that according to equation 16 the fractions of both the native and denatured proteins converge to zero, but never reach it. Therefore the statement "at physiological temperatures the protein is in the native state" must be interpreted more precisely as meaning that "at physiological temperatures the native state is predominant".

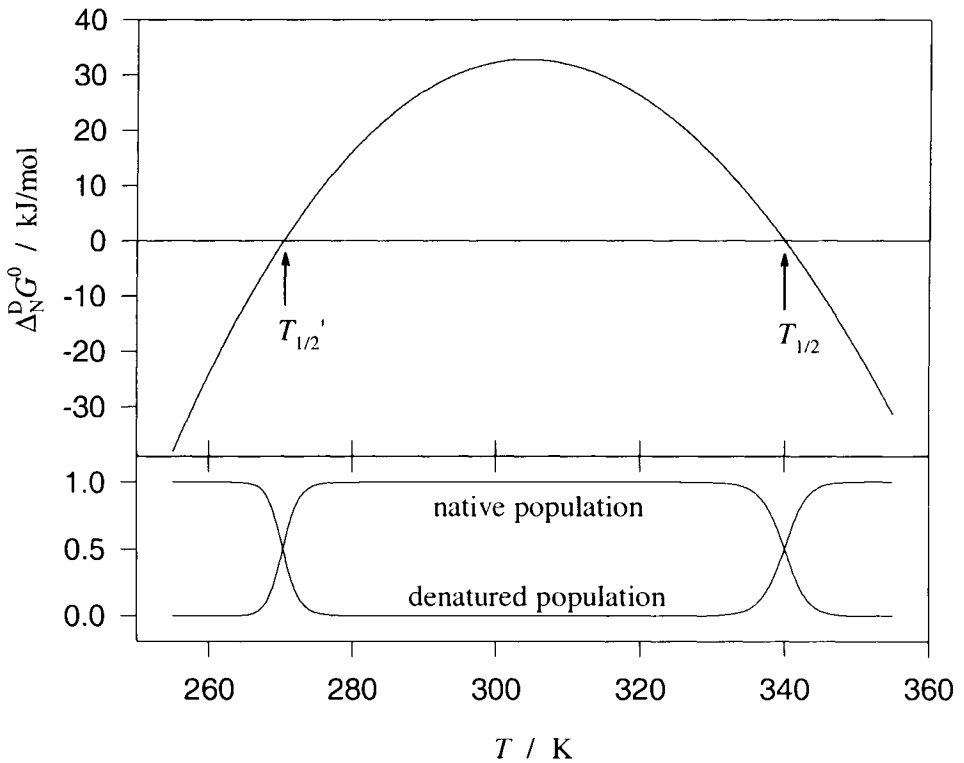

Figure 2. Protein stability curve for a two state N $\rightleftharpoons$ D transition. At positive $\Delta_N^D G^0(T)$ values the native state occurs predominantly, at negative $\Delta_N^D G^0(T)$ values the denatured state. A $\Delta_N^D C_p$ value > 0 causes the typical bending of the curve that leads to both cold denaturation at $T'_{1/2}$ and heat denaturation at $T_{1/2}$. In most cases cold denaturation is not observed, because it would occur below the freezing point of water. The lower part of the figure shows the variation with temperature of the fractional populations of native and denatured protein molecules. The parameters used for the calculations according to equation 23 are the same as in Figure 1.

Equation 13 is valid for the simple two-state 1:1 transition mechanism involving a constant $\Delta^{\mathrm{D}}_{\mathrm{N}}C_p$ value. For different transition stoichiometries or a temperature dependent $\Delta^{\mathrm{D}}_{\mathrm{N}}C_p$ value the stability equation will assume a more complex form (see below).

3.3 The heat capacity peak

Figure 3 illustrates the determination of the calorimetric enthalpy, ΔH_{cal}, from the area between the transition peak and the sigmoidal or linear (dotted line) baseline. In a later section the sigmoidal baseline under the transition peak will be shown to contain only ΔC_p-terms and no enthalpy terms, while for the heat capacity peak the opposite applies. The value for ΔH_{cal} is obtained by numerical integration of the peak. This quantity is equated to the standard enthalpy change at $T_{1/2}$, $\Delta^{\mathrm{D}}_{\mathrm{N}}H^0(T_{1/2})$. Strictly speaking this is only true for a simple N $\rightleftharpoons$ D reaction, because the bell shaped curve becomes asymmetric for higher stoichiometries. However, within experimental error this assumption is in most cases valid.

Another approximation provides usually also satisfactory results. This is the use of a linear baseline (dotted line in Figure 3) instead of the sigmoidal curve. This simplification might introduce significant errors only for very broad or asymmetric peaks [16].

ΔH_{cal} and $\Delta H_{\mathrm{v.H.}}$ should be identical if the transition proceeds as a two-state reaction. The latter quantity is the so-called van't Hoff enthalpy and represents the standard enthalpy change of a one-step reaction. For a reaction of the type $\mathrm{N}_n \rightleftharpoons n\mathrm{D}$ the van't Hoff enthalpy can be approximately calculated by

$$\Delta H_{\mathrm{v.H.}} = \frac{(1+\sqrt{n})^2 R T^2_{1/2}\left(< C_p >_{1/2} - \frac{\Delta^{\mathrm{D}}_{\mathrm{N}}C_p\sqrt{n}}{1+\sqrt{n}}\right)}{\Delta H_{\mathrm{cal}}}, \qquad (17)$$

where $< C_p >_{1/2}$ is the difference between the heat capacity at $T_{1/2}$ and the extrapolated $C_{p,\mathrm{N}}$ value of the native state at $T_{1/2}$ [17]. The ratio $\Delta H_{\mathrm{cal}}/\Delta H_{\mathrm{v.H.}}$ is a measure of the size of the cooperative unit of the transition. It should be equal to unity, if 1) the stoichiometry assumed for the transition is correct, 2) the reaction shows true two-state character and 3) the reaction is reversible.

Since the van't Hoff enthalpy is a measure of the sharpness of the peak, any flattening of the heat capacity curve, associated e.g. with sequential

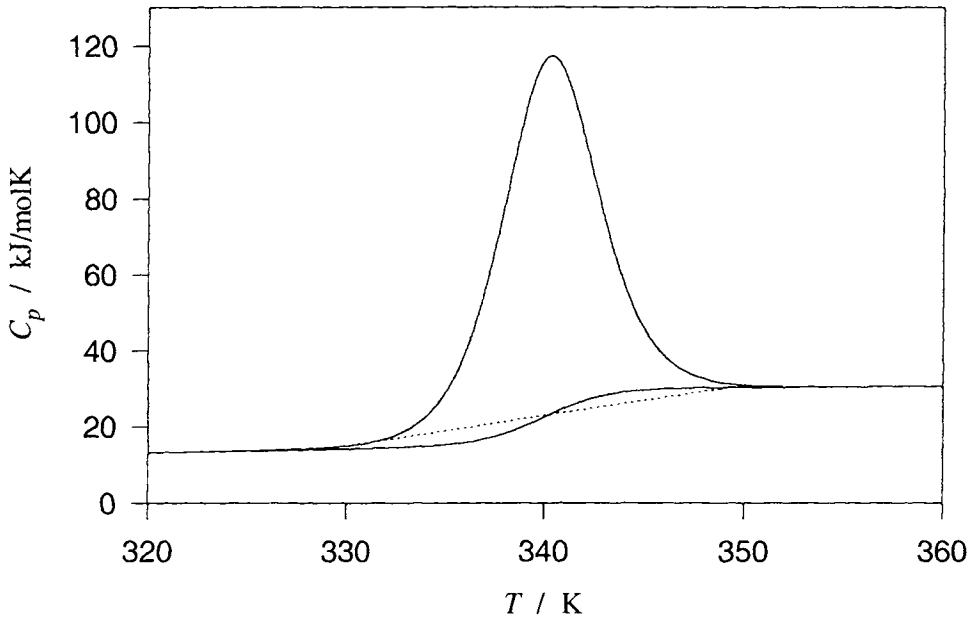

Figure 3. Illustration of the determination of the calorimetric enthalpy ΔH_{cal} by integration of the heat capacity peak. The error of taking a linear baseline for integration (dotted) instead of the sigmoidal curve is in most cases negligible. Positive and negative errors in the area compensate each other. The parameters used in the calculations (equation 44) are given in Figure 1.

reactions, decreases $\Delta H_{\mathrm{v.H.}}$ and therefore increases the size of the cooperative unit above 1. If the ratio $\Delta H_{\mathrm{cal}}/\Delta H_{\mathrm{v.H.}}$ is found to be smaller than one, this may indicate a stoichiometry that is higher than assumed. Alternatively the reaction may also contain irreversible steps. Then the second law of thermodynamics states that

$$\frac{\delta Q}{T} = \delta S_{\mathrm{transfer}} = \mathrm{d}S - \delta S_{\mathrm{irreversible}} \leq \frac{dQ_{\mathrm{rev}}}{T} \tag{18}$$

[18], i.e. the entropy $\delta S_{\mathrm{transfer}}$ observed experimentally becomes smaller by the internally produced entropy $\delta S_{\mathrm{irreversible}}$ than the total entropy change in the system $\mathrm{d}S$ [19]. Therefore also the enthalpy change observed, ΔH_{cal}, will be smaller than under reversible conditions.

3.4 Cold denaturation

From the stability curve for an N $\rightleftharpoons$ D transition shown in Figure 2 it is evident that there may be two points at which the standard Gibbs energy change $\Delta_{\mathrm{N}}^{\mathrm{D}}G^0(T)$ vanishes. This implies the existence of two transition temperatures $T_{1/2}$, for heat denaturation, and $T'_{1/2}$ for low temperature unfolding. This latter reaction is generally referred to as "cold denaturation". Cold denaturation has been discussed by Brandts [20] on the basis of spectroscopic measurements, but was observed calorimetrically first by Privalov et al. [3].

Figure 4 shows DSC measurements on myoglobin which we performed under conditions similar to those applied by Privalov et al. [3]. The experimental curve is indicated by the open circles and the calculated heat capacity functions for the native and unfolded state are given by the dashed-dotted and dotted lines respectively. The experimental curve can be simulated accurately using equation 44 – see section 5.4.1. The $C_{p,\mathrm{N}}(T)$ and $C_{p,\mathrm{D}}(T)$ function have been obtained from equations 65 and 66 – see section 5.5.

The cold denaturation phenomenon can be analysed thermodynamically by comparing the two contributions to the stability $\Delta_{\mathrm{N}}^{\mathrm{D}}G^0(T)$: the transition enthalpy $\Delta_{\mathrm{N}}^{\mathrm{D}}H^0(T)$, and the entropic contribution to the Gibbs energy change which is given by $T\Delta_{\mathrm{N}}^{\mathrm{D}}S^0(T)$. These contributions are shown in Figure 5. The graph illustrates impressively the marginal stability of proteins. $\Delta_{\mathrm{N}}^{\mathrm{D}}G^0$ is given at each temperature by the difference $\Delta_{\mathrm{N}}^{\mathrm{D}}H^0 - T\Delta_{\mathrm{N}}^{\mathrm{D}}S^0$ between the solid and the dotted line. Both $\Delta_{\mathrm{N}}^{\mathrm{D}}H^0(T)$ and $\Delta_{\mathrm{N}}^{\mathrm{D}}S^0(T)$ are temperature dependent because of the heat capacity difference $\Delta_{\mathrm{N}}^{\mathrm{D}}C_p$ between the native and the denatured protein. As mentioned before $\Delta_{\mathrm{N}}^{\mathrm{D}}C_p$ is responsible for the curvature of the $\Delta_{\mathrm{N}}^{\mathrm{D}}G^0(T)$ curve and therefore also for the occurrence of cold denaturation. There are only few calorimetrically investigated proteins, which show cold denaturation without addition of destabilising agents in an experimentally accessible temperature range. The two classical examples are myoglobin [3] and staphylococcal nuclease [21].

If $\Delta_{\mathrm{N}}^{\mathrm{D}}C_p$ is zero there is no cold denaturation, because only one temperature exists at which $\Delta_{\mathrm{N}}^{\mathrm{D}}G^0$ vanishes. For a reliable extrapolation of protein stability over a long temperature interval it is therefore of utmost importance to know accurately the heat capacities of the native and denatured state of the protein in the same temperature region.

Often ΔC_p has been determined by performing measurements at differ-

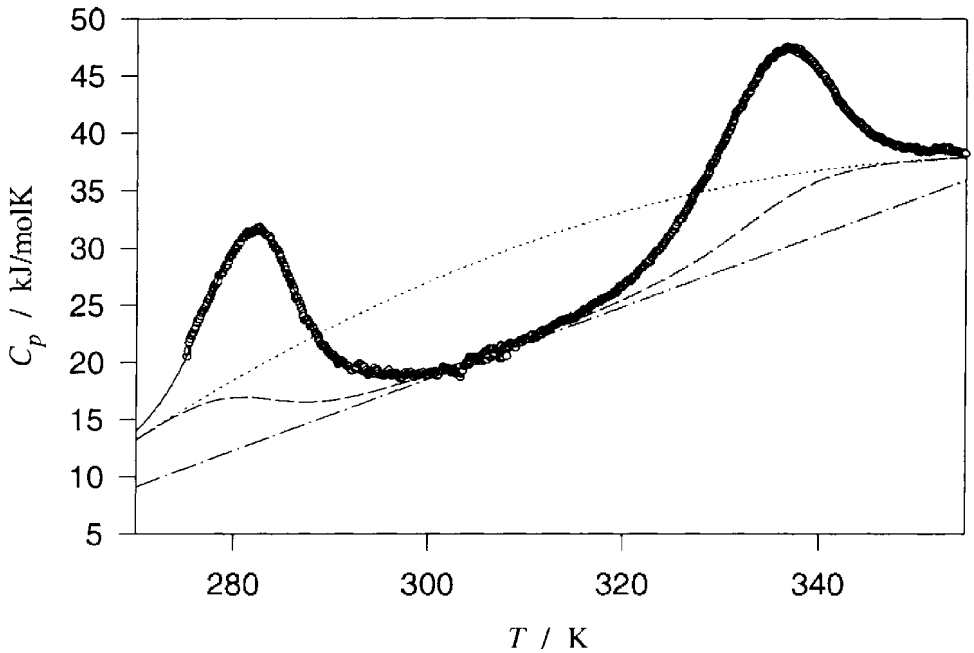

Figure 4. Heat capacity of myoglobin at acidic pH. Two peaks can be distinguished that are assigned to cold- and heat-denaturation, respectively. From a fit (solind line) of the experimental data (dots) according to equation 44 the heat capacities of native $C_{p,\mathrm{N}}$ (dash-dotted) and denatured state $C_{p,\mathrm{D}}$ (dotted line) were obtained. The heat capacity function of the native state has been linearly extrapolated on the basis of the experimental $C_{p,\mathrm{N}}(T)$ curve. The heat capacity of the unfolded state is found to be non-linear. The fit parameters at $T_{1/2}$ = 333.4 K are: ΔH^0 = 212 kJ/mol, $C_{p,\mathrm{N}}$ = 29 kJ/molK, $\partial_T C_{p,\mathrm{N}}$ = 315 J/molK^2, $C_{p,\mathrm{D}}$ = 36 kJ/molK, $\partial_T C_{p,\mathrm{D}}$ = 160 J/molK^2 and $\partial_T^2 C_{p,\mathrm{D}}$ = -6.2 J/molK^3

ent pH values and plotting ΔH_{cal} vs. the transition temperatures $T_{1/2}$. The slope of this curve is then assumed to correspond to ΔC_p according to equation 6. But this procedure is problematic, since the slope of the plot is not only determined by the intrinsic change in heat capacity of the polypeptide chain, but also by ligation effects which include protonation changes [9,22]. Furthermore ΔC_p generally cannot be expected to be temperature independent, due to the curvature in the $C_{p,\mathrm{D}}$ function and the linearity of $C_{p,\mathrm{N}}$ [23].

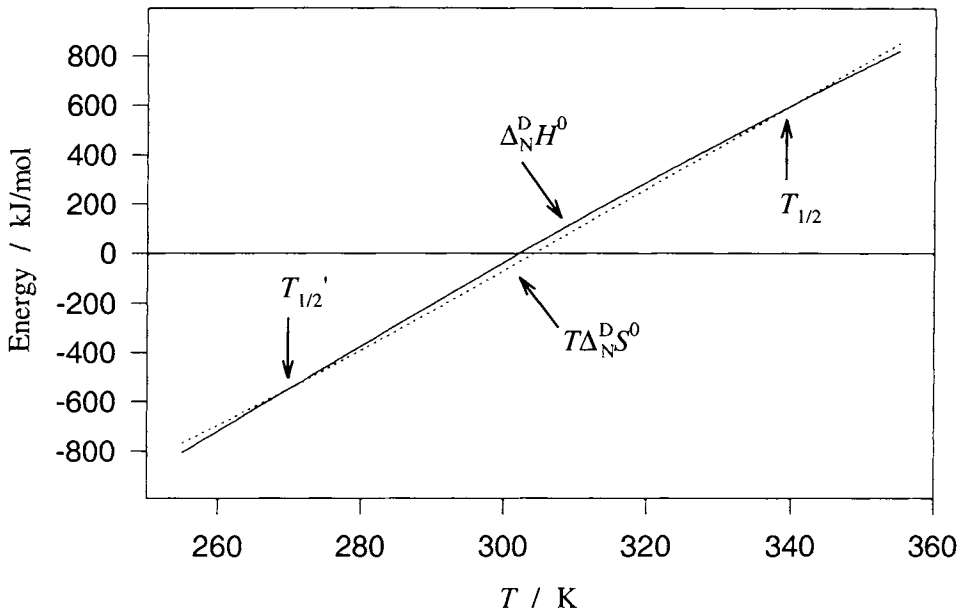

Figure 5. Simulated enthalpy and entropy curves. Around $T_{1/2}$ both $\Delta_N^D H^0(T)$ and $\Delta_N^D S^0(T)$ are positive, i.e. the denatured state has a higher enthalpy and entropy than the native one. At $T'_{1/2}$ the situation is reversed. The marginal difference $\Delta_N^D H^0(T) - T \cdot \Delta_N^D S^0(T)$ provides the value for the protein stability $\Delta_N^D G^0(T)$. The parameters used with equations 7 and 9 are those given in Figure 1.

3.5 The temperature dependence of $\Delta_N^D C_p(T)$

So far we have considered the simplest case that $\Delta_N^D C_p$ is temperature independent to a first approximation. This assumption is still useful and is based on the first significant DSC studies on proteins [24-27]. There it had been demonstrated that within the accuracy obtainable at that time the heat capacity of unfolded proteins was a linear function of temperature similar to that of native proteins, but parallel shifted by a constant, positive $\Delta_N^D C_p$ value. However, inspection of Figure 4 reveals clearly that $\Delta_N^D C_p$ is temperature dependent. Furthermore model compound studies that allow calculation of the variation with temperature of the heat capacity $C_{p,D}(T)$ of the unfolded state of proteins, indicate unambiguously that $C_{p,D}(T)$ is not linear [28-30]. Therefore it is necessary to incorporate these features

into the calculation of the stability curve. We shall go a step further by providing a formula for a generalised stability curve that makes allowance for the incorporation of effects of stoichiometry.

To derive such a stability relation for a two-state transition $N_n \rightleftharpoons nD$ of an oligomeric protein, N_n, consisting of n non-covalently linked monomers (subunits), we proceed in the following manner. $\Delta_N^D G^0(T)$ is written as a Taylor series

$$\Delta_N^D G^0(T) = \sum_{k=0}^{n} \frac{\Delta_N^D G^0(T_{1/2})^{(k)}}{k!}(T - T_{1/2})^k + \frac{1}{n!}\int_{T_{1/2}}^{T} (T-t)^n \Delta_N^D G^0(t)^{(n+1)} \mathrm{d}t \tag{19}$$

[31]. The index (k) indicates the number of derivatives with respect to T. For $n = 1$ eq. 19 yields

$$\Delta_N^D G^0(T) = \Delta_N^D G^0(T_{1/2}) - (T - T_{1/2})\Delta_N^D S^0(T_{1/2}) - \int_{T_{1/2}}^{T} \frac{T-t}{t}\Delta_N^D C_p(t)\mathrm{d}t \tag{20}$$

Because of the thermodynamic relations

$$\Delta_N^D G^0(T_{1/2}) = -RT_{1/2}\ln\left(K(T_{1/2})\right)$$

and

$$\Delta_N^D G^0(T_{1/2}) = \Delta_N^D H^0(T_{1/2}) - T_{1/2}\Delta_N^D S^0(T_{1/2})$$

one obtains

$$\Delta_N^D G^0(T_{1/2}) - \Delta_N^D S^0(T_{1/2}) \cdot (T - T_{1/2}) = -RT\ln\left(K(T_{1/2})\right) - \Delta_N^D H^0(T_{1/2})\frac{T - T_{1/2}}{T_{1/2}}. \tag{21}$$

For the $N_n \rightleftharpoons nD$ model with monomer concentration $c = n[N] + [D]$ remaining constant in the transition the equilibrium constant $K(T_{1/2})$ can be expressed as

$$K(T_{1/2}) = \frac{[D(T_{1/2})]^n}{[N_n(T_{1/2})]} = \frac{(c/2)^n}{c/(2n)} = n\left(\frac{c}{2}\right)^{n-1} \tag{22}$$

[32]. If a curvature of $C_{p,D}(T)$ has to be taken into account, it is advisable to employ the second derivative of $\Delta_N^D C_p(T)$. With these relations the

following expression for the temperature dependence of $\Delta_N^D G^0(T)$ has been obtained

$$\begin{aligned} & \Delta_N^D G^0(T) = \\ - \quad & RT \ln \left(n \left(\frac{c}{2} \right)^{n-1} \right) - \Delta_N^D H^0(T_{1/2}) \frac{T - T_{1/2}}{T_{1/2}} \\ + \quad & \Delta_N^D C_p(T_{1/2}) \cdot \left(T - T_{1/2} - T \ln \frac{T}{T_{1/2}} \right) \\ + \quad & \Delta_N^D C_p^{(1)}(T_{1/2}) \cdot \left(\frac{T_{1/2}^2 - T^2}{2} + T T_{1/2} \ln \frac{T}{T_{1/2}} \right) \\ + \quad & \frac{\Delta_N^D C_p^{(2)}(T_{1/2})}{2} \\ & \left(\frac{T^3 - T_{1/2}^3}{3} + \frac{(T - T_{1/2})^2 T}{2} - T_{1/2}^2 T \ln \frac{T}{T_{1/2}} \right) \end{aligned} \tag{23}$$

[1]. The equation reduces to the commonly used formula (equation 13) for isomeric transitions of the type N $\rightleftharpoons$ D having a 1:1 stoichiometry, since in that case $K(T_{1/2}) = 1$. For 1:2 stoichiometry, such as dimer to monomer transitions of the form $N_2 \rightleftharpoons 2D$, one obtains $K(T_{1/2}) = c$. Inspection of equation 23 shows that only for the N $\rightleftharpoons$ D transition the temperature of 50% conversion, $T_{1/2}$, coincides with the temperature T_G, which by definition occurs at $\Delta_N^D G^0(T_G) = 0$ [9]. In all other cases, there is a difference between $T_{1/2}$ and T_G. It is the steepness of the $\Delta_N^D G^0(T)$ curve that determines how far these two temperatures are apart, and the steepness, in turn, is dominated by the magnitude of $\Delta_N^D H^0$, as can be seen from equation 23 [1].

4. PREDICTING THE C_p VALUE OF THE DENATURED STATE ON THE BASIS OF MODEL COMPOUNDS

From the thermodynamic data obtained by DSC at $T_{1/2}$ an extrapolation of the thermodynamic quantities to other temperatures can be performed. For a valid extrapolation, however, the accuracy of $C_{p,N}(T)$ and $C_{p,D}(T)$ is critical. Usually the thermodynamic parameters at temperatures below $T_{1/2}$ are of interest. The heat capacity of the native state can be determined directly by DSC from the experimental protein heat capacity in this temperature range. The heat capacity of the denatured state, however, has

to be estimated over a very large temperature interval using information from above $T_{1/2}$. This is not problematic if, at low temperatures, the cold denatured state becomes observable and permits the measurement of the heat capacity of the denatured state as in the case of myoglobin at low pH (Figure 4). However, that situation applies only to a few proteins as mentioned above. Therefore the $C_{p,\mathrm{D}}$ function has to be determined by alternative procedures.

One such method is to estimate the heat capacity of the denatured state by using low molecular weight compounds that model the protein backbone chain and the amino acid side-chains. Such model compounds can be small organic molecules with structures that are similar to those of the side chains. For example CH_3OH has been used to model the side chain of serine [28]. Probably better estimates of side chains are given by using small peptides as model compounds [29,30,33]. The basic assumption in this procedure is that the contributions of the monomeric units are additive – at least in random-coil like protein states [28,34]. Provided this assumption holds, which is most likely, a comparison of measured and predicted heat capacities of the denatured state yields information on how closely the given protein resembles a random coil in the denatured state. Since the heat capacity change associated with protein denaturation is assumed to be proportional to the increase in the solvent accessible area [35] the experimental $C_{p,\mathrm{D}}(T)$ curve should be higher than the native state heat capacity function $C_{p,\mathrm{N}}(T)$ but lower than the calculated heat capacity curve $C_{p,\mathrm{D}}^{\mathrm{calculated}}(T)$. Only in the case that the unfolded protein assumes a random coil structure and therefore maximal hydration, should the experimental and calculated heat capacity curves for the denatured state coincide.

An example of a protein for which the calculated and measured $C_{p,\mathrm{D}}(T)$ are very similar has been given by Schöppe et al. [2] (Figure 6). The heat capacity predicted from the model peptides [29,30] shows only minor deviations from the experimental curve. In contrast, calculations based on parameters derived from the small organic model compounds [28] provide much lower values.

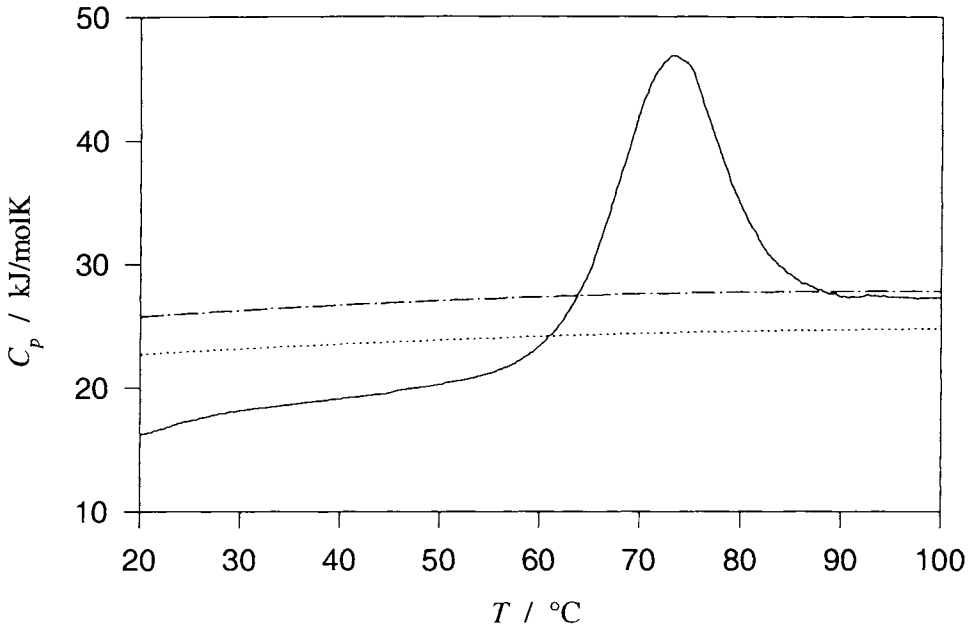

Figure. 6. Heat capacity of barstar wt and heat capacities predicted from the two model systems: small organic molecules [28] (dotted line) and peptides (dash-dotted line). The figure is taken from Schöppe et al. [2].

4.1 Oligopeptide-based model compounds

4.1.1 The glycyl group

The partial molar heat capacity of the glycyl group, $C_p(CH_2CONH)$, of a polypeptide has been evaluated in a recent study using partial molar heat capacity data for a series of peptides of amino acid sequence ala(gly)$_n$, n = 2-4 [29]. The coefficients a, b, c and d of the polynomial

$$C_p = a + b(T - 273.15) + c(T - 273.15)^2 + d(T - 273.15)^3 \qquad (24)$$

that represents the temperature dependence of the heat capacity of the backbone peptide group CHCONH and the end groups are given in Table 1.

4.1.2 The side chains

The partial molar heat capacities of the amino acid side-chains can be estimated using the partial molar heat capacity data for tripeptides of the form glycyl-X-glycine. The partial molar heat capacity, $C_p(R)$, of any

Table 1: Coefficients of the temperature polynomials for the calculation of the partial molar heat capacities of the glycyl group, the peptide backbone unit and the ionic end-groups

Group	a (J/molK)	b (J/molK^2)	c (J/molK^3)	10^4d (J/molK^4)
CH_2CONH	68.1	0.80	-0.0012	-0.23
CHCONH	-15.3	1.02	-0.0009	-0.24
$NH_3^+ + CH_2CO_2^-$	-65.0	4.56	-0.0647	3.69
$NH_3^+ + CHCO_2^-$	-148.4	4.77	-0.0644	3.68

side-chain of amino acid X is given by the equation

$$C_p(\mathrm{R}) = C_p(\mathrm{glyXgly}) - C_p(\mathrm{glyglygly}) + C_p(\mathrm{H}), \tag{25}$$

where C_p(glyXgly) and C_p(glyglygly) are, respectively, the partial molar heat capacities at infinite dilution for the peptides gly-X-gly and triglycine, and C_p(H) is the heat capacity of the hydrogen atom of the methylene moiety of triglycine. It has been noted that there are several rather disparate values for C_p(H) in the literature [30]. However, it should be noted that, using the peptide as model compounds, any uncertainties in the absolute value of C_p(R) resulting from the choice of C_p(H) data used in the calculations are not manifested in the value of the partial molar heat capacity of an unfolded protein. This is because the heat capacity of the backbone peptide group CHCONH is derived from the partial molar heat capacity of the glycyl group CH_2CONH by subtracting the estimated heat capacity of the H atom

$$C_p(\mathrm{CHCONH}) = C_p(\mathrm{CH_2CONH}) - C_p(\mathrm{H}) \tag{26}$$

[29]. A comparison of equations 25 and 26 shows that the sum of C_p(R) and C_p(CHCONH) is independent of the value chosen for C_p(H) when tripeptides are used as model compounds.

Similar to equation 24 the temperature dependence of the partial molar heat capacity of each amino acid side chain can be represented by a third order polynomial. The polynomial coefficients are given in Table 2.

Table 2: Coefficients of the temperature polynomials that represent the heat capacity for each of the amino acid side-chains.

Side-chain	a (J/molK)	b (J/molK^2)	c (J/molK^3)	10^4d (J/molK^4)
gly	83.4	-0.22	-0.0003	0.011
ala	204.3	-0.99	0.0078	-0.24
val	359.9	-1.64	0.0186	-1.16
leu	444.8	-1.47	0.0107	-0.60
ile	451.3	-1.38	0.0067	-0.47
ser	151.6	-0.58	0.0106	-0.87
thr	247.7	-0.64	0.0094	-0.70
asn	160.8	1.28	-0.0253	1.49
gln	206.2	0.16	0.0050	-0.67
phe	427.3	-1.63	0.0155	-0.83
tyr	336.7	0.26	-0.0044	0.081
trp	440.4	-0.21	-0.0128	0.92
his	235.4	0.67	0.0428	-3.52
cys	256.9	-1.73	0.0207	-1.22
met	342.0	-1.23	0.0177	-1.47
pro	206.2	-1.40	0.0256	-1.25
asp	157.8	0.54	-0.0112	0.18
glu	219.3	-0.17	0.0058	-0.77
lys^+	360.6	-0.26	0.0148	-0.27
arg^+	241.0	0.63	-0.0095	0.27

5. ANALYSIS OF HEAT CAPACITY CURVES BY STATISTICAL PHYSICS

5.1 General considerations

The classical statistical thermodynamic approach to protein folding considers a protein solution as a canonical ensemble of small mesoscopic systems. The single protein can be involved in conformational changes or ligand binding equilibria [36-47]. This description of a protein solution is most useful and is in agreement with the postulates of statistical physics. It is only necessary to define the relevant terms for the protein solution in a consistent manner.

Usually DSC experiments are performed on ideally diluted aqueous solutions of proteins in which each macromolecule can be assumed to experience minimal interactions with the others. This means that such a solution can be viewed to a good approximation as an ensemble of non-interacting small microscopic systems in the Gibbsian sense.

We are able to control the number of systems in the ensemble by controlling the number of proteins in our solution. Furthermore we can control the variables "pressure" and "temperature" of the protein solution. Actually what is adjusted is a mean volume and a mean energy by controlling the intensive variables pressure and temperature. In statistical thermodynamical terms this is called a "harmonic canonical ensemble" [48]. Its partition function is defined as $Y(\beta, p)$ [49]. It depends on pressure p and $\beta = 1/k_B T$, where k_B is the Boltzmann constant and T the absolute temperature.

So far we have not precisely defined the term "protein". For the statistical thermodynamic treatment we differentiate between protein and bulk buffer. In a thermodynamic sense the term "protein" or "protein system" is meant to refer to the polypeptide chain plus the hydration shell. The hydration shell is considered to have physical properties different from those of the "bulk buffer". The term "bulk buffer" refers to those parts of the protein solution that have the same physical properties as the pure buffer without protein chains. The dimensions of the hydration shell are generally assumed to be in the order of one monolayer [50]. Recently the hydration shell of RNase was estimated by dielectric relaxation studies. It was found that the amount of water accounting for hydration effects was smaller than the number of water molecules calculated for full monolayer coverage of the surface [51].

From the very beginning the heat capacity measured by DSC was recognised to be a partial molar quantity [52]. This means that every change in the properties of the solution caused by addition of a protein molecule is ascribed to this molecule. This is manifested in the procedure by which the raw data are treated to calculate the heat capacity. The value used for the mass of the protein, m_{protein}, in equation 2 is that of the dry polypeptide chain and not that of a hydrated polypeptide chain. Only if the dry mass is employed in the calculations, does one obtain agreement between the van't Hoff enthalpy values, $\Delta H_{\text{v.H.}}$, and the calorimetric enthalpies ΔH_{cal}. This is good evidence for the correctness of the choice.

This procedure implies that, in the statistical thermodynamical treatment of the influence of hydration, the hydration water need not to be considered as a term that increases the mass of the polypeptide chain. Rather it must be taken into account by the introduction of interaction terms in the corresponding Hamiltonian [53].

The single protein with its hydration shell will be referred to as the "protein-microsystem", while the collective sum of protein microsystems will be addressed as the "protein-macrosystem".

5.2 Definition of relative partition functions

The relevant partition function consists of the contributions of both the protein systems and the buffer and is composed of the product of the individual partition functions

$$Y(\beta, p) = Y_{\text{B}}(\beta, p) \cdot Y_{\text{P}}(\beta, p), \tag{27}$$

$$Y(\beta, p) = \exp(-G\beta) \tag{28}$$

where $Y_{\text{B}}(\beta, p)$ refers to the partition function of the bulk buffer and $Y_{\text{P}}(\beta, p)$ refers to the partition function of the protein-macrosystem. The enthalpy of the protein solution can be calculated from the temperature derivative of the partition function $Y(\beta, p)$ [49] according to equation 29

$$H = -\frac{\partial \ln Y}{\partial \beta} = -\frac{\partial \ln Y_{\text{B}}}{\partial \beta} - \frac{\partial \ln Y_{\text{P}}}{\partial \beta} = H_{\text{B}} + H_{\text{P}}. \tag{29}$$

Thus, the enthalpy H_{P} of the protein-macrosystem can be obtained, if the enthalpy of the protein solution, H, and the enthalpy of the pure buffer, H_{B}, can be determined. The enthalpy value H_{P} corresponds to an ensemble average of the protein-macrosystem. Due to ergodicity the value is also equivalent to the time average behaviour the single protein-microsystem [19]. Therefore we may drop the differentiation between the

protein-microsystems and the protein-macrosystem and simply refer to "the protein" instead.

The partition function $Y_P(\beta, p)$ for the simple two-state equilibrium $N \rightleftharpoons D$, is given by the expression

$$Y_P(\beta, p) = Y_N(\beta, p) + Y_D(\beta, p) \tag{30}$$

where Y_N refers to the contribution of the native, biologically active state, and Y_D to that of the denatured state. The reaction scheme can be easily extended to treat the occurrence of intermediates according to the equation

$$N \rightleftharpoons I_1 \rightleftharpoons I_2 \rightleftharpoons \cdots \rightleftharpoons D.$$

The partition function Y_P consists in such a case of the sum of the contributions Y_i of all states

$$Y_P = \sum_{i=1}^{n} Y_i. \tag{31}$$

If the enthalpy of the protein-system H_P is formulated relative to the enthalpy H_N of the fraction of proteins in the native state N one obtains the relation

$$H_P - H_N = -\frac{\partial \ln Y_P}{\partial \beta} + \frac{\partial \ln Y_N}{\partial \beta} = -\frac{\partial \ln \frac{Y_P}{Y_N}}{\partial \beta} = -\frac{\partial \ln Q}{\partial \beta}. \tag{32}$$

$Q := Y_P/Y_N$ is defined as a relative partition function.

Since the population sizes of the species N_i are given by the relation

$$N_i = N\frac{Y_i}{Y_P}, \tag{33}$$

with $N = \sum_i N_i$ referring to the total number of proteins considered, the relative partition function Q can be expressed by the population sizes of the various species according to equation 34

$$Q = \frac{Y_P}{Y_N} = \frac{\sum_i N_i}{N_N}. \tag{34}$$

It is important to note here that this is possible if and only if the sizes of all protein populations are divided by a single reference species, in this case by that of the native state N_N. Not every combination of concentrations is a partition function.

The definition of the relative partition function Q renders it very easy to identify the first and second temperature derivative of Q with experimentally accessible parameters. The first derivative of $\ln Q$ with regard to

temperature provides the enthalpy relative to the native state

$$H_{\mathrm{P}} - H_{\mathrm{N}} = -\frac{\partial \ln Q}{\partial \beta} = k_B T^2 \frac{\partial \ln Q}{\partial T} \tag{35}$$

and the second derivative with regard to temperature yields the heat capacity of the protein relative to the native state

$$C_{p,\mathrm{P}} - C_{p,\mathrm{N}} = \frac{\partial (H - H_{\mathrm{N}})}{\partial T} = -\frac{\partial}{\partial T}\frac{\partial \ln Q}{\partial \beta}. \tag{36}$$

The Boltzmann constant k_B in eq. 35 is valid for the single protein-microsystem. It must be replaced by R for the determination of molar quantities. In the following we will suppress the index P for the protein. C_p as well as H will refer to the protein only.

5.3 Calculation of the partition function by integrating heat capacity curves

From equation 36 it is evident that a direct integration of a $C_p(T)$-curve yields the relative partition function Q [37,41,42]. Before numeric integration of the experimental $C_p(T)$-curve the heat capacity of the reference species has to be subtracted. For practical reasons this usually works best, if either the heat capacity of the native or that of the denatured state is used as reference heat capacity. For a reliable deconvolution of the experimental heat capacity curve it is essential that either $C_{p,\mathrm{N}}$ or $C_{p,\mathrm{D}}$ can be extrapolated accurately into the transition region. Depending on whether the native or the denatured state is taken as reference state equation 34 shows that the following relations hold

$$\frac{1}{Q} = \frac{N_{\mathrm{N}}}{\sum_i N_i} = \alpha_{\mathrm{N}} \qquad \text{or} \qquad \frac{1}{Q} = \frac{N_{\mathrm{D}}}{\sum_i N_i} = \alpha_{\mathrm{D}}. \tag{37}$$

The reciprocal value of the relative partition function is related to either the fraction of the native or denatured state. Figure 7 shows the numerical integration procedure for the heat capacity curve of the two-state unfolding transition of ROP wt protein [53,54]. This is a homo-dimeric small protein that unfolds according to the mechanism $\mathrm{N}_2 \rightleftharpoons 2\mathrm{D}$. The straight line indicates the extrapolation of the native state heat capacity $C_{p,\mathrm{N}}(T)$. According to eq. 36 the enthalpy has been calculated relative to the native state by integration of the heat capacity difference $C_p(T) - C_{p,\mathrm{N}}(T)$

$$H(T) - H_{\mathrm{N}}(T) = \int_{295K}^{T} \left[C_p(T) - C_{p,\mathrm{N}}(T)\right] dT. \tag{38}$$

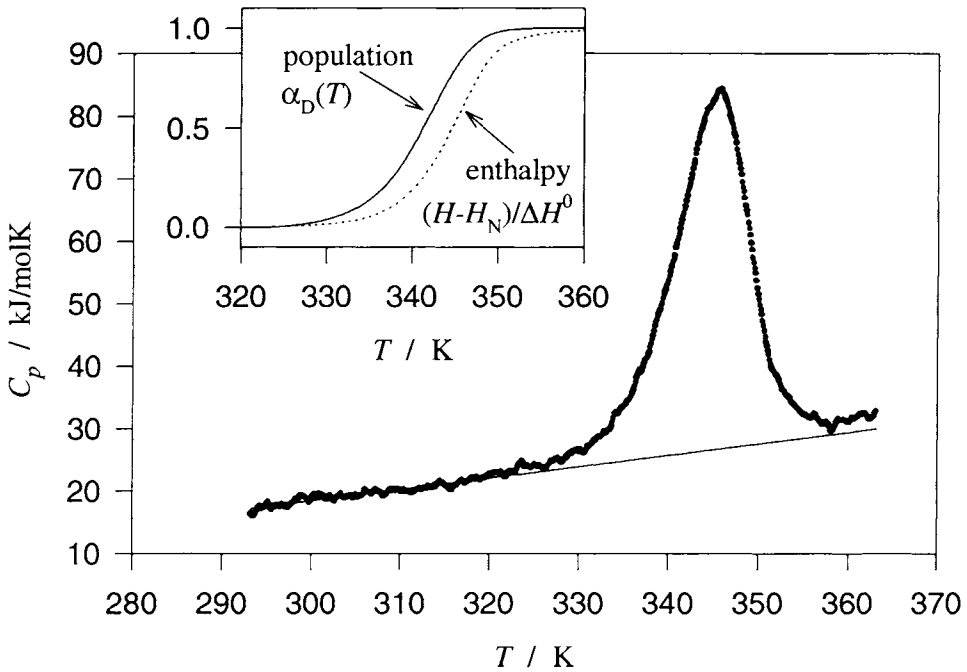

Figure 7. Numerical integration of a C_p-curve to determine the population sizes using equations 38 and 39. Note that for obtaining the population one has to integrate twice, while the enthalpy is obtained after the first integration. Therefore it cannot be expected that the two quantities vary in the same manner with temperature. This discrepancy between $\alpha_D(T)$ and $H(T) - H_N(T)$ is actually seen in the denaturation transition of the dimeric ROP protein. It should occur generally in transitions of oligomeric proteins. The C_p-curve of ROP protein was taken from Steif et al. [54]. The insert shows a comparison of the variation with temperature of the population $\alpha_D(T)$ of unfolded proteins and of the relative enthalpy change $(H - H_N)/\Delta H^0$ calculated using equations 38 and 39.

The integral can be substituted by a sum over the measured heat capacities times ΔT, since usually the temperature difference between two neighbouring points ΔT (e.g. 0.1K) is sufficiently small. The temperature dependence of the fraction of native proteins $\alpha_N(T)$ is readily calculated

using eq. 35 and eq. 37

$$\alpha_{\mathrm{N}}(T) = \frac{1}{Q(T)} = \exp\left[-\int_{295K}^{T} \frac{H - H_{\mathrm{N}}}{RT^2}\, dT \right] \tag{39}$$

Inspection of the insert in Figure 7 shows that the shift in population is not directly proportional to the change in enthalpy [1,53]. This intriguing result differs from those reported previously by Freire [43] and Brandts & Lin [44]. That it is correct can be easily seen from equations 38 and 39 which show that the enthalpy change corresponds to the first integration, but the population shift to the second integration. Therefore, in general they cannot be assumed to be equal. This conclusion is also supported by the analytical solutions for some folding models given below.

Freire and Biltonen [37] have shown for RNase A, by integrating first with regard to the native state and then with regard to the denatured state as reference, that there is a difference in the two integration results. This difference has been interpreted as being suggestive of a few percent of intermediates being present at $T_{1/2}$. The occurrence of such small intermediate populations is assumed to be the reason for the finding that the cooperative unit of reversibly folding proteins (defined by $\Delta H_{\mathrm{cal}}/\Delta H_{\mathrm{v.H.}}$) is frequently observed to be slightly larger than unity [52].

5.4 Fitting of heat capacity curves

The integration method relies heavily on the accuracy of the heat capacity data of the native or the unfolded state and on the possibility to extrapolate these data into the transition range. Application of the method shows that results are significantly altered if the reference integration baseline (either $C_{p,\mathrm{N}}(T)$ or $C_{p,\mathrm{D}}(T)$) is only slightly varied. Therefore it is a better approach to fit the data to analytical equations derived for the various folding models. This approach has two advantages. On the one hand the compatibility of the model with the data can be tested, and on the other hand – if the model is compatible – a maximum of thermodynamic information can be extracted.

In the following we shall give enthalpy and heat capacity equations for some typical folding models. For each model the relative partition function is given as well as the enthalpy and the heat capacity functions resulting from the temperature derivatives according to equations 35 and 36. In this

process the van't Hoff equation

$$\frac{\partial K}{\partial T} = \frac{K\Delta_{\mathrm{N}}^{\mathrm{D}}H^0}{RT^2} \tag{40}$$

has been used and the corresponding population sizes have been calculated according to equation 41

$$\alpha_i = \frac{Q_i}{\sum Q_i} = \frac{Q_i}{Q} = \frac{N_i}{\sum N_i}. \tag{41}$$

Only those models are presented for which a complete analytical solution can be given. Stoichiometries of $n:1$ require the solution of polynomials of n-th order, which is analytically problematic for n=3 or 4 and impossible for $n>4$.

5.4.1 Two-state model, 1:1 Stoichiometry

The relative partition function for this model is

$$Q = \frac{[\mathrm{N}] + [\mathrm{D}]}{[\mathrm{N}]} = 1 + K \tag{42}$$

with N being the reference state. The equilibrium constant $K(T)$ is readily calculated from $\Delta_{\mathrm{N}}^{\mathrm{D}}G^0(T)$ using the standard thermodynamic relationship $K(T) = \exp(-\Delta_{\mathrm{N}}^{\mathrm{D}}G^0(T)/RT)$. The enthalpy relative to the native state is obtained from eq. 35

$$H - H_{\mathrm{N}} = RT^2\frac{\partial \ln Q}{\partial T} = \frac{K}{1+K}\Delta_{\mathrm{N}}^{\mathrm{D}}H^0(T) = \alpha_{\mathrm{D}}\Delta_{\mathrm{N}}^{\mathrm{D}}H^0(T) \tag{43}$$

[39]. α_{D} is the population of the denatured state (equation 41). Therefore, the difference in the mean energy between the native and denatured state $\Delta_{\mathrm{N}}^{\mathrm{D}}H^0(T) = H_{\mathrm{D}} - H_{\mathrm{N}}$ is directly weighted by the population α_{D} of the denatured molecules. Intuitively this result seems to be reasonable, but it leads to errors if used uncritically for transitions involving stoichiometries other than 1:1 [1]. The heat capacity C_p is the variation of the enthalpy with temperature and is given by the following expression

$$\begin{aligned} C_p &= C_{p,\mathrm{N}} + \frac{\partial(H - H_{\mathrm{N}})}{\partial T} \\ &= C_{p,\mathrm{N}} + \Delta C_p\frac{K}{1+K} + \frac{[\Delta_{\mathrm{N}}^{\mathrm{D}}H^0(T)]^2}{RT^2}\,\frac{K}{1+K}\,\frac{1}{1+K} \\ &= C_{p,\mathrm{N}} + \Delta C_p\alpha_{\mathrm{D}} + \frac{[\Delta_{\mathrm{N}}^{\mathrm{D}}H^0(T)]^2}{RT^2}\,\alpha_{\mathrm{D}}\,\alpha_{\mathrm{N}}. \end{aligned} \tag{44}$$

$C_{p,\mathrm{N}}(T)$ is the heat capacity function of the native state, $\Delta C_p(T) = C_{p,\mathrm{D}}(T)$-$C_{p,\mathrm{N}}(T)$ is the difference between the extrapolated heat capacity functions of the denatured and native states at temperature T, and the term $\Delta C_p \alpha_\mathrm{D}$ describes the sigmoidal baseline under the transition peak. The term $[\Delta_\mathrm{N}^\mathrm{D} H^0(T)]^2 \alpha_\mathrm{D} \alpha_\mathrm{N}$ characterises the heat absorption peak. The product $\alpha_\mathrm{N}\alpha_\mathrm{D} = \alpha_\mathrm{N}(1 - \alpha_\mathrm{N})$ is responsible for the appearance of the characteristic shape of the heat capacity peak. Typical curves are given in Figures 1 and 4.

5.4.2 Three-state model, 1:1:1 Stoichiometry

This simple sequential two-step unfolding reaction is described by the following equations

$$\mathrm{N} \rightleftharpoons \mathrm{I} \rightleftharpoons \mathrm{D} \qquad K_1 = \frac{[\mathrm{I}]}{[\mathrm{N}]} \qquad K_2 = \frac{[\mathrm{D}]}{[\mathrm{I}]}. \tag{45}$$

The relative partition function is defined by equation 46

$$Q = \frac{[\mathrm{N}] + [\mathrm{I}] + [\mathrm{D}]}{[\mathrm{N}]} = 1 + K_1 + K_1 K_2. \tag{46}$$

Differentiating $\ln Q$ with regard to temperature according to equation 35 results in the enthalpy

$$\begin{aligned} H - H_\mathrm{N} &= \Delta_\mathrm{N}^\mathrm{I} H_1^0(T)(\alpha_\mathrm{I} + \alpha_\mathrm{D}) + \Delta_\mathrm{I}^\mathrm{D} H_2^0(T)\alpha_\mathrm{D} \\ &= \Delta_\mathrm{N}^\mathrm{I} H_1^0(T)\alpha_\mathrm{ID} + \Delta_\mathrm{I}^\mathrm{D} H_2^0(T)\alpha_\mathrm{D} \end{aligned} \tag{47}$$

and the second derivative yields again the heat capacity

$$\begin{aligned} C_p = C_{p,\mathrm{N}} &+ \Delta_\mathrm{N}^\mathrm{I} C_{p,1}\alpha_\mathrm{ID} + \Delta_\mathrm{I}^\mathrm{D} C_{p,2}\alpha_\mathrm{D} \\ &+ \frac{(\Delta_\mathrm{N}^\mathrm{I} H_1^0)^2}{RT^2}\alpha_\mathrm{N}\alpha_\mathrm{ID} + \frac{(\Delta_\mathrm{I}^\mathrm{D} H_2^0)^2}{RT^2}\alpha_\mathrm{NI}\alpha_\mathrm{D} \\ &+ 2\frac{\Delta_\mathrm{N}^\mathrm{I} H_1^0 \Delta_\mathrm{I}^\mathrm{D} H_2^0}{RT^2}\alpha_\mathrm{N}\alpha_\mathrm{D}. \end{aligned} \tag{48}$$

It is worth noting that we obtain for the two-step reaction three enthalpy terms, one for each of the two transitions $\mathrm{N} \rightleftharpoons \mathrm{I}$ and $\mathrm{I} \rightleftharpoons \mathrm{D}$ and the third term is due to the overall reaction.

5.4.3 Two-state model, 1:2 Stoichiometry

The reaction scheme for this model is

$$\mathrm{N}_2 \rightleftharpoons 2\mathrm{D} \qquad K = \frac{[\mathrm{D}]^2}{[\mathrm{N}_2]}. \tag{49}$$

Mass conservation dictates that the total concentration of monomers, $c = 2[N_2] + [D]$, remains constant. Therefore the concentration of denatured molecules [D] can be calculated from the equilibrium expression and expressed in terms of c and the equilibrium constant K

$$[D] = \frac{K}{4}\left(\sqrt{1+\frac{8c}{K}} - 1\right). \tag{50}$$

Using this expression for [D] the relative partition function for this model is

$$Q = \frac{[N]+[D]}{[N]} = \frac{2[N_2]+[D]}{2[N_2]} = 1 + \frac{2}{\sqrt{1+\frac{8c}{K}} - 1}. \tag{51}$$

Q has been calculated an the basis of subunit monomer concentrations. From the relative partition function Q we immediately get the relations

$$\sqrt{1+\frac{8c}{K}} - 1 = \frac{2}{Q-1} \qquad \text{and} \qquad \frac{8c}{K} = \frac{4Q}{(Q-1)^2}, \tag{52}$$

which are needed for the following calculations. The temperature derivative of Q is

$$\begin{aligned} \frac{\partial Q}{\partial T} &= \frac{-2}{\left(\sqrt{1+\frac{8c}{K}} - 1\right)^2} \frac{1}{2\sqrt{1+\frac{8c}{K}}} \frac{-8c\Delta_N^D H^0}{KRT^2} \\ &= \frac{8c\Delta_N^D H^0}{KRT^2\left(\frac{2}{Q-1}\right)^2\left(\frac{2}{Q-1}+1\right)} = \frac{\Delta_N^D H^0}{RT^2}\frac{Q(Q-1)}{Q+1}. \end{aligned} \tag{53}$$

With the use of these equations the enthalpy relative to the native state can be calculated:

$$H - H_N = RT^2\frac{\partial \ln Q}{\partial T} = \Delta_N^D H^0 \frac{Q-1}{Q+1} = \Delta_N^D H^0 \frac{\alpha_D}{1+\alpha_N} \tag{54}$$

It is important to emphasise that $\Delta_N^D H^0$ is not directly weighted by α_D but by the ratio $\alpha_D/(1+\alpha_N)$ as mentioned before (Figure 7). As a result of the different stoichiometry of the transition the direct proportionality between α_D and the enthalpy change is lost. The heat capacity function for this model is given by equation 55

$$\begin{aligned} C_p &= C_{p,N} + \Delta C_p \frac{Q-1}{Q+1} \\ &\quad + (\Delta_N^D H^0)^2 \frac{(\partial_T Q)(Q+1) - (\partial_T Q)(Q-1)}{(Q+1)^2} \end{aligned} \tag{55}$$

$$= C_{p,\mathrm{N}} + \Delta C_p \frac{Q-1}{Q+1} + \frac{(\Delta_{\mathrm{N}}^{\mathrm{D}} H^0)^2}{RT^2} \frac{2Q(Q-1)}{(Q+1)^3}$$

$$= C_{p,\mathrm{N}} + \Delta C_p \frac{\alpha_{\mathrm{D}}}{1+\alpha_{\mathrm{N}}} + \frac{(\Delta_{\mathrm{N}}^{\mathrm{D}} H^0)^2}{RT^2} \frac{2\alpha_{\mathrm{N}}\alpha_{\mathrm{D}}}{(1+\alpha_{\mathrm{N}})^3}.$$

Again it must be noted that the transition term involving $(\Delta_{\mathrm{N}}^{\mathrm{D}} H^0)^2$ is weighted by a factor different from that reported before.

5.4.4 Three–state model, 1:2:2 Stoichiometry

This model is similar to the preceeding one, but it contains in addition the native monomers I as intermediates,

$$\mathrm{N}_2 \rightleftharpoons 2\mathrm{I} \rightleftharpoons 2\mathrm{D} \qquad K_1 = \frac{[\mathrm{I}]^2}{[\mathrm{N}_2]} \qquad \sqrt{K_2} = \frac{[\mathrm{D}]}{[\mathrm{I}]}. \tag{56}$$

The relative partition function is now

$$Q = \frac{2[\mathrm{N}_2] + [\mathrm{I}] + [\mathrm{D}]}{2[\mathrm{N}_2]} = 1 + Q_{\mathrm{I}}(1 + \sqrt{K_2}) \tag{57}$$

$$Q_{\mathrm{I}} = \frac{2}{\sqrt{(1+\sqrt{K_2})^2 + 8c/K_1} - (1+\sqrt{K_2})}$$

$$Q_{\mathrm{D}} = Q_{\mathrm{I}}\sqrt{K_2}.$$

We will give only the results, since the principles of the calculations are the same as for the other models. The enthalpy and the heat capacity expressions are, respectively:

$$H = H_{\mathrm{N}} + \Delta_{\mathrm{N}}^{\mathrm{I}} H_1^0 \frac{\alpha_{\mathrm{I}} + \alpha_{\mathrm{D}}}{1+\alpha_{\mathrm{N}}} + \Delta_{\mathrm{I}}^{\mathrm{D}} H_2^0 \frac{\alpha_{\mathrm{D}}}{1+\alpha_{\mathrm{N}}}. \tag{58}$$

$$\begin{aligned} C_p &= C_{p,\mathrm{N}} + \Delta C_{p,1} \frac{1-\alpha_{\mathrm{N}}}{1+\alpha_{\mathrm{N}}} + \Delta C_{p,2} \frac{\alpha_{\mathrm{D}}}{1+\alpha_{\mathrm{N}}} \\ &+ \frac{(\Delta_{\mathrm{N}}^{\mathrm{I}} H_1^0)^2}{RT^2} \frac{2\alpha_{\mathrm{N}}(1-\alpha_{\mathrm{N}})}{(1+\alpha_{\mathrm{N}})^3} + 2\frac{\Delta_{\mathrm{N}}^{\mathrm{I}} H_1^0 \Delta_{\mathrm{I}}^{\mathrm{D}} H_2^0}{RT^2} \frac{2\alpha_{\mathrm{N}}\alpha_{\mathrm{D}}}{(1+\alpha_{\mathrm{N}})^3} \\ &+ \frac{(\Delta_{\mathrm{I}}^{\mathrm{D}} H_2^0)^2}{RT^2} \frac{\alpha_{\mathrm{D}}(2\alpha_{\mathrm{N}} + \alpha_{\mathrm{I}})}{(1+\alpha_{\mathrm{N}})^3} - \frac{1}{2}\frac{(\Delta_{\mathrm{I}}^{\mathrm{D}} H_2^0)^2}{RT^2} \frac{\alpha_{\mathrm{D}}(1-\alpha_{\mathrm{D}})}{(1+\alpha_{\mathrm{N}})^3}. \end{aligned} \tag{59}$$

Interestingly, the heat capacity expression seems to imply a negative peak. But this is not the case. Inspection of the last line of the heat capacity formula shows that actually the negative term compensates for overcounting the transition enthalpy $(\Delta_{\mathrm{I}}^{\mathrm{D}} H_2^0)^2$ in the first term. (At a temperature at which D is populated the following approximation should hold:

$2\alpha_N + \alpha_I \approx \alpha_N + \alpha_I = 1 - \alpha_D$). Overcounting originates from the definition of $\Delta_I^D H_2^0$ as the enthalpy of the reaction $2I \rightleftharpoons 2D$. Microscopically this reaction is of course equivalent to two times the reaction $I \rightleftharpoons D$ with $2\Delta_I^D H_{mic}^0 = \Delta_I^D H_2^0$. Therefore the proper enthalpy term that should be used in equation 59 is

$$\begin{aligned}(\Delta_I^D H_2^0)^2 - \frac{1}{2}(\Delta_I^D H_2^0)^2 &= \frac{1}{2}(\Delta_I^D H_2^0)^2 \\ &= \frac{1}{2}(2\Delta_I^D H_{mic}^0)^2 = 2(\Delta_I^D H_{mic}^0)^2,\end{aligned} \tag{60}$$

since there are two denaturing monomers per dimer. Altogether there are three types of peaks reflected in the C_p expression. The $(\Delta_N^I H_1^0)^2$–peak is associated with the dissociation of the dimers into native-like monomers, the $(\Delta_I^D H_2^0)^2$–peak relates to the denaturation of the monomers and the $\Delta_N^D H_1^0 \Delta_I^D H_2^0$–peak is due to the direct denaturation of the native dimers to the denatured monomers.

5.4.5 Three-state model, 1:1:2 Stoichiometry

A very similar reaction scheme is presented in equation 61. The difference to the previous model is that here the intermediate occurs as dimer I_2 and not as monomer I.

$$N_2 \rightleftharpoons I_2 \rightleftharpoons 2D \qquad K_1 = \frac{[I_2]}{[N_2]} \qquad K_2 = \frac{[D]^2}{[I_2]}. \tag{61}$$

The relative partition function is

$$Q = \frac{2[N_2] + 2[I_2] + [D]}{2[N_2]} = 1 + K_1 + \frac{2(1+K_1)}{\sqrt{1 + 8c(1+K_1)/K_1K_2} - 1}. \tag{62}$$

The equations for the enthalpy and the heat capacity functions are then:

$$H - H_N = \Delta_N^I H_1^0 \frac{2\alpha_I + \alpha_D}{1 + \alpha_{NI}} + \Delta_I^D H_2^0 \frac{\alpha_D}{1 + \alpha_{NI}} \tag{63}$$

$$\begin{aligned}C_p = C_{p,N} &+ \Delta_N^I C_{p,1} \frac{2\alpha_I + \alpha_D}{1 + \alpha_{NI}} + \Delta_I^D C_{p,2} \frac{\alpha_D}{1 + \alpha_{NI}} \\ &+ \frac{(\Delta_N^I H_1^0)^2}{RT^2} \left[\frac{2\alpha_N(2\alpha_I + \alpha_D)}{(1+\alpha_{NI})^3} + \frac{2\alpha_N\alpha_I}{(1+\alpha_{NI})^2} \right] \\ &+ \frac{(\Delta_I^D H_2^0)^2}{RT^2} \frac{2\alpha_{NI}\alpha_D}{(1+\alpha_{NI})^3} + \frac{\Delta_N^I H_1^0 \Delta_I^D H_2^0}{RT^2} \frac{4\alpha_N\alpha_D}{(1+\alpha_{NI})^3}\end{aligned} \tag{64}$$

5.5 Fit strategy

Obviously the results become increasingly complex with the number of intermediates being increased. A fit of an experimental curve seems to be hardly useful for more complicated models unless most of the fit parameters can be directly estimated from the experimental curve. This is, for example, possible, if all peaks are well separated.

An effective fit strategy starts with the extrapolation of the heat capacities of the pure native and denatured states

$$C_{p,\mathrm{N}}(T) = C_{p,\mathrm{N}}(T_{1/2}) + (T - T_{1/2}) \left(\frac{\partial C_{p,\mathrm{N}}}{\partial T} \right)_{T_{1/2}} \tag{65}$$

and

$$\begin{aligned} C_{p,\mathrm{D}}(T) &= C_{p,\mathrm{D}}(T_{1/2}) + (T - T_{1/2}) \left(\frac{\partial C_{p,\mathrm{D}}}{\partial T} \right)_{T_{1/2}} \\ &\quad + (T - T_{1/2})^2 \left(\frac{\partial^2 C_{p,\mathrm{D}}}{\partial T^2} \right)_{T_{1/2}} \end{aligned} \tag{66}$$

As noted above, frequently the second temperature derivative need not be taken into account. Fit parameters are then $T_{1/2}$, $C_{p,\mathrm{N}}(T_{1/2})$, $C_{p,\mathrm{D}}(T_{1/2})$ and their slopes, given by $(\partial C_{p,\mathrm{N}}/\partial T)_{T_{1/2}}$ and $(\partial C_{p,\mathrm{D}}/\partial T)_{T_{1/2}}$. A rough estimate of $T_{1/2}$ can be easily obtained by searching for the maximum of the C_p-curve. Also the heat capacities of the pure states are determined easily. The area under the peak gives an approximate value of $\Delta^{\mathrm{D}}_{\mathrm{N}} H^0(T_{1/2})$.

By performing several measurements at different protein concentrations it can be shown, whether an oligomerization step is involved in the transition of the protein. If the protein is oligomeric, we get for $T = T_{1/2}$ according to equation 23

$$\Delta G^0(T_{1/2}) = -RT_{1/2} \ln \left(n \left(\frac{c}{2} \right)^{n-1} \right) \tag{67}$$

Additionally, using the relation $\Delta G^0(T_{1/2}) = \Delta H^0(T_{1/2}) - T_{1/2} \Delta S^0(T_{1/2})$, it is seen that the transition temperature $T_{1/2}$ increases with increasing protein concentration according to

$$\frac{1}{T_{1/2}} = \frac{R \ln \left(n \left(\frac{c}{2} \right)^{n-1} \right)}{\Delta H^0(T_{1/2})} - \frac{\Delta S^0(T_{1/2})}{\Delta H^0(T_{1/2})}. \tag{68}$$

Therefore the stoichiometry n of the transition can be estimated from a plot of $1/T_{1/2}$ vs. $\ln(c)$.

The situation is more complex if more than one peak is involved. How far two unfolding steps can be observed separately depends on the difference between the transition temperatures $T_{1/2}$. Figure 8 illustrates this by showing different transition curves with all parameters identical except for the two $T_{1/2}$ values. Only if $T_{1/2}^{(1)}$ of the first transition is lower than $T_{1/2}^{(2)}$ of the second transition two peaks will be resolved in the calorimetric measurement.

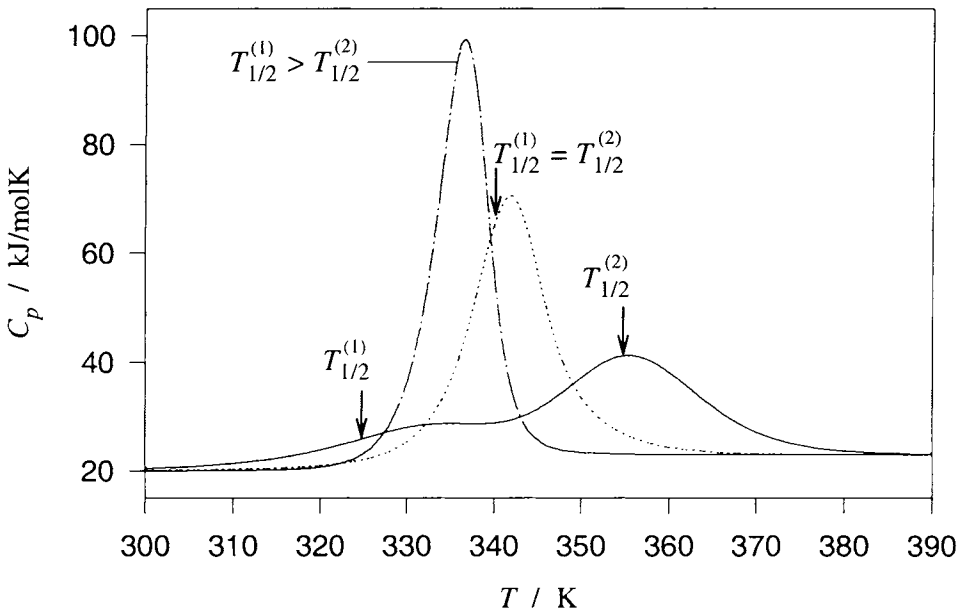

Figure 8. Influence of the difference between the two transition temperatures $T_{1/2}$ and their order of occurrence on the shape of heat capacity curve of a protein with two-step unfolding ($N_2 \rightleftharpoons 2I \rightleftharpoons 2D$). Except for the transition temperatures all parameters $\Delta H_1^0 = 200$ kJ/mol, $\Delta H_2^0 = 400$ kJ/mol, $C_{p,N} = 20$ kJ/molK, $C_{p,D} = 23$ kJ/molK and $c = 0.4$ mM were kept constant in the calculations of the three transition curves according to eq. 59. line: $T_{1/2}^{(1)} = 325$K, $T_{1/2}^{(2)} = 355$K; dash-dotted line: $T_{1/2}^{(1)} = T_{1/2}^{(2)} = 340$K; dotted line: $T_{1/2}^{(1)} = 355$K, $T_{1/2}^{(2)} = 335$K. It is remarkable that the situation in which the transition temperature for the second transition is below that of the first transition the sharpest transition peak is observed, since the the sum of the enthalpies is involved.

When the $T_{1/2}$ values for the two transitions are exchanged a simple one-step reaction is observed (dash-dotted curve). The low stability of the monomers would favour early denaturation, however, the stability of the oligomerized native state (dimer) dominates the overall transition. If such a peak were decomposed into two transitions using a fitting routine, the transition temperatures $T_{1/2}^{(1)}$ and $T_{1/2}^{(2)}$ as well as the transition enthalpies ΔH_1^0 and ΔH_2^0 would be obtained with large uncertainties.

6. TREATMENT OF IRREVERSIBLE TRANSITIONS

6.1 First order kinetics

Denatured proteins often show irreversible behaviour at high temperature. A mathematical procedure for the analysis of heat capacity curves affected by irreversible first order unfolding was suggested by Sanchez-Ruiz et al. [12]. However, in that study the unfolding reaction was treated only as a kinetic phenomenon. Therefore no equilibrium parameters could be obtained. In a later paper [13] other treatments of the C_p-curves were suggested which allowed for the extraction of equilibrium parameters from the non-equilibrium C_p-curve.

Their simple model assumes that each denatured protein molecule transforms irreversibly in a first order reaction into a species from which the native form cannot be recovered. This model is called Lumry-Eyring model [55] since Lumry and Eyring were among the first to propose that proteins unfold in two steps, a reversible unfolding equilibrium of the tertiary structure followed by a first order, irreversible step involving secondary structure unfolding.

$$\mathrm{N} \overset{K}{\rightleftharpoons} \mathrm{D} \overset{k}{\rightarrow} \mathrm{F} \qquad K = \frac{[\mathrm{D}]}{[\mathrm{N}]} \tag{69}$$

If the magnitude of the rate constant k is small compared to the rate constants dominating the reversible folding equilibrium characterised by the equilibrium constant K, the equilibrium should be well approximated by the ratio of the fractions of unfolded α_D and native molecules α_N

$$K = \frac{\alpha_\mathrm{D}}{\alpha_\mathrm{N}}. \tag{70}$$

Because the sum of the fractional populations is $\alpha_\mathrm{N} + \alpha_\mathrm{D} + \alpha_\mathrm{F} = 1$ the

fraction α_D of the denatured protein can be expressed by

$$\alpha_D = \frac{1-\alpha_F}{1+K} \cdot K = \alpha_D^{eq} \cdot (1-\alpha_F). \tag{71}$$

Therefore the rate of formation of the final state is

$$\frac{\partial \alpha_F}{\partial t} = k\alpha_D = k\alpha_D^{eq}(1-\alpha_F). \tag{72}$$

The time t can be transformed to temperature T by introducing the heating rate $r = \mathrm{d}T/\mathrm{d}t$. Integration of equation 72 yields then

$$\alpha_F = 1 - \exp\left(-\int_{T_0}^{T} \frac{k\alpha_D^{eq}}{r}\mathrm{d}T\right) \tag{73}$$

$$\Rightarrow \frac{\partial \alpha_F}{\partial T} = \frac{k\alpha_D^{eq}}{r} \exp\left(-\int_{T_0}^{T} \frac{k\alpha_D^{eq}}{r}\mathrm{d}T\right) \tag{74}$$

Since the transition exhibits 1:1 stoichiometry, the enthalpy change is proportional to the corresponding population sizes

$$\begin{aligned} H - H_N &= \Delta_N^D H^0(\alpha_D + \alpha_F) + \Delta_D^F H \alpha_F \\ &= \Delta_N^D H^0[\alpha_D^{eq}(1-\alpha_F) + \alpha_F] + \Delta_D^F H \alpha_F. \end{aligned} \tag{75}$$

The heat capacity is obtained from the temperature derivative of equation 75

$$\begin{aligned} C_p &= C_{p,N} + \Delta_N^D C_p(\alpha_D + \alpha_F) + \Delta_D^F C_p \alpha_F \\ &\quad + \frac{(\Delta_N^D H^0)^2}{RT^2} \alpha_N^{eq} \alpha_D^{eq}(1-\alpha_F) \\ &\quad + \frac{\partial \alpha_F}{\partial T}\left[(1-\alpha_D^{eq})\Delta_N^D H^0 + \Delta_D^F H\right] \\ &= C_{p,N} + \Delta_N^D C_p(\alpha_D + \alpha_F) + \Delta_D^F C_p \alpha_F \\ &\quad + \frac{(\Delta_N^D H^0)^2}{RT^2} \alpha_N^{eq} \alpha_D^{eq} \exp\left(-\int_{T_0}^{T} \frac{k\alpha_D^{eq}}{r}\mathrm{d}T\right) \\ &\quad + \left[(1-\alpha_D^{eq})\Delta_N^D H^0 + \Delta_D^F H\right] \frac{k\alpha_D^{eq}}{r} \exp\left(-\int_{T_0}^{T} \frac{k\alpha_D^{eq}}{r}\mathrm{d}T\right). \end{aligned} \tag{76}$$

For the fit of experimental data to this model, simply the same parameters as for an equilibrium curve have to be employed plus a value of k and optionally also for $\Delta_D^F H$. The rate constant is assumed to show Arrhenius behaviour

$$k(T) = k(T_{1/2}) \exp\left[-\frac{E_a}{R}\left(\frac{1}{T} - \frac{1}{T_{1/2}}\right)\right]. \tag{77}$$

It turns out that within the peak region $k(T)$ can be considered constant as long as the activation energy E_a is smaller than approximately 300 kJ/mol.

Figure 9 gives some examples for the influence of the irreversible first order step on the equilibrium C_p-curve. If a protein shows this type of irreversibility the van't Hoff enthalpy yields the equilibrium value (Figure 10), provided it is calculated by equation 78

$$\Delta H_{\text{v.H.}} = \sqrt{(1+\sqrt{n})^2 R T_{1/2}^2 \left(< C_p >_{1/2} - \frac{\Delta_N^D C_p \sqrt{n}}{1+\sqrt{n}} \right)} \tag{78}$$

[17], which is equivalent to equation 17, where the identity $\Delta H_{\text{v.H.}} = \Delta H_{\text{cal}}$ has been applied.

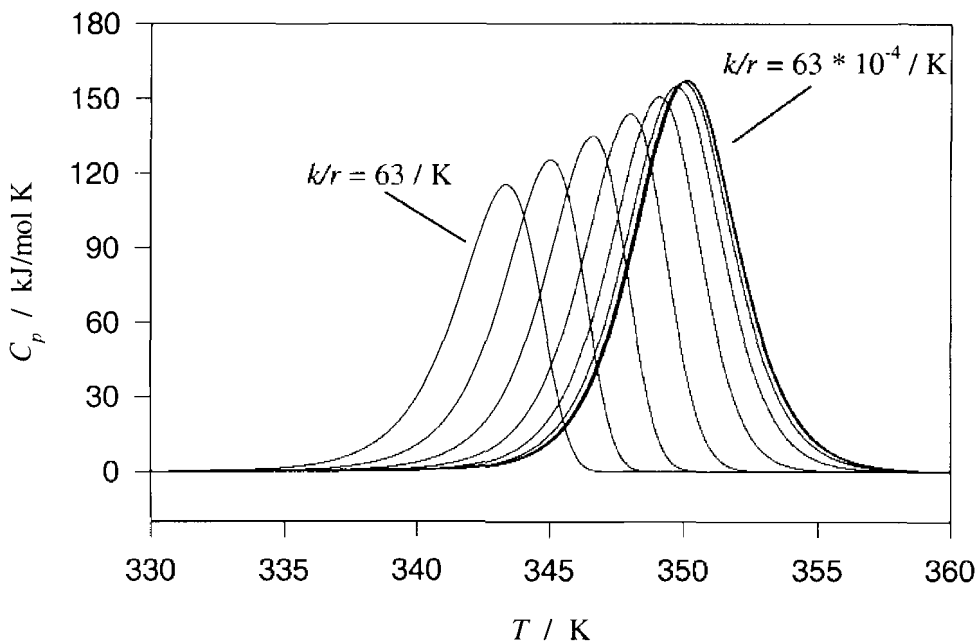

Figure 9. Influence of a first order irreversible step on the shape and the position of the heat capacity peak according to equation 76. The ratio, k/r, of the first order rate constant, k, and the heating rate, r, has been varied from a value of $63 \cdot 10^{-4}$/K on the right side to 63/K on the left side. For each curve the ratio differs by a factor of 3.16. Low k/r ratios leave the equilibrium curve practically unchanged. The parameters used in equation 76 are $T_{1/2}$ = 350K, $\Delta_N^D H^0(T_{1/2})$ = 800kJ/mol, E_a = 0 and $\Delta_N^D C_p$ = 19kJ/molK.

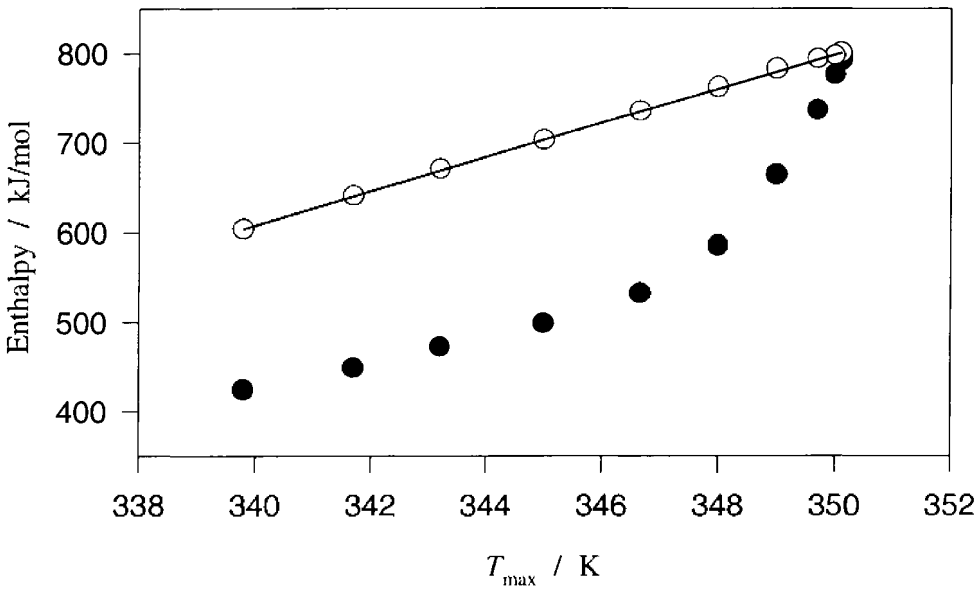

Figure 10. Influence of a first order irreversible step on the calorimetric enthalpy ΔH_{cal} (closed circles) and the van't Hoff enthalpy $\Delta H_{v.H.}$ (open circles). The peaks given in Figure 9 were integrated numerically to obtain ΔH_{cal} and their height $< C_p >_{1/2}$ was used for the determination of $\Delta H_{v.H.}$ with equation 78 (n=1, $\Delta^{F}_{D}H$=0). It is worth emphasising that the van't Hoff enthalpies are identical to the equilibrium value (solid line) at the respective temperature, whereas the calorimetric enthalpy, obtained from the integration of the peaks in Figure 9, is smaller at all temperatures.

6.2 Aggregation processes

Since irreversibility can often be associated with aggregation processes a modified model is also useful:

$$N \overset{K}{\rightleftharpoons} D \qquad nD \overset{k}{\rightarrow} F_n \qquad K = \frac{[D]}{[N]} \tag{79}$$

The kinetics are assumed to be of n-th order, where n should range between 1 and 2, since higher order encounters are probably rare. If there is only little aggregation (e.g. because aggregation kinetics is slow compared

to the heating rate), n will be equal to two because a two particle collision is required. In contrast, if aggregation is the dominating reaction, n should become smaller than 2 because the single denatured protein molecule will more probably react with the already existing network of aggregated proteins than with another individual denatured protein. This means that the apparent order n of the aggregation will change with heating rate.

In analogy to equations 71 to 74 we get

$$\alpha_F = 1 - \left[1 + n(n-1)\int_{T_0}^{T} \frac{k}{r}(\alpha_D^{eq})^n dT\right]^{\frac{1}{1-n}} \tag{80}$$

and

$$\frac{\partial \alpha_F}{\partial t} = nk(\alpha_D^{eq})^n \left[1 + n(n-1)\int_{T_0}^{T} \frac{k}{r}(\alpha_D^{eq})^n dT\right]^{\frac{n}{1-n}} \tag{81}$$

The enthalpy and heat capacity functions are therefore

$$H - H_N = \Delta_N^D H^0(T)[\alpha_D^{eq}(1-\alpha_F) + \alpha_F] \tag{82}$$

$$C_p = C_{p,N} + \Delta_N^D C_p[\alpha_D + \alpha_F] + \Delta_N^D H^0 \left\{ \frac{\Delta_N^D H^0}{RT^2}\alpha_D \alpha_N^{eq} \right. \tag{83}$$

$$\left. + \alpha_N^{eq} n \frac{k}{r}(\alpha_D^{eq})^n \left[1 + n(n-1)\int_{T_0}^{T} \frac{k}{r}(\alpha_D^{eq})^n dT\right]^{\frac{n}{1-n}} \right\}.$$

7. RESPONSE OF THE CALORIMETER

Since electronic devices such as DSC instruments have a limited response time the intrinsic C_p-signal may be distorted by the response behaviour of the calorimeter. In general the output signal $g(t)$ is the convolution of the ideal input signal $f(t)$ and the response function $k(t)$ of the calorimeter:

$$g(t) = f(t) \otimes k(t) := \int_0^t k(t-\tau) f(\tau) d\tau \tag{84}$$

[56]. Usually $g(t)$ is known and $f(t)$ has to be reconstructed. The response of typical microcalorimeters is of first order [15] with a relaxation time b. The response function and its derivative with regard to time can then be expressed by the equations

$$k(t) = \frac{a}{b}\exp(-t/b) \qquad \Rightarrow \qquad k'(t) = -\frac{a}{b^2}\exp(-t/b). \tag{85}$$

The factor a equals 1 and is only required for a simulation of a distortion according to equations 84 and 85, if the time difference between two sample points is large compared to the instrumental relaxation time b. A convenient method to recover $f(t)$ from $g(t)$ is provided by the use of Laplace transforms. The Laplace transform $K(s)$ of $k(t)$ is

$$\begin{aligned} K(s) &= \mathcal{L}\{k(t)\} \stackrel{\text{def}}{=} \int_0^\infty k(t)\exp(-st)\mathrm{d}t \qquad (86)\\ &= \int_0^\infty \frac{a}{b}\exp\left(-(t/b)-st\right)\mathrm{d}t = \frac{a}{1+bs}. \end{aligned}$$

According to the rules of Laplace transformation [56] the time derivative of equation 84 is given by

$$\begin{aligned} g'(t) &= k(0^+)f(t) + \int_0^t k'(t-\tau)f(\tau)\mathrm{d}\tau \qquad (87)\\ \Leftrightarrow f(t) &= \frac{g'(t)}{k(0^+)} - \int_0^t \frac{k'(t-\tau)}{k(0^+)}f(\tau)\mathrm{d}\tau, \end{aligned}$$

with $k(0^+) = \lim_{t\searrow 0} k(t)$. By Laplace transform this equation becomes

$$F(s) = \Gamma(s) + M(s)F(s) = \frac{\Gamma(s)}{1-M(s)} = \Gamma(s) + \frac{M(s)}{1-M(s)}\Gamma(s), \qquad (88)$$

with $\mathcal{L}^{-1}\{\Gamma(s)\} = \gamma(t) := \frac{g'(t)}{k(0^+)}$ and $\mathcal{L}^{-1}\{M(s)\} = \mu(t) := -\frac{k'(t-\tau)}{k(0^+)}$. Moreover there is

$$\frac{M(s)}{1-M(s)} = \frac{\mathcal{L}\{\frac{1}{b}\exp(-t/b)\}}{1-\mathcal{L}\{\frac{1}{b}\exp(-t/b)\}} = \frac{1}{bs} = \mathcal{L}\Big\{\frac{\varepsilon(t)}{b}\Big\}, \qquad (89)$$

with $\varepsilon(t) = 1$ for $t > 0$, 0 in all other cases. The function $f(t)$ is therefore given by the equation

$$\begin{aligned} f(t) &= \gamma(t) + \int_0^t \frac{\varepsilon(t-\tau)}{b}\gamma(\tau)\mathrm{d}\tau = \frac{1}{a}\Big[bg'(t) + \int_0^t g'(\tau)\mathrm{d}\tau\Big] \qquad (90)\\ &= \frac{1}{a}\Big[bg'(t) + g(t) - g(0)\Big]. \end{aligned}$$

The input function is $f(t) = C_p(t) - C_p(0)$. Therefore eq. 90 can be written

$$\begin{aligned} C_p(t) &= g(t) + b\left(\frac{\partial g(t)}{\partial t}\right) \qquad (91)\\ &\approx g(T) + b\cdot r\frac{\Delta g(T)}{\Delta T}, \end{aligned}$$

where $g(T)$ is the observed distorted heat capacity signal, r the heating rate, and ΔT and $\Delta g(T)$ the temperature and heat capacity differences, respectively, between two neighbouring data points. A simulation that illustrates to which extent relaxation times can influence the heat capacity signal is given in Figure 11.

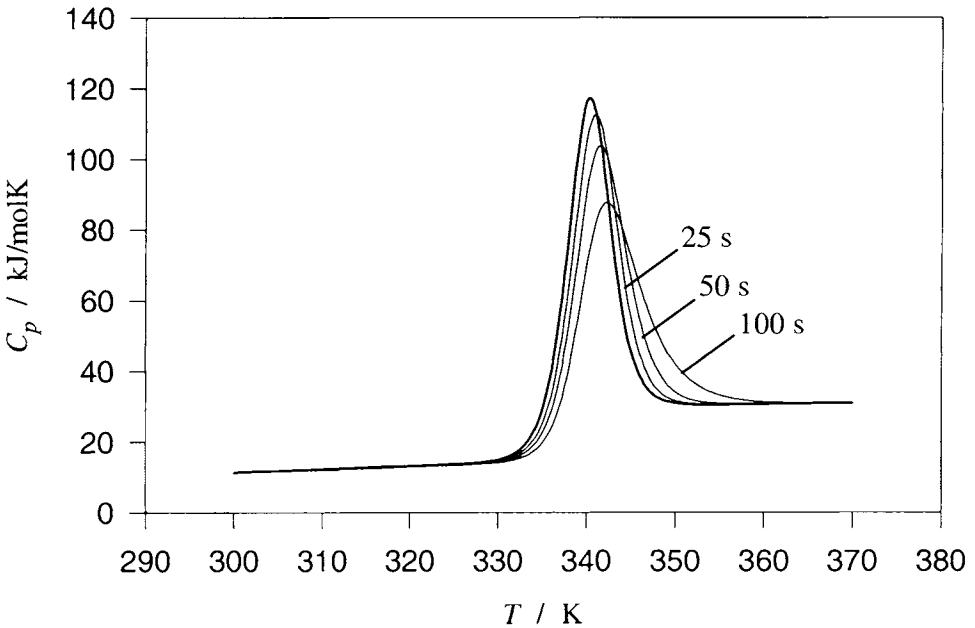

Figure 11. Distortion of a C_p-curve by the response time of the calorimeter at a heating rate of 1K/min. The different relaxation times are indicated by the numbers. For the calculations equations 84 and 85 were used.

8. DSC CALORIMETER TYPES, PRACTICAL HINTS

8.1 The influence of differences in the shape of calorimeter cells

Experience with different types of DSC-instruments shows that in certain instances, particularly in cases where aggregating systems are observed, the C_p-signals are distorted in a way that depends on the shape of the calorimetric cell. The differences are most pronounced between pill-shaped cells and tubular cells. In pill shaped cells the signal has been observed

to oscillate or drop precipitously out of the control range in an undefined manner. These effects are not observed when using the same solutions in instruments with tubular cells.

8.2 Calibration

In some calorimeters power [μW] is the output signal. Therefore the difference ΔP_{app} between the buffer scan and the protein scan simply has to be divided by the heating rate r [degree/s] prior to application of equation 2 in order to get the proper heat capacity units:

$$C_{p,\text{protein}} = C_{p,\text{buffer}} \cdot \frac{v_{\text{protein}}}{v_{\text{buffer}}} - \frac{\Delta P_{\text{app}}}{m_{\text{protein}} \cdot r}. \tag{92}$$

Calorimeters that yield voltage as output signal have to be calibrated. This should be done during the baseline scan. The sample cell is heated by an additional and defined power P_{cal}. The calorimeter reacts to the power input by a change in voltage ΔU_{cal} that is used for the calculation of the calibration constant K_{cal}

$$K_{\text{cal}} = \frac{P_{\text{cal}}}{\Delta U_{\text{cal}} \cdot r}. \tag{93}$$

If the difference in voltage between the protein scan and the baseline is called ΔU the protein heat capacity is calculated by the equation

$$C_{p,\text{protein}} = C_{p,\text{buffer}} \cdot \frac{v_{\text{protein}}}{v_{\text{buffer}}} - \frac{\Delta U \cdot K_{\text{cal}}}{m_{\text{protein}}}. \tag{94}$$

9. FIT MACROS

Finally we shall give some macros for calculating and fitting heat capacity curves. A frequently used program that should work on all platforms is "Gnuplot". The program is excellent for performing non-linear least square fits but its graphical capabilities are not as refined as those of other (commercial) programs. Furthermore it cannot be employed in spread-sheet analysis. It is available without charge on the Internet on many sites for example at the homepage: http://www.cs.dartmouth.edu/gnuplot_info.html. Additionally a few macros are given for another – commercial – program "Sigmaplot". In the following commands are written in `typewriter style` and they have to be typed as given.

9.1 Macros for the denaturation of a monomeric protein

The reaction scheme is N⇌D.

9.1.1 Macro using Gnuplot

In Gnuplot comments are characterised by double crosses #. Experimental data are given in the file `data.tab` (e.g. as tab-delimited columns). The first step in using the program is to change the numerical values of the heat capacities and enthalpies given in the Gnuplot file to values that are approximately appropriate to the respective protein. To obtain an idea of whether the choice of parameters was reasonable, a plot of the heat capacity curve on the basis of these parameters can be plotted by typing `gnuplot`, to start the program, followed by `load "fitfile.gnu"`, where `fitfile.gnu` is the macro given below. It must be saved on the hard disk after the changes of the parameters have been made. If the calculated heat capacity function seen in the plot appears to fit approximately the data, the optimisation of the parameters can be initiated by removing the #-sign in front of the fit-statement and by typing `load "fitfile.gnu"`. At the end of the fitting routine the fit parameters are given as well as the confidence interval and the covariance matrix. The results are automatically saved in a file called "`fit.log`".

If the data require to consider the second derivative of the heat capacity of the denatured state `DDcpd`, this term has to be added to the fit statement.

The following macro is called `fitfile.gnu`

```
# G N U P L O T
# Linux version 3.5 (pre 3.6)
# patchlevel beta 319
#
# Copyright(C) 1986 - 1993, 1996
# Thomas Williams, Colin Kelley and many others
#
cpd(x)=Cpd+(x-tm)*DCpd+((x-tm)**2)/2*DDCpd
cpn(x)=Cpn+(x-tm)*DCpn
dcpn(x)=DCpn
dcpd(x)=DCpd+(x-tm)*DDCpd
dG1(x)=-dHm/tm*(x-tm)+(cpd(tm)-cpn(tm))*(x-tm-x*log(x/tm))
dG2(x)=(dcpd(tm)-dcpn(tm))*((tm**2-x*x)/2+x*tm*log(x/tm))
dG3a(x)=(x**3-tm**3)/3+(x-tm)*(tm*x-x*x)/2
dG3b(x)=-tm**2*x*log(x/tm)
```

```
dG3(x)=DDCpd/2*(dG3a(x)+dG3b(x))
dG(x)=dG1(x)+dG2(x)+dG3(x) # standard gibbs enery change
K(x)=exp(-dG(x)/R/x)       # equilibrium constant
dH1(x)=dHm+(x-tm)*(cpd(tm)-cpn(tm))
dH2(x)=((x-tm)**2)/2*(dcpd(tm)-dcpn(tm))
dH3(x)=DDCpd/6*(x-tm)**3
dH(x)=dH1(x)+dH2(x)+dH3(x) # standard enthalpy change
Q(x)=1+K(x)     # relative partition function
an(x)=1/Q(x)    # fraction of native proteins
ad(x)=K(x)/Q(x) # fraction of denatured proteins
cpbase(x)=(cpd(x)-cpn(x))*ad(x)+cpn(x)
cppeak(x)=dH(x)**2/R/x/x*ad(x)*an(x)
cpprot(x)=cpbase(x)+cppeak(x) # heat capacity of the protein
# Parameters at the transition temperature
Cpd = 24598.6  # heat capacity of the denatured state
DCpd = 236.6   # first temperature derivative of Cpd
DDCpd = -3.1   # second temperature derivative of Cpd
Cpn = 23548.2  # heat capacity of the denatured state
DCpn = 165.8   # first temperature derivative of Cpn
dHm = 100173.4 # standard enthalpy change
tm = 309.8     # transition temperature
R = 8.31441    # gas constant
plot cpprot(x), cpbase(x), "data.tab"
# the next line is the fit statement
# fit cpprot(x) "data.tab" via dHm, tm, Cpn, Cpd, DCpn, DCpd
# EOF
```

9.1.2 Macro using Sigmaplot

As for the gnuplot macro reasonable start parameters should be introduced at the beginning. In the Sigmaplot spreadsheet the data temperature [K] and heat capacity [J/molK] should be placed in columns 1 and 2. The parameters `htm`[J/mol], `tm`[K], `Cpd`[J/molK], `DCpd`[J/molK^2], `Cpn`[J/molK], `DCpn`[J/molK^2], `DDCpd`[J/molK^3] should be written in column 3 in exactly the same order as given below. For example the estimated transition temperature `tm` is in line two of column three etc.

```
[Parameters]    ;should be given in column 3
htm=col(3,1,1)  ;enthalpy h(tm)
tm=col(3,2,2)   ;transition temperature
```

```
Cpd=col(3,3,3)  ;heat capacity of the denatured state
DCpd=col(3,4,4) ;first temperature derivative of Cpd
Cpn=col(3,5,5)  ;heat capacity of the native state
DCpn=col(3,6,6) ;first temperature derivative of Cpn
[Variables]
t=col(1)  ;temperature in column 1
cp=col(2) ;experimental heat capacity data in column 2
[Equations]
DDCpd=col(3,7,7) ;second temperature derivative of Cpd
;standard free gibbs energy change
g1=-h/tm*(t-tm)+(t-tm-t*ln(t/tm))*(Cpd-Cpn)
g2=((tm^2-t^2)/2+t*tm*ln(t/tm))*(DCpd-DCpn)
g3a=(t^3-tm^3)/3
g3b=(t-tm)*(-t^2+t*tm)/2-tm^2*t*ln(t/tm)
g3=(g3a+g3b)*c/2 ;dddelta cp
g=(g1+g2+g3)
;equilibrium constant
K=exp(-g/(8.31441*t))
;standard enthalpy change
h1=htm+(Cpd-Cpn)*(t-tm)+(DCpd-DCpn)/2*(t-tm)^2
h2=1/6*DDCpd*(t-tm)^3
h=h1+h2
;Delta Cp
dcp=Cpd-Cpn+(DCpd-Cpn)*(t-tm)+DDCpd/2*(t-tm)^2
;Cp Kurve Protein
base=K/(K+1)*dcp+Cpn+DCpn*(t-tm) ;heat capacity baseline
peak=K/(8.31441*t^2)*(h/(K+1))^2 ;heat capacity peak
cpprot=base+peak ;calculated protein heat capacity
fit cpprot to cp
```

9.2 Macros for the denaturation of a dimeric protein

The reaction scheme is $N_2 \rightleftharpoons 2D$. These macros are used in analogy to the previous ones.

9.2.1 Macro using Gnuplot

```
cpd(x)=Cpd+(x-tm2)*DCpd+((x-tm2)**2)/2*DDCpd
cpn(x)=Cpn+(x-tm2)*DCpn
dcpn(x)=DCpn
```

```
dcpd(x)=DCpd+(x-tm2)*DDCpd
dG1(x)=-dHm/tm*(x-tm)+(cpd(tm)-cpn(tm))*(x-tm-x*log(x/tm))
dG2(x)=(dcpd(tm)-dcpn(tm))*((tm**2-x*x)/2+x*tm*log(x/tm))
dG3a(x)=(x**3-tm**3)/3+(x-tm)*(tm*x-x*x)/2
dG3b(x)=tm**2*x*log(x/tm)
dG3(x)=DDCpd/2*(dG3a(x)-dG3b(x))+R*x*ln(c)
dG(x)=dG1(x)+dG2(x)+dG3(x)
dH1(x)=dHm+(x-tm)*(cpd(tm)-cpn(tm))
dH2(x)=((x-tm)**2)/2*(dcpd(tm)-dcpn(tm))+DDCpd/6*(x-tm)**3
dH(x)=dH1(x)+dH2(x)
K(x)=exp(-dG(x)/R/x)
Q(x)=1+2/((1+8*c/K(x))**0.5-1)
an(x)=1/Q(x)
ad(x)=1-an(x)
nenn(x)=1+an(x)
cpbase(x)=(cpd(x)-cpn(x))*(2*ad(x))/nenn(x)+cpn(x)
cppeak(x)=dH(x)**2/R/x/x*2*an(x)*ad(x)/nenn(x)**3
cpprot(x)=cpbase(x)+cppeak(x)
# parameters at the transition temperature
Cpd = 24598.6   # heat capacity of the denatured state
DCpd = 236.6    # first temperature derivative of Cpd
DDCpd = -3.1    # second temperature derivative of Cpn
Cpn = 23548.2   # heat capacity of the native state
DCpn = 165.8    # first temperature derivative of Cpn
dHm = 100173.4  # standard enthalpy of the transition
tm = 309.8      # transition temperature
R = 8.31441     # gas constant
c = 7.1e-05     # protein concentration
plot cpprot(x), cpbase(x), "datafile"
# fit cpprot(x) "datafile" via dHm, tm, Cpn, Cpd, DCpn, DCpd
# EOF
```

9.2.2 Macro using Sigmaplot

```
[Parameters]
htm=col(3,1,1)   ;enthalpy of transition
tm=col(3,3,3)    ;transition temperature
Cpn0=col(3,5,5)  ;heat capacity of the native state
Cpn1=col(3,6,6)  ;first temperature derivative of Cpn
```

```
Cpd0=col(3,7,7)  ;heat capacity of the denatured state
Cpd1=col(3,8,8)  ;first temperature derivative of Cpd
[Variables]
t=col(1)  ;temperature in column 1
cp=col(2) ;experimental heat capacity data in column 2
[Equations]
Cpd2=col(3,9,9) ;second temperature derivative of Cpd
c=col(3,10,10)  ;protein concentration
R=8.31441       ;gas constant
cpn=Cpn0+(t-tm2)*Cpn1
cpd=Cpd0+(t-tm2)*Cpd1+(t-tm2)^2*Cpd2
g1=(t-tm-t*ln(t/tm))*(Cpd0-Cpn0)-htm/tm*(t-tm)+R*t*ln(c)
g2=((tm^2-t^2)/2+t*tm*ln(t/tm))*(Cpd1-Cpn1)
g3a=(t^3-tm2^3)/3+(t-tm2)*(-t^2+t*tm2)/2
g3b=-tm2^2*t*ln(t/tm2)
g3=(g3a+g3b)*Cpd2/2
g=g1+g2+g3
K=exp(-g/(R*t))
dh1=h+(Cpd0-Cpn0)*(t-tm2)+(Cpd1-Cpn1)/2*(t-tm2)^2
dh2=1/6*Cpd2*(t-tm2)^3
dh=dh1+dh2
q=1+2/((1+8*c/K)^0.5-1)
f1=(cpd-cpn)*qd/(1+q)+cpn
f2=dh^2/(R*t^2)*2*q*(q-1)/(q+1)^3
f=f1+f2
fit f to cp
```

REFERENCES

[1] J. Rösgen, B. Hallerbach and H.-J. Hinz, Biophys. Chem. 74 (1998) 153

[2] A. Schöppe, H.-J. Hinz, V.R. Agashe, S. Ramachandran and J.B. Udgaonkar, Prot. Sci. 6 (1997) 2196

[3] P.L. Privalov, Y.V. Griko, S.Y. Venjaminov and V.P. Kutyshenko, J. Mol. Biol. 190 (1986) 487

[4] H.F. Stimson, Am. J. Phys. 23 (1955) 614

[5] O. Kratky, H. Leopold and H. Stabinger, Meth. Enzymol. 27 (1973) 98

[6] H.-J. Hinz, T. Vogl and R. Meyer, Biophys. Chem. 52 (1994) 275

[7] H. Durchschlag, in H.-J. Hinz (Ed.), Thermodynamic Data for Biochemistry and Biotechnology, Springer Verlag, Berlin, 1986, p. 45
[8] G.S. Kell, J. Chem. Eng. Data 12 (1967) 66
[9] W.J. Becktel and J.A. Schellman, Biopolymers 26 (1987) 1859
[10] I.M. Plaza del Pino, C.N. Pace and E. Freire, Biochemistry 31 (1992) 11196
[11] S.A. Potekhin and E.L. Kovrigin, Biophys. Chem. 73 (1998) 241
[12] J.M Sanchez-Ruiz, J.L. Lopez-Lacomba, M. Cortijo and P.L. Mateo, Biochemistry 27 (1988) 1648
[13] J.M Sanchez-Ruiz, Biophys. J. 61 (1992) 921
[14] D. Grasso, C. La Rosa, D. Milardi and D. Fasone, Thermochim. Acta 265 (1995) 163
[15] O. Lopez Mayorga and E. Freire, Biophys. Chem. 87 (1987) 87
[16] A. Tamura, K. Kimura, H. Takahara and K. Akasaka, Biochemistry 30 (1991) 11307
[17] P.L. Privalov and S.A. Potekhin, Meth. Enzymol. 131 (1986) 4
[18] G.N Lewis and M. Randall, Thermodynamics, McGraw-Hill, New York, 1961
[19] B. Hallerbach and H.-J. Hinz, Biophys. Chem. 76 (1999) 219
[20] J.F. Brandts, J. Am. Chem. Soc. 86 (1964) 4291
[21] Y.V. Griko, P.L. Privalov, J.M. Sturtevant and S.Y. Venyaminov, Proc. Natl. Acad. Sci. USA 85 (1988) 3343
[22] S.-I. Kidokoro, Y. Miki and A. Wada, (1990) in M. Hatano (Ed.), Protein Structural Analysis, Folding and Design, Japan Scientific Societies Press and Elsevier, 1990, p. 75
[23] M.W. Lassalle, H.-J. Hinz, H. Wenzel, M. Vlassi, M. Kokkinidis and G. Cesareni, J. Mol. Biol. 279 (1998) 987
[24] T.Y Tsong, R.P Hearn, D.P. Wrathall and J.M. Sturtevant, Biochemistry 9 (1970) 2666
[25] P.L. Privalov, N.N. Khechinashvili and B.P. Atanasov, Biopolymers 10 (1971) 1865
[26] P.L. Privalov, FEBS-Lett. 40 (1974) 140
[27] P.L. Privalov and N.N. Khechinashvili, J. Mol. Biol. 83 (1974) 665
[28] G.I. Makhatadtze and P.L. Privalov, J. Mol. Biol. 213 (1990) 375
[29] M. Häckel, G.R. Hedwig and H.-J. Hinz, Biophys. Chem. 73 (1998) 163
[30] M. Häckel, H.-J. Hinz and G.R. Hedwig, Thermochim. Acta 308 (1998) 23

[31] O. Forster, Analysis 1, Vieweg Verlag, Braunschweig, 1989
[32] L.A. Marky and K.J. Breslauer, Biopolymers 26 (1987) 1601
[33] T. Vogl, H.J. Hinz and G.R. Hedwig, Biophys. Chem. 54 (1995) 261
[34] C. Jolicoer, B. Riedel, D. Desrochers, L.L. Lemlin, R. Zamojska and O. Enea, J. Solution Chem. 15 (1986) 109.
[35] S.J. Gill, S.F. Dec, G. Olofsen and I. Wadsö, J. Phys. Chem. (1985) 3758
[36] R. Lumry, R. Biltonen and J.F. Brandts, Biopolymers 4 (1966) 917
[37] E. Freire and R.L. Biltonen, Biopolymers 17 (1978) 463
[38] E. Freire and R.L Biltonen, Biopolymers 17 (1978) 481
[39] J. Wyman, S.J. Gill and A. Colosimo, Biophys. Chem. 10 (1979) 363
[40] A. Cooper, Prog. Biophys. molec. Biol. 44 (1984) 181
[41] S.-I. Kidokoro and A. Wada, Biopolymers 26 (1987) 213
[42] S.-I. Kidokoro, H. Uedaira and A. Wada, Biopolymers 27 (1988) 271
[43] E. Freire, Comments Mol. Cell Biophys. 6 (1989) 123
[44] J.F. Brandts and L.-N. Lin, Biochemistry 29 (1990) 6927
[45] J. Wyman, S.J. Gill, Binding and linkage, University Science Books, Mill Valley, 1990
[46] M. Straume and E. Freire, Anal. Biochem. 203 (1992) 259
[47] E. Di Cera, Thermodynamic theory of site-specific binding processes in biological macromolecules, Cambridge University Press, New York, 1995
[48] H. Römer and T. Filk, Statistische Mechanik, VCH Verlagsgesellschaft, Weinheim, 1994
[49] M. Toda, T. Kubo and N. Saitô, Statistical Physics I, Springer-Verlag, Berlin, 1983
[50] S.N. Timasheff, Annu. Rev. Biophys. Biomol. Struct. 22 (1993) 67
[51] T. Abou-Aiad, U. Becker, R. Biedenkap, R Brengelmann, R. Elsebrock, H.-J. Hinz and M. Stockhausen, Ber. Bunsenges. Phys. Chem. 101 (1997) 1921
[52] P.L. Privalov, Adv. Prot. Chem. 33 (1979) 167
[53] J. Rösgen and H.-J. Hinz, Phys. Chem. Chem. Phys. (1999) in press
[54] C. Steif, P. Weber and H.-J. Hinz, Biochemistry 32 (1993) 3867
[55] R. Lumry and H. Eyring, J. Phys. Chem. 58 (1954) 110
[56] H. Weber, Laplace-Transformation, Teubner, Stuttgart, 1990

Handbook of Thermal Analysis and Calorimetry. Vol. 4: From Macromolecules to Man.
R.B. Kemp, editor.

Chapter 3

LIPID MODEL MEMBRANES AND BIOMEMBRANES

A. Blume and P. Garidel

Martin-Luther-University Halle-Wittenberg, Institute of Physical Chemistry, Muehlpforte 1, D-06108 Halle, Germany

1. INTRODUCTION

1.1. Lipid bilayers as model membranes

The major components of biological membranes are lipids and proteins. The lipids are arranged in a bimolecular leaflet. The proteins are either incorporated into the bilayer or are bound to the surface by electrostatic interactions, the two protein classes being called intrinsic (or integral) and extrinsic (or peripheral) membrane proteins. The current membrane model is still based on the proposal by Singer and Nicolson from 1972 [1]. Figure 1 shows a cartoon of a biological membrane with its intrinsic proteins.

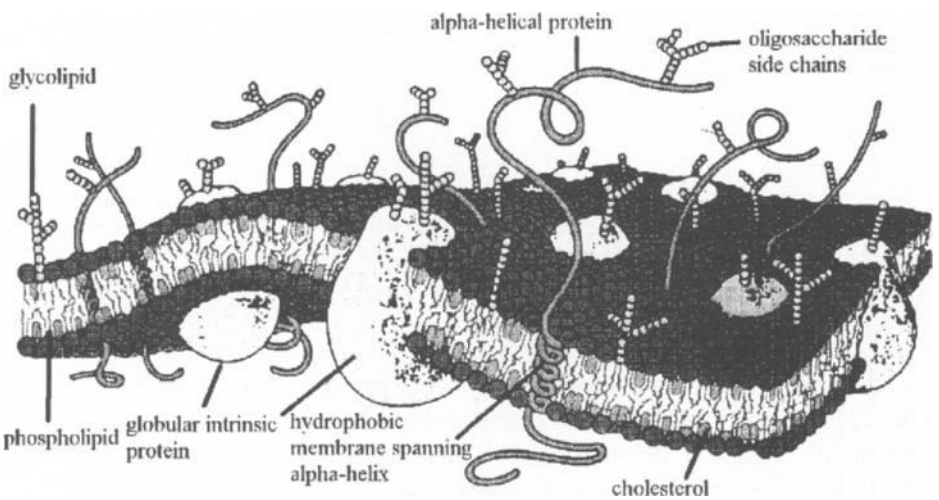

Figure 1. Fluid-mosaic membrane model (adapted from reference [5]).

Extrinsic proteins can be separated by treating membranes with aqueous salt solutions of high ionic strength whereas intrinsic proteins can only be isolated by solubilizing the membranes in micellar surfactant solutions. Recently, this model has been modified taking into account that the lipid matrix is more complicated and that the lipid transverse and also the lateral distribution might not be uniform, but essentially it is still widely accepted [2-5].

The lipids isolated from natural membranes by extraction with organic solvents are usually complex mixtures of different membrane forming amphiphilic molecules. One of the major lipid classes are phospholipids, glycerol compounds with two fatty acids esterified to the glycerol and a short polar headgroup containing a phosphodiester moiety (see below). Because of their hydrophobic fatty acyl chains, phospholipids in their pure from do not dissolve in water but spontaneously form aggregates, the bimolecular lamellae being the most common aggregation form. These aggregates can be prepared in the form of closed spherical vesicles and liposomes that serve as useful model systems for biological membranes. Liposomes can be prepared in a size range between 25 nm to 20 μm, either in unilamellar or multilamellar form. Figure 2 shows a schematic drawing of a unilamellar bilayer vesicle and for comparison some idealized vesicle forms and their generally used abbreviations [6-8].

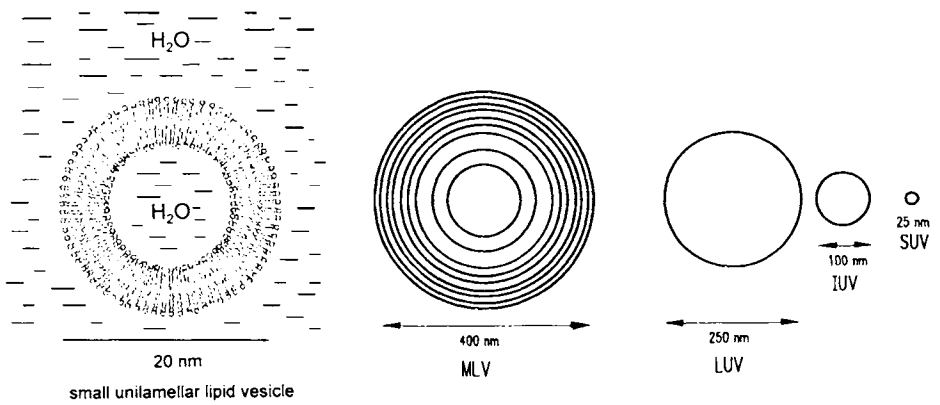

Figure 2. Left: Schematic drawing of a unilamellar bilayer vesicle. Right: Sketches of vesicles and liposomes of different size. The following abbreviations are commonly used: MLV: multilamellar vesicles, LUV: large unilamellar vesicles, IUV: intermediate unilamellar vesicles, SUV: small unilamellar vesicles.

The composition of a vesicle membrane can be manipulated in a wide range using different lipid classes and different lipid chain lengths. A prerequisite is that the lipids form well hydrated lamellar phases and that the vesicles are stable against aggregation and fusion. When these prerequisites are fulfilled, even membrane proteins can be incorporated into the synthetic membranes using appropriate procedures, such as detergent dialysis. Therefore, most physico-chemical studies of membrane properties of bilayers of defined composition have been performed with liposomes of the multilamellar or unilamellar type.

In this contribution, there will be described the principal type of calorimetric experiments which can be performed to elucidate the behavior of lipid model membranes. Most of the examples come from work performed in the author's laboratory. Numerous other groups are involved with calorimetric studies on these model membrane systems and there exists a vast amount of literature, because calorimetry has become a standard analytical method in the last ten to twenty years. It is our goal to present the principles of the method and not an extensive review over the current literature. Therefore, this chapter is necessarily biased towards work from the author's laboratory and apologies are extended to all those whose work is not adequately represented here.

1.2. Chemical structure of lipids

As mentioned above, phospholipids are abundant in eukaryotic and also bacterial membranes. Phospholipids are diesters of *sn*-glycero-3-phosphoric acid as shown in Figure 3 for a variety of different lipid classes, all with the same palmitoyl chain.

The fatty acids esterified to the glycerol vary in length between 14 and 24 carbon atoms and also in the degree of unsaturation (1-4 double bonds). In natural phospholipids, usually two different fatty acids occur, the fatty acid in *sn*-2 position having a higher degree of unsaturation. The phosphate group is in almost all cases esterified by a short alcohol. The headgroup of the phospholipid can therefore be zwitterionic or negatively charged at neutral pH, depending on the type of alcohol [2,10]. The alkyl chains can also be connected to the glycerol backbone via ether linkages. These phospholipids are consequently chemically more stable than the ester derivatives.

Plasmalogens are phospholipids in which the chain in the *sn*-1 position is linked to the glycerol via an α-β-unsaturated ether linkage. The plasmalogens have similar headgroups as the diester phospholipids and their physico-chemical behavior is also closely related to their normal counterparts with diacyl chains.

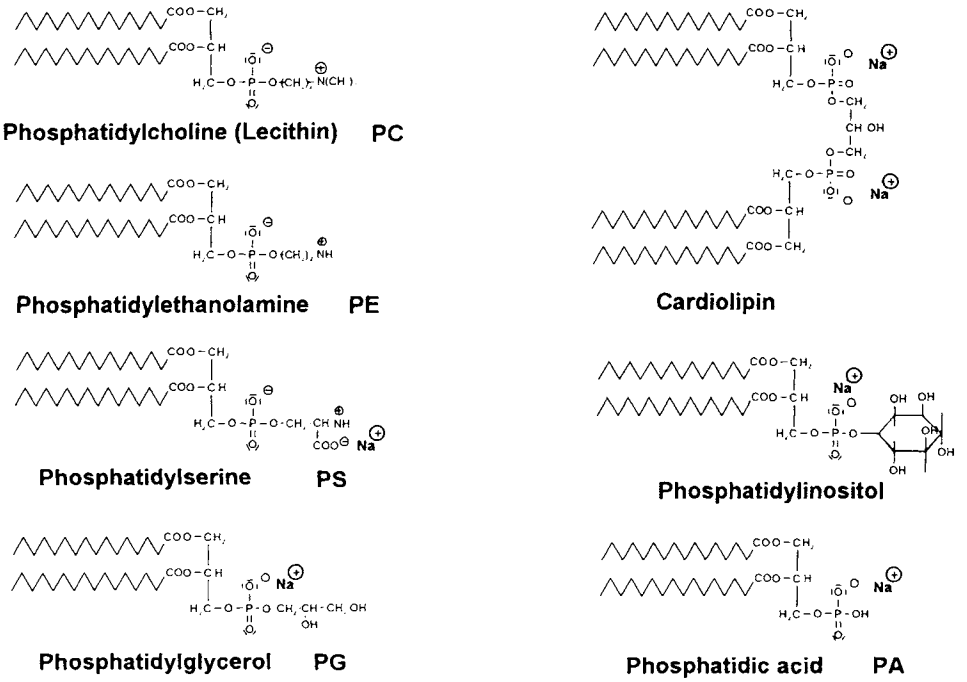

Figure 3: Chemical structure of different phospholipids together with their abbreviations. PC: phosphatidylcholine, PE: phosphatidylethanolamine, PS: phosphatidylserine, PG: phosphatidylglycerol, PA: phosphatidic acid.

Sphingolipids are derived from the long chain aminoalcohol sphingosine. One of the hydroxyl groups is usually esterified with another long chain fatty acid, whereas the other is bound to a polar moiety. Sphingolipids can occur as phospho- or glycosphingolipids. Figure 4 shows as an example the structure of sphingomyelin, a phosphosphingolipid, and of the glycosphingolipid glucosylceramide belonging to the general class of glucocerebrosides.

Gangliosides are more complicated sphingolipids, they carry linear and/or branched oligosaccharides as headgroup. Gangliosides are particularly important lipid molecules because they are involved in different recognition processes at the cell surface. Their various oligosaccharide headgroups function as receptors for a variety of proteins. Figure 4 shows as a representative example for lipids of this important class the ganglioside GM1 [2,10].

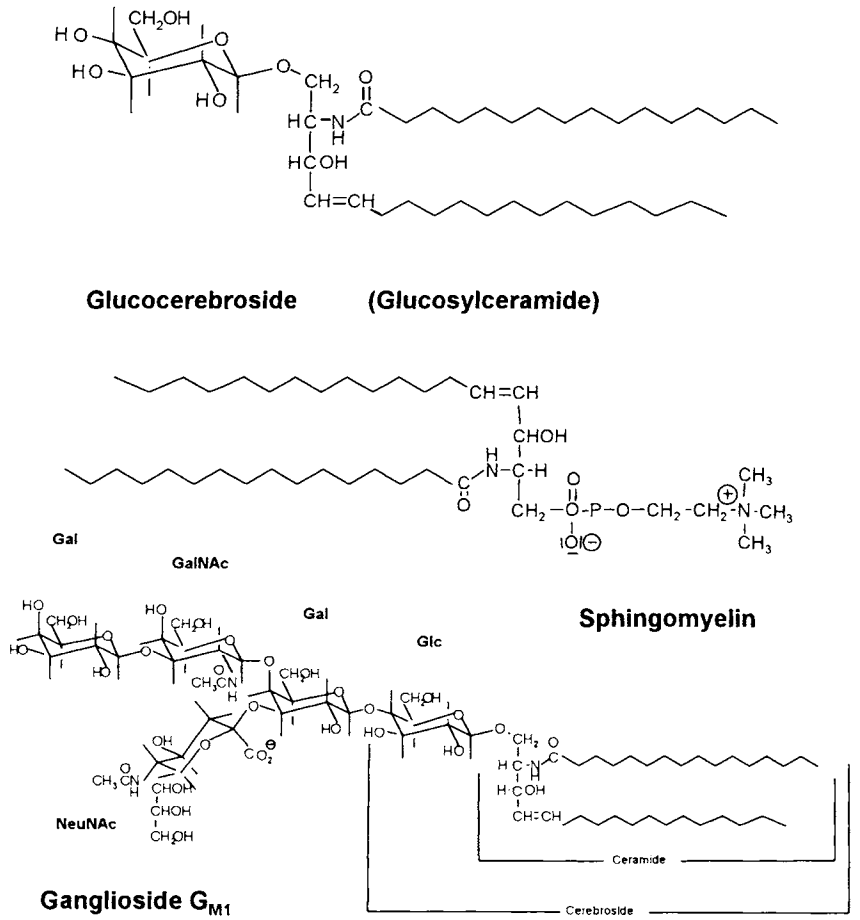

Figure 4. Chemical structure of phospho- and glycosphingolipids.

1.3. Thermotropic and lyotropic phase behavior of lipids

Lipids are amphiphilic molecules with hydrophobic hydrocarbon chains and a hydrophilic headgroup. The water solubility of double-chained lipids is very low, usually below 10^{-10} M. When brought into contact with water, they form a variety of aggregate structures, depending on the balance between hydrophobic and hydrophilic parts and on the steric requirements of the hydrophilic group. The major driving force for the aggregation is the decrease in chemical potential of hydrophobic groups when they are removed from contact with water and brought into an apolar medium. This decrease amounts to ~ 3.4 kJ·mol^{-1} per CH_2-group, as

determined from the water solubility of a variety of long chain alkyl compounds [11-13].

The major lyotropic phases encountered with double-chain phospholipids are lamellar, inverted hexagonal, and cubic phases. Single chain lipids have surfactant properties and can also form spherical and cylindrical micelles. Figure 5 shows some of the possible aggregation structures. Phospholipids not only show lyotropic mesomorphism, i. e. different phases as a function of water content, but also thermotropic mesomorphism, i. e. transitions between different phases can be induced by varying the temperature.

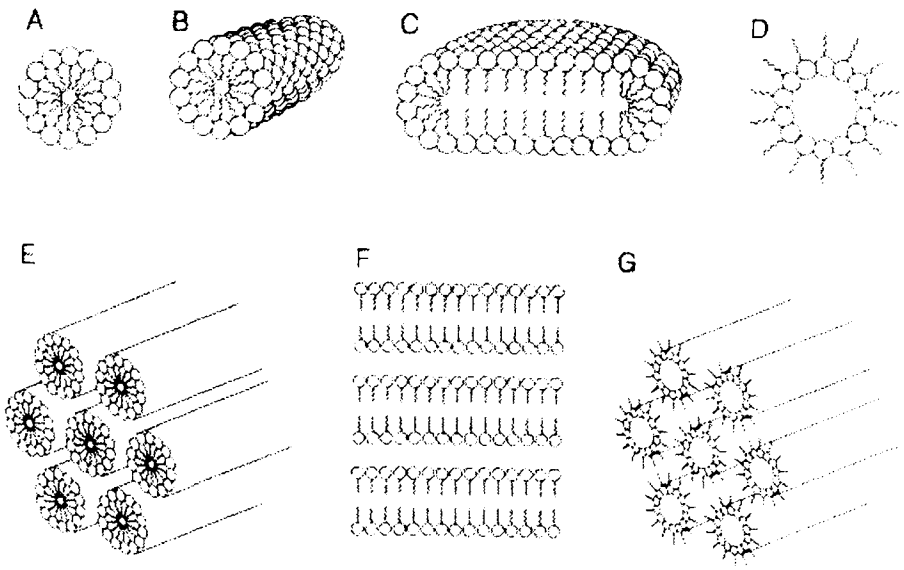

Figure 5. Aggregation structures of amphiphilic molecules. A: spherical micelle, B: rod-like micelle, C: disk-like micelle, D: inverse micelle, E: hexagonal I phase of infinite rod-like micelles, F: lamellar phase of infinitely stacked bilayer sheets, G: hexagonal II phase of infinite inverse rod-like micelles (adapted from reference [7]).

By far the most intensively studied phase transitions induced by temperature are those between different lamellar phases. This is so, because the bimolecular leaflets of the lamellar phases serve as biomembrane models (see above). Lamellar phases with various degrees of order of the hydrocarbon chains can occur. The high temperature lamellar phase (L_α-phase) is a so-called liquid-crystalline phase. This consists of bimolecular lipid leaflets separated by water layers of defined

thickness. If excess water is present, it will form a separate phase. The molecules in the bilayers are liquid in the sense that they can diffuse freely in the plane of the bilayers and can also rotate around their molecular long axis. The lipid headgroups can adopt a large number of different conformations and the hydrocarbon chains are very flexible. Trans-gauche isomerization of the chains leads to a variety of different gauche conformers. The flip-flop of molecules from one side of the bilayer to the other, however, is slow with half-times in the range of hours to days. The liquid-crystalline L_α-phase is the state which most biomembranes adopt and its properties are therefore of particular importance for understanding biological membranes functions. Liquid-crystalline L_α-phases in excess water can be mechanically treated by shaking, shearing, or by ultrasonication, to produce lipid vesicles of various sizes and lamellarity, which can serve as model systems for biological membranes [6-8].

When the temperature is lowered, the liquid-crystalline lamellae show a phase transformation to an ordered lamellar phase, the so-called "gel phase". This expression was coined for the gel-like appearance of lipid-water samples with 50 or more weight% of lipid. This gel-like behavior is caused by an ordering of the lipid chains and a considerable reduction in dynamics of all types of motional modes. The hydrocarbon chains are almost in an all-trans conformation, but the orientation of the molecular long axis of the molecule with respect to the bilayer normal can vary. Gel phases with different tilt angles and hydrocarbon chain packing can be formed, depending on the headgroup structure, the length and degree of unsaturation of the chains, and the mismatch between the two chains in the *sn*-1 and *sn*-2 position. Figures 6 and 7 show different types lamellar phases. Also, interdigitated gel phases are found, for instance for the ether lipid dihexadecylphosphatidylcholine or for PCs with a large mismatch in chain lengths [14-16].

Besides the lamellar phases, a variety of other lyotropic phases, such as hexagonal and cubic phases exist [17]. These are formed by lipid molecules preferring curved interfaces. When a larger mismatch between the cross-sectional area of the chains and the headgroup exists, positively or negatively curved surfaces are energetically favorable. This effect can be described by a simple geometric model proposed by Israelachvili [18], where a packing parameter $V/(l \cdot A)$, (V = volume of the molecule, l = effective length, A = effective surface area at the interface) is introduced. When $V/(l \cdot A) > 1$, an inverted hexagonal (H_{II}) phases can be formed, which is composed of water filled cylinders in a hexagonal array, the lipid chains of the cylinders being in contact with each other. These phases are often formed by unsaturated PEs at higher temperatures (see Figure 6).

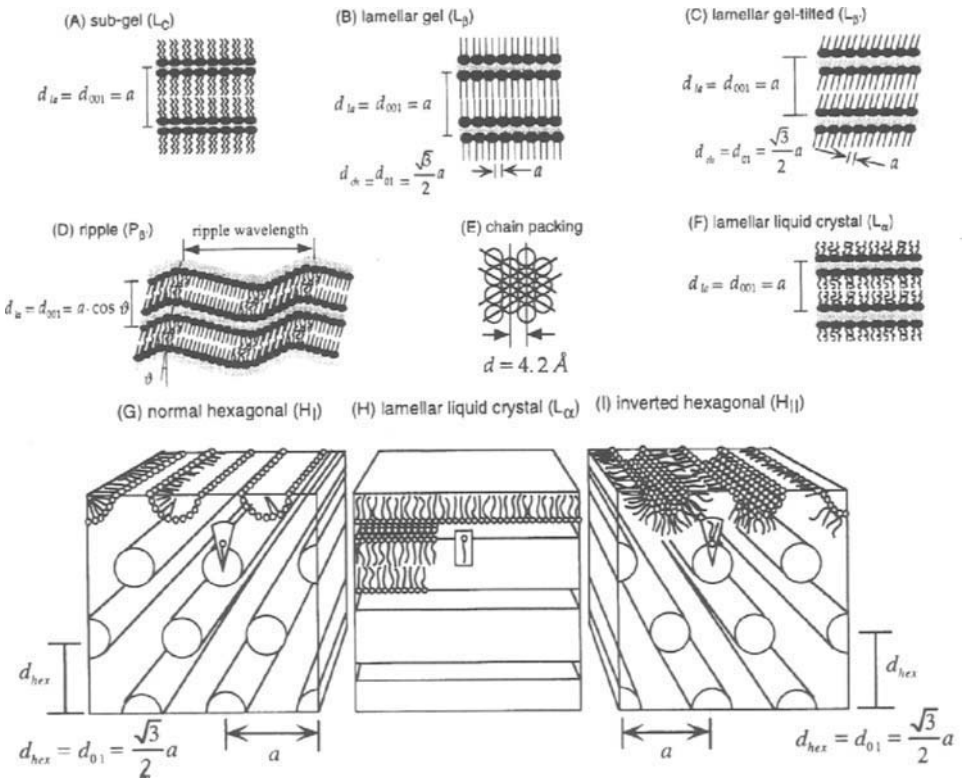

Figure 6. Different types of lyotropic lamellar and hexagonal phases with their characteristic repeat distances as observed by x-ray scattering (adapted from reference [19]).

In mixed lipid/water systems the formation of cubic phases is also quite common. These phases often occur in the phase diagram between lamellar L_α- and hexagonal H_{II}-phases. Several different cubic phases of different symmetry have been found, where the lipid molecules are arranged on periodic minimal surfaces [3,17,19] (see Figure 8). The phases shown in the figure are bicontinuous phases and are formed by lipid/water mixtures at low water content. For the cubic phase Ia3d (Q^{230}) the three-dimensional network of continuous water rods is shown. This phase is also called gyroid phase, whereas phase Pn3m (Q^{224}) is called double-diamond, and phase Im3m (Q^{229}) has the name "plumber's nightmare".

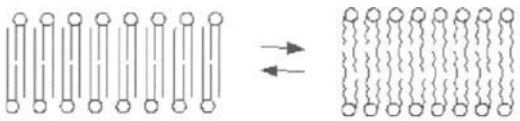

1-Octyl-2-stearoyl-phosphatidylcholine (OSPC)

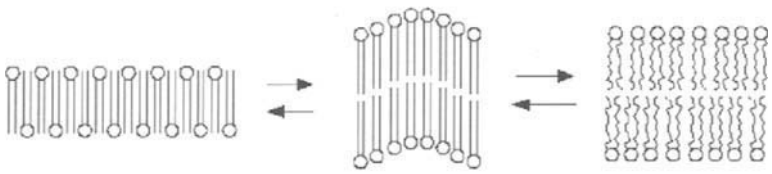

1,2-Dihexadecyl-phosphatidylcholine (DHPC)

Figure 7. Interdigitated phases formed by phosphatidylcholines with two chains of unequal length or by phosphatidylcholines with ether linkages [14-16].

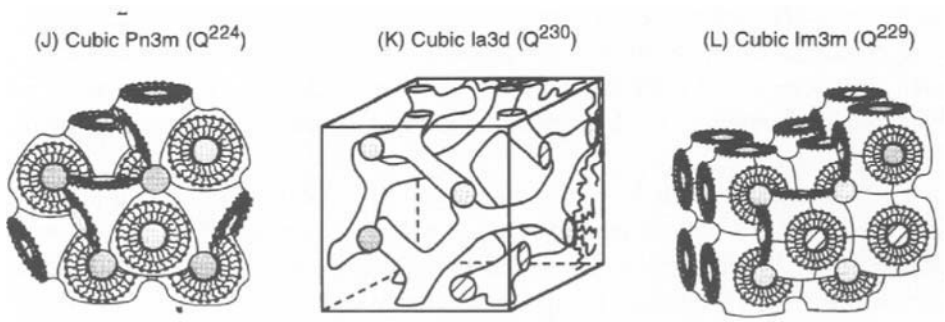

Figure 8. Cubic (Q) phases formed by amphiphilic molecules and their different nomenclature (adapted from reference [19]).

The conversion of lipid/water systems from one type of phase to another can be induced by physical and chemical parameters. The phase structure depends, for instance, on the water content of the sample, but also on temperature and pressure. For systems with more than one lipid component, the lipid composition is, of course, also important. The phase transformation can be easily studied by differential scanning calorimetry (DSC) for a temperature induced transition, and

by isothermal titration calorimetry (ITC) for a composition induced transition. In the next two sections, examples for these two types of calorimetric experiments will be presented and it will be shown how information on the thermodynamic state functions and on structure and conformation of the molecules in these lyotropic phases can be obtained from the analysis of the observed heat effects.

2. DIFFERENTIAL SCANNING CALORIMETRY OF MEMBRANES

2.1. Thermotropic phase transitions of pure lipids in excess water

In this section we will describe some examples for the application of DSC to the study of phase transition in dilute aqueous lipid suspensions. As mentioned above, many lipids display not only thermotropic but also counterion induced lyotropic mesomorphism. In binary lipid/water mixtures with one specific pure lipid component a variety of lyotropic phases can be formed depending on temperature and the lipid/water ratio. We only describe phase transitions occurring in dispersions with high water content (excess water). These systems are really two-phase systems, where an almost pure water phase coexists with a lipid/water phase of a certain composition [20]. Increasing the temperature of an ordered lamellar phase to the liquid-crystalline lamellar phase is usually accompanied by a change in water content of the lamellar phase. In lipid systems in excess water it is an eutectic melting reaction. The prime example, which has been studied in much detail is the system dipalmitoyl-phosphatidylcholine (DPPC)/water. The phase diagram obtained by differential scanning calorimetry is shown in Figure 9 [20].

For a dispersion at high water content and low temperature, a two-phase region exists, where almost pure water coexists with an $L_{\beta'}$-phase with a water content of ca. 20 weight%. Increasing the temperature leads to a eutectic melting reaction at 33°C to another two-phase region where a $P_{\beta'}$-phase coexists with pure water. Further increasing the temperature finally leads to the so-called melting at the main phase transition temperature T_m, a higher water content which is again a eutectic melting reaction. The liquid-crystalline L_α-phase has and is again in coexistence with pure water. However, to simplify the thermodynamic analysis, the excess water phase and the change in hydration of the lamellae upon heating it into the L_α-phase is often neglected and the dilute lipid/water dispersion is described as a one component lipid system. The observed eutectic melting transitions for DPPC are then called pre-transition and main transition. In analogy with this simplification, mixtures of two lipids in excess water are described as pseudo-binary systems.

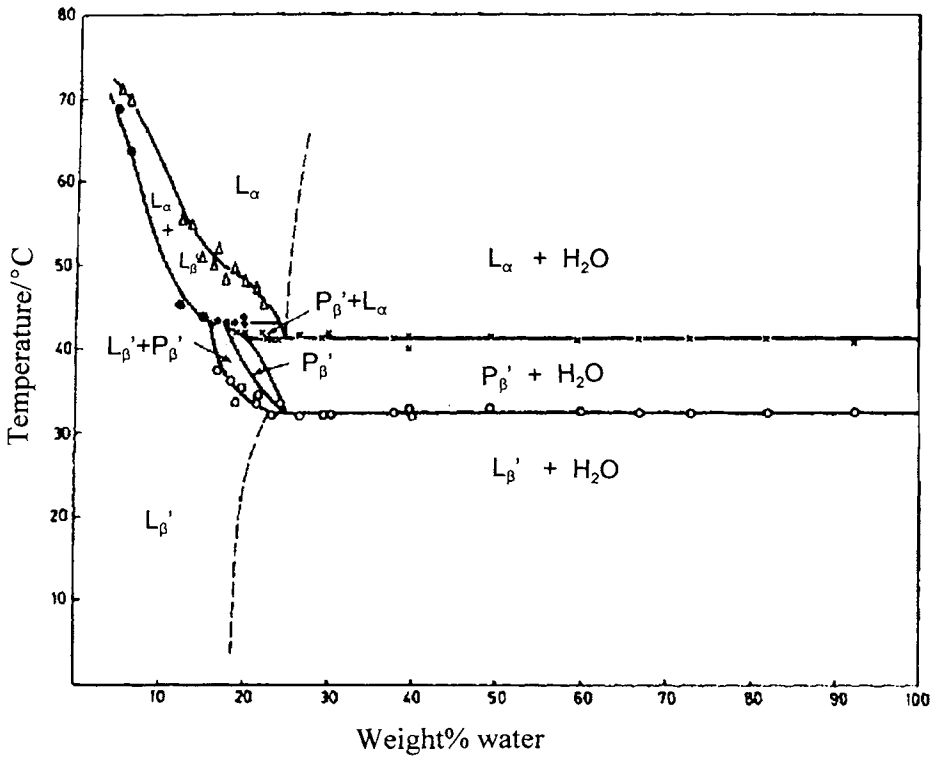

Figure 9. Phase diagram of the DPPC/water system (adapted from reference [20]).

The DSC instrumentation needed for studies of very dilute lipid suspensions are so-called high-sensitivity DSC-instruments, mainly of the adiabatic type, with cell volumes of usually 0.5 - 1.5 mL. The lipid concentration needed for these instruments is in the range of 0.1 - 10 mg/mL, depending on the width of the endotherms. The reader is referred to Volume I of this handbook for instrumental details.

One of the newly developed highly sensitive differential scanning calorimeters is the VP-DSC by MicroCal, Inc., Amherst, MA, USA. Typical DSC curves of the phospholipid distearoylphosphatidylcholine (DSPC) measured with this instrument are shown in Figure 10 [21]. DSPC has a similar phase diagram as DPPC, only the difference in T_m between the pre- and the main phase transition is smaller.

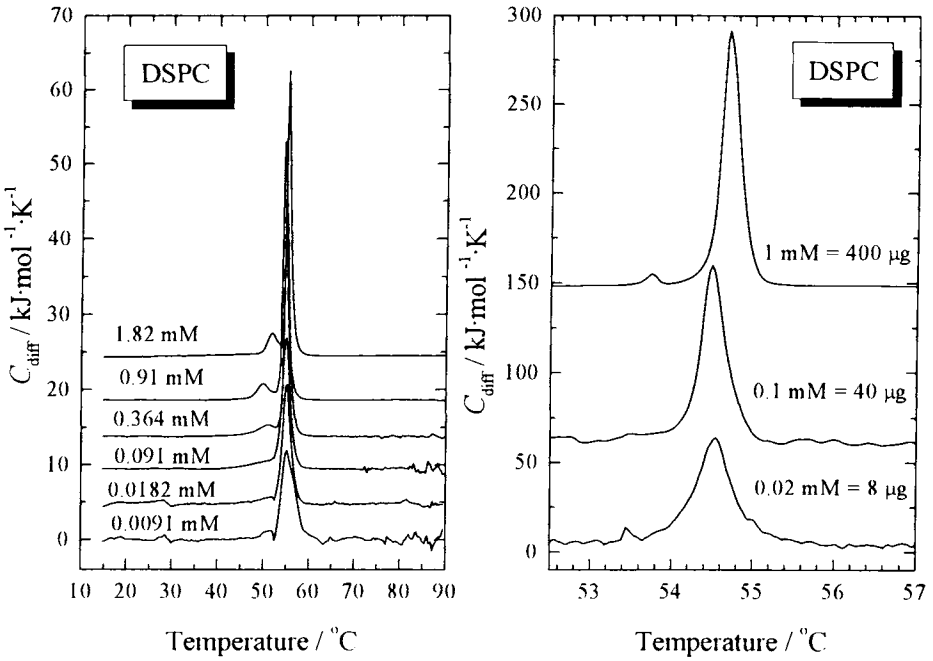

Figure 10. DSC curves of DSPC obtained with the VP-DSC by MicroCal, Inc. Cell volume = 0.5 mL. Left: heating rate: 60°C, passive mode. The peaks are broadened but the sensitivity is high enough to pick up the signal of ca. 3.7 µg of DSPC. Right: heating rate: 30°C, highest feedback gain. The peaks are no longer broadened, but the noise is somewhat increased. The sub-main transition at 53.8°C is clearly seen [22].

The cell volume of this instrument is 0.5 mL. The sample was prepared at a concentration of 1.82 mM and then diluted and repeatedly re-scanned. For a check of the instrumental sensitivity we performed two tests. Firstly, we set the heating rate to 60°C/h and ran the instrument in the "passive mode". This leads to a broadening of the transition but improved sensitivity. Secondly, we increased the feedback to the fastest response but decreased the heating rate to 30°C/h to reproduce more accurately the very sharp transition of these phospholipids. The sharpness of the transition is now well resolved, but the instrumental noise is somewhat increased. The recently found sub-main transition is clearly resolved as a small additional peak at ca. 53.8°C [22]. The instrumental sensitivity is such

that the transition of 3-8 μg of DSPC can easily be picked up, however at the cost of either broadening of the peak or increased base line noise [21].

2.1.1. Influence of headgroup structure and hydrocarbon chain length

For a phospholipid with a particular headgroup, for instance, the common phosphocholine headgroup, the transition temperatures for the gel-gel and gel-liquid-crystalline transition depend on the nature of the hydrocarbon chains. For straight chain saturated fatty acids the chain length dependence is such that with increasing chain length the transition temperatures increase, but not in a linear fashion. This has been described for many phospholipids with saturated chains and the relevant data have been collected in a data base [12,13,23]. Figure 11 shows the T_m-values for the gel-liquid-crystalline phase transition for a number of different phospholipids as a function of chain length.

It can be seen that the increase in T_m is decreasing with increasing chain length. This is understandable, because the influence of the van der Waals-interactions between the hydrocarbon chains increases with chain length and then dominates the thermotropic transition behavior so that the transition temperatures should reach a limit. For shorter chain phospholipids, significant differences in the transition temperatures are observed, depending on the chemical structure and charge at the headgroup, because here the headgroup effects are more important. Small headgroups and the possibility for intermolecular interactions via hydrogen bonds tend to increase T_m, while increasing negative charge of the headgroup usually decreases T_m due to repulsive electrostatic interactions between headgroups and a concomitant increase in hydration of the headgroup. Figure 12 shows as an example DSC-curves of phospholipids at *pH* 7 with different headgroup structures and two different chain lengths obtained with the MicroCal MC-2 instrument at a heating rate of 60°C/h.

While the precision in the determination of phase transition temperatures is generally excellent, so that T_m-values obtained with different instruments by different groups agree fairly well, this is not so for the transition enthalpies ΔH, the other thermodynamic quantity obtainable by calorimetry. The agreement between data reported by different groups and with different instruments is usually not better than ± 5% for the ΔH-values. There are several reasons for these discrepancies, namely different purity of samples, different preparation procedures of the liposomal suspensions, inaccuracies in sample concentrations (the concentration is usually calculated from dry weight or from phosphorous analysis), different scanning speeds and incubation times at low temperature, and finally, differences in base line subtraction procedures.

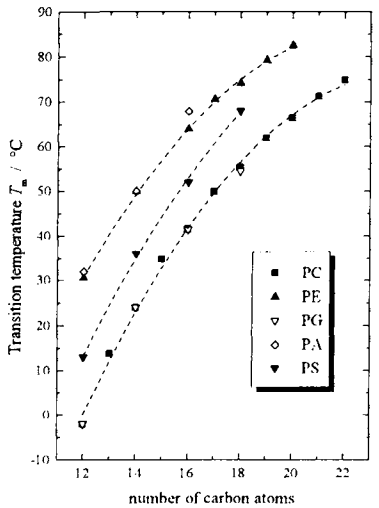

Figure 11. Transition temperature T_m for the main phase transition of different phospholipids. Compiled from various sources [12,13,23-25].

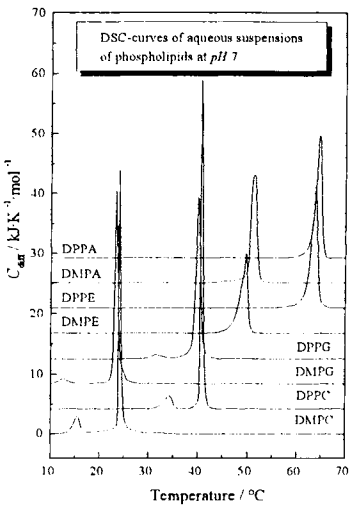

Figure 12. DSC curves of aqueous phospholipid dispersions obtained with the MicroCal MC-2 (c = 1-2 mM).

The effect of different base line subtraction procedures on the ΔH-value becomes particularly important when the mid-point temperatures of several transitions are close together. This is the case for phosphatidylcholines, where the $L_{\beta'} \rightarrow P_{\beta'}$ and the $P_{\beta'} \rightarrow L_{\alpha}$ transition is observed as shown in Figure 13 for distearoylphosphatidylcholine (DSPC). Here, the gel-gel phase transition is so closely located near the main phase transition that a clear separation is not possible and the procedure for dividing the total ΔH between pre- and main transition becomes somewhat arbitrary. One possible procedure is to calculate the integral over both transitions and then separate the ΔH for the pre-transition at a temperature halfway between the T_m-values of the pre- and main transition from the ΔH for the $P_{\beta'} \rightarrow L_{\alpha}$ transition (see Figure 13). As indicated in the figure, a linear base line was used for the integration. This is not the only possibility. Particularly, when the apparent heat capacity below and above the transition are significantly different, a base line of sigmoidal shape should be used.

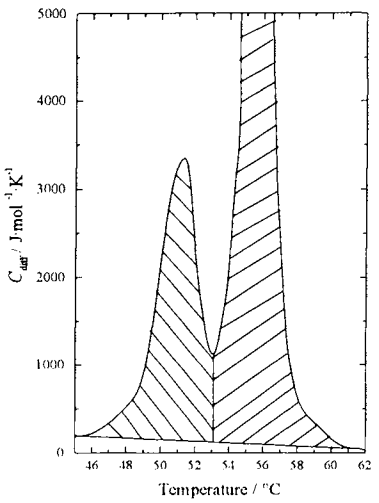

Figure 13. Enlarged view of a DSC curve of DSPC showing the method of integration and separation between the transition enthalpies of the pre- and main transition.

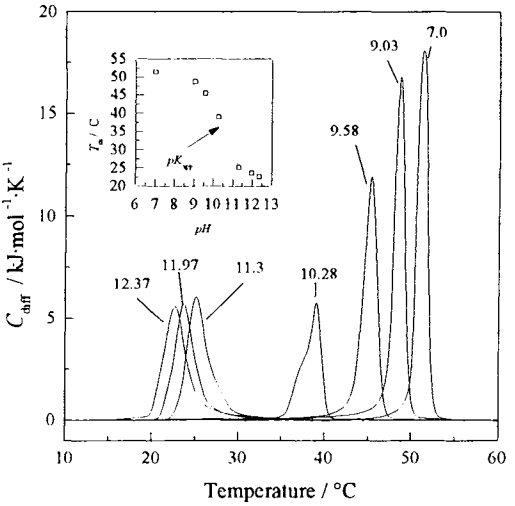

Figure 14. DSC curves of dimyristoyl phosphatidic acid as a function of *pH*. The insert shows the *pH*-dependence of the transition temperature T_m and the apparent *pK*-value for the dissociation of the second proton (adapted from reference [30]).

In general, for a series of phospholipids with identical headgroups an almost linear increase of ΔH with increasing chain length is observed with a value of ca. 1.92-2.1 kJ·mol^{-1} per CH_2-group. For the transition entropies $\Delta S = \Delta H / T_m$, the linear increase is similar, because the changes in T_m on an absolute temperature scale are small. The ΔS increase is 5.5 J·K^{-1}·mol^{-1} per CH_2-group [12,13,24].

2.1.2. Influence of pH and ion binding

For some phospholipids with ionizable headgroups, the gel phase structures and the transition temperatures depend on the charge of the headgroups. For instance, for phosphatidic acids (PA), phosphatidylglycerols (PG), and phosphatidylserines (PS), a variation of *pH* can change the number of charges on the headgroup [12,13,26-32]. Figure 14 shows as an example the *pH* induced changes in T_m for DMPA when the second proton dissociates from the phosphate headgroup.

Changes in headgroup charge also lead to changes in transition enthalpies and entropies. Doubly negatively charged PAs have significantly lower ΔH- and ΔS-

values than the singly charged forms. [31]. In the low *pH* regime, the phosphate groups of phospholipids become protonated, the thermotropic and lyotropic behavior changes drastically when the headgroups become uncharged as is the case for PAs and PGs. For PAs, the bilayers become dehydrated and quasi-crystalline lamellar phases are formed. This is immediately evident by a visual inspection of the diluted aqueous dispersion which becomes strongly turbid after a change of *pH* to 2. The dispersion is no longer stable and precipitates. This effect is also observed for PGs. In the case of PCs, PEs and PSs, the headgroups still carry a positive charge at low *pH*-values, so that this dehydration effect is not observed.

Figure 15 shows some examples for DSC curves at different *pH*-values for phospholipids with different headgroups.

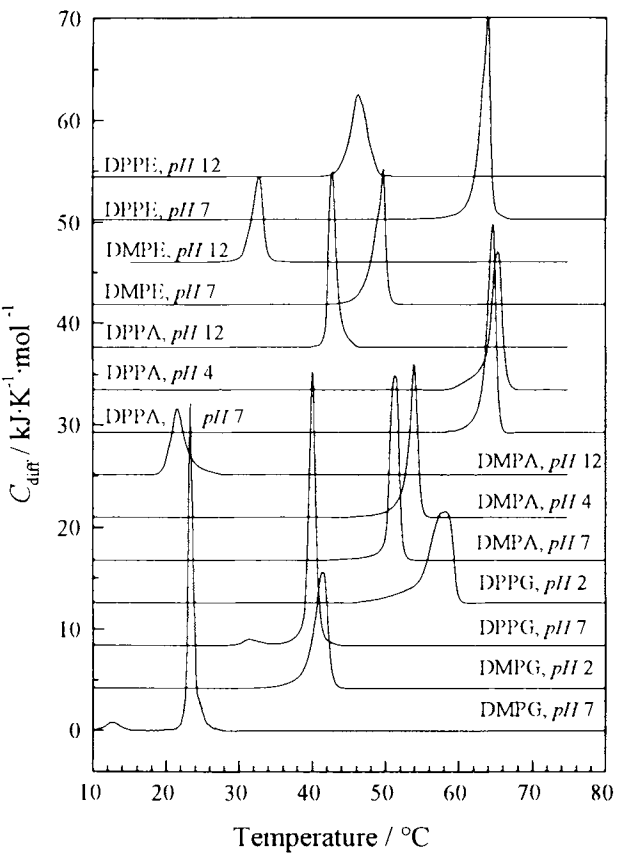

Figure 15. DSC curves of dilute aqueous dispersions (1 mM) of different phospholipids (PGs in 0.1 M KCl) obtained with the MicroCal MC-2 instrument.

The headgroups of PCs and PEs are zwitterionic at *pH* 7. The negatively charged phosphodiester group can bind positively charged ions. Binding will modulate the hydration of the phosphate moiety and therefore the transition behavior will change. The binding constants of monovalent cations are small and the effects of increasing the ionic strength with NaCl or KCl is negligible. For divalent and trivalent cations, much larger binding constants are observed and in an excess of salt with divalent cations the transition temperatures shift to higher values. This effect has been studied in some detail only for phosphatidylcholines [33-38].

Figure 16 shows DSC scans of DMPC in the presence of Fe^{2+} and Fe^{3+} illustrating the difference in binding between di- and tri-valent Fe cations. For Fe^{3+} even at 10^{-4} M, i.e. a lipid to Fe^{3+} ratio of 10:1, shifts of the main phase transition temperature are observed indicating much stronger binding of the trivalent cation compared to the divalent cation. Similar effects have been observed with other trivalent cations such as La^{3+} [36-38].

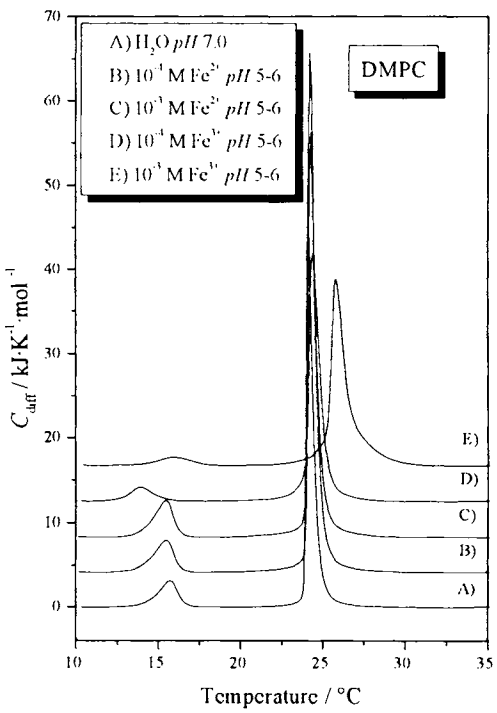

Figure 16. DSC curves of DMPC in the presence of different concentrations of Fe^{2+} and Fe^{3+}, the DMPC concentration was 1 mM.

The binding of mono- and multivalent cations to negatively charged phospholipids at *pH* 7 is much stronger and drastic changes in phase behavior are observed particularly when di- or trivalent cations are bound to PAs or PGs. In a first approximation, the influence of monovalent cations can be viewed as purely of electrostatic origin as described by the simple Gouy-Chapman theory [27,31, 39,40]. Increasing ionic strength leads to a screening of negative surface charges and a decrease of the electrostatic repulsive interactions between headgroups. As a consequence, the phase transition temperature increases. However, specific binding at higher concentrations also occurs, so that the effects of Li^+, Na^+, and K^+ are different. Figure 17 shows the effect of increasing concentrations of NaCl on the phase transition of $DMPG^-$ and $DMPA^-$.

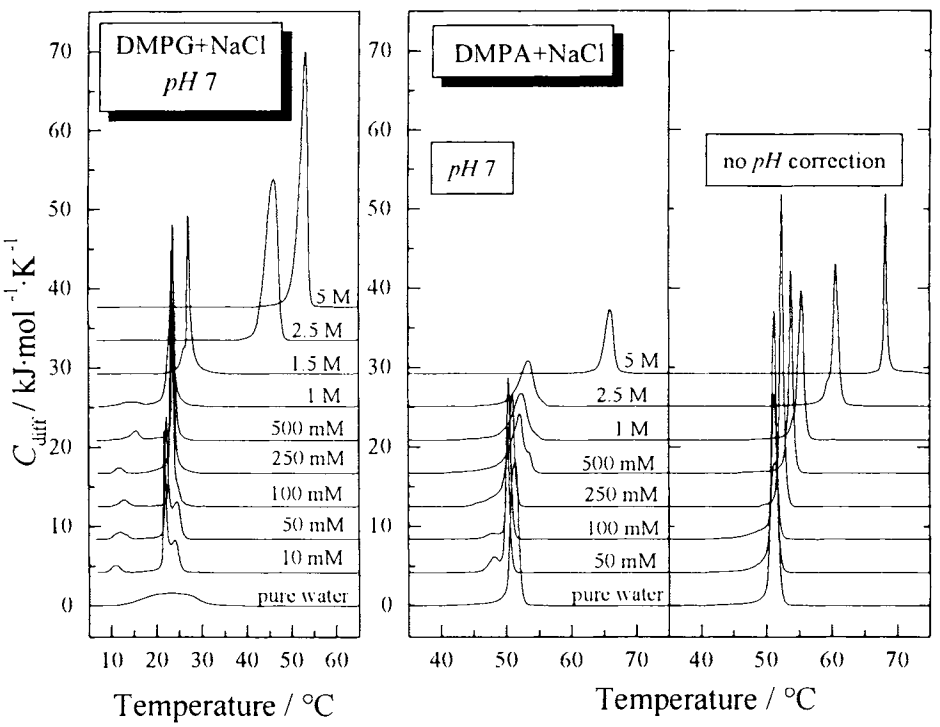

Figure 17. Left: DSC curves of DMPG suspensions at *pH* 7 as a function of NaCl concentration. Right: DSC curves of DMPA suspensions at *pH* 7 after *pH* correction and uncorrected in unbuffered suspensions. Here, the *pH* changes slightly to lower values due to a partial dissociation of the second proton.

In the case of the phosphatidic acid DMPA, an additional effect, namely the shift in the apparent pK_2-value for the dissociation of the second proton has to be taken into account [31]. In unbuffered dispersions the *pH*-value decreases slightly upon salt addition, the headgroup mainly stays in its singly charged form. When the dispersion is kept at *pH* 7 by low concentrations of buffer or by *pH* adjustment, the addition of salt leads to an increase in the formation of the doubly charged form of DMPA due to a shift of the apparent pK_2 from 10.5 at low ionic strength to ca. 7 at high ionic strength. The thermograms at high NaCl concentration are therefore of a mixture of singly and doubly charged DMPA. The thermograms are consequently broader and the increase in T_m is less pronounced as when the DMPA molecules stay in their singly charged form.

The formation of the Ca^{2+} salts of these phospholipids leads to a strong dehydration of the lipid headgroup region and the formation of liquid-crystalline L_α-phases occurs only at very high temperatures. In addition, in the case of PA, the binding of divalent cations can again induce the dissociation of the second proton, so that the formation at 1:1 complexes of the doubly charged form with a divalent cation such as Ca^{2+} occurs even at *pH* 7 or lower due to a shift of the apparent pK_2 [41-47].

For PAs and PGs there is a clear dependence of the binding behavior on the nature (i.e. probably the size) of the divalent cation. Ca^{2+} behaves differently compared to Mg^{2+} or Sr^{2+}, the phases formed in an excess of divalent cations are probably not the same and the thermotropic behavior is complicated by the formation of metastable phases [48]. As an example, DSC-curves of DMPA at various PA:M^{2+} ratios is shown in Figure 18 for the case of Ca^{2+} and Mg^{2+} binding. The DSC scans at *pH* 3.5 always correspond to the singly charged form of DMPA, i.e. 2:1 DMPA:M^{2+} complexes, whereas at *pH* 7 1:1 complexes are formed.

Larger organic cations can also bind to lipid bilayers. These ions can "partition" into the interface region and not only act via their charges but also through their apolar parts which perturb the hydration of the interface and also the packing of the chains. Figure 19 shows the effects of the organic salt choline chloride on DMPC and DMPE bilayers. Binding of monovalent cations to zwitterionic lipids is normally weak, and choline chloride is no exception. However, in contrast to inorganic monovalent cations, the organic cations has a notable effect, depending on the lipid headgroup. Whereas for DMPE the effect is negligible, the perturbation of the interface region in the case of PC is clearly evident from the broadening and the shift of the pretransition and, to a lesser extent, also the main phase transition temperature.

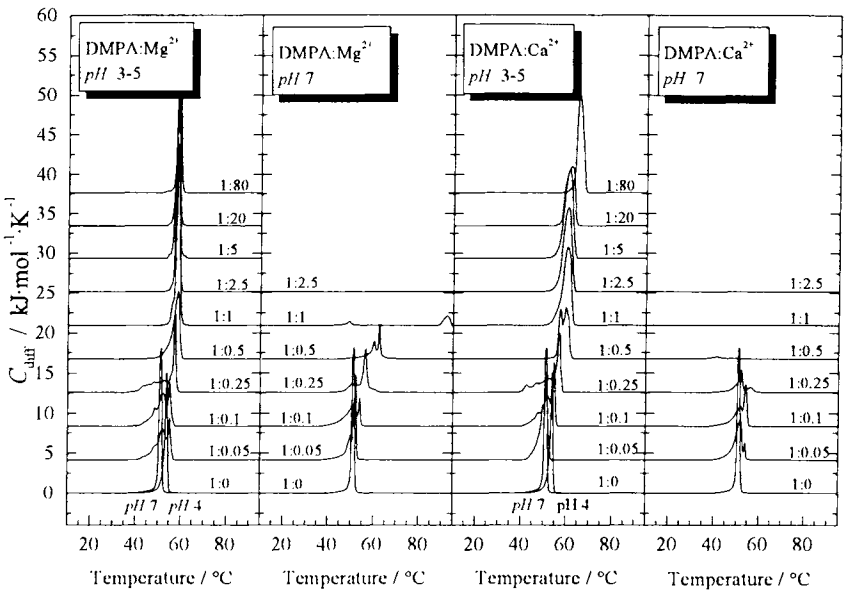

Figure 18. DSC scans of DMPA with Mg^{2+} and Ca^{2+} at different molar lipid:cation ratios. The 1:1 complexes formed at *pH* 7 do not show any phase transition below 95°C, whereas the 2:1 complexes formed at *pH* 3-5 clearly display melting transitions at 60-65°C.

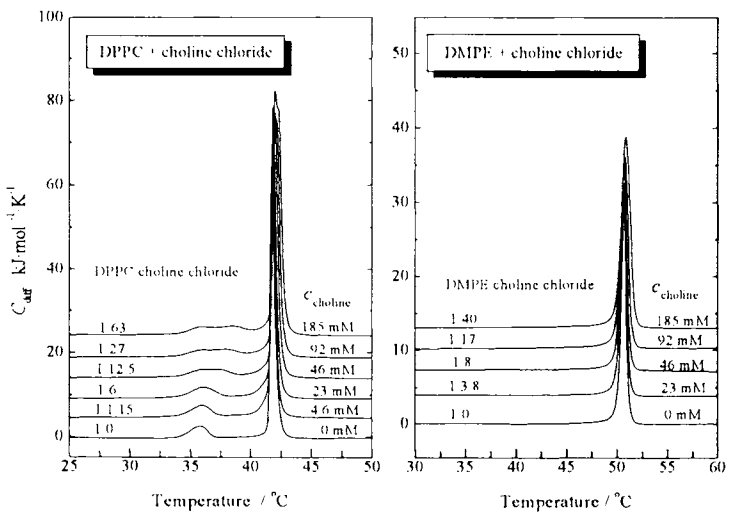

Figure 19. DSC scans of DPPC and DMPE in the presence of various concentrations of choline chloride.

2.2. Phase transitions of lipid mixtures

Lipids of biological membranes are a complex mixture of various classes of lipids with different headgroups and chain length. The composition of membranes of eukaryotic cells can differ substantially, depending on the location and the function of the cells in the body. In addition, significant differences are found between the lipid composition of the plasma membrane of a cell and intracellular membranes building up the various compartments inside a eukaryotic cell. It is for this reason that the analysis of lipid miscibility has gained much attention in the last years. The question whether lipid immiscibility in the liquid-crystalline L_α-phase is possible is of particular relevance to the function and organization of biological membranes. It has been a long debated question whether biological membranes show lateral inhomogeneities or domain formation, thus providing membrane proteins with different lipid surroundings necessary for their function as enzymes or ion channels [49-53].

It has been known for quite a while that certain types of membrane located enzymes show a specificity for the binding of certain lipids but it still is unclear whether lateral domain formation is mainly caused by proteins or whether pure lipid mixtures can show this phenomenon by themselves [54-60].

Biological membranes and the lipid mixtures extracted from them are far too complex to gain suitable information on their mixing behavior by calorimetric methods. Therefore, the systematic investigation of mixtures of two or more lipids, preferentially synthetic ones, in aqueous dispersion is the method which has led to important conclusions about lipid miscibility in these quasi-two-dimensional lamellar phases. The analysis of the phase diagrams obtained from the investigation of the thermotropic transitions of suspensions with different lipid compositions in excess water in terms of the curvature and the location of the phase boundaries provides the necessary information about non-ideality parameters.

2.2.1. Lipid-cholesterol mixtures

Cholesterol is abundant in many membranes of eukaryotic cells, the total percentage reaching up to 50% of the total lipid content. The behavior of lipid-cholesterol mixtures has therefore attracted much attention. Despite the vast amount of publications on the thermotropic behavior of phospholipid-cholesterol mixtures, the macroscopic description of lipid-cholesterol systems using phase diagrams is still very much debated, because different analytical methods such as NMR-, ESR-, fluorescence- and FT-IR-spectroscopy monitor changes in physicochemical behavior of lipid-cholesterol mixtures as a function of composition and temperature which cannot easily reconciled with observations using DSC [61-72].

The general effect of cholesterol with its rigid ring system is to "condense" the molecules in the L_α-phase and to "fluidize" the lipids in the gel phase. The lipid molecules are transferred into some intermediate state where the acyl chains have much less gauche conformations than usually found for the liquid-crystalline state. However, the rotation of the molecules around their long axis and the speed of lateral diffusion remains fast, so that this state has been termed "liquid-ordered" state, meaning that the ordering effect of cholesterol is restricted to the trans-gauche-isomerization of the chains, whereas all other properties are still characteristic for a "liquid" state. The temperature and the particular cholesterol content at which this transition to the liquid-ordered state occurs depends on the chemical structure of the phospholipid, i.e. its chain length, degree of unsaturation or branching, and its headgroup type.

For saturated phosphatidylcholines, DSC thermograms of samples with increasing cholesterol content show a broadening of the peaks and a decrease of the total transition enthalpy. Only with high sensitivity DSC instruments can the thermograms at cholesterol contents above 40 mol% be analyzed with sufficient accuracy and reliability, because the transition becomes extremely broad, encompassing a range of 40-70 degrees. At cholesterol contents of up to 20 mol%, the DSC endotherms can be decomposed into a narrow and a broad component. The narrow component decreases in area and disappears at 20-40 mol% cholesterol, while the broad component remains the only "peak" above this concentration. It gradually broadens and decreases in area when the cholesterol content is increased further. Above 40-60 mol% cholesterol, usually no endothermic transition is observed. This seems to be the limit of cholesterol uptake of the bilayer phase for many phospholipids. Further increase of cholesterol content leads to a phase separation of pure cholesterol, probably in the form of suspended hydrated crystallites in water, and a cholesterol saturated bilayer phase.

As an example, Figure 20 shows DSC curves of DSPC-cholesterol mixtures as a function of cholesterol content. The DSC curves at high mol% cholesterol have been enlarged to show the broad transition which is still visible even at 50 mol% cholesterol. Figure 21 shows the total enthalpy as a function of composition, which decreases non-linearly, the break in the plot indicating the percentage at which the narrow transition has disappeared. This superposition of broad and narrow components in the endotherms is shown in Figure 22 together with simulations used for decomposing the observed endotherm into its components. It can be seen that even at 40 mol% cholesterol, the total DSC curve can be decomposed into two components. The broad component covers a temperature range from 20 to 90°C. This broad transition can only be observed, if the DSC instru-

ment used shows excellent base line reproducibility as the older DSC DASM 1 and 4 instruments and the newer VP-DSC.

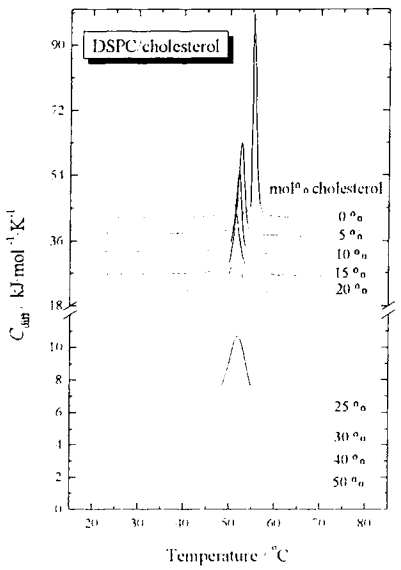

Figure 20. DSC curves of DSPC/cholesterol mixtures as a function of cholesterol content (adapted from reference [67]).

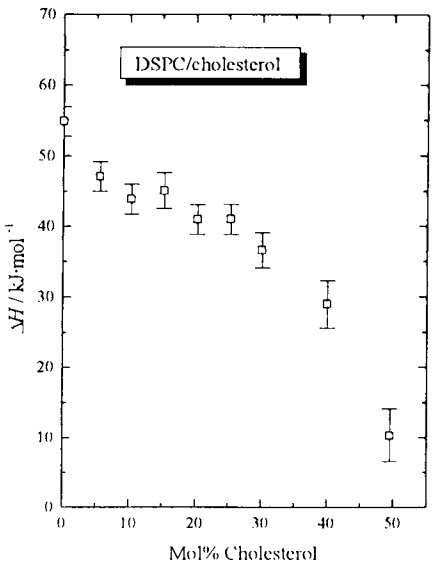

Figure 21. Total transition enthalpy for DSPC/cholesterol as a function of cholesterol content (adapted from reference [67]).

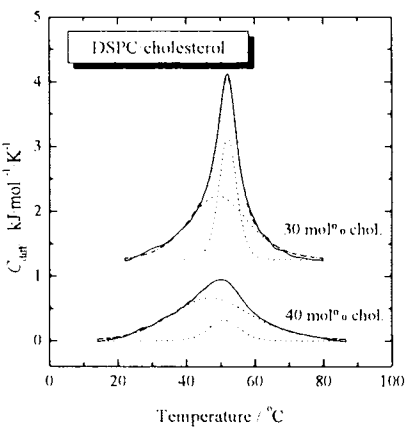

Figure 22. DSC curves of DSPC at high cholesterol content, showing the decomposition into two components [67].

The effect of cholesterol on other phospholipid mixtures is qualitatively similar. For PCs with saturated chains, it is observed that the mid point temperature of the broad transition is higher than that of the sharp transition when the PC carries shorter chains, such as in DMPC. For DAPC with its C20 chains, the broad transition is shifted to a lower temperature compared to the sharp transition [67,68].

It is extremely difficult to construct a phase diagram on the basis of DSC measurements alone. Other techniques, such as spectroscopic methods mentioned above, have to be used. However, despite all efforts, a consistent description of the behavior of lipid-cholesterol mixtures, using the information obtained by these various methods was not very successful. Using a microscopic interaction model, a theoretical phase diagram has been calculated, which shows many of the features observed in lipid-cholesterol mixtures, though the location of the phase boundaries suggested by this model is often not found [62,66,67]. This is shown in Figure 23. The different regions of liquid-disordered (ld), liquid-ordered (lo), and solid-ordered (so) state vary for the different phospholipids studied so far. In general, however, the appearance of the phase diagrams for different phospholipid/cholesterol mixtures is similar.

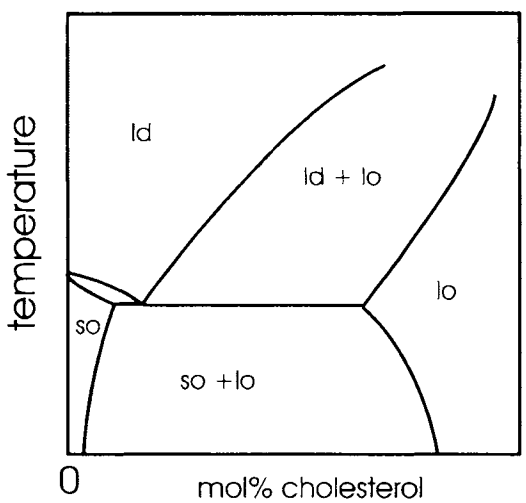

Figure 23. Schematic phase diagram of phospholipid/cholesterol mixtures showing the regions of the solid-ordered (so), liquid-ordered (lo), and liquid-disordered (ld) phases [62,66].

The difficulties in interpretation of experimental results in terms of a phase diagram apparently arise, because the suggested phase separation between phases

of different composition often does not occur on a "macroscopic" scale, i.e. some μm, where it should be observable, but only on a scale of several molecular distances. This means that these micro domains are not easily observable, particularly when methods are used which are sensitive to averaging by lateral diffusion between different domains. This is the case for ^{2}H-, ^{31}P-, and ^{13}C-NMR methods, though the time scales are somewhat different, and also for the different fluorescence measurements, where lateral diffusion is probed with fluorescent labels [64,67,72].

In conclusion, DSC-experiments on lipid-cholesterol mixtures are easily performed and have revealed important information. However, the interpretation of these DSC data in terms of a simple phase diagram is not easy.

2.2.2. Binary phospholipid mixtures

As already mentioned above, biological membranes can be a complex mixture of various lipid classes, i.e. phospholipids, sphingolipids, cholesterol, etc. The analysis of simple pseudo-binary phospholipid mixtures is a first attempt to describe the miscibility in the much more complex biological membranes. The phase behavior of mixtures of two different phospholipids in excess water is usually treated in a similar way as the mixing behavior of two compounds in volume phases [73-80]. The third component, water, is not explicitly taken into account, i.e. the pure water phase is neglected. Also the change in water content of the lamellar phases occurring during the transition from the gel to the liquid-crystalline state is neglected. The mixing of two lipids is in this approach viewed as being restricted to the quasi-two-dimensional bilayers and treated similarly as the solid-liquid equilibrium in three-dimensional bulk phases. This approach works quite well, despite the fact that the phase transitions of pure lipids from ordered to disordered phases are not true first order phase transitions but in a strict thermodynamic sense eutectic melting reactions.

The large variety of mixing behavior found for three-dimensional bulk phases can also be found for the quasi-two-dimensional systems. The type of phase diagrams found for mixtures of two lipid components are shown in Figure 24. The types of diagrams range from those indicating ideal mixing in both phases, over diagrams with lower or upper azeotropic points, to those types of systems which show limited miscibility in the low temperature ordered phase with mono-, peritectic, or eutectic behavior. Limited mutual miscibility in the ordered lamellar phases is quite common, when the structures of the phases formed by the pure lipids differ significantly, whereas homogeneous mixing, though possibly non-ideal, is common for the liquid-crystalline L_{α}-phase.

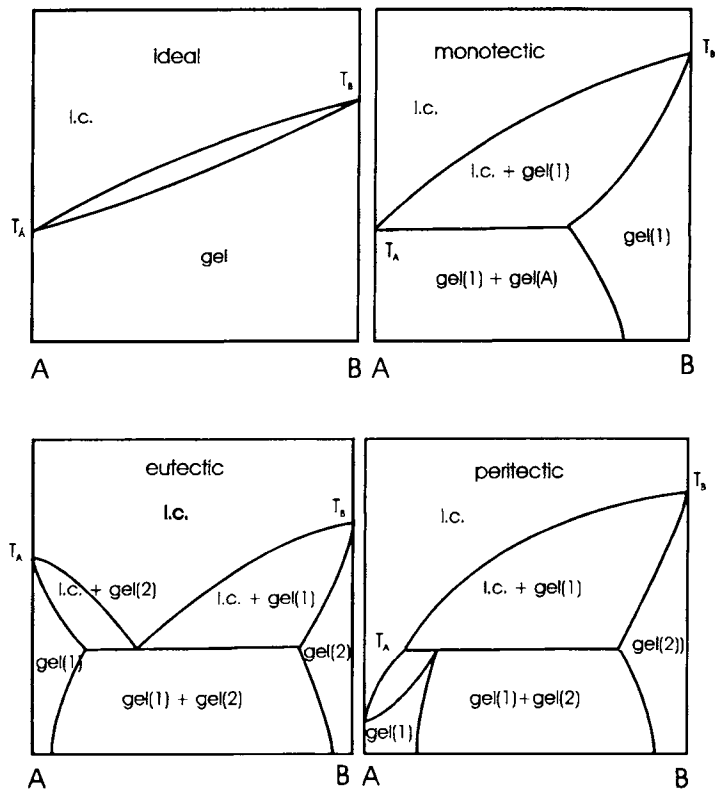

Figure 24. Simplified schematic diagram of possible types of phase diagrams observed for pseudo-binary phospholipid mixtures.

When phase diagrams are constructed from DSC curve, the procedure is usually the following: DSC curves at different molar ratios of the two components are recorded. The temperatures for the onset $T(-)$ and end $T(+)$ of the phase transition are determined from the deviations of base line at low and high temperatures. The problems arising by this procedure are immediately obvious. Because the transitions are very broad, the experimental determination of these temperatures can be very inaccurate unless an instrument with high sensitivity and a very reproducible base line is used. In addition, even the transitions of pure lipids are broadened due to limited cooperativity of the transition. To obtain singular values for the melting temperatures for both pure components, their finite width of the transition is measured and then subtracted from all other $T(-)$ and $T(+)$ values of the mixtures, weighted with the respective mole fractions of the mixture [76,81-

83]. This leads to phase diagrams, which end in angular points on both sides and a somewhat reduced width of the coexistence range in between. However, reducing the width of the transition range of mixtures by this procedure assumes that the cooperativity of the transition simply scales with the composition in linear fashion. This is unlikely, as theoretical calculations show. In mixtures, the cooperativity is likely to be much lower than in the pure compounds [84].

We have therefore devised a new method for the determination of the temperatures for onset and end of melting, which is based on a simulation of the experimental DSC-curves. This procedure uses a regular solution model for non-ideal mixing in both, the ordered and the liquid-crystalline phase, and incorporates the additional broadening by assuming a simple two-state transition of limited cooperativity, with the cooperative unit size *c.u.* as an adjustable parameter. This model is still a simplification of the real situation as it is based on the assumption that the cooperativity does not depend on temperature [84]. Nevertheless, this procedure seems to be more reliable for the determination of the phase boundaries as the arbitrariness in determining the onset and end of melting temperatures is replaced by a more objective procedure.

The method for calculation of the heat capacity curves will now be outlined in a condensed form. The reader is referred to the original publications for further details [80,85-87].

For a binary system with components A and B the molar enthalpy H in the phase transition region from the gel (g) to the liquid-crystalline (l) phase can be described by:

$$H = \varphi H_g + (1 - \varphi) H_l \qquad (1)$$

with H_g and H_l being the enthalpies in the gel and liquid-crystalline phase, respectively, and φ the degree of transition going from 1 to 0 in the liquid-crystalline phase. φ can be calculated from the lever rule:

$$\varphi = \frac{x - x_l}{x_g - x_l} \qquad (2)$$

with x_g and x_l being the mole fractions of component B in the solid and liquid-crystalline phase in equilibrium at a given temperature.

For non-ideal mixing in the two phases we can formulate two equations for the enthalpies H_g and H_l as a function of composition introducing an excess enthalpy ΔH^E:

$$H_g = x_A \cdot H_{g,A} + x_B \cdot H_{g,B} + \Delta H^E_g \; ; \; H_l = x_A \cdot H_{l,A} + x_B \cdot H_{l,B} + \Delta H^E_l \qquad (3)$$

Using the Gibbs-Helmholtz equation $\Delta G^E = \Delta H^E - T\Delta S^E$, two cases have been considered, the case with $\Delta S^E = 0$ gives $\Delta G^E = \Delta H^E$, the so-called regular solution [88] and the case with $\Delta H^E = 0$ is the athermal solution [89].

For the simulation of the *cp*-curves we will only use regular solution theory. The non-ideality of the system is caused by a non-zero ΔH^E.

The free excess enthalpy ΔG^E of mixing as a function of mole fraction x can be written as:

$$\Delta G^E = \Delta H^E = x \cdot (1-x) \cdot \{\rho_1 + \rho_2 \cdot (2x-1) + \rho_3 \cdot (2x-1)^2 + \rho_4 \cdot (2x-1)^3 + \ldots\} \qquad (4)$$

ρ_i are the non-ideality parameters describing the deviations from ideal mixing behavior. Positive non-ideality parameters indicate a tendency towards cluster formation of like mixing and with increasing ρ the system finally shows a miscibility gap and phase separation into two phases of different composition. Negative non-ideality parameters lead to complex formation of unlike molecules.

For the simulation of the *cp*-curves we have used a symmetrical formulation for the excess enthalpy for both phases:

$$\Delta G^E = \Delta H^E = x \cdot (1-x) \cdot \rho \qquad (5)$$

The *solidus* and *liquidus* curves are now calculated from the following two transcendental equations:

$$T = \frac{\Delta H_B + \rho_1 \cdot (1-x_1)^2 - \rho_g \cdot (1-x_g)^2}{\frac{\Delta H_B}{T_B} - R \cdot \ln\{x_1 / x_g\}} \qquad (6)$$

$$T = \frac{\Delta H_A + \rho_1 \cdot (x_1)^2 - \rho_g \cdot (x_g)^2}{\frac{\Delta H_A}{T_A} - R \cdot \ln\{(1-x_1)/(1-x_g)\}} \qquad (7)$$

with $x_A = (1 - x)$, $x_B = x$, ΔH_A and ΔH_B being the calorimetrically measured main transition enthalpies, and T_A and T_B the main transition temperatures of the pure components A and B [73,76,80].

With the definition of $cp_{id} = (\partial H\ \partial T)_p$ the heat capacity curves can be calculated from Equations. 1, 3 and 5 once the segments of the *liquidus* and *solidus* curves of the phase diagram are known.

The calculated cp_{id}-curves are calculated for true first order phase transitions with infinite cooperativity. In reality, the transition curves for pure lipids are broadened due to limited cooperativity which is even more decreased in lipid mixtures [84].

As the simplest model we assume a two-state transition between the solid and the liquid state:

$$G \rightleftharpoons L \tag{8}$$

where G and L denote the gel and the liquid-crystalline phase. The equilibrium constant for such a process is then defined as:

$$K = \frac{[L]}{[G]} = \frac{1-\Theta}{\Theta} \tag{9}$$

The brackets represent the amount of lipids in one of the states and Θ is the degree of transition going from 1 (all lipids in the gel state) to 0. With the van't Hoff equation

$$\left(\frac{\partial \ln K}{\partial T}\right)_p = \frac{\Delta H_{vH}}{R \cdot T^2} \tag{10}$$

we can calculate an expression for $(\partial\Theta/\partial T)$, describing the width of the transition as a function of the van't Hoff transition enthalpy ΔH_{vH} [24,80]. The cp_{id}-curve for infinite cooperativity is now convoluted with the broadening function $(\partial\Theta/\partial T)$ to obtain a corrected heat-capacity curve cp_{sim}:

$$cp_{sim} = cp_{id} \otimes \left(\frac{\partial Q}{\partial T}\right) \tag{11}$$

As a first example we show the experimental and calculated heat capacity curves for a system with almost ideal mixing behavior, namely the system DMPC/DPPC (see Figure 25). The dotted curves obtained from the simulations give good fits to the experimental curves.

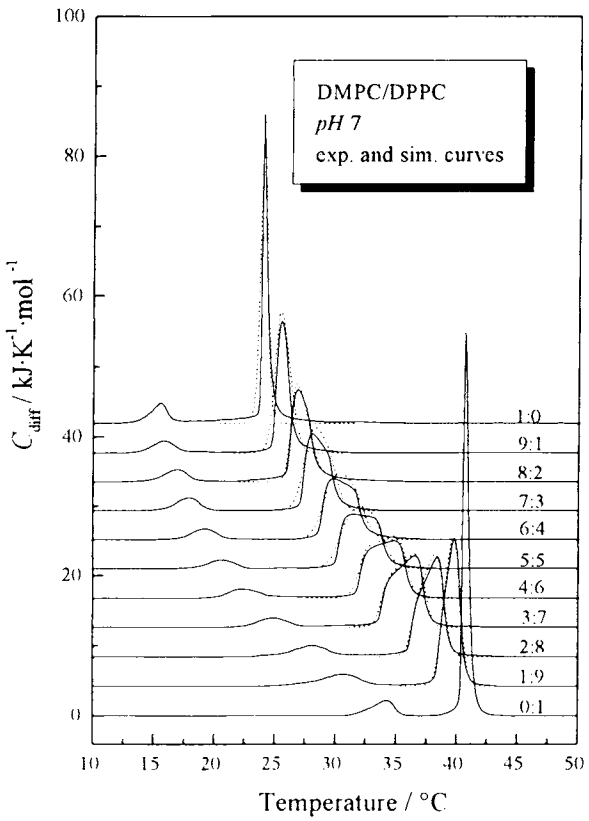

Figure 25. DSC curves of DMPC/DPPC mixtures as a function of composition (molar ratios). The dotted lines are the simulated curves calculated with the model described in the text [90].

Even for this almost ideal mixture the non-ideality parameters obtained from the simulation of the heat capacity curves show a concentration dependence, indicating that the mixing is non-ideal and non-symmetric. Figure 26 shows the phase diagram for this mixture. The up and down triangles are the temperatures *T(-)* and *T(+)* obtained from the simulations while the open and filled circles are the temperatures for onset and end of melting obtained by the usual empirical procedure described above. It is evident that the temperature values obtained from simulations lead to a phase diagram with a narrower coexistence range.

Because the simulation of the *cp*-curves indicated a non-symmetric, non-ideal mixing behavior, we recalculated the phase diagram using a regular solution model which accounts for this non-symmetric mixing behavior in both phases, yielding four non-ideality parameters:

$$\Delta G^{E} = \Delta H^{E} = x(1\text{-}x)[\,\rho_1 + \rho_2(2x - 1)] \qquad (12)$$

The equations of coexistence are in this case more complicated and are not shown here. The two parameter ρ_1 and ρ_2 for each phase describe the non-ideality as a function of x, where the parameter ρ_2 is responsible for the asymmetry.

The non-ideality parameters shown in Figure 26 were obtained by fitting the equations describing the coexistence curves to the *T(-)* and *T(+)* values (up and down triangles). Fitting to the empirical temperature values would lead to larger non-ideality parameters.

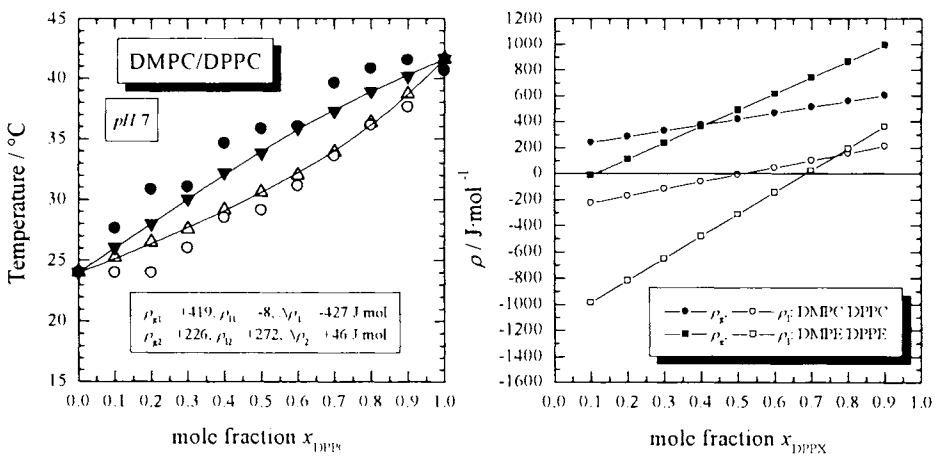

Figure 26. Left: Phase diagram obtained for DMPC/DPPC mixtures. The points for onset and end of melting obtained by the usual empirical procedure are indicated by open and filled dots, the triangles were obtained from the simulation of the DSC curves. The solid lines are fit curves through the triangles using the four parameter model described in the text. Right: Non-ideality parameters as a function of composition as obtained from the simulation of phase diagrams of DMPC/DPPC and DMPE/DPPE (not shown) [90].

In almost all cases of pseudo-binary phospholipid mixtures, we found that the non-ideal mixing is also non-symmetric, so that this four parameter model gave the best fits to the experimental data. An illustration of how the shape of the phase diagram can change, when the asymmetry of mixing is increased due to increased ρ_{g2} and ρ_{l2} values for the gel and liquid-crystalline phase, respectively, is shown in Figure 27.

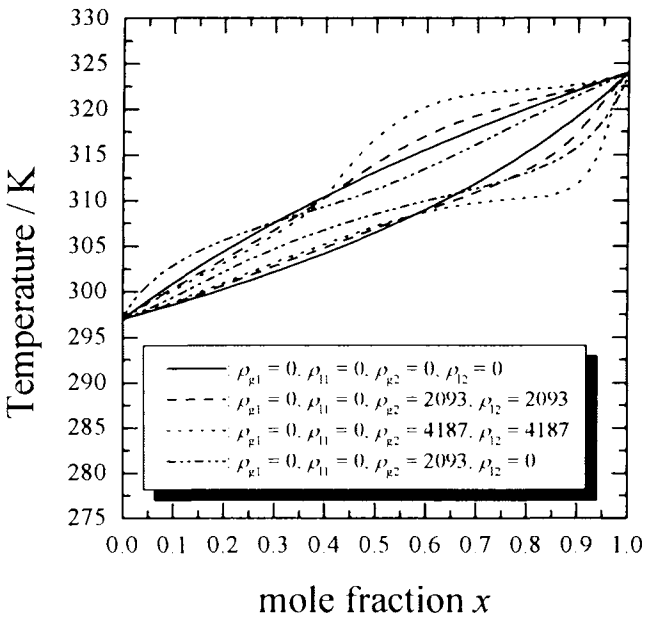

Figure 27. Calculated phase diagrams with different values for the asymmetry parameter ρ_{l2} and ρ_{g2} in J·mol^{-1}.

We have systematically investigated various mixtures of phospholipids differing in headgroup structure and chain length. The details of these investigations are found in the relevant publications [80,85-87,90].

Some important aspects of the mixing behavior of selected systems should be mentioned. Non-ideal mixing is not only found for lipids in the ordered gel phases but also for liquid-crystalline lipids. Gel phase immiscibility and phase diagrams which are of the peritectic or eutectic type are regularly observed when the two lipids in the mixture have differences in chain length of 4 or more CH_2-groups or when the gel phase structures are different. For instance, lipids that form inter-

digitated gel phases or quasi-crystalline L_c- or $L_{c'}$-phases usually do not mix with lipids forming L_β- or $L_{\beta'}$-phases. An example for gel phase immiscibility with probably eutectic behavior is shown in Figure 28 for the system 1,2-di-11-cyclohexylundecanoyl-phosphatidylcholine (11cyPC) and 1,2-di-13-cyclohexyltridecanoyl-phosphatidylcholine (13cyPC), both lipids with ω-cyclohexyl fatty acids of different chain length. The gel phase structure of these lipids is still not known but probably of the $L_{c'}$-type with strongly tilted chains to accommodate the simultaneous packing of the alkyl chains and the ω-cyclohexyl rings at the chain ends. Numerous other examples of gel phase immiscibilities of lipids are now known and the reader is referred to the original publications [91-98].

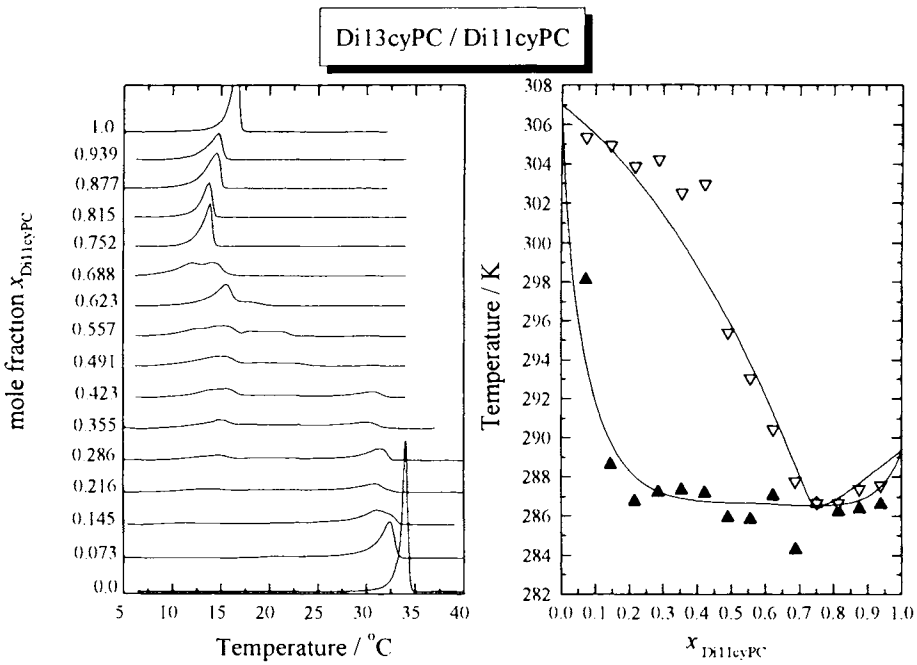

Figure 28. DSC curves and phase diagram of 1,2-di-11-cyclohexylundecanoyl-phosphatidylcholine (11cyPC) and 1,2-di-13-cyclohexyltridecanoyl-phosphatidylcholine (13cyPC), showing eutectic behavior [87,91].

The mixing behavior in systems, where one of the compounds is charged can be strongly influenced by varying the *pH* of the suspension and thus the headgroup charge. In mixtures of DMPA with DPPC, partial protonation of the PA component leads to phase diagrams with an upper azeotropic point or even a miscibility gap in the liquid-crystalline L_α-phase [85]. The non-ideality parameter for

the liquid-crystalline phase is strongly positive. The DSC thermograms and the resulting phase diagram for this system is shown in Figure 29.

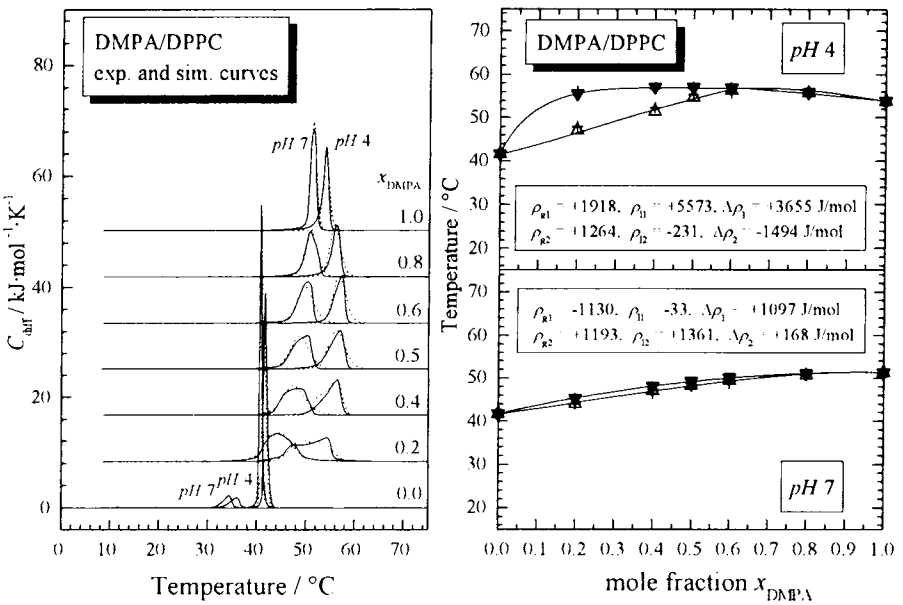

Figure 29. Left: DSC curves of DMPA/DPPC mixtures at *pH* 7 and at *pH* 4, in the partly protonated form of DMPA. Right: Phase diagrams and non-ideality parameters obtained from calculations based on the *T(-)* and *T(+)*-values obtained from the simulation of the *cp*-curves (left: dotted lines). At *pH* 4, the shape of the phase diagram indicates lipid immiscibility in the liquid-crystalline phase (adapted from reference [85]).

The finding that positive non-ideality parameters can be found for liquid-crystalline lipid mixtures and that even immiscibility in the liquid-crystalline phase is possible is particularly important in relation to the mixing behavior of lipids in biological membranes. This and other examples show that in pure lipid systems clustering of like lipids and even domain formation and demixing can be induced by modifications of the headgroup interactions [85,86]. The previously observed immiscibility in lipid bilayers was always restricted to gel state bilayers and occurred in those systems, where either large chain length differences were present, or the gel phases formed by the two pure compounds were incompatible. Immiscibility in the fluid L_α-phase, however, is not so much caused by differ-

ences in chain length or chain structure of the two lipids, but mainly by differences in headgroup interactions, and these can be modulated by molecules or ions present in the water phase.

2.2.3. Lipid-protein interactions

Biological membranes are composed of lipids and proteins, the lipids building up the bimolecular leaflet, which is the major permeability barrier, and the proteins providing the essential biological functions. The proteins can be either intrinsic proteins embedded in the lipid bilayers and having accessible polar surfaces on both sides of the bilayer, or they are mainly bound to the bilayer surface by electrostatic interactions. When proteins are incorporated into lipid bilayers or bound to the surface of the lamellae, the lipid packing in the gel phase is perturbed and the transition profiles obtained by DSC are changed in a characteristic way. Numerous studies of lipid-protein interactions have been performed in the past and the effects on the DSC transition curves have been modeled [99-104].

The effects observed with various proteins depend on the nature of the interaction. Intrinsic proteins can either preferentially associate with gel state lipids or with liquid-crystalline lipids. When a preferential association with gel state lipids occurs, the DSC peaks become a more and more pronounced shoulder at the high temperature side of the peaks. For a preferential association with liquid-crystalline lipids, this effect is reversed. However, peripheral association of proteins or peptides to the surface of the bilayers, can also lead to high temperature shoulders, so that a distinction between different modes of binding becomes difficult. In reality, larger proteins can bind to the surface with their hydrophilic domains through electrostatic interactions, but at the same time also insert hydrophobic sequences into the bilayer. The overall effect on the shape of the DSC peaks is then difficult to predict. Therefore, DSC measurements on lipid-protein interactions mainly serve as a qualitative indicator for protein binding or insertion, as judged from the change of the shape of the DSC peaks.

As an example for the change occurring when proteins are bound to the surface of lipid vesicles we show DSC curves of unilamellar vesicles of DMPC with various other lipids before and after binding of the GM2 activator protein, which is essential for the enzymatic processing of the ganglioside GM2 in lysosomes by the protein β-hexose-aminidase [105,106]. This activator protein binds specifically to gangliosides, but also by electrostatic interactions to negatively charged surfaces. Figure 30 shows some examples for different mixtures. In all cases, the DSC curves show shoulders on the high temperature side of the original peak. This can be interpreted that mainly binding to the

surface occurs and no insertion into the lipids bilayers [107]. Experiments with lipid monolayers support these findings.

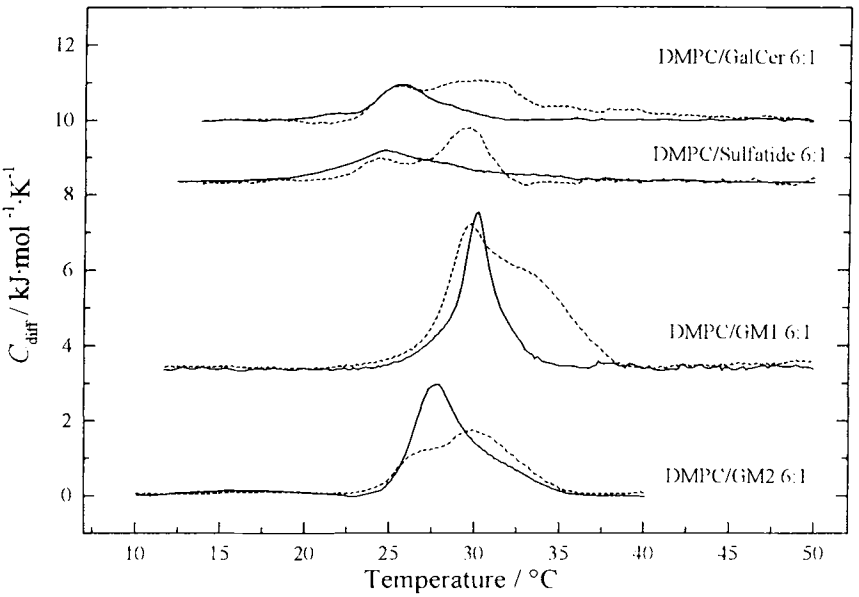

Figure 30. DSC curves of unilamellar vesicles of DMPC with different proportions of other lipids as indicated. Solid curves: before, dotted curves: after addition of the GM2 activator protein. With pure DMPC vesicles, only a minor shift of the DSC peak to slightly lower temperature is observed [107].

2.2.4. Lipid-surfactant mixtures

Lipid-surfactant mixtures have gained much interest in context with the solubilization of membranes and with the problem of reconstituting membrane proteins into artificial membrane systems such as unilamellar vesicles. For the "solubilization" of membranes, a sufficiently high concentration of an aqueous micellar solution has to be added to the membrane suspension, so that the bilayers are transformed into mixed micelles containing surfactant, membrane lipids, and membrane proteins. This "solubilization" process is quite complicated and the necessary amounts of surfactant for complete solubilization depends on the nature of the surfactant, the type of membrane, and the total concentration of lipid and surfactant.

For a better understanding of this process, experiments with model membrane systems have been undertaken and an overall picture has emerged for the low concentration regime of lipid and surfactant, which can be described as follows.

Addition of surfactant molecules to lipid vesicles first leads to a partitioning of the surfactant into the lipid bilayers, an equilibrium is established, the partition coefficient depending on the nature of the lipids in the membrane and the chemical structure of the surfactant. Further increase of the total surfactant concentration leads finally to a saturation of the bilayers with surfactant molecules and first mixed micelles of a different surfactant to lipid ratio appear. Over a certain concentration range mixed bilayers and mixed micelles coexist until finally all bilayers have been transformed into micelles.

This process can be easily followed by titration calorimetry, as described below. In particular, the partition coefficients and the boundaries of the coexistence region can be determined. In addition, the thermodynamic quantities obtained from these calorimetric experiments provide new insight into the molecular interactions in these systems.

DSC studies of lipid-surfactant mixtures in the regime of low surfactant concentrations provide some insight into the partition coefficient of the surfactant molecule between water and the bilayer. We have systematically studied the behavior of DMPC/octylglucoside (DMPC/OG) mixtures by ITC and DSC. The results of the ITC experiments will be described below. Figure 31 shows as an example some DSC curves of DPPC/OG mixtures as a function of total OG concentration. First, a decrease of the transition temperature due to preferential OG partitioning into the L_α-phase bilayers is observed.

In principle, the partition coefficient can be calculated from this decrease in T_m [108]. However, ITC experiments and also experiments using fluorescent probes have shown that the partition coefficient is a function of OG concentration in the bilayer, decreasing with increasing surfactant saturation of the bilayer. The approach using DSC curves therefore leads to incorrect results. A further increase of the OG concentration to values where partial or complete micellization for liquid-crystalline bilayers is observed, still leads to DSC curves with a clear endothermic peak, which is now almost independent of total OG concentration. Obviously, the mixed micelles formed at higher temperatures convert to bilayer phases upon cooling and the phase behavior at lower temperature is more complicated.

Systematic studies of the phase behavior of lipid-surfactant systems have been performed particularly on mixtures of surfactants of the $C_{12}EO_n$ type and phosphatidylcholines with different chain lengths and saturation [109-113]. The phase diagrams of these pseudo-binary mixtures in excess water are complicated and become even more so when the water content is varied.

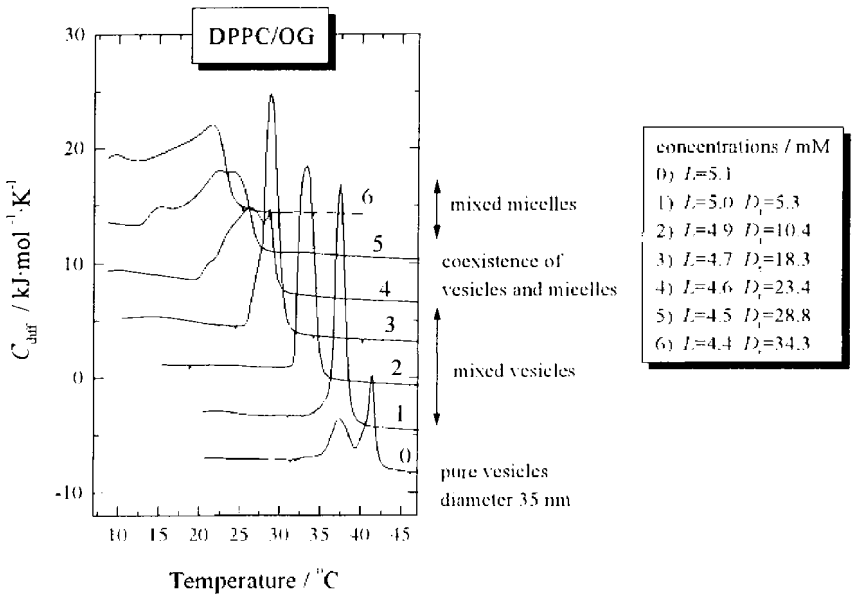

Figure 31. DSC curves of DPPC/OG mixtures at different concentrations and mixing ratios as indicated on the right hand side in the box (L = DPPC, D_1 = OG). The arrows indicate the ranges where vesicles and micelles are the stable form at a temperature above the T_m value of pure DPPC, i.e. at 50°C (M. Keller and A. Blume, unpublished).

3. ISOTHERMAL TITRATION CALORIMETRY (ITC)

High sensitivity isothermal titration calorimetry has become more and more popular for studying heats of reaction observed upon binding of ions and molecules to membranes and the incorporation or partitioning of molecules into membranes. Also, phase changes in lyotropic systems triggered by the addition of molecules or ions to the aqueous lipid dispersion can be studied. Examples are *pH*-induced phase transitions in lamellar phases and surfactant induced micellization of lamellar phases. The application of ITC for biological questions has particularly benefited from the availability of commercial instruments, such as those developed by MicroCal Inc., namely the OMEGA and the MCS-ITC systems [114].

In titration calorimetry, the experimental procedure is usually as follows: The cell (volume of ca. 1-2 mL) is filled with reactant A, and the other reactant B is injected into the solution in aliquots of 2-25 μL using a microliter syringe. Approximately 10-25 injections are usually performed with waiting times between injections of 5-20 min, depending on the kinetics of the reaction. The observed heat signals are then evaluated as a function of concentration of B in the cell or as a function of molar ratio B/A. These experiments can be performed in a temperature range between 2 and 80°C to determine the temperature dependence of the reaction enthalpy.

Depending on the specific problems to be studied, it is often advantageous to perform also the reversed type of experiment, namely adding reactant A to a solution of B in the cell. Here, the heat of reaction is determined as a function of concentration of A. Both experiments are complementary and the data should be fitted with one and the same particular binding model.

In many cases where the solubility of one of the components is very low, only one of the two experiments is possible, the solution of the reactant with the low solubility has to be filled into the cell, because otherwise the heats of reaction are too low to be detectable.

3.1. Isothermal phase transitions

As already mentioned above, some phospholipids show a *pH*-dependent phase behavior. For instance, phosphatidic acids can be deprotonated at high *pH*-values, the phase transition temperatures of the $L_\beta \rightarrow L_\alpha$ phase transition is lowered [29,30]. Therefore, it is possible to trigger the phase transition from the L_β- to the L_α-phase by injecting NaOH into a suspension of DMPA-vesicles at constant temperature. The titration experiment performed in this way as a function of temperature yields the heat of dissociation in the L_α-phase (high temperature) or the L_β-phase (low temperature). In between these temperatures, the heat of reaction for the dissociation is superimposed by the phase transition heat. An example is shown in Figure 32 for the reaction [30]:

$$DMPA^- + OH^- \rightarrow DMPA^{2-} + H_2O \qquad (13)$$

The titration curves in the high and low temperature region, where no phase transition is induced by the reaction can be simulated to determine the intrinsic pK_2-value for the dissociation of the second proton of DMPA. For a simulation it is necessary to use the Gouy-Chapman theory to calculate the proton concentration in the vicinity of the bilayer surface. This is different from the bulk concentration due to the formation of the electrical double layer. Using this approach, the intrin-

sic pK_2, which is lower than the apparent pK-value, can be calculated. Simulated titration curves fitting the experimental data with the pK-values indicated are shown in Figure 33. The intrinsic pK_2 turns out to be dependent on the state of the bilayer and is slightly lower than the value expected from solutions of phosphodiesters, such as glycerophosphate, particularly at high temperature [30].

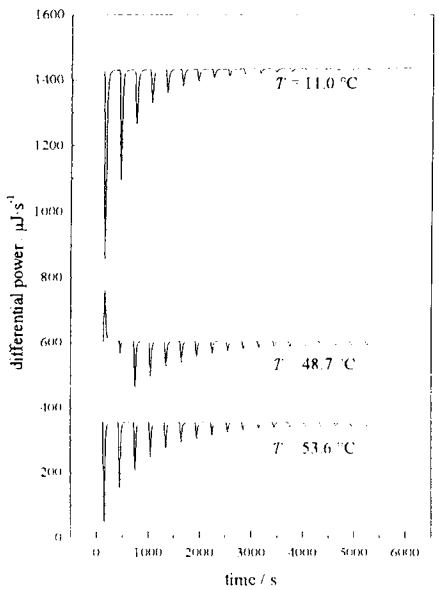

Figure 32. Titration curves of 1.4 mL 1 mM DMPA vesicles with 0.1 N NaOH. The curve at 48.7°C has a deviation due to the *pH* induced transition from the gel to the liquid-crystalline phase (adapted from reference [30]).

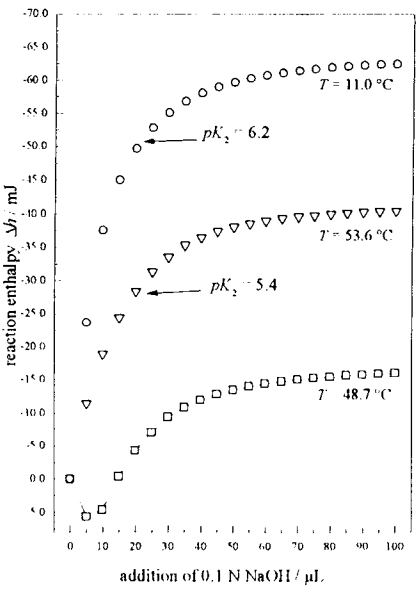

Figure 33. Integral reaction enthalpies from the experiment shown in Figure 32. The dotted curves were calculated using the Gouy-Chapman theory. The curve at 48.7°C could not be simulated due to the contribution of the transition enthalpy (adapted from reference [30]).

In the reversed type of experiment, the DMPA vesicle suspension is injected into an aqueous solution at *pH* 12. In this type of experiment the OH^- concentration is so high that it does not change significantly during the titration, because only small amounts of DMPA are titrated into the solution. The titration peaks then all have the same area. The total heat of reaction observed here is comprised

of the heat of neutralization, the heat of dissociation, and, depending on temperature, the phase transition heat (see equation (13)). Figure 34 shows the heat of reaction as a function of temperature after subtraction of the heat of neutralization.

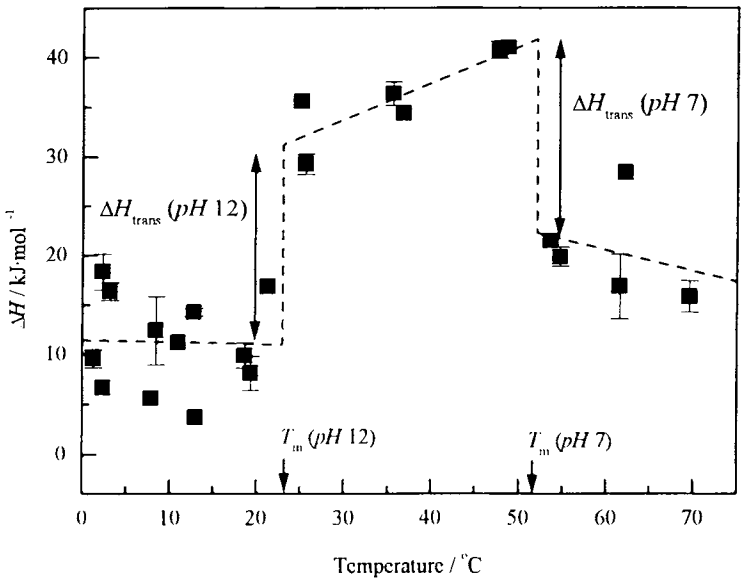

Figure 34. Total heat of reaction after subtraction of the heat of neutralization of the reaction of equation (13). The double arrows denote the transition enthalpies from the gel to the liquid-crystalline phase for $DMPA^-$ and $DMPA^{2-}$ (adapted from reference [30]).

It is clearly evident that in the temperature interval from 25-50°C, an additional endothermic effect due to the transition from the gel to the liquid-crystalline phase is superimposed. The difference between the higher and lower levels of the reaction heat corresponds to the transition enthalpies of the singly and doubly charged DMPA, respectively. The temperature dependence of the heat of dissociation in the low and high temperature region is small. This is characteristic for ionic reactions. However, in the intermediate temperature range, where the transition enthalpy is superimposed, the slope is positive and much more significant. The positive Δcp observed here can be explained by changes in hydration of the interfacial region of the bilayers, including hydrophobic surfaces, due to the triggering of the gel to liquid-crystalline phase transition. Additional hydration of the

doubly charged phosphate group would only lead to negative Δcp-values. Apparently, this is overcompensated by the hydration of hydrophobic parts of the molecule when the lipid molecules become less tightly packed in the liquid-crystalline phase.

3.2. Heats of ion binding

Similar experiments as with OH^- can be performed with other ions, such as Mg^{2+}, Ca^{2+}, Sr^{2+}, or trivalent cations, which bind to negatively charged phospholipid headgroups and more weakly to zwitterionic headgroups. In most cases, the phase transition temperatures are shifted to higher values, when cations are bound. Therefore, induced by cation binding, the heats for isothermal phase transitions are observed, in addition to the heat of cation binding. In contrast to experiments where acid or base is injected into the cell, the addition of aliquots of a Ca^{2+} solution to $DMPA^-$ vesicles leads to badly reproducible results. After binding of Ca^{2+} to the outside of the vesicles, these become susceptible to fusion and aggregation. The dispersion settles and further addition of aliquots of a Ca^{2+} solution to the already precipitated dispersions is difficult, a thermodynamic equilibrium cannot be reached despite continuous stirring of the solution in the cell.

Because of these effects, only the reversed experiment is possible, the addition of lipid vesicles to a solution of excess Ca^{2+} in the cell. Here, the reaction proceeds fast enough, because the vesicles are immediately ruptured by the ion binding due to the osmotic gradient. The total heat of reaction observed for each of the injections is reproducible and the same. In Figure 18, the effect of Mg^{2+} on the phase behavior of $DMPA^-$ was shown as revealed by DSC. Clearly, a shift of the phase transition to higher values was observed in an excess of Mg^{2+}.

The results of ITC experiments for binding of Mg^{2+} to $DMPA^-$ is shown in Figure 35 [90]. Three different temperature regimes are evident. Below 50°C, Mg^{2+} binding to $DMPA^-$ is endothermic and the binding enthalpy decreases with temperature. Between 50°C and 57°C the exothermic reaction enthalpy is mainly caused by the transition enthalpy from the L_α to the gel phase (L_β ?). This is again an isothermal phase transition, induced by ion binding, but in this case from a fluid to a gel phase, in contrast to the phase transition induced by OH^- described above. At temperature higher than 57°C, the binding enthalpy is slightly endothermic and increases with temperature. In this temperature range the bilayers remain in the L_α-phase after Mg^{2+} binding under these particular experimental conditions.

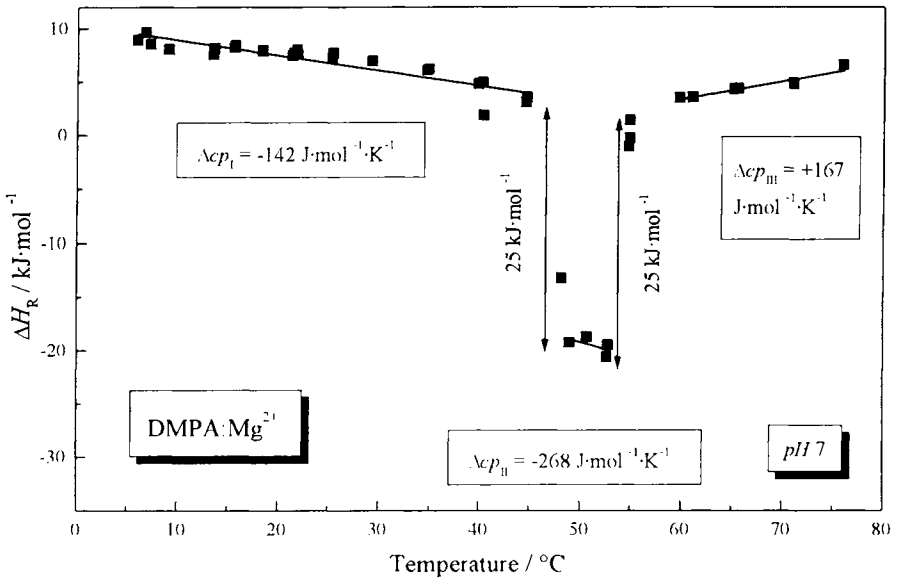

Figure 35. Total reaction enthalpy observed when titrating a 20 mM DMPA vesicle suspension at *pH* 7 into 100 mM $MgCl_2$. The heat of dilution was determined in a separate experiment and subtracted [90].

The slope of the ΔH vs. T curves is due to differences in the heat capacity Δcp of the two forms. The negative Δcp found at low temperature for binding of Mg^{2+} to gel phase bilayers is characteristic for all negatively charged phospholipid systems studied so far. The binding of divalent cations to phosphoester and phosphodiester groups of water soluble molecules, such as mono- and polynucleotides, or glycero-1-phosphate and glycero-1-phospho-glycerol, the latter being representative of the lipid headgroups of PA and PG, is normally endothermic and has a positive Δcp of 30-85 J·mol^{-1}·K^{-1} [90]. This positive Δcp is explained by the liberation of water from the negatively charged phosphate groups when the divalent cations bind and share the water of hydration. The negative Δcp found for binding to lipid bilayers can only be explained when it is assumed that also water in contact with hydrophobic surfaces is released. This is quite likely, because binding of divalent cations usually induces tighter packing of the chains in the hydrophobic region. This effect is even increased in the intermediate tem-

perature regime where a transition from the liquid-crystalline to the gel phase is induced. At high temperature, the slope becomes positive. Here Δcp is positive and similar to the values found for cation binding to water soluble model compounds.

The ITC experiments agree well with the DSC experiments shown in Figure 18 for the change of the phase transition as a function of Mg^{2+} concentration. This applies to the transition temperatures as well as to the ΔH-values of the phase transition (double arrows in Figure 35). The binding of Sr^{2+} produces similar effects. Only Ca^{2+} is again different, it induces metastable phases in the high temperature region, an effect also observed in the DSC curves [90].

3.3. Heats of incorporation of hydrophobic molecules

Purely hydrophobic compounds partition easily into bilayers. Because of their low water solubility, however, it is difficult to perform titration experiments. The only possible experimental approach is the titration of a lipid vesicle suspension into a very dilute aqueous solution of the hydrophobic compound in the cell. Many experiments have been performed with simple model compounds, such as indole derivatives using dialysis methods [115]. The enthalpy of incorporation was then determined from the temperature dependence of the partition coefficient. This is inherently less precise than a direct calorimetric determination. On the other hand, when the concentrations of the hydrophobic molecules are small, then a determination of the partition coefficients becomes difficult. The transfer enthalpies are then still accessible, though with limited precision.

Figure 36 shows titration experiments of 0.1 mM indole, N-methyl-indole, and 3-methyl-indole with 2 mM POPC vesicles. The transfer enthalpies are negative with -4.2, -2.5, and -5.0 $kJ \cdot mol^{-1}$ for these three hydrophobic molecules. These values are smaller than those determined from the temperature dependence of the partition coefficient [115]. The Gibbs free energies for transfer are -32, -34, and -36 $kJ \cdot mol^{-1}$, respectively. This means that the partitioning is mainly driven by entropy, because the $T\Delta S$ term is strongly positive with ~29.3 $kJ \cdot mol^{-1}$. This is not surprising, because at room temperature the preferential partitioning of hydrophobic molecules into organic solvent or other hydrophobic surroundings is almost exclusively driven by an entropy gain [11] due to the restructuring of water molecules previously in contact with hydrophobic surfaces. Similar effects are found for the self-association of surfactants into micelles (see below).

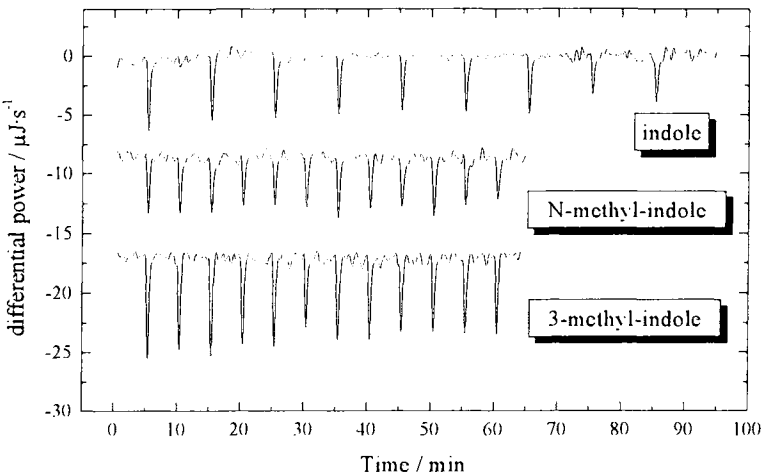

Figure 36. Titration experiments with indole derivatives at 0.1 mM in the calorimetric cell, titrated with 2 mM POPC in 10 mM Hepes, 50 mM KCl, *pH* 7 at a temperature of 25 °C (M.A. Requero and A. Blume, unpublished results).

Polyene antibiotics such as amphotericin, nystatin, or filipin are examples of mainly hydrophobic molecules that also have polar groups. In water, these cyclic molecules tend to aggregate to shield their hydrophobic surfaces from water. These compounds are readily incorporated into natural as well as model membranes and tend to aggregate in the bilayer, now in a reversed manner, i.e. shielding their polar groups from the hydrophobic interior of the membrane. The antibiotics form complexes with sterols and act as membrane active compounds in the sense that the bilayers become leaky [116,117].

Figure 37 shows experimental data for filipin incorporation into DMPC membranes as a function of the total DMPC concentration. The data can be fitted with a model assuming partitioning of the filipin molecules into the membranes with an exothermic reaction enthalpy and aggregation of filipin to tetramers in the membrane. This model seems still to be to crude too describe the experimental data in full detail, but in principle, an analysis is possible. Using a simple partitioning equilibrium without aggregation in the membrane does not give better fits. We chose this model, because it is known that these polyene antibiotics aggregate in the membrane. However, it is likely that there are already aggregates in water which have to dissociate before they can enter the membrane. The exothermic reaction enthalpy for partitioning can be explained by the assumption that the in-

corporation of these molecules leads to partial ordering of the lipid chains [117]. Purely hydrophobic effects would lead to much smaller enthalpies of incorporation (see above).

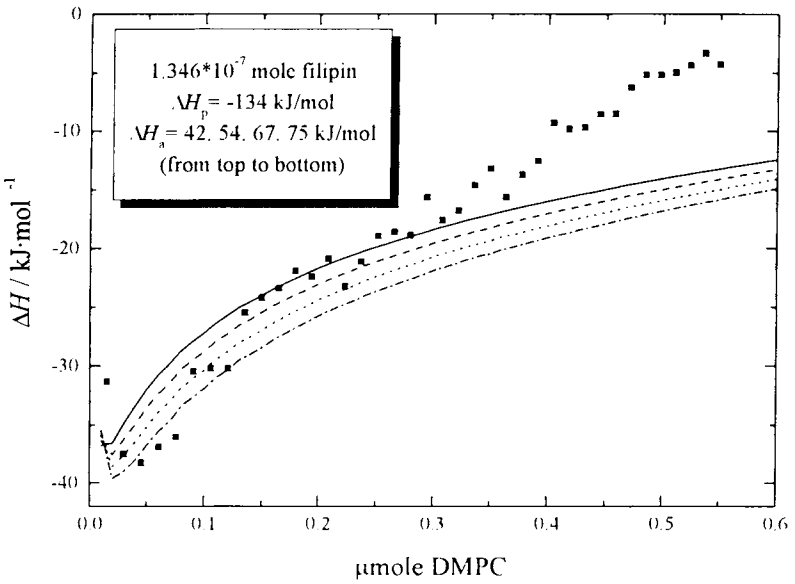

Figure 37. Experimental points and calculated curves for the titration of filipin with DMPC vesicles at 30°C. The model calculations used a fixed partition coefficient of 4000 and a tetramer aggregation constant of 10 $(L/mol)^3$. The aggregation enthalpy ΔH_a was varied and the enthalpy for transfer from water to the bilayer ΔH_p was kept constant (adapted from reference [117]).

3.4. Lipid-surfactant interactions

3.4.1. Demicellization of surfactants

By far the most detailed thermodynamic analysis of binding to or incorporation of molecules into membranes has up to now been formulated for the binding or incorporation of surfactants into lipid bilayers, including the solubilization phenomenon. There is a simple reason for this: surfactants and synthetic lipids of high purity are available in large quantities and the experimental titration curves are highly reproducible because the reactants remain "soluble" in the sense that no macroscopic settling occurs. In addition, the reactions are fast on the time

scale of the experiments so that short waiting times can be used and the integration of the calorimetric peaks is precise.

The heat effects observed when surfactants are incorporated into membranes arise mainly from changes in "hydrophobic hydration", i.e. a change of the water exposure of hydrophobic groups when a surfactant monomer in water is transferred into a hydrophobic surrounding, i.e. the bilayer. This heat of reaction is strongly temperature dependent and usually changes sign at a temperature of 20-30°C when no other heat effects are superimposed.

An example where these characteristic changes are easily observable, are titration experiments with micellar solutions of surfactants which are titrated into the vessel filled with pure water. Initially, dilution of the micellar solution leads to complete demicellization. When the concentration of monomers in the cell approaches the critical micellar concentration (*cmc*), the heat effect connected with the transfer of surfactants from the micelle to the aqueous solution disappears and the heat of reaction approaches zero [118-123].

Figure 38 shows the results of demicellization experiments with the negatively charged surfactant sodium lauroyl-alaninate (SLA) at different temperatures (A. Blume, M. Ambühl, and H. Watzke, unpublished results). It can be seen that the heat effect due to demicellization changes sign close to a temperature of 35°C. Similar curves are obtained for a variety of other surfactants. However, the temperature where $\Delta H = 0$ varies with the headgroup structure of the surfactant. For anionic and cationic surfactants the temperature is usually between 20 and 30°C, whereas for non-ionic surfactants, such as octylglucoside (OG), it is close to 50 °C [123]. The *cmc* can be easily and precisely determined from the first derivative of the curves shown in Figure 38. The *cmc* is slightly temperature dependent and has a minimum where the demicellization enthalpy is zero.

From the temperature dependence of the *cmc* as well as the enthalpy of demicellization it is possible to calculate the demicellization entropy and its temperature dependence using the Gibbs-Helmholtz relation $\Delta G \quad \Delta H - T\Delta S$. A plot of all three thermodynamic parameters as a function of temperature is shown in Figure 39 for the anionic surfactant sodium lauroyl-alaninate (SLA). It is clearly evident that the ΔG-value for demicellization of SLA shows only a weak temperature dependence whereas the two terms ΔH and $T\Delta S$ are strongly temperature dependent in a similar way. This type of "enthalpy-entropy" compensation is quite common for phenomena where changes in "hydrophobic hydration" are involved, because a considerable increase in heat capacity occurs when hydrophobic groups are exposed to water (see below) [124-131].

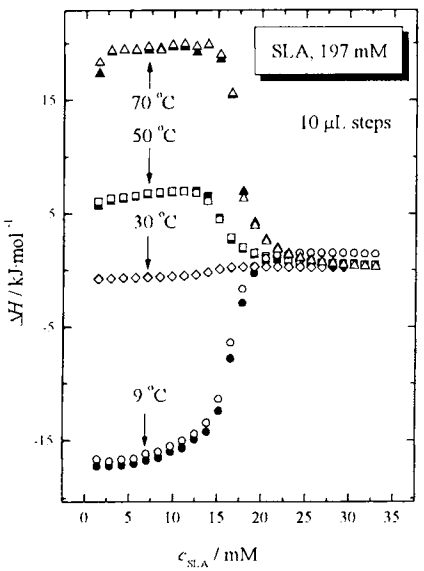

Figure 38. Heats of reaction observed by dilution of 197 mM micellar SLA into water (A. Blume, M. Ambühl, H. Watzke, unpublished results).

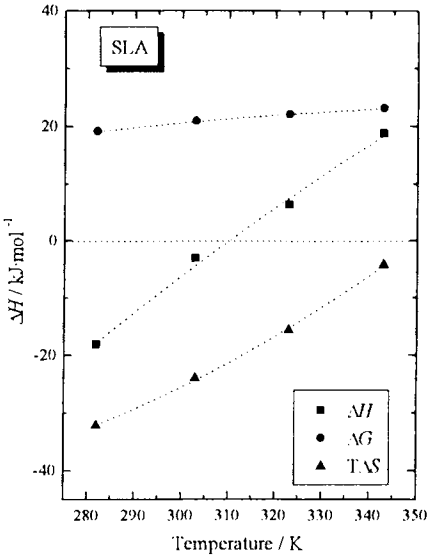

Figure 39. Enthalpy, Gibbs free energy, and entropy term for the demicellization of SLA as a function of temperature (A. Blume, M. Ambühl, H. Watzke, unpublished results).

The $T\Delta S$ term approaches zero at a relatively high temperature where a maximum of ΔG is observed. At the temperature where ΔH is zero, the driving force for micellization is purely entropic in nature. This strong increase in ΔS, observed when hydrophobic moieties are removed from contact with water by self-association, is often described as a characteristic feature of the hydrophobic effect and is thought to be the only driving force for self-association. It is assumed that this is caused by a change in the properties of water molecules in the surrounding of hydrophobic groups, i.e. that they are more ordered than in bulk water. However, this explanation is too simple. Up to now, no direct experimental proof has been found for a higher order of water around hydrophobic moieties. In addition, as can be seen from Figure 38, the tendency for self-association is highest at high temperatures (130-150°C), where $\Delta S = 0$. Here, the driving force for self-association is purely enthalpic in nature [123,124,128,130].

From the slope of the ΔH vs. T curve the change in heat capacity Δcp can be determined. In a first approximation, Δcp is constant, at least over a temperature

range of 50°C. Δcp is positive, which is characteristic for the hydrophobic effect. This positive Δcp is the only reliable thermodynamic function which immediately makes it clear that a transfer of hydrophobic groups from a nonpolar solvent to water is taking place. It has been found for a large variety of compounds and different transfer reactions that Δcp is directly proportional to the hydrophobic surface exposed to water. For instance, for CH_2 - groups, Δcp was found to amount to 65-70 $J \cdot mol^{-1} \cdot K^{-1}$ per CH_2 group [132,133]. For the demicellization of surfactants, Δcp -values are observed which are lower than calculated from the number of CH_2-groups in the molecule. This means that already in the micelles some CH_2-groups are exposed to water, which agrees with the loose packing of surfactant molecules in the micelles and their highly curved surfaces [123,124].

3.4.2. Partitioning of surfactants into bilayers

When surfactants are added to lipid vesicles or natural membranes, they are incorporated into the membranes and, when the surfactant concentration is high enough, the membranes are disrupted or solubilized and mixed micelles of surfactant and membrane lipids are formed. These processes can easily be studied by ITC, provided a temperature is chosen, where the transfer enthalpies are not zero. The solubilization of lipid bilayer vesicles by surfactants has been commonly described by a model, in which three different stages occur and this is depicted in Figure 40 [134-137].

Starting at a certain concentration of lipids, the addition of surfactant first leads to a partitioning of the surfactant molecules into the lipid bilayers. This equilibrium can be described by a partition coefficient $P = x_b \; x_W$, the mole fraction ratio of surfactant in the bilayers x_b and in water x_W.

Further increase of the surfactant concentration leads to disruption of some vesicles at a concentration called D_t^{sat} and first mixed micelles are formed. The mole fraction at saturation of the vesicles is called x^{sat} and the mole fraction of surfactant in the micelles is x^{sol}. Therefore, we find a coexistence region of mixed vesicles of composition determined by x^{sat} and mixed micelles with composition x^{sol}.

Still further increase of surfactant concentration leads to a disappearance of vesicles till finally above the line called D_t^{sol} all vesicles have been transformed into micelles. The two lines enclosing the coexistence region are described by the equation

$$D_t^{\#} = R_e^{\#} \cdot L + D_W^{\#} \qquad (14)$$

where the # sign stands for "sat" or "sol", respectively and $R_e = D_b / L$ is the ratio of the surfactant concentration in the bilayer over the lipid concentration. The change in concentration of surfactant and lipid observed during this type of titration is shown as arrow (2) in Figure 40.

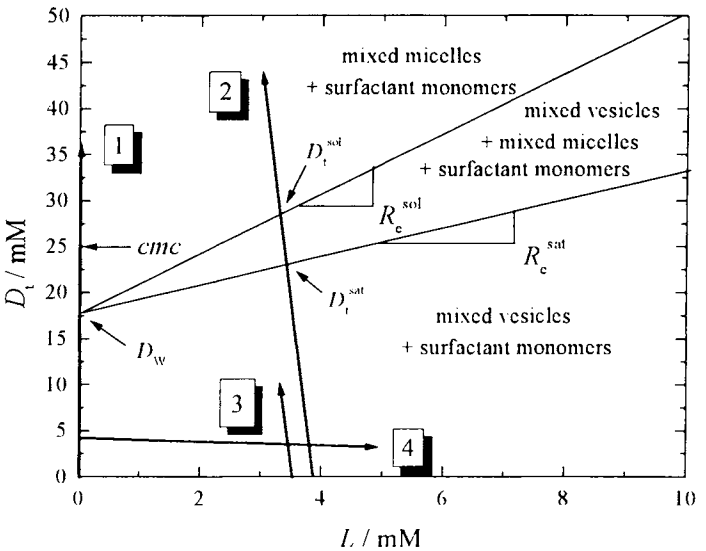

Figure 40. Schematic diagram describing the behavior of lipid/surfactant systems in the region of high water content. Arrow (1) describes the demicellization experiment, arrow (2) the solubilization, and arrows (3) and (4) the partitioning experiments.

Depending on the *cmc* of the surfactant and its partition coefficient P, experiments for determining P in the concentration regime where the vesicles are still stable, can again be performed in two different ways, namely titration of lipid vesicles to a monomeric surfactant solution or vice versa (arrows (3) and (4) in Figure 40). For the surfactant octylglucoside, both experiments are possible due to the high critical micellar concentration of this surfactant (ca. 25 mM). Figure 41 shows a partition experiment, where a solution of monomeric OG is titrated with DMPC vesicles at two different temperatures. Again, the characteristic change in sign of the transfer enthalpy ΔH^T is evident. At 70°C, $\Delta H^T < 0$, whereas at 27°C $\Delta H^T > 0$. It turns out that the transfer of an OG molecule from water to a lipid bilayer is connected with very similar heat effects as a transfer into a pure OG micelle, particularly when unsaturated PCs such as egg-PC or soy bean PC are used. For transfer into DMPC a slight difference is observed, appar-

ently caused by the more ordered hydrocarbon environment of DMPC with its saturated chains [138].

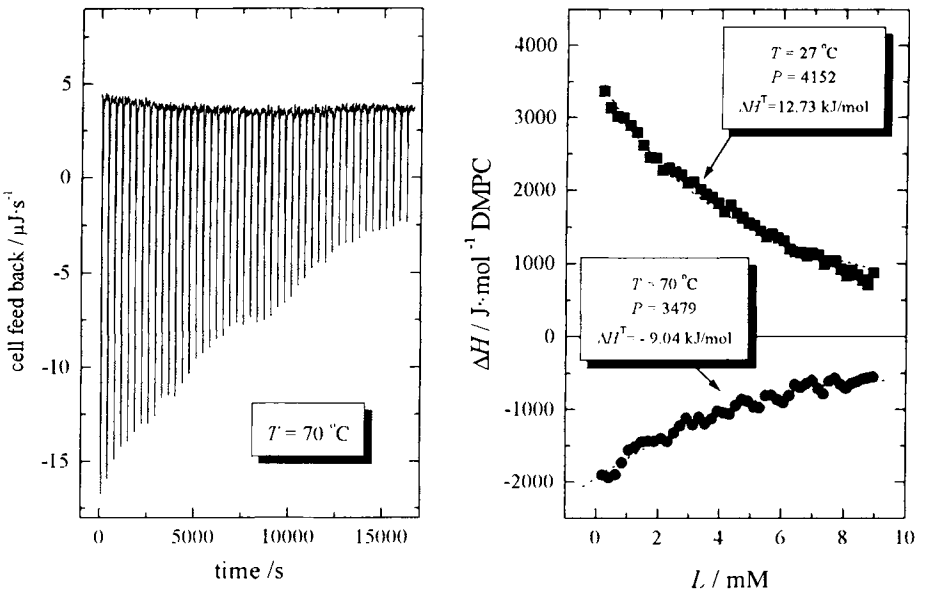

Figure 41. Left: Titration peaks obtained by titrating a 50 mM DMPC vesicle suspension into a 3 mM OG solution. Right: Normalized heats of reaction at 27 and 70°C. The dotted lines were fitted to the experimental points on the basis of equation (17). The obtained parameters are the partition coefficient P and the enthalpy of transfer ΔH^{T} [138].

From the titration curves, the relevant parameters of the partition coefficient P and the transfer enthalpy ΔH^{T} can be extracted using the appropriate models. These have been described in detail in the original publications as well as in a recent review [138-141]. Here we will only give a shortened version of the derivation. The definition of the partition coefficient in mole fraction unit is:

$$P = \frac{D_b \cdot (D_W + W)}{(D_b + L) \cdot D_W} \tag{15}$$

With $D_W = D_t - D_b$ with D_t being the total surfactant and W the water concentration and using the approximation $D_W + W \approx W$ one finds [138,139]:

$$D_b = \frac{1}{2P}\left[P \cdot (D_t - L) - W + \sqrt{P^2 \cdot (D_t + L)^2 - 2 \cdot P \cdot W \cdot (D_t - L) + W^2}\right] \tag{16}$$

To determine the change of the surfactant concentration D_b in the lipid bilayer occurring upon injection of ΔL moles of lipid to the surfactant monomers, we have to differentiate equation (5) with respect to L:

$$\frac{\Delta D_b}{\Delta L} = -\frac{1}{2} + \frac{P \cdot (D_t + L) + W}{2 \cdot \sqrt{P^2 \cdot (D_t + L)^2 + 2 \cdot P \cdot W \cdot (L - D_t) + W^2}} \tag{17}$$

Two effects are considered to contribute to the observed heat of reaction Q. One is the incorporation of the surfactant monomers into the lipid bilayer and the other is the dilution of the vesicular dispersion. The observed heat of reaction Q is then related to equation (17) by [138,139]:

$$Q = \frac{\Delta D_b}{\Delta L} \cdot \Delta H^T + \Delta H_{dil} \tag{18}$$

The term ΔH_{dil} accounts for the dilution enthalpy observed upon titration of lipid vesicles into the surfactant solution and can be determined in a separate experiment by titrating lipid vesicles into water. When the reversed experiment is performed, i.e. the titration of a monomeric surfactant solution to a vesicles suspension in the cell, then equation (16) has to be differentiated with respect to D_t and one obtains:

$$\frac{\Delta D_b}{\Delta D_t} = +\frac{1}{2} + \frac{P \cdot (D_t + L) - W}{2 \cdot \sqrt{P^2 \cdot (D_t + L)^2 + 2 \cdot P \cdot W \cdot (L - D_t) + W^2}} \tag{19}$$

The observed heat of reaction is then calculated in an analogous manner to equation (18). Here the dilution term is determined from diluting surfactant monomers into water.

These equations are only valid, if the partition coefficient is not a function of concentration of the surfactant in the bilayer and the heat of transfer is also independent on the surfactant concentration, i.e. assuming ideal behavior. These assumptions usually apply only over a small concentration regime of x_b. For titration curves covering a wider range up to the saturation concentration x^{sat} one has to

take into account non-ideality effects. This can be done in several ways, the simplest ones are to introduce a non-ideality parameter ρ and use a regular solution or athermal solution model for non-ideal mixing of surfactant with bilayers. The partition coefficient then becomes concentration dependent in the following form [138]:

$$P = P(x_b = 1) \cdot \exp\left[-\rho \cdot (1 - x_b)^2 / RT\right] \tag{20}$$

The equations and their derivatives become then more complicated, the formulations of the relevant equations are found in the original publications [138-146].

3.4.3. Solubilization of membranes by surfactants

The solubilization of membranes can be achieved by titrating a more concentrated micellar surfactant solution to lipid vesicles, an experiment according to arrow (2) in Figure 40. Because a micellar solution is titrated to lipid vesicles, the heat effects observed for the first injections arise from demicellization and consecutive incorporation of the detergent into the bilayers. At the saturation concentration, a sudden deviation from the almost linear behavior of the heat effects is observed, before the heat signals show another sudden change at the solubilization concentration. A typical curve for the solubilization of DMPC by OG at 70°C is shown in Figure 42. From the first derivative of this curve, the values D_t^{sat} and D_t^{sol} can be determined as shown in the figure. When these solubilization experiments are performed at different lipid concentrations, the coexistence lines can be determined. A typical example for these types of phase diagrams is shown in Figure 43 for the solubilization of DMPC vesicles (left) and soy bean PC (SBPC) vesicles (right). Notable is that the coexistence lines do not meet upon extrapolation to $[L] = 0$ at one point on the ordinate. The assumed model therefore seems to be too simple to describe the vesicle-micelle transition in the regime of low lipid concentration.

The difference in the solubilization behavior of DMPC versus SBPC is evident from Figure 43. The coexistence range of mixed vesicles and mixed micelles is much wider for SBPC. Experiments with other PCs with saturated chains have shown that the width of the coexistence region depends on the chain length and on the degree of unsaturation.

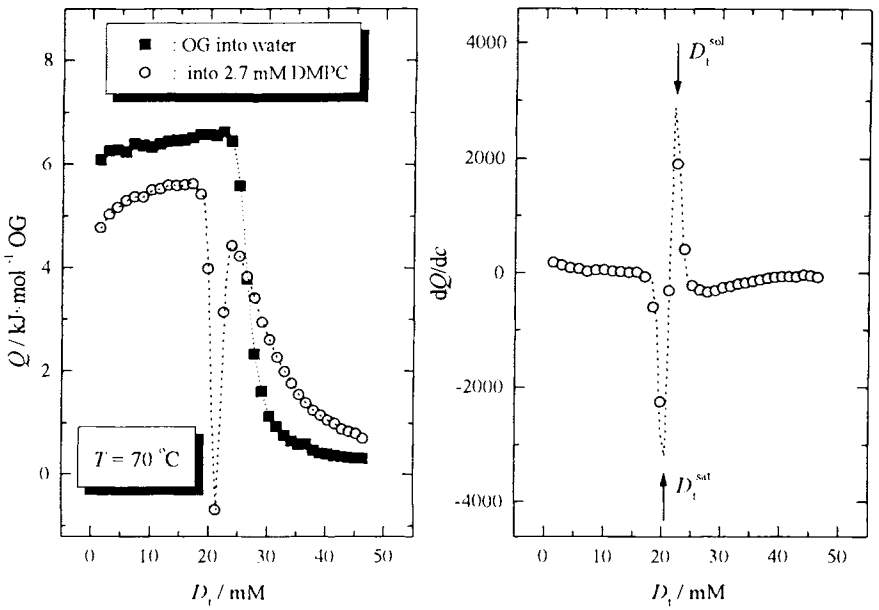

Figure 42. Titration of OG into water and into a 2.7 mM DMPC vesicle suspension leading to solubilization of the vesicles at the indicated concentrations determined from the first derivative curve on the right hand side [138].

But also the chemical structure of the headgroup and its charge have a strong influence on the values of R_e^{sat} and R_e^{sol}, the slopes of the coexistence lines and on the value of D_w, the monomer concentration in coexistence with the bilayers or micelles. For instance, for phosphatidylglycerols (PG), D_w and also R_e^{sat} are much lower than for the corresponding PCs, and for phosphatidylethanolamines the opposite behavior is found. Figure 44 shows for a comparison the coexistence lines for phospholipids with different headgroups as determined from isothermal titration calorimetry.

The physical basis for these differences is at present not well understood. Qualitatively, one can say that headgroups interactions via hydrogen bonds and electrostatic interactions have a large influence. Phosphatidylglycerols with their negatively charged and well hydrated headgroup are much more easily solubilized than the corresponding PCs. Phospholipids with strong intermolecular interactions between headgroups, such as phosphatidylethanolamines which prefer negatively curved interfaces, are difficult to force into a positively curved surface

of a micelle. In the case of phosphatidic acids, these two influences of electrostatic repulsion and attractive forces via hydrogen bonds partially compensate.

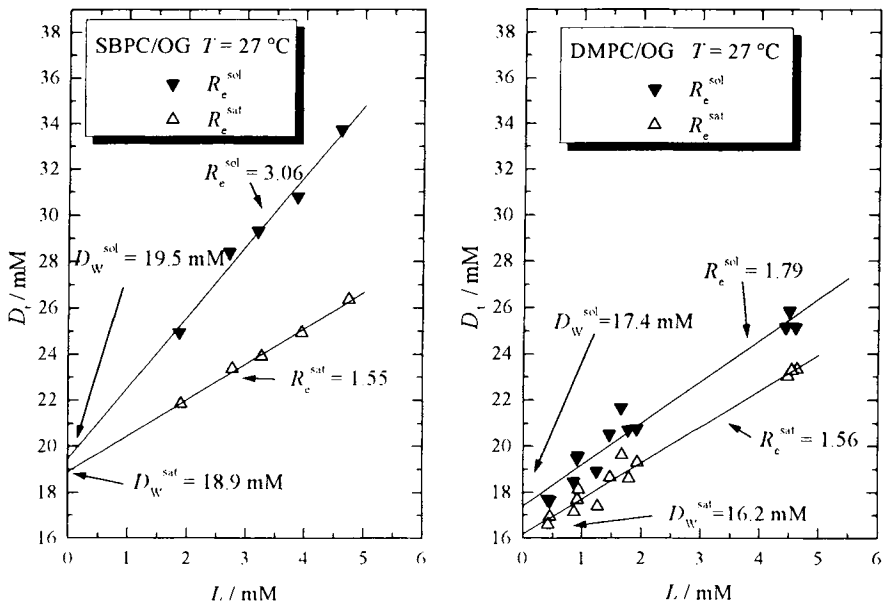

Figure 43. Phase diagram in the low concentration regime for SBPC/OG and DMPC/OG at 27°C. The slopes of the upper coexistence lines are different for the two phospholipids (adapted from reference [138]).

The experiments using ITC presented here are only a few examples for a whole range of experimental protocols which can be performed for studying lipid-surfactant interactions [143-146]. The reversed process, namely the formation of vesicles starting from mixed micelles can also be easily followed by simply diluting a micellar solution into a cell filled with water. Also, a vesicle solution can be added to solution of surfactant monomers just below the *cmc*, etc. These experimental protocols correspond to different paths in the phase diagram shown in Figure 40 which are not indicated there. In this way, a complete description of the behavior of the system can be obtained including all thermodynamic transfer functions. These experiments have to performed at several temperatures when information on the differences in hydrophobic hydration of the micellar and vesicular lipid-water interface is needed. Only these experiments can provide values for Δcp the only reliable thermodynamic function for estimating contributions by the hydrophobic effect.

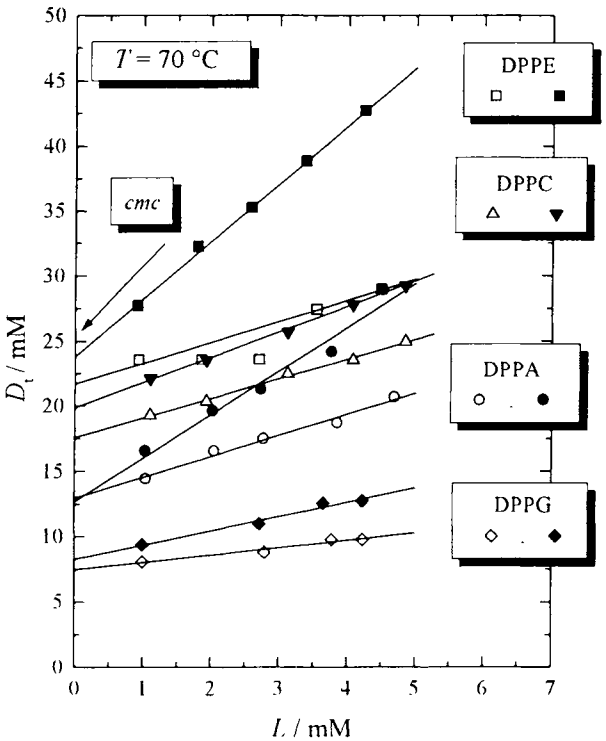

Figure 44. Phase diagrams in the low concentration regime obtained by ITC experiments for octylglucoside and phospholipids with different headgroups (M. Keller and A. Blume, unpublished results).

3.5. Lipid-protein and lipid-peptide interactions

The use of ITC to study protein-lipid interactions is mainly limited to the study of water soluble proteins, which can bind to the surface of lipid vesicles. In many cases, at higher concentrations even water soluble proteins tend to aggregate. Therefore, the interpretation of calorimetric data becomes difficult, because a variety of effects contribute to the observed heat of reaction. Even for smaller, better soluble oligopeptides, the situation is in principle complex. The interaction of binding can be formally separated into several steps, namely electrostatic adsorption to the membrane surface (if the bilayers are negatively charged and the peptide carries positive charges), hydrophobic interaction with the headgroup region or with the more hydrophobic chains, changes in conformation of the peptide, and also conformational changes in the lipid molecules, i.e. possible ordering

or disordering of chains. All these events can contribute to the observed heat effect. Also, changes in hydration of the peptide and the lipids can occur, and particularly when water is released from hydrophobic sites, or vice versa, large heat effects can be observed, depending on temperature (see section 3.4.).

The calorimetric methods for studying lipid-peptide interactions have been recently reviewed by Seelig [147]. The experimental protocols used for studying lipid-peptide interactions are essentially similar to those presented above for lipid-surfactant interactions and the data analysis proceeds along the same lines except that the ΔG-value is now related to a binding constant and not a partition coefficient [147,148]. Depending on the model used, this binding constant can be interpreted as a constant for binding to specific sites, for "surface partitioning" due to electrostatic interactions, for cooperative binding, or for simple adsorption described by a Langmuir adsorption isotherm [147]. The simulation of the experimental titration curves have then to be adapted to the specific model. In general, when the ligand is titrated to the lipid suspension, an expression relating the change of bound ligand to the change in total ligand concentration is needed. For the reversed experiment the equation contains the change of bound ligand relative to the change in total lipid concentration. When charged ligands and charged lipids are used, the electrostatic effects have to be considered. Normally, the application of the simple Gouy-Chapman theory for the electrical double layer gives satisfactory results [40, 147,149-151].

As an example, Figure 45 shows titration experiments of DMPG-vesicles with the oligopeptide lys_3 at different temperatures as a function of lys_3 to DMPG ratio. With increasing temperature, the binding enthalpy becomes more exothermic, the binding constant changes only marginally. The most simple mass action model yields binding constants of ca 500 M^{-1} at both temperatures and binding enthalpies of -32.6 kJ·mol^{-1} at 50°C and -36.8 kJ·mol^{-1} at 60°C. The binding constants agree fairly well with those obtained by other methods, which were reported to be 190 M^{-1} and 5400 M^{-1} for lys_3 and lys_5, respectively. This corresponds to Gibbs free energies of binding of -12.6 and -20.9 kJ·mol^{-1}[152].

We also studied the binding of lys_3 to mixed DMPC/DMPG (1:1) bilayers and found no significant differences in binding constants and enthalpies. For a series of oligopeptides from lys_2 to lys_5 we found increasingly more negative binding enthalpies. For lys_5 , for instance ΔH = -41.8 kJ·mol^{-1} at 50°C and the temperature dependence is similar as for lys_3. For lys_2 the binding enthalpies are very small and no reliable data could be obtained.

The negative temperature dependence of the binding enthalpy is expected for electrostatic binding connected with the release of water from polar binding sites. This has regularly been observed for the binding of other inorganic cations to

negatively charged phospholipids (see above). However, the negative binding enthalpies for simple oligopeptides such as lys_3 and lys_5 we found here is at variance with previous results [149] and has not been found before.

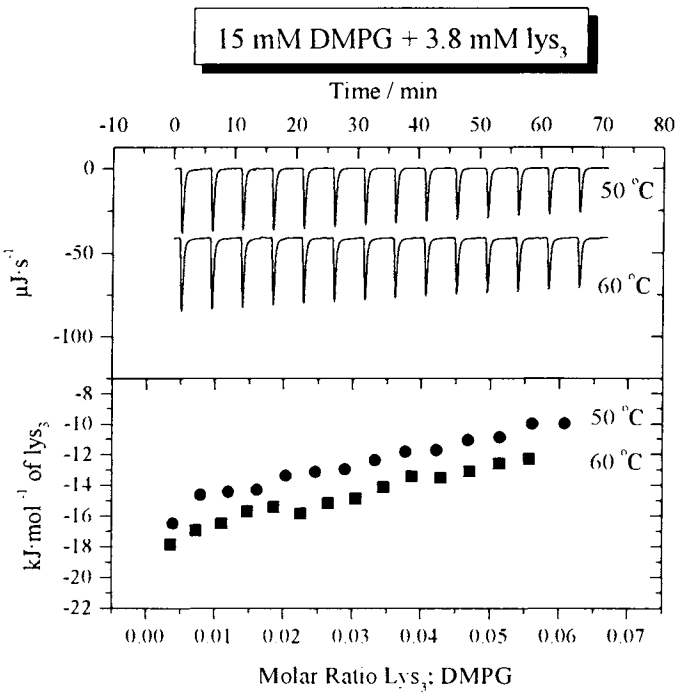

Figure 45. Titration of 15 mM unilamellar DMPG vesicles with lys_3 at two different temperatures at *pH* 7 (M.A. Requero and A. Blume, unpublished results).

For a variety of other peptides and also for more hydrophobic drugs, negative enthalpies for binding or incorporation have been observed. For these molecules, as discussed above for the incorporation of filipin into bilayers, the observed heat effects contain contributions from other than purely hydrophobic effects. Therefore, the only thermodynamic function containing reliable information on changes of "hydrophobic hydration" is Δcp. However, in many cases, the temperature dependence of the heat of reaction has not been determined.

For the binding of lys_3 and lys_5 to DMPG and DMPC/DMPG bilayers the ΔH-values are more negative than the ΔG-values. Using the Gibbs-Helmholtz equation $\Delta G = \Delta H - T\Delta S$, negative ΔS-values for electrostatic binding of lys_3 and lys_5 are found. This leads to the surprising result that binding of these peptides

seems to be mainly driven by enthalpy. This is in contrast to the finding for the binding of simple inorganic cations [37,90] where ΔH is always much smaller. The negative ΔS-values can be assumed to arise from the loss of degrees of freedom of these oligopeptides when adsorbed to the surface of the bilayers. This effect seems to overcompensate the positive entropy increase which is usually found for stronger electrostatic binding due to the release of bound water from hydration sites. It is possible that the water structure at the bilayer surface is in a first approximation unaffected by the oligopeptide binding. From model calculations it was suggested that a 0.25 nm water layer should exist between the van der Waals surfaces of the peptide and the bilayer [152]. This seems to indicate that the headgroups of the lipids are still sufficiently hydrated whereas upon binding of divalent inorganic cations water is released from the surface as FT-IR-spectroscopic measurements have shown [90].

4. CONCLUSIONS

Differential Scanning Calorimetry (DSC) and Isothermal Titration Calorimetry (ITC) have become standard techniques in the field of thermodynamic investigation of natural membranes and model membrane systems. Due to the new developments of more sensitive DSC instruments, studies of lipid-protein systems have become feasible, which could previously not be performed because of the limitations on amount of material. It is to be expected that DSC methods will again make a large progress because of these improvements in sensitivity.

ITC methods have now been used with great success in the last 8-10 years and numerous papers have appeared describing the interaction of various molecules with membranes. The quantitative interpretation of ITC data relies on model assumptions and can be quite complicated. Various effects contribute to the observed heat effect. This complicates the analysis and requires rather systematic studies of the heats of reaction as a function of concentration of both reactants and as a function of temperature. For synthetic molecules available in high purity and large quantities, such as phospholipids and surfactants, this presents no problem. The quantitative analysis of the heat effects observed when these types of molecules interact has therefore made the largest progress in the past two years.

It can be expected that the sensitivity of the titration calorimeters will also dramatically increase in the next two years. Therefore, the ITC method will certainly be much more applied in the near future to study interactions in biological systems, where nowadays the limitations on the available amount of biological material is still preventing many interesting experiments.

ACKNOWLEDGMENTS

The work described in this article was supported by grants from the Deutsche Forschungsgemeinschaft (Bl 182/7-2,7-3,12-1), the Fonds der Chemischen Industrie, and by the Biotechnology Research Program of the State of Rhineland-Palatinate. We want to thank these organizations for their financial support.

REFERENCES

1. S.J. Singer, G.L. Nicolson, Science 175 (1972) 720.
2. R.B. Gennis, Biomembranes. Molecular Structure and Function, Springer-Verlag, New York, 1989.
3. R. Lipowsky and E. Sackmann (eds.) Handbook of Biological Physics, Vol 1, Structure and Dynamics of Membranes. From Cells to Vesicles, Elsevier, Amsterdam, 1995.
4. K.M. Merz, Jr. and B. Roux (eds.) Biological Membranes. A Molecular Perspective from Computation and Experiment, Birkhäuser, Boston, 1996.
5. M.S. Bretscher, Spektr. Wissensch. 12 (1985) 99.
6. R.R.C. New (ed.) Liposomes, a Practical Approach, IRL Press, Oxford, 1990.
7. D.D. Lasic, Liposomes, from Physics to Applications, Elsevier, Amsterdam, 1993.
8. D.D. Lasic and Y. Barenholz (eds.) Handbook of Nonmedical Applications of Liposomes Vol. I-IV, CRC Press, Boca Raton, 1996.
9. M. Rosoff (ed.) Vesicles, Surfactant Science Series, Vol. 62, Marcel Dekker, New York, 1996.
10. D.B. Datta, A Comprehensive Introduction to Membrane Biochemistry, Floral Publ., Madison, 1987.
11. C. Tanford, The Hydrophobic Effect, Wiley, New York, 1980.
12. G. Cevc and D. Marsh, Phospholipid Bilayers. Physical Principles and Methods, Wiley, New York, 1987.
13. G. Cevc (ed.) Phospholipids Handbook, Marcel Dekker, New York, 1993.
14. C. Huang and J.T. Mason, Biochim. Biophys. Acta, 846 (1986) 423.
15. J. Shah, P.K. Sripada, and G.G. Shipley, Biochemistry, 29 (1990) 4254.
16. J.T. Mason and F.A. Stephenson, Biochemistry, 29 (1990) 590.
17. J. Seddon, Biochim. Biophys. Acta, 1031 (1990) 1.
18. J. Israelachvili, Intermolecular and Surface Forces, Academic Press, London, 2nd ed.,1991.
19. M. Caffrey and A. Cheng, Curr. Opin. Struct. Biol., 5 (1995) 548.
20. C. Grabielle-Madelmont and R. Perron, J. Coll. Interf. Sci., 95 (1983) 471.

21. V.V. Plotnikov, J.M. Brandts, L.-N. Lin, and J.F. Brandts. Anal. Biochem., 250 (1997) 237.
22. K. Jorgensen, Biochim. Biophys. Acta, 1240 (1995) 111.
23. M. Caffrey, Chem. Phys. Lipids, 61 (1992) 1.
24. A. Blume, Thermochim. Acta, 193 (1991) 299.
25. R.N.A.H. Lewis, N. Mak, and R.N. McElhaney, Biochemistry, 26 (1987) 6118.
26. H. Träuble and H. Eibl, Proc. Natl Acad. Sci., 71 (1974) 214.
27. H. Träuble, M. Teubner, P. Woolley, and H. Eibl, Biophys. Chem., 4 (1976) 319.
28. P. Woolley, M. Teubner, Biophys. Chem.,10 (1979) 335.
29. A. Blume and H. Eibl, Biochim. Biophys. Acta, 558 (1981) 13.
30. A. Blume and J. Tuchtenhagen, Biochemistry, 31 (1992) 4636.
31. G. Cevc, Biochim. Biophys. Acta, 1031 (1990) 311.
32. F. Jähnig, K. Harlos, H. Vogel, and H. Eibl, Biochemistry, 18 (1979) 1459.
33. F. Castelli, A. Raudino, and S. Gurrieri, Chem. Phys. Lipids, 52, (1990) 129.
34. A. McLaughlin, C. Grathwohl, and S. McLaughlin, Biochim. Biophys. Acta, 513 (1981) 388.
35. H.D. Doerfler, P. Miethe, and H.W.Meyer, Chem. Phys. Lipids, 54 (1990) 181.
36. B.Z. Chowdry, G. Lipka, A.W. Dalziel, and J.M. Sturtevant, Biophys. J., 45 (1984) 633.
37. R. Lehrmann and J. Seelig, Biochim. Biophys. Acta, 1189 (1994) 89.
38. F. Hwang, D.-q. Zhao, J.-w. Chen, X.-h. Chen, and J.-z. Ni, Chem. Phys. Lipids, 82 (1996) 73.
39. S. McLaughlin, Curr. Top. Memb. Trans., 9 (1977) 71.
40. S. McLaughlin, Ann. Rev. Biophys. Biophys. Chem., 18 (1989) 113.
41. I. Graham, J. Gagné, and J.R. Silvius, Biochemistry, 24 (1985) 7123.
42. M.J. Liao and J.H. Prestegard, Biochim. Biophys. Acta, 645 (1981) 149.
43. T. Nakashima, M. Shigematsu, Y. Ishibashi, G. Sugihara, and T. Inoue, J. Coll. Interf. Sci., 136 (1990) 447.
44. G. Laroche, E.J. Dufourc, J. Dufourcq, and M. Pézolet, Biochemistry, 30 (1991) 3105.
45. J.S. Vincent and I.W. Levin, Biophys. J., 59 (1991) 1007.
46. T. Inoue, H. Minami, R. Shimozawa, and G. Sugihara, J. Coll. Interf. Sci., 152 (1992) 493.
47. H. Takahashi, T. Yasue, K. Ohki, and I. Hatta (1995) Biophys. J., 69 (1995) 1464.
48. J.M. Boggs and G. Rangaraj, Biochemistry, 22 (1983) 5425.
49. G. Benga and R.P. Holmes, Prog. Biophys. Mol. Biol., 43 (1984) 195.

50. D. Marsh, FEBS-Lett., 268 (1990) 371.
51. D. Marsh, in: New Comprehensive Biochemistry, Vol. 25 (A. Watts, ed.), Elsevier, Amsterdam, 1993, p. 41.
52. J.F. Tocanne, L. Cézanne, A. Lopez, B. Piknova, V. Schram, J.-F. Tournier, and M. Welby, Chem. Phys. Lipids, 73 (1994) 139.
53. D. Marsh, Eur. Biophys. J., 26 (1997) 203.
54. M. Glaser, Curr. Opin. Struct. Biol., 3 (1993) 475.
55. W.L.C. Vaz, Biophys. Chem., 50 (1994) 139.
56. R. Welti and M. Glaser, Chem. Phys. Lipids, 73 (1994) 121.
57. W.L.C. Vaz, Mol. Membr. Biol., 12 (1995) 39.
58. A.K. Hinderliter, J. Huang, and G.W. Feigenson, Biophys. J., 67 (1994) 1906.
59. K. Gawrisch, J.A. Barry, L.L. Holte, T. Sinnwell, L.D. Bergelson, and J.A. Feretti, Mol. Membr. Biol., 12 (1995) 83.
60. P. Garidel, C. Johann, and A. Blume, Biophys. J., 72 (1997) 2196.
61. P.L. Yeagle, Biochim. Biophys. Acta, 822 (1985) 267.
62. J.H. Ipsen, G. Karlstrom, O.G. Mouritsen, H.W. Wennerström, and M.J. Zuckermann, Biochim. Biophys. Acta, 905 (1987) 162.
63. M. Bloom and O.G. Mouritsen, Can. J. Chem., 66 (1988) 706.
64. M.R. Vist and J.H. Davis, Biochemistry, 29 (1990) 451.
65. J.B. Finean, Chem. Phys. Lipids, 54 (1990) 147.
66. J.L. Thewalt and M. Bloom, Biophys. J., 63 (1993) 1176.
67. T.-H. Huang, C.W.B. Lee, S.K. Das Gupta, A. Blume, R.G. Griffin, Biochemistry, 32 (1993) 13277.
68. T.P.W. McMullen, R.N.A.H. Lewis, and R.N. McElhaney, Biochemistry, 32 (1993) 516.
69. P.F.F. Almeida, W. L. C. Vaz, and T. E. Thompson. Biophys. J., 64 (1993) 399.
70. T.P.W. McMullen, R.N.A.H. Lewis, and R.N. McElhaney, Biophys. J., 66 (1994) 741.
71. T.P.W. McMullen and R.N. McElhaney, Biochim. Biophys. Acta, 1234 (1995) 90.
72. J.A. Virtanen, R. Ruonala, M. Vauhkonen, and P. Somerharju, Biochemistry, 34 (1995) 11568.
73. A.G. Lee, Biochim. Biophys. Acta, 472 (1977) 285-344.
74. A.G. Lee, Biochim. Biophys. Acta, 507, (1978) 433.
75. P.H. von Dreele, Biochemistry, 17 (1978) 3939.
76. B. Tenchov, Prog. Surf. Sci., 20 (1985) 273.
77. S. Ali, H.-N. Lin, R. Bitman, and C.H. Huang, Biochemistry, 28 (1989) 522.
78. E.E. Brumbaugh and C. Huang, Methods Enzym., 210 (1992) 521.

79. J. Huang and G.W. Feigenson. Biophys. J., 65 (1993) 1788.
80. C. Johann, P. Garidel, L. Mennicke, and A. Blume. Biophys. J., 71 (1996) 3215.
81. S. Mabrey and J.M. Sturtevant, Biochemistry, 73 (1976) 3862.
82. T. Inoue, T. Tasaka, and R. Shimazowa, Chem. Phys. Lipids, 63 (1992) 203.
83. Y. Nibu, T. Inoue, and I. Motoda, Biophys. Chem., 56 (1995) 273.
84. I.P. Sugár, J. Phys. Chem., 91 (1987) 95.
85. P. Garidel, C. Johann, and A. Blume, Biophys. J., 72 (1997) 2196.
86. P. Garidel, C. Johann, L. Mennicke, and A. Blume, Eur. Biophys. J., 26 (1997) 447.
87. L. Mennicke, PhD thesis (1995) University of Kaiserslautern (Germany).
88. H. J. Hildebrandt, J. Am. Chem. Soc., 51 (1929) 66.
89. E.A. Guggenheim, Proc. Roy. Soc. [London] Ser. A, 183 (1944) 203.
90. P. Garidel, Ph.D.Thesis (1997) University of Kaiserslautern (Germany).
91. A. Blume, K. Habel, A. Finke, and T. Frey, Thermochim. Acta, 119 (1987) 53.
92. J.T. Mason, Biochemistry, 27 (1988) 4421.
93. A. Ortiz, J. Villalain, and J.C. Gomez-Fernandez, Biochemistry, 27 (1988) 9030.
94. H.N. Lin and C.H. Huang, Biochim. Biophys. Acta, 946 (1988) 178.
95. R.D. Koynova, H.L. Kuttenreich, B.G. Tenchov, and H.J. Hinz, Biochemistry, 27 (1988) 4612.
96. R.B. Sisk and C.H. Huang, Biophys. J., 61 (1992) 593.
97. F. Lopez-Garcia, V. Micol, J. Villalain, and J.C. Gomez-Fernandez, Biochim. Biophys. Acta, 1153 (1993) 1.
98. M. Wegener, R. Neubert, W. Rettig, and S. Wartewig, Chem. Phys. Lipids, 88 (1997) 73.
99. O.G. Mouritsen and M. Bloom, Biophys. J., 46 (1984) 141.
100. M.M. Sperotto and O.B. Mouritsen, Eur. Biophys. J., 19 (1991) 157.
101. M.M. Sperotto and O.B. Mouritsen, Eur. Biophys. J., 22 (1993) 323.
102. T. Heimburg and R.L. Biltonen, Biophys. J., 70 (1996) 84.
103. O.G. Mouritsen and P.K.J. Kinnunen in: Biological Membrane (K.M. Merz and B. Roux (eds.) Birkhäuser, Boston, 1996, p. 463.
104. T. Heimburg and D. Marsh in: Biological Membranes (K.M. Merz and B. Roux, eds.) Birkhäuser, Boston, 1996, p. 405.
105. W. Fürst and K. Sandhoff, Biochim. Biophys. Acta, 1126 (1992) 1.
106. K. Sandhoff and A. Klein, FEBS-Lett., 346 (1994) 103.
107. A. Giehl, T. Lemm, O. Bartelsen, K. Sandhoff, and A. Blume, Eur. J. Biochem. 261 (1999) 650.

108. T.M. Bayerl, G.D. Werner, and E. Sackmann, Biochim. Biophys. Acta, 984 (1989) 214.
109. T. Inoue, R. Motoyama, K. Miyakawa, and R. Shimozawa, J. Coll. Interf. Sci., 164 (1993) 318.
110. B. Maedler, G. Klose, A. Moeps, W. Richter, and C. Tschierske, Chem. Phys. Lipids, 71 (1994) 1.
111. S. Funari and G. Klose, Chem. Phys. Lipids, 75 (1995) 145.
112. G. Klose, S. Eisenblaetter, and B. König, J. Coll. Interf. Sci., 172 (1995) 438.
113. B. Maedler, H. Binder, and G. Klose, J. Coll. Interf. Sci., (1997) in press.
114. T. Wiseman, S. Williston, J.F. Brandts, and L.N. Lin, Anal. Biochem., 179 (1989) 131.
115. W. Wimley and S.H. White, Biochemistry, 32 (1993) 6308.
116. S. Omura and H. Tanaka in Macrolides Antibiotics: Chemistry, Biology and Practice (S. Omura, ed.) Academic Press, New York, 1984, p.351.
117. J. Milhaud, J.M. Lancelin, B. Michels, and A. Blume, Biochim. Biophys. Acta, 1278 (1996) 223.
118. K.S. Birdi, Colloid. Polymer. Sci. 45 (1983) 261.
119. N.M. von Os, G.J. Daane, and G. Haandrikman,. J. Colloid Interface Sci. 141 (1991) 199.
120. Y. Moroi, R. Matuura, T. Kuwamura, and S. Inokuma, Colloid Polymer. Sci. 266 (1988) 374.
121. A. Blume, J. Tuchtenhagen, and S. Paula, Progr. Coll. Polymer Sci. 93 (1993) 118.
122. K. Weckström, K. Hann, and J.B. Rosenholm, J. Chem. Soc. Faraday Trans. 90 (1994) 733.
123. S. Paula, W. Süs, J. Tuchtenhagen, and A. Blume, J. Phys. Chem. 99 (1995) 11742.
124. K. Shinoda, J. Phys. Chem., 81 (1977) 1300.
125. R. Lumry and S. Rajender, Biopolymers, 9 (1970) 1125.
126. D. F. Evans and B. W. Ninham, J. Phys. Chem., 87 (1983) 5025.
127. D. F. Evans and B. W. Ninham, J. Phys. Chem., 90 (1986) 226.
128. P. L. Privalov and S. J. Gill, Pure Appl. Chem., 61 (1989) 1097.
129. B. Lee, Biopolymers, 31 (1991) 993.
130. W. Blokzijl, and J.B.F.N. Engberts, Angew. Chem., 105 (1993) 1610.
131. B. Lee, Biophys. Chem., 51 (1994) 271.
132. C. Jolicoeur and P.R. Philip, Can. J. Chem., 52 (1974) 1834.
133. S.J. Gill and I. Wadsö, Proc. Natl. Acad. Sci. USA, 73 (1976) 2955.
134. D. Lichtenberg, R.J. Robson, and E.A. Dennis, Biochim., Biophys. Acta, 737 (1983) 285.

135. D. Lichtenberg, Biochim. Biophys. Acta, 821 (1985) 470.
136. S., Almog, B. Litman, W. Wimley, J. Cohen, E.J. Wachtel, J. Barenholz, A. Ben Shaul, and D. Lichtenberg, Biochemistry, 29 (1990) 4582.
137. D. Lichtenberg, in Biomembranes: Physical Aspects (Shinitzky, M. ed.) VCH, Weinheim, 1993, p 63.
138. M. Keller and A. Blume, Biochim. Biophys. Acta, 1326 (1997) 178.
139. H. Heerklotz, G. Lantzsch, H. Binder, G. Klose, and A. Blume, J. Phys. Chem., 100 (1996) 6764.
140. H. Heerklotz, H. Binder, G. Lantzsch, and G. Klose, Biochim. Biophys. Acta, 1196 (1994) 114.
141. H. Heerklotz, G. Lantzsch, H. Binder, G. Klose, and A. Blume, Chem. Phys. Lett. 235 (1995) 517.
142. H. Heerklotz, H. Binder, G. Lantzsch, G. Klose, and A. Blume, J. Phys. Chem. B, 101 (1997) 639.
143. H. Heerklotz and H. Binder in Recent Research Developments in Phys. Chem., 1, Transworld Research Network, Trivandrum, India, 1997, (in press).
144. M.R. Wenk, T. Alt, A. Seelig, and J. Seelig, Biophys. J., 72 (1997) 1719.
145. E. Opatowski, M.M. Kozlov, and D. Lichtenberg, Biophys. J., 73 (1997) 1448.
146. E. Opatowski, D. Lichtenberg, and M.M. Kozlov, Biophys. J., 73 (1997) 1458.
147. J. Seelig, Biochim. Biophys. Acta, 1331 (1997) 103.
148. H.F Fisher and N. Singh, Methods Enzym., 259 (1995) 194.
149. G. Beschiaschvili and J. Seelig, Biochemistry, 31 (1992) 10044.
150. J. Seelig, S. Nebel, P. Ganz, and C. Bruns, Biochemistry, 32 (1993) 9714.
151. G. Montich, S. Scarlata, S. McLaughlin, R. Lehrmann, and J. Seelig, Biochim. Biophys. Acta, 1146 (1993) 17.
152. N. Ben-Tal, B. Honig, R.M. Peitzsch, G. Denisov, and S. McLaughlin, Biophys. J., 71 (1996) 561.

This Page Intentionally Left Blank

Handbook of Thermal Analysis and Calorimetry. Vol. 4: From Macromolecules to Man.
R.B. Kemp, editor.

Chapter 4

COMBUSTION CALORIMETRY

I. Lamprecht

Institut für Biophysik, Freie Universitat Berlin, Thielallee 63, D-14195 Berlin, Germany

1. INTRODUCTION

1.1. Historical Aspects

Although combustion calorimetry can be traced back to the early experiments of Lavoisier, Crawford and Blake in the middle and at the end of the 18th century and to Count Rumford's (B. Thompson's) combustion determinations on wood, oils and spirits in the beginning of the 19th century, the area of bomb calorimetry started not before one century later 1885 with Berthelot's combustion bomb filled with pure oxygen under high pressure. His calorimeter developed over many decades to a kind of a universal instrument of high precision and reliability, versatile for many types of investigations, not only for the oxidation of organic and in-organic substances. In the same extent it has been used for any other reaction in which a quick and complete transformation takes place between a gas under in-creased pressure and a solid or liquid substrate [1]. Techniques and applications of bomb calorimetry are described in a number of monographs, usually from a chemical point of view [1 – 101], and mentioned only a few times in a biological context [11-17].

1.2. Instrumentation

Combustion calorimetry is the only technique to determine the energy content of fuels and thus is of great economic importance. Therefore, this method as well as its evaluation techniques have been standardized at both national and international levels (ASTM, DIN, ISO; see Volume 1 of this Handbook, Chapter 10 *Combustion Calorimeters* by the same author [18]). Several bomb calorimeters are commercially available and have been described previously [18]. Usually, they are suited for sample sizes of approximately 1 g or with combustion heats of up to 30 kJ. Since it is often difficult in biology or bioche-

mistry to collect samples or synthesize compounds in such amounts, there is some interest in the scientific community for microbomb or at least semi-microbomb calorimeters. Some equipment is on the market for 1-g calorimeters to reduce the

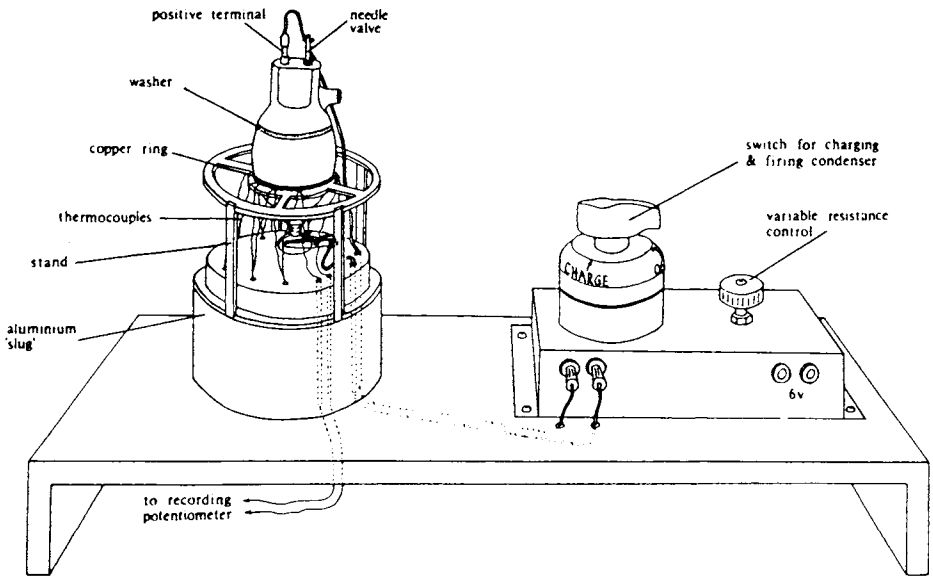

Figure 1. Phillipson's miniature bomb calorimeter [22].

necessary sample dry mass to 50 to 200 mg [18]. An early microbomb calorimeter for sample sizes of about 10 mg was described by Mackle and O'Hare [19]. Moreover, a bomb vessel is available for the classical Calvet calorimeters [20,21]. But the instrument most often cited in the biological literature is that of Phillipson [22]. Because of its importance in bioscience it is shown in Figure 1 taken from the original paper. It was developed for small sample sizes of 5 to 100 mg dry weight typical in biological and especially ecological investigations, with the idea to be easily constructed and without any use of water, stirrers, vacuum insulation and other necessary prerequisites as in larger instruments. It was commercially available in earlier years but is no longer on the market today. Many of the Phillipson calorimeters are custom-made with various modifications. The present author found it useful to exchange the spherical bottom part of the bomb with its poor thermal contact to the support and heat flux sensor against a flat bottom. This is in perfect contact to a square Seebeck (commercial Peltier) element as heat flow sensor which increases the sensitivity of the calorimeter by a factor of about 10.

1.3. Chemical and Thermodynamical Aspects

It is well-known that all energy available in the biosphere originates from the photolysis of water by solar radiation leading to energy rich reduction products of carbon dioxide, mainly carbohydrates and fats [23]. These compounds contain the "reduced bonds": C-C, C-H, N-C and N-H which can be oxidized during energy metabolism. The energy content in a C-C or C-H bond is approximately 880 kJ/mol (or 110 kJ per equivalent of electrons), in a double bond twice as much. C=O groups render about 82, CHOH and CH_2OH groups about 54 kJ/mol. C-O and O-H bonds are the same as in the final metabolic products carbon dioxide and water and do not add any further energy. Kharasch [24,25] published a very comprehensive compilation for combustion heats of organic compounds containing carbon, hydrogen and oxygen. He observed a strong linearity between the number of valence electrons and the combustion heat q with a slope of 110 kJ per equivalent of electrons. This compilation was extended for organic compounds with nitrogen.

The same author proposed a theoretical approach to the caloric values of carbohydrates calculated from the number N of valency electrons in a certain compound [25]. When C, H and O describe the numbers of carbon, hydrogen and oxygen , resp., in a molecule, N can be derived from the formula

$$N = 4 \times C + 1 \times H - 2 \times O$$

and the heat of combustion of that pure organic compound is estimated to $109.0 \times N$ kJ/mol. With corrections for structural features of certain molecules, for double bonds or aromatic rings, calculations can be performed with an accuracy of about 1 % [26].

When the elemental composition of cells is known as weight fractions of carbon (C), hydrogen (H) and oxygen (O) a modified form

$$q \text{ (kJ/g cells)} = 33.76 \times C + 144.05 \times (H - O/8)$$

of the Dulong equation can be applied, e.g. for microorganisms. Another approach uses the Giese equation and the numbers of carbon (N_C), hydrogen (N_H) and oxygen atoms (N_O) in an empirical molecular formula for cells. Together with the "reduction level" RL given by

$$RL = (2N_C + N_H/2 - N_O)/(2N_C)$$

one arrives at

q (kJ/g cells) = 460.24 × RL × N_C / M

with M = molecular weight of the cells [27]. For a yeast cell with a mean molecular formula of $CH_{1.68}O_{0.49}$ [16] the Dulong equation renders a caloric value of 23.52 kJ/g, the Giese equation 25.13 kJ/g. Usually, the Dulong equation is supposed to be less accurate than other approaches. A more detailed description of energy calculation is given in [28] and in Chapter 18 *Quantitative Calorimetry and Biochemical Engineering* by von Stockar and coworkers of this Handbook.

It was shown by Erickson [29] that the energy content of biomass q_0 can be calculated from the carbon weight fraction σ_b and the degree of reductance, γ_b. γ_b is given as the equivalent of available electrons per g·atom C. Using analytical and energetical data from the literature the author found that q_0 values of the major cell constituents fall into a fairly narrow range between 105.9 and 118.9 kJ/equiv in agreement with other authors who observed a coefficient of variation of just 4 %.

Based on a "stoichiometric" equation for the combustion of biomass and the oxygen consumption during combustion, Ho and Payne arrived at a very simple equation for the combustion enthalpy only depending on the mass fraction of carbon f_{CT} calculated for biomass without ash and water [30]:

$\Delta H_0 = 44.852\ f_{CT}$.

This equation has been applied to the energy content of prototrophic bacteria with astonishing good results.

Several authors pointed to the possibility to evaluate the caloric content of organic matter – mainly in the field of ecology – from an elemental CHN analysis and a determination of the ash content (e.g. [31]). Such data provide a means to calculate the proximate biochemical composition (carbohydrates, lipids, proteins) and the bomb calorimetric values. The N:C ratios indicate the relative protein content when a conversion factor of 5.8 ± 0.13 for nitrogen to protein is used [31]. Subtracting protein carbon from the total amount of C renders non-protein C, i.e. C fixed in carbohydrates and lipids. These two substrates can be further divided by application of the non-protein respiratory quotient RQ. It is important to take into account the residual water absorbed by hygroscopic material, chemically bound or retained during drying. The advantage of such an "indirect" method for evaluating combustion heats is that automatic CHN analyzers for samples of about 1 mg are commercially available. Table 1 presents the corresponding values for standard carbohydrates (glycogen and starch), lipids (plant oil and mussel fat bound as triacylglycerol) and proteins [31].

Table 1
Elemental composition and combustion enthalpies of carbohydrates, lipids and proteins [31].
(C_i, H_i, N_i: mass fractions of carbon, hydrogen and nitrogen in the substrates i; $\Delta_c h_i$: specific combustion enthalpy for the substrates i; $\Delta_c h_C$: specific combustion enthalpy based on the mass of carbon; $\Delta_c H_C$: molar combustion enthalpy based on the mass of carbon)

Substrate i	C_i	H_i	N_i	$\Delta_c h_i$	$\Delta_c h_C$	$\Delta_c H_C$
				kJ/(gi)	kJ/(gC)	kJ/(molC)
Carbohydrate	0.444	0.0062	0.000	-17.5	-39.4	-473
Lipid	0.776	0.114	0.000	-39.5	-50.9	-611
Protein	0.529	0.070	0.173	-23.9	-45.2	-543

The "heat of combustion" is that amount of energy which is dissipated during the complete combustion of one mass unit of a substance under the condition that (i) the combustion products are cooled down to the initial temperature, i.e. that the heat of condensation of water vapour is included; (ii) that carbon dioxide and sulphur dioxide are in a gaseous state and that (iii) there is no oxidation of nitrogen (DIN 51900). In all biological applications condition (i) is sufficiently exactly fulfilled, while the two other conditions have nearly no influence on the results [32].

It has to be kept in mind that combustion heat is determined calorimetrically under constant volume conditions, while biological reactions proceed under constant pressure. Hence the combustion heat corresponds to the change in energy ΔE, the reaction heat to that of enthalpy ΔH. Their difference is given by the volume energy ΔnRT. Δn is the change in number of moles of gases during the reaction, R the general gas constant (8.314 J/K/mol) and T the absolute temperature:

$$\Delta H = \Delta E + \Delta nRT.$$

In general, the chemical composition of the burnt biological material is not known so that Δn cannot be calculated. However, combustion of many defined organic compounds showed that the volume energy ΔnRT varies between 0 and 80 J/g so that ΔE is a good estimate of ΔH in most biological applications [32]. Although the change in Gibbs' free energy ΔG

$$\Delta G = \Delta H - T\Delta S$$

would be the most interesting value in many ecological questions the lack of the entropy term ΔS for biological materials prohibits a calculation of ΔG [33].

Caloric contents are usually presented with an accuracy of 5 J/g, often even 0.5 J/g. Runge [32] pointed out that combustion heats are only ΔE values. When they are used as approximations for the ΔH values of energy storage or energy flow in biocoenoses, this accuracy is meaningless since the ΔnRT term only allows for a correct figure of the last but one digit (corresponding to 50 J/g). Nevertheless, caloric values converted from kcal/g to kJ/g and presented in the following sections show the same number of digits as published in the original papers.

The official unit for energy is Joule (J), but cal, kcal or even the "big calory" Cal are still used in many biological and specially ecological applications. Throughout this chapter all original calorie values have been converted into the new SI unit "J" by 1 cal_{IT} = 4.1868 J, and all weight specific caloric contents will be given as "kJ/g". If not otherwise noted (e.g. afdw for ash free dry weight) "g" means dry weight (dw).

1.4. Biological Aspects

Bomb calorimetry was used in its first applications to determine thermodynamically significant quantities such as heats of formation, energy contents of pure or well-defined substances or energies stored or lost during chemical reactions [34]. The later applications - mainly those of biological sciences - became more diffuse and difficult to describe in thermodynamical terms. Energy content of biomatter determined by bomb calorimetry did not mean that it was usuable energy for consumers since - e.g. - many structural carbohydrates in plants are not digestable and thus not available for an animal. Nuts are often cited as an example for a fruit of high energy content in its shell plus kernel but of rather low energy gain for the consumer. Quite often, plant material is toxic and therefore avoided by most animals so that its energy should not be counted in ecological balances.

Specific combustion energy values are given per mass ("weight"). In most cases it will be "dry weight" after the sample dried in an oven from 8 to 48 h and at temperatures between 60 and 110 °C and storing in a desiccator till burning. Sometimes it is just cited as "oven-dry" without further specification. In these cases the combustion heats will be given as "per g" in this chapter. But one should keep in mind that such dried samples quickly gain weight by absorbing moisture from the air. Therefore, samples from the desiccator have to be pre-equilibrated to air (about 30 min) before burning and corrected for the weight increase. A more exact and more useful denomination for comparison of different matter is

that of "ash-free dry weight" (here "afdw") after the determination of the ash content directly from the bomb or better in separate ashing experiments.

When combustion values are given per g biomass, it should be stated by the authors what is meant by "biomass" as the significance of the different constituents of biomass may vary from experiment to experiment. It makes sense to exclude the non-living parts such as water or salts, the calcareous matter of the integument or skeleton and the protective structures not connected with the body (e.g. shells of hermit crabs, tubes of polychaetes or anemones). Also inorganic sediments found in the guts of sediment feeders such as echinoids or polychaetes are no part of the biomass [35]. The problem with organic epidermal structures (e.g. of shells) is more difficult to solve. The extracellular matrix may form a considerable part of an animal's mass, not only in or on the epidermis, but often it might be impossible to separate the cellular and extracellular components of an organism. Because the demarcation between living and non-living material is flexible, it should be clearly stated which parts are included in the "biomass" so that the comparison of results from different authors is facilitated.

Besides the thorough biochemical investigation of a sample for its elemental composition or the fractions of the major components (carbohydrates, proteins, lipids) another way to derive biomass is to assume a proportionality between the nitrogen content of a sample and the amount of living matter. The chemical analysis of nitrogen which can be performed with a number of methods and an appropriate conversion factor (see above) then render the wanted amount of biomass.

Combustion experiments are only meaningful when they proceed in an explosion-like manner to a final, thermodynamically well-defined state. The main question for biological matter concerns the state of water in the bomb: liquid or vapour. In the case of vapour, the heat of evaporation is lost from the combustion energy. One talks about the "gross heating value" or the "high heat value" (HHV) when all water (moisture + water formed by combustion) is in liquid form, otherwise about the "low heat value" (LHV). Depending on the amount of water these two values may differ considerably (see e.g. [36] and Chapter *Wood* in this volume).

At the end of this section an essential *caveat* should be kept in mind. Caloric values less than 17.6 kJ/g afdw should be considered with suspicion. Carbohydrates burn with the lowest energy content of 17.6 kJ/g, proteins and lipids with higher values (see Table 1). Combustion heats lower than 17.6 kJ/g afdw may be due to a wrong determination of the ash fraction or to contributions of inorganic reactions during burning (see e.g. [37]).

2. SAMPLE PREPARATION

2.1. General Sample Preparation

Handling and preparation of samples vary between different authors and applications of combustion calorimetry. Samples of larger quantities are often oven-dried for 24 h at 100 °C, pulverized in a Wiley Mill and sieved with 60 mesh-to-the inch sieves.

Battley and DiBiase [38] proposed a preparation technique based on lyophilization in a vacuum desiccator with concentrated sulfuric acid. 5 mm-layers of thick cell suspension are placed in glass Petri dishes in the desiccator. During evacuation the water in the suspension evaporated and the suspension froze. Any water vapour was absorbed by the sulfuric acid leaving a white powder that can be compressed into pellets. But there are two *caveats* for this method (Battley 1998, personal communication): (i) The desiccator should be placed in a protective cover as once there was a strong implosion during the experiments blowing around pieces of glass and droplets of concentrated acid! (ii) Lyophilized bacteria should be harvested under a hood because the bacterial product is very light and may disperse into air. Therefore, this method is not recommended for pathogenic bacteria, but works well with yeasts and fungi.

Von Stockar and coworkers [28,39] describe a very exact and gentle procedure to prepare biomass for the determination of combustion enthalpy as well as elemental composition. They are convinced that the large scatter in the literature data is due to an inadequate preparation of the cells for combustion. Although developed for microbial cells, their procedure can be applied just as well to other biological samples such as pure substances or tissues. The authors recommend to first freeze-dry (lyophilize) the matter and then to oven-dry it for 24 h at 100 °C. Moreover, methods for the evaluation of residual moisture and ash content are presented.

One may find a good and detailed technical introduction into bomb calorimetry and sample preparation in a paper of Paine [26] that does not intend to be a "cookbook". The author discussed possible pitfalls and explained reasons for wrong results. His sentence is still valid today and should be kept in mind by the newcomer or the frustrated specialist that: "Any preparatory reading done in the extensive fuel technology literature is apt to return high dividends." [26]

Lieth [13] gave a comprehensive survey about the *Measurement of Caloric Values* with all necessary information and many useful hints about collecting and sampling of biological matter in the field and about subsequent preparations. He specially pointed to the fact that the variability of the energy estimates almost entirely depended on the accuracy of the dry-matter determination. Its variability is 20 to 100fold higher than that of the energy evaluation. Many caloric values are

calculated from the chemical composition of biological matter. For that purpose the caloric contents of typical chemical compounds found in ecological research are listed in Table 6 (see below). Following Lieth [13] energy contents based on ash-containing matter should be used for the calculation of ecological efficiency, those based on ash-free matter for studies of translocation and growth. Further information how to handle combustion calorimeters - especially the Phillipson microbomb - was presented by Fraschetti et al. [40].

Schindler and coworkers [41] found considerable differences between samples of freshwater zooplankton which were prepared either from fresh or frozen and samples from formalin-preserved material, while the method of drying (heat- or freeze-dried) had no influence. Storing samples of the copepod *Diaptomus oregonensis* in formalin for 4 months reduced the caloric content by 19 % from 28.11 to 22.88 kJ/g. Somewhat controversial observations were published by Dauvin and Joncourt [42] who found significant differences in caloric contents of fresh or formalin fixed samples when dried at 60 °C, but not at 110 °C, and not for fresh samples at 60 and 110 °C. Therefore, these authors applied 10 % neutral formalin for fixation and a temperature of 110 °C for drying. Cuendet [43] showed that earthworms of 13 species stored in 4 % formalin for 1 to 4 weeks lost 10 to 30 % of their fresh weight. This fact is important when studying energy contents of these animals (about 22 kJ/g) and energy balances in ecosystems, because earthworms are the predominant part of the animal biomass in terrestrial ecosystems.

In general, one has to reflect that fixation solutions may extract water or fat and thus change the relation between wet and dry weight, the chemical composition and the energy content of the samples.

2.2. Drying of Samples

Lovelady and Stork [44] described an alternative method to prepare samples for bomb calorimetry in the field of medical/nutritional investigations. Instead of applying the usual oven drying over 48 h till weight constancy with repeated weighing of the sample, they prepared slurries of human faeces, pre-freezed and then lyophilized them. This procedure took only 16 h and rendered a powder without any odour. Moreover, there was no temperature elevation during drying and thus no loss of volatile energetic compounds.

Table 2 presents a compilation of some drying procedures found in the literature. It shows that there are quite big differences between the various investigations and that it makes sense to establish an individual approach tailored to the special problem under investigation.

Table 2
Drying procedures found in the cited literature. (ly: lyophilized; t.c.w.: to constant weight; n.i.: no information)

Author	Reference	Temperature	Duration	Sample
		°C	h	
Prochazka et al.	[45]	105	2 x 24	Microorganism
Andlid et al.	[46]	105	24	Microorganism
		ly	ni	Microorganism
Cordier et al.	[28]	ly	24	Microorganism
		105	24	Microorganism
Nunez et al.	[36,47]	105	12	Plants
Abrahamson	[48]	60	72	Plants
Bliss	[49]	80	n.i.	Plants
Lieth	[13]	80	<24	Plants
Darling	[50]	90	t.c.w.	Plants
Sweeney et al.	[51]	60	48	Insects
Campbell et al.	[52]	70	48	Insects
Myrcha et al.	[53]	40	t.c.w.	Animals
Vitt et al.	[54]	70	t.c.w.	Animals
Tinkle, Hadley	[55]	105	t.c.w.	Animals

2.3. Determination of the Ash Content

For comparison of tissues from different origin it is often not enough to present the energy content per dry weight but more meaningful per ash free dry weight, as the ash contents vary considerably between biological objects and even within them. Neenan and Steinbeck [56] showed that the ash content of hard-wood changed from 0.41 to 0.96 % with a mean of 0.65 %, that of bark from 4.2 to 9.5 % with a mean of 5.9 % in the same plant.

The ash content is usually determined by weighing the combustion crucible before and after combustion (when sample sizes of about 1 g are used). It is often recommended to determine the ash content of a sample separately by burning it in a muffle furnace, but it is known that the ash content estimated in this way is slightly higher than that found by burning in a bomb. One has to assume that different residues are formed by combustion in the bomb and in the furnace or that not all residues are collected in the crucible. Odum and coworkers [57] supposed that this might be due to the explosive character of burning in the calorimeter. But Runge [32] showed that there is a strong linear correlation between the ash contents determined by bomb and furnace with a slope of 1.14 for all material burnt.

Runge hence recommended to use the easily obtained bomb values and to correct them to the true ash content by this correlation.

Battley [58] pointed out that ash-free dry weights lead to a 5 to 6 % smaller amount of CHON-containing cell mass than determined by means of the total cellular composition. This is due to the fact that the salts of phosphorus and sulfur add a higher weight to the ash than the elements contribute to the weight of the cellular fabric. Such differences have to be taken into account when comparing caloric values of different authors.

As with drying, different recipes for a separate ashing procedure in a muffle furnace are given in the literature. Darling proposed a temperature of 450 °C and a duration of 4 h [50] (see also Fritzsche [59]), Neenan and Steinbeck applied 530 °C for more than 6 h [56], Tinkle and Hadley [55] as well as Vitt [60] 550 °C for 24 h and Campbell and coworkers [52] 550 °C for 2 h when investigating insects. Paine [26] used 500 °C since at that temperature no volatilization of mineral material takes place which would reduce the final ash content, and significantly higher temperatures could produce difficulties. Moreover, he recommended scepticism against caloric values obtained at ash contents of more than 25 % [26]. Further informations on the ash content of samples burnt in a bomb calorimeter or with standard ignition techniques can be found in the paper of Reiners and Reiners [61].

2.4. Acid Corrections

Only in a few investigations cited here, acid corrections were applied. Schroeder [62] gave a detailed description of the method and discussed the application to combustion heat of several materials of ecological interest (leaves, faeces, Lepidoptera larvae, zooplankton). Moreover, he compared the results obtained with a Parr semimicro bomb with that of a Phillipson type bomb and established a negative mass dependence.

During combustion of organic matter, acids are formed from non-metallic oxides, mainly H_2SO_4, HNO_3 and HCl. They are collected in bomb washings with methyl red saturated deionized water and titrated with 0.0725 M Na_2CO_3 to the methyl red endpoint as recommended in the Parr manual. Investigations showed that 4 J ($\approx$ 1 cal) per ml Na_2CO_3 have to be subtracted from the observed heats of combustion. Schroeder determined a mean acid correction of -0.33 % with sample masses of 0.10 g and of -0.14 % at 0.30 g in the semimicro bomb and of -0.57 % (5 mg) and - 0.31 % (20 mg) in the Phillipson type bomb. Acid corrections are less pronounced for plant than for animal matter and more important with the more accurate semimicro bomb as they form 20 to 30 % of the technique variations in this instrument [62].

2.5. Application of Fillers

Phillipson [22] argued that one needs at least sample sizes of 200 mg dw for commercial bombs, amounts which are often difficult to attain in biology, and that filler materials are necessary in such cases. Benzoic acid was recommended by Richman [63] and Millipore membranes by Comita and Schindler [64]. But it is difficult to know the exact percentage of the filler in a small pellet. Moreover, the caloric value is not really constant in the case of the Millipore membranes. Additionally, a small difference between two large figures has to be determined so that significant errors have to be expected when small biological samples are mixed with a large portion of filler. Microbombs with small sample sizes are preferable under such circumstances [22].

Moreover, samples with an organic content smaller than about 25 % should be burnt with additional, known amounts of benzoic acid (up to 30 %) to guarantee complete combustion and to promote ignition [37]. Paine [26] recommended to add mineral oil of known combustion heat to samples to bind the pulverized material together and to increase the temperature difference after burning. Cross and coworkers [65] used equal amounts of activated charcoal to burn wasp cocoons with an extremely high ash content of 84 % (see below 5.1.2).

Sometimes, pellets tend to break when removed from the sample press. If this happens, it is recommended to add a small amount of water to give a much greater cohesiveness to the pellets. The samples have to be dried again after the succesful removal [66].

3. COMBUSTION OF MICROBIAL SAMPLES

In addition to the recipes of sample preparation given above some special techniques are found in papers on microbial combustion calorimetry. A few of them shall be cited here.

(i) Cells are harvested, 3 x washed, dried for 24 h at 105 °C, pulverized and dried again for 24 h at 105 °C [67].

(ii) Cells are freeze-dried for combustion experiments, their dry weight is determined after 24 h drying at 105 °C [46].

(iii) Cells are harvested in the exponential growth phase in ice cooled water to prevent lysis, followed by a threefold washing in ice-cold water. The cell paste is then transfered into Petri dishes as a thin layer, frozen overnight at -20°C and then lyophilized for 24 h. After powdering the paste is again lyophilized for 6 h and held under vacuum.
As the tablets of cell paste take up considerable amounts of moisture when taken out of the desiccator, they should be equilibrated for 15 to 30 min to

the ambient air, then weighed, dried at 105 °C for 24 h and weighed again. Only equilibrated tablets should be burnt [28].

In a paper on microbial cell preparation for combustion, it was shown that the large scatter in literature data on caloric values might be due to inappropriate preparation of biomass [28]. With their procedure the authors found a significant difference between bacteria (23.13 ± 0.52 kJ/g) and yeasts (21.21 ± 0.47 kJ/g). Moreover, they showed that there was no influence of the dilution rate of continuous cultures on the combustion heat of *Kluyveromyces fragilis* in agreement with results of Ho and Payne [30]. The results of the latter authors were surprisingly good when they assumed in their theoretical calculations that only the C-content of cells is relevant for their caloric value [30].

In reply to Erickson's paper about elemental composition and energy content of biomass [29] Payne wrote a paper entitled *Is the heat of combustion of microbial cells predictable solely from chemical bounding?* [68]. Without presenting data he argued that mainly thermophilic microorganisms are exceptions from the general rules. These cells, their component structures and their isolated macromolecules are significantly more stable than those of mesophilic organisms. Macromolecular foldings, structural overlappings and perhaps inorganic-organic bindings might provide heat stability and thus resistance to combustion [68].

Gustafsson and coworkers described bomb calorimetric experiments on the oleaginous yeast *Rhodotorula fragilis* [46]. The energy content of these cells increased from 23.0 to 30.6 kJ/g during the lipid-accumulation phase, directly correlated with their lipid content. The results are in good agreement with the theoretical values derived from a chemically determined lipid content and a combustion enthalpy of 38.91 kJ/g for triacylglycerols. Therefore, these authors remarked that combustion calorimetry could be used as an effective indirect method to evaluate the lipid content of *R. fragilis* [46].

In investigations on microorganisms the yield of a growth experiment may be given as amount of dry mass, of nitrogen or products of interest. Prochazka and coworkers [45,67] suggested to use the energy content of the culture as an alternative measure of the yield. They found mean values for different species of bacteria, fungi and yeasts as given in the following Table 3. The mean of all microorganisms amounted to 22.80 kJ/g with a range of 21.22 to 26.90 kJ/g, the latter value being singular.

The energy transformation of straw as substrate (lignocellulose) into the fruit bodies of a wood-rotting fungus (the oyster mushroom *Pleurotus ostreatus*) was estimated by means of bomb calorimetry [69] and compared with the transformation of plant energy into animal protein. With a caloric value of 11.97 kJ/g in *Pleurotus* fruit bodies and a mean biological energetic efficiency of 23.3 % this

fungus competed with common animal products. 0.111 kJ of energy was fixed in the protein fraction of the mushroom per 1 kJ consumed plant matter. The corresponding figures for some domestic animals were 0.113 kJ/kJ for chicken, 0.031 for pork and 0.030 for beef. While animals needed grains or forage feeds for such a transformation, *Pleurotus* grew on "waste" material (wheat, rice or rape straw, leaves and wood waste) that otherwise was only composted and not used in the food chain directly.

Table 3
Energy content of different microorganisms [67]

	Number of Species	Mean Value kJ/g	Range kJ/g
Bacteria	15	22.65	21.31 - 23.79
Fungi	9	23.48	21.28 - 26.90
Yeasts	8	22.29	21.22 - 24.12
Mean	32	22.80	21.22 - 26.90

Further information about the energy content of microorganisms derived from experimental and theoretical data can be found in Chapter *Quantitative Calorimetry and Biochemical Engineering* by von Stockar and coworkers in this Volume.

4. COMBUSTION OF PLANT MATERIAL

For a long time, investigations on plants and special plant materials played an important role in bomb calorimetry, in ecological aspects as well as in questions of energy storage and renewable energy production. Perhaps *that* classical work in this area is the paper of Gottlieb [70] who published data on the elemental composition and caloric content of some wood species, among them the oak *Quercus pedunculata*, the hornbeam *Carpinus betulus*, the beech *Fagus silvatica*, the birch *Betula alba*, the Scotts pine *Pinus sylvestris* and the spruce *Picea abies*. Ovington and Heitkamp [71] gave an introduction to energy accumulation in British forest plantations and Golley [72] compiled combustion data on 600 different plants. A truly comprehensive literature review is found in Pipp and Larcher [73,74] for caloric and ash contents of more than 1500 plant species. These authors concluded that the energy content is lower in herbaceous than woody plants, that dicotyledonous plants are less energy rich than coniferes, but richer than monocotyledons and that generative tissues contain more energy than vegetative ones. Further data on caloric contents of woody plants are cited in Chapter

Wood of this Handbook, not only determined by bomb calorimetry but also by DTA and DSC.

Darling [50] made an intensive investigation of the caloric values of a group of perennial desert and arid woodland plants and observed values of 13.36 to 22.50 kJ/g. His main result was that tissues (mainly leaves) with low energy contents had high ash percentages (up to 22.3 and 16.7 % in leaves or cactus pads; up to 16.9 and 17.7 in bark) and considerable concentrations of oxalate salts. Figures as high as 38 % oxalate are cited from corresponding literature [50]. Since the oxidation reactions of oxalate or oxalic acid to carbonate show only small exothermic heat productions of about 1/10 of that of biomass, the high content of the oxalates reduces the total specific combustion energy considerably. This underlines the fact that ash determinations in plant tissues are essential prerequisites in the evaluation of true and really comparable caloric values.

Allocations of biomass, energy and nutrient elements were determined in two plants (*Verbascum* and *Solidago*) from different populations [48]. The results show that these allocations may vary between each other in different parts of the plant, that biomass allocation renders no information about that of nutrient elements and that none of them is the best measure of resource allocation patterns. But there is a strong correlation between biomass and energy in *Solidago* so that the authors followed an earlier emphasis [75] that bomb calorimetry can be avoided when plants are investigated which store mainly carbohydrates in their seeds - this is in agreement with the equation of Ho and Payne [30] for energy calculation just from the C content (see above).

Energy allocation in different male and female parts of the reproductive structures of Amaryllis flowers was determined by oxygen bomb calorimetry [76]. Highest caloric values were found for pollen with 24.3 kJ/g (as high as that of peanuts!) and for mature seeds with 22.2 kJ/g while the other parts showed significantly smaller values between 17.3 and 18.9 kJ/g. Since flowers produced about 15 times more mass of seeds than of pollen (550:33 mg per flower) seed production is much more costly for the plant. This is in agreement with the idea that seeds have to carry an energy source for the germination of the next generation [76].

Kriebitzsch [77] determined the net primary production (NPP) of two light and two shadow plant species by means of bomb calorimetry and calculated their efficiencies as percentage of energy fixed in dry matter related to solar radiation energy. Efficiency was more homogeneous among the four species in a shaded area (0.9 to 2.2 %) than in the open field (0.4 to 2.7 %) with a maximum NPP of about 860 MJ/(ha.d).

Collin and Jones [78] investigated the caloric content of pollen from wind- and insect-pollinated dicotyles and of wind-pollinated monocotyles and found no sig-

nificant differences between these three groups. This was against the expectation of the authors since pollen is utilized by many pollinators as direct food source and thus should have a higher, "rewarding" energy content in the insect-pollinated plants. The results are given in Table 4.

Table 4
Caloric content of pollen from mono- and dicotyles [78]

	Mean ± SD kJ/g	Range kJ/g
Wind-pollinated dicotyles	24.62 ± 1.88	21.73 – 28.26
Insect-pollinated dicotyless	24.16 ± 0.67	23.28 – 25.00
Wind-pollinated monocotyles	21.77 ± 0.75	20.56 – 25.46

SD = Standard Deviation

It was supposed that the thick lipophilic resin layer (20 % dm) on the leaves of the fire-adapted species *Elytropappus rhinocerotis* from the Cape Province/South Africa is connected with the well-known flammability of this plant. Proksch and coworkers [79] could show by bomb calorimetry that the caloric value of the resin alone is 13.89 kJ/g, of the resin per g branch 2.78 kJ/g and that of young branches 21.81 kJ/g. Therefore, the authors suggest that the high flammability is due to the fine branch structures and the dense growth rather than to the contribution of this non-volatile resin.

A natural grassland in Jhansi/India was investigated for its caloric values and ecological efficiency [80]. Plants were divided in 4 compartments (live, standing dead, litter, roots) and harvested monthly throughout the year. Biomass showed a mean value of 14.60 ± 0.65 kJ/g afdw with the main contribution by the roots (15.54 ± 1.16) and the lowest by litter (13.33 ± 1.59). Energy density per m^2 changed less during the year below ground (3350 to 11000 kJ/m^2) than above ground (670 to 13000 kJ/m^2) with the highest contribution by green standing crop of 11500 kJ/m^2. The ecological efficiency, i.e. the energy captured by vegetation divided by solar radiation, was 1.17 %. These values have to be used with some care since some of the data are considerably lower than the limit of 17.6 kJ/g afdw of carbohydrate combustion given above for senseful biological caloric values.

Hellmold and Schmidt [81] determined the caloric content of the four most important plant species in a species-rich beech forest on calcareous soil and found values of 16.1 to 19.1 kJ/g for the surface part and of 16.9 to 18.5 kJ/g for rhizomes and roots. While the energy content of leaves and shoots decreased during the season the underground part increased its caloric value. Largest values were

observed in the daugther bulbs with 20.1 kJ/g. This is in agreement with results of Boscher [82] that elevated combustion heats in reproductive organs (seeds, bulbs) correlate with high concentrations of nitrogen and fatty acids.

Decomposition studies on forest plant material were carried out with morphological, chemical and thermoanalytical methods (combustion calorimetry, DTA, DTG) [83]. Bomb calorimetry rendered a constant increase of the caloric value of the plant material from 21.13 to 22.29 kJ/g afdm after three years of decomposition. With the help of DTA/DTG experiments this effect can be explained by the prevailing decrease of low-energy compounds due to microbial activities.

As part of the International Biological Program Oszlanyi [84,85] determined the caloric content of several important coniferous and deciduous tree species in four different forest areas in Slovakia. Wood, bark, leaves/needles and underground biomass showed significantly different heats of combustion with highest values in leaves and needles, lower ones in bark and smallest in wood. Variations in connection with branch or stem thickness brought less pronounced differences. In general, the above-ground biomass had energy contents between 18 and 21 kJ/g.

Different tropical forest types from Panama showed a lower caloric content with a mean value of 16.98 kJ/g (15.12 to 19.20 kJ/g) than forests from temperate or alpine regions [72,86]. Mean values were highest (17.88 kJ/g) for mangroves (presumed as an adaptation to the daily environmental fluctuations in flooding and desiccation) and lowest for gallery forest (16.59 kJ/g). The author found caloric differences between the 9 various vegetation compartments (canopy leaves and stems, understory leaves and stems, canopy and understory fruit, epiphytes, litter and roots), but they were really pronounced only in the tropical moist forest. In this context, Verduin [34] criticized that much of the energy in plant parts is not available to the plant and that it is not clear how the free energy would help the plant to adapt to desiccation. In the same way he supposed that the higher energy content in alpine plants is just an accidental result as the slow growth under these conditions shifts the photosynthates into other metabolic pathways producing energy rich, highly reduced substances like fats, oils or resins.

Seeds of 9 common plant species collected from 5 areas at four different sites in northeastern Kansas exhibited a mean energy content of 21.27 $\pm$ 2.30 kJ/g (18.23 - 25.20 kJ/g) [87]. More oily seeds had a higher caloric value in good correlation to their elevated fat content. The mean energy values were significantly different in all nine species between the 5 areas within the sites, while nothing like this could be observed for the sites. Comparison of the values of this paper with literature data indicate that caloric values of the same plant may change from year to year presumably depending on the specific climatic factors (mainly: available water during the seed production period).

Sedum lanceolatum, a herbacious perennial, typical of western North America, was collected in the Rocky Mountains at 4 sites in altitudes between 2257 and 3726 m above sea level and dissected into 6 tissues: roots, stems and rhizomes, leaves, flowers, peduncle, and peduncle leaves [88]. Comparing the same type of tissue, no differences could be found in caloric values at all chosen altitudes, but differences existed between tissues. Flowers (18.59 ± 0.29 kJ/g afdw) and leaves (17.33 ± 0.33) had the highest energy contents, peduncle leaves (15.32 ± 0.25) and stems/rhizomes (15.11 ± 0.17) the lowest, while the mean value amounted to 17.06 kJ/g afdw (which is again rather low, see above). The proportional investment in sexual tissues was significantly smaller (- 37.6 %) at the lowest altitude than the average value for the three upper altitudes. This underlines the frequent observation that there is a trend of increased energy allocation to sexual tissues at higher elevations and may be in contrast to biomass allocation. Thus, the author warned to exclusively use biomass when different plant populations are compared for their resource allocation. Data about energy content, metabolic cost, nutrients and number of structures should be taken into consideration [88].

Table 5
Caloric values of 55 plant species collected at Mt. Washington, NH/USA. SD = standard deviation [49].

Group	Number of Species	Mean ± SD kJ/g afdw	Range kJ/g afdw
Evergreen shrubs	11	21.34 ± 0.20	20.31 – 23.27
Deciduous shrubs	9	20.65 ± 0.14	19.33 – 21.57
both together	20	21.03 ± 0.14	19.33 – 23.27
Herbs	20	19.26 ± 0.12	18.16 – 21.54
Mosses	7	18.46 ± 0.29	17.63 – 20.01
Lichens	8	18.10 ± 0.25	17.07 – 19.33

Data on 40 species of alpine Tracheophytes and 15 species of alpine lichens and mosses collected at Mt. Washington, NH/USA showed significantly higher caloric values than those known for corresponding plants from temperate and tropical zones [49]. This may be mainly due to the increased lipid fraction in the alpine plants and is in good agreement with observations of other authors. The obtained values are compiled in Table 5 which shows that there are no significant differences (at the 5 % confidence level) between evergreen and deciduous shrubs, but between shrubs and the other three groups.

In a subsequent paper Hadley and Bliss [89] investigated nine of the principal alpine species of the same mountain. They found that new shoots of 4 herbaceous

species had lower caloric and lipid and higher protein contents than evergreen and deciduous shrubs, while all three values were lower in rhizomes and roots than in shoots of the same species. Thus it may be supposed that stored energy reserves in these perennial plants are mainly carbohydrates in the roots and rhizomes, while lipids and perhaps carbohydrates are stored in the old shoots of evergreen shrubs [89].

Boyd [90] investigated vascular aquatic macrophytes and observed that the concentration of each amino acid was very similar in 11 species and at different locations while the total protein content varied greatly. Nevertheless, the caloric values were relatively uniform with figures between 16.35 and 18.07 kJ/g. *Typha latifolia* (the "cattail") collected at different stages of maturity increased its energy content from 17.42 to 19.06 kJ/g, but the protein content showed much higher variations. Of course, the digestibility of aquatic macrophytes is not known. Since several of these plants have high concentrations of cellulose and lignin the available energy content is much smaller than the caloric values given above [90].

5. COMBUSTION OF ANIMAL MATERIAL

A classical, often cited paper by Slobodkin and Richman [91] listed caloric contents of 17 animal species of 6 different phyla. They ranged from 18.4 to 29.3 kJ/g afdw, but concentrated between 22.6 and 25.5 kJ/g afdw for 70 % of the species. The authors state that the observed skewed distribution with the modal frequency at or near the lower range limit could be anticipated. Selection always went for progeny and only in few cases for a high-energy content of the body. Moreover, there might be some unique combination of biochemical components which is essentially the same for all animals [91].

It was shown by several authors that there is a good agreement between direct and indirect determinations of the energy content of animal tissue. Under the assumption that carbohydrates play no role in animal tissues it is just necessary to measure the fat and the nitrogen contents and to transform them to energy units. With a conversion factor of 6.25 (5.8 given by Gnaiger and Bitterlich [31]) between the amount of nitrogen and that of protein and with combustion heats of 39.4 kJ/g for fat and 23.7 kJ/g for protein the energy content of rat carcasses was determined to 24.5 ± 1.2 kJ/g by combustion calorimetry and to 24.9 by calculation [92]. The authors argue that the chemical approach is more simple and less time consuming than bomb calorimetry.

5.1. Terrestrial Animals

5.1.1. Vertebrates

Contents of water, ash and energy have been determined for nestling starlings (*Sturnus vulgaris*) during the time from hatching till leaving the nest after 21 days [53]. Caloric content per g fresh weight increased twofold, because the relative water content decreased significantly. Energy content per g dry weight showed a slight increase during this period around a mean value of 22.2 kJ/g. Ash content was constant about 12 % dw. The published data are in agreement with similar literature values for starlings, Tree and House Sparrows (*Passer domesticus*), Barn Swallows (*Hirudo rustica*) and Redwinged Blackbirds (*Agelaius phoeniceus*).

Gorecki [93] discussed literature data for caloric values of animals with special interest in the large differences between non-migrating and migrating birds as well as before and after migration in the latter. He found that fat content of body tissues had a significant influence on their caloric content since animal fat usually exceeds 38 kJ/g while proteins (and carbohydrates) range between 17 and 21 kJ/g only.

Odum and coworkers [57] compared the caloric content of birds prepared for long-distance migration, returning from migration and for non-migrants. The first group showed contents of 33.1 to 34.8 (mean 33.9) kJ/g afdw as result of a very high fat index around 2.5 (g fat/g nonfat dw) and a mean caloric value of the extracted fat of 37.7 kJ/g afdw. Returning migrants varied between 23.9 and 31.0 (mean 29.3) kJ/g afdw with a fat index of 0.8, while the lean non-migrants figured between 25.1 and 28.9 (mean 26.4) kJ/g afdw and a fat index of 0.3. While the 32 investigated birds from 20 species varied considerably in their fat index (0.11 to 3.42) and in their total caloric content (23.9 to 34.8 kJ/g afdw) the caloric contents were similar when calculated on an ash-free non-fat dry weight base (22.9 kJ/g) with no significant differences between the three groups. It should be mentioned that none of the birds was specially sacrificed for these investigations, but that most of them were killed during their nocturnal flights colliding with a television tower in Florida/USA.

In the line of ecological and bioenergetical investigations on savanna animals in Venezuela 26 young and adult armadillos (*Dasypus sabanicola*) were investigated for their caloric content during development. Figures of 16.7 and 18.0 kJ/g and of 22.2 and 23.9 kJ/g afdw were determined for young and grown-up individuals, respectively [94]. There were some seasonal (dry/rainy) differences between females and males. The mean gross body composition amounted to 52.4 % dw protein, 17.5 % fat and 30.1 % ash, with higher protein contents (62.6 %) and lower fats (4.2 %) in juveniles which are in accordance with the observed caloric contents.

Bomb calorimetric data on various reptile tissues were compiled by Gorecki [93] up to 1969 and presented by Vitt [60] for ash-corrected energy content in 19 lizard and 4 snake species in connection with attempts to estimate the reproductive efforts in these animals (see also [95]). Although the differences between species and populations are significant, they are so small that mean values can be used for all species: 27.4 kJ/g afdw for eggs and 23.3 kJ/g for bodies. Vitt [60] gave conversion equations from dry or wet weight of clutch/eggs and bodies to caloric contents which should be valid for most lizards and snakes. He supposed that such energetic values are relatively conservative features in the biology of reptiles. Further calorimetric data on body tissue and eggs of various reptiles were presented by Congdon et al. [96] in connection with energy budgets and life histories of reptiles. These values showed that the caloric content of eggs was 30 % higher in the mean (25.6 kJ/g) than that of the bodies (20.0 kJ/g). The differences between these two sets of data may be partly due to the calculation per g dry weight or ash-free dry weight.

A less pronounced difference in the energy content of eggs (30.4) and whole bodies (25.7 kJ/g afdw; 18 % increase) was observed in the viviparous montane lizard *Sceloporous jarrovi*. This lizard exhibited a strong correlation between energy input into eggs (reproductive effort) and body length and hence energy for growth. The ratio of reproductive to total body calories remained relatively constant during development [55].

Lizards are well-known among vertebrates for their tail autotomy (self-mutilation) and their quick regeneration of the tail to increase escape and to reduce mortality from predation. Bomb calorimetry together with respiration experiments was performed on several lizard species to determine the energetics of tail regeneration and the metabolic allocation between main body and tail [54,96]. There were no significant differences between the metabolic rates of tailed and un-tailed geckos (*Coleonyx variegatus*). After the metabolic experiments the lizards were sacrificed, freeze-dried and investigated by bomb calorimetry. Highest caloric values were observed in regenerated tails (28.0 kJ/g afdw) and in original tails (26.4), even higher than for most eggs of other lizard species [55,95]. The body showed a caloric content of only 24.7 kJ/g afdw, but with a strongly increased ash content of 16.70 %, compared with 7.06 and 9.01 % for the regenerated and the original tail, respectively. The results underline that tail autotomy is highly significant as predation defence strategy [96].

Energy contents of sloughed skins of 92 individual snakes from three families were determined by a nonadiabatic bomb calorimeter to estimate their contribution to the total daily energy metabolism [97]. The energy content of 175 skins varied between 19.9 and 25.1 kJ/g and showed a total mean value of 21.53 kJ/g

with significant differences between the families: 21.1 kJ/g for Viperidae, 21.7 kJ/g for Colubridae and 23.9 kJ/g for Boidae.

Maiorino [98] established an energy budget for a *Boa constrictor* by determining the caloric content of food, faeces (17.7 kJ/g) and products like the shed skin (24.7 kJ/g) by bomb calorimetry taking the difference between food and faeces as the assimilated energy.

5.1.2. Invertebrates

Six coexisting species of *Ephemerella* mayflies from Pennsylvania/USA showed energy contents between 20.2 and 27.3 kJ/g afdw for larvae, adults and eggs with highest figures in eggs and a significant increase from larvae to adults, presumably due to a disproportionate incorporation of lipids [51]. Four of the six species had similar assimilation rates per g larvae mass (slightly above 40 kJ/g afdw) and an even partition of energy between growth and respiration, while the two other species exhibited completely different patterns with a strongly reduced respiration in favour of growth.

Chemical and caloric contents of a chrysomelid beetle (*Agelastica alui*) - living exclusively on alders and feeding on alder leaves - were determined throughout the vegetation period [99,100]. There were no significant fluctuations around the mean value of 22.6 kJ/g although the lipid content changed considerably. The mean value was near to that of all Arthropods (except Crustaceae) of 21.7 kJ/g as presented in [101]. Because of this constancy in the caloric content and the small deviation from the mean of the systematic group the author raised the question which additional information about ecological systems could be obtained by bomb calorimetry.

The development of three weevil species (*Rynchaenus fagi*, *Strophosomus* sp., *Otiorhynchus singularis*) in two beech stands has been monitored by means of various ecological methods in the framework of the Solling project, among them bomb calorimetry [102]. Caloric contents of larvae, pupae and imagos varied between 20.9 and 27.6 kJ/g afdw. Assimilation rates of average individuals were calculated from the sum of body mass production and respiration. The ecological efficiency defined as production divided by consumption amounted to 7.0 to 8.5 % for all weevil adults. With an energy turnover of 176×10^3 kJ/ha/yr in the 60-year old beech stand, *R. fagi* counted to the dominant phytophagous insects.

Drutschmann (1998, personal communication) observed a caloric content of 37.5 kJ/g in imagos of the wax moth *Galleria mellonella*, a figure which is very near to that of fat. The content of growing larvae was significantly smaller with 27.5 kJ/g in the first stages, 31.9 in the last larval stage and 34.2 kJ/g for the pupae. As *Galleria* pupae and imagos no longer feed this further energy concen-

tration in the last two stages must be due to a prevailing consumption of proteins and carbohydrates.

An intensive bomb calorimetric investigation was performed on the energy transfer between a wasp, the organ-pipe mud-dauber *Trypoxylon politum*, and its sole prey, living paralyzed spiders [65]. Energy contents of the spiders (20.9 kJ/g), the prepupae (21.7 kJ/g), the pupae (20.5 kJ/g), adults of both sexes (males: 19.8, females: 19.6 kJ/g) and faeces (19.4 kJ/g) were determined. Cocoons exhibited an extremely high ash content of about 84 % and could be burnt only after a 1 : 1 addition of activated charcoal. As the wasp's life cycle is short, the entire mean consumption of the prey (spiders: 4.38 kJ) led to a rather high consumption rate of 11.3 mW. 0.41 kJ were required for the cocoon formation, 1.02 kJ were egested in total so that a maximum efficiency of 76 % was found.

Caloric values of twenty oribatid mite species varied in an extremely broad spectrum between 13.4 and 22.2 kJ/g afdw [103]. Figures below the critical level of 17.6 kJ/g afdw (see Introduction) were found in those mites with high ash contents up to 50 % dw. It was discussed that the energy-poor exoskeleton (which is burnt together with the rest of the mite) could be responsible for such low values. But it should be remebered that the exoskeleton is formed by chitin, a nitrogen containing polysaccharide. Hence, the given explanation seems vague and errors in the determination of the ash content more probable (see Paine [26]).

A combination of radiotracer and gravimetric measurements with bomb calorimetry has been applied in a rather early paper to determine the ingestion and assimilation rates of the isopod *Armadillidium vulgare* under field and laboratory conditions [104]. Caloric contents of food (leaves of the thistle *Silybum marianum*) and of faeces were rather small below 17.6 kJ/g afdw and the ash fractions relatively high between 16 and 21 % dw. Together with the radiotracer and gravimetric determinations it was found that the caloric content of the food assimilated was higher than that of food ingested so that an energy concentration took place in the isopod.

5.2. Aquatic Animals

Prus [105] gave a literature review about caloric contents of aquatic animals. Contents between 17.6 and 28.5 kJ/g afdw were found in 63 species of aquatic animals with a majority of 37 species between 21.8 and 25.1 and a common mean of 23.4 kJ/g afdw. Variations of 4 to 8 kJ/g were cited within several species dependent on season, food availability, sex, physiological state and developmental stage. High values were observed in stages before reproduction, food shortage or diminished energy inflow.

These observations have been confirmed for freshwater zooplankton from three Canadian lakes. Investigations were carried out by means of a modified Phillip-

son bomb applicable to small samples sizes of 1 to 10 mg [41]. The authors observed significant differences in the energy content depending on species, lake, season and year. The caloric values for two copepods from all three lakes varied between 22.88 and 30.88 kJ/g with ash contents between 0.5 and 2.8 %.

Wacasey and Atkinson [37] listed energy values of 121 species of marine benthic invertebrates from the Canadian Arctic and discussed the possibility to derive caloric values from the percentage of organic dry matter. They found a mean caloric value of 22.7 kJ/g afdw for that community which is quite similar to the value published for lower latitudes [101] and near to that of proteinaceous material (23.9 kJ/g). Although the mean organic content in the 12 investigated taxa varied considerably from 18.1 to 88.4 % dw the mean caloric values concentrated in a narrow range with one exception (*Ascidiacea*) [37].

Bast and von Oertzen listed energy contents of about 100 aquatic organisms with special attention to those found in the Baltic Sea [106]. Data were obtained by combustion in a modified Phillipson microcalorimeter (MBC-3) or taken from the literature and showed a range from about 12 to 29 kJ/g afdw. Highest values were observed in eggs (26.7 ± 0.3 kJ/g afdw) and in larvae with yolk sacs (26.8 kJ/g afdw), smallest values on the lowest trophic level and in sediments [106].

In connection with metabolic investigations and influences by changing salinities, Fritzsche determined the energy contents of two polychaetes, *Marencelleria viridis* and *Hediste diversicolor*, found in the "Darß-Zingster Boddenkette" of the German part of the Baltic Sea as well as in the Dollart of the North Sea [59]. There were no differences between the two species nor between the two habitats. The energy contents varied between 22.20 and 24.02 with a mean of 23.08 kJ/g afdw. This figure is near to the mean value of 23.4 kJ/g afdw for 63 aquatic animals given by Prus [105] and in the range of 22.60 to 23.9 kJ/g afdw for 121 species of marine invertebrates found by Wacasey and Atkinson [37]. In the latter investigation polychaetes had a mean value of 23.30 kJ/g afdw. Neuhoff observed a caloric range of 20.99 to 21.19 kJ/g afdw for *H. diversicolor* depending upon the degree of salinity [107].

Caloric values of three soft corals (*Alcyonium paessleri, Clavularia frankliniana, Gersemia antarctica*) from the McMurdo Sound/Antarctica have been evaluated indirectly by determination of ash, carbohydrate and protein contents as well as that of the "refractory material" (insoluble protein) and converted to energy values by usual data from the literature [108]. The ash content, indicative for the relative sclerite fraction, varied between 30 and 50 % dw. Lipid and carbohydrate levels were relatively low and protein accounted for more than 65 %, leading to considerable energy contents up to 17.3 kJ/g. Although such energy values should be interesting for higher trophic levels, the three investigated corals contain bioactive compounds that protect against predation by seastars and fishes.

Similar results were obtained for the antarctic ascidian *Cnemidocarpa verrucosa* with high energy contents, 2 - 3 times that of other sessile antarctic marine invertebrates (such as sponges, e.g.) but well protected by a tough tunic noxious to pelagic and benthic fish [109]. 16 antarctic sponges showed high and variable ash contents (32 to 79 % dw), protein levels up to 56 % and low energy contents around 9.8 kJ/g [110]. More than half of them were toxic in various degrees, so that sponge-eating predators had the chance to choose the more abundant, non- to mildly-toxic species. Finally, the energetics of the antarctic sea star *Odontaster validus* have been investigated by the same approach rendering biomass and energy density estimates per m^2 and energy distribution in the body [111]. Highest values around 25 kJ/g have been found in the pyloric cecum, mainly associated with insoluble protein, i.e. high amounts of structural material.

Bomb calorimetry and biochemical analysis of holothurian (sea-cucumber) body tissues showed significant differences in the caloric contents of testis, gut, and body wall [112] which may be partly due to the calcium-carbonate content of the tissues (specially of the body wall). Holothurians with an average energy content of about 25 kJ/g afdw represent an important store of energy in the deep sea.

Nagata [113] determined the energy transformation in an intertidal population of three gastropods (snails) which formed the more pronounced part of biomass and density in this habitat. Respiration and combustion measurements exhibited highly different contributions from 27.6 to 496 kJ/m^2/year of these herbivores to the energy flow. The author regarded the caloric content of shell to zero because published combustion heats of 80 to 250 J/g were negligible compared with 13 to 21 kJ/g for flesh measured by him.

An energy budget was established for the European ormer *Haliotis tuberculata*, a large gastropod mollusc of marine habitats [114]. The authors showed that the mucus production formed a considerable part of the budget of up to 30 % in large individuals so that it had an important influence on the other energy components changing them up to 50 %. In a corresponding energetic investigation of a Malaysian gastropod population (*Natica maculosa*) the author was not able to determine faeces and mucus because both dispersed too rapidly in the sea water [115]. Bomb calorimetry rendered 19.3 kJ/g for *Natica* and 20.1 kJ/g for its gastropod prey *Umbonium vestiarium*.

Energy content of the flesh of the gastropod *Crepidula fornicata* (a marine snail from the bay of Marennes-Oléron/France) was determined to values between 15.1 and 19.3 kJ/g afdw (mean 17.7 kJ/g) by means of a Phillipson microbomb [116-118]. These values were higher for males than for females throughout the period of reproduction. Eggs of *C. fornicata* showed a significantly larger energy content than flesh with a mean value of 22.4 kJ/g afdw.

120 species of macrobenthic invertebrates from the Western English Channel were investigated by a similar calorimeter [42]. The authors found caloric contents between 11.16 and 22.09 kJ/g (with an overall mean of 18.65 ± 2.10) and between 17.75 and 23.57 kJ/g afdw (mean 20.52 ± 1.69). 83.5 % of the species ranged between 19 and 22 kJ/g afdw. The general mean value for the whole community was 10 % lower than a corresponding value for Arctic invertebrates [37] which is in accordance with the observation that the lipid and energy content of several zooplankton species increased with higher lattitudes.

It was found that the amphipod *Corophium volutator* collected in the Gulf of Gdansk/Poland experienced strong seasonal variations in its caloric content around a mean value of 18.2 kJ/g afdw for the females which are predominant in the population [119].

Energy flow through a population of fiddler crabs (*Uca pugnax, U. minax*) and marsh periwinkles (*Littorina irrorata*) was monitored by bomb calorimetry and respiration figures taken from literature, and was partitioned into the different components in an ecological energy transformation equation [120]. Caloric contents of both crabs were similar with 11.2 and 10.7 kJ/g, their faeces contained 10.1 kJ/g. The corresponding values for the snail (*L. irrorata*) were 21.0 kJ/g and 6.4 kJ/g, respectively, averaged over the season and different body sizes. The periwinkels consumed approximately one-tenth of the total net production of the marsh, the combined crab populations about one-fourth. The observed energy contents (given per dry weight) of both crabs are rather low, possibly due to a high ash content.

Freshwater animals from a New Zealand lake were calorimetrically investigated for seasonal changes and differences between size classes in their caloric content [66]. The author showed that it cannot be recommended to use a single energy value for an animal to describe its importance in energy flow evaluations, because spring values may be 17 % higher than those in summer and more than 60 % higher than that in winter.

Similar seasonal variations of up to 20 % in the caloric values of some littoral benthic invertebrates were seen between summer and autumn [121]. Equivalent observations were published on the marine gastropod *Crepidula fornicata* for the biochemical composition and the energy content of the flesh. These changes were connected with two periods of spawning in females and one of reproduction in males. The mean caloric content changing between 15.1 and 19.3 kJ/g afdw was generally higher in the males than in the females, but the highest figures were found in eggs with 22.4 kJ/g afdw.

A combination of combustion calorimetry and respiration rate determination was used to establish an energy balance for an aquatic host-parasite system [122]: the three-spined stickleback *Gasterosteus aculeatus* infected by the pseudophyl-

lidean tapeworm *Schistocephalus solidus*. Caloric contents of the balance components were determined with a Phillipson microbomb for small sample sizes and with an adiabatic bomb calorimeter for samples above 40 mg dw. Fish exceeding 60 mg dw showed a mean energy content of 19.81 ± 0.22 kJ/g with an increase for growing fish. Values of the parasite varied between 18.84 and 25.54 kJ/g with a mean of 20.95 ± 0.26 kJ/g, the feed content amounted to 23.22, that of the stickleback faeces to 18.31 kJ/g. Significant differences could be established between uninfected and infected fish in their energy turnover, because the parasites were more efficient in energy transformation than their hosts.

Bomb calorimetric measurements were performed together with determinations of dry weight, carbon and nitrogen content for eggs, larvae and juveniles of the walleye pollock *Theragra chalcogramma* from the North Pacific [123]. They rendered the following energy values for eggs: 15.57 to 21.85 kJ/g (mean 19.28 ± 1.86), for larvae: 17.35 to 24.65 kJ/g (mean 21.26 ± 1.73) and for juveniles: 17.48 to 39.85 kJ/g (mean 23.28 ± 3.58). The larger scatter in the juveniles resulted from the fact that younger fish converted energy mainly into proteins and older to lipids. As pollocks underwent seasonal and yearly fluctuations, body weight alone was an insufficient means to predict body composition and energy content, while Fulton's cube law condition factor index - a special combination of wet weight and body length of the fish - showed a strong linear correlation.

Gross energy content of the African catfish *Clarias gariepinus* together with its feed and faeces was determined to test the applicability of three different methods to establish the energy content: (i) bomb calorimetry, (ii) chemical composition, and (iii) chemical oxygen demand [124]. The methods rendered significantly different results between the three sample classes and within the classes, and the authors concluded that calorimetry was the most appropriate for this purpose. The energy contents obtained by a Gallenkamp ballistic bomb calorimeter were: 24.10 ± 0.19 kJ/g (fish), 21.95 ± 0.09 kJ/g (faeces) and 21.76 ± 0.27 kJ/g (feed).

6. COMBUSTION OF ECOLOGICAL MATERIAL

6.1. General Aspects

It was often stated that energy allocation in ecological systems can be described by dry mass distribution and that it is not necessary to perform calorimetric experiments. Other authors hold that "For the ecologist dealing with specific time and energy budgets or population energetics, direct calorimetry of representative members of the population is a prerequisite for accuracy" [26]. Hickman and Pi-

telka [75] analysed four ecologically diverse plant species and found no significant differences between energy allocations based on calories or on dry weight of plant parts (roots, stems, leaves, flowers, pods and seeds). Figure 2 adapted from their Table 2 shows the linear correlation between energy content and dry mass for the different plant parts and species (slope = 0.997; r^2 = 0.995). The authors concluded that dry matter suffices for allocation description in the case when mainly carbohydrates are stored in plants and lipids play a secondary role. But they continue: "It must be emphasized that the usefulness of calorimetry depends upon the question being pursued. Calorimetry will remain essential for many ecological studies, but not for all those concerned with energy budgets." [75].

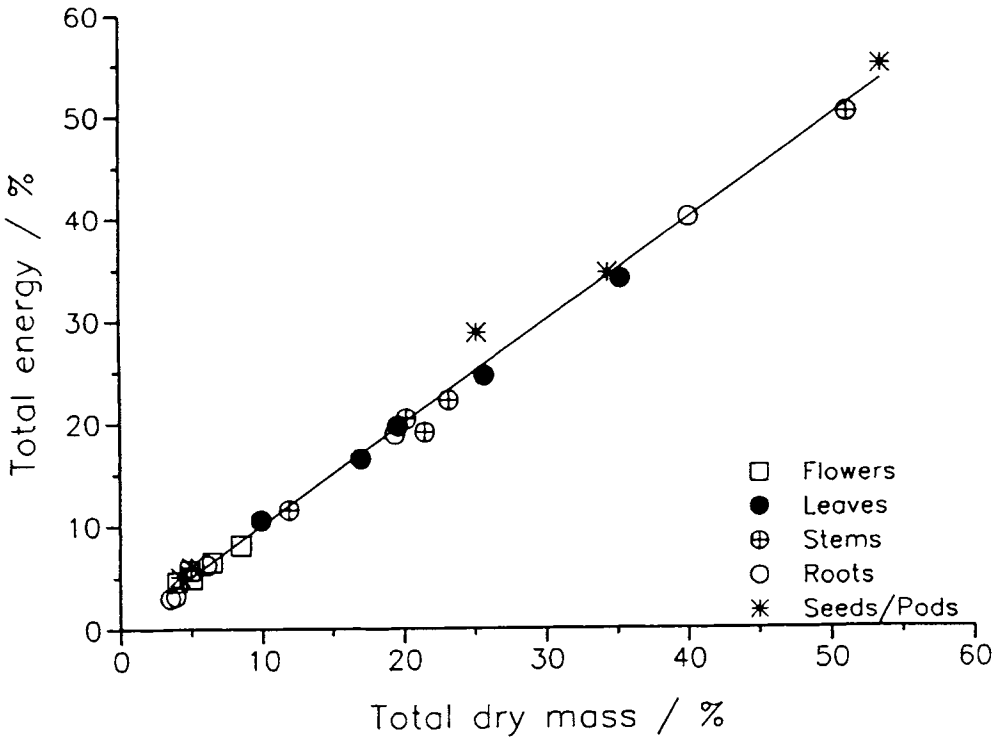

Figure 2. Linear correlation between energy content and dry mass for different plant parts and species (slope = 0.997; r^2 = 0.995) [75].

Boyd and Goodyear [125] showed that determinations of just energy flow or energy transfer are too coarse simplifications for ecological systems. Carnivorous nutriments are of huge food value due to their content of proteins and thus form a rich diet while the food value of herbivorous diet is much lower with an interme-

diate figure for omnivorous diets. Carbohydrates have to be divided into structural and non-structural compounds. Structural carbohydrates like cellulose, hemicellulose or lignin are difficult to digest, while non-structural ones like starches, sugars or fructosans are easily degraded. These differences are important in the determination of the food value [125].

McClintock [126] pointed out that the amount of energy in food for consumers is essential in different ecological questions, that combustion calorimetry renders only the gross energy content and that a more realistic picture is obtained via the organic content. By subtracting contributions by insoluble and indigestible components, a "useable" energy is obtained. Structural or insoluble carbohydrates in plants and insoluble proteins in animals (e.g. keratin, collagen) form such non-useable organic contributions. They reduce the available energy in 5 plant species to figures between 5.7 and 65.7 % (mean 32.3 %) of the caloric value and in 5 animal species to figures between 45.3 and 91.8 % (mean 69.7 %) of the total energy. One obtains a strong overestimation of energy flows in ecology if such reductions are not taken into account as "The guts of animals are not bomb calorimeters." It is thus necessary to include the determination of percentages of soluble/insoluble carbohydrates and proteins into the evaluation, in addition to that of lipids and ash. Only then one gets an accurate indirect measurement of the total energy levels of plant and animal prey [126].

Applied to herbivorous diet some general rules can be stated:

(i) 80 to 90 % of the nitrogen in plants is bound in proteins, so that a nitrogen determination renders a crude estimation for the protein content and from this for the nutritive value of such a diet.

(ii) Toxic compounds in a plant make it unpalatable for man or most animals and bring the nutritive value down to zero in spite of a possibly high energy content.

(iii) Roots and rhizomes contain a high percentage of non-structural carbohydrates and a low amount of proteins, while seeds present fats, proteins and non-structural carbohydrates.

(iv) The total energy content of plants is fairly constant with 16.7 to 17.6 kJ/g dw.

(v) Unfortunately, a separation into available and non-available fractions is not possible.

(vi) For general ecological purposes, a determination of the protein content (total nitrogen $\times$ 6.25 [125] or 5.8 [31]) and of the non-cell wall material is sufficient for a good estimate of the quality of net production [125].

In general, one can state that bomb calorimetry is more suitable for estimating the digestable energy content of animal than of plant material [125].

Table 6.
Caloric content of some typical chemical compounds and classes of matter, used in ecological calculations [13].

Compound or matter class	Caloric content kcal/g	Caloric content kJ/g
Starch	4.18	17.5
Cellulose	4.2	17.6
Saccharose	3.95	16.5
Glucose	3.7	15.5
Raw fiber	4.2	17.6
N-free extract	4.1	17.2
Glycine	3.1	13.0
Leucine	6.5	27.2
Raw protein	5.5	23.0
Oxalic acid	0.67	2.8
Ethanol	7.1	29.7
Tripalmitin	9.3	38.9
Palmitinic acid	9.4	39.3
Isoprene	11.2	46.9
Lignin	6.3	26.4
Fat	9.3	38.9

In 1942 Lindeman [127] proposed the use of energy as the common "currency" to compare ecological systems and their trophic-dynamic aspects. Quite a number of bomb calorimetric investigations were performed in this field and the importance of caloric values confirmed (e.g. Lieth [13]) but there are several authors who prefer the chemical analysis of biomatter and an energy calculation by known combustion heats of essential compounds or classes of substances (Table 6). Both sides will be presented in the following sections.

The very large and comprehensive data collection on caloric values of biological material performed by Cummins and Wuycheck [101] is of great help for all ecological investigations. It shows significant differences between various phyletic or ecological categories. A few of these values are presented in Table 7.

6.2. Applications

In the seventies an interdisciplinary research project was carried out by several German universities in a mountain range south of Hannover/Germany ("Solling project"). Energy contents and turnovers were determined in different biocoenoses of forest, meadow and arable field. Caloric contents of most plants varied between 17.2 and 23.0 kJ/g with one extreme exception of 36.8.kJ/g in a spruce

sample with high resin fraction. Highest energy contents were observed in a spruce stand (650 MJ/m^2), lowest in the meadow (< 23 MJ/m^2). Highest net primary production was found in fields of the grass *Lolium multiflorum* with about 33 MJ/m^2/year, corresponding to 1 % of the yearly global radiation. It could be further shown that most of the fixed energy is distributed directly between detritus pathways and exploitation by man ("economic yield") while just 1 to 2 % are used by herbivores [32].

Table 7.
Caloric values *q* of biological matter, given in kcal/g and kJ/g on an ash-free basis, from the compilation of Cummins and Wuycheck (1971) after Payne [26]. (n = number of samples).

Category	n	Caloric value kcal/g	Caloric value kJ/g
Primary producers	342	4.681	19.60
Detritus consumers	44	4.885	20.45
Macroconsumers	357	5.821	24.37
Aquatic	155	5.465	22.88
Terrestrial	202	6.099	25.54

An interesting early paper of ecological research by bomb calorimetry was published by Long [128]. He made an intensive investigation into preparing plant material and into its caloric and ash contents. In the giant cactus (*Carnegiea gigantea*) the ash content may be as high as 25.5 % in special parts, while *Rose*, *Rubus* and *Prunus* show only 6 %. A great diversity of weights and energies was observed for adjacent leaves which looked quite similar, partly due to shading and partly to competition. Minimum caloric values were observed at the bottom and the top of a plant with a maximum in the upper third of the sunflower *Helianthus annuus*. If plants were grown in competitive units those at the edges and specially at the corners developed best and showed the highest energy content, even on a per weight basis. When the light intensity was changed in the growth period calories stored in the plant dropped dramatically (due to the much smaller final mass of the plant), but also per g dry weight (by as much as 20 %). Sandy soil in contrast to loam and even to adobe led to a lower caloric value (down to only 83 %) for all investigated plants, as a consequence of a reduced water content in soil.

In investigations of two extreme Greek ecosystems, the very dry phrygonic and the relatively wet maquis system, the energy content of dominating evergreen and decidious plants were determined for the whole plant as well as for leaves, bark and wood [129,130]. Leaves of phrygonic plants show intermediate caloric con-

tents (18.8 kJ/g) between those of evergreen sclerophyllous (19.5 kJ/g) and of deciduous ones (18.3 kJ/g). No significant differences are seen between evergreen and deciduous individuals from the maquis in their energy values for bark (about 17.6 kJ/g) and wood (19.3 kJ/g). Calculating the mass contribution of leaves, bark and wood to the above-ground biomass and the mass distribution between evergreen and deciduous plants, a maquis ecosystem contains 18.1 kJ/g (18.7 kJ/gafdw) of energy, very similar to the Greek phrygonic system.

Lieth [14,15] used plant caloric values together with growth of biomass to assess the primary productivity in different areas of the Earth. Although the approximate average combustion values changed only slightly between their maximum in Mediterranean sclerophyll forest (20.5 kJ/g) and their minimum in tropical grassland (16.7 kJ/g), the mean annual energy fixation per m^2 dropped from a 48.1 MJ/m^2 in the tropical rain forest to 1.3 MJ/m^2 for desert scrub. These calculations were laid down in several global maps for energy density, evaporation and productivity based on different parameters (see e.g. Figure 5 in Chapter *Wood* in this volume).

By means of bomb calorimetry and respirometry Jensen [131] determined the population density and various energy categories for the slug *Arion ater* in a Danish beech stand from May to October. Monthly biomass amounted to 0.269 g/m^2 or 5.9 kJ/m^2, the production to 11.9 kJ/m^2, the consumption to 149 kJ/m^2 and the assimilation to 114 kJ/m^2. The respiration based measurements resulted in a much smaller assimilation (32.6 kJ/m^2) presumably due to an overestimation of the consumption in the direct approach.

Graminivorous insects establish an important pest of stored grain and lead to severe losses in worldwide food supply. Bomb calorimetric and respirometric investigations have been used to understand the energy flow within insect infected grain bulk ecosystems [52, 132-135]. The granary weevil, *Sitophilus granarius*, and the rice weevil, *S. oryzae*, were grown in single wheat kernels through their whole development from the egg to larva, prepupa, pupa and adult insect and the energy contents of these different states determined. Figure 3 shows how the energy content of an individual increased from 0.16 to 24.53 J of the prepupa and to final 18.25 J for the adult. During this 50-day period about 197 J or 37 % of the initial caloric content of the wheat kernel (528 J) were ingested by the insect with a rather high overall assimilation efficiency of about 80 %. Figure 4 presents an energy budget for the rize weevil indicating the partition of energy between the different aspects of life.

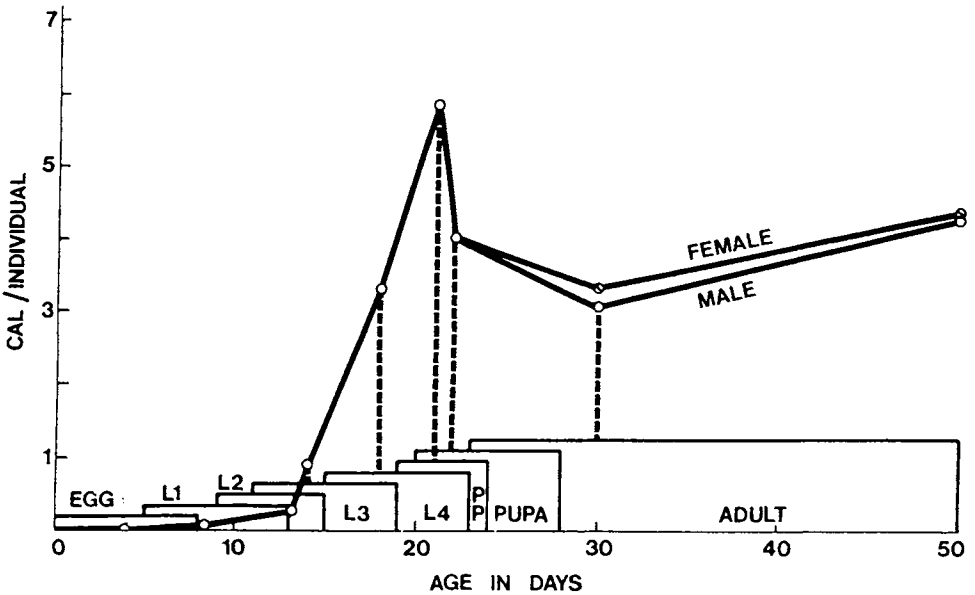

Figure 3. Caloric content of one individual rice weevil (*S. oryzae*) during its development in a wheat kernel from the egg through four larval stages (L1...L4), the prepupal (PP) and the pupal stage to the adult insect [132].

Ecological energetic information about hot springs is rare in literature, but one early contribution is cited here, the determination of energy flow of the dipterous herbivore *Hedriodiscus truquii* in two hot springs (35 and 47 °C) [136]. Lipid content and hence caloric values vary strongly in the larval body during the season. Energy budgets could be established in three instar stages and with a census for the whole population. Only up to 1 % of the algal primary production was consumed by *Hedriodiscus* although it acted as the dominant herbivore of these hot springs.

6.3. Fuel Alternatives

While fuelwood is marginal in the rich countries with a contribution of about 5 % to the total energy consumption (see also Chapter 10 *Wood*), about 40 % of the Third World's total fuel originates from biomass [137]. Biomass fuels - that are stems, branches, barks and roots of trees, shrubs, crop residues like straw, corn stover, cane or cotton stalks, leaves or grasses and dry animal dung in many countries - can be calculated to fuel by a mean caloric value of 15 kJ/g. Worldwide yearly consumption of this biomass - which could be applied far more use-

fully and efficiently in agriculture as fertilizer or amelioration factor in exhausted soils - amounts to 40 × 10^{18} J or an equivalent of 900 million tons of crude oil, compared to about 1400 million tons of all commercial energies in the Third World [137].

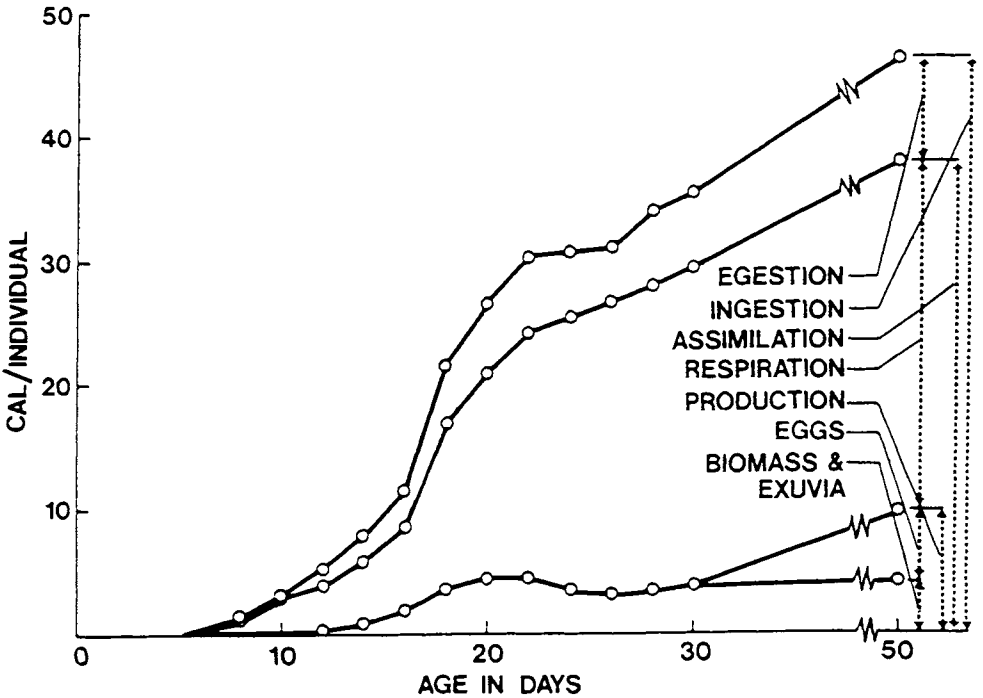

Figure 4. Cumulative energy budget for the rize weevil (*S. oryzae*) during its development from the egg to the adult. For the different larval and pupal stages see Figure 3 [132].

Count Rumford (1813) was one of the first scientists to study the combustion heat of wood, of course not yet in an oxygen bomb calorimeter [138]. He determined that the combustion heat of 1 pound of very dry oak wood burning without smoke and smell and with an "inappreciable quantity of ashes and no charcoal" is able to increase the temperature of 31.457 pounds of water by 180 °F. In our modern terminology the caloric value of this oak wood amounts to 13.17 kJ/g wet weight. Moreover, Count Rumford observed a striking similarity between his results and those of Lavoisier and Crawford. The original Table 1 of the author is presented in Figure 5.

Number of Experiments.	Quantity of Wood burned.	Elevation of the Temperature of the Calorimeter.	Result. Pounds of Water heated 180° with one Pound of Combustible.
1	5·10 gr.	$10\frac{1}{4}$ F.	31·051 lb.
2	5·13	$10\frac{1}{2}$	31·623
3	5·12	$10\frac{3}{5}$	31·941
4	4·95	10^{3}	31·212
Mean Result.....			31·457
Result according to Lavoisier and Crawford's experiments			31·684

It is rare to find experiments made by different persons at distant periods, and with very different apparatus, which agree better together.

But experiments which are well made, can never fail in agreeing in their results, whatever be the difference of the methods employed: it is nevertheless necessary to remark, that the coincidence in question could not be so perfect as it appears, for every thing depends upon the equality of the humidity which may exist in the wood and charcoal employed, a circumstance which it is impossible to establish.

Figure 5. Combustion heat of "very good dry oak wood" and comparison with the results of Lavoisier and Crawford [138].

Wood of the balsam fir (*Abies balsamea*) was investigated that was either living or killed by the bud spruce budworm. Gross heat of combustion averaged around 20.0 kJ/g with no significant differences between living and killed material [139]. Due to the strongly reduced moisture content of dead material the usuable heat increased greatly with the time of being dead from about 7.0 kJ/g for living samples to more than 11.0 kJ/g for 22-months dead ones.

Nine hardwood species were investigated as fuelwood in short-rotation forestry with the astonishing result that the observed differences in the caloric values of woods were just 4 % (mean 20.0 kJ/g) and that only bark (with less importance as fuel due to its small contribution to biomass) showed larger variations of up to 13 % (mean 20.08 kJ/g) [56]. Highest energy contents were found in leaves (21.13 kJ/g ovendry). Thus, biomass yield and ecological tolerance will have more influence on the specific harvest than the caloric values.

The energy potential of leafy spurge (*Euphorbia esula*) has been investigated to prove whether this perennial weed of the northern Great Plains of USA can be used as an alternative fuel crop [140]. Under optimal agronomic conditions the whole plant biomass showed a caloric content of 18.45 kJ/g and a 6.8 % oil content of 41.95 kJ/g, similar to the combustion heat of crude oil. Compared to other renewable energy sources leafy spurge produced 4 times more energy per year and hectare than straw and 8 times more than lodgepole pine and is thus an interesting alternative energy source.

In a series of papers Nunez-Regueira and coworkers [36,47,141,142] investigated the caloric values and flammabilities of forest species in Galicia/Spain and the use of forest waste as an alternative (municipial) energy source. The mean heat content of all wood species studied amounted to about 19.0 kJ/g similar to values observed for municipial solid waste so that these forest residues can be used as an additional fuel. Collecting forest material would for sure reduce the risk of forest fires [141,142], but the question remains open how the ecologic system reacts to this interference (see also Chapter *Wood* in this volume).

Municipal solid waste (MSW) is a huge problem for many communities due to lack of deposition places, danger of infections and annoyance by odour. Problems are reduced by the common technique of MSW incineration which at the same time renders heat to be transformed into electric energy. Thus, it is of great economic importance to know the energy contents of MSW and perhaps of its different fractions. They are determined by conventional combustion calorimetry on samples of about 1 g. Franjo and coworkers [143] found typical high heat values (HHV, see Introduction) of 22.440 kJ/g and low heat values (LHV) of 20.672 kJ/g. Paper contributed about 50 %, plastics 30 % (due to their high heat of combustion) and fermentables (food, garbage) 20 % to the LHV with minor or negligible heats of the other components.

However, it is often criticized that multi-ton quantities cannot be reduced representatively to 1 g samples burnt in conventional bombs and that milling MSW to 2 mm particles alters the composition. To check this criticism a - compared with the usual instruments - huge combustion calorimeter was constructed at the National Institute of Standards and Techniques in Gaithersburg, MD/USA [144]. With a combuster of about 0.2 m^3 volume in a calorimeter of 1.33 m outer diame-

ter and 2.60 m height it was suitable for burning 2.5 kg samples in a flow of oxygen near atmospheric pressure. The results show that the difference in combustion heats of unprocessed and processed MSW may be up to ± 3 % (mainly due to the difficulties to prepare "exactly identical" kg samples), while the differences between the conventional and the "huge" calorimeter is just ± 1 %. Careful preparation of MSW for combustion thus guarantees that reliable results are possible with conventional bomb calorimeters [145].

7. CONCLUSIONS

In this chapter on bomb calorimetry, possible applications from different biological fields have been presented, sometimes in competition with other methods such as analysis of elemental or chemical composition (carbohydrates, proteins, lipids) and the degree of reductance. In many cases it may depend upon the facilities of an investigator or an institute which approach is chosen or thought to be "more simple". Instead of expressing a personal considered opinion about the value of combustion calorimetry compared to other techniques, citations shall be presented from a few of the papers discussed in the preceding pages.

- "It must be emphasized that the usefulness of calorimetry depends upon the question being pursued. Calorimetry will remain essential for many ecological studies, but not for all those concerned with energy budgets." [75].
- "Whereas this type of calorimetry has been extremely valuable in obtaining heats of combustion of pure substances of known composition, the general literature shows that there is considerable variability associated with measuring the heat of combustion of biomass. The difficulties may be associated with an inability to account for exactly what is going on in the calorimeter by means of reaction equation giving all the reactants and products. Also, uncertainties may exist as to what comprises "ash", and what comprises the organic component, so that it becomes equally uncertain what the mass is that loses heat." [146].
- "However, bomb calorimetry is more simple and direct. It might be expected that the simpler method would be theoretically the more accurate. Practically, the direct and indirect methods of calorimetry appear to be similar in this respect if appropriate data for the latter are available." [146]
- "These data warn against exclusive use of biomass when resource allocation is the basis for comparing populations of plants... Plant resource allocation patterns...can best be obtained by the combined use of methods

based on biomass, calorimetry, metabolic costs, nutrients, and number of structures." [88].

- "Results with *Solidago* show strong correlation between biomass allocation and energy allocation. This reemphasizes Hickman and Pitelka's (1975) conclusion that calorimetry is not necessary to determine energy allocation patterns within populations in plants with primarily carbohydrate seed reserves." [48].
- "...combustion calorimetry provides the most general reference in ecological energy budget calculations." [31]
- "Because of this constancy in the caloric content and the small deviation from the mean of the systematic group the author rose the question which additional information about ecological systems can be obtained by bomb calorimetry." [100]
- "For the ecologist dealing with specific time and energy budgets or population energetics, direct calorimetry of representative members of the population is a prerequisite for accuracy." [26].
- "The guts of animals are not bomb calorimeters." [110]
- "At present the most useful measurement of energy in an ecological community is still caloric values (= heat of combustion) since they are relatively easy to determine and are good estimates of the energy available in a non-conservative growth reaction." [33]
- "The results" (of three different methods) "indicate that the gross energy content of feed and faeces can be determined most accurately by combustion." [124].

REFERENCES

1. W.A. Roth and F. Becker, Kalorimetrische Methoden zur Bestimmung chemischer Reaktionswärmen, Vieweg, Braunschweig, 1956, p. 114.
2. W.P. White, The Modern Calorimeter, Chemical Catalog Company, New York, 1928.
3. T.M. Sturtevant, in: Weissberger's Physical Methods of Organic Chemistry, 2nd ed., Interscience, New York, 1945, 311.
4. M. Kleiber, in: F. Uber (Ed.), Biophysical Research Methods, Interscience, New York, 1950.
5. F.D. Rossini (Ed.), Experimental Thermochemistry, Vol. 1. Interscience, New York, 1956.

6. E. Calvet, in: H.A. Skinner (Ed.), Experimental Thermochemistry, Vol. 2, Interscience, New York, 1962, p. 385.
7. H.A. Skinner (Ed.), Experimental Thermochemistry, Vol. 2., Interscience, New York, 1962, p. 457.
8. J.D. Cox, in: Thermodynamics and Thermochemistry, Butterworths, London, 1964.
9. S. Sunner and M. Mansson (Eds.), Combustion Calorimetry, Pergamon Press, Oxford, 1979, p. 428.
10. W. Hemminger and G. Höhne, Calorimetry - Fundamentals and Practice, Verlag Chemie, Weinheim, 1984, p. 310.
11. H.A. Skinner, in: H.D. Brown (Ed.), Biochemical Microcalorimetry, Academic Press, New York, London, 1969, p. 1.
12. H. Lieth and R.H. Whittaker (Eds.), Primary Productivity of the Biosphere, Springer, Berlin, 1975.
13. H. Lieth, in: H. Lieth and R.H. Whittaker (Eds.), Primary Productivity of the Biosphere, Springer, Berlin, 1975. p. 119.
14. H. Lieth, in: O.L. Lange, L. Kappen and E.D. Schulze (Eds.), Ecological Studies. Analysis and Synthesis, Vol. 19. Water and Plant Life, Springer, Berlin, 1976, p. 392.
15. H. Lieth, in: I. Lamprecht and B. Schaarschmidt (Eds.), Application of Calorimetry in Life Sciences, de Gruyter, Berlin, 1977, p. 325.
16. I. Lamprecht, in: A.E. Beezer (Ed.), Biological Microcalorimetry, Academic Press, London, 1980, p. 43.
17. J.A. McLean and G. Tobin, Animal and Human Calorimetry, Cambridge University Press, Cambridge, 1987, p. 338.
18. I. Lamprecht. in: Handbook of Thermal Analysis and Calorimetry, Vol. 1, Elsevier Science, Amsterdam, 1998.
19. H. Mackle and P.A.G. O'Hare, Trans. Farady Soc., 59 (1963) 2693.
20. E. Calvet, P. Chovin, P. Moureau and H. Tachoire, J. Chim. Phys., 57 (1960) 593.
21. H. Tachoire, Compt. Rend., 255 (1962) 2950.
22. J. Phillipson, Oikos, 15(1) (1964) 130.
23. G.B. Stokes, TIBS, 13 (1988) 422.
24. M.S. Kharasch, J. Res. Bur. Nat. Stand., 2 (1929) 359.
25. M.S. Kharasch and B. Sher, J. Phys. Chem., 29 (1925) 625.
26. R.T. Paine, Ann. Rev. Ecol. System., 2 (1971) 145.
27. J.H.T. Luong and B.Volesky, Adv. Biochem. Eng., 28 (1983) 1.
28. J.L. Cordier, B.M. Butsch, B. Birou and U. von Stockar, Appl. Microbiol. Biotechnol., 25 (1987) 305.
29. L.E. Erickson, Biotechnol. Bioengin., 22 (1980) 451.

30. K.P. Ho and W.J. Payne, Biotechnol. Bioeng., 21 (1979) 787.
31. E. Gnaiger and G. Bitterlich, Oecologia (Berlin), 62 (1984) 289.
32. M. Runge, Scripta Geobot., 4 (1973) 3.
33. D. Scott, Ecology, 46(5) (1965) 673.
34. J. Verduin, Ecology, 53 (1972) 982.
35. D. Crisp, in: N.A. Holme and A.D. McIntyre (Eds.), Methods for the Study of Marine Benthos, Blackwell, Oxford, 1984, p. 387.
36. L. Nunez-Regueira, J.A.R. Anon and J.P. Castineiras, Biores. Technol., 57 (1996) 283.
37. J.W. Wacasey and E.G. Atkinson, Mar. Ecol. Progr. Ser., 39 (1987) 243.
38. E.H. Battley and G. DiBiase, Biotechnol. Bioengin., 22 (1980) 2417.
39. T. Gurakan, I.W. Marison, U. von Stockar, L. Gustafsson, E. Gnaiger, Thermochim. Acta, 172 (1990) 251.
40. S. Fraschetti, M. Robertson, G. Albertelli, R. Capelli and A. Eleftheriou, Oebalia, 20 (1994) 117.
41. D.W. Schindler, A.C. Clark and J.R. Gray, J. Fish Res. Bd. Canada, 28(4) (1971) 559.
42. J.C. Dauvin and M. Joncourt, J. Mar. Biol. Ass. UK, 69 (1989) 589.
43. G. Cuendet, Rev. Suisse Zool., 92 (1985) 795.
44. H.G. Lovelady and E.J. Stork, Clin. Chem., 16(3) (1970) 253.
45. G.J. Prochazka, W.J. Payne and W.R.Mayberry, J. Bacteriol., 104 (1970) 646.
46. T. Andlid, C. Larsson, C. Liljenberg, I. Marison and L. Gustafsson, Appl. Microbiol. Biotechnol., 42 (1995) 818.
47. L. Nunez-Regueira, J.A.R. Anon and J.P. Castineiras, Biores. Technol., 61 (1997) 111.
48. W.G. Abrahamson and H. Caswell, Ecology, 63(4) (1982) 982.
49. L.C. Bliss, Ecology, 43(4) (1962) 753.
50. M.S. Darling, Oecologia (Berlin), (1976) 127.
51. B.W. Sweeney and R.L. Vannote, Ecology, 62 (1981) 1353.
52. A. Campbell, N.B. Singh and R.N. Sinha, Can. J. Zool., 54(5) (1976) 786.
53. A. Myrcha, J. Pinowski and T. Tomek, Bull. Acad. Pol. Sci. Ser. Sci. Biol. Cl. II, 21(10) (1973) 649.
54. L.J. Vitt, J.D. Congdon and N.A. Dickson, Ecology, 58 (1977) 326.
55. D.W. Tinkle and N.F. Hadley, Copeia, 2 (1973) 272.
56. M. Neenan and K. Steinbeck, Forest Sci., 25(3) (1979) 455.
57. E.P. Odum, S.G. Marshall and T.G. Marples, Ecology, 46(6) (1965) 901.
58. E.H. Battley, Appl. Environm. Microbiol., 61(4) (1995) 1655.

59. D. Fritzsche, Leistungsanalytische und resistenzökologische Untersuchungen zur Emanzipation des Polychaeten *Marenzelleria viridis* (Verrill 1873) gegenüber den Faktoren Salinität und Sauerstoffpartialdruck. Thesis, Rostock 1995.
60. L.J. Vitt, J. Herpetol., 12 (1978) 66.
61. W.A. Reiners and N.M. Reiners, Ecology, 53 (1972) 132.
62. L.A. Schroeder, Oecologia (Berlin), 28 (1977) 261.
63. S. Richman, Ecol. Monogr., 28 (1958) 273.
64. G.W. Comita and D.W. Schindler, Science, 140 (1963) 1394.
65. E.A. Cross, A.E.-S. Mostafa, T.R. Bauman and I.J. Lancaster, Environm. Entomol., 7 (1978) 647.
66. P.A. Ryan, N. Z. J. Mar. Freshw. Res., 19 (1982) 283.
67. G.J. Prochazka, W.J. Payne and W.R. Mayberry, Biotechnol. Bioengin., 15 (1973) 1007.
68. W.J. Payne, Biotechnol. Bioengin., 22 (1980) 1095.
69. A. Ginterova and A. Lazarova, Folia Microbiol., 34 (1989) 141.
70. E. Gottlieb, J. prakt. Chem., 2 (1883) 385.
71. J.D. Ovington and D. Heitkamp, J. Ecol., 48 (1960) 639.
72. F.B. Golley, Ecology, 42 (1961) 581.
73. E. Pipp and W. Larcher, Smn 196-4. Sitzber. Öster. Akad. Wiss., Math. Nat. Kl. Abtl. 1, 196(1-4) (1987) 37.
74. E. Pipp and W. Larcher, Smn 196-13. Sitzber. Öster. Akad. Wiss., Math. Nat. Kl. Abtl. 1, 196(5-10) (1987) 249.
75. J.C. Hickman and L.F. Pitelka, Oecologia (Berlin), 21 (1975) 117.
76. C.A. Smith and W.E. Evenson, Amer. J. Bot., 65(6) (1978) 714.
77. W.U. Kriebitzsch, Verhdlg. Ges. Ökol., 9 (1981) 117.
78. L.J. Collin and C.E. Jones, Amer. J. Bot., 67(2) (1980) 210.
79. P. Proksch, M. Proksch, P.W. Runde and E. Rodriguez, Biochem. System. Ecol., 10(1) (1982) 49.
80. B.K. Trivedi and G.P. Mishra, Ann. Arid Zones, 22(2) (1983) 107.
81. C. Hellmold and W. Schmidt, Verhdlg. Ges. Ökol., 17 (1989) 177.
82. J. Boscher, Oikos, 37 (1981) 328.
83. H. Dziadowiec and A. Kwiatkowska, Ekol. Polska, 28(1) (1980) 111.
84. J. Oszlanyi, Biologia (Bratislava), 34(10) (1979) 775.
85. J. Oszlanyi, Ekologia (CSSR), 1(3) (1982) 289.
86. F.B. Golley, Ecology, 50 (1969) 517.
87. S.R. Johnson and R.J. Robel, Ecology, 49(5) (1968) 956.
88. C.L. Jolls, Oecologia (Berlin), 63 (1984) 57.
89. E.B. Hadley and L.C.Bliss, Ecol. Monographs, 34(4) (1964) 331.
90. C.E. Boyd and C.P. Goodyear, Arch. Hydrobiol., 69(2) (1971) 256.

91. L.B. Slobodkin and S. Richman, Nature, 191 (1961) 299.
92. G.H.M. Keller, F.J.M. Schouten and L.M. Dalderup, Clin. Chem., 17 (1971) 121.
93. A. Gorecki, in: W. Grodzinski, R.Z. Klekowski and A. Duncan (Eds.), Methods for Ecological Bioenergetics, Lippincott, Philadelphia, 1975, p. 275.
94. A. Fergusson-Laguna and J. Pacheco, Acta Cient. Venez., 32 (1981) 239.
95. R.E. Ballinger and D.R.Clark, J. Herpetol., 7(2) (1973) 129.
96. J.D. Congdon, L.J. Vitt and W.W. King, Science, 184 (1974) 1379.
97. C.R. Blem and M.P. Zimmermann, Comp. Biochem. Physiol., A83(4) (1986) 661.
98. D.M. Maiorino, Bull. N. J. Acad. Sci., 22(2) (1977) 49.
99. W. d'Oleire-Oltmanns, Verhdlg. Ges. Ökol., 5 (1976) 181.
100. W. d'Oleire-Oltmanns, in: I. Lamprecht and B. Schaarschmidt (Eds.), Application of Calorimetry in Life Sciences, de Gruyter, Berlin, 1977, p. 315.
101. K.C. Cummins and J.C. Wuycheck, Verh. Theor. Angew. Limnol., 18 (1971) 1.
102. R. Grimm, Oecologia (Berlin), 11 (1973) 187.
103. M. Luxton, Pedobiol., 15 (1975) 161.
104. S.P.Hubbell, A. Sikora and O.H. Paris, Health Phys., 11 (1965) 1485.
105. T. Prus, Pol. Arch. Hydrobiol., 17 (1970) 183.
106. H.D. Bast and J.A. von Oertzen, Wiss. Ztschr. Wilhelm-Pieck-Universität Rostock, 25 (1976) 295.
107. H.G. Neuhoff, Mar. Ecol. Progr. Ser., 1 (1979) 255.
108. M. Slattery and J.B. McClintock, Mar. Biol., 122 (1995) 461.
109. J.B. McClintock, J. Heine, M. Slattery and J. Weston, J. Exp. Mar. Biol. Ecol., 147 (1991) 163.
110. J.B. McClintock, Mar. Biol., 94 (1987) 479.
111. J.B. McClintock, J.S. Pearse and I. Bosch, Mar. Biol., 99 (1988) 235.
112. M. Walker, P.A. Tyler and D.S.M. Billett, Mar. Biol., 96 (1987) 277.
113. M. Nagata, Bull. Jap. Soc. Sci. Fish., 49(1) (1983) 33.
114. L.S. Peck, M.B. Culley and M.M. Helm, J. Exp. Mar. Biol. Ecol., 106(2) (1987) 103.
115. A.J. Berry, J. Exp. Mar. Biol. Ecol., 66 (1983) 93.
116. J.-M. Deslous-Paoli and M. Héral, Oceanol. Acta, 9(3) (1986) 305.
117. J.-M. Deslous-Paoli, M. Héral and H. Massé, Bilan énergétique d'une population de *Crepidula fornicata* dans le bassin de Marennes-Oléron. in: Bases Biologiques de l'Aquaculture. Montpellier 1983, IFREMER, Actes Colloq. n^0 1, p. 109.

118. M. Héral and J.-M. Deslous-Paoli, Oceanol. Acta, 6 (1983) 193.
119. A. Dobrzycka and A. Szaniawska, Thermochim. Acta, 251 (1995) 11.
120. L.M. Cammen, E.D. Seneca and L.M. Stroud, Am. Midl. Nat., 103(2) (1980) 238.
121. D.W. Rodgers and S.U. Quadri, Can. J. Zool., 55(5) (1977) 881.
122. M. Walkey and R.H. Meakins, J. Fish Biol., 2 (1970) 361.
123. R.K. Harris, T. Nishiyama and A.J. Paul, J. Fish Biol., 29 (1986) 87.
124. A.M. Henken, H. Lucas, P.A.T. Tijssen and M.A.M. Machiels, Aquaculture, 58 (1986) 195.
125. C.E. Boyd and C.P. Goodyear, Arch. Hydrobiol., 69(2) (1971) 256.
126. J.B. McClintock, Oecologia (Berlin), 70 (1986) 161.
127. R.L. Lindeman, Ecology, 23 (1942) 399.
128. F.L. Long, Plant Physiol., 9 (1934) 323.
129. S. Adamandiadou, L. Siafaca and N.S. Margaris, Flora, 167 (1978) 574.
130. L. Siafaca, S. Adamandiadou and N.S. Margaris, Oecologia (Berlin), (1980) 276.
131. T.F. Jensen, Natura Jutlandica, 18 (1975) 10.
132. N.B. Singh, A. Campbell and R.N. Sinha, Ann. Entomol. Soc. Am., 69(3) (1976) 503.
133. N.B. Singh and R.N. Sinha, Ann. Entomol. Soc. Am., 70(1) (1977) 107.
134. R.N. Sinha, Ann. Technol. Agric., 22(3) (1973) 351.
135. R.N. Sinha, Environm. Ecol., 6 (1977) 185.
136. J.G. Stockner, J. Fish. Res. Bd. Canada, 28 (1971) 73.
137. V. Smil, Energy, Food, Environment - Realities, Myths, Options. Clarendon Press, Oxford, 1987, p.369.
138. Count Rumford, Phil. Mag., 42 (1813) 296.
139. D.P. Barnes and S.A. Sinclair, Wood Fiber Sci., 16(4) (1984) 518.
140. B.D. Maxwell, S.M. Wiatr and P.K. Fay, Econom. Bot., 39(2) (1985) 150.
141. J.A.R. Anon, M.G. Anon, F. Fraga, J. Palacios and L. Nunez-Regueira, J. Therm. Anal., 41 (1994) 1393.
142. J.A.R. Anon, F.F. Lopez, J.P. Castineiras, J.P. Ledo and L. Nunez-Regueira, Bioresource Technol., 52(3) (1995) 269.
143. F.C. Franjo, J.P. Ledo, J.A.R. Anon and L. Nunez-Regueira, Environm. Technol., 13(11) (1992) 1085.
144. K.L. Churney, A.E. Ledford, M.L. Reilly and E.S. Domalski, J. Res. Natl. Bur. Stand., 91(5) (1986)277.
145. E.S. Domalski, K.L. Churney, A.E. Ledford, J.C. Colbert, S.S. Bruce, T.J. Buckley, R.C. Paule and M.L. Reilly, Pure Appl. Chem., 63(10) (1991) 1415.

146. E.H. Battley, Thermochim. Acta, 250 (1995) 337.

Handbook of Thermal Analysis and Calorimetry. Vol. 4: From Macromolecules to Man.
R.B. Kemp, editor.

Chapter 5

THE THERMODYNAMICS OF MICROBIAL GROWTH

Edwin H. Battley

Department of Ecology and Evolution, State University of New York at Stony Brook, Stony Brook, NY 11794-5245, USA.

1. INTRODUCTION

There are several reasons for studying the thermodynamics of microbial growth. The most important of these is that such studies may increase our comprehension of the extent to which energy becomes transferred from substrate to cellular substance during the process of growth. Microorganisms are the most simple and convenient tools for studying this because of the limited nutrient requirements of many of them. Information obtained in this manner can be used as a basis for studying the thermodynamics accompanying the growth of cells from multicellular organisms. Another reason is that such studies may tell us something about the way in which energy becomes recycled in the biosphere. This is an important aspect of microbial ecology, which is the study of relationships of all kinds between the microorganisms that accomplish energetic and material recycling, and their environments. A third is that the knowledge gained may be of some practical use in biotechnology. A fourth reason is simply that carrying out such studies involves a challenging combination of biology, physics, and chemistry, and the pulling together of all sorts of ideas from these different disciplines. When this is done, in spite of the biochemical complexity of the process of cellular growth, its thermodynamics appears to be relatively simple and capable of being described without recourse to extensive theoretical treatment involving irreversible thermodynamics. It must be emphasized that the same methods for the culture of microbial cells may not be applicable directly to the growth of other types of cells, especially animal cells and protists lacking cell walls. This will be further emphasized in the text. It is the nutritional simplicity of microbial growth that makes microorganisms useful tools for thermodynamic studies, quite apart from other interests in them as a group. Thermodynamics is a universal phenomenon and the principles of energy transfer worked out with microbes should be applicable in some manner to the

growth of all kinds of cells.

Any complete, thermodynamic study must include measurements or determinations of the free-energy, enthalpy, and entropy changes accompanying the transition of a system from a defined initial state to a defined final state. This is no less true for studies of the spontaneous process of microbial growth.

2. MATERIAL GROWTH PROCESS SYSTEMS.

A thermodynamic system is a bounded space containing what is being studied. A growing cell is an open system, but because cells are usually extremely small it is not often practical to study them as individuals. The simplest method of studying them is to treat cells in the aggregate as a biomass product that develops as the result of the process of growth. The bounded space can then be chosen as a culture vessel (reactor) containing a suitable culture medium in which the cells being studied are grown. What takes place in the vessel during growth is usually called a "growth process" because it is vastly more complex than a simple reaction. Thermodynamic changes take place as this growth process system proceeds from a thermochemically defined initial state to a thermochemically defined final state. The formation of a mass of cells is one of the consequences of this process. For microbial systems low concentrations of reactants can be used, so that there is no significant exchange of materials between the system and the environment. The culture medium within the culture vessel can be regarded then as a thermodynamically closed system of which the process of growth is a part. This is not true for cultures of animal cells, in which a constant partial pressure of $O_2(g)$ and $CO_2(g)$ must be maintained by passing these gases through the system, and in this respect such cultures are at least in part open systems. On the other hand, if this is done at a constant rate, a steady state condition can be maintained involving a constant energy exchange. Although in theory it ought to be possible to deal with all kinds of growing cells, the least difficult system for studying the thermodynamics of cellular growth makes use of a pure culture of microorganisms that can be grown on a single substrate, or of plant or animal cell lines that have minimal culture requirements. But even for these latter other, more specific, aspects of the culture system must be observed. Cells not possessing cell walls must be provided constantly with enough energy to prevent water from entering the cytoplasm by the Gibbs-Donnan effect, and this and other energy requirements for the maintenance of the cell are in addition to those for growth. A batch culture system is preferable for studying the thermodynamics of microbial growth only in that it best simulates what occurs naturally. Also, during the exponential phase of a batch culture the average composition of the cells is constant. Microorganisms living in a natural environment respond to the presence of a food source by growing exponentially until this substrate becomes exhausted,

after which the biomass that has been formed dies and/or becomes a food source for the next higher level of the food chain. This condition of exponential growth until no further substrate remains is most simply reproduced by batch culture. To measure the heat of growth it is necessary to enclose the system in a calorimeter. The calorimetric methods used can be either adiabatic, whereby the increase in temperature of the growth process system is measured, or isothermal, whereby a measurement is made of the quantity of heat transferred out of the calorimeter at a constant temperature.

2.1. The initial state of a growth process system.

For microbial growth process systems the simplest initial state consists of an aqueous solution of the necessary inorganic macro- and micronutrients, vitamins, and a single organic substance, or substrate, that serves both as a carbon source and an electron donor. The macro- and micronutrients are those required by all cells. These are $NH_4^+(aq)$ or $NO_3^-(aq)$, $H_2PO_4^-(aq)$, $SO_4^{2-}(aq)$, $K^+(aq)$, $Mg^{2+}(aq)$, and $Ca^{2+}(aq)$ as macronutrients, and $H_2BO_3^-(aq)$, $Cu^{2+}(aq)$, $Cl^-(aq)$, $Fe^{3+}(aq)$, $Mn^{2+}(aq)$, $Co^{2+}(aq)$, and $Zn^{2+}(aq)$ as micronutrients. For some cells $MoO_4^{2-}(aq)$ or $SiO_4^{2-}(aq)$, may also be required. Micronutrients can often be supplied as impurities accompanying the macronutrients. Requirements for vitamins, if any, differ with different micro-organisms and have to be known in advance if these are to be included in the culture medium. Many single substrates are both carbon sources and electron donors, the most common being sugars, amino acids (which can serve also as a source of nitrogen), and small molecular weight alcohols and fatty acids. It is important that the osmolality of the culture medium, the pH, and the temperature are suitable (preferably optimal) for the cells being studied, so that the only thing limiting the extent of growth is the quantity of the substrate. The prepared medium should be completely clear, so that no precipitates or suspended nutrients will interfere with the accurate determination of the cellular yield, which is obtained by centrifuging the cells from suspension, washing twice, and determining their dry weight. Finally, the initial state must contain a few cells capable of growth in the culture medium being used. These are added to the medium in order to initiate an experiment. Growth occurs because the cells are self-reproducing catalysts. The inoculum can be made sufficiently small that its biomass is negligible. It is thus excluded from the initial state for purposes of calculating a mass balance. The initial state must be sterile in order to limit the growth-process to the organism being studied, and precautions to ensure sterility must be observed until a growth experiment is over.

Animal cell culture systems all require at least two substrates as carbon and/or nitrogen sources, and electron donors [1] and usually require more [2], as illustrated by reference [3]. Higher plant cell culture systems are equally complex [4]. This complicates efforts to understand what is the source of energy that enters into

their growth processes, quite apart from the energy source for cellular maintenance. In autotrophic cell cultures the source of electrons (oxidizable inorganic substances, or light) is different from the source of carbon, which is CO_2(aq). It is evident that growth process systems other than those involving heterotrophic microorganisms offer increased challenges with respect to understanding the thermodynamics of cellular growth processes.

2.2. The final state of a growth process system.

This consists of the cells that have grown and other products of the growth process, plus anything that is not completely utilized such as extra macro- and micronutrients and vitamins. Batch culture experiments can be constructed so that the substrate is the only limiting factor and becomes exhausted, resulting in the complete cessation of growth. In aerobic systems the products are often only CO_2(aq) and H_2O(l), although partially oxidized substrates can also occur as products depending on the cells being studied. In anaerobic systems additional products typically consist of substances resulting from the dismutation of the substrate. Among these there can be CO_2(aq), alcohols, organic acids, or ketones.

2.3. A cautionary note.

In studies on the thermodynamics of microbial growth it is important that only growth is being considered and not growth plus something else. Microbial cells take advantage of any opportunities either to grow or to accumulate storage materials, or both. Cells in an environment that is growth-limiting in some respect (for example, an insufficiency of nitrogen or a given macro- or micro nutrient, or too low a temperature) but in which there is an ample supply of energy will accumulate storage materials for use in future metabolism. This can occur aerobically or anaerobically and is called, respectively, oxidative or fermentative assimilation. Descriptions of these processes have been summarized recently with respect to micro-organisms [5]. It was pointed out originally in 1900 [6] and emphasized more recently [7,8] that microbial storage products are not a part of the structure, or fabric, of microbial cells, and are really internal substrates that become utilized when an external substrate becomes exhausted. For an accurate elemental analysis of cellular structure cells must be free of storage substances. This appears to happen when microbial cells are grown exponentially in batch culture at their highest specific growth rate (μ_{max}), as shown by the abrupt cessation of the heat production accompanying a growth process, following the exhaustion of the substrate [9,10]. The presence of storage substances can have an effect not only on the elemental composition of cells but especially on what is interpreted to be the yield of cells on a given quantity of substrate. For example, oxidative or fermentation assimilation results in the synthesis of inositol and glycogen as the principal storage

products in yeast. Yeast cells can be grown aerobically on glucose. However, if only 20% of the glucose were to be oxidatively assimilated, this would result in an increase in cellular dry weight of 52 % over what would occur if growth were the only process taking place, giving a corresponding erroneous increase in the apparent yield of cells [11].

Cells other than microorganisms present other difficulties. Growing animal cells may or may not contain storage substances. When they do not, they are capable of utilizing their structural materials for purposes of maintenance, becoming smaller in this process. Growing higher plant cells may also contain storage substances. There is the additional problem with both plant and animal cells of how to distinguish between the energetic changes that accompany growth and those accompanying differentiation. If cells to be analyzed for their elemental composition do contain storage substances, the mass of these latter can be determined chemically at the end of growth and subtracted from the rest of the biomass. However, it is apparent that the more complex the growth process system, the more difficult it will be to analyze the thermodynamics of that process.

2.4. Growth process equations.

A growth process equation represents the material balance of a system that contains exponentially growing microbial cells. The left and right sides of the equation represent the initial and the final states of the system, as well as the required compliance with the Law of the Conservation of Mass. A growth-process is an extremely complex oxidation-reduction (O-R) phenomenon, and in common with all O-R reactions or processes the composition and quantity of each of the reactants and products must be known. However, it is not necessary to measure all of these. In the simplest cases, both the quantity of a known substrate introduced into the system and the composition of each of the reactants is known. It is the products of the growth process that have to be determined, including the cells and small molecular weight organic substances if these latter are formed. Unless there is evidence to the contrary, it is assumed that the inorganic products are CO_2(aq), H_2O(l), and NH_3(aq) if a nitrogenous substrate is used. Otherwise, the quantities of these substances can be determined. In theory, growth process equations can be written for all kinds of cells.

2.4.1. Harvesting the cells.

Typically, after growth has ceased most microbial cells can be centrifuged from suspension, washed twice by suspending them in distilled water followed by recentrifugation, and then lyophilized. All this can be done in a previously weighed centrifuge tube, with the lyophilization being carried out by placing the tube in a desiccator over concentrated H_2SO_4 followed by evacuation [12]. There is a more

conventional method that can also be used in which samples to be lyophilized are placed in glass ampules and frozen quickly by immersion in liquid nitrogen, followed by a connection at room temperature to an evacuation system in which there is a reservoir immersed in liquid nitrogen which traps the water removed by sublimation from the samples [13]. It has been recommended that following lyophilization the sample should be held at 100 °C for 24 hours prior to weighing or other experimentation [13].

2.4.2. Determining cellular composition.

Once the total quantity of cells produced during a growth process is known, the cellular composition can be determined. The question arises here as to whether a cell grown on one substrate has intrinsically a different composition from the same kind of cell grown on a different substrate. This was initially thought to be true [9], in that analyses of *Saccharomyces cerevisiae* cells grown on different substrates did indeed appear to be slightly different. However, these analyses were performed at a time when microchemical determinations in general were just beginning to be performed, and it may have been that the small differences were the result of experimental error. Different enzymes are involved at the beginning of a metabolic reaction chain in the utilization of different substrates by a given kind of cell. But, these enzymes are proteins, and at present it seems completely reasonable to assume that the fabric of a cell of a given species grown at μ_{max} on one substrate (exclusive of storage products) is identical to that of a cell of the same species grown at μ_{max} on a different substrate (also exclusive of storage products). It is equally reasonable to assume that the cellular composition (again, exclusive of storage products) of one microbial species may be slightly different from that of another species.

Cellular composition has been obtained formerly by using combustion analysis to determine the percentages of C, H, N, and ash in a given mass of dried cells, the quantity of O being calculated by difference from the total dry weight. Descriptions of what constitutes "ash" differ in the literature. Ash can be considered what remains after total combustion, and consists of the salts or oxides of the inorganic substances in cells. It has been accounted for largely as the oxides of P, K, Na, Mg, Ca, Si, S, and Fe, with Cl presumably as a salt of the cations [14]. In more recent compendia [15,16] the minerals found in yeasts are listed on a per cent solids basis, without reference to the oxides or carbonates that are the actual products of combustion. Thus, there is a present tendency to regard "ash" as the substance and form in which minerals exist *within* the cells. Although the ash (mineral content) is a fraction of the cellular dry weight it has always been regarded as being energetically non-functional, and "should not be considered as part of the elemental composition or enthalpy of combustion."[13]. This implies that "ash" consists of the inorganic part of the cell, as is. It also implies that the weight

of the inorganic substances comprising part of the cellular composition does not change on combustion. However, using *Escherichia coli* K-12 as a model it has been shown that the atoms other than C, H, O, and N contribute greater weight to ash as oxides and salts than they do as part of the cellular fabric [17]. An accurate formula representing the proportions of C, H, O, N, P, and S within a unit mass of cells, and a knowledge of the kind and quantity of cellular ions associated with this biomass is essential to obtain accurate values of cellular thermodynamic properties. A better method of doing this is to determine the percentages of C, H, O, N, P, and S directly, the difference between the sum of these and 100 per cent being the weight of *inorganic ions*. Compressed Red Star "universal" baker's yeast (*Saccharomyces cerevisiae*, manufactured by General Foods Corporation, Milwaukee, Wisconsin 53218, U.S.A.) can be used to describe the methods for determining cellular composition because it contains the smallest quantity of stored carbohydrates of any of the commercial preparations tested. This yeast is grown on a solution of clarified molasses and nutrients and washed twice during concentration from the fermenters by being passed through a separator (effectively a zonal centrifuge). Other culture methods are used for different kinds of cells, although harvesting methods on a greater or lesser scale are all similar. Because of the culture methods used, compressed yeast does contain variable amounts of glycogen and inositol which must be removed in order to obtain an accurate elemental analysis of the cellular fabric. This is done by suspending the yeast in distilled water in a 1:1, wt:vol ratio and incubating the suspension at 30 °C to ferment away any residual carbohydrate storage material. Aliquots of this suspension can be tested at intervals to determine if any residual carbohydrate is present. The Warburg or other manometric technique can be used for this purpose, with the gas phase in the vessels being filled with an inert gas. Another simple technique is the Durham tube [18] method, which is illustrated in Figure 1. It should be emphasized that this is a qualitative, not quantitative technique. For the Red Star yeast, when no further fermentation was observed (usually about 16 hrs), the cells were centrifuged from suspension and lyophilized [12]. An empirical analysis of these cells is given in Table 1. In this particular analysis the weight of ash is calculated to be 8.62 %. The sum of the percentages of C, H, N, and ash is then 69.18 %. If this value is subtracted from 100 %, the value for O as determined by difference is then 30.82 %, whereas the actual value for the O content as determined directly by chemical analysis is 34.03%. This illustrates the necessity for determining O this way, rather than by difference. The results of an analysis of cell composition in this manner, even of cells of the same species, may vary slightly with the strain of yeast cells used, the manner of preparation of the cells for analysis, and the analyst. Micro nutrients having a relative mass compared to one g atom of carbon of less than 0.001 are not included because the formula representing the cells would then become

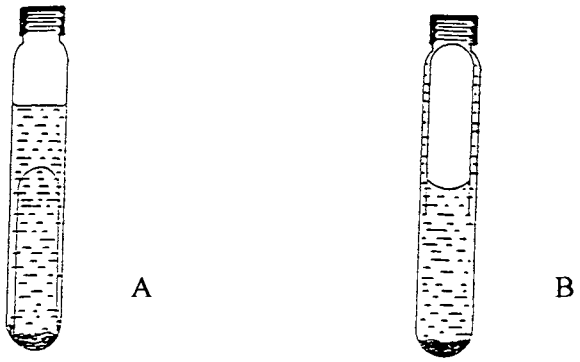

Figure 1. An illustration of the Durham tube method. A Durham tube consists of a smaller test tube inverted inside a larger tube, both of which are sterile. To test for the presence of intracellular *fermentable* carbohydrate the larger tube is three-quarters filled with a suspension of cells, the smaller tube is inserted into the larger tube, and the cap is screwed tight. The assembly is then inverted to fill the enclosed smaller tube with the suspension, righted, and incubated at an appropriate temperature (30 °C is good for yeasts) as shown for tube A. If fermentable carbohydrates are present in the suspended cells, gas will accumulate in the top of the inverted smaller tube, causing it to float inside the larger tube, as shown for tube B.

too cumbersome to work with. An analysis of Red Star yeast results in the following empirical formula.

$$C_{3.820}H_{6.161}O_{2.127}N_{0.605}P_{0.045}S_{0.012}K_{0.083}Mg_{0.010}Ca_{0.003} \quad (A)$$

However, a formula such as this is not particularly convenient to deal with, and the use of a unit-carbon formula (UCF) was adopted [9], the concept of which has been in general use ever since. Formula (A) then becomes

$$CH_{1.613}O_{0.557}N_{0.158}P_{0.012}S_{0.003}K_{0.022}Mg_{0.003}Ca_{0.001} \quad (B)$$

Actually, this would better be called an ion-containing unit-carbon formula (ICUCF), since it accounts for almost all of the cellular mass. This is necessary if accurate measurements of cellular entropy are to be made. Formula (B) represents a biomass having an ion-containing unit carbon formula weight (ICUCFW) of 26.202 g. Although the term "unit-carbon formula weight" (UCFW) or its derivatives has historical precedence, the term "carbon mol" (Cmol) recently has come into wide use in the literature describing the same thing, an example of which is reference [19]. This latter acronym is easier to say or use, and will be adopted here along with the acronym for one ion containing carbon mol (ICCmol). The acronym ICUCF remains the same, since it does not represent a mass.

Table 1
Analysis of the elements in 100 g dry wt of *Saccharomyces cerevisiae* cells.[a]

Elements	g % dry weight	average (g %)	g % as ash
STRUCTURAL			
Carbon[b]	45.78, 45.68, 45.93, 46.12	45.88	
Hydrogen[b]	6.42, 6.26, 6.03, 6.14	6.21	
Oxygen[b]	34.55, 34.86, 33.11, 33.61	34.03	
Nitrogen[b]	8.48, 8.45, 8.65, 8.28	8.47	
Phosphorous[b]	1.27, 1.44, 1.41, 1.39	1.38	3.16 as P_4O_{10}(cr)
Sulfur[c]		0.39	2.12 as K_2SO_4(cr)
Subtotal structural elements:		96.36	
IONIC:			
Potassium[d]		0.95	as K_2SO_4(cr)
		2.29	2.76 as K_2O(cr)
Magnesium[d]		0.25	0.41 as MgO(cr)
Calcium[d]		0.12	0.17 as CaO(cr)
Subtotal cellular ions:		3.61	
TOTAL:		99.97	8.62

Empirical formula: $C_{3.820}H_{6.161}O_{2.127}N_{0.605}P_{0.045}S_{0.012}K_{0.083}Mg_{0.010}Ca_{0.003}$
Ion-containing unit carbon formula: $CH_{1.613}O_{0.557}N_{0.158}P_{0.012}S_{0.003}K_{0.022}Mg_{0.003}Ca_{0.001}$
Ion-containing unit carbon formula weight: 26.202 g; AE = 4.079; eq = 4.577

[a] Red Star baker's yeast (General Foods Corp., Milwaukee, Wisconsin 53218, USA).

[b] These values were determined by MHW labs, P.O.Box 15149, Phoenix, AZ 85018, with oxygen being determined directly using the method of Aluise, et al [20].

[c] This value was taken from Reed and Nagodawithana [16].

[d] The values for K^+, Mg^{++}, and Ca^{++} add up to the difference between 96.36 % structural material and 99.97 %. According to the data of Reed and Nagodawithana [16], the trace elements amount to about 0.03 g % dry weight and about 0.83% of the total ion content. The ratios of K^+:Mg^{2+}:Ca^{2+} are 1.000:0.079:0.036. The product of *bomb calorimetric* sulfur oxidation is taken here as K_2SO_4(cr). This may not be entirely correct if some of the sulfur remains as SO_2(g) or SO_3(g). The products K_2O(cr), MgO(cr) and CaO(cr) are assumed from the data of Gurakan et al [13], which showed that at 600 °C there was no carbon in the ash. On the other hand, when plant-like products are burned in air the mineral products of combustion are carbonates.Thus, if part or all of the combustion inside a bomb calorimeter were to take place at a temperature of less than 600 °C (for example, at 400 °C), the products would be more correctly K_2CO_3(cr), $MgCO_3$(cr), and $CaCO_3$(cr). The ash weight calculated here is similar to the 8.12 % dry wt obtained for *S. cerevisiae* by Gurakan et al [13] and might not be expected to be exactly the same in that the ash content of cells depends on the strain of cells used and how they are grown.

Most microbial cells do not ferment cellular storage substances but oxidize them. Obligately anaerobic and facultative microorganisms (some yeasts and bacteria) are the exceptions. Analysis of the structural material of aerobically-grown cells that contain storage substances requires a different procedure. Here use can be made of a Warburg respirometer, a biological oxygen demand (BOD) determination, or an oxygen electrode, to determine when endogenous respiration ceases. However, the most convenient method is still to grow the cells exponentially at μ_{max} using optimal growth conditions, whereupon microbial cells apparently do not store substances by fermentative or oxidative assimilation.

2.4.3. Constructing growth-process equations representing the system.

Conventionally, the total dry weight of cells formed from the quantity of substrate used in a given growth experiment is converted into the quantity that would be formed from one mol of substrate. This is the molar growth yield, having the dimensions of grams dry weight of cells grown per mol of substrate utilized. The molar growth yield divided by one ICCmol gives the molar yield coefficient (MYC), which is the number of ICCmols formed from one mol of substrate. Alternatively, because it is a *unit*-carbon formula that is used to represent the cells, the MYC can be determined directly from the quantity of carbon incorporated into the cells from one mol of substrate. MYCs can also be determined in the same manner for any other organic product of a growth-process. The quantities of CO_2(aq) and H_2O(l) formed as products are determined by difference. The quantities of the N, P, S, K, Mg, and Ca sources that are utilized during growth are determined by multiplying the MYC by the quantities of these elements in the cells or other product. These methods apply whether growth is aerobic or anaerobic. Whereas during aerobic growth the organic products are often only the cells, with anaerobic growth there are always organic products in addition to the cells, and these have to be determined individually. Organic products are treated operationally in the same manner as the cells.

2.4.4. Representing anabolism and catabolism.

A growth-process equation as a whole represents metabolism, and is the sum of the equations representing the other processes that take place concurrently. For the heterotrophic growth exhibited by yeasts, these latter can be regarded most simply as the processes of anabolism, which is cellular synthesis, and of catabolism, which provides the energy to bring about anabolism. A part of the substrate is utilized as

a carbon source and an electron donor for anabolism, and the other part is used as an electron donor for the complex, catabolic oxidation-reduction processes that generate ATP used to provide the activation energy for anabolism. This, of course, is a simplification.

Among microorganisms there are many types of metabolism that are all variations on the same overall biochemical scheme. Something has to serve as a source of energy, something as an electron donor, and something as a source of carbon. Thus, the yeast described here is a chemoorganoheterotrophic microorganism in that its source of energy is chemical, and its source of electrons is a small number of organic compounds that can also serve as a carbon source. Some electron donors can be anaerobically fermented, but others can only be oxidized. Most commonly known bacteria, and all the fungi and protozoa exhibit these types of metabolism. Some bacteria are chemolithoautotrophic. Here, the source of energy is chemical, the source of electrons is a small number of inorganic substances, and the source of carbon is CO_2(aq). The electron donor is aerobically oxidized. Among these are those bacteria that oxidize H_2(aq), H_2S(aq), $S_2O_3^{2-}$(aq), NH_4^+(aq), NO_2(aq), etc. In photoorganoheterotrophic growth the source of energy is light and the source of electrons is a small number of organic acids and alcohols which also serve as the carbon source. This type of metabolism occurs in the non-sulfur purple photosynthetic bacteria. Photolithoautotrophic growth also occurs, and here the source of energy is light, the source of electrons is a small number of reduced sulfur compounds, and the source of carbon is CO_2(aq). The purple and green sulfur photosynthetic bacteria carry on this type of metabolism. Note that here the sources of energy, electrons, and carbon are all different, and not combined as in chemoorganoheterotrophs. Many microorganisms carry out the oxygenic photosynthesis characteristic of higher plants, and these might best be called photohydroautotrophs. Here the source of energy is light, the source of electrons is water, and the source of carbon is CO_2(aq). The equation representing anabolism is similar for all of the above types of metabolism, in that the anabolic substrate can be written as an organic substance that either originates in the environment, or is the product of CO_2(aq) reduction. Equations representing catabolism differ. CO_2(aq) reduction is neither anabolism nor catabolism, and should be introduced in a separate equation as providing an organic substrate for anabolism. The point is that equations representing anabolism, catabolism, and CO_2(aq) reduction where these occur, can be written to represent any type of growth metabolism in order to study the thermodynamics of microbial growth. What is presented in this Chapter is only the

beginning of what is possible.

2.4.5. Available electrons and equivalents.

All biological substances capable of being oxidized contain electrons that can be transferred to $O_2(aq)$, the number transferred being a function of the kind of oxidation. Biologically important organic substances can contain C, H, O, N, P, and S, and the products of their *biological* oxidation are $CO_2(aq)$, $H_2O(l)$, $NH_3(aq)$, $H_2PO_4^-(aq)$ and $H_2S(aq)$. Because organic N and S are not oxidized biologically to $N_2(g)$ and sulfur oxides as would occur in a bomb calorimeter, the number of electrons transferred to $O_2(aq)$ is less, i.e., a lesser number is "available." These are said to be "available electrons" (AE), and the understanding is that these are what are contained in substances that are oxidized biologically [21]. The number of AE in a biologically important substance can be calculated readily by means of the following equation [22],

$$AE = 4nC + nH - 2nO - 3nN + 5nP - 2nS \qquad (1)$$

where nC, nH, nO, nN, nP, and nS are the numbers of C, H, O, N, P, and S atoms in the formula representing the substance. If a given atom is not present in a substance, it is ignored, and ions are not included since they are not involved in the transfer of electrons. Using equation (1) glucose, $C_6H_{12}O_6$, contains 24 AE, and the biomass represented by formula (B) contains 4.079 AE. The electrons transferred to $O_2(g)$ during a non-biological oxidation, as in a bomb calorimeter, conventionally are called equivalents (eq). These reactions differ from those described by equation (1) in that N in an organic substance becomes oxidized to $N_2(g)$ and S to a gaseous oxide (SO_3?) which might combine with $K_2O(c)$ to produce $K_2SO_4(c)$.The equation representing the number of equivalents transferred to $O_2(g)$ is then [23, 24]

$$eq = 4nC + nH - 2nO - 0nN + 5\,nP + 6\,nS \qquad (2)$$

Atoms that are not present in a substance are ignored. For substances such as glucose not containing N, P, or S, AE = eq. On the other hand, for the biomass represented by formula (B) eq = 4.577, which is considerably higher than 4.079 AE. This is because of the further oxidation of nitrogen and sulfur. Phosphorous is already in its highest oxidation state in biologically important substances. Ions such as Mg^{2+}, Ca^{2+}, and K^+ do not contribute electrons since they do not become further oxidized.

The difference between the idea of eq and AE is sometimes not recognized, and can lead to differences in the interpretation of data.

2.4.6. Representing anabolism.

Because the electrons in the biomass can only come from that portion of the substrate that is used to construct the biomass, this quantity of substrate can be calculated as

$$S_{an} = \frac{MYC_{cells} \cdot AE_{cells}}{AE_{sub}} \tag{3}$$

In equation (3) S_{an} represents the anabolic substrate, which is the fraction of one mol of substrate that is utilized for cell production; MYC_{cells} is the molar yield coefficient; AE_{cells} has been defined previously; and AE_{sub} is the number of AE in one mol of substrate. As an example given in Table 2, the MYC_{cells} for the growth of *S. cerevisiae* aerobically on glucose is 1.914. The quantity of electrons in this biomass can only have come from that portion of the substrate that is utilized for biomass construction. Using equation (3), this quantity of substrate is then $(1.914 \cdot 4.079) \div 24 = 0.325$ mol glucose. The mass of the ions as represented in formula (B) has to be considered in entropy determinations, which is why they are included in an ICUCF. Once the quantity of substrate and the quantity of cells are determined, the quantities of the other reactants can be calculated. The nature of these latter is known because of their having been added to the culture medium in the form of a nitrogen, a phosphorous, and a sulfur source. In addition to carbon, hydrogen, and oxygen, these elements comprise the fabric of the cells. Here, these other reactants are $NH_3(aq)$, $H_2PO_4^-(aq)$, and $SO_4^{2-}(aq)$. Unless otherwise determined, the inorganic products of an aerobic growth process are taken to be $CO_2(aq)$ and $H_2O(l)$. The coefficients for the reactants other than the substrate are obtained by multiplying the quantities of N, P, and S in the cells by the MYC. The quantity of $CO_2(aq)$ is calculated as the difference between S_{an} multiplied by the number of C atoms in the substrate, and the MYC of the cells (since the quantity of C in the cells is always 1). The ions in the cells are supplied by ions in solution as reactants, the quantities of which are calculated by multiplying the quantities of K, Mg, and Ca in the cells by the MYC. The electrostatic balance of the equation is accomplished by adding $H^+(aq)$ or $OH^-(aq)$ as a reactant or product, in common with the construction of any O-R equation. For the example of the aerobic growth of *S.*

cerevisiae on glucose in Table 2, the equation representing anabolism then becomes

$$0.325\ C_6H_{12}O_6(aq) + 0.302\ NH_3(aq) + 0.023\ H_2PO_4^-(aq) + 0.006\ SO_4^{2-}(aq) \quad (4)$$
$$+0.042\ K^+(aq) + 0.006\ Mg^{2+}(aq) + 0.002\ Ca^{2+}(aq) + 0.023\ OH^-(aq) \rightarrow 0.036\ CO_2(aq)$$
$$+ 0.925\ H_2O(l) + 1.914\ CH_{1.613}O_{0.557}N_{0.158}P_{0.012}S_{0.003}K_{0.022}Mg_{0.003}Ca_{0.001}(cells)$$

Note that in equation (4) *no $O_2(aq)$ enters into the anabolic process*. This applies whether the system is aerobic or anaerobic. Except for the synthesis of steroids and for a few other processes in eukaryotic cells for which a very small quantity of oxygen is required, there is no requirement for this element biochemically for anabolism except as a constituent of molecular structure. In addition, the absence of $O_2(aq)$ as a participant in anabolism can be considered an evolutionary holdover. During the initial evolutionary stages of the development of cellular forms some 3.5 billion years ago, the available evidence suggests that there was no gaseous oxygen present on this planet. For this reason all anabolism was (and still is) effectively anaerobic. Anabolism can certainly be considered one of the most conservative of all biological processes, even though most catabolic processes are aerobic.

2.4.7 Representing organic product formation.

With anaerobic growth processes there will be organic products other than the cells. Each of these must be known as to kind and quantity, and each can be treated in exactly the same manner as the cells in anabolism. There is thus no oxygen involved in any anaerobic equations. The quantity of substrate utilized to form other organic products of a growth-process is calculated in the same manner as the cells, as shown in the following equation.

$$S_{prod} = \frac{MYC_{prod} \cdot AE_{prod}}{AE_{sub}} \quad (5)$$

where S_{prod} represents the fraction of one mol of substrate that is used to form the product, MYC_{prod} is the molar yield coefficient for the product, AE_{prod} is the number of AE in one mol of product, and AE_{sub} has been defined previously. An example of product formation is found in the anaerobic glucose data set in Table 2, in which glycerol is produced. It is listed as a separate process, simply to distinquish it from anabolism. The formation of organic products other than the cells during aerobic

metabolism can be considered the result of anabolism.

It is often useful to determine the "reductance degree" (γ) of a substrate so that it can be compared with that of the biomass. This is the number of AE that can be transferred to O_2(aq) per gram atom of C in a substance [25]. For CO_2(aq) γ is 0, for CH_4(aq) (completely reduced C) it is 8, and for all other organic substances it is in between. A value for γ is calculated by dividing the number of AE in a substance as obtained using equation (1) by the number of C-atoms in the substance. For glucose γ is 4.000, and for *S. cerevisae* cells using formula (B) it is 4.079. Such information is useful for constructing anabolic equations in that with substrates less reduced than the biomass, such as glucose, CO_2(aq) is always a product of anabolism. The process of anabolism under this condition is similar to that of a chemical dismutation, where a part of the substance is reduced at the expense of the other part, which becomes oxidized. Fermentations are examples of dismutations. Effectively, a part of the substrate becomes reduced to the average level of the cellular fabric. The rest is oxidized to CO_2(aq). With substrates more reduced than glucose, such as ethanol ($\gamma = 6$), CO_2(aq) is always a reactant in anabolism. This is because CO_2(aq) serves as an oxidant to oxidize the substrate to the level of the biomass. Examples of growth on substrates either more or less reduced than the biomass are found in Table 2. Occasionally, a substrate is incompletely oxidized to CO_2(aq) and H_2O(l) during catabolism. An example of this is the oxidation of ethanol only to acetic acid during the aerobic growth of some acetic acid bacteria. Here, acetic acid is a product, but of catabolism. The process of CO_2(aq) reduction in autotrophy is neither anabolism nor catabolism. Rather, it can be regarded as a completely different process that provides organic substrate material for chemoorganoheterotrophic growth.

2.4.8. Another way of representing anabolism.

Other than using the electron equivalence of the substrate and the biomass to construct anabolic equations as described in Section *2.3.6*, carbon equivalence has also been used, examples of which are found in references [26, 27]. In this latter method, the carbon in the quantity of substrate used to form the biomass is equivalent to the quantity of carbon in the biomass. Whereas this can be done as a chemical representation, the problem exists that unless the substrate and the cells have exactly the same degree of reduction, O_2(aq) will be either a reactant or a product of anabolism. Except to the negligible extent noted in Section *2.4.6.*, O_2(aq) does not enter into anabolism.

2.4.9. Representing catabolism.

Regarded in the manner presented here, catabolism provides the activation energy for anabolism to occur. It takes the form of a process equation in which that part of the substrate that is not utilized in anabolism is fermented under anaerobic conditions or oxidized under aerobic condition, either process providing ATP for cellular synthesis. Thus, in the catabolism of *S. cerevisiae* glucose is fermented to carbon dioxide and ethanol in a dismutation reaction, and aerobically it is oxidized to carbon dioxide and water. The ethanol formed during anaerobic growth is a product, and can be treated as such. Since growth-process equations are written conventionally in terms of growth on one mol of substrate, the quantity of substrate used in catabolism, (S_{cat}) is calculated as ($1 - S_{an} - \sum S_{prod}$). The summation sign refers to anaerobic processes in which anabolic fermentation products other than the cells are formed. If cells are the only products of a growth process, this term is ignored. For the example in Table 1 of the aerobic growth of *S. cerevisiae* on glucose ($1 - S_{an}$) = S_{cat} = 0.675 mol, and the equation representing catabolism becomes

$$0.675\ C_6H_{12}O_6(aq) + 4.050\ O_2(aq) \rightarrow 4.050\ CO_2(aq) + 4.050\ H_2O(aq) \qquad (6)$$

2.4.10. Representing metabolism.

Metabolism is the sum of anabolism and catabolism. Adding equations (4) and (6) gives

$$C_6H_{12}O_6(aq) + 0.302\ NH_3(aq) + 4.050\ O_2(aq) + 0.023\ H_2PO_4^-(aq) + 0.006\ SO_4^{2-}(aq) + 0.042\ K^+(aq) + 0.006\ Mg^{2+}(aq) + 0.002\ Ca^{2+}(aq) + 0.023\ OH^-(aq) \rightarrow 4.086\ CO_2(aq) + 4.975\ H_2O(l) + 1.914\ CH_{1.613}O_{0.557}N_{0.158}P_{0.012}S_{0.003}K_{0.022}Mg_{0.003}Ca_{0.001}(cells) \qquad (7)$$

Adding the equations representing the formation of each of the organic products (i.e., cells plus any other organic substances) gives the process equation representing anaerobic metabolism, as illustrated by the equations for the anaerobic growth of *S. cerevisiae* on glucose in Table 2.

2.4.11. Points to consider.

The brief description given above on the construction of growth process equations is intended to give some idea of the overall aspects of what goes on when cells are grown. It is not necessary to go through the construction of anabolic and catabolic process equations if one is interested only in metabolism. Once the kinds and quantities of the organic reactants and products of metabolism are known (as

they must be) as well as the nitrogen source, the quantities of CO_2(aq) and H_2O(l) produced can be determined easily by difference. The mass balance of any growth process equation will never be exact because of the necessity of dealing with coefficients and subscripts that are not small, whole numbers. However, with some care the elemental balances can often be obtained to within 1%. A detailed description of these methods is given in reference [28].

2.4.12. Examples.

Examples of growth process equations representing the growth of *S. cerevisiae* anaerobically on glucose and aerobically on glucose, acetate, and ethanol are given in Table 2. The only reason for choosing this particular group of growth processes as examples is that there is an internal consistency with respect to three of the data sets. Each growth process equation may require a number of analyses, any of which may be subject to inaccuracies. Except by carrying out these analyses many times, it is impossible to know the accuracy of a given growth process equation.Thus, any check on this accuracy is useful. The strain of *S. cerevisiae* used for studying these growth processes did not grow aerobically on the glycerol formed during anaerobic growth on glucose, but it did grow on the ethanol. Therefore, the addition of the MYC for anaerobic growth on glucose (0.590 ICCmol) plus that for aerobic growth on the ethanol formed during anaerobic growth [1.300 mol ethanol x 1.030 ICCmol mol ethanol^{-1}] = 1.339 ICCmol] should equal that for aerobic growth of glucose. The addition gives 1.929 ICCmol. This is an agreement of 0.78% with that determined experimentally for aerobic growth on glucose (1.914 ICCmol), which gives some credence as to the accuracy of the respective growth-process equations and makes these useful as examples. Such checks cannot be made with respect to the acetic acid growth process equation.

It is apparent that equations representing the growth of different kinds of cells may be different and more complex than those represented here. This is true for some animal cell cultures where a minimum of two substrates is required, even though the culture medium may be otherwise defined. It is even more complex when it is necessary to use a culture medium containing several essential amino acids or lipids, or is completely undefined, as in the use of serum for animal cell cultures, or coconut milk for plant cell cultures. Here, the representation of the components of a growth process in an equation becomes a difficult procedure. The only way of solving this problem is to determine individually those substances in the initial state that are consumed during growth, and this is usually impractical to do.

Table 2
Equations and thermodynamic changes at 298.15 K and 1 atm representing the growth of *Saccharomyces cerevisiae* anaerobically on glucose and aerobically on glucose, ethanol, and acetic acid, with ammonia as the nitrogen source [a]

Anaerobic growth on glucose

Non-conservative process:

Alcoholic glucose fermentation: $C_6H_{12}O_6(aq) \rightarrow 2\ CO_2(aq) + 2\ C_2H_6O(aq)$, $AE_{NC} = 8.000$
$\Delta_pG'_{NC} = -270.75$ kJ mol^{-1}; $\Delta_pH'_{NC} = -138.57$ kJ mol^{-1}; $T\Delta_pS'_{NC} = 132.18$ kJ mol^{-1} [b]

Conservative process:

Anabolism: $0.100\ C_6H_{12}O_6(aq) + 0.093\ NH_3(aq) + 0.007\ H_2PO_4^-(aq) + 0.002\ SO_4^{2-}(aq) + 0.013\ K^+(aq) + 0.002\ Mg^{2+}(aq) + 0.001\ Ca^{2+}(aq) + 0.008\ OH^-(aq) \rightarrow 0.012\ CO_2(aq) + 0.285\ H_2O(l) + 0.590\ CH_{1.613}O_{0.557}N_{0.158}P_{0.012}S_{0.003}K_{0.022}Mg_{0.003}Ca_{0.001}$(cells)
$\Delta_pG'_{an} = -11.05$ kJ; $\Delta_pH'_{an} = -13.71$ kJ; $T\Delta_pS'_{an} = -2.66$ kJ [b]

Glycerol formation: $0.252\ C_6H_{12}O_6(aq) + 0.216\ H_2O(l) \rightarrow 0.432\ C_3H_8O_3(aq) + 0.216\ CO_2(aq)$
$\Delta_pG'_{cat} = -23.37$ kJ; $\Delta_pH'_{cat} = -1.62$ kJ; $T\Delta_pS'_{cat} = 21.75$ kJ [b]

Catabolism: $0.650\ C_6H_{12}O_6(aq) \rightarrow 1.300\ C_2H_6O(aq) + 1.300\ CO_2(aq)$
$\Delta_pG'_{cat} = -175.99$ kJ; $\Delta_pH'_{cat} = -90.07$ kJ; $T\Delta_pS'_{cat} = 85.92$ kJ [b]

Metabolism: $C_6H_{12}O_6(aq) + 0.093\ NH_3(aq) + 0.007\ H_2PO_4^-(aq) + 0.002\ SO_4^{2-}(aq) + 0.013K^+(aq) + 0.002\ Mg^{2+}(aq) + 0.001\ Ca^{2+}(aq) + 0.008\ OH^-(aq) \rightarrow 0.432\ C_3H_8O_3(aq) + 1.300\ C_2H_6O(aq) + 1.528\ CO_2(aq) + 0.069\ H_2O(l) + 0.590\ CH_{1.613}O_{0.557}N_{0.158}P_{0.012}S_{0.003}K_{0.022}Mg_{0.003}Ca_{0.001}$(cells)
$\Delta_pG'_{met} = -210.41$ kJ mol^{-1}; $\Delta_pH'_{met} = -105.40$ kJ mol^{-1}; $T\Delta_pS'_{met} = 105.01$ kJ mol^{-1} [b]

Aerobic growth on glucose

Non-conservative process:

Glucose oxidation: $C_6H_{12}O_6(aq) + 6\ O_2(aq) \rightarrow 6\ CO_2(aq) + 6\ H_2O(l)$, $AE_{NC} = 24.000$
$\Delta_pG'_{NC} = -2905.47$ kJ mol^{-1}; $\Delta_pH'_{NC} = -2862.17$ kJ mol^{-1}; $T\Delta_pS'_{NC} = 43.30$ kJ mol^{-1} [b]

Conservative process:

Anabolism: $0.325\ C_6H_{12}O_6(aq) + 0.302\ NH_3(aq) + 0.023\ H_2PO_4^-(aq) + 0.006\ SO_4^{2-}(aq) + 0.042\ K^+(aq) + 0.006\ Mg^{2+}(aq) + 0.002\ Ca^{2+}(aq) + 0.023\ OH^-(aq) \rightarrow 0.036\ CO_2(aq) + 0.925\ H_2O(l) + 1.914\ CH_{1.613}O_{0.557}N_{0.158}P_{0.012}S_{0.003}K_{0.022}Mg_{0.003}Ca_{0.001}$(cells)
$\Delta_pG'_{an} = -35.76$ kJ; $\Delta_pH'_{an} = -44.31$ kJ; $T\Delta_pS'_{an} = -8.55$ kJ [b]

Catabolism: $0.675\ C_6H_{12}O_6(aq) + 4.050\ O_2(aq) \rightarrow 4.050\ CO_2(aq) + 4.050\ H_2O(l)$
$\Delta_pG'_{cat} = -1961.19$ kJ; $\Delta_pH'_{cat} = -1931.96$ kJ; $T\Delta_pS'_{cat} = 29.23$ kJ [b]

Metabolism: $C_6H_{12}O_6(aq) + 0.302\ NH_3(aq) + 4.050\ O_2(aq) + 0.023\ H_2PO_4^-(aq) + 0.006\ SO_4^{2-}(aq) + 0.042\ K^+(aq) + 0.006\ Mg^{2+}(aq) + 0.002\ Ca^{2+}(aq) + 0.023\ OH^-(aq) \rightarrow 4.086\ CO_2(aq) + 4.975\ H_2O(l) + 1.914\ CH_{1.613}O_{0.557}N_{0.158}P_{0.012}S_{0.003}K_{0.022}Mg_{0.003}Ca_{0.001}$(cells)
$\Delta_pG'_{met} = -1996.95$ kJ mol^{-1}; $\Delta_pH'_{met} = -1976.27$ kJ mol^{-1}; $T\Delta_pS'_{met} = 20.68$ kJ mol^{-1} [b]

Table 2 (cont.)

Aerobic growth on ethanol

Non-conservative process

Ethanol oxidation: $C_2H_6O(aq) + 3\ O_2(aq) \rightarrow 2\ CO_2(aq) + 3\ H_2O(l)$, $AE_{NC} = 12.000$
$\Delta_pG'_{NC} = -1317.36$ kJ mol^{-1}; $\Delta_pH'_{NC} = -1361.80$ kJ mol^{-1}; $T\Delta_pS'_{NC} = -44.44$ kJ mol^{-1} [b]

Conservative process

Anabolism: $0.350\ C_2H_6O(aq) + 0.163\ NH_3(aq) + 0.330\ CO_2(aq) + 0.012\ H_2PO_4^-(aq) + 0.003\ SO_4^{2-}(aq) + 0.022\ K^+(aq) + 0.003\ Mg^{2+}(aq) + 0.001\ Ca^{2+}(aq) + 0.012\ OH^-(aq) \rightarrow 0.490\ H_2O(l) + 1.030\ CH_{1.613}O_{0.557}N_{0.158}P_{0.012}S_{0.003}K_{0.022}Mg_{0.003}Ca_{0.001}$
$\Delta_pG'_{an} = 28.86$ kJ; $\Delta_pH'_{an} = 1.45$ kJ; $T\Delta_pS'_{an} = -27.41$ kJ [b]
Catabolism: $0.650\ C_2H_6O(aq) + 1.950\ O_2(aq) \rightarrow 1.300\ CO_2(aq) + 1.950\ H_2O(l)$
$\Delta_pG'_{cat} = -856.28$ kJ; $\Delta_pH'_{cat} = -885.17$ kJ; $T\Delta_pS'_{cat} = -28.89$ kJ [b]

Metabolism: $C_2H_6O(aq) + 0.163\ NH_3(aq) + 1.950\ O_2(aq) + 0.012\ H_2PO_4^-(aq) + 0.003\ SO_4^{2-}(aq) + 0.022\ K^+(aq) + 0.003\ Mg^{2+}(aq) + 0.001\ Ca^{2+}(aq) + 0.012\ OH^-(aq) \rightarrow 0.970\ CO_2(aq) + 2.440\ H_2O(l) + 1.030\ CH_{1.613}O_{0.557}N_{0.158}P_{0.012}S_{0.003}K_{0.022}Mg_{0.003}Ca_{0.001}$(cells)
$\Delta_pG'_{met} = -827.42$ kJ mol^{-1}; $\Delta_pH'_{met} = -883.72$ kJ mol^{-1}; $T\Delta_pS'_{met} = -56.30$ kJ mol^{-1} [b]

Aerobic growth on acetic acid

Non-conservative process:

Acetic acid oxidation: $C_2H_4O_2(aq) + 2\ O_2(aq) \rightarrow 2\ CO_2(aq) + 2\ H_2O(l)$, $AE_{NC} = 8.000$
$\Delta_pG'_{NC} = -857.84$ kJ mol^{-1}; $\Delta_pH'_{NC} = -889.82$ kJ mol^{-1}; $T\Delta_pS'_{NC} = -31.98$ kJ mol^{-1} [b]

Conservative process:

Anabolism: $0.316\ C_2H_4O_2(aq) + 0.098\ NH_3(aq) + 0.007\ H_2PO_4^-(aq) + 0.002\ SO_4^{2-}(aq) + 0.014\ K^+(aq) + 0.002\ Mg^{2+}(aq) + 0.001\ Ca^{2+}(aq) + 0.009\ OH^-(aq) \rightarrow 0.012\ CO_2(aq) + 0.297\ H_2O(l) + 0.620\ CH_{1.613}O_{0.557}N_{0.158}P_{0.012}S_{0.003}K_{0.022}Mg_{0.003}Ca_{0.001}$(cells)
$\Delta_pG'_{an} = 24.10$ kJ; $\Delta_pH'_{an} = 6.78$ kJ; $T\Delta_pS'_{an} = -17.32$ kJ [b]
Catabolism: $0.684\ C_2H_4O_2(aq) + 1.368\ O_2(aq) \rightarrow 1.368\ CO_2(aq) + 1.368\ H_2O(l)$
$\Delta_pG'_{cat} = -586.76$ kJ; $\Delta_pH'_{cat} = -608.64$ kJ; $T\Delta_pS'_{cat} = -21.88$ kJ [b]

Metabolism: $C_2H_4O_2(aq) + 0.098\ NH_3(aq) + 1.368\ O_2(aq) + 0.007\ H_2PO_4^-(aq) + 0.002\ SO_4^{2-}(aq) + 0.014\ K^+(aq) + 0.002\ Mg^{2+}(aq) + 0.001\ Ca^{2+}(aq) + 0.009\ OH^-(aq) \rightarrow 1.380\ CO_2(aq) + 1.665\ H_2O(l) + 0.620\ CH_{1.613}O_{0.557}N_{0.158}P_{0.012}S_{0.003}K_{0.022}Mg_{0.003}Ca_{0.001}$(cells)
$\Delta_pG'_{met} = -562.66$ kJ mol^{-1}; $\Delta_pH'_{met} = -601.86$ kJ mol^{-1}; $T\Delta_pS'_{met} = -39.20$ kJ mol^{-1} [b]

---

[a] These equations have been constructed by replacing the original UCFs from Battley [9] with that from Table 1. This does not change the carbon balance of these former, and includes a formula representing cells for which both Δ_fH' and Δ_fS' values have been obtained (see Table 3).
[b] These values for $T\Delta_pS'$ were calculated using the Gibbs free energy equation and the values above for Δ_pG' and Δ_pH' for the respective processes. Slightly different values would be obtained if the Δ_pS' values were to be calculated directly, because of carrying the fractional values of Δ_pG' and Δ_pH' to only two decimal places.

3. THE THERMODYNAMICS OF GROWTH PROCESS SYSTEMS.

Classical (equilibrium) thermodynamics deals with systems that come to a reversible equilibrium condition after the passage from an initial to a final state. This implies the existence of a thermodynamic equilibrium constant. And, in general, even if the equilibrium is very far to the right, the classical treatment is still thought to be valid. In theory, all reactions or processes can be considered to be reversible, at least to some extent. Whether this is applicable to cellular growth is dubious because, for all practical purposes, growth (anabolism) is a completely irreversible phenomenon. This may not be true for the reactions in aqueous solution that provide the reactants for anabolism. The biologically acceptable forms of substances used as reactants in metabolism that are products of a dissociation in aqueous solution become replaced as they are consumed, and these are certainly equilibrium phenomena. For anabolism or catabolism there is no equilibrium constant that can be calculated, and this suggests that classical equilibrium thermodynamics cannot be applied. Cells cannot be "ungrown", and catabolized substrates are never reformed. Theoretical attempts have been made to approach the problem of irreversibility in the form of "near-equilibrium" or "non-equilibrium" thermodynamics [29, 30], but in general these have been applied more in theory than in fact to the phenomenon of cellular growth. Whether the energy exchanges accompanying growth are better treated using equilibrium, near-equilibrium, or irreversible thermodynamics or by any number of theoretical treatments may be irrelevant. Provided that the thermodynamic properties of the reactants and products participating in anabolism, catabolism, or metabolism are known, the energy changes accompanying these processes can always be calculated as the difference between the energies of the initial and the final states. This idea was applied in the early 1900s by Rubner [31] in his classical studies on the heat of microbial growth, long before the modern methods of treating thermodynamics came into use.

3.1. The Gibbs free energy equation.

Most microbial cells grow under the physical conditions of constant or nearly constant temperature and pressure during the time taken to pass through a life cycle, or can be caused to do so experimentally. The exchanges of energy that take place as a growth process system passes spontaneously from its initial to its final state can then be described by the Gibbs free-energy equation, as follows

$$\Delta G = \Delta H - T\Delta S \quad (8)$$

where ΔG, ΔH, and ΔS represent the free energy, enthalpy, and entropy changes, respectively, accompanying a reaction or process at a constant temperature and pressure. Derivations of these quantities can be found in Volume 1 of this *Handbook*. Equation (8) is valid for many kinds of applications. Values for ΔG, ΔH, and ΔS can be calculated for growth process equations only if the values for the thermodynamic properties of the reactants and products are known.

3.2. Thermodynamic properties for substances participating in growth processes.

Cells metabolize in an aqueous environment and, except for those of the cells, the thermodynamic properties of the reactants and products of growth-processes are those of these substances in aqueous solution. Values for the free energy, enthalpy, and entropy of formation of all substances from the elements at 298.15 K and 1 atm are referred to as "thermodynamic properties." These can be found in several compendia [32-34] listed for quantities of one mol in a given standard state. In aqueous solution, all substances are taken to be at a concentration of one mol at unit activity for values of $\Delta_f G^{o\prime}$, and of a hypothetical one mol at infinite dilution for $\Delta_f H^{o\prime}$. Values for $\Delta_f S^{o\prime}$ can be calculated using the following form of the Gibbs free energy equation, where the superscript refers to the aqueous standard state.

$$\Delta_f G^{o\prime} = \Delta_f H^{o\prime} - T\Delta_f S^{o\prime} \quad (9)$$

However, standard state concentrations are usually osmotically unfavorable for the growth of cells and must be reduced to concentrations that are more physiologically appropriate for the initial state of a growth process. During the process of cellular growth under the kinds of conditions found in nature and in batch cultures, the reactants of a growth process become utilized to form the cells and other products. This means that the concentrations of all substances participating in a growth process will change, those of the reactants decreasing and those of the products rising. There is one exception to this in the form of continuous cultures in which, because of the way in which continuous culture equipment is designed to work, the concentrations of reactants and products are constant at the steady state. This is an advantage with regard to being able to establish constant values for thermodynamic properties in the aqueous environment of growing cells. On the other hand, except

when the dilution rate equals μ_{max} in continuous cultures, the cells are growth-rate limited as opposed to being non-limited in batch cultures. Depending on how far below μ_{max} the growth rate is under continuous culture conditions, it is possible that storage products may be formed within the cells during the G_1 phase of the cell cycle. This is because under conditions in which the rate of growth is lowered because of some limiting factor, the cells may store internal substrate until such time as enough of the limiting factor has been accumulated to permit cell division. As stated in Section 2.3, this can result in apparent cellular yields that are too large, and to an inaccurate analysis of the elemental composition of the cellular fabric.

3.2.1. Values for the enthalpy, free energy, and entropy of formation in aqueous solution of substances utilized or produced during growth, excluding cells.

Values for the enthalpy of formation of substances in aqueous solution at a concentration of other than 1 *m* are designated by the symbol $\Delta_f H'$ since these are not in the standard state. These do not change as a function of concentration from those of $\Delta_f H^{\circ\prime}$ because these latter are at hypothetical infinite dilution. What is stated above for values of $\Delta_f H'$ is *not* true of values for the free energy of formation of substances in aqueous solution at concentrations other than that of the standard state. These are designated by the symbol $\Delta_f G'$, and *do* change with concentration. Thus, as the reactants of a growth process become utilized during growth, their concentration becomes less and the value for $\Delta_f G'$ becomes more negative as a function of dilution. The reverse is true for products in solution that are formed during growth. The free energy change accompanying dilution can be expressed as follows,

$$\Delta_{dil}G' = \frac{-RT}{1000} \ln \frac{\text{conc. in std. state} \cdot \text{activity coeff. in std. state}}{\text{lower conc.} \cdot \text{activity coeff. at lower conc.}} \qquad (10)$$

where $\Delta_{dil}G'$ is in kJ mol^{-1}. The standard state is a hypothetical 1 *m* solution which corresponds to the limiting condition implied by Henry's Law, in which the solute has an activity of one (unity). The numerator inside the logarithm in equation (10) thus equals 1. If the concentration of the solute in the denominator is sufficiently low, its activity coefficient also approaches 1, and the activity can be taken equal to the concentration. Under these conditions at 298.15 K,

$$\Delta_{dil}G' = -2.479 \ln \left(\frac{1}{a_c}\right) \text{kJ mol}^{-1} \qquad (11)$$

where a_c represents the activity of the solute at a concentration, c, that is less than 1 *m*. The non-standard free energy of formation of a solute under these conditions then becomes

$$\Delta_f G' = \Delta_f G^{\circ\prime} + (-2.479 \ln \frac{1}{a_c}) \text{ kJ mol}^{-1} \quad (12)$$

It is apparent from equation (12) that, if a_c becomes sufficiently small, $\Delta_f G'$ will approach minus infinity; and this is what is to be expected theoretically as the substrate of a growth process becomes consumed. The same is true but in reverse for products formed *de novo* at the beginning of a growth process. In either case, the true value for $\Delta_f G'$ can be found only by integration of the successive $\Delta_f G'$ values as a function of dilution, the graph of either of which deals with minus infinity. Obviously, this will not work practically. However, at a concentration of about 0.001 *m* solute, molecules or ions are sufficiently isolated from one another that further dilution has little effect on their thermodynamic interactions [35]. This has been adopted as the basis of a "microbiological" aqueous standard state that would be of more practical use than the conventional aqueous standard state [36]. Substrate concentrations of 0.001 *m* are adequate for growing microbial cells and are similar to concentrations of intermediary metabolic solutes found inside of cells. At this concentration the assumption can be made realistically that the activity is equal to the concentration. At 0.001 *m* the $\Delta_f G'$ values for solutes will be more negative than those for $\Delta_f G^{\circ\prime}$ by - 17.11 kJ mol^{-1}. The Gibbs free energy equation with respect to the energies of formation of solutes at concentrations less than that of the standard state then becomes

$$\Delta_f G' = \Delta_f H' - T\Delta_f S' \quad (13)$$

Because $\Delta_f H' = \Delta_f H^{\circ\prime}$, when $\Delta_f G'$ becomes more negative, $\Delta_f S'$ will become more positive, as it would be expected to do because of the dilution of the solute.

Although the use of a "microbiological" (cellular) standard state with respect to 0.001 *m* can be considered an improvement over the use of the conventional aqueous standard state, it may not represent the final solution to the problem of the changing concentrations of soluble reactants and products during growth in a batch culture. This is because there is no evidence at present as to the extent to which the energies of dilution of soluble reactants as they are utilized during growth, or the energies of concentration of soluble products as they are formed during growth, have anything

to do with the growth process itself.

3.2.2. Values for cellular enthalpy, entropy, and free energy of formation.

At the present time, values for the thermodynamic properties of cells cannot be found in compendia in the literature. Cells are not pure substances. They have some of the properties of precipitates in that they are insoluble (i.e., they are visible)[37], and do not have standard thermodynamic properties in the usual sense. Nevertheless, a unit mass of anything, impure or otherwise, does have a finite enthalpy, entropy, and free-energy of formation, and this also applies to cells. The unit mass is taken as the ICCmol, represented here by formula (B). Such a formula accounts for more than 99% of the total mass, and formulae of this kind are probably the best that can be obtained for something as complex and as variable as different kinds of cells.

To obtain a value for cellular enthalpy of formation, $\Delta_f H_{cells}$, it is necessary to measure the heat of combustion and to construct an equation representing the combustion of a unit mass of cells. For the cells represented by formula (B) an appropriate combustion equation is as follows.

$$CH_{1.613}O_{0.557}N_{0.158}P_{0.012}S_{0.003}K_{0.022}Mg_{0.003}Ca_{0.001}(\text{cells}) + 1.151\ O_2(g) \rightarrow 1.000\ CO_2(g) + 0.806\ H_2O(l) + 0.079\ N_2(g) + 0.003\ P_4O_{10}(cr) + 0.003\ K_2SO_4(cr) + 0.008\ K_2O(cr) + 0.003\ MgO(cr) + 0.001\ CaO(cr) \quad (14)$$

Larsson [38] has determined the heat of combustion , $\Delta_c H$, of *S. cerevisiae* cells to be -19.44 ± 0.17 ($n = 7$) kJ (g of *whole cells*)$^{-1}$. By "whole cells" is meant living cells that have been dried, and not the usual method of cellular representation in terms of kJ (g ash-free dry wt)$^{-1}$. Multiplying this by 26.202 g ICCmol^{-1} for the mass of cells represented by formula (B) gives -509.37 kJ ICCmol^{-1} as the heat of combustion for the oxidation represented by equation (14). Using this and the appropriate values from Table 3, $\Delta_f H_{cells}$ is calculated to be -133.13 kJ ICCmol^{-1}. The accuracy of this value is a function of the correctness of the combustion equation and the accuracy of the heat determination. Equation (14) represents that the K^+, Mg^{2+}, and Ca^{2+} that were present as ions in the cell are present at the end of the combustion as $K_2SO_4(cr)$, $K_2O(cr)$, $MgO(cr)$, and $CaO(cr)$. This may or may not be true. It has been shown [13] that yeast cells combusted in a muffle furnace at 600 °C give an ash that contains little or no carbon, but that cellular combustion at lower temperatures does result in carbon-containing ash. This

Table 3
Thermodynamic properties at 298.15 K and 1 atm. [a]

Substance	Formula	State	$\Delta_f G^\circ$ (kJ mol^{-1})	$\Delta_f G'$, [b] (kJ mol^{-1})	$\Delta_f H^{\circ(\prime)}$ (kJ mol^{-1})	$\Delta_f S'$ (J K^{-1} mol^{-1})
Acetic acid	$C_2H_4O_2$	aq		-421.20	-485.26	
Ammonia	NH_3	aq		-43.68	-80.29	
Biphosphate ion	$H_2PO_4^-$	aq		-1105.66	-1296.29	
Calcium ion	Ca^{2+}	aq		-570.65	-542.83	
Calcium oxide	CaO	cr	-604.04		-635.09	
Carbon dioxide	CO_2	g	-394.36		-393.51	
		aq		-403.13	-413.80	
Yeast cells	ICUCF	s		-88.00	-133.13	-151.37
	IFUCF	s		-98.91	-143.58	-149.82
	KCUCF	s		-86.62	-131.75	-151.36
Ethanol	C_2H_6O	aq		-198.07	-287.02	
Glucose	$C_6H_{12}O_6$	aq		-931.65	-1263.07	
Glycerol	$C_3H_8O_3$	aq		-514.59	-676.55	
Hydrogen ion	H^+	aq		-17.11	0	
Hydroxyl ion	OH^-	aq		-174.40	-229.99	
Magnesium ion	Mg^{2+}	aq		-471.91	-466.85	
Magnesium oxide	MgO	cr	-569.44		-601.70	
Nitrogen	N_2	g	0		0	
Oxygen	O_2	g	0		0	
		aq		-0.79	-12.09	
Potassium ion	K^+	aq		-300.37	-252.38	
Potassium oxide	K_2O	cr	-321.84		-363.15	
Potassium sulfate	K_2SO_4	cr	-1319.59		-1437.70	
Phosphorous decoxide	P_4O_{10}	cr	-2697.84		-2984.03	
Sulfur trioxide	SO_3	g	-371.08		-395.72	
Sulfate ion	SO_4^{2-}	aq		-761.74	-909.27	
Water	H_2O	l	-237.18		-285.83	

[a] The data for inorganic substances except for oxygen were taken from reference [32], those for the organic substances and for oxygen from reference [33], and for K_2O and K_2SO_4 from reference [34]. The methods for calculating the thermodynamic properties of yeast cells are found in Section *3.2.2* of the text.

[b] It has been recommended [35,36] that $\Delta_f G'$ values calculated on the basis of a 0.001 *m* real concentration are more closely representative of the thermodynamic properties of biological systems than conventional $\Delta_f G^{\circ\prime}$ values. This has been adopted here, and the values in this column are therefore 17.11 kJ more negative than those of the aqueous standard state.

latter is presumably in the form of carbonates, since potassium carbonate (potash) is the major product of the burning of plant materials in a conventional combustion using atmospheric oxygen. If combustion in a calorimeter takes place at a temperature appreciably lower than 600 °C the ash may include or consist mostly of K, Mg, and Ca carbonates, which is going to give a slightly different heat of combustion, even if all the organic carbon has become completely oxidized. The organic sulfur in the cells may be oxidized to gaseous oxides, or may form sulfates. In addition, the P_4O_{10}(cr), which is highly deliquescent, may absorb water as the calorimeter comes to a temperature equilibrium after a combustion experiment with dried cells, with the formation of H_3PO_4(cr), H_3PO_4(l), or a salt of potassium phosphate. It is apparent that there is some uncertainty with respect to what goes on within a bomb calorimeter during and immediately after the combustion of cellular material. The use of a rotating bomb calorimeter would be preferable in this respect, but has not been used as yet for this purpose.

On the other hand, calculations using equations similar to (14) but with carbonates rather than oxides have relatively little effect on the heat of formation per unit mass of cells. The value for $\Delta_f H$ of -509.37 kJ ICCmol^{-1} applies to lyophilized cells, and not to cells in their hydrated state as represented in Table 2. It has been determined experimentally that the hydration of lyophilized yeast cells results in an enthalpy change of less than 90 J g^{-1} [39]. At the most, this is about 2.36 kJ ICCmol^{-1} of yeast cells as represented by formula (B), which is only 0.46 % of the enthalpy change accompanying combustion and well within the standard error of Larsson's [38] analyses. For this reason and as a first approximation, the enthalpy change accompanying cellular hydration is neglected, although the idea of energies being involved in hydration should not be forgotten.

The physical entropy of any mass is a function of the quantity of thermal energy it must absorb in order to exist at a given temperature above absolute zero, the standard temperature usually being taken at 298.15 K for biological purposes, as represented by the following equation.

$$S = \int_0^{298.15} C_p \, \mathrm{d} \ln T \tag{15}$$

where C_p is the heat capacity at a constant pressure of 1 bar of a given mass of substance. To obtain a value for cellular entropy, S_{cells}, it is necessary to use a low-temperature calorimeter to measure the heat capacities of a mass of dried cells as a function of temperature from the practical lower limit of about 7 K up to slightly

more than 298.15 K. An extrapolation of the data to 0 K using the Debye equation and a subsequent total integration of the heat capacity data gives the entropy for the cellular mass used in the determination. Details of this procedure can be found in Volume 1 of this *Handbook*. Low-temperature calorimeters are intricate and expensive, and there are not many of them compared to conventional combustion calorimeters. Measurements of complex biological materials have seldom been made by the physical chemists who use these instruments. This is largely because substances such as cells, proteins, nucleic acids, etc., usually do not occur in the form of pure, crystalline solids. Nevertheless, everything has an entropy. At the present time, only one cellular entropy determination has been made, using the yeast cells represented by formula (B) [40]. The value measured was 1.304 J $K^{-1}g^{-1}$ at 298.15 K which, when multiplied by one ICCmol of 26.202 g, gives a total entropy of 34.167 J K^{-1} $ICCmol^{-1}$. However, this value is that of the "absolute" entropy of this mass of cells, and not of the entropy of formation, $\Delta_f S_{cells}$. This latter is necessary to calculate a value for the free energy of formation, $\Delta_f G_{cells}$. A value for $\Delta_f S_{cells}$ is obtained by means of the following equation,

$$\Delta_f S_{cells} = S_{cells} - 5.740\,n\mathrm{C} - 65.34\,n\mathrm{H} - 102.57\,n\mathrm{O} - 95.81\,n\mathrm{N} - 41.09\,n\mathrm{P} - 31.80\,n\mathrm{S} - 64.18\,n\mathrm{K} - 32.68n\mathrm{Mg} - 41.42\,n\mathrm{Ca} \quad (16)$$

where S is the entropy of one ICCmol of dried *S. cerevisiae* cells, and n is the subscript for each atom in formula [B] for the cells. The constants 65.34, 102.57, and 95.81 are one half the standard entropies of $H_2(g)$, $O_2(g)$, and $N_2(g)$, respectively. The other constants are the standard entropies of solid graphite, white phosphorous, rhombic sulfur, potassium, magnesium, and calcium. All constants have the dimensions of J $K^{-1}g$ at^{-1}. The terms $\Delta_f S$ and S have no superscripts in that they represent an impure, solid substance. Using equation (16), $\Delta_f S_{cells}$ is calculated to be -151.37 J K^{-1} $ICCmol^{-1}$. The cells to which these entropies apply were lyophilized, and there are no experimental data with respect to entropy changes accompanying cellular hydration. Just as with the enthalpy of hydration, the entropy of hydration is taken to be small, and as a first approximation can be neglected.

It is apparent from the descriptions above that both $\Delta_f H_{cells}$ and $\Delta_f S_{cells}$ are thermal quantities that can be calculated as a result of calorimetric determinations. This is not true of the cellular free energy of formation, $\Delta_f G_{cells}$, which is *not* a thermal quantity. However, because of the equivalence of all forms of energy, the free

energy of formation of cells can be calculated by means of equation (8) as follows.

$$\Delta_f G_{cells} = -133.13 \text{ kJ·ICCmol}^{-1} - (298.15 \text{ K X } -0.15137 \text{ kJ·K}^{-1}\text{·ICCmol}^{-1})$$
$$= -88.00 \text{ kJ·ICCmol}^{-1} \quad (17)$$

The above values for $\Delta_f G_{cells}$, $\Delta_f H_{cells}$, and $\Delta_f S_{cells}$ are entered into Table 3, along with the thermodynamic properties of other substances participating in growth processes.

3.2.3. Examples of thermodynamic changes accompanying growth processes.

Calculations of the thermodynamic changes accompanying the growth processes in Table 2 can be made using the appropriate thermodynamic properties in Table 3. Values for these changes are also included in Table 2, using the symbols $\Delta_p G'$, $\Delta_p H'$, and $\Delta_p S'$, where the subscript "p" refers to "process", in recognition that growth is a process consisting of a great many reactions, and not a simple reaction. These symbols represent what can be regarded as the "true" thermodynamic changes, i.e., *those occurring within the immediate aqueous environment of the cell suspension.* The "observed" values would be expected to be slightly different because of side reactions that take place within the aqueous environment as the reactants are utilized and the products are synthesized. These side reactions also include the thermodynamic changes accompanying the reactions $O_2(g) \rightarrow O_2(aq)$ and $CO_2(aq) \rightarrow CO_2(g)$ as gas exchanges occur within the culture vessel. Thus, the observed enthalpy of growth would be that actually measured if the growth process were carried out inside a calorimeter. A close estimate of the observed thermodynamic changes can be obtained by using the thermodynamic properties of $O_2(g)$ and $CO_2(g)$ in the equations in Table 2, rather than those for $O_2(aq)$ and $CO_2(aq)$. Of the thermodynamic changes represented in Table 2, it is only $\Delta_p H'_{met}$ that can be measured experimentally. This was done with respect to the growth of *S. cerevisiae* on the four substrates for which growth process equations are shown. The average agreement of the calculated values of $\Delta_p H'_{met}$ in Table 2 for these four growth processes is 1.17 % lower than those that were measured experimentally [41]. However, the experimental data show a wide variation, possibly because of the use of primitive calorimetric equipment at the time of measurement. In the forty years since then the technical aspects of biological calorimetry have improved enormously, largely due to the use of solid state circuitry which has resulted in a remarkable stability for calorimetric instruments.

3.3. Alternate ways of representing cellular substance.

A careful analysis of the percentages of C, H, O, N, P, and S is absolutely essential for accurate thermodynamic studies in that the cellular fabric comprises these elements. However, an equally careful analysis of the ions comprising the residuum of the cellular dry weight may constitute an unnecessary tedium.

3.3.1. Values for the enthalpy, entropy, and free energy of formation of cells from which the ions have been theoretically removed.

Although the data in Table 2 represent most closely the mass and energy changes that take place during cellular growth using *S. cerevisiae* as an example, it can be argued that the inorganic substances that are present in the cells do not contribute to the thermodynamics of growth to any great extent. Because inorganic ions exist in solution within the cells as well as outside them in the environment, they can be considered to contribute little to overall cellular thermodynamics, even though they do contribute to the measured cellular dry weight and entropy. Theoretically removing the ions from an ICUCF would leave a formula representing only the organic cellular fabric. The ICUCF for *S. cerevisiae* would then become

$$CH_{1.613}O_{0.557}N_{0.158}P_{0.012}S_{0.003} \qquad (C)$$

This is an ion-free unit carbon formula (IFUCF) representing an ion-free carbon mol (IFCmol) having a corresponding wt of 25.229 g.

A value for $\Delta_f H$ of the cellular fabric represented by formula (C) can be obtained by a theoretical oxidation of the cellular fabric using the following equation.

$$CH_{1.613}O_{0.557}N_{0.158}P_{0.012}S_{0.003}(\text{cells}) + 1.144\ O_2(g) \rightarrow 1.000\ CO_2(g) + 0.806\ H_2O(l) + 0.079\ N_2(g) + 0.003\ P_4O_{10}(cr) + 0.003\ SO_3(g) \qquad (18)$$

Assuming that the heat of combustion of -19.44 ± 0.17 ($n = 7$) kJ (g of *whole, dry cells*)$^{-1}$ (i.e., on a not-ash-free, dry wt basis) [38] is due only to the organic part of the cells, the heat of combustion for one IFCmol of cells would then become -19.44 kJ g^{-1} 25.229 g IFCmol^{-1} = -490.45 kJ IFCmol^{-1}. When this value is used in equation (18) together with other appropriate values from Table 3, the value for $\Delta_f H_{\text{IFcells}}$ becomes -143.58 kJ. It is apparent that this value is significantly larger than that calculated using the full ICUCF.

A value for $\Delta_f S_{\text{IFcells}}$ of -149.82 J K^{-1}Cmol^{-1} is obtained using formula (C)

and equation (16) but deleting the terms for K, Mg, and Ca. Using equation (8), the value for $\Delta_f G_{IFcells}$ then becomes -98.91 kJ IFCmol^{-1}. Thermodynamic properties of the ion-free cells are therefore different from those of ion-containing cells, because of the use of a different UCF.

3.3.2. Values for the enthalpy, entropy, and free energy of formation of cells, assuming that all ions can be represented by potassium ion.

Attempting to eliminate the ions theoretically, as in section 3.2.1, requires knowing what they are. However, another simplifying assumption can be made that the difference between the percentages of C, H, O, N, P, and S as determined directly, and the total dry weight is due entirely to potassium ion. This is justified in that, as shown in Table 1, potassium constitutes 90% by weight of the cellular ions. If potassium ion is taken to be the only ion present, the cellular mass can be represented by the following formula.

$$CH_{1.613}O_{0.557}N_{0.158}P_{0.012}S_{0.003}K_{0.024} \qquad (D)$$

Formula (D) can be called a potassium-containing unit-carbon formula (KCUCF). One potassium-containing carbon mol (KCCmol) is then 26.166 g, as opposed to 26.202 g for an ICCmol as shown in Table 1, a difference of only 0.13%. A value for $\Delta_f H$ of one KCCmol can be obtained by a theoretical oxidation of the cellular fabric using the following equation.

$$CH_{1.613}O_{0.557}N_{0.158}P_{0.012}S_{0.003}K_{0.024}(cells) + 1.150\,O_2(g) \rightarrow 1.000\,CO_2(g) + 0.079\,N_2(g) + 0.806\,H_2O(l) + 0.003\,P_4O_{10}(cr) + 0.003\,K_2SO_4(cr) + 0.009\,K_2O(cr) \qquad (19)$$

Again using the value of -19.44 ± 0.17 (n=7) kJ (g of *whole, dry cells*)$^{-1}$ [38], the heat of combustion of the cells as represented by equation (19) becomes -19.44 kJ g^{-1} 26.166 g KCCmol^{-1} = -508.67 kJ KCCmol^{-1}. When this value is used in equation (19) together with other appropriate values from Table 3, the value for $\Delta_f H_{KCcells}$ becomes -131.75 kJ KCCmol^{-1}.

A value for $\Delta_f S_{KCcells}$ of -151.36 J K^{-1} KCCmol^{-1} is obtained using formula (D) and equation (16), but deleting the terms for Mg and Ca. Using equation (17), the value for $\Delta_f G_{KCcells}$ is calculated to be -86.62 kJ KCCmol^{-1}.

Whether approximations such as these can be used to calculate thermodynamic changes is purely a matter of the accuracy desired.

3.3.3. Comparative values for $\Delta_p G'_{met}$ and $\Delta_p H'_{met}$ using different representations of the unit carbon formula.

Growth process equations can be written that are similar to those in Table 2, but which make use of the modifications in the composition of the cells as described in Sections *3.3.1* and *3.3.2*. For the IFUCF represented by formula (C) the reactants K^+(aq), Mg^{2+}(aq), and Ca^{2+}(aq) are omitted from the equations and the thermodynamic properties of ion-free cells are used together with other appropriate values from Table 3. For the KCUCF represented by formula (D) the simplifying assumption is made that only a small error will be introduced if all ions are taken to be K^+(aq), and the thermodynamic properties of the K-containing cells are used together with other appropriate values from Table 3. The results are given in Table 4. It is apparent that directly measuring the percentages of C, H, O, N, P, and S (which should be done in any case), and then taking the difference between the sum of these percentages and the total dry weight to be K to give a KCUCF, gives values that are very close to those obtained knowing more about the kind and quantity of other ions with respect to aerobic growth. Of these, $\Delta_f H_{KCCmol}$ is the most important because of its potential practical use in biotechnology in determining the heats of growth of micro-organisms in bioreactors and the quantity of energy required to remove it. Values for $\Delta_f G_{KCCmol}$ and $\Delta_f S_{KCCmol}$ have more interest academically with respect to an understanding of what is going on thermodynamically during growth processes. As shown in Table 4, the values obtained with an IFUCF in general deviate more from those obtained with an ICUCF than do those obtained with a KCUCF. They are therefore not as useful as this last in making thermodynamic interpretations.

3.4. Other methods of calculating thermodynamic changes accompanying growth.

If they happen to be available, it is always best to use calorimetric instruments to measure the thermal exchanges accompanying microbial growth, the combustion of dried cells, or entropy determinations. These sorts of procedures have been described above. On the other hand, if calorimetric instruments are not available, there are indirect ways of calculating thermodynamic changes that do not require direct thermal measurements. These methods constitute what has come to be called "indirect calorimetry." Indirect calorimetry does not require the expensive calorimetric devices required for direct measurement. Even if calorimeters are available, the measurements may not mean a great deal if it is not known

Table 4
Comparison of the calculated thermodynamic changes accompanying growth using an ion-containing unit carbon formula (ICUCF), an ion-free unit carbon formula (IFUCF), and a potassium-containing unit carbon formula (KCUCF) for the cells.

Growth on:	ICUCF		IFUCF		KCUCF	
	$\Delta_p G'_{met}$ (kJ mol^{-1})	$\Delta_p H'_{met}$ (kJ mol^{-1})	$\Delta_p G'_{met}$ (kJ mol^{-1})	$\Delta_p H'_{met}$ (kJ mol^{-1})	$\Delta_p G'_{met}$ (kJ mol^{-1})	$\Delta_p H'_{met}$ (kJ mol^{-1})
glucose anaerobically	-210.41	-105.40	-216.84	-111.56	-209.59	-104.58
glucose aerobically	-1996.95	-1976.27	-2017.83	-1996.27	-1994.31	-1973.62
ethanol	-827.42	-883.72	-838.66	-894.48	-826.00	-882.29
acetic acid	-562.67	-601.86	-569.43	-608.13	-561.81	-601.00

what is generating the heat and what side effects are affecting the observed measurements. Knowing what contributes to the total observed heat exchange is useful in this respect.

3.4.1. Thornton's Rule.

In 1917 Thornton [42] published the generalization that $\Delta_c H°$ for many organic substances is directly proportional to the number of atoms of O consumed during a combustion. This, in various forms, has come to be called "Thornton's Rule." Shortly thereafter [43] the same idea was extended to correlate the heat of combustion with the number of electrons transferred to oxygen, with the finding that $\Delta_c H$ could be approximated closely by multiplying this number by 108.99 kJ. More recently, Thornton's Rule was reviewed and calculations made with 488 substances of all kinds containing C, H, O, and N for which $\Delta_c H°$ is known [44]. An average of these data gave a value of -111.40 kJ eq^{-1} and a linear regression a value of -110.88 kJ eq^{-1}. Since there was no reason to believe that one of these results was "better" than the other, these values were averaged to give -111.14 kJ eq^{-1} as a general value that could be used for organic substances of all kinds [8]. Cellular fabric contains P and S in addition to C, H, O, and N, but P is present in its highest oxidation state and the quantity of S is always very small, even though it is oxidized during combustion. The ions in cells are not further oxidized. When -111.14 kJ eq^{-1} is multiplied by four electrons required to reduce O_2(g) to H_2O(l), a value of -444.56 kJ mol^{-1} O_2(g) consumed during combustion is obtained, called the oxycaloric equivalent, ($\Delta_c H°_{O_2}$), where the subscript "c" indicates that the value came from bomb calorimetric combustion. It is important to distinguish

distinguish between bomb calorimetric and biological oxidations, as pointed out in Section *2.4.5.*, because of the greater number of electrons transferred to oxygen during a bomb calorimetric oxidation.

3.4.2. Using Thornton's Rule to calculate $\Delta_f H_{cells}$.

Multiplying the $\Delta_c H$ value for the combustion of *dried S. cerevisiae* cells of -19.44 kJ g^{-1} [38] by the mass of one ICCmol of cells from Table 1 gives a value of -509.37 kJ $ICCmol^{-1}$. Using equation (2), 4.577 eq are transferred to $O_2(g)$ during the bomb calorimetric combustion of one ICCmol of cells. Dividing -509.37 kJ $ICCmol^{-1}$ by 4.577 eq $ICCmol^{-1}$ gives -111.29 kJ eq^{-1}. This is within 0.13 per cent of the value of -111.14 kJ eq^{-1} from Section *3.4.1*, indicating that this latter can be used to calculate a $\Delta_c H$ value for one ICCmol of whole, dried cells in general. When this is used with the appropriate data from Table 3 in an equation similar to equation (19), a value can be calculated for $\Delta_f H_{cells}$. This latter value can then be used together with appropriate values from Table 3 in process equations such as those in Table 2 to calculate values for $\Delta_p H_{an}$ or $\Delta_p H_{met}$ for aerobic or anaerobic growth processes without the necessity of using a calorimeter. If it is accuracy that is desired, these are the methods of choice.

3.4.3. Another way to calculate $\Delta_p H'_{met}$.

Although it is best to pay attention to all possible detail in comprehending the various aspects of the thermodynamics of microbial growth, this is not always practical to do. If maximum accuracy is not required and only a close approximation is needed, it is more convenient to obtain an estimate of $\Delta_p H'_{met}$ directly, rather than to go through the steps outlined in Section *3.4.2.* This is to measure the oxygen consumption of a microbial culture directly and to use an oxycaloric equivalent, $\Delta_k H'_{O_2}$, to calculate the quantity of heat produced [45], where the subscript "k" indicates that this heat exchange is the result only of the catabolism that takes place during metabolism. The assumption is made that the contribution of $\Delta_p H'_{an}$ to $\Delta_p H'_{met}$ is negligible, and this is true within about two per cent for most aerobic growth processes. The value used for $\Delta_k H'_{O_2}$ can be obtained most accurately by writing the equation representing the oxidation in the *aqueous* state of the substrate being utilized, calculating the accompanying non-conservative heat production using appropriate values from Table 3, and dividing this value by the number of O_2 molecules participating in the oxidation. For example, in Table 2, $\Delta_p H'_{NC}$ for glucose oxidation is -2862.17 kJ mol^{-1} which, when divided by 6 molecules of $O_2(aq)$ utilized in the oxidation gives a value for $\Delta_c H'$ of -477.03 kJ mol^{-1} of

O_2(aq). If this is equated with $\Delta_k H'_{O_2}$ and multiplied by 4.050 mol of O_2(aq) consumed during metabolism, the value for $\Delta_k H'_{O_2}$ becomes -1931.97 kJ. The same value is obtained for aerobic glucose catabolism in Table 2. On the other hand, the value of $\Delta_p H'_{met}$ for aerobic growth on glucose from Table 2 is -1972.94 kJ. The value for $\Delta_k H'_{O_2}$ is thus about 2% too low if this is going to approximate that of metabolism, which is not at all unreasonable, considering the ease with which it can be obtained. Values for $\Delta_k H'_{O_2}$ obtained by calculation using equations representing oxidation do vary, those for ethanol and acetic acid being -453.93 kJ and -444.91 kJ, respectively. These procedures work well when the nature of the substrate is known and values for thermodynamic properties are available. If a complex rather than a defined culture medium is used and the nature of the substrate is not known, as with nutrient broth, yeast extract, blood, coconut milk, etc., a reasonable estimate for $\Delta_k H'_{O_2}$ must be used. The value for $\Delta_c H^o_{O_2}$ of -444.56 kJ from Section *3.4.1* is not suitable in that it represents a bomb calorimetric rather than a biological oxidation, which would give a more negative value. The $\Delta_k H'_{O_2}$ value of -477 kJ obtained for glucose is high compared to that of other common substrates such as those above for ethanol and acetic acid as representatives of more reduced and more oxidized substrates. Simply averaging the highest (glucose) and the lowest (acetic acid) in this case would give a reasonable value for $\Delta_k H'_{O_2}$ of -460 kJ that could be applied without an error of more than 4 per cent to most culture conditions involving undefined substrates. On the other hand, a $\Delta_k H'_{O_2}$ value of -450 kJ ± 22 kJ $Cmol^{-1}$ has been calculated for protein [45], and a $\Delta_c H_{O_2}$ value of -455 ± 15 kJ mol^{-1} for the bomb calorimetric combustion of the major compounds in plant metabolism [46].

3.4.4. Calculating values for $\Delta_f G_{cells}$, $\Delta_p G'_{an}$ *and* $\Delta_p G'_{met}$.

These values are not thermal quantities and cannot be measured calorimetrically. They can be determined experimentally only by measuring the heat of combustion and the entropy of one ICCmol of cells, and using the Gibbs free energy equation to calculate values for $\Delta_f G_{cells}$, $\Delta_p G'_{an}$, and $\Delta_p G'_{met}$. On the other hand, the same methods used for determining the value of $\Delta_c H_{cells}$ to be -111.14 kJ eq^{-1} can be used for determining a value for $\Delta_c G_{cells}$, where the subscript "c" indicates that this value came from bomb calorimetric combustion. This was done with respect to 288 pure substances containing C, H, O, and N for which $\Delta_c G^o$ is known [47]. The average value of $\Delta_c G^o$ was -108.74 kJ eq^{-1} and a linear regression run through these data gave -107.06 kJ eq^{-1}. As with $\Delta_c H$ eq^{-1}, one of these values is

no "better" than the other, and these were averaged to give a general value of -107.90 kJ eq^{-1} [48]. It might seem that because this technique appears to work well for determining values for $\Delta_f H_{cells}$ using equation (18) and appropriate values from Table 3, it would also work for determining values for $\Delta_f G_{cells}$. It doesn't! The value for $\Delta_f G_{cells}$ from Table 3 was calculated with the Gibbs free energy equation using values for $\Delta_f H_{cells}$ and $\Delta_f S_{cells}$ that were calculated from experimental thermal measurements. On the other hand, multiplying -107.90 kJ eq^{-1} by 4.577 eq ICCmol^{-1} gives a value for $\Delta_c G_{cells}$ of -493.96 kJ ICCmol^{-1}. Using this value and other appropriate values from Table 3, $\Delta_f G_{cells}$ is calculated to be -108.61 kJ ICCmol^{-1}, which is high compared with similar values in Table 3. Using this and the value for $\Delta_f H_{cells}$ of -133.09 kJ ICCmol^{-1} from Table 3, $\Delta_f S_{cells}$ is calculated as follows.

$$\Delta_f G_{cells} = \Delta_f H_{cells} - T\Delta_f S_{cells} \qquad (20)$$

-108.61 kJ ICCmol^{-1} = -133.09 kJ ICCmol^{-1} - 298.15 K $\Delta_f S_{cells}$, from which

$\Delta_f S_{cells}$ = -82.11 J K^{-1} ICCmol^{-1}

In equation (20) superscripts are not used because cells have no standard state. The value for $\Delta_f S$ calculated above is about half of that obtained from experimental measurements, which are taken to be correct. The reason for the failure of this calculation is uncertain. The experimental measurements of cellular entropy were of polymerized cellular fabric (i.e. proteins, phospholipids, nucleic acids, cell wall material, etc.), whereas the value found with equation (19) made use of $\Delta_c G^\circ$ values for small molecular weight molecules to obtain a general value for $\Delta_c G$ eq^{-1} that could be used to calculate a value for $\Delta_f G_{cells}$. Adding the free energy of polymerization would increase the value for $\Delta_c G^\circ$ and would lower the value for $\Delta_f G_{cells}$. On the other hand, there was no need to do this when calculations were made using the methods described in Section *3.4.2.*

3.5. The efficiency of growth.

The quantity of biomass or other organic substance produced during growth is more or less proportional to metabolic or catabolic free energy change, or metabolic or catabolic enthalpy change. Entropy changes have never been considered in this respect. Efficiency can be expressed as the fraction of energy

initially available that becomes conserved within the substance of a biomass and/or organic product. Thus, for the conservation of energy in a growth process

$$\eta_G = \frac{\Delta_p G'_{NC} - \Delta_p G'_{met}}{\Delta_p G'_{NC}} \tag{21}$$

where η_G represents the efficiency of free energy conservation within the biomass and other organic products [49]. Similarly,

$$\eta_H = \frac{\Delta_p H'_{NC} - \Delta_p H'_{met}}{\Delta_p H'_{NC}} \tag{22}$$

where η_H represents the efficiency of enthalpy conservation within the biomass and other organic products [41]. Other types of efficiencies are also possible, and a description of these can be found in reference [19]. Efficiencies of entropy conservation have not been dealt with largely because their units are three orders of magnitude smaller than those of free energy or enthalpy, and small inaccuracies in either of these latter cause large inaccuracies in the calculation of entropy changes.

3.5.1. Calculating electron conservation efficiencies for aerobic growth processes.

The difficulty with efficiencies as represented by equations (21) and (22) is that they have different values, whereas it would be expected that some form of energy conservation efficiency exists having one value from which all other efficiencies can be derived by using appropriate constants. The answer to this appears to be the electron conservation efficiency [50-55]. This is the number of electrons conserved within a biomass or other organic product during a growth process. The transfer of electrons from electron donor to electron acceptor is the common denominator for all O-R reactions, including the growth of microorganisms. If cells are the only product, as often happens in aerobic growth, the electron efficiency can be represented as follows.

$$\eta_{AEcells} = \frac{MYC_{cells}\, AE_{cells}}{AE_{sub}} \tag{23}$$

where η_{AE} is the efficiency of electron conservation within the cellular fabric formed during a growth process. A similar equation would apply to the efficiency of electron

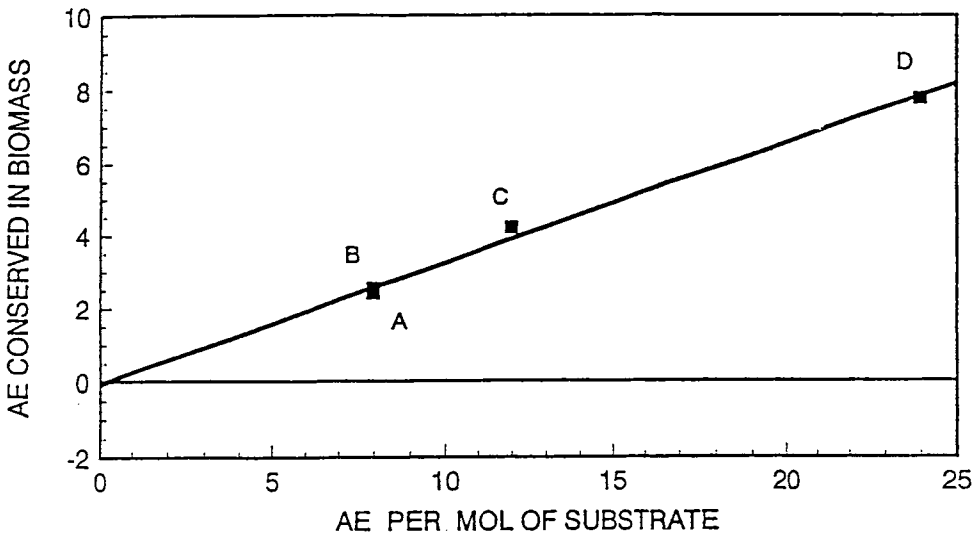

Figure 2. A linear regression in which the number of electrons conserved in the fabric of the cells is plotted against the number of available electrons per mol of substrate for the growth of *S. cerevisiae* anaerobically on glucose [A] and aerobically on acetic acid [B], ethanol [C], and glucose [D]. The slope of the line is 0.331, the Y-intercept is -0.072, and the correlation coefficient is 0.997. Note that points A and B are almost identical. This is because the respective non-conservative processes both transfer eight available electrons, and because the composition of the cells is the same for both growth processes.

conservation within the substance of other organic products.

3.5.2. Calculating free energy conservation efficiencies for aerobic growth processes.

For the aerobic growth of *S. cerevisiae* on glucose as represented in Table 2

$$\eta_{AEcells} = \frac{MYC_{cells}\, AE_{cells}}{AE_{sub}} = \frac{1.914\ (4.079\ AE\ )}{24} = 0.325 \qquad (24)$$

It is apparent that this is numerically the same value as S_{an}, which is to be expected in that 0.325 mol of glucose contains 0.325 of the number of electrons in one mol of glucose. Figure 2 shows that the conservation of AE within cellular fabric is independent of the nature and of the overall metabolism of the electron donor. This is true even during autotrophic growth when the electron donor is an inorganic substance such as $H_2(aq)$ and the carbon source is $CO_2(aq)$, so that there is

no substrate performing the functions of electron donor and carbon source in the usual sense [56]. However, equation (23) will not by itself enable a calculation to be made of the free energy and enthalpy conserved because it does not take into account the energy charges per electron of different electron donors.

The equations in Table 2 representing anabolism are constructed so that the quantity of anabolic substrate and the quantity of cells produced are electron equivalent. This means that if all electrons have the same energy charge, there would be no thermodynamic changes accompanying anabolism, and $\Delta_p G'_{an}$, $\Delta_p H'_{an}$, and $\Delta_p S'_{an}$ would all be zero. This is not the case because the energy charge of the electrons within a substance is different, depending on the substrate [55]. For example, in the biological oxidation of glucose 24 electrons are transferred to $O_2(g)$ with an accompanying $\Delta_c G'$ of -2905.47 kJ mol^{-1}. The average free energy charge of each electron is therefore -121.06 kJ eq^{-1}. For the biological oxidation of ethanol and acetic acid these values are -109.78 kJ eq^{-1} and -107.23 kJ eq^{-1}, respectively. These differences are reflected in the sign of the energy changes accompanying anabolism. The following equation represents the *biological* oxidation of one ICCmol of cells represented by formula (B).

$$CH_{1.613}O_{0.557}N_{0.158}P_{0.012}S_{0.003}K_{0.022}Mg_{0.003}Ca_{0.001}(\text{cells}) + 1.026O_2(aq) \rightarrow 1.000\,CO_2(aq) + 0.547\,H_2O(l) + 0.158\,NH_3(aq) + 0.012\,H_2PO_4^-(aq) + 0.003\,HS^-(aq) + 0.022\,K^+(aq) + 0.003\,Mg^{2+}(aq) + 0.001\,Ca^{2+}(aq) + 0.015\,OH^-(aq) \quad (25)$$

With the appropriate data from Table 3, the free energy change ($\Delta_c G'_{cells}$) accompanying the process represented by equation (25) is calculated to be -475.44 kJ $ICCmol^{-1}$. Using equation (1) the biomass represented in equation (25) contains 4.079 AE. The average free energy charge for this biomass is then -475.44 kJ $ICCmol^{-1} \div 4.079$ AE $ICCmol^{-1} = -116.56$ kJ AE^{-1}. If $\Delta_c G' AE^{-1}$ for the substrate is less than that of the biomass, free energy will be required for anabolism and the sign of $\Delta_p G'_{an}$ will be positive. If $\Delta_c G'$ AE^{-1} for the substrate is greater than that of the biomass, free energy will be lost as heat and entropy during anabolism and the sign of $\Delta_p G'_{an}$ will be negative. These relationships will also apply to the production of an organic product during metabolism. The quantity $\Delta_c G' AE^{-1}$ is a constant for any given substance, as is $\Delta_c H' AE^{-1}$. A calculation of η_G can be made using equation (23) if AE_{cells} is multiplied by $\Delta_c G'_{cells}$ AE^{-1} and if AE_{sub} is multiplied by $\Delta_c G'_{sub}$ AE^{-1}. For the aerobic growth of *S. cerevisiae* on glucose as shown in Table 2

$$\eta_{Gcells} = \frac{MYC_{cells}\, AE_{cells}}{AE_{sub}} \cdot \frac{(\Delta_c G'_{cells}\, AE^{-1}_{cells})}{(\Delta_c G'_{sub}\, AE^{-1}_{sub})} \qquad (26)$$

This reduces to

$$\eta_{Gcells} = \frac{MYC_{cells}\, \Delta_c G'_{cells}}{\Delta_c G'_{sub}} = \frac{1.914\ (-475.44\ \text{kJ ICCmol}^{-1})}{-2905.47\ \text{kJ mol}^{-1}} = 0.313 \qquad (27)$$

Because η_G represents the fraction of the free energy from one mol of substrate that is conserved within the structure of the cells, if there are no other organic products of the growth process the fraction $(1 - \eta_G)$ must be that of the free energy that is lost during metabolism. Thus

$$\Delta_p G'_{met} = (1 - \eta_G)\, \Delta_p G'_{NC} = (1 - 0.313)(-2905.47\ \text{kJ mol}^{-1})$$

$$= -1996.06\ \text{kJ mol}^{-1}\ \text{of glucose consumed.} \qquad (28)$$

This value is nearly identical to that of -1996.95 kJ mol^{-1} in Table 2. It should be the same and probably differs because of the use of fractional numbers rather than small whole numbers in the calculations.

3.5.3. Calculation of enthalpy conservation efficiencies for aerobic growth processes.

The same methods used above in Section *3.5.2.* for calculating free energy conservation efficiencies can be used to calculate enthalpy conservation efficiencies. Using appropriate data from Table 3, the enthalpy change ($\Delta_c H'_{cells}$) accompanying the process represented by equation (25) is calculated to be -463.89 kJ ICCmol^{-1}. For the growth of *S. cerevisiae* aerobically on glucose as represented in Table 2:

$$\eta_{Hcells} = \frac{MYC_{cells}\, \Delta_c H'_{cells}}{\Delta_c H'_{sub}} = \frac{1.914(-463.89\ \text{kJ ICCmol}^{-1})}{-2862.17\ \text{kJ mol}^{-1}} = 0.310\ ; \text{ and} \qquad (29)$$

$$\Delta_p H'_{met} = (1 - \eta_H)\Delta_p H'_{NC} = (1 - 0.310)(-2862.17\ \text{kJ mol}^{-1})$$

$$= -1974.89\ \text{kJ mol}^{-1}\ \text{of glucose consumed.} \qquad (30)$$

This value is nearly identical to that of -1976.27 kJ mol^{-1} in Table 2.

It is evident from equations (23), (26), and (29) that there are three different values for efficiency with respect to the aerobic growth of *S. cerevisiae* on glucose. However, both η_G and η_H can be derived from η_{AE} through the use of the appropriate constants and therefore η_{AE} must be considered the most basic efficiency of the three. It can be asked, even if this is true, what good is it? The answer can only be that for one purpose or another, it may be useful, and at the least, dealing with this concept will increase our general comprehension.

3.5.4. Calculating electron conservation efficiencies for anaerobic growth processes.

For anaerobic growth processes no AE are transferred to O_2(aq) as a result of a biological oxidation, even though a biological oxidation does occur. Nevertheless, AE can be used to indicate the *relative* energies in substances. This can be demonstrated using as an example the anaerobic growth of *S. cerevisiae* on glucose which is represented in Table 2. Here, all the organic substances formed during growth must be considered products. The efficiencies of electron conservation for anaerobic growth are calculated just as for aerobic growth processes.

$$\eta_{AEcells} = \frac{MYC_{cells}\, AE_{cells}}{AE_{sub}} = \frac{0.590\ (4.079\ \text{kJ ICCmol}^{-1})}{24} = 0.100 \qquad (31)$$

$$\eta_{AEgly} = \frac{MYC_{gly}\, AE_{gly}}{AE_{sub}} = \frac{0.432\ (14.000\ \text{kJ ICCmol}^{-1})}{24} = 0.252 \qquad (32)$$

$$\eta_{AEeth} = \frac{MYC_{eth}\, AE_{eth}}{AE_{sub}} = \frac{1.300\ (12.000\ \text{kJ ICCmol}^{-1})}{24} = 0.650 \qquad (33)$$

$$\text{Total } \eta_{AE} = \overline{1.002}$$

The total electron conservation efficiency equals 100 per cent (or should) because no AE have been lost from the system. The efficiency comparable to that for the aerobic growth of *S. cerevisiae* on glucose would be expected to reside in those organic products of the growth process that are different from that produced in the

anaerobic catabolic process, which in this case is ethanol. Thus, the sum of 0.100 and 0.252 as the efficiencies calculated with equations (31) and (32), respectively, gives 0.352, which is reasonably close to that of 0.325 from equation (24). Here, the same substrate is being used to form cells with the same composition both aerobically and anaerobically. Theoretically the two values might be expected to be the same. That they are not is because only a part of the electrons is conserved in the cells. The rest is conserved in another product, glycerol, which is much more reduced than the cells ($\gamma = 4.666$), which raises the value of the *total* electron conservation efficiency. Or, it may be due to an inaccurate analysis either in the quantity of glycerol, or in failing to find small quantities of other products.

3.5.5. Calculating free energy conservation efficiencies for anaerobic growth processes.

Values for the free energy and enthalpy conservation efficiency during anaerobic growth can also be calculated using the same methods as for aerobic growth. To calculate free energy conservation efficiencies

For the cells produced during growth

$$\eta_{G\text{cells}} = \frac{\text{MYC}_{\text{cells}}\,\Delta_c G'_{\text{cells}}}{\Delta_c G'_{\text{sub}}} = \frac{0.590\ (-475.44\ \text{kJ ICCmol}^{-1})}{-2905.47\ \text{kJ mol}^{-1}} = 0.097 \qquad (34)$$

For the glycerol produced during growth

$$\eta_{G\text{gly}} = \frac{\text{MYC}_{\text{gly}}\,\Delta_c G'_{\text{gly}}}{\Delta_c G'_{\text{sub}}} = \frac{0.432\ (-1640.75\ \text{kJ mol}^{-1})}{-2905.47\ \text{kJ mol}^{-1}} = 0.244 \qquad (35)$$

For the ethanol produced during growth

$$\eta_{G\text{eth}} = \frac{\text{MYC}_{\text{eth}}\,\Delta_c G'_{\text{eth}}}{\Delta_c G'_{\text{sub}}} = \frac{1.300\ (-1317.36\ \text{kJ mol}^{-1})}{-2905.47\ \text{kJ mol}^{-1}} = 0.589 \qquad (36)$$

Total η_G 0.930

The sum of the above values represents the total free energy conservation

efficiency. The fraction of the free energy that is lost during metabolism must then be (1 - 0.930). From this

$$\Delta_p G'_{met} = (1 - 0.930)\,\Delta_c G'_{NC} = 0.070\,(-2905.47\ \text{kJ mol}^{-1})$$

$$= -203.38\ \text{kJ mol}^{-1}\ \text{of glucose consumed.} \qquad (37)$$

This value agrees satisfactorily with that for $\Delta_p G'_{NC}$ of -210.41 kJ mol^{-1} in Table 2.

3.5.6. Calculating enthalpy conservation efficiencies for anaerobic growth processes.

For the cells produced during growth

$$\eta_{H\text{cells}} = \frac{\text{MYC}_{\text{cells}}\,\Delta_c H'_{\text{cells}}}{\Delta_c H'_{\text{sub}}} = \frac{0.590\,(-463.89\ \text{kJ ICCmol}^{-1})}{-2862.17\ \text{kJ·mol}^{-1}} = 0.095 \qquad (38)$$

For the glycerol produced during growth

$$\eta_{H\text{gly}} = \frac{\text{MYC}_{\text{gly}}\,\Delta_c H'_{\text{gly}}}{\Delta_c H'_{\text{sub}}} = \frac{0.432\,(-1665.85\ \text{kJ mol}^{-1})}{-2862.17\ \text{kJ mol}^{-1}} = 0.251 \qquad (39)$$

For the ethanol produced during growth

$$\eta_{H\text{eth}} = \frac{\text{MYC}_{\text{eth}}\,\Delta_c H'_{\text{eth}}}{\Delta_c H'_{\text{sub}}} = \frac{1.300\,(-1361.80\ \text{kJ mol}^{-1})}{-2862.17\ \text{kJ mol}^{-1}} = 0.618 \qquad (40)$$

Total η_H 0.964

The sum of the efficiency values above represents the total enthalpy conservation efficiency. The fraction of the enthalpy that is lost during metabolism must then be (1- 0.964). From this

$$\Delta_p H'_{met} = (1 - 0.964)\,\Delta_c H'_{NC} = 0.036\,(-2862.17\ \text{kJ mol}^{-1}) \qquad (41)$$

$$= -103.04\ \text{kJ mol}^{-1}\ \text{of glucose consumed.}$$

This value agrees satisfactorily with that of - 105.40 kJ mol^{-1} from Table 2.

3.5.7. Why calculate efficiencies?

The calculation of efficiencies is largely of academic interest, although this can have a practical application. It is apparent from this section that there are several types of efficiencies that are useful, depending on what one wants to do with them. The electron conservation efficiency is certainly the most basic in that the other efficiencies can be derived from this using the appropriate constants. The very high correlation coefficient with respect to the data in Figure 2 indicates a strong relationship between the number of AE in the substrate and that in the cells that are grown. This suggests that at least for microorganisms different organic substrates become converted to one or a few common forms of about the same level of reduction, which then enter into anabolism. Biochemists have known this for years, but have not applied it to the overall synthesis of cellular fabric. Calculating the efficiency of free energy conservation focuses on the idea that during a growth process non-thermal energy becomes converted into thermal energy, and the available free energy is the only source of this heat. But, the free energy changes accompanying anabolism can be either plus or minus a certain amount, and it is not the absolute value of the free energy change that is important. Calculating the efficiency of enthalpy conservation or loss has obvious practical advantages with respect to the quantity of heat given off during growth in a culture vessel or a bioreactor.

3.6. A comment on entropy.

Recently there has been a resurgence of interest in the function of entropy in living systems, initiated by the fiftieth anniversary of the publication by Schrödinger of his well known book entitled "What is Life" [57].

In the process equations in Table 2 an attempt has been made to present the changes both in substance and in energy that accompany the growth of *S. cerevisiae* as a representative micro-organism. One of these energy changes is that of entropy and it is evident that, as with any closed system, the entropy changes that occur as a growth process system proceeds from its initial to its final state can be plus, minus, or zero, although this last is not seen here.

For better or worse, many meanings have arisen as to the concept of "entropy." The principal idea that is usually expressed is that entropy represents a degree of "randomness," or "probability" with respect to something being studied. This

idea presents the problem of comprehension that neither randomness nor probability has dimensions, and no obvious connection with the values of $T\Delta S$ found in Table 2. In statistical mechanics the dimensions of J K^{-1} mol^{-1} (of whatever mass) are introduced into equations having probabilities through the use of the Boltzman constant. But, it is difficult even to conceive of what the probability states of a cell might be. That physical entropy is a quantity of heat is often not emphasized. Heat is thermal energy that is exchanged between two masses because of a temperature difference between them. It is also the form of energy that must be absorbed by a given mass in order for it to exist at a given temperature above absolute zero, as mentioned in Section *3.2.2.* At any temperature above 0 K *everything* has an entropy that is a function of its heat capacity. Thus, entropy is *absorbed* thermal energy. If it isn't absorbed, it is heat. Entropy can be acquired by a mass or lost from it as a result of a temperature change. This phenomenon is one of the few, perhaps the only one, that can be considered completely reversible. Exactly the same quantity of heat is always required to be absorbed by a given mass in order to raise it by a given temperature increment, or is lost from it if the temperature of the mass is lowered by a given increment. Entropy cannot be considered to be "bound" energy in the sense that chemical energy is. Entropy is thermal energy. Chemical energy is non-thermal energy. If work can be defined as non-thermal energy that is exchanged between two masses because of a force exerted between them, then no work is required when a mass acquires entropy, or when entropy is lost from a mass. At a constant temperature, growth process system entropy changes do occur, as seen in Table 2. This is not because of temperature differences, but because of a change in the physical nature of the system. If a given quantity of a substrate such as glucose disappears from a growth process system because it is metabolized at a given temperature, an exact quantity of entropy is lost into the system as heat. If organic substances are produced during metabolism, such as cells, in order for these to exist at the constant temperature of the system heat must be absorbed, and this thermal energy becomes an exact quantity of entropy. The overall change in entropy of a growth process system as it proceeds from an initial to a final state is because of the disappearance of reactants and the formation of products, all of which have their own specific physical and thermodynamic properties. Thus, if more entropic heat were to be lost from the reactants than was absorbed by the products, there would be a quantity of heat contributing to the enthalpy change in addition to that due to the change in free energy, and the total quantity of heat transferred would be greater than the quantity of free energy

degraded into heat. The reverse would be true if less entropic heat were to be lost from the reactants than absorbed by the products at the given temperature. This is expressed by turning around the Gibbs free energy equation.

$$\Delta_p H = \Delta_p G + T\Delta_p S \tag{42}$$

If $T\Delta_p S$ is negative, $\Delta_p H > \Delta_p G$; if $T\Delta_p S$ is positive, $\Delta_p H < \Delta_p G$. This is simply to point out that there are two components to the enthalpy change. If the sign of $\Delta_p G$ is negative all of this non-thermal energy becomes converted into thermal energy. For growth processes this quantity of heat is always large enough that a positive $T\Delta_p S$ will not cause $\Delta_p H$ also to become positive. For example, in the case of anaerobic growth on glucose in Table 2 the enthalpy change is only about half that of the free energy change because of a large, positive entropy change.

It is important to realize that the physical entropy considered here is not something that is consumed or produced. Entropy can only exist as *absorbed* thermal energy. Lost entropy is heat. As entropy, it cannot be transported across the limiting boundaries of a closed system. If entropy is transported, it can only be as thermal energy absorbed by a given mass at a given T. If the mass cannot be transported across a limiting boundary, neither can the entropy associated with it What *is* transported across this limiting boundary is heat, because of a transient temperature difference between a growth process system and the environment. This continues until the final state, after which temperature equilibrium with the environment becomes re-established.

What happens to the thermal energy when it enters the environment is anyone's guess. Conventional theory maintains that it heats up the universe, thereby increasing its entropy. However, this could only happen if the heat energy lost from the system is absorbed; otherwise, it remains as radiant energy. Another question is whether or not the entropy change of a spontaneous process taking place within a system *must* be negative, in order that the entropy of the universe will increase and, as a result, become more random. This does not happen in the case of yeast cells growing on glucose, in which the entropy changes accompanying metabolism are positive, as shown in Table 2. On the other hand, they are negative for growth on ethanol and acetic acid. This indicates that the passage of a growth process system from its initial state to its final state is not dependent on the sign of the entropy change of

the system. What is more likely is that growth is dependent on the tendency of electrons in the outer orbitals of the atoms in a growth process system to become rearranged or transferred from a less probable to a more probable condition (state), irrespective of the entropies and the related entropies of formation of the reactants and products, including cells [55]. The question then becomes whether the less probable electron configuration in the initial state represents a greater organization than the more probable electron configuration in the final state.

Acknowledgements:

The author wishes to express his grateful thanks to Dr. Christer Larsson, Lundberg Laboratory, Department of General and Marine Microbiology, Medicinareg. 9C, S-413 90 Göteborg, Sweden, for the use of his unpublished data on the heat of combustion of whole cells of *S. cerevisiae.*

REFERENCES

1. R.B. Kemp, personal communication.
2. H.P.J. Bonarius, V. Hartimanikatis, K.P.H. Maesters, C.D. de Gooijer, G. Schmid, and J. Tramper, Biotechnol. Bioeng., 50 (1996) 299.
3. G.E. Jones (Ed.), Human Cell Culture Protocols, Humana Press, Totawa, New Jersey, 1996.
4. A.D. Krikorian, Bot. Revs., 62 (1996) 41.
5. E.H. Battley, Energetics of Microbial Growth, Wiley-Interscience, New York, 1987, Sections 5.1 and 5.2.
6. E. Duclaux, Traité de Microbiologie, III, Masson et Cie, Paris, 1900, p.378.
7. E.H. Battley, Energetics of Microbial Growth, Wiley-Interscience, New York, 1987, p.254.
8. E.H. Battley, Pure & Appl. Chem., 65 (1993) 1881.
9. E.H. Battley, Physiol. Plant., 13 (1960) 192.
10. Z. Dermoun and J.-P. Belaich, J. Bacteriol., 140 (1979) 377.
11. E.H. Battley, Energetics of Microbial Growth, Wiley Interscience, New York, 1987, p.393.
12. E.H. Battley and G. DiBiase, Biotechnol. Bioeng., 22 (1980) 2417.
13. T. Gurakan, I. Marison, U. von Stockar, L. Gustafsson, and E. Gnaiger, Thermochim. Acta, 72 (1990) 251.
14. A.A. Eddy, in A. H. Cook (ed.), The Chemistry and Biology of Yeasts, Academic Press, New York, 1958, p.158.

15. A. Halász and R. Lászity, Use of Yeast Biomass in Food Production, CRC Press, Boca Raton, 1990, p.39.
16. G. Reed and T.W. Nagodowithana, Yeast Technology, 2nd edn., Van Nostrand Reinhold, New York, 1991.
17. E.H. Battley, Appl. Environ. Microbiol., 61 (1995) 1655.
18. H.G. Schlegel, Allegemeine Mikrobiologie, Georg Thieme Verlag, Stuttgart, 1969, p.242.
19. U. von Stockar and I.W. Marison, Thermochim. Acta, 229 (1993) 157.
20. V.A. Aluise, R.T. Hall, F.C. Staats, and W.W. Becker, Anal. Chem., 19 (1947) 347.
21. W.R. Mayberry, G.J. Prochazka, and W.J. Payne, Appl. Microbiol.,15 (1967) 1332.
22. E.H. Battley, Biotechnol. Bioeng., 37 (1991) 334.
23. M.S. Karasch and B. Sher, J. Phys. Chem., 29 (1925) 625.
24. E.H. Battley, Biotechnol. Bioeng., 39 (1992) 5.
25. I.G. Minkevitch and V.K. Eroshin, Izv.Akad. Nauk. SSSR., Ser. Biol. 3(1973) 414.
26. Z. Dermoun and J.P. Belaich, J. Bacteriol., 143 (1980) 742.
27. M. Rutgers, H.M.L.Van der Gulden, and K.Van Dam, Biochim. Biophys. Acta, 973 (1989) 302.
28. E.H. Battley, Energetics of Microbial Growth, Wiley Interscience, New York, 1987, Section 10.5.
29. H.V. Westerhof, Pure & Appl. Chem., 65 (1993) 1899.
30. E. Gnaiger, Pure & Appl. Chem., 65 (1993) 1983.
31. M. Rubner, Arch. Hyg., 48 (1904) 260.
32. R.C. Weast, (Ed.), Handbook of Biochemistry and Biophysics, CRC Press, Boca Raton, FL, 63rd edn, 1982, p. D-45. This is a compilation of selected values taken from D.D. Wagman, W.H. Evans, V.B. Parker, R.H. Schumm, S.M. Bailey, I. Halow, K.L. Churney, and R.L. Nuttall, National Bureau of Standards Notes 270-3, 270-4, 270-5, 270-6, 270-7, and 270-8, Superintendent of Documents, U.S.Government Printing Office, Washington, D.C. 20402.
33. R.C. Wilhoit, in H.D. Brown (Ed.), Biochemical Microcalorimetry, Academic Press, New York, 1969, Appendix, p.305.
34. M.W. Chase, Jr., C.A. Davies, J.R. Downey, Jr., D.J. Fririp, R.A. McDonald, and A.N. Syverud, J. Phys. Chem. Ref. Data, 14 (1985) Supplement No. 1.
35. G.N. Lewis and M. Randall, Thermodynamics; revised by K.S. Pitzer and L.Brewer, McGraw-Hill, New York, 2nd edn, 1961, p.239.

36. E.H. Battley, Energetics of Microbial Growth, Wiley Interscience, New York, 1987, p.374.
37. E.H. Battley, Biotechnol. Bioeng., 38 (1991) 480.
38. C. Larsson, personal communication.
39. U.von Stockar, L.Gustafsson, C. Larsson, I. Marrison, P.Tissot, and E. Gnaiger, Biochim. Biophys. Acta , 1183 (1993) 221.
40. E.H. Battley, R.L. Putnam, and J. Boerio-Goates, Thermochim. Acta, in press.
41. E.H. Battley, Physiol. Plant., 13 (1960) 628.
42. W.M. Thornton, Phil. Mag., 33 (1917) 196.
43. M.S. Karasch and B. Sher, J. Phys. Chem., 29 (1925) 625.
44. S.A. Patel and L.E. Erickson, Biotechnol. Bioeng., 23 (1981) 2051.
45. E. Gnaiger and R.B. Kemp, Biochim. Biophys. Acta, 1016 (1990) 328.
46. L. D. Hansen, M. S. Hopkin, D. K. Taylor, T. S. Anekonda, D.R. Rank, R.W. Breidenbach, and R.S.Criddle, Thermochim. Acta, 250 (1995) 215.
47. L.N. Erickson and S.A. Patel, CRC Crit. Rev. Biomed. Eng., 8 (1982) 311.
48. E.H. Battley, Pure & Appl. Chem., 65 (1992) 1881.
49. E.H. Battley, Physiol. Plant., 13 (1960) 674.
50. L.E. Erickson and M.D. Öner, Ann. N.Y. Acad. Sci., 413 (1983) 99.
51 L.E. Erickson, in L.E. Erickson and D.Y.-C. Fung (Eds.), Handbook on Anaerobic Fermentations, Marcel Dekker, Inc., New York, 1988, p.119.
52. L.E. Erickson, in L.E. Erickson and D.Y.-C .Fung (Eds.), Handbook on Anaerobic Fermentations, Marcel Dekker, Inc., New York, 1988, p.325.
53. L.E. Erickson, S.S. Yang, and M.D. Öner, in L.E. Erickson and D.Y.-C. Fung (Eds.),Handbook on Anaerobic Fermentations, Marcel Dekker, Inc., New York, 1988, p.463.
54. M.D. Öner, L.E. Erickson, and S.S.Yang, in L.E. Erickson and D.Y.-C. Fung (Eds.), Handbook on Anaerobic Fermentations, Marcel Dekker, New York, 1988, p.293.
55. E.H. Battley, Can. J. Microbiol., 41 (1995) 388.
56. E.H. Battley, Can. J. Microbiol., 42 (1996) 38.
57. E. Schrödinger, What is Life? The Physical Aspect of the Living Cell, Cambridge University Press, Cambridge, 1945.

Handbook of Thermal Analysis and Calorimetry. Vol. 4: From Macromolecules to Man.
R.B. Kemp, editor.

Chapter 6

QUANTITATIVE CALORIMETRY AND BIOCHEMICAL ENGINEERING

Philippe Duboc*, Ian Marison and Urs von Stockar

Institute of Chemical Engineering and Bioengineering
Swiss Federal Institute of Technology
CH-1015 Lausanne
Switzerland

1. INTRODUCTION: APPLICATIONS OF CALORIMETRY IN BIOCHEMICAL ENGINEERING

1.1. Cooling requirements

Heat production by microorganisms addresses the important problem of heat removal in industrial large scale bioreactors. In fact, the heat flow rate increases with the reactor volume, whereas transfer of heat to the environment increases only with the surface. The volume/surface ratio decreases with increasing reactor size, and may even be limiting. Adequate heat removal requires the installation of large cooling coils in industrial systems.

A yeast continuous culture growing aerobically on glucose (feed concentration of 20 g dm^{-3}) produces 3.4 W dm^{-3} at a dilution rate of 0.10 h^{-1} (for a heat yield on substrate of 185 kJ C-mol^{-1}). If the heat is not removed (adiabatic reactor), the temperature of the reactor will increase by as much as 2.6°C h^{-1}. These figures show the necessity to remove efficiently heat in aerobic processes [11]. If the same culture is grown anaerobically, the heat flow rate will significantly decrease due to the low heat yield on glucose. However, the rate of temperature increase is about 2.5°C h^{-1} for a feed concentration of 300 g dm^{-3} (e.g. molasses), indicating that anaerobic processes on glucose are subjected to heat

*present address: Center for Process Biotechnology, Denmark Technical University, DK2800 Lyngby, Denmark

removal problems as soon as the substrate concentration is high. An example is "heat accident" in wine making when adiabatic fermentor temperature increases above an unfavorable value for fermenting yeast.

1.2. Data consistency

Gross measurement errors are easier to detect when several elemental balances (for carbon, nitrogen, degree of reduction) can be checked. Because heat (enthalpy) is an extensive variable, an energy balance can be set-up around the reactor boundary considered as an open system. Therefore heat can be used to check that no major substrate or product has been neglected.

1.3. On-line monitoring and control of bioreactors

The heat flow rate corresponds to the heat released by the growth reaction. By analogy with chemical processes, heat flow rate is used to monitor [2,3] or control [4] biotechnological processes, and is of special interest as few other on-line measurements are available (e.g. during methanogenesis).

1.4. Thermodynamics of living systems: What is measurable ?

Biological activity is the result of the coupling between fueling reactions (catabolism) which are exergonic and biosynthetic reactions (anabolism) which are endergonic. The Gibbs energy function, $\Delta_r G$, is the respective driving force generated and dissipated by these reactions. Although $\Delta_r G$ is the fundamental thermodynamic variable sustaining growth, only enthalpy change of reaction ($\Delta_r H$) is measurable by calorimetry (temperature change or heat flow). The fundamental relation between $\Delta_r G$ and $\Delta_r H$ is,

$$\Delta_r G = \Delta_r H - T\Delta_r S \qquad (1)$$

where T is the system temperature and $\Delta_r S$ the entropy change of the reaction.

Growth is a redox process associated with Gibbs energy dissipation [5]. In general, negative $\Delta_r G$ changes are associated with negative $\Delta_r H$ measurements and thus with heat flow rate (if no work is performed). Heat is released by almost all biological processes as a consequence of Gibbs energy dissipation to sustain thermodynamically unfavorable reactions. Dissipation is the cost to perform non-spontaneous redox reactions. However, thermodynamic analysis of growth concerns only Gibbs energy, the driving force of chemical reactions.

Historically, Lavoisier was the first who related respiration to combustion, a famous picture being his experiment of placing a bird under a glass bell. After a couple of minutes the bird died under the sorry eyes of the assistant, as a candle

stops to burn. Similarly, he reported the relation between heat generation and metabolic activity. In fact, heat flow rate provides an estimator of the biological activity.

The aim of this contribution is to show the application of fundamentals of thermodynamics to biochemical engineering. The connection between different measurements is inspected at the reactor scale. The reader is referred to references [6,7] for a discussion of notations and terminology.

2. HEAT FLOW RATE MEASUREMENT

Only the enthalpy of reaction is measurable in calorimeters by measuring the energetic change in the reaction broth. A review of the different types of calorimeters is available in [8-10] and in this Volume. Some types of calorimeters used for biotechnological applications will be briefly described.

2.1. Heat conduction calorimeters

In heat conduction calorimeters, the heat flow rate produced inside the reactor is transferred to the surrounding thermopile wall [11-13], leading to a voltage signal (V) proportional to the heat flow rate ($\mathrm{d}Q/\mathrm{d}t$),

$$V = k \frac{\mathrm{d}Q}{\mathrm{d}t} \tag{2}$$

where the proportionality constant k can be experimentally determined by calibration. Heat conduction calorimeters have a low detection limit, but identification of any change in the heat flow rate is slow. Therefore this type of calorimeter is suited to slow processes producing low amounts of heat.

In order to circumvent the low flexibility of use of the heat conduction calorimeters, a conventionally equipped bioreactor is coupled to a small heat conduction calorimeter [14]. The by-pass enters the calorimeter and heat production is measured by the difference between the voltage signal measured between the reaction chamber and the reference vessel. The advantage of this configuration is the concurrent operation of the bioreactor in a classical fashion and the measurement the heat flow rate with a low detection limit (2-3 mW dm^{-3}). However, the by-pass leads to a time delay, heat losses are possible and there is no proof that environment conditions in the calorimetric chamber are those in the bioreactor. In particular, pH and substrate concentrations are certainly different.

2.2. Heat accumulation calorimeters

Heat accumulation calorimeters are based on a precise evaluation of all the heat exchange terms between the reactor and its environment [15-17]. For example, Cooney et al. [18] measured the temperature increase of an insulated reactor at regular intervals while the cooling system was switched off. The temperature increase is due to the heat production of growth. Constant contributions (e.g., heat losses, feed, ...) were calibrated before inoculation. Improvements and modifications by accurate estimation and modeling of all heat fluxes were proposed by References [19,20].

2.3. Heat compensation calorimeters

Heat measurement is based on a enthalpy balance around the reaction vessel run at constant temperature. The first application to calorimetry of living organisms is certainly the measurement of the heat generated by a Guinea pig reported in 1780 by Lavoisier and de Laplace [21]. They placed the animal in a chamber surrounded by ice and an insulation layer (Figure 1). It was assumed that ice was the only heat sink and the metabolic activity of the animal the only heat source. Therefore, the amount of water collected was proportional to the heat produced by the Guinea pig.

An example of an heat compensation calorimeter is the "reaction calorimeter" RC-1 developed by Mettler-Toledo (Greifensee, CH). It consists of a 2 dm^3 glass reactor surrounded by a double jacket through which oil circulates at high flow rate (2 dm^3 s^{-1}). The temperature of the oil (T_J) is controlled by a PI controller so that the reactor temperature is maintained at its set-point. The T_J-controller regulates an electronic valve mixing warm and cold oil. The difference between the measured reactor temperature and the reactor temperature set-point determines the jacket temperature set-point by a proportional controller. Therefore, heat production in the reaction broth leads to an immediate reactor temperature increase which is compensated for by a decrease in the jacket temperature. The two control loops are shown in Figure 2, as is the working principle of the biocalorimeter [9,10]. The large flow rate and high heat capacity of the oil circulating ensure that the temperature difference between incoming and outgoing oil (due to heat removal) is negligible. The difference $T_R - T_J$ is proportional to the heat flow rate through the exchange surface:

$$\Phi_Q = UA(T_R - T_J) \tag{3}$$

where U is the heat transmission coefficient (W m^{-2} K^{-1}) and A the effective heat transfer area (m^2). The coefficient UA can be experimentally determined

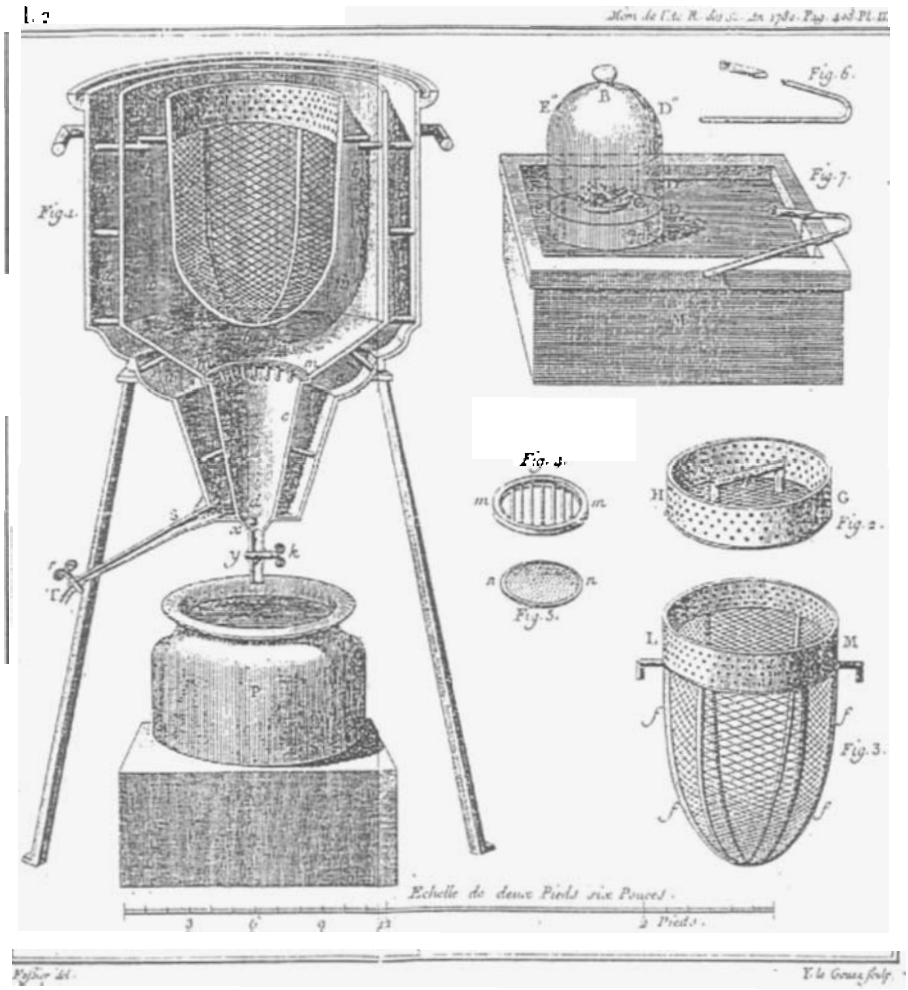

Figure 1: The first isothermal reaction calorimeter developed by Lavoisier and de Laplace in 1780 [21].

by monitoring the temperature difference necessary to compensate for a given heat output generated by an internal calibration heater.

If there is no heat accumulation in the liquid phase (T_R constant), the measured flow rate (Φ_Q) is equal to the heat generated by the microbial growth reac-

(Φ_t) plus constant contributions ($\Phi_{base\text{-}line}$ = stirring, losses, ...) that can be measured under working conditions before the inoculation.

The advantage of this type of reaction calorimeter is that it is run exactly as if it were a bioreactor with the constraint that all incoming and outgoing thermal flows are monitored or constant (and determined during calibration procedure). The set-up shown in Figure 3 includes heating of the top plate to avoid water and ethanol condensation, heating and saturation with water of the gas by a simple bubble column, thermostating incoming medium flow in continuous culture. In addition, torque measurement is possible to correct the base line for viscosity change during the culture.

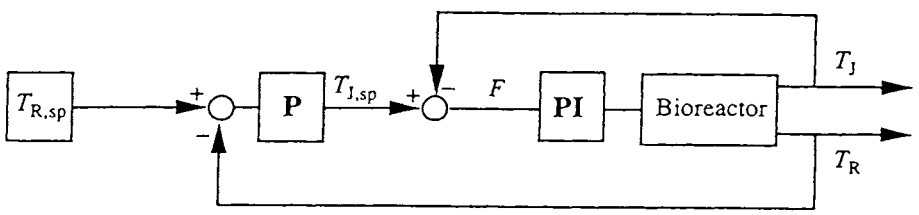

Figure 2: Principle of the two control loops for the reactor and the jacket oil temperature.

2.4. Dynamic response of the calorimetric measurements

2.4.1. Comparison of the dynamic response of various on-line measurements

Heat flow measurement can be performed at steady state growth conditions (in that case the heat flow signal does not vary with time and is not affected by the dynamics of the measurements) or under dynamic growth conditions, for example after a pulse of substrate or during a batch experiment. Under dynamic growth conditions, an important characteristics of the calorimeter is to provide at a given time a signal representing the actual metabolic activity of the culture. The heat flow rate indicated by the calorimeter should change as fast as the heat

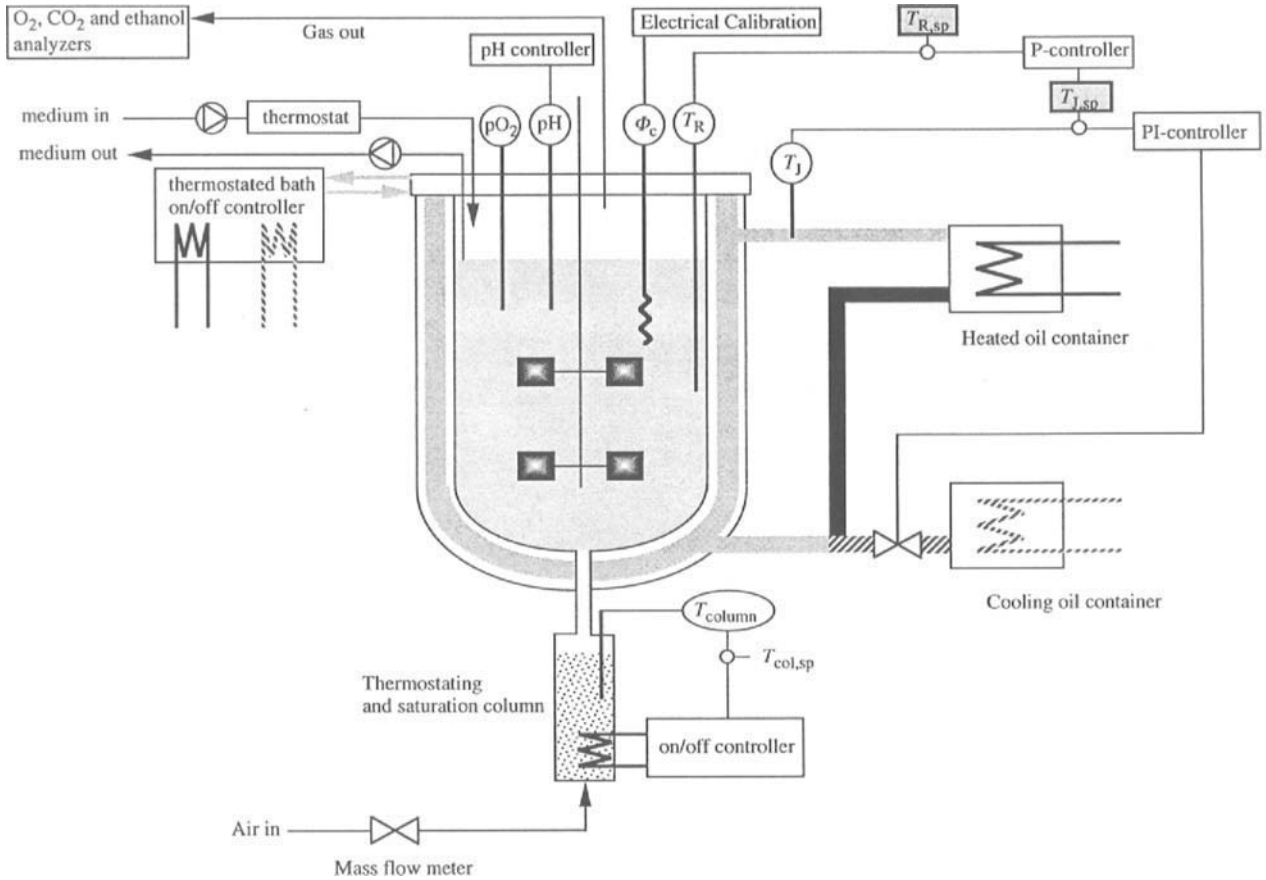

Figure 3: Set-up of the RC-1 calorimeter modified for biotechnological applications.

flow rate of the culture. The difference between the measured heat flow rate and the heat production rate of growth reaction is due to the dynamic of energy transfer through the inner wall of the calorimeter, the dynamics of oil circulation, the dynamics of the temperature probes etc. It was shown in references [22,23] that the time constants of these phenomena are small. It is therefore not a problem to assimilate the measured heat flow rate with the true one.

The response of the r_{O_2}, r_{CO_2}, pO_2, Φ_r, and y_E (ethanol in gaseous phase) measured in an aerobic continuous culture of *S. cerevisiae* subjected to a sudden increase in the dilution rate is shown in Figure 4 for an isothermal reaction calorimeter (RC-1, Mettler Toledo) [24]. The rapid increase of the metabolic activity should be detected by all the variables. For simplicity of interpretation, the measurements were scaled between 0, the steady state level at low dilution rate, and 1, the level reached 30 min after the shift-up. The pO_2 profile is parallel to the r_{O_2} profile. It is clear that the heat measurements give the fastest response: transient response lasted less than 4 min., about half that of the oxygen measurements. In fact, heat measurements are affected by the heat transfer through the wall and the temperature controller, whereas measurements based on gas phase analysis are affected by the time delay until the detection cell, mixing in the reactor and mixing in the head space. Dissolved oxygen measurements are affected by bubble mixing and gas-liquid transfer.

2.4.2. Time constant of heat transfer

The time constant of the heat transfer through the glass wall is calculated from the physical properties of the wall [25],

$$\tau_W = \frac{L_W^2 \rho_W c_{p,W}}{\lambda_W} \tag{4}$$

where L_W is the reactor wall thickness (m), ρ_W the density of the reactor wall (kg m^{-1}), $c_{p,W}$ the heat capacity (J kg^{-1} K^{-1}) and λ_W the heat conductivity of the reactor wall (W K^{-1} m^{-1}). For the RC-1 calorimeter, a typical value is $\tau_W = 0.82$ min.

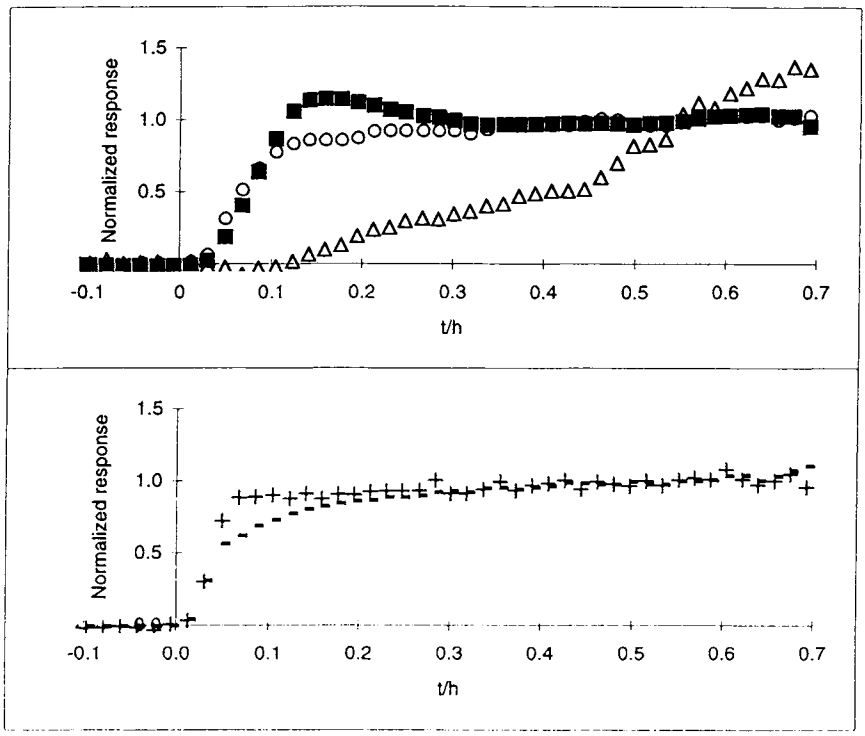

Figure 4: Dynamic response of a continuous culture of *S. cerevisiae* after a sudden increase of the dilution rate from 0.05 to 0.18 h^{-1}. (■) CO_2 production rate; (O) O_2 consumption rate; (Δ) ethanol vapor content; (–) dissolved oxygen; (+) heat flow rate, which gives the fastest response [24].

2.4.3. Time constant of temperature control

The operating principle of the RC-1 has already been presented. The jacket set-point temperature is controlled by a proportional controller by the reactor temperature. In turn, the jacket temperature is controlled by a PI controller by mixing warm and cold oil together.

The proportional controller affects the estimation of the heat flow rate from the temperature measurements during dynamic experiments, i.e. when some heat may be accumulated. In fact, the accumulation term in the heat equation is

negligible as soon as the system evolves smoothly. However, it may be important during rapid changes in the metabolic activity, for example a fast growing batch culture or during transient continuous culture. The energy balance equation reads:

$$\Phi_Q = UA(T_R - T_J) + m\,c_p \frac{dT_R}{dt} = \Phi_r + \Phi_{base\text{-}line} \tag{5}$$

The question is to know whether the term $UA(T_R - T_J)$ gives a good estimation of the term Φ_Q, and therefore any change in Φ_r provokes a rapid change in T_R and all the heat is evacuated by the wall and not accumulated. The control of T_J reads:

$$T_{J,sp} = T_{R,sp} + p\,(T_{R,sp} - T_R) \tag{6}$$

where p is the gain of the proportional controller. Equations (5) and (6) lead to the following solution,

$$\Phi_Q = UA(1 + p)(T_R - T_{R,sp}) + mc_p \frac{dT_R}{dt} \tag{7}$$

Thus, the time constant of the T_R control loop is :

$$\tau = \frac{mc_p}{UA(1 + p)} \tag{8}$$

Application with: $m = 1600$ g ; $c_p = 4.18$ J g^{-1} K^{-1}; $p = 10$; $UA = 7.9$ W K^{-1}

$\tau = 77$ s

The low time constant of the control loop shows that rapid changes in Φ_Q cause rapid changes in T_R: Φ_Q can be estimated from the difference between T_R and T_J, and the heat accumulation term will be negligible.

For a constant Φ_Q the temperature tends to the following steady state value:

$$T_R \rightarrow T_{R,sp} + \frac{\Phi_Q}{UA(1 + p)} \tag{9}$$

$$T_J \rightarrow T_{R,sp} - \frac{\Phi_Q}{UA}\frac{p}{(1+p)} \tag{10}$$

T_R is not equal to its set-point even in T_R-mode. An offset is introduced by the proportional controller. The higher the value of p, the lower the difference between set-point and the measured value. The difference in T_J is p times higher than the difference in T_R.

Application: during calibration, $\Phi_Q = \Phi_{calibration} = 9.7$ W
for $UA = 7.9$ W K^{-1} and $p = 10$
$T_R \rightarrow T_{R,sp} + 0.112$
$T_J \rightarrow T_{R,sp} - 1.116$

The reactor can also be run in T_J-mode, i.e. the jacket temperature is kept constant. This limits the heat evacuation and the reactor temperature will certainly increase more than observed in T_R-mode. The heat equation reads as Equation (5), but the jacket temperature T_J is constant. If T_J and Φ_Q are constant, the solution of the heat equation reads,

$$\frac{\Phi_Q}{UA} + T_J = T_R + \frac{mc_P}{UA}\frac{dT_R}{dt} \tag{11}$$

The time constant of the system is :

$$\tau = \frac{mc_p}{UA} \tag{12}$$

T_R tends to the limit :

$$T_R \rightarrow T_{R,sp} + \frac{\Phi_Q}{UA} \tag{13}$$

Application: $m = 1600$ g ; $c_p = 4.18$ J g^{-1} K^{-1}; $p = 10$; $UA = 7.9$ W K^{-1}
$\tau = 845.5$ s

The high time constant of the system shows that a rapid change in Φ_Q will give a slow change in T_R: heat accumulates and Φ_Q cannot be immediately estimated from $UA(T_R - T_J)$.

In conclusion, the heat compensation calorimeter RC-1 run in T_R-mode provides an excellent on-line signal to monitor rapid changes in the metabolic activity. Especially, it is faster than the gas analyses.

3. MOLE AND ENTHALPY BALANCES IN OPEN SYSTEMS

Heat flow rate does not only addresses the important problem of heat removal in industrial large scale bioreactors, it also provides an estimate of the biological activity. The objective of setting-up balances is to measure accurately any flow in order to quantify the growth reaction rate.

3.1. System boundary

Mass and energy balances hold only around the boundary of a system, which is normally defined as one microorganism or the bioreactor [6]. Clearly, heat flow rate can only be measured for a bioreactor, not for a single microorganism. Therefore, molar and energy balances will be measured only for reactors for which both matter and energy flow in and out. By comparison, a single microorganism is also an open system and energy flow can be calculated. Figure 5 depicts the boundary around the reaction vessel considered as an open system exchanging matter and energy with its surroundings. The state of the feed is liquid for the medium feed and gaseous for the oxygen and CO_2. Biomass flows out suspended in the liquid phase.

By comparison, all nutrients are taken up in the liquid state by biomass, as are the products released (Figure 6). The gas-liquid transfer as well as the acid-basic equilibrium of $CO_{2,liq}/HCO_3^-{}_{,liq}$ does not take place inside the cell but at the interface of the liquid and gaseous phases in the reactor. The heat related to these transfer phenomena is produced outside the cells but inside the reactor boundary. The uptake or release of species in the liquid phase (in dynamic equilibrium with the gaseous phase) is due to the cellular metabolism.

The bioreactor is usually at non-steady-state since accumulation of extensive quantities occurs. The fundamental relation for any conserved species (atoms or energy) in one phase is:

$$\text{ACCUMULATION} = \text{INPUT} - \text{OUTPUT} + \text{REACTION} + \text{TRANSFER} \qquad (14)$$

The system is assumed to be well mixed so that no gradients exist inside the reactor broth. Mole and energy balance can also be considered around a single cell. In this case, the reference state as well as the concentration change for the species supplied in gaseous form to the reactor.

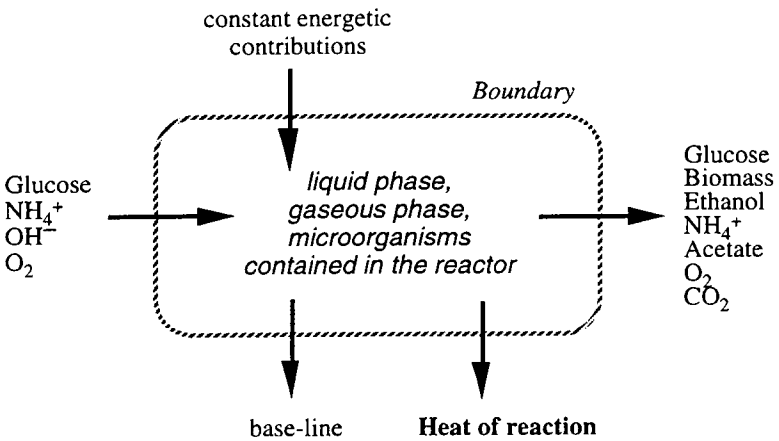

Figure 5: Boundary around the bioreactor for the set-up of molar and energy balances.

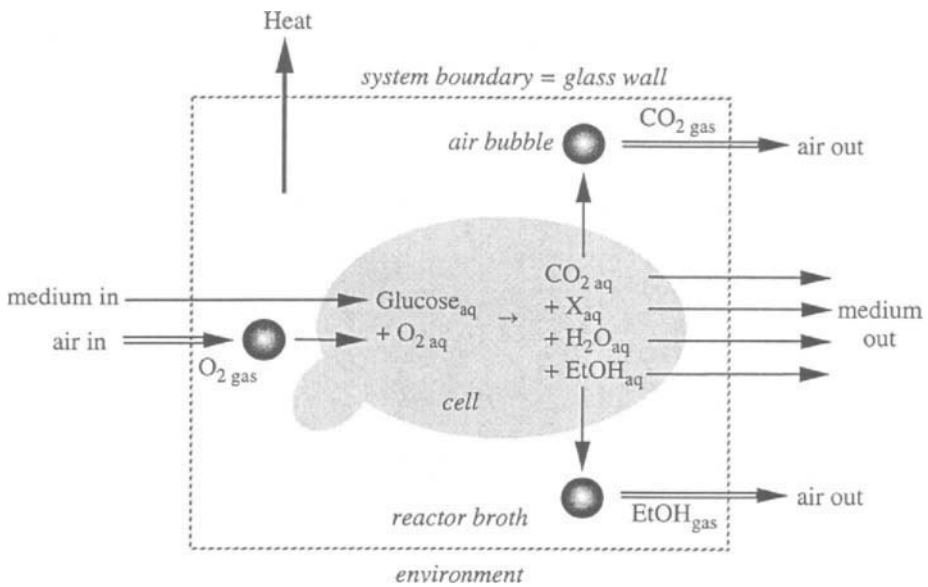

Figure 6: Change of phase for substrates entering the reactor in gaseous phase and consumed in liquid phase by the microorganism (gray ellipsis). aq = aqueous; gas = gaseous.

3.2. Molar balance

The relation (14) holds for molar balances expressed in rates (mol s^{-1}) or quantities (mol). Reaction and transfer terms are positive (for products) or negative (reactants). For example, the reaction rate r_i of a species i found in the liquid phase is calculated from Equation (14) as:

$$r_i = -F_{\text{liq,in}} c_{i,\text{liq,in}} + F_{\text{liq,out}} c_{i,\text{liq}} - k_{i,\text{liq}} a V_l \left(c^*_{i,\text{liq}} - c_{i,\text{liq}} \right) + \frac{\mathrm{d}\left(V_{\text{liq}} c_{i,\text{liq}} \right)}{\mathrm{d}t} \qquad (15)$$

and

$$\frac{\mathrm{d}V_{\text{liq}}}{\mathrm{d}t} = F_{\text{liq,in}} - F_{\text{liq,out}} \qquad (16)$$

The accumulation term cancels at steady state and in the case of a batch reactor the volume change is negligible. The mass balance for biomass, glucose, oxygen in the liquid and in the gaseous phase for a continuous culture at steady state are listed in Table 1. No oxygen is consumed in the gaseous phase, since only the transfer to liquid phase occurs so that $r_{O_2,g} = 0$.

The difference between the incoming and the outgoing liquid flow rate is due to base and acid adjunction for pH correction, metabolic water production and water vaporization. Let us consider a continuous culture of yeast (*Saccharomyces cerevisiae* for example) growing aerobically on glucose (20 g dm^{-3}) at a dilution rate of 0.10 h^{-1}. If one mole of water is produced per C-mol glucose consumed, the metabolic water volumetric production rate will be 1.2 ml dm^{-3} h^{-1}, i.e. 1.2 % of the incoming flow. For base addition compensating ammonium consumption due to biomass formation, a biomass yield of 0.6 C-mol C-mol^{-1} and a biomass nitrogen content of 0.15 mol C-mol^{-1} are used. Thus, the base consumption rate is 6 mmol dm^{-3} h^{-1}, corresponding to 3 ml dm^{-3} h^{-1} for a base stock solution of 2 M. Water vaporization is normally not a problem if the reactor is equipped with a condenser and if the water reflux is total. Nevertheless, in the worst case off-gases are not condensed and the water vapor content at 30°C is 4.2%, corresponding to an outflow of 2.03 ml dm^{-3} h^{-1} for a volumetric aeration rate of 1 vvm. Therefore, the liquid outflow rate will vary between 107.2 and 105.2 ml h^{-1} for an inflow rate of 100 ml h^{-1} depending upon the water reflux to the reactor. The difference between inflow and outflow terms is therefore relatively important.

Table 1: Dynamic mass and energy balances of the process variables in steady state continuous culture.

- Glucose: $r_G(t) = -F_{liq,in}c_{G,in} + F_{liq,out}c_G(t)$
- Biomass: $r_X(t) = F_{liq,out}c_X(t)$
- O_2 in gaseous phase:
  $r_{O_2,g}(t) = -F_{g,in}c_{O_2,g,in} + F_{g,out}(t)c_{O_2,g}(t) + k_{O_2,liq}aV_{liq}\left(c^*_{O_2,liq} - c_{O_2,liq}(t)\right)$
- O_2 in liquid phase:
  $r_{O_2,liq}(t) = -F_{liq,in}c_{O_2,liq,in} + F_{liq,out}c_{O_2,liq}(t) - k_{O_2,liq}aV_{liq}\left(c^*_{O_2,liq} - c_{O_2,liq}(t)\right)$

3.3. Enthalpy balance

Since enthalpy change is measurable by direct calorimetry, a balance can be set-up and verified with the experimentally determined reaction rates. At constant pressure (which is the case of bioreactors) and if no work is performed, the energy balance reads:

$$mc_P \frac{dT_R}{dt} = \Phi_Q + \sum_i r_i \Delta_{c,aq} H_i^o \qquad (17)$$

where Φ_Q is the measured heat flow rate and $\Delta_{c,aq}H_i^o$ is the standard enthalpy of combustion of the species i in aqueous state.

The correct choice of the state of the compounds is crucial to obtain a correct enthalpy balance [6]. For the energy balance around the reactor depicted in Figure 5, the following state of the carrier flow of each species must be as listed in Table 2 and the modified enthalpy of combustion is listed for some compounds in Table 3.

For biomass, the enthalpy of hydration is about 0.05-0.10 J g^{-1}, i.e. about 1.3-2.8 kJ C-mol^{-1}, proving that the enthalpy of combustion determined for dry biomass can be used without further correction to calculate the enthalpy balance for wet biomass.

Table 2: State of substrates for energy balance around the bioreactor.

Species	State
Glucose in or out	aqueous
Oxygen in or out	gaseous
CO_2 in or out	gaseous
Aqueous ethanol out	aqueous
Gaseous ethanol (stripping)	gaseous

Table 3: Enthalpy of combustion of various substrates and products. Reproduced from reference [6] with permission from the author and publisher.

Species	state	$\Delta_c H^*$ (kJ (C)-mol^{-1})	γ^*
O_2	gaseous	0	- 4
H_2O	aqueous	0	0
CO_2	gaseous	0	0
NH_3	aqueous	- 348	0
NH_4^+	aqueous	- 296	+ 1
glucose	aqueous	- 469	+ 4
ethanol	aqueous	- 678	+ 6
glycerol	aqueous	- 550	+ 4.67
acetic acid	aqueous	- 437	+ 4
CH_4 (1 bar)	aqueous	- 892	+ 8
H_2 (1 bar)	aqueous	- 286	+ 2
biomass [#]		- 456.7	+4.31

[#] see Table 11 and Table 17

Enthalpy balance calculation require the choice of a reference state. For convenience we choose to work with enthalpy of combustion rather than with enthalpy of formation. Thus, terms concerning water, O_2 and CO_2 disappear because they flow as gas through the system boundary (cf. Figure 5). The reference state of the substances in solution is aqueous, infinitely diluted at 30°C. The thermal effect of CO_2 hydration is discussed in [26].

3.4. Growth reaction stoichiometry

The reaction rate r_i of a species i has been defined in Equation (15). The rate at which a given reaction proceeds, called the advancement rate, is defined as:

$$\dot{\xi} = \frac{1}{\nu_i} r_i \tag{18}$$

where ν_i is the stoichiometric coefficient of i.

The molar yield of j on i is calculated as:

$$Y_{j/i} = \left| \frac{r_j}{r_i} \right| = \left| \frac{\nu_j}{\nu_i} \right| \tag{19}$$

and the enthalpy yield of the reaction is defined per C-mol of substrate as:

$$Y_{Q/i} = \left| \frac{\Phi_r}{r_i} \right| \tag{20}$$

Growth is the result of a large network of biochemical reactions that can be brought together because the reaction rate of the individual biochemical reaction remains proportional one to another. However, the overall growth reaction may change when the environmental conditions are changed, for example as the supply rate of any substrate is changed. A typical growth reaction under aerobic conditions with biomass and product formation is written on a C-molar basis as,

$$\begin{aligned} &- CH_2O - Y_{O_2/G} O_2 - Y_{NH_3/G} NH_3 + Y_{X/G} C_1 H_{x_H} O_{x_O} N_{x_N} \\ &+ Y_{CO_2/G} CO_2 + Y_{P/G} C_1 H_{p_H} O_{p_O} N_{p_N} + Y_{w/G} H_2O = 0 \end{aligned} \tag{21}$$

There are 6 yields in this stoichiometry in addition to the enthalpy yield, which are subjected to 5 conservation balance constraints (for the atoms C, H, O, N, and for energy). Therefore, the degree of freedom of the system is 7 - 5 = 2. Experimental determination of two yields is required to calculate any other yield. However, water production cannot be monitored so that the balances on C, H, O and N are linearly combined to define the degree of reduction γ in a way such that the degree of reduction of water is zero.

The degree of reduction of a compound i of elemental formula $C_1 H_{e_H} O_{e_O} N_{e_N} S_{e_S} P_{e_P}$ is equal to the number of electrons exchanged during its oxidation (*available electrons*). By definition, the degree of reduction of the fi-

nal products of combustion is zero. Therefore, the degree of reduction is calculated by difference with the final products of combustion, and several reference states are conceivable. The thermodynamic combustion reference state is : H_2O, CO_2, N_2, SO_3 and P_2O_5 (Table 4) and corresponds to the thermodynamically most favored products [27]. Consequently, the valence of C, H, O, N, S and P are +4, +1, –2, 0, +6 and +5, respectively [28]. This combustion state defines the Kharasch degree of reduction of *i*,

$$\gamma_i = 4 + e_H - 2e_O + 6e_S + 5e_P \tag{22}$$

If the compound does not contain carbon, the degree of reduction is defined per mole as:

$$\gamma_i = e_H - 2e_O + 6e_S + 5e_P \tag{23}$$

The degree of reduction of ash is obviously zero, since ash is the solid residue of combustion of biomass. This simple observation will be helpful to discuss the degree of reduction of biomass.

$$\gamma_{ash} = 0 \tag{24}$$

Nevertheless, other references are possible, and in particular the commonly named *generalized degree of reduction* [29,30] uses NH_3 as the reference of nitrogenous compounds combustion (the valence of nitrogen is set to –3). Strictly speaking, this is a degree of hypothetical reduction, which corresponds to the hypothetical combustion to CO_2, H_2O and NH_3 (Table 4) with an enthalpy of hypothetical combustion $\Delta_c H^{\circ *}$ and free energy change of hypothetical combustion $\Delta_c G^{\circ *}$. The superscript * on γ is preferred to the common prime in order to have an homogenous notation for γ^*, $\Delta_c H^{\circ *}$ and $\Delta_c G^*$ without confusion with the standard thermodynamic reference at pH = 7. With this reference, the generalized degree of reduction is calculated as follows,

Table 4: Kharasch and generalized degree of reduction definition for ammonia and biomass.

reference state	combustion products	NH_3	biomass
Kharasch (γ)	H_2O, CO_2, N_2, SO_3 and P_2O_5	- 3	$4 + x_H - 2x_O + 6x_S + 5x_P$
generalized (γ^*)	H_2O, CO_2, NH_3, SO_3 and P_2O_5	0	$4 + x_H - 2x_O - 3x_N + 6x_S + 5x_P$

$$\gamma_i^* = 4 + e_H - 2e_O - 3e_N + 6e_S + 5e_P \quad (25)$$

Any reference state can be used as long as the same calculation procedure is applied to all the species involved in the reaction (Table 4). The choice of the reference state determines if ammonia consumption has to be monitored (with the choice of γ) or the biomass nitrogen content determined (with the choice of γ^*). Table 4 summarizes the application of the degree of reduction calculation when the value of the nitrogen valence is changed from 0 to - 3. If nitrate is the nitrogen source, another generalized degree of reduction can be defined with the valence of nitrogen set to + 5 so that the degree of reduction of the nitrogen source will be zero [30]. However, the value of the degree of reduction of biomass is affected by this reference change [31].

The calculation of the degree of reduction has two main applications. First, to predict the enthalpy of combustion (and compare different compounds more or less reduced), and second, to calculate elemental balances.

After introduction of the degree of reduction, there remain 6 molar yields ($Y_{O_2/G}$, $Y_{NH_3/G}$, $Y_{X/G}$, $Y_{P/G}$, $Y_{CO_2/G}$ and $Y_{Q/G}$) which are subjected to 4 conservation constraints (on C, N, γ^* and energy). The balances on yields for carbon, nitrogen, available electrons and energy read:

$$1 = Y_{X/G} + Y_{P/G} + Y_{CO_2/G} \quad (26)$$

$$Y_{NH_3/G} = Y_{X/G} x_N + Y_{P/G} p_N \quad (27)$$

$$\gamma^*_G - \gamma^*_{O_2} Y_{O_2/G} = \gamma^*_X Y_{X/G} + \gamma^*_P Y_{P/G} \quad (28)$$

$$\Delta_c H^\circ_G = Y_{X/G} \Delta_c H^{\circ *}_X + Y_{P/G} \Delta_c H^{\circ *}_P + Y_{Q/G} \quad (29)$$

3.5. Cumulated quantities

The reaction rate of a species is simply calculated by monitoring the input and output rates at steady state in Equation (14). Estimation of the reaction rate during transient experiments is however more difficult since the accumulation rate, which might not be negligible, is difficult to estimate because it requires the calculation of a time derivative. A method was presented by [32,33] to circumvent this problem: Equation (14) is integrated to determine the cumulated

amount of moles of the species i that have been consumed or produced. In fact, the reaction rate of i is related to the cumulated quantity by derivation:

$$r_i = \frac{\mathrm{d}n_i}{\mathrm{d}t} = \dot{n}_i \tag{30}$$

Note the n_i does not represent the number of moles present in the reactor but the variation of mole number due to the reaction since the reference observation at time t_1. The mass balance Equation (15) can be integrated between two observations at times t_{j-1} and t_j :

$$\begin{aligned} n_i(t_{j-1} \rightarrow t_j) = [c_i(t)V_{\mathrm{liq}}(t)]_{t_{j-1}}^{t_j} - \int_{t_{j-1}}^{t_j} c_{i,in}(t)F_{\mathrm{liq},in}(t)dt \\ + \int_{t_{j-1}}^{t_j} c_i(t)F_{\mathrm{liq},out}(t)dt \end{aligned} \tag{31}$$

Each term is estimated by the method of trapezoids. Let us call $n_i(j)$ the number of moles involved (consumed or produced) in the reaction since the beginning of the experiment: by definition no reaction has been observed before the first sample at time t_1. The cumulated quantity $n_i(j)$ involved between the observations at time t_j and t_1 (beginning of the experiment) is easily calculated by the sum of the increments:

$$n_i(j) = n_i(t_1 \rightarrow t_2) + n_i(t_2 \rightarrow t_3) + \ldots + n_i(t_{j-2} \rightarrow t_{j-1}) + n_i(t_{j-1} \rightarrow t_j) \tag{32}$$

$n_i(j)$ is expressed in moles or grams.

The quantity increases if the species is produced and conversely decreases when the species is consumed. The quantity remains constant when the net production rate is zero, i.e. when the species is neither consumed nor produced, or when consumption and production rates are equal.

Similar to the calculation of the cumulated amount of a species that has reacted, calculation of the total amount of heat produced during a dynamic experiment is useful to calculate yields and check elemental balances.

Let $\Phi_r(t)$ represent the heat flow rate measured by a calorimeter related to growth reaction. Thus, the heat produced between the first observation at time t_1 and the jth observation at t_j is:

$$Q(j) = \int_{t_0}^{t_j} \Phi_r(t)\mathrm{d}t \tag{33}$$

and is approximated by the method of rectangles by integrating between short time intervals.

An example of calculation of the cumulated quantities is given in the paragraph 6.4 together with the calculation of the atom and energy balances.

4. ELEMENTAL COMPOSITION

The set-up of elemental and enthalpy balances constitutes the basis for the consistency check of experimental data from biotechnological processes. For that purpose, the exact composition and physico-chemical characterization of all species involved in the process under study has to be determined including biomass. Another use is the design of the growth medium or the investigation of possible stoichiometric limitation by the medium supply. We chose to take into account all atoms bound in the main macromolecules whereas other atoms, mainly present as ions in biomass (K^+, Ca^{2+}, Na^+ ...), are not incorporated in the elemental formula [28]. One C-mol of biomass is defined as $C_1H_{x_H}O_{x_O}N_{x_N}S_{x_S}P_{x_P}$.

4.1. Sample preparation, humidity and ash determination

Culture samples are collected and centrifuged for 10 min at 4°C, and then carefully washed twice with demineralized water. Collected biomass corresponding to 2–3 g dry weight is freeze-dried [34].

Since the samples are very hygroscopic, humidity determination has to be performed in parallel to elemental analyses. For that purpose, samples are equilibrated at room ambient conditions in Petri dishes for several hours just before use. Aliquots of 0.5 to 1 g are weighted and dried for 24 h at 100°C to determine the humidity content (f_{moisture}) in triplicate. The CHN content obtained from the analyzer for each element k ($f_{k,\text{hum}}$) are corrected for humidity content as follows to obtain the mass fraction of the element on dry weight,

$$f_k = \frac{f_{k,\text{hum}}}{1 - f_{\text{moisture}}} \tag{34}$$

Hydrogen content also has to be corrected for water content,

$$f_H = \frac{f_{H,\text{hum}} - \frac{2}{18} f_{\text{moisture}}}{1 - f_{\text{moisture}}} \tag{35}$$

4.2. CHN measurement

The elemental analyzer measures the C, H and N content of biomass upon its combustion at 925°C in a pure oxygen environment by monitoring the volatile compounds (C in CO_2, N in N_2, H in H_2O). The results are reproducible but largely dependent on the growth conditions; the solid residue of combustion is ash and contains oxides and salts. Mass fractions of biomass can be expressed as:

$$f_C + f_H + f_N + \sum_{k=1}^{k=J} f_k + f_{ash} = 1 \tag{36}$$

Oxygen is found both in the gaseous (CO_2, H_2O, N_2) and solid phase (ash). Quantification of mass fraction of oxygen in gas is usually calculated by subtraction using Equation (36) assuming that that no element other than C, H, N and O will show up in the gaseous phase, and that no external oxygen is taken-up to form ash. However, it has been shown that sulfur does not remain in ash as sulfate [28]. Thus, the mass balance should be strictly written as:

$$f_C + f_H + f_N + f_S + f_O = 1 - f_{ash} \tag{37}$$

Hence, the oxygen fraction of biomass is overestimated when calculating f_O without taking into account the S fraction. However, experimental values show that the overestimation of the oxygen content is only about 2% as illustrated later on.

4.3. Elemental formula and molar mass

Atomic coefficient of element k in biomass formula (x_k) is calculated as follows:

$$x_k = \frac{f_k}{f_C} \frac{M_C}{M_k} \tag{38}$$

where M_k is the mass of one mol of k. The nitrogen atomic coefficient remains correct even if moisture content is neglected since both carbon and nitrogen analyses are similarly affected.

Calculation of the degree of reduction and generalized degree of reduction was presented in equations (22) and (25), respectively. The low value of the atomic coefficient of sulfur in biomass has a low influence on the degree of reduction.

The mass of 1 C-mol of biomass is calculated from the carbon content as,

$$M_X = \frac{1}{f_C} M_C \tag{39}$$

4.4. Dry weight or ash-free biomass ?

The mass of one C-mol biomass depends only on the carbon content according to Equation (39). Although it is tempting to calculate M_X from the elemental formula as the sum of the mass of its elements, this estimation is incorrect since some atoms have not been analyzed, in particular those that are found in ash. $M_{X,ash\text{-}free}$ corresponds to the mass of the elemental formula without ash, i.e. to an hypothetical biomass,

$$M_{X,ash\text{-}free} = M_X(1 - f_{ash}) \tag{40}$$

Since dry weight measurements always include ash, only M_X calculated according to Equation (39) should be used to calculate elemental or energy balances and never the hypothetical ash-free molar mass.

4.5. Sulfur, phosphorus and ions content of biomass

The sulfur content of biomass varies largely from one microorganism to another: the mass fraction is 0.28 g per 100 g biomass for *Saccharomyces cerevisiae* and up to 0.49 g per 100 g in *Methanobacterium thermoautotrophicum* (Table 5). Similarly, the phosphorus and potassium content of biomass showed large variations among different organisms as illustrated in Table 5 and Table 6. Phosphorus is mainly found in biomass as phosphate groups in RNA and DNA whereas potassium is present as ion. The potassium content of *M. thermoautotrophicum* is 4.3%, twice that of *S. cerevisiae*.

Röntgen fluorescence spectroscopy and plasma atomic emission allow quantitative measurement of S, P as well as many other elements. The ion mass fraction of *Kluyveromyces marxianus* and *M. thermoautotrophicum* are listed in Table 7. The large difference in iron and nickel content is related to the metabolism. In fact, these two ions are cofactors of key enzymes in methanogenesis [35]. The total mass of ions found in biomass is 6.36 g per 100 g biomass for *M. thermoautotrophicum* and 3.14 for *K. marxianus* (phosphorus is not taken into account since it is not present as free ion in biomass). The values are in good agreement with [36].

Table 5: Mass fractions (g g^{-1}) of C, H, N, S, P and ash in different microorganisms. Reproduced from Reference [28] with permission of the author and publisher.

microorganism	f_C (a)	f_H (a)	f_N (a)	f_S (b)	f_P (b)	f_{ash} (c)
Saccharomyces cerevisiae	0.4243	0.0617	0.0641	0.0028	0.0202	0.0926
	(0.0004)	(0.0001)	(0.0003)			(0.003)
Kluyveromyces marxianus	0.445	0.065	0.073	0.0042	0.0135	0.071
Methanobacterium thermoautotrophicum	0.4201	0.0589	0.1088	0.0049	0.0371	0.1735
	(0.0025)	(0.0003)	(0.0011)			(0.0002)
Saccharopolyspora erythraea	0.4315	0.0623	0.0921	0.0028	0.0107	0.1445
	(0.0008)	(0.0004)	(0.0012)			(0.0002)

(a) average values of measures in triplicate, standard deviation is indicated in parenthesis.
(b) absolute error estimated to ± 0.0001, (c) determination in duplicate

The ion content of living biomass (K^+, Na^+, Cl^- etc.) differs from the ash content which consists mainly of phosphorus and potassium oxides. Several sulfur- and non sulfur-containing chemicals and a few macromolecules were combusted. No ash remained after combustion of $(NH_4)_2SO_4$, NH_4Cl, methionine, cysteine or Bovine Serum Albumin at 600°C. These results suggest that independently of whether the compound was of organic or inorganic origin, no S is present in the solid residue of combustion. This was also confirmed by sulfate determination in ash after combustion of biomass since sulfur could only be present as sulfate. The amount of sulfur determined in ash of yeast extract, *M. thermoautotrophicum* and *S. cerevisiae* was as low as 0.3, 0.4 and 0.9%, respectively of the amount of sulfur initially present in the samples. These results clearly indicate that no sulfate is found in ash [28].

The contribution of phosphorus and potassium oxides to the formation of ash is easily estimated from the biomass composition; it is found that both oxides are the main constituents of the ash (between 68 and 92.7% of the ash fraction of the organisms in Table 5). An important question to estimate the biomass oxygen content is whether oxygen bound to phosphorous as phosphate ions in biomass is sufficient to form all the oxides found in ash, or if external oxygen is taken up during the combustion. Knowing the P content of biomass, the amount of oxygen available from the phosphate groups is estimated. This was done for

Table 6: Potassium and calcium mass fractions (g g^{-1}) of different microorganisms. Detection limits of K and Ca are 100 and 80 μg g^{-1}, respectively. Reproduced from Reference [28] with permission of the author and publisher.

microorganism	f_K	f_{Ca}
Saccharomyces cerevisiae	0.0229	$144.7\ 10^{-6}$
Kluyveromyces marxianus	0.029	$174.6\ 10^{-6}$
Methanobacterium thermoautotrophicum	0.0431	$96.4\ 10^{-6}$
Saccharopolyspora erythraea	0.0021	$2229.5\ 10^{-6}$

M. thermoautotrophicum and *K. marxianus*. Adding the mass of oxygen bound to P to the total mass of all trace elements (Table 7) results in 17.59 g per 100 g of biomass for *M. thermoautotrophicum* and 7.33 g for *K. marxianus*. These values are very close to the corresponding mass fraction of ash (7.1 and 17.35 g per 100 g biomass), suggesting that no external oxygen has been taken up during combustion of biomass, and therefore the measured mass fractions of ash only takes into account elements that were originally present in biomass samples.

4.6. Integration of S and P into the elemental composition

The sulfur mass fraction influences the estimation of the oxygen mass fraction calculated by difference according to Equation (37). Elemental composition of the bacterium *M. thermoautotrophicum* is $CH_{1.681}O_{0.426}N_{0.222}$, neglecting f_S , and changes to $CH_{1.681}O_{0.418}N_{0.222}S_{0.0044}$ when f_S is included into the calculation of the oxygen mass fraction. Thus, neglecting f_S in the calculation of the oxygen fraction of biomass only introduces a minor error even for a microorganism containing a large amount of S. It can be concluded that the quality of the determination of elemental composition of C, H, N, O is not greatly affected when the S content is not measured.

On the other hand, phosphorus is bound as phosphate in macromolecules and is exclusively found in ash, which has a degree of reduction of 0. The oxygen bound to P has not been taken into account in the estimation of f_O since it is found in ash. Hence, if one wants to include P in the elemental formula, one has to add 2.5 O per P included. This is illustrated in Table 8 where the elemental

Table 7: Ion mass fractions of *K. marxianus* and *M. thermoautotrophicum* determined by plasma atomic spectroscopy. Reproduced from Reference [28] with permission of the author and publisher.

Element	unit	*M. thermo-autotrophicum*	*K. marxianus*	*Detection limit*
K	g per 100 g	4.3	2.9	0.01
Mg	g per 100 g	0.23	0.13	0.001
Na	g per 100 g	0.97	0.03	0.01
B	µg/g	$80^{\varnothing}$	110	50
Ca	µg/g	$80^{\varnothing}$	200	80
Co	µg/g	15	$220^{\varnothing}$	5
Cr	µg/g	$20^{\varnothing}$	$5^{\varnothing}$	5
Cu	µg/g	$13^{\varnothing}$	13	2
Fe	µg/g	820	100	10
Mn	µg/g	$2^{\varnothing}$	7	1
Mo	µg/g	5	50	5
Ni	µg/g	180	$10^{\varnothing}$	10
Zn	µg/g	$60^{\varnothing}$	80	10
Total	g per 100 g	6.23	3.14	

Superscript $^{\varnothing}$ indicates that the element was not present in the medium. It can be provided by yeast extract (for *K. marxianus*) or through leaching of steel parts of the reactor. Most of the concerned values are close to detection limit.

formula is calculated once without taking notice of the P-content of biomass, and once with respect to P content in biomass. In addition, including phosphorus does not change the degree of reduction: added P is compensated by simultaneously added oxygen because $\gamma_{P_2O_5} = 0$.

In conclusion, correct elemental composition determination requires special care both for experimental work and for calculations. The mass of one C-mole of biomass should be calculated from the carbon content of biomass and not from the elemental formula in order to take into account all the cell elements (especially ash). The carbon and nitrogen content used to check conservation of atoms during the growth process must be expressed as gram of element per gram dry weight biomass. The generalized degree of reduction with NH_3 as the

Table 8: Atomic formula of the different microorganisms. Reproduced from Reference [28] with permission of the author and publisher.

Microorganism		x_C	x_H	x_O	x_N	x_S	x_P	M_X	γ^*
S. cerevisiae	(a)	1	1.745	0.627	0.129	0.0025	0	28.28	4.12
	(b)	1	1.745	0.673	0.129	0.0025	0.018		
K. marxianus	(a)	1	1.753	0.576	0.141	0.0035	0	26.97	4.20
	(b)	1	1.753	0.605	0.141	0.0035	0.012		
M. thermo-autotrophicum	(a)	1	1.681	0.418	0.222	0.0044	0	28.56	4.21
	(b)	1	1.681	0.488	0.222	0.0044	0.034		
S. erythraea	(a)	1	1.732	0.464	0.183	0.0025	0	27.81	4.27
	(b)	1	1.732	0.503	0.183	0.0025	0.0096		

(a) including only C, H, O, N, S
(b) including C, H, O, N, S and P.

reference state (γ^*) is more useful than the degree of reduction (γ) to calculate the available electrons balance. Additionally, determination of ash, C, H and N content of biomass is sufficient to calculate a good approximation of the oxygen content and of the degree of reduction. Sulfur can be neglected and incorporation of phosphorus in the elemental formula is not necessary since it is fully recovered in ash with the oxygen bound to it to form the phosphate groups.

4.7. Composition of bacterial strains, algae, filamentous fungi and yeast

Elemental analysis was performed at least in triplicate for various microorganisms grown in batch [37,38]. All the mass fractions listed in Table 9 are expressed as gram of element per 100 g dry weight biomass. The standard deviation (σ) of the measurements is given in parenthesis. If x is the average of n determinations, a 95% confidence interval of the expected value is given by $x \pm \sigma\, t_{n-1,0.95}/\sqrt{n}$, where $t_{n-1,0.95}$ is the Student distribution with $n - 1$ degrees of freedom and a probability for a type 1 of error of 0.05. Some values are indicated in Table 10 for a different population size.

The results for bacteria, algae, filamentous fungi and yeast are listed in Table 9 for the different strains and in Table 11 for each group of microorganisms. Differences and similarities were statistically investigated. First, it is very important to note the good reproducibility of the results for each strain. The standard deviation of any determination performed in triplicate is always low com-

pared to the average value. Thus, the values given in Table 9 are statistically significant. However, the results vary greatly from one microorganism to another as discussed below.

The carbon and hydrogen content of bacteria is relatively constant (43.81% and 6.04%, respectively) of dry weight. By comparison, the nitrogen content varies greatly from one species to another: the minimum is 8.47% for *B. flavum*, and the maximum was found for *Lactobacillus helveticus*. The average nitrogen content was 10.63 and the standard deviation 1.5%, i.e. as high as 14.1% of the average value. The variability in the average N content is due to the difference between each strain since each determination was performed at least in triplicate and showed a good reproducibility. Similarly, the ash content varied greatly from one strain to another: the average value is 15.44% and the standard deviation 9.67%, indicating that the measurements of the different microorganisms were widely dispersed for each group.

The carbon, hydrogen, nitrogen and ash content of 7 different algae is listed in Table 9. As for bacteria, the carbon and hydrogen content is rather similar among the algae (51.6% and 7.01%, respectively), but the nitrogen content varies greatly between 2.66% and 7.75%, with an average value of 5.33% (g/g) and an absolute standard deviation of 2.04% (g/g). Interestingly, the average nitrogen content of algae is significantly lower than the nitrogen content of bacteria, as well as the ash content. The good reproducibility of the analyses for each strain indicates that the differences between the strains is not due to scatter but to systematic different nitrogen or ash content between the different groups of microorganisms.

The ash content dispersion was even greater for filamentous fungi. The average ash content was 9.54% and the standard deviation for the group of filamentous fungi is as high as 6.14%. The average carbon content was 49.0% and the average H content 7.0% with only little difference between the strains.

As found for the other organisms, ash and nitrogen content of yeast strains varied largely from one strain to another. The average content was 7.25 for both ash and nitrogen, and the standard deviations were 2.48 and 2.13% (g/g), respectively, i.e. as high as 34.2 and 29.4% of the average value.

Table 9: Elemental analysis of microorganisms. Mass fractions are expressed as g per 100 g biomass. M_X is the mass of one C-mole of biomass, and γ^* the generalized degree of reduction. The standard deviation is indicated in parenthesis [37,38].

Organism	f_{ash}	f_C	f_H	f_N	elemental formula	M_X	γ^*
BACTERIA							
Lactobacillus helveticus	9.03 (0.12)	47.54 (0.04)	6.25 (0.03)	12.79 (0.07)	$C_1H_{1.58}O_{0.39}N_{0.23}$	25.24	4.12
F. dehydrogenans	13.53 (0.05)	45.16 (0.11)	6.15 (0.03)	10.87 (0.09)	$C_1H_{1.63}O_{0.40}N_{0.21}$	26.57	4.21
Saccharopolyspora erythraea (a)	9.32 (0.11)	45.86 (0.10)	6.16 (0.08)	10.05 (0.06)	$C_1H_{1.61}O_{0.47}N_{0.19}$	26.17	4.11
Saccharopolyspora erythraea (b)	4.83 (0.01)	48.48 (0.05)	6.80 (0.05)	9.22 (0.08)	$C_1H_{1.68}O_{0.47}N_{0.16}$	24.75	4.24
B. flavum	30.23 (0.37)	38.54 (1.13)	5.78 (0.14)	8.47 (0.09)	$C_1H_{1.80}O_{0.33}N_{0.19}$	31.15	4.57
Escherichia coli	11.27 (0.02)	47.83 (0.07)	6.95 (0.04)	12.30 (0.07)	$C_1H_{1.74}O_{0.34}N_{0.22}$	25.09	4.40
Bacillus cereus	9.98 (0.04)	46.05 (0.03)	5.73 (0.03)	11.98 (0.14)	$C_1H_{1.49}O_{0.43}N_{0.22}$	26.06	3.97
Corynebacterium glutamicum	32.09 (0.08)	33.65 (0.89)	5.00 (0.05)	9.33 (0.15)	$C_1H_{1.78}O_{0.44}N_{0.24}$	35.68	4.18
Methanobacterium thermoautotrophicum	18.65 (0.40)	41.20 (0.16)	5.58 (0.04)	10.67 (0.07)	$C_1H_{1.63}O_{0.43}N_{0.22}$	29.12	4.09
ALGAE							
Rocan 1	6.15 (0.03)	51.18 (0.05)	5.96 (0.01)	2.66 (0.03)	$C_1H_{1.40}O_{0.50}N_{0.04}$	23.45	4.26
Rocan BUV 2	11.67 (0.19)	44.52 (0.11)	5.78 (0.03)	2.84 (0.08)	$C_1H_{1.56}O_{0.59}N_{0.05}$	26.95	4.21
Chlamydomonas	4.20 (0.23)	53.26 (0.36)	7.34 (0.07)	7.25 (0.14)	$C_1H_{1.65}O_{0.39}N_{0.12}$	22.53	4.52
Chrorella sp. ATCC 7516 (medium 5)	5.43 (0.03)	55.05 (0.11)	8.06 (0.14)	5.47 (0.06)	$C_1H_{1.76}O_{0.35}N_{0.09}$	21.80	4.79
Chlorella Spain sp. ATCC 7516 (medium S)	4.31 (0.05)	53.90 (0.13)	8.00 (0.11)	7.75 (0.12)	$C_1H_{1.78}O_{0.36}N_{0.12}$	22.26	4.69
Selenastrum capricornutum	5.65 (0.27)	52.38 (0.21)	7.00 (0.06)	4.69 (0.21)	$C_1H_{1.60}O_{0.43}N_{0.08}$	22.91	4.51
Scenedesnus obtusiusculus	5.22 (0.13)	51.04 (0.02)	6.97 (0.03)	6.66 (0.08)	$C_1H_{1.64}O_{0.44}N_{0.11}$	23.51	4.42

Table 9 (cont.)

FILAMENTOUS FUNGI							
Neurospora crassa	8.48 (0.02)	48.17 (0.07)	7.22 (0.02)	7.14 (0.03)	$C_1H_{1.80}O_{0.45}N_{0.13}$	24.91	4.52
Penicillium chrysogenum	21.13 (0.90)	51.14 (0.13)	7.95 (0.02)	4.78 (0.05)	$C_1H_{1.87}O_{0.22}N_{0.08}$	23.47	5.18
Mucor rouxii	9.57 (0.01)	50.35 (0.21)	7.52 (0.06)	3.91 (0.05)	$C_1H_{1.79}O_{0.43}N_{0.07}$	23.83	4.74
Aspergillus niger	8.77 (0.05)	46.18 (0.30)	6.17 (0.13)	5.16 (0.25)	$C_1H_{1.60}O_{0.55}N_{0.10}$	25.98	4.22
Aspergillus niger (spores)	3.18 (0.14)	49.15 (0.10)	6.14 (0.03)	6.70 (0.07)	$C_1H_{1.50}O_{0.53}N_{0.12}$	24.42	4.09
YEAST							
Candida kefyr NCYC 1441	4.70 (0.06)	51.18 (0.11)	7.13 (0.02)	7.07 (0.24)	$C_1H_{1.66}O_{0.44}N_{0.12}$	23.45	4.42
Candida utilis ATCC 9950	9.68 (0.02)	45.97 (0.01)	6.39 (0.02)	3.76 (0.05)	$C_1H_{1.66}O_{0.56}N_{0.07}$	26.10	4.33
Debaryomyces hansenii	8.74 (0.06)	44.41 (0.01)	6.36 (0.06)	5.27 (0.05)	$C_1H_{1.71}O_{0.6}N_{0.10}$	27.02	4.21
D. nepaliensis CBS 5921	4.51 (0.01)	45.67 (0.16)	6.78 (0.10)	4.74 (0.09)	$C_1H_{1.77}O_{0.63}N_{0.09}$	26.27	4.24
Saccharomyces cerevisiae Whi 2+	7.04 (0.06)	45.16 (0.11)	6.27 (0.08)	7.41 (0.03)	$C_1H_{1.65}O_{0.57}N_{0.14}$	26.57	4.09
S. cerevisiae Whi 2-	8.64 (0.01)	45.44 (0.05)	6.24 (0.04)	9.46 (0.05)	$C_1H_{1.64}O_{0.5}N_{0.18}$	26.41	4.1
S. cerevisiae CBS 426a	9.55 (0.12)	45.05 (0.17)	5.89 (0.11)	8.51 (0.19)	$C_1H_{1.56}O_{0.52}N_{0.16}$	26.64	4.04
S. cerevisiae CBS 426b	3.06 (0.01)	47.77 (0.02)	6.11 (0.06)	10.38 (0.40)	$C_1H_{1.52}O_{0.51}N_{0.19}$	25.12	3.93
Kluyveromyces marxianus NRRL 665	10.05 (0.03)	43.85 (0.13)	6.35 (0.05)	8.68 (0.02)	$C_1H_{1.73}O_{0.53}N_{0.17}$	27.37	4.16
Zygosaccharomyces bailii NCYC 563	6.50 (0.013)	46.26 (0.09)	6.32 (0.05)	7.20 (0.04)	$C_1H_{1.63}O_{0.55}N_{0.13}$	25.94	4.14

(a) exponential growth phase, (b) erythromycin production phase

Table 10: Value of the Student distribution for a population of size n.

n	$t_{n-1,0.95}/\sqrt{n}$
3	2.48
4	1.59
5	1.24
10	0.72
20	0.47
30	0.37

4.8. Statistical comparison of the composition of bacteria, algae, filamentous fungi and yeast

The average content of the strains listed in Table 9 are summarized in Table 11 [38]. It is first important to compare the standard deviation of each group to the average value to assess the dispersion of the results. It was already mentioned that each determination in Table 9 is accurate, and the value given in Table 12 indicate that the carbon and hydrogen content of all the strains in each group are close to the average value (σ/x lower or close to 10%). Thus, the average value for a whole group is in turn a good estimation of the C and H content of any strain listed in Table 9, and by extrapolation, of any other microorganism related to the list. By comparison, ash and nitrogen contents are widely dispersed among each group and between the groups, so that an average value is a poor estimate of the ash or N content of a given microorganism. For example, a 95% confidence interval for the ash and nitrogen content is calculated in Table 12 using the values given in Table 10 and Table 11.

The difference in nitrogen content is mainly due to the difference in protein content of the microorganisms. In fact, protein is the main cellular component containing nitrogen (in addition to RNA, DNA, free amino acids pool). The elemental composition of the main macromolecules is given in Table 11: protein contribute mainly to the N content, and RNA (5-15% cellular mass) and DNA (about 2% of cell mass) contribute to ash formation due to the phosphorus oxides.

Table 11: Average elemental composition of the four groups of microorganisms. For comparison, the elemental composition of BSA, glycogen (storage polysaccharide), RNA and DNA are indicated. *n* is the number of strains in each group from the Table 9 and the standard deviation is indicated in parenthesis [38].

Group	*n*	f_{ash}	f_C	f_H	f_N	elemental formula	M_X	γ^*
Bacteria	9	15.44 (9.67)	43.81 (5.01)	6.04 (0.61)	10.63 (1.50)	$C_1H_{1.66\ (0.10)}O_{0.41\ (0.05)}N_{0.21\ (0.02)}$	27.76 (3.63)	4.21 (0.18)
Algae	7	6.09 (2.56)	51.62 (3.44)	7.01 (0.90)	5.33 (2.04)	$C_1H_{1.63\ (0.13)}O_{0.44\ (0.08)}N_{0.09\ (0.03)}$	23.35 (1.71)	4.48 (0.21)
Filamentous fungi	5	9.54 (6.14)	49.00 (1.94)	7.00 (0.81)	5.54 (1.35)	$C_1H_{1.71\ (0.15)}O_{0.44\ (0.13)}N_{0.10\ (0.03)}$	24.52 (0.99)	4.55 (0.44)
Yeast	10	7.25 (2.48)	46.08 (2.09)	6.38 (0.35)	7.25 (2.13)	$C_1H_{1.65\ (0.07)}O_{0.54\ (0.05)}N_{0.14\ (0.04)}$	26.09 (1.11)	4.17 (0.14)
All microorganisms	31	9.84 (6.99)	47.14 (4.45)	6.53 (0.74)	7.52 (2.78)	$C_1H_{1.66\ (0.11)}O_{0.46\ (0.09)}N_{0.14\ (0.06)}$	25.46 (2.14)	4.31 (0.27)
BSA	3	1.20 (0.06)	52.79 (0.13)	7.10 (0.02)	16.57 (0.02)	$C_1H_{1.61}O_{0.32}N_{0.27}$	22.73	4.17
glycogen (a)		0	44.4	6.18	0	$C_1H_{1.67}O_{0.83}$	27	4.0
RNA (b)		16.5 (1.95)	33.9 (0.33)	3.75 (0.07)	15.8 (0.08)	$C_1H_{1.328}O_{0.666}N_{0.399}$	35.40	2.80
DNA (b)		19.3 (0.95)	36.35 (0.07)	4.01 (0.02)	16.22 (0.21)	$C_1H_{1.325}O_{0.498}N_{0.382}$	33.01	3.18

(a) calculated on the basis of a glucose polymer of elemental formula $C_6H_{10}O_5$.
(b) data from [28]

Table 12: 95% confidence interval of the average ash and nitrogen content of the population of bacteria, yeast and for all the microorganisms. n is the size of the population [38].

group	n	f_{ash}	f_N
bacteria	9	$8.15 < f_{ash} < 22.73$	$9.50 < f_N < 11.76$
yeast	10	$5.46 < f_{ash} < 9.04$	$5.72 < f_N < 8.78$
all microorganisms	31	$7.23 < f_{ash} < 12.45$	$6.48 < f_N < 8.56$

The average elemental composition of all the microorganisms is given in Table 11. As a consequence of the nitrogen content dispersion (Table 13), the atomic coefficient of nitrogen is poorly determined, which shows that the average formula that can be proposed is not a good estimation for a specific strain:

$C_1H_{1.66\,(0.11)}O_{0.46\,(0.09)}N_{0.14\,(0.06)}$

$f_{ash} = 9.84\%$ ($\sigma = 6.99\%$)

and $M_X = 25.46$ ($\sigma = 2.14$) g C-mol^{-1}

It is obvious from a direct evaluation of the data that there exist large differences between the strains and between the groups. These observations are confirmed by a statistical test. In fact, the good reproducibility of each elemental analysis performed with 3 or 4 repetitions gives a strong indication that differences between the strains (Table 13) and between the groups are significant. The aim of the t-test is to compare two populations (e.g. bacteria and algae) of average value x_1 and x_2, with standard deviations of σ_1 and σ_2, and size n_1 and n_2, respectively. The tested hypothesis is $x_1 = x_2$, and the test function is

$$z = \frac{|x_1 - x_2|}{\sqrt{\frac{\sigma_1^2}{n_1} + \frac{\sigma_2^2}{n_2}}} \qquad (41)$$

The hypothesis is rejected for $z > t_{n1+n_2-2,0.95}$, with $t_{n1+n_2-2,0.95}$ corresponding to the Student distribution for $\alpha = 1-0.95 = 0.05$ and (n_1+n_2-2) degrees of freedom. For example, the threshold value is about 2.1 for $n_1 + n_2$ about 20.

In this context, each group was compared to any other for each of the 6 properties: f_{ash}, f_C, f_H, f_N, M_X, γ^*. The hypothesis that the average value of one group is equal to the average value of another group is rejected for z values higher than 2.1. The results are listed in Table 14. From the statistical test, the ash

Table 13: Dispersion of the results for elemental composition, molecular mass and degree of reduction. Standard deviation of the population as percentage of the average value for different properties calculated from Table 11 [38].

group	ash	C	H	N	M_X	γ^*
bacteria	62.6	11.4	10.1	14.1	13.1	4.3
algae	42.0	6.7	12.8	38.3	7.3	4.7
filamentous fungi	64.4	4.0	11.6	24.4	4.0	9.7
yeast	34.2	4.5	5.5	29.4	4.3	3.4
All microorganisms	71.0	9.4	11.3	37.0	9.1	6.3

Table 14: t-test to compare the average of two populations. The tested hypothesis is that the average values of the two populations are equal for the different criteria. Results above the threshold value are indicated in bold and correspond to the rejection of the hypothesis [38].

hypothesis	bacteria = algae	bacteria = filamentous fungi	algae = filamentous fungi	bacteria = yeast	algae = yeast	yeast = filamentous fungi
f_{ash}	**2.78**	1.39	1.19	**2.47**	0.93	0.80
f_C	**3.69**	**2.76**	1.68	1.26	**3.80**	**2.68**
f_H	**2.45**	**2.31**	0.02	1.47	1.76	1.64
f_N	**5.77**	**6.49**	0.21	**4.03**	1.88	1.89
M_X	**3.21**	**2.51**	1.49	1.33	**3.73**	**2.78**
γ^*	**2.71**	1.65	0.33	0.54	**3.41**	1.88

content of bacteria is different from the ash content of algae, and only the nitrogen content of algae and filamentous fungi are similar. The results shown in Table 14 confirm that there exist significant differences between the groups and that an average composition is a very poor estimate of the composition of a specific strain, especially concerning the ash and the nitrogen content. The molecular weight is tightly correlated to the carbon content by Equation (39) which explains the similar results found for M_X and f_C in Table 14.

In conclusion, the carbon and hydrogen content of the various microorganisms is rather similar. The average values are 47.1 and 6.5% of the dry weight. As a consequence, the molecular mass varies moderately and is about 25.5 g C-mol^{-1}. However, ash and nitrogen content shows significant variation both inside each group and between the groups. In particular, the average ash and N content of bacteria is about twice the content of yeast. Therefore, the averaged value cannot be used to estimate precisely the nitrogen content of biomass, for example to calculate N balance.

4.9. Influence of growth conditions

It is of interest to investigate the change of elemental composition with growth conditions, mainly the dilution rate or the nature of the limiting substrate. For example, the nitrogen content increased almost linearly with the dilution rate in an aerobic glucose-limited continuous culture of *K. marxianus* grown at dilution rates ranging from 0.05 to 0.32 h^{-1} [39]. The ash fraction reached a constant value after a dilution rate of 0.125 h^{-1} as shown in Figure 7. Therefore, using an average elemental composition for different growth conditions may lead to incorrect conclusions. Similarly, the ash content and the nitrogen content of a glucose-limited continuous culture of *S. cerevisiae* increased with the dilution rate (Figure 8) [40]. The cellular content of an

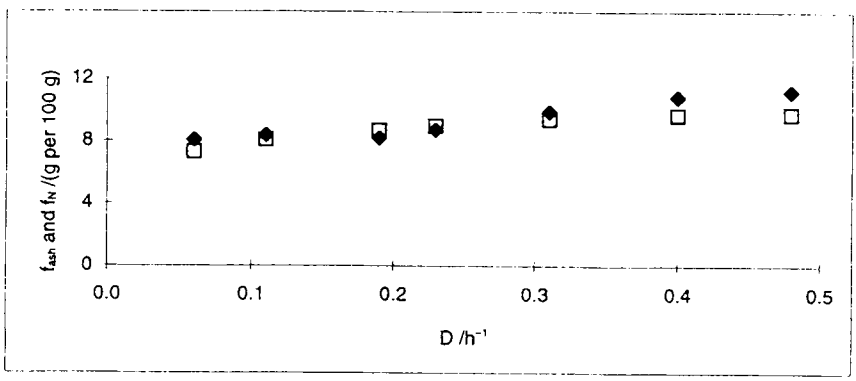

Figure 7: Evolution of the nitrogen (□) and ash (◆) content of *K. marxianus* grown in aerobic glucose-limited continuous culture. (Redrawn from Reference [39] with permission of the author and publisher).

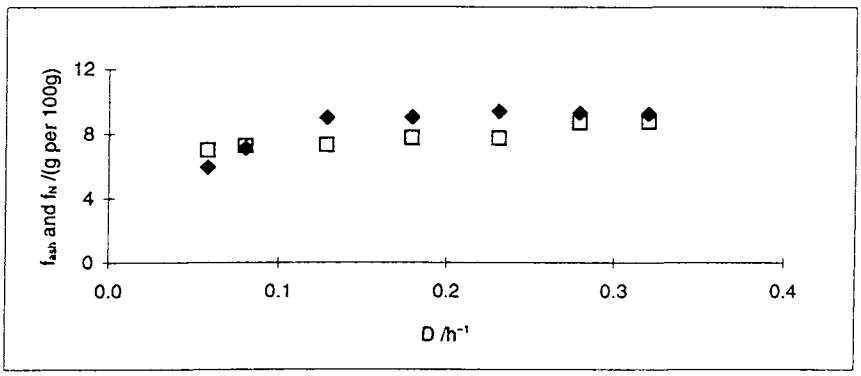

Figure 8: Evolution of the nitrogen (□) and ash (◆) content of *S. cerevisiae* grown in aerobic glucose-limited continuous culture. (Recalculated from Reference [40]).

anaerobic glucose-limited continuous cultures of *S. cerevisiae* CBS 8066 [41] is presented in Table 15. Protein and RNA content increases linearly with dilution rate, and conversely the total carbohydrate content decreases linearly with *D*. Glycogen and trehalose were almost undetectable from $D = 0.30\ h^{-1}$ onward. In addition, large changes in elemental composition were found under nitrogen-limitation, during aerobic [39,40,42] or anaerobic [41] experiments, with *S. cerevisiae* or *K. marxianus* (also denominated *K. fragilis*). For example, Figure 9 shows the evolution of the atomic coefficient of nitrogen (x_N) in the elemental formula as a function of the dilution rate for *S. cerevisiae* grown under glucose or glucose and ammonium limitation in aerobic continuous cultures [40]. Obviously, the protein content increases with the dilution rate but the carbohydrate content increases under nitrogen limitation. This figure exemplifies the large variation in elemental composition that can be observed when environmental conditions vary.

By comparison, the elemental composition of *M. thermoautotrophicum* grown in continuous cultures with hydrogen as energy source and CO_2 as carbon source remained remarkably constant for various growth conditions. Since

Table 15: Macromolecule content (g per 100 g biomass) during anaerobic glucose-limited continuous cultures of *S. cerevisiae* CBS 8066 [41].

	D (h^{-1})			
	0.10	0.20	0.30	0.40
Protein	45.0	50.0	55.5	60.1
Glycogen	8.4	4.2	0.6	0.0
Trehalose	0.8	0.2	0.0	0.0
Mannan	13.1	12.9	12.0	13.3
Other carbohydrates	18.4	15.4	12.6	3.7
RNA	6.3	8.2	10.1	12.1
DNA	0.4	0.4	0.5	0.6
Free amino acids	1.1	1.3	1.1	2.0
Lipids	2.9	3.0	3.8	3.4

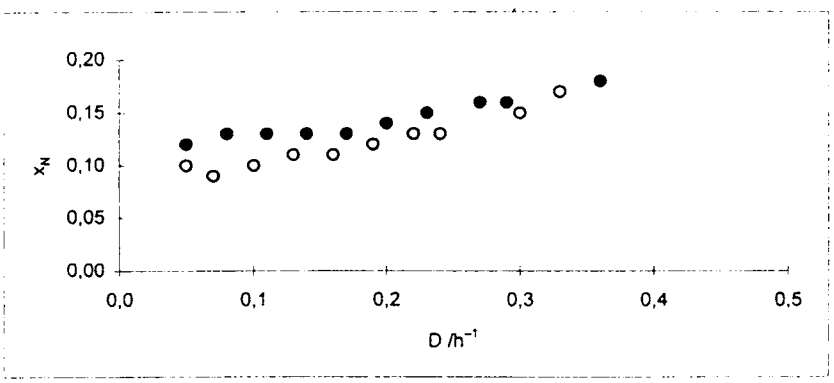

Figure 9: Evolution of the coefficient x_N for aerobic glucose-limited (●) or glucose and nitrogen limited (○) continuous cultures of *S. cerevisiae*. (Redrawn from Reference [40] with permission of the author and publisher).

the hydrogen is supplied by the gas phase, it is possible to vary the hydrogen supply independently of the dilution rate, and therefore, of the growth rate value [35]. Two continuous culture experiments were performed under hydrogen limitation at a gassing rate of 1 vvm and 0.5 vvm at dilution rates ranging from 0.06 to 0.30 h^{-1} (between 7 and 9 samples were analyzed in triplicate for each aeration rate). Alternatively, the culture can be limited by the iron supply when the medium composition is changed. A third continuous culture was performed under iron-limited conditions at a gassing rate of 0.5 vvm and a dilution rate of 0.096 h^{-1} and 7 different values of limiting-iron feed supply. The biomass composition was remarkable constant (especially for N and Fe content) for all the growth conditions, independently of the nature of the limiting substrate (either hydrogen as energy source or iron as biosynthetic nutrient), or of the dilution rate. Thus, the averaged elemental composition can be used for all the experiments, in contrast to what was found for yeast grown on glucose. In addition, this indicates the specific protein content is constant (because f_N is constant) even if the specific metabolic activity increases. The average biomass composition of *Methanobacterium thermoautotrophicum* for all the samples is:

$$C_1H_{1.68\,(0.08)}O_{0.39\,(0.02)}N_{0.24\,(0.01)}$$
$$\gamma^* = 4.18\ (\sigma = 0.10)$$
$$M_X = 25.87\ (\sigma = 0.37)\ \text{g C-mol}^{-1}$$

5. ENHALPY OF COMBUSTION OF BIOMASS

The enthalpy of combustion of a compound is always negative. By definition, the end products of combustion (CO_2, H_2O, N_2, SO_3, P_2O_5, ash in general) have an enthalpy of combustion of zero. This defines the combustion reference [6].

5.1. Sample preparation, and principle of measurement

The samples are prepared as for elemental analyses and the moisture content of the sample has to be determined in parallel. The principle of enthalpy of combustion measurement consists of burning a sample in a pure oxygen environment and then measuring the temperature increase of the surrounding water bath [34,43,44]. The ignition is initiated by a copper wire, and the measurements are corrected for moisture content of biomass, nitrous and sulfuric acid formation. A complete description of the measurement instruction can be found in references [28,34].

5.2. Modified enthalpy of combustion

The enthalpy balance equation (Equation(17)) shows that nitrogen source consumption has to be monitored since the reference state of combustion of nitrogenous compounds is N_2, whereas the nitrogen source is usually NH_3. In order to avoid the determination of nitrogen source consumption for data evaluation, the nitrogen consumption is estimated from biomass nitrogen content, as long as no nitrogenous compound is produced. Alternatively, enthalpy of combustion of biomass is reduced for the nitrogen source (NH_3) contribution to define the modified enthalpy of combustion, which corresponds to the same reference as the generalized degree of combustion. Both are marked by an asterisk to be consistent.

$$\Delta_c H_X^{o*} = \Delta_c H_X^o - x_N \Delta_c H_{NH_3}^* \tag{42}$$

The modified enthalpy of combustion corresponds to a hypothetical biomass that would not incorporate nitrogen, or it can be interpreted as assuming NH_3 instead of N_2 as final product of nitrogenous compounds combustion.

The ratio between the enthalpy of combustion and the degree of reduction is the oxycaloric quotient, Q_O. Similarly, the modified oxycaloric quotient is defined as:

$$Q_{O,i}^* = \frac{\Delta_c H_i^{o*}}{\gamma_i^*} \tag{43}$$

and is expressed in kJ e^--mol^{-1}.

The interest of this notion is that several authors [27,28,30,45-47] have reported an almost constant value of the oxycaloric quotient for CHON compounds. Since enthalpy of combustion is defined with respect to a reference state [48], this state must be the same as for the degree of reduction, i.e. for any species *i*:

$$\gamma_i^* = 0 \Leftrightarrow \Delta_c H_i^{\circ *} = 0 \tag{44}$$

where $\Delta_c H_i$ is the enthalpy of combustion of species *i* with the same reference state of combustion as for γ_i (for example, the enthalpies of combustion of CO_2, H_2O, N_2, SO_3 and P_2O_5 are zero). Considering different states for $\Delta_c H$ and γ may lead to erroneous conclusions [30]. Therefore, the oxycaloric quotient can be defined based on the standard enthalpy of combustion with the modified definition. In addition:

$$Q^*_{O,i} \approx Q^*_O \approx Q_O \quad (45)$$

where Q_O denotes the general average oxycaloric quotient of CHON compounds. This relation, known as Thornton's rule, estimates the enthalpy of combustion from the degree of reduction, i.e. from the elemental analysis. Analysis of various chemical compounds containing C, H, O, N, S and P atoms have shown that a 99% confidence interval of the slope of $\Delta_c H$ versus γ is -104.8 ± 2.8 kJ/ e^--mol, which is an estimate of Q_O [28].

5.3. Enthalpies of combustion of bacteria, algae and filamentous fungi and yeast

The enthalpy of combustion of the strains analyzed for CHN content is given in Table 16 [37,38]. Each determination was performed 3 to 5 times. The average values obtained for each group are summarized in Table 17. The enthalpy of combustion of all the microorganisms are rather close one to another and there is no clear difference between the 4 groups (Table 17). The differences are clearer for the modified enthalpy of combustion due to different nitrogen contents (see Table 11).

The average oxycaloric quotient is -112.4 kJ e^--mol^{-1} for the 30 strains. Thus, a good estimate of the enthalpy of combustion is obtained with Thornton's rule. The low variability in γ^* among the different strains (Table 11) is reflected by the similar modified enthalpy of combustion of bacteria (-460.3 kJ $Cmol^{-1}$) and yeast (-481.1 kJ C-mol^{-1}). Thus, an average value can be used to calculate the energy balance in a first approximation.

6. DETECTION AND CORRECTION OF MEASUREMENT ERRORS

6.1. Constraints on rates or cumulated quantities

It is necessary to check the data consistency before performing any calculation. In fact, it is difficult to describe accurately the metabolism or to quantify biochemical pathways if some relevant species is omitted or biased [49-51].The recovery of an entity k (such as carbon or nitrogen atoms) is defined as the ratio between its production rate and its consumption rate. Assuming that $x_{k/i}$ represents the amount of k per mole of chemical species i, the recovery is calculated as:

Table 16: Enthalpy of combustion, modified enthalpy of combustion and oxy-caloric quotient of biomass [37,38].

Organism	$\Delta_c H^\circ_X$ kJ C-mol^{-1}	$\Delta_c H^*_X$ kJ C-mol^{-1}	$Q^*_{O,X}$ kJ e$^-$-mol^{-1}
BACTERIA			
L. helveticus	- 537.5	- 469.3	- 114.1
F. dehydrogenans	- 519.7	- 458.8	- 109.0
Saccharopolyspora erythreus P1060 (a)	- 519.2	- 463.6	- 112.8
Saccharopolyspora erythreus P1060 (b)	- 527.2	- 479.0	- 112.9
B. flavum ATCC 14067	- 491.7	- 435.9	- 95.4
E coli	- 530.0	- 464.8	- 105.6
B. cereus	- 507.8	- 441.9	- 111.4
M. thermoautotrophicum	- 537.6	- 468.8	- 114.6
ALGAE			
Rocan 1	- 473.3	- 460.1	- 107.9
Rocan BUV 2	- 474.8	- 458.6	- 109.0
Chlamydomonas	- 535.4	- 500.9	- 110.9
Chrorella sp. ATCC 7516 (medium 5)	- 553.7	- 528.5	- 110.3
Chlorella Spain sp. ATCC 7516 (medium S)	- 583.3	- 546.8	- 116.7
Selenastrum capricornutum	- 564.3	- 541.6	- 120.2
Scenedesnus obtusiusculus	- 525.9	- 492.8	- 111.6
FILAMENTOUS FUNGI			
Neurospora crassa	- 583.4	- 545.8	- 120.9
Penicillium chrysogenum	- 636.9	- 613.2	- 118.3
Mucor rouxii	- 537.6	- 517.9	- 109.3
A niger	- 498.5	- 470.2	- 111.4
A. niger (spores)	- 418.7	- 384.1	- 94.0
YEAST			
C. kefyr NCYC 1441	- 527	- 491.5	- 111.2
C. utilis ATCC 9950	- 514	- 493.3	- 113.9
D. hansenii	- 538	- 508.4	- 120.8
D. nepaliensis CBS 5921	- 525	- 498.4	- 117.6
S. cerevisiae Whi 2+	- 494	- 452.6	- 110.7
S. cerevisiae Whi 2-	- 513	- 459.8	- 112.1
S. cerevisiae CBS 426a	- 518	- 470.7	- 116.5
S. cerevisiae CBS 426b	- 529	- 472.8	- 120.3
K. marxianus NRRL 665	- 505	- 454.7	- 109.3
Z. bailii NCYC 563	- 547	- 508.6	- 122.8

(a) exponential growth phase; (b) erythromycin production phase

Table 17: Average enthalpy of combustion, modified enthalpy of combustion and oxycaloric quotient of biomass. The standard deviation for each group is indicated in parenthesis [38].

Group	$\Delta_c H^\circ_X$ kJ C-mol^{-1}	$\Delta_c H^*_X$ kJ C-mol^{-1}	$Q^*_{O,X}$ kJ e$^-$-mol^{-1}
Average bacteria	- 521.35 (15.62)	- 460.29 (14.50)	- 109.46 (6.41)
Average algae	- 530.08 (42.59)	- 504.19 (36.45)	- 112.36 (4.44)
Average filamentous fungi	- 535.01 (83.06)	- 506.26 (85.67)	- 110.77 (10.52)
Average yeast	- 521.00 (15.59)	- 481.09 (21.59)	- 115.52 (4.76)
Average all microorganisms	- 525.55 (38.65)	- 485.13 (42.70)	- 112.37 (6.52)
BSA	- 536.4	- 456.9	- 109.5

$$R_k = \frac{\sum_{\text{products}} x_{k/i} r_i}{-\sum_{\text{substrates}} x_{k/i} r_i} \tag{46}$$

The minus sign indicates that $r_i < 0$ for substrate so that $R_k > 0$. Recovery should equal one, and it is lower than one if a product formation rate is underestimated (or neglected), or if a substrate consumption rate is overestimated. The enthalpy recovery take into account all the products and substrates as well as the heat dissipated and the heat of combustion of the hydroxide ions and the heat of vaporization of gaseous ethanol [32].

Another way to judge the correctness of the balance is to compute the balance for the elements. For each entity the net consumption rate in the reactor must be equal to the net production rate. For s different species containing the element k the balance for that element can be expressed by rates ($\dot{\varepsilon}_k$) or by cumulated quantities (ε_k) as follows [32,33],
on rates:

$$\dot{\varepsilon}_k = \sum_{i=1}^{i=s} r_i \, x_{k/i} \tag{47}$$

on cumulated quantities:

$$\varepsilon_k = \sum_{i=1}^{i=s} n_i \, x_{k/i} \tag{48}$$

The constraint is that the balance should equal zero.

It is possible to investigate the balances individually (each balance should equal zero) or simultaneously. In that case the combined balance is a vector of which each element is one of the balances and the constraint is that each element of the vector should equal zero. We construct the matrix **X** of element fraction of which each element X_{ki} is equal to $x_{k/i}$. The vector of balances is noted $\underline{\varepsilon}$ and the general formula using matrix notation is:

$$\underline{\varepsilon} = \mathbf{X} \, \underline{n}^T \tag{49}$$

where the subscript T denotes the transposition operator.

Similarly, the energy balance is calculated on rates ($\dot{\varepsilon}_Q$ in W) or cumulated quantities (ε_Q in J),
on rates:

$$\dot{\varepsilon}_Q = \Phi_r + \sum_{i=1}^{i=s} r_i \Delta_c H_i^o \tag{50}$$

on cumulated quantities:

$$\varepsilon_Q(j) = Q(j) + \sum_{i=1}^{i=s} n_i(j) \Delta_c H_i^o \tag{51}$$

where s is the number of species. By definition $Q(0) = 0$ and for any species $n_i(0) = 0$ because nothing has occurred before the first reaction.

6.2. Statistical test

Even if there is no gross error measurement, any balance will not be exactly equal to zero due to the random noise on the measures. The most simple test for checking if the balance is acceptable is to compare it with the input. This gives the fraction of the feed that is missing or that is in excess. It can be compared with the estimated accuracy on the measurements and gives a first criterion for evaluating a balance. Recoveries should be comprised between 98-102%. Nevertheless, this method does not provide an absolute threshold value to reject or accept the balance. Statistics are more suitable to detect errors. Several authors

[49,50,51] proposed a statistical test to investigate the balances once we have accepted a certain level of noise on the experimental data. We assume that the experimental data are normally distributed with a known variance-covariance matrix ψ. Under these assumptions, the balances $\underline{\varepsilon}$ are normally distributed and the variance-covariance of $\underline{\varepsilon}$ is Σ:

$$\Sigma = X^T \Psi X \tag{52}$$

We want to test if the balance is close enough to zero so that we can attribute the residual distance to zero to the random noise. For that purpose we calculate the distance to the target (here to zero) weighted by the inverse of the variance-covariance matrix Σ of $\underline{\varepsilon}$. Now we calculate the statistic function h:

$$h = \underline{\varepsilon}^T \Sigma^{-1} \underline{\varepsilon} \tag{53}$$

It is distributed as a central Chi-squared distribution with K degrees of freedom (equal to the number of balances) if the hypothesis that the balances are equal to zero is correct. The test function h calculated with K balances is also called the Mahalanobis distance because it is the weighted distance to the target zero and it is compared to a χ^2 distribution with K degrees of freedom and a level of significance $1-\theta$. This gives us an Upper Control Limit (UCL). If $h > \chi^2(1-\theta, K)$ the hypothesis concerning the balances is rejected, conversely if $h < \chi^2(1-\theta, K)$ the hypothesis cannot be rejected. For a level of significance of 95% the UCL is 2.71 for one degree of freedom, 4.61 for 2 degrees of freedom, 6.25 for 3 degrees and 7.78 for 4 degrees of freedom.

When calculated on cumulated quantities, balances and statistical test are recursively calculated for each observation. Thus on obtains the profile of h versus time, which indicates subsets of data for which the hypothesis might be rejected. The first observations usually do not satisfy the statistical test because even low level of noise have a large effect on the h value. A significant result necessitates at least 10 observations.

6.3. Example of calculation of the test function

For a dynamic experiment [32,33] where the vector of species is

$\underline{n}$ = [glucose ethanol biomass CO_2 acetate]

the change in mole number at the end of the experiment (in moles) was:

$\underline{n}$ = [-0.461 0.331 1.055 0.991 0.014]

The carbon constraint is simply the molar carbon content of each species :

$\mathbf{X} = [6 \;\; 2 \;\; 1 \;\; 1 \;\; 2]$

and the carbon balance is

$\varepsilon = (-0.461) \times 6 + 0.331 \times 2 + 1.055 + 0.991 + 0.014 \times 2 = -0.0116$ C-mol.

The distance to zero is:

$\varepsilon^2 = (0.0116 - 0) \times (0.0116 - 0) = 0.000134$

Under the assumption that all the variables are measured with 3% error the variance-covariance matrix of the measures, Ψ, is a diagonal matrix with the elements:

$\Psi_{1,1} = (-0.461 \times 0.03)^2$, $\Psi_{2,2} = (0.331 \times 0.03)^2$, $\Psi_{3,3} = (1.055 \times 0.03)^2$ etc...

The variance-covariance of the balance is a scalar Σ equal to 0.0092. The test function is calculated with the Equation (53). The numerical value is:

$$h = \frac{0.000134}{0.0092} = 0.0146$$

This value must be compared with a χ^2 distribution with one degree of freedom (one balance on carbon) and a level of significance of 90%. h is far below the Upper Control Limit of 2.71. It means that the distance to zero is not large enough to reject the hypothesis that the carbon balance is equal to zero. The level of noise that we have accepted (3%) on the data is sufficient to explain the difference of the simplified carbon balance to zero.

6.4. Example of balance calculation during dynamic experiment

A glucose-limited continuous culture was grown aerobically at an initial dilution rate of 0.1 h^{-1} and the dilution rate was then at *time* = 1.5 h shifted to 0.40 h^{-1}, close to the maximum specific growth rate and far above the critical dilution rate [24]. Ethanol and acetic acid production immediately set in. The biomass concentration decreased due to products formation and to a transient imbalance between the growth rate and the dilution rate. 5.5 hours after the shift-up, and before the new steady state was reached, the dilution rate was decreased to 0.05 h^{-1}. Cells started to grow on glucose and ethanol.

6.4.1. Concentrations and cumulated quantities profiles

The profile of concentration for biomass, ethanol, glucose and acetic acid is shown in Figure 10, and indicates clearly that the reactor was not at steady state. For example the decrease in ethanol concentration after time = 7 h is due to dilution, stripping and may be due to consumption by the microorganisms. Only inspection of the profile of the cumulated amount of ethanol that has reacted, shown in Figure 11, illustrates the consumption by the microorganisms.

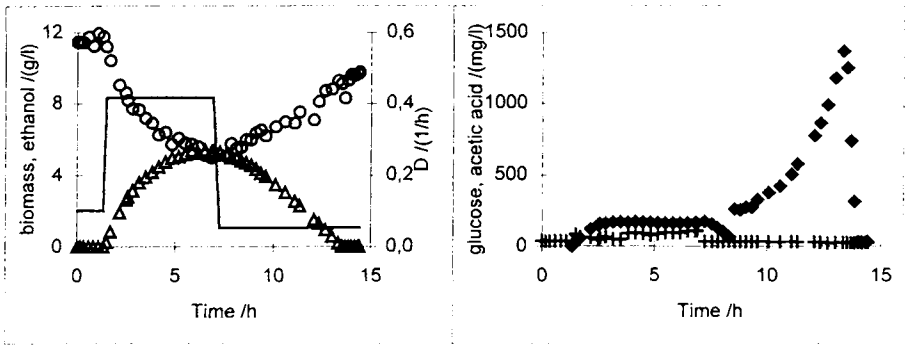

Figure 10: Biomass concentration (O), ethanol concentration (Δ), glucose (+) and acetic acid (◆). The dilution rate was changed from 0.10 to 0.40 h^{-1} at time = 1.5 h, and then decreased from 0.40 to 0.05 h^{-1} at time = 7 h. The profile of the concentrations show clearly that the reactor was not at steady state [24].

Based on the cumulated amount of each species (Figure 11), mole balances were calculated between the beginning of the experiment and each observation.

6.4.2. Atom balance

The mole balances took into account: glucose, ethanol in the liquid and the gaseous phase, acetic acid, CO_2, biomass and NH_3.

Over the whole experience, the recoveries presented in Table 18 for carbon, nitrogen and available electrons were 1.003, 0.982 and 0.99, respectively. The loss of carbon by ethanol stripping amounted to 1.5% of the carbon supplied by glucose. Some error in the nitrogen recovery may be due to a changing biomass composition with the dilution rate whereas a constant nitrogen content was considered.

Although the recoveries are close to one, the balances were individually checked with the χ^2 test. The test function *h* listed in Table 18 was calculated for a relative error on the measurement of 3% and must be compared with a threshold value of 2.71 for 1 degree of freedom and a significance level of 90%.

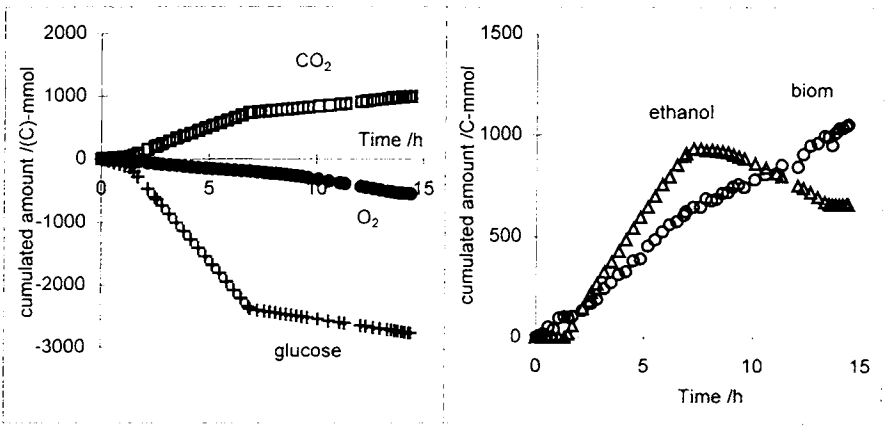

Figure 11: Cumulated quantity of glucose (+), oxygen (●), CO_2 (□);biomass (O) and ethanol (Δ). The cumulated quantity decreases for substrates, and conversely increases for products. See the change in the slope of the cumulated amount of ethanol. Since the test function is always significantly lower than the threshold value, there is no indication that the data are erroneous [24].

Table 18: Mole and energy recoveries and test function of the χ^2 test during a transient experiment for carbon, nitrogen, degree of reduction and enthalpy. The χ^2 test was performed for a level of significance of 90% and a relative error of 3% on the measurement for the chemical species and of 1% for heat. The Upper Control Limit was 2.71 [24].

balance	recovery	*h*
carbon	1.003	0.01
nitrogen	0.982	0.90
available electrons	0.990	0.18
enthalpy	1.007	0.04

6.4.3. Balance profiles

Cumulated quantities and carbon balance have been calculated for each sampling time. The cumulated amount of carbon contained in the substrate (glucose) is almost always equal to the sum of the carbon present in the products (biomass, CO_2, ethanol, acetate) as shown by the profile in Figure 12, indicating that the balance on cumulated quantities for carbon and available electrons was low through the experiment. A similar conclusion holds true for the nitrogen balance. The profile of the cumulated amount of carbon (or available electrons, Figure 12) consumed and produced is a powerful tool to detect systematic errors when the two curves diverge systematically.

The statistical test was performed for each observation and the result is shown in Figure 13 for the carbon balance. The χ^2 test shows the hypothesis that the deviation of the carbon balance from zero is due to random error is never rejected, except for some observations at the beginning of the experiment where small errors have a large influence on the result. Similar results are obtained with the test function calculated for the degree of reduction balance. In comparison to the carbon content which remains almost constant for various growth conditions, the nitrogen content of biomass changes with the dilution rate. It is therefore not surprising that the nitrogen balance is not as good as the carbon balance since a constant nitrogen content was used. Nevertheless, determining the nitrogen content of biomass during transient experiments is not easy since it requires to take large volumes of sample. Thus, it can be suspected that the nitrogen balance is not very good because the biomass composition used to calculate the balance does not reflect the actual characteristics of biomass.

6.4.4. Energy balance

The balance includes the following contributions: glucose, ammonium ions, NaOH consumed, biomass produced, ethanol in the liquid phase and in the gaseous phase and acetate. The enthalpy of combustion of gaseous ethanol was corrected for the heat of vaporization and the enthalpy of combustion of biomass was corrected for the nitrogen content.

At the end of the experiment there is an excess enthalpy as low as 0.7% (J/J) compared to the glucose consumed (Table 18). A statistical analysis facilitates the interpretation of the errors. The $\chi 2$ test was performed assuming an error of 1% on the heat measurement and the quantity of added base. Errors on the other

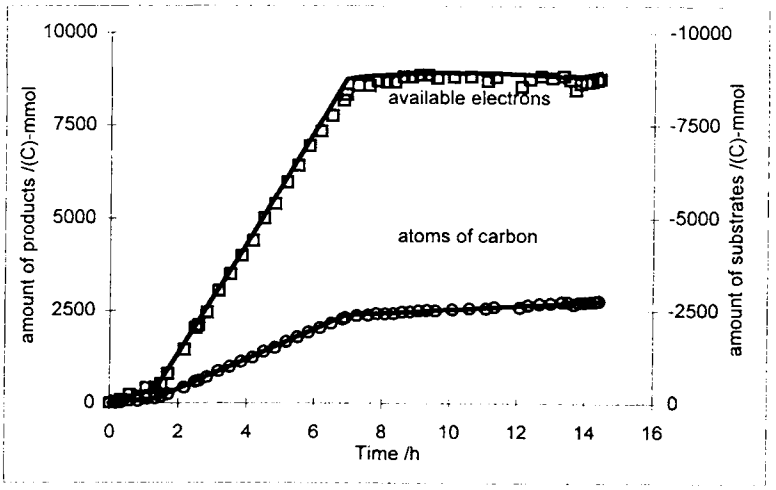

Figure 12: Profile of the cumulated amount of carbon contained in the substrate (glucose, bold line) and sum of the cumulated amount of carbon contained in the products (biomass, ethanol, CO_2 and acetate, open circles). The two curves are very close one to another. Similarly, the sum of the available electrons contained in the substrates consumed (glucose and O_2, bold line) is almost always equal to the sum of the available electrons found in the products (biomass, ethanol, acetate; open squares). Cumulated amount decreases for substrates, and conversely increases for products [24].

species involved were assumed to be 3%. The test function on energy balance was only 0.041 at the end of the experiment, compared to the cutoff value of 2.71 (χ^2 distribution with one degree of freedom and 90% significance level), and consequently here is no reason to reject the energy balance.

6.5. Data reconciliation

If the data consistency is acceptable, data can be reconciliated in order to remove the acceptable error [51]. The distance to the true estimate of the cumulated value is:

$$\hat{\delta} = \Psi X^T \Sigma^{-1} \varepsilon \tag{54}$$

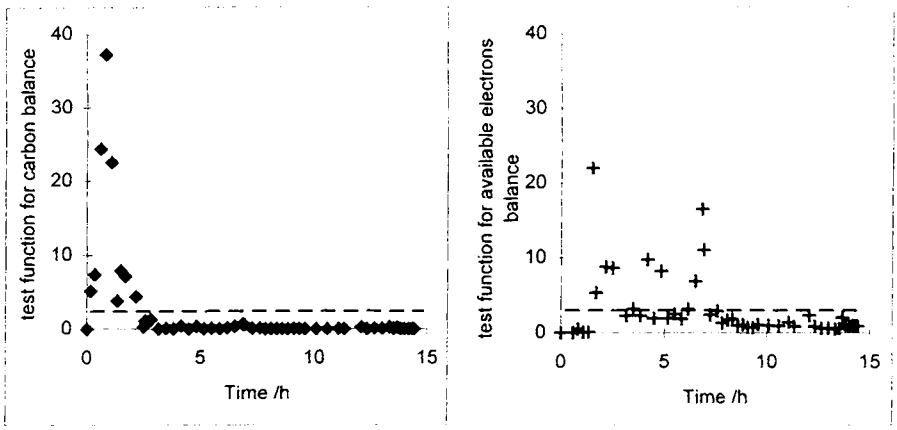

Figure 13: Profile of the χ^2 test for the carbon balance (◆) and for the nitrogen balance (+). For the carbon balance the test is rejected only for the first observations where the amount of carbon involved in the balance is low whereas for nitrogen balance the test is rejected more often, which is certainly due to a poor estimation of the nitrogen content of biomass. The dotted line indicates the Upper Control Limit (2.71) [24].

and the experimental measurements are corrected as follows to estimate the true values which satisfy the elemental constraints,

$$\hat{x} = x_{meas} + \hat{\delta} \tag{55}$$

The same procedure is applicable to reconcilation of reaction rates using the error $\dot{\varepsilon}$.

6.6. Indirect balancing

If n is the number of measurements (e.g. yield) and m the number of constraints (balances applicable), then the degree of freedom of the system is $m - n$. If $m > n$, one cumulated mole number or one yield can be estimated from the other if it is was not measured or if it is erroneous.

For example, Okabe et al. (1992) [52] report the following growth stoichiometry for the sulfate reducing bacteria *Desulfovibrio desulfuricans* growing on lactic acid and sulfate, and producing biomass, acetic acid, CO_2 and H_2S.

$$CH_2O + 0.127\ H_2SO_4 \rightarrow$$

$$0.023\ X + 0.653\ CH_2O + 0.32\ CO_2 + 0.093\ H_2S \qquad (56)$$

There are 6 measurements (yields) and 3 balances (C, γ* and S).

1. Carbon recovery: $R_C = 0.996$
2. Sulfur recovery: $R_S = 0.73$ (assuming an atomic coefficient in biomass $x_S = 0.0044$ as for *M. thermoautotrophicum*).
3. γ-recovery: $R_\gamma = 0.86$ (the combustion reference state is CO_2, H_2O, NH_3, SO_3 and P_2O_5)

It is clear that the available electrons and the sulfur balances are not correct, whereas the carbon balance is very satisfactory. In fact, biomass is negligible in these calculations and it is difficult to estimate accurately H_2S produced during the experiment. Thus, the yield $Y_{H_2S/HLac}$ can be estimated by solving the available electron balance:

$$4 = 0.023\ \gamma_X + 0.653\ \gamma_{HAc} + Y_{H_2S/HLac}\ \gamma_{H_2S}$$

with $\gamma^*_X = 4.2$, $\gamma_{HAc} = 4$ and $\gamma_{H_2S} = 8$.

One finds $Y_{H_2SO_4/HLac} = 0.161$ mol C-mol^{-1}. Therefore, the more probable stoichiometry is:

$$CH_2O + 0.161\ H_2SO_4 \rightarrow$$

$$0.023\ X + 0.653\ CH_2O + 0.32\ CO_2 + 0.161\ H_2S \qquad (57)$$

Another example of indirect balancing is the estimation of the specific growth rate during cell cycle oscillations of *S. cerevisiae* grown in continuous culture [53]. First, it was shown that carbon, degree of reduction and enthalpy balances were correct during cell cycle oscillations. In addition, residual glucose, ethanol and acetate had little impact on the balance calculation, so that they could be omitted without significant error. Therefore, an approximate calculation of the balances involves glucose and oxygen consumption rates, and CO_2, heat and biomass production rates. The four first terms are directly measurable, so that the biomass production rate (r_X) may be indirectly determined with the three balances on C, γ and enthalpy:

$$\hat{r}_{X,C}(t) = \frac{-\left(x_{C/G} r_G(t) + x_{C/CO_2} r_{CO_2}(t)\right)}{x_{C/X}} \qquad (58)$$

$$\hat{r}_{X,\gamma}(t) = \frac{-\left(\gamma_G^* r_G(t) + \gamma_{O_2}^* r_{O_2}(t)\right)}{\gamma_X^*} \tag{59}$$

$$\hat{r}_{X,Q}(t) = \frac{-\left(\Delta_c H_G^{o} r_G(t) + \Phi_r(t)\right)}{\Delta_c H_X^{o*}} \tag{60}$$

Estimates of r_X based upon such rate measurements are very close to one another (Figure 14) except during the S-phase. In fact, the estimates are not correct when ethanol or acetic acid are being produced or consumed because they are neglected in the balances (see Equations (58)-(60)) whereas they contain carbon, electrons and enthalpy.

The specific growth rate may be calculated from the biomass production rate as follows:

$$\hat{\mu}(t) = \frac{\hat{r}_X(t)}{c_X(t) V_{liq}} \tag{61}$$

Figure 15 shows that the growth rate varies between 0.08 h^{-1} and 0.12 h^{-1} for a dilution rate of 0.10 h^{-1}. The specific growth rate is low during the S phase and high during the G2, M and G1 phases, and the shape of the curve is roughly square. A calculation of the biomass specific growth rate from atomic and energy balances thus provides good estimations while this method is less sensitive to data scatter and experimental problems (linearity) than calculations based upon optical density measurements [54].

Similarly, the instantaneous molar biomass yield was not constant since it is defined as:

$$Y_{X/G} = \frac{r_X(t)}{r_G(t)} \tag{62}$$

The yield varied between 0.45 and 0.75 C-mol C-mol^{-1} because the rate of glucose consumption was constant and the biomass formation rate varied as depicted in Figure 15. An average yield coefficient of 0.63 C-mol C-mol^{-1} was calculated from the cumulated amounts of glucose consumed and biomass produced. By comparison in a non-oscillating continuous culture grown at a

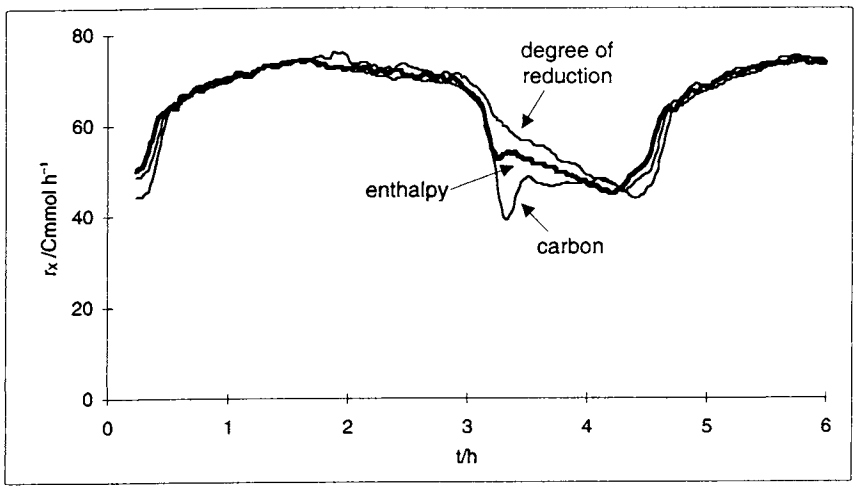

Figure 14: Estimation of the biomass formation rate from the carbon, degree of reduction and enthalpy balances during cell cycle oscillations at a dilution rate of 0.10 h^{-1}. (Redrawn from Reference [53] with permission of the author and publisher).

dilution rate of $D = 0.10\ h^{-1}$ at steady state, the growth rate μ is constant and equal to D by definition, and the molar yield is constant about 0.6 C-mol C-mol^{-1} [29]. The data indicates that oscillations do not improve the average biomass yield over one period of oscillation as compared to homogenous population at steady state.

7. ENERGETICS OF MICROORGANISMS

Energetics of growth can be investigated at the level of the microorganism or at the level of the reactor vessel. In both cases, the system considered is:

— open: matter and energy flow across the boundary of the system
— far from equilibrium: reactions go on continuously
— irreversible: it is not possible to change the conditions in order to return to the initial state.

In the case of the reactor, the content of the vessel consists of the liquid phase, the gaseous phase and the microorganisms. The reactor is treated as pseudo-homogenous, i.e. well mixed and the measurements represent the average of the response of the individual cells or entities in the reaction vessel.

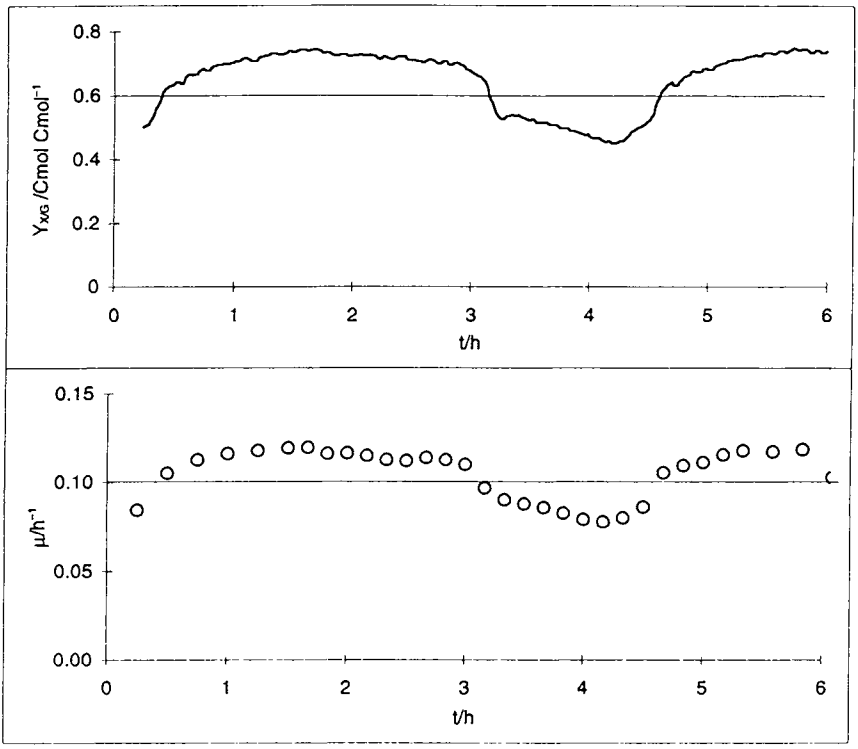

Figure 15: Variation of the specific growth rate and the biomass yield on glucose during cell cycle oscillations. Biomass formation rate was estimated by indirect balancing using the enthalpy balance. (Redrawn from Reference [53] with permission of the author and publisher).

7.1. Driving force of biochemical reactions

'This is the stuff our dreams are made of'
No doubt, Shakespeare was thinking of Gibbs energy change.

There is often a confusion between enthalpy, $\Delta_r H$, and Gibbs energy, $\Delta_r G$ defined in Equation (1). Negative values of $\Delta_r G$ correspond to exergonic reactions that proceed spontaneously in the direct sense, and conversely, positive values of $\Delta_r G$ correspond to endergonic reaction that will not proceed unless they are

coupled to another exergonic reaction. Change in Gibbs energy is the driving force of any chemical or biochemical reaction and consequently, this variable is fundamental, but unfortunately not directly accessible. On the other hand, enthalpy change does not give any information on the possibility of a chemical reaction, since it represents the amount of energy that can only be transformed in heat [7]. However, this variable is easily measured by direct calorimetry.

Growth consists of the coupling between fueling exergonic reactions (catabolism) and biosynthetic endergonic reactions (anabolism) as shown in Figure 16. The decrease in Gibbs energy of the former is the driving force of biosynthesis. Energy is transduced by ATP formation and hydrolysis. The Gibbs energy of growth is the sum of the Gibbs energy of catabolism plus the Gibbs energy of anabolism.

$$\Delta_r G_{growth} = \Delta_r G_{catabolism} + \Delta_r G_{anabolism} \qquad (63)$$

$$< 0 \qquad << 0 \qquad > 0$$

In fact, a fraction of the $\Delta_r G$ generated by fueling reactions is not conserved in biosynthesis but dissipated since the growth reaction rate would be zero for $\Delta_r G_{growth} = 0$ (equilibrium of growth reaction).

The fueling reaction consists of the oxidation of the energy source (electron donor) and the reduction of an electron acceptor (Figure 17). Typical oxido-reduction couples are listed in Table 19. For example, the two half reactions for the oxidation of glucose read as follows,

$$CH_2O + H_2O \rightarrow CO_2 + 4\ e^- + 4\ H^+$$
$$O_2 + 4\ e^- + 4\ H^+ \rightarrow 2\ H_2O$$
$$\overline{CH_2O + O_2 \rightarrow CO_2 + H_2O}$$

For the reductive catabolism of glucose to ethanol, glucose is bismuted, i.e. partially oxidized to CO_2 and partially reduced to ethanol, so that the degree of reduction of the final products are respectively lower and higher than the degree of reduction of glucose:

$$1/3\ CH_2O + 1/3\ H_2O \rightarrow 1/3\ CO_2 + 4/3\ e^- + 4/3\ H^+$$
$$2/3\ CH_2O + 4/3\ e^- + 4/3\ H^+ \rightarrow 2/3\ CH_3O_{0.5} + 1/3\ H_2O$$
$$\overline{CH_2O \rightarrow 2/3\ CH_3O_{0.5} + 1/3\ CO_2}$$

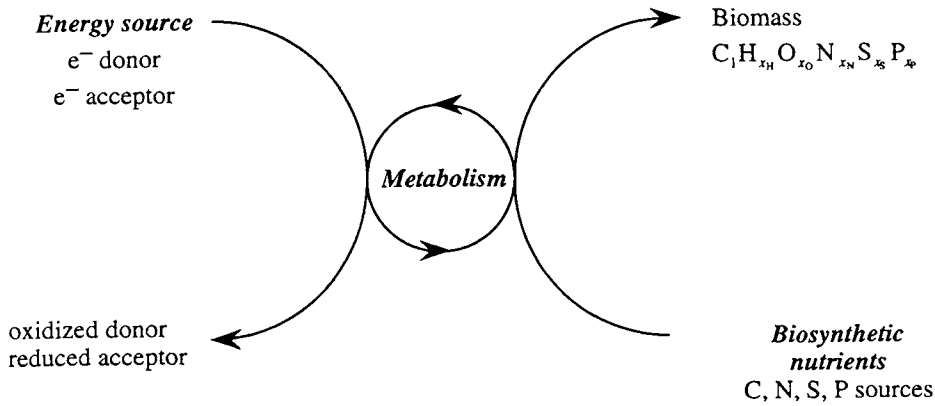

Figure 16: Coupling between fueling reactions (catabolism) and biosynthetic reactions (anabolism).

The flux of electrons is illustrated in Figure 17 showing the electron donor oxidation to a final product of degree of reduction zero, and the electron acceptor is reduction. Two domains are possible: $\gamma_{acceptor} < 0$ which defines the aerobic metabolism, and $\gamma_{acceptor} \geq 0$ which defines the anaerobic metabolism.

Biosynthesis implies a carbon source, and nitrogen, sulfur, phosphorus sources among others (cf. elemental composition and Figure 16). It was shown that the degree of reduction of bacteria and yeast is about 4.2 (Table 11), which is different from most of the carbon sources. Thus, a biosynthetic reaction is also a redox reaction and thus may involve an electron acceptor. As a result of the coupling between fueling (catabolic) reactions and biosynthetic (anabolic) reactions, a part of the Gibbs energy initially available from the energy source is conserved into biomass, and another part is dissipated to generate the driving force.

7.2. ATP production and utilization

Microorganisms have been considered as a black box in the former sections. Growth was represented by a macrochemical reaction without further investigation of the biochemical pathways. Considering the metabolism of the microorganisms may however provide some useful information on the growth energetics. The example treated here concerns the energetic metabolism of *S. cerevisiae* during aerobic or anaerobic growth.

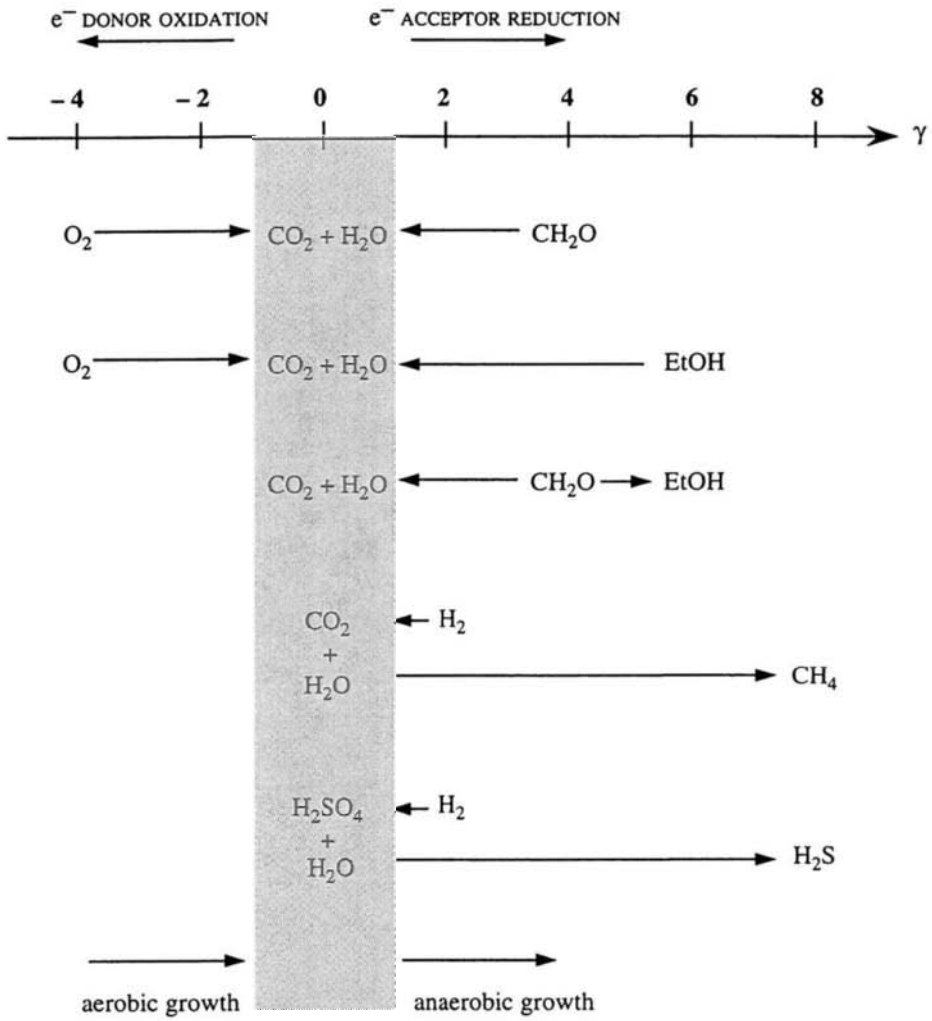

Figure 17: Flux of electrons between the electron donor (energy source) and the electron acceptor [24].

Table 19: Catabolic reactions for different electron donors and acceptors [24].

catabolic reaction	e^- donor	+	e^- acceptor	→	oxidized product	+	reduced product
oxidative catabolism of glucose	CH_2O	+	O_2	→	CO_2	+	H_2O
oxidative catabolism of ethanol	$CH_3O_{0.5}$	+	3/2 O_2	→	CO_2	+	3/2 H_2O
reductive catabolism of glucose	1/3 CH_2O	+	2/3 CH_2O	→	1/3 CO_2	+	2/3 $CH_3O_{0.5}$
methanogenesis	H_2	+	1/4 CO_2	→	1/2 H_2O	+	1/4 CH_4
sulfate reduction (a)	CH_2O	+	1/2 H_2SO_4	→	CO_2	+	1/2 H_2S

(a) energy source is lactic acid ($\gamma = 4$) which can only be partially degraded to 2/3 of acetic acid (also $\gamma = 4$) and 1/3 of CO_2, so that the catabolic half reaction reads (the valence of S is +6):

$CH_2O + 1/3\ H_2O \rightarrow 2/3\ CH_2O + 1/3\ CO_2 + 4/3\ e^- + 4/3\ H^+$

which simplifies to $CH_2O + H_2O \rightarrow CO_2 + 4\ e^- + 4\ H^+$

7.2.1. ATP requirements for biosynthesis

The ATP requirements to form one C-mole biomass is called the yield $Y_{ATP/X}$ and the growth reaction reads:

$$\frac{\gamma_X^*}{\gamma_G} CH_2O + Y_{ATP/X} ATP \rightarrow X + \left(1 - \frac{\gamma_X^*}{\gamma_G}\right) CO_2 + Y_{ATP/X}(ADP + P) \qquad (64)$$

where X represents one C-mole of biomass.

ATP is required for growth and maintenance [55]. If maintenance is considered to be non growth-associated, the yield of ATP on biomass, corrected for maintenance, is calculated from the following relation [56,57,58]:

$$q_{ATP} = Y_{ATP/X}^{biosynthesis} D + k_{ATP} \qquad (65)$$

where q_{ATP} is the specific ATP production rate, $Y_{ATP/X}^{biosynthesis}$ the ATP yield on biomass synthesized, and k_{ATP} the maintenance coefficient.

Maintenance is considered as ATP hydrolysis not coupled to another endergonic reaction. It is due to futile cycles, maintenance of gradients, and maintenance of metabolic machinery.

The energetic cost of biomass formation can be estimated from biochemical data concerning the energetic cost of amino-acid synthesis and polymerization, as well as the cost to synthesize polysaccharides, RNA, DNA, lipids, etc. and

ion transport. The effective value determined during anaerobic experiments is always higher than the energetic cost predicted from cell components.

Table 20 indicates the cost expressed in mmol ATP for anaerobic glucose-limited continuous culture at $D = 0.20\ h^{-1}$ on mineral media [41]: protein polymerization and solute transport account for 70% of the total cost. The predicted ATP requirement is 38.5 mmol per gram biomass. This value represents the minimal cost predicted from biochemistry and does not take into account sub-optimal energy coupling at the cell level.

7.2.2. ATP production by reductive metabolism

The cost of biomass synthesis is easily determined in anaerobic cultures since oxidative phosphorylation is not active. The only ATP synthesis step is ethanol formation from pyruvate, and glycerol synthesis consumes one mole of ATP per mole formed. The ATP yield of anaerobic catabolic reactions is low as shown in Table 21. In fact, degradation of glucose is incomplete and the

Table 20: ATP requirement for macromolecule synthesis and ion transport for an anaerobic glucose-limited continuous culture at $D = 0.20\ h^{-1}$ on mineral media ([41], modified for lipid content).

	ATP (mmol per gram biomass)
Protein polymerization	18.1
Transport	8.91
Carbohydrates	3.49
amino acids synthesis	3.24
RNA nucleic acids synthesis	1.89
Lipids	1.43
RNA turnover	0.8
RNA polymerization	0.46
DNA nucleic acids synthesis	0.16
DNA polymerization	0.01
Total	38.485

Table 21: Anaerobic catabolic reactions.

Pathway	Reaction
ethanol fermentation	Glucose + 2ADP + $2P_i$ → 2 ethanol + $2CO_2$ + 2ATP
acetate fermentation	Glucose + 2ADP + $2P_i$ + $4NAD^+$ → 2 acetate + $2CO_2$ + 2ATP + 4NADH
glycerol fermentation	Glucose + 2ATP + 2NADH → 2Glycerol + 2ADP + $2P_i$ + $2NAD^+$

standard free energy of the products is almost equal to that of the substrate. For example, only two moles of ATP are formed per mole ethanol synthesized.

Thus, the specific ATP production rate in anaerobic continuous culture of *S. cerevisiae* on glucose is calculated by balance from Table 21 [59],

$$q_{ATP} = \frac{r_{ATP}}{c_X V} = q_E / 2 - q_{GlOH} / 3 \tag{66}$$

Glycerol is formed to close the redox balance since some intermediates are used for biosynthesis [60]. For *S. cerevisiae* CBS 426, the yield $Y_{ATP/X}$ was determined to be 1.59 ± 0.07 mol C-mol^{-1} biomass, with a maintenance k_{ATP} of 0.018 ± 0.014 mol C-mol^{-1} h^{-1} [24].

7.2.3. ATP production by aerobic catabolism

Mechanistic P/O ratio Oxidation of reducing equivalents produced during glycolysis and in the TCA cycle takes place in the mitochondria (oxidative phosphorylation). The maximal ATP production rate, coupled with electrons exchanged, is determined by the mechanism of sites III and IV in the electron transport chain. The mechanistic *P/O* ratio is equal to the number of moles ATP synthesized by the oxidation of one mole of NAD(P)H+H$^+$ by 0.5 mole O_2. The electrochemical potential change in site III of the respiratory chain is 41.4 kJ per mole NAD(P)H+H$^+$ oxidized and 99.6 kJ mol^{-1} for the site IV, whereas the standard energy of ADP phosphorylation to ATP is 30.5 kJ mol^{-1}. Thus, a maximum of 1 mole of ATP can be produced in site III per mol NAD(P)H+H$^+$ oxidized, and a maximum of 2 moles ATP in site IV, leading to a maximal mechanistic *P/O* ratio of 3. However, it is not demonstrated that the mechanistic *P/O* ratio of oxidative phosphorylation is effectively 3 due to the inefficiency of sites III and IV.

Effective P/O ratio If spilling reactions exist, part of the ATP formed by oxidative phosphorylation is degraded to ADP+P, thus lowering the apparent

yield of ATP used for biosynthesis per 0.5 mole O_2 consumed. The effective *P/O* ratio is defined as the ratio between the ATP production used for biosynthesis and the O_2 consumption for oxidative catabolism:

$$\mathrm{NAD(P)H} + \mathrm{H^+} + 1/2\ \mathrm{O_2} + P/O(\mathrm{ADP} + \mathrm{P}) \rightarrow \mathrm{NAD(P)} + \mathrm{H_2O} + P/O\ \mathrm{ATP} \tag{67}$$

In aerobic experiments on glucose, the effective *P/O* and $Y_{ATP/X}$ yields are related to the biomass yield on biomass by ATP balance. Since the cells do not exchange ATP with the environment, Equations (64), (67) and the yield $Y_{X/G}$ are subjected to the constraint:

$$P/O = \frac{Y_{ATP/X} Y_{X/G}}{2\left(1 - \frac{\gamma_X}{\gamma_G} Y_{X/G}\right)} \tag{68}$$

For *S. cerevisiae* CBS 426, an aerobic biomass yield on glucose of 0.6 C-mol C-mol^{-1} and a yield $Y_{ATP/X}$ of 1.6 mol C-mol^{-1} [24] impose that the effective *P/O* ratio is equal to 1.29, which is close to the effective *P/O* ratio of 1.2 proposed in reference [61] for *S. cerevisiae* CBS 8066 and the value identified as 1.09 in reference [62].

7.3. Enthalpy and Gibbs energy dissipation

In the previous sections, energetics of growth has been considered in terms of ATP production and utilization for biosynthesis and spilling. Now growth will be considered at a more fundamental level of Gibbs energy and enthalpy dissipation. Since Gibbs energy is dissipated during growth, the term $\Delta_r H_{growth} - T\Delta_r S_{growth}$ must be negative for changes in enthalpy and/or changes in entropy. The ratio between the heat flow rate ($\Delta_r H_{growth}$) and the biomass production rate (r_X), defining the heat yield of growth (negative value if heat is produced), was experimentally determined or calculated (for *Ms. acetivorans* and *D. desulfuricans*) for several microorganisms and growth conditions (Table 22). In most cases the heat yield is negative, i.e. heat is produced during growth. However, it is predicted using an energy balance that heat will by taken-up from the environment during growth of the aceto-methanogen *Ms. acetivorans*. This phenomenon is not common, but not forbidden by any thermodynamic law [5].

Since it is not measurable, the Gibbs energy dissipation per C-mole biomass formed was calculated from the growth stoichiometry. As expected, the change in Gibbs energy is always negative and with no exception. The $\Delta_r G_{growth}$ dissipation per C-mol biomass formed varied between 321 kJ C-mol^{-1} for aerobic or anaerobic glucose-limited continuous cultures of *S. cerevisiae* and 3050 kJ C-mol^{-1} for iron-limited continuous cultures of *M. thermoautotrophicum*. The difference between $\Delta_r G_{growth}$ and $\Delta_r H_{growth}$ is small for aerobic processes, and may be considerable for anaerobic growth. For example $\Delta_r G_{growth}/r_X$ is similar for aerobic and anaerobic growth of *S. cerevisiae* whereas the heat dissipation, $\Delta_r H_{growth}/r_X$, of the aerobic process is twice that of the anaerobic process (−305.3 and −141.5 kJ per C-mol biomass, respectively). The observation that the Gibbs energy dissipation per amount of biomass formed is the same in aerobic and anaerobic conditions gives good support that the ATP cost of biosynthesis $Y_{ATP/X}$ will be identical for both aerobic and anaerobic conditions as well.

An empirical relation was proposed in reference [5] to relate the specific Gibbs energy dissipation to the number of atom of carbon of the energy source (C) and the degree of reduction (γ_C) of the carbon source,

$$-\frac{\Delta_r G_{growth}}{r_X} = 200 + 18(6 - C)^{1.8} + \exp\left\{\left[3.6 + 0.4C\right] \cdot \left|3.8 - \gamma_C\right|^{0.32}\right\} \qquad (69)$$

The advantage of this relation is to require only black-box information and it gives a good prediction. However, some cases are badly represented, for example it is predicted that −277 kJ C-mol^{-1} is dissipated during aerobic growth on acetate, whereas the experimental value is about 3 times higher (−732 kJ C-mol^{-1}).

The entropy change during growth calculated by the difference between $\Delta_r H_{growth}$ and $\Delta_r G_{growth}$ is often positive (entropy production). In such a case, the Gibbs energy dissipation is larger than the enthalpy dissipation so that only a part of the driving force ($\Delta_r G_{growth}$) can be experimentally detected as heat production ($\Delta_r H_{growth}$). Thus, in the case of an entropy increase, $\Delta_r G_{growth}/\ \Delta_r H_{growth} > 1$. However, the term $T\Delta_r S_{growth}$ is not systematically positive as illustrated by the growth of *M. thermoautotrophicum* [35]. In the case of a hydrogen-limited continuous culture, the enthalpy dissipation is 4.7 times higher than the Gibbs energy dissipation, so that most of the heat dissipation was due to entropy

Table 22: Enthalpy and Gibbs energy dissipation per C-mole biomass during growth. $\Delta n/n_X$ indicates the change in mole number of the growth reaction per C-mole biomass [24].

Microorganism	growth conditions	$\Delta_r H_{growth}/r_X$ kJ C-mol^{-1}	$\Delta_r G_{growth}/r_X$ kJ C-mol^{-1}	$T\Delta_r S_{growth}/r_X$ kJ C-mol^{-1}	$\Delta n/n_X$
S. cerevisiae	aerobic, glucose-limited	- 305.3	- 321.6	+ 16.3	- 0.2
S. cerevisiae	aerobic, ethanol-limited	- 643.3	- 623.0	- 11.3	- 1.7
S. cerevisiae	aerobic, acetate-limited	- 704.1	- 731.9	+ 27.8	- 1.3
S. cerevisiae	anaerobic, glucose and oxygen limited	- 89.0	- 322	+ 233	+ 4.8
M. thermoautotrophicum	anaerobic, H_2-limited	- 3730 (a)	- 802	- 2928	- 20
M. thermoautotrophicum	anaerobic, iron-limited	- 7141 (a)	- 3049	- 4092	
Ms. acetivorans	anaerobic, acetate-limited	+ 201.5	- 745.1	+ 946.6	+ 25
D. desulfuricans	anaerobic, sulfate-limited	- 809.2 (b)	- 1012.5	+ 206.3	+ 14.3

(a) [35]
(b) calculation based on the reconciliated data of [52]

dissipation (-2926 kJ C-mol^{-1}). In the case of an entropy decrease the Gibbs energy dissipation is larger than the enthalpy dissipation. The figures presented in Table 22 show that Gibbs energy dissipation is not always associated with entropy production or negentropy consumption as proposed by Schrödinger [63] in "What is Life ?" in 1944. Microorganisms are constrained to dissipate Gibbs energy to grow, but they are constrained neither to dissipate enthalpy nor to increase entropy.

The calculation of the ratio $\Delta_r G_{growth}/\Delta_r H_{growth}$ depends on the biomass yield and therefore requires a minimum amount of knowledge on the process. However, it was demonstrated [64] that the ratio could be estimated from the change of the catabolic reaction and not of the complete growth reaction ($\Delta_r G_{growth}/\Delta_r H_{growth} = \Delta_r G_{catabolism}/\Delta_r H_{catabolism}$), which is easier. Therefore, the contribution of the entropy term is predictable from the catabolic reaction stoichiometry. The entropy generation ($\Delta_r S_{growth} > 0$) or destruction ($\Delta_r S_{growth} < 0$) per C-mol biomass can be assessed by looking at the change in the number of

molecules per C-mol biomass formed. The molar mass of biomass must be estimated to perform this calculation. As a pseudo-chemical entity, the molar mass of biomass can be calculated as the molar mass of its constituents (protein, carbohydrates, RNA, DNA, ions etc.) weighted by their mole fraction in biomass:

$$M_{\text{biomass}} = \sum x_{m/X} M_m \tag{70}$$

where M_{biomass} is the mass of one mole of biomass, $x_{m/X}$ is the mole fraction of molecule m in biomass (mole per C-mol biomass) and M_m the molar mass of m (g per mole) [24]. Since biomass consists mainly of macromolecules (protein, carbohydrates, RNA, DNA) of high molecular mass, M_{biomass} can be considered as very large when compared to the molecular mass of the other species involved in growth. As a consequence, the number of moles of biomass produced is always negligible. For example, the stoichiometry for aerobic growth reads on a C-molar basis (X represents one C-mole of biomass):

$CH_2O + 0.37\ O_2 \rightarrow 0.6\ X + 0.4\ CO_2$

which gives expressed in mole of each species (*Biomass* represents one mole of biomass):

$C_6H_{12}O_6 + 2.22\ O_2 \rightarrow \varepsilon\ Biomass + 2.4\ CO_2$

where ε although corresponding to 3.6 C-moles is close to zero moles of biomass.

Thus, $\Delta n = 2.4 - 1 - 2.22 = -0.82$

and $\Delta n/n_X = -0.23$ mol per C-mol biomass.

It can be seen in Table 22 that a decrease in entropy is observed when the number of moles $\Delta n/n_X$ decreases (e.g., for *M. thermoautotrophicum*, for *S. cerevisiae* grown on ethanol) and conversely, entropy increases when the number of molecules increases (for *S. cerevisiae* grown anaerobically, for acetomethanogens, for sulfate reducing bacteria).

Therefore, growth is fundamentally associated with Gibbs energy dissipation. Changes in enthalpy, as well as in entropy, can be negative or positive. Although in most cases heat is produced and entropy increases during growth, this does not correspond to any thermodynamic constraint by itself. The only thermodynamic constraint is that $\Delta_r G_{\text{growth}}$ must be negative.

7.4. Thermodynamic constraints on biomass and product yields

Metabolism is subjected to the absolute thermodynamic constraint of $\Delta_r G_{\text{growth}}$ dissipation and to the existing biochemical pathways. However, it is

tempting to calculate the theoretical limit of the value of biomass, CO_2 or O_2 yields on glucose allowed by the thermodynamic constraint of Gibbs energy dissipation [30]. Of course, it is well known from biochemistry that neither CO_2 can be taken-up nor O_2 produced by *S. cerevisiae*. However, this part will show that this would not systematically violate the thermodynamic constraint.

During growth on glucose under aerobic or anaerobic conditions, the yields of biomass, CO_2 and oxygen, the enthalpy of reaction and Gibbs energy of reaction are related by the conservation constraint of extensive entities (carbon, available electrons, enthalpy and Gibbs energy). For simplicity, the elemental balance on nitrogen is not considered so that the generalized degree of reduction of biomass is used as well as the enthalpy of combustion modified for the nitrogen source [65].

During oxido-reductive growth of *S. cerevisiae* or *K. marxianus* on glucose, the reductive metabolism may be forced by decreasing the oxygen supply or by increasing the dilution rate above the critical value for *S. cerevisiae* [66-69]. The general expression of the growth stoichiometry is:

$$-CH_2O - Y_{O_2/G}O_2 + Y_{X/G}X + Y_{E/G}CH_3O_{0.5} + Y_{CO_2/G}CO_2 = 0 \tag{71}$$

where the yields are subjected to the four linear constraints of carbon conservation, degree of reduction, enthalpy and Gibbs energy:

$$1 = Y_{X/G} + Y_{E/G} + Y_{CO_2/G} \tag{72}$$

$$\gamma_G - \gamma_{O_2} Y_{O_2/G} = \gamma^*_X Y_{X/G} + \gamma_E Y_{E/G} \tag{73}$$

$$\Delta_c H_G = Y_{X/G}\Delta_c H^*_X + Y_{E/G}\Delta_c H^*_E + \Delta_r H_{growth} \tag{74}$$

$$\Delta_c G_G = Y_{X/G}\Delta_c G^*_X + Y_{E/G}\Delta_c G^*_E + \Delta_r G_{growth} \tag{75}$$

Four limit cases can be considered:

- case 1: $Y_{O_2/G} = 0$
- case 2: $Y_{CO_2/G} = 0$
- case 3: $\Delta_r H_{growth} = 0$
- case 4: $\Delta_r G_{growth} = 0$

and are represented on the plot of $Y_{X/G}$ as a function of $Y_{E/G}$ in Figure 18A. All the experimental points must be to the left of the thermodynamic constraint of

$\Delta_r G_{growth} = 0$. The profile of the experimental points obtained in glucose and oxygen limited cultures are located close to the line corresponding to a Gibbs energy efficiency of 60% [48,65]. Points located on the line $Y_{O_2/G} = 0$ correspond to anaerobic experiments, and the points to the left of this line are from partially aerobic experiments ($Y_{O_2/G} > 0$). The limit case $Y_{O_2/G} = 0$ corresponds to the lowest values of $Y_{X/G}$ and $Y_{E/G}$, and by comparison the limit $Y_{CO_2/G}$ corresponds to the largest values of $Y_{X/G}$ and $Y_{E/G}$, except for high $Y_{X/G}$. The fact that the line $\Delta_r H_{growth} = 0$ is always to the left of the line $\Delta_r G_{growth} = 0$ shows that the entropy contribution to $\Delta_r G_{growth}$ will be positive (entropy production) whatever is the biomass yield. A similar plot for *M. thermoautrophicum* would show that the relative position of the lines is different: $\Delta_r H_{growth} = 0$ is at the right of the line $\Delta_r G_{growth} = 0$ for the biomass yield observed, so that entropy is effectively consumed ($T\Delta_r S_{growth} < 0$) during growth.

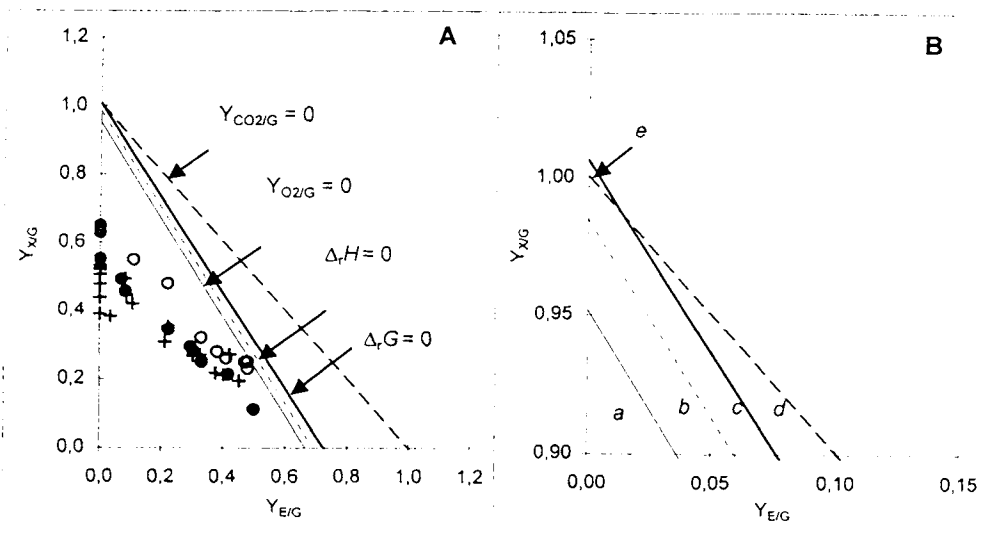

Figure 18: Limit lines corresponding to $Y_{O_2/G} = 0$ (faint line); $Y_{CO_2/G} = 0$ (bold dotted line); $\Delta_r H_{growth} = 0$ (faint dotted line); $\Delta_r G_{growth} = 0$ (bold line) [24].

(A) Thermodynamics forbids to cross the line $\Delta_r G_{growth} = 0$. Experimental data obtained during oxido-reductive metabolism of *S. cerevisiae* (+; O) or *K. marxianus* (●). (Redrawn from References [66], [67], [68], respectively, with permission of the author and publisher).

(B) Detail of the limit lines for high biomass yield and low ethanol yield.

Since the only theoretical constraint that cannot be violated is $\Delta_r G_{growth} < 0$, in theory experimental points could be located anywhere to the left of this limit line, in particular to the right of the other limit lines as will be discussed below. Figure 18B shows 5 areas labeled *a* to *e*.

a: This corresponds to the usual oxido-reductive growth: some oxygen is consumed, CO_2 and heat are produced. The limit case is obtained for $Y_{O_2/G} = 0$, which corresponds to pure anaerobic growth.

b: Oxygen is produced since the point is to the right of the line $Y_{O_2/G} = 0$, but is thermodynamically possible since it is to the left of the constraint $\Delta_r G = 0$. Some heat is still produced, as well as CO_2 (point to the left of the limit lines).

c: Oxygen is produced and heat is consumed. The growth reaction is still spontaneous since some Gibbs energy is dissipated.

d: Growth is not possible above the limit line corresponding to $\Delta_r G = 0$. The limit case is obtained for $\Delta_r G = 0$ which corresponds to thermodynamic equilibrium, which is by far not the usual state of a biological system.

e: Growth is possible since the point is below the line $\Delta_r G = 0$. However, the point is above the line $Y_{CO_2/G} = 0$, which means that CO_2 is taken-up from the environment. Similarly, heat is absorbed ($\Delta_r H > 0$) and oxygen is produced.

The cases *b*, *c* and *e* show that there is no thermodynamic constraint that prevents observation of heat consumption, oxygen production or CO_2 uptake with yeast, but however, there are biochemical limits. The case of oxygen production would correspond to oxidation of part of the glucose to O_2, i.e. in Figure 17 the catabolic reaction would start at $\gamma = 4$ and arrive at $\gamma = -4$. Nevertheless, the cases *b* to *d* are totally impossible in practice with yeast. In fact, how would it be possible to produce oxygen without consumption by the microorganisms themselves? This shows the limit to such speculations. However, heat uptake by aceto-methanogens is possible because the limit line corresponding to $\Delta_r H_{growth} = 0$ is situated to the left of the limit line for $Y_{O_2/G} = 0$ on which the data are situated during the anaerobic growth [24].

8. CALORIMETRIC INVESTIGATION OF MULTIPLE LIMITED GROWTH

In a general case, a continuous culture is limited by the nutrient *i* [24,70]. If the supply of another nutrient *j* is decreased, the supply rate will decrease below

the minimum level required to metabolize i as before under single i-limitation (with the yield $Y_{j/i,i\text{-lim}}$). Two extreme limit behaviours can be envisaged:

i) the metabolism of the organism remains constant, as does the stoichiometric coefficient $Y_{j/i}$. Since it is now the supply of species j which limits the culture, the consumption of i will be given by $r_i = Y_{j/i}\, r_j$ and will now become smaller or equal than the supply of i. Some unused i will show-up in the broth.

ii) the organism is able to adapt its metabolism in such a way as to consume all of the supply of both i and j. The yield $Y_{j/i}$ is then modified to be equal to the ratio of the supply rates of i and j. This condition is called a double limitation.

In reality, an intermediate between i) and ii) is observed. The limitation of the j supply compared to the i uptake is quantified by comparing the actual yield of j on i ($Y_{j/i}$)to $Y_{j/i,i\text{-lim}}$ [24]. This is a generalization of the aerobicity concept first presented in reference [67] for glucose and oxygen limitations. The supply restriction parameter, $\rho_{j/i}$, is defined as,

$$\rho_{j/i} = \frac{q_j}{q_i}\frac{1}{Y_{j/i,i-\text{lim}}} = \frac{Y_{j/i}}{Y_{j/i,i-\text{lim}}} \tag{76}$$

In addition, it is often found that the residual concentration in the liquid phase of the limiting nutrient is very low, and thus negligible compared to the inlet concentration in the calculations.

8.1. Glucose and oxygen limitation

Application of calorimetry to oxygen-limited continuous cultures has been presented in detail in references [67,71,72]. In fact, reductive metabolism is almost athermic as compared to aerobic metabolism. In addition, it is possible to set the oxygen limitation to the desired value by changing the oxygen gas feed composition [67,73]. The level of oxygen limitation is quantified by the ratio $\rho_{O_2/G}$ (called aerobicity and also denoted Ω [74]):

$$\rho_{j/i,\text{supply}} = \frac{c_j^*}{c_{i,\text{in}}}\frac{k_{i,\text{liq}}a}{D}\frac{1}{Y_{j/i,i-\text{lim}}} \tag{77}$$

The value of $\rho_{O_2/G}$ is 1 during purely aerobic metabolism and 0 under anaerobic conditions. Values comprised between 0 and 1 correspond to oxido-

reductive metabolism. The glucose consumption rate is partitioned between the oxidative and the reductive pathways as follows:

$$r_{G,ox} = \rho_{O_2/G}\, r_G \tag{78}$$

$$r_{G,red} = (1-\rho_{O_2/G}) r_G \tag{79}$$

with the glucose consumption rate estimated from the glucose supply rate at moderate dilution rate,

$$r_G \approx F_{liq,in}\, c_{G,in} \tag{80}$$

The heat flow rate is calculated from the oxidative and reductive contributions:

$$\Phi_r = Y_{Q/G,ox}\, r_{G,ox} + Y_{Q/G,red}\, r_{G,red} \tag{81}$$

Thus, noting the $Y_{Q/G,red} << Y_{Q/G,ox}$ and introducing Equation (80),

$$\Phi_r \approx \rho_{O_2/G}\, Y_{Q/G,ox}\, F_{liq,in}\, c_{G,in} \tag{82}$$

or in terms of yield,

$$Y_{Q/G} \approx \rho_{O_2/G}\, Y_{Q/G,ox} \tag{83}$$

Similarly, the other yields are expressed as a function of $\rho_{O_2/G}$ assuming a linear response of the metabolism between $\rho_{O_2/G} = 0$ and $\rho_{O_2/G} = 1$ (glycerol formation is neglected),

$$Y_{X/G} = \rho_{O_2/G}\, Y_{X/G,ox} + (1-\rho_{O_2/G}) Y_{X/G,red} \tag{84}$$

$$Y_{EtOH/G} = (1-\rho_{O_2/G}) Y_{EtOH/G,red} \tag{85}$$

$$Y_{CO_2/G} = \rho_{O_2/G}\, Y_{CO_2/G,ox} + (1-\rho_{O_2/G}) Y_{CO_2/G,red} \approx Y_{CO_2/G,ox} \approx Y_{CO_2/G,red} \tag{86}$$

and by definition,

$$Y_{O_2/G} = \rho_{O_2/G}\, Y_{O_2/G,ox} \tag{87}$$

This simple approach is illustrated in Figure 19 for a continuous culture of *K. marxianus*. The evolution of the biomass yield on glucose is linear for the whole range of oxygen limitation.

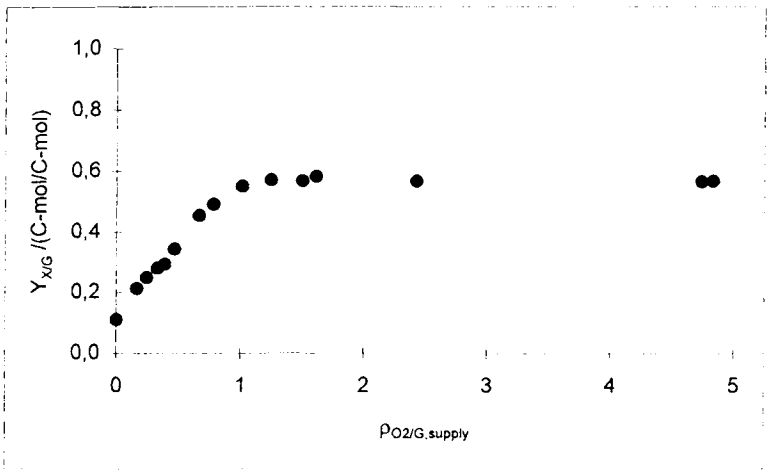

Figure 19: Variation of the yield of biomass on glucose as a function of $\rho_{O_2/G,supply}$ (ratio between oxygen transfer to glucose supply scaled by the glucose-limited yield) for the growth of *K. marxianus*. The culture is double limited by glucose and oxygen for $\rho_{O_2/G,supply} < 1$. Redrawn from Reference [68] with permission of the author and publisher.

8.2. Glucose and ammonium limitation

In comparison with oxygen, ammonium is absolutely required for growth if no other nitrogen source is available. In fact it is a non-substitutable nutrient for biosynthesis whereas oxygen is an electron acceptor that can be substituted by glucose (reduced to ethanol). If glucose conversion is not complete due to ammonium limitation, the restriction of ammonium supply compared to glucose uptake is expressed as:

$$\rho_{j/i} = \frac{c_{j,\text{in}}}{c_{i,\text{in}} - c_i} \frac{1}{Y_{j/i,i-\text{lim}}} \tag{88}$$

Four observations were made from experiments performed with *S. cerevisiae* and *K. marxianus* grown in continuous cultures on glucose with different ammonium feed concentration [39-41]:

- There is a domain of double limitation where both glucose and ammonium residual concentrations are very low (Figure 20).
- Biomass concentration is not proportional to the ammonium feed concentration. In fact, polysaccharides are accumulated under N-limitation [41].
- The fraction of glucose that is used for fueling reactions increases dramatically under nitrogen limitation [75]. This has a significant effect on the yield of heat produced per C-mol biomass (Figure 21 and Figure 22).
- Ethanol formation occurs at severe N limitation for *S. cerevisiae* and was not detected for *K. marxianus*. However, glucose conversion was not complete for *K. marxianus*. In fact, the oxidative capacity of *S. cerevisiae* is limited whereas that of *K. marxianus* is not. Therefore, the uncoupling increase is subjected to a maximal constraint in *S. cerevisiae*.

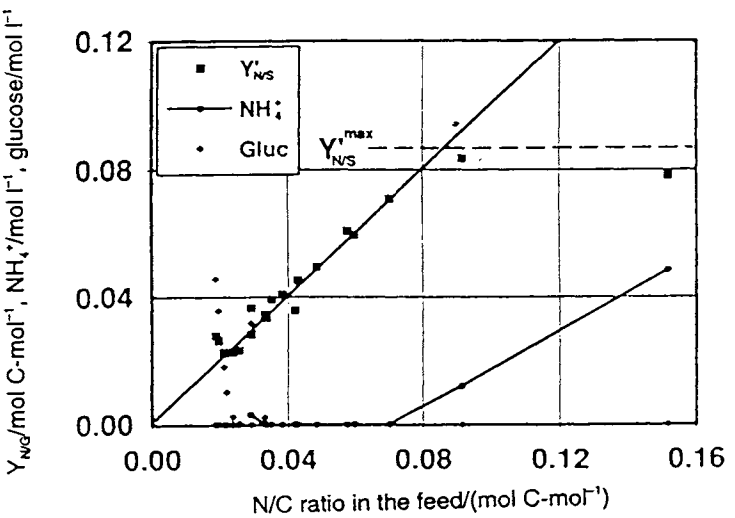

Figure 20: Residual glucose concentration, residual ammonium concentration and nitrogen yield on glucose as a function of the N/C ratio of the feed medium for *S. cerevisiae*. (Redrawn from Reference [40] with permission of the author and publisher).

It is thus clear that the increase in glucose consumption by the fueling reaction allowed a complete conversion of the glucose supply when growth was limited by the ammonium supply. The heat yield on biomass depicted in Figure 21 for *S. cerevisiae* illustrates the catabolic decoupling: the heat dissipation per C-mole biomass formed doubled as the ammonium supply was reduced by 50% of the minimum requirement to avoid a N-limitation. Then, the apparent heat yield on biomass decreased since a part of the glucose was metabolized reductively with ethanol formation (this reaction is almost athermic). A similar trend is found for *K. marxianus* as shown in Figure 22: the heat yield on biomass increased up to two times with decreasing ammonium supply.

In conclusion, calorimetric measurements are very sensitive to ammonium limitations since decoupling increases dramatically. In addition to decoupling, biomass composition changes showing the large flexibility of the metabolism to consume excess glucose. Changes in elemental composition correspond to storage carbohydrate accumulation. However, nitrogen-limited continuous cultures illustrate the non specificity of the heat flow rate measurements. The increase in heat production is due to a higher catabolic activity, not to a higher biosynthetic activity, which produces only a low amount of heat. This addresses the fundamental dilemma of calorimetry: measurements concern the flow of substrate that is dissipated, not the flow of substrate invested in biomass.

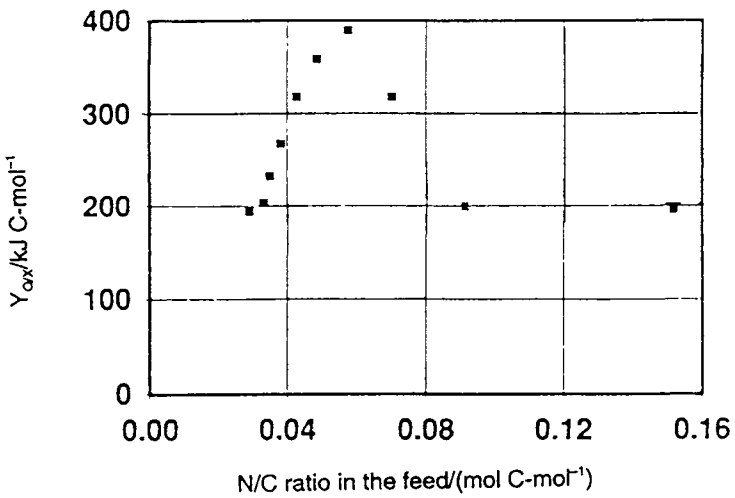

Figure 21: Heat yield on biomass as a function of the N/C ratio for *S. cerevisiae* feed medium. (Redrawn from Reference [40] with permission of the author and publisher).

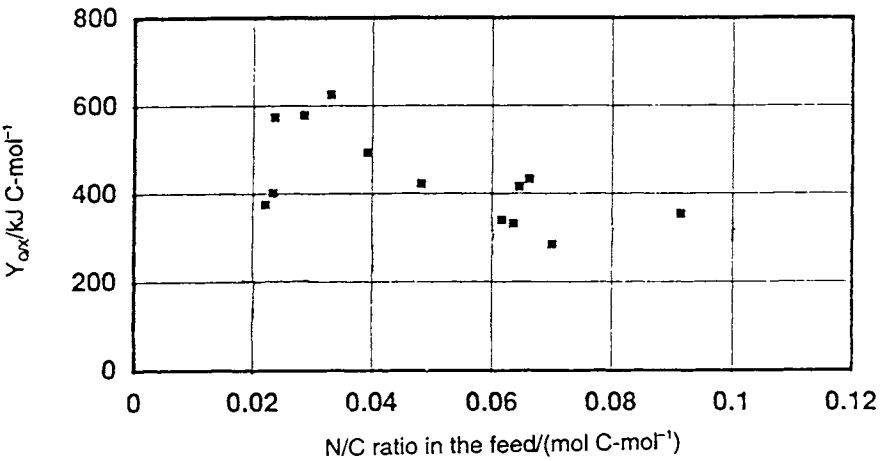

Figure 22: Heat yield on biomass as a function of the N/C ratio for *K. marxianus* feed medium. (Redrawn from Reference [39] with permission of the author and publisher).

9. MONITORING OF AEROBIC BIOPROCESSES BY CALORIMETRY

Calorimetric measurements are used in addition to other on-line measurements such as r_{O_2}, r_{CO_2}, pO_2 or pH evolution. The information is both qualitative, to detect physiological events, and quantitative.

9.1. Aerobic batch culture on glucose

An aerobic batch culture of *Saccharomyces cerevisiae* was performed on glucose with an initial substrate concentration of 20 g dm^{-3}. The profile of the on line measurements is shown in Figure 23. During the first oxido-reductive phase ①, a part of the glucose uptake is metabolized oxidatively, and the remaining glucose uptake is metabolized reductively. As a consequence, oxygen is consumed and at the same time ethanol is produced. The heat flow rate is low, and it can be estimated that the contribution of the reductive metabolism to the heat flow rate accounts for as much as that of the oxidative metabolism. The ethanol production rate stops as glucose is exhausted (②); the decrease in metabolic activity is clearly detectable on the heat production decrease. The small peak of activity indicated by ③ on the Figure 23 corresponds to rapid pyruvate exhaustion, and ethanol consumption starts almost immediately after glucose

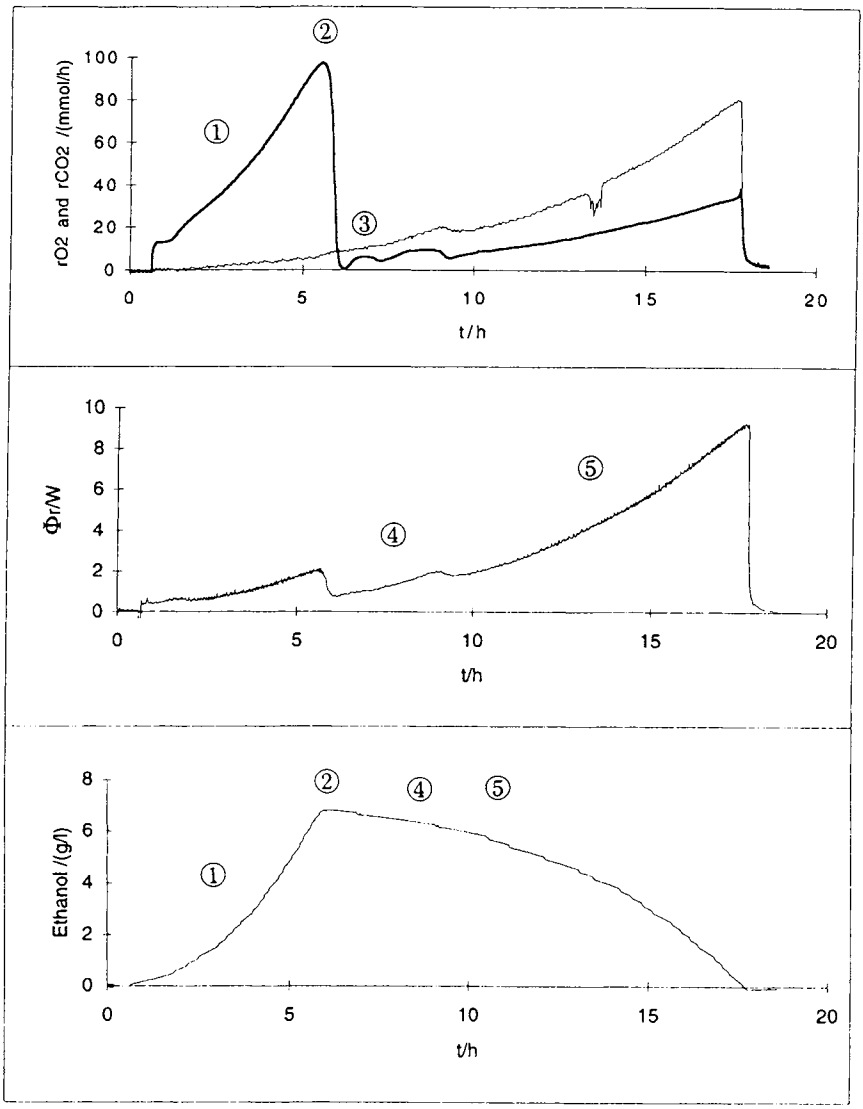

Figure 23: Aerobic batch culture of *S. cerevisiae* on glucose. ① = oxido-reductive metabolism on glucose; ② = glucose exhaustion; ③ = pyruvate consumption; ④ = consumption of ethanol and acetate; ⑤ = consumption of ethanol.

exhaustion during the phases ④ and ⑤. During the phase ④, acetic acid is also consumed which results in additional heat flow rate. During phase ⑤, ethanol is the only carbon source.

9.2. Glucose pulse

The dynamic response of *S. cerevisiae* and *C. utilis* grown in aerobic glucose continuous culture after a glucose pulse was investigated by van Kleeff et al. [20]. The oxidative metabolism of *C. utilis* was able to increase very rapidly in the presence of excess glucose (1 g dm^{-3}). The heat flow rate profile of this Crabtree negative yeast showed a sharp increase. Oxygen consumption and heat production decreased slowly once excess glucose was exhausted and the residual concentration had reached the steady state value. No by-product could be detected. By comparison, the behavior of *S. cerevisiae* was very different. The oxygen consumption rate increased slowly when the culture was subjected to an excess of glucose. Reductive metabolism set in and ethanol, as well as acetic acid, were detected in the broth. The heat flow rate reflects the metabolic adaptation to glucose oxido-reductive metabolism whereas it is undetectable with r_{CO_2}. The ethanol consumption phase as the excess glucose was exhausted was also clearly detectable by the heat signal.

9.3. Shift-up in dilution rate in aerobic continuous culture

The response of the culture to a dilution rate increase from 0.05 to 0.20 h^{-1} was an immediate increase of the glucose consumption rate so that the residual glucose concentration was always negligible (between 20 to 50 mg dm^{-3}, not shown) [24]. The time profile of the heat flow rate, Φ_r, shown in Figure 24 clearly indicates that the oxidative metabolism must have increased immediately after the shift since only the oxidative metabolism is significantly exothermic. However, it is surprising that the evolution of the oxygen consumption rate r_{O_2} is delayed as compared to the heat flow rate. The difference in the dynamic response between Φ_r and r_{O_2} is due to gas-liquid transfer and mixing dynamics. Oxygen measurements provide a slow indication of metabolic changes. The immediate increase in Φ_r shown in Figure 24 corresponds to the potential for immediate adaptation of the oxidative capacity, denoted $q_{O_2}^{jump}$. The response of the respiratory capacity (q_{O_2}) measured 10 min. after the shift-up is represented in Figure 25.

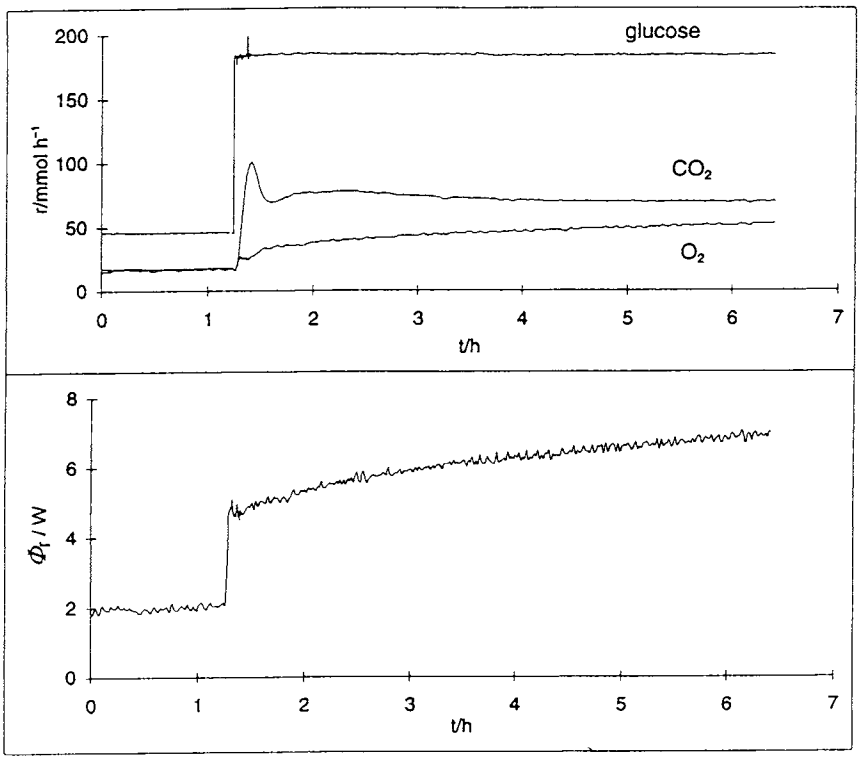

Figure 24: Profile of the on-line measurements (glucose uptake rate, CO_2 production rate, O_2 consumption rate, heat flow rate) after a shift-up in aerobic continuous culture of *S. cerevisiae* from 0.05 to 0.20 h^{-1} [24].

The jump of q_{O_2} was not sufficient to fully oxidize the glucose taken-up just after the shift-up. Thus reductive metabolism immediately set in as reflected by the large increase of r_{CO_2}, as compared to r_{O_2} (Figure 25), and the accumulation of ethanol in the broth (up to 1.82 g dm^{-3}). Figure 25 shows that the biomass concentration decreased from 10.5 to 8.2 g dm^{-3} due to the low biomass yield of the reductive pathway. The adaptation of the oxidative metabolism is shown on the q_{O_2} profile which reached a maximal value, $q_{O_2}^{max}$, within a couple of hours.

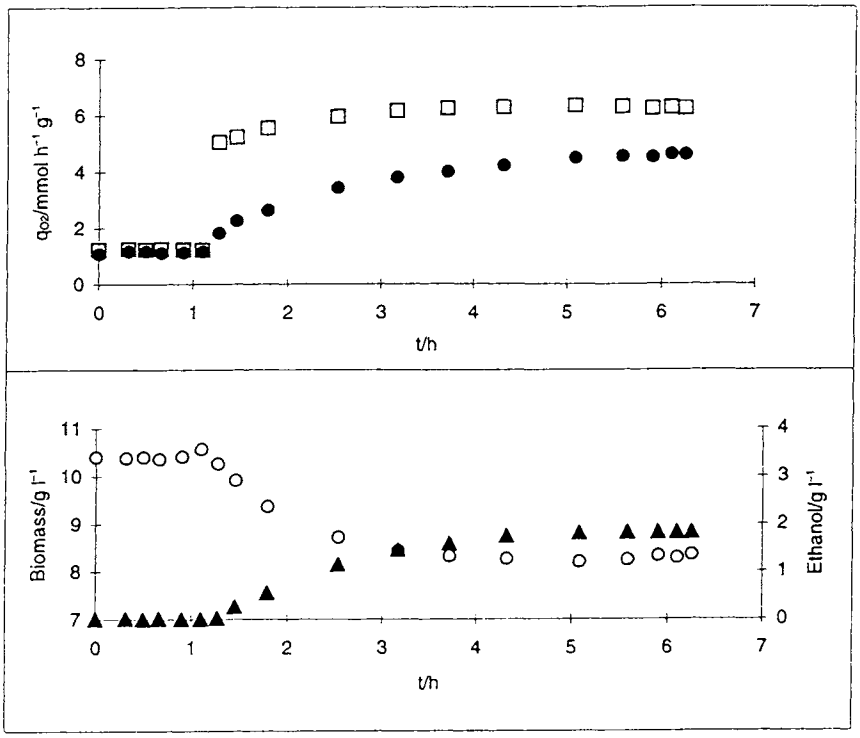

Figure 25: Shift-up in dilution rate in aerobic continuous culture of *S. cerevisiae*. D was increased from 0.05 to 0.20 h^{-1}. Evolution of the specific oxygen consumption rate (●), biomass concentration (○) and ethanol concentration (▲) [24]. The q_{O_2} needed to fully oxidize the specific glucose uptake is estimated as $q_G\, q_{O_2/G,ox}$ (□).

9.4. Cell cycle oscillations of *Saccharomyces cerevisiae*

Synchronized populations of *Saccharomyces cerevisiae* CBS 426 growing at a dilution rate of 0.10 h^{-1} are characterized by autonomous oscillations of process variables [53]: CER varied between 25 and 60 mmol h^{-1} and rapidly increased as the oxygen consumption rate increased from 25 to 55 mmol h^{-1} for a continuous culture grown at a dilution rate of 0.10 h^{-1}. High rates of gas exchange occurred during the S-phase when buds emerged. The heat flow rate was in the range 3.5 to 7 W. The dissolved oxygen concentration oscillated between 60 and 85% of air saturation. The increase in CER was also accompanied by a slow decrease (10%) in the biomass concentration which indicates that the culture was not at steady-state and that biomass accumulation (positive

or negative) was significant. As compared to the S phase, the biomass production rate was high during the G_2, M and G_1 phases and less glucose was oxidized, leading to low OUR, CER and heat flow rate (see Figure 14 and Figure 15).

Elemental analysis showed that the carbon and hydrogen mass fractions were constant over a single oscillation with average values of 42.68 ± 0.21 and 6.25 ± 0.15% respectively [53]. They did not show any systematic evolution with the position in the cell cycle. The average N mass fraction was 6.58 ± 0.32%. Since the reactor is not at steady state, the elemental and energy balances were calculated on cumulated quantities, i.e. the integral of the reaction rates. Recoveries of carbon, degree of reduction and of energy were determined to be respectively 102.5, 98.3 and 98.8% over one period of oscillation (Table 23).

10. MONITORING OF ANAEROBIC BIOPROCESSES BY CALORIMETRY

10.1. Anaerobic batch of *S. cerevisiae*

An anaerobic batch experiment with *S. cerevisiae* grown on glucose was performed in a bench scale calorimeter [24]. The nitrogen sparging rate was 0.6 dm^3 min^{-1} and the initial glucose concentration was 10 g dm^{-3}. The molar yields on glucose are indicated in Table 24.The amount of ethanol stripped accounted only for 3% of the initial glucose of this experiment because the nitrogen sparging rate was low (0.4 vvm) and the experiment was short (it lasted only 7 h). During this experiment, only 2.6% of the enthalpy contained in glucose was found as heat and 4.2% was found in gaseous ethanol. In addition, the heat used for ethanol vaporization was 0.6 kJ per C-mol of glucose, i.e. 5% of the heat flow rate. Additionally, this example shows that indirect estimation of the heat flow rate from product yield requires a precise determination of the ethanol production in the liquid and the gaseous phase. The heat yield on glucose is in good agreement with the value proposed by von Stockar and Birou [68]. In comparison with these results, Meier-Schneiders et al. [76] found a heat yield on glucose of about 18 kJ $C\text{-}mol^{-1}$.

10.2. Methanogens

The energy source of the archaebacterium *Methanobacterium thermoautotrophicum* is hydrogen and is supplied by the gaseous phase, as well as the

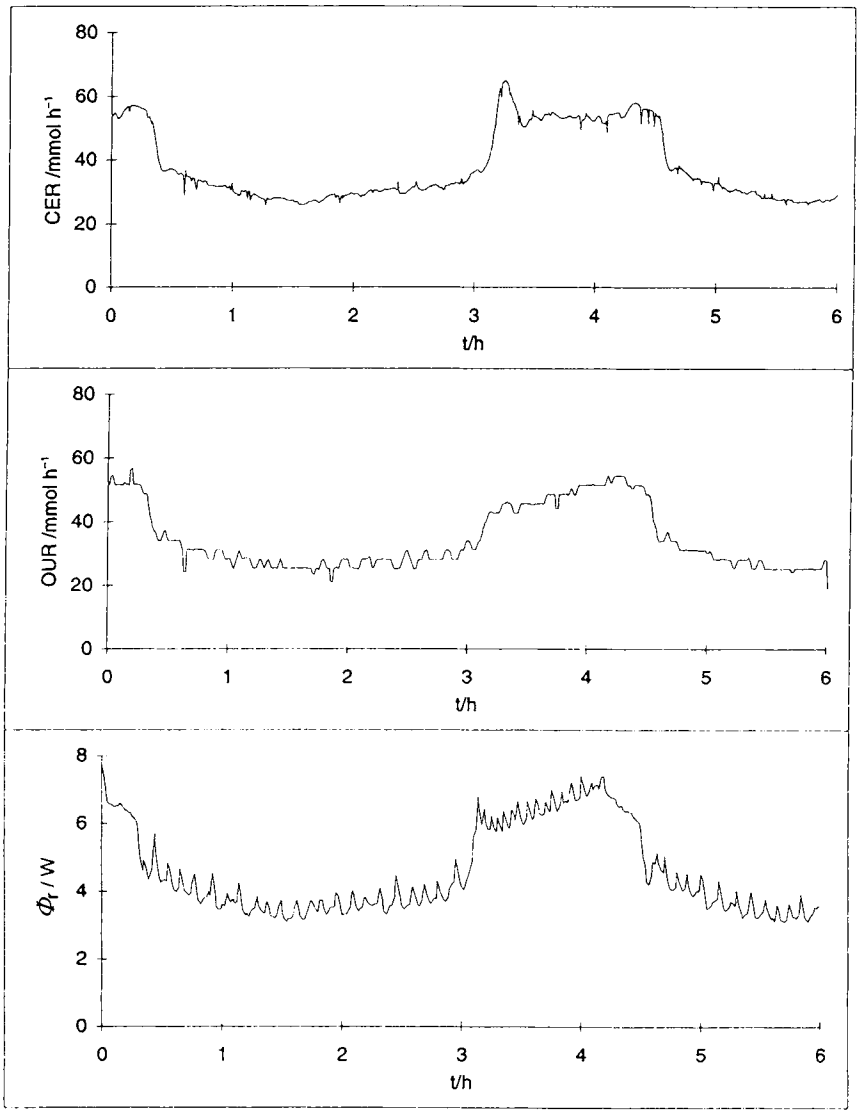

Figure 26: Profile of the heat flow rate (Φ_r), oxygen uptake rate and CO_2 production rate during cell cycle oscillations occurring at a dilution rate of 0.10 h^{-1}. (Redrawn from Reference [53] with permission of the author and publisher).

Table 23: Inputs and outputs during one oscillation period at a dilution rate of 0.10 h^{-1}. The number of available electrons per C-mol is +4 for glucose and acetic acid, –4 for oxygen, +4.13 for biomass, +6 for ethanol and zero for CO_2 and NaOH. The reference state for the enthalpy of combustion and the degree of reduction is CO_2, H_2O and NH_3. (Redrawn from Reference [53] with permission of the author and publisher).

Species	Carbon (C-mmol)	Available electrons (mmol)	Enthalpy (kJ)
Glucose	- 435.4	- 1741.6	- 204.2
Oxygen	0.0	+ 589.2	0.0
Biomass	273.8	1128.1	128.9
Ethanol	0.49	2.9	0.33
Acetic acid	0.4	1.6	0.17
CO_2	171.8	0.0	0.0
Heat	0.0	0.0	74.2
NaOH	0.0	0.0	- 1.9
Balance	+ 11.1	- 19.8	- 0.5
Recovery (%)	102.5	98.3	100

Table 24: Molar yields on glucose for anaerobic batch. Growth conditions: T_R = 30°C, N_2 flow rate = 0.6 dm^3 min^{-1}. Product yields are expressed in C-mol C-mol^{-1} and heat yield in kJ C-mol^{-1} [24].

Molar yield (C-mol C-mol^{-1})	
$Y_{X/G}$	0.138
$Y_{E/G}$	0.506
$Y_{CO_2/G}$	0.292
$Y_{GlOH/G}$	0.074
$Y_{HAc/G}$	0.017
$Y_{NaOH/G}$	0.019
Heat yield (in kJ C-mol^{-1})	
$Y_{Q/G}$	12 kJ C-mol^{-1}
Recoveries (mol mol^{-1} or J J^{-1})	
R_C	1.027
R_{dr}	1.007
R_Q	1.003

carbon source, CO_2. The gas-liquid transfer determines the biomass concentration, whereas the growth rate is determined independently of the carbon and energy sources supply by the dilution rate. It has been shown [35] that some nutrient provided by the liquid phase is exhausted once a certain amount of biomass has been formed. Often, iron or sulfide is the limiting substrate and stops growth. The growth stoichiometry reads:

$$-4H_2 - Y_{CO_2/H_2}CO_2 - Y_{NH_3/H_2}NH_3 + Y_{X/H_2}X + Y_{CH_4/H_2}CH_4 = 0 \qquad (89)$$

A typical experiment is shown in Figure 27: growth is exponential until one nutrient from the liquid phase (probably iron) is exhausted [77]. On-line monitoring by calorimetry is illustrated in Figure 28. The heat flow rate is parallel to the profiles of r_{H_2}, r_{CO_2} and r_{CH4}. It is important to note the high heat dissipation obtained during this anaerobic growth. The linearity between heat dissipation and electron exchange from the fueling reactions is depicted in Figure 29. It can be seen that 224.4 kJ are produced per mole of hydrogen consumed ($\gamma_{H_2} = 2$), which corresponds to -112.2 kJ per mol of electron. Therefore, calorimetric data is an important signal that can be used to monitor and control anaerobic bioprocesses in addition to the few available on line measurements: CO_2 in the off-gases, dissolved hydrogen.

11. CONTROL OF BIOPROCESSES BASED ON CALORIMETRIC MEASUREMENTS

11.1. Fed-batch of *S. cerevisiae*

Reductive metabolism sets in as soon as the glucose uptake exceeds the oxidative capacity of *S. cerevisiae*. Ethanol is formed and biomass yield decreases. It is therefore of interest to control the feed rate function of a fed-batch experiment in order to avoid ethanol formation. The heat flow rate measurement is sensitive to the onset of the reductive metabolism since the reductive enthalpy yield on glucose is much lower than the oxidative yield (12 versus 190 kJ C-mol^{-1} glucose).

11.1.1. Estimation of the respiratory quotient

Randolph et al. [78] developed a control strategy based on the estimation of the respiratory quotient of *S. cerevisiae* from heat flow rate measurements and r_{CO_2}. In fact, the oxygen consumption rate can be estimated from Φ_r and the oxycaloric quotient, Q_O, since almost all the heat released is due to the

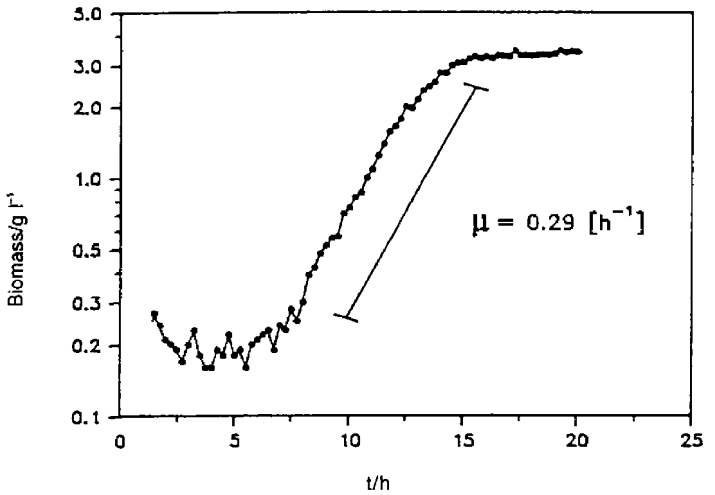

Figure 27: Biomass concentration during an anaerobic batch of *M. thermoautotrophicum* with hydrogen as energy source. (Redrawn from Reference [77] with permission of the author and publisher).

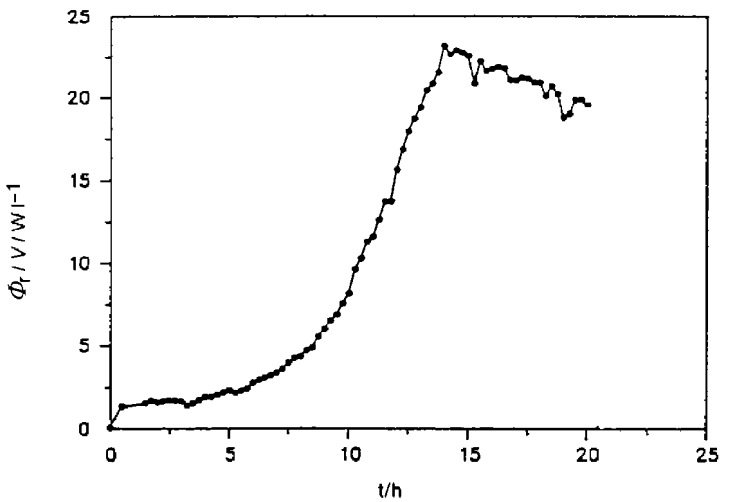

Figure 28: Heat flow rate during an anaerobic batch of *M. thermoautotrophicum* with hydrogen as energy source [77].

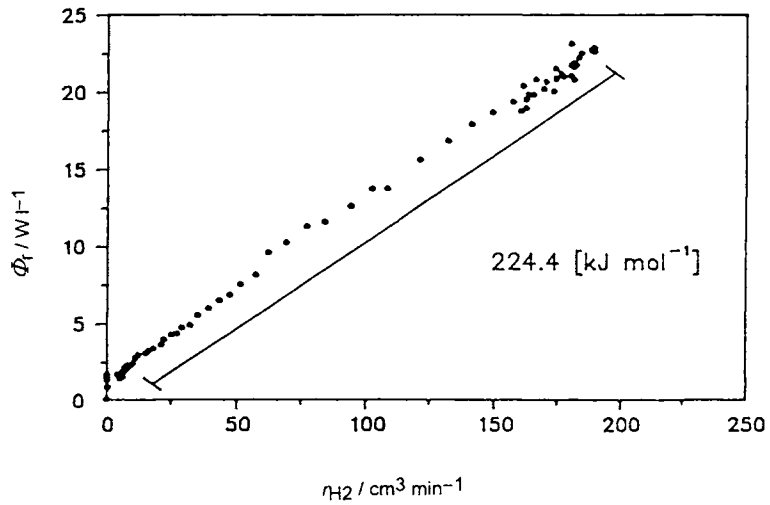

Figure 29: Linear relation between the heat produced and the amount of hydrogen consumed. Because the degree of reduction of hydrogen is 2, the slope is close to two time the oxycaloric quotient Q_O. (Redrawn from Reference [77] with permission of the author and publisher).

oxidative metabolism. First, an exponential feed trajectory was defined to increase the feed rate at a selected dilution rate. The feed rate was corrected by a proportional feed back controller to correct deviations from oxidative metabolism as detected by the *RQ* increase. The results are shown in Figure 30. The heat flow rate increased exponentially as expected and the respiratory quotient remained near its set-point value (Figure 31). Fluctuations in r_{CO_2} were decreased by reducing the controller gain.

11.1.2. Controlled glucose pulses

A more simple control strategy was proposed in reference [14] which consisted of pulsing 0.6 g of glucose to a culture of *S. cerevisiae* when glucose was depleted. In fact, the heat flow rate increased immediately after addition of a glucose pulse to a starving culture. Then, heat production decreased as glucose was exhausted once again. Addition of the next pulse was controlled by comparing the heat flow rate during the last 50 s to the heat flow rate during the previous 250 s. The medium pump was activated if the heat production

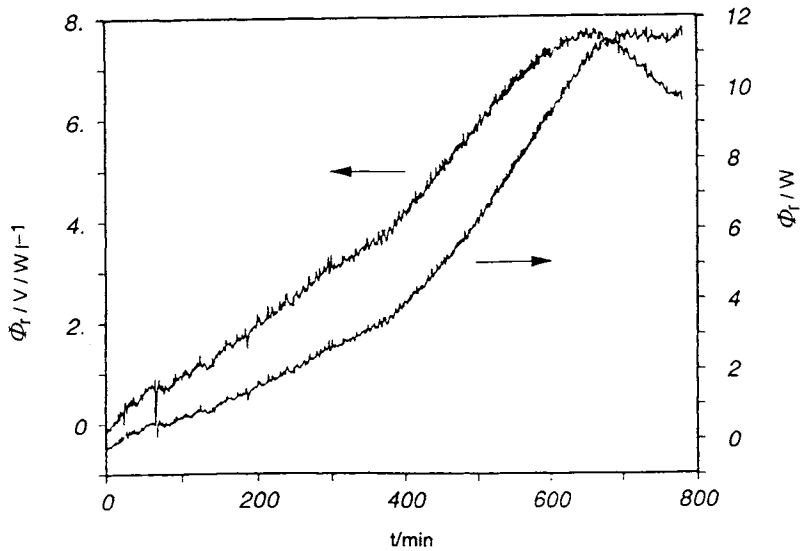

Figure 30: Heat flow rate and volumetric heat flow rate during controlled fed-batch cultivation. (Reproduced from Reference [78] with permission of the author and publisher).

decreased below a threshold value. The profile of the heat measurement is shown in Figure 32 with repeated sharp increases followed by a slow decrease. The control of the glucose addition resulted in a biomass yield increase of about 40% as compared to a batch experiment. However, ethanol formation could not be avoided by this simple control strategy.

11.1.3. Control based on RQ and heat flow rate measurements

Several control strategies were studied in reference [79] to correct the feed rate of a fed-batch cultivation subjected to a pulse of glucose (growth rate was about 0.15 h^{-1}). The pulse of glucose corresponding to a final concentration of 2 g dm^{-3} was similar to a large perturbation, and resulted in ethanol formation followed by ethanol consumption. A control strategy based on heat flow rate and *RQ* measurements gave a shorter duration of the disturbance as compared to a control strategy based only on heat flow rate, or only on *RQ* measurements. In fact, *RQ* measurements are very sensitive to the onset of reductive metabolism, but are slow. By comparison, heat measurements give a faster response to a change in the metabolic activity.

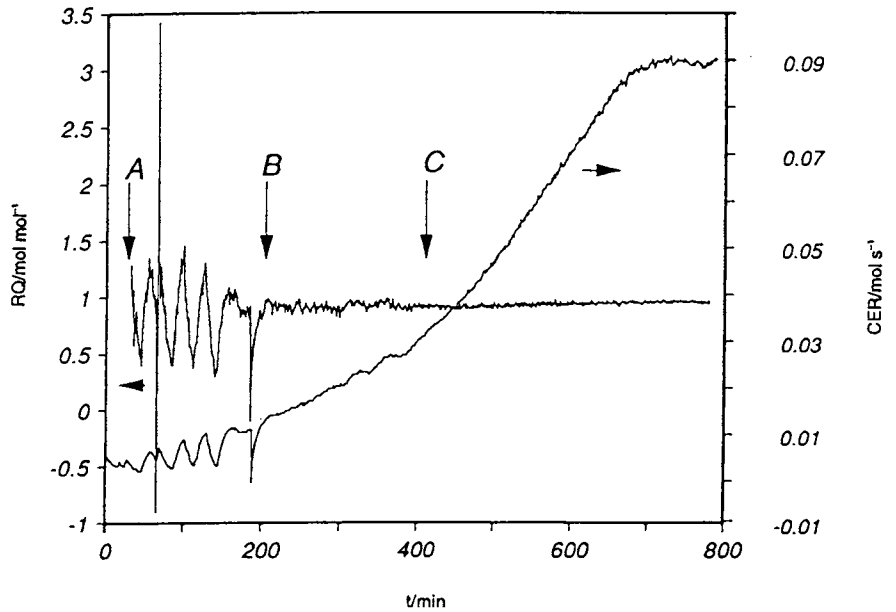

Figure 31: Estimation of the Respiratory Quotient from heat flow rate and CO_2 evolution rate during controlled fed-batch cultivation for different values of the controller gain. A, B, and C correspond to values of the controller gain of 1.23, 0.85 and 0.45, respectively. (Reproduced from Reference [78] with permission of the author and publisher).

11.2. Fed-batch culture for erythromycin production

Calorimetry has been applied by Menoud [80,81] to monitor and control fed-batch cultures of the filamentous bacteria *Saccharopolyspora erythraea* [82]. The objective was to use the heat flow rate as quantitative indicator of the exhaustion of one of the nutrients (ammonium ions or glucose). In fact, the low product yield (about 10-30 C-mmol per C-mol glucose) did not allow to calculate an indirect balance for a compound of degree of reduction of 5.03. A main prerequisite for monitoring filamentous cultures is to correct the power release signal for non-biological effects due to modification of the broth rheology. With the RC-1 calorimeter, the rheology of the broth affects i) the heat transmission coefficient *UA* through the glass wall, which must be known for

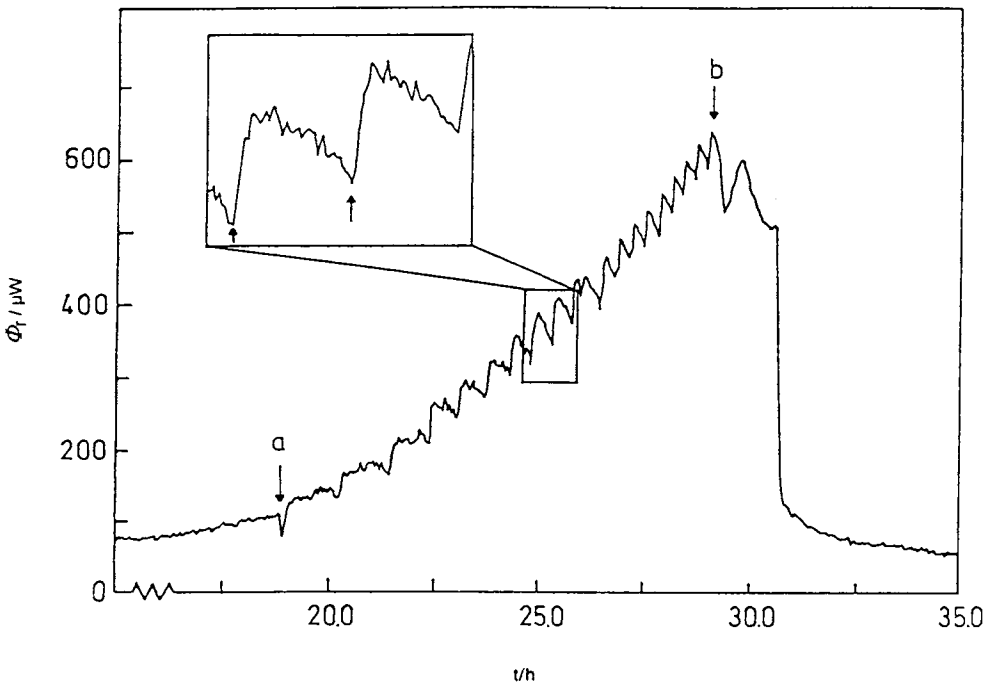

Figure 32: Heat flow rate during repeated glucose pulses to a culture of *S. cerevisiae*. (Reproduced from Reference [14] with permission of the author and publisher).

evaluating the measurement and ii) the thermal dissipation by the stirrer, which will be picked up by the calorimeter together with the biological signal.

Although $U \cdot A$ can in principle, be measured during the culture through calibration, this proved unnecessary because it remained virtually not affected by viscosity change. However, the power uptake by the agitator underwent important variations and thus was measured by a torque meter [80]. As can be seen from the example given in Figure 33, the torque drastically decreased 25 hours into the culture due to the appearance of foam, causing also a decrease in the Φ_r measurement (disturbance 1). At 65 h, an antifoam agent was added, causing disturbances no 2 and 3 in the thermogram.

When the calorimetric base-line was corrected for the power introduced by the stirrer, disturbances 1-3 disappeared (see Figure 34).

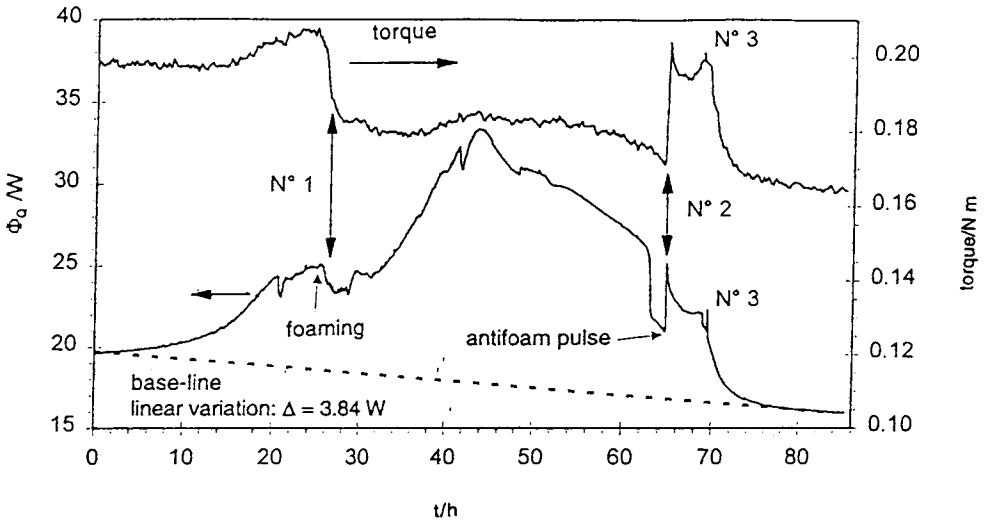

Figure 33: Heat dissipation rate (Φ_Q) and torque profile during batch culture of *Saccharopolyspora erythraea*. The heat flow rate measured with the calorimeter is affected by torque variation and a linear base-line correction due to reactor volume decrease (sampling). Numbers ① to ③ indicate disturbances due to torque variation as described in the text. (Redrawn from Reference [81] with permission of the author and publisher).

Figure 35 shows the thermogram of a typical culture of *S. erythraea* on a complex, industrial medium containing glucose (50 g dm^{-3}), ammonium sulfate (4.5 g dm^{-3}), and a complex extract of cotton-seed flower (30 g dm^{-3}). The thermal profile contains a set of characteristic features, found in a qualitatively similar way in all thermal profiles, and which could be used to identify particular events. At the time point labeled ⓪ , a characteristic decrease of 1.4 ± 0.14 W occurred for 45 min. which was probably due to the exhaustion of an unidentified substrate contained in the cottonseed flower extract. When the residual ammonium concentration became limiting, a characteristic peak of about 1 W followed by a period of high heat flow rate was systematically observed (see label ①). This is most probably due to the tendency of microbial energy metabolism to uncouple under energy sufficient conditions [42]. This intensive heat flow rate continued for about 2 hours until the ammonium ions

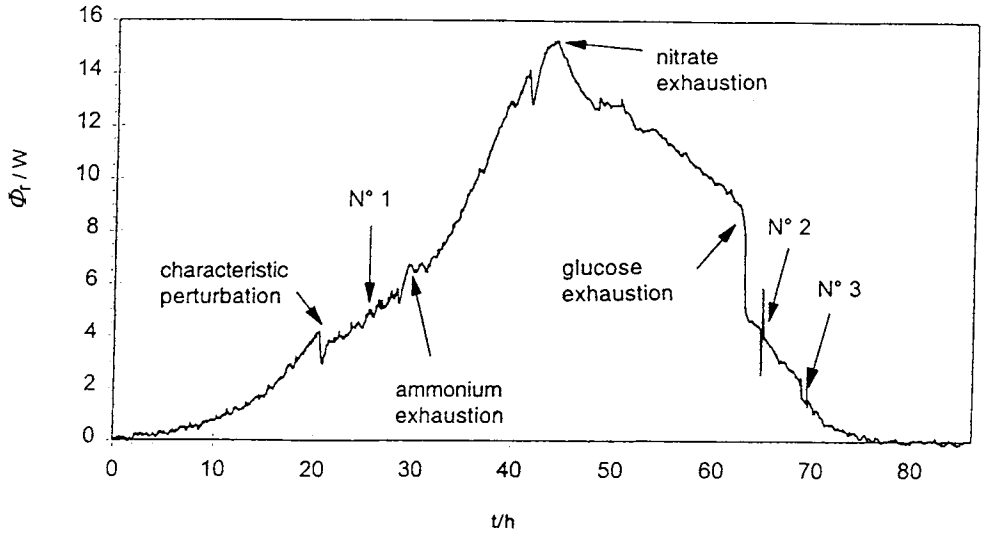

Figure 34: Heat flow rate of growth reaction (Φ_r) of a batch culture of *Saccharopolyspora erythraea* after correction for base-line variation and torque variation. In comparison with Figure 33, Φ_r represents the heat flow rate dissipated by the microorganisms. Metabolic changes due to ammonium, nitrate or glucose exhaustion are clearly detectable. (Redrawn from Reference [81] with permission of the author and publisher).

were completely exhausted (see Figure 35), after which the heat flow rate started gradually to decrease (②). After these events growth continued only slowly, growing on an unidentified nitrogen source in the cottonseed flour. Although some erythromycin was produced before the events ① and ②, the main production usually occurred after these and continued until glucose became exhausted and biosynthesis came to a halt. Glucose exhaustion was also revealed precisely by the thermal profile in the form of an almost instantaneous drop in heat flow rate, marked ③, after which the heat flow rate slowly decreased to the base line.

Repeating the experiment reported in Figure 35 at several initial ammonium ion concentrations showed that increasing the concentration of $(NH_4)_2SO_4$ from 1.75 to 8 g dm^{-3} leads a higher build-up of biomass and a clear decrease of the specific erythromycin productivity during the growth phase (before event ②).

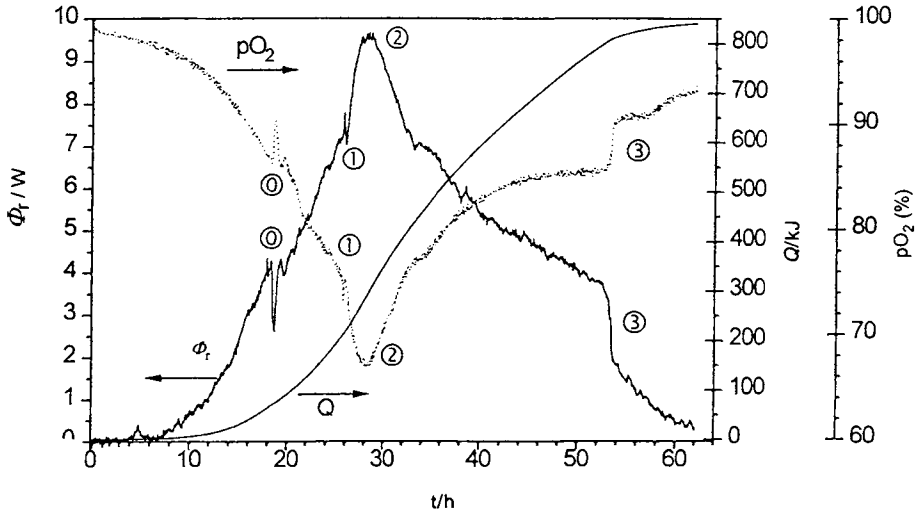

Figure 35: Heat flow rate, pO_2 and total heat released during a batch culture of *Saccharopolyspora erythraea* on glucose and ammonium (4.47 g dm^{-3} initial concentration). ⓪ and ① indicate two characteristic perturbations that were observed for all the experiments, ② indicates ammonium exhaustion and ③ glucose exhaustion. (Redrawn from Reference [81] with permission of the author and publisher).

As a result, the overall product yield decreased and the final concentration of erythromycin decreased from 900 to 423 mg dm^{-3}.

There would therefore be room for improvement by adding $(NH_4)_2SO_4$ in a fed-batch manner, with the aim of building up high cell densities, and yet keeping the ammonium ion concentration low at all times. The result of such a fed-batch culture is shown on Figure 36. It was started with an initial ammonium sulfate concentration of only 0.5 g dm^{-3} but with a high glucose concentration of 100 g dm^{-3}. The thermal power release indicated the on-set of growth and it went through the characteristic disturbance (⓪) observed in previous experiment. When it indicated ammonium ion limitation by going through the pronounced maximum labeled ①, the ammonium sulfate concentration was restored to 0.5 g dm^{-3} by automatic addition (Figure 36). A period of readjustment with low activity followed (③). Then, growth vigorously resumed and the heat flow rate went through the characteristic rapid peak (①) and the period of

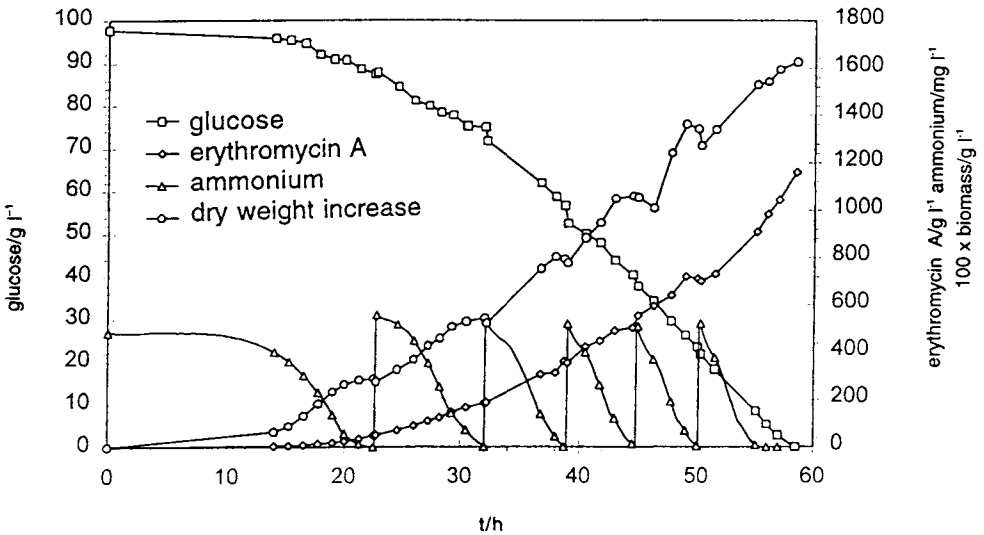

Figure 36: Controlled fed-batch culture of *Saccharopolyspora erythraea* by pulsing ammonium. Ammonium depletion was detected by the heat flow rate signal and was compensated for by an ammonium pulse. (Redrawn from Reference [81] with permission of the author and publisher).

intense heat production (①) indicating again imminent ammonia exhaustion. After 5 pulses leading to 5 similar cycles the exhaustion of glucose caused a rapid break-down of the heat flow rate by about 6 W, but the erythromycin can be seen to have reached a level of 1200 mg dm^{-3}. This concentration is not surprising in the view of the large amount of glucose processed, but the specific productivity was maintained at the high values typical for cultures with low ammonia content.

The same culture was used to investigate whether the biomass formed could be stimulated to continue producing antibiotics by feeding it with additional glucose. A total of 46.3 g dm^{-3} of additional glucose was delivered to the culture in 6 pulses, which were added each time the characteristic drop in the thermogram indicated exhaustion of glucose. As can be seen in Figure 37, the glucose pulses restored the heat flow rate to the state immediately before they drop, but the slow overall decline of the thermal activity typical for the production phase after nitrogen exhaustion could not be halted. Biomass concentration stayed constant at about 15 g dm^{-3} during these pulses, but the erythromycin concentration doubled to 2300 mg dm^{-3}. This type of extended fed-batch

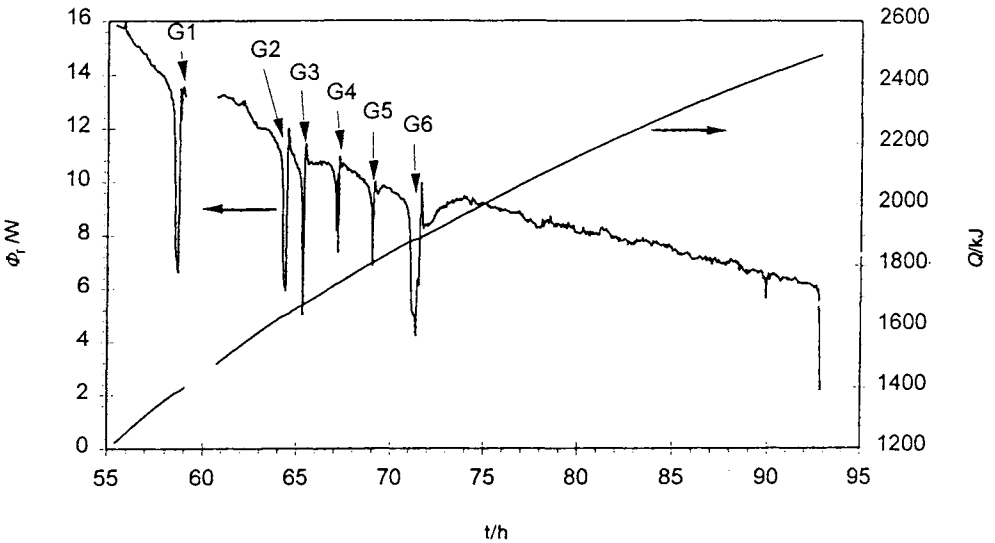

Figure 37: Heat flow rate and total heat released during controlled fed-batch culture of *Saccharopolyspora erythraea* by pulsing glucose after ammonium depletion of the culture shown in Figure 36. The depletion of glucose was easily detected by the sharp heat flow rate decrease immediately followed by the injection of a glucose pulse. (Redrawn from Reference [81] with permission of the author and publisher).

culture on glucose is expected to be especially attractive because of the catabolite repression and adverse rheology effects that would occur if all the glucose were present in the medium from the beginning.

11.3. Control of dilution rate increase in continuous culture

Continuous cultures subjected to a sudden increase in the dilution rate (shift-up) showed that the glucose uptake rate increased immediately to the new feeding rate, but that the oxygen consumption could not follow fast enough to ensure a completely oxidative metabolism. Thus, part of the glucose assimilated was degraded by the reductive metabolism, resulting in a temporary decrease of biomass concentration, even if the final dilution rate was below the critical dilution rate. The dynamic increase of the specific oxygen consumption rate, q_{O_2}, was characterized by an initial immediate jump followed by a first order in-

crease to the maximum value. It could be modeled using 3 parameters denoted $q_{O_2}^{jump}$, $q_{O_2}^{max}$, and a time constant τ_{ox} [83]. The values for the first two of the parameters varied considerably from one shift to another, even if they were performed under identical conditions.

Based on this model, a time-dependent feed flow rate function was derived that should permit an increase in the dilution rate from one value to another without provoking the appearance of reductive metabolism [83]. The idea was to increase the glucose supply in parallel with the dynamic increase of the oxidative capacity of the culture, so that all of the assimilated glucose could always be oxidized. Nevertheless, corresponding feed-profile experiments showed that deviations into the reductive metabolism could not be completely suppressed due to variability in the model parameters.

A nonlinear proportional controller was used to correct the feed profile. The controlled variable was the heat flow rate because it gives the fastest response to a metabolic switch. As for open-loop feed profile experiments, the profile feed rate was calculated with $q_{O_2}^{max}$ set to 5.8 mmol g^{-1} h^{-1}, τ_{ox} = 1.9 h and the initial respiratory potential $q_{O_2}^{jump}$ was identified by a short initial step-up (20 min). The controller gain α was 0.01 dm^3 h^{-1} W^{-1}. Other experiments with α equal to 0.03 and 0.04 dm^3 h^{-1} W^{-1} were also performed in order to study the effect of the controller gain.

From Figure 38 it is apparent that the heat flow rate was higher than the set-point during 1 h after the dilution rate increase so that there was no feed flow rate correction. Then, at t = 2.1 h, the controller activates because the heat flow rate became lower than the set-point. This is shown in Figure 38 where the feed rate decreased at this moment. Controller action confirms that the culture was forced to work at its highest specific O_2 consumption rate, but at the same time ethanol production was extremely low (Figure 39). Moreover, the heat flow rate measured was almost equal to its set-point value towards the end of the experiment resulting in little modification of the flow rate. As a consequence, feed rate increase was the fastest possible under the constraint of q_{O_2} adaptation.

Biomass concentration remained almost constant throughout the entire experiment and the maximum ethanol concentration observed was 490 mg dm^{-3} (Figure 39). This is a considerable improvement as compared with shift-up experiments where ethanol concentration reached 1.82 g dm^{-3} and biomass concentration decreased from 10.5 to 8.2 g dm^{-3} for the same final dilution rate. As further evidence that the maximal specific O_2 consumption rate was reached at

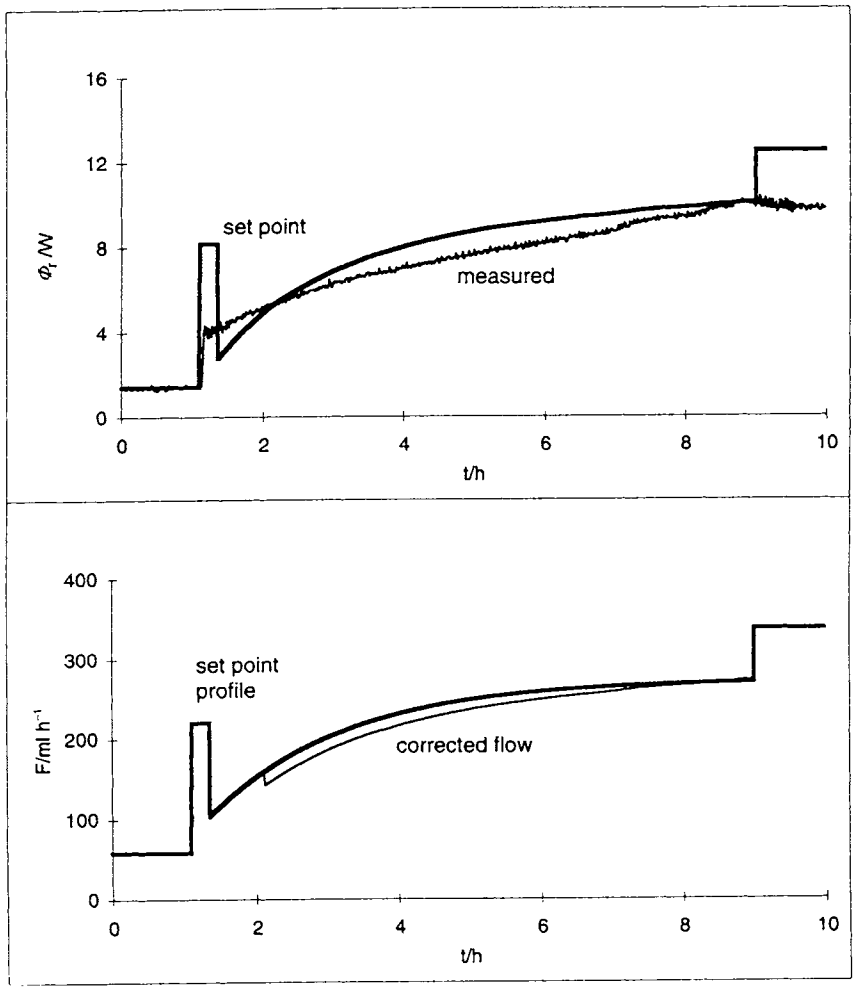

Figure 38: Feedback control experiment of continuous culture of *Saccharomyces cerevisiae* aimed at controlling the dilution rate increase. The feed flow rate was corrected when the heat flow rate was lower than the set-point value (at t = 2.1 h). Correction stops towards the end of the experiment. A further dilution rate shift was imposed at the end of the experiment to check that the oxidative capacity was at its maximal value (second arrow). (Redrawn from Reference [83] with permission of the author and publisher).

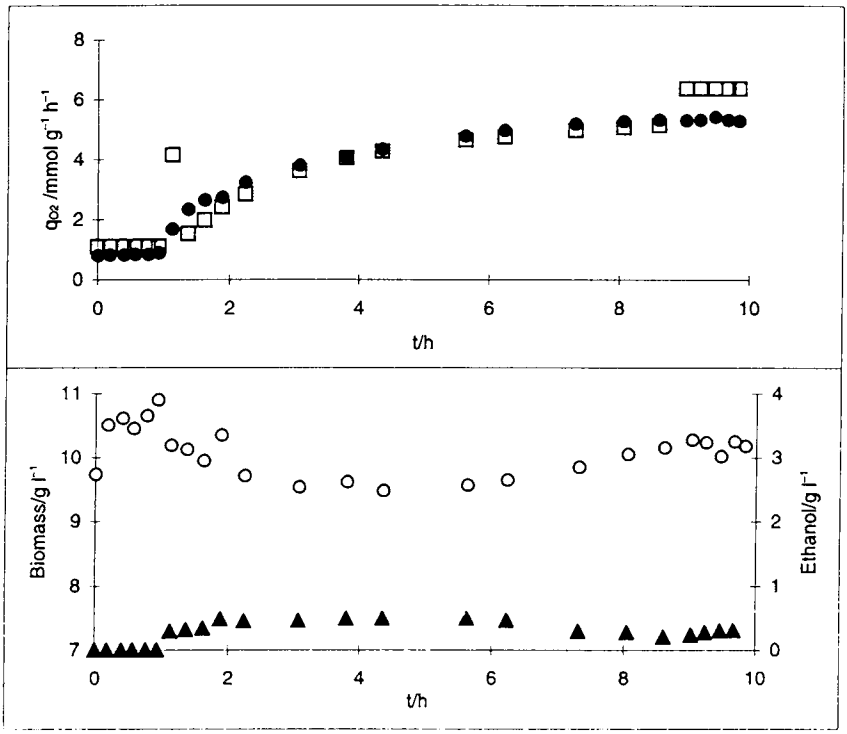

Figure 39: Feedback control experiment of continuous culture of *Saccharomyces cerevisiae*. The experimental q_{O_2} (●) is compared to the value needed to fully oxidize the glucose supply ($q_G Y_{O_2/G,ox}$, □). The very small difference results in low ethanol (▲) accumulation and a low biomass concentration (○) decrease. The shift occurred at 1.2 h, and a second shift was performed at 9 h to check that q_{O_2} was saturated. (Redrawn from Reference [83] with permission of the author and publisher).

the end of the profile, the reactor was subjected to a second shift in dilution rate to 0.4 h^{-1} at $t = 9$ h. No further increase in the specific oxygen consumption rate occurred, but ethanol was produced as expected (Figure 38 and Figure 39).

However, it was not expected that the heat flow rate would be higher than the set-point during the first hour after the dilution rate increase. Also, biomass concentration was not supposed to slightly decrease (from 10.5 to 9.5 g dm^{-3}) in the absence of significant ethanol production or glucose accumulation. Similarly, the prediction underestimated other on-line measurements (r_{O_2}, r_{CO_2}) at the

beginning of the experiments. Since no other substrate is available, this can only be explained by a decrease in biomass yield of the oxidative metabolism during the transition without ethanol formation; it appears that respiration (glucose combustion) uncouples slightly just after the shift as compared to steady state [19]. Since the elemental balances are correct, the slight biomass decrease must be due to higher catabolism rather than reductive metabolism, thus not violating our objective. Higher catabolism is equivalent to oxidative spilling of substrate, not overflow towards reductive pathways. It leads to a higher heat yield on substrate, and conversely a lower biomass yield.

The choice of a controller gain α equal to 0.03 or 0.04 l h^{-1} W^{-1} gave good results. Ethanol concentration varied between 0.10 and 0.55 g dm^{-3} for a final dilution rate close to 0.20 h^{-1}. The controller action always resumed towards the end of the experiments. Note that the initial step used to determine experimentally $q_{O_2}^{jump}$ contributes, to a large extent, to the ethanol formation, but is necessary to ensure a fast enough increase in the feed rate.

12. CONCLUSIONS

Calorimetry has been successfully applied to bioreactor monitoring and to bioprocess control. Because heat production rate is associated with the growth of most of the organisms, direct calorimetry is based on the quantification of the heat flow rate that has to be removed from the reactor to keep the system at a constant temperature. Under the condition of well controlled environment, the measurement of the heat flow rate removed is not only a qualitative indicator but a quantitative measure of the biological activity.

Due to the relative sophistication of the biocalorimeters, such reactors can be considered as High Performance Bio-Reactors, and allow to check for the enthalpy balance in addition to the carbon and degree of reduction balances. In order to calculate correctly the balances, there now available a large set of data concerning elemental composition and enthalpy of combustion of biomass for various growth conditions.

Direct calorimetry gives insight in the thermodynamics of growth. Although Gibbs energy dissipation, which is the fundamental thermodynamic variable to determine, can not be directly measured, the difference with enthalpy production, which is determined by direct calorimetry, is small for aerobic processes, or can be calculated for anaerobic processes.

Further developments of the equipment are required for applications to weakly exothermic organisms (animal cells for example), to improve the long

term stability, and to reduce the price of the bio-calorimeters which can limit the application of this technique. More fundamentally, the field of cellular energetics and bioenergetics remains open.

REFERENCES

1. B. Birou, I. Marison and U. von Stockar, Biotechnol. Bioeng., 30 (1987) 650.
2. M. Meier-Schneiders, W. Weikmann, U. Grosshans, C. Busch and A. Steinbüchel, Can. J. Microbiol., 14 (1995) 267.
3. L. Auberson, T. Kanbier and U. von Stockar, J. Biotechnol., 29 (1993) 295.
4. C. Larsson, A. Blomberg and L. Gustafsson, Biotechnol. Bioeng., (1990)
5. J.J Heijnen and J.A. van Dijken, Biotechnol. Bioeng., 39 (1992) 833.
6. U. von Stockar, E. Gnaiger, L. Gustafsson, C. Larsson, I. Marison and P. Tissot, Biochim. Biophys. Acta, 1183 (1993) 221.
7. E. Gnaiger, Pure Appl. Chem., 65 (1993) 1983.
8. E.H. Battley, Energetics of Microbial Growth. Wiley Interscience, New York, 1987.
9. U. von Stockar and I. Marison, Adv. Biochem. Eng./Biotechnol., 40 (1989) 93.
10. U. von Stockar and I. Marison, Thermochim. Acta, 193 (1991) 215.
11. Y. Ishikawa, M. Shoda and H. Maruyama, Biotechnol. Bioeng., 23 (1981) 2629.
12. Y. Ishikawa and M. Shoda, Biotechnol. Bioeng., 25 (1983) 1817.
13. Y. Ishikawa, Y. Nonoyama and M. Shoda, Biotechnol. Bioeng., 23 (1981) 2825.
14. C. Larsson, G. Lidén, C. Niklasson, L. Gustafsson, Bioproc. Eng. 7 (1991) 151.
15. B. Heinritz, in R.B. Kemp (Ed.), Biological Calorimetry. Themochim. Acta, 172 (1990).
16. I.G. Minkevich, F. Baumann, G. Rogge and B. Heinritz, Acta Biotechnol., 9 (1989) 435.
17. B. Volesky, J.H.T Luong and K.V. Thambimuthu, Can. J. Chem. Eng., 56 (1978) 526.
18. C.L. Cooney, D.I.C. Wang and R.I. Mateles, Biotechnol. Bioeng., 11 (1968) 269.

19. B.H.A. van Kleeff, J.G. Kuenen and J.J. Heijnen, Biotechnol. Bioeng., 41 (1993) 541.
20. B.H.A. van Kleeff, J.G. Kuenen and J.J. Heijnen, Biotechnol. Prog., 12 (1996) 510.
21. A. Lavoisier and P. de Laplace, Histoire de l'Académie des Sciences, (1780) 355.
22. P. de Vallière, State and Parameter Estimation in Batch Reactors for the Purpose of Inferring On-line the rate of Heat Production, PhD. Thesis, ETH Zürich, 1989.
23. D. Bonvin, P. de Vallière and D. Rippin, Comp. Chem. Engineering, 13 (1989) 1.
24. P. Duboc, Transient Growth of *Saccharomyces cerevisiae*, a Quantitative Approach, Ph.D. Thesis, EPF Lausanne, 1997.
25 L.G. Karlsen and J. Villadsen, Chem. Eng. Sci., 42 (1987) 1165.
26. M. Meier-Schneiders, F. Schäfer, U. Grosshans and C. Busch, Thermochim. Acta, 251 (1995) 85.
27. M.S. Kharasch and B. Sher, J. Phys. Chem., 29 (1925) 625.
28. P. Duboc, N. Schill, L. Menoud, W. van Gulik and U. von Stockar, J. Biotechnol., 43 (1995) 145.
29. J.A. Roels, Energetics and Kinetics in Biotechnology, Elsevier Biomedical Press, Amsterdam, 1983, p. 25.
30. S.I. Sandler and H. Orbey, Biotechnol. Bioeng., 38 (1991) 697.
31. J. Nielsen and J. Villadsen, Bioreaction Engineering Principles, Plenum Press, New York, 1994, p. 38.
32. P. Duboc and U. von Stockar, Themochim. Acta, 251 (1995a) 119.
33. P. Duboc and U. von Stockar, Themochim. Acta, 251 (1995b) 131.
34. T. Gurakan, I. Marison, U. von Stockar, L. Gustafsson and E. Gnaiger, Thermochim. Acta, 172 (1990) 251
35. N. Schill, Continuous Cultures of *Methanobacterium thermoautotrophicum*: Thermodynamic Analysis, Growth Physiology and Modeling, Ph.D. Thesis, EPF Lausanne, 1996.
36. J.S. Harrison, in D.J.D. Hockenhull (Ed.), Progress in Industrial Microbiology, Vol. 10, Churchill Livingstone, London, 1971, p. 129.
37. C. Larsson, P. Duboc, T. Gurakan, R.M. Buccino, I. Marison and U. von Stockar, J. Biotechnol., (1997), submitted.
38. P. Duboc, T. Gurakan, R.M. Buccino, I. Marison and U. von Stockar, J. Biotechnol., (1997), submitted.
39. M. Cooney, I. Marison, W. van Gulik and U. von Stockar, Appl. Microb. Biotechnol., 44 (1996) 643.

40. C. Larsson, U. von Stockar, I. Marison and L. Gustafsson, J. Bacteriol., 175 (1993) 4809.
41. U. Schulze, Anaerobic Physiology of *Saccharomyces cerevisiae*, Ph.D. Thesis, Technical University of Denmark. 1995.
42. U. von Stockar, C. Larsson, I. Marison and M. Cooney, Thermochim. Acta, 250 (1995) 247.
43. DIN 51 900, Beuth Verlag, Berlin, 1979.
44. NF M 03-005, AFNOR, Paris, 1982.
45. W.M. Thornton, Philos. Mag., 33 (1917) 196.
46. M.S. Kharasch, Bur. Stand. J. Res., 2 (1929) 359.
47. J.L. Cordier, B. Butsch, B. Birou and U. von Stockar, Appl. Microbiol. Biotechnol., 25 (1987) 305.
48. U. von Stockar, C. Larsson and I. Marison, Pure Appl. Chem., 65 (1993) 1889.
49. T.T.J.M. van der Heijden, J.J. Heijnen, C. Hellinga, B. Romein and K.Ch.A.M. Luyben, Biotechnol. Bioeng., 43 (1994) 3.
50. T.T.J.M. van der Heijden, J.J. Heijnen, C. Hellinga, B. Romein and K.Ch.A.M. Luyben, Biotechnol. Bioeng., 43 (1994) 11.
51. N.S. Wang and G. Stephanopoulos, Biotechnol. Bioeng., 25 (1983) 2177.
52. S. Okabe, P.H. Nielsen and W.G. Characklis, Biotechnol. Bioeng, 40 (1992) 725.
53. P. Duboc, I. Marison and U. von Stockar, J. Biotechnol., 51 (1996) 57.
54. C. Chen and K. McDonald, Biotechnol. Bioeng., 36 (1990) 28.
55. S.J. Pirt, Proc. Roy. Soc. London, 163B (1965) 224.
56. A.H Stouthamer, Ant. van Leeuwenhoek, 39 (1973) 545.
57. A.H. Stouthamer and H.W. van Verseveld, in M. Moo-Young, (Ed.), Comprehensive Biotechnology, Plenum Press, Oxford, 1985.
58. D.W. Tempest and O.M. Neijssel, Ann. Rev. Microbiol., 38 (1984) 459.
59. C. Verduyn, E. Postma, W.A. Scheffers and J.P van Dijken, J. Gen. Microbiol. 136 (1990) 405.
60. E. Albers, C. Larsson, G. Liden, C. Niklasson and L. Gustafsson, Appl. Env. Microbiol., 62 (1996) 3187.
61. W. van Gulik and J.J. Heijnen, Biotechnol. Bioeng., 48 (1995) 681.
62. P.A. Vanrolleghem, P. de Jong-Gubbels, W. van Gulik, J.T. Pronk, J.P. van Dijken and S. Heijnen, Biotechnol. Prog., 12 (1996) 434.
63. E. Schrödinger, What is Life ? The physical aspect of the living cell, Cambridge University Press, Cambridge, 1944.
64. J.J. Heijnen, M.C.M. van Loosdrecht and L. Tijhuis, Biotechnol. Bioeng., 40 (1992) 1139.

65. U. von Stockar and I. Marison, Thermochim. Acta, 229 (1993) 157.
66. J. Dekkers, H. De Kok and J.A. Roels, Biotechnol. Bioeng., 23 (1981) 1023.
67. L. Auberson and U. von Stockar, Biotechnol. Bioeng., 40 (1992) 1243.
68. U. von Stockar and B. Birou, Biotechnol. Bioeng., 34 (1989) 86.
69. J.P. Barford and R.J. Hall. Biotechnol. Bioeng., 23 (1981) 1735.
70. U. von Stockar and L. Auberson, J. Biotechnol., 22 (1992) 69.
71. B. Birou, Etude de la Chaleur Degagée par des Cultures Microbiennes dans un Fermenteur de Laboratoire, Ph.D. Thesis, EPF Lausanne, 1986.
72. U. von Stockar and L. Auberson, J. Biotechnol., 22 (1992) 69.
73. N. Schill, W. van Gulik, D. Voisard and U. von Stockar, Biotechnol. Bioeng., 51 (1996) 645.
74. L. Auberson, Calorimetry and Metabolic Switches in the Bottleneck Metabolism of *Saccharomyces cerevisiae*, Ph.D. Thesis, EPF Lausanne, 1990.
75. C. Larsson, U. von Stockar, I. Marison and L. Gustafsson, Thermochim. Acta, 251 (1995) 99.
76. M. Meier-Schneiders, U. Grosshans, C. Busch and G. Eigenberger, Appl. Microbiol. Biotechnol., 43 (1995) 431.
77. E. Gerhard, Optimisation et étude calorimétrique de cultures de *Methanobacterium thermoautotrophicum*, Ph.D. Thesis, EPF Lausanne, 1991.
78. T. Randolph, I. Marison, D. Martens and U. von Stockar, Biotechnol. Bioeng., 36 (1990) 678.
79. B.H.A van Kleeff, Heat Flow Measurements for the Study and Control of Biotechnological Processes, Ph.D. Thesis, pp. 99-119, Technische Universiteit Delft, 1996.
80. L. Menoud, I.W. Marison and U. von Stockar, Thermochim. Acta, 251 (1995) 79.
81. L. Menoud, Developpement de l'utilisation de la calorimétrie à flux de chaleur pour le suivi et le controle en ligne de bioprocédés: application à la production de l'antibiotique érythromycine par la bactérie filamenteuse *Saccharopolyspora erythraea,* Ph.D. Thesis, EPF Lausanne, 1996.
82. U. von Stockar, P. Duboc, L. Menoud and I. Marison, Thermochim. Acta 300 (1997), in press.
83. P. Duboc, L. Casão-Pereira and U. von Stockar, Biotechnol. Bioeng., (1997), in press.

This Page Intentionally Left Blank

Handbook of Thermal Analysis and Calorimetry. Vol. 4: From Macromolecules to Man.
R.B. Kemp, editor.

Chapter 7

CALORIMETRY OF MICROBIAL PROCESSES

Christer Larsson and Lena Gustafsson

General and Marine Microbiology, Lundberg Laboratory, Göteborg University, Medicinaregatan 9C, 5-41390 Göteborg, Sweden

1. BACKGROUND

Microbial processes can be monitored and quantified by means of calorimetric measurements [1-15]. Even though life processes are extremely complex, and may be composed of thousands of individual metabolic reactions, data obtained by calorimetry can be interpreted because the net metabolic process can be described and thermodynamically treated as a rather simple physico-chemical reaction [2,4, 12, 15].

What is measured by calorimetry is the sum of the net heat change resulting from the biological process (Q_{met}; see Figure 1) and from physico-chemical side-reactions. Microbial processes can usually be considered to take place at constant temperature and pressure. Under such conditions, the net heat change is equal to the enthalpy change [12].

The continuous net energy change (or more specifically, enthalpy change) is equal to the sum of the enthalpy change of all the reactions that occur per unit of time during, for example, microbial growth and may therefore be used in continuous monitoring of growth processes. Enthalpy change determinations can also be used in quantitative descriptions of microbial processes and enable determinations of the energy exchange between living matter and its environment and for elucidating mechanisms about bioenergetics and biological growth efficiency [2, 16-18].

The great advantage of calorimetric measurements for biological studies is that the technique is completely non-specific but it is also completely universal. This assumption is based on the fact that more or less all the biological reactions are connected to the enthalpy changes and, consequently, any biological activity can be measured calorimetrically. The drawback, which also lies in the non-

specificity, is that a calorimetric measurement does not give the origin of the enthalpy change in terms of a specific reaction. It is therefore important to combine heat measurements with other methods.

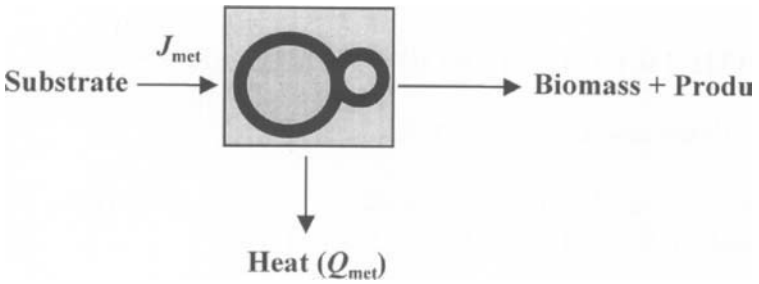

Figure 1. Open system exchanging matter and energy with its environment. The system is represented by a microorganism, metabolising at a flux of J_{met}. The total heat production of the bioprocess is Q_{met}.

The advantage of combining measurements will be illustrated in the following *example.* In order to study the complete microbial energy conversion from substrates to products at steady state conditions in response to the environmental conditions, a chemostat study with the yeast *Saccharomyces cerevisiae* was performed [19]. The microorganisms were grown in defined medium with glucose as the only carbon and energy source and an ammonium salt as the nitrogen source. Glucose was used as the limiting substrate and the range of dilution rates was 0.08 to 0.22 h^{-1} (Figure 2). At steady state, all metabolic flow rates as well as the chemical composition of the biomass should be constant. Consequently, also the enthalpy change should be constant at each particular steady state. The enthalpy change was measured calorimetrically as the heat change by a multichannel microcalorimeter (Bioactivity Monitor LKB 2277, Thermometric AB, Järfälla, Sweden) of the heat conduction type [20].

The flow-through mode of the microcalorimeter was used by pumping a flow of the culture-liquid from the fermenter, mixed with a flow of humidified air, through the measuring vessel of the microcalorimeter. In the flow-through mode, the measuring cell is a gold spiral with an inner volume of about 0.7 ml. The effective volume has to be determined, since it is dependent on the flow rate.

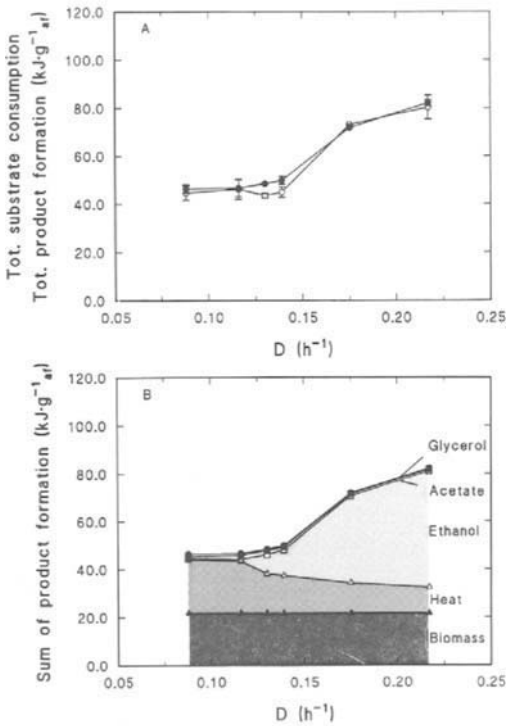

Figure 2. (A) Total substrate consumption (O) and total product formation (●), expressed in energy units per unit of ash-free (*af*) biomass produced, versus dilution rate (D) during steady state growth of *S. cerevisae* in a chemostat and in defined medium. The area defined by the non-overlapping regions of the substrate consumption and product formation curves describes the imbalance in energy recovery. (B) Sum of product formation during growth of *S. cerevisiae* in defined medium. Symbols: ▲ , biomass; Δ , plus heat; □ , plus ethanol; ■ ,plus acetate; ● , plus total (intracellular and extracellular) glycerol. Reproduced with permission from reference [19] copyright © American Society for Microbiology.

In the ideal case, all heat evolved in the measuring cell should be transferred to the surrounding heat sink. However, because this transfer is not perfect, the losses have to be corrected by calibration. Although electrical tests can easily be performed on a regular basis by an external located (relative to the flow vessel) resistance, there must also be internal calibration. In this case a

chemical mixture providing an almost constant and known rate of heat production is pumped through the measuring cell, for which the exact effective volume can be calculated [21].

The advantage of this type of calorimeter is the sensitivity of the instrument. The drawback, however, may be that the heat change is measured not directly in the fermentor, but in an external loop. This may mean that the culture conditions are not exactly the same as in the fermenter, especially when the fermenter is used as a chemostat, which means that one substrate component is limiting. During the time delay caused by the transport of the culture fluid between the fermenter and the measuring cell, the concentration of the limiting substrate may be decreased to a level which causes a changed metabolism of the microorganisms. It is therefore very important to validate the experimental set up. Various tests were performed in order to check this for the heat data obtained in the study represented in Figure 2. (*1*), To simulate the rate of glucose consumption in the flow line, samples were taken from the culture in the fermenter and the rate of glucose consumption was determined. A linear decrease in the glucose concentration was demonstrated during the first minutes. However, this decrease was in this case at most 20%, compared to the concentration in the fermentor after a time lapse corresponding to the transport time between the fermenter and the calorimetric cell. (*2*), Stopped-flow measurements were made in order to check for glucose availability. The flow through the calorimeter cell was stopped at intervals, and the rate of heat production was monitored. (*3*), Two flow-through cells were connected in series. This resulted in a slightly lowered rate of heat production from the second cell. The decrease in the heat signal was extrapolated to time zero, simulating the level of the heat signal in the fermenter. For this study, with its particular conditions, these tests resulted in a correction of the measured heat signal by a factor of 1.02. Thus, under the prevailing experimental conditions and with the chosen experimental organism, the time delay between the fermenter and the calorimetric measuring cell had only a minor influence on the rate of heat production. For microorganisms with a high metabolic activity and at high cell densities, however, care has to be taken so that the conditions in the calorimetric measuring cell and the fermenter are comparable.

When appropriate conditions cannot be reached in the calorimetric measuring unit because of limiting substrate(s) and/or high cell densities, a bench-scale calorimeter in which the fermenter and the calorimeter is one unit may be preferable. For example, in the chemostat study by Larsson et al. [22] a 2-liter bench-scale calorimeter (model RC-1; Mettler-Toledo AG, Greifensee,

Switzerland) modified for biological work was used (for different studies using this type of bench-scale calorimeter, the reader is referred to the chapter by Duboc et al. in this volume). This instrument is less sensitive than the microcalorimeter. To some extent, however, the higher detection limit is compensated for by the much larger volume of the calorimetric unit. With any type of instrument used, the validity of the heat data may be verified by the energy balance attained (Figure 2), *i.e.* the sum of the energy content of the different substrates and products should be equal. In other words, according to Hess's law of energy conservation, the energy calculations can be performed on the basis of either the total amount of substrate used or the total amount of products formed (including heat), enabling reliability tests of the data. Consequently, if an experimental energy balance is achieved this verifies that all essential substrates and products (as illustrated in Figure 2B) are identified and correctly quantified. For correctly performed energy (enthalpy) balance calculations, the reader is referred to the work done by von Stockar et al. [12], in which thermodynamic considerations in constructing energy balances for cellular growth is dealt with in detail.

In the following of this chapter, several examples from the authors' own work, often with yeast as the model organism will be presented. However, the approaches described are mostly general and therefore equally well suited for other types of microorganism, such as bacteria.

2. THE ORIGIN OF HEAT PRODUCTION IN METABOLISM

2.1. Anabolism versus catabolism

It is a common statement that life is always connected to the production of heat. That is true in most cases, perhaps with one (known) exception, *i.e.* the anaerobic production of CH_4 and CO_2 from acetate. In this process the entropy term outweighs the heat term and, at least in theory, life could be connected to net heat absorption [23]. However, if we ignore this exception and instead concentrate on what part of metabolism generates the heat. Is it due to catabolic or anabolic reactions? The answer is in fact both catabolism and anabolism is involved.

When the substrate is converted in catabolic routes part of the liberated enthalpy is conserved in the production of ATP and another part is evolved as heat (Q_{cat}) (Figure 3). The ATP formed in the catabolic reactions is consumed in the anabolic reactions and heat is evolved also in this step (Q_{anab}). The result

of the overall process is that part of the substrate is broken down to catabolic products, *i.e.* CO_2 and H_2O and/or fermentation products and another part of the substrate is used for biomass formation (Figure 3). The measured total heat production of metabolism (Q_{met}) is the sum of Q_{cat} and Q_{anab}. This definition of Q_{anab} is not equivalent to the term heat of anabolism [2]. The total heat production, Q_{met}, is the same but Q_{anab} is higher than heat of anabolism since the former also includes the heat evolved when ATP hydrolysis is used to fuel anabolic reactions. (Consequently, Q_{cat} is lower than what can be calculated from the reaction J_{cat} due to synthesis of ATP).

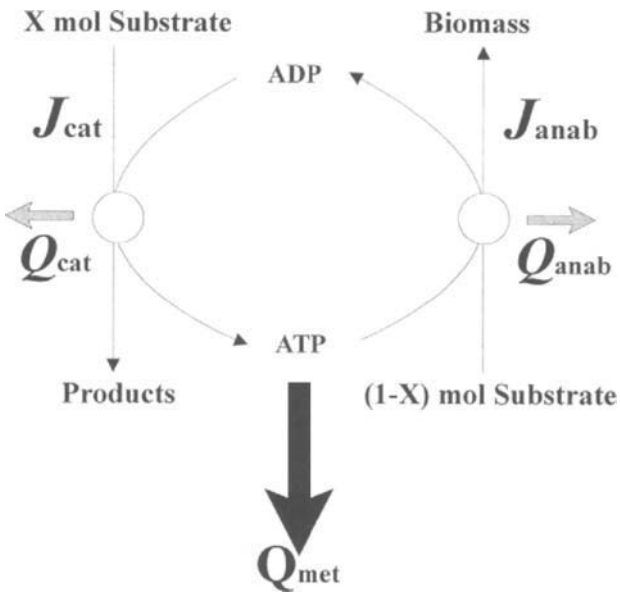

Figure 3. Overview of heat production in a simplified metabolic scheme during heterotrophic (organisms using organic substrates both as source of carbon and electron donor, *i.e.* energy source) growth. For simplicity, energy transformations are only exemplified by ATP turnover, *i.e.* the ATP/ADP cycle. The flow of carbon from 1 unit of substrate through the catabolic (J_{cat}) and anabolic (J_{anab}) routes is of simplicity presented as two separate routes.

It is important to realise that heat generation is not a consequence or measurement of the rate of ATP turnover. In an aerobic process the heat production rate is directly proportional to the oxygen consumption rate. Whether there are 6 (P/O ratio = 3) or just 1 (P/O ratio = 0.5) ATP formed per

O_2 consumed is totally irrelevant for the amount of heat produced. (On the other hand, if the stoichiometry was known the rate of ATP turn over could be calculated). There may be indirect effects, of course, such that an increased ATP formation per O_2 may reduce the rate of oxygen consumption and hence the heat production rate or that an increased ATP formation per O_2 results in an increased growth yield and hence a decreased heat production (see below).

As already stated, the fact that heat evolution occurs when ATP is used to power the anabolic reactions should not be confused with the term heat of anabolism [2]. Heat of anabolism in this sense means the heat accompanying the anabolic reactions when the overall growth equation is separated into catabolism and anabolism and the heat dissipation due to ATP consumption (in the anabolic pathways) is not included (see section 2.2.1 for examples). It is generally believed that heat of anabolism is close to zero at least during growth on carbohydrates having a similar degree of reduction as biomass [2, 24]. However, this term may increase if carbon sources are used that differ significantly in their degree of reduction from that of the biomass [24]. Furthermore, the enthalpy change could be both exothermic and endothermic depending on whether it is the substrate or biomass which is the most reduced. An alternative way of looking at this is that the degree of reduction of the substrate affects the extent of catabolism needed for production of biomass. For instance, highly oxidized carbon sources, the extreme being CO_2, require both considerable reducing power in the form of NADPH but also energy in the form of ATP, hence the catabolic activity has to be high per unit of biomass produced. Similarly, if the biomass is very reduced compared to the substrate, such as for *e.g.* oleaginous yeast [25], a high catabolic activity is required to produce the necessary amounts of reducing power. With a reduced substrate such as ethanol the situation is very different. During ethanol utilisation not only the catabolic but also the anabolic pathways leads to a considerable formation of NADH. In that sense one could argue that anabolism in this case, with a reduced substrate, leads to anabolic heat production. However, with such an argument NADH oxidation and O_2 reduction in the respiratory chain has been defined as anabolism, and that is rather unorthodox. The conclusion from this is that it is very difficult or even impossible to separate the metabolism of a cell into two entirely separate activities, like anabolism and catabolism. Nevertheless, the heat production of a cell always originates from the sum of catabolic and anabolic reactions, *i.e.* Q_{met} (Figure 3).

2.2. Coupled versus uncoupled metabolism

The maintenance energy demand is usually considered small or even negligible under optimal growth conditions (Figure 4) [26-28]. The amount of energy required to run maintenance reflects the amount of Gibbs energy needed. The maintenance energy turn-over may increase substantially under conditions of external stress such as, *e.g.* high osmolarity [19, 28], low pH [29, 30] and presence of weak acids [27, 31, 32]. Another phenomenon that is frequently observed in microbiology is metabolic uncoupling [22, 33-40]. What will be discussed in the following, however, is the metabolic energy turn-over measured as an enthalpy change.

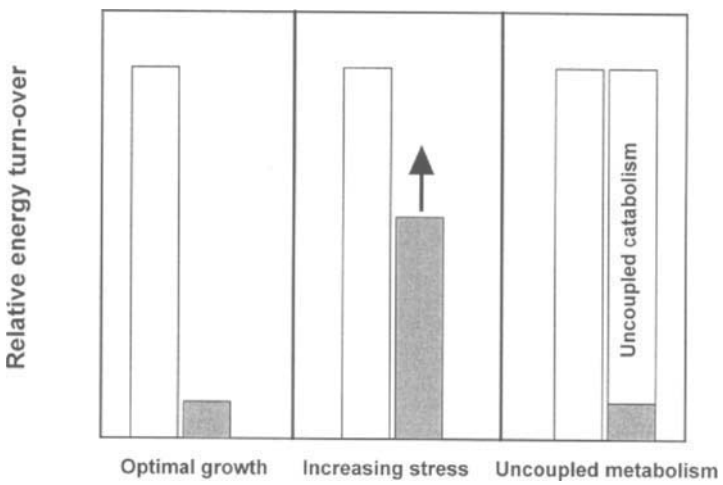

Figure 4. Theoretical segregation between total metabolic energy turnover (open column) and maintenance energy turn-over (grey columns) under different growth conditions.

This is not an effect of an increased maintenance energy turn-over, instead it is due to uncoupling between the ATP requirements for anabolism and maintenance and the catabolic ATP production (Figure 4). The rationale behind this behaviour is not known but, at least concerning the yeast *Saccharomyces cerevisiae*, a poor regulation of the sugar transport system might be involved. However, this seemingly wasteful type of metabolism may in natural environments be of competitive value. Metabolic uncoupling in *S.*

cerevisiae has been reported both aerobically [22, 41] as well as anaerobically [41, 42]. The magnitude of excessive ATP formation is not known under aerobic conditions, since this depends on the P/O ratio. Anaerobically, however, where there is a strict coupling between ATP and product formation, it is clear that a substantial fraction of the ATP production is not required and has to be removed. The mechanism(s) utilised by the cells for consuming excess ATP is not known but several different suggestions have been put forward including the existence of futile cycles, increased turnover of cellular constituents, etc. [35, 39, 40].

2.2.1. Heat yield determinations

The extent of metabolic uncoupling and the magnitude of stress imposed on the cells is visualised by a decreasing growth yield but it could also be quantified by determining the so-called heat yield, *i.e.* the amount of heat produced per amount of biomass formed. This parameter has the advantage of being independent of growth rate or biomass concentration but it is, however, critically dependent on the metabolism and growth yield of the cells. For instance, if a hypothetical aerobic case is considered in which glucose is used as carbon and energy source and ammonium as nitrogen source with the following assumptions, growth yield 0.60 C-mol/C-mol of glucose, energy content 560 kJ/C-mol of biomass and a biomass composition according to $CH_{1.85}O_{0.50}N_{0.15}$. Then, by using the guidelines suggested by von Stockar et al. [12] a catabolic and an anabolic reaction is described as:

Anabolic

$0.66\ C_6H_{12}O_6(aq) + 0.54\ NH_4^+(aq) \rightarrow 3.60\ CH_{1.85}O_{0.50}N_{0.15}(?) + 0.36\ CO_2(g) + 1.44\ H_2O(l) + 0.54\ H^+(aq)$

Catabolic

$0.34\ C_6H_{12}O_6(aq) + 2.04\ O_2(g) \rightarrow 2.04\ CO_2(g) + 2.04\ H_2O(l)$

The resulting heat yield could be calculated, by using the heat of combustion values provided by von Stockar *et al.*[12] according to:

0.34 mol x -2814 kJ/mol / 3.60 C-mol = -266 kJ/C-mol

which is equal to -266 kJ/C-mol /24 g/C-mol = -11.1 kJ/g

It might seem contradictory to separate metabolism into a catabolic and an anabolic part since it was concluded that to do this is very difficult or even impossible (see section 2.1.). However, for the sake of heat yield calculations it does not matter how the split is done, *i.e.* the result is the same if oxygen is used instead of CO_2 to balance the anabolic reaction. If oxygen is used the reactions would be:

Anabolic

$0.60\ C_6H_{12}O_6(aq) + 0.54\ NH_4^+(aq) \rightarrow 3.60\ CH_{1.85}O_{0.50}N_{0.15}(?) + 0.36\ O_2(g) + 1.08\ H_2O(l) + 0.54\ H^+(aq)$

Catabolic

$0.40\ C_6H_{12}O_6(aq) + 2.40\ O_2(g) \rightarrow 2.40\ CO_2(g) + 2.40\ H_2O(l)$

The heat production during respiration of glucose is equal to -469 kJ/ mol O_2 (with the conditions given in the above equation). In order to produce 3.60 C-mol of biomass, 2.40 mol O_2 is consumed in the catabolic reaction. At the same time 0.36 mol O_2 is produced (by this way of separating anabolism and catabolism) in the anabolic reaction. Consequently the heat yield could be calculated according to:

(2.40 - 0.36) mol O_2 x -469 kJ/mol O_2 / 3.60 C-mol biomass = -266 kJ/C-mol or -11.1 kJ/g

which is exactly the same result as when CO_2 was used to balance the anabolic reaction. Furthermore, in these calculations the excess NADH accompanying biomass formation [43, 44] has been neglected but neither does this affect the heat yield calculations. This is due to the fact that excess NADH requires more glucose in the anabolic reaction and consequently less is available for catabolism and heat production. However, the excess NADH is respired at the expense of oxygen and the concomitant heat production will exactly balance the lower heat production caused by the diversion of glucose from catabolism to anabolism. These calculations also illustrate the difficulty in trying to determine the heat of anabolism by separating anabolism from catabolism. The result will depend very much on how the split is done. In the first case where CO_2 is produced in the anabolic reaction the enthalpy change accompanying the anabolic reaction is essentially zero. However, if instead it is assumed that O_2 is produced in the anabolic reaction a heat uptake of 169 kJ could be

calculated for this reaction (this value is of course equivalent to 0.36 O_2 x -469 kJ/mol O_2 = -169 kJ). However, as shown above, for the sake of heat yield determinations the separation between anabolism and catabolism is irrelevant. A change in growth yield, on the other hand, has a big impact on the heat yield. As stated previously the type of metabolism also has a big influence on the heat yield. If instead an anaerobic system is considered where ethanol is formed from glucose, *e.g.* by *S. cerevisiae*, and with a growth yield of 0.10 C-mol/C-mol, the growth equations will be:

Anabolic
0.11 $C_6H_{12}O_6$(aq) + 0.09 NH_4^+(aq) → 0.60 $CH_{1.85}O_{0.50}N_{0.15}$(?) + 0.06 CO_2(g) + 0.24 H_2O(l) + 0.09 H^+(aq)

Catabolic
0.89 $C_6H_{12}O_6$(aq) → 1.78 C_2H_5OH(aq) + 1.78 CO_2(g)

The heat production accompanying ethanol formation is -100 kJ/mol glucose [12]. Consequently the heat yield could be calculated according to:

0.89 mol x -100 kJ/mol / 0.60 C-mol = -148 kJ/C-mol

which is equal to -148 kJ/C-mol / 24 g/C-mol = -6.2 kJ/g

However, the excess NADH formed due to anabolic reactions has to be taken into account under anaerobic conditions. For instance, *S. cerevisiae* uses glycerol formation as a way of disposing a surplus of NADH anaerobically [45-47] and this will of course affect the heat production. By using the value of 0.3 mol NADH per C-mol biomass formed [43], the growth equations will change to:

Anabolic
0.125 $C_6H_{12}O_6$(aq) + 0.09 NH_4^+(aq) + 0.18 NAD^+ → 0.60 $CH_{1.85}O_{0.50}N_{0.15}$(?) + 0.15 CO_2(g) + 0.15 H_2O(l) + 0.18 NADH + 0.27 H^+(aq)

Catabolic
0.875 $C_6H_{12}O_6$(aq) + 0.18 NADH + H^+ → 1.57 C_2H_5OH(aq) + 0.18 $C_3H_8O_3$(aq) + 1.78 CO_2(g) + 0.18 NAD^+

The heat yield is decreased to:

(0.875 x -2814) -((1.57 x -1357) + (0.18 x -1649)) / 0.60 = -58 kJ/C-mol
or -58 /24 = -2.4 kJ/g

Quite a number of publications concerning the meaning and experimental determinations of heat yields under different conditions have been published, *e.g.* references[15, 16, 19, 22, 29, 30, 35, 43, 48-53]. The studies have included various microorganisms growing on different substrates [49], the difference between aerobic and anaerobic conditions [53], but also the effect of different stress conditions such as low pH [29, 30], osmotic stress [16, 19] or nitrogen limitation [22, 33, 35]. As expected, depending on the conditions, the reported heat yield values are quite diverse. Fully aerobic growth on glucose seem to result in values approximately between -10 to -15 kJ/g [22, 30, 49, 50], whereas anaerobically values as low as -4 to -5 kJ/g were observed [43, 50]. At the other extreme is growth at low pH where values between -70 to -80 kJ/g have been reported [29, 51].

3. FUTURE AREAS OF APPLIED CALORIMETRY

3.1. Continuous registration and control of fermentations

Analysis and control of batch and fed-batch fermentations by calorimetry has been performed in, *e.g.* references [29, 54-56]. The heat production rate can of course be used as a control parameter. In addition, calorimetry can be very useful in continuous culture studies as a convenient way of monitoring when steady-state is established [22, 33, 57]. The advantage of using calorimetry for registration and control is its non-destructive nature and that it can easily be applied as a continuous on-line measurement. Since all reactions in a cell give rise to a heat change, a constant heat production rate indicates a constant total activity and hence steady-state conditions. Calorimetry has also been used to study the energetic consequences in terms of efficiency during oscillatory growth [16], which is frequently observed in continuous cultures of *S. cerevisiae*. Different ways of calculating efficiencies were presented and the results showed that oscillatory growth caused a reduction in efficiency compared to steady-state conditions [16]. A related field of research is the heat flux measurements during glycolytic oscillations in yeast cells (see section *3.2.3.*). Another area where calorimetry has proven to be a useful tool is in medium optimisation studies [15, 49, 52, 55]. The possibility of detecting poor

growth and activity due to medium limitation will most probably become increasingly important. This is because increased competition and increasingly sophisticated bioprocesses in the field of biotechnology makes accurate control strategies necessary for process reproducibility and to make the bioprocesses economically feasible. A new problem has arisen in recent years because it is common practice in modern molecular biology to use amino acid auxotrophy as selective markers. As a consequence, growth arrest or metabolic disorders that are frequently observed is due to medium limitation of the specific amino acids for which the organisms are auxotrophic.

This will be illustrated in the following *example.* When using auxotrophic mutants it is of course necessary to supplement the medium with the required amino acids. Unfortunately it has turned out to be very difficult to determine the amounts needed by the organism, at least concerning the yeast *S. cerevisiae.* This yeast shows an extensive over-consumption of added amino acids, in particular leucine, but depending on the strain also tryptophan may be consumed in excess of anabolic requirements (Larsson & Gustafsson, unpublished). Leucine limitation causes growth arrest but the cells still maintain a high catabolic activity which could be detected by calorimetry (Figure 5).

It is often suggested to use 30 mg/l leucine when cultivating these mutants. However, when using 5 g/l glucose as carbon and energy source, the concentration was increased to 120 mg/l. Nevertheless, even this concentration turned out to limit growth (Figure 5). If the added leucine was used solely for the purpose of protein synthesis this amount should be sufficient to produce more than 2 g/l of biomass (50% protein content and approximately 10% of the protein consists of leucine). In the study described (Larsson & Gustafsson, unpublished), the growth limitation was initiated well below a biomass concentration of 1 g/l. As can be seen by the rapid response when leucine was added (Figure 5), calorimetry is a simple way of both detecting the presence of a limitation as well as to determine what substance is responsible.

The study presented in Figure 5 exemplifies the use of calorimetry in medium design, not only for auxotrophic mutants, but generally in any kind of medium design for microbial processes, independent of organism and substrate complexity.

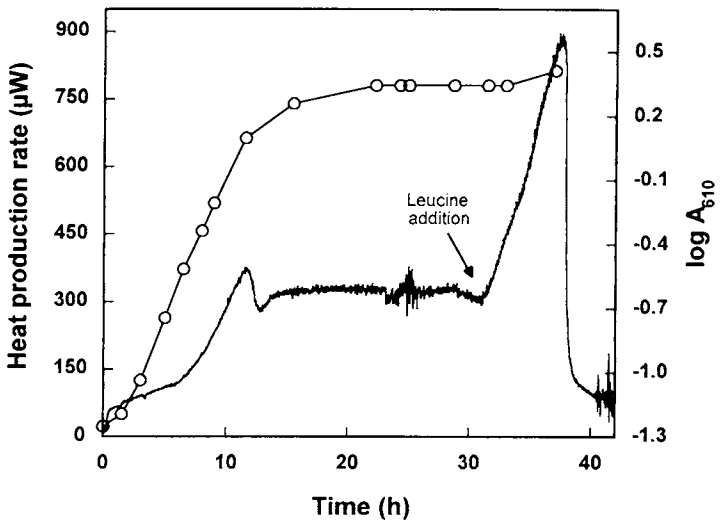

Figure 5. Growth and heat production rate during a leucine limited aerobic batch culture of a *leu2* deletion mutant of *S. cerevisiae* with a synthetic medium containing 120 mg/l leucine and 5 g/l glucose as carbon and energy source. The arrow indicates addition of a further portion of leucine. Log A_{610} (○) and heat production rate (–) (Larsson & Gustafsson, unpublished).

3.2. Analysis of metabolic fluxes in non-growing/starved cells

Although the dominant portion of microorganisms in nature probably reside during most of their life cycle in a non-growing state, most studies with microorganisms have been performed with growing organisms. There is most certainly a lot to learn about metabolism in non-growing and starved cells. Because of different reasons, however, the non-growing state is more difficult to study. One reason is the low rate of metabolic flux. For some approaches, sensitive microcalorimeters have proved useful.

3.2.1. Catabolic flux distribution

Calorimetry measures the total metabolic activity. In order to quantify the contributions of different metabolic fluxes, sequential inhibition of respective metabolism by inhibitors may be used. If an organism, for example, has the ability to perform both respiration and fermentation as part of their catabolism, inhibitors of respiration and fermentation may be used in order to quantify

their respective importance under a certain condition [58]. It should be kept in mind though, that blocking either metabolism, for example respiration, might have secondary effects on the other metabolism, for example fermentation, *i.e.* the fermentative activity may increase in a situation when respiration is blocked or *vice versa*. This has to be checked in control experiments.

This will be illustrated in the following *example*. The combination of calorimetry and inhibitors of fermentation and respiration was used to distinguish between the fermentative and respiratory activity, respectively, after glucose pulsing to carbon or nitrogen starved cultures of *S. cerevisiae* (Figure 6; Nilsson, Påhlman, Larsson & Gustafsson, unpublished). Respiration and fermentation were sequentially inhibited by azide, and iodoacetic acid, respectively. Azide is an inhibitor of the respiratory chain, while iodoacetic acid is an inhibitor of glycolysis.

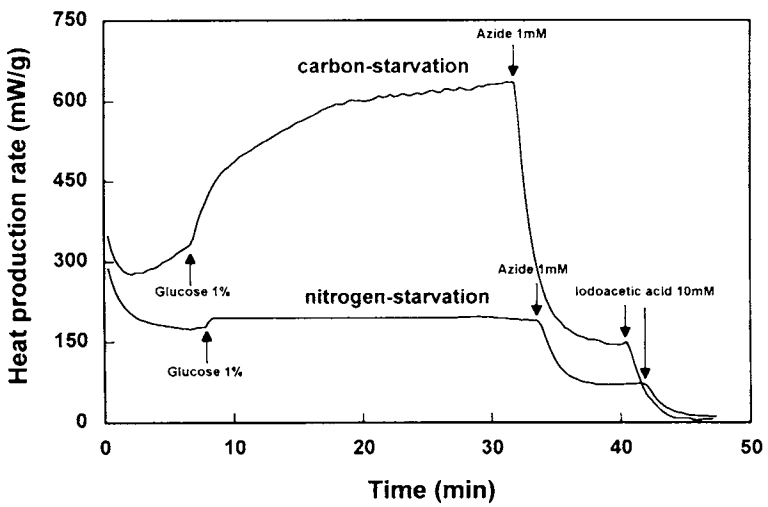

Figure 6. Changes in heat production rate after addition of 1% glucose to *S. cerevisiae* cultures starved for carbon or nitrogen, respectively. Azide was added in order to inhibit respiration, while iodoacetic acid inhibits glycolysis (Nilsson, Påhlman, Larsson & Gustafsson, unpublished).

The difference in heat production before and after addition of azide represents respiratory activity while the fermentative activity is obtained from

the difference in heat production in the presence of azide and the subsequent addition of iodoacetic acid (Figure 6; Nilsson, Larsson, Påhlman & Gustafsson, unpublished). Test experiments showed good agreement in fermentative activity when comparing calorimetric and direct measurements of ethanol production for carbon-starved cells but not for nitrogen-starved cells [58]. The reason for the difference between carbon and nitrogen starved cells is not understood.

For these studies, the multichannel microcalorimeter described in section 1 was used in the flow-through mode. Temperature controlled and stirred Ehrlenmeyer flasks, containing starved yeast cultures in synthetic salt solution, were connected to the microcalorimeter and a mixed flow of liquid-culture and humidified air was pumped through the measuring vessel of the microcalorimeter. The yeast cells were pulsed with glucose as an energy source (no nitrogen was added). The cells responded immediately to the energy source, although very differently depending on whether they were originally starved for nitrogen or carbon. As can be seen, carbon starvation provoked a much higher respiratory as well as fermentative activity after a glucose pulse compared to nitrogen starved cells. This difference in response has recently been verified in studies excluding the use of inhibitors, but with a combination of respirometry and calorimetry, (Nilsson, Påhlman, Larsson & Gustafsson, unpublished). The main reason for this is probably the fact that nitrogen starvation results in a rapid inactivation of glucose transporting enzymes in *S. cerevisiae* [59].

Calorimetric studies of this kind, in combination with specific techniques, may be valuable in resolving metabolic responses of non-growing/starved microorganisms. For an example see section *3.2.4.*, where a combination of calorimetry and respirometry on starved bacteria is presented.

3.2.2. The control of catabolic flux

Although the biochemistry of glycolysis has been known for a long time, the regulation of glycolysis is far from fully understood. At least in yeast, it has been suggested that glucose transport exerts a high control on the glycolytic flux [60]. In Metabolic Control Analysis (MCA), the extent to which an enzyme controls a flux is quantified by a flux control coefficient (for review, see [61]).

This will be illustrated in the following *example.* The complexity of the sugar transport system in *S. cerevisiae* is very great and consequently not

simply accessible to modifications. This problem was addressed in a study by Teusink and collaborators [62]. The activity of the sugar transport system was modulated by changing the external glucose concentration, *i.e.* the substrate concentration (glucose) was used as a parameter instead of as a variable. Non-growing cells of *S. cerevisiae* were used and only fermentative metabolism was allowed, since respiration was blocked by the addition of cyanide. Since the ethanol produced per glucose consumed was constant after a glucose pulse throughout a parallel experiment, it was assumed that also the heat produced per glucose consumed stayed constant. The glucose consumption could therefore be calculated from the heat flux. Microcalorimetry was used to accurately measure the heat flux through glycolysis (see section *3.2.3.* for some further details concerning the experimental approach). The interpretation of data obtained was that the extent to which the glycolytic flux in resting yeast cells is controlled by the glucose transport system depends very much on the conditions and can largely differ from case to case.

3.2.3. Heat flux and metabolic dynamics

The use of microcalorimetry as a complementary method to study regulation and control of metabolic fluxes has great potential, since microcalorimetry with a high precision measures an average of all metabolic fluxes rather than the time dependence of the concentration of specific metabolic intermediates. It is therefore possible to use microcalorimetry as an accurate "fluxmeter" for studies of metabolic dynamics [63].

This will be illustrated in the following *example.* Sustained oscillations of glycolytic intermediates have been shown in the yeast *S. cerevisiae,* both in cell free extracts [64, 65] and in whole cell cultures [63, 66]. Oscillatory growth is also a well-documented phenomenon in this yeast (see reference [16]) for further references). In the latter case, there may be an oscillatory shift in proportion of the respiratory and fermentative catabolism, during continuous aerobic growth on glucose. The oscillatory behaviour has been documented as an oscillation of substrate consumption rates and product formation rates rather than as an oscillation of metabolic intermediates [16]. An oscillatory behaviour may be of short (duration less than 1 min. [62, 63, 66]), medium (duration less than 1 hour; [64]), or long term duration (duration of several days; [16]).

Glycolytic oscillations in yeast have been known for a long time (for review see reference [67]). The fact that sustained oscillations can be observed in a population, implies that some synchronisation mechanisms prevents the cells

from running out of phase. Recently acetaldehyde was identified as a metabolite that has the potential of triggering a sustained glycolytic oscillation. Acetaldehyde thereby couples the individual cells (see reference [63] for further references). The metabolic oscillations are readily monitored through NAD(P)H fluorescence, but these do not give a measure of the total metabolic flux. This, however, may be performed by microcalorimetry. In the study by Teusink *et al.* [63], the time duration of the oscillations were less than 1 min.

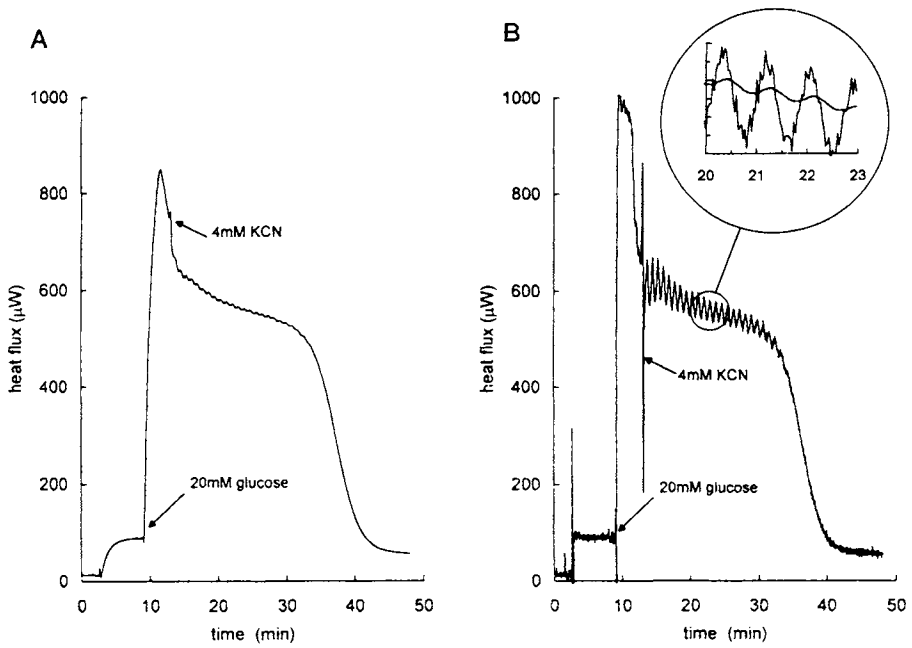

Figure 7. Oscillations in the heat production rate measured by the microcalorimeter without (A) and with correction (B). At t=3 min, the cells enter the calorimeter; glucose and cyanide were added as indicated by the arrows. The inset in panel B is an enlargement of the uncorrected and the corrected data. For details see [63]. Reproduced with permission from reference [63] copyright © American Society for Biochemistry and Molecular Biology.

The main obstacle to making calorimetric investigations on glycolytic oscillations is that it requires an instrument which is at the same time highly sensitive but also allows for rapid measurements since the time period of the

oscillations may as in this case be less than 1 min. A procedure was therefore developed for correction of the distortion of amplitude and phase of the heat signal caused by the relatively slow response of the calorimeter (Figure 7; [63]). The correction was based on the Tian equation. By applying this correction procedure it was possible to study oscillations in heat production rate with a period duration of less than 1 minute. The flow-through mode of the multichannnel microcalorimeter (BAM) of the heat conduction type was used as described in section 1 [20].

The study was performed with resting cells in Erlenmeyer flasks at a temperature of 21°C. At this temperature the period of the oscillations was approximately 50 s. To induce oscillations, glucose and subsequently cyanide were added. The culture-liquid was pumped to the measuring cell of the microcalorimeter and then returned to the Erlenmeyer flask (Figure 7).

In this study [63], the heat flux and the concentrations of glycolytic metabolites were simultaneously determined. The data showed that the oscillations in heat production rate were in phase with the oscillations in NADH concentration. The heat flux measurements also enabled the recognition of (i) changes in metabolic capacity that may affect glycolytic dynamics, (ii) implications of glucose carrier kinetics for glycolytic dynamics and (iii) the continued requirement for an acetaldehyde trapping agent for sustained oscillations in *S. cerevisiae.*

3.2.4. Mechanisms of ageing

As long as the environment support self-replication, microorganisms appear to be immortal. Yet, microorganisms die if circumstances arrest multiplication, although depending on the type of organism and conditions they may survive prolonged periods of starvation. Specific genetic programmes are suggested to have evolved to prolong survival of microorganisms under adverse conditions (see reference [68] for further reading). It has been shown that utilizable energy from endogenous material allows protein synthesis in bacteria. Strategies evolved to protect the microorganisms from starvation death are now intensively studied, especially with use of molecular biology techniques.

This will be illustrated in the following *example.* In the bacterium *Escherichia coli,* one of the global regulatory systems is the two-component ArcA-ArcB system, which is activated when the environment contains no external electron acceptor or only poor ones; ArcA being the regulator and ArcB the sensor component [69]. The importance of the ArcA regulator for the

starvation response of *E. coli* was studied [68]. This investigation used a combination of respirometry (Oroboros Oxygraph; A. Paar KG, Graz, Austria) [70], microcalorimetry (similar fermenter-calorimetry system as described in section *3.2.1.* was used) and molecular biology techniques. It was shown that the Δ*arcA* mutant failed to decrease the synthesis of several TCA cycle enzymes during starvation. This was manifested by an elevated rate of respiration and total metabolic activity compared to the wild-type during starvation conditions. By combining calorimetry and respirometry it was found that the mutant had a higher total activity but also that the respiratory activity accounted for more than 80% of the total energy turnover in the mutant whereas in the wild-type only 40% of the total energy expenditure was due to respiratory activity. These differences between the wild type and the mutant were only found under starvation conditions. Exponential growth resulted in a similar total metabolic activity and respiratory activity in the Δ*arcA* mutant and the wild-type [68]. The inability to survive prolonged periods of starvation could at least in part be overcome by overproducing the superoxide dismutase SodA. This suggests that the increased respiratory activity in the Δ*arcA* mutant enhances the level of toxic oxygen radicals, thus reducing the survival. However, the beneficial effect of overproduced SodA is dramatic during 2-3 days of starvation but prolonged periods renders these cells as sensitive as non-overproducers. A plausible explanation might be that the incapability of reducing the metabolic activity when there is no exogenous carbon and energy source will drain the cells of energy. In fact, if the high activity of the mutant as reported by Nyström *et al.* [68] were to be maintained for a long time, the total energy content of the whole cells would very quickly be consumed.

3.2.5. Maintenance energy flux

Maintenance energy flux in non-growing/starved cells is not easily studied. There are at least two difficulties (*i*) the low rate of metabolic flux; and (*ii*) the complexity of potential intracellular energy sources. Microcalorimetry may be an appropriate technique for studies of maintenance energy flux, both because it is not restricted to the metabolsm of any particular substrate and it is a relatively sensitive method (see also section 2.2.; for a review see [4]). Care must be taken, however, in how these experiments are performed. It is quite common to concentrate and/or transfer the cells to a new (starvation) medium for these types of determinations. At least in yeast such a transfer has been shown to trigger some kind of endogenous metabolism [26], which should not be confused with maintenance metabolism since periods of an increased

metabolism may occur in response to a disturbance in the environment. In contrast, maintenance energy is here defined as the lowest level of energy turnover during survival of non-growing cells. When performing calorimetric measurements on stationary phase cells of *S. cerevisiae*, heat production rates below the instrumental detection limit of 4 to 5 J/g h was obtained [26]. If, however, these cells were harvested by centrifugation and transferred to a salt solution, an endogenous activity amounting to 36 J/g h could be measured. In addition to changes in metabolic activity also the intracellular nucleotide levels were shown to be affected by this transfer [71]. Hence great care should be taken in the design of such experiments. Unfortunately, not even microcalorimeters may be sensitive enough to measure the low metabolic rates persisting in starved microorganisms. However, the volume of the measuring cell may be increased by using for example a perfusion vessel [20] instead of the flow-through vessel.

3.3 Bioadhesion

Studies of bioadhesion have in recent years become increasingly important. One explanation for this is that bioadhesion offers a large number of applications in the field of biotechnology. Usually the non-growing state in nature is maintained because of nutrient limitation and as a consequence of the search for food, microorganisms often adhere to different surfaces. It has actually been estimated that the predominant mode of growth occurs on surfaces compared to a free-living mode in liquid-suspension. This seems to be true for all kinds of environments, *i.e.* in fresh water and in marine ecosystems as well as in terrestrial environments or in association with higher organisms. As a consequence of adhesion, the organisms seem to be more active compared to when they reside in the free-living state [72]. An increased metabolic rate would be detected by calorimetric measurements. This expectation was confirmed in a study by Humphrey and Marshall [73] where a rapid increase in the rate of heat production of the marine bacterium *Vibrio* DW1 was obtained when a surface was introduced. The heat output was directly measured in a flow-microcalorimeter. Earlier data from studies with *Vibrio* DW1 showed that the presence of an air-water interface or a solid surface (dialysis membrane) in the absence of an energy substrate, induced among other responses, a reduction of cell-size [74] and a substantial increase in oxygen consumption [75]. Conflicting data are, however, found in other parts of the literature [76-78]. The explanation for this may be partly that surfactants at surfaces can induce various cell responses. Furthermore,

different surface active substances may be extracted to a different extent and surfactant properties may differ in their effect on the microorganisms [73].

There are so far very few studies covering calorimetric quantification or monitoring of the metabolic activity of adhered cells compared to free-living ones. Calorimetric measurements have, on the other hand, been used in order to pin-point physiological states of microorganisms which differ with respect to adhesion properties. For example, different states of the growth cycle have been monitored by flow calorimetry, both in defined laboratory media and in diluted mucus from the intestine of higher organisms [79-82]. Different yeast strains isolated from fish were shown to decrease in cell surface hydrophobicity (CSH) when switching from exponential growth to non-growth in the stationary phase. It was suggested that hydrophobic interactions are important for the initial events of fish colonisation by yeast [82].

For colonisation to occur subsequent to adhesion, growth of bacteria and yeast has been considered a necessity. The different fish-isolated yeast strains were able to utilise fish mucus as the sole source of nutrients (including the energy source) for growth (Figure 8). The occurrence of one major peak in the monitored rate of heat production indicates that only one type of compound was used as the major energy source [79]. A great advantage of this type of growth studies in mucus, is that, unlike nephelometry, calorimetry is not sensitive to opaque media. Consequently, calorimetry enables a possibility to register growth continuously, both in coloured and non-transparent media.

The bacterium *Escherichia coli* can also utilise ileal mucus lipids as the sole carbon/energy and nitrogen source [83]. To further elucidate nutrient utilisation during growth on mucus and mucus lipids, a mutant was constructed that was deficient in the fatty acid degradation [84]. By monitoring the metabolic activity of *E. coli* 1107 (wild-type) and *E. coli* 1107*fad* AB^- (mutant) in a flow-microcalorimeter during growth in piglet ileal mucus, it was possible to demonstrate that the fatty acids were used by the wild type during stationary phase (Figure 9). The consumption of fatty acids did not seem to be connected to additional net growth. It was concluded that possible cell growth may have been balanced by death of the cells or, alternatively, the energy produced was used as maintenance energy. This illustrates one of the strengths with calorimetry, *i.e.* to show the occurrence of unknown metabolic activities, not always easily detected with other techniques.

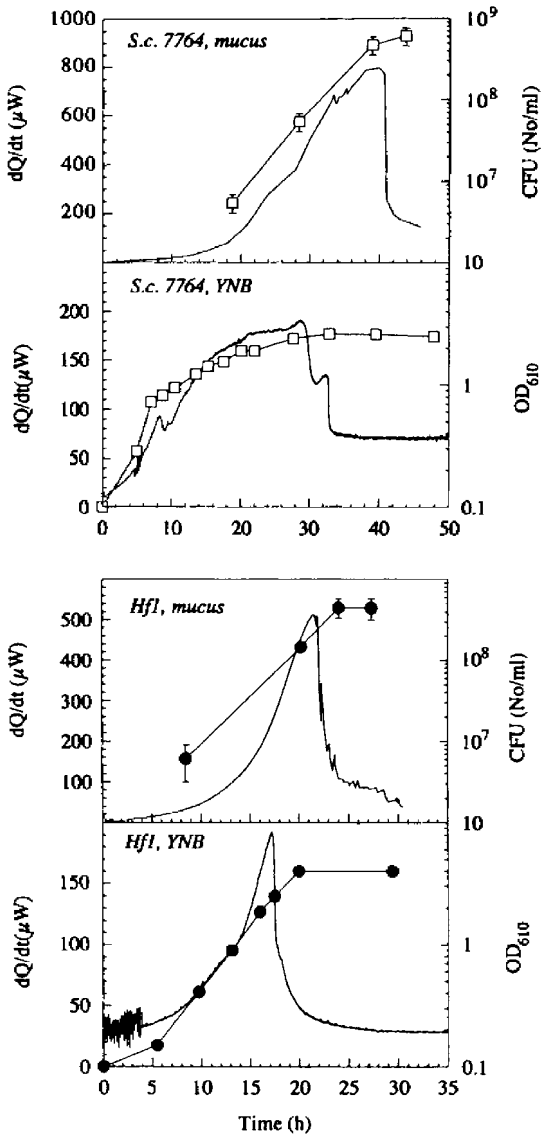

Figure 8. Growth of *S. cerevisae* CBS7764 (open symbols) and *D. hansenii* Hf1 (filled symbols) in intestinal mucus and in YNB. Rate of heat production (-), CFU ( ) and OD_{610} (O). Reproduced with permission from reference [79].

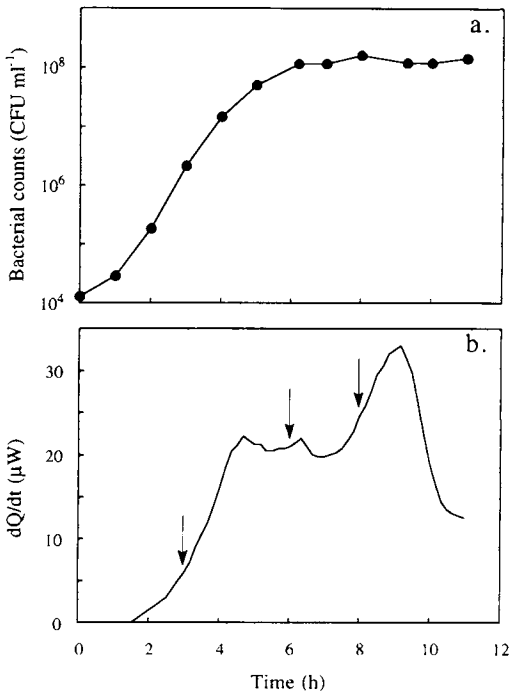

Figure 9. Growth (a) and rate of heat production (b) of *E. coli* K88 during anaerobic growth in piglet ileal mucus. Growth was measured as the increase in CFU per ml, and the rate of heat production (d*Q*/d*t*) was measured with a microcalorimeter. The arrows indicate times of ^{35}S-methionine labelling of the *E. coli* K88 culture during growth: 3 h, exponential growth phase; 6 h, early stationary phase, 8 h, late stationary phase. Reproduced with permission from reference [84] copyright © American Society for Microbiology.

3.4 Ecosystem studies

Organisms in the natural environment often have, as already pointed out, to cope with low substrate concentrations or periods better characterised as starvation for a particular or for several nutrients (see also sections 3.2. and 3.3.). For example, in the marine environment, heterotrophic microorganisms are often considered to be starved of energy. In addition to non-optimal conditions for growth and survival of the organisms caused by the level of nutrient supply, there may appear physical or chemical stress factors, such as non-optimal temperature, osmotic potential, redox potential or accumulation of

toxic substances. To increase even more the constraints on the organisms, both the chemical and the physical characteristics of the environment may fluctuate at a varying frequency as well as amplitude.

Energy is needed for any type of biological activity used to meet different environmental conditions. The available energy may, however, be limited. Consequently, the strategy of energy regulation and the efficiency of energy utilisation is of utmost importance for the survival and growth of the different organisms and for the competition or co-operation between the organisms constituting any natural habitat. The capacity and strategy in regulating the energy flow will, consequently, have an impact on the composition and behaviour of the ecological community and, thereby, on the total energy flow in the community (quoted from [85]). Included in the environmental changes that may cause an altered flow, on both intra- and inter-organismic levels, are man's activities in causing pollutants of different biological toxicity to be distributed to the environment.

Although calorimetry in principle can be a very powerful tool in ecological studies, relatively few studies have been performed with this technique (for reviews see references [3, 86]). The great potential of calorimetry in ecological studies lies in that it gives a total measure of the metabolic activity in a natural sample, which certainly will provide additional information compared to other more specific methods used, like gas and enzyme activity measurements. By *combining* oxygen consumption measurements with heat measurements, on the other hand, different types of energy metabolism may be distinguished, *e.g.* anaerobic (anaerobic respiration and fermentation) and aerobic respiratory metabolism.

Explanations for the scarce use of calorimetry in ecological studies are for example the cost of the equipment, the difficulty to perform measurements on undisturbed samples, uncontrollable physico-chemical side-reactions, difficulties in interpreting obtained data and a general poor knowledge of what actually is the biological meaning of the measured heat signal.

3.4.1. Sample handling

Several authors have used the calorimeter for measurements of metabolic activity in soil [80, 87-99]. One of the difficulties with measurements of natural samples are of course the complexity of the system, in which many physico-chemical reactions may contribute substantially to the measured heat output. By using sterilised soil samples, a contribution of 10% of the total heat output was shown to originate from non-biological reactions [95]. The

proportion of the non-biological contribution may of course correlate to the size of the contribution of the biological reactions, but the ratio of the respective contribution (biological/non-biological) may also be markedly changed, for example by increasing the humidity of the sample [89]. Other physical factors that during the experiment may severely affect the total heat output (biological and non-biological) and introduce changes in the microbial population is the temperature and the type and size of the gas phase. Consequently, control experiments under relevant conditions have to be performed for every specific sample. Until now, examples that have been described in any detail in this chapter, have made use of the flow-through mode of microcalorimeters. For experiments on natural samples, however, measuring vessels of the ampoule type are usually more appropriate. If closed ampoules are used during the calorimetric measurements, either oxygen may be limiting or an increased carbon dioxide concentration may cause an inhibition. The latter turned out to be the case during long term experiments (2 to 3 months). Closed ampoules are, however, not the only alternative for studies of soil or sediment samples. In a study where the total activity in sediment samples were compared in closed ampoules and an open perfusion vessel in which the water phase was continuously aerated, the aeration led to an increased and maintained rate of heat production [100].

This will be illustrated in the following *example.* In the study by Gustafsson and Gustafsson [100], the earlier mentioned multichannel microcalorimeter (BAM) of the heat conduction type [20] was used. However, in these studies the ampoule and not the flow-through mode was used. The channels were fitted with either an ampoule or a perfusion vessel. The vessels (of acid-proof stainless steel) had a volume of 6.5 ml and were loaded with 6 ml sediment-water mixture. After sedimentation the vessels contained around 1.5 ml sediment. In the closed ampoule there was no possibility to aerate the sample during measurements whereas in the newly designed perfusion vessel [101] it was possible to stir and aerate the sample. The stirring propeller was placed 0.5 - 1 cm above the sediment surface. After sealing, the vessel was completely filled by pumping in relevant river or lake water. During the experiment the water over the sediment was gently stirred and aerated through the stirring axle with water saturated air. That the treatment of the sample in the perfusion vessel showed a higher and constant rate of heat production, does not necessarily mean that the microbial population in the sediment was devoid of

oxygen in the closed ampoule. Instead or additionally, the beneficial effect may have been due to the removal of otherwise accumulating carbon dioxide.

In experiments reported by Sparling [96-98], the heat output from the soil biomass was remarkably uniform, and soil treatments such as storage or amendment resulted in larger effects on the heat output, than did the type of soil sample. Pamatmat and collaborators [102, 103] measured a fairly steady level of heat output from anaerobic layers of sediments (1-2 cm depth or deeper). In contrast, the heat output decreased with depth. The heat output from the uppermost aerobic layers (0-1 cm), on the other hand, decreased with time of measurement because of aeration insufficiency. These studies demonstrate the necessity of using relevant conditions and control experiments, in order not to hide real effects behind effects originating from improper sample handling. This of course also includes the texture of the soil or sediment sample. Laserre and Tournier [104], however, reported identical microcalorimetric responses with undisturbed and disturbed sediments. They established microcosms from the superficial layer of sediments and water, representing different ecosystems located on the Atlantic coast of France and added peptone in order to imitate an acute eutrophication process. During the transition phase that followed peptone addition, correlations were obtained between rates of heat production, oxygen consumption and $^{14}CO_2$ turnover. Correlations in response, however, disappeared when steady state conditions were achieved.

3.4.2. Mixed metabolisms on organism and population level

Combination of heat and oxygen measurements are particularly valuable, since this provides information about the extent of aerobic compared to anaerobic metabolism. For a variety of different conditions and substrates, such as carbohydrates, lipids and proteins, the oxycaloric equivalents range from -430 to -480 kJ $(mol\ O_2)^{-1}$ [105, 106], *i.e.* the enthalpy change per mole oxygen consumption. Transferring this relation to experimental conditions, it equals the ratio between the rate of heat production and oxygen consumption during fully respiratory catabolism, under most biological conditions, *i.e.* constant pressure and temperature. From this follows that simultaneous calorimetry and respirometry provides a tool in ecological studies. For purely aerobic metabolism, calorimetric measurements may substitute for oxygen measurements (indirect calorimetry) or *vice versa*. For a mixture of anaerobic and aerobic metabolism the extent of the two may be quantified by combining

calorimetry and oxygen measurements. The combination of different methods (including respirometry) with calorimetry is illustrated in a study [107] with the aim to evaluate different methods for their potential in the development of a toxicity test system.

This will be illustrated in the following *example.* The primary aim of the study was to use natural samples as a ecotoxicity test system [107]. Changes in heat production, respiratory activity, ATP pool, and the most probable number of microorganisms of different categories were measured in natural sediment samples. The model substance used in the toxicity test was a quaternary amine, Aliquat 336. Some of the results are presented in Figure 10. For the test, sediment and water were sampled from a river. Care was taken to sample only the upper layer. Experiments were repeated five times during two periods of a summer in Sweden. The sampled sediment and water were aerated at the laboratory for 20 h and thoroughly mixed. The aim of the work was not to simulate the activity of the samples to that of the natural location from which the samples originated, but rather, as already said, to set up a reproducible test system for toxic compounds. Consequently, care was taken to receive as homogenous test material as possible. After mixing, the sediment and water mixture was divided into portions, which were differently treated with the toxic compound, Aliquat 336. The ampoule mode of the microcalorimeter already described (BAM) was used. Two channels of the calorimeter were used in order to permit simultaneous determinations on aliquat-treated sediment and control sediment. The glass ampoules that were used had a volume of 3 ml and were loaded with 2 ml sediment-water mixture; 6 ampoules for control samples and 2 for each concentration of Aliquat-treated samples. After sedimentation the ampoules contained 1.2 to 1.5 ml sediment and 0.8 to 0.5 ml water. The ampoules were equipped with teflon covered caps with sealing rings. Between measurements, the water phase was aerated with water-saturated air (110 ml per h) through injection needles. This experimental set up allowed relatively many samples to be handled simultaneously and also made possible fairly extended experimental time periods. Qualitatively good agreement was obtained between heat production and respiratory activity, as well as between the different types of relative biomass, determined as ATP-pool and most probable number of microorganisms. The test variables chosen were considered to offer a sound approach for testing potentially toxic compounds.

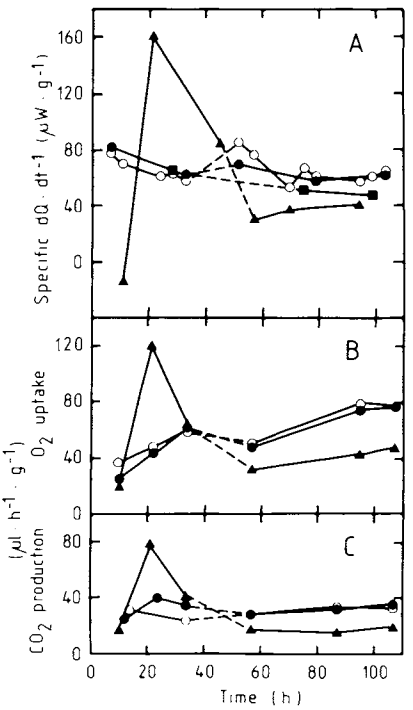

Figure 10. Activities of samples, untreated or treated with Aliquat. The broken lines combine start- and end-experiments. Symbols: (○) control; (●) 10; (■) 100; and (▲) 1000 mg Aliquat per l. A. Specific heat production, during incubation in calorimetric ampoules. B. Oxygen uptake rate and C. Carbon dioxide production rate during incubation in manometer vessels. Reproduced with permission from reference [107] copyright © OIKOS.

In another study, the use of the calorimetric:CO_2 ratio for measurements of aerobic and anaerobic soil microbial activity was illustrated [87]. Depending on the substrate, the value of the calorimetric:O_2 ratio and the calorimetric:CO_2 ratio may be equal (carbohydrates), while an increased value of the calorimetric:CO_2 ratio compared to the calorimetric:O_2 ratio is to be expected for more reduced substrates (lipids, ethanol) than carbohydrates. In other words, more oxygen is consumed per carbon in more reduced substrates (see also [87] for a comparison and discussion of different values reported in

literature). In the study by Albers and co-workers [87], a mean value of -435 kJ mol^{-1} CO_2 was obtained in different soils supplied with glucose under aerobic conditions, which indicates a complete oxidation of the substrate to CO_2. In wet soil aggregates, in which the gas exchange may be limited by diffusion processes, the heat output per unit of carbon dioxide evolved was reduced by 35% under aerobic conditions.

The calorimetric:CO_2 ratio obtained under aerobic conditions was subsequently compared with the calorimetric:CO_2 ratio obtained under anaerobic conditions when the samples where incubated under a N_2 atmosphere. During anaerobic conditions the value of the ratio was further reduced by 50% reflecting an increased fermentative metabolism which excludes the possibility that the anaerobic metabolism was completely represented by different types of anaerobic respiratory metabolism. This interpretation was strengthened by the results of addition of a substrate rich in NO_3^-, which provided the soil organisms with an alternative electron acceptor to oxygen. Indeed, under such conditions the calorimetric:CO_2 ratio stayed at its highest level, comparable to the value obtained during conditions providing fully aerobic metabolism, also in samples with relatively large soil aggregates. This study strongly demonstrates the value of the combination of heat and gas analyses, but also to the usefulness of combining additional analyses, such as N_2O production, to give a measure of the extent of anaerobic respiration in the form of denitrification. A similar approach was used in a study with pure cultures. During anaerobic growth of the denitrifying bacterium *Pseudomonas fluorescens,* heat measurments were combined with electron acceptor analyses (Figure 11; [108]). In this study thermodynamic quantification was also performed. A theoretical treatment is, unfortunately, not always straightforward because lack of tabulated thermodynamic values of all possible substrates and products that may be of interest. However, where possible, a theoretical calculation of expected enthalpy change values may in comparison with experimentally obtained data, verify or falsify a hypothesis of, for example, population compositions and activities.

This will be illustrated in the following *example.* In the study by Samuelsson and collaborators [108], the multichannel microcalorimeter (BAM) was used in the flow-through mode. The aim of the study was to compare the growth of a dentrifier (catabolic endproduct: nitrogen gas), *Pseudomonas fluorescens,* and a dissimilatory ammonium producer (catabolic endproduct: ammonium), *Pseudomonas putrefaciens,* during anaerobic growth in nitrate- or nitrite-

limited medium. The bacteria were cultured in liquid media with added nitrogenous electron acceptors in sealed flasks. In order to achieve anaerobic cultivation conditions, the flasks were evacuated and flushed with helium gas and the tubes connecting the flasks with the measuring cells of the microcalorimeter were made of stainless steel. Part of the tube line was made of silicon, *i.e.* the part that was fitted to the pumps. In order to exclude air diffusion of the silicon tubes, the pumps were placed in a plastic hood, which was internally flushed with helium gas. Unfortunately, this experimental set up was not ideal, since it may almost be regarded as a closed system, *i.e.* except that some gas diffusion was possible in the short piece of the flow line that was made of silicon, no material (not even gases) exchange with the environment was possible. Because of gas production due to metabolic activities, pressure changes occurred in the experimental system, which affected the heat determinations. The solution is to use some device that provides pressure equilibration or even better, to use an open system, in which the fermenter is continuously flushed with gas (see for example reference [43]). *P. fluorescens* behaved differently in relation to its possible "anaerobic" electron acceptors, if there were some oxygen available in comparison with pure anaerobic conditions. During purely anaerobic growth, *P. fluorescens* produced some nitrite when using nitrate as the electron acceptor. During the second half of the growth process, however, the nitrite was consumed simultaneously with the rest of the nitrate. This resulted in only one maximum in the heat production curve. In contrast, during growth with traces of oxygen diffusing into the system, oxygen was the primary electron acceptor used. Nitrate was subsequently consumed and finally nitrite that was produced during the whole nitrate consuming phase, was utilised. This subsequent use of the electron acceptors was clearly indicated from the calorimetric curve (Figure 11). Actually, in an early stage of this study the calorimetric approach indicated that there was an additional electron acceptor available, *i.e.* oxygen, despite all precautions described above to exclude oxygen from the system. Inexplicable high growth yields were, however, obtained. This was from the beginning the reason for applying calorimetry which, as already mentioned, indicated leakage of oxygen. The study was finally extended as to include quantitative enthalpy change measurements, in addition to the use of the calorimeter as a "flux meter" for monitoring metabolic shifts.

The great advantage of calorimetry is that any type of metabolism can be monitored, while all specific methods have limitations. Taking heterotrophic growth as an example, aerobic respiration, anaerobic respiration (external

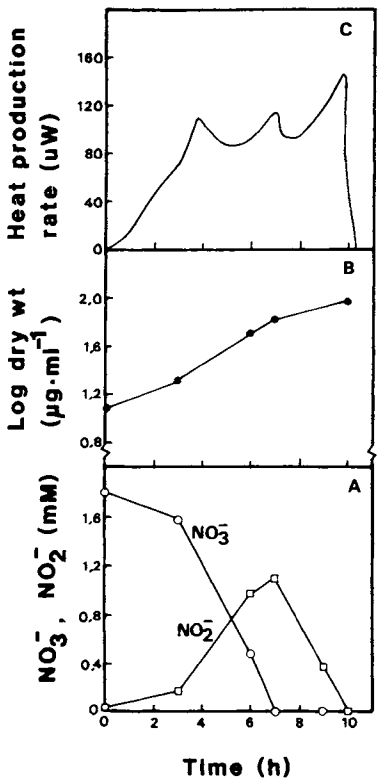

Figure 11. (A) Concentrations of NO_3^- (O) and NO_2^- (□). (B) Log dry weight (●). (C) Heat production rate for *P. fluorescens* grown on complex medium with 2 mM NO_3^- under mixed aerobic and anaerobic conditions. The first maximum in the heat signal results from consumption of impurities of oxygen. Reproduced with permission from reference [108] copyright © American Society for Microbiology.

electron acceptor other than oxygen is used) and fermentation can all be monitored quantitatively by calorimetry. Respirometry is of course only valid for organisms catabolising via aerobic respiration, while carbon dioxide monitoring like calorimetry may be appropriate in all three cases. Of course, there are many types of fermentations that do not lead to carbon dioxide evolution. Such fermentations are still possible to monitor by calorimetry, but consequently excludes the use of carbon dioxide measurements.

3.4.3. Final thermodynamic remark

Pamatmat [103] stated that "total heat flux is an indication of the rate of degradation of potential energy originally fixed by photosynthesis and represents benthic energy flow". This statement may be true, but only under strictly aerobic conditions that provide fully respiratory metabolism [105]. It is only under a fully aerobic metabolism that the entropy term becomes negligible and the energy in terms of Gibbs energy equals the enthalpy change or heat change provided that the system works at constant temperature and pressure.

4. CONCLUSIONS

Calorimetry may be useful for a diverse spectra of microbial studies, including physiological studies of pure cultures incubated in defined media to ecological studies of natural samples with a mixed population of microorganisms feeding on a large variety of nutrient sources. Calorimetric data can in combination with other methods be used in mechanistic studies, in which the black box is opened up in order to study intracellular regulatory mechanisms. The very great advantage of calorimetry is that it is completely non-specific, which means that almost any type of biological reaction or process may be measurable with calorimetry. The limit may be the sensitivity of the instrument. The lower limit is set by the activity of the microorganisms, *i.e.* the higher the metabolic activity is, the lower cell concentration it is possible to use. Both qualitative and quantitative calorimetric measurements may be useful, depending on the purpose of the measurement. For keeping track of energy flows, energy balance determinations may be valuable. However, for accurate quantitative determinations care has to be taken in the interpretation of the data. All substances have to be treated in the correct actual state, and corrections have to be made for physico/chemical side reactions [12]. For continuous registration of metabolic activity, calorimetry may be very useful in order to control bioprocesses, *e.g.* for reproducible sampling, harvesting and dynamic control of feeding streams. The different types of calorimeters are relatively robust instruments, which are fairly easy to handle. The authors of this chapter do believe that new areas of usefulness of the technique will be discovered, when more and more sophisticated techniques are used in combination with calorimetry.

REFERENCES

1 A. Beezer, Biological Calorimetry, Academic Press, London, 1980.
2 E.H. Battley, Energetics of Microbial Growth, John Wiley & Sons, Inc., New York, 1987.
3 L. Gustafsson, in M.A. Sleigh (Ed.), Microbes in the Sea, Ellis Horwood, Limited, Chichester, 1987, p.167.
4 L. Gustafsson, Thermochim. Acta 193 (1991) 145.
5 R.B. Kemp and A. Schön, Thermochim. Acta 172 (1990)
6 I. Lamprecht, W. Hemminger and G. Höhne, Thermochim. Acta 193 (1991).
7 I. Lamprecht and B. Schaarschmidt, Applications of Calorimetry in Life Sciences, Walter de Gruyter, Berlin, 1977.
8 W.W. Forrest, in J.R. Norris and D.W. Ribbons Eds.), Methods in Microbiology, Academic Press, London and New York, 1972, p.285.
9 B.F. Perry, R.J. Miles and A.E. Beezer, Calorimetry for Yeast Fermentation, Monitoring and Control., Springer-Verlag, Berlin, 1990.
10 C. Spink and I. Wadsö, Methods Biochem. Anal. 23 (1976) 1.
11 U. von Stockar and I.W. Marison, Thermochim. Acta 193 (1991) 215.
12 U. von Stockar, L. Gustafsson, C. Larsson, I. Marison, P. Tissot and E. Gnaiger, Biochim. Biophys. Acta 1183 (1993) 221.
13 D.R. Wilkie, Progr. Biophys. Biophys. Chem. 10 (1960) 259.
14 I. Lamprecht and A.I. Zotin, Thermodynamics of Biological Processes, Walter de Gruyter, Berlin and New York, 1978.
15 U. von Stockar and I.W. Marison, in A. Fiechter (Ed.), Advances in Biochemical Engineering, Springer-Verlag, Berlin, 1989, p.94.
16 R. Ölz, K. Larsson, C. Larsson, E. Gnaiger and L. Gustafsson, in S. Schuster (Ed.), Modern Trends in Biothermokinetics, Plenum Press Ltd, New York, 1993, p.53.
17 U. von Stockar and I.W. Marison, Thermochim. Acta 229 (1993) 157.
18 U. von Stockar, C. Larsson and I.W. Marison, J. Pure Appl. Chem. 65 (1993) 1889.
19 R. Ölz, K. Larsson, L. Adler and L. Gustafsson, J. Bacteriol. 175 (1993) 2205.
20 J. Suurkuusk and I. Wadsö, Chem. Scr. 20 (1982) 155.
21 A. Chen and I. Wadsö, J. Biochem. Biophys. Meth. 6 (1982) 297.
22 C. Larsson, U. von Stockar, I. Marison and L. Gustafsson, J. Bacteriol. 175 (1993) 4809.
23 J.J. Heijnen and J.P. van Dijken, Biotechnol. Bioeng. 39 (1992) 833.
24 C. Larsson. (1990), Ph.D Thesis, University of Göteborg, Sweden.

25 T. Andlid, C. Larsson, C. Liljenberg, I. Marison and L. Gustafsson, Appl. Microbiol. Biotechnol. 42 (1995) 818.
26 A. Nilsson, C. Larsson and L. Gustafsson, Thermochim. Acta 250 (1995) 233.
27 C. Verduyn, E. Postma, W. Scheffers and J. van Dijken, J. Gen. Microbiol. 136 (1990) 405.
28 T. Watson, J. Gen. Microbiol. 64 (1970) 91.
29 C. Larsson, A. Blomberg and L. Gustafsson, Biotechnol. Bioeng. 38 (1991) 447.
30 L. Gustafsson and C. Larsson, Thermochim. Acta 172 (1990) 95.
31 C. Verduyn, E. Postma, W.A. Scheffers and J.P. van Dijken, Yeast 8 (1992) 501.
32 A.D. Warth, Appl. Environ. Microbiol. 54 (1988) 2091.
33 M.J. Cooney, I.W. Marison, M.W. van Gulik and U. von Stockar, Appl. Microbiol. Biotechnol. 44 (1996) 643.
34 S. Hueting and D.W. Tempest, Arch. Microbiol. 123 (1979) 189.
35 C. Larsson, U. von Stockar, I. Marison and L. Gustafsson, Thermochim. Acta 251 (1995) 99.
36 G. Lidén, A. Persson, L. Gustafsson and C. Niklasson, Appl. Microbiol. Biotechnol. 43 (1995) 1034.
37 O.M. Neijssel and D.W. Tempest, Arch. Microbiol. 107 (1976) 215.
38 O.M. Neijssel and D.W. Tempest, in A.T. Bull, D.C. Ellwood and C. Ratledge (Eds.), Microbial Technology: Current State, Future Prospects. 29th Symposium of the Society for General Microbiology, Cambridge University Press, London, 1979, p.53.
39 O.M. Neijssel, E.T. Buurman and M.J. Teixeira de Mattos, Biochim. Biophys. Acta 1018 (1990) 252.
40 D.W. Tempest and O.M. Neijssel, FEMS Microbiol. Lett. 100 (1992) 169.
41 C. Larsson, A. Nilsson, A. Blomberg and L. Gustafsson, J. Bacteriol. 179 (1997) 7243.
42 G. Liden, A. Persson, L. Gustafsson and C. Niklasson, Appl. Microbiol. Biotechnol. 43 (1995) 1034.
43 E. Albers, C. Larsson, G. Lidén, C. Niklasson and L. Gustafsson, Appl. Environ. Microbiol. 62 (1996) 3187.
44 J. van Dijken and W. Scheffers, FEMS Microbiol. Rev. 32 (1986) 199.
45 A. Blomberg and L. Adler, Adv. Microb. Physiol. 33 (1992) 145.
46 K. Nordström, J. Inst. Brew. 74 (1968) 429.
47 E. Oura, Proc. Biochem. 12 (1977) 19.

48 L.C.M. Auberson and U. von Stockar, Biotechnol. Bioeng. 40 (1992)
49 B. Birou, I.W. Marison and U. von Stockar, Biotechnol. Bioeng. 30 (1987) 650.
50 B. Birou and U. von Stockar, Enzyme. Microb. Technol. 11 (1989) 12.
51 A. Blomberg, C. Larsson and L. Gustafsson, J. Bacteriol. 170 (1988) 4562.
52 I. Marison and U. von Stockar, Enzyme. Microb. Technol. 9 (1987) 33.
53 U. von Stockar and B. Birou, Biotechnol. Bioeng. 34 (1989) 86.
54 C. Larsson, G. Liden, C. Niklasson and L. Gustafsson, Bioproc. Eng. 7 (1991) 151.
55 M. Meier-Schneiders, U. Grosshans, C. Busch and G. Eigenberger, Appl. Microbiol. Biotechnol. 43 (1995) 431.
56 T.W. Randolph, I.W. Marison, D.E. Martens and U. von Stockar, Biotechnol. Bioeng. 36 (1990) 678.
57 C. Larsson, C. Morales, L. Gustafsson and L. Adler, J. Bacteriol. 172 (1990) 1769.
58 C. Larsson, A. Nilsson and L. Gustafsson, in E. Gnaiger, F. Gellerich, M. Wyss, R. Steinlechner and G. Azzone (eds.), What is Controlling Life, Vol. 3, Innsbruck University Press, Innsbruck, 1994, p.232.
59 R. Lagunas, FEMS Microbiol. Rev. 104 (1993) 229.
60 C. Gancedo and R. Serrano, in A. Rose and J. Harrison (Eds.), The Yeasts, Academic Press, 1989, p.205.
61 D. Fell, Understanding the Control of Metabolism, Portland Press, London and Miami, 1997.
62 B. Teusink, M. Walsh, K. van Dam, L. Gustafsson and H. Westerhoff. in H.V. Westerhoff, J.L. Snoep, J.E. Wijker, F.E. Sluse and B.N. Kholodenko (eds.), Modern Trends in BioThermoKinetics, Vol. 7, BioThermoKinetics Press, Amsterdam, 1996 p.417.
63 B. Teusink, C. Larsson, J. Diderich, P. Richard, K. van Dam, L. Gustafsson and V. Westerhoff, J. Biol. Chem. 271 (1996) 24442.
64 K. Drong. (1991) , Freie Universität, Berlin.
65 T. Grospietsch, K. Drong and I. Lamprecht, Experientia 51 (1995) 117.
66 P. Richard, B. Teusink, H.V. Westerhoff and K. van Dam, FEBS Lett. 318 (1993) 80.
67 B. Hess, J. Exp. Biol. 47 (1979) 271.
68 T. Nyström, L. Larsson and L. Gustafsson, The EMBO J. 15 (1996) 3219.
69 S. Iuchi and E.C.C. Lin, Proc. Natl. Acad. Sci. USA 85 (1988) 1888.
70 T. Haller, M. Ortner and E. Gnaiger, Anal. Biochem. 218 (1994) 338.

71 C. Larsson, A. Nilsson, I. Påhlman and L. Gustafsson, in H.V. Westerhoff, J.L. Snoep, J.E. Wijker, F.E. Sluse and B.N. Kholodenko (eds.), Modern Trends in BioThermoKinetics, Vol. 7, BioThermoKinetics Press, Amsterdam, 1996 p.407.
72 M.C.M. van Loosdrecht, in O.M. Neijssel, R.R. van der Meer and K.C.A.M. Luyben, (eds.), The European Congress on Biotechnology Vol. 4, Elsevier Science Publishers B.V., Amsterdam, 1987
73 B.A. Humphrey and K.C. Marshall, Arch. Microbiol. 140 (1984) 166.
74 S. Kjelleberg, B.A. Humphrey and K.C. Marshall, Appl. Environ. Microbiol. 43 (1982) 1166.
75 S. Kjelleberg, B.A. Humphrey and K.C. Marshall, Appl.Environ. Microbiol. 46 (1983) 978.
76 J.J. Bright and M. Fletcher, Appl. Environ. Microbiol. 45 (1983) 818.
77 A.S. Gordon, S.M. Gerchakov and J. Millero, Appl. Environ. Microbiol. 45 (1983) 411.
78 D. Kirchman and R. Mitchell, Appl. Environ. Microbiol. 43 (1982) 200.
79 T. Andlid. (1995) Ph.D Thesis, General and Marine Microbiology , Göteborg University, Göteborg.
80 H. Vandenhove, R. Merckx, H. Wilmots and K. Vlassak, Soil Biol. Biochem. 23 (1991) 1133.
81 R. Vázquez-Juárez, T. Andlid and L. Gustafsson, Mol. Marine Biol. Biotechnol. 6 (1996) 64.
82 R. Vázquez-Juárez, T. Andlid and L. Gustafsson, Colloids and Surfaces 2 (1994) 199.
83 L. Blomberg. (1992) Ph.D Thesis, General and Marine Microbiology , Göteborg University, Göteborg.
84 L. Blomberg, L. Gustafsson, P. Cohen, P. Conway and A. Blomberg, J. Bacteriol 177 (1995) 6695.
85 L. Gustafsson, Thermochim. Acta 251 (1995) 69.
86 U. Reh, Thermochim. Acta 193 (1991) 107.
87 B.P. Albers, F. Beese and A. Hartmann, Biol. Fertil. Soils 19 (1995) 203.
88 F.A. Hesselink van Suchtelen, Archiv fur Pflanzenbau 7 (1931) 519.
89 K. Ljungholm, B. Norén, R. Sköld and I. Wadsö, OIKOS 33 (1979) 15.
90 K. Ljungholm, B. Norén and I. Wadsö, OIKOS 33 (1979) 24.
91 K. Ljungholm, B. Norén and G. Odham, OIKOS 34 (1980) 98.
92 T. Konno, Netsu 3 (1976) 148.
93 T. Kimura and K. Takahashi, J. Gen. Microbiol. 131 (1985) 3083.
94 B. Heilmann and F. Beese, Soil. Sci. Soc. J. 56 (1992) 596.

95 U. Mortensen, B. Norén and I. Wadsö, Bulletins from the Ecological Research Committee (Stockholm) 17 (1973) 189.
96 G.P. Sparling, Soil Biology and Biochemistry 13 (1981) 93.
97 G.P. Sparling, Soil Biology and Biochemistry 13 (1981) 373.
98 G.P. Sparling, J. Soil Science 34 (1983) 381.
99 H. Vandenhove. (1992) Ph.D Thesis, Katholieke Universiteit te Leuven, Leuven.
100 K. Gustafsson and L. Gustafsson, J. Microbiol. Meth. 4 (1985) 103.
101 G. Nordmark, M. Laynez, A. Schön, J. Suurkuusk and I. Wadsö, J. Biochem. Biophys. Meth. 10 (1984) 187.
102 M.M. Pamatmat, G. Graf, W. Bengtsson and C.S. Novak, Marine Ecology - Progress Series 4 (1981) 135.
103 M.M. Pamatmat, Science 215 (1982) 395.
104 P. Laserre and T. Tournier, J. Exp. Marine Biology and Ecology 74 (1984) 123.
105 E. Gnaiger, in E. Gnaiger and H. Forstner Eds.), Polarographic Oxygen Sensors, Springer-Verlag, Berlin, 1983, p.337.
106 E. Gnaiger and R.B. Kemp, Biochim. Biophys. Acta 1016 (1990) 328.
107 K. Gustafsson and L. Gustafsson, OIKOS 41 (1983) 64.
108 M.-O. Samuelsson, P. Cadez and L. Gustafsson, Appl. Environ. Microbiol. 54 (1988) 2220.

Handbook of Thermal Analysis and Calorimetry. Vol. 4: From Macromolecules to Man.
R.B. Kemp, editor.

Chapter 8

CALORIMETRY OF SMALL ANIMALS

I. Lamprecht and E. Schmolz

Institut für Biophysik, Freie Universität Berlin, Thielallee 63, D-14195 Berlin, Germany

1. INTRODUCTION

1.1. General aspects

Animal calorimetry and thus calorimetry in general started more than 200 years ago when Lavoisier and Laplace presented their famous *Memoire sur le Chaleur* to the French Academy of Sciences [1]. They described their well-known ice calorimeter and reported about the metabolism and the heat production of guinea-pigs. Nearly simultaneously, Adair Crawford in Edinburgh investigated biological material by combustion calorimetry before he changed to heat production rates of living matter [2]. He showed for the first time that there is a rough proportionality between oxygen consumption and heat dissipation and thus founded the basis of modern indirect calorimetry. But it was Lavoisier with his experiments on guinea-pigs who made the essential step. Simultaneously to the amount of melted ice he determined the consumption rate of oxygen as a measure of the animal's respiratory gas exchange. His famous *La vie est donc une combustion* can be cited in more detail as *Life is a slow combustion maintained through respiration. Animal bodies are composed of combustible elements. Food replaces the loss of body substances resulting from the combustion of some of the matters present in the body* (cited from [3]).

After these essential first steps into modern scientific thinking and away from alchemistic ideology it took a long time before the next sound experiments on animals were performed by e.g. Despretz [4], Rubner [5], Laulanie' [6], by Krehl and Soetbeer [7] and by Atwater and Rosa [8] on man. More details about the historical development of animal calorimetry can be found in Kleiber's classical book *The Fire of Life* [9].

Biological calorimetry made a great progress in the last decades including a continuous transition from customer produced instruments to commercially available, versatile and highly sophisticated machines [10]. The field of medium sized animals remained more or less excluded since - on the one hand - suitable calorimeters with active volumes of several hundred millilitres are missing on the market. On the other hand the philosophy still exists that *indirect* calorimetry like manometry, polarography, tracer techniques, metabolite determinations or monitoring of heart beat, e.g., renders similar results in an easier, less expensive and quicker way (section 2.). This is partly correct, but often these approaches demand sacrificing the animals or show only a reduced picture when anaerobic metabolism is included. Direct calorimetry is for sure the most general and integrative method with many advantages, though also with some pitfalls.

Direct and indirect calorimetry covered the whole size spectrum of animals from the fruit fly *Drosophila melanogaster* with 1 mg to large domestic animals like horses, cows and oxen with more than 500 kg. Since this article is dedicated to small animals these upper boarders will not be touched. But there are excellent monographs and review articles dealing with these aspects of animal calorimetry which may be consulted for further information [11,12]. The whole field of human calorimetry is also excluded although many methodological, technical and fundamental parallels exist to our present paper. Again many monographs may be considered. Moreover, a recent review by Schutz about direct and indirect calorimetry with special orientation to man renders a good introduction and a comprehensive literature compilation [3].

The present paper concentrates on *small animals*. The term *small* needs some clarification since *small* is a rather arbitrary decision. For a long time the 100 mL-Calvet calorimeters were the only commercial instruments applicable for animals while the next larger choice were so-called whole body apparatus for poultry and domestic animals like cats and dogs. Thus, *small* in our sense means organisms that can be easily investigated in vessels of about 100 mL. Exceptions are stable colonies or swarms of social insects reared in simple calorimetric boxes (section 3.5.) to study the energetics of their social life and interactions in parallel to the usual calorimetric investigations of isolated members of different castes or of small groups of them (see below).

A further - technical - discrimination goes for terrestrial and aquatic animals since they demand considerably different experimental conditions. Terrestrial animals, especially insects, are easy to breed, to keep, to handle and to investigate and usually need no care during the investigation and no sophisticated equipment. Aquatic animals are surrounded by a medium of high specific heat capacity so that the instrumental response becomes slow, temperature equilibration periods long and experiments tedious. But the most important difference con-

cerns the oxygen supply of the animal under investigation. With an oxycaloric equivalent of -450 kJ per mol oxygen corresponding to 20 J/mL oxygen for a typical metabolism and a heat production rate of 2 mW = 2 × 10^{-3} J/s the animal has an oxygen consumption rate of 1 × 10^{-2} mL/s. In a 100 mL-vessel with air there are about 20 mL oxygen (about 1 mmol) available. During an experiment of 10 000 s (about 3 h) only 1 mL O_2 (5 %) is consumed so that the initial concentration drops from 21 to just 20 % which has no significant influence on the metabolic rate of the animal. Due to the low solubility of oxygen in fresh water (237 µmol/l at 30 °C) the situation is completely different in aquatic experiments. The above mentioned 2 mW of heat production transforms to 4.5 10^{-9} mol/s (1 × 10^{-2} mL/s) and to an oxygen consumption of 45 µmol in 10000 s. This is nearly twice the amount of oxygen dissolved in 100 mL of water (23.7 µmol). These calculations show that aquatic animals soon come to hypoxic and even microoxic or anoxic conditions which considerably change their metabolism. Thus, aeration of the experimental vessel or a steady flow of air saturated water through the vessel are necessary for meaningful and successful experiments. But both approaches have their disadvantages: the first introduces evaporation effects with high energetic contributions if the incoming air is not completely saturated with water vapour. The second one may exhibit mixing heat if the inflowing water is not exactly temperature equilibrated beforehand. It becomes clear that investigations with aquatic animals are more tricky and demand for more sophisticated equipment than those with terrestric species. These problems will be discussed below in more detail.

Papers on calorimetry of (smaller) animals are spread over rather different journals from very general ones like Nature and Science to very specific ones for marine biology or ecology so that it is difficult to get a comprehensive view. Several review articles on special fields [13-15] and some monographs appeared in recent years. Although not preferably dedicated to the present questions a broad collection of papers on direct and indirect animal calorimetry can be found in two monographs of Zotin [16,17] and another four by Zotin and Lamprecht [18-21] about Biological Calorimetry.

All calorimetric data cited in this chapter deal with intact, living animals which are not sacrificed for or during the experiment. That means that

- All weights and weight specific rates in this chapter are given as or per wet weight and as dry weight only if stated.
- All results obtained by combustion calorimetry are excluded and reserved for the corresponding chapter *Combustion Calorimetry* in this volume of the handbook.

- Calorimetric papers dealing with whole organs of animals (e.g. [22-24]) like hearts of frogs [25], muscles [26-28], nerves [22,23] or perfused organs [29,30] may be found in other compilations.
- Although much calorimetric work has been performed with original animal tissues such as brown fat [22] or human skin [31,32] and on animal cells in culture (see Chapter *Isolated Animal Cells* by R. Kemp in this handbook), they are not the topic of the present review.

When heat production rates are given per body mass (mW/g) in the following chapter, one has to keep in mind that such a *weight specific rate* - corresponding to *specific gravity* or *specific heat* - is doubtful. Kleiber has shown that metabolic rates are not linearly correlated with body weight, but with a broken power of it (often about 0.75). Thus, a weight specific heat production rate would vary with weight and would not be a constant as those two other *specific* examples [9,33]. Therefore, metabolic rates per animal should be prefered, or a *metabolic weight* should be used which incorporates the broken power (section 7.2.). Nevertheless, the information *mW/g* will be applied here since it facilitates the energetic comparison between animals of very different families and sizes.

1.2. Time constant

The commercially available Calvet microcalorimeters with batch vessels of 100 mL active volume have rather high time constants of the thermal signal so that a *smearing* of the power-time curves occurs. If one is not only interested in the mean heat output of an animal during prolonged periods, but also in the amplitudes of locomotor activities desmearing techniques have to be applied to the registered slope. The classical approach is performed by the Tian equation

$$q(t) = \alpha\,[\Theta(t) + \tau \times \mathrm{d}\Theta(t)/\mathrm{d}t] \qquad (1)$$

where $q(t)$ is the thermal power, t the time, α the heat exchange coefficient, Θ the temperature difference between the active and the reference vessel and τ the time constant of the calorimeter [34-36]. Modern techniques - simplified by computer application to calorimetry - include the well known Fast Fourier Transform [36,37]. Figure 1 gives an example for the desmearing effect due to the Tian equation for the power-time curve of a Milos wall lizard (*Podarcis milensis*) (section 4.). The bursts of activity become more pronounced and structures become visible which were hidden in the original trace. But it should be remembered that the heat output represented by the corresponding area under the curve remains unchanged by desmearing.

1.3. Remarks on calorimetric nomenclature

Modern biological calorimetry differentiates between *quantitative* and *analytical* calorimetry. The first is the classical one bound to the determination of thermodynamical data of enthalpy, entropy and heat capacity. The more modern *analytical calorimetry* looks *whether* heat producing processes are occurring and with which kind of time profile. This type is of great interest during metamorphosis of insects, adaptation phenomena to environmental factors or periodically repeated activities. Examples of such different applications of analytical calorimetry will be given below.

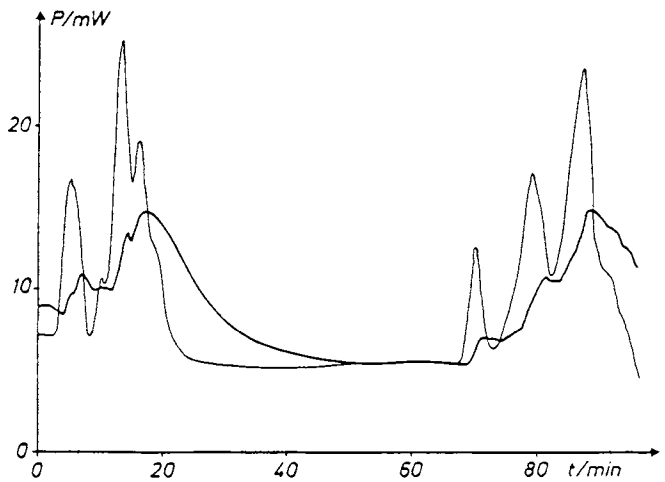

Figure 1. Recorded power-time curve (solid line) of a Milos wall lizard (*Podarcis milensis*) and the *desmeared* original signal (thin line) calculated with the Tian equation [38].

Sometimes there is confusion due to different use of terms. Thermodynamics calls a process *exothermic* when heat is given off by the system and *endothermic* when it consumes heat. In biology, warm-blooded (*homeothermic*) animals like mammals and birds that produce heat to keep their body temperature constant are called *endotherms* and their behaviour *endothermic*, in contrast to the thermodynamical direction. Their counterparts with changing body temperatures are *ectotherms* (not exotherms) or cold-blooded (*poikilothermic*) animals. Nevertheless, all of them produce heat as a by-product of their metabolism so that they can be monitored by (exothermic) calorimetry.

The term *thermogram* was used in the older literature for the calorimeter signal as function of time. *Thermogram* is now reserved by nomenclature for changes of

enthalpy or heat capacity as a function of varying temperature or for images of infrared thermo-cameras. Therefore, *thermogram* is substituted by *power-time curve* throughout this text. Other terms like *heat flow versus time*, *heat flux versus time* or *heat dissipation curve* are also used in the literature.

Physiologists are rather conservative people and like to publish still in old units that do not agree with the SI norm. Even the *large calorie* Cal is sometimes found in the literature. In this survey all original data are transformed to the official power unit Watt (W) and the corresponding energy unit Joule (J). To facilitate the comparison of data Table 1 shows the appropriate conversion factors - but unidirectional!

Table 1.
Conversion of some frequently used old or odd units of energy and power into the correct SI units.

Old/Odd Unit	SI Energy Unit J	SI Power Unit W
cal	4.1868	
Cal	4.1868×10^{3}	
cal/h		1.163×10^{-3}
Cal/h		1.163
cal/d		48.46×10^{-6}
Cal/d		48.46×10^{-3}
J/h		277.8×10^{-6}
J/d		11.58×10^{-6}

2. DIRECT AND INDIRECT CALORIMETRY

The quantity of heat produced when a given portion of pure air is altered by the respiration of an animal is nearly equal to that which is produced when the same quantity of air is altered by the combustion of wax or charcoal. (Crawford, 1778) [2]. These early words of Crawford together with Laplace's indirect observation of respiration rates of guinea-pigs in his ice calorimeter established the fundaments for the great success of indirect calorimetry.

Indirect calorimetry was originally bound to the manometric or voluminetric determination of the respiratory metabolism of an animal, i.e. its oxygen consumption and carbon dioxide production rate. Nowadays, it includes a manifold of different metabolic approaches, as briefly mentioned in the *Introduction*.

Battley [39] presented a critical survey about advantages and drawbacks of direct and indirect techniques for different types of calorimetry. Kleiber [33] stated that *Indirect calorimetry measures the heat production of an animal; direct calorimetry measures the heat loss. Heat gain and heat loss are equal only when heat capacity and body temperature remain constant.* One may define indirect calorimetry as the determination of heat production rates by means of some methods other than direct calorimetry. But one has to bear in mind that *with the exception of the determination of heat production by ergometry, all indirect methods of calorimetry depend ultimately on previously made direct calorimetric measurements of one kind or another that are used in the calculation of the heat produced.* [39]

If one has the choice to make direct or indirect calorimetric determinations one has to consider their strong and weak points. For analytical calorimetry, i.e. the proof if some process is proceeding and how fast, the direct approach is preferable, e.g. for temporal structures or periodicities in animal activity or for special developmental transitions like pupation and moulting of insects (section 5.3.). Although calorimeters are more expensive than most indirect techniques they are also advantageous for quantitative analysis of heat loss provided that the necessary corrections can be performed for the true heat dissipation. If one wants to know the reason(s) for an observed heat loss, indirect calorimetry may be the approach of choice. But in any case when both methods are at hand, it will be best to determine the possible heat loss in an indirect way and confirm it later with the direct one [39].

Oxygen consumption is most frequently used to determine the energy metabolism of animals, as the energetically coupled transfer of electrons from the substrate to the terminal acceptor oxygen is the most important mechanism of energy transformation under normoxic conditions. When dealing with higher terrestric animals, there will be a strong correlation between heat production and oxygen consumption, but this is not necessarily true for aquatic animals (section 7.1.). From the known substrate and the oxycaloric equivalent of heat production per mol of oxygen the heat dissipation of an animal can be calculated when the oxygen uptake is determined (indirect calorimetry). Oxycaloric equivalents change between 430 and 500 kJ/mol O_2 with a main value of about 450 kJ/mol. Several authors showed that indirect and direct calorimetry render the same results under atmospheric conditions.

However, there are often situations in the life of animals (e.g. strong locomotor activities, decrease of oxygen concentration in their environment) that force them to switch over partly (perhaps also temporarily) or completely to anaerobic metabolism without oxygen consumption. Under such conditions direct calorimetry - which monitores all enthalpy changes in the animal and not only the aerobic ones

- provides a full picture of energetic flows and the only means to determine metabolic rates directly [40].

Although this handbook is dedicated to *true* calorimetric techniques and results, it is necessary to present here some survey about indirect calorimetry as it plays such an important role in the determination of animal metabolism.

2.1. Determination of gas metabolism

Animals need external energy to keep their homeostasis and numerous gradients across cellular membranes as well as for biosynthesis and muscular activities. Such biochemical processes are coupled with a significant heat dissipation that can be monitored via oxygen consumption, carbon dioxide production and nitrogen excretion.

The classical Warburg method of manometric indirect calorimetry (see e.g. [41]) determined the oxygen consumption rate by a reduction of volume and the carbon dioxide production by a volume increase in the gaseous environment of an organism under research. The ratio of carbon dioxide production and oxygen consumption, the so-called respiratory quotient RQ, rendered information about the substrate(s) used in this specific metabolism. Table 2 presents the RQ values for various pure or mixed substrates and the expected heat production or gas exchanges.

Table 2.
Respiratory quotient RQ, expected enthalpy change and gas exchanges for pure and mixed substrates in animal calorimetry. Adapted from [3]

Substrate	RQ	ΔH kJ/g	V_{O2} L/g	V_{CO2} L/g
Glucose	1.00	15.6	0.746	0.746
Starch	1.00	17.5	0.829	0.829
Ethanol	0.667	29.6	1.460	0.973
Lactic acid	1.00	15.1	0.746	0.746
Protein	0.835	19.7	1.010	0.844
Lipid	0.707	39.6	2.019	1.427

This simple approach for only two kinds of gases was later refined to include methane production and excretion of nitrogen with urine (see [3] for review). Brouwer [42] proposed the following equation for mammals

$$\Delta H\,(\mathrm{kJ}) = 16.17\ V_{O2}\,(\mathrm{l}) + 5.02\ V_{CO2}\,(\mathrm{L}) - 2.17\ V_{CH4}\,(\mathrm{L}) - 5.99\ W_{N}\,(\mathrm{g}) \qquad (2)$$

where V_{O2}, V_{CO2} and V_{CH4} are volumes of oxygen, carbon dioxide and methane, resp., given in litres exchanged during the experimental period and W_N the mass of nitrogen in gram in the urinary excreta. For many animals the contribution V_{CH4} of methane can be neglected so that Romijn and Lokhorst [43] found a relation for birds

$$\Delta H\,(\mathrm{kJ}) = 16.20\ V_{O2}\,(\mathrm{L}) + 5.00\ V_{CO2}\,(\mathrm{L}) - 9.93\ W_N\,(\mathrm{g}). \quad (3)$$

If the RQ value is determined, the equation of Kleiber [9] can be applied

$$\Delta H\,(\mathrm{kJ}) = V_{O2}\,(14.25 + 7.86 / \mathrm{RQ}). \quad (4)$$

It becomes obvious from the above equations that the contribution of V_{O2} to the energy dissipation is the most important one.

Such equations are often applied in metabolic investigations. To cite just a few references from the literature: Miller and coworkers [44] determined the energy metabolism of mice (*Mus mus*) and kestrels (*Falco tinnunculus*), Bennet and Dawson [45] that of lizards and snakes, and Dauncey and Ingram [46] that of young pigs under the influence of drugs. Moreover, such relations are used in one way or another to estimate substrate expenditure rates under the assumption that all substrates of endogenous and exogenous origin are completely oxidized to water and carbon dioxide and that urea is the main endproduct of nitrogen metabolism [3].

It was shown by Lovrien and coworkers [47] that overall oxygen demand overestimated the basal metabolic rate because it included transient bursts of heat with an own oxygen consumption (Figure 2). Direct calorimetry discerns the quiet or resting periods with apparently no locomotor or other activities, while in several techniques oxygen demand as an integral method shows nearly no temporal structures and thus includes the phases of higher energy exchange also. Therefore, analytical calorimetry as a tool for monitoring activities, different metabolic levels or transient states of an animal should be carried out by direct calorimetry and not by manometry or polarography.

2.2. Metabolic investigations by tracer techniques

The following method is often counted separately and complementary to indirect calorimetry (see e.g. [3]). Nevertheless, we will introduce it here as it renders metabolic information in addition to direct calorimetry with more detail about metabolic pathways than the classical indirect approach.

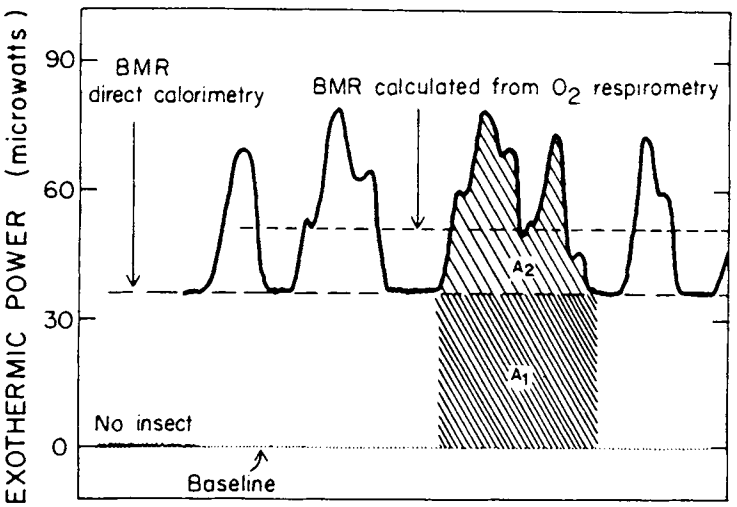

Figure 2. Typical power-time curve of an insect showing the basal metabolic rate (BMR) of low level and transients of increased heat output that are included in the mean oxygen demand [47].

Radioactive or non-radioactive labelling of substrates offers an independent approach to study animal metabolism. Most common are ^{14}C and ^{3}H radioactive isotopes and deuterium ^{2}H, carbon ^{13}C, nitrogen ^{15}N and oxygen ^{18}O as stable ones. The concentration of the latter can be increased artificially to facilitate their detection. The stable isotopes are preferable as they are harmless to the animals as well as to the scientist. In the case of nitrogen this isotope is the only choice for labelling. They are still rather expensive and need a lot of skill in mass spectrometry detection.

Lifson and coworkers [48] used isotope dilution techniques in form of the double-labelled water method to evaluate the CO_2 production and the origin of the oxygen expired in CO_2. In the *carbon dioxide entry technique* CO_2 production is determined and transformed to energy units by means of the RQ value [49]. Both techniques were applied to larger animals, but they are not applicable to short time investigations.

2.3. Heart rate and metabolism

The correlation between heart rate and oxygen consumption or heat production was sometimes used as an indirect approach to metabolic rates after corresponding calibration. Smaller animals like rodents (e.g. squirrels, rats, mice, hamster

[50]) or bats [51,52] and large ones like sheep [53] were investigated by this means. The oxygen consumption rate dV_{O2}/dt of the latter could be calculated by

$$dV_{O2}/dt = (HR \times SV) \times (c_A - c_V) \quad (5)$$

with the heart rate HR, the stroke volume SV, and the oxygen concentrations c_i in the arterial (A) and the venous blood (V), resp. [53]. By direct calorimetry Nagasaka and coworkers presented a heat production/heart rate correlation of

$$M\,(W/m^2) = 0.194\ HR\ (beats\ per\ min) - 17.7 \quad (6)$$

for resting rats at various temperatures between 14 and 27 °C [54]. These temperatures resulted in a wide range of M and HR values.

Most of the animals cited in this review are too small to apply this heart rate technique. But heart beat can be measured by other methods in small invertebrates so that this approach might stimulate the fantasy of some calorimetrists for further investigations.

3. ADDITIONAL EQUIPMENT

3.1. Optical monitoring

Power-time curves of animals are not at all generally smooth and on a constant level, but rather show significant and characteristic temporal structures (see e.g. Figures 2,4,5,9,10,12,14,16,18,20). These structures are mainly due to locomotor activities which may be rather strong despite of the reduced space in the calorimetric vessel. To facilitate the interpretation of different activity levels, Lamprecht and Becker developed a combination of a 100-mL Calvet microcalorimeter with an endoscopic system [55]. A rigid endoscope of appropriate length and diameter, with a Hopkins optic and an aperture of 67° was incorporated into the supporting rod of the calorimetric vessel. Illumination was performed via a light guide by a coldlight projector. Different filter combinations could be used to dimm the light or to select the near infrared. Animals were observed by the eye or by a video system of camera, recorder and monitor. In the case of near infrared, an infrared night vision system was applied between endoscope and video camera. As honeybees change their behaviour under light and as the usual calorimetric investigations were performed in the dark, near infrared illumination - invisible to the bees - was used for their observation [56,57].

The projector output (50 to 100 mW heat production due to illumination in the calorimetric vessel) was dimmed down to about 1 mW for visual observation and 10 mW for video monitoring. For comparison: snails produced about 0.4 mW, crickets around 2 mW, honeybees 16 mW and lizards 8 mW. After electrical stabilization of the projector, illumination resulted in a constant shift of the base-line and did not disturb the calorimetric experiments. Figure 3 shows a water snail (*Biomphalaria glabrata*) on the bottom of the vessel. The vertical lines on the vessel wall were used for orientation to determine the exact position of the animal [55].

Figure 3. Endoscopic view of a water snail (*B. glabrata*) on the bottom of the calorimetric vessel. The helix of the snail-shell is decorated with white lines to facilitate the determination of its orientation in the vessel when observing periodic movements [55].

A significantly refined system was published by Addink and coworkers to analyse the movement of fish in a flow-through differential calorimeter of 1 liter (section 7.2.) [58]. This system consisted of an automatic video tracking and motion analysis system and a rigid endoscope of 90° aperture, separated from the water in the vessel by a small window. The radiation of the coldlight source was split into two halfs to illuminate both, the active and the reference vessel. Together with a water-cooled glass filter this twin setup reduced the parasitic heat production rate to just ± 5 μW. Neverteless, the necessary illumination increased the metabolic rate of fish that were usually kept in complete darkness for more

than one week. The video signals were analyzed by digital image processing and allowed to observe rather complex movements of fish under normoxic and anoxic conditions and to gain additional behavioral information about the locomotor activity of the animals and their kind of metabolism (section 7.2).

3.2. Acoustic monitoring

Insects often try to fly in the calorimetric vessel and move their wings as sign of unrest or means of warming up. As these activities are connected with a production of sound, they may be easily monitored and analyzed by audio techniques. Incorporation of a microphone in the vessel does not disturb the calorimetric output. Acoustic signals can be directly perceived via a loudspeaker or registered on a tape recorder for later analysis by a sound spectrograph connected with a film camera [57]. As the power-time curves change rather slowly with time it is possible to ascribe a distinct frequency spectrum to a specific point in the trace (Figure 4). This facilitates the interpretation of locomotor activities of the animal in the vessel. Moreover, a strict correlation between sound generation and the metabolic heat output could be shown for bumblebees [59]. These results will be discussed below (section 5.4.3.).

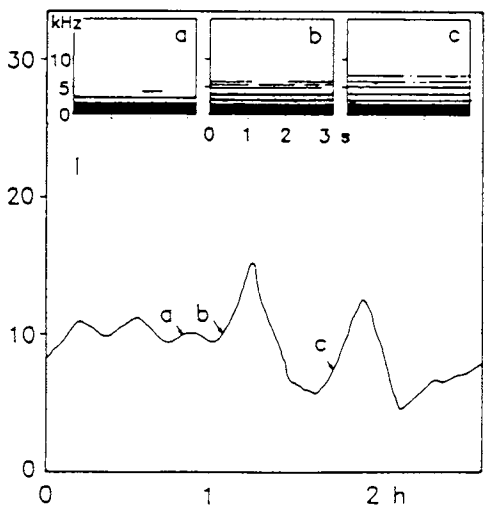

Figure 4. Power-time curve of a virgin honeybee queen (*Apis mellifera carnica*) at 25 °C together with 3 frequency spectra for the points *a*, *b* and *c*. Besides the ground noise, there are nearly no higher frequencies for point *a* of resting metabolism, while at *b* and *c* higher frequencies dominate prior to the heat increase in the curve [57].

Another example of sound monitoring was given in the power-time curve of a cricket (*Acheta domesticus*) [60]. At the beginning of the experiment it showed an extreme unrest with high locomotor activity. After calming down to a level of half the initial intensity the animal periodically produced the typical sound of crickets. The song periods were seen as times of reduced metabolism and activity. This result was in agreement with the observation that crickets stridulate by moving their forwings above each other in a resting position, even at the unpleasant and restricted environment of a calorimetric vessel: *Music can soften pain to ease* (Alexander Pope, *Chorus to Brutus*).

3.3. Gas monitoring

For a long time, indirect calorimetry in the sense of respirometry was supposed to be an easy, cheap and equivalent approach in energy metabolism compared to direct measurements. This is reflected in a far larger number of gas measuring types and devices described in the literature and sold on the market than calorimeters. Only those which are used in connection with direct calorimetry are of interest here. They exclude the classical Warburg manometry, but include gas determination by polarographic (e.g. Clark) electrodes, by electronic pressure transducers or by semiconductor chips. Most of them are specially dedicated to monitoring oxygen concentrations, besides that of course to CO_2 and to a smaller extent NH_3. Some of these techniques were combined with calorimeters. Pressure transducers, oxygen electrodes and semiconductor chips are specially suited for closed batch vessels with terrestric animals. Paramagnetic oxygen and infrared CO_2 sensors are advantageous for *dry* flow experiments where the flow of air through the calorimetric vessel is monitored for the concentrations of its components. Polarographic oxygen sensors are successfully applied to aquatic animals and flow calorimeters of the sorption type.

3.3.1. Gas sensors

Life is intimately coupled to the presence of oxygen, although systems have developed that can exist for shorter or longer periods or even exclusively under anoxic conditions. Aerobic metabolism is by far more effective in an energetical sense than the anoxic variant, so it plays a predominant role on Earth. Molecular oxygen forms about 20 % of the atmosphere, but only an essentially smaller amount is dissolved in water: 0.24 mmol/L water compared with 8.9 mmol/L air at 30 °C. This makes oxygen concentration so important for aquatic animals and so interesting for scientists working in this field.

Indirect calorimetry as an addition to or substitute for direct heat measurements is mainly respirometry, i.e. again mainly determination of oxygen consumption rates. This is why so many oxygen detecting systems are on the market and applied for such investigations. Only a few of them have been directly integrated in or coupled to calorimetry. Some examples of them will be discussed in this section.

Polarographic oxygen electrodes are most frequently applied for aquatic animals. In his book *Polarographic Oxygen Sensors* [61] Gnaiger described the combination of flow calorimeters with a twin-flow microrespirometer developed in his group at the University of Innsbruck [62]. An LKB flow sorption microcalorimeter with a sorption chamber of 0.5 mL was best suited for this purpose. A few examples were given for the successful application of this combination for investigations of aquatic animals, among them water fleas and fish larvae (section 7.3.). This specific microrespirometer is used in many laboratories. Other oxygen sensing systems applied in connection with direct calorimetry may be found in the corresponding literature (e.g. [63]).

However, the same type of sensor can also be used in terrestric investigations, yet with a strongly reduced sensitivity. A Beckman-Monitor-System (type 123301 O_2/T) was adapted to 100-mL vessels of a Calvet microcalorimeter. The electrode was placed high enough above the heat flux meter that no interference between the two signals could be observed. This system was - e.g. - applied during investigations of crabs [64] or snakes and lizards [38,65].

In parallel to this device an oxymeter plus transoxode - normally applied for transcutaneous determination of oxygen tension in blood - was used in experiments similar to those mentioned above. The transoxode was incorporated in the top cover of the calorimetric vessel or used with larger separate containers for a long-term monitoring of respiration in animals with weights of more than 1 g.

Moreover, lately developed galvanic oxygen sensors (GS Japan Storage Battery Co., Japan) were adapted to 100 mL vessels of a Calvet calorimeter. These sensors have just the correct diameter for the calorimeter, life times between 5 and 10 years, voltage outputs of 40 to 180 mV in pure oxygen, linear correlations between voltage and oxygen concentration and reaction times of 5 to 60 s for 90 % of the final signal, depending upon the type chosen. Mounted on top of the vessel they introduced no disturbance of the heat flow signal. The type KE-50 was successfully applied in investigations of bee groups, especially under the influence of alarm pheromones (H. Gehrs, E. Schmolz and I. Lamprecht, unpublished results).

Further information on a broad spectrum of non-polarographic gas sensors may be found in the book *Gas Sensors* by G. Sberveglieri [66].

In a calorimetric investigation of bumblebees Schultze-Motel applied a paramagnetic oxygen analyzer (OXYNOS-1, Leybold-Heraeus, Germany) connected to a Calvet calorimeter in flow-through mode [67,68]. The air stream through the vessel was chosen at such a level that the oxygen concentration never dropped below 20 %. Nevertheless, changes in the oxygen tension of 0.01 % could be easily detected in the analyzer signal. Moreover, an infrared carbon dioxide analyzer (BINOS, Leybold-Heraeus, Germany) was shunted in the same air stream to determine the CO_2 production and from it the respiratory quotient RQ. For a comparison of the temporal behaviour of the three signals, all had to be desmeared (sections 1.2. and 5.4.3.) with their specific time constants: calorimeter 581 s, CO_2 analyzer 239 s and O_2 analyzer 77 s. This triple combination rendered fruitful information about locomotor activity, discontinuous ventilation, sound generation and heat production as well as general metabolism. It could be further used for hibernating hornet queens [69] and activity investigations on several other insects.

3.3.2. Pressure monitoring

To perform simultaneous indirect calorimetry in a closed batch system, an electronic pressure transducer with integrated amplifier (Pressure Transducer LX 1601f or LX 1602a, National Semiconductors) was integrated into a Calvet microcalorimeter of 100 mL active volume [70]. To avoid any disturbance of the heat signal due to the measuring current of the transducer or the absorption of CO_2 in potassium hydroxide, absorber container and transducer were placed a few centimeter above the calorimetric vessel. The transducer output was fed to the same recorder so that heat production rate and pressure change due to oxygen consumption could be compared directly in the graph. Figure 5 illustrates the obtained results of the power-time curve Q, its integrated analog Q for the total amount of heat production and the oxygen consumption V_{O2} for a noninfected water snail (*Biomphalaria glabrata*, see below). [70].

3.4. Electrical stimulation

Lizards and snakes are known to use anaerobic energy sources during the initial stages of activity bursts, even in the presence of oxygen [71]. To investigate these anaerobic contributions during aerobic heat production, electric shock stimulation of the animals was applied [38]. Two electrodes extended into the full length of the 100 mL vessel of a Calvet microcalorimeter, leaving enough space for the animals to move around freely (Figure 6). An additional polarographic oxygen electrode was placed on top of the vessel. A current source and a voltme-

ter were connected to the electrodes. To avoid dangerous high voltages the animals were smeared with an electrode cream like that for electrocardiograms in human medicine. Prior to stimulation, the voltmeter was used to find a moment of "appropriate" position of the animal by means of the electrode resistance. It figured around some MΩ in an "open" state without contact and dropped to some kΩ when the animal was in contact with both electrodes. In this moment a pulse of slowly oscillating 30 V and 30 s was given, sufficient to induce a strong burst of activity with a large anaerobic contribution to heat dissipation. Further information is given in section 4.

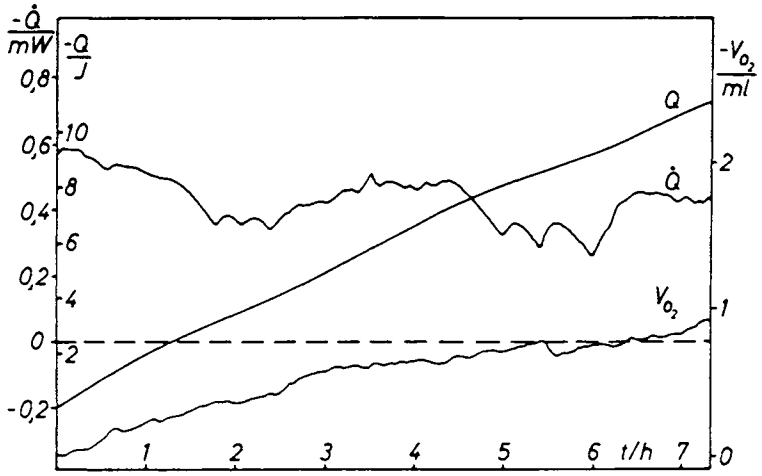

Figure 5. Different metabolic rates for a noninfected water snail. See text [70].

3.5. Poor man's calorimeter PMC

There yawns a large gap between commercial (micro)calorimeters with maximum vessel volumes of 25, 30 or 100 mL and instruments of many litres for smaller domestic animals. The only exception known to the authors is the Setaram GF 108 1-L instrument used in the Leyden group [72]. A low-price solution for an intermediate size calorimeter was found in cooling/warming boxes sold as picnic equipment for less than US$ 200 [73]. They are equipped with a Peltier battery as a heat pump between the inner volume of the box and the environment. In the same way the heat pump can work as a Seebeck heat flow sensor to determine heat production rates inside the box. The inner walls of the box may be additionally covered by copper foil of high thermal conductivity to facilitate heat flow to the sensor.

The first 8-L version of such a PMC (Figure 7) was applied to metabolic investigations on medium sized animals, among them the Japanese quail *Coturnix coturnix japonica* [74]. The calorimeter box - additionally equipped with a polarographic oxygen sensor, a humidity detector and a digital thermometer - showed a sensitivity of 8.0 mV/W and a very large time constant of 41 min. (But this was of no meaning for the investigations in such PMCs as the signals showed no short-term fluctuations.) Moreover, the instrument was placed in an insulating box for better thermal stability. Air flow through the PMC amounted to 10 L/h in experiments with quails between 130 and 180 g.

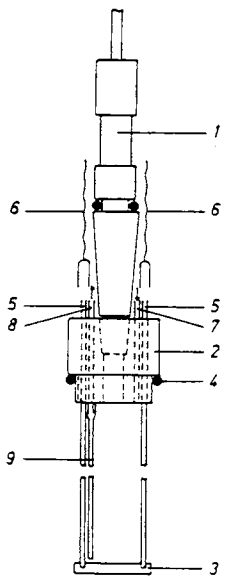

Figure 6. Stimulation device for 100 mL vessels of Calvet microcalorimeters consisting of two electrodes (5) with electric connections, air in- and outlet (7,8/9) and a Beckman polarographic oxygen sensor (1) on top.

In further developments for the investigation of social insects such camping boxes were used for the metabolic observation of whole bumblebee colonies throughout a season [67] and in a differential twin setup with boxes of 24 L for the observation of hornet nests or honeybee winter clusters [75,76]. More information about results with these instruments are given below (section 5.5.).

Winckler produced a modification of the PMC for aquatic organisms [77]. A camping cooler of 18 L served as an air-bath thermostat for the main calorimetric

vessel of 1 L. All 6 sides of the rectangular metallic vessel were equipped with Peltier batteries as heat flow sensors which carried large metallic heat sinks as usually applied for cooling of power transistors. The open parts of the vessel surface were covered with polyurethane foam to force the main heat flow through the Peltier batteries. The sensitivity of this calorimeter amounted to 130 mV/W, its time constant to about 20 min. First results were obtained with the cichlid fish *Cichlasoma nigrofasciatum* of several gram in relation to developmental progress.

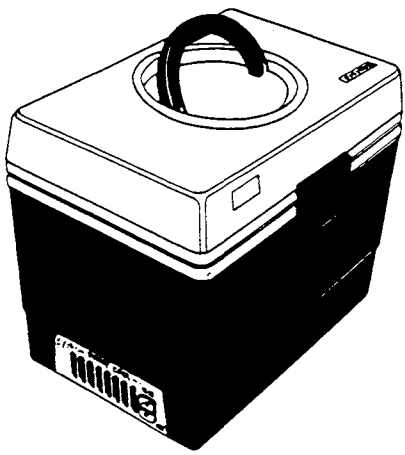

Figure 7. Sketch of the first camping box used as a *Poor Man's Calorimeter* (*PMC*) [73].

4. AMPHIBIA AND REPTILIA

Many animals answer to the stress of hypoxia and anoxia with a reduced metabolism and a strongly decreased heat production. While this effect is frequently investigated in aquatic animals (section 7), such data about air-breathing animals are rare in the literature. The common frog *Rana temporaria* was studied in a flow-through batch calorimeter under defined gas compositions [78,79]. The frog - immobilized by curare - dropped its normoxic metabolism of about 5 mW (0.16 mW/g) to a final steady state of 25 % during hypoxia and anoxia, a reduction comparable with that of other vertebrates. Reoxygenation after 2 h led to a steady state of many hours, higher than that before the stress.

Most metabolic research on reptiles was performed by indirect calorimetry of respiration or biochemical analysis. The first direct calorimetric results were

published in 1899 [7]. Hill reported quantitative data for a grass snake [80]. Although several authors pointed out that direct calorimetry would be a prospective or even indispensible tool for metabolic research in reptiles, no such data from other groups were found in the literature.

Schaarschmidt and coworkers investigated three snake species (*Coluber gemonensis*, *Coronella austriaca* and *Elaphe longissima*) in a 100 mL Calvet microcalorimeter combined with a Beckman oxygen electrode for indirect measurements [65]. The obtained power-time curves were desmeared using the Tian equation (section 1.2. and Figure 1) to obtain the true amplitudes of locomotor activities. Snakes with a weight of about 13 g showed a mean heat production rate of 0.61 mW/g, a 50 % higher maximum rate and a 26 % lower minimum rate at 25 °C. Simultaneous direct and indirect measurements led to oxycaloric equivalents of -457 kJ/mol O_2 for the mean and -638 kJ/mol for the maximum metabolic rate with one extremely high value of -856 kJ/mol for *C. austriaca* at locomotor activities. The figure of -457 kJ/mol O_2 was in good agreement with literature data [81]. The differences between the maximum and the mean value indicated to which extent the snakes used anaerobic metabolism during their short bursts of activity.

The energy metabolism of three lizard species (*Podarcis milensis*, *Podarcis muralis* and *Lacerta agilis*) was investigated by means of simultaneous microcalorimetry and respirometry. It rendered mean maximum values of 3.9 mW/g and mean average rates of 2.1 mW/g at animal weights between 2 and 10 g [82]. Analyses of time desmeared power-time curves showed that the resting metabolism contributed with about 60 % to the mean routine heat dissipation. The remainder originated from locomotor activity, mainly from anaerobic metabolism. Comparison of respiration and heat production led to an oxycaloric equivalent of 18.6 J/mL O_2 or -417 kJ/mol which increased to 26.6 J/mL O_2 (-596 kJ/mol) during bursts of activity. These values were close to those published by McDonald [81]. The only other calorimetric experiment on lizards found in the literature is 100 years old: Krehl and Soetbeer [7] determined the heat production rate of a much larger *Lacerta viridis* (110 g) to 0.95 mW/g at 25.3 °C. Applying a published allometric metabolism/mass relationship [83], their result coincided with the data given above.

Moreover, temperature dependence of energy metabolism could be investigated with the setup described in section 3.4. It rendered the known parabolic behaviour of heat production rate as function of temperature with a maximum around 32 °C. Due to aerobic metabolism in the closed vessel the oxygen concentration dropped permanently. Lizards were able to cope with these changing conditions when longer lasting periods below 9.3 kPa pO_2 were avoided [83].

Electric stimulation of lizards in this device (section 3.4.) induced large bursts of anaerobic metabolism [38]. Figure 8 shows the traces of simultaneous calorimetry (structured curve) and respirometry (smooth curve). The power-time curve before stimulation fluctuated due to locomotor activities of the animal but was constant in the mean slightly above 20 mW. In the moment of stimulation a strong increase in heat output was observed which returned to the previous level within 40 min. This additional peak amounted to 22.9 J provoked in 30 s, i.e. to an additional power of 763 mW or a 35-fold higher rate than prior to stimulation (100.1 mW/g compared with 2.9 mW/g under normal conditions). This result agreed with observations of Cragg [84] who found a 25-fold stimulation in *Lacerta viridis* from 7.06 mW/g at rest to 173.7 mW/g. Moreover, it is seen in Figure 8 that the change in the oxygen consumption rate started immediately at stimulation but took more than 40 min to return to a constant value comparable to that observed before. During this period the *oxygen debt* was paid back. The oxycaloric equivalent of 20.8 J/mL O_2 (-466 kJ/mol) indicated that glucose was used for compensation.

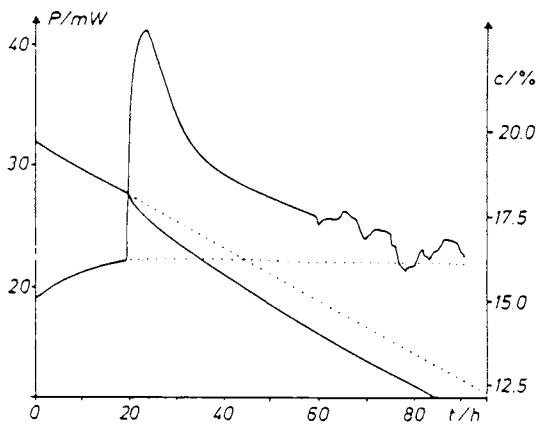

Figure 8. Power-time curve (structured graph) and oxygen consumption of an Ocellated lizard (*L. agilis*) before, during and after an electric stimulation of 30 V and 30 s [38]. (The time scale should read "min", not "h".)

These experiments showed the great advantage of calorimetry plus respirometry for metabolic investigations as no animal was really harmed during the experiment. This is in contrast to biochemical experiments where animals have to be sacrificed in order to determine the increased level of lactate in blood and tissue after stimulation.

5. INSECTS

5.1. Insects in General

On account of their small size and frequent aptitude for living under confined conditions, insects constitute an excellent material for microcalorimetric investigations. [85]

In his review about *Calorimetry of Higher Organisms* Prat presented a few introducing examples of microcalorimetry on insects, including economy periods (of basal metabolism) and spontaneous and provoked paroxism, development, aging and metamorphosis as well as of group effects [85]. Most investigations were run in a more analytical than quantitative manner, although some heat production rates were given and further might be found in the original literature. Figure 9 shows a power-time curve of a male cockroach (*Periplaneta americana*) with a few sponatenously occuring paroxisms (A_2 to A_5) and 3 paroxisms (B_1 to B_3) provoked by olfactory stimulation with whiffs of alcohol vapour. The first stimulation (Z_1) led to a sevenfold increase in heat output, the second (Z_2) to a more than twentyfold increase with a new higher steady state afterwards and Z_3 to a thirtyfold jump. Such increasing sensitization of an animal may result in a permanent perturbation and in death through exhaustion. Similar stimulations were observed with sexual odours from female cockroaches.

A rather large compilation of respiration rates of insects can be found in an article of Keister and Buck [86]. They observed a typical value of 1 mL O_2/(g·h) for the resting metabolism of many insects, which transforms to about 6 mW/g.

A rough estimate of the hexose metabolism of flying insects which is about 100-fold higher than at rest is given by Sacktor [87]. A 50 mg insect should consume in the average an amount of 30 µmol hexose/(g·min) in flight and have a yield of -1300 kJ/mol O_2.

Evaporation of water as a strong endothermic effect (with 2.27 kJ/g water) plays an important role in life (and calorimetry). However, insects are often well protected against water loss by their cuticula and special forms of behaviour like discontinuous ventilation during resting metabolism. This situation changes when insects fly, breath regularly and use liquids for cooling purposes. Nevertheless, even in power-time curves of resting metabolism short-term endothermic transients were observed (see below) which were mainly due to active water loss for cooling or passive loss at ventilation.

Comparing the calorimetrically obtained heat output - corrected for the value of evaporation - with that found in respirometry of the mealworm *Tenebrio molitor*, Peakin registered no significant differences between both methods and observed the familiar U-shaped curve of metabolism during pupation [88]. He argued that

respirometry put some degree of stress on the investigated insects because potassium hydroxide, used for the absorption of CO_2, also lowered the relative humidity of the experimental atmosphere; and moreover, that modern calorimetry - in contrast to respirometry - would be able to offer any specific atmosphere necessary for the natural welfare of the animal.

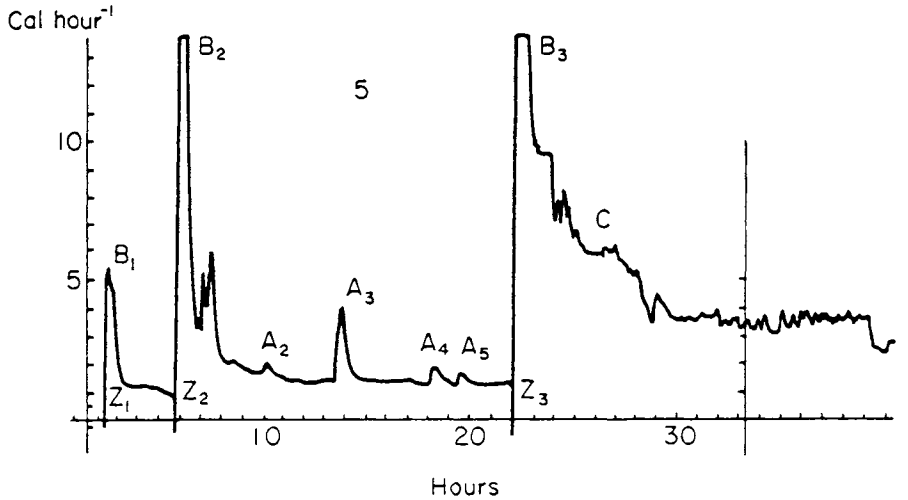

Figure 9. Power-time curve of an adult male cockroach (*P. americana*) stimulated by 3 whiffs of alcoholic vapour (Z_1 to Z_3) [85].

Group effects are rather common among insects, leading to a reduced mass specific heat production rate compared to that of an isolated animal when several individuals of the same species are put together in the calorimeter. Prat [85] showed that the heat dissipation of a female fruit fly (*Drosophila*) of about 1 mg dropped from 0.12 mW to 0.08 mW when together with 4 further fruit flies. This effect is even more pronounced in social insects like honeybees which produce a collective thermogenesis resulting in social homeothermy.

When insects are used for metabolic experiments, handling introduces an unavoidable stress to the animals which can last for minutes, hours or even days and interfere with the intended investigations. The mealworm *T. molitor* was used to show that insects may be grouped calorimetrically by their irritability during pretreatment and that such groups render significantly different results [89]. For this end a combination of differential calorimeter and an automatic electrolytic microrespirometer-actograph was applied. Four groups of mealworms could be distinguished calorimetrically by their breathing patterns, abdominal pulsations,

hyperactivity and wriggling movements. The group with chaotic rhythms of CO_2 release, irregular pulsations, larger water loss and high irritability contained those animals which were most susceptible to toxicants and chemical stress.

5.2. Calorimetric investigations on special insects

To our knowledge, the first calorimetric experiments on insects were published by Tian and Cotie in 1924 [90]. The authors used a single heat detector setup (a predecessor of the famous twin differential Tian-Calvet microcalorimeter) placed in a cellar to get a constant ambient temperature and a stable base line. The authors collected 23 flies (*Musca domestica*) in a glass vessel of 5.4 cm^3 and sealed it. After a period of 90 min of high heat production the rate decreased, returned to a small secondary peak at 2 h and dropped steeply to the base line. Due to the consumption of oxygen in the closed vessel the flies at first reduced their metabolism (90 min), made an effort to escape (peak at 2 h) and then entered a state of asphyxia of strongly reduced metabolism which could not be separated from the experimental zero line. Brought back to oxygen the flies became active again. The paper ended with a sentence that could be the motto of a textbook of biological calorimetry: *Nous ne connaissons pas de méthode qui êut permis de suivre avec une égale facilité et une pareille précision dans le détails une observation biologique du genre de celle que nous venons d'exposer.*

Several insect species were investigated by means of a Calvet-type microcalorimeter, among them 5 species of grasshoppers (*Melanoplus* sp.), 2 different moths (*Galleria mellonella, Tineola* spec.), the fruit fly *Drosophila melanogaster* and the cockroach *Periplaneta americana* [91]. The author observed strong fluctuations in the power-time curves of the insects at the time of moulting, during metamorphoses and at egg deposition. Diurnal rhythms could be detected in some cases which were most pronounced in *P. americana* with a maximum of heat dissipation in the afternoon.

Early calorimetric investigations were performed on pupae of the wax moth *Galleria mellonella* by means of a differential adiabatic setup [92]. *Galleria* represents an important pest for weak honeybee colonies where it feeds on wax, honey, pollen and other organic material. Individual pupae were kept in small Dewar flasks of 5 cm^3 for measurements of 10 to 60 min, which were repeated in regular intervals through the whole pupal metamorphosis of about 7 days. The calorimetric experiments alternated with manometry (indirect calorimetry) to evaluate the RQ and to find hints about the type of metabolism. Heat dissipation was monitored by electrical heating of the reference flask to keep the temperature difference between both Dewars close to zero. In this way composite curves for male and female moths and both direct and indirect calorimetry were established.

Moreover, the manometric data were transformed to heat dissipation and compared with the direct values. The considerable differences between both might be due to evaporation and to a wrong assumption that only fat and no protein was metabolized during metamorphosis. Sex differences as well as an U-shaped course of energy turnover during pupal metamorphosis occured, observed also by other authors.

A similar combination of microcalorimetry and respirometer/actograph as that cited above was applied to investigations on the influence of plant extracts on the metabolism of diapausing pupae [93]. The system chosen as an example for chemical ecology consisted of the cabbage butterfly *Pieris brassicae* and an extract of the painted daisy *Pyrethrum roseum*, a long- and well-known neurotoxic substance for plant protection. The distinct cycles of gas exchange seen in the power-time curves and similar to those found in *T. molitor* were abolished and changed to chaotic rhythms. Moreover, body mass losses per day increased by more than 40 % in treated pupae and the further pupal development was changed or stopped.

The Mediterranean fruit fly *Ceratitis capitata* represents a serious threat in the fruit-growing industry, especially during the time of shipping. Seo and coworkers made a somewhat exotic indirect calorimetric investigation on the heat production and thermal conductivity of fruit fly pupae at different temperatures [94]. From oxygen consumption and carbon dioxide production rates of 44 g of pupae enclosed in a copper cell they determined a RQ of about 1.0, assumed carbohydrate metabolism and calculated mass specific heat production rates of 0.80 to 8.02 mW/g for temperatures between 10 and 35 °C. Because irridiated pupae enclosed in polyethylene bags in millions or more showed poor emergence after shipping in earlier experiments, the question of an inactivation by prolonged metabolic heat exposure was raised. The authors determined a maximum conductivity of 1.70 mW/(°C·cm) and a maximum critical radius for the bags of 3.4 cm at 32.2 °C.

The same organism was used much earlier by Fourche and Lemaitre comparing heat production and respiration during metamorphosis [95]. Pupae are specially suited for such investigations as they do not feed any more and just show gas exchange with the environment during metamorphosis. A Calvet-type microcalorimeter at 26 °C was charged with 20 pupae that dissipated a maximum heat of about 90 mW per individual at the beginning of the phase. A clear U-shaped slope of heat production as well as oxygen consumption rate was obtained as with the wax moth *G. mellonella* and the mealworm *T. melitor* with a minimum rate of 12.4 mW/pupa corresponding to a reduction to about 7 %. After this minimum the heat dissipation increased till the emergence of the imago to 41.4 mW/pupa or 45 % of the initial value.

Two insects, the locust *Locusta migratoria* and the hawk moth *Manduca sexta*, which are known for their different tolerance against hypoxia and anoxia were studied by microcalorimetry in a flow-through mode for defined gas mixtures [79,96]. Both showed no alterations in behaviour or heat production during hypoxia down to oxygen concentrations of 2 %. In the *critical oxygen range* between 2 and 1 % the insects became agitated, hyperventilated and tried to escape. A few minutes later they were completely immobile. During that time the heat production rate was just 5.3 % of the normoxic value for *Locusta* and 3.6 % for *Manduca*. More pronounced differences were seen between the two species in the tolerable length of the anoxic period and in their response when gas flow was switched back to air after some hours of anoxia.

Wilson and colleagues used a Tian-Calvet-type microcalorimeter [97,98] to investigate the German cockroach *Blattella germanica* which is the most important insect pest infecting households, hospitals, restaurants and hotels, being resistant against many pesticide chemicals [99]. The interest of the authors concentrated on a calorimetric determination of circadian rhythms, followed over several days. They kept individual male cockroaches in a small gelatine capsule inside the calorimeter vessel of about 10 cm^3 in complete darkness (as in most calorimetric experiments with insects!). Although there were considerable differences in heat flow transients and frequencies between the insects, a basic rhythm was established for all of them. Phases of activity lasted about 12 h, mainly during the night. In these periods the total heat output was 2.7 times higher than during daytime. In general, heat dissipation was considerably larger in unentrained than in entrained animals, supposedly due to strong locomotor activities.

Periodically occuring exothermic peaks (Figure 10) in power-time curves of pupae of the mealworm *T. molitor* and the wax moth *G. mellonella* could be traced to muscular activities which act as tracheal ventilation, accelerate the hemolymph circulation and support the heartbeat [100]. In these two insects they amounted to only 1 % of the total heat output during pupal metamorphosis and could be neglected. In contrast to these observations the same authors found significantly increased heat flows during ventilation in the Colorado beetle *Leptinotarsa decemlineata* and the weevil *Hylobius abietis* with contributions of 12 to 18 % [101,102]. Endothermic peaks which were also observed in the calorimeter curves resulted from water vapour liberated with CO_2 [101,102].

Custom-made simple thermocouple calorimeters of 0.25 mL active volume and a sensitivity of 20 μV/mW were applied to study the growth regulating and toxic effects of *Ledum palustre* extracts on the growth of pupae of *T. molitor* [103]. They exhibited the U-shaped course of mass-specific heat production rate (max. 2.8 mW/g, min. 1.2 mW/g) as described also by other authors (e.g. [88,92]). Superimposed on the slope were longer-lasting clear endothermic structures during

ecdysis and additional leaking of exuvial fluid, while muscular hyperactivity prior to ecdysis rendered strong exothermic effects. The individual power-time curves of the pupae showed strong fluctations due to bouts of rhythmic abdominal movements and to cyclic emission of CO_2 from tracheae. These structures were considerably changed by application of *L. palustre* extracts with a less pronounced U-shape, only partial ecdyses, shortening of the interecdysial periods, changes in the bending movements and disappearance of intermittent CO_2 release.

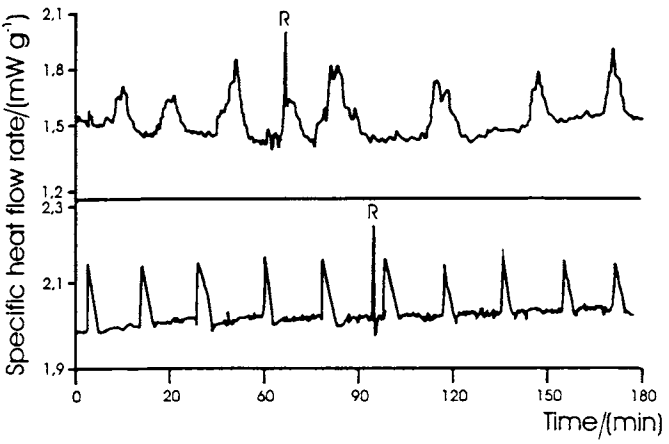

Figure 10. Periodically occuring exothermic peaks in the heat production in pupae of *G. mellonella* (above) and *T. molitor* (below) due to muscular activities and rotating or twisting movements R [100].

Microcalorimetric experiments were used to analyse the well-known drastic temperature increase in laboratory cultures of *Galleria mellonella* during larval development. The authors showed that the temperature rise was due to an approximately threefold increase in mass specific heat production rates from about 50 mW/g for the larval stage L3 to about 140 mW/g for L4 and L5 (followed by a drop to 75 mW/g for L6) [104]. The observed aggregation of larvae inside silken tubes was thus unlikely to be responsible for the temperature jump from 32 to 40 °C during stages L4 and L5 which are typical for *G. mellonella* in laboratory cultures.

A very sensitive differential calorimeter (~ 150 μV/mW) with Seebeck thermopiles [105], two flat cylindrical glass vessels of about 5 cm^3 and gasification and exhaust trains was described for investigations on insects [106,107], shown in Figure 11. Basal metabolic rates and heating or cooling transients were monitored for single individuals of the yellow fever mosquito *Aedes aegypti* and the

German cockroach *Blattella germanica* [107]. The insects were confined in the glass vessels but free to move around. The obtained power-time curves showed the expected steady line for the basal metabolism superimposed by transients. The basal metabolism of blood fed mosquitos amounted to 4.6 mW/g, the cooling transients to 6 mJ (corresponding to 16 µg water or 0.6 % body mass) and the heating transients to 15 mJ (corresponding to 24 µg of hexose - if carbohydrates were metabolized). The latter figure is threefold higher than before feeding so that the observed effect might be understood as a *specific dynamic action*, the extra heat production by an organism after feeding [108].

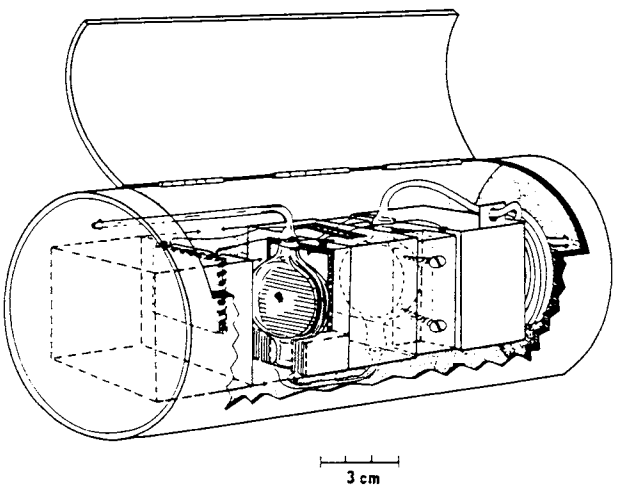

Figure 11. Sketch of the twin microcalorimeter applied for insect investigations (see text) [107].

With the same calorimeter, *B. germanica* was investigated for its answer to anaesthesia with CO_2. The basal metabolic rate amounted to about 1.3 mW/g at 25 °C. Introduction of CO_2 into the gas flow induced an irritation of the insect and a subsequent cessation of heat production. A re-aeration 2 h later led to an enormous increase of heat production up to more than 9 mW/g and later 6 mW/g which returned to the initial level of basal metabolism only after a few days [107].

The same calorimeter was applied for monitoring embryogenesis of the flour beetle *Tribolium confusum*, a worldwide pest in stored grains. These beetles survive a manifold of adverse storage conditions, and their embryos cannot be killed by contact insecticides due to their wax layer. Eggs of this beetle were investigated in sample sizes of 600 eggs (about 36 mg) to obtain a detectable signal during the first day [106]. Fourty h before hatching the eggs showed a constant

heat production rate of 5.9 mW/g which increased more than twofold after hatching with longer lasting spikes of threefold turnover.

A further application of this calorimeter was for airborn irritations like attractants, toxic compounds, anaesthetics or allochemicals on individual insects [47]. Larvae of the cabbage looper (*Trichoplusia ni*) were tested against microgram amounts of benzene. They produced a strong, but short exothermic effect because the benzene was washed out by the air stream. A young male of the rootworm *Diabrotica longicornis* answered with a pronounced exothermic heat output to the exposure to pheromones prepared as extracts from female corn rootworms. Moreover, the male moved immediately towards the source of the stimulant.

Pregnant females of the viviparous cockroach *Nauphoeta cinerea* showed a significantly ($p < 0.001$) smaller mass specific heat production rate (0.80 mW/g) than males (1.45 mW/g) or virgin females (1.53 mW/g) [109]. Thus, the general expectance that pregnancy increases the metabolic turnover could not be confirmed. As the power-time curves of the animals were rather constant with only a few fluctuations, reduced locomotor activities in pregnant females could not be responsible for this effect. The mass specific data of males and virgin females fitted well to an allometric equation established by Coelho and Moore [110] via indirect calorimetry for resting cockroaches, while the pregnant females were significantly out of the range [109]. Preliminary investigations on the much heavier *Gromphadorina portentosa* (mass between 4.9 and 7.8 g with a mean of 6.5 g) proved that their metabolism also obeyed the mentioned equation with 0.60 mW/g at 30 °C and 0.19 mW/g at 15 °C (H. Zwettler, personal communication 1997).

The Mexican jumping bean, the larva of the moth *Laspeyresia saltitans* (earlier named *Carpocapsa saltitans*) is better known as a curiosity or a *gimmick* than as an object of scientific interest (but see e.g. [111]). However, it may be used to show calorimetrically its low level of basal metabolism and the high heat output during locomotor activities. The larva inside the empty bean tries to find a place of convenient temperature by rocking and jumping in a temperature gradient. Jumps up to a few centimeters are possible. Figure 12 demonstrates the large differences between rest and activity with long quiet periods (I. Lamprecht, unpublished results). With mean masses of 70 and 5 mg for the bean and the larva, resp., and taking into account that the maximum amplitudes are smeared by the time constant of the calorimeter one arrives at specific heat production rates around 100 mW/g, comparable to those of flying insects.

5.3. Flight calorimeter for small insects

An isoperibolic heat flow calorimeter (sensitivity 63.6 μV/mW) was constructed for direct monitoring of heat production rate during flight of smaller insects [112]. It incorporated a roundabout of small friction with a diameter of 144 mm, light guide illumination, microphone for acoustical investigations and an inductive proximity sensor for counting the revolutions per minute and determination of the flight speed. Figure 13 presents a sketch of the instrument which is housed in an LKB air bath thermostat. Preliminary experiments were performed with various insects, among them honeybees, hornets, flies, moths and several beetles. For some of them illumination was not strong enough so that they resisted to fly. Hornets were most willing to cooperate with flight times up to several hours without break. However, their speed and thus also their heat output rates were lower than expected, presumably because of the low light level and the narrow radius of the carousel.

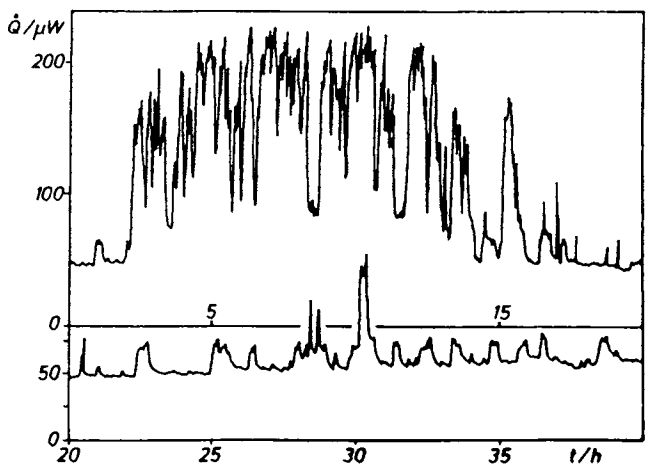

Figure 12. Power-time curve of a Mexican jumping bean of about 70 mg at 25 °C.

5.4. Insect Development

Prat [85] presented two calorimetric examples of development and aging in his survey article about calorimetry of higher organisms. One concerned the growth of the wax moth *Galleria mellonella* from hatching of the egg through larval and pupal stages until emergence of the adult butterfly with different metamorphoses and the energetically accentuated period of transition from the pupa to the imago.

The larval development of the same insect was followed recently also by means of Calvet microcalorimeters [104]. Individual larvae could be monitored continuously over 40 days in their metabolic behaviour. Figure 14 shows the strong increase in heat production rate up to the larval stage L7, the subsequent drop to the extremely low level of pupal metabolism and the intensive fluctuations in heat dissipation because of locomotor activities. Moreover, moulting phases were indicated by a drastic decrease of heat production down to 7 to 20 % of the preceding value followed by a rapid increase to the next maximum. These results should be compared with the very early investigations of Taylor and Crescitelli [92] on the same organism (section 5.2.).

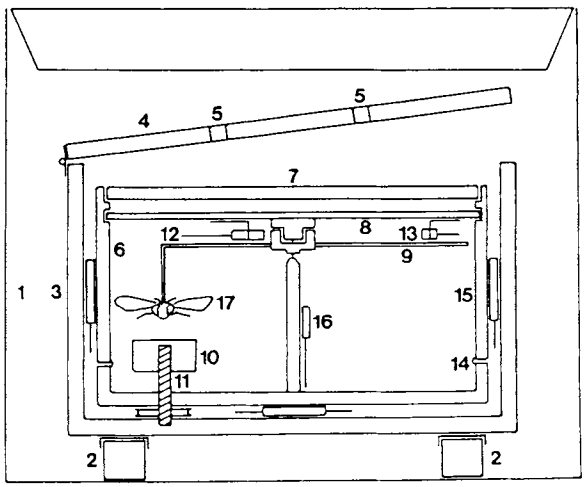

Figure 13. Schematic sketch of a carousel calorimeter for small insects with 1: LKB air bath thermostat, 9: flight carousel, 12: proximity sensor, 13: microphone, 14: light guides, 15: Peltier heat flux sensors and 17: insect [112].

In a line of theoretical investigations concerning biological thermodynamics of irreversible processes and heat dissipation functions, *T. molitor* and *B. germanica* were followed manometrically and calorimetrically through their complete development [113,114]. Aperiodic fluctuations of heat output due to spontaneous locomotor activities were found in power-time curves of both insects, and *B. germanica* showed additional periodical heat bursts during the night which were connected with discontinuous ventilation (*spontaneous paroxysm*). *T. molitor* exhibited changes in its mass specific heat production rates during development with a distinct maximum in the larval stage (around 20 mW/g), clear indication of moulting and metamorphosis and a strong decrease to the low metabolic level of

the adult larva (about 2 mW/g). The U-shaped course of pupae development as published by other authors [88,92,103] could not be seen.

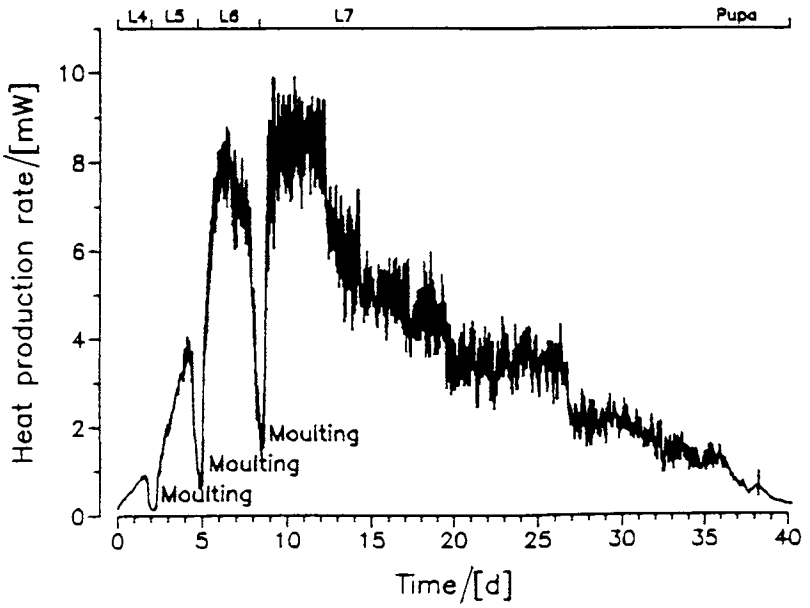

Figure 14. Power-time curve of an individual wax moth larva (*G. mellonella*) during the development. For further details see text [104].

5.5. Social Insects

5.5.1. Some general features

Most existing animals are poikilotherm, i.e. the temperature of their body follows that of the environment. Only birds and mammals developed the technique of homeothermy (constant body temperature) which made their metabolic processes independent of the ambient temperature. A corresponding homeothermy is found in social insects, but not aimed at the individuals as in birds or mammals, but at the social community such as bee hives or clusters, hornet colonies or bumblebee nests. There exists no control center (as the hypothalamus of the brain of higher animals), but each single social insect forms the control center and the performing organ. Homeothermy in social insects is used to keep the nest temperature constant in less favourable climates and to ensure a quick and effective breeding of offspring. For this end, heat production rates in small (bee) populations are as high as that of small mammals. Different physiological and

behavioural techniques were developed in these insects to protect their colonies against overheating and - more important - against undercooling in unfavourable periods. Increase in metabolic activity, periodic contractions of the flight muscles on the physiological side, insulation by special paper-like envelopes (hornets, wasps) or clustering (honeybees) on the mechanical/behavioural side are applied for this end.

5.5.2. Honeybees

Although a large body of metabolic investigations on honeybees has been performed due to their economical, ecological and scientific importance, only very few calorimetric experiments are found in the literature. The usual research on energy turnover in honeybee larvae, pupae and adults of different castes are performed in the indirect way via O_2 consumption and CO_2 production by Warburg or other techniques, assuming a respiratory quotient of exactly 1.00, an oxycaloric equivalent of 21.1 J/mL O_2 and an energy content of 15.8 kJ/g in sugar. Other approaches include sugar consumption or difference measurements between the temperature of the bee thorax and that of the environment. For a literature survey see [56,57,115].

True calorimetric experiments have been performed only a few times in the past [116-118]. A number of papers, both on the European (*Apis mellifera carnica*) and the Egyptian honeybee (*A. m. lamarckii*) appeared during the last 10 years from the Berlin group [56,57,75,76,115,119-121]. They concerned metabolic differences between the two races, investigations on heat production rates during development and of the castes: queens (virgin and laying), drones, workers, larvae and pupae, locomotor activities and their observation by endoscopic and acoustic techniques as well as seasonal and temperature dependences.

Communication in the bee hive and among its different members occurs by various means, among them mixtures of chemical compounds called *pheromones* for different informations. Alarm pheromones were chosen in microcalorimetric experiments as they were known for their dramatic effects. Groups of 30 bees were collected in 100 mL vessels of a Calvet calorimeter working in a flow-through mode (H. Gehrs, E. Schmolz and I. Lamprecht, unpublished results, see also [76]). After establishment of the base line the pheromone or single components of it were introduced into the air flow and strongly enforced heat outputs occured immediately which returned to the former level after a few minutes, or even lower due to an exhaustion of the honeybees. Desmearing of the calorimetric signal (section 1.2.) rendered an instantaneous, nearly steplike upward jump of the heat production at the pheromone addition.

In connection with the discussion about Africanized *killer bees* in America, it was interesting to compare metabolism and activity of the usual European honey-

bee *Apis mellifera carnica* (about 120 mg) with the much smaller Egyptian race *A. m. lamarckii* (about 78 mg). The latter one is more alert and ready for attack than the calmer European race. Such differences were reflected in the heat production rates of both subspecies at all investigated temperatures between 20 and 40 °C. As expected the most pronounced difference was seen at 20 °C with a 80 % higher mass specific rate in *A. m. lamarckii* than in *A. m. carnica* [76,120].

Although the weight of a worker honeybee was approximately constant throughout its life, slightly above 100 mg, the weight specific heat production rate increased from around 30 mW/g at 30 °C for a freshly hatched bee to around 180 mW/g for an adult forager bee [57,115]. Temperatures of 20 and 25 °C produced higher values than 30 °C with a maximum around 12 days of age [57]. Caste specific differences were seen at all temperatures and are presented for 25 °C in Table 3. The heavy drones increased their metabolic turnover 3.4 times at 30 °C and even 19.7 times at 20 °C during life time. Virgin queens had a significantly higher weight specific heat dissipation than the 21 days old egg laying queen. Lowest values were found in brood of workers and drones.

Table 3.
Mean heat production rates *p* of isolated members of the different castes of the European honeybee *Apis mellifera carnica* at 25 °C. SD = Standard Deviation. [57]

Caste	Age	Weight mg	*p* mW/g	SD mW/g
Workers	hatched	105	56	24
	young	120	142	23
	adult	100	209	21
Drones	juvenile	236	68	19
	fertile	205	184	37
Queens	virgin	176	117	16
	laying	258	102	12
Brood	larvae	155	4.4	0.6
	pupae	120	1.8	0.4

Energetic data for single individual honeybees are open to criticism as these social insects exhibit a high degree of unrest when they are separated from their nest mates. To study such effects, honeybee groups of increasing number were transfered to 100 mL vessels of a Calvet calorimeter and monitored by heat dissipation and endoscopic observation [56,57]. Larger groups than 18 animals were difficult to handle and had to be anaesthetized by CO_2 or cooling down. As such

handling had severe influences on the metabolic response of the bees, it was avoided. Figure 15 shows the strong decline in the weight specific heat dissipation rate down to a final steady value of 5 to 7 % of the rate of an isolated bee. Corresponding effects had been reported by Roth [117,118]. Similar reductions could be obtained when small groups of 6 workers were investigated together with a queen or brood which both induced social activities and calmed down the bees. Groups of 12 drones behaved as workers with a reduction of heat dissipation down to 12 %, quietly sitting on the bottom of the vessel or the climbing stick.

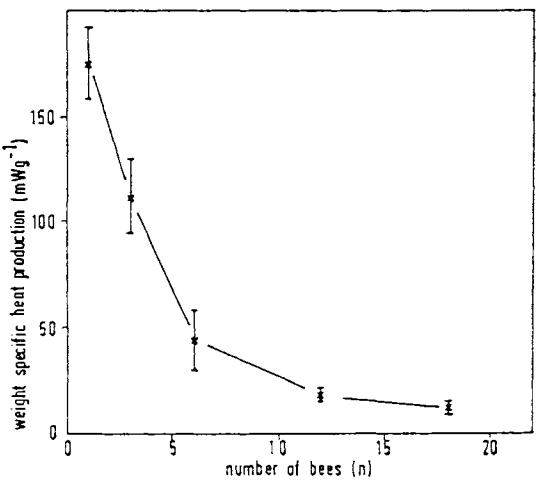

Figure 15. Weight specific heat production rate of honeybee workers (*A. m. carnica*) at 30 °C as function of the group size [56].

5.5.3. Bumblebees

Bumblebees form smaller colonies than honeybees which exist through the summer season and die out in the autumn. Only inseminated queens survive the following winter and establish new colonies in the spring. But they have many other features in common with honeybees so that it is worthwile to study bumblebee colonies by means of calorimetry. Although the temperature balance of their nests has been evaluated extensively, there are no investigations on whole colonies reported in the literature.

Small initial nests of the bumblebee *Bombus lapidarius* were translocated from the outside into a calorimetric (cooling) box as described in detail above (section 3.5.) placed in the basement of the institute [67,68]. The queen and a few already

existing workers could continue their normal life as the box was connected to the environment by a walkway of 60 cm. Temperatures outside and inside the box near to incubated brood cells were monitored continuously together with the heat production rate of the nest. The brood temperature remained almost constant during the day between 30 and 32 °C while the heat flow showed a diurnal rhythm with a maximum around 1.6 W in the early morning and a minimum of 0.9 W in the night. After the death of the queen heat dissipation and brood temperature decreased significantly.

The heat production rate of workers exhibited a U-shaped form during the development of the nest with high values at the beginning and the end of the season and a pronounced minimum during the main nest phase. In this period the heat loss per individual ranged from 5 to 30 mW (30 to 200 mW/g). The results obtained in this investigation indicated that bumblebees are capable of finely adapting their metabolic heat production to guarantee a constant nest temperature for the brood [67,76].

Endoscopic observations on bumblebees in the Calvet calorimeter showed that there was a one-to-one correlation between sound production and wing movements so that it was interesting to investigate this correlation in some more details [59]. Power-time curves rendered distinct periods of increased heat production connected with strong sound generation (Figure 16). Between the periods the heat output dropped from more than 200 mW/g to a basal value of 10 mW/g, while during continuous wing buzzing rates of more than 350 mW/g were determined - as high as those of insects in free flight. It was observed that the increase in heat dissipation started 5 min earlier than the first sound generation presumably due to a warm-up of the muscles before wing movements. The results underline that the simultaneous monitoring of calorimetric and acoustic signals is a suitable method to get more insight into insect metabolism and locomotor activity.

5.5.4. Hornets

Social thermogenesis is common for many wasps and often studied by thermometry. But no information about the nest metabolism - obtained by direct or indirect calorimetry - is presented in the literature. Nevertheless, such data would be interesting for energy balances of a complete nest during the season and the contributions from the different castes of the wasps, the environmental temperature, the size of the nest and the insulating properties of the envelope. To find an answer to such questions, experiments similar to those with bumblebee nests were performed on the hornet *Vespa crabro.*

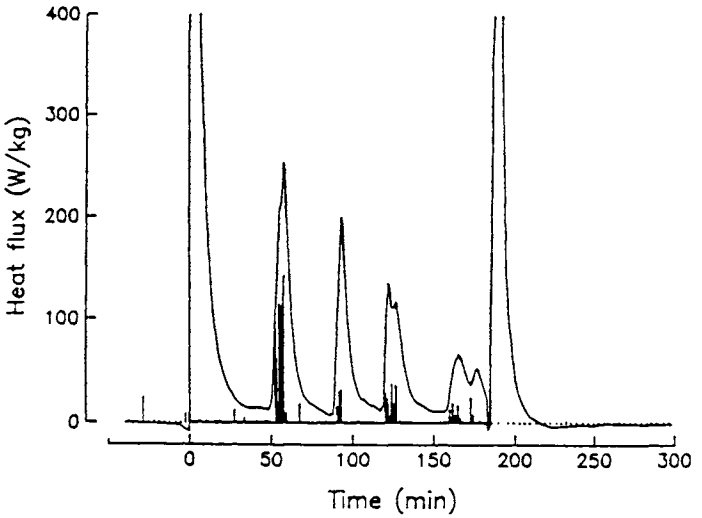

Figure 16. Heat production and sound generation of a bumblebee worker (*B. lapidarius*) of 105 mg. The vertical lines represent the sound generation as the voltage output of the microphone. The strong heat flux rates at the beginning and the end of the trace are artifacts due to heat of friction during introduction and removal of the calorimetric vessel [59].

To this end, young, intact hornet colonies were transfered from their natural locations into camping cold boxes (section 3.5.) of 24 L volume equipped with a free access to the outdoor environment [75]. The hornets continued to construct the vertically hanging combs and the multilayered nest envelope during the season so that continuously growing colonies could be studied. The heat output for a typical nest ranged from 1.2 W at the end of the season in October to 12.5 W at the time of maximum insect number. Hornet workers contributed with 70 to 90 % at 49 mW/g at 20 °C, drones with 36 mW/g [122,123]. Heat flux from the nest showed a diurnal rhythm like that of bumblebees but shifted in time to a maximum around noon. Comparing hornet nests of different sizes rendered a clear positive correlation between size and internal temperature as well as heat production rate.

The nest envelope constructed from paper-like material was produced by the hornets from small pieces of wood (about 7 mg) collected in the environment. 15 min were needed in the mean to collect one piece, so that 725 h of flight were invested in a nest envelope of 22 g. The total energy consumed amounted to 780 kJ, equivalent to the energy used in 5 days heating of the nest. As the envelope established a significant temperature gradient between the nest interior and the

environment and thus reduced the heat flow considerably, the advantage of such an insulation became obvious [76].

At the end of the season, hornet colonies die out and only the inseminated queens survive hibernating in protected places. During this period they show a strongly reduced metabolism to save energy and especially water to escape death from desiccation. Discontinuous ventilation is a means to avoid water loss. This behaviour was investigated via heat and CO_2 production in isolated queens at different temperatures [69,124]. The periodic release of CO_2 was visible in the power-time curves as sudden drops of heat flow by 30 to 50 μW, presumably due to water loss and evaporation. The CO_2 production showed temporally corresponding bouts from near zero up to 160 μL/h. The frequency of these bouts increased from 0.05 h^{-1} at 5 °C to 5 h^{-1} at 20 °C. The mean heat output amounted to 0.91 mW at 15 °C. The weight loss of the queens was monitored during the whole hibernating period and was assumed to result from metabolic combustion of fat (39.8 kJ/g). Thus, this weight loss corresponded to a heat production rate of 1.05 mW equivalent to that determined directly.

5.5.5. Wood ants

Socially living ants establish above-ground and underground colonies to guarantee an effective development of their brood in varying climates. These colonies are often characterized by hills of considerable size and an appropriate shape to collect solar irradiation. Measurements show that the temperature in the central brood zone remains rather constant inspite of fluctuating ambient values. Moreover, these temperatures are significantly above the environment, typically around 25 °C in nests of the wood ant *Formica polyctena*. Several theories were developed to explain the increased temperature in the nest:

- The main source of energy is solar irradiation.
- Heat is transported into the nest by sun-bathing ants (heat carriers).
- The adult ants are responsible for the necessary heat production.
- Most heat in the nest is produced by microbial degradation of nest material.

All earlier investigations on ant hills were carried out by thermometry of the nests and indirect calorimetry of the developmental stages of the ants. Later it was shown in the Berlin group by means of direct isoperibolic and quasi-adiabatic calorimetry that the heat production rates at 20/30 °C for adult ants (2.6/5.2 mW/g) and pupae (0.8/1.9 mW/g) were significantly higher than those of the nest material taken from the periphery (0.18/0.45 mW/g) or even from the center (0.32/0.65 mW/g) [125-128]. However, due to the 40 to 100 times higher mass of the nest material in the different layers (I: periphery, II: intermediate zone, III: center) the heat balance was shifted to the microbial degradation as shown in Table 4. As a rough estimate one could state that about 85 % of the biological

heat production of the ant hill resulted from microbial activity. These results were doubted by other scientists [129-132] partly due to the assumption that the inner part of the nest is kept sterile by the ants and that the humidity in the nest is not high enough for the development of microorganisms. Further investigations are necessary to clarify these contrary opinions.

Table 4.
Temperature Θ, mass of nest material m_N, number of ants n_A, mass of ants m_A and heat production rates by nest material P_N and ants P_A in the 3 layers of a typical German ant hill (*Formica polyctena*) in summer. [125]

Layer	Θ °C	m_N kg	n_A	m_A kg	P_N W	P_A W	P_N/P_A
Layer I	16	52.0	52 100	0.521	7.80	1.04	7.5
Layer II	20	25.5	45 000	0.450	6.25	1.17	5.3
Layer III	24	4.8	11 500	0.115	2.16	0.41	5.3
Total		82.3	108 600	1.086	16.21	2.62	6.2

To establish a more complex picture of an ant hill throughout the active season, a nest in the forest was investigated from early spring to late autumn monitoring all demographic, biological, physical and meteorological parameters. Equalized heat flow balances were found for sunny and rainy days with the important - and nearly constant - biological heat production. The following contributions were determined (Table 5):

Table 5.
Heat contribution P by different sources to the energy balance of a hill of the wood ant *Formica polyctena* on a summer day [127].

Heat gain by	P/W
Direct irradiation	15
Heat carriers	0.3
Microbial metabolism	16
Ant metabolism and activity	3

Negative contributions stemmed from evaporation, back radiation, convective heat loss at the surface and heat conduction to the soil [127].

6. PROTOZOA

Although in modern systematics the taxon "Protozoa" is no longer existent, we included heterotrophic protists in this chapter as all metazoons (multicellular animals) originate from a part of this taxon.

As the (single cellular) protozoon *Amoeba proteus* is used as research object in many aspects, Nässberger and Monti [133,134] thought it worthwile to apply microcalorimetry to it. Samples of 0.1 to 1.0 mL with 1500 to 4800 cells were filled in 1.1 mL ampoules of a standard LKB microcalorimeter at 25 °C. The metabolic heat output strongly depended on the duration of a preceding starvation and amounted to 0.84×10^{-9} W/cell, comparable to a figure of 3.3×10^{-9} W/cell for another protozoon, the ciliate *Tetrahymena pyriformis* [135]. Moreover, a pronounced *crowding effect* was observed at increasing cell numbers in the calorimetric vessel with a reduction to 60 % when doubling the cell concentration. Stimulated pinocytosis - the uptake of soluble materials from the environment - led to a significantly increased heat production rate as shown in Figure 17 for a stimulation by lysozyme [134].

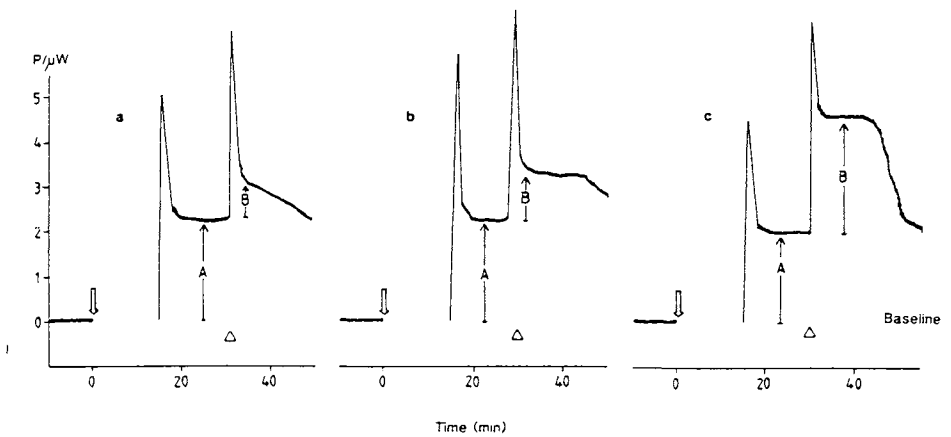

Figure 17. Lysozyme stimulated pinocytosis in *Amoeba proteus*. Changes in heat output due to different lysozyme concentrations (0.04, 0.21 and 0.43 mg/mL). The baseline is indicated before the arrow, *A* represents the basic metabolism, B the heat output during pinocytosis [134].

7. AQUATIC ANIMALS

7.1. General Considerations

While most terrestrial animals are investigated in batch systems, sometimes supplied with a flow of air, oxygen or gas combinations, the type of applied calorimeter is more important for aquatic animals. In a closed batch system, the oxygen concentration in the water will continuously drop during the experiment. As the oxygen solubility in water is rather small with only 2 to 5 % of the concentration in air, this reduction may occur rapidly. Moreover, excretion of products from the anaerobic metabolism changes the ambient conditions considerably, often in an uncontrolled manner.

Flow calorimeters can help to avoid such problems and to guarantee a constant or controlled environment for the aquatic organisms. Flow-through vessels of different sizes are available nowadays which are constructed in such a way that the steady flow of water does not influence the calorimetric signal to a significant extent and that constant conditions can be pertained for indefinite periods. If such flow systems are applied in anoxic experiments the usual teflon tubings have to be exchanged for gold capillaries which prevent gaseous diffusions.

Hypoxic conditions are typical in aquatic systems. They are partly man-made by surface pollution and eutrophication, partly they occur seasonally under ice, especially when it is covered with snow and photosynthesis is prohibited, during summer stagnation in smaller lakes or as stratification in larger lakes (Lake Tanganyika, e.g.) and by overstocking of fish ponds. Aquatic organisms exhibit different responses to hypoxia which may be investigated by calorimetry, respirometry or a combination of both, in some cases supported by ^{31}P-NMR [136]. Examples of such experiments are given below.

A further burden for aquatic systems is an acidification of weakly buffered water, mainly by acid rain. The pH value of the water may drop from a nearly neutral value around 7.0 to extreme figures below pH 5.6. Fish populations may answer in different ways, among them changes in metabolic rates, ionic balances or substrates, behavioral modifications, reduced reproductivity and increased mortality. As such variations are seen in the metabolism of the objects, calorimetry is a suitable tool for corresponding research [136].

In an early review article on microcalorimetric monitoring of ecological, toxicological and pharmacological effects on aquatic animals Gnaiger discussed problems where direct calorimetry provided an indispensable technique [137]. He paid special attention to oxygen depleted micro-habitats and anoxic aquatic environments and compiled data of several other authors.

There are a few problems encountered in calorimetric determinations of metabolism of aquatic animals. The instrument must guarantee that rapid media chan-

ges are possible to study responses to varying environments. This implies that the active volume has to be as small as possible for the investigated species. Spaargaren recommended a minimum of 10 mL for a 2 g shrimp [40]. Moreover, the heat production rate of aquatic animals is often rather small with a typical figure of 0.2 mW/g for poikilotherms [138]. Due to the large heat capacity of water such rates lead to only small temperature rises at large time constants which introduces a smearing of the thermal signal.

Antibiotics are often used against microorganisms in experiments with aquatic animals without concern about their influence on the animals themselves. Gnaiger showed that streptomycin, penicillin and neomycin or combinations of them may have stimulatory as well as inhibitory effects, both depending on the organism, the oxygen concentration in the water and on possible combinations of the drugs [139]. Biological samples for this combined direct and indirect calorimetry were aquatic oligochaetes, zooplankton, or fish eggs and larvae. Gnaiger's investigation underlines that one has to be careful in the interpretation of metabolic results when antibiotics have been applied.

Spaargaren presented a simple, low-cost, sensitive and rapidly responding flow-through microcalorimeter based on temperature difference measurements by a thermocouple [140] (see also [40,141]). The volume of the instrument could be easily adapted to the mass of the aquatic animal under investigation. Flow rate were adjusted between 1 and 10 mL per minute so that short-term changes in the environment could be realized.

Electric heaters are usually applied for calibration of calorimeters, especially for heat-flow instruments equipped with thermopiles or *Peltier sensors*. But often a chemical calibration is more appropriate and matching the experimental conditions more closely. For this end Wadsö and coworkers recommended the hydrolysis of triacetin in imidazole/acetic acid buffer with stable, long-lasting heat production rates between 7 and 90 μW/mL at 37 °C [142,143]. Some other possible reactions were cited and discussed in connection with the most important types of calorimetric vessels, batch forms as well as flow-through containers.

7.2. Fish

Direct calorimetry of fish is scarce, and indirect calorimetry started even later. Davies [144] determined heat production rates for goldfish, Smith and coworkers [145] investigated those of 4 salmonids at different temperatures. *Group effects* (see section 5.1.1. and 5.4.2.) could also be observed. Van Waversfeld and colleagues presented an approximate rate of 700 J/h/mw (0.20 W/mw) for fish at 20 °C where mw indicates the metabolic weight, i.e. the body mass m in kg to a broken power of 0.85 ($mw = m^{0.85}$) [146].

A broad spectrum of investigations on fish were carried out in a 1-litre differential flow-through calorimeter (Sétaram GF 108) developed and described by Addink and his group [63,72]. Thanks to the continuous perfusion it is suited for long-term monitoring of aquatic animals between 1 and 50 g under stress-free constant normoxic or hypoxic conditions. The water flowing through the calorimeter can be saturated with air for the usual normoxic metabolism or with nitrogen for reduced oxygen concentrations (hypoxia) or even anoxia. The calorimeter works with a sensitivity of 100 mV/W and a time constant of 33 min. A part of the outflowing water is sent to an oxygen sensor for simultaneous indirect calorimetric recordings. The smearing of the thermal signal due to the high time constant was compensated by a deconvolution procedure described in [147]. This calorimeter was used for investigations on groups of the goldfish *Carassius auratus* [146-150] and tilapia (*Oreochromis mossambicus*) [58,63]. Recently the calorimeter was equipped with a video tracking and motion analysis system (section 3.1.) which allowed to follow complex movements of the fish like accelerations, fin movements or branchial ventilation [63].

Goldfish (*C. auratus*) are very tolerant to anaerobic conditions and survive anoxia up to 16 h. They are thus very suited for calorimetric studies of normoxia and hypoxia in fish [146-150]. Goldfish in groups of 4, long-time acclimated to the experimental conditions, were introduced to the flow-through calorimeter for more than one week. Only after 2 days the normoxic metabolism was determined so that all handling stress for the animals vanished before, which usually led to an overestimation of heat output in usual short-term experiments. Simultaneous indirect calorimetry and metabolite determinations showed that glycogen storage appeared to be crucial for surviving under anoxia. The normoxic metabolic rate of about 0.20 W/mw was reduced to 0.06 W/mw under anoxia. During this period only 5 % of the metabolizable energy was used for the energy metabolism, while about 60 % and 40 % were converted to ethanol and fat, resp. [149].

By means of the video tracking system it was possible to observe the behavioural response of tilapia (*O. mossambicus*) during severe hypoxia [58]. The authors found no differences to the normoxic state so that the calorimetrically determined 50 % reduction of the heat production rate had to be ascribed to a lowered cellular energy metabolism which is known as *metabolic depression*. Moreover, strong fluctuations between aerobic and anaerobic periods were observed in the power-time curves. A slow acidification of the water had no influence on heat production, oxygen consumption and oxycaloric equivalent of tilapia under normoxic conditions. And even an additional stepwise hypoxia showed no potentiating effect [136,151].

7.3. Aquatic Invertebrates

Heat production rates of juvenile mussels (*Mytilus edulis*) of about 10 mg were determined by direct calorimetry for mussels feeding on algae at different rates [152,153]. Heat dissipation was partitioned into the cost of food acquisition, maintenance, absorption/digestion and growth and compared with theoretical estimates. Total heat output varied between 3.83 and 7.15 mW/g at 15 °C and 3.3 % salinity, depending on the rate of feeding.

Combined calorimetry and polarography on another mussel (*Modiolus demissus*) were described for a closed system and for a setup in which the calorimetric vessel could be flushed from time to time to reconstitute the original oxygen tension [154]. Pronounced metabolic cycles were seen in the power-time curves each lasting for about 10 h. They were connected with the periodic opening and closing of the shell, the consumption of oxygen trapped in the shell and an approach to basal aerobic or even anaerobic metabolism in the intervals. More detailed information may be found in [155,156].

Microcalorimetric investigations of the host-parasite relationship between the water snail *Biomphalaria glabrata* and the pair-worm *Schistosoma mansoni* were performed to evaluate the energetic influence between the parasite and the host [70] (see also [157]). No differences in the heat production rates of infected and uninfected snails were found as long as they were compared on a wet weight basis, while they became highly significant per dry weight (12.63 to 8.94 mW/g dw, resp., $p < 0.0001$). The same results were obtained with indirect calorimetry by means of the Warburg technique. As such manometric experiments are at best in parallel, an electronic pressure transducer was incorporated into the calorimeter to allow for truely simultaneous indirect measurements (section 3.3.2.). Because both indirect approaches rendered identical values, these results were used. They showed that aerobic metabolism sufficed to explain the observed heat production rates and that no anaerobic contributions took place. Periodic structures were seen in the calorimetric traces, but not in the indirect signals as they have integral character in contrast to the derivative one of calorimetry. The authors explained the observed structures with oscillations in the glucose concentration of the snail's hemolymph. Later endoscopic observations of the snail in the calorimeter underlined that the periodic fluctuations were not connected with any locomotor activities [55].

In a further calorimetric paper on *B. glabrata* infected or uninfected by *S. mansoni*, Becker showed that there was no difference between the active metabolism of both groups while animals in a relaxed state - due to an injection of succinylcholine chloride - differed significantly ($p \leq 0.001$) in their heat production rates (1.02/0.22 mW/g for unrelaxed/relaxed uninfected snails and 0.96/0.30 mW/g for infected snails) [158]. This could be explained by a reduced locomotor

activity in infected snails to such an amount that the active metabolism remained equal. Figure 18 presents the energetic states of relaxation, recovery (arrow) and activity for an infected animal.

The semiterrestrial fiddler crab *Uca pugilator* experiences periodically changing salinities in its tidial environment. *Uca* developed effective mechanisms to regulate its hemolymph concentrations in the sense of an excellent osmoregulator. Simultaneous direct and indirect calorimetry on these crabs were performed at 3 different salinities: 33, 100 and 167 % of sea water salt concentration before, during and after some days of adaptation to the new conditions [64]. The metabolic heat output was approximately doubled at both altered salinities compared with that of standard salt concentration (0.29 mW/g). The basal metabolic rate as well as the locomotor activity were specially raised at high salinity, and less pronounced at low values.

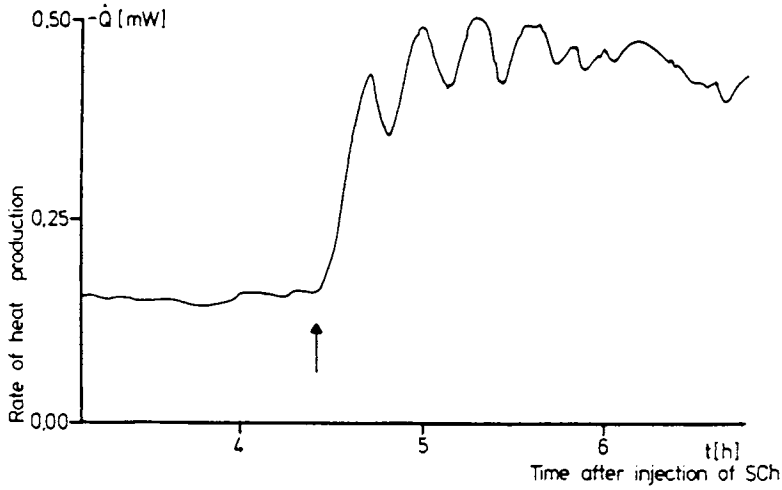

Figure 18. Power-time curve of a snail (*B. glabrata)* infected by *S. mansoni* and relaxed by an injection with succinylcholine chloride at time 0 h (out of scale) [158].

The brine shrimp *Artemia franciscana* is a frequently used model organism for metabolic investigations as its embryos exhibit an astonishing tolerance to anoxia over prolonged periods. A number of direct calorimetric experiments are found in the literature [159-166]. Hand and Gnaiger showed that the energy flow is reduced to 2.4 % in the reversible transition of brine shrimp embryos from aerobic development to anaerobic dormancy [160]. This is supposedly due to changes of the intracellular pH and mobilization of trace amounts of trehalose. In

longer periods of anaerobiosis the metabolic depression went down to extreme, but still detectable 0.5 % of the aerobic level [163]. In a later paper of Hontoria and coworkers it was shown that with their calorimetric equipment no heat dissipation could be detected in encysted embryos after 1.5 h of anoxia [164]. But in a reexamination of his earlier experiments Hand used higher amounts of brine shrimps and observed 8 μW for 2.3 g shrimps after 50 h of anoxia and 60 μW for 20 g, while the blanks resulted to 0.5 μW [166]. The 60 μW were in contrast to 35 mW for fully aerobic embryos indicating a reduction to 0.17 % in the anaerobic state and a heat dissipation of 12.8 μW/g dry weight against 6.35 mW/g under aerobic conditions.

The freshwater amphipod *Gammarus pulex* and the brackish-water amphipod *G. tigrinus* - typical for large German rivers intensely salt-polluted by potash-mining - were investigated by flow-microcalorimetry and ^{31}P NMR spectroscopy to determine their energetic behaviour under salt stress [167]. After addition of KCl, both answered with an immediate increase in heat production which was driven by forced aerobic metabolism. In both animals a second increase occured after about 1 h. After a more or less pronounced plateau both heat production rates dropped, in *G. tigrinus* to a value 20 % above the basal metabolism, while in *G. pulex* aerobic and anaerobic metabolic capacity were not high enough to cope with the salt stress. The animal died. Nevertheless, the energy output continued on a level similar to that of the basal metabolism before stress. This effect might be partly due to microbial contamination and intracellular degradation processes but could not be fully explained by the authors [167]. In contrast to these observations a vanishing of locomotor activities and a subsequent gradual decrease to the baseline was seen in the death of the terrestric pillbug *Armadillidium vulgare* [60].

The medicinal leech *Hirudo medicinalis* was investigated under normoxic and severe hypoxic conditions by direct and indirect calorimetry and biochemical analysis [168]. Animals showed a reduction of heat production down to 13 % and of ATP turnover to about 30 % of the aerobic rate under artificial or self-induced hypoxia (Figure 19). The mean heat production rate under long-term aerobic incubation amounted to 0.13 mW/g, that at the end of the hypoxic phase to about 0.03 mW/g in the mean. This reduction ensured the survival during environmental anaerobiosis. Biochemical analysis of substrates and endproducts provided a means to calculate heat dissipation indirectly and to compare it with the calorimetric results. Under long-term hypoxia only 71 % of the observed heat production rate could be explained biochemically.

The aquatic worm *Sipunculus nudus* is counted as an *oxyconformer* since its oxygen consumption rate declines linearly with the ambient oxygen tension with an onset of anaerobic metabolism at low concentrations. At extreme hypoxia it

exhibited a metabolic rate of 6.0 μW/g which could be fully explained by the enthalpy changes during formation of anaerobic end products [169].

The aquatic oligochaete *Lumbriculus variegatus* is known to survive long periods of anoxia so that it represents a suited object for various calorimetric investigations. Groups of 10 individuals of this species with 1 to 2 mg dry weight were placed in a perfusion chamber of a flow calorimeter connected to a twin-flow respirometer (section 3.3.1.) for simultaneous direct and indirect calorimetry [170]. They were exposed to normoxic and anoxic conditions and showed a drastic reduction of heat dissipation under anoxia down to 15 % of the aerobic rates. Switching back to aerobic conditions, heat dissipation increased immediately.

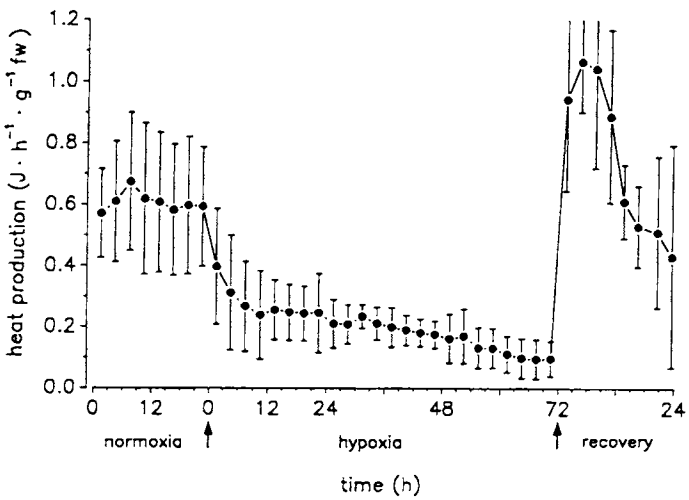

Figure 19. Power-time curve of a medicinal leech (*Hirudo medicinalis*) under normoxic and hypoxic conditions and in the subsequent recovery phase. The pronounced heat production (*overshoot*) after introduction of air is clearly visible [168].

The same organism was investigated calorimetrically over periods of up to 7 days under aerobic and anoxic conditions [171]. While animals showed synchronized peaks of activity under aerobic conditions, flat and smooth power-time curves without structures were observed during anoxia. Aerobic heat production of 0.44 mW/g at 12 °C dropped to 0.19 mW/g under anoxia, and from 0.86 to 0.30 mW/g at 20 °C. The aerobic heat production rates could be fully explained by the oxygen consumption, but only less than 50 % of the anoxic heat production was recovered by the formation of secondary end products from glycogen

fermentation. The rest remained unexplained, similar to results of the bivalve *Mytilus edulis* [172-174].

Simultaneous direct and indirect calorimetry was applied to monitor decreased oxygen concentrations in combination with hydrogen sulphide contaminations of freshwater on two annelides, *Limnodrilus hoffmeisteri* and *Tubifex tubifex* [175,176]. Such combined adverse conditions are typical for polluted lakes and rivers with high organic load. Complete anoxia reduced the normoxic heat production rates (0.83 and 0.56 mW/g for *L. hoffmeisteri* and *T. tubifex*, resp.) to less than one fourth. Presence of 100 µmol/l H_2S depressed the heat dissipation in *L. hoffmeisteri* at each oxygen level, mainly due to the strict inhibition of aerobic respiration. In contrast, heat dissipation increased in *T. tubifex* (up to 170 %) because of its detoxification system which protects respiration.

Pronounced levels of hydrogen sulphide are not only found in water, but also in sediments as a consequence of polytrophic conditions. The polychaete *Marenzelleria viridis* from the southern Baltic Sea was chosen as a representative of the group of sediment living aquatic animals influenced by H_2S [177]. Direct (and indirect) calorimetry showed a significantly enhanced heat production rate in the presence of sulphide under hypoxic conditions, due to changing detoxification processes dependent on the presence or absence of oxygen. Figure 20 exhibits a typical power-time curve of *M. viridis* without and with H_2S in its environment.

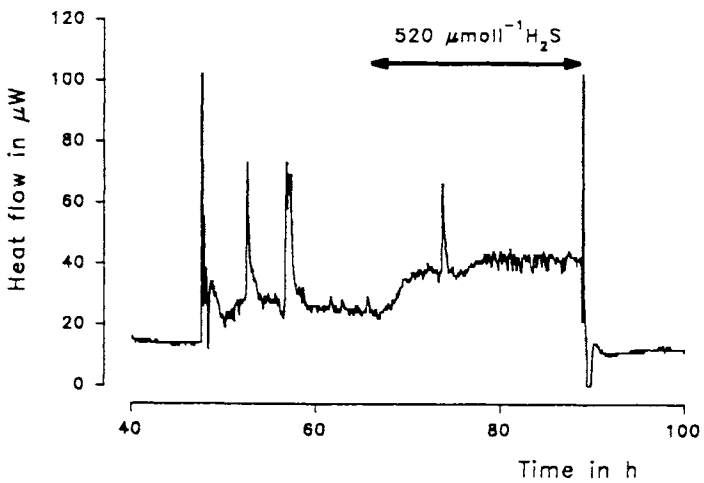

Figure 20. Power-time curve of a polychaete (*M. viridis*) of 71 mg at 10 °C, a salinity of 5 ‰ and a moderate hypoxia. The larger bouts of heat production are due to locomotor activities, the smaller to ventilation. The period of pollution by sulphide is indicated [177].

Moreover, the metabolism of *M. viridis* was investigated by simultaneous flow-through calorimetry and respirometry at different temperatures, salinities and oxygen partial pressures. It was compared to that of the indigenous species *Nereis* (*Hediste*) *diversicolor* [178]. Larvae of *M. viridis* showed no change in their metabolism at decreasing oxygen concentrations down to severe hypoxia, while adults gradually lowered their activity. They followed an oxyconformer model when an additional hyposmotic stress of 0.5 ‰ salinity was applied. The metabolic behaviour of larvae and adults is demonstrated in Figure 21.

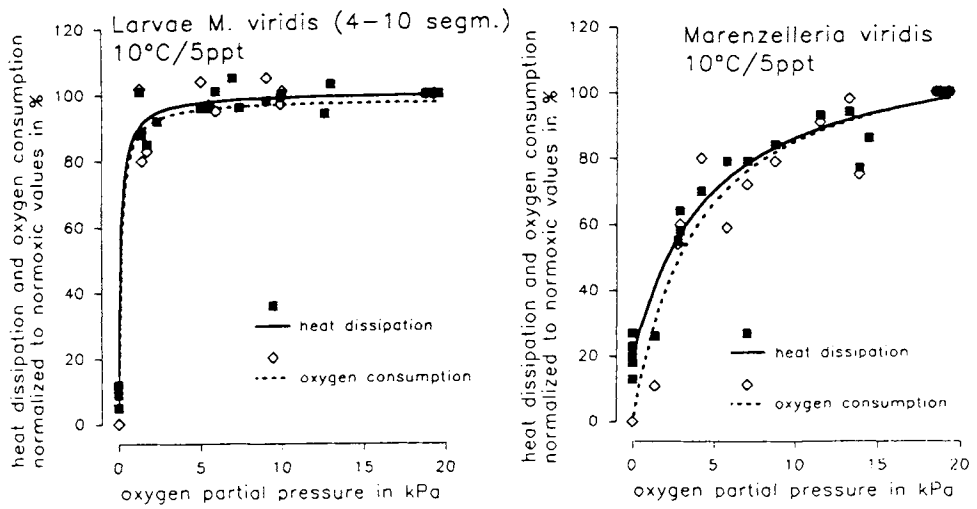

Figure 21. Heat dissipation and oxygen consumption rates of the polychaete *M. viridis* at varying oxygen partial pressures at an average biotope salinity of 5 ‰. Left: Larvae follow an oxyregulator model down to severe hypoxia. Right: Adult animals react more according to an oxyconformer model with decreasing metabolic rates at progressing hypoxia [178].

The sediment living polychaete *Neanthes virens* is frequently used as a test organism for toxic chemicals in the marine environment. Therefore, direct calorimetric experiments were performed to show the stress induced on these worms when they are kept without sediments as often done in environmental monitoring [179]. Alternating periods of hyperactive and resting animals found in the power-time curves indicated that *N. virens* was in an abnormal state, not useful for significant toxicity tests.

The same author investigated a model soft-bottom ecosystem consisting of flooded clean sand with food, microorganisms, nematodes (*Diplolaimella chitwoodi*) and polychaetes (*Capitella capitata*) and looked for their mutual inter-

actions [180]. He could show that direct calorimetry was an elegant and suitable tool for such experiments, but that it was difficult to partition the energy flows in this system without uncoupling interactions.

8. ECOLOGY

When we talk about ecosystems, rather complex entities of different trophic levels and a manifold of interacting organisms are meant, plants as well as microbes and animals. Of course, it is impossible to investigate a complex ecosystem in total by means of calorimetry, but only isolated members of it without connection to the rest of their environment. In this sense, all the calorimetric determinations - direct, indirect or by combustion - are just first approximations to a full energetic picture of the system. Nevertheless, separated animals may be used to monitor changes in the system or influences by xenobiotic substances or pollutions. Again, direct calorimetry renders a more comprehensive description because aerobic plus anaerobic metabolism is determined while the latter is lost in respiration tests.

Widdows presented an introduction to microcalorimetric methods in ecology and discussed applications from microbial ecology to investigations of aerobic and anoxic metabolism in aquatic invertebrates or fish and to toxicological and pharmacological experiments [181]. A number of special examples might be found on those pages. Reh listed a manifold of direct calorimetric experiments connected with ecological questions [13]. They ranged from microorganisms and microbial degradation of litter or sludge over aquatic and terrestrial animals to populations under the influence of xenobiotic pollutions. Many further investigations have been run with indirect or combustion calorimetry. Another short introduction to this field is given in [182].

Some of the papers mentioned in section 5.1. may be cited here as also ecologically orientated. These are the investigations of Seo and colleagues [94] on the Mediterranean fruit fly *Ceratitis capitata*, of the Estonian group around Kuusik about the interaction between plants and insects [103] and of Lovrien and his coworkers on the effects of toxic compounds on beetles [47]. Another example results from combustion calorimetry (see *Combustion Calorimetry* in this volume of the handbook) on chrysomelid beetles (*Agelastica alni*) exclusively feeding on alder leaves [183,184].

The sorption chamber of an LKB sorption flow calorimeter was enlarged from the usual 0.5 mL to the maximal possible size of 3 mL to house single individuals of the freshwater snail *Planorbis corneus* during toxicity tests with the heavy

metal cadmium [185]. Low flow rates of 9.5 mL/h did not disturb the thermal signal, did not cause the animals to draw back in their shells and facilitated the exposure to cadmium concentrations between 0.01 and 1000 µg/L. Heat dissipation of snails amounted to 0.45 mW/g under normal conditions and dropped significantly at all chosen Cd concentrations. The typical result of intoxication showed an immediate short fluctuation due to the forced introduction of contaminated medium, a more or less constant *shoulder* and a steady decline to a new constant level (Figure 22). As the physiological action of cadmium is rather complex, the calorimetric response remained unspecific with no attribution to a special chemical or metabolic event. Nevertheless, the results with 0.01 µg/ Cd underline the high sensitivity of the applied method and the short-time availability of the answer.

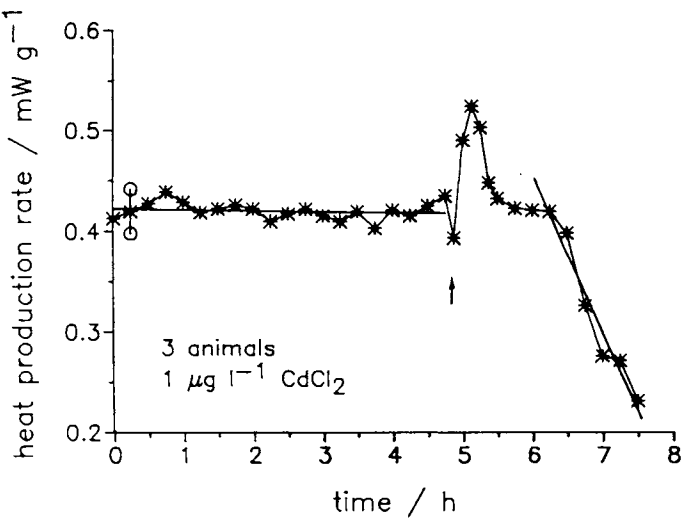

Figure 22. Typical power-time curve for the action of cadmium intoxication on a freshwater snail (*Planorbis corneus*). At the arrow, contaminated water is introduced to the sorption chamber at a higher flow rate to guarantee for a quick and effective water exchange. The bar near the ordinate indicates the standard deviation for a superposition of 3 individual traces [182].

Pentachlorophenol (PCP) is one of the most intensively used pesticides in the world because of its fungicide, herbicide, insecticide, molluscicide and defoliant action [186]. As a technical product it is contaminated with a number of impurities which make PCP even more toxic than the pure substance. This has to be kept in mind when laboratory results are compared with data from environmental pollution. In a line of direct calorimetric experiments, different members of a fo-

rest ecosystem were investigated for their metabolic response to a treatment with increasing concentrations of PCP [182,187,188]. Besides soil and litter several typical animals found in such a biotope were included in the investigation. As PCP is known to be a strong decoupler of oxydative phosphorylation [189] a stimulating action on the heat production rates was expected at low concentrations and a fatal poisoning only at higher ones. This expectation was met by the power-time curves without and with PCP as shown in Figure 23 for the earthworm *Eisenia foetida*. Similar traces were found for the pill bug *Armadillidium vulgare*, the wood louse *Oniscus asellus* and the carabid beetle *Nebria brevicollis*. Typical stimulations resulted in an increase of about 30 % under medium PCP concentrations. Problems arose with the best way of PCP application. Bathing the animals for a few minutes in a PCP solution rendered the most homogeneous results and a linear uptake with time, but stressed the animals considerably, while kreeping around on filter paper sucked with the solution was stress free but less reproducible.

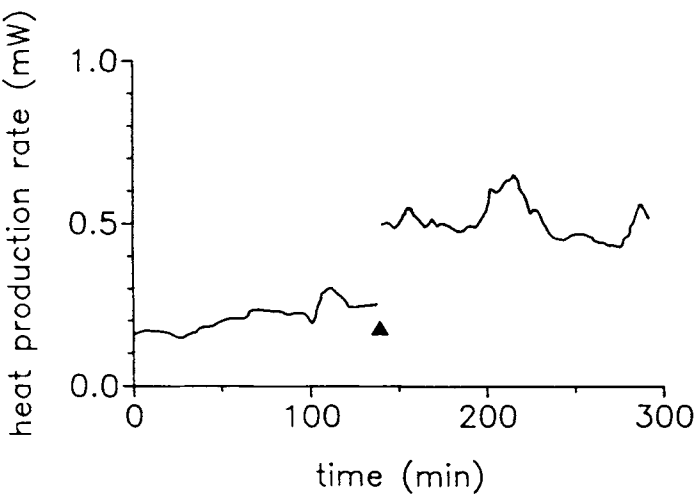

Figure 23. Power-time curve of an earthworm (*Eisenia foetida*) before and under the stimulating influence of pentachlorophenol (PCP). For further details see text [182].

The ground-beetle *Pterostichus oblongopunctatus* is a typical representative of terrestrial ecosystems, frequently investigated and used as an indicator for sound or polluted biotops. It was chosen for preliminary batch calorimetric experiments under normal conditions and under the influence of lead-contaminated food and SO_2-loaded air [190]. SO_2 exposition as high as 100 times the usual level resulted in nearly no change in heat output (1 mW/g), while Pb led to a significantly in-

creased metabolic turnover to more than twice of normal values. Combined action of both poisons lowered the stimulation by Pb, so that no synergistic effect became visible.

9. CONCLUSIONS AND PERSPECTIVES

The preceding pages have shown that *Calorimetry of Small Animals* is a wide field with investigations of little aquatic invertebrates like *Tubifex tubifex* (section 7.3.) as well as of larger reptiles (section 4.) or whole colonies of social insects (section 5.5.). Nevertheless, it became clear from the compilation of results that the choice of examples was a very personal one of the authors guided by their specific interests, experimental possibilities and existing co-operations. These examples were just a reduced sector of the broad spectrum of potential applications. Neither small mammals nor birds were mentioned in the text although mice, rats and hamsters could have been included. But they are usually investigated in research groups working in the medical area or with larger domestic animals.

Moreover, the different sections demonstrated that direct calorimetry in contrast to the various indirect methods mentioned in section 2. is indispensible in situations when organisms experience severe hypoxia or anoxia. Such states are often supposed to be only typical for aquatic systems - at least periodically or seasonally (section 7.3.). On the contrary, hypoxic situations may also occur for terrestric organisms. It was shown recently that significantly reduced oxygen concentrations can be used by honeybees to reduce and regulate their metabolism in the core of winter clusters [191]. On the other hand, geophysical data point to the fact that atmospheric concentrations of oxygen and carbon dioxide have changed dramatically during palaeontological periods [192]. Organisms were forced to adapt their metabolism to such varying environmental conditions. As it is well-known that physiological traits are often highly conservative in evolution it makes sense in this respect to look for metabolic adaptations of extant forms to artificial states of modified atmospheric parameters, although these animals will never experience such conditions in their normal life. But these investigations may render further insight into metabolism, its adaptation and regulation.

Future investigations on small animals will depend on further development of calorimeters and of combinations with indirect methods. Until now, no calorimetric experiments were performed with specimens under higher pressure. But some data on metabolic research and pressure are found in the literature [193-195]. In the opinion of the authors, an experimentally difficult, but fascinating field opens here. Invertebrates (like gammarides, worms or snails) from deep freshwater (e.g.

Lake Baikal with depth down to 1 700 m, temperatures just above zero and high oxygen tensions) could be compared with corresponding marine organisms, e.g. the astonishing Pompeii worm (*Alvinella pompejana* [196]) from hydrothermal vents in several thousand meter depth at temperatures up to 80 °C. On the other hand, it could be interesting to study the influence of low pressure or the transition to lower pressure in terrestric animals, e.g. insects living in high altitudes of the Alps or other mountaineous systems.

Microorganisms have been used for a long time to investigate the actions of drugs or of man-made xenobiotics by means of calorimetry. In the same sense, small animals will become valuable calorimetric test systems for all kinds of environmental pollutions, terrestrial as well as aquatic. Many of them are easy to breed and to keep in large numbers under standardized conditions so that highly reproducible results can be expected. Control experiments of drugs for human application or of environmental disturbances which are performed with higher vertebrates nowadays, should be shifted to this invertebrate range and might thus reduce ethic scruples about the usual "animal experiments".

Many experiments on small animals were performed in a (too?) short-term manner, so that the question remained if artifacts were measured or true physiological phenomena. Flow-through systems with air or water as applied by some scientists for fish (section 7.2.), aquatic invertebrates (section 7.3.) or insects (section 5.) would help to avoid such mistakes - if the animals are kept in an adequate state and environment during prolonged experimental periods. In any case, one has to have a *great staying power* for working calorimetrically with animals, keeping in mind the old Persian proverb:

You can find out all about a man in two days,
about an animal in four.

10. REFERENCES

1. A.L. Lavoiser and P.S. de LaPlace, Mémoire sur la Chaleur, Mémoires de la Académie Royale, 1780.
2. A. Crawford, Experiments and Observations on Animal Heat and the Inflammation of Combustible Bodies being an Attempt to Resolve these Phenomena into a General Law of Nature, Edinburgh, 1778.
3. Y. Schutz, Diabetes/Metabolism Reviews, 11(4) (1995) 383.
4. C. Despretz, J. Physiol. Exp. Path., 4 (1824) 143.
5. M. Rubner, Biol., 30 (1894) 73.
6. F. Laulanié, Arch. Physiol., (1896) 572.
7. L. Krehl and F. Soetbeer, Arch. Ges. Physiol., 77 (1899) 611.
8. W.O. Atwater and E.B. Rosa, Description of new respiration calorimeter and experiments on the conservation of energy in the human body, U.S. Dept. Agr. Off. Exp. Sta. Bull., 63 (1899).
9. M. Kleiber, The Fire of Life, Wiley, New York, 1961, p. 454.
10. I. Wadsö, Thermochim. Acta, 300 (1997) 1.
11. K. Blaxter, Energy metabolism in animals and man, Cambridge University Press, Cambridge, 1989, p. 336.
12. M.J. Dauncey, Thermochim. Acta, 193 (1991) 1.
13. U. Reh, Thermochim. Acta, 193 (1991) 107.
14. I. Lamprecht, Thermochim. Acta, 94 (1985) 113.
15. I. Lamprecht, Pure Appl. Chem., 70(3) (1998) 695.
16. A.I. Zotin, Thermodynamic Aspects of Developmental Biology, Karger, Basel, 1972, p. 159.
17. A.I. Zotin, Thermodynamic Bases of Biological Processes - Physiological Reactions and Adaptations, de Gruyter, Berlin, 1990, p. 293.
18. I. Lamprecht and A.I. Zotin (Eds.), Thermodynamics of Biological Processes, de Gruyter, Berlin, 1978, p. 428.
19. I. Lamprecht and A.I. Zotin (Eds.), Thermodynamics and Kinetics of Biological Processes, de Gruyter, Berlin, 1982, p. 536.
20. I. Lamprecht and A.I. Zotin (Eds.), Thermodynamics and Regulation of Biological Processes, de Gruyter, Berlin, 1985, p. 573.
21. I. Lamprecht and A.I. Zotin (Eds.), Thermodynamics and Pattern Formation in Biology, de Gruyter, Berlin, 1988, p. 518.
22. P. Boivinet, in: I. Lamprecht and B. Schaarschmidt (Eds.) Application of Calorimetry in Life Sciences, de Gruyter, Berlin, 1977, p.159.
23. R.C. Woledge, in: A.E Beezer (Ed.) Biological Microcalorimetry, Academic Press, London, 1980, p.145.

24. R.B. Kemp, in: A.M. James (Ed.), Thermal and Energetic Studies of Cellular Biological Systems, Wright, Bristol, 1987, p. 147.
25. P. Boivinet and B. Rybak, Life Sciences 8 (1969) 11.
26. R.C. Woledge, in: I. Lamprecht and B. Schaarschmidt (Eds.), Application of Calorimetry in Life Sciences, de Gruyter, Berlin, 1977, p. 183.
27. G.W.H. Höhne, A.E. Bader and S. Hönle, Thermochim. Acta, 251 (1995) 307.
28. S. Tewe and G.W.H. Höhne, Thermochim. Acta, 309 (1998) 145.
29. F. Baisch, in: I. Lamprecht and B. Schaarschmidt (Eds.), Application of Calorimetry in Life Sciences, de Gruyter, Berlin, 1977, p. 209.
30. F. Baisch, Thermochim. Acta, 22 (1978) 303.
31. A. Anders, H. Schaefer, B. Schaarschmidt and I. Lamprecht, Arch. Dermatol. Res., 265 (1979) 173.
32. M. Pätel, U. Reichert, B. Schaarschmidt and I. Lamprecht, in: W. Hemminger (Ed.), Thermal Analysis, Vol. 2, Birkhäuser, Basel, 1980, p. 559.
33. M. Kleiber, J. Theor. Biol., 53 (1975) 199.
34. E. Calvet and H. Prat, Microcalorimétrie - Applications physico-chimiques et biologiques, Masson et Cie, Paris, 1956, p. 395.
35. S.L. Randzio and J. Suurkuusk, in: A.E. Beezer (Ed.), Biological Microcalorimetry, Academic Press, London, 1980, p. 311.
36. W. Hemminger and G. Höhne, Calorimetry - Fundamentals and Practice, Verlag Chemie, Weinheim, 1984, p. 310.
37. K.H. Müller and T. Plesser, Thermochim. Acta, 119 (1987) 189.
38. I. Lamprecht and F.R. Matuschka, Thermochim. Acta, 94 (1985) 161.
39. E.H.B. Battley, Thermochim. Acta, 250(2) (1995) 337.
40. D.H. Spaargaren, Comp. Biochem. Physiol., 112A (1995) 433.
41. W.W. Umbreit, R.H. Burris and J.F. Stauffer, Manometric & Biochemical Techniques, 5th editon, Burgess, Minneapolis, 1972, p. 387.
42. E. Brouwer, in: K.L. Blaxter (Ed.), Energy Metabolism, Academic Press, London, 1965, p. 441.
43. C. Romijn and W. Lokhorst, Proc. 2nd Symposium on Energy Metabolism, Wageningen, 1961.
44. B.G. Miller, J.K. Kirkwood, K. Howard, A. Tuddenham and A.J.F. Webster, Labor. Anim., 51 (1981) 313.
45. A.F. Bennett and W.R. Dawson, in: C. Gans (Ed.), Biology of the Reptilia, Academic Press, London, vol 5A/3, 1976, p. 127.
46. M.J. Dauncey and D.L. Ingram, Br. J. Nutr., 41 (1979) 361.
47. R.E. Lovrien, T.J. Kurtti, R. Tsang and M. Brooks-Wallace, J. Biochem. Biophys. Meth., 5 (1981) 307.

48. N. Lifson, G.B. Gordon, M.B. Visscher and A.O. Nier, J. Biol. Chem., 180 (1949) 803-811.
49. B.A. Young, R.A. Leng, R.G. White, G.L. McClymont and J.L. Corbett, Publ. Eur. Ass. Anim. Prod., 12 (1969) 435.
50. J.E. Morhardt and S.S. Morhardt, Am. J. Physiol., 221 (1971) 1580.
51. P. Leitner, Comp. Biochem. Physiol., 19 (1966) 431.
52. R.E. Carpenter and J.B. Graham, Comp. Biochem. Physiol., 22 (1967) 709.
53. A.J.F. Webster, Br. J. Nutr., 21 (1967) 769.
54. T. Nagasaka, K. Hirata, H. Shibata and Y. Sugano, Jap. J. Physiol., 30 (1980) 799.
55. I. Lamprecht and W. Becker, Thermochim. Acta, 130 (1988) 87.
56. L. Fahrenholz, I. Lamprecht and B. Schricker, Thermochim. Acta, 151 (1989) 13.
57. L. Fahrenholz, I. Lamprecht and B. Schricker, J. Comp. Physiol. B, 161 (1992) 119.
58. V.J.T. van Ginneken, A.D.F. Addink, G.E.E.J.M. van den Thillart, F. Körner, L. Noldus and M. Buma, Thermochim. Acta, 291 (1997) 1.
59. P. Schultze-Motel and I. Lamprecht, J. Exp. Biol., 187 (1994) 315.
60. I. Lamprecht, in: W. Hemminger (Ed.), Thermal Analysis, Vol. 2, Birkhäuser, Basel, 1980, 3.
61. E. Gnaiger and H. Forstner (Eds.), Polarographic Oxygen Sensors - Aquatic and Physiological Applications, Springer, Berlin, 1983, p. 370.
62. E. Gnaiger, in: E. Gnaiger and H. Forstner (Eds.), Polarographic Oxygen Sensors - Aquatic and Physiological Applications, Springer, Berlin, 1983, p. 134.
63. V.J.T. van Ginneken, A. Gluvers, R.W. van der Linden, A.D.F. Addink and G.E.E.J.M. van den Thillart, Thermochim. Acta, 247 (1994) 209.
64. G.B. Joachimsohn, I. Lamprecht and K. Graszynski, Thermochim. Acta, 94 (1985) 151.
65. B. Schaarschmidt, F.R. Matuschka and I. Lamprecht, Thermochim. Acta, 251 (1995) 261.
66. G. Sberveglieri (Ed.), Gas Sensors - Principles, Operation and Development, Kluwer Academic Publishers, Dordrecht, 1992, p. 409.
67. P. Schultze-Motel, Thermochim. Acta, 193 (1991) 57.
68. P. Schultze-Motel, Verh. Dt. Zool. Ges., 84 (1991) 427.
69. E. Schmolz, I. Lamprecht and B. Schricker, Apidologie, 27(4) (1996) 319.
70. W. Becker and I. Lamprecht, Z. Parasitenk., 53 (1977) 297.
71. A.F. Bennett and P. Licht, J. Comp. Physiol., 81 (1972) 277.

72. A.D.F. Addink, G. van den Thillart, H. Smit and J. van Waversfeld, Thermochim. Acta, 193 (1991) 41.
73. T. Wesolowski, B. Schaarschmidt and I. Lamprecht, J. Therm. Anal., 30 (1985) 1403.
74. P. Schultze-Motel and I. Lamprecht, Thermochim. Acta, 119 (1987) 157.
75. E. Schmolz, I. Lamprecht and B. Schricker, Thermochim. Acta, 251 (1995) 293.
76. I. Lamprecht, Thermochim. Acta, 300 (1997) 213.
77. K. Winckler, Thermochim. Acta, 251 (1995) 255.
78. C. Schulz, M. Thuy and G. Wegener, Thermochim. Acta, 187 (1991) 71.
79. T. Moratzky, G. Burkhardt, W. Weyel and G. Wegener, Thermochim. Acta, 229 (1993) 193.
80. A.V. Hill, J. Physiol., 43 (1911/1912) 379.
81. H.S. McDonald, in: C. Gans (Ed.), Biology of the Reptilia, Vol. 5A/2, Academic Press, London, 1976, p. 19.
82. I. Lamprecht, F.R. Matuschka and B. Schaarschmidt, J. Exp. Biol., 156 (1991) 375.
83. A.F. Bennett and W.R. Dawson, in: C. Gans (ed.) Biology of Reptilia, vol. 5A/3, Academic Press, London, 1976, p. 127.
84. P.A. Cragg, Comp. Biochem. Physiol., 60A (1978) 399.
85. H. Prat, in: H.D. Brown (Ed.), Biochemical Microcalorimetry, Academic Press, New York 1969, p.181.
86. M. Keister and J. Buck, in: M. Rockstein (Ed.), The Physiology of Insecta, 2nd ed., Academic Press, New York 1974, p. 470.
87. B. Sacktor, in: D. Candy and B. Kilby (Eds.), Insect Biochemistry and Function, Chapman and Hall, London 1975, p.1.
88. G.J. Peakin, Experientia, 29(7) (1973) 801.
89. M. Harak, A. Kuusik. K. Hiiesaar, L. Metspalu, A. Luik and U. Tartes, Thermochim. Acta, 309 (1998) 57.
90. A. Tian and J. Cotie, C. R. Acad. Sci. (Paris), 178 (1924) 1390.
91. H. Prat, Canad. J. Zool., 32 (1954) 172.
92. I.R. Taylor and F. Crescitelli, J. Cell. Comp. Physiol., 10 (1937) 93.
93. M. Harak. Heat production and respiration during the normal and defective metamorphosis of holometabolous insects by direct and indirect calorimetry, PhD Thesis, Tartu, 1997.
94. S.T. Seo, D.L. Williamson and M.S.Fujimoto, J. Econ. Entomol., 83(3) (1990) 896.
95. J. Fourche and C. Lemaitre, Bull. Biol. France Belg., 108 (1974) 97.
96. G. Wegener and T. Moratzky, Thermochim. Acta, 251 (1995) 209.

97. H.D. Brown, in: H.D. Brown (Ed.), Biochemical Microcalorimetry, Academic Press, New York, 1969, p. 291.
98. W.J. Evans, in: H.D. Brown (Ed.), Biochemical Microcalorimetry, Academic Press, New York, 1969, p. 257.
99. B.R. Wilson, L.E. Hagmann, S.K. Chattopadhyay and H.D. Brown, Chronobiol., 8(3) (1981) 243.
100. M. Harak, I. Lamprecht and A. Kuusik, Thermochim. Acta, 276 (1996) 41.
101. A. Kuusik, L. Metspalu, K. Hiiesaar, A. Kogerman and U. Tartes. Proc. Est. Acad. Sci. Biol., 42 (1993) 94.
102. A. Kuusik, U. Tartes, M. Harak, K. Hiiesaar and L. Metspalu, Eur. J. Entomol., 91 (1994) 297.
103. A. Kuusik, M. Harak, K. Hiiesaar, L. Metspalu and U. Tartes, Thermochim. Acta, 252 (1995) 247.
104. E. Schmolz and O. Schulz, Thermochim. Acta, 251 (1995) 241.
105. R. Gawtry and R. Lovrien, Calorim. Conf. Abstr., 30 (1975) 48.
106. F. Dunkel, C. Wensman and R. Lovrien, Comp. Biochem. Physiol., 62A (1979) 1021.
107. T. Kurtti, M.A. Brooks, C. Wensman and R. Lovrien, J. Thermal Biol., 4 (1979) 129.
108. A. White, P. Handler and E. Smith, in: Principles of Biochemistry. McGraw-Hill, New York 1964, p. 290.
109. P. Schultze-Motel and H. Greven, Entomol. Gener., 22(3/4) (1998) 199.
110. J.R. Coelho and A.J. Moore, Comp. Biochem. Physiol., 94A (1989) 587.
111. C. Heckrotte, J. therm. Biol., 8(4) (1983) 333.
112. E. Schmolz, B. Schricker and I. Lamprecht, J. Therm. Anal., 52 (1998) 33.
113. K.D. Loehr, P. Sayyadi and I. Lamprecht, in: I. Lamprecht and A.I. Zotin (Eds.), Thermodynamics of Biological Processes, de Gruyter, Berlin, 1978, p. 197.
114. K.D. Loehr, P. Sayyadi and I. Lamprecht. Experientia, 32 (1976) 1002.
115. L. Fahrenholz, I. Lamprecht and B. Schricker, J. Comp. Physiol. B, 159 (1989) 551.
116. R. Chauvin (Ed.), Traité de Biologie de l'Abeille, Vol. 5, Masson et Cie, Paris, 1968, p. 152.
117. M. Roth, C. R. Acad. Sci., 258 (1964) 5534.
118. M. Roth, Ann. Abeille, 8 (1965) 5.
119. M. Lemke and I. Lamprecht, J. Theor. Biol., 142 (1990) 143.
120. R. Dewitz, I. Lamprecht, E. Schmolz and B. Schricker, Apidologie, 25(5) (1994) 476.

121. I. Lamprecht, Thermochim. Acta, 234 (1994) 179.
122. E. Schmolz, I. Lamprecht and B. Schricker, Thermochim. Acta, 229 (1993) 173.
123. E. Schmolz. I. Lamprecht and B. Schricker, Apidologie, 24(5) (1993) 526.
124. E. Schmolz, B. Schricker and I. Lamprecht, Verh. Dt. Zool. Ges., 90(1) (1997) 147.
125. D. Coenen-Staß, B. Schaarschmidt and I. Lamprecht, Ecology, 61(2) (1980) 238.
126. I. Bachem, I. Lamprecht and B. Schaarschmidt, in: W. Hemminger (Ed.), Thermal Analysis, Vol. 2, Birkhäuser, Basel, 1980, p. 571.
127. I. Bachem and I. Lamprecht, J. Gen. Biol., 44(1) (1983) 114 (in Russian).
128. D. Coenen-Staß, Mitt. Dtsch. Ges. Allg. Angew. Ent., 6 (1988) 140.
129. K. Horstmann, Ins. Soc., 29 (1982) 402.
130. K. Horstmann and H. Schmid, Entomol. Gener., 11 (1986) 229.
131. K. Horstmann, Zool. Beitr. N. F., 33(1) (1990) 105.
132. R. Rosengren, W. Fortelius, K. Lindström and A. Luther, Ann. Zool. Fennici, 24 (1986) 147.
133. L. Nässberger and M. Monti, Protoplasma, 123 (1984) 135.
134. L. Nässberger and M. Monti, J. Protozool., 34(2) (1987) 123.
135. D. Lloyd, C.A. Phillips and M. Straham, J. Gen. Microbiol., 106 (1978) 19.
136. V.J.T. van Ginneken. Influence of hypoxia and acidification on the energy metabolism of fish: An *in vivo* ^{31}P-NMR and calorimetric study. PhD-Thesis, University of Leiden, 1996.
137. E. Gnaiger, Science Tools, 30 (1983) 21.
138. C.L. Prosser, in: C.L. Prosser (Ed.), Comparative Animal Physiology, Saunders, Philadelphia, 1973, p.165.
139. E. Gnaiger, Thermochim. Acta, 49 (1981) 75.
140. D.H. Spaargaren, 9th Europ. Mar. Biol. Symp., 1975, p. 475.
141. D.H. Spaargaren, Acta Biotheor., 42 (1994) 263.
142. A. Chen and I. Wadsö, J. Biochem. Biophys. Meth., 6 (1982) 297.
143. L.E. Briggner and I. Wadsö, J. Biochem. Biophys. Meth., 22 (1991) 101.
144. P.M.C. Davies, Comp. Biochem. Physiol., 17 (1966) 983.
145. R.R. Smith, G.L. Rumsey and M.L. Scott, J. Nutr., 108 (1978) 1017.
146. J. van Waversveld, A.D.F. Addink, G. van den Thillart and H. Smit, J. Therm. Anal., 33 (1988) 1019.
147. V.J.T. van Ginneken, A.D.F. Addink and G.E.E.J.M. van den Thillart, Thermochim. Acta, 249 (1995) 143.

148. J. van Waversveld, A.D.F. Addink and G. van Thillart, J. Exp. Biol., 143 (1989) 325.
149. J. van Waversveld, A.D.F. Addink and G. van den Thillart, J. Comp. Physiol., 159 (1989) 263.
150. J. van Waversveld. The energy metabolism of goldfish at different oxygen levels determined by simultaneous direct and indirect calorimetry. PhD-Thesis, University of Leiden, 1988.
151. V.J.T. van Ginneken, A.D.F. Addink, G.E.E.J.M. van den Thillart, Thermochim. Acta, 276 (1996) 7.
152. J. Widdows, in: W. Wieser and E. Gnaiger (Eds.), Energy Transformations in Cells and Organisms, Thieme, Stuttgart, 1989, p. 145.
153. J. Widdows and A.J.S. Hawkins, Physiol. Zool., 62(3) (1989) 764.
154. M.M. Pamatmat, in: E. Gnaiger and H. Forstner (Eds.), Polarographic Oxygen Sensors, Springer, Berlin, 1983, p. 167.
155. M.M. Pamatmat, Mar. Biol., 48 (1978) 317.
156. M.M. Pamatmat, Mar. Biol., 53 (1979) 223.
157. C.T. Hurst and C.A. Walker, Amer. Nat., 69 (1935) 461.
158. W. Becker, J. Comp. Physiol., 135 (1980) 101.
159. E. Gnaiger, J. Exp. Zool., 228 (1983) 471.
160. S.C. Hand and E. Gnaiger, Science, 239 (1988) 1425.
161. S.C. Hand and E. Gnaiger, in: W. Wieser and E. Gnaiger (Eds.), Energy Transformations in Cells and Organisms, Thieme, Stuttgart, 1989, p. 155.
162. J.S. Glasheen and S.C. Hand, J. Exp. Zool., 145 (1989) 263.
163. S.C. Hand, J. Comp. Physiol. B, 160 (1990) 357.
164. F. Hontoria, J.H. Crowe, L.M. Crowe and F. Amat, J. Exp. Biol., 178 (1993) 149.
165. S.C. Hand, K.E. Kwast and T.J. Anchordoguy, Modern Trends in Bio-Thermokinetics, 3 (1994) 251.
166. S.C. Hand, J. Exp. Zool., 273 (1995) 445.
167. J.H.E. Koop, J. Zange and M.K. Grieshaber, Thermochim. Acta, 251 (1995) 45.
168. H. Schmidt, A. Wichmann, I. Lamprecht and I. Zerbst-Boroffka, J. Comp. Physiol. B, 166 (1996) 205.
169. I. Hardewig, A.D.F. Addink, M.K. Grieshaber, H.O. Pörtner and G. van den Thillart, J. Exp. Biol., 157 (1991) 143.
170. E. Gnaiger and I. Staudigl, Physiol. Zool., 60(6) (1987) 659.
171. E. Gnaiger, FEBS Lett., 112 (1980) 239.
172. A. De Zwaan and T.C.M. Wijsman, Comp. Biochem. Physiol., 54B (1976) 313.

173. J.H. Kluytmans, M. van Graft, J. Janus and H. Pieters, J. Comp. Physiol., 123 (1978) 163.
174. M.M. Pamatmat, in: K.R. Tenore and B. Coull (Eds.), Marine Benthic Dynamics, Belle W. Baruch Libr. Marine Sci. no. 11, Univ. South Carolina Press, Columbia SC, 1980.
175. A. Schneider, I. Lamprecht and M.K. Grieshaber, Mitt. Dtsch. Ges. Limnol., 36 (1992) 314.
176. A. Schneider, Die Sulfidtoleranz der Schlammröhrenwürmer *Limnodrilus hoffmeisteri* (Cl.) und *Tubifex tubifex* (M.), PhD-Thesis University Düsseldorf 1994, Shaker, Aachen, 1994, p. 122.
177. A. Schneider, Thermochim. Acta, 271 (1996) 31.
178. D. Fritzsche and J.A. von Oertzen, Thermochim. Acta, 251 (1995) 1.
179. M.M. Pamatmat, Mar. Poll. Bull., 13(10) (1982) 364.
180. M.M. Pamatmat and S. Findlay, Mar. Ecol. Progr. Ser., 11(1) (1983) 31.
181. J. Widdows, in A.M. James (Ed.), Thermal and Energetic Studies of Cellular Biological Systems, Wright, Bristol, 1987, p. 182.
182. K. Drong and I. Lamprecht, Pure Appl. Chem., 65(9) (1993) 1967.
183. W. d'Oleire-Oltmanns, Verhdlg. Ges. Ökol., 5 (1976) 181.
184. d'Oleire-Oltmanns, in: I. Lamprecht and B. Schaarschmidt (Eds.), Application of Calorimetry in Life Sciences, de Gruyter, Berlin, 1977, p. 315.
185. G.B. Joachimsohn, I. Lamprecht and B. Schaarschmidt, J. Therm. Anal., 35 (1989) 659.
186. K.R. Rao (Ed.), Pentachlorophenol - Chemistry, Pharmacology, and Environmental Technology, Plenum Press, New York, 1979.
187. I. Lamprecht, C. Motzkus, B. Schaarschmidt and D. Coenen-Staß, Thermochim. Acta, 172 (1990) 87.
188. K. Drong, I. Lamprecht, C. Motzkus and B. Schaarschmidt, Thermochim. Acta, 193 (1991) 125.
189. W.G. Hanstein, Biochim. Biophys. Acta, 456 (1976) 129.
190. U. Rink, Struktur und Phänologie der Fauna von Laufkäfern (Coleoptera: Carabidae) und Kurzflügelkäfern (Coleoptera: Staphylinidae) in immissionsbeeinflußten Kiefernbeständen des Berliner Grunewaldes und deren Belastung. PhD-Thesis, Free University Berlin, Berlin, 1991.
191. K. Van Nerum and H. Buelens, Comp. Biochem. Physiol., 117A (1997) 445.
192. R. Dudley, J. Exp. Biol., 201 (1998) 1043.
193. J.J. Childress, TREE, 10(1) (1995) 30.
194. K.L. Smith and R.J. Baldwin, in E. Gnaiger and H. Forstner (Eds.), Polarographic Oxygen Sensors - Aquatic and Physiological Applications, Springer, Berlin, 1983, p. 298.

195. M.A. Cheney, L.D. Hansen, R.W. Breidenbach, E. Wilhelmsen and R.S. Criddle, Comp. Biochem. Physiol., 114B (1996) 69.
196. S.C. Cary, T. Shank and J. Stein, Nature, 391 (1998) 545.

This Page Intentionally Left Blank

Handbook of Thermal Analysis and Calorimetry, Vol. 4: From Macromolecules to Man.
R.B. Kemp, editor.

Chapter 9

CALORIMETRIC APPROACHES TO ANIMAL PHYSIOLOGY AND BIOENERGETICS

Steven C. Hand

Department of Environmental, Population and Organismic Biology,
University of Colorado,
Boulder, Colorado 80309-0334 USA

1. INTRODUCTION

In addition to the established applications in the fields of chemistry and biochemistry, isothermal calorimetry offers a number of experimental advantages in studies of animal physiology. Key applications include the measurement of energy flow under conditions of oxygen limitation, where availability of the common electron acceptor for eukaryotic respiration is sufficiently low that fermentative pathways are recruited. Flux through fermentative pathways is invisible to estimators of energy metabolism that rely on oxygen consumption as the rate indicator. Calorimetry, when combined with simultaneous measurements of oxygen consumption, allows the noninvasive assessment of aerobic to anaerobic poise of an animal or tissue via the use of the calorimetric-respirometric ratio (CR ratio; heat dissipated in kJ per mole of oxygen consumed). The CR ratio provides an independent measure of the contribution of fermentative pathways to the energetic requirements of an animal, in parallel to direct biochemical measurements of the accumulation of anaerobic end products. In the complete absence of oxygen, calorimetry permits a quantitative biochemical accounting of anaerobic processes by generating an independent enthalpy baseline for comparison. Further, heat dissipation may provide insight into the existence and quantitative importance of alternative electron acceptors.

As this review will attempt to document, the compelling rationales mentioned above for calorimetry have been experimentally executed using a diversity of developmental stages and adult forms with substantial benefit to the biological questions posed. The areas of investigation where weaknesses in the calorimetric

approach have been exposed will also be noted. For example, when rates of heat dissipation are extremely depressed (i.e., below 0.5% of the maximal aerobic metabolic rate), is possible that other exothermic events unrelated to pathways coupled to ATP turnover can make quantitatively significant contributions to the measured heat flow. Thus under such conditions, assumptions that heat dissipation is indicative of metabolic activity must be evaluated carefully. Studies where measurements of heat dissipation have been simply substituted for respiratory rate, when respiration would have easily and accurately provided the same information, are not insightful ways to employ calorimetry -- particularly when one considers the time-consuming nature of the technique. Similarly, if a study calls for broadly surveying the metabolic rate of numerous species, then respirometry may be more convenient, providing non-limiting oxygen supply is a feature of the experimental regime contemplated.

Heat conduction calorimeters [cf. 1] that provide sensitivity in the microwatt range are primarily the ones used in the investigations discussed below. This review is not intended to be exhaustive in its scope, but rather will highlight applications where microcalorimetry has been most useful in animal bioenergetics and physiology.

2. METABOLIC STATUS AND THE CR RATIO

Isothermal calorimetry has been applied to bioenergetic studies of both aquatic and terrestrial animals to assess changes in heat dissipation in response to various physical/chemical changes in their immediate environment. However, it is appropriate to emphasize at the outset that heat dissipation by itself does not does not provide an absolute measure of metabolic rate across all conditions, if one takes as a definition of metabolism the rate of ATP turnover. The heat dissipated per mole of ATP generated can differ depending on the biochemical pathway, or combination of pathways, in operation at any given time [2]. In order to relate heat dissipation rate to metabolism rate for a given tissue or organism, information about the operative metabolic pathways and the end products generated must be available. For example, when an organism undergoes a transition from aerobic production of ATP to complete reliance on glycolytically generated ATP as may happen under anoxia, a 50% drop in heat dissipation would not indicate a depressed metabolism, but rather that the rates of dissipative ATP turnover for the two conditions are very comparable. This phenomenon is due to the lower caloric equivalent of ATP turnover under anoxia (approximately -40kJ mol^{-1} ATP) compared to that seen for aerobic metabolism (approximately -80 kJ mol^{-1} ATP) [cf. 2,3]. Similarly, if heat dissipation rate were unchanged across an aerobic-anaerobic transition, then to

account for this observation in an organism exclusively utilizing carbohydrate fuels, glycolytic carbon flux would need to have increased over 8-fold under anoxia (-2879 kJ mol^{-1} of glycosyl unit catabolized aerobically, versus -331 kJ mol^{-1} glycosyl unit catabolized anaerobically to succinate) [2,3]. Still, when heat dissipation data is combined with biochemical and respirometry measurements, the results can provide real-time insights not attained with any other approach.

Another noteworthy point is that under cellular conditions where there is no net change in the levels of adenosine phosphates and phosphagens (i.e., ergobolic reactions are in steady-state), there is not a quantitatively significant contribution of ATP turnover to measured heat dissipation [2]. In this situation, the heat released during ATP hydrolysis is balanced by heat uptake during ATP synthesis. Thus, at constant ATP, the vast majority of measured heat flux derives from the oxidation of the carbon substrates, not ATP hydrolysis. Conversely, at times when *net* hydrolysis of ATP does occurs, a portion of the overall heat dissipation is attributable to the ATP hydrolysis reaction, but typically its contribution is small. For example, one of the largest and most rapid declines in ATP level occurs in brine shrimp embryos as they enter anoxia. ATP falls below 10% of control (aerobic) values in less than 1 h [4-6]. Yet this net ATP hydrolysis contributes only 6% of the total heat dissipated from the embryos during the initial 30-minute transition into anoxia [7]. This point may be obvious to some, but misinterpretations arising from the notion that cellular heat dissipation results from ATP hydrolysis are not uncommon.

One of the more useful applications of microcalorimetry is to evaluate the degree to which an animal depends on aerobic metabolism to supply its energetic needs. The experimentally determined ratio of kilojoules of heat dissipated per mole of oxygen consumed (i.e., the calorimetric-respirometric ratio, or CR ratio) should approximate within experimental error the theoretical oxycaloric equivalent when dissipative metabolism is fully aerobic. For an aquatic organism, the oxycaloric equivalents are -444 kJ mol O_2^{-1} for oxidation of lipid, -450 for protein catabolism to ammonia (-443 for protein to urea), and -477 for carbohydrate substrates [8]. Thus the oxycaloric equivalents differ approximately 9% depending on the identity of the substrate. In principle this difference could be utilized to experimentally evaluate the predominant fuel oxidized by an organism under normoxic conditions, but the experimental error inherent in determining the CR ratio makes this application impractical. The oxycaloric equivalent is also influenced by the buffering capacity of the intracellular milieu, and for aquatic species, the external environment if acid equivalents are excreted [2,8]. The enthalpies of neutralization (binding of protons) at 25°C for imidazole groups are -30 kJ mol^{-1} H^+ and for bicarbonate -9 kJ mol^{-1} H^+; a knowledge of the buffering characteristics of the animal system in question is necessary to fine-tune the appropriate value for the oxycaloric

equivalent. Considering the variety of metabolic substrates and cellular conditions, the theoretical oxycaloric equivalent can range from -430 to -480 kJ mol O_2^{-1} [8]. The experimental CR ratio for a fully aerobic animals would be expected to fall within the above range.

If the CR ratio is markedly higher (i.e. more negative) than -430 to -480 kJ mol O_2^{-1}, then an anaerobic contribution to energy production is indicated. The capacity of an organism to utilize a combination of aerobic and anaerobic metabolism is not uncommon even under normoxic conditions. Such a situation is common in isolated cells [cf. 8,9]. Mixed aerobic-fermentative metabolism can be a routine feature of an animal under normoxia, promoted by physiological hypoxia via an imbalance between oxygen delivery consumption, or caused by environmental hypoxia. Examples of CR ratios well above the oxycaloric equivalent in response to oxygen limitation include adult specimens of *Mytilus edulis* (-1250 kJ mol O_2^{-1}) [10] and prodissoconch larvae of the oyster *Crassostrea virginica*, where the CR ratios increase stepwise from a normoxic value of -450 to -694 kJ mol O_2^{-1} under severe hypoxia [11].

Conversely, if the CR ratio value is significantly below -430 kJ mol O_2^{-1}, as can occur during aerobic recovery from anoxia, then a number of factors can be responsible including reoxygenation of body fluids, the restoration of high-energy phosphate pools, and gluconeogenesis from organic acids like succinate [cf. 12-14]. The theoretical oxycaloric equivalent for gluconeogenic succinate clearance is estimated to be about -200 kJ mol O_2^{-1}, and the oxycaloric equivalent for the partial oxidation of succinate to malate or aspartate is projected to be quite low as well [13]. Similarly, when net biosynthesis of total protein is occurring in a cell, the CR ratio would not be expected to match the oxycaloric equivalent, because anabolic pathways are endothermic. Concepts of coupled and uncoupled metabolic half-cycle reactions in dissipative and conservative metabolism have been described [e.g., 2,15].

Representative CR ratios for multicellular organisms under normoxic conditions are provided in Table 1. The overall average for the 31 species in the list is -463 $\pm$ 39 (SD) kJ mol O_2^{-1}. In cases where more than one value was available for the same species (encompassing multiple developmental stages on occasion), they were averaged to obtain a single value prior to calculating the mean for all species. A second feature observable in Table 1 (part 'B') is the substantially lower CR ratios measured for organisms undergoing aerobic recovery after exposure to oxygen limitation. The CR ratios during the first hour of recovery can fall to the range of -180 to -280 kJ mol O_2^{-1}. As recovery progresses over the next several hours, CR ratios climb and eventually approach the average oxycaloric equivalent again (-450 kJ mol O_2^{-1}). This trend is observed for both adult and larval forms.

Table 1
Calorimetric-respirometric (CR) ratios in kJ mol O_2^{-1} for representative animals

Status and Organism	CR Ratio	Reference
A. NORMOXIC CONDITIONS		
Porifera		
Eunapius fragilis (freshwater sponge)		
diapause gemmules	-470	16
post-diapause gemmules	-495	16
Cnidaria		
Actinia equina (sea anemone)		
intertidally acclimated	-412	17
subtidally acclimated	-549	17
Anthopleura elegantissima (sea anemone)		
aerial exposure	-473	18
Annelida		
Hirudo medicinalis (medicinal leech)	-472	19
Lumbriculus variegatus		
(freshwater oligochaete)	-451	20
Lysilla alba (polychaete)	-489	21
Tubifex tubifex (freshwater oligochaete)	-482	22
Sipunculida		
Sipunculus nudus (peanut worm)	-423	23
Arthropoda		
Artemia franciscana (brine shrimp)		
embryos	-495, -484	7,14
Cherax quadricarinatus (Australian crayfish)	-440	24
Formica polytena (wood ant)		
pupae (at preferred temp.)	-420	25
adult workers (at preferred temp.)	-317	25
Tenebrio molitor (darkling beetle)		
pupae (avg., 8 age groups)	-489	26
Tribolium confusum (flour beetle)		
embryos	-342	27
first instar larvae	-516	27
Uca pugnax (fiddler crab)	-432	28
Mollusca		
Abra tenuis (infaunal bivalve)	-579	29

Table 1

Status and Organism	CR Ratio	Reference
Arion hortensis (slug)		
standard metabolism	-433	30
active metabolism	-483	30
Cardium edule (cockle)	-455	10
Crassostrea gigas (Japanese oyster)		
pediveliger larvae	-478	31
Crassostrea virginica (American oyster)		
prodissoconch larvae (avg., 2 size classes)	-464	11
pediveliger larvae	-469, -446	11,31
juveniles (spat)	-486	11
Geukensia demissa (= *Modiolus demissus*) (ribbed mussel)	-474	32
Mytilus edulis (bay mussel)		
prodissoconch larvae (avg., 4 size classes)	-601	33
adult	-470, -455	34,35
Oreohelix spp. (pulmonate snail)		
standard metabolism	-461	36
active metabolism	-487	36
estivating	-464	36
Tagelus plebeius (veneroid bivalve)	-450	21
Tellina alternata (veneroid bivalve)	-550	21
Chordata		
Carassius auratus (goldfish)	-442, -464, -464	37
	-443, -404, -418	38,39,40
Fundulus heteroclitus (mummichog)		
embryos	-458	41
Lacerta agilis (sand lizard)	-411	42
Podaris milensis (Milos wall lizard)	-422	42
Podarcis muralis (common wall lizard)	-426	42
Scophthalmus maximus (turbot)		
embryos	-472	43
larvae	-452	43
Salvelinus alpinus (arctic char)		
embryos	-451	44

Table 1

Status and Organism	CR Ratio	Reference
Average for 31 species:	-463 ± 39 (SD)	
B. AEROBIC RECOVERY FROM ANOXIA		
Porifera		
Eunapius fragilis (freshwater sponge)		
post-diapause gemmules		
(8 h anoxia/3 h recovery)	-363	16
Mollusca		
Crassostrea virginica (American oyster)		
pediveliger larvae		
(11 h anoxia/1 h recov.)	-180	11
(11 h anoxia/2 h recov.)	-377	11
(11 h anoxia/3 h recov.)	-500	11
(11 h anoxia/3-6 h recov.)	-583	11
(11 h anoxia/beyond 6 h recov.)	-486	11
Mytilus edulis (bay mussel)		
adults		
(6 h anoxia/0.5-1 h recov.)	-360	13
(72 h anoxia/0.5-1 h recov.)	-340	13
(120 h anoxia/0.5-1 h recov.)	-210	13
veliconch larvae		
(8 h anoxia/0.75 h recov.)	-219	33
(8 h anoxia/3 h recov.)	-457	33
Annelida		
Hirudo medicinalis (medicinal leech)		
(72 h severe hypoxia/0-6 h recov.)	-268	19
(72 h severe hypoxia/0-24 h recov.)	-396	19
Sipunculida		
Sipunculus nudus (peanut worm)		
(24 h anoxia/first few hours)	-335	23
Arthropoda		
Artemia franciscana (brine shrimp)		
embryos		
(144 h anoxia/0.75 h recov.)	-226	14
(144 h anoxia/1.17 h recov.)	-277	14

Table 1

Status and Organism	CR Ratio	Reference
(144 h anoxia/1.58 h recov.)	-310	14
(144 h anoxia/2.0 h recov.)	-346	14

3. HEAT FLUX AND OXYGEN LIMITATION

The potential usefulness of direct calorimetry in determining the aerobic-anaerobic balance for invertebrate facultative anaerobes in response to oxygen limitation has been appreciated for over 20 years [45,46]. Instrumental prototypes used in initial attempts to quantify heat flux in invertebrates, as well as some experimental results, began to appear in the late 1970s and early 1980s [17,28,32,47-52]. For example, the Pamatmat calorimeter was based on the principles and designs of Wadsö [53], where the semiconductor thermopiles were used in a twin calorimeter design in order to reduce baseline drift. The voltage output from the thermoelectric modules was directly proportional to the rate of heat dissipation from the animal. Suurkuusk, Wadsö and colleagues [54-56] continued to refine these designs ultimately leading to commercial instruments with more experimental flexibility, sensitivity and stability. The idea of coupling direct and indirect calorimetry in a twin-flow respirometry-calorimetry system was developed by Gnaiger [30,44,57].

3.1. Molluscs

Intertidal bivalves have been used extensively to study bioenergetic responses of organisms to oxygen limitation. Of particular note is the excellent series of papers on the bay mussel *Mytilus edulis* [10,12,35,58,59], which soundly established the utility of calorespirometry and provided an excellent experimental data base and theoretical concepts for future testing. Useful reviews of this work exist [3,13], so I will not reevaluate the work and its implications here, except to point out that the studies contributed to, among other issues, the ongoing debate over the existence of an anaerobic exothermic gap in invertebrates (see section 3.2)

More recently, the energy metabolism of the infaunal bivalve *Abra tenuis* was evaluated at various oxygen partial pressures to partition aerobic and anaerobic contributions [29]. As seen in Figure 1, total heat dissipation rate and oxygen uptake began to decline when p_{O2} was lowered below about 10 kPa. Under

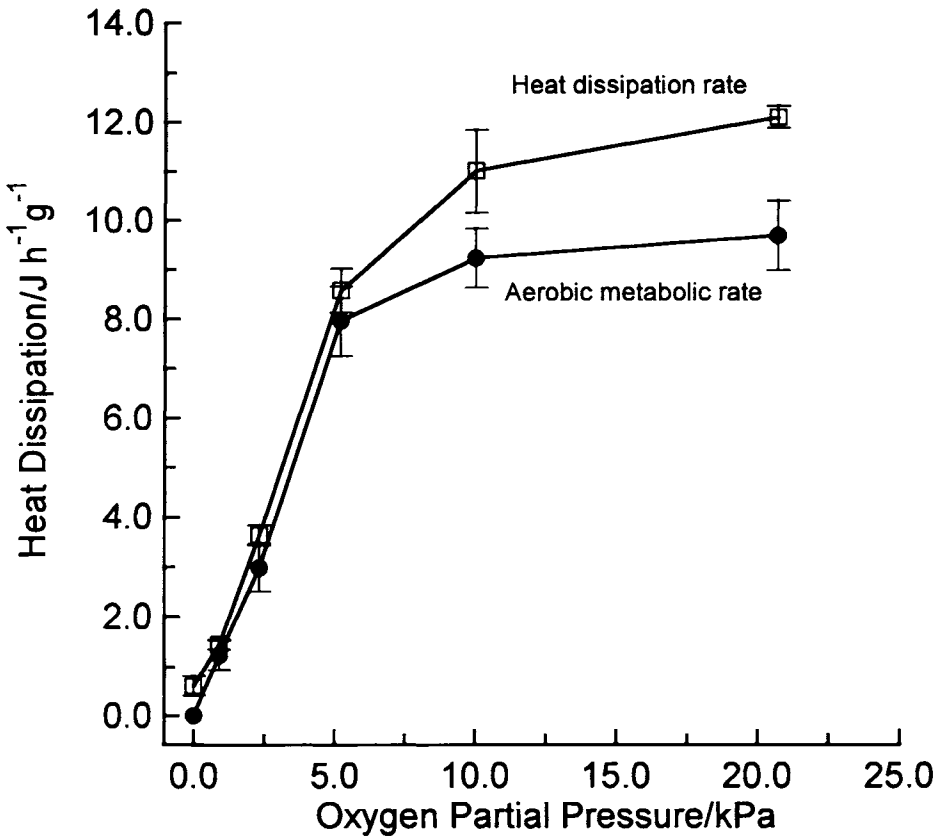

Figure 1. Rates of heat dissipation and oxygen consumption at various levels of p_{O2} for the bivalve *Abra tenuis* [redrawn from 29].

anoxia, the rate of heat dissipation reached 5-6% of the normoxic rate, which is similar to a number of other bivalves [3]. A marked departure from the typical depression of heat dissipation under anoxia was observed for the coot clam *Mulinia lateralis* [60], where heat dissipation hardly changed at all after 8 h of anoxia (97% of the normoxic controls). This bivalve is a deposit feeder and is known to maintain substantial feeding and locomotory activity under anoxia [60]. The unchanged rate of heat dissipation under anoxia relative to normoxia implied a substantial elevation of glycolytic flux in the absence of oxygen. A re-evaluation of anoxic heat dissipation in *M. lateralis* also demonstrated a rather high anoxic heat dissipation, but far lower than originally

reported (18-28% of aerobic controls) [61]. In *A. tenuis* a substantial anaerobic component (approximately 20%) to the total heat dissipation under normoxia was observed, which was apparently caused by intermittent shell closures and changes in ventilation patterns. Such sporadic variation in valve closure has been noted previously in a number of calorimetric studies [see references in 3; also 62,63]. Wang and Widdows [29] speculated that the particularly high frequency of valve closures in *A. tenuis* is associated with its infaunal burrowing mode of life.

A novel application of calorimetry to molluscan energetics was described in a report by Lui et al. [64], in which changes in the rate heat of dissipation under anoxia were used to evaluate the costs of osmotic regulatory events in the southern oyster drill *Thais haemastoma*. Anoxic heat flux increased by 55% after transfer from 10 ppt to 30 ppt salinity, which suggested that a significant amount of energy was necessary for the initial phase of acclimation to hyperosmotic conditions. In contrast, heat flux did not vary significantly under anoxia when snails were transferred from 30 ppt to 10 ppt. The latter result suggests either that the cost of intracellular isosmotic regulation was undetectably small or that the snails did not regulate during the first 24 h after transfer. As the authors pointed out, the undetectable change in heat flux after hypoosmotic challenge could not be ascribed to energy limitation under anoxia, because of the large anoxic scope observed between the hyperosmotic and hypoosmotic challenges.

3.2. Exothermic gap under anoxia

The possibility was initially raised by Gnaiger [50] that a substantial discrepancy existed between direct calorimetric measurement of anoxic heat dissipation and the indirect biochemical estimation of heat dissipation based on accumulated end products and associated biochemical events, i.e., the so called "exothermic gap." He compared heat dissipation data gathered under anoxia for *Lumbriculus variegatus* with previously published biochemical data on anaerobic end products for *Tubifex ssp.* [65] and concluded that less than 50% of the measured heat dissipation could be explained by the biochemical data. This conclusion was latter criticized by Hardewig et al. [23] because of the two species comparison that was used. Evidence from later studies with *Mytilus edulis* also supported the existence of an exothermic gap [59]. The exothermic gap was statistically insignificant over the first 12 h of anoxia, but during 48 h of anoxia the exothermic was 63% (i.e., 63% of total anoxic heat flux was unexplained biochemically). Famme and Knudsen [22] reported a close match between the measured and calculated heat values for *Tubifex tubifex* over an anoxic bout of approximately 20 h. However, in a re-evaluation of these data

by Gnaiger and Staudigl [20], the caloric equivalent for excreted acids used by Famme and Knudsen was criticized as being too high, and a recalculation suggested that 34% of the heat dissipated under anoxia was biochemically unexplained. More recently, Hardewig et al [23] reported good agreement between the calculated value of heat dissipation (23.4 mJ h^{-1} g^{-1} fresh mass) and the measured heat production (21.5±3.5 mJ h^{-1} g^{-1} fresh mass) for a 24 h period of anoxia in the peanut worm *Sipunculus nudus*. Thus, for this marine coelomate worm, there is not an exothermic gap over this duration of anoxic exposure. Finally, a similar comparison of the calculated and measured heat dissipation rates was made for the freshwater leech *Hirudo medicinalis* [19] over 0-8 h and 8-72 h periods of severe hypoxia. During the short-term anoxic period, the calculated heat dissipation fully accounted for the measured heat flux. However, over the 8-72 h period, 29% of the measured heat dissipation could not be explained; the difference between calculated and measured heat flux was statistically significantly across this period ($P = 0.03$).

At this juncture, based on the work with *M. edulis*, *S. nudus* and *H. medicinalis*, a statistically significant exothermic gap cannot be measured during early phases of anoxia (i.e., ≤24 h). However, with increased anoxic duration, an exothermic gap is measurable in *M. edulis* and *H. medicinalis* (extended periods of anoxia have not been evaluated in this context with *S. nudus*). For *T. tubifex* an exothermic gap is perhaps measurable within a 20 h period of anoxia, if the re-evaluation of Gnaiger and Staudigl [20] is followed. Clearly interspecific differences exist, and the experimental duration of anoxia used is an important determining factor. It appears that an exothermic gap is present in certain cases. The implication is that additional biochemical events that are not thermally-neutral must still be evaluated in order to obtain a complete enthalpy balance for all species.

3.3. Arthropods

Meade et al. [24] reported the responses of heat and oxygen flux to varying levels of environmental oxygen for the Australian crayfish *Cherax quadricarinatus*. When crayfish were exposed to p_{O2} values less than approximately 5 kPa, both heat dissipation and oxygen uptake were depressed. However, the depression of heat dissipation was only transient, and it recovered to normoxic values within 4 h, which suggested some form of metabolic compensation. CR ratios at or below the critical p_{O2} were not determined, so the quantitative contribution of anaerobic pathways to any compensation could not be estimated. These juvenile crayfish were incapable of surviving a 1-2 h anoxic treatment at 28°C.

Calorespirometry of the freshwater copepod *Cyclops abyssorum* [44]

demonstrated pronounced variation in spontaneous activity under normoxia; aerobic metabolism almost exclusively sustained this activity pattern as judged by comparisons of heat and oxygen flux. Anoxic perfusion for 19 h at 6°C caused a drop in heat dissipation to approximately 60% of normoxic rates. Adults apparently survived the treatment, but nauplius larvae did not.

Environmental hypoxia among terrestrial insects is not a common occurrence. However, it is clear that at some point during the evolution of this group, the capacity for substantial hypoxia tolerance was genetically favored in response to selective pressure. Insects withstand degrees of hypoxia that cannot be tolerated by any mammal [66]. At 2% oxygen, adult locusts maintain normal body posture [66], but enter an immobile quiescent condition with minutes after exposure to anoxia [66,67]. Anoxia can be tolerated for several hours at room temperature with no adverse effects [66,67]. Upon reoxygenation, the desert locust *Schistocerca gregaria* regains locomotion, and after 30 min or so, these large insects walk normally [67]. A large depression of overall energy metabolism accompanies these bouts of anoxia. Microcalorimetric studies showed that for *S. gregaria*, heat dissipation declined within about 1.5 h to 6-7% of normoxic values. This new steady-state rate of heat dissipation was constant for the remainder of the anoxic test period (4.5 h) [67]. Wegener [68] reported comparable data for the migratory locust *Locusta migratoria*. Within 2.5 h of anoxia, whole body levels of ATP in *S. gregaria* declined to 13% of control (aerobic) values. Similarly, in the cerebral ganglion of *L. migratoria*, ATP declined after 30 min of anoxia (25°C) to approximately 10% of aerobic levels [69-71] and in flight muscle to 1% of normoxic levels after 2 h [72]. Calculated ATP turnover for *S. gregaria* during anoxia dropped to about 4% of the normoxic values [67]. Levels of ATP rebounded rapidly during aerobic recovery.

3.4. Vertebrates

The diving turtle *Trachemys (=Pseudemys) scripta* shows a remarkable tolerance to prolonged periods of anoxic submergence. It can survive two weeks of anoxia at 18°C and 4-5 months at 3°C [73,74]. During 4 h of forced submergence in anoxic water at 24° C in a 1.2 l chamber, there was an 85% reduction in heat dissipation relative to control (air-breathing) turtles [75]. Oxygen stores in the lung and blood were not fully depleted by the end of the dive. Thus with longer submergence times, one might predict that heat flux would fall to even lower levels.

In addition to turtles, the goldfish (*Carassius auratus*) and the crucian carp (*Carassius carassius*) are among the few vertebrates with substantial anoxia tolerance. Carp can survive days of anoxia at room temperature, and if the

temperature is lowered to near 0°C, several months survivorship is possible [76]. Calorimetric studies of goldfish have yielded substantial insights into their metabolic status during normoxia and oxygen limitation [37-40,77,78]. Under normoxia goldfish were fully aerobic, as indicated by CR ratios (Table 1). During hypoxia (10% and 5% air saturation), heat dissipation was reduced to approximately 59% and 53% of the normoxic level, respectively [37]. The CR ratio was -620 kJ mol O_2^{-1} at 10% hypoxia and -1208 kJ mol O_2^{-1} at 5% hypoxia [37]. These data indicated a contribution of anaerobic metabolism to the overall metabolic rate in response to hypoxia. The anaerobic heat production during 5% hypoxia equaled that measured under anoxia, whereas anaerobic heat production during 10% hypoxia was only half the anoxic rate. Consequently, anaerobic metabolism was fully activated at 5% hypoxia in goldfish. This conclusion is consistent with data on ethanol formation, where the 5% hypoxic production rate of ethanol was equivalent to that under anoxia, but at 10% hypoxia, ethanol production was only 60% of that seen under anoxia [37]. Heat dissipation was reduced to 29% of the normoxic level during anoxia [37,77,79]. The predicted (biochemically calculated) heat dissipation was 40% less than the value directly measured during anoxia [37], but as pointed out by the authors, this discrepancy was likely explained by lactic acid production and creatine phosphate breakdown. Neither of these components was included in the analysis.

3.5. Isolated tissues and organelles

The high sensitivity of the mammalian brain to anoxia and ischemia [80] has led to interest in the turtle brain as a comparative model for anoxia tolerance. A low normoxic metabolic rate and the ability to depress metabolism further during anoxia are viewed as central to the extended tolerance of turtle brain to anoxia [for reviews, see 81,82]. To test the latter premise directly, cortical slices were prepared from the turtle *Chrysemys picta* and evaluated calorimetrically during transitions from normoxia to anoxia [83]. When compared to values for control slices (perfused with artificial cerebrospinal fluid saturated with 95% O_2:5% CO_2), heat flux was depressed 37% during perfusion with 95% nitrogen:5% CO_2 and 49% under pharmacological anoxia (1 mmol l^{-1} NaCN added) (Table 2). Both treatments produced rapid declines in heat dissipation, but a more rapid effect was seen with pharmacological anoxia due to the slow washout of oxygen from the flow-through system. Nitrogen perfusion followed by normoxia promoted a return to the predicted control levels in all trials (Figure 2).

Calculations of ATP utilization rate based on heat dissipation (Table 2) estimated the depressions in metabolism to be 30% (nitrogen) and 42% (pharmacological anoxia) compared to normoxic controls. Even larger

Table 2
Comparison of heat flux and ATP utilization in turtle cortical slices [after 83]

	Initial[a,b] (N=8)	Nitrogen[a] (N=4)	Chemical anoxia[a] (N=3)
Heat Dissipation/ mW g^{-1}			
Control[c]	2.26±0.08	1.79±0.03	1.87±0.04
120 min	---	1.14±0.05	0.95±0.05
Calculated ATP Utilization/μmol g^{-1} min^{-1}			
Control	1.72±0.06	1.36±0.03	1.42±0.03
120 min	---	0.97±0.04	0.82±0.04
Heat Depression/ % of control[c]			
120 min	---	36.5±2.6	49.3±1.7

[a]All values are means ± SEM
[b]Initial values represent the first accurately recorded heat values of the normoxic tissue.
[c]Control values are the predicted normoxic values at 120 min based on curve-fitting procedures.

metabolic depressions (>80%) have been estimated from lactate accumulation in vivo for whole brain [84,85]. This difference is likely due to the lack of spontaneous electrical activity in tissue slices. Current evidence suggests that one mechanism for metabolic depression in turtle brain is reduction of spontaneous electrical activity [82]. Brain slices consume approximately 50% less oxygen than the intact tissue [86], which may be ascribed to the loss of electrical activity in slices (for further discussions, see [83,87]). Thus, the metabolic depression seen in vitro with anoxic brain slices apparently involves other biochemical mechanisms. Possibilities include anoxic depression of both internal ion leakage [88] and protein synthesis [89].

Similar calorimetric results to those reported for turtle cortical slices have been obtained for telencephalic slices from crucian carp [87]. In response to anoxia, heat flux decreased by 37%, which corresponded to a 31% fall in ATP

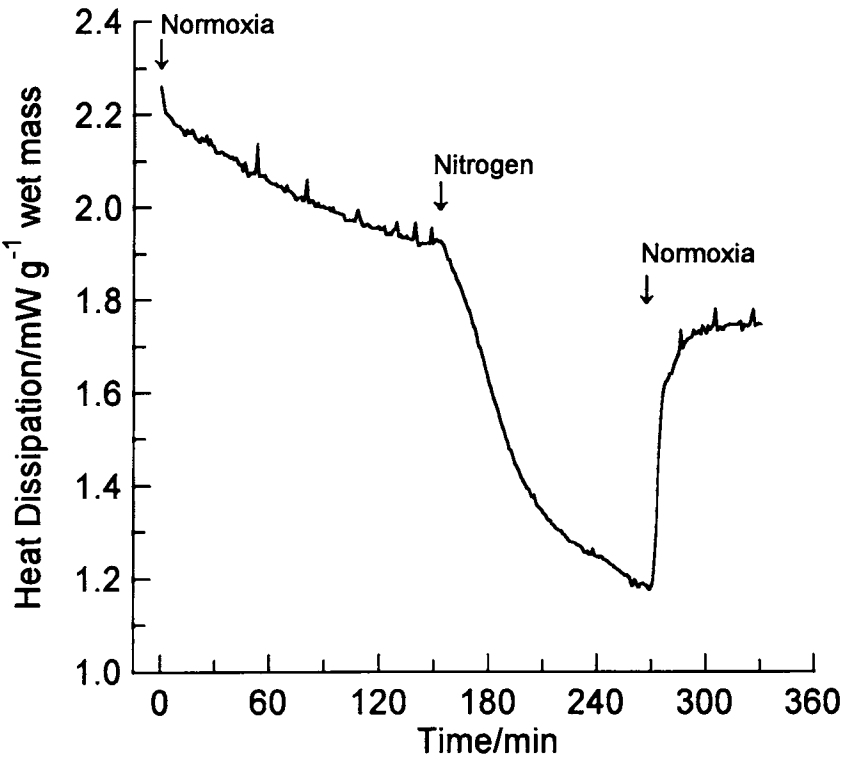

Figure 2. Heat flux from turtle cortical slices during normoxia and perfusion with nitrogen-saturated medium (25°C) [redrawn from 83].

utilization rate. Adenylate phosphates were well maintained, and substantial lactate (but not ethanol) was produced in the slices during the 20 h bout of anoxia. Based on the expected heat dissipation from the catabolism of glucose to lactate under anoxia (-70 kJ mol^{-1}) [2] and the total amount of lactate generated by the brain slices, the predicted heat dissipated across the anoxic period was 36.7 J, which compared favorably with the total heat dissipation measured directly (35.4 J).

Heat flux and oxygen flux were measured simultaneously in excised gills of the bay mussel *Mytilus edulis* as a function of p_{O2} [90,91]. The energy demand of the gill was modulated by the application of the neurohormone serotonin, which stimulates ciliary activity by promoting phosphorylation of axomenal proteins via a cAMP-dependent pathway [92]. Across the range oxygen partial pressures investigated (20.7 to 4.1 kPa), the measured heat flux was supported

almost exclusively by aerobic metabolism. CR ratios across this range were variable but not statistically different from the value measured under normoxia. Neither was there any statistical difference in CR ratio elicited by application of serotonin. The mean CR ratio for all treatments was -468 kJ mol O_2^{-1}. At each p_{O2} tested, the addition of 10 μM serotonin approximately doubled the heat flux and oxygen flux. One implication of the data is that the depression of heat and oxygen flux seen at low p_{O2} in control gills, possibly due to unstirred layers, was relieved with serotonin. The resultant increase in ciliary activity could have reduced the unstirred layers and enhanced oxygen flux to the mitochondria. The added oxygen flux apparently matched the increased energy demand, because anaerobic metabolism was not recruited judging from the CR ratios.

Oxygen levels at the mitochondrion in cells are often much lower than those selected for studying P:O ratios and phosphorylation efficiencies in isolated mitochondria. Yet, very few studies have attempted to analyze phosphorylation efficiencies under oxygen limitation in isolated mitochondria [93], in part due to the insensitivity of classical respirometric techniques. Evidence for downregulation of proton leakage through the mitochondrial membrane has been obtained from comparisons of P:O ratios under normoxia versus severe hypoxia in isolated mitochondria from rat liver and from embryos of the brine shrimp *Artemia franciscana* [94]. To measure phosphorylation efficiencies of isolated mitochondria at oxygen partial pressures several fold below the p_{50} of the mitochondrion, Gnaiger et al. [94] developed the approach of oxygen injection calorespirometry. With this method, oxygen consumption was initiated and a steady-state maintained by continuous injection of air-saturated solution into the previously anoxic incubation medium. Thus the mitochondrial oxygen consumption was experimentally dictated by the rate-limiting oxygen supply. The steady-state oxygen levels that resulted were well below the mitochondria p_{O2}. Simultaneously, heat flux was measured directly with microcalorimetry. The difference in heat flow between coupled and uncoupled (2,4-dinitrophenol) states provided a measure of ATP synthesis. The ATP synthesized was calculated by dividing this heat quantity by 44 kJ mol ATP^{-1}, i.e., the amount of heat conserved per mole ATP synthesized under the experimental conditions used. Dividing the ATP value by the total oxygen consumed yielded the P:O ratio.

Whereas phosphorylation efficiency dropped during ADP limitation under normoxia, P:O ratios were conservatively five-fold higher under severe hypoxia, when oxygen consumption was limited by oxygen supply. A reduction in proton leakage across the inner membrane under hypoxia could potentially explain the observation, which would decrease state 4 respiration. The proton permeability of the inner mitochondrial membrane is dependent on the physical properties of

the lipid bilayer and can be influenced by the degree of fatty acid saturation; a higher proportion of unsaturated fatty acids decreases the proton conductance of the membrane [95]. However, changes of membrane composition in response to anoxia have not yet been reported. Shigenaga et al. [96] showed that oxidative damage to mitochondria, which raises the levels of peroxidized lipids, increases the membrane permeability. Thus it is possible that reductions in free radical formation under severe hypoxia could translate into decreased membrane permeability. Reduction of the cellular membrane conductivity for inorganic ions is well recognized as an important adaptive mechanism [82,97] during hypoxia. A similar process involving reduced proton leakage through mitochondrial membranes might also occur during this hypometabolic state [94].

4. DEVELOPMENTAL PHYSIOLOGY

The expanding field of developmental physiology brings functional, molecular, and biophysical approaches to bear on mechanistic and integrative questions important for developmental stages of animals. Included here are topics like larval bioenergetics and intermediary metabolism, developmental arrest, chemical sensing, signals and transduction pathways controlling metamorphosis, and nutrient acquisition in developmental stages. Parallelling its utility for adult forms, calorimetry is also helping to solve physiological and energetic problems relevant to embryos and larvae.

4.1 Invertebrate larvae

Hypoxia and anoxia in estuarine and coastal habitats, stagnant bodies of freshwater, and organic-rich sediments in aquatic environments of all types can present bioenergetic challenges to invertebrate embryos and larvae. Information is only beginning to accumulate on the responses of developmental stages to oxygen limitation. Widdows and colleagues have investigated this issue for larvae of the American oyster *Crassostrea virginica* and the bay mussel *Mytilus edulis* [11,33,98]. Oyster larvae tolerate anoxia, and the tolerance increases with larval development [11]. A particularly important finding from this study was that the increased anoxia tolerance appeared to be related to an increased ability to lower the total heat dissipation rate, thereby conserving energy expenditures under anoxia. Figure 3 illustrates this tight correlation between metabolic depression and anoxic survival time. Early larval stages maintained heat dissipation under anoxia at 34% of normoxic rates, while later stages depressed heat dissipation to 3% of normoxic values. Latter stages displayed at least an order of magnitude longer anoxia tolerance than early ones. A very similar relationship has been observed for adult facultative anaerobes [89]. At

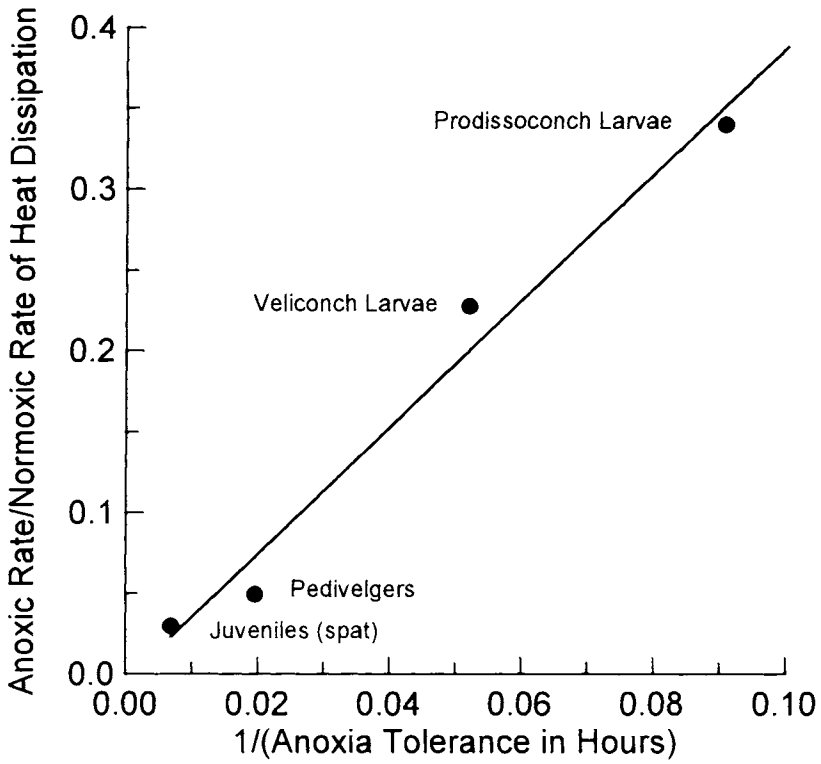

Figure 3. Relationship between the fractional depression of heat dissipation under anoxia and anoxia tolerance (expressed as 1/median mortality time in hours) for larvae and juveniles of *Crassostrea virginica* [redrawn from 11].

the lowest level of p_{O2} (0.67 kPa), the rate of heat dissipation by all larvae had a statistically significant anaerobic component. For juveniles, the increase in CR ratio was significant relative to the normoxic value at 0.67, 1.33 and 2 kPa. Either anaerobic capacity was greater in juveniles or the increased distances for oxygen diffusion limited oxygen delivery in these larger forms, or perhaps both. Finally, as seen in Table 1, CR ratios of oyster pediveligers during aerobic recovery from anoxia displayed a similar trend to that observed for adult bivalves. Values were low (-180 kJ mol O_2^{-1}) early in recovery, increased with time, and reached typical normoxic values after several hours [11]. As pointed out by the authors, more biochemical information is needed on larvae before the importance of these recovery profiles for CR ratios can be fully interpreted [11].

Parallel studies to those for *C. virginica* larvae have been completed for

Mytilus edulis larvae [33]. The trend was similar for *M. edulis* larvae regarding the increased anoxia tolerance in later developmental forms, as was the recovery profiles for CR ratios. However, there was a significant anaerobic component in the total energy expenditure of larvae under normoxic conditions (Table 1), which the authors suggested was due to periods of valve closure and quiescence under normoxia that diminished under moderate hypoxia. In addition to calorimetric data on *M. edulis* larvae, measurements are also available for gametes [98]. These data showed that mass-specific heat dissipation increased five-fold as development proceeded from the unfertilized egg to the D-stage (3-day) larva, but then declined thereafter.

The energetics of larval metamorphosis is another topic to which calorimetry has been applied [31]. Metamorphosis in marine invertebrates is a complex suite of behavioral, morphological, physiological and biochemical changes. Mortality is generally quite high during metamorphosis, but the precise reasons are often only inferred rather than empirically demonstrated. Intrinsic factors like genetic incompatibilities, energetic deficiencies, and internal developmental constraints to fitness are poorly understood [31]. Haws et al. [31] induced metamorphosis in pediveligers of *Crassostrea virginica* and *C. gigas* (the Japanese oyster) by administering 0.1 mmol l^{-1} epinephrine, which has the advantage of promoting high synchrony without noted side effects [99]. Induction of metamorphosis in pediveligers was greater than 95% for each calorimetric run, and mortality was less than 4% during the experimental time course. Epinephrine exposure caused an immediate drop in both heat flux (Figure 4) and oxygen flux by approximately 30-40%. The decline was likely a result of cessation in swimming activity. There was a close agreement between alterations in oxygen flux and heat dissipation. Larvae reached a metabolic minimum 50 min after epinephrine infusion and remained quiescent for an additional hour. There was a sharp rise in metabolism which reached a plateau about 5 h after addition of epinephrine. Mean premetamorphic CR ratios indicated a fully aerobic metabolism for pediveligers of both species (*C. virginica*, -446 kJ mol O_2^{-1}; *C. gigas* -478 kJ mol O_2^{-1}). Only minor changes were noted after metamorphic induction, where the CR ratios were -490 kJ mol O_2^{-1} and -423 kJ mol O_2^{-1} for *C. virginica* and *C. gigas*, respectively. The measured values of heat dissipation for *C. virginica* pediveligers are in agreement with Widdows et al. [11], but calorimetric data for post metamorphosis induction are unavailable for comparison. Data on carbohydrate, lipid and protein stores indicated that all the measured usages would have to result from aerobic catabolism in order to begin to explain the observed heat dissipated over the same time period [31]. Carbohydrate reserves and utilization were positively correlated with metamorphic survival.

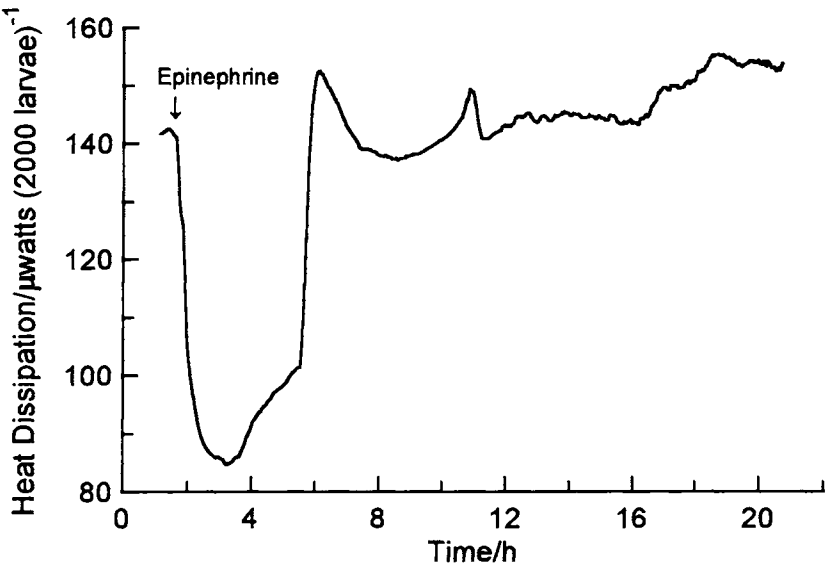

Figure 4. Heat flux for pediveliger larvae of *Crassostrea gigas* during induction of metamorphosis with epinephrine [redrawn from 31].

4.2 Vertebrate embryos and larvae

Developmental stages of several fish species have been evaluated with calorespirometry. The CR ratios for developing turbot (*Scophthalmus maximus)* embryos and larvae [43] fell within the theoretical scope for oxycaloric equivalents that reflected a fully aerobic metabolism (Table 1). The total measured heat dissipation over the first 19 h post-fertilization matched the expected heat dissipated calculated from aerobic glycogen consumption across the same period (measured, -1.80 to -1.91 mJ; biochemically predicted, -1.90 mJ). Lactate was low and constant across this period of development. The energetic role played by carbohydrates diminished after commencement of epiboly. Similar CR ratios to those of the turbot (Table 1) have been reported for embryos of the arctic char [44].

The mummichog *Fundulus heteroclitus* has been used extensively for studies of genetic variation within and among populations. Specifically, much attention has been given to variation in allelic frequencies for the *Ldh-B* locus among populations of this marine teleost distributed across a temperature cline along the Atlantic coast of North America [e.g., 100,101]. The allelic enzymes encoded

by the locus differ in kinetic properties and have been functionally correlated with differences physiological performance and development [reviewed in 41]. Fish homozygous for the *Ldh-B*^{a} allele develop faster than those homozygous for *Ldh-B*^{b} [102,103]. Differences in metabolic rates between the two homozygous genotypes were investigated using calorespirometry [41]. Heat flux increased dramatically over the first 24 h post-fertilization in *Ldh-B*^{a} homozygotes, particularly between hours 10 and 15, but *Ldh-B*^{b} homozygotes did not. Lactate levels in the oocyte were high (40-48 mmol l^{-1}), and approximately 100-fold more lactate was utilized during the first 24 h of development than was glucose. The CR ratio was similar for both genotypes, with the average value being -458 kJ mol O_2^{-1} (Table 1). Thermochemical calculations indicated that the predicted heat dissipation based on measured disappearance of lactate was 2-fold to 30-fold higher than the actual measured heat flux across a series of time intervals (Table 3). Thus, a significant portion of the lactate utilized during development

Table 3
Predicted heat dissipation by *Fundulus heteroclitus* embryos during early development versus the measured heat flux[1] [after 41]

Genotype and Developmental Time/h	Predicted Heat Dissipation[2]/μW			Observed Heat Dissipation/μW
	Lactate	Glucose	Combined	
Ldh-B^a*B*^{a}				
5	4.25	0.075	4.32	0.14
10	1.87	0.32	2.19	0.29
15	0.79	0.82	1.61	0.77
Ldh-B^b*B*^{b}				
5	2.68	0.032	2.71	0.14
10	1.08	0.098	1.18	0.31
15	0.44	0.35	0.79	0.46

[1]All values expressed per embryo.
[2]Utilization rates were based on biochemical measurements and radiolabeling studies, and values then converted to heat dissipation assuming complete aerobic catabolism to CO_2 and H_2O.

was not catabolized to CO_2 and H_2O, but rather was apparently used for other processes that were less exothermic. The close associations among *Ldh-B* genotype, lactate utilization and metabolic rate suggested that genotype has a significant effect on developmental rate in *Fundulus*.

5. QUIESCENCE AND DIAPAUSE

Consistent with the terminology of Keilin [104] and Mansingh [105], quiescence and diapause represent two major categories of animal dormancy that are observed in many phylogenetically diverse organisms. As will be illustrated below, these states are characterized by deep metabolic depression, and in some situations, energy flow is essentially undetectable by conventional measures. A transient depression of energy flow is not sufficient to define a state of dormancy. The potential must exist for an extended duration of the hypometabolic state -- i.e., on the order of weeks, months or years [106]. Normally, arrest of developmental processes accompanies this protracted metabolic depression when embryonic or immature stages are involved. Quiescence is a metabolic and/or developmental arrest imposed by an unfavorable environmental condition like desiccation, anoxia, or temperature extremes [106]. It is controlled simply by application or removal of the relevant physical insult. Diapause is also a state of metabolic and/or developmental arrest, but two distinctive differences exist relative to quiescence. Firstly, diapause (obligate, endogenous, constitutive dormancy) is controlled by some type of endogenous physiological factor, so that the diapausing organism remains dormant even under optimal environmental conditions that would otherwise promote normal metabolism and development. Release from diapause (activation, diapause breakage) requires exposure to a specific stimulus or cue, or combination of cues. Secondly, diapause generally *precedes* any environmental insult (e.g., onset of the winter season, dry season, etc.). Both diapause and quiescence serve as arrested states in the life cycles of animals (particularly invertebrates) and provide an important means to survive deleterious environmental conditions. Additional advantages of latent stages include recolonization of an environment, transport and dissemination of the species, synchronization of favorable environmental conditions with the active stage of the organism, and avoidance of predators [106].

5.1. Anaerobic quiescence in brine shrimp embryos

Embryos of the brine shrimp *Artemia franciscana* are perhaps the quintessential example of an animal capable of acute metabolic arrest during

anoxia [107]. Anoxia is common in the hypersaline and often high-temperature lakes into which these embryos are released, and the condition is often prevalent within the thick windrows of cysts (and decaying algal mats) that accumulate along shorelines [108]. The embryos enter a state termed anaerobic quiescence, and in this condition can withstand anoxia at room temperature for four years with remarkable survivorship [109]. The largest pH_i transition ever measured for living cells occurs within minutes after exposure to anoxia. pH_i drops by at least one full unit to 6.7 within 20 min [110,111], and to as low as 6.3 after several hours [110]. The pH_i recovers to aerobic control values within minutes of reoxygenation, and this pattern is superimposable on the metabolic recovery after short term anoxia [7,112].

A qualitatively and quantitatively similar state of metabolic arrest can be promoted artificially by exposing the embryos to elevated levels of CO_2 in the presence of oxygen (aerobic acidosis) [113]. The pH_i of embryos under the artificial condition of aerobic acidosis is 6.8 [113], and the biochemical features describing the shutdown of carbohydrate metabolism are virtually identical to anoxia [5]. Protein synthesis and degradation are arrested under both anaerobic quiescence and aerobic acidosis [for review, see 89], and mRNA levels are stabilized [114,115]. ATP levels plummet during anoxia [4,5], but under aerobic acidosis ATP does not change from control values for several hours [5,116]. Thus the observed metabolic depression is not a result of low ATP levels. These latter observations provide compelling support for pH_i as a key cellular signal in the metabolic switching. Selecting an organism that has evolved such remarkable capacities for long-term dormancy might enhance the chances of clarifying mechanisms essential to tolerance of dormancy in other animals.

Heat flow is depressed to extremely low levels [7,14,117] as embryos enter anaerobic quiescence. The overall pattern for heat flux during an anoxic bout is shown in Figure 5 [7]. Addition of ammonium chloride during the anoxic bout served to elevate pH_i by approximately one pH unit [113] and stimulated heat dissipation (Figure 5), presumably by relieving the pH-induced blockage of the glycolytic pathway seen under acidotic conditions in these embryos [5]. As shown in Figure 6, calorimetric studies with sealed ampoules revealed heat dissipation dropped to 0.2% of aerobic values after 50 h of anoxia and was still declining when experiments were terminated [118]. While the profile of heat dissipation was similar, the absolute level of depression was lower with sealed ampoules than with the open-flow system (0.49%) where embryos were perfused with nitrogen-saturated medium [14]. Thus, it is possible that trace quantities of oxygen (below the detection level of the polarographic oxygen sensors) were presence in the flow-through studies. At these low heat flux values, processes like protein degradation can make a quantitatively significant (16%) contribution

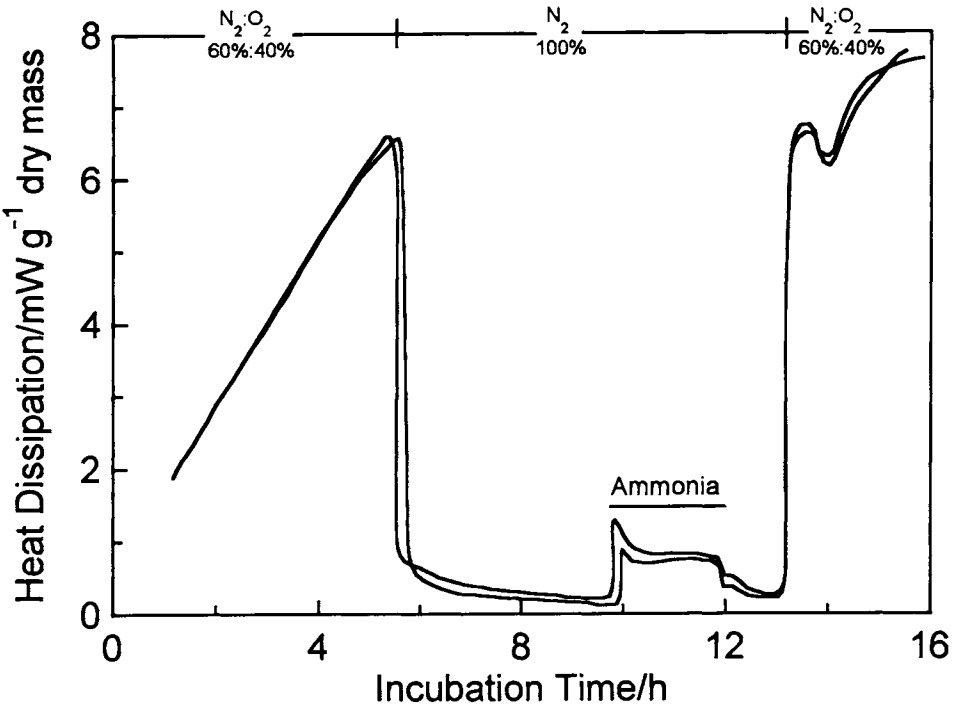

Figure 5. Superimposed traces of two independent experiments showing heat dissipation of *Artemia franciscana* embryos during nornoxia and during perfusion with nitrogen-saturated medium. Ammonia was introduced under severe hypoxia, which served to alkalinize intracellular pH and stimulate heat flux [redrawn from 7].

to the heat flow [118]. These are the lowest heat dissipation values thus far reported for organisms under anoxia (cf. [2,3]). Values approached undetectable levels, and at some point the embryos likely reach an ametabolic state under anoxia. CR ratios under aerobic conditions were consistent with a fully aerobic metabolism (Table 1). Exposure to aerobic acidosis, which dramatically depressed heat flow, did not appreciably alter the CR ratio (-481 kJ mol O_2^{-1}) [7]. Thus, nonoxidative metabolism was not stimulated to compensate for the depression of aerobic metabolism under aerobic acidosis [7]. CR ratios during aerobic recovery from anoxia (Table 1) were similar to those discussed previously for other invertebrates.

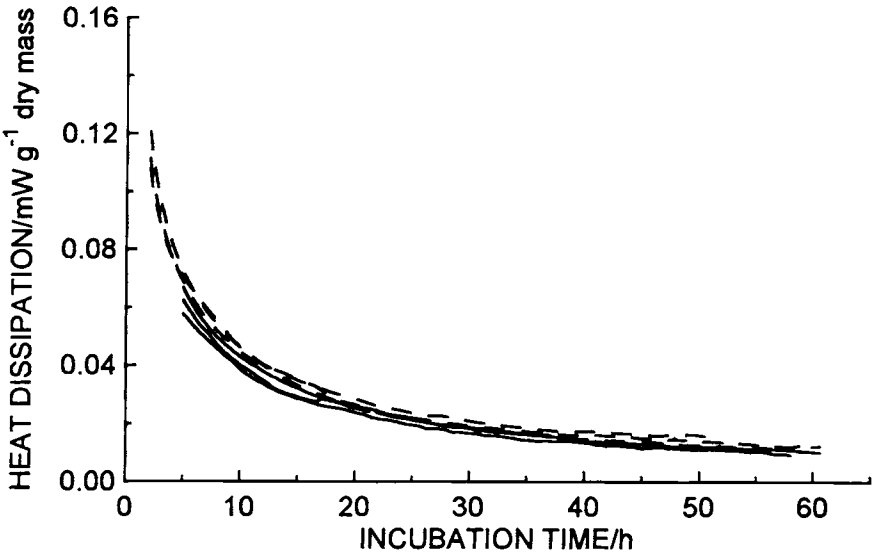

Figure 6. Heat dissipation under anoxia in sealed ampoules for *Artemia franciscana* embryos. Data are from experiments using 5 cm^3 (dashed lines) and 25 cm^3 (solid lines) ampoules [redrawn from 118]. Measurable heat flux is still present after 50-60 h.

5.2. Anhydrobiosis in brine shrimp embryos

A second quiescent state in *A. franciscana* embryos that has been studied calorimetrically is anhydrobiosis, or life without water. These embryos are one of the most intensely studied anhydrobiotic systems (for reviews, see [119,120]), in part because their hydration state can be precisely controlled. Embryos enter a profound, yet reversible, state of metabolic arrest in response to cellular dehydration. While the metabolic transitions appear to be a function of water content, the controlling mechanisms involved are not fully understood.

Glasheen and Hand [121] used open-flow microcalorimetry to monitor changes in energy flow of *A. franciscana* embryos (Great Salt Lake, Utah) undergoing cycles of dehydration-rehydration in NaCl solutions. Because these encysted embryos are completely impermeable to inorganic salts, hydration state can be altered accurately by immersing embryos in solutions of varying ionic strength. Calorimetry avoids the technical difficulties that arise when oxygen consumption is chosen as a means to estimate aerobic metabolism in solutions of high salt concentration. Electrolyte solutions within polarographic electrodes

dehydrate under such conditions [122].

Heat dissipation from developing embryos rose steadily during the first 4 h in control 0.25 M NaCl (Figure 7). When the perfusion medium was switched

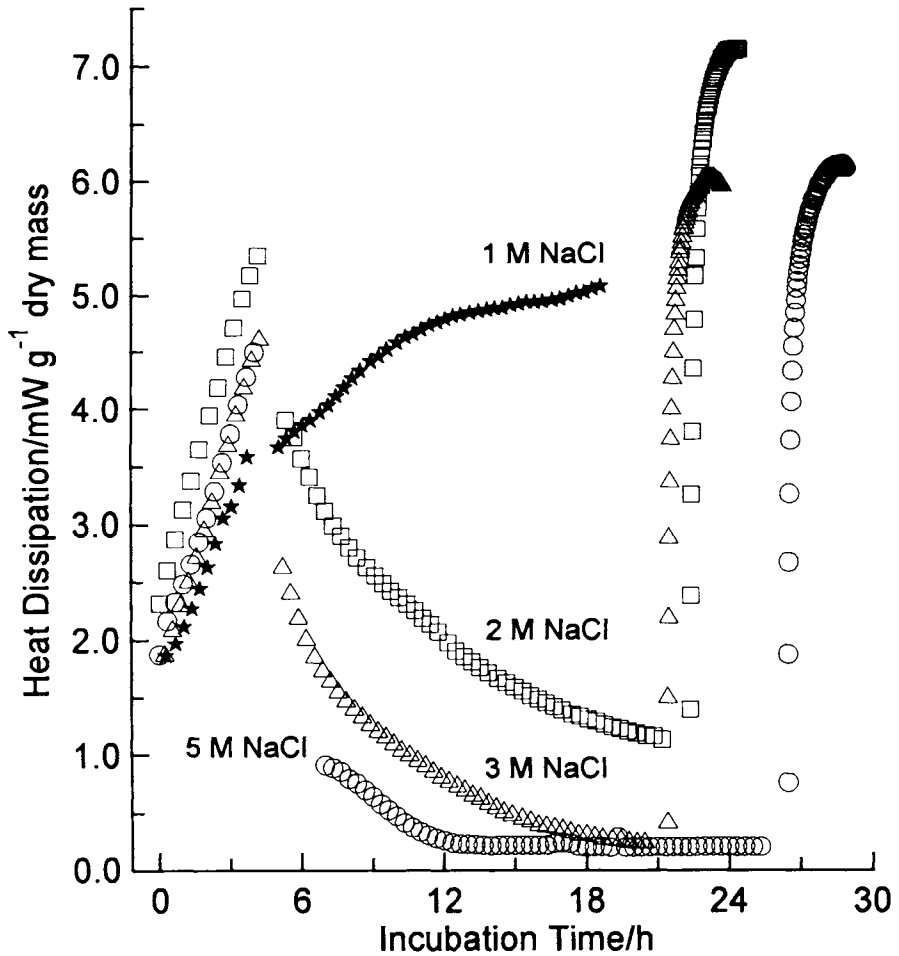

Figure 7. Heat flux of *Artemia franciscana* embryos during normoxic incubations in various concentrations of NaCl solutions, which served to progressively dehydrate the embryos. For each run, the embryos were initially incubated for 4 h in 0.25 mol l^{-1} NaCl and then switched to the indicated experimental solution. At approximately hours 20-25, embryos were returned to control conditions (0.25 mol l^{-1} NaCl) and the recovery period monitored [redrawn from 121].

to 1.0 M NaCl, energy flow continued to rise, reaching 137% of control (hour 4) values. However, when control medium was switched to 2.0 M NaCl, energy flow fell exponentially to 21% of control values after approximately 18 h. In experiments with 3 M NaCl, heat dissipation fell sharply to 6%. At higher ionic concentrations, heat dissipation declined to as low as 3%, or to an absolute rate of 0.14 mW g^{-1} dry mass (Figure 7). Thus metabolism in developing embryos was disrupted at a critical hydration level promoted by an external NaCl concentration between 2.0 and 3.0 M. When embryos were returned to control perfusion after dehydration, recovery of energy flow was rapid, showing the reversibility of the metabolic arrest (Figure 7)

These metabolic transitions were correlated with embryo hydration levels measured across the same dehydration series [121]. Fully hydrated embryos had a water content of 112 $\pm$ 2.6 g H_2O per 100 g dry mass in 0.25 M NaCl. At the first point where heat dissipation was markedly depressed (the 2.0 M incubation), cyst water content was 72.8 $\pm$ 0.9 g H_2O/ 100 g dry mass. This water content is similar to the hydration level required to depress carbohydrate catabolism and respiration of *A. franciscana* embryos from San Francisco Bay [123,124]. Embryos rely exclusively on trehalose catabolism for energy at this stage of development. Analysis of glycolytic intermediates suggested that the dehydration-induced inhibition was localized at the trehalase, hexokinase and phosphofructokinase reactions [125]. One possibility is that the metabolic shutdown observed during progressive dehydration is explained by perturbation of vicinal or macromolecular-associated water after bulk water has been removed [120]. Alternatively, metabolic arrest may involve disruption of macromolecular assemblies (e.g., enzyme-cytostructural interaction) owing to the elevated ionic strengths of intracellular contents in dehydrated embryos (cf.[121].

5.3. Estivation in land snails

Many terrestrial pulmonate snails respond to desiccating conditions by entering estivation, a behavior that minimizes evaporative water loss [126]. The quiescent state may last up to several years. Studies of the metabolism of estivating snails have generally employed respiration, which of course assumes completely aerobic metabolism. Yet ventilation is discontinuous during entry into estivation, and prolonged periods of apnea can result in pulmonary oxygen tissues as low as 0.35 kPa [127]. It is possible at such low oxygen tensions that anaerobic metabolism might be recruited to supplement aerobic energy production, and as a result, respiration would underestimate metabolic rate.

Rees and Hand [36] utilized simultaneous respirometry and calorimetry to measure energy flow in snails before and during a short period of estivation. Within four days following entry into estivation, heat dissipation and oxygen

consumption by *Oreohelix spp.* decreased by 83% compared to standard non-estivating rates (Table 4). CR ratios indicated that over the first two days of estivation, anaerobic pathways were not recruited to supplement declining metabolic rates (Table 1), although it is clearly possible that anaerobiosis occurred later as dormancy progressed. This observation is in accord with the observation that end products of anaerobic metabolism did not accumulate in the

Table 4
Heat dissipation, respiration, and respiratory exhange ratios (R) for non-estivating and estivating *Oreohelix spp.* [after 36]

	Heat Dissipation/ J g^{-1} dry mass h^{-1}	Respiration/ μmol O_2 g^{-1} dry mass h^{-1}	R/ mol CO_2 mol^{-1} O_2
Standard (N=5)[a]	16.5±1.3[c]	35.8±3.0	0.99±0.02
Active (N=5)[a]	34.3±1.3	70.4±2.5	0.93±0.01
Estivating (N=5)[b]	2.9±0.3	6.2±0.5	0.95±0.03

[a]Values for standard and active states are from control periods (perfusion with 100% relative humidity air) characterized by the lowest and highest heat dissipation rates, respectively.
[b]Values determined approximately two days after induction of estivation.
[c]All values are means±SEM.

land snail *Otala lactea* over three days of estivation, but lactate was measurable in this snail after three weeks of estivation [128]. Activity bouts under non-estivating conditions were supported aerobically, again as judged by the fact that CR ratios fell within a range consistent with oxidative metabolism (Table 1). Respiratory exchange ratios (Table 4) suggested a primary dependence upon carbohydrate metabolism both in non-estivating and estivating snails. Biochemical measurements of the utilization of stored fuels during estivation in *Oreohelix* confirmed the primary usage of carbohydrate over the first month of estivation [129]. Protein catabolism commenced latter in estivation and resulted in the accumulation of large quantities of urea (≥200 mmol l^{-1}) in the snails' tissues after several months [129].

A correlate of the reduced respiration rates is a decrease in evaporative water loss [127]. There is a close relationship between the extent reduction in respiration for a given snail species and its capacity to tolerate desiccating environments [36]. Remarkably, after seven months of estivation, the percent tissue water in *Oreohelix* had not change significantly, although total water declined in parallel with body dry mass [129].

5.4. Diapause in sponge gemmules

All of the examples of dormancy discussed thus far have fallen into the category of quiescence. A particularly good example of diapause is exhibited by gemmules of the freshwater sponge *Eunapius fragilis*. Gemmules are asexually produced reproductive bodies composed of undifferentiated cells surrounded by a collagenous capsule. Such structures serve as the overwintering stage in the life cycle of sponges. Newly formed gemmules are in an obligate state of developmental arrest (diapause). If diapausing gemmules are held in water at room temperature they will not develop. However, vernalization in the cold for 2-3 months releases gemmules from diapause and allows them to resume development when warmed to 20-23°C. *E. fragilis* is well suited for the study of entry and exit from diapause, because unlike the case with many sponge species, diapause and quiescence are not intertwined [130]. Some species of sponges do not enter diapause at all and exhibit only quiescence (e.g., *Ephydatia fluviatilis*) [131].

Recently, Loomis et al. [16] characterized metabolic changes during germination of *E. fragilis* gemmules and compared the results with diapausing gemmules. Upon warming post-diapause gemmules to 21°C, heat dissipation (Figure 8) and oxygen consumption increased 600% during the ensuing 48-72 h, during which time gemination culminated in the emergence of a new sponge from the gemmule capsule. Energy flow was two-fold lower in diapausing gemmules that had not experienced cold vernalization, and heat dissipation was unchanged over the same period of incubation (Figure 8). The diapausing gemmules did not develop or germinate during this incubation at 21°C.

The CR ratio of post-diapause gemmules increased significantly from -354 kJ mol O_2^{-1} during the first hours of germination to -541 kJ mol O_2^{-1} after 57 h (Figure 9) [16]. The average across the entire germination period was approximately -495 kJ mol O_2^{-1}. The CR ratio at hour 12.5 was statistically different from the oxycaloric equivalent for aerobic carbohydrate metabolism (-477 kJ mol O_2^{-1}), which was chosen as a basis of comparison because sorbitol is the primary energy source during germination [132]. The lower CR ratio near the beginning of the incubation might be attributable to the fact that these gemmules were stored at 4°C without aeration for months prior to the start of

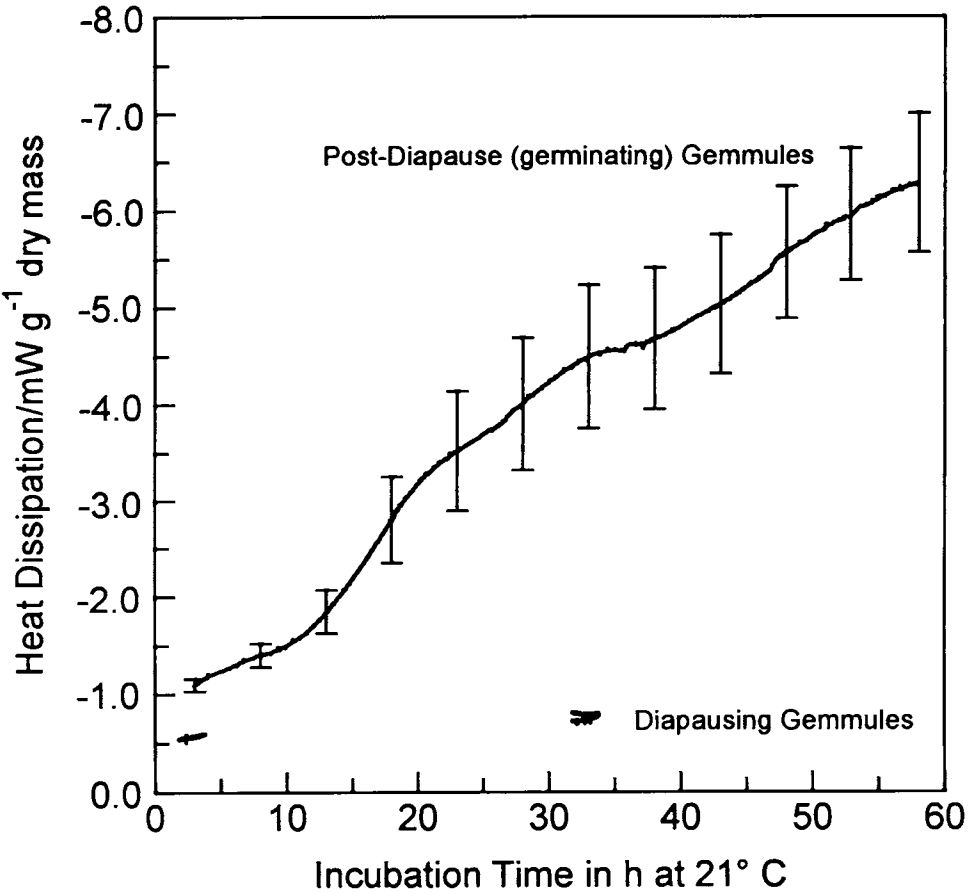

Figure 8. Heat flux of germinating and diapausing gemmules of *Eunapius fragilis* under normoxia. Data for germinating gemmules are expressed as means of three independent experiments. Error bars represent ± one SEM at the indicated time points. Values for diapausing embryos are presented for two independent experiments [redrawn from 16].

the incubation. Thus they may have experienced hypoxia and at the beginning of the experiment were undergoing aerobic recovery. This speculation was supported by the low CR ratio (-363 kJ mol O_2^{-1}) measured 2.5-3.5 h after the anoxic bout shown in Figure 10. For comparison, immediately prior to the onset of anoxia the CR ratio was -438 kJ mol O_2^{-1}. After 3.5-6.5 h of aerobic recovery, the value had risen to -457 kJ mol O_2^{-1} and to -527 kJ mol O_2^{-1} after

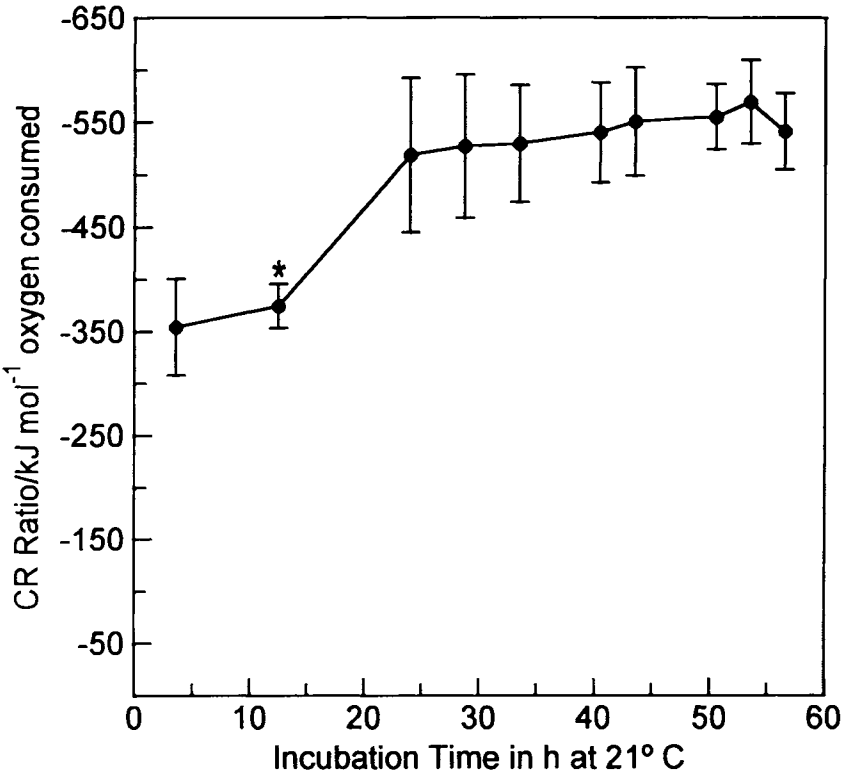

Figure 9. CR ratios measured for post-diapause (germinating) gemmules of *Eunapius fragilis*. Values are means for 3-h intervals (except for a 1.25-h interval at the first time point). Error bars represent ± one SEM (N=3), except at hours 50.5 and 56.5 where N=4. The asterisk denotes a significant difference from the theoretical oxycaloric equivalent for carbohydrate (-477 kJ mol O_2^{-1}) [redrawn from 16].

10.5-13.5 h of recovery. The CR ratio for diapausing gemmules was approximately -490 kJ mol O_2^{-1} at the end of the experiment in Figure 8.

Post-diapause gemmules tolerated severe hypoxia for at least 7.5 h (Figure 10), during which time heat dissipation was reduced to 6% of the aerobic value. Upon return to aerobic conditions, the heat dissipation climbed rapidly, and gemmules resumed development and emerged. Anoxia tolerance in gemmules may well be quite advantageous, because the natural habitat of these gemmules during winter can include burial in pond sediments of low oxygen tension.

Virtually nothing is known about metabolic processes in anoxic gemmules.

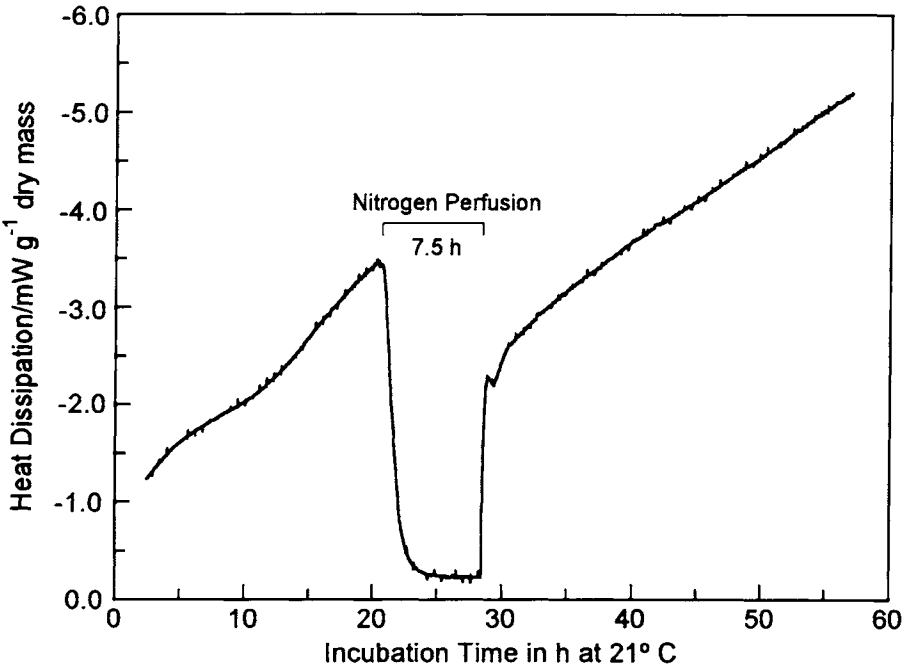

Figure 10. Interruption of heat dissipation from post-diapause gemmules of *Eunapius fragilis* resulting from perfusion with nitrogen-saturated water [redrawn from 16].

6. NITRATE RESPIRATION IN A CLAM-BACTERIUM SYMBIOSIS

The last example of a physiological application of calorimetry represents a distinct departure from the preceding studies and is novel from two perspectives. First, the biological issue involves a marine bivalve, *Lucinoma aequizonata*, which forms a symbiotic association with chemautotrophic bacteria [133,134]. The invertebrate host has undergone morphological and physiological modifications to intracellularly house the bacteria in its greatly enlarged gills. The bacteria provide nutrition to the host by translocation of carbon compounds and through intracellular digestion of the bacteria by the gill cells [135,136]. The symbionts fix CO_2 and use a reduced sulfur compound as an electron donor for respiration. The electron acceptor is commonly oxygen, but sometimes

nitrate. Respiratory reduction of nitrate to nitrite (i.e., nitrate respiration) is common in bacteria but has never been found in higher animals [137]. The symbionts of *L. aequizonata* are exceptional in that nitrate respiration has completely replaced oxygen respiration, and as a result, the process is constitutive and not inhibited by oxygen [138]. Thus, while nitrate respiration has been identified in this symbiosis, its quantitative significance had not been determined until recently [139]. Second, the application of calorimetry to this symbiosis offered methodological advantages for the purpose of quantifying the contribution of nitrate respiration to the overall metabolism of the host's gill tissue. Further, it allowed specific questions to be addressed: does nitrate respiration in the symbionts of *L. aequizonata* result in measurable heat production, and if so, how does it compare with heat flux of the animal tissue. Heat flux is a metabolic indicator capable of detecting changes in the presence of the alternative electron acceptor (nitrate) under both aerobic and anoxic conditions, something that is not possible with respiration rate.

Hentschel et al. [139] measured heat production and nitrate respiration rates simultaneously in the gill tissue of *L. aequizonata* to answer the above questions. After an aerobic trace had been established, perfusion conditions were switched to anoxia. Upon the addition of nitrate to the anoxic perfusion medium of the open-flow calorimeter, an immediate increase in heat dissipation was seen (Figure 11). A second point to be observed from Figure 11 was that the nitrate-stimulated heat production was proportional to the concentration of nitrate added (30 μmol l^{-1} to 1 mmol l^{-1}). Nitrite appearance in the effluent seawater followed the same pattern as the heat dissipation (data not shown). Half-maximal stimulation of heat production by nitrate was achieved at 0.81 mmol l^{-1} nitrate. The mean experimental ratio of heat produced per mole nitrite was -130$\pm$22.6 kJ mol^{-1} nitrite (N=13, $\pm$SEM). Gill tissue from *Mytilus edulis*, which does not contain symbionts, was used as a negative control. A change in heat flux was not observed upon exposure to 1 mmol l^{-1} nitrate. Similarly, a calorimetric run without gill tissue showed that nitrate or nitrite had no effect on the baseline.

From the data of Figure 12, it is clear that the addition of nitrate had comparable effects on heat dissipation under aerobic conditions as well. This result is consistent with the properties of nitrate respiration previously described and its constitutive nature in these symbionts [138]. At nitrate concentrations between 0.5 and 5 mmol l^{-1}, the total heat production was increased 2-fold relative to the unstimulated anoxic baseline. Thus, nitrate respiration makes a distinctly measurable contribution to the energy flow of the gill. The symbiosis of *L. aequizonata* was particularly useful for establishing this point, because of the ability to distinguish between animal tissue metabolism and symbiont

metabolism: symbionts respire on nitrate, but not oxygen, and the animal uses oxygen, but never nitrate. The preferred use of nitrate by the symbionts is thought to provide a selective advantage to the clam in its natural environment, because the animal does not have to compete with its symbionts for oxygen. The clam is exposed to permanently hypoxic conditions in the mud in which it lives [140].

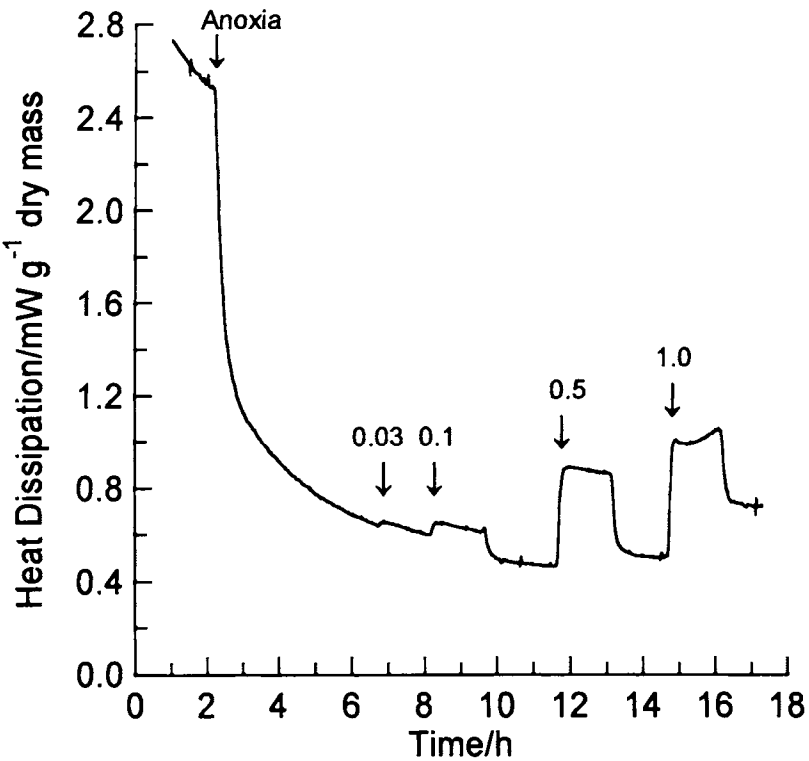

Figure 11. Heat flux of *Lucinoma aequizonata* gill tissue containing intracellular bacterial symbionts in the presence of added nitrate. After a normoxic baseline was established, perfusion with nitrogen-equilibrated sea water was begun at hour 2.5. Arrows indicate stepwise additions of nitrate for 1.5 h each under nominally oxygen-free conditions. Concentrations are given in units of mmol l^{-1}. Each addition of nitrate was followed by a nitrate-free period, except after the 0.03 mmol l^{-1} addition. Simultaneous appearance of nitrite in the effluent seawater showed similar stepwise increases as seen with the heat flux (data not shown) [redrawn from 139].

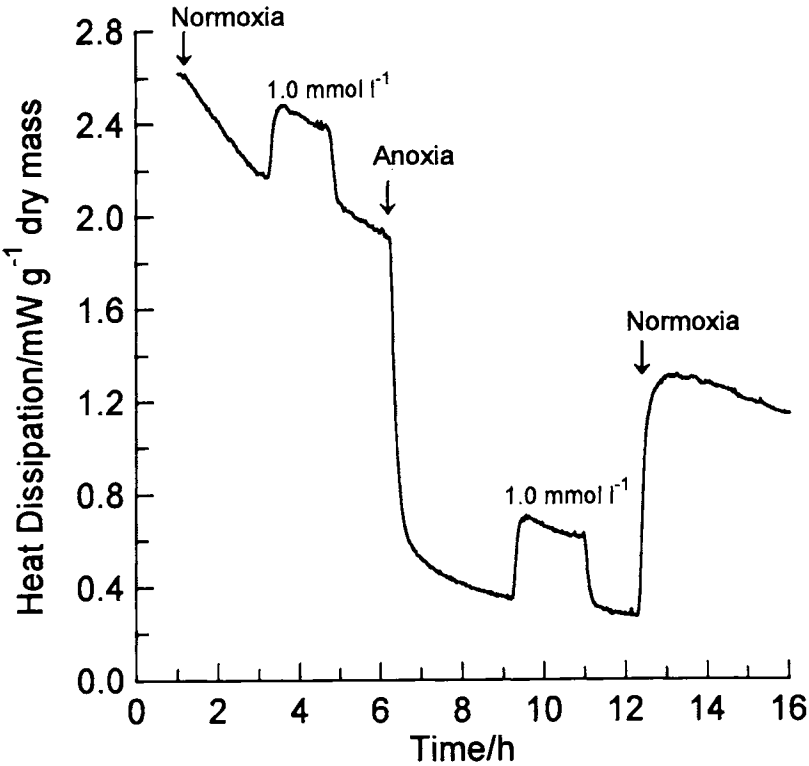

Figure 12. Heat dissipation of *Lucinoma aequizonata* gill tissue showing quantitatively similar stimulations by 1.0 mmol l^{-1} nitrate under both normoxic and anoxic conditions. Time periods are indicated for the additions of nitrate. Aerobic recovery was initiated at hour 12.5 [redrawn from 139].

7. CONCLUSIONS AND FUTURE DIRECTIONS

Calorimetry has proven to be of high utility for providing insights into questions of animal physiology and bioenergetics. The approach is not simply an alternative to respiration rate measurements, but can provide information that cannot be obtained with oxygen consumption (see example of *Lucinoma aequizonata*, section 6). The simultaneous measurement of heat flux and oxygen flux (calorespirometry) has been important for determining the proportions of aerobic and anaerobic metabolism recruited under a variety of environmental conditions to which both adult and developmental stages can be exposed. Thus from the perspective of an animal physiologist, calorimetry has

been, and continues to be, an invaluable tool in bioenergetics and metabolic adaptation studies. While some believe the impact of microcalorimetry in the area of cell biology "has not yet been of much importance for the intended target areas" [1], the same cannot be said for the field of physiology. However, physiological researchers that have employed calorimetry in their work are well aware of the how vulnerable microcalorimetric measurements can be to systematic errors [cf. 1], including evaporation, condensation, adsorption, incomplete mixing, corrosion of stainless steel surfaces (particularly in flow-through systems), concerns with electrical calibration, and methods for correcting instrumental response times.

There are innovations still to come that may make calorimetry even more applicable for physiological work. Particularly noteworthy is the possibility of positioning analytical sensors in the calorimetry reaction vessel without significant disturbance [141]; miniaturized oxygen and pH electrodes have been used in conjunction with calorimetric measurements of T-lymphoma cells. There are exciting advancement underway in the general field of miniature sensors. Companies like 3M Health Care (Tustin, CA USA) and Puritan Bennett (Carlsbad, CA USA) are actively developing probes based on the concept of optical fluorescence microsensing that are small enough to position intra-arterially. Excitation light is sent down an optical fiber to the probe, which has a fluorescent dye coating; the dye at the tip reacts to the excitation light and analyte concentration and a fluorescence emission signal is returned via the same fiber to a monitor [142-145]. Other coating work on light absorbance principles. Apparently, pH, p_{O2} and p_{CO2} can be monitored in this way. Initial attempts have been made to position such probes in calorimetric ampoules (David W. Kraus, Dept. of Biology, University of Alabama, Birmingham, USA; personal communication). Combinations of isothermal calorimetry with new analytical approaches and instrumentation offer intriguing research prospects for the future.

ACKNOWLEDGEMENTS

All research cited from the laboratory of SCH was supported by National Science Foundation (USA) grants IBN-9723746, IBN-9306652, DCB-9018579, DCB-8702615, and DCB-8316711. The author gratefully acknowledges this support.

REFERENCES

1. I. Wadsö, Chem. Soc. Rev., 26 (1997) 79.
2. E. Gnaiger, J. Exp. Zool., 228 (1983) 471.

3. J. Widdows, in A.M. James (Ed.), Thermal and Energetic Studies of Cellular Biological Systems, IOP Publishing Limited, Bristol, 1987, p. 182.
4. D.M. Stocco, P.C. Beers and A.H. Warner, Dev. Biol., 27 (1972) 479.
5. J.F. Carpenter and S.C. Hand, J. Comp. Physiol. B, 156 (1986) 451.
6. T. Anchordoguy and S.C. Hand, Am. J. Physiol., 267 (1994) R895.
7. S.C. Hand and E. Gnaiger, Science, 239 (1988) 1425.
8. E. Gnaiger and R.B. Kemp, Biochim. Biophys. Acta, 1016 (1990) 328.
9. R.B. Kemp, Thermochim. Acta, 193 (1991) 253.
10. J. Widdows and J.M. Shick, Mar. Biol., 85 (1985) 217.
11. J. Widdows, R.I.E. Newell and R. Mann, Biol. Bull., 177 (1989) 154.
12. J.M. Shick, E. Gnaiger, J. Widdows, B.L. Bayne and A. De Zwaan, Physiol. Zool., 59 (1986) 627.
13. J.M. Shick, J. Widdows and E. Gnaiger, Am. Zool., 28 (1988) 161.
14. S.C. Hand, J. Comp. Physiol. B, 160 (1990) 357.
15. E. Gnaiger, Thermochim. Acta, 40 (1980) 195.
16. S.H. Loomis, S.C. Hand and P.E. Fell, Biol. Bull., 191 (1996) 385.
17. J.M. Shick, Mar. Biol. Lett., 2 (1981) 225.
18. J.M. Shick and J.A. Dykens, Biol. Bull., 166 (1984) 608.
19. H. Schmidt, A. Wichmann and I. Lamprecht, J. Comp. Physiol. B, 166 (1996) 205.
20. E. Gnaiger and I. Staudigl, Physiol. Zool., 60 (1987) 659.
21. J.E. Doeller, D.W. Kraus and J.M. Colacino, Comp. Biochem. Physiol., 97A (1990) 107.
22. P. Famme and J. Knudsen, J. Comp. Physiol., 154 (1984) 587.
23. I. Hardewig, A.D.F. Addink ,M.K. Grieshaber, H.-O. Pörtner and G. van den Thillart, J. Exp. Biol., 157 (1991) 143.
24. M.E. Meade, J.E. Doeller, D.W. Kraus and S.A. Watts, J. Exp. Zool., 270 (1994) 460.
25. D. Coenen-Stass, B. Schaarschmidt and I. Lamprecht, Ecology, 61 (1980) 238.
26. G.L. Peakin, Experienta, 29 (1973) 801.
27. F. Dunkel, C. Wensman and R. Lovrien, Comp. Biochem. Physiol., 62A (1979) 1021.
28. M.M. Pamatmat, Mar. Biol., 48 (1978) 317.
29. W.X. Wang and J. Widdows, Mar. Biol., 116 (1993) 73.
30. E. Gnaiger, J.M. Shick and J. Widdows, in C.R. Bridges and P.J. Butler (Eds.), Techniques in Comparative respiratory Physiology: An Experimental Approach, Cambridge University Press, Cambridge, 1989, p. 113.
31. M.C. Haws, L. DiMichele and S.C. Hand, Mol. Mar. Biol. Biotech., 2

(1993) 207.
32. M.M. Pamatmat, J. Exp. Zool., 228 (1983) 405.
33. W.X. Wang and J. Widdows, Mar. Ecol. Prog. Ser., 70 (1991) 223.
34. P. Famme, J. Knudsen and E.S. Hansen, Mar. Biol. Lett., 2 (1981) 345.
35. J. Widdows and A.J.S. Hawkins, Physiol. Zool., 62 (1989) 764.
36. B.B. Rees and S.C. Hand, J. Exp. Biol., 152 (1990) 77.
37. J. van Waversveld, A.D.F. Addink and G. van den Thillart, J. Comp. Physiol. B, 159 (1989) 263.
38. A.D.F. Addink, G. van den Thillart, H. Smit and J. van Waversveld, Thermochim. Acta, 193 (1991) 41.
39. V.J.T. van Ginneken, A. Gluvers, R.W. van der Linden, A.D.F. Addink and G.E.E.J.M. van den Thillart, Thermochim. Acta, 247 (1994) 209.
40. V.J.T. van Ginneken, J. Vanderschoot, A.D.F. Addink and G.E.E.J.M. van den Thillart, Thermochim. Acta, 249 (1995) 143.
41. K.T. Paynter, L. DiMichele, S.C. Hand and D. Powers, J. Exp. Zool., 257 (1991) 24.
42. I.H.D. Lamprecht, F.-R. Matuschka and B. Schaarschmidt, J. Exp. Biol., 156 (1991) 375.
43. R.N. Finn, J. Widdows and H.J. Fyhn, Mar. Biol., 122 (1995) 157.
44. E. Gnaiger, in E. Gnaiger and H. Forstner (Eds.), Polarographic Oxygen Sensors. Aquatic and Physiological Applications, Springer-Verlag, Berlin, 1983, p. 134.
45. C.S. Hammen, in M. Wiley (Ed.), Estuarine Processes, Academic Press, New York, 1976, p. 347.
46. E. Gnaiger, in I. Lamprecht and B. Schaarschmidt (Eds.), Applications of Calorimetry in Life Sciences, Walter de Gruyter, New York, 1977, p. 281.
47. J.P. Herold, Comp. Biochem. Physiol., 58A (1977) 251.
48. M.M. Pamatmat, Mar. Biol., 53 (1979) 223.
49. E. Gnaiger, Experientia Suppl., 37 (1979) 155.
50. E. Gnaiger, FEBS Lett., 112 (1980) 239.
51. C.S. Hammen, Comp. Biochem. Physiol., 62A (1979) 955.
52. C.S. Hammen, Comp. Biochem Physiol., 67A (1980) 617.
53. I. Wadsö, Science Tools, 21 (1974) 18.
54. J. Suurkuusk and I. Wadsö, Chemica Scripta, 20 (1982) 155.
55. M.G. Nordmark, J. Laynez, A. Schön, J. Suurkuusk and I. Wadsö, J. Biochem. Biophys. Meth., 10 (1984) 187.
56. Thorén, J. Suurkuusk and B. Holma, J. Biochem. Biophys. Meth., 18 (1989) 149.
57. E. Gnaiger, Science Tools, 30 (1983) 21.
58. J. Widdows, B.L. Bayne, D.R. Livingstone, R.I.E. Newell and P.

Donkin, Comp. Biochem. Physiol., 62A (1979) 301.
59. J.M. Shick, A. De Zwaan and A.M. Th. De Bont, Physiol. Zool., 56 (1983) 56.
60. S.E. Shumway, T.M. Scott and J.M. Shick, J. Exp. Mar. Biol. Ecol., 71 (1983) 135.
61. J.M. Shick, E. Gnaiger, S. Tyler and M.S. Woodward, Am. Zool., 27 (1987) 167 (abstract).
62. T.F. Pedersen, Ophelia, 36 (1992) 203.
63. I.J. Holopainen and O.-P. Penttinen, Oecologia, 93 (1993) 215.
64. L.L. Liu, W.B. Stickle and E. Gnaiger, Mar. Biol., 104 (1990) 239.
65. U. Schöttler and G. Schroff, J. Comp. Physiol., 105 (1976) 243.
66. G. Wegener, in A.P. Gupta (Ed.), Arthropod Brain: Its Evolution, Development, Structure and Functions, John Wiley and Sons, Inc., New York, 1987, p. 369.
67. P.W. Hochachka, J.C. Nener, J. Hoar, R.K. Saurez and S.C. Hand, Canadian J. Zool., 71 (1993) 1267.
68. G. Wegener, in P.W. Hochachka, P.L. Lutz, T. Sick, M. Rosenthal and G. van den Thillart (Eds.), Surviving Hypoxia: Mechanisms of Control and Adaptation, CRC Press, Boca Raton, 1993, p. 417.
69. G. Wegener, R. Michel and M. Thuy, Zool. Beitr., 30 (1986) 103.
70. G. Wegener, in H. Acker (Ed.), Oxygen Sensing Tissues, Springer-Verlag, Berlin, 1988, p. 13.
71. G. Wegener, N.M. Bolas and A.A.G. Thomas, J. Comp. Physiol. B, 161 (1991) 247.
72. W. Weyel and G. Wegener, Experientia, 52 (1996) 474.
73. X.J. Musacchia, Physiol. Zool., 32 (1959) 47.
74. G. Ultsch, Comp. Biochem. Physiol., 81A (1985) 607.
75. D.C. Jackson, J. Appl. Physiol., 24 (1968) 503.
76. J. Piironen and I.J. Holopainen, Ann. Zool. Fennici, 23 (1986) 335.
77. J. van Waversveld, A.D.F. Addink, G. van den Thillart and H. Smit, J. Therm. Anal., 33 (1988) 1019.
78. J. van Waversveld, A.D.F. Addink, G. van den Thillart and H. Smit, J. Exp. Biol., 138 (1988) 529.
79. J. van Waversveld, A.D.F. Addink and G. van den Thillart, J. Exp. Biol., 142 (1989) 325.
80. A.J. Hansen, Physiol. Rev., 65 (1985) 101.
81. C.J. Doll, in P.W. Hochachka, P. Lutz, T. Sick, M. Rosenthal and G. van den Thillart (Eds.), Surviving Hypoxia, CRC Press, Boca Raton, 1993, p. 389.
82. P.L. Lutz, Annu. Rev. Physiol., 54 (1992) 619.
83. C.J. Doll, P.W. Hochachka and S.C. Hand, J. Exp. Biol., 191 (1994)

141.
84. D.A. Kelly and K.B. Storey, Am. J. Physiol., 255 (1988) R774.
85. P.L. Lutz, P.M. McMahon, M. Rosenthal and T.J. Sick, Am. J. Physiol., 247 (1984) R740.
86. P. Lipton and T.S. Whittingham, in R. Dingledine (Ed.), Brain Slices, Plenum Press, New York, 1984, p. 113.
87. D. Johannsson, G.E. Nilsson and E. Tornblom, J. Exp. Biol., 198 (1995) 853.
88. P.E. Bickler, Am. J. Physiol., 263 (1992) R1298.
89. S.C. Hand and I. Hardewig, Annu. Rev. Physiol., 58 (1996) 539.
90. J.E. Doeller, D.W. Kraus, E. Gnaiger and J.M. Shick, Thermochim. Acta, 172 (1990) 171.
91. J.E. Doeller, D.W. Kraus, J.M. Shick and E. Gnaiger, J. Exp. Zool., 265 (1993) 1.
92. P. Satir and M.A. Sleigh, Annu. Rev. Physiol., 52 (1990) 137.
93. R.C. Cole, P.C. Sukanek, J.B. Wittenberg and B.A. Wittenberg, J. Appl. Physiol., 53 (1982) 1116.
94. E. Gnaiger, G. Mendez and S.C. Hand, Biophys. J., 64 (1993) M-pos 489 (abstract).
95. M.D. Brand, D. Steverding, B. Kadenbach, P.M. Stevenson and R.P. Hafner, Eur. J. Biochem., 206 (1992) 775.
96. M.K. Shigenaga, T.M. Hagen and B.N. Ames, Proc. Natl. Acad. Sci. USA, 91 (1994) 10771.
97. P.W. Hochachka, Science, 231 (1986) 234.
98. M. Sprung and J. Widdows, Mar Biol., 91 (1986) 41.
99. S.L. Coon, D.B. Bonar and R.M. Weiner, J. Exp. Mar. Biol. Ecol., 94 (1985) 211.
100. A.R. Place and D.A. Powers, Proc. Natl. Acad. Sci. U.S.A., 76 (1979) 2354.
101. L. DiMichele, D.A. Powers and J.A. DiMichele, Am. Zool., 26 (1986) 201.
102. L. DiMichele and D.A. Powers, Nature, 296 (1982) 563.
103. L. DiMichele and D.A. Powers, Physiol. Zool., 57 (1984) 52.
104. D. Keilin, Proc. Roy. Soc. London B, 150 (1959) 149.
105. A. Mansingh, Can. Entomol., 103 (1971) 983.
106. S.C. Hand, Adv. Comp. Environ. Physiol., 8 (1991) 1.
107. G.E. Hofmann and S.C. Hand, Am. J. Physiol., 258 (1990) R1184.
108. J.S. Clegg, Trans. Amer. Micros. Soc., 93 (1974) 481.
109. J.S. Clegg, J. Exp. Biol., 200 (1997) 467.
110. W.B. Busa, J.H. Crowe and G.B. Matson, Arch. Biochem. Biophys., 216 (1982) 711.

111. K. Kwast, J.I. Shapiro, B.B. Rees and S.C. Hand, Biochim. Biophys. Acta, 1232 (1995) 5.
112. S.C. Hand, Pure Appl. Chem., 65 (1993) 1951.
113. W.B. Busa and J.H. Crowe, Science, 221 (1983) 366.
114. G.E. Hofmann and S.C. Hand, J. Exp. Biol., 164 (1992) 103.
115. I. Hardewig, T. Anchordoguy, D. Crawford and S.C. Hand, Mol. Cell. Biochem., 158 (1996) 139.
116. T. Anchordoguy and S.C. Hand, J. Exp. Biol., 198 (1995) 1299.
117. F. Hontoria, J.H. Crowe, L.M. Crowe and F. Amat, J. Exp. Biol., 178 (1993) 149.
118. S.C. Hand, J. Exp. Zool., 273 (1995) 445.
119. J.S. Clegg, J. Exp. Zool., 215 (1981) 303.
120. J.S. Clegg, Am. J. Physiol., 246 (1984) R133.
121. J.S. Glasheen and S.C. Hand, J. Exp. Biol., 145 (1989) 263.
122. J.M. Hale, in E. Gnaiger and H. Forstner (Eds.), Polarographic Oxygen Sensors. Aquatic and Physiological Applications, Springer-Verlag, Berlin, 1983, p. 3.
123. J.S. Clegg, Comp. Biochem. Physiol., 53A (1976) 83.
124. J.S. Clegg, Comp. Biochem. Physiol., 53A (1976) 89.
125. J.S. Glasheen and S.C. Hand, J. Exp. Biol., 135 (1988) 363.
126. J. Machin, in V. Fretter and J. Peake (eds.), The Pulmonates, Academic Press, London, 1975, p. 105.
127. M.C. Barnhart, Physiol. Zool., 59 (1986) 733.
128. T.A. Churchill and K.B. Storey, Physiol. Zool., 62 (1989) 1015.
129. B.B. Rees and S.C. Hand, Biol. Bull., 184 (1993) 230.
130. P.E. Fell, Int. J. Invertebr. Reprod. Dev., 11 (1987) 305.
131. R. Rasmont, Compt. Rend. Acad. Sci., 261 (1965) 845.
132. S.H. Loomis, L.F. Ungemach, B.R. Branchini, S.C. Hand and P.E. Fell, Biol. Bull., 191 (1996) 393.
133. C.M. Cavanaugh, Biol. Soc. Wash. Bull., 6 (1985) 373.
134. C.R. Fisher, Rev. Aquat. Sci., 2 (1990) 399.
135. D.L. Distel and H. Felbeck, J. Exp. Zool., 247 (1988) 11.
136. A.E. Boetius and H. Felbeck, Mar. Biol., 122 (1995) 105.
137. V. Stewart, Microbiol. Rev, 52 (1988) 190.
138. U. Hentschel and H. Felbeck, Appl. Env. Microbiol., 61 (1995) 1630.
139. U. Hentschel, S.C. Hand and H. Felbeck, J. Exp. Biol., 199 (1996) 427.
140. S.C. Cary, R.D. Vetter and H. Felbeck, Mar. Ecol. Prog. Ser., 55 (1989) 31.
141. P. Bäckman and I Wadsö, J. Biochem. Biophys. Meth., 23 (1991) 283.
142. W. Marshall and R. Foster-Smith, Progress Notes (Puritan-Bennett), 4

(1992) 6.
143. P. Pantano and D.R. Walt, Anal. Chem., 67 (1995) 481.
144. J.L. Gehrich, D.W. Lübbers, N. Opitz, D.R. Hansmann, W.W. Miller, J.K. Tusa and M. Yafuso, IEEE Trans. Biomed. Eng., BME-33 (1986) 117.
145. W.R. Seitz, Anal. Chem., 56 (1984) 16.

Handbook of Thermal Analysis and Calorimetry. Vol. 4: From Macromolecules to Man.
R.B. Kemp, editor.

Chapter 10

WHOLE BODY CALORIMETRY

Uwe Frenz

Department Biochemistry and Physiology of Nutrition,
German Institute of Human Nutrition,
Arthur-Scheunert-Allee 114-155, 14558
BergholzRehbrücke,
Germany

1 INTRODUCTION

Calorimetric methods have long been used for research in many fields like physics, chemistry, medicine, physiology and nutritional sciences. Calorimetry in biology-related fields is used to investigate metabolism and metabolites of biological objects. Objects can be humans, animals, plants and even single organs or cell clusters of them. Metabolites are usually investigated using direct calorimetric techniques like bomb calorimetry. This results in the oxidation enthalpy of food, food components and excreta. Whole body calorimetry instead is used to investigate the metabolism of complete and intact living beings. It is employed for different purposes:

- characterising the requirements of food energy and food components for individuals and different population groups,
- investigating metabolic pathways and regulation mechanisms in physiology,
- monitoring the metabolism of critically ill patients in medicine and
- exploring reasons and progression of obesity, hypertension and diabetes in nutrition research.

The application of (direct) calorimetry on living beings started about 200 years ago, when Lavoisier and Crawford independently from each other performed their trailblazing experiments on respiration and heat loss. Lavoisier measured the heat loss of animals sitting in a cage surrounded with ice and isolated from the environment. Later he introduced indirect calorimetry by means

of measuring oxygen consumption of his subjects. The next important step was the classification of food and its components carbohydrate, fat and protein as the 'fuel' for the body, introduced by Liebig.

The modern usage of calorimetry started around the turn of this century, when two groups of researchers succeeded in constructing calorimeters to measure the energy expenditure of living beings in combination with an accurate balance of matter. Rubner and his group found that the energy conservation law could be applied to living beings too, when he investigated the energy balance of dogs [1]. Atwater and later Benedict too performed their experiments [2,3], which are still impressive in quality and quantity of analysis. They found not only the energy conservation being fulfilled, but were able to calculate changes in the body's fat stores by a careful C-N-H balance.

Calorimetry is still in use today, but the emphasis in biological and medical research went from direct to indirect calorimetry in the last decades. This was mainly caused by two reasons. The first one is a huge improvement in gas analysis instrumentation compared with that of the instrumentation of direct calorimetry. The second reason is, that indirect calorimetry provides not only with measures of energy expenditure, but the substrate oxidation rates too. This is in biology related fields probably of at least the same significance than energy expenditure alone.

Direct and indirect calorimetry have almost only the denomination "calorimetry" in common, but cover quite different measurements. Direct calorimetry assesses the heat loss (HL) of subjects. The direct heat transfer through chamber walls surrounding the subject is measured as well as hidden heat delivered in form of evaporised water and heated air. Indirect calorimetry in contrast assesses the energy expenditure (EE) of a subject by measuring the gaseous exchange and nitrogen excretion. In this method it is assumed that the food consists only of three main substrates (carbohydrate, fat and protein) with known chemical composition and known stoichiometry of oxidation. So substrate oxidation can be calculated from gaseous exchange and nitrogen excretion. This can be expressed as the amount of chemical energy transferred into heat in the subject's body. Both values, heat loss and energy expenditure, are tightly related to each other, but not equivalent. They use different pools with different dynamic properties inside the body as well as in the calorimetric chamber. So the methods to access both values measure different items utilising different sensors with different specifics.

2. BASICS

The physical law of energy conservation applies to living beings too. So any food energy, ingested by a living being, is balanced by energy losses from its body and energy stores within it. This can be described by the following (word) equation:

Food energy = energy in faeces
+ energy in urine
+ energy in gaseous excretions (CH_4, H_2)
+ lost heat
+ mechanical work (locomotor activity)
+ retained energy (syntheses, stores, 'growth', biological production)

Energy intake of free living subjects is not easy to access - it can be difficult to do it quite accurately in the case of normal diets. Some of the energy balance components like the remaining energy in faeces and urine can easily be assessed by means of bomb calorimetry or can even be assumed as a fixed part of the overall food energy. Other components like energy in gaseous excretions have great individual variations, but are usually very small compared with the other components. So the energy balance equation can be rewritten by replacing the gross food energy minus energy in faeces, urine and gases by the metabolisable or net energy:

Net energy = lost heat
+ mechanical work
+ retained energy

All remaining components on the right side of the equation are quite difficult to assess. The lost heat is determined either by direct or indirect calorimetry or by other methods, that have been calibrated by calorimetric methods. The mechanical work performed by the subject can easily be measured as long as it is real work, performed on a bicycle ergometer or something similar. But to perform the normal, unconscious day-to-day movements of the subject also needs energy. The portion of energy needed for the locomotor activity in calorimetric chambers is usually measured utilising motion detectors. Their results together with the overall energy expenditure are used to estimate the portion of locomotor activity by regressive methods. Integrating the energy needed for all

unconscious and unrecognised work commonly results in much higher values than just the energy used for physical work.

The retained energy can not easily be assessed in humans and large animals. Even measuring it in smaller laboratory animals may be relatively inaccurate. There are two approaches to assess the retained energy in laboratory animals. The first solution includes long-term feeding and balancing of the individuals. It can also be applied to humans and large animals. The second method is a comparison of two groups of animals. Their carcasses are chemically analysed before and after application of test diets over some ten days.

The retained energy is very important for nutritional research, emergency recovery situations and efficiency of animal production. So normally the energy balance equation is used to calculate the retained energy from net energy intake, locomotor activity and heat loss. Heat loss however is measured directly or indirectly with calorimetric methods.

3. METHODS AND EQUIPMENT

Energy metabolism of living beings can be measured by several means, including direct and indirect calorimetry. The former is the detection of the heat loss of the subject; the latter allows the determination of the overall heat produced by the oxidative processes of the subjects metabolism. The physical law of energy conservation together with the limited heat storage capacity of the subject's body requires heat production to be equivalent or tightly related to heat loss - at least within short periods of some sec to min, depending on the species. Under standard conditions and over longer periods of at least a full day - both methods give identical results. After a meal, at changing levels of exercise or even during the day there is a change in body core temperature. This results in changes of the heat content of the body that may cause differences between direct and indirect calorimetry. Under standard conditions and over 24 h periods however, both methods can be employed to assess the energy expenditure of intact subjects and so to measure the energy balance.

There are some other methods to determine energy metabolism like the doubly labelled water (DLW) method [4-7] or other isotope dilution techniques [8], heart rate monitoring [9,10] or activity protocols. They all have at least one big disadvantage. Some methods (DLW) integrate over very long periods of some days to weeks compared to metabolically relevant periods of some seconds to a full day. Other methods need expensive individual calibrations against calorimetric measurements (heart rate monitoring) or produce relatively high

errors. The isotope dilution techniques require additional information provided by indirect calorimetry or food intake surveys. Finally there are only the two calorimetric methods as reference methods or standard.

Whole body calorimetry is not necessarily confined to a calorimetric chamber, although this type of equipment is dominant. Direct calorimetry is also possible with a water cooled garment [11]. Indirect calorimetry can perfectly be done in a chamber, but also by using a mask, a canopy or a ventilated hood. A canopy is a hard cover for the head or the upper part of the body, usually applied to patients laying on a bed. Calorimetry on animals is usually done in a calorimetric chamber or cage; on farm animals masks have also been used.

A calorimetric chamber is used for periods of between a day and a week or even longer. So the chamber has to be as similar to a living room as possible, although its volume has to be limited to improve the response time and accuracy of the system. Chambers contain, in addition to the necessary sensors, air locks for the transfer of food, excreta and blood samples, etc. and some utilities for comfortable housing the subjects. This includes a foldable bed, personal hygiene facilities, a desk and chair, some consumer electronics and typically some workout equipment like a bicycle ergometer. An example of a chamber is shown in Figure 1.

3.1. Direct Calorimetry

Direct calorimetry is the measurement of the heat loss (HL) of a subject. It is usually be done in specialised calorimetric chambers [12-14], but was done with heat exchanging body suits [11] too. Heat dissipation may occur in different ways. It can be direct heat transfer to the stationary environment (usually the chamber) or heat transfer to the air being pumped through the chamber. Another way is heat used to vaporise body water (and probably other water from inside the chamber like washing water or sweat, previously stored in clothing or chamber interior):

$$HL = HL_{NE} + HL_S + HL_L \qquad (1)$$

In equation (1) HL denominates the overall heat loss of the subject, HL_{NE} the nonevaporative, radiate heat loss of the subject to the environment, HL_S the sensible heat loss of the subject (heat transfer by warmed air) and HL_L the latent (evaporative) heat loss (heat transfer by vaporised water.

To assess all heat losses to the environment it is necessary to encapsulate the subject with a chamber, which may be of quite different size. Nevertheless it has a heat capacity and the only thing that can be measured is the heat loss of the chamber, containing the subject:

$$HL = HL_{CE} + \Delta HL_{Ch} + HL_S + HL_L \quad (2)$$

Here HL_{CE} means the heat loss from the chamber to the environment and ΔHL_{CH} the change in heat content of the chamber.

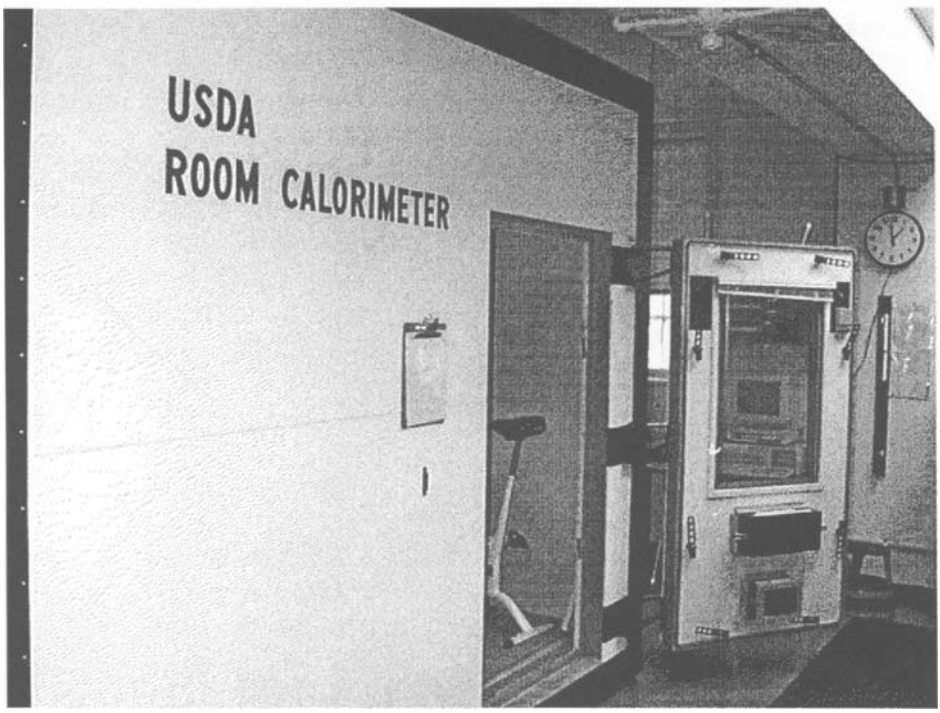

Figure 1. View of the combined direct and indirect calorimetric chamber at USDA Beltsville, MD, USA. The gas in- and outlet is located on the left wall. The door includes a window and two locks for transfer of food and waste. The whole system is controlled by a PC

The heat content of the chamber depends under well-defined conditions only on chamber temperature. This is, however, not always balanced with the air temperature in the chamber. If the chamber temperature remains constant the heat content can be assumed to be constant, especially if the experimental schedule is comparable for different measurements. This constant heat content is than added to HL_{CE} resulting in the nonevaporative heat loss of the subject. Most experimentors did so in the past; however, there are some papers dealing with heat storage compensation in the calorimetric chamber [13,15]

3.1.1. Principles of Measurement

The nonevaporative heat loss can be measured in two ways. The active way is to control a heat sink in such a manner, that the temperature gradient across the well-insulated chamber walls is maintained very near to zero (heat sink calorimeter). The passive way is to measure the temperature gradient across the poorly insulated chamber walls, that have to be passed by the heat (gradient layer calorimeter). In addition temperature changes of the exchanged air have to be taken into account. The evaporative heat loss is measured either by condensing the water appearing in the chamber to maintain a constant water content, or by measuring an increased water content in the chamber and the removal of water by the outgoing air. Water is a fundamental problem, because it adheres to the inner surface of the chamber (and even diffuses into some of the chamber materials). So water may not be measurable exactly and quickly enough, compared to the other parameters. Typical time constants of the nonevaporative heat loss of direct calorimeters can be improved by mathematical compensation of heat dilution and storage in the chamber. The time constant of the evaporative heat loss however still lacks these improvements and remains at values of h and even days, depending on the calorimeter's features.

3.1.2. Equipment

Gradient layer calorimeters are covered with walls constructed from materials with a relative low heat resistance. This results in a temperature gradient across this covering of only a very few degrees even while measuring subjects with relatively high actual heat loss rates. The temperature gradient is measured by sensors distributed over both the inner and outer surface of the covering layer. It can very effectively be constructed by using glass-reinforced epoxy resin plates with thin copper films on both sides [16]. By etching meandrous structures into the copper film one can form a reasonable resistor with a temperature dependent resistance, that averages the temperature on the whole surface. Both sides of the layer can be compared utilising a Wheatstone bridge to monitor very small temperature differences of up to about 0.01°C. Other applications use thermocouple panels [14] mounted on the inner surface of the chamber. These panels are electrically connected in series to achieve easy measurable voltages and to average over the whole chamber surface. The relation between the measured electrical signal and the heat flux can empirically be found by calibrating the chamber with electrical heaters or with combustion of calibration substances like alcohol or butane.

There is, however, a problem due to the heat capacity of the chamber. Temperature changes in the environment result in heat fluxes to or from this heat

capacity. To avoid these problems the chamber is often surrounded by a water jacket. This stabilises the temperature change rate of the outer side of the chamber to ± 1 mK/min and limits the absolute temperature change within a day to ± 0.5 K. The same result could be achieved by modelling and correcting for the heat flux to and from the stores of the chamber material [1].

Heat sink calorimeters do actively remove that amount of heat from the chamber, that was released by the subject [13,17]. This is achieved by recirculating the air within the chamber over a heat exchanger, which is controlled by the temperature gradient across the chamber walls. The gradient is maintained near zero, which minimises the uncontrolled heat transfer through the chamber walls. The walls themselves have to be well insulated with a low heat capacity to be very sensitive to heat transfers with a short reaction time. The heat loss of the chamber can be determined through heat exchangers in different approaches. One solution was to determine the flow rate of water and the increase in water temperature across the heat exchanger. Another approach was to measure the ratio of temperature increase across the heat exchanger and that across an electrical heater in the same water flow. A third solution monitors the power consumption of an electrically driven (Peltier-) heat exchanger. Due to the much higher thermal resistance of the chamber walls the heat exchange between chamber and environment caused by environmental temperature changes is much less than in gradient layer calorimeters. So the environmental temperature must be controlled only to ± 0.5 K, avoiding the need for a water jacket around the calorimeter.

Evaporative heat measurements can be done by two different ways. The increase in water content can be assessed by condensing the water in the outgoing air. The other way is to monitor the flow rate and water content of both incoming and outgoing air. Estimating the evaporative heat loss by condensing the water in the outgoing air requires conditioning the incoming air to a constant dew point. So the fresh air has to be saturated and then passed over a heat exchanger. After leaving the chamber the air is again passed over an identical heat exchanger. The evaporative heat loss can be calculated from the condensation heat of the condensed water, corrected for the temperature difference between the subject's body and the heat exchanger. The second possibility to measure the evaporative heat requires just a rough dew point conditioning, but needs the accurate measurement of the heat content of the incoming and outgoing air and the air flow through the chamber. Dew point measurements of air are preferably done with optical condensing instruments instead of capacitive sensors due to their better accuracy and stability. Water production multiplied with the evaporation heat at body temperature is the evaporative heat loss.

The dew point of the incoming air has to be chosen very carefully to have a comfortable climate in the chamber as well as not to saturate the chamber air during heavy working periods of the subjects (sweating).

Direct calorimeters for human calorimetry can be very accurate and fast responding instruments (Table 1). They provide a good environment for performing controlled studies. They are, on the other hand, very expensive to both construct and operate. It is necessary to adjust for every source of incoming and outgoing heat like heated food and warm excreta, as well as light-, TV-, audio- and PC power consumption. Direct calorimeters have almost been replaced by indirect ones in most of the facilities performing calorimetric research on humans and large animals. This was done due to the more useful results in physiologic related research (insight view into net substrate oxidation) and the better features (less expensive, easier to operate) of indirect calorimeters. Due to the availability of consumer electronic equipment to the subjects indirect chambers are probably more convenient for them.

Table 1
Parameters of some direct calorimeters in facilities around the world: direct calorimeters are very accurate and fast responding instruments.

facility	published	value	rate of recovery [%]	calibrated against	τ [min]	compensation?
Beltsville [15]	1997	HL		locomotor activity measured by IR sensors	2-5	yes
Beltsville [14]	1991	HL	99.7 ± 2.6	alcohol combustion	~90	no
Lausanne [42]	1985	HL	97 ..103	simultaneous indirect calorimetry	~20	no
Odense [13]	1985	HL_{NE}	100 ± 0.6	electrical heaters	~15	yes
ditto	ditto	HL_{evap}	100 ± 0,7	weighing of water evaporizers	~15	yes
Cambridge [12]	1977	Q_S	99.87	electrical heaters	< 10	
ditto	ditto	Q_L	100 ± 2	water pump & electrical heater		
Yellow Springs [11]	1972	HL_{NE}	100 ± 1.5	electrical heater in a dummy	~13	no

3.2. Indirect Calorimetry

Indirect calorimetry is the determination of the overall heat production by the oxidative processes in the subject's body. Heat production is calculated from respiratory gas exchange, i.e. the amount (mass) of oxygen consumption (M_{O2}) and carbon dioxide production (M_{CO2}). This calculation is based on the assumption that only three kinds of well-known substrates (carbohydrates (CHO), fat and protein) are completely oxidised. There is a third value to be determined for the equation system to be solvable, which is usually the nitrogen excretion rate (N_{ex}). The protein oxidation rate is calculated utilising the energy content of urea in the urine excreted. Assuming a well-known protein mixture being oxidised one can determine the urea produced and consequently the nitrogen excreted. N_{ex} combined with M_{O2} and M_{CO2} are the measured values in indirect calorimetry. They allow the determination of not only energy expenditure (EE), but of the substrate oxidation rates as well.

3.2.1. Theoretical Basis

The theoretical basis of indirect calorimetry has been described several times [18,19]. First it is necessary to determine which are the typical main substrates assumed to be oxidised. Glucose ($C_6H_{12}O_6$) is almost always used as the typical carbohydrate, especially because higher carbohydrate molecules are oxidised very similarly to several molecules of glucose. It is necessary to adjust for the different energy content of disaccharides (lactose etc.) and polysaccharides (starch etc.) due to the energy of hydrolysis. Palmitoyl-stearoyl-oleoyl-glycerol ($C_{55}H_{104}O_6$) is used as typical fat, because it is very similar to the triacylglycerol formed from three 'mean' fatty acids of the human body as found by Hirsch [20]. There is no standard available for typically oxidised proteins. In the following reaction equations results given by Ferranini and Consolazio [18,21] have been used. Writing down the stoichiometry of the oxidation reaction of these three main substrates one gets:

$$1\,G + 6\,O_2 \rightleftarrows 6\,CO_2 + 6\,H_2O \qquad (3)$$

(RQ = 1.000, ΔH = minus 2818 kJ·mol^{-1})

$$1\,F + 78\,O_2 \rightleftarrows 55\,CO_2 + 52\,H_2O \qquad (4)$$

(RQ = 0.705, ΔH = minus 33740 kJ·mol^{-1})

$$1P + 5.1O_2 \rightleftarrows 4.1CO_2 + 5.6H_2O + 0.6Urea \quad (5)$$

(RQ = 0.805, ΔH = minus 1989 $kJ \cdot mol^{-1}$)

Here G denominates the glucose oxidation rate, F the fat (Palmitoyl-stearoyl-oleoyl-glycerol) oxidation rate, P the protein oxidation rate and RQ the respiratory quotient, which is the quotient of carbon dioxide production and oxygen consumption: $RQ = CO_2/O_2$. The RQ is not only a theoretical quotient characterising each of the metabolites, but a very important factor in whole body calorimetry, characterising the actual ratio of the oxidised substrates.

To simplify the calculations it is easier to change the units from mole to g or l for the respiratory gases:

$$1\,g\,G + 0.746\,l\,O_2 \rightleftarrows 0.746\,l\,CO_2 + 0.600\,g\,H_2O \quad (6)$$

(ΔH = minus 15.64 kJ)

$$1\,g\,F + 2.029\,l\,O_2 \rightleftarrows 1.431\,l\,CO_2 + 1.124\,g\,H_2O \quad (7)$$

(ΔH = minus 39.17 kJ)

$$1\,g\,P + 0.966\,l\,O_2 \rightleftarrows 0.782\,l\,CO_2 + 0.450\,g\,H_2O \quad (8)$$

(ΔH = minus 9.95 kJ)

Nitrogen is about 16 % of protein by weight:

$$P = 6.250\,N \quad (9)$$

Equation (9) transforms equation (8) into equation (10):

$$1\,g\,N + 6.038\,l\,O_2 \rightleftarrows 4.888\,l\,CO_2 + 2.81\,g\,H_2O \quad (10)$$

Summarising the components (gases, nitrogen and energy) used to oxidise 1 g of every substrate from equations (6), (7) and (10) results in:

$$O_2 = 0.746\,G + 2.029\,F + 6.038\,N \tag{11}$$

$$CO_2 = 0.746\,G + 1.431\,F + 4.888\,N \tag{12}$$

$$\Delta H = 15.640\,G + 39.167\,F + 105.42\,N \tag{13}$$

Equations (11) and (12) can be solved for substrate oxidation rates and subsequently for energy expenditure or chemical energy transferred to heat:

$$G = 4.55\,CO_2 - 3.21\,O_2 - 2.87\,N \tag{14}$$

$$F = -1.67\,CO_2 + 1.67\,O_2 - 1.92\,N \tag{15}$$

$$EE = 16.17\,O_2 + 5.03\,CO_2 - 5.98\,N \tag{16}$$

$$RQ = \frac{CO_2}{O_2} \tag{17}$$

$$NPRQ = \frac{CO_2 - 4.888\,N}{O_2 - 6.038\,N} \tag{18}$$

In equation (18) the acronym NPRQ denotes the non-protein-RQ. It indicates a theoretical value of the actual RQ, which was adjusted to remove the influence of the protein oxidation on the metabolism. The NPRQ is a good indicator for the main source of energy in a subjects metabolism at a given time.

Equation (16) is called the Weir-equation; it is the basic equation of indirect calorimetry. Its coefficients vary slightly between different authors and whether measurements were performed on humans or animals due to their different food composition and tissue composition. It shall be notified, that the portion of the oxygen term alone on EE in equation (16) is about 73 - 80 %. If the RQ can be roughly estimated from food intake, food composition and work load of the subjects, it is possible to estimate CO_2 from O_2. Taking into account the possible error in estimating the RQ, the remaining error of EE is usually very small [22].

3.2.2. Principles

Normal and comfortable living conditions have to be maintain in the calorimetric chamber, at least under normal conditions and for humans. This requires

the concentration of oxygen and carbon dioxide in the breathing air remaining within small ranges of about 18-21% for O_2 and 0-2.5% for CO_2; with a typical measure of the gas concentration being about 20% for O_2 and 0.8% for CO_2. This is achieved by choosing the flow rate (F), of which fresh air is pumped through the chamber being about 100 times the expected value of oxygen consumption of the subjects.

Respiratory gases are diluted in the chamber air. This can be described [23,24] by:

$$\frac{dC(t)}{dt} = -\frac{F}{V} * C(t) = -\frac{1}{\tau} * C(t) \tag{17}$$

Here dC(t)/dt denominates the first derivative of the concentration of a gas in the chamber, F the flow rate of fresh air pumped through the chamber, V the chamber volume and τ the time constant of the system ($\tau = V/F$).

The heat loss (HL) of a warm-blooded animal cannot be proportional to its body mass (BM), but to its surface area and the heat conductivity to the environment. Assuming a constant density of the animals body it is possible to estimate the ratio of body surface area and body volume being somehow proportional to $BM^{0.67 \text{ to } 1}$. Empirical investigations led to a power factor of about 0.75. So the term $BM^{0.75}$ was introduced and called metabolic body mass (MBM), which is, in fact, proportional to HL within a species or related species. Assuming a proportionality of HL and MBM the heat balance of the body requires a proportionality between EE and MBM too. This, however, introduces a differentiation of indirect calorimetric measurements by body mass. On first hand there is calorimetry on humans and large (farm) animals, often done in relatively large (and convenient) calorimetric chambers with volumes (V) of up to 25 m^3. On the other hand there is indirect calorimetry on small (laboratory) animals, even organ tissue or cell clusters. Small animal calorimetry can perfectly be done in relative small cages with volumes of just a few litres, whereas tissues or cell clusters can be investigated in small ampoules [25].

The body mass of mice, rats, humans and horses varies from about 20 g, 250 g, 75 kg to 1000 kg, repectively. This is about 50,000 times. The typical chamber (cage) volume is somehow related to body mass and has a comparable variation. On the other hand the metabolic body mass varies only between 0.02 $kg^{0.75}$, 0.35 $kg^{0.75}$, 25.5 $kg^{0.75}$ and 118 $kg^{0.75}$ about 3333 times. So does EE, O_2 and the flow rate of the system too. This implements typical time constants between some min in small animal measurements to up to some 5 h in human measurements. So human calorimetrists had to employ equation (17) to improve

the time resolution of their measurements. This in fact increases the requirement to the stability of the gas analysing system.

Other techniques have been developed to avoid these timing-versus-accuracy problems using masks or canopies instead. This is often used for short term measurements or for critically ill persons [26,27]. But wearing such masks or laying under a canopy is not very convenient. It can not be expected from healthy subjects for more than about 8 h. Metabolism is largely controlled by many rhythmic stimuli like daily meals, sleep and even dark-light cycle. This creates the need to perform measurements over very long periods, best at least a full day. There are approaches like the factorial method to employ mask calorimetry for the estimation of the 24 h EE. A full determination of the 24 h EE and its actual rhythmicity however can only be fulfilled with chamber calorimetry.

3.2.3. Equipment

Central elements of an indirect calorimetric system are the air mixing and sampling system and the gas analysers. The gas mixing system has to provide a fast responding and well-mixed atmosphere within the chamber without disturbing the subject by heavy noise or noticeable whiffs. To improve the effect of the mixing system and to reduce the influence of covered volumes in the corners of the chamber, the air inlet and outlet are often made using comb-like structures [14]. These structures are formed from parallel pipes or ducts with many small wholes. The inlet is often distributed on or in the floor, whereas the outlet and sampling system is distributed on the ceiling. Most of the air pumped through this system is probably recycled and just a small part is really exchanged and analysed.

In mask-, canopy- or ventilated hood systems there are small mixing chambers used to average the concentration changes of the expired air, that may occur during the single breaths. They would probably be too fast to be analysable by typical sensors and would give no useful information to the experimentors.

The gas analysers have to be chosen specifically for the type of measurements to be performed. For indirect calorimetry it is sufficient to analyse the respiratory gas for changes in the concentration of oxygen and carbon dioxide. Nevertheless it is often of some interest to analyse for other gases too, like methane, hydrogen, pentane and alcohol. Even the remaining components of air (N_2, Ar, H_2O) are sometimes analysed. Typical oxygen analysers employed in indirect calorimetric systems make use of the temperature dependency of the paramagnetism of oxygen (example: Magnos 4G by Hartmann & Brown or Oxymat 5 by Siemens). The commonly used CO_2-analysers utilise the infrared

absorption of the CO_2-molecule (example: Uras 3G by Hartmann & Braun or Ultramat 5 by Siemens) [28]. For short-term investigations, experimentors and physicians often use complete systems including gas analysers as well as flow meters, humidity detection and a computer to control the system, acquire the data and analyse it. Such systems often utilise the electrochemical characteristic of oxygen. These sensors are less expensive, but need cyclic refreshments within periods of some h or at least days.

Having the need to analyse for more than just oxygen and carbon dioxide it may be useful to employ a multiple gas analysing system, based on a mass spectrometer [14]. These systems can analyse for many components of gases in a wide range of concentrations, enabling the simultaneous analysis of the subject's respiration, gut fermentation processes and alcohol metabolism. These analysers have largely been improved in the last years; as well in their stability and analytical range as in their value-per-cost ratio.

If employing equation (17) to improve the time resolution of large calorimetric chambers it is extremely important to have a gas analysing system producing very stable rather than very accurate signals. Any signal noise and instability would be largely amplified by the first derivation of the signal. A systematic inaccuracy instead could easily be corrected by periodic recalibration and system checks performed within the measurements.

The next very important measure is the gas flow or volume measurement. There have been achieved many improvements in this field too. Standards are still sensors that measure the differential pressure over a long throttle with a laminar gas flow. Other sensors employ small turbines that have their advantages in peak flow measurements. They are often used in mask calorimeters. These two types of flow meters measure the gas volume instead of its mass. Pressure, temperature and humidity of the air also have to be acquired to correct to standard temperature and pressure under dry conditions (STPD) in order to get the amount of gas flown through the chamber.

The most recent types of sensors in this field are mass flow meters or even mass flow controllers (MFC). They utilise the heat transfer capacity of the gas molecules of the air. The heat transport in the gas flow is measured with two consecutive sensors wired in a Wheatstone bridge. The temperature difference between the sensors is proportional to the number of gas molecules having passed the sensors. Although the heat transport capacity is slightly specific for the different gas molecules in air, there is no need to adjust for changes in air composition because these changes are very small. If the gas analysers are not pressure specific it is possible to avoid the (exact) measurement of pressure and temperature of the air.

Temperature measurements have to be done in any case - at least to document the conditions of the experiments performed. There are many types of sensors available; just a simple thermometer would probably not be good enough. Best is a couple of electronic sensors (thermocouples or integrated thermosensors) distributed within the chamber and at gas in- and outlets. This allows to correct the measured air volume to standard conditions and get an idea on how well the air is mixed within the chamber.

Air pressure measurements can be done by any kind of sensors that provide a signal for the data acquisition system. The relative error of pressure sensors is very small because its absolute inaccuracy is related to relatively high absolute measures. There is no need for a very sophisticated instrument - it has just to be recalibrated several times within a year.

Accurate humidity measurements are very expensive, compared with their significance for indirect calorimetry. So some experimentors just do not perform these measurements and precondition the air in case of temperature and humidity. The humidity in the chamber is, as stated before, not easy to measure and even harder to control. This is caused by the large variations of the water vapour production of the subject, especially during different phases of locomotor activity (increased breathing, sweating) and the water storage within the chamber. The water vapour tends to adhere to (and even diffuse into) the inner surface of the chamber and furniture and can not be measured exactly and quickly enough.

Humidity must be measured to document the experimental conditions and may be so to correct the air flow measurements to STPD conditions, if applicable. The significance of errors in humidity measurements on the accuracy of the detection of the gaseous exchange and EE, however, is relatively small.

All these sensors have to be regularly calibrated and checked as specified by the producer. Nevertheless they do drift within relatively small periods of time. Many experimentors have included regular checks and recalibrations into their calorimeter control software to deal with these drifts [12,28-30]. This is especially important for the gas analysing system. There have been developed very sophisticated solutions to recalibrate the gas analysers with calibration gases or burning alcohol or butane. There are even systems that use catalytic oxidation of alcohol to generate calibration gases useful for small animal calorimetry.

The overall performance and accuracy of the system must be checked regularly. This is commonly be done by alcohol combustion [14] or injection of a well-known mixture of nitrogen and carbon dioxide [13,30]. Both techniques have

their advantages and disadvantages. In the case of alcohol combustion it is important to ensure that the combustion is complete and no alcohol has left the combustion system without being oxidised. In human or large animal calorimetry a simple alcohol lamp is used as combustion system. Calorimetry on small laboratory animals lacks this opportunity, because the smallest possible open flame is consuming much more oxygen than the typical animals. Here are - if at all- catalytic alcohol oxidation methods used.

The RQ of alcohol is 0.667 and outside the range of the oxidation of the substrates being burned in living beings. On the other hand this type of calibration system is easy to operate, the amount of alcohol processed can easily be assessed simply by weighing of the lamp or the alcohol tank. This calibration system can be used for both direct and indirect calorimeters [14]. The insertion of a mixture of CO_2 and N_2 (which 'dilutes' the other gases and mainly O_2 in the chamber) instead is harder to process; the amount of the virtual oxygen consumption is more difficult to determine. But it is possible to 'generate' every needed value of RQ.

3.2.4. Timing problems

Utilising equation (17), the time resolution of gaseous exchange measurements can be improved to some min. In the Weir-equation (16) on the other hand the nitrogen excretion rate is also needed to calculate EE. Although the importance of the N_{ex}-term in the Weir-equation is only about 1 % of EE, it is important for the determination of the substrate oxidation rates in equation (14) and (15).

In normal calorimetric measurements, N_{ex} is usually determined by collecting urine and measuring its nitrogen content. Urine collection can not be done properly for periods shorter than about 6 - 8 h because of the urea pools and the storage of urine in the bladder. So the sampled nitrogen has to be distributed over the sampling period. This is usually done by two methods, assuming either a constant protein oxidation rate over time or a constant contribution of protein to energy supply. Both methods can be criticised, but give acceptable results under normal conditions. Problems arise using indirect calorimetry in answering the question whether there is a significant lipogenesis from CHO in humans. This would require the NPRQ rising above 1.0, which usually happens rarely, just for a few measured cycles and just slightly above 1.0. So it could be held to be an error in measurement or not, depending on a qualified distribution of nitrogen on the measured cycles.

3.3. Applications

3.3.1. Experimental Scheduling

Living beings are influenced by the various rhythms of their surrounding environment. The most important ones affecting energy metabolism are the daily change of light and darkness, the working periods and the meals usually taken several times a day. So the energy expenditure varies widely within a day, making just short 'snapshots' almost useless (Figure 2).

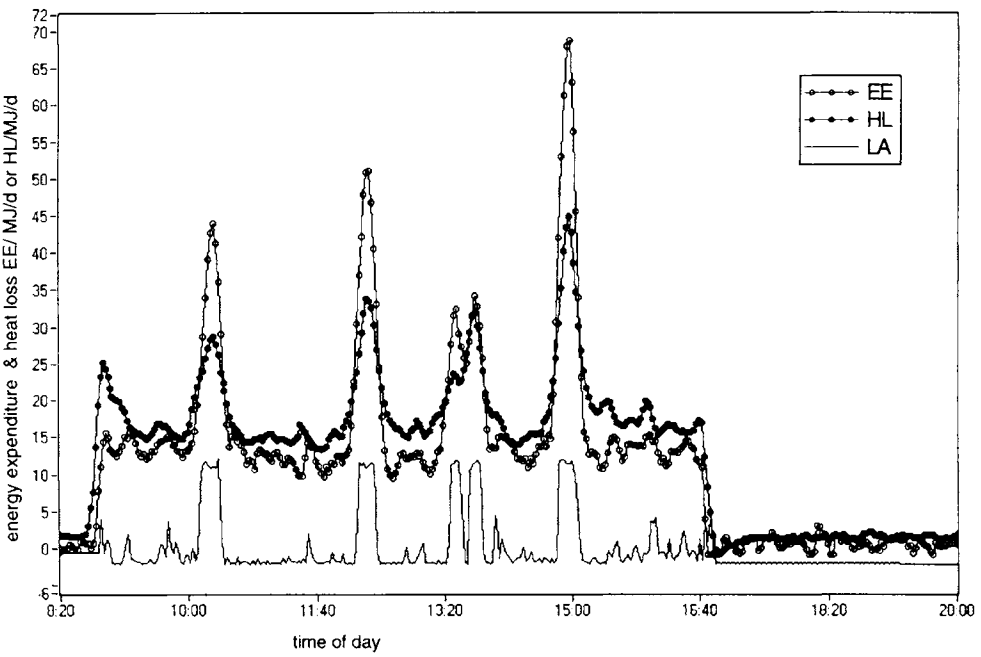

Figure 1: Example of simultaneous measurements of HL and EE of a human subject

Depending on the objective of a study the time and duration of calorimetric measurements have to be defined; typical measurements in calorimetric chambers are about a full day or even several full days. Experimentors often use comparative methods to measure physiological, pharmacological or dietetic values.

Daily energy expenditure can be separated into the basal metabolic rate (BMR), the postprandial thermogenesis (ppTh), also called dietary induced thermogenesis (DIT) and the energy needed for locomotor activity (LA). Locomotor

activity can change very fast and the respective change in EE can be measured with a systematic delay of typically some min, depending on the methods. The value of energy needed for heavy work load can reach up to 5 times the BMR. Reactions on diet intake (ppTh) occur within some ten min and can be assessed with the same systematic delay. The duration of the postprandial phase lasts for up to several h, depending on the kind and amount of food eaten. Typical experimental schedules for the measurement of ppTh last for 6 to 8 h. The respective value of ppTh can reach up to about 30 % of BMR at peak level - it is typically about 15 % of energy intake of a day.

In order to get reasonable results a specific experimental schedule has to be devised, including periods to settle down after entering the chamber and relax before leaving it finally. The activity of the subjects in the chamber needs to be controlled and measured very tightly to specify the amount of energy that was used for locomotor activity. Typical LA-sensors can not detect the work performed while moving something in the chamber, but detect the movement. There can be heavy misinterpretations, especially while reading (and moving) newspapers or making the bed. So the activity needs to be exactly scheduled to admit comparisons. The same applies for the amount of food and the time it is eaten in the chamber. Due to the impact of activity and especially dietary energy intake both activities need to be controlled in a period of about 12 h before entering the chamber for food intake and at least 30 min for locomotor activity. A controlled pre- and post-measurement period is especially important in direct calorimetry because of the heat storage in the subject's body and in the chamber. This stored heat is not easy to estimate. In order to enable comparison of the results standardised pre-measurement conditions have to be enforced. This is to ensure comparable amounts of heat being stored in the subject's body.

3.3.2. Investigating Metabolism

Calorimetry together with special dietary regimes, experimental (timing) schedules and treatments can be used to obtain insight into specific parts of the metabolism. Using indirect calorimetry this can be expanded to more specific insights into substrate metabolism.

Acheson et al. [31] performed an experiment to answer the question, if a net de-novo lipogenesis is of importance in humans. They preloaded the body glycogen stores of their subjects by feeding them for 3 to 6 days with either a high-fat, mixed or high-CHO diet. In an indirect calorimetric experiment the subjects were given 250 g Dextrin Maltose at 1 h and twice 25 g at 3 and 6 h after the start of measurement. The CHO oxidation as well as its conversion to body fat was much lower in the high-fat group than in the others. Most of the subjects of

this group had no net lipogenesis at all, their NPRQ remained below 1.000. The other groups had quite well filled stores of glycogen at the beginning of the measurements. This resulted in an excess of CHO for the metabolism. The high-CHO group reached the level of NPRQ $\geq$ 1.000 just after the intake of the second dose of CHO, while the mixed-diet group needed the third dose to cross that line significantly.

Aust et al. [32] investigated the available energy and the absorption time of different kinds of different dietary fibre. They fed adult rats with their standard diet for about 4 weeks. Every fifth day the rats were kept hungry for 14 h to empty their glycogen stores. The rats were than given a basic diet supplying only about 50 % of their energy requirements. As an addition, they got another about 35 % of their energy requirements by the test substance (dietary fibre). The increase of net CHO oxidation compared to that of only the basic supply was interpreted to be the result of the added test substance, because of the limited energy supply and the pre-deflated glycogen stores. Having given starch as test diet the increases of CHO oxidation of the other test diets could be compared to that of starch. This resulted in utilisation factors quite similar to that found in long lasting feeding experiments. The time course of RQ changed significantly between the different fibres, which was interpreted as the result of different absorption and transfer times.

The overall energy utilisation factor of rats was estimated by Frenz et al. [33]. They performed indirect calorimetry on rats for 3 or 4 consecutive days with different levels of energy intake (EI). The increase in energy balance (EI - EE) versus EI was interpreted as the energy utilisation factor. It was determined to be between 75 to 90 % for different protein enriched diets. The coefficients of determination (CD) of the regression between energy balance and energy intake were found to be surprisingly high at levels of 99 to 100 % [29].

The same method could also be applied to the net substrate oxidation rates. Due to the - at least partial - mutual exchangeability of the substrates as source of energy, this approach was not fully functional for the substrates. In [29] a diet containing 37 % of protein, 4 % of fat and 51 % of CHO (The remainder consists of dietary fiber, water, minerals, etc.) was used. In this case by increasing the protein intake by 1 g the CHO intake was automatically increased by 1.4 g. And in energy metabolism CHO is preferred, as long as there is enough CHO from both intake and body stores available. So the relation of the substrates as fuel differed at different levels of diet intake. This resulted in a fat utilisation factor of up to 800 % and CHO utilisation factors of as low as 33 %. The CD's, however, remained at levels of 92 - 99 %. Only for carbohydrate and

with an incomplete supply this method resulted in utilisation factors and coefficients of determination, that could be interpreted physiologically relevant.

The degree of saturation of the body glycogen stores may be an important modulator of appetite because of its very limited storage capacity for it. Indirect calorimetry is the only non invasive method to assess the glycogen status in man. Murgatroyd et al. [34] published a method to measure the net carbohydrate flux from liver and muscle. Subjects had been given a standard diet of one third of their energy requirement before entering a calorimetric chamber at 20:00 h. Calorimetry was performed until the end of the experimental schedule next day. The subjects slept through the night. Their CHO oxidation was assumed to be primarily derived from the meal directly in the first 4 h after the meal and from hepatic stores thereafter. This assumption was made because of the relative inactiveness of the subjects. The CHO oxidation in this part of the night was remarkably constant at all subjects.

On the next day they started an alternated cycle of 30 min working on a bicycle ergometer at 45 % of their maximal oxygen uptake capacity and 30 min of rest. This cycle was repeated until the subjects felt complete exhaustion. This activity schedule was assumed to deplete the muscle glycogen. Their CHO oxidation decreased from about 80 g/h at the first exercise cycle to about 20 g/h at the last one. At the same time the fat oxidation at active times doubled. Fitting the CHO depletion data versus time to a quadratic regression resulted in excellent regression coefficients. This regression equation was used to extrapolate to the point at which the glycogen stores would have been completely emptied. So the total glycogen storage capacity could be estimated by a simple integration of the CHO oxidation. The results fitted very well with others derived from biopsies or blood glucose measurements, although the method assessed the total net substrate oxidation rather that of single organs.

In almost every calorimetric study the subjects sit most of the time in the chamber. Even in a normal western population people sit most of their active time in the day. But 'active' sitting (reading, writing, working on a PC, etc.) is energetically different from 'passive' sitting (relaxing, 'dreaming' with open eyes). In a direct calorimetry study performed by Kurzer [35], this difference was measured. Subjects had a standardised diet at morning and entered the chamber 1 h later. After another 1 h of settling down and reading books they started a 3-h schedule of activity or inactivity. The first and third hour the subjects had been asked to sit as relaxed as possible, not to read or do gross movements. In the second hour the subject remained sitting, but performed a standardised activity schedule including working with dictionaries and performing arm and legs stretching. This hour was chosen to approximate the maximum

activity of subjects in calorimeter studies. The total heat loss of the subjects changed from about 1.1 x BMR while sitting passive to 1.46 x BMR while sitting active. In calorimetric studies where the subjects spent 50 % of their time sitting this difference could lead to a difference in total EE of up to 15 %. So the sitting behaviour must be controlled in comparative calorimetric studies.

3.4. Comparisons

Both methods, direct and indirect calorimetry have their own advantages and disadvantages. Direct calorimetry does not rely on assumptions about the metabolism. It can react as quickly as (or even quicker than) indirect calorimetry. It is necessary to correct for (or at least take into account) the heat storage and the active heat transport and heat regulation systems of the subjects. Corrections have to be made for heat transfer with food, drink, excreta, light and electrical devices. Direct calorimetry provides (only) information on heat loss and heat production; and therefore on energy metabolism. It does not provide information about the source of energy, the main substrates being burned. Direct calorimeters are more complicated and probably more expensive both to establish and to operate. This holds true at least for calorimetric chambers as usually used for nutritional and metabolic research. They can not easily be combined with other (invasive) research methods like blood sampling or infusions.

Indirect calorimeters on the other hand rely on the main assumptions of complete oxidation of the main substrates and the intermediate pools maintaining constant. This may not always be true, especially for short-term measurements or in acute reaction of external influences (like leaps in locomotor activity - 'escape' -reactions). This has to be kept this in mind while interpreting the results. The main advantage of indirect against direct calorimetry is the provision of information on the burned substrates and therefore a deeper insight into the metabolism of the subject. The method itself is quite simple, but accurate and precise. It is easier to establish and cheaper to operate than direct calorimetry. It can easier be combined with other physiologic methods like blood drawing, infusions or microdialysis. There is sufficient expertise available from researchers world-wide to provide advice how to construct indirect calorimetric chambers and what to avoid. In the most recent survey [28] there have been given 16 world-wide locations operating indirect calorimetric chambers, but only 5 facilities operating direct chambers. At least two of them are combined direct and indirect chambers. The system in Beltsville [14] is one of them. Due to the physiological and nutritional questions dealt with in this group the calorimeter is in fact much more often used just as indirect chamber than as direct or combined one.

Some parameters of direct and indirect chambers are given in Table 2 to simplify a comparison of both methods.

Table 2: Advantages, disadvantages and common features of direct and indirect calorimetry

	indirect calorimetry	direct calorimetry
advantages	• detects substrate oxidation • relatively simple in principle • much world-wide expertise	• detects heat loss directly • less expertise / less facilities
disadvantages	• The main assumptions of complete oxidation may not always be true • complicated to maintain and operate	• complicated and sophisticated to construct, maintain and operate • HL is not always balanced by heat production; HL(chamber) not always equal to HL(subject) • no information on the substrate oxidation is provided
common features	• accurate precise and fast responding methods, but require extensive electronic, computing and mathematical skills to operate • best possible sensor systems required • chambers provide a good environment for strictly controlled studies, but they are an artificial environment • 24h-supervision for subjects under measurement is required • It is more cost effective to run two to four chambers simultaneously than just a single one. • A complete system with chamber, analysis and computing systems, housing and feeding for the subjects and some additional measurements costs about a six-digit number of US-$.	

3.5. Locomotor Activity

The chemical energy in the diet is distributed into different pools. Some energy is maintained in the faeces or is used to synthesise urea. The remaining metaboliseable energy is used for three purposes. Some energy is used to maintain the dynamic equilibrium of the subject's body and to perform all the

necessary transformations (basal metabolic rate - BMR). These processes are ineffective, there is some residual energy, which is transformed into heat. This heat is under normal situations sufficient to maintain the needed body temperature, but there are sometimes extra heat producing mechanisms like cold induced thermogenesis of rodents or shivering. Other energy is used in the muscles to perform mechanical work, even to move the body or parts of it. The remaining energy, which is the balance between energy intake and EE, can be used for growth (increase in body mass) or production of milk, eggs, wool, foetuses, etc.. So locomotor activity is an important factor in balancing energy metabolism and its value has to be estimated. It is even used for a rough estimation of energy expenditure by heart rate measurements [10].

There have been several approaches to estimate LA while performing calorimetry or independently from this method. A survey of the different methods used in this area has been given by Grobbecker [36]. The method commonly used to measure locomotor activity of human subjects employs infrared or microwave motion detectors. Also in use have been motion detectors employing the Doppler effect of ultrasound. There have also been older reports of animal cages placed or hanging on simple switches. In other cases cages have been placed in the magnetic field of a coil or in the electric field of a flat capacitor. More modern approaches use video or still video cameras, often combined with some special mark sign on the animals. The positions of the animal or that sign at given times and the distances between them are detected. A very sophisticated solution was presented by Aust et al. [37]. The bottom of a cage was placed on three electronic weight sensors. A computer calculated the actual position of the rat's centre of gravity at a frequency of 60 Hz. The position changes have been found being proportional to the work that was performed. This approach could easily be used in human chambers too. Another solution [33] was found utilising the distinctive rhythmicity of rat behaviour, that had well-defined periods of activity and rest. The good timing resolution of the calorimetric system enabled detection of local minima in the time course of EE within periods of 120 min, which represented a level of EE while the rat was at rest. A smooth connection of these local minima by moving averages within the same period separated the energy used within the active phase from the remaining energy (Figure 3).

The industrial motion detectors commonly used in human experiments are often modified to fit this application. This alteration decreases the threshold of motions being detectable to assess even small movements. Standard detectors activate a switch for a given period of about some seconds to minutes with every motion they have detected. This period is dramatically decreased to parts

of a second. Thus short movements result in just one activation, but longer movements in multiple ones. The number of activations within a given measurement period is counted and accounted for as being proportional to the locomotor activity of the subject in this period.

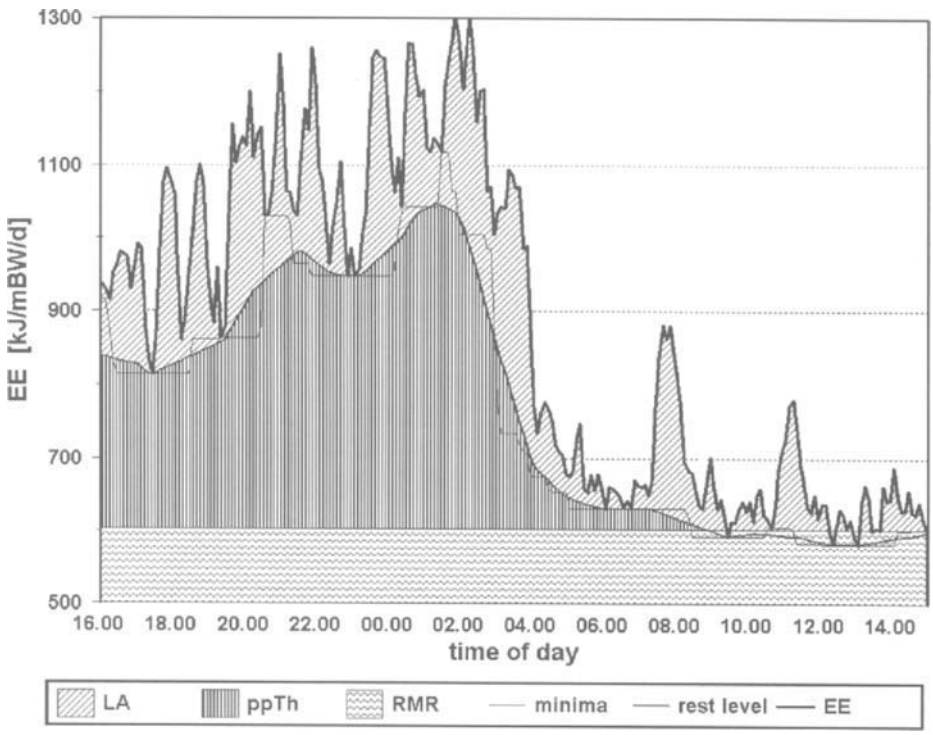

Figure 3: Separation of LA from EE utilising the rhythmicity of rats

The locomotor activity measured by such motion detectors is not necessarily proportional to the energy used for this motion. This energy depends also on the body mass of the subject and, for example, on the work load (tension) of a bicycle ergometer. Nevertheless there is a solution to estimate this proportionality, if the time resolution of the calorimetric system is better than the resting periods between different types of activity. This is done by simply detecting the increase of both EE and LA from period to period. This results at least in an estimation of the portion of EE used for LA. Extrapolation to a value of zero LA results in a separation of the overall EE into LA and the remaining energy

without activity (EE-LA). If the subjects reach a postabsorptive status within the measurement period this remaining energy expenditure can probably be used to separate BMR and ppTh from each other. This approach assumes that the postabsorptive phase of a meal is limited and that it takes some time of hunger to change metabolism into a hunger status with decreased EE and other metabolic changes. So there is a period, where the remaining energy expenditure represents the basal metabolic rate BMR. It is just necessary to include this period in the measurement period.

Both values, BMR and ppTh, have been found to be good indicators for the effectiveness of energy metabolism and possible reasons for the development of obesity.

3.6. Other Methods to assess EE

There are many other methods to estimate a value for the energy metabolism of living beings. They are somehow related to metabolites themselves or to the balance of body mass, body energy, body water or other components of the body.

The *balance methods* have to deal with the different pools of metabolites in the body, which cannot easily be detected. They limit the accuracy of estimation of EE or require relatively long lasting measurements. On the other hand they rely on the measurement of energy or food *intake* instead of energy expenditure and heat production or heat loss. Every food intake can be accounted for as energy and matter. Parts of this food is metabolised and used to generate energy for the body. Unused energy has to be stored within the body while insufficient energy supply has to be met by endogenous resources. This results in changing body contents of the main substrates. Such changes can be detected as alterations in the body composition and the overall body mass, if they exceed the daily variations.

As an example, an adult male weighing 80 kg may have an EE of 12 MJ/d. A positive balance of just 5 % is about 650 kJ/d. This energy can be stored as glycogen or fat, which is about 41 g CHO or 16 g fat. Glycogen needs at least double the weight of water to be storable, resulting in about 120 g/d. The glycogen storage capacity of mammals is limited to about the normal CHO intake of a day. In this example its capacity is about 1 kg. The day-to-day variation of body weight of a person is up to 1.5 %, which is also up to 1.2 kg in this example. So a period of at least 10 to 30 days of energy balancing with an average energy excess of 5 % or some parallel measurements are needed to get

reliable results. So exact energy intake measurements often become very expensive in time, costs and cooperation of the subjects.

Glycogen is the only significant kind of carbohydrates that can be stored in the body. The storage capacity for it is limited at about 1 % of the body mass. Adults do not change their protein content very fast, at least under normal conditions. Thus, almost all excess food energy in long term feeding and balancing experiments must be stored as fat in the body and almost all the missing food energy must be supplied from endogenous fat. But fat is a very effective way to store energy per mass, which results in very small changes in body mass at usual energy imbalances.

The typical metabolism in animals is aerobic[1], although there are many anaerobic reactions in the metabolic pathway. Oxygen and carbon dioxide as well as many other reagents have to be transported by the circulating blood, which is pumped by the heart. So the *heart beat rate* (HR) can be a good measure of metabolic activity [9,10]. Spurr found a high determination (CD ~ 0.98) of oxygen consumption by the heart rate of subjects at different levels of locomotor activity. The determination was much weaker for subjects at resting status (CD ~ 0.88). The actual HR is also determined by many other circumstances like age, fitness, ambient temperature, postprandial status, etc. It can, however, be used to calculate EE after some individual calibration, if HR is recorded in short intervals. This enables a discrimination between phases of sleep, rest and activity, which have different relations between HR and EE.

Modern equipment to measure HR limit the impairment to the subject. There are electrocardiograph tape recorders or telemetry systems to store the results of measurements. Finger clips with optical sensors for the blood pulse and some kinds of cuffs (like used to monitor the blood pressure) may be used to sense the heart rate over long periods. The individual relation between heart rate and EE measurements can be calibrated in whole body calorimeters as well as with mask calorimeters, performing different levels of activity. This calibration can later be used to estimate EE of free living subjects and/or over relatively long periods (up to some days).

There may be temporarily phases of anaerobic reactions not being fully compensated by aerobic ones. These phases have to be quite short because of the very limited tolerance of the body to the reaction products of anaerobic metabolism (lactic acid). This type of reaction has to be compensated later to regain normal balanced conditions. Indirect calorimetry would, if at all, just see short changes in RQ and EE. Heart beat measurements would see it as a peak of energy metabolism.

Another commonly used method to determine EE of free living subjects utilises doubly labelled water ($^2H_2{}^{18}O$) [4-8]. Although the term doubly labelled water is not correct, it is commonly used. It denominates water consisting of a known portion of molecules where at least one of the hydrogen atoms of water is replaced by deuterium and/or the oxygen is replaced by its stable isotope ^{18}O. Most of the water molecules are - if at all - just single labelled. But both labels are available in the water probes.

A well-determined amount of this chemically pure and simple water is drunk and subsequently used as a reagent in metabolism. The deuterium labels only the water pool of the body, whereas the oxygen isotope labels both the water and the bicarbonate pools. The term 'labels' denominates the fact that some of the isotopes in the body reaction pools are exchanged by the heavier ones coming from the doubly labelled water. Both pools are exchanged with normal water during time and the labelling is diluted and gradually removed again from the body. The disappearance rate of labelled hydrogen in urine provides a measure of the water turnover rate in the body. The disappearance rate of ^{18}O is measured in urine and/or in the carbon dioxide compartment of the respiratory gases. Both values are detected by isotope ratio mass spectrometry (IRMS), coupled with some other methods (catalytic reduction of water on zinc or equilibration with pure oxygen over the water probe) to transfer the metabolites into gaseous state. In case of deuterium the water probe is equilibrated with normal hydrogen, which is analysed for its isotope ratio. The isotope ratio of the stable isotope of oxygen is usually determined in carbon dioxide. The disappearance rates of both heavier isotopes from the body pools provide a measure of both the water- and the bicarbonate turnover. The difference between both disappearance rates is interpreted as bicarbonate turnover, which can be transferred into EE using classical indirect calorimetric formulas. One of the most important limitations of this method is in fact this transformation. As shown in section 3.2.1, the determination of EE by O_2 is about 80 %, leaving just about 18 % to CO_2. To calculate EE from CO_2 a mean value of RQ for the subjects has to be assumed. This RQ must be chosen very carefully depending on the type of diet consumed in the last days before measurement and the amount of diet compared to the energy requirement during the measurement. The International Dietary Consultance Group (IDECG) has specified default values [44]. These are used to standardise the doubly labelled water method and to establish the comparability of the results. For western diets a typical RQ of 0.85 was chosen.

The biological half-lives of the oxygen and hydrogen isotopes in the body are about 3 to 8 days. So the probes have to be taken daily for 7 to 14 days, depending on the metabolic activity of the subject. The subjects are not affected at all,

they just have to provide their urine sample, in the beginning of a measurement twice a day, later once daily or even less frequently. The probes can be analysed within some days after sampling, because the water as well as the isotopes are stable. So this method is very useful for field studies under free living conditions. On the other hand it integrates over periods of about two days or more, thus making the method not very time specific.

The indirect calorimetry formulas require two measures to calculate EE and RQ. So the doubly labelled water method relies on some extra detections of the RQ, the oxygen consumption or, as usual, some assumptions on the mean RQ during the measurements. Besides the standard values provided from the IDECG, very satisfactory assumptions can be made by taking into account the food composition during the measuring period and changes in the fat content of the body [38].

Labelled bicarbonate on its own can be used to assess EE instead of doubly labelled water. This technique is valuable for short intervals of about 1-3 days because of the shorter biological half life of bicarbonate compared with water. It is applicable to humans only, if stable marked bicarbonate ($NaH^{13}CO_3$) is used. This substance is less expensive than doubly labelled water, but relies like DLW on the quite expensive technology of IRMS. The bicarbonate is constantly infused and will reach rapidly an equilibrium with the CO_2-pool of the subject's body. CO_2-production will dilute this pool. The CO_2 production rate can be calculated from the variations in the dilution of labelled CO_2 and the infusion rate. The method assumes no isotope exchange or fixation and a constant pool of bicarbonate. It is not as accurate as the doubly labelled water method; Elia [39] found individual accuracies of up to ± 6%, validated against whole body calorimetry in a calorimetric chamber.

4. WHOLE BODY CALORIMETRY IN BIOLOGICAL AND NUTRITIONAL RESEARCH

Energy exchange and transformation are the driving force for all processes. This, of course, holds true for living beings too. Investigating them ultimately raises questions of energy supply, requirement and balance. An adequate food energy supply is very important for animals as well as humans to avoid under or overnutrition. Permanent or long lasting undernutrition severely damages the subject. Overnutrition on the other hand leads to the increase in body weight due to the accumulation of body fat. Overweight people (and animals too) tend to suffer from various diseases like hypertension and cardiovascular problems.

This status is linked with a higher risk of other illnesses and longer lasting periods of being ill with more severe progression. Obese people have a higher mortality risk compared with normal weight subjects.

A balanced diet constitutes not only of carbohydrates, fat and protein, but of water, dietary fibre, vitamins, minerals and micronutrients too. The demand of these diet components depends on various conditions like age and growth status, locomotor activity (work load), environmental temperature and probably on the season. The determination of the requirements of these nutrients under different conditions gives very important information on how to provide a balanced diet but to avoid overnutrition. Whole body calorimetry is probably the most accurate and so the most important method both to estimate substrate and energy requirements and to calibrate other alternative methods to assess the energy metabolism like long-term heart rate measurements or the isotope dilution methods.

4.1. Energy Balance and Components

Living beings have to maintain an energy balance: energy intake must balance losses and energy flows to and from internal stores. A balance must also be maintained for the three main substrates used as fuel components, viz. carbohydrate, protein and fat. But for the substrates there are metabolic transformations of some of them to others, if the internal storage capacity is over- or underrun by demand and supply. Nevertheless these transformations are detected by indirect calorimetry, at least as oxidation of the original substrate. If for instance protein is broken down to generate glucose as fuel for the brain, this is recognised by calorimetry as protein oxidation. On the other hand if CHO was used to synthesise fatty acids, which were stored in the adipose tissue, this is recognised as a negative fat oxidation.

4.1.1. Energy Sinks and Energy Intake

Energy sinks occur in the form of heat loss, mechanical work performed and biological 'production'. The latter term describes growth (increase in body size and - content) as well as the replacements of body parts lost during day-to-day live (hair, nail, skin and gut cells and enzymes lost). It also involves foetuses and maternal milk. To clarify the different energy sinks and not to mix possible different pathways of substrates at different metabolic situations the energy losses are usually divided into:

- basal metabolic rate: Energy needed to maintain basal functionality of the body (blood circulation and breathing under basal conditions, thermoregulation, unconscious

movements, renewal of body parts like skin and mucous membranes, nail and hair growth, etc.).

- locomotor activity: Energy needed for physical work at any activity level above rest (any conscious moves, physical and mental work, etc.).
- postprandial thermogenesis: Any increase in energy expenditure related to and occurring after an intake of food. This may be caused by the mechanical work of processing the food (biting, transferring through the digestive tract) and transferring the digested food components into the body stores.
- growth and production: Increase in body mass and energy content of the body and energy spent to produce things like milk, eggs, foetuses and wool.

Energy intake on the other hand is the energy contained in the food eaten in the period of interest. It involves not only the energy in solid food, but also the hidden energy and substrates in soft drinks and alcoholic beverages.

4.1.2. Calorimetric Results - Extrapolation to Free Living Conditions

Whole body calorimetry provides a measure of the subject's total energy expenditure within the measured period, but in an artificial environment. The calorimeter is usually coupled with instruments to estimate locomotor activity. Setting up a useful activity schedule the measurements include a period of rest, resulting in a value of the basal metabolic rate. The energy balance is calculated by carefully taking into account every piece of food entering and every product leaving the chamber. Living in the calorimeter is somehow artificial. Living beings behave quite different as compared to their common living conditions. Many studies showed, that subjects tend to underreport their previous energy intake during normal live. They also may reduce their food intake while living in the chamber. The capability to do sports is very limited within the calorimeter. Activity on a bicycle ergometer, stepper or other activity devices is usually scheduled to compensate for this. But then untrained subjects may have higher than normal activity levels while trained ones comparatively lack activity. All these problems raise questions on the extrapolation of calorimetric results to free living conditions. There is however no better and more accurate method to investigate energy expenditure and energy requirements than whole body calorimetry. There are just some additional methods like questionnaires, heart rate monitoring or the doubly labelled water method. These can be calibrated by whole body calorimetry and then used under free living conditions.

4.1.3. Substrate Balance

Energy balance is closely connected to the substrate balance of the subject's body. Fat, CHO and protein intake in a given period have to balance the respective oxidation minus storage. Some side conditions have to be fulfilled too: Glycogen as the only storable form of CHO is stored in company with at least the same amount of water. A significant glycogen storage can easily be detected as body mass increase. Protein balance can easily be measured as nitrogen balance; this measurement is independent from gaseous exchange measurements. The most problematic substrate balance to investigate is that of fat because of the high energy content per mass of it and the typical slow changes in fat stores. Typical daily changes in the fat stores are much lower than the daily variation of water content of the body.

There are some transformations between the substrates in the body. Carbohydrates are hydrolysed to glucose and than stored as glycogen in the skeleton muscles and the liver. Since glycogen storage capacity is very limited, an oversupply of carbohydrates will soon initiate a transformation of carbohydrates to fatty acids (lipogenesis). Fat can be stored in nearly unlimited amounts in the body's adipose tissue. Under normal dietary circumstances, however, lipogenesis is not very significant in humans. Besides the regulation of CHO and fat turnover there is also a considerable turnover of proteins and amino acids. The degree of it depends on the energy and food supply and the status of the subject's body, whether it is growing, is pregnant or lactating, is ill or is in a normal condition. Amino acids can also be broken down to generate glucose, if there is an insufficient supply of it. Glucose is essential for the energy supply of the brain. Fat from the food is mainly first stored in the adipose tissue, until there is a higher demand of energy. During the day the glycogen stores are partially emptied and the fatty acids are activated again. In the case of higher energy demand there is an extra activation of fatty acids to be used as the main energy source for the body, except for the brain. The adipose tissue in humans is usually be filled mostly by fatty acids derived from the fat content of the food. Many animals, especially those living in environments with very seasonal food supply, do generate a huge fat depot to survive the poor season.

Lipogenesis from carbohydrates in humans is not a very common metabolic situation. It would require observed RQ-values to be higher than 1. This is sometimes seen, but almost always within the range between 1.00 and 1.05. This could also be interpreted as measurement errors or noisy results. Lipogenesis would require a temporary oversupply of carbohydrates, that could not be absorbed into the glycogen stores. This situation usually happens within some h after a big meal. It also requires a relatively low energy expenditure like in

resting periods. A very stable calorimetric system with a high time resolution is needed to detect such situations by indirect calorimetry.

4.2. Methods to Assess Energy Balance Components

Energy intake and energy expenditure of living beings are under normal conditions in a very good regulated balance. Experimentors interested in this area are sitting 'between the chairs'. They can either study subjects under 'normal' free living conditions or those undergoing standardised methods, probably in artificial environments. The first will provide more applicable results - the latter enables comparison with results from other groups.

4.2.1. Long-term Balancing

There are many different approaches to determine the components of energy (food) intake and energy expenditure (substrate oxidation). One approach is to balance food intake and to measure the body mass of the subject over long periods. This is a very time consuming type of experiment. It needs a great effort and accuracy in weighing the food supplied to and returned from the subjects. The subjects need good instructions and a good will for cooperation. There may be some influence on the results coming from a different food composition of the supplied food compared with the typical diet of the subjects.

Another approach is to fill in a dietary diary and/or some guided questionnaires. This would eliminate possible errors induced by the standardised diet supplied by the lab, but would introduce systematic errors resulting from misreporting by the subjects.

Long term recording of body weight and possibly body composition would result in data for the substrate flow to or from body stores. The dietary food intake can be assessed by questionnaires or prediction formulas, provided by earlier measurements. So energy expenditure and substrate oxidation rates can be calculated from energy and substrates balances. All these approaches would not need calorimetry at all; it could however be used to verify some of the results of these methods. Body composition can be assessed by various established methods like dual energy X-ray analysis (DEXA), skin fold measurements, underwater weighing and body impedance measurements.

4.2.2. Calorimetric Detection of BMR and ppTh

The basal metabolic rate is best determined by calorimetric methods. There have been used two different approaches to measure BMR, depending on the available instruments. In every case the subjects are instructed or enforced not to eat overnight. In case of a canopy or mask system the subjects are connected

to the system and are required to relax and rest for at least 30 min. Then energy expenditure is measured in a period of 30 min to 2 h, while the subjects are laying awake on a bed or sitting relaxed on a chair. If a calorimetric chamber is used the measurement of BMR is usually scheduled after a nights sleep just after the wake-up call, but before getting up.

A comparable method is used to measure postprandial thermogenesis (also called 'thermic effect of food' or 'dietary induced thermogenesis' - DIT). The subjects are prepared as mentioned above, but given a standardised test diet. Energy expenditure is measured over a much longer period, usually about 6 to 8 h, depending on the amount and composition of the test diet. To enable comparison between the results of different labs' these measurements have often been performed with about 1 MJ of glucose or casein as test diet. Normal mixed diets however would result in more applicable numbers. In calorimetric systems employing masks or canopy's the measurements of BMR and ppTh are often coupled to reduce the effort both for experimentors and subjects. They measure the BMR first, followed by giving the test diet and then assessing ppTh. In calorimetric chambers the schedule is often switched performing the measurements of ppTh first after some settling down in the chamber. BMR is commonly the last measurement performed just before the release of the subjects from the chamber.

Subjects not explicitly enforced to rest and relax within the measurement of ppTh do perform some locomotor activity. Even instructed subjects have considerable difficulties to stay relaxed but awake for periods of 6 to 8 h without performing some physical workout. So there is another approach in which it is assumed that BMR and the uncontrolled locomotor activity of subjects are comparable in days with or without food. The ppTh is then calculated simply from the difference of EE on a fed and an unfed day.

4.2.3. Detection of LA

It is hard to detect the energy used for locomotor activity. The typical method to determine LA is to measure a number proportional to the physical activity. This is usually be done by motion detectors, step counters or other activity monitors. The results however are values for the activity of the subject, not of the work performed. A typical known problematic situation using motion detectors is reading newspapers or making the bed. These activities are connected with large movements of lightweight objects, which need only marginal work to perform. The sensors however detect large movements. Other problems are known using step counters, which would not detect work performed sitting. So these measurements have to be calibrated against EE by some standard activity

schedules containing a typical mix of activities. Doing these calibrations individually would considerably increase the effort for the experimentors. Calibrating globally for a given population would ignore possible individual differences in effectivity of moving or in moved body masses. For example a step could be performed in a wide, fast and active or a small, slow and tired way and would be counted as a single step. But both variants would need a considerable different amount of energy.

An interesting approach to determine the energy used for locomotor activity of rats was given in ref. [33]. Those rats had a distinctive rhythmicity with at least one activity peak and one rest within any given period of between 98 and 112 min. Detecting the moving temporary minima of EE within a period of 2 h resulted in the actual energy expenditure at rest (EE - LA). These local minima have been connected by a moving average algorithm. This resulted in an assumption of the separation of the energy used for locomotor activity from EE. The remaining part of energy consists only of BMR and ppTh. Humans however may not show this rhythmic behaviour. But they may be forced into a given activity schedule while being measured in the calorimetric chamber. The data received from the motion detectors could be used to detect periods without locomotor activity. Connecting the values of EE at these periods by an assumed function (the simplest function would be a straight line) would result in an estimation of the energy used for locomotor activity. The differences between the levels of EE with and without activity can be used to calculate a calibration curve. The slope of energy increase versus activity increase could possibly be used to differentiate between the different types of activity (reading a newspaper should have a distinguishable lower slope than riding a bicycle ergometer).

Some empirically interconnections have been found between locomotor activity and energy expenditure in free living subjects of a given lifestyle. But these connections are too weak to be used in calorimetric experiments. They are often used in balanced food intake experiments or studies performed utilising the doubly labelled water method.

4.3. Energy utilisation

Energy utilisation is of interest in nutrition as well as in medicine and physiology. It determines the individual energy requirements and the availability and demand of different kinds of food. Usage of indigestible or partially digestible carbohydrates (dietary fibre) may become a method to reduce the amount of energy intake in the western hemisphere. An increased intake in dietary fiber would also improve the function of the digestive tract and its health. This may reduce the social problems related to obesity and other diseases as well as

individual problems of obese people. Energy utilisation is also important for balancing energy in situations with high energy requirements like sports or military training.

Evaluation of energy utilisation requires the measurements of both energy intake and energy balance. The latter could be determined by measuring the retained energy. This is related with lots of problems, which have been described before. It is much easier to use calorimetry for the determination of the energy balance by measuring energy intake and energy expenditure. This could be done at different levels of energy intake to calculate a linear regression of energy balance versus energy intake. This method [33] was performed on 44 growing rats, that have been divided into 4 different dietary groups. All the rats had been given 4 individual levels of energy intake (about 0,75 %, 100 % and 1 25 % of the individual energy requirement). The individual coefficients of determination of the mentioned regression have been found extremely high at 99.5 to 100 % [29] (Figure 4). The slopes of the individual regressions have been interpreted as energy utilisation factors.

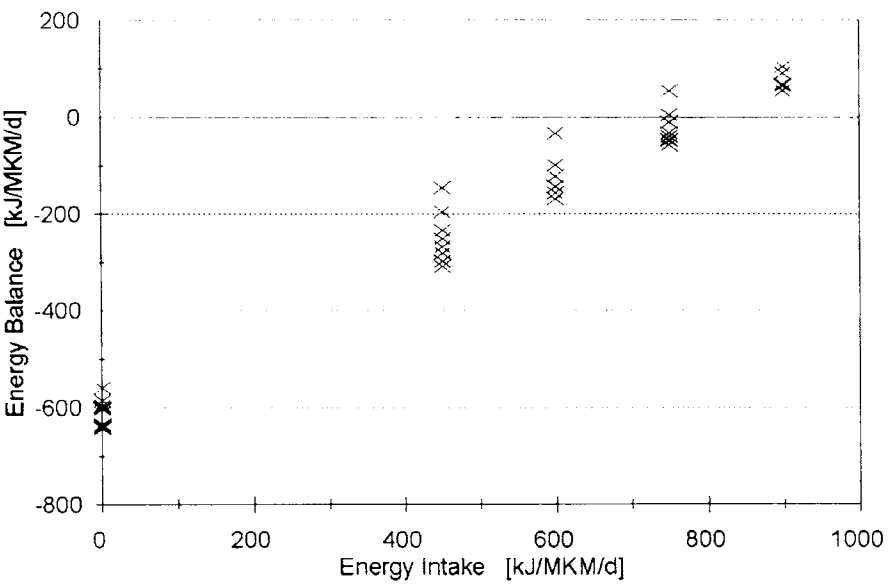

Figure 4: Energy balance of rats fed with a protein enriched diet at different levels of energy intake:

The same principle could also be used to determine the utilisation of single substrates. This will not work quite well, however, because of the partially mutual substitution of the different substrates as sources of energy [31]. This is especially important in the exchange of CHO and fat. CHO is always preferred as a source of energy, as long as it is available. This fact has been utilised to determine the utilisation of different types of carbohydrates [32]. Between 8 and 28 rats, depending on the expected differences between the diet groups, in different groups were fed over periods of up to four weeks with their standard diet. Every fifth day indirect calorimetry was performed after a fasting period of 14 h. For the calorimetric measurement the rats were only given a basic supply of 50 % of their energy requirement as their standard diet supplemented with another about 35 % of the special carbohydrate diet. It was assumed that all given CHO was metabolised during the measurement. Two of the additions were microcristalline starch (assumed to be indigestible) and wheat starch (assumed to be fully digestible). The increase of CHO oxidation for a given diet was compared to the corresponding increase of cellulose and starch. The relation of the increases was interpreted as CHO utilisation and was found to be very well related to utilisation factors determined with feeding experiments on other rats. This method was used to determine the digestibility of resistant starch in rats.

4.4. Other Applications of Whole Body Calorimetry

In whole body calorimetry it is generally assumed that the measured gas and heat exchange are solely due to the subject's body. Its intestine however contains huge numbers of bacteria. Their metabolism is included in the results of calorimetric measurements. In some situations it may be of interest to characterise the metabolism of this intestinal microflora too.

Another area of interest to physiologist is thermoregulation. Energy metabolism and heat loss of a body have to be very well balanced to prevent it from overheating or cooling. Studying the dynamic properties of energy metabolism, heat loss and body temperature may improve knowledge about the thermoregulation processes of the body.

As a third area of application, energy metabolism of a subject is very important to characterise the physiological and psychological status of that subject. This connection can be used not only in medicine but to monitor the behaviour of a subject or behavioural changes due to the influence of stress or different drugs.

4.4.1. Gut Fermentation

The number of microbes (mostly bacteria) in the intestinal tract is about the same or even greater than the number of cells in the human body. Although the relation of the different species in the intestinal tract is relatively stable, their fermentation activity may vary widely due to the food history in the last about 10 days and some other reasons like drug intake. Food containing large amount of dietary fibre increases the fermentation capacity of some species that utilise fibre and transform it to short chain fatty acids. This metabolic activity is coupled with the generation of hydrogen, which then may be partially transformed to methane. These gases are than mostly removed, either through the blood circulation and the lung or as flatulence. So the intestinal microflora together with the diet history of the last weeks may have a great influence on the energy metabolism of the microflora, which is located inside the subject. Due to the transformation of normally indigestible (at least for the subject of the calorimetric measurement) food components into fatty acids the intestinal microflora has a large influence on the overall energy utilisation. There are some other influences of the microflora on the intestinal tract and the whole subject too. They produce some necessary dietary components like, for example, folic acid and at least acts like a store for some of these components. They also improve the passage time of food through the digestive tract.

Direct calorimetry measures the heat flow coming from the subject, whereas indirect calorimetry measures the gas exchange of the subject. The former can not be separated into the parts coming purely from the subject's cells or from the microflora. The latter however can distinguish the gas production of the intestinal microflora by measuring its gas production. This production is usually very small compared with the gaseous exchange of the subject (less than 10 l/d, compared with more than 300 l/d of oxygen consumption for a person with about 75 kg of body mass). The microflora have - in contrast to the subject - an anaerobic metabolism. They produce gases like hydrogen, methane or pentane, which can be used to characterise their metabolic activity. The gas analysis needs to be very sophisticated to achieve a sufficient accuracy at the very low concentrations of those gases ($\sim 10^{-4}$ % for methane or hydrogen, even lower concentrations for pentane). This analysis could be done in parallel to the conventional gas analysis in indirect calorimetry. A mass spectrometer is very useful in such experiments, because it could perform all the analysisses. In ref. [14] a MS was used to measure the methane concentration in parallel to indirect calorimetric measurements.

4.4.2. Thermoregulation

Mammals need to control and usually maintain their body temperature within a narrow range. These control processes have to be very powerful, fast reacting and independent of the actual energy expenditure or heat loss. Studying thermoregulation can be of interest in different sciences. Sports and work physiologists may get information on the possible work load of subjects depending on the actual heat loss to the environment. They may study the subject's reactions upon heavy work loads, because large amounts of sweat are difficult to handle in artificial environments like calorimetric chambers, submarines or space stations. Thermoregulation influences the energy requirement of the subject due to active heat removal or generating heat by shivering. This is of interest for nutritionists and physiologists.

Thermoregulation can be studied from both sides, heat production and heat loss, together with monitoring the subject's heat content. This can be done by monitoring the body's core temperature. Here we probably find the 'native ground' for combined direct and indirect calorimetry because they assess both heat production and heat loss. The dynamic properties of direct and indirect calorimetry have to be taken into account. They have been compared in different facilities [15,40] (see also Table 1). By using mathematical methods to compensate for gas dilution and heat storage the time resolution of the calorimeters could be improved to only a few min. There is, however, a systematic delay between the generation of a peak in energy expenditure and its detection by the calorimeter. This delay is caused by the transportation, dilution and storage of gases and heat within the subject and the chamber. There is also some technical delay in the calorimetric system, caused by the data acquisition, filtering and mathematical compensations. In contrast a burst in locomotor activity can be detected on-time. So the effective delay can be determined by calculating a cross correlation between LA and EE or HL [15]. The position of the maximal correlation factor indicates the effective delay. The resolution of the detection was improved by fitting the 5 highest correlation factors to a quadratic function and detecting its maximum.

The technical delay as well as chamber size and usually the gas flow rate through the chamber are constant. So any changes in the effective delays are caused by alterations in the body's internal transportation mechanisms. An experiment had been performed [15] comparing two similar days of calorimetry at relatively low activity levels. On one of the days two periods of 30 min light activity on a bicycle ergometer had been added to the activity schedule. On the second day the subjects rested in these periods. The effective delay of HL versus LA widely increased on the 'active' days compared with the others. This can

be explained by the subject sweating. Water can not easily be removed from the chamber because it adheres to all surfaces and even diffuses into some chamber material. This increases the effective dilution volume for water and consecutively adds some extra delay for the detection of HL. The lag of EE versus LA decreased in the same situation. This is possibly due to the faster blood circulation and the higher respiration rate.

4.4.3. Behavioural research

The behaviour of subjects is hard to measure, it is often just subjectively rated in comparison to somehow 'normal' behaviour. Changes in the mental status of a subject are in one way or the other expressed in its locomotor activity. A depressive or a passive status is characterised by fewer and smaller spontaneous movements, whereas an enthusiastic or active status is characterised by wide and sometimes fidgety movements. These changes in locomotor activity can easily be detected by calorimetric methods as stated before (see sections 3.5 and 4.2.3.). These measurements can be done without interruption over very long periods. Such long-term measurements integrate even the smallest differences between subjects of different activity levels. Those different activity level may be caused by different treatments or different instructions to the subjects.

To test the difference between 'active' and 'passive' sitting Kurzer performed a study on 9 male and 8 female young volunteers [35]. They entered a calorimetric chamber in the morning after a fasting period of 10 h and after they had a standardised breakfast. In the chamber they performed a standardised activity schedule of 4 h. The first hour was scheduled to settle down. In the second and fourth hour the subjects were asked to relax and sit as passively as possible. In the third hour they were ask to perform a standardised activity comprising of defining words from a dictionary or finding locations in an atlas. Kurzer found differences in the total heat loss between the 'active' and the 'passive' hours of 31 ± 10 %. The evaporative heat loss even increased by 54 ± 21 %. In a calorimetric study where 50 % of the day is performed 'sitting' this variance between 'active' and 'passive' sitting may add up to a total difference in HL over the day of up to 15 %. This variation is higher than typical expected differences in calorimetric studies.

4.4.4. Pharmacological Research

Living beings are very tightly regulated systems. This is achieved by many interconnected multistage regulatory systems with some feedback between them. The activation of regulatory systems as well as the reaction of the body to such activation needs energy, which is provided as ATP by the energy metabolism.

So any influence of drugs on the regulatory system will cause some changes in the energy metabolism, which might be detectable by calorimetry, if they are large enough.

A calorimetric experiment was performed on rats, that have been treated with different doses of dexfenfluramine [41,42]. This drug is a releaser and re-uptake inhibitor of serotonin, which in fact is a neurotransmitter in the hypothalamus of the brain. It is among others involved in the control of eating behaviour, eating preferences and activity status. Five groups of rats were given dexfenfluramine (dF) at doses of 0, 1, 2.5, 5 and 10 mg/kg of body weight over 12 days. A treatment with 0 mg/kg contained just saline. This group was used as a control. Many different reactions were observed that depended on the dose and time of treatment. The rats treated with at least 2.5 mg/kg dF decreased their food intake by 10 to 75 % compared with the control group. The weight gain of the group treated with 10 mg/kg was decreased by about 10 %. This caused a lower body weight of this group, which was maintained for the whole period of observation. This treatment also reduced energy expenditure at increased degrees with higher doses (Figure 5).

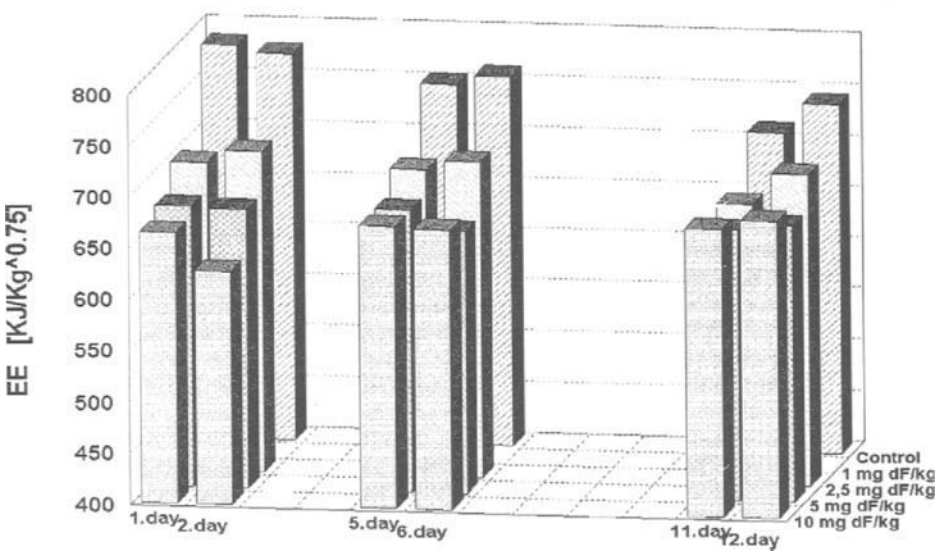

Figure 5: Energy expenditure of rats treated with different doses of dF

EE was reduced from 780 kJ/kg$^{0.75}$ in the control group to 660 kJ/kg$^{0.75}$ in the group with the highest treatment. The influence of dF decreased with time. Surprisingly fat oxidation rate was increased while EE was decreased (Figure 6).

Thus most of the remaining energy after the application of dF was obtained from fat oxidation.

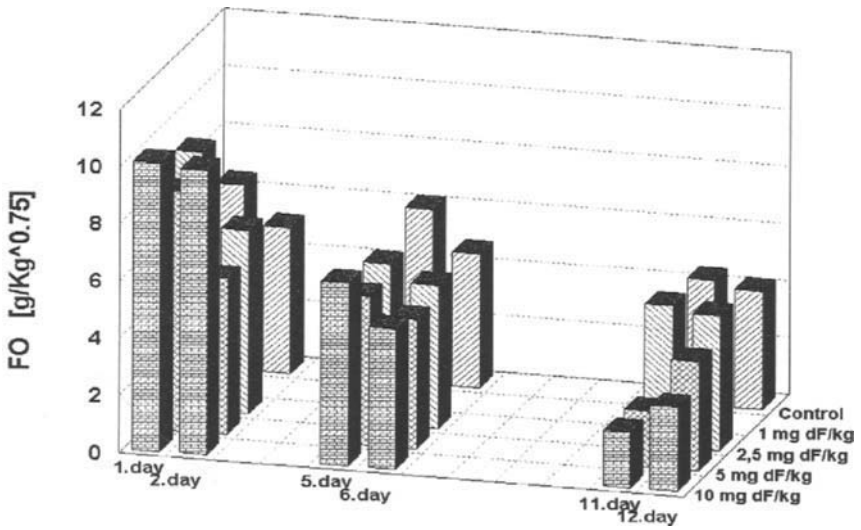

Figure 6: Fat oxidation of rats treated with dF at different doses over 12 days

Pair feeding experiments showed, that the observed results were not only caused by decreased food intake but also by central nervous influences. A treatment with dF also changed the behaviour of the treated rats. Normally rats are active at night and inactive at days. After the treatment with dF on the afternoon the rats remained inactive for about 15 hours and did hardly eat their food. After that period they started to nibble and to be more active. Thus dF also decreased the activity status of those rats besides its influence on EE and substrate oxidation.

As a result of research performed by different groups dexfenfluramine was introduced as a drug for obesity treatment in the USA in 1995. Whole body calorimetry contributed to this approach. Evidence has been found later for dF being involved in generating valvular insufficiency. So in 1997 it was (at least) temporarily withdrawn from the market.

5. CONCLUSION

Whole body calorimetry is an important tool for physicians, physiologists and nutritionists. The application of calorimetry started about 200 years ago. Its theoretical base was established in the last 100 years. The technique of calorimeters and calorimetric methods have been largely improved until nowadays. Modern whole body calorimeters are very accurate and fast responding instruments. They reach recovery rates of about 100 ± 3 % and a delay of measurement of as short as 3 min. Two calorimetric techniques are established, direct and indirect calorimetry. The former is the measurement of the heat loss of a subject; the latter determines the heat production by metabolic processes. This gives a deeper insight into the metabolic status of the subjects. So indirect calorimetry is nowadays more frequently used than direct one.

Clinical applications are often done using indirect mask calorimeters. These types of calorimeters are also preferred by sports and work physiologists. Long term measurements are preferably be done in calorimetric chambers or by isotope dilution techniques. Calorimetric chambers and specialised activity and dietary schedules can be used to detect different compartments of the overall energy expenditure. This techniques and the use of indirect calorimetry are also used to determine the compartments of the energy and substrate balance. These results can be used to get a deeper insight into metabolism and its regulation processes. This is probably the most important application of whole body calorimetry in modern physiology.

REFERENCES

1. M. Rubner, Zeit. f. Biol., 30 (1894) 73
2. W. O. Atwater and F. G. Benedict, Agricultural Bulletin No. 136, US Department of Agriculture, Washington, DC 1903.
3. W. O. Atwater and F. G. Benedict, A respiratory calorimeter with appliances for the direct determination of oxygen, Carnegie Inst. Washington DC, (1905).
4. N. Lifson and R. McClintock, J. Theoret. Biol., 12 (1966) 46
5. D. A. Schoeller and E. van Santen, J. Appl. Physiol., 53 (1982) 955
6. E. Jequier and Y. Schutz, Proc. Nutr. Soc., 47 (1988) 219.
7. J. L. Seale, W. V. Rumpler, J. M. Conway and C. W. Miles, Am. J. Clin. Nutr., 52 (1990) 66.

8. J. A. Romijn , E. F. Coyle, J. Hibbert and R. R. Wolfe, Am. J. Physiol., 263 (1992) E64.
9. P. Avons, P. Garthwaite, H. L. Davies, P. R. Murgatroyd and W. P. James, Eur. J. Clin. Nutr., 42 (1988) 185.
10. G. B. Spurr, A. M. Prentice, P. R. Murgatroyd, G. R. Goldberg, J. C. Reina and N. T. Christman, Am. J. Clin. Nutr., 48 (1988) 552.
11. P. Webb, J. F. Annis and J. Troutman, J. Appl. Physiol., 32 (1972) 412.
12. M. J. Dauncey, P. R. Murgatroyd and T. J. Cole, Br. J. Nutr., 39 (1978) 557.
13. S. Jacobsen, O. Johansen and L. Garby, Am. J. Physiol., 249 [Endocrinol. Metab. 22] (1985) E416.
14. J. L. Seale, W. V. Rumpler and P.W. Moe, Am. J. Physiol., 260 (1991) E306.
15. U.W. Frenz and W.V. Rumpler, Thermochim. Acta, 292 (1997) 1.
16. G. Spinnler, E. Jequier, R. Favre, M. Dolivo and A. Vannotti, J. Appl. Physiol., 35 (1973) 158.
17. E. Tschegg, A. Sigmund, V. Veite, P. Schmid and K. Issigler, Metabolism, 28 (1978) 764.
18. E. Ferrannini, Metabolism, 37 (1988) 287 and 1185.
19. K. N. Frayn, J. Appl. Physiol., 55 (1983) 628.
20. J. Hirsch, Handbook of physiology Am. Physiol. Soc. Washington DC, 1965, 181.
21. F. J. Consolazio, R. E. Johnson and L. J. Pecora, Physiological measurements of metabolic functions in man / respiratory metabolism, McGraw-Hill, New York, 1963.
22. J. B. Weir, J. Physiol., 109 (1949) 1.
23. D. Brown, T. J. Cole, M. J. Dauncey, R. W. Marrs and P. R. Murgatroyd, Med. & Biol. Eng. & Comput., 22 (1984) 333.
24. P. B. Frappell, H. A. Blevin and R. V. Baudinette, J. theor. Biol., 138 (1989) 479.
25. H. Böttcher, J. Nittinger, S. Engel and P. Fürst, J. Biochem. Biophys. Meth., 23 (1991) 181.
26. J. C. Handley, S. A. Spencer, S. Rakowski and P. Rolfe, Earl. Hum. Dev., 26 (1991) 167.
27. W. Höltermann, L. Leuchter, P. Lukasewitz, H. Pfeiffer and H. Lennartz, Anest. Intens. Notfallmed. Schmerzther., 26 (1991) 165.
28. P. R. Murgatroyd, P. S. Shetty and A. M. Prentice, Int. J. Obes., 17 (1993) 549.

29. U. Frenz, Bestimmung der Energie- und Makronährstoff-Verwertung bei Ratten unter Diäten mit leicht unterschiedlichen Aminosäuregehalten Neue optimierte Methoden der indirekten Kalorimetrie, PhD-thesises, Verlag Dr. Köster Berlin, 1995.
30. P. R. Murgatroyd, H. L. Davies and A. M. Prentice, Br. J. Nutr., 58 (1987) 347.
31. K. J. Acheson, Y. Schutz, T. Bessard, E. Ravussin, E. Jequier and J. P. Flatt, Am. J. Physiol., 246 (1984) E62.
32. L. Aust, U. Frenz, A. Täufel, R. Noack, Ernährungs-Umschau, 40 (1995) 59 (Abstr.).
33. U. Frenz, L. Aust and R. Noack, Thermochim. Acta, 251 (1994) 271.
34. P. R. Murgatroyd, B. J. Sonko, A. Wittekind, G. R. Goldberg, S. M. Ceesay and A. M. Prentice, Act. Physiol. Scand., 147 (1993) 91.
35. M. S. Kurzer, Hum. Nutr. Clin. Nutr., 41C (1987) 403.
36. P. Grobbecker, Messung der motorischen Aktivität von Versuchstieren in Respirationskammern in Verbindung mit Wärmeproduktionsmessungen, PhD-thesises, AdL der DDR, 1989.
37. L. Aust, K. H. Brocke, W. E. Heyer, R. Noack, und J. Proll, Z. Versuchstierk., 28 (1986) 119.
38. A. E. Black, A. M. Prentice and W. A. Coward, Hum. Nutr. Clin. Nutr., 40C (1986) 381.
39. M. Elia, N.J. Fuller and P.R. Murgatroyd, Am. J. Physiol., 263 (1992) E676.
40. E. Jequier und J. P. Felber, Bailliere's Clin. Endocrin. & Metab., 1 (1987) 911.
41. M. Boschmann, U. Frenz, R. Noack, L. Aust and C. M. Murphy, Int. J. Obes., 18 (1994) 235.
42. U. Frenz, L. Aust, M. Boschmann and R. Noack, Int. J. Obes., 17 (1993) 27.
43. E. Jequier, in J. S. Garrow and D. Halliday, (Eds.), Substrate and energy metabolism in man. Libbey, London, 1985.
44. A.M. Prentice, (Ed.) The Doubly-Labelled Water Method for Measuring Energy Expenditure. Technical Recommendations for Use in Humans, ed. International Dietary Energy Consultancy GroupVienna: IDECG/IAEA, NAHRES-4 1990.

This Page Intentionally Left Blank

Handbook of Thermal Analysis and Calorimetry. Vol. 4: From Macromolecules to Man.
R.B. Kemp, editor.

Chapter 11

MICROCALORIMETRIC STUDIES OF ANIMAL TISSUES AND THEIR ISOLATED CELLS.

R. B. Kemp and Y. H. Guan

Institute of Biological Sciences, University of Wales, Aberystwyth, SY23 3DA, Wales, UK.

1. INTRODUCTION

The physiological properties and the underlying biochemical mechanisms of animal tissues have been studied by calorimetry since the pioneering studies of A.V. Hill ninety years ago [1]. For most of that time, the instruments were handmade in University workshops and it was not until the advent, more than thirty years ago, of commercial versions to measure heat flow rate in the microwatt range that studies of cells isolated from animal tissues became relatively commonplace. Much of this can be attributed to the simple and accessible range of heat conduction microcalorimeters designed by Wadsö [2] and manufactured in Sweden. As will be seen in this chapter, the instruments of several other Companies have also been employed and the properties of all of them are stated in a chapter written for Volume 1 of this Handbook [3]. Thus, this aspect of the calorimetric studies will only be touched upon when it is necessary to draw attention to the advantages of a specific type of instrument for a particular kind of investigation.

It is sufficient to write at this stage that there are two main types of heat conduction calorimeter [3]. One is the batch instrument, in which either a vessel containing the experimental material is inserted into the measuring chamber (sometimes called ampoule drop) or a substance is introduced to a vessel fixed within the instrument, usually by a titration pump. The other is the flow type in which the material is pumped by peristalsis from an outside container through transmission tubing to the measuring vessel. The choice will depend on the nature of both the biological sample and the required information [4]. In brief, tissues and organs are usually studied in stirred or unstirred batch vessels,

sometimes with perfusion. The cells freshly obtained by dissociation from such sources or cloned to form cell lines, are, by their very nature, "sticky" and most appropriately grown adherent to a suitably treated surface. This is usually an insert to the vessel, a Petri dish or a tenterframe, or a stirred suspension of beads that acts as a substratum. Such a suspension can be pumped through a flow vessel but it is more common for this procedure to be adopted for cells adapted to grow in suspension, usually for pharmaceutical use in a bioreactor. Details will be given in the appropriate Sections of this Chapter.

By its very character, a handbook is intended to be a companion to the scientist at the bench and not a comprehensive review of the work that has been done in the field. For this the reader is guided to the many articles available in the literature (see, for instance References [5-11]). For the incontrovertible reason of the greater expertise held by another, calorimetric studies of the cells constituting blood tissue will be neglected in this chapter in favour of Monti's contribution to this Volume. It is worth bearing in mind, however, that much of the technical information given in the present chapter is highly relevant to work with blood. It should also be accepted that one of the disadvantages of the traditional calorimeter, compared even to the age-old Warburg respirometry, is the relatively slow throughput of data. This is a particular irritation to the Pharmaceutical Industry in which competitive pressure has resulted in the adoption of combinatorial chemistry techniques with the many resultant substances requiring biological assay on 1536-well microtitre plates! The response must be to shape thermosensitive devices into such multiplexed detectors [12,13] and/or to resort to thermal imaging [14]. For these studies and for many using conventional calorimetry, it is suffice to know that living matter produces heat but for the most penetrating investigations in physiology, it is important to appreciate the nature and sources of heat production.

2. THERMODYNAMICS

Most calorimetrists (even biologists!), and those aspiring to be so, have a knowledge of classical thermodynamics in which the system is at equilibrium [15,16]. It is unnecessary, therefore, to elaborate on the fundamental relationship between the changes (Δ) in the states of Gibbs energy (G), enthalpy (H) and entropy (S),

$$\Delta H = \Delta G + T\Delta S \qquad (1)$$

It is axiomatic, however, that living systems are not at equilibrium and therefore cannot be described completely by classical thermodynamics. In the strict sense

then, non-equilibrium thermodynamics (NET) is required [17], though it is by no means certain that, at the level of direct and indirect calorimetry, analysis of the data using the principles of the classical laws, gives the wrong answer. The extensive research and data analysis done by Battley on the energetics of growing microorganisms was seemingly very successful using only equilibrium thermodynamics (see for instance References [18,19]). For these experiments, he made sure there was a closed system even for gaseous exchange. In life on this planet and in the experiments of most researchers, the living system under examination is open to the exchange of energy and materials; thermodynamically this is an open system. All living material is growing or at least it is synthesising new macromolecules in a renewal process. When undertaking in vitro experiments on an open system, it is necessary to define its thermodynamic boundary and then do the calculations within this constraint, having described the parameters [20] (see also Duboc et al., this Volume). The boundary or control volume [21] can be the vessel alone in batch calorimetry but in a flow instrument it usually includes the reservoir or culture vessel/bioreactor acting as the source for the living material.

The irreversible process of growth and renewal requires energy, a relatively small amount of which is stored in the accumulation, replacement (recycling) and structuring of matter [22]. The rest of the energy is expended on maintaining the physiological state of the cell [23]. For all cells this includes performing the internal work concerned with the functions of the cytoskeleton, such as intracellular vesicular transport. In muscle cells, there is also the predominant external work involved in periodic contraction. For all these processes, cells consume substrates that, in terms of energy analysis, possess the high quality, useful Gibbs energy. During the energy transformations required for maintenance and contractile activity (internal and external in the case of muscle), the quality is decreased and the remaining energy is dissipated as heat. With the notable exception of muscle, the differential amount of work ($\mathrm{d}W$) in animal cells is usually small and the energy conservation in biomass accumulation may be modest. Thus, in terms of irreversible thermodynamics [24], the growth of non-muscle cells can be said to be a dissipative rather than a completely irreversible process, $\mathrm{d}D$ [25],

$$\mathrm{d}G = \mathrm{d}W + \mathrm{d}D \tag{2}$$

In these terms, the dissipated energy is related to the differential change in heat by,

$$\mathrm{d}Q = \mathrm{d}D + \mathrm{d}B \tag{3}$$

where dB is the bound energy which is the change in entropy times the absolute temperature ($dB = TdS$). Equation (3) is recognised in the following form in relation to the rate of change in enthalpy, dH [25],

$$dH = dG + dB \tag{4}$$

Thus, the growth rate of animal cells can be measured using calorimetry when the absolute magnitude of the molar bound energy is small. It is important to realise, however, that it is coupled processes that lead to growth. In terms of Gibbs energy, this is the coupling of exergonic fuelling reactions (catabolism) to endergonic biosynthetic reactions. Gibbs energy is the driving force generated and dissipated by these reactions, i.e. it sustains the redox process of growth (see Duboc et al. in this Volume).

The key to understanding the information that is obtained from calorimetry lies in two crucial points. First, inherent within its design, a heat conduction calorimeter measures the rate of heat flow ($\Phi = dQ/dt$, Watts, W). In other words, it gives the kinetics of the process. Secondly, this flow can be regarded as the rate of thermal (th) advancement, $d_{th}\xi/dt$ in the energy transformations [26]. Advancement, or the extent of reaction as it is also known, is an important concept in energy transformation because it is explicit to the stoichiometric coefficients, ν_i, of the of the i-th species in the reaction. In the case of a reaction, advancement, $d\xi_B$, is,

$$d\xi_B = dn_i \nu_i^{-1} \tag{5}$$

where dn_i is the change in the amount of a reactant or a product, i and the subscript B denotes $|\nu_B| = 1$. Therefore, $d\xi_B$ is side-independent.

"Metabolic activity" is a convenient expression for the rate of advancement of a reaction in living cells, $d\xi_B/dt$, or its flux when the rate is expressed as being specific to mass, $(1/x)(d\xi_B/dt)$, where x represents the amount of biomass). The thermal advancement of energy transformation, $d_{th}\xi$, is related to $d\xi_B$ by the expression,

$$d_{th}\xi = \nu_i \Delta H_{B,i} d\xi_B \tag{6}$$

where $\Delta H_{B,i}$ is the molar enthalpy of the reaction system in terms of species i. The change in thermal advancement, $d_{th}\xi$, is exactly equivalent to the more

Equation (6) can be exploited in a variety of ways that will be demonstrated in this chapter, not least in the enthalpy balance approach (see Section 5.2.4). For this method, it is necessary to have the following information: (i) the experimental reaction flux, J_B (mol s^{-1} m^{-3}),

$$J_B = d\xi_B / x dt \tag{7}$$

is obtained for each species in a chemical reaction; and (ii) the calculated molar reaction enthalpy, ΔH_B (J mol^{-1}), is found using the molar enthalpy of formation for each species i, that is,

$$\Delta H_B = \sum_i \nu_i H_i \tag{8}$$

By combining Equation (7) and Equation (8), the resulting reaction enthalpy flux, J_H, (W m^{-3}) is given by,

$$J_H = J_B \Delta H_B \tag{9}$$

where J_B is the reaction molar flux (mol s^{-1} per amount of biomass). J_H is directly comparable to the experimentally measured (scalar) heat flux, J_Q. From this, it can be appreciated that heat flux gives thermodynamic information as well as kinetic data. This is the great advantage of studies with heat conduction calorimeters.

Although in thermochemical terms, metabolic activity, $d\xi_B / x dt$, can be expressed using equation (5) and equation (6), its meaning in terms of the biochemical pathways is essentially concerned with the rate of ATP turnover [22]. Under the steady or quasi steady state conditions of cells growing in good environmental conditions in vivo or in vitro, the endothermic ATP generation (supply) is tightly coupled to the exothermic ATP utilisation (demand). Thus, under these stable conditions, the ATP cycle has a net enthalpy change of zero. Furthermore, the catabolic process is coupled to ATP supply and the ATP demand is coupled to the anabolic process that, under aerobic conditions, has a very small overall enthalpy change [27]. These considerations essentially mean that heat flux is a reflection of catabolic flux. This is the understanding of "metabolic activity" in the biochemical sense.

3. REASONS FOR SYSTMATIC ERRORS IN CALORIMETRY

Experimental animal physiologists will understand the need for the appropriate environmental conditions to obtain the correct data. Of course, this imperative extends to studies undertaken with living material. Some of the attraction of the modern calorimeter is the low detection limit, often associated with a high degree of sensitivity [3]. However, these attributes reinforce the need for careful experimentation to eliminate systematic errors. The well-known virtue of heat measurements is that all sources are registered, even under conditions that preclude optical measurements. This is also a major cause of error, however, because all the types of side-reaction are registered and, because there is no heat "spectrum", these can be indistinguishable from the heat of the chosen system. It is vital, therefore, to make a careful experimental design, bearing in mind the following non-exclusive list of possible error sources. Some errors are peculiar to specific types (batch/flow) and makes of calorimeter.

3.1. Physical environment

The list of possible physical factors in this Section is brief because many of them are peculiar to individual designs and then have been well documented by Wadsö [28,29]. Two important general aspects must be drawn to the attention of the inexperienced user.

3.1.1. Conditions that cause tissue/cell damage

Commercial batch and flow calorimeters are mainly designed and built for physicochemical studies. It is essential, therefore, for investigations of living matter in its bathing medium to ensure that the vessels are made of compatible materials. For instance, cells and any protein in the medium may stick to glass and not be removed or be precipitated in a washing procedure. The use of a silicone coating is recommended in this case. It is also important to check on the possible interaction of bioactive chemicals added to the living system to elicit a specific response. As an illustration, although gold might be considered the ideal material for a calorimetric vessel, it has been found that the cardiac glycoside, ouabain, is adsorbed to it and continues to act, even after thorough washing.

There are a number of problems specific to flow calorimeters arising from the fact that they have been designed in the first place for studying the thermal properties of pure chemicals. The vessel is generally fabricated from 24-carot gold [3,28] but the transmission tubing to and from it can be of different materials, both metal and plastic. This requires the formation of several joints. While this apparently causes no problems for the circulation of yeast [30,31] and the normally non-adherent blood cells (see Monti in this Volume), the unions together with the coils of the upward flow vessel act as sites for blockage by

tissue cells [10]. In the Thermometric TAM flow calorimeter, this problem was partly alleviated by changing the flow from upward through the vertical, measuring vessel to downward [32] (see Figure 1). The only way to deal with the joints, however, was to eliminate them.

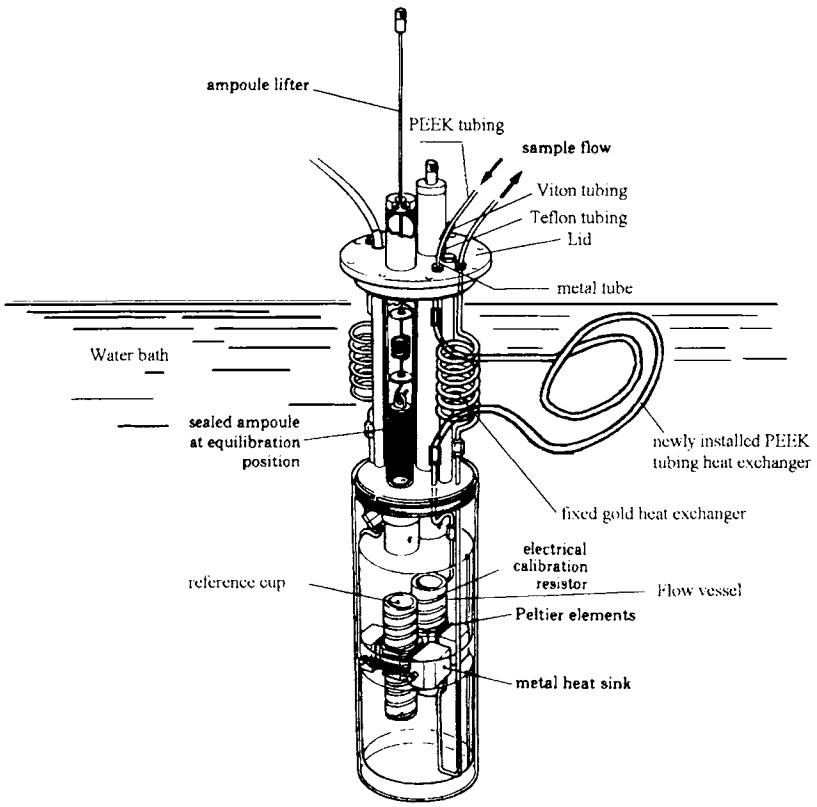

Figure 1. The standard Thermometric flow microcalorimeter has been modified for downward flow through the measuring vessel which consists of gold tubing wound round the standard cup of the batch microcalorimeter. With the changed flow direction, it was necessary to install a new heat exchanger. This is simply a coil of PEEK tubing (1 mm I.D.) inserted between the lid and the cup. The previous gold heat exchanger is retained downstream of the measuring flow vessel. The reference cup normally contains a sealed ampoule that is not moved when the instrument is in regular use (Reproduced from Reference [32] with permission).

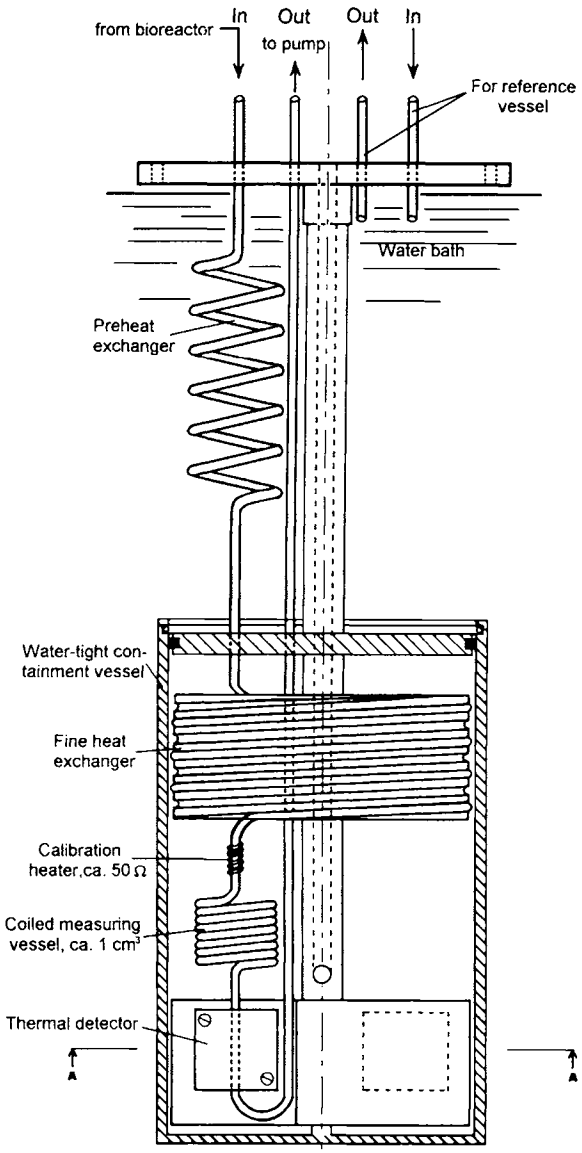

(A)

Figure 2(A). A pictorial representation of the new flow module for the Thermometric 2277 Thermal Activity Monitor. The section labeled by A–A is illustrated in Figure 2(B).

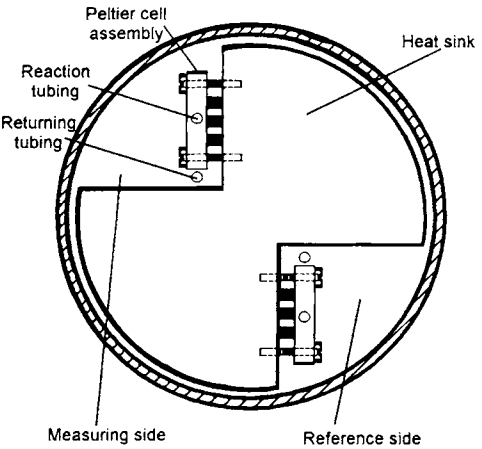

(B)

Figure 2(B). A sectional view of the layout of the thermal detector in the new flow module for Thermometric 2277 TAM. The vertical position of this section is labeled in Fig. 2(A) as A–A. (Reproduced from Reference [33] with permission).

There was an added incentive to simplify the transmission lines because an increasing number of cell cultures consist of adherent cells carried on beads. In order to use a flow calorimeter to monitor their heat production, the transmission tubing and flow vessel needed to be wide bore. These requirements stimulated the design and construction by Thermometric AB of a flow module optimised for use with cells originating in solid tissue [33] (see Figure 2). High quality stainless steel was used because of its malleability, low reactivity and negligible gas permeability. For thermodynamic studies in which the boundary of the open system must be considered, changes in gas composition from the use of, for instance silicon tubing, must be eliminated to allow a correct interpretation of the results (Section 5.2.2).

The pumps required for flow calorimetry have to be carefully considered because they can be sources of error. Accentuated or irregular pulsing can cause severe baseline perturbation and the pump rollers can damage the cells. The choice of flow rate is crucial for several reasons. If it is too fast, heat will be carried away from the measuring vessel in the distal transmission tubing. If it is too slow, then there may well be problems of cell sedimentation and oxygen

deprivation leading to sub-normoxic conditions. If the cell suspension is pumped at an inappropriate linear flow velocity, this may cause trauma to the cells. In the customised flow module described above (Figure 2), this was one of the major design considerations.

It is more common to use batch vessels for cellular studies possibly because such calorimeters are available in greater numbers. In early studies, cells in suspension were simply placed in an unstirred batch vessel. The heat effect was measured as the cells sedimented on top of one another ("crowding" effect – see Section 3.2.1) and formed an adverse microenvironment with decreasing oxygen tension, resulting an increasing concentration of toxic products (see for instance Reference [34]). It is essential that suspended animal cells are stirred but even this can lead to systematic errors according to the type of stirrer and the speed of gyration [29].

For studies of anchored cells, modifications need to be made in many cases. For instance, cultures on tenterframes [35] have been inserted into the 100-cm^3 batch vessel of a Calvet calorimeter [3] and glass plates with cell monolayers on them have been stacked in the ampoules of a Thermometric BAM instrument [36]. In one recent case [37], the stirrer blades of a Thermometric perfusion vessel were modified to act as monolayer plates. It would seem preferable these days to attach the cells to beads that are suspended in a stirred ampoule (see for instance Reference [38]).

3.1.2. Inaccurate/non-existent electrical and chemical calibration

Because it is in the Manuals of commercial instruments, it is well recognised these days that electrical calibration using the Joule effect must be carried out on a regular basis. What is not so well appreciated is that all vessels must be chemically calibrated using a suitable reaction. Biological processes are slow and Wadsö [28,29,39] has long advocated using the slow, imidazole-catalysed hydrolysis of triacetin for this purpose (see Reference [3]). This seems to have fallen on deaf ears for, apart from a study of the kinetics of the reaction in a simple unstirred ampoule [40], there are no reports of the experimental calibration of the vessels used in tissue/cell investigations. It was a surprise, therefore, to find that the conventional TAM flow vessel with the recommended maximum flow rate of 35 cm^3 h^{-1} had a thermal volume of 0.77 cm^3 as opposed to its physical volume of 0.6 cm^3 [32]. Larsson et al. [31] pumped an aerated yeast suspension at 90 cm^3 h^{-1} through the same type of flow vessel as just described and obtained good enthalpy balance data. It is suspected that the "cooling" effect of the fast pumping rate compensated for the thermal overestimation. The thermal volume (1.05 cm^3) for the customised Thermometric flow module described in Section 3.1.1. was close to the nominal

volume of 1 cm^3 at 100 cm^3 h^{-1} pumping rate [33] but there is some evidence that different flow rates give altered values [41]. In other words, flow calorimeters must be chemically calibrated at the pumping rate used for the experiment.

Preliminary data for a stirred Thermometric perfusion vessel indicate the same necessity [41]. A 1-cm^3 aliquot of triacetin mixture in a 3-cm^3 sealed glass ampoule had a thermal volume of 0.998 cm^3. This compared favourably with the previous results obtained elsewhere [40]. A perfusion vessel with the same spacial volume of the calibrant stirred at 30 rev min^{-1} had a thermal volume of 0.81 cm^3 but at 90 rev min^{-1} it was 0.99 cm^3.

3.2. Physiological environment

3.2.1. Oxygen tension

It is often not realised that oxygen is a hydrophobic gas with a consequentially low solubility in water (210.2 μmol dm^{-3} in air-saturated pure water [42]). It is even less soluble in physiological solutions because the salting out effect reduces solubility considerably and sometimes by more than 10%, depending on the complexity of the medium. This is particularly important in closed vessels and especially in those without an air space. It is also a contributory cause of hypoxia and the progression to anoxia in excised tissues and cell suspensions. There is a decrease in specific heat production with increasing sample size that is known in both direct and indirect biocalorimetry as the "crowding effect". This has been mathematically modelled for tissue biopsies by Singer et al. [43] – see Figure 3. The same phenomenon occurs in unstirred layers of cells (see for instance Reference [34]) in which the physiological conditions in the interstices between them are so poor in terms of low oxygen tension, inappropriate pH, high ammonia concentration, etc., that they cause a decrease in metabolic activity [44].

3.2.2. pH

Tissues and cells originating in the homeostatic conditions in tissues cannot tolerate a pH outside the range of 7.2 ± 0.2 without deleterious effect. Besides the physical effect, it has been shown in several papers from Wadsö's laboratory (see for instance References [45-47]) that the heat dissipated by cells is very sensitive to changes in pH (see Figure 4) and, at least for T-lymphoma cells, it peaks in the above range (see Figure 5). Bäckman [46] indicated that pH-dependency was common to many cell types but that they varied in the degree of it. This phenomenon included erythrocytes that have no mitochondria and so it was reasoned that the changes in bulk phase pH affected glycolysis [45], presumably by altering cytosolic pH through the Na^+, H^+ exchange in the plasma

membrane [48]. One of the reasons why lactate is so harmful to cells [4,22,44] could be that it lowers the pH of the medium when excreted from them – negative feedback.

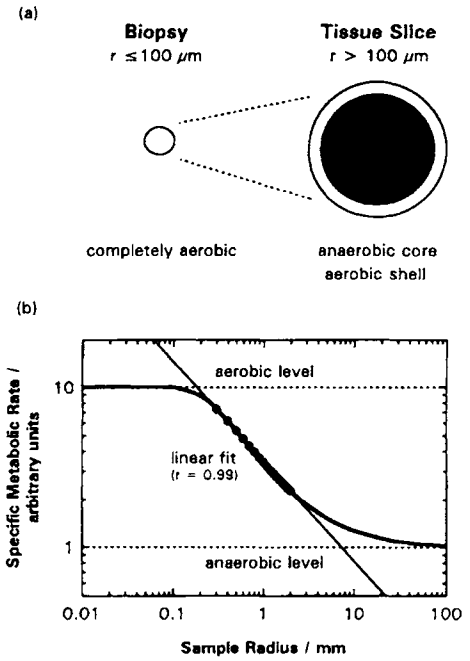

Figure 3. Influence of the sample size on the metabolic rate (crowding effect). (a) Whereas a small biopsy is completely aerobic, a large tissue slice consists of an an aerobic shell and an anaerobic core. (b) Thus, with increasing sample radius, the heat output per unit of volume shows a sigmoidal decrease from the higher aerobic to a lower anaerobic level. When plotted on log scales, the steep portion of this transition fits a linear regression. Both the critical depth of tissue aerobiosis (100 μm) and the relationship of anaerobic to aerobic metabolism (1:10) are rough assumptions (Reproduced from Reference [43] with permission).

3.2.3. Temperature

It may seem obvious that cells from warm-blooded animals should be maintained at 37 °C but the importance of so doing is nicely illustrated by

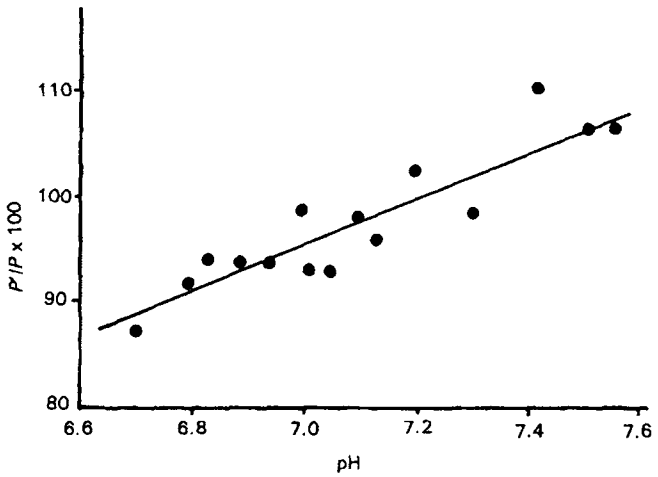

Figure 4. Influence on the heat flow rate value of changes in the pH of a suspension of T-lymphoma cells. P'/P is the quotient between heat flow rate values determined at the indicated pH value (P') and that determined at pH 7.20 (P) (Reproduced from Reference [45] with permission).

Bäckman [46] and depicted in Figure 6. The specific heat flow rate (heat flux) of T-lymphoma cells varied considerably between 25 °C and 42 °C (Figure 6a) with a pH-corrected, temperature dependence at 37 °C of ~1 pW/°C (Figure 6b). Although temperature is easily controlled in calorimetric experiments, a problem may arise in comparative studies. In this case, some of the results may be obtained under less stringent temperature control, for instance in biochemical analyses. In the case of T-lymphoma cells, Bäckman [46] recommends that the temperature control for these ex situ experiments should be within 0.1 °C of the calorimetric value. He then plotted heat flux against $1/T$ (Figure 6b). Based on the similarities between this plot and an Arrhenius plot, an apparent activation energy (E'_a) was calculated from the slope between 25 °C and 37 °C and found to be 87 kJ mol^{-1}. There was a rapid decline in the value of E'_a at temperatures above 37 °C. Although it may not be possible to relate to the activation energy of some specific rate-limiting step, there is remarkable linearity.

3.2.4. Osmotic pressure

When reading the Materials and Methods section of papers, it is frequently noted that calorimetric data were obtained for cells in simple, hypo-osmotic

media. While this may be acceptable for very short periods, it is essential that the incubation medium remains iso-osmotic in the range of 260-280 mOsm for experiments lasting longer than a few minutes.

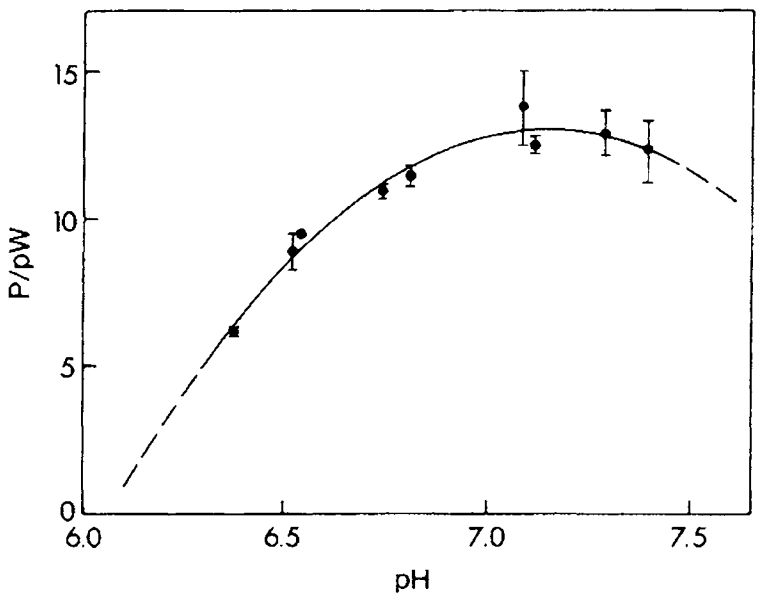

Figure 5. The heat flow rate per T-lymphoma cell, P_{cell}, as a function of the medium pH (Reproduced from Reference [46] with permission).

3.2.5. Substrates

Careful thought should go into choosing the medium to use for calorimetric experiments on tissues and cells. In essence, it is the catabolic process coupled to the ATP cycle that is measured by this technique (see Section 2). Therefore the choice of substrate(s) will affect the rate of heat flow and the amount of a particular substrate will determine the duration of a particular quasi steady state. Cells can be maintained for a considerable period on a simple, glucose-containing physiological solution but most cells do not actually grow without the amino acid glutamine. This is a vital precursor for nucleic acids and can also act as the amino donor in the de novo formation of other amino acids and amino sugars [49]. Glutamine can also be oxidised to provide energy for the cell [44,50]. In many cases, oxidation is only partial and lactate is an end product.

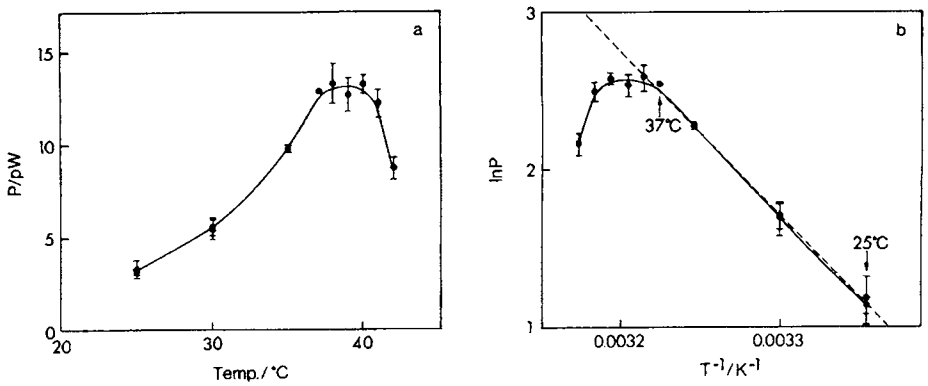

Figure 6. (a) Changes in P_{cell}, as a function of temperature. (b) A plot of $\ln P_{cell}$ vs. $1/T$ based on the values in Figure 6(a). All values are corrected to pH 7.2 using the results from Figure 5 (Reproduced from Reference [46] with permission).

In order to simulate body fluids, tissues and cells are often incubated in the presence of serum. This provides a wide variety of micronutrients, hormones, growth factors and co-factors as well as fatty acids bound to, or part of, serum proteins. These are all essential for long term growth but, packaged in unknown amounts as components of serum, they cause culture variability and render it impossible to conduct precise thermobiochemical calculations in, for instance, the enthalpy balance method (see Section 5.2.4). Serum is also the most common source of mycoplasma infection. For these reasons, it has been replaced by complex, defined media with specified amounts of constituents for the growth and production of heterologous proteins by genetically engineered cells and hybridomas (see Section 5.2.5). A further advantage of a defined medium has become apparent in recent years in that the composition can be adjusted rationally in order to optimise cell growth and protein production (see Section 5.5).

All the factors in this section will affect the metabolic activity and, consequently, the heat flux (see Reference [44,51]).

3.2.6. Waste products

The major catabolic products that are toxic to isolated cells or those in tissues are ammonia [52] and lactate [53], the by-products of glutaminolysis [54] and glycolysis. Uniquely, glutamine has two amino groups and the ammonia arising from the degradation of the amino acid has adverse effects on intracellular

organelles, cytosolic and lysosomal enzyme activity and vesicular transport. It diffuses freely across the plasma membrane and the intracellular membranes in the unprotonated form and, amongst a range of deleterious consequences, it affects the post-translational glycosylation process in the formation of glycoproteins. This is an important consideration for those manufacturers producing recombinant proteins. It is well established that this amino acid is thermolabile and that it decays rather quickly at 37 °C. The ammonia diffuses into the cell and it adds to the amount arising from the conversion of glutamine to glutamate during the transport of it through the plasma membrane [44]. Hence, there is a search for more stable forms of the acid, such as the dipeptides, GlutaMAX™ I and II (GibcoBRL – Life Technologies Ltd., Paisley, PA4 9RF).

Lactate is freely transported from the cytosol through the plasma membrane to the environment where it decreases the bulk phase pH. This is one of the reasons why a Mycoplasma infection, so dreaded by those who culture cells, is harmful to them. These organisms are glycolytic "engines" [10] and adhere to the cell surface, pumping out lactate in relatively large amounts.

3.2.7. Size

The heat flow rate is an extensive quantity. For comparative studies or those in which heat is only one of the chosen variables, it is essential to make the measurement specific to the size of the system. In classical Monod terminology for microbial growth, this would be called the specific rate. The term for size specificity in the field of bioenergetics, however, is "flux", J. For living cells in suspension, size is usually equated with volume, V. On the other hand, size is usually expressed as mass, m, for cells in monolayer and for excised tissues/organs. It will be noted that, in both cases, the denominator is a cubic expression and thus they are the scalar fluxes. This term should be expressed as $J = \mathrm{d}Q/\mathrm{d}t\,V^{-1}$ in terms of volume. There are techniques available to measure the volume of cells. These can be classified as on-line, that is in the culture vessel, including laser nephalometry [55] and dielectric spectroscopy [56]; and the more familiar off-line techniques of Coulter counting and flow cytometry [57]. These assessments of volume are directly related to mass providing the mass density is constant, $\rho = m/V$ [44]. This may not be the case at different phases of the cell cycle and it is affected by the osmotic pressure of the medium (see Section 3.2.4). For measures of the mass of tissues and their biopsies as well as for organs, wet or preferably dry weight or protein content is used, whereas the latter is almost ubiquitous for estimating the mass of adherent cells. It is not known which of the two measures, mass or volume, most closely reflects metabolic activity, but the closeness of the relationship probably

depends on the cellular location of the predominant catabolic pathways, the cytosol (e.g. red blood cells) or the mitochondria, for a particular cell type.

Kleiber [58] originally showed that the oxygen flux of animals decreased with the increasing size of them. This Rule was shown to apply to the direct calorimetric data for Vero cells growing on Cytodex 1 beads in a stirred vessel [38]. As will be seen in Figure 7, the low value of the weight exponent (0.4) reflects a very marked influence of cell size on the metabolic flux, expressed as per unit protein [59]. Thus, cell number concentration may be an important factor in determining the value for the heat flow rate. In general, as cells become confluent on the substratum, exemplified in the above case by the surface of the solid beads, there is a declining rate of cell growth. This is because, after division, daughter cells exhibiting contact inhibition of growth are arrested in early G_1 phase while they are still small and then become "resting" cells (G_0).

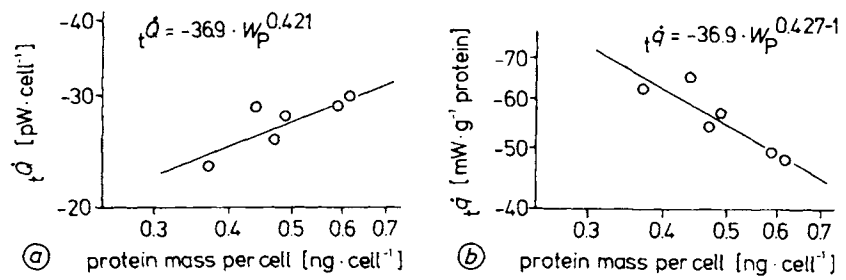

Figure 7. Double-logarithmic plots of cellular heat flux (*a*) and protein mass per cell (*b*), both of them as functions of protein mass per cell, W_p. Vero cells grown on microcarriers at 37 °C and pH 7.2 (original data from Reference [38]) (Reproduced from Reference [59] with permission).

One of the properties of cancer cells in vivo is that they have escaped the contact inhibition of growth. This is retained in cells dissociated from tumours and grown in vitro. Instead of ceasing to grow on contact, cancer cells grow over one another and form layers that, in the example of human renal carcinoma cells [43], reflect the increasingly anaerobic conditions by having a reduced heat flux (see Figure 8A and Section 3.2.8). As predicted in the mathematical model discussed earlier (see Figure 3), Singer et al. [43] also showed that Kleiber's Rule can apply to explanted tissue samples (Figure 8B). For liver, the heat flux

increased with decreasing sample size apparently because the condition in the larger explants was more anaerobic than that in the smaller, "biopsy-like" samples. There is evidence that anaerobic glycolysis is the reason for the decrease in metabolic activity, at least in lymphocyte hybridoma cells [60]. Reworking the direct and indirect calorimetric data for unstirred cells (see Figure 9) showed that the calorimetric-respirometric ratio (CR ratio – see Section 5.5) became more negative, from –570 kJ mol^{-1} O_2 to –770 kJ mol^{-1}, with increasing cell density. Thus, it is likely that the apparent agreement with Kleiber's Rule in some cases is due to adverse environmental conditions rather than to an allometric relationship per se [44].

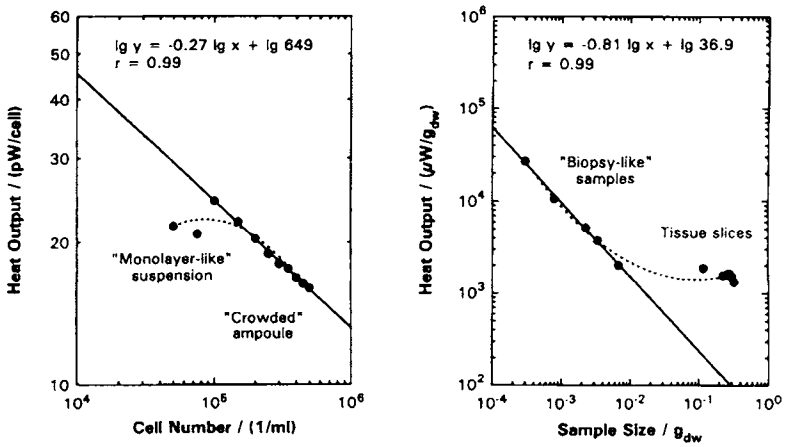

(A) (B)

Figure 8. (A) Influence of sample size on the heat output per cell in a suspension of human renal carcinoma cells. Note that it decreases with increasing cell number. This may be expressed by a continuous transition from aerobiosis in a "monolayer-like" suspension to increasingly anaerobic conditions in a "crowded" ampoule. (B) Influence of sample size on heat output per unit dry weight (dw) in rat liver tissue samples. It increases with decreasing sample size. This is apparently due to a continuous transition from mainly anaerobic conditions in large tissue slices to an increasing amount of aerobiosis in "biopsy"-like" samples. The two curves complement each other giving a sigmoidal relationship, whose steep portion fits a linear regression when plotted on log scales (Reproduced from Reference [43] with permission).

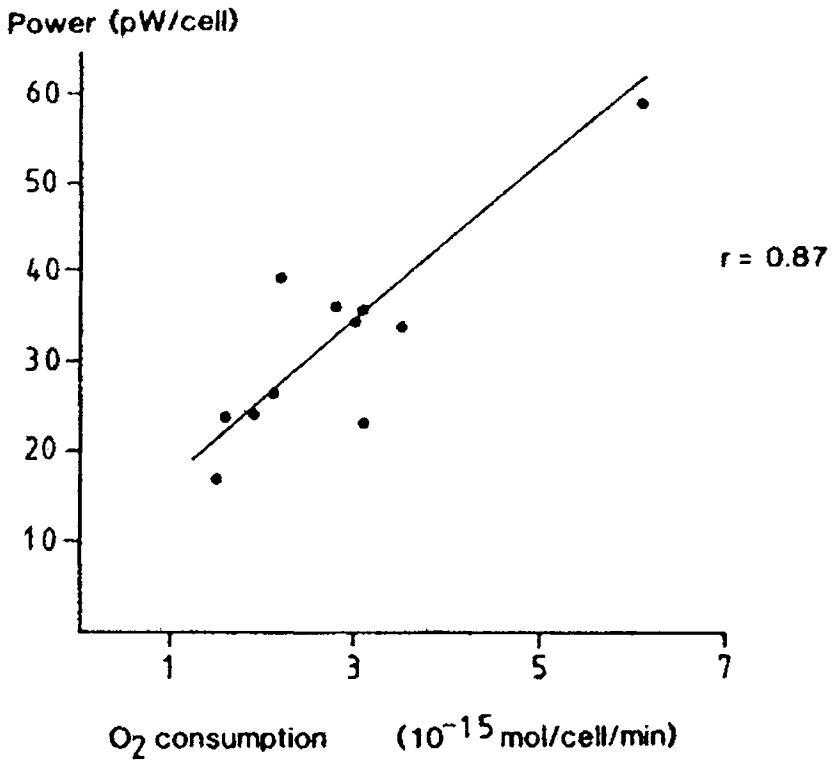

Figure 9. Relationship between the heat production and the oxygen consumption ($n = 11$) in lymphocyte hybridoma cells (Reproduced from Reference [60] with permission).

3.2.8. Metabolism

It has already been established that heat flow rate is a manifestation of the catabolic process on its own (see Section 2). Thus, one needs only to consider respiration – namely, the citric acid cycle and oxidative phosphorylation – the pentose phosphate pathway (PPP), β-oxidation of fatty acids, glycolysis and glutaminolysis. With the exceptions of glycolysis, the PPP and some of the steps in the catabolic degradation of glutamine, these pathways are mitochondrial and, thus, do not take place in, for instance, blood cells without mitochondria. In the erythrocytes, the demand for ATP is met by the reduction of glycolytic pyruvate to lactate. In the phagocytic white blood cells, NADPH is required for the formation of the oxygen metabolites that kill the microbes responsible for many

infections. This is produced from glucose by the PPP with the pyruvate being completely oxidised to give the same enthalpy change as for the respiration of this substrate, according to Hess's Law. Without any of the side-reactions that occur because the overall reaction takes place in the cellular physiological environment, the molar (m) reaction enthalpy of glucose oxidation, ΔH_m is -2814 kJ mol^{-1}. Cells deriving ATP from glycolysis alone consume 16 times more glucose than those obtaining it by oxidation, but produce less heat per mol ATP. To illustrate the point for cells incubated in a glucose-containing, bicarbonate-buffered medium [44], it is necessary to assume an ATP stoichiometric coupling coefficient in glucose oxidation ($\nu_{ATP/Glc}$). The classical textbook value is 36 mol ATP per mol glucose (glc) but there is an estimate as low as 30 [61]. The most convincing calculated value, however, is that of Beavis, 33 [62]. In the given example, the stoichiometric coefficient for ATP coupling in glycolysis is 2, the molar reaction enthalpies were calculated from Wilhoit [63] and the heats of neutralisation were taken from Gnaiger and Kemp [64]. Then, the heat yield for ATP by the oxidation of glucose is $-3044/33 = -92.2$ kJ mol^{-1} ATP and that by glycolysis is $-161/2 = -80.5$ kJ mol^{-1} ATP.

3.2.9. Growth

For populations of cells in vitro, growth implies an increase in density (number concentration). Cells from normal (non-cancerous) tissues mimic their antecedents in the tissue. They only divide and grow until the onset of the well-known phenomenon of contact inhibition. Thus, most of the cells in tissues in vivo and in confluent monolayers in vitro are in the cell cycle phase of G_0. This is a homeostatic mechanism to regulate the size of tissues and organs. The exceptions in the body are the stem cells that are continuously renewing epithelia and some tissues, for instance blood tissue, and certain other cells that maintain cell numbers in the tissue by duplication. Explants from these tissues/organs simulate wound healing and the cells constituting them grow out from the bulk. In such cells, as with freshly sub-cultured cells in vitro, the molecular mechanism of the cell cycle must be re-assembled before the cell can resume the growth that is characteristic of the G_1 phase. This is one of the principal reasons for the lag phase in the growth of animal cells in culture.

The cells in primary and secondary tumours as well as their descendants in culture have lost the mechanism causing contact inhibition. Thus, they continually grow and divide, overwhelming other tissues in vivo and forming multiple layers in culture dishes. Actively growing normal and cancerous cells have a higher metabolic activity than those that are in G_0 phase or have

differentiated and can no longer undertake growth and division. Most of these cells only require ATP for maintenance purposes whereas those in growth are synthesising considerable amounts of biomass and undertaking the energetically demanding process of cell division. Much of the ATP utilised by cells is in protein synthesis, and this requires approximately 4-5 ATP molecules per peptide bond.

4. TISSUES/ORGANS

The greatest amount of work in this field has been done on the heat production of striated muscle starting with the pioneering studies by A.V. Hill that began nearly 90 years ago [1]. It continued in his hands for more than 50 years [65] and then passed to others [5-7]. Smooth and cardiac muscle received comparatively less attention till recent times. The reverse is true of heat dissipation in nerve cells in which there was some remarkable early work [8] and little in later years. After some interesting fundamental studies on the heat output of other tissues earlier this century [6], the more contemporary studies in this area have been stimulated by the need to know about the physiology of medical conditions, including cancer (see for instance Reference [66]).

4.1. Muscle

4.1.1. Striated muscle

The basic facts about heat production in striated muscle have been known for some time [7,65]. Although some of the crucial data has been obtained using calorimeters, it must be said that many results were obtained by inserting thermopiles into the muscle tissue in vitro [65]. This technique is more highly sensitive than calorimetry and has a rapid response time but it cannot be used while the tissue is immersed in a solution [6]. By use of thermopiles, it is known that the heat flow rate of striated muscle during contraction is 100 to 1000 times greater than at rest. This initial heat lasts for a few seconds and is followed by a recovery period of up to an hour during which there is the continuous production of a smaller amount of heat. Then, the heat flow rate returns to that of the resting condition. Unlike in purely chemical reactions, a considerable amount of work is done by this contractile system. In order to account for the enthalpy of the heat and the external work, h, in terms of the chemical reactions, therefore, a modified form of Equation (8) must be used,

$$H = \sum n_i \Delta h_i \tag{10}$$

where n_i is the number of moles of reaction *i*. In this way, it was shown that much of the initial heat was derived from the tightly coupled conversion of the phosphogen, creatine phosphate to ATP to give the energy for the contraction. During this process, the external work was done on the system [7]. The amount of heat produced was independent of whether the muscle was under normoxic or anoxic conditions. It was during the second, longer phase of lesser heat production that the degree of oxygenation became important because this was when the level of creatine phosphate was restored to normal using ATP synthesised by the catabolic pathways. Normally, the supply and demand for ATP is tightly coupled but dominating this transient period is the endothermic (and endergonic) process of phosphorylating ADP and creatine (43 kJ mol^{-1} – see Reference [25] and also Section 5.5) by harnessing the catabolic process. This means that, during this period of restoring the steady state, an enthapy of 6 × 43 = 258 kJ is metabolically conserved in fully coupled net phosphorylation for each mol of oxygen utilised in the respiration of glucose. This increases the enthalpy change for fully uncoupled respiration from maximally –469 kJ mol^{-1} to –211 kJ mol^{-1}.

Making an account of the chemical reactions by the enthalpy balance approach during the contraction-relaxation cycle failed to explain all the sources of the heat [67]. In frog sartorius muscle, for instance, the unexplained heat was 21% of the total produced during isometric tetanic contractions at 0 °C [68] (see Figure 10). To consider the source of this unexplained heat, it must be recalled that contraction is initiated by the depolarisation of the sarcolemma spreading to the T-tubule system. This causes the Ca^{2+} bound to calsequestrin in the sarcoplasmic reticulum to be released into the sarcoplasm (cytosol) and bind to troponin C [4]. It is the entropy change caused by the movement of the Ca^{2+} ions that accounts for at least some of the unexplained heat. Another source of it that is difficult to quantify accurately is the splitting of ATP in the pumping of Ca^{2+} ions back to the sarcoplasmic reticulum to mark the end of the contraction cycle. The exact stoichiometry of this relationship is not known but it is maximally 2 ATP per Ca^{2+} ion.

The active Na^+,K^+ pump restores the resting potential in the depolarised sarcolemma. Thirty years ago, it was thought that this pump made a considerable contribution to the overall amount of heat generated during contraction. In order to reinvestigate this claim, Chinet et al. [69] designed and built a combined direct and indirect calorimeter to measure the heat flow rate and the oxygen uptake rate (OUR) of perfused tissue (see Figure 11). It actually consisted of four heat conduction instruments and it was commercialised by SL Secfroid S.A. (Aclens, Switzerland). The cardiac glycoside ouabain was employed to inhibit the Na^+, K^+ ATPase of rat soleus muscle and thus it was

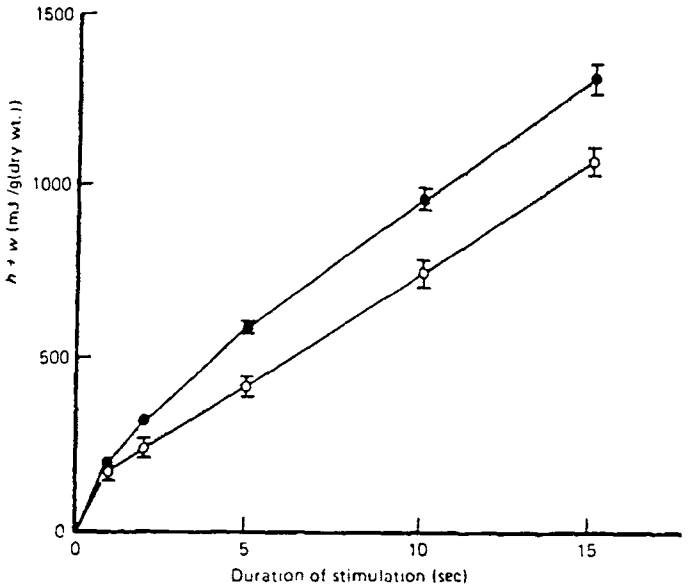

Figure 10. This shows the heat + work produced (•) during a 15 sec tetanus of a frog sartorius muscle at 0° C and the heat + work that is due to the measured PCr splitting (O). The bars show 1 SEM (Original data from Reference [68]) (Reproduced from Reference [67] with permission).

found that the pump only made a small contribution of 4.7% to heat production. The authors then calculated that the Gibbs energy transferred to the ions as they were transported across the sarcolemma (*W*) was 0.04 mW g (wet wt.)$^{-1}$ min^{-1}. Using this finding as an example, the overall thermodynamic efficiency, ε, [5] of the process at steady state conditions is,

$$\varepsilon = \frac{\mathrm{d}W/\mathrm{d}t}{\mathrm{d}\xi/\mathrm{d}t}\Delta_r G \tag{11}$$

where $\Delta_r G$ is the total rate of expenditure of Gibbs energy involved in the process. Since the entropy change for substrate oxidation is small compared with the enthalpy change [24], the heat flux is approximately equal to the Gibbs energy flow rate and so it was possible to calculate the thermodynamic efficiency to be 34%. On the premise that the maximum efficiency of the

cellular energy conservation process is 65%, it was estimated that the minimum energetic efficiency of ATP utilisation by the active Na^+, K^+ transport process in mammalian striated muscle is 52%.

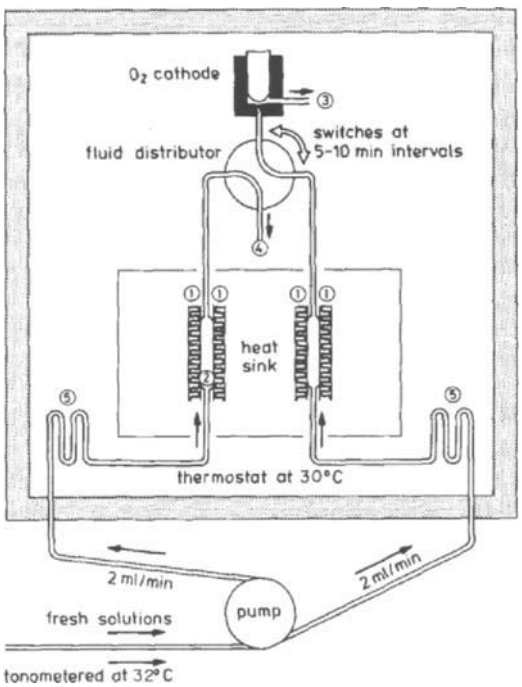

Figure 11. Scheme of one of the microcalorimeters used for the simultaneous measurements of O_2 consumption and heat production rates in perfused preparations. The thermal gradient layers (1) are made of semiconductor thermocouples mounted in series on each chamber. The preparation (2) is placed near the upstream extremity of one of the 8-cm long tantalum chambers, so that most of the heat it produces is transmitted to the surrounding aluminium block that functions as a heat sink. The four-way distributor, driven from outside the thermostatic jacket by a torsion bar and a pneumatic valve, directs the effluents of the preparation chamber and the control chamber to the drain, alternately via a jet in front of the O_2 cathode (3) or directly (4) every 2 to 5 min. Immediately upstream of the calorimeter chambers, the downstream components of the heat exchangers (5) are wound together, in co-current, in close contact with an extension of the aluminium block (not represented on the drawing) (Reproduced from Reference [70] with permission).

It is possible, of course, to use direct calorimetry, often in combination with the indirect approach (OUR) to investigate the properties of muscle under different physiological conditions and in the diseased state. Chinet's group [70] found that the slow- and fast-twitch skeletal muscle fibres from the murine model of Duchenne muscular dystrophy had a reduced sarcoplasmic energy metabolism as measured by the combined direct and indirect calorimeter [69]. The possibility that this could be due to diminished glucose availability was then examined [71] but was dismissed in favour of decreased oxidative utilisation of glucose and free fatty acids, conceivably due to defective mitochondria.

In recent years, there has been increasing interest in the use of calorimetry to study the effects of drugs on muscle biopsies. The first consideration must be to establish calorimetric conditions that minimise artefacts. The Thermometric family of heat conduction calorimeters [72] was designed with the needs of the biologist in mind and the perfusion vessel is suitable for use with tissue samples [73]. In its standard form, this vessel has a stirrer but this was replaced by a basket to hold the muscle biopsies (Figure 12). The stirring rate was 24 rev/min and the medium perfusion rate was 20 $cm^3\ h^{-1}$. As an example of the type of experiment that can be done [74], human striated muscle was taken from the lateral vastus (proximal thigh) of volunteers given the β-adrenceptor blocker, propranolol and of the controls without medication. The calorimetric data showed that blockade of the sympathetic β_2-receptors decreased muscle thermogenesis (see Figure 13) and impaired isokinetic endurance.

4.1.2. Smooth muscle

In contrast to striated muscle, there has not been a sustained study of the sources of the heat flow rate in the smooth type. Some interesting work, for instance on rat anococcyeus muscle [75], has been performed, but the potential of calorimetric studies in this respect will be illustrated by the example of guinea-pig taenia coli smooth muscle [76]. The strips were chemically skinned in a solution based on Triton X-100 and then mounted isometrically on the hooks of a muscle holder in the modified titration vessel of a Thermometric heat conduction calorimeter (see Figure 14). The holder acted as the turbine stirrer and the tissue was incubated in a carefully designed solution containing 3.2 mM MgATP and creatine phosphate, pH 6.9. Unlike the striated type, there is only a very small phosphogen store in smooth muscle and so the heat flow rate of skinned muscle should accurately reflect ATP turnover.

One disadvantage of skinned muscle is that Ca^{2+} must be added to cause contraction. The resulting heats of mixing and binding must be backed off from the results. This was done successfully and it was found possible to titrate the effects of increasing the Ca^{2+} concentration using a Hamilton syringe and also

demonstrate the effects on parallel experiments of force generation recorded with Grass FT03 force transducers. The results depicted in Figure 15 indicate that, as the heat flow rate increased with the stepwise increments in $[Ca^{2+}]$ from p*Ca* 9 to 4.8, the energetic cost of force maintenance tended to increase at higher $[Ca^{2+}]$. After Ca^{2+} activation, the forces still increased beyond the point at which the heat flow rate had reached its maximum. Skinning eliminated oxidative and glycolytic catabolism as well as abolishing any expression of the Ca^{2+} pump. So, the calorimetric data were consistent with the observed breakdown of creatine phosphate.

Because the chemical environment in skinned muscle is well defined, energy balance studies do not lead to "unexplained" heat values [4]. This is not to dismiss studies on native smooth muscle. It has been shown [77], for instance, that maintenance of tension in the smooth muscle in the pig coronary artery does not entail the dissipation of large amounts of Gibbs energy and is not dependent on the presence of normal Ca^{2+} pools.

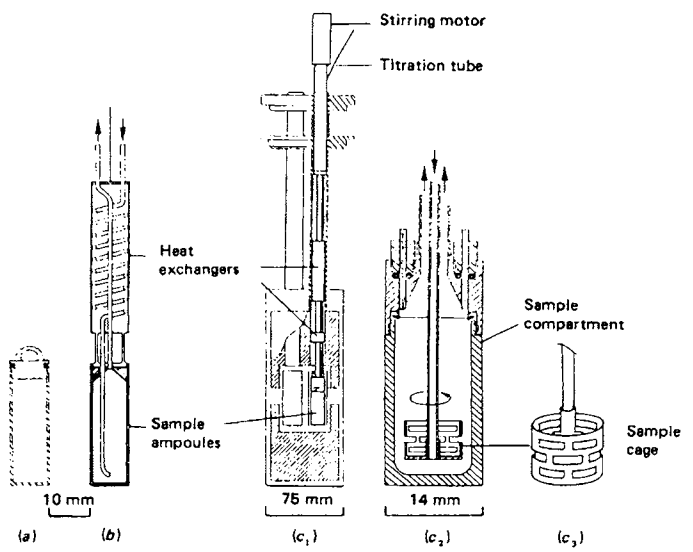

Figure 12. Schematic representation of some parts of the calorimetric equipment: (*a*) Simple cylindrical calorimetric vessel; (*b*) a type of perfusion vessel; and (*c*) another type of perfusion vessel with a simplified picture of the perfusion vessel inserted in the measurement position (c_1), a section through the sample compartment (c_2), and the sample cage (c_3) (Reproduced from Reference [73] with permission).

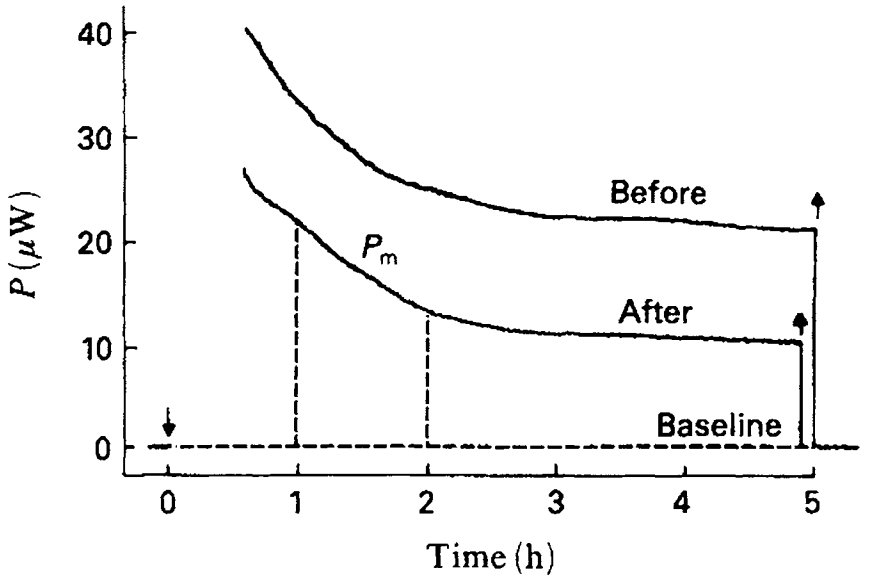

Figure 13. Representative measurements of heat flow rate (P) on biopsy samples from the vastus lateralis muscle, obtained from one subject before and after medication with propranolol. The sample ampoule was inserted into the microcalorimeter at ↓, and taken out at ↑. P_m = the mean value during the second hour of registration (Reproduced from Reference [74] with permission).

4.1.3. Cardiac muscle

There has not been an intensive study to discover all the sources of heat production by all the different muscles in the heart. There have been, however, many recent papers building on the early work reviewed by Woledge [6] and focussed principally on the energetic consequences of lifelong contraction (see for instance References [78-80]). Some of them have also illustrated the powerful nature of combine direct/indirect calorimetry. In this respect, Chinet et al. [81] examined a specific example of the energetics of rat heart papillary muscles. It had been thought possible that energy dissipation and the bearing of tension during ionic contracture in the myocardium may not result from one and the same process. The OUR data were converted by an oxycaloric equivalent to being the indirect heat flow rate and compared with the direct calorimetric results. These obviously included the anaerobic pathways as well as respiration. It was shown that over a 15-min contracture plus a 45-min recovery cycle, both sets of rates were consistently larger than the basal rate (see Figure 16). During

contracture, the direct heat flow rate was higher than the indirect rate by 24% and in the recovery by 21%, meaning that the myocardium incurs the maximum oxygen debt compatible with complete oxidative recovery. From this result, it was suggested that the contracture tension was maintained at low energy cost whereas the heat was mainly related to the homeostasis of the intracellular calcium.

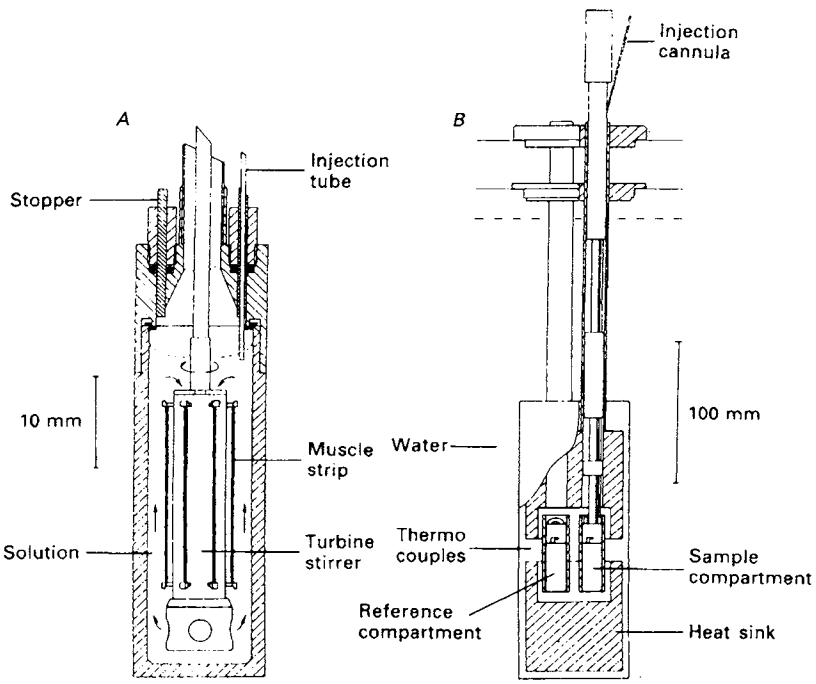

Figure 14. *A*, the specially modified sample compartment in the Thermometric TAM microcalorimeter showing the turbine with the muscle strips attached to it; *B*, the twin heat conduction calorimeter with the insertion vessel and an identical set-up without the sample in the reference compartment. Note that the calorimeter may be used for titration (Reproduced from Reference [76] with permission).

4.2. Nerve

Generation of the action potential in a nerve is accompanied by a biphasic change in heat flow rate, the first is exothermic and the second is endothermic

(Figure 17). For a crab non-myelinated nerve, the initial exothermic heat after a single impulse was found to be -11.7 mJ g^{-1} and the subsequent endothermic heat was $+10$ mJ g^{-1} [82]. A similar experiment for rabbit non-myelinated fibres gave quantitatively different values of -102.5 and $+92.9$ μJ g^{-1}, respectively [83]. The dissimilarity is probably due to surface area differences. In both cases, the nerves possessed a residual heat flow rate of 1.7 mJ g^{-1} for the crab and 9.6 μJ g^{-1} for the rabbit. This situation continued for over 200 s compared with the short biphasic peak for the action potential of 0.5 s. The relatively large amounts of heat produced and absorbed during this transient impulse cannot be explained by chemical reactions in the nerve.

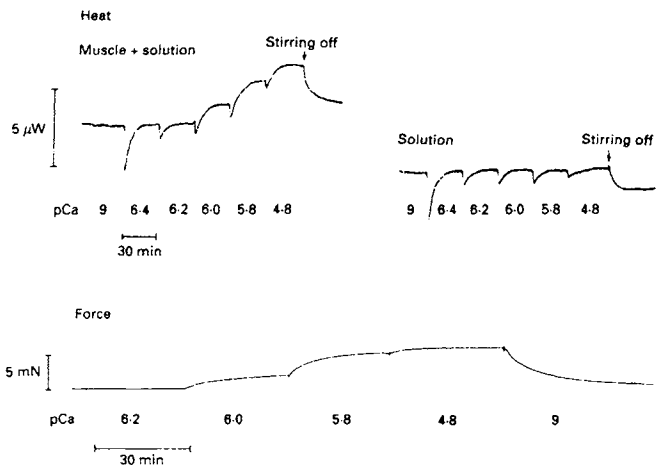

Figure 15. Muscle titrated with $CaCl_2$ solution. The upper panel shows heat rate records with and without muscle, respectively. The lower panel shows the corresponding force development from muscle fibres taken from the same preparation (Reproduced from Reference [76] with permission).

Ritchie [8] likened the electrical properties at the membrane of a nerve to those of a condenser. He reasoned that the biphasic thermal peak was due to the changes in entropy that accompany the charging and discharging of such a condenser. He maintained that the change in enthalpy on discharging a condenser of capacity C at a thermodynamic temperature T (K) may differ considerably from the change in Gibbs energy by an amount $T\Delta S$, that can be shown to equal $\Delta G(T/C)(\Delta C/\Delta T)$. If $\Delta C/\Delta T$ is positive, heat will be released on

the discharge; and if $\Delta C/\Delta T$ is negative, the entropy change will lead to the absorption of heat. In terms of the dielectrics, the permittivity, ε, varies with the thermodynamic temperature (see Figure 18). For any substance, $\varepsilon/\Delta T$ is zero near the absolute zero of temperature.

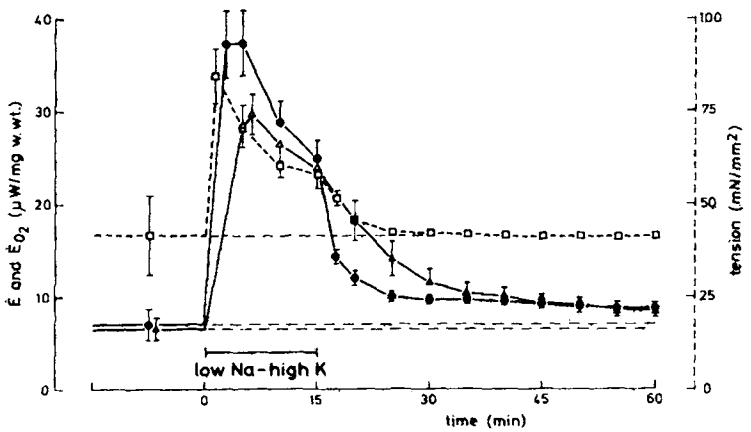

Figure 16. Effects of a 15-min exposure to a low-Na, high-K solution on the direct (dots) and indirect (triangles) calorimetric fluxes expressed in μW/mg wet weight, and on isometric tension (squares) expressed in mN/mm^2. All three variables were measured simultaneously, at 30 °C, on nine right papillary muscle preparations (vertical bars denote SEM). $\dot{E}_{O_2}$ values were computed from mean $\dot{E}_{O_2}$ determinations over 2 to 5-min periods and a standard energetic equivalent of –450 kJ/mol O_2 (Reproduced from Reference [70] with permission).

From Figure 18 it can be seen that, as the temperature increases, ε also increases at first but starts to decrease after reaching a certain critical temperature, so that $\varepsilon/\Delta T$ is positive in the range from zero temperature until the critical temperature is reached, and thereafter it is negative. Below the critical temperature [8,44], electrical polarisation of the dielectric increases entropy (see Figure 18); above it, polarisation decreases entropy. From this generalised consideration, it will be seen the situation depends on the exact relationship between the membrane capacity and the thermodynamic temperature for a

particular nerve. This is not known in the cases of the crab and rabbit for technical reasons, but the squid giant axon was shown to have a positive temperature coefficient for permittivity [8]. If this is also true for the nerves in question, it means that the entropy changes on the discharge of the condenser would indeed account for the bulk of the heat produced by them. In addition, it seems likely that the small residual heat was due to the activity of the sodium pump (Na^+, K^+-ATPase) (see Section 4.1.1. and References [8,69]). Hydrolysis of ATP is of course required for the movement of ions against a concentration gradient and the heat generated is presumably due to the need for re-phosphorylation of ADP by the oxidative process in the mitochondria.

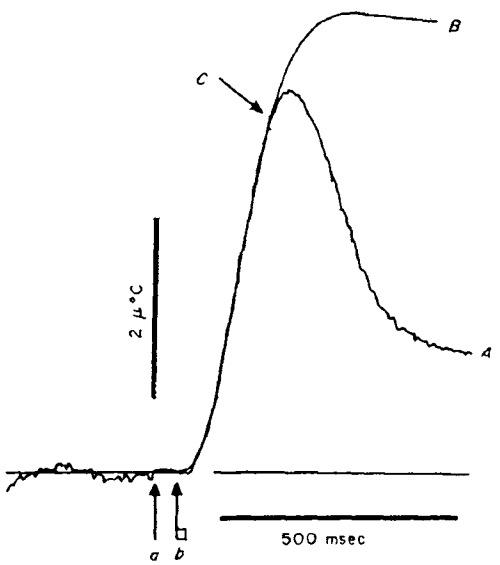

Figure 17. Curve *A*: the changes in temperature of the non-myelinated fibres of a rabbit desheathed vagus nerve at 4.2 °C in response to a single maximal stimulus of 2 msec in duration applied at *a*. The record is the result of averaging 20 records electronically. Curve *B*: the rise in temperature of the same nerve, after it had been rendered inexcitable by isotonic KCl, in response to a block of heat (twenty-one 200 μsec pulses of current applied between the two ends of the nerve at 1 msec intervals) beginning at *b*. The amplification was about a tenth of that in *A* and was adjusted to make the early part of the rising phase of *B* coincide with the early part of Curve A (Reproduced from Reference [8], after Reference [83], with permission).

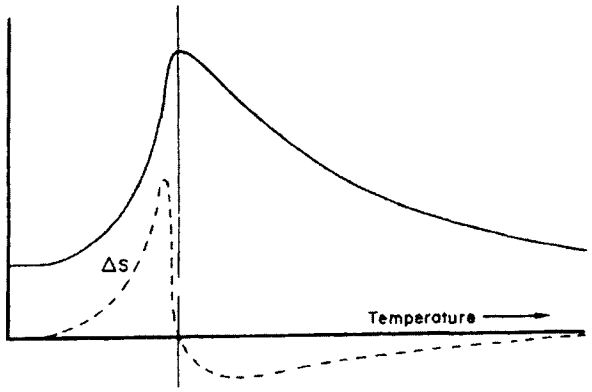

Figure 18. The variation of the permitivity, ε, with temperature. The broken line shows the increase in entropy (ΔS) associated with the electrical polarisation of the dielectric (Reproduced from Reference [8] with permission).

4.3. Diseased and damaged human tissues

Attention has only recently focussed on the potential of calorimetry for studying the differences in metabolic activity caused by the diseased state and by such procedures as transplantation. In this respect, attention has already been drawn to an investigation into Duchenne muscular dystrophy (see Section 4.1.1). A disease that affects a far larger proportion of the population, however, is cancer. One of the most serious problems in treating neoplasia lies in the initial detection of it. Some of the methods rely to an extent on subjective criteria and it would be a great advantage if there were a more objective approach.

For reasons identified previously (see the various subdivisions in Section 3), isolated neoplastic cells in vitro have a greater metabolic activity than their normal counterparts, as detected by calorimetry (see Table 1). Singer's group [84] has shown that this characteristic is a feature of many different tumour tissues from the human urogenital tract. Using a range of tissue biopsies to compare the tumour state with the normal one, it was shown that the use of calorimetry can allow such a distinction because heat production in the tumour tissue was as much as 8.4-fold higher than that for normal tissue. Furthermore, it proved possible to differentiate between the various histological gradings for the tumour tissue using microcalorimetry.

After successful detection, the next stage is to secure a cure. One suggestion has been to heat tumour tissue by microwaves to 60 °C and kill the cells by coagulation of their proteins – thermotherapy [85]. For this to have some chance

Table 1
Heat flux, $J_{\Phi/N}$, for mammalian cells with ranges or standard deviations for some cell types. The tabulation is based on data in References [4,6,7,8] that give the original sources (Reproduced from Reference [44] with permission).

Cell type	$J_{\Phi/N}$ /pW per cell
Human erythrocytes	0.01
Human platelets	0.06
Bovine sperm	1.3 ± 0.1
Human neutrophils	2.5 ± 0.3
Human lymphocytes	5
Horse lymphocytes	8
Human T-lymphoma	8 ± 1
3T3 mouse fibroblasts	17
Chinese hamster ovary (CHO) 320 (recombinant)	~23
KB	25
Vero	27 ±2
Mouse lymphocyte hybridoma	30 – 50
HeLa-53G	31.2
Mouse macrophage hybridoma, 2C11-12	32 ± 2
LS-L929 fibroblasts	34 ± 3
Chinese hamster ovary (CHO)-K1	38
Human foreskin fibroblast	40 ± 10
Rat white adipocytes	40
Human white adipocytes	49 ± 15
Human melanoma, H1477	80
Human keratinocytes	83 ± 12
Hamster brown adipocytes	110
SV-K14 (transformed) keratinocytes	134 ± 35
Rat hepatocytes	329 ± 13

of success, many of the physical properties of the tumour must be better understood, including (i) optical properties in terms of the scattering and absorption of photons and (ii) thermal properties such as specific heat capacity and thermal conductivity. The specific heat capacity, C_p, can be calculated [86],

$$C_p = E\Delta U/m\beta \tag{12}$$

where the calibration factor, $E = 279.8$ mW V^{-1}, the differential voltage ΔU, the heating rate $\beta = 3$ K min^{-1} and the mass, m. The differential voltage is determined by differential scanning calorimetry (see Reference [87] in Volume 1 of this Handbook) with the value being taken from the thermogram (Figure 19) at a temperature of 37 °C. This profile is typical for a lung tumour. In Figure 19, the difference between the reference curve and the measured curve gave a differential voltage of 10.67 mV.

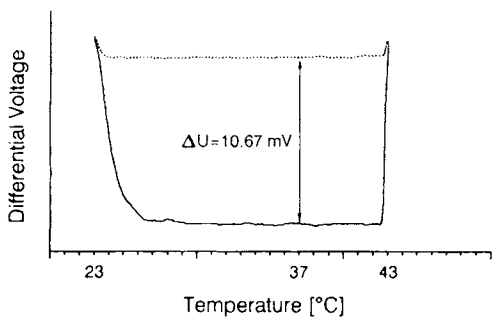

Figure 19. Thermogram of tissue from a tumorous lung. The continuous line is the measured curve and broken line is the reference curve (Reproduced from Reference [86] with permission).

On a different topic, there is increasing pressure to improve the success rate of organ transplantation. As an example of the contribution that calorimetric measurements can make to this field, attention is drawn to a study on ischaemic liver. Tissue injury to liver due to hypoxia or ischaemia during surgery and transplantation is a serious problem and it is difficult to predict recovery from it. It has been suggested [88] that calorimetry, as an indicator of metabolic activity, might have role in prediction. One of the traditional indices of the ischaemic

state is ATP concentration but the ATP cycle is very dynamic and dependent on many factors. For this reason, measurements of static tissue concentrations during the ischaemic time course cannot fully represent the true cellular energetic state, and is certainly not a useful predictive variable for recovery after reperfusion [88]. As explained in Section 2, calorimetry measures the rate of heat flow and therefore indicates the dynamic metabolic condition of the cells. A positive indication of the advantage of calorimetry over other biochemical estimations can be seen in Figure 20 in which there is a good correlation between the time course of the heat flux and the functional recovery after reperfusion [88].

5. CELLS

5.1. Cell types and their differing adhesion

In the animal body, of course most of the cells stick to one another to form solid tissues and organs. The cells of one particular tissue, blood, are derived from stem cells in the haemopoietic tissue but are non-adhesive for the majority of their short, mature lives. Thus, blood was an early subject for calorimetric study, largely by some of the clinical scientists in Lund, the city that is the "spiritual" home of the LKB/Thermometric calorimeters. In the early days when batch vessels had no stirrers and were only rotated, the cells were pumped through a flow calorimeter because sedimentation in batch vessels caused the "crowding effect" (see Section 3.2.1) due to the onset of anoxic conditions.

Whole blood has rarely been examined (but see References [89,90]) and most of the investigations have been on various fractions of blood tissue, including cells purified as single types. As such, they are covered in a separate Chapter by Monti in this Volume and are only considered in this chapter to illustrate certain generic points. The rest of Section 5 is devoted to cells from tissues other than blood and includes the one non-adhesive normal type of cell apart from the blood cells, that is the gamete. This area of research has been reviewed several times over the years by Kemp (see References [4,9-11,16]).

To investigate cells from solid tissues/organs, in many cases they have to be dissociated by an enzyme. The most common one is trypsin, with or without the chelating agent, ethylene diamine tetra acetic acid, EDTA [91]. Calorimetric studies have only rarely involved freshly dissociated cells [92,93] because the tissue debris formed during the preparation can be very troublesome and causes great variation in the results. The use of established cell lines has been more common. Most of these are of course still adhesive and stick to surfaces. This fact can been ignored in some cases when using stirred vessels. For instance, the heat production of leukaemic KM-3 cells routinely grown on the surface of T-

flasks [94] was measured in the stirred insertion vessel designed in Wadsö's laboratory [95] (see Reference [3] for details).

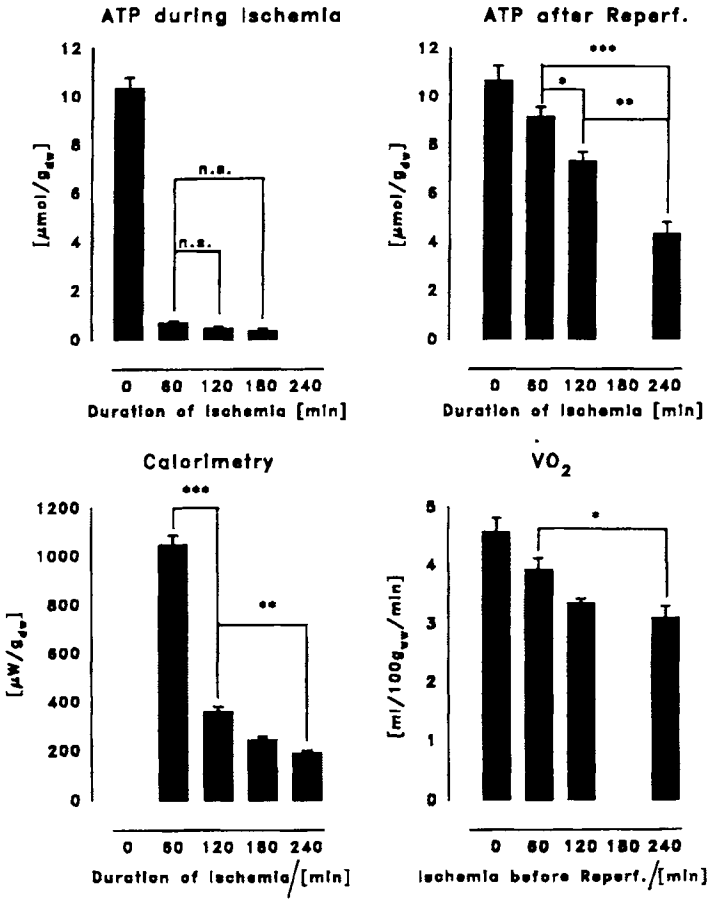

Figure 20. Synopsis of the metabolic parameters measured during ischaemia (ATP concentration and calorimetry) and during or after reperfusion (ATP concentration and oxygen consumption). The metabolic recovery is dependent on the duration of the preceding ischaemic storage. This kind of dependency could be predicted by the time course of the metabolic rate but not by measurement of ATP concentration at specified time points during ischaemic storage. Data are mean ± SEM (Reproduced from Reference [66] with permission).

As briefly mentioned earlier in this chapter (see Section 3.1.1), several different strategies have been adopted for obtaining data for the heat production of cells attached to a substratum. Human keratinocytes were grown to confluency on the collagen coated hydrophilic membrane of a Petriperm dish [96], a piece was cut out and then inserted into the chamber of a large capacity Calvet calorimeter (see Reference [3] for details of it) to record the heat production. In another approach, rabbit macrophages were grown as two-tiered monolayers in the stainless steel vessels of a Thermometric TAM calorimeter [36]. In another ingenious approach, Ba/F3:6 lymphoid cells have been allowed to attach to the blades of a modified stirrer in a Thermometric insertion vessel [37]. Although the 4-cm^3 vessel can be used for this purpose, in practice it is less mechanically demanding to employ the 20-cm^3 one for this purpose. These days, it would seem preferable to take advantage of one of the several types of beads that have been designed to act as the substratum for growing cells at high density. Examples include chick fibroblasts attached to relatively large, solid glass beads [92], Vero cells adherent to solid Cytodex 1 microcarriers from Pharmacia AB [38] and CHO 320 cells stuck to the multiple surfaces of macroporous Cytopore 1 carriers [97]. It is crucial, however, that whatever strategy is employed, it avoids the problem of the "crowding" effect that leads to anoxic conditions (see Section 3.2.1). One ingenious approach to avoid this problem resulting from cell sedimentation was to add Percoll (Pharmacia) to the culture medium and thus increase its density to allow the cells to "float" in the medium [98]. The alternative that is normally employed for suspension cell cultures in both bench and industrial reactors is to stir the cells at an appropriate rate.

5.2. Heat flow rate as a variable in animal cell bioreactors

Over the past 15 years, there has been an increasing use of animal cells, principally from insects and mammals, to produce medically important substances such as monoclonal antibodies from hybridomas, recombinant proteins from genetically engineered cells and vaccines. The cells are grown in carefully controlled bioreactors with on-line monitoring of parameters such as temperature, pH and dissolved oxygen. With the exception of biomass measurements by laser nephalometry and dielectric spectrometry, there has been a paucity of reliable biosensors to measure metabolic variables such as changes in the concentration of materials [55]. With one notable exception, there has been little recognition among biochemical engineers that heat flow rate is in fact potentially the perfect biosensor since, as shown in Section 2, Equation (6), it is a function of the metabolic rate [4].

5.2.1. The bioreactor as a calorimeter

It has long been recognised that one problem always to be resolved in the design of an industrial scale calorimeter is the dissipation of heat produced by the cells. If the rate of heat production is measured, then this is an excellent way to assess metabolism. With this in mind, von Stockar's group has adapted a 2-L Mettler RC-1 heat accumulation calorimeter used mostly for the safety testing of chemical reactions in industrial plants (see Reference [3] in Volume 1 for calorimeter types) to measure the heat produced by cell cultures. In this guise, it has been used predominately for microbial studies (see Duboc et al. in this Volume for details) but a first attempt to exploit its potential for animal cells was in 1989 when a hybridoma cell line was used as the experimental system [99]. Two techniques for delivering air to the cells were compared, namely "under surface aeration" and sparging by air (see Figure 21). When combined with data on the consumption of glc and the production of lactate (lac), the results showed that the culture with under surface aeration had a yield of heat to glc, $Y_{Q/S}$, of 41.49 kJ c-mol^{-1}. For the sparged culture $Y_{Q/S}$ was much higher at 66.6 kJ c-mol^{-1}. This meant that the sparged culture was more aerobic, a conclusion borne out by the fact that it contained less lac and gave a lower $Y_{lac/glc}$ yield (0.96 c-mol/c-mol) than did the one that was gassed by under surface aeration ($Y_{lac/glc} = 1.24$ c-mol/c-mol). At that time, the detection limit for the reaction calorimeter was ~2×10^6 cells per cm^3. It should be noted that the starting point for cell cultures is generally an order of magnitude lower than less than this density, rising perhaps to approximately 1×10^6 cm^{-3}. It is only recently that improvements to the calorimeter (see Duboc et al. in this Volume; also References [100,101]) have resulted in a sufficiently low detection limit to follow the course of a conventional batch culture of animal cell culture. While the improved Mettler calorimeter allows model experiments on the bench scale, it is not intended to act as a biosensor for industrial scale bioreactors.

5.2.2. Combination of bioreactor with flow microcalorimeter

A solution has been found for the requirement to measure heat production in industrial bioreactors by circulating the cell suspension from the bioreactor to a flow calorimeter [102]. A 3-L Applikon bioreactor that contained a stirred suspension of CHO 320 cells genetically engineered to produce interferon-γ (IFN-γ) was taken to be the model for an industrial scale plant. It was connected by thermostated PEEK transmission tubing to an ex situ and on-line Thermometric flow microcalorimeter (Figure 22; see Reference [32]) with a standard gold flow-through vessel (0.6 cm^3) that had been modified for downward flow to minimise blockage (Figure 1). The thermal volume was

calibrated by the triacetin reaction (see Section 3.1.2) to be 0.77 cm^3 at pumping rate of 35 $cm^3\ h^{-1}$. Because the results were to be used for enthalpy balance studies on this thermodynamically open system (see Reference [20]), it was important to (i) define the boundary of the system and (ii) ensure that the conditions were the same throughout that system. For the first requirement, it was decided that the infinitely thin boundary was in the walls, of, in sequence, the glass bioreactor, the PEEK transmission tubing, the Viton (or Aliprene) of the pump tubing and the gold of the flow vessel. For the second imperative, the transmission tubing was thermostated at the same temperature as the bioreactor and the calorimeter while the PEEK transmission lines and the Viton/Aliprene pump tubing were selected for their low gaseous diffusivity. In addition, the pumping rate was found experimentally to be sufficiently fast to ensure that the dissolved oxygen in the medium remained at normoxic levels because the cell suspension passed through the calorimetric measuring vessel at the dilute cell densities typical for animal cell culture.

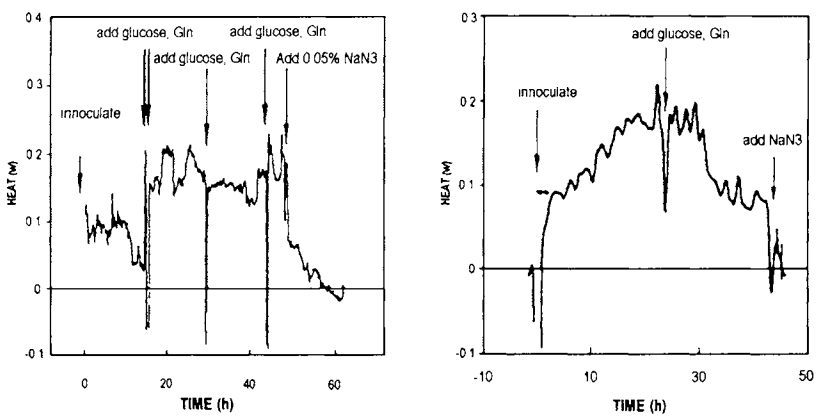

(A) (B)

Figure 21. (A) Heat produced by a hybridoma suspension culture with under-the-surface aeration. (B) Heat production by the same type of culture with sparging by air (Reproduced from Reference [99] with permission).

The continuous heat flow rate and the numbers of viable cells at discrete time intervals were recorded during a batch culture of CHO 320 cells. These measurements gave the important result that the metabolic rate declined while

there were still increases in the cell number concentration (see Figure 23). The implications were that the heat flow rate could be an even more sensitive reflection of cellular metabolism if it were made specific to biomass, i.e. scalar heat flux.

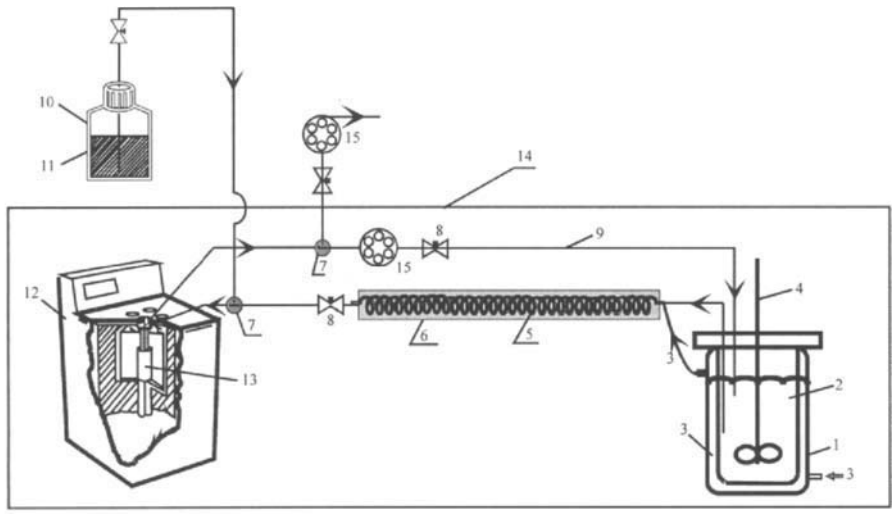

Figure 22. A schematic diagram for the measurement of the heat flow rate of bioreactor-cultured animal cells using a flow microcalorimeter. 1 – bioreactor; 2 – cultured cells; 3 – jacket water for temperature control in the bioreactor; 4 – agitator; 5 – the outlet tubing of the jacket water is used for warming the cell suspension in the tubing leading to the microcalorimeter; 6 – a non-conductive sponge-plastic pipe is used to reduce heat dissipation along the outlet jacket water attached to the PEEK tubing transmitting the cell suspension to the calorimeter; 7 – PEEK T-piece; 8 – PEEK two-way valve; 9 – PEEK tubing (1 mm I.D.); 10 – glass bottle holding sterilized medium for washing the flow vessel of the microcalorimeter through short-time interruption of the heat flow measurement; 11 – sterile medium for cleaning the flow vessel free of possible accumulated animal cells, that would result in an overestimation of the heat flow rate for the cells in the bioreactor; 12 – a representation of the 4-channel Thermometric calorimeter (TAM); 13 – the gold flow vessel assembly; 14 – the dotted boundary, enclosing essentially the bioreactor and the flow vessel of the microcalorimeter, is an open thermodynamic system for enthalpy balance studies; 15 – the peristaltic pump (Reproduced from Reference [32] with permission).

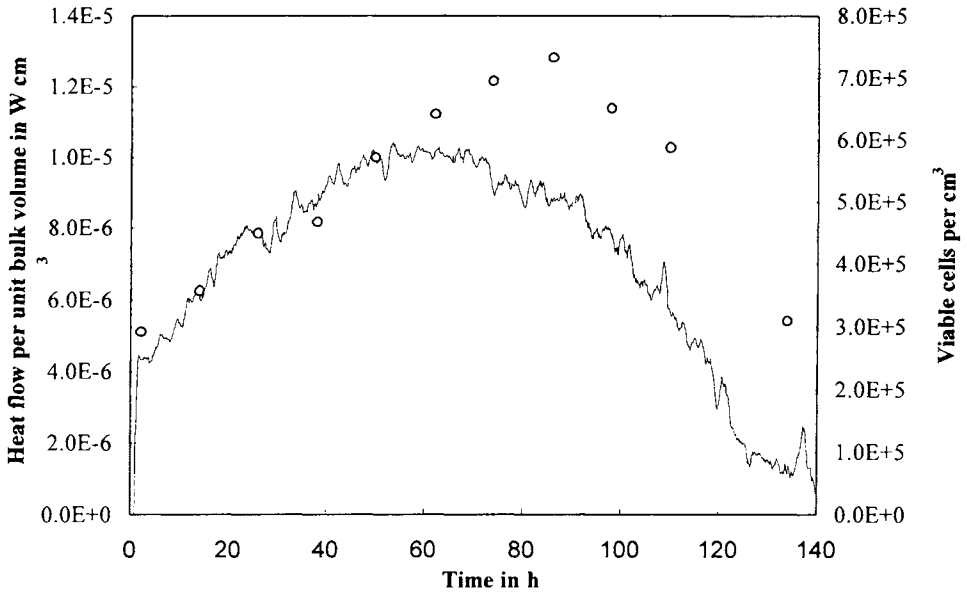

Figure 23. The heat flow rate of growing cells measured on-line by the microcalorimeter and scaled to the unit bulk volume of RPMI 1640-based culture medium buffered with 20 mM HEPES and 4 mM bicarbonate (—). Estimates were made for the number of viable cells per cm^3 bulk volume (o) at discrete time intervals (Reproduced from Reference [44] with permission).

It was found that the biomass could be measured with the in situ, on-line probe of a radio frequency (0.5 MHz) dielectric spectrometer (Viable Cell Monitor; Aber Instruments Ltd., Aberystwyth, Wales, UK). The capacitance (C, in Farads, F) measurements made with this instrument have been shown both theoretically [56] and by calibration with a flow cytometer [103] to record the volume fraction of the viable cells, when there is no change in conductivity. Providing there is also no alteration to the cell volume during the culture period, therefore, monitoring the change in capacitance indicates the variation in biomass. The Applikon BioXpert software [103] zeroed the capacitance for the value obtained with the culture medium, smoothed the two signals by the moving average technique and divided the digitised capacitance signal by that of biomass to give the flux. The resulting trace, $J_{\Phi/C}$, compared favourably with one in which the heat flow rate at discrete times during the culture was divided by the cell number concentration (N) obtained off-line with a Coulter counter,

$J_{\Phi/C}$, (Figure 24) and it had the advantage of being continuous, on-line [44,103]. Then the on-line heat flux profile was compared with the discrete changes in the concentrations of the major substrates, glucose and glutamine, measured by off-line methods (Figure 25). The significant finding was that the biosensor detected a decline in the metabolism of the CHO 320 cells before there was an apparent alteration in the consumption of the two substrates. This result also confirmed the fact that, despite evidence of reduced metabolic flux, the cells continued to grow (see Figure 23) and produce IFN-γ. What such measurements of concentrations cannot show, however, is any variation in the rates of material change. This requires the use of differentiation between at least two time points, t_1 and t_2, for each period of the batch culture and then it only gives the average relative rate. The research of Tikhonov [104] allows an alternative approach that employs an integration equation to furnish the instantaneous rate in preference to the conventional differential equation that only gives the average rate between two time points. So far, the Tikhonov functional has not been applied to data for material flows.

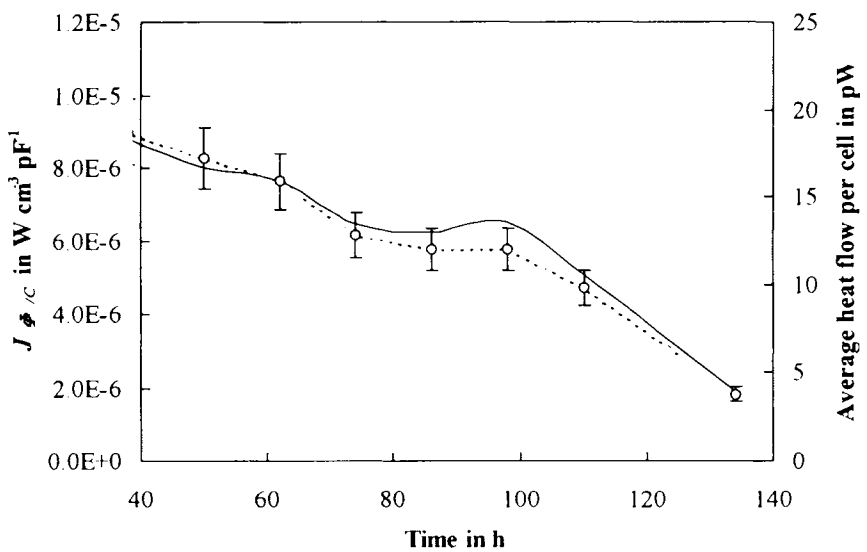

Figure 24. On-line heat flux measurements adjusted to per cm^3 bulk volume (—) and heat flow per viable CHO 320 cell (o) over 140 h of a batch culture. In the expression of $J_{\Phi/C}$, the values are given in terms of 1 cm^3 bulk medium volume (Reproduced from Reference [44] with permission).

For the work on CHO 320 cells described by Guan et al. [103], the average relative rates were obtained and made specific to cell number concentration. The data then showed (see Figure 26) that indeed the specific growth rate (μ) and the fluxes of the major substrates and products, including IFN-γ, did begin to decline at the relatively early time indicated by the heat flux biosensor. In fact, by plotting the fluxes for the major materials against the heat flux (Figure 27), it is clearly seen that there is a monotonic relationship to describe the fact that heat flux is a function of the material fluxes. This means that it can be regarded as an on-line, real time biosensor that (i) has a rigorous thermodynamic foundation to it, (ii) gives the instantaneous metabolism flux, (iii) is non-invasive as well as being non-destructive and (iv) is robust with no consumable components. Its use can be extended to medium design and fed-batch cultures in which heat flux is the control variable.

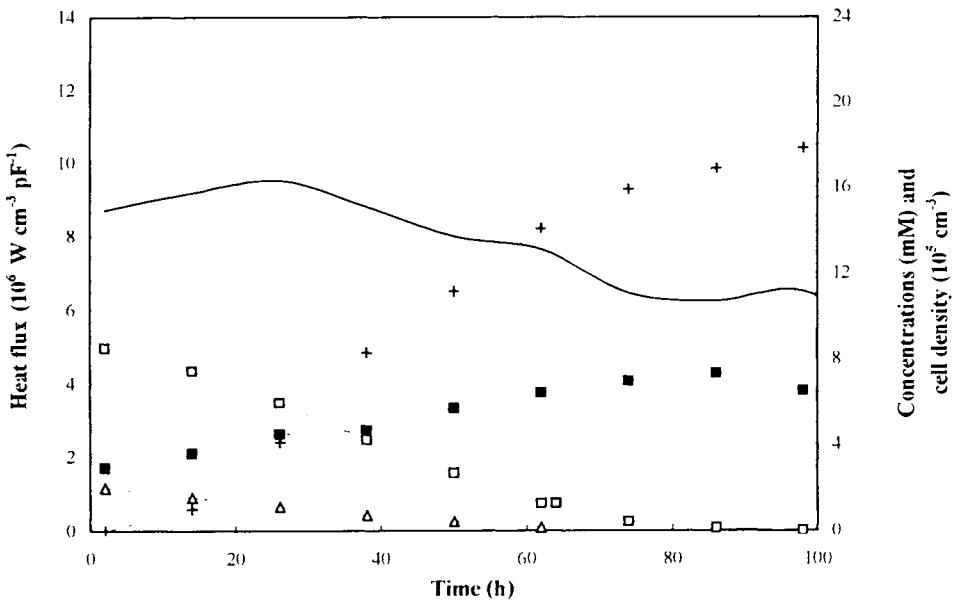

Figure 25. On-line measurement of heat flow rate and capacitance calculated on-line as heat flux (—) with off-line measurements of cell density (■) and changes in the concentrations of glucose (□), glutamine (Δ) and IFN-γ (+) for a batch culture of CHO 320 cells (Reproduced from Reference [22] with permission).

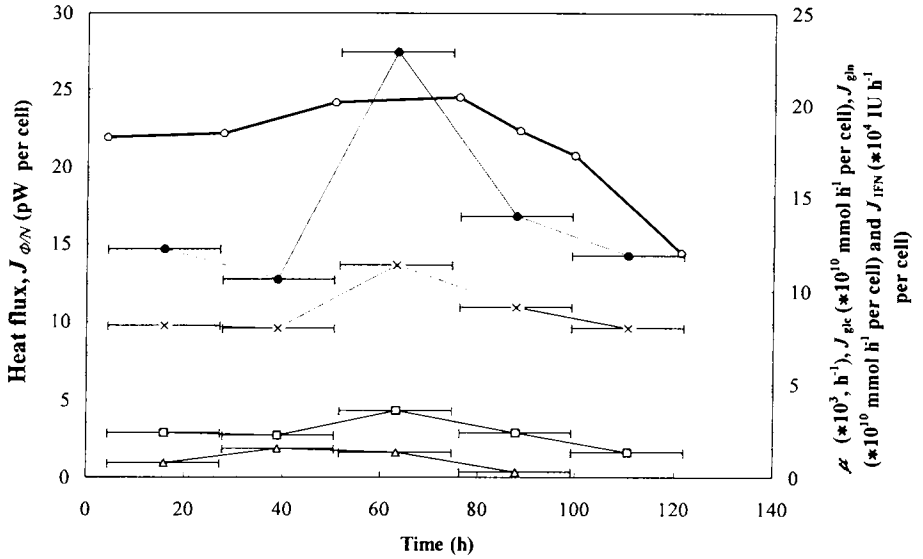

Figure 26. Comparison of the heat flux ($J_{\Phi N}$) with the fluxes of glucose (J_{glc}), glutamine (J_{gln}) and IFN-γ (J_{IFN}), as well as the specific growth rate (μ) during the batch cultivation of CHO 320 cells in suspension. Heat flux (O), glucose flux (□), glutamine flux (Δ), IFN-γ flux (×) and specific growth rate (•). The bars indicate the period over which the discrete off-line measurements were made to give the individual average values for fluxes (Reproduced from Reference [44] with permission).

5.2.3. Heat flux and the growth reaction

The growth of cells from substrates is a chemical reaction, albeit a complex one, and is accompanied by a change in enthalpy. In Chapter 10 of his famous book, Battley [18] describes the general procedures for writing microbial growth-process equations and the three simple rules in principle can be extended to the information necessary to construct the growth reaction for higher organisms:

(i) The elemental composition and the quantity of the substrates used as a source of carbon and energy for growth;

(ii) The elemental composition and quantity of any organic products of the growth process. This includes the cells and, especially in the case of cells

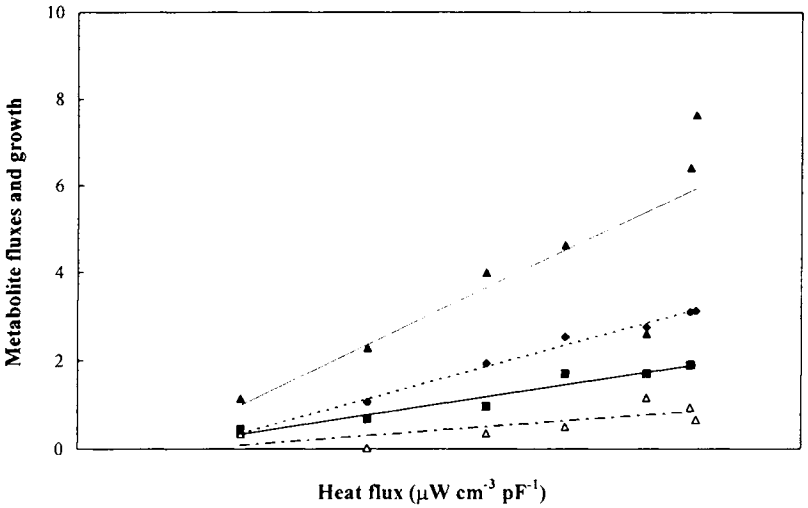

Figure 27. Heat flux is plotted as a function of the specific growth rate (■) showing the monotonically decreasing relationship. This dependence extends to the fluxes for 10^4 × IFN-γ production flux, IU s^{-1} per cell, (▲) and the major catabolites, 10^7 × glucose consumption flux, mol s^{-1} per cell, (◆) and 10^7 × glutamine consumption flux, mol s^{-1} per cell (Δ) (Reproduced from Reference [22] with permission).

producing heterologous proteins, any secondary product. The elemental composition of the cells (biomass) should consist of the ash-free proportions of C, H, O and N and is usually expressed as in terms of C-mol. The formula has the form $CH_{n_H}O_{n_O}N_{n_N}$, where n_H, n_O, and n_N represent the relative numbers of hydrogen, oxygen and nitrogen atoms, respectively, when the number of carbon atoms is taken as one.

(iii) The elemental composition of the nitrogen sources. In animal cells, these are the amino acids.

The validity of the constructed growth reaction can be tested by the enthalpy balance method (see Sections 2 and 5.2.4). The metabolism of animal cells is much more complex than that of microbes but it has been found that in practice the components of the growth reaction can be simplified sufficiently to make the exercise a feasible one for cells grown in a defined medium without serum [44]. Although there are still many nutrients without this complex additive, it has been shown that the micronutrients can be neglected and that, for enthalpy balance studies, it is justifiable to ignore the amino acids [105] because the

enthalpy of anabolism is negligible, at least for microbes [18]. Considering all these factors, Guan and Kemp [105] decided that the following stoichiometric equation was a justifiable basis for constructing the growth reaction of cells producing heterologous proteins and was also appropriate for an enthalpy balance approach,

$$\nu_{Glc}C_6H_{12}O_6(Glc) + \nu_{Gln}C_5H_{10}N_2O_3(Gln) + \nu_O O_2 \rightarrow CH_\alpha O_\beta N_\gamma(cell) + \nu_L C_3H_6O_3(Lac) + \nu_C CO_2 + \nu_N NH_3 + \nu_H H_2O + \left(\int_{t_1}^{t_2} J_{H,r}\,dt\right) \quad (13)$$

The following conditions should be noted for Equation (13): (a) molecular formulae are used to aid the subsequent material and energy balances; (b) any target protein (e.g. IFN-γ) is combined with the biomass which is expressed by a C-molar formula as customarily utilised for microbial biomass (see the Chapter by Duboc et al. in this Volume and also Reference [20]); and (c) the stoichiometric coefficient of the cell mass is set at unity and so the enthalpy change of the growth reaction now is based on unit number of C-molar biomass [105]. It has been shown from experimentation (see Figure 27) that there is a one-to-one monotonic relationship between the metabolic flux (see Equation (7)) and the stoichiometry of the growth equation (Equation (13)). This can be expressed by:

$$\frac{1}{x}\frac{d\xi}{dt} \leftrightarrow \vec{\nu} \quad (14)$$

It means that the metabolic activity of the cell determines the stoichiometry of the growth equation and a particular set of stoichiometric coefficients for this equation corresponds to a value of the metabolic activity for the same amount of viable cell mass. Thus, for Equation (13), the growth reaction is characterised by its set of stoichiometric coefficients [105], that is,

$$\vec{\nu} = \left(\nu_{S_1} \quad \nu_{S_2} \quad \nu_O \quad 1(cell) \quad \nu_L \quad \nu_C \quad \nu_N \quad \nu_H \quad \nu_x\left(\int_{t_1}^{t_2} J_{H,r}\,dt\right)\right) \quad (15)$$

Looking at Equation (14) in the light of Equation (15), it is explicit that the cellular metabolic requirement can be determined by measuring the metabolic flux, specifically represented by the heat flux variable [105]. Since the metabolic flux varies with time in culture, the stoichiometry expressed by Equation (14) must change to reflect it. If the variable is measured for the culture on-line and

in real time, the cellular nutritional demand must be reflected in the growth equation. In the first place, however, it is necessary to incorporate the experimental data into the growth equation and to validate it by the enthalpy balance method.

5.2.4. The growth reaction and the enthalpy balance method

The Mayer enthalpy balance method is a device for checking that the construction of an equation to describe a chemical reaction is correct. There is no limit to the complexity of the equation and the calculations must obey Hess's Law that the net heat evolved or absorbed in any chemical change depends only on the initial and final states, being independent of the stages by which to reach the final state. Thus, the method is invaluable for checking the validity of the growth reaction, including the assumptions underlying it in terms of, for instance, the effect of excluding micronutrients (see Section 5.2.3).

In terms of the growth reaction, the enthalpy balance is achieved when the sum of the enthalpy changes of all the reactions occurring during growth is equal to the heat production measured by calorimetry [16,20,44,105]. As described in equation (9), the enthalpy change of the growth reaction can be calculated as the sum of all the individual reaction enthalpy fluxes, J_H, for the constituents in Equation (13) from their measured reaction fluxes and the molar reaction enthalpies. In the case of CHO 320 cells, the former is calculated from the type of data depicted in Figure 25 for the concentrations of the materials.

Some of the molar reaction enthalpies are well known but they still have to be corrected for the side reactions present under the environmental conditions of the culture, for instance the enthalpies of neutralisation of the products. For calculating those reaction enthalpies not expressly in the literature, the most comprehensive reference work is the Appendix to Wilhoit [63] and it may be necessary to make the calculations on the basis of balanced reaction stoichiometries and the known enthalpies of formation, $\Delta_f H^\circ$, in dilute aqueous solution. There are, however, other useful sources of information in, for instance, References [18,20,64].

The ratio of the heat flux to the enthalpy flux, J_Q/J_H, is known as the enthalpy recovery (see review in Reference [102]). If the ratio is balanced, then it confirms the description of the (growth) reaction. If the value is greater than unity, then there is at least one unaccounted reaction in the system. If it is less than unity, then there is at least one unnoticed endothermic reaction.

The direct application of the enthalpy balance method to growth reactions such as Equation (13) requires knowledge of the enthalpy of combustion for the cell mass. It is a major difficulty to obtain a clean sample of animal cell biomass

free of protein and other environmental macromolecules in the medium because the plasma membrane is relatively delicate and easily lysed during washing procedures. In addition, the large amount required for combustion, three dried samples of 0.5 g each, is a formidable proposition in terms of amount of animal cells, unlike for microbes (see procedures outlined by Gurakan et al. [106]). Because it is now possible to grow cells in completely protein-free medium, this is an experiment waiting to be done, for which Kemp [3] in Volume 1 of this Handbook tells the reader about bomb calorimeters.

For those without the required instrumentation, an alternative indirect approach is to calculate the enthalpy of combustion, $\Delta_c H_i$, for compound *i*, in this case biomass, from the known Thornton regularity of the heat evolved per equivalent of oxygen, Q_o, [107] using the relationship [108],

$$\Delta_C H_i = Q_o \gamma_i \tag{16}$$

where γ_i is the degree of reductance for any compound *i* of the generalised C-molar formula $CH_{e_{i1}}O_{e_{i2}}N_{e_{i3}}$ defined by

$$\gamma_i = 4 + e_{i_1} - 2e_{i_2} - 3e_{i_3} \tag{17}$$

This meaning makes γ_i four times the number of moles of oxygen required to oxidise one C-mole of compound *i* to CO_2, H_2O and N_2. There is a relatively small range for the value of the heat released per mole O_2 during combustion [109] and the best estimate appears to be –115 kJ deg^{-1} of reductance [108,109]. There is still a problem, however, in that this approach requires knowledge of the degree of reductance calculated from the elemental analysis of the biomass. Sample preparation can still be an issue for the reasons stated above but the size of the lyophilised sample is small at ~3 mg. "Empirical" formulae for the elemental composition of biomass are beginning to appear in the literature and Bushell et al. [110] has given the formula for the murine hybridoma , PQXB1/2, as $CH_{1.7}O_{0.25}N_{0.25}$. From equation (17), the degree of reductance of the biomass (γ_b) is 4.45. More recently, there have been determinations of the biomass formula for the SP2/0-Ag 14 myeloma cell line at $CH_{1.78}O_{0.43}N_{0.25}$ [111] that gives $\gamma_b = 4.17$ and for the *Zac3* hybridoma at $CH_{1.64}O_{0.36}N_{0.24}$ [112] to give $\gamma_b = 4.2$. Erickson [109] regards 4.291 as an acceptable generalised degree of reductance when the elemental formula is unknown. Using the generalised value

for Thornton's regularity (above) and applying the calculated degrees of reductance to Equation (16), the enthalpy of combustion appears to lie in the range –480 to –512 kJ mol^{-1} O_2 with the likelihood of it being towards the lower side. Since the substrates (s), glc ($\gamma_s = 4$) and gln ($\gamma_s = 3.6$), are less reduced than the biomass, CO_2 is a net product of anabolism as opposed to being a reactant in the process, e.g. in anaplerotic reactions.

It is well-established that culture media are generally not optimised for the production of biomass in terms of the supply of the correct stoichiometric quantities of amino acids [49,54,103] and the cells require biosynthetic precursors from glucose via the glycolytic pathway. In addition, glutamine is oxidised to provide energy by glutaminolysis [113–115] as well as being directly (purine and pyrimidine synthesis) and indirectly (transamination to give other amino acids and amino sugars) incorporated into biomass. Although many of the valence electrons (high quality energy – Gibbs energy) of the major substrates are (i) lost as H_2O in the oxidation to CO_2 and (ii) excreted from the cell as lactate, the degree of reductance found for animal cell biomass means that a considerable number of them is conserved in the biomass (see Section 2 for the theoretical background). So, much of the substrate Gibbs energy is dissipated as chemical entropy in the biomass (see Equation (2)) rather than as heat. This opens the whole question of the efficiency of biomass production that has been rather well addressed for microbial systems (see Duboc et al. in this Volume and References [23,108,109,116]). It has not really been addressed for animal cell systems, largely because medical products produced under patent are not price-sensitive at this time.

5.2.5. The application of the growth reaction to medium design

The exhaustion of one substrate before the others seen in Figure 25 with respect to glc and gln is a typical occurrence in cell culture because, in general, an empirical approach has been adopted in formulating culture media, rather than a rational one based on demand by the cell [44]. Xie and Wang [114] have made a complete stoichiometric analysis of the medium requirements for a particular type of hybridoma cell but this is a very lengthy and expensive exercise. Bonarius et al. [113] have employed a mass balance method to improve the medium for another type of hybridoma cell. Yet another way is to use frequency statistics for medium optimisation by applying Plackett-Burmann equations [117]. A plausible alternative to these three methods would be to employ the procedure of constructing a growth reaction. In its fullest sense, this would require either knowledge of the enthalpy of combustion for the particular cell type or sufficient confidence in the regularities detailed above to employ a

reasonable approximation to it. In their absence, it has been demonstrated that an indirect application of the enthalpy balance approach has its merit [105].

Using growing CHO 320 cells as the example of the advocated method, the growth reaction given in Equation (13) is divided into two half-reactions, namely the catabolic half-reaction, Equation (18), and the anabolic half-reaction, Equation (19),

$$(\nu_{S_1})_{cat}\,\text{Glucose} + (\nu_{S_2})_{cat}\,\text{Glutamine} + \nu_O O_2 \rightarrow \nu_L\,\text{Lactate} + (\nu_C)_{cat}\,CO_2 + (\nu_N)_{cat}\,NH_3 + (\nu_H)_{cat}\,H_2O + \nu_x\left(\int_{t_1}^{t_2} J_{H,x}\right)_{cat} \tag{18}$$

$$(\nu_{S_1})_{ana}\,\text{Glucose} + (\nu_{S_2})_{ana}\,\text{Glutamine} \rightarrow \text{Biomass} + (\nu_C)_{ana}\,CO_2 + (\nu_N)_{ana}\,NH_3 + (\nu_H)_{ana}\,H_2O \tag{19}$$

The criteria for the separation are well-established (see Reference [105] for details) but, for the genetically engineered cells used in this example, the anabolic half-reaction is taken to include both (i) substrate degradation to form biosynthetic precursors and (ii) the subsequent syntheses from them of the diverse macromolecules constituting the biomass and the heterologous protein, IFN-γ. For the reason stated in Section 5.2.4, carbon dioxide was incorporated into the right hand side of this half-reaction, together with the consequent H_2O. Equation (19) implicitly involves the relation [105],

$$\Delta_r H_{ana} \cong 0 \tag{20}$$

The enthalpy change for the anabolic half-reaction is neglected on good circumstantial evidence for microbes reviewed in References [18,105]. In one case, it can be seen from the calculations that there is a small but significant enthalpy of anabolism for cultured *Saccharomyces cerevisiae* cells [27] but, even so, the assumption in Equation (20) would only fail by a few percent.

Acceptance of Equation (20) means that, as stated in Section 2, the heat flux of the growth reaction is entirely reflected by that of the catabolic half-reaction (Equation (18)). The details of the methodology are too lengthy for inclusion in this Chapter and are given in Reference [105] but in essence the enthalpy of the catabolic half-reaction constructed as shown in Equation (18) is calculated in the way stated in Section 5.2.4 from the experimental reaction flux data. If this value balances the observed heat flux, then the complete description of the growth reaction is correct and the enthalpy recovery is unity. It should be remembered, however, that batch cultures are not in steady state. The metabolic activity and therefore the heat flux changes in terms of the environmental

conditions include substrate availability and the accumulation of toxic products. This can be seen for CHO320 cells by the differing fluxes during the batch culture (see Figure 26). For the intervals between each sample to assay for changes in the material, the necessary equations for the metabolic, catabolic and anabolic reactions were constructed and are shown in Table 2. The data not unexpectedly reflect the alterations in metabolism with the dynamically changing environment. In particular, they show the demand for substrates with time. As an illustration, when cells were in early "exponential" growth (4-28 h), the demand for glc:gln was 3:1, not 5:1 as provided in the medium. Thus, this is one of the bases for a strategy to supply nutrients in fed-batch culture (see Section 5.2.6). More immediately, it was the impetus to design a new medium for improved growth of CHO320 cells and their production of a heterologous protein [51].

5.2.6. The role of the heat flux biosensor in fed-batch culture

In a batch culture, cells grow in number until one or more of the substrates are depleted, whereupon metabolic activity declines, the cells stop growing and eventually there is death. If the cells are producing medically important substances in the pharmaceutical industry, there is a disadvantage in terms of overall production if cultures have to be started at frequent intervals. Since there is a limit to the concentrations of metabolites in the medium in terms of osmotic pressure, the adopted strategy is to retain the relatively low levels of materials in the batch culture but then feed the cells more nutrients when the growth rate is in decline. The problem has been to detect this retardation because of the paucity of on-line probes that measure a variable related to the slow-down [55]. Heat flux is a good candidate in this respect because, as shown in Equation (14), there is a monotonic relationship between the metabolic flux and the stoichiometry of the growth reaction (see for example that calculated in Equation (13)). Since heat flux, J_{th} is a form of metabolic flux, Equation (14) can be converted as,

$$v_i = f\left(J_{th}\right) \tag{21}$$

The strength of this relationship was illustrated from data for cells grown in batch culture with the improved medium (Figure 28 – see Reference [51]). The utilisation of glucose, glutamine and oxygen was calculated in relation to heat flux for the following stoichiometric ratios,

$$v_{Glc}/v_O = 0.0581J_{th}^2 - 2.0949J_{th} + 19.663 \tag{22}$$

$$v_{Gln}/v_O = 0.0279J_{th}^2 - 1.045J_{th} + 9.8561 \tag{23}$$

Table 2
A typical set of split metabolic reactions for CHO320 cells in suspended batch culture

Period (h)	Metabolic Reactions	Heat Flux (pW per cell) Exp	cal	Enthalpy Recovery
4-28 h	Catabolism: $C_6H_{12}O_6 + 0.24C_5H_{10}N_2O_3 + 0.75O_2 \rightarrow 2.12C_3H_6O_3 + 0.872CO_2 + 0.50NH_3 + 0.14H_2O$	22.1	22.4	101.4%
	Anabolism: $0.35C_6H_{12}O_6 + 0.20C_5H_{10}N_2O_3 \rightarrow 3.10CH_{2.0}N_{0.13}O_{0.87}$			
	Metabolism: $C_6H_{12}O_6 + 0.33C_5H_{10}N_2O_3 + 0.56O_2 = 1.57C_3H_6O_3 + 0.646CO_2 + 0.37NH_3 + 0.10H_2O + 2.30CH_{2.0}O_{0.87}N_{0.13}$			
28-51 h	Catabolism: $C_6H_{12}O_6 + 0.12C_5H_{10}N_2O_3 + 0.50O_2 \rightarrow 2.01C_3H_6O_3 + 0.561CO_2 + 0.23NH_3 + 0.22H_2O$	24.2	25.4	105.0
	Anabolism: $C_6H_{12}O_6 + 0.416C_5H_{10}N_2O_3 \rightarrow 18.02CH_{2.0}N_{0.267}O_{0.733}$			
	Metabolism: $C_6H_{12}O_6 + 0.268C_5H_{10}N_2O_3 + 0.25O_2 = 1.005C_3H_6O_3 + 0.281CO_2 + 0.115NH_3 + 0.11H_2O + 9.01CH_{2.0}O_{0.733}N_{0.267}$			
51-76 h	Catabolism: $C_6H_{12}O_6 + 0.084C_5H_{10}N_2O_3 + 0.64O_2 \rightarrow 1.91C_3H_6O_3 + 0.68CO_2 + 0.17NH_3 + 0.43H_2O$	24.4	24.4	100.0%
	Anabolism: $0.47C_6H_{12}O_6 + 0.47C_5H_{10}N_2O_3 \rightarrow 5.17CH_{2.0}N_{0.18}O_{0.82}$			
	Metabolism: $C_6H_{12}O_6 + 0.377C_5H_{10}N_2O_3 + 0.44O_2 = 1.30C_3H_6O_3 + 0.46CO_2 + 0.12NH_3 + 0.29H_2O + 3.52CH_{2.0}O_{0.82}N_{0.18}$			
76-100 h	Catabolism: $C_6H_{12}O_6 + 0.14C_5H_{10}N_2O_3 + 0.79O_2 \rightarrow 1.94C_3H_6O_3 + 0.863CO_2 + 0.28NH_3 + 0.45H_2O$	22.5	21.8	96.9%
	Anabolism: $0.39C_6H_{12}O_6 + 0.039C_5H_{10}N_2O_3 \rightarrow 2.54CH_{2.0}N_{0.03}O_{0.97}$			
	Metabolism: $C_6H_{12}O_6 + 0.129C_5H_{10}N_2O_3 + 0.57O_2 = 1.40C_3H_6O_3 + 0.621CO_2 + 0.20NH_3 + 0.32H_2O + 1.83CH_{2.0}O_{0.97}N_{0.03}$			
100-122 h	Catabolism: $C_6H_{12}O_6 + 0.13C_5H_{10}N_2O_3 + 1.25O_2 \rightarrow 1.77C_3H_6O_3 + 1.32CO_2 + 0.25NH_3 + 0.94H_2O$	17.6	17.4	98.9%
	Anabolism: non-detectable			
	Metabolism: $C_6H_{12}O_6 + 0.13C_5H_{10}N_2O_3 + 1.25O_2 \rightarrow 1.77C_3H_6O_3 + 1.32CO_2 + 0.25NH_3 + 0.94H_2O$			

Reproduced from Reference [105] with permission)

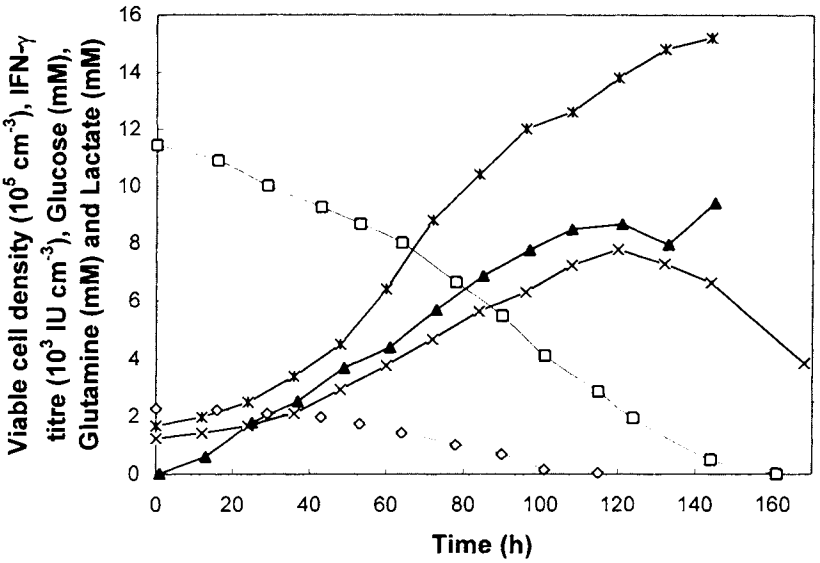

Figure 28. Changes in the concentrations of the major catabolites during the batch culture of CHO 320 cells grown in the improved medium. Cell growth (×) is shown together with the concentrations of glucose (□), glutamine (◊) and lactate (▲) at each time. Also shown is the constitutive secretion of IFN-γ (✱) (Reproduced from Reference [51] with permission).

When expressed graphically over the 120-h period of the culture, it can be seen in Figure 29 drawn from Equation (22) and Equation (23) that heat flux is a monotonically increasing function of these ratios and therefore an apparently valid probe of metabolic activity.

Direct experimental proof of the relationship, however, can only be achieved by using continuous cultures in which theoretically there is a metabolic steady state at each dilution rate [118]. Unlike such cultures of microbial cells, however, a given dilution rate for animal cell culture can still give variation in the concentrations of substrates and products because of their metabolic complexity. This is where the measuring system that monitors on-line both heat flow rate and the viable cell mass to give heat flux [103] has an advantage over most others. A constant value for the former indicates steady state metabolic activity and the latter, as shown in Reference [103], is a good reflection of viable cell mass. In experiments on CHO320 cells [119], the specific metabolic activity as shown by the heat flux plateaux for different dilution rates, was at steady state

and its value increased with increasing dilution rate (see Figure 30). For a given steady state, glucose was at a low concentration and glutamine was depleted entirely in most cases. The concentration of lactate appeared to vary for the dilution rate, $D = 0.016\,h^{-1}$. However, the heat flux for each of the periods selected (usually each period lasts from 4 to 7 days) means that the steady states were properly achieved without long transition periods. This is the first time that a direct measurement of steady state has been made for cultured animal cells. The result is very instructive and opens up a new avenue for addressing and exploring the changes of metabolic fluxes in response to the cellular environment. It is as important, especially from the aspect of employing heat flux as a possible control variable, to realise that Figure 30 gives the required proof of the strict relationship between the material stoichiometric coefficients and their equivalent in terms of heat.

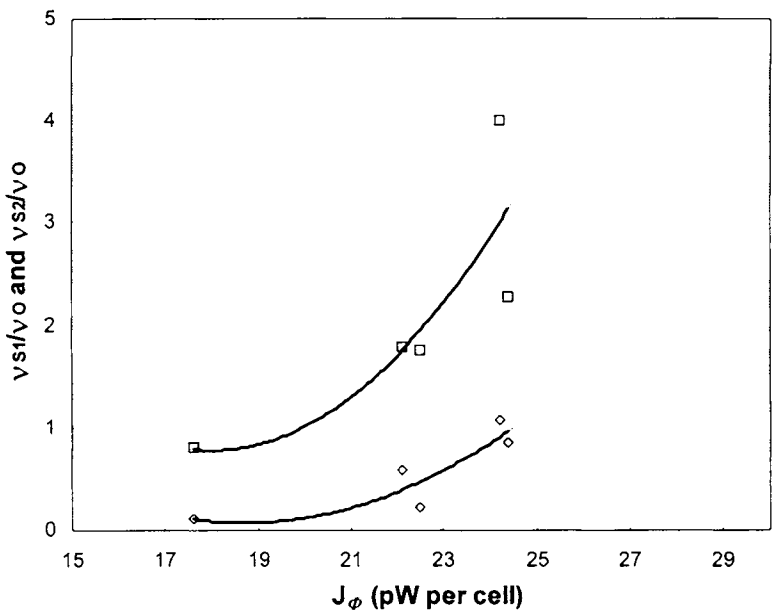

Figure 29. The heat flux over a specified set of values is compared against the stoichiometric ratios for the consumption of glucose (s_1) and glutamine (s_2) to oxygen. The data for the two specific cases [see Equations (22) and (23)] show that the relationship of heat flux to glucose (□) and glutamine (◊) fluxes (Reproduced from Reference [51] with permission).

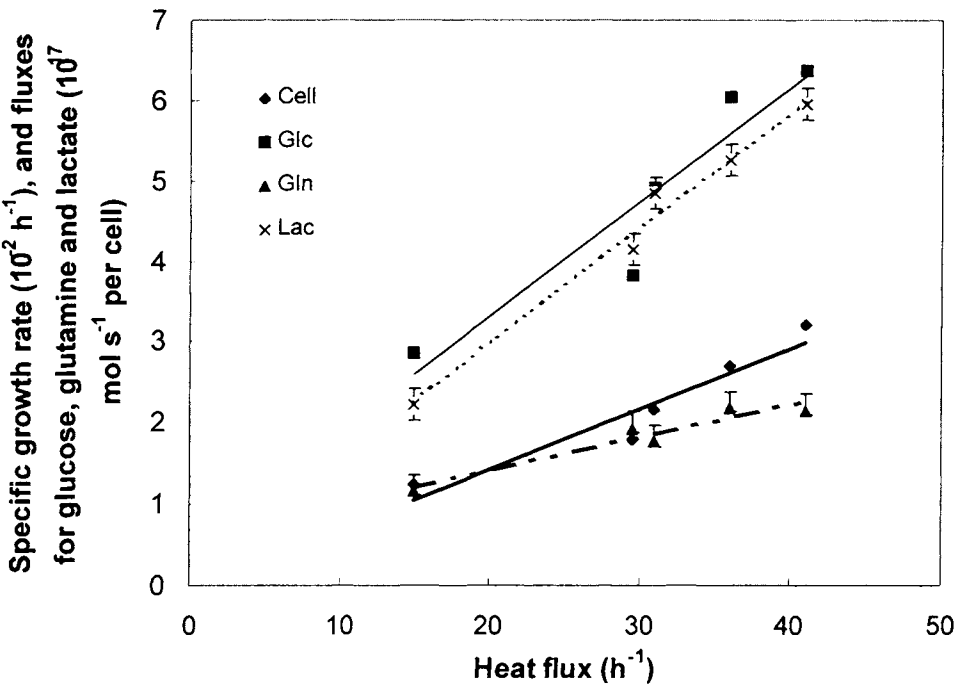

Figure 30. The cell specific growth rate, and fluxes for glucose, glutamine and lactate were correlated to heat flux at different dilution rates in a continuous culture (Reproduced from Reference [119] with permission).

It is suggested from the above results that, once a culture system has been defined in metabolic terms, the heat flux probe is indeed the ideal way for early intervention to control feeding by an automated on-line technique. With this background, the fed-batch experiments were conducted with the averaged decrease in on-line heat flux over a 1-h period being taken as the biosensor signal in the Applikon BioXpert software to trigger the feeding of a nutrient cocktail (glucose, 50 mM; glutamine, 16 mM) to the cells. The results depicted in Figure 31 showed that biosensor-controlled nutrient feeding effectively restored the metabolic activity at cell concentrations below ca. 10^6 cm^{-3}. Above this level, feeding slowed the deterioration in metabolism to a degree dependent on the time in culture. These results give incontrovertible evidence that heat flux is a robust and reliable biosensor that can be used to control nutrient feeding in batch culture.

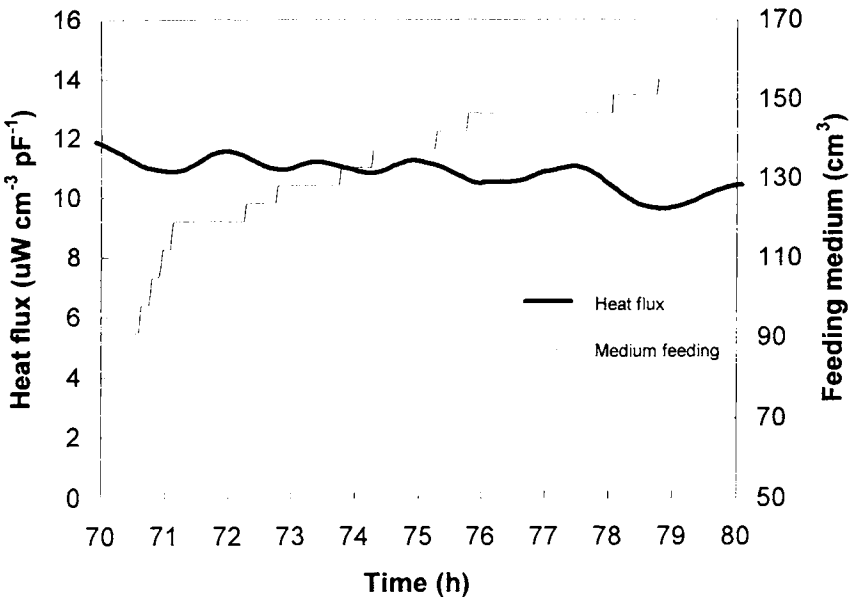

Figure 31. This shows a small section of the heat profile for a fed-batch culture (from 70 to 80h) to illustrate that the medium feeding was triggered by the declining heat flux values over 1-h assessment periods. The heat flux was restored, to a varied extent, by this feeding strategy (Reproduced from Reference [119] with permission).

5.3. Metabolic studies to identify and quantify pathways in cells

As indicated earlier (see Section 5.2.4), it is enthalpy balance studies that permit the identification and characterisation of metabolic pathways. The earliest use of the method for cells in vitro was by Eftimiadi and Rialdi [120] who studied the metabolic events following the triggering of human neutrophils by phorbol-12-myristate-13-acetate to give the respiratory burst. This mimics natural messengers that cause the cell to produce oxygen metabolites such as hydrogen peroxide that destroy the foreign organisms infecting tissues. The cells require NADPH for the process. Radioisotopic tracing was combined with the use of classical metabolic inhibitors. The data depicted in Figure 32 indicated that triggered cells employ both aerobic and anaerobic pathways to provide sufficient NADPH to give the oxygen metabolites as well as ATP for energy. The cells have few mitochondria and so most of the oxidation is in the hexose monophosphate (HMP) shunt.

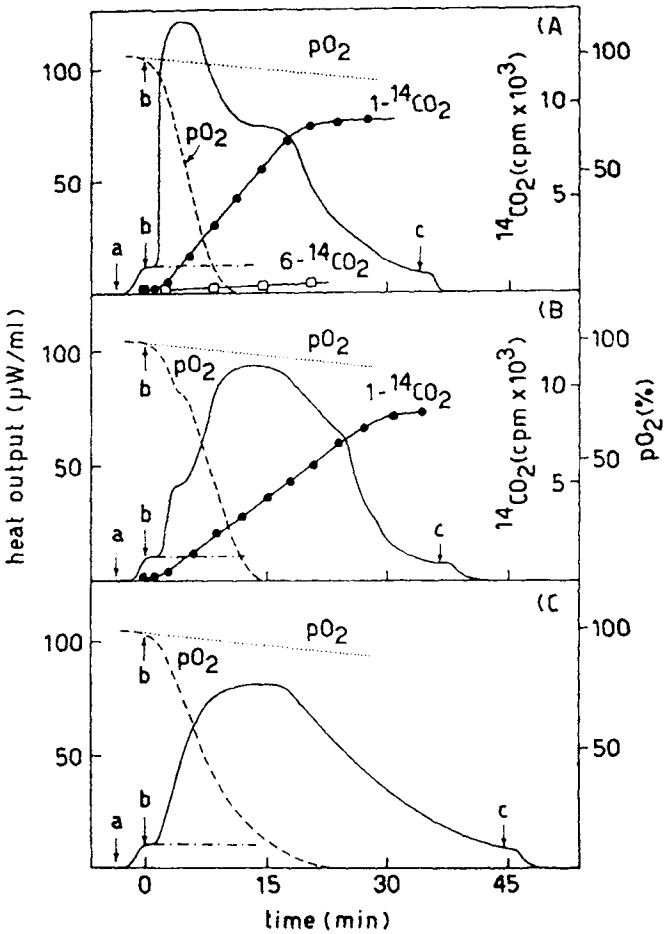

Figure 32. Power-time curves of human neutrophils activated with 10 ng cm^{-3} PMA(—). Arrows indicate additions at times indicated: (a) neutrophils (5×10^6 cells/cm^3; (b) PMA; (c) saline. Representative patterns of power-time curves obtained with the blood donors investigated: A (9 donors), B (10 donors), C (11 donors). Power-time curve of resting neutroplils (– · –). (···) $pO2 = pO2$ in basal state; (---) pO_2 after addition of PMA. [1-$^{14}CO_2$] = $^{14}CO_2$ produced during the oxidation of [1–^{14}C] glucose (–•–); [6–$^{14}CO_2$] produced during oxidation of [6-^{14}C] glucose (–□–). Each point of $^{14}CO_2$ represents the mean of closely agreeing duplicate determinations; the data are from single experiments that are representative of four separate experiments; basal values have been subtracted from the reported values (Reproduced from Reference [120] with permission).

Calculations from the data indicated that oxidative metabolism produced heat of 1 pW per cell. The Embden-Meyerhof pathway to furnish lactate was estimated to give 1.8 pW per cell. Using an elderly LKB model 10700-1 flow calorimeter (see Reference 28) to pump the cell suspension from a stirred vessel, the heat production was found to be 2.5 pW per cell. Compared to the calculated value of 2.8 pW per cell, the similarity was considered to be within the experimental error to justify that all the catabolic pathways had been held to account for the respiratory burst.

A similar study with the same type of calorimeter was later carried out on 2C11-12 mouse macrophage hybridoma cells that undergo a phorbol-triggered respiratory burst after activation with a lipopolysaccharide (LPS) mixture and recombinant interferon-γ [121]. In this case, mitochondria were introduced to the cells from the cytoplasm of the lymphosarcoma cells required in the hybridoma fusion process and so there was an intense involvement of oxidative phosphorylation with a consequent reduced proportion of oxidative metabolism through the HMP shunt. The calculated enthalpy flux from the conventional metabolic data using well-authenticated molar reaction enthalpy values [63,122] was then compared with the experimental value for heat flux (Table 3). It is clear that some important pathways were not discovered for the activated cells and that the same was true to a lesser extent for the phorbol-triggered hybridomas. Unsurprisingly, the increased heat flux of these cells was mostly due to the oxidation of glucose and there was in fact a small decrease in glycolysis.

The study on the macrophage hybridoma cells highlighted the role of glutamine in energy production (see References [49,50,54]). The data were analysed more intensely for the significance of glutaminolysis in metabolism (see Table 4). These stoichiometric calculations revealed that, after allowing for the deamination of glutamine, 16.3 pmol s^{-1} per 10^6 cells was available to the LPS-activated cells. If all the oxygen were consumed in glutamine oxidation, then only 12.6 pmol s^{-1} per 10^6 cells of it could be fully oxidised and none of the glucose. Furthermore, the CO_2 production was lower than would be expected from the glutamine oxidation with a respiratory quotient (RQ) of 1.11. The balance for the ammonium ions also showed that deamination and complete oxidation of glutamine was less than could be suggested from its consumption [121].

There is an alternative to pumping cell suspensions through a flow calorimeter from a culture and measuring changes in the concentrations of metabolites off-line. At the microanalytical scale, it is to make on-line estimations using probes situated in the calorimetric vessel. The Thermometric TAM has a series of different batch insertion vessels with a small volume (see Reference [3]). One type of vessel is designed for tissue perfusion and has a 4-

cm^3 volume. It has been modified to include polarographic microsensors for pH and oxygen (Figure 33 – see Reference 123). It was used to monitor the metabolic activity of immortalised T-lymphoma cells (CCRF-CEM) stirred in suspension. In one experiment, the vessel was regarded similarly to a bioreactor, there being a headspace (0.6 cm^3) so that oxygen could be recruited at the air-liquid interface. The results showed that the cells grew over approximately 30 h while there was a decrease in both the DO and the pH (Figure 34). The authors commented on the fact that the increase in heat production was not exponential, but this is often the case for animal cells rather than microbes [103]. It was attributed to the decline in bulk phase pH because they had already established that this has a detrimental effect on the rate of glycolysis (see Section 3.2.2. and References [45-47,124]). The pH of the HEPES-buffered medium was probably affected by the excretion of lactate produced partly in response to the poorly

Table 3
Flux of 2C11-12 mouse macrophage hybridoma cells calculated from the measured reaction flux and the theoretical molar reaction enthalpy for each reaction pathway

	Molar reaction enthalpy $\Delta_r H_B$ (kJ mol^{-1})	Reaction enthalpy flux J_{th} (μW per 10^6 cells)	
		Activated cells	Triggered cells
Actual heat production		34	58
Calculated heat production for			
(a) Oxidation of			
(i) Gln to CO_2	-2084	-(4.6)	-(2.5)
(ii) Gln to Lac	-695	-3.5–6.3	-2.4–2.8
(iii) Gln to Pyr	-890	-0.2	-0.05
(iv) Glc to CO_2	-3018	-11.6	-45.3
(b) Glycolysis of			
(i) Glc to Lac	-153	-4.2	-2.3
Total		-20.9	50.25

Reproduced from Reference [121] with permission.

Table 4

Stoichiometric calculations[a] for the respiration of glutamine to CO_2 and NH_4^+

Theoretical oxygen flux (J_{O_2})	J_B /pmol s^{-1} per 10^6 cells	
	Activated cells	Triggered cells
Gln transamination (tam) flux $J_{tam} = J_{Asp} + J_{Ser} + J_{Ala}$	$0.83 + 2.67 + 1.5 = 5.0$	$0.47 + 0.76 + 2.6 = 3.83$
Gln deamination (dam) flux to Glu $J_{dam} = J_{Glu} = J_{tam}$	$6.4 - 5.0 = 1.4$	$5.1 - 3.8 = 1.3$
Gln oxidation flux $J_{Gln(ox)} = J_{Gln} - J_{Glu}$	$22.7 - 6.4 = 16.3$	$18.7 - 5.1 = 13.6$
These values are used to calculate the enthalpy change for complete oxidation of glutamine		
Oxygen consumption related to $J_{Gln(ox)}$ $O_2/Gln = 1/0.22 = 4.55$ $J_{O_2}(Gln) = J_{Gln(ox)} \times O_2/Gln$	$16.3 \times 4.55 = 74$	$13.6 \times 4.55 = 62$
Actual value	57	109
Complete Gln oxidation based on O_2 uptake $RQ/Gln = 1.11$		
Ammonium balance $NH_4^+/O_2 = 0.44$		
$J_{NH_4^+}(Gln - ox) = J_{O_2}(Gln) \times NH_4^+/O_2$	$74 \times 0.44 = 32.6$	$62 \times 0.44 = 27.3$
$J_{NH_4^+}(theor) = J_{NH_4^+}(dam) + J_{NH_4^+}(Gln - ox)$	$1.4 + 32.6 = 34$	$1.3 + 27.3 = 28.6$
Actual value	22	18

[a] The theoretical oxycaloric equivalent for glutamine $\Delta_k H_{O_2}$ is –452 kJ per mol O_2 at pH 7 and an enthalpy of neutralization, $\Delta_b H_{H^+}$, of –8 kJ mol^{-1}. Assuming an enthalpy of neutralization of the intracellular buffer $\Delta_b H_{H^+}$ of –21 kJ mol^{-1} [64] and $H^+/O_2 = 0.46$, the standard oxycaloric equivalent ($-452 - [0.46 \times (-8)] = -448$ kJ mol^{-1}) becomes the actual value ($-448 + [0.46 \times (-21)] = -456$ kJ mol^{-1}).

Reproduced from Reference [121] with permission.

designed medium that resulted in the need for recruiting biosynthetic precursors from catabolic pathways (see Section 5.5 and References [51,103,114,115]). The reason for the slight decrease in DO was unclear but, of course, OUR is usually measured in a sealed vessel [125].

In order to discover the longer term effects of incubating cells in medium without a gas phase for oxygen recruitment [123], the perfusion vessel was firstly equilibrated to 37 °C with stirred medium. Then, 100 µl of concentrated cell suspension was introduced to the vessel using a Hamilton microsyringe attached to a high precision, motor-driven pump [126]. This model is no longer available but a substitute with at least an equal specification is the Titration-Injection microPump – TIP – produced by Oroboros Alge (Alge Elektronik GmBH, A-6893 Lustenau, Austria). It was used for the titration experiments on CHO320 cells [22].

The metabolic results found for T-lymphoma cells injected into the vessel after it had been equilibrated to 37 °C for 5 h are shown in Figure 35. With a closed vessel, a reliable estimation was made of OUR as well as heat flow rate until microxic conditions prevailed at 10 h, whereupon there was a rapid decrease in the heat production (Figure 35A). As depicted in Figure 35B, the enthalpy balance calculations revealed that oxidative processes accounted for 60% of the heat flow rate with the remainder being due to anaerobic pathways. Presumably, the main candidate would be glycolysis to produce lactate. The calorimetric-respirometric ratio during the first phase was -776 ± 15 kJ mol^{-1} O_2 (for interpretation of this finding, see Section 5.5).

After 10 h, the second phase was characterised by a gradual increase in heat flow rate that was restored to its former value by 13 h (see Figure 35A). This was entirely due to anaerobic processes (Figure 35B). The carbon flux was found to be double the level in phase 1. This was presumably due to the much lower yield of ATP by such processes that would be dominated by the reduction of pyruvate to lactate in substrate phosphorylation, with the net synthesis of 2 mol ATP per mol Glc. The increased glycolytic flux would result in a decreased pH as seen in Figure 35A. It was not possible of course to monitor the viability of the cells over the 20-h period but one would imagine that the accumulation of toxic lactate [53] would have a profound effect on the cells. Indirectly, this may be supposed from the fact that the heat flow rate during this phase was approximately at the same level as in phase 1, despite the fact that 15× more carbon is required to produce the same quantity of ATP as by oxidative phosphorylation. For the purpose of this speculation, the reliable number calculated by Beavis [62] for the stoichiometric yield of ATP per glc of 33 has been chosen, but there are many other values to be found in the literature (see Section 3.2.8).

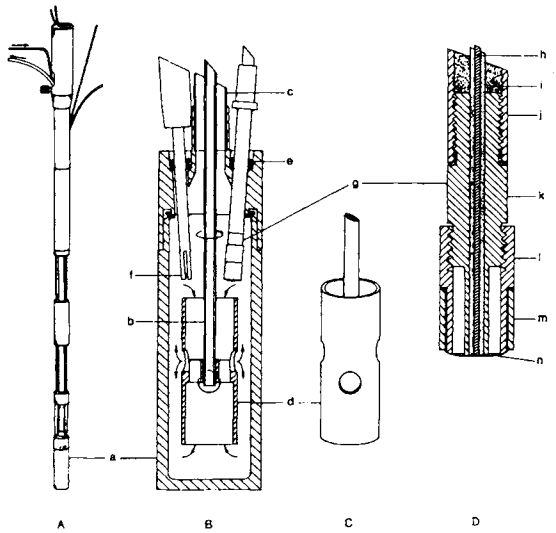

Figure 33. (A) A combined titration/perfusion vessel equipped with a stirring device, a polarographic oxygen sensor and a combination pH-electrode (MI-414). (B) Section through the 3-cm^3 sample compartment with the electrodes mounted. The sample compartment is shown in the perfusion mode, with the turbine stirrer mounted on a hollow stirrer shaft. (C) Turbine stirrer made of Kel-F or stainless steel. (D) Section through the tip of the oxygen sensor. a – sample compartment; b – hollow stirrer shaft; c – outer steel casing; d – turbine stirrer; e – O-rings; f – combination pH-electrode with the glass membrane protected by stainless steel tube; g – polarographic oxygen sensor; h – glass-coated platinum cathode; i – epoxy resin; j – stainless steel tubing; k – silver anode; l – stainless steel membrane holder; m – Kel-F collar; n – double teflon membrane (Reproduced from Reference [123] with permission).

On occasions, it may be preferable to increase the resolution of the respirometric measurements by using much larger electrodes than could fit in the 4-cm^3 vessel. This was the case for a study of reversible metabolic suppression induced by anoxia in isolated turtle hepatocytes [127]. The cells were freshly prepared and were incubated in a phosphate- and HEPES-buffered physiological solution containing BSA but without glucose in order to record the endogenous metabolism from the glycogen stored in them. As seen in Figure 36, hepatocytes in a normoxic environment had a higher heat flow rate than did

those in argon-induced anoxia. Furthermore, only normoxic cells responded to the respiratory inhibitor, cyanide, introduced with a motorised Hamilton syringe. Measurement of OUR with a high resolution Paar Oroboros Oxygraph with Orbisphere electrodes [128] showed that the oxidative processes fully accounted for the heat production. In other words, there was no "unexplained" heat (see Sections 2, 4.1.1. and 5.2.4. for an explanation of "unexplained" heat in terms of the enthalpy balance method), in contrast to the situation for the anoxic hepatocytes. Using the caloric equivalent of glycogen reduction to lactate, it was found that the heat flux for lactate production accounted for 36% of the anoxic heat flux [127]. The enthalpy change associated with the release of free glucose from glycogen breakdown accounted for an additional 6%. The remaining 58% of anoxic heat flux constituted the "unexplained" gap for future investigation.

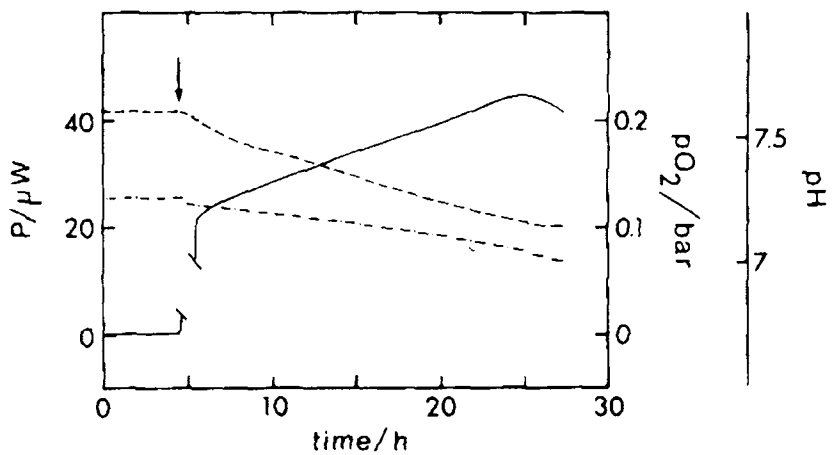

Figure 34. Variation in heat production rate (——), oxygen activity (– – –) and pH (·····) in a suspension of growing T-lymphoma cells. After obtaining baseline values for the medium (RPMI-1640) alone, the cell suspension was added as indicated by the arrow. During the experiment, a gas phase (air) of 0.6 cm^3 was present above the cell suspension (Reproduced from Reference [123] with permission).

For experiments of the above type these days, it would be preferable to use the 20-cm^3 vessels available from Thermometric and CSC (see Reference [3] in Volume 1 of this Handbook). There are now many other possibilities for

biosensors, some based for instance on polarography and others with light guides on changes in fluorochromes. One of the possible criticisms of the work described above is the lack of knowledge of what was happening to the cell suspension in terms of growth and viability. This information could be obtained using a light guide (see Figure 37), such as advocated by Wadsö [129]. In fact, quartz rods were used some years ago as light guides to measure the optical density and thereby the amount of biomass, but this was for yeast [130]. It may now be possible to assess the quantity of viable biomass by dielectric spectroscopy [56] as used in bioreactors [103]. Clearly, it is important to maintain the cells in suspension and thus avoid the "crowding" effect that occurs on sedimentation (see Section 3.2.1). As mentioned previously, if stirring is not possible, then the alternative should be examined to suspend the cells by increasing the specific density of the medium using the PVP-coated silica gel Percoll manufactured by Pharmacia. This has been utilised for BHK fibroblasts that were found to float in 20% (w/v) Percoll and had a heat flux of 15 pW per cell [98].

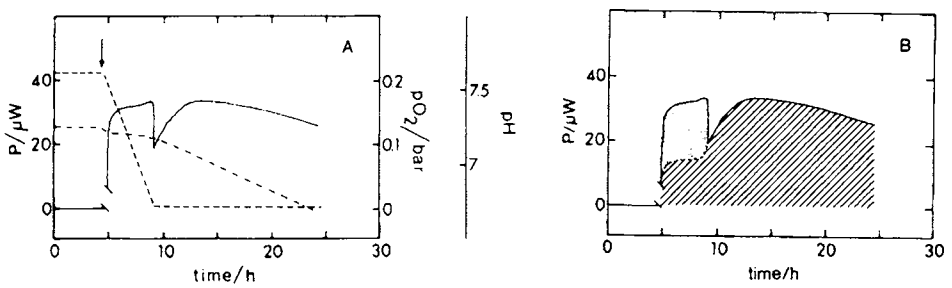

Figure 35. (A) Parallel measurements of the heat production rate (——), oxygen activity (– – –) and pH (·–·–·) obtained from a suspension of T-lymphoma cells growing in RPMI-1640 medium. No gas phase was present during the experiment. Once the baseline had been established, the experiment was started (as indicated by the arrow) by the injection of 100 μl of concentrated cell suspension. (B) The total heat production divided into an oxygen-related part (shaded; calculated as described in the text), and a part not related to oxygen (hatched) (Reproduced from Reference [123] with permission).

Of course, motile cells do not require stirring or flotation. The best example in multicellular organisms is the haploid spermatozoan. In the 1980s,

Hammerstedt's group undertook a series of metabolic studies on bull sperm using a heat conduction microcalorimeter designed and built by Lovrien (Figure 38; also see Volume 1 of the Handbook [3] and Reference [131]). The work was reviewed earlier [10] but, as an example of their studies, Inskeep et al. [132] looked at the differences in metabolism between ejaculated sperm (EJS), that had interacted with the fluids of the accesory sex glands, and newly matured sperm from the cauda epididymus (CES). The total heat dissipation from the former (224 μW per 10^8 cells) was significantly higher than that of the latter (92 μW per 10^8 cells) when both were incubated in vitro with glucose.

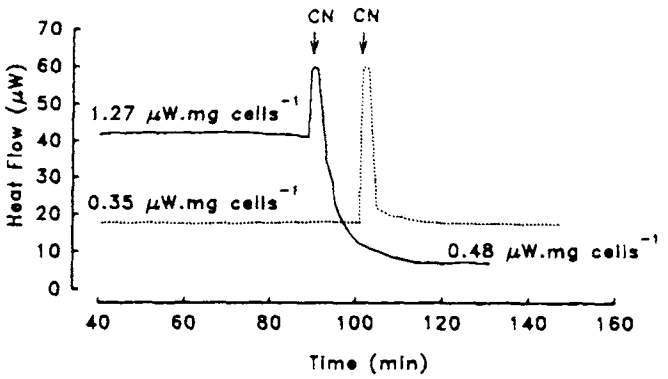

Figure 36. A simultaneous calorimetric trace of normoxic (solid line) and anoxic (dotted line) hepatocytes at 25 °C. Cyanide (CN, 0.5 mM) was added to each incubation at the time indicated by the arrow. The anoxic cells are measured at twice the concentration of the normoxic cells to decrease the error at the low heat flow rate that was close to baseline. The normoxic cells have a linear heat output over the particular concentration range (Reproduced from Reference [127] with permission).

Under similar conditions outside the calorimeter [132], OUR was threefold higher for EJS (414 pmol s^{-1} per 10^8 cells) than for CES (152 pmol s^{-1} per 10^8 cells). On the other hand, the adenylate energy charge (EC = [ATP + ½ADP]/[ATP + ADP + AMP]) was identical for both sets of sperm. Inskeep et al. [132] calculated, however, that the rate of ATP synthesis was greater for EJS (3.6 nmol s^{-1} per 10^8 cells) than for CES (1.39 nmol s^{-1} per 10^8 cells). Less than 0.56 nmol s^{-1} per 10^8 cells for sperm from each source was derived from the

degradation of endogenous reserves. Thus, ejaculation would appear to be accompanied by a large increase in the catabolic rate coupled to the ATP cycle, that is satisfied by the breakdown of glucose. It was also found that the additional ATP generated by the ejaculated sperm was partly utilised in increased motility (85 nmol s^{-1} as against 58 nmol s^{-1} for CES). The remainder may possibly be due to substrate cycling in glucose metabolism at the inter-conversions in the Embden-Meyerhof pathway between glucose/glucose 6-phosphate and fructose 6-phosphate/fructose 1,6-bisphosphate.

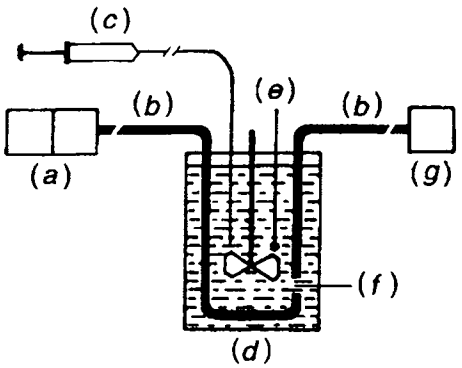

Figure 37. This shows the principle arrangement of a microcalorimetric titration vessel equipped for light absorption. An electrode is also positioned in the vessel. (*a*) lamp and the other optical equipment, (*b*) light guide, (*c*) titration syringe, (*d*) microcalorimetric vessel, (*e*) electrode, (*f*) light path in the medium, (*g*) spectrometer (Reproduced from Reference [129] with permission).

As stated earlier (Section 3.1.1)), it has always been a calorimetric problem to study the metabolism of cells adherent to a substratum. The obvious solution these days is to use beads in a "bioreactor-type" vessel. An early application of such a technique was the use of solid Cytodex 1 microcarriers (Pharmacia) to measure the heat production of anchorage-dependent green monkey kidney (Vero) cells [38] in a Thermometric stirred perfusion vessel [95]. As seen in Figure 39, the heat production was proportional to the number of cells assessed by counting in a Bürker chamber the number of nuclei released from cells and stained with a hypotonic solution of citrate containing crystal violet [38]. In recent years, different kinds of microcarriers have been manufactured that are optimised for specific cell types.

5.4. Pharmacological studies

It would seem obvious that a technique measuring the net metabolic activity of living material should have potential both as a screen for likely drugs and as a tool in seeking to establish the mode of action of natural products and synthetic compounds. Indeed, there has been sufficient research in this direction to show the value of heat measurements and, to illustrate the point, reference is now made to a few of the major studies.

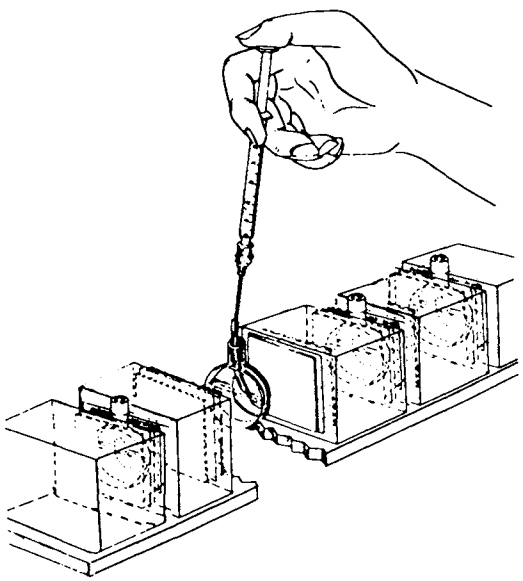

Figure 38. A Lovrien three-channel batch heat conduction microcalorimeter for solution-solution or solution-suspension mixing. Each vessel (5 cm^3 total) has two compartments. The smaller chamber (shown being loaded with the syringe) holds 0.5-1.0-cm^3, while the larger chambers can receive 1.0-2.0 cm^3. After thermal equilibration, 6 to 15 min, the assembly is inverted to mix all the vessels' contents and thus start the reactions. Two Seebeck thermopiles make contact with the sides of each vessel. The reference vessel's thermopiles are connected in opposition to the thermopiles of all the three sample vessels. Thus, the heat of the reference or control experiment is electrically subtracted from the heat of each of the three sample vessels. Port closures may be fitted for the gas purging necessary for either aerobic or anaerobic conditions. The mixing vessel materials are glass, 18 K gold or stainless steel (Reproduced from Reference [131] with permission).

5.4.1. Cancer drugs

The potential for the calorimetric prediction of the action of antineoplastic drugs was first realised in 1988 by Schön and Wadsö [133]. The inhibitory drug methotrexate (MTX) is very well known in genetic engineering because its target enzyme, dihydrofolate reductase (DHFR), is often incorporated into plasmids for co-amplification. It effectively stops DNA synthesis by arresting de novo synthesis of purine and pyrimidines. In the experiments under discussion, it was injected into a suspension of neoplastic cells of the T-lymphoma line stirred in a Thermometric perfusion vessel by a Kel-F turbine [45]. As seen in Figure 40, the drug had an effect on heat flow rate within 2 h. A satisfactory dose-response curve was then constructed from the calorimetric data over the range of 0.02 – 2.00 μM MTX.

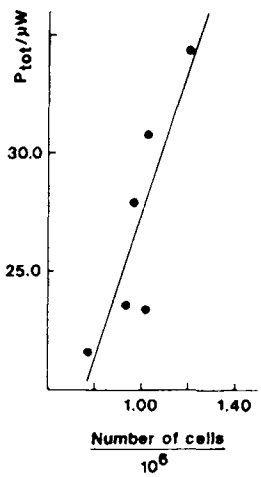

Figure 39. Heat flow rate values plotted against the number of cells (Reproduced from Reference [133].

In a later, more comprehensive study, the effect of the purine and pyrimidine antagonist, 6-thioguanine (6-TG), was examined in detail [134]. The dose-dependent effect of 6-TG on the heat flow rate of T-lymphoma CCRF-CEM cells was examined and the results are depicted in Figure 41. The transient spike at the time of introducing the drug represents the heat of dilution of the drug and, more particularly, of the vehicle to dissolve the 6-TG, that is dimethylsulphoxide (DMSO).

Bermudez et al. [134] formulated equations to give a response value (R) based on the heat profiles shown in Figure 41. From these values they have constructed a dose-response line by fitting an exponential curve to the experimental data. This is depicted in Figure 42A. They also re-examined the inhibition by MTX and found a similar response to the dose (Figure 42B). One of the disadvantages of using MTX is that cells can readily become resistant to it owing to a defect in membrane transport. This is characteristic of the CFM/MTX subline and it makes these cells a positive control to ensure that the inhibitory effect is due to the action of MTX (see Figure 42C). In the case of CCRF-CEM cells, the saturation values for the response to both drugs were very similar, with the R_{max}-values of ~2.4 that reflect the extent to which the culture can be inhibited, whereas R_{max} for the resistant CEM/MTX cells was <1.3. Using the more familiar 50% effect as the endpoint [134], the sensitivity of the cells to the drugs was described as half the maximal response, D_{50}. For CCRF-CEM, the D_{50} was equal to 0.38 μM for 6-TG and 0.05 μM for MTX. In other words, these cells were more sensitive to MTX than to 6-TG. In contrast, the CEM/MTX cells gave a D_{50} for MTX of ~8 μM.

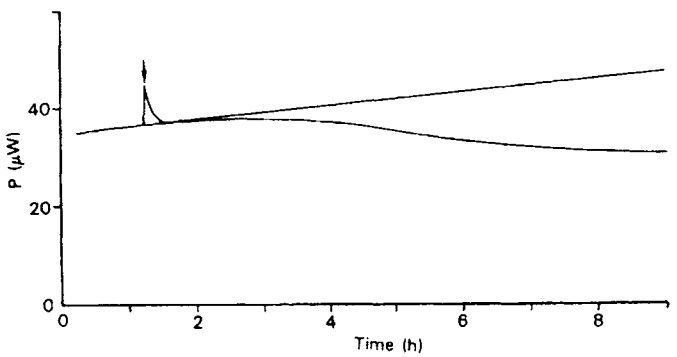

Figure 40. Heat flow rate for a sample of T-lymphoma cells where methotrexate (MTX) is injected (bottom line) and for a reference sample (top) run in parallel. The addition of MTX to a final concentration of 0.18 μM was made at the time indicated by the arrow (Reproduced from Reference [133] with permission).

It is well known that chemotherapy for neoplasia involves combinations of drugs in order to overcome variable cell biochemistry. Among other experiments, Roig and Bermudez [135] studied the effect of combining MTX

and 6-TG on the heat flow rate of T-lymphoma cells. In Figure 43 the time to the maximum effect (t_D) was plotted against the molar concentrations of the anti-metabolites. This provided information on the elapsed time for the cellular response to the individual drugs and their combination. This variable decreased continuously with increasing concentrations of MTX but it was saturated for 6-TG at doses higher than 2 μM (see Figure 43). When both drugs were administered to the cells in combination, the response appeared earlier and t_D was also saturated for combination doses above 3 μM (2 μM 6-TG + 1 μM MTX).

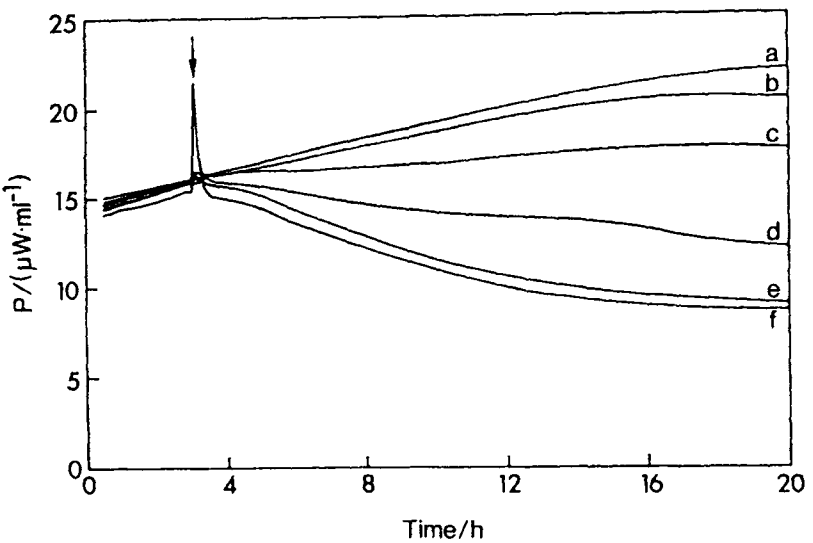

Figure 41. The heat flow rate (P) for CCRF-CEM cells exposed to 6-thioguanine (6-TG). The arrow indicates the point at which 6-TG was injected, the vessels being inserted into the calorimeter at time zero. Mechanical disturbance occurring during the first hour has been omitted. The final drug concentrations were (a) 0, (b) 0.2, (c) 0.5, (d) 1.0, (e) 2.0, and (f) 4.0 μM (Reproduced from Reference [134] with permission).

It is of course well justified in the context of cancer to dose the body heavily with "harmful" drugs. However, it must be expected that the other tissues, especially the liver, might be affected and possibly to a serious extent. Taxol is a natural product with potent anticancer activity because it is able to break the

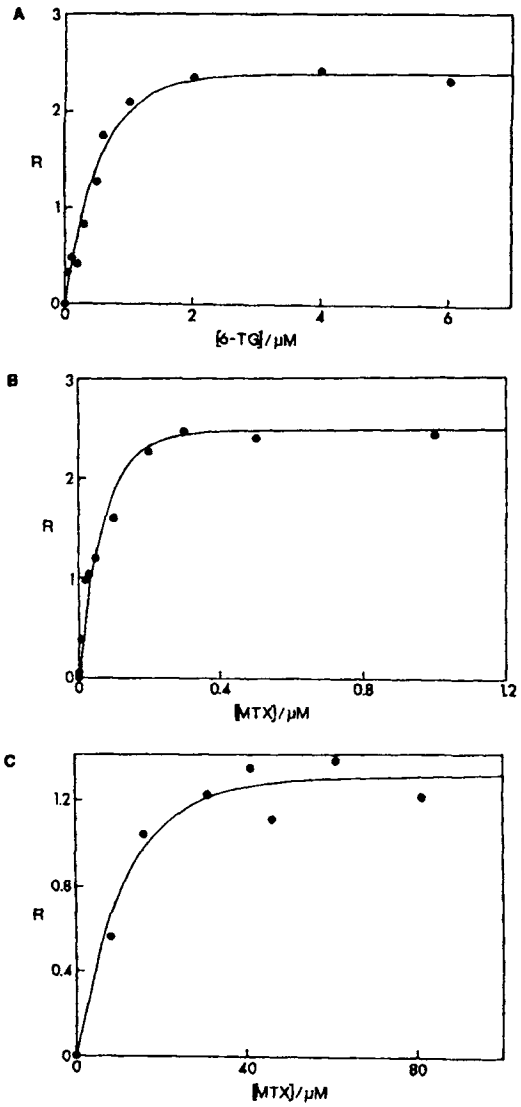

Figure 42. The calorimetric dose-response curves constructed as the relative response, *R*, vs the concentration of the drug. A and B show the effect on CCRF-CEM cells of 6-thioguanine (6-TG) (A) and methotrexate (MTX) (B), respectively. C shows the effect of MTX on the subline, CEM/MTX. The solid line in each section represents the best fit to the experimental points. (Reproduced from Reference [134] with permission).

protection afforded to neoplastic cells that overexpress the *bcl* gene. It does so in some way by interfering with the microtubule-mitochondrion interaction, causing a post-translational change to bcl protein by inducing phosphorylation of it [136]. Manzano et al. [137] studied the metabolic effects of taxol on isolated rat hepatocytes and found that it occasioned a decrease OUR more than in the heat flow rate and increased lactate production. The reduced aerobic metabolism caused a reduction in ATP production that was then supplemented by a higher glycolytic flux yielding ATP from the reduction of pyruvate to lactate. Measurement of ATP content indicated that substrate phosphorylation was insufficient to meet ATP demand and meant that taxol reduced the overall metabolic activity.

Because of the known action of taxol, Manzano et al. [137] initiated state 3 respiration in isolated mitochondria by the addition of 0.8 mM ADP together with one specific substrate of each respiratory chain complex. These were 10 mM pyruvate (NADH-ubiquinone oxidoreductase, complex I), 1 mM succinate (succinate dehydrogenase, complex II) or 0.2 mM ascorbate and 10 μM tetramethyl-*p*-phenylenediamine (cytochrome oxidase). The addition of taxol strongly reduced the respiratory capacity of complex I and complex II by 58% and 45%, respectively, without affecting cytochrome oxidase. Thus, they found a direct effect on respiratory metabolism. This is presumably because the change to mitochondrial bcl protein in the intermembrane space caused the release of cytochrome c [138] and can lead to the apoptotic cascade (see Section 5.2.2).

These few scientifically acceptable examples of a type of study show that drug interaction with cells can be detected by changes in heat flux as an index of metabolic activity. The problem from the point of view of the pharmaceutical industry is that conventional calorimetry cannot cope with the extremely high throughput of potential drugs produced in a field impelled by genomics and combinatorial chemistry. To a small extent, the answer may be to make a truly multi-channel calorimeter. Takahashi [139] has designed a 24-channel instrument (Biothermal Analyser H-201) that is produced by the Nippon Medical and Chemical Instruments Co. Ltd. (Osaka, Japan). It is intended, however, for the detection of the heat flow rate from microbial preparations and is not sensitive enough (17.2 μW/μV) for animal cell suspensions (10^6 cells produce ~20 μW). The throughput of such a system would be unacceptable in any case since the Pharmaceutical Industry talks in terms of screening tests using 284-well or even 1536-well microtitre plates with robotic control.

In terms of thermoelectric devices, the approach of Pizziconi and Page [12] may indicate a possibly fruitful path. They have engineered a microfabricated hybrid biosensor, in which both the cellular and macromolecular constructs are

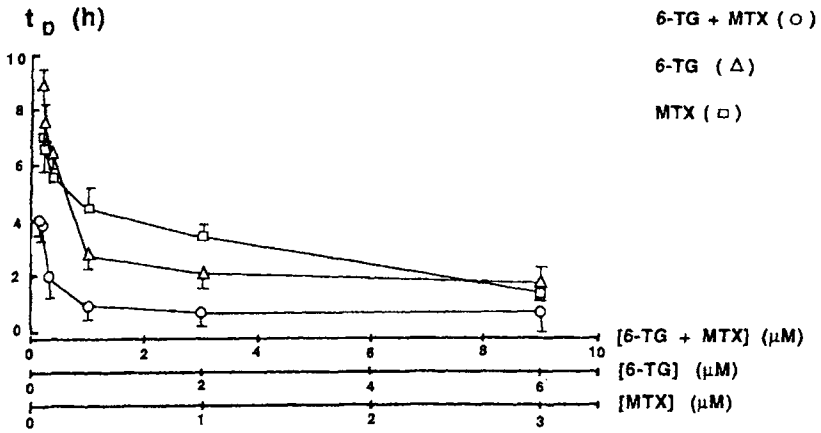

Figure 43. The time of maximum effect (t_D) of 6-thioguanine (6-TG), methotrexate (MTX) and their combination at $D_{MTX}/D_{6\text{-}TG} = 0.5$ ratio. t_D values were obtained for different doses of 6-TG (Δ), MTX (□) and the combination of both drugs (O). Symbols show the mean ± SEM for 3-5 experiments (Reproduced from Reference [135] with permission).

integrated with a thermopile acting as an advanced transducer. As a model interactive system, they chose the mast cell recognition of immunoglobulin E (IgE) that attaches with high affinity to the cell surface. The cells are activated with the specific antigen and this causes the release of histamine. The representative immunoassay system (see Figure 44) thus consists of (A) living mast cells, with (B) the IgE antigen recognition, bound by natural extracellular matrix proteins at the cell/transducer interface (C) to a highly sensitive, thin-film thermopile transducer (D). It is possible to amplify the heat produced by reaction of the mediators with known ligands (E). It is of course important to multiplex the system using a sensing array, as shown conceptually in Figure 44.

The prototype thermopiles were constructed as thin films of antimony and bismuth metals in regular patterns to form pairs of thermocouple junctions on a thin (38 μm) Mylar ® support [12]. They were modified to accommodate the living cells by incorporating a small microwell, placed directly over both the active and the reference junctions, to contain the culture medium. The cells were immobilised with fibronectin placed over the active thermopile junctions only (see Figure 45), so that the thermopile electromotive force is proportional only to the temperature difference between the active and reference junctions. A

small stirrer was used to minimise the local temperature gradients. In the actual experiments, the cells were activated chemically using the calcium ionophore, A23187. There was a relatively rapid increase in the heat flow rate within 20 min to give a value that was validated by conventional calorimetry. Further improvements were made in later papers (see for instance Reference [140]).

A non-thermoelectric approach to the need for the rapid throughput of many samples is that of Paulik et al. [14] using thermal imaging to measure the thermogenesis by cells in microtitre plates. Heat dissipation was recorded with a thermo-electrically cooled Agema Thermovision System AB (Danderyd, Sweden) equipped with a SW scanner and a 40° × 25° lens that detects a 2–5.4 μ spectral response and has a focal distance of 6 cm. The scanner had an internal calibration system with an accuracy of 0.08 °C. Images were captured using a recurs function set at 16. The data were analysed using OS-9 advanced systems and ERICA 2.00 software (Agema). Thermography of the human subcutaneous adipocytes was performed at 37 ± 0.02 °C in a strictly controlled incubator that contained the apparatus (Figure 46).

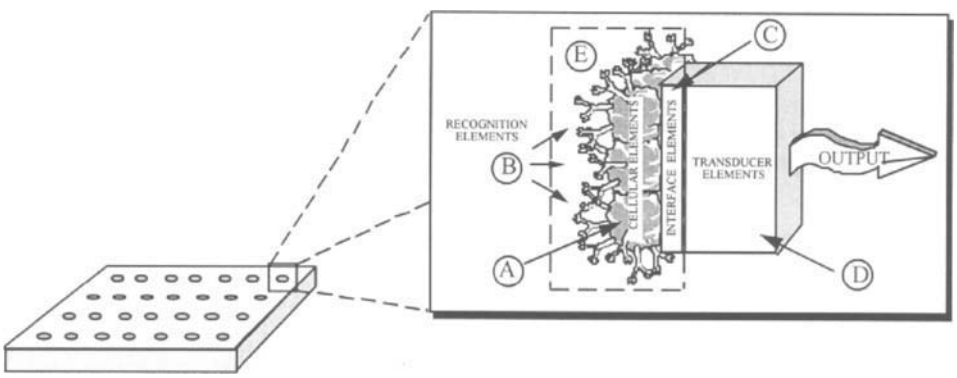

Figure 44. The cell-based hybrid biosensor immunoassay system. The inset depicts the arrangement of the key hybrid sensor components. The details of the system A to E are in the text (Reproduced from Reference [12] with permission).

The adipocytes used as the test system for mammalian cells were grown in 96-well plates with the well-known respiratory uncoupler, carbonyl cyanide p-(trifluoromethoxy)phenylhydrazone (FCCP) or the inhibitor of the respiratory chain, rotenone. The results reproduced in Figure 47 validated the analytical

system by correctly showing that FCCP caused increased thermogenesis and rotenone inhibited heat dissipation. The authors also found that more heat was produced when the cells were stimulated by CL316243, a β_2-adrenoceptor agonist being developed by GlaxoWellcome to treat obesity. On the other hand the antidiabetic agent, troglitazone, suppressed the heat production by the adipocytes.

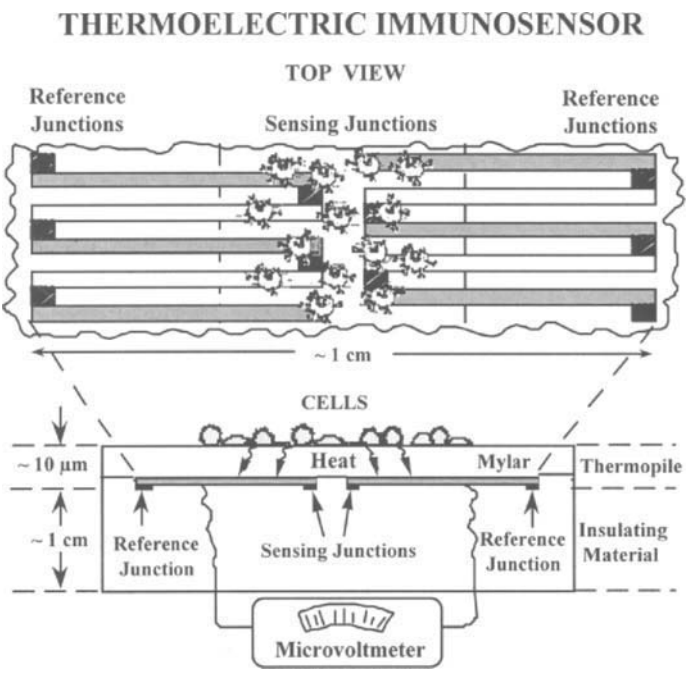

Figure 45. Schematic representation of the prototype of a thin-film whole cell biosensor. The top view shows the placement of living cells over active sensing junctions (Reproduced from Reference [12] with permission).

5.4.2. Clinical studies

The potential to employ calorimetry as a diagnostic tool in medicine has been exposed largely by Monti and his co-workers in the University Hospital in Lund (see Chapter by him on Blood tissue in this Volume). As an example of the insight that calorimetry can give to clinical problems and to continue the theme at the end of the preceding Section, attention is drawn briefly to "bad" fat. This is the white adipose tissue associated with obesity (see review in Reference [10]

and Section 5.5 for "good" fat, brown adipose tissue). White adipocytes were dissociated with collagenase from human subcutaneous adipose tissue and suspended in (floated on) a Krebs-Ringer-bicarbonate buffer containing glucose, insulin and albumin [141]. It was perhaps surprising to find that the adipocytes from 14 obese patients had a lower average heat flux than those from the same number of normal controls (see Figure 48A). The average for the former was 26 ± 12 (SD) pW per cell compared with the latter at 49 ± 15 pW per cell.

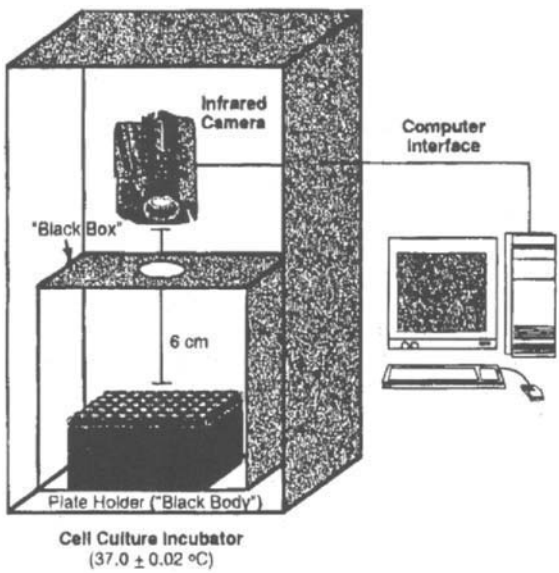

Figure 46. Apparatus for measuring infrared thermography in cell culture. The "black box" and the "black body" minimize the thermal noise (*i.e.* reflection and air currents) from the culture plates and the surrounding environment. The use of an incubator also prevents fluctuations in the surrounding temperatures and improves cellular responses and viability. The camera monitors the real-time heat production from the cells in culture with images recorded by a central processing unit for further data analysis (Reproduced from Reference [14] with permission).

Adipocytes from obese patients mirrored their "owners" in being considerably larger than those cells from normal people, so the difference between the two groups was emphasised by expressing it in terms of tissue weight (Figure 48B).

"Obese" fat tissue produced 40 $\mu W\ g^{-1}$ whereas the normal tissue evolved 133 $\mu W\ g^{-1}$. The investigators stated that "there is increasing evidence that obesity is associated with an increased metabolic efficiency" [141]. Now this is not a particularly new idea for, over 40 years ago, a corpulent Latin master said, when criticising a typically poor translation of Ovid, "Kemp, you and I have only one characteristic in common – a highly efficient digestive system" [10]. The research in Lund was expanded to include for instance (i) the effects of fasting and horizontal gastroplasty on the heat produced by adipocytes by the obese patients [10]; and (ii) the differences that occur in such clinical conditions as the painful adiposis dolorosa in which the fat cells are larger than normal and produce less heat [142]. These effects were not as marked as those found in obesity but there was also the observation of an increased proportion of monounsatuated fatty acids at the expense of saturated ones.

5.4.3. Cell signalling

One of the more interesting current topics in Cell Biology at this time is the detection of cell signals and the energetic costs of the cascades subsequent to the binding of primary messengers (hormones, growth factors, etc.) to their cell surface receptors. Since many of the cascades after membrane transduction of the message involve a series of phosphorylations in the cytosol, it is reasonable to assume that there is more demand for ATP and thus metabolism coupled to its supply must increase in a proportionate manner. In an experiment reported in 1993 [94], apoptosis was induced in a human pre-B acute lymphocytic leukaemia cell line, KM-3. On the surface of these cells is a 37 kDa cell surface antigen (BAL) that acts as a receptor, perhaps similar to what is now called the death inducing receptor (CD95), for an unknown primary messenger, possibly a cytokine. A mouse monoclonal anti-BAL antibody was raised and the cells were treated with it. It had no effect on the heat flux of a cell suspension stirred in a Thermometric insertion vessel (see Reference [3]) until the receptors, "extended" by the antibody molecules, were crosslinked by a rabbit anti-mouse Ig antibody. Within 20 min of its addition, the heat flow rate increased (Figure 49) and, following an inflexion, this enhanced rate of +3.5% continued for at least 4 h. No change in heat production was observed in cells without the secondary antibodies. These cells did not show any of the classical symptoms of apoptosis. On the other hand, the cells treated with the crosslinking antibodies within hours exhibited the growth inhibition (Figure 50A) and the DNA fragmentation typical of apoptosis (Figure 50B).

In order to discover the source of the increased metabolism, OUR was measured and was said by the authors [94] to be unaffected by the induction of

apoptosis. No data were presented but it was shown that lactate formation increased by ~10%. It might be suggested from these results that the additional requirement for ATP was met by aerobic glycolysis and, from this, it could be inferred that the respiratory capacity of the mitochondria was at its maximum in the control cells. The absence of the OUR data precludes analysis of the data in terms of the enthalpy balance method and the intensity of the glycolysis in aerobic conditions that requires knowledge of the calorimetric-respirometric ratio (see Reference [65] and Section 5.5).

This is the only comprehensive report of the effect of signalling but there was a recent abstract stating the effect of the human growth hormone (hGH) on the human lymphoid cells, Ba/F3:6, growing on the improvised glass blades of the stirrer used in the Thermometric insertion vessel [37]. hGH in a 1 nM solution caused an immediate, if rather slow increase in metabolic activity, measured by the change in heat flow rate of about +10%. It would appear likely that the difference is an expression of the energetic cost of cell signalling in terms of a phosphorylation cascade.

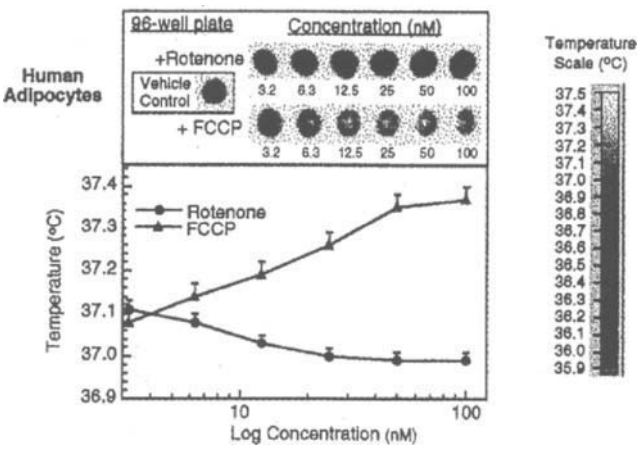

Figure 47. Black and white scan of an infrared image of human adipocyte cultures treated with rotenone and FCCP. Confluent human adipocytes were cultured in 96-well microtitre plates (50 µl/well). Dose responses are shown on the thermogenic effects of rotenone and FCCP on human adipocytes. The cells were treated for 10 min with either agent before the images were analyzed by infrared thermography. Representative data are presented from experiments performed in triplicate (Reproduced from Reference [14] with permission).

5.5. The calorimetric-respirometric ratio

In most cases, scientists that wish to investigate intermediary metabolism in tissues choose indirect calorimetry, OUR, as one of their analytical tools and perhaps also measure lactate concentrations as an indicator of the intensity of aerobic glycolysis. Even when needing to express the results in terms of heat flux, for respiratory metabolism they apply the appropriate oxycaloric equivalent, $\Delta_k H_{O_2}$, to the data for oxygen flux (J_{O_2}),

$$J_Q = \Delta_k H_{O_2} J_{O_2} \tag{24}$$

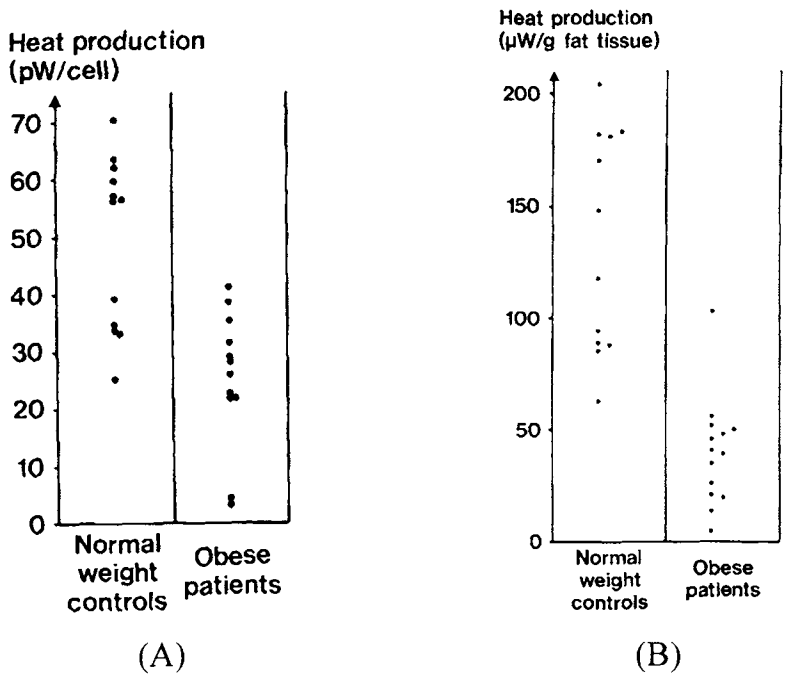

Figure 48. The heat flow rate of adipocytes in obese patients and in lean control subjects, expressed as μW per cell (A) and as μW per gram of tissue (B). (Reproduced from Reference [141] with permission).

Oxycaloric equivalents are the theoretical values for the enthalpy changes of the catabolic half-cycle, e.g. glc to HCO_3^- and H^+, and do not include any coupled processes such as ATP production. This means that no work is done, so

the net efficiency is zero. These equivalents can be calculated from standard enthalpies of formation (see Section 5.2.4) and, for given substrates, are the same as values obtained by bomb calorimetry. Combustion in a bomb calorimeter is dissipative and thus totally inefficient, not being coupled to any energy conserving mechanism. In practice, it has been found that the oxycaloric equivalents for all substrates are similar [64] according to Thornton's Rule (see Section 5.2.4). This is because of the regularity for the heat evolved per equivalent of oxygen consumed in terms of available electrons [107-109]. For a variety of substrates and conditions, Gnaiger and Kemp [64] have calculated that the theoretical oxycaloric equivalents range from –430 to –480 kJ mol^{-1} O_2; on average $\Delta_k H_{O2} = -450$ kJ mol^{-1} ± 15% (see Table 5).

Table 5
Oxycaloric equivalents of aerobic respiration for various substrates in aqueous solution at pH 7.

$\Delta_k H^{\circ}_{O_2}$ and $\Delta_k H^{'}_{O_2}$ (kJ/mol O_2) are calculated with enthalpies of neutralisation of 0 and –9 kJ/mol H^+, respectively, and with all reactants dissolved in water. $\Delta_k H_{O_2}$ refers to the same conditions as $\Delta_k H^{'}_{O_2}$, except that O_2 and CO_2 are exchanged with the gas phase. The CO_2/O_2 ratio is the molar gas exchange ratio or respiratory quotient. Values for triacylglycerols, $(C_{18\,8}H_{33}O_2)_3$, and protein, $(C_{4\,79}H_{7\,51}O_{1\,49}N_{1\,34}S_{0\,032})_n$, are calculated from average fatty acid and amino-acid compositions of organisms, with aqueous urea or ammonium ion as nitrogenous end-product.

Substrate	CO_2/O_2	$\Delta_k H^{\circ}_{O_2}$	$\Delta_k H^{'}_{O_2}$	$\Delta_k H_{O_2}$
Glucose	1.0	-469	-476	-469
Glycogen	1.0	-469	-477	-469
Palmitic acid	0.70	-431	-435	-434
Triacyglycerols	0.72	-439	-444	-442
Protein → urea	0.84	-436	-442	-438
Protein → NH_4^+	0.97	-443	-450	-443

Reproduced from Ref. [64] with permission.

The theoretical oxycaloric equivalent is the expected ratio of the calorimetric heat flux and the respirometric oxygen flux, the CR ratio,

$$\text{CR ratio} = J_Q / J_{O_2} \tag{25}$$

For whole animals in normoxic conditions, homeostatic mechanisms ensure that the CR ratio is the same as the above generalised oxycaloric equivalent [143] with the Cori cycle in the liver converting to glucose any lactate formed in the tissues and subsequently excreted into the circulating blood. As noted some years ago [10,59], it is rare indeed for tissue cells grown in culture to have a CR ratio close to the generalised oxycaloric equivalent. The only authenticated report is for hamster mature brown adipocytes that have a CR ratio of –490 kJ mol^{-1} O_2 when treated with noradrenaline [144]. This hormone stimulates thermogenesis in brown fat by acting on the 33-kDa uncoupling protein (UCP; also known as thermogenin) in the inner mitochondrial membrane to open channels between the cytosol and the matrix [145]. Thus it causes the dissipation of the protonmotive force. In the same way established for the familiar lipophilic uncouplers such as dinitrophenol, electron transport from NADH to O_2 now proceeds at a maximal rate not coupled to the demand for ATP. There is a proportionate increase in both heat production and OUR as a result of the relatively uncontrolled catabolic flux. This is analogous to the situation in the bomb calorimeter (see above) because uncoupling results in a totally inefficient process that permits no energy conservation, i.e. there is no oxidative phosphorylation to produce ATP. Without another source of ATP, there must be the rapid death of uncoupled cells.

Clark et al. [146] were interested in the hypertrophy of brown fat in rats fed on highly palatable "junk-type cafeteria" food as a mechanism to dissipate the additional energy by increased thermogenesis. They measured heat flow rate in a rotating LKB batch calorimeter [28,147] and OUR in a stirred respirometer. The results for the dissociated brown adipocytes shown in Figure 51 demonstrate that the injection of noradrenaline stimulated the heat flow rate more than OUR and apparently gave a considerably more exothermic CR ratio of –1477 kJ mol^{-1} O_2. This result was interpreted to mean that the necessary ATP production had a reduced efficiency.

In a series of papers using the same combination of direct and indirect calorimetry, Clark's group also studied isolated rat hepatocytes (see review in Reference [10]). Judging from calculations later undertaken by Kemp [10], the research showed that dihydroxyacetone and fructose both caused considerably more negative CR ratios; from –542 kJ mol^{-1} O_2 to approximately –650 kJ mol^{-1} O_2 [147]. They attributed these findings to the increased rates of substrate cycling between glucose/glucose 6-phosphate, fructose 6-phosphate/fructose 1,6-bisphosphate and pyruvate/phosphoenolpyruvate to decouple the catabolic process from ATP production and lower the efficiency of ATP production.

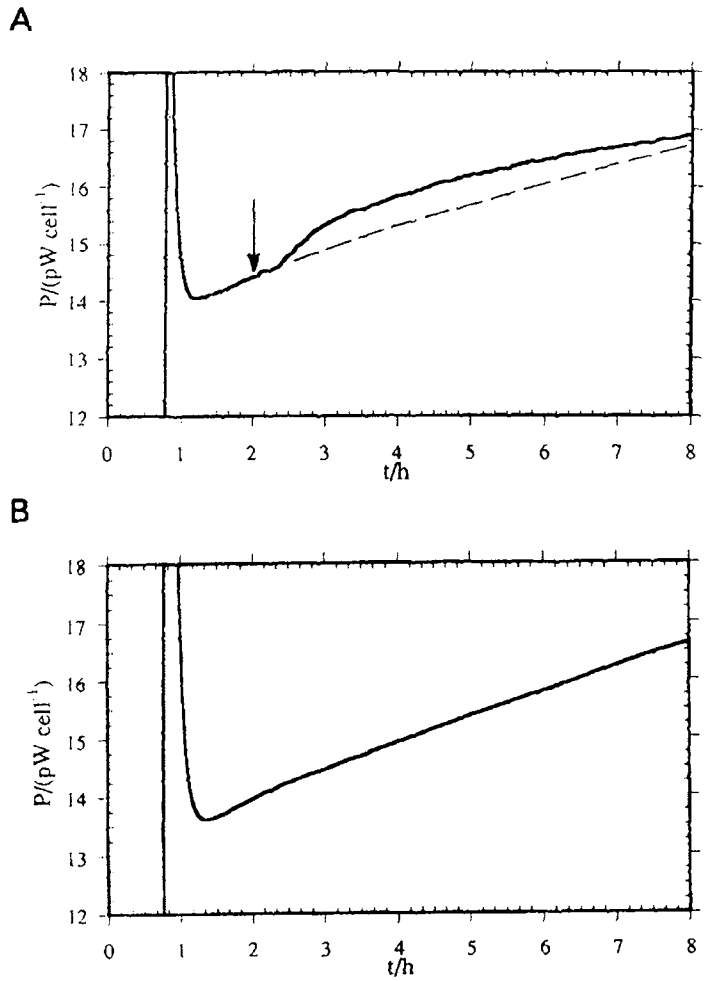

Figure 49. Calorimetric measurements of KM-3 cells. The heat flux at 37.0 °C was plotted as a function of time (t). The early portion that is out of range, corresponds to lowering and thermal equilibration of the calorimetric vessel. During this 1-h stage, the temperature of the cell suspension reached 36.9 °C in less than 6 min; (A) KM-3 cells incubated in the presence of the anti-BAL from t = 0 h. At t = 2 h, 48 µl secondary antibody was injected as marked by the arrow. The difference between the original and the extrapolated dotted line is the excess heat flux (ΔP) in response to cross-linking; (B) the same as in (A), but without the cross-linking secondary antibody (Reproduced from Reference [94] with permission).

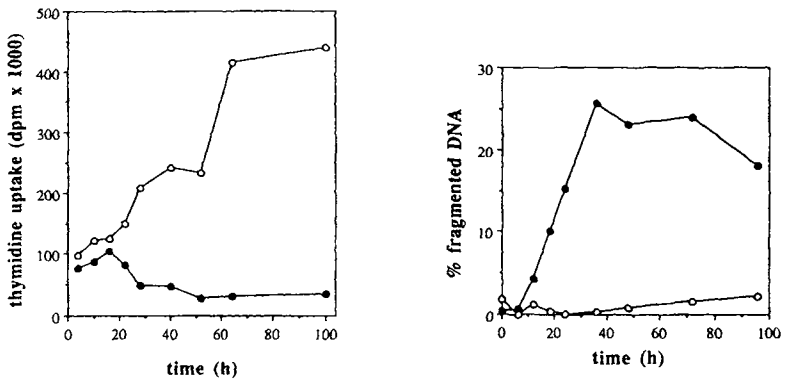

Figure 50. (A) The uptake of [^{3}H]thymidine as a function of time in KM-3 cells, treated with anti-BAL and secondary antibody (•) or without these antibodies (o). The indicated times represent the period between the addition of the secondary antibody and the end of the 4-h [^{3}H]thymidine pulse. The data points are expressed as the mean value of five experiments. (B) The kinetics of DNA fragmentation in KM-3 cells after cross-linking of anti-BAL antibodies (•) and in untreated KM-3 cells (o). KM-3 cells were incubated with anti-BAL antibodies for 2 h before addition of secondary antibodies at $t = 0$ h The degree of DNA fragmentation represents the percentage of DNA that was present in the cytoplasmic fraction in the cells. Samples were run in duplicates (Reproduced from Reference [94] with permission).

It is important to examine the claims that CR ratios more negative than the corresponding oxycaloric equivalent, are due to decreased efficiency. As established in Section 4.1.1. (see also Reference [25]), an enthalpy of 258 kJ (i.e. 6 × 43) is metabolically conserved for each mole of oxygen utilised in the respiration of glucose. Therefore, the highest thermodynamic efficiency for ATP production is 0.55 (i.e. 258/469), using the oxycaloric equivalent of –469 kJ mol^{-1} O_2 [64]. The enthalpy change per mol O_2 for the fully coupled reaction is –211 (–469 + 6 × 43) kJ mol^{-1} O_2. The ATP/O_2 ratio decreases with uncoupling. So, the thermodynamic efficiency is lowered, and the enthalpy change per mol O_2 decreases from –211 to a maximum of –469 kJ mol^{-1} for fully uncoupled respiration. Since it has been established above that this value represents zero efficiency, then uncoupling (see Figure 52 for detailed explanation) and decoupling (see Figure 53 for reasoning) to give highly exothermic CR ratios

cannot be due to the lower efficiency of ATP production. The reasons for these CR ratios more must be sought elsewhere.

Gnaiger and Kemp [64] established that highly exothermic CR ratios were due to the integration of anaerobic pathways with aerobic metabolism and it is common knowledge that the most common anaerobic end product in mammalian cells is lactate. Net production of lactate from glucose is accompanied by a dissipative catabolic enthalpy change, $\Delta_k H_{Lac}$, of –80 kJ mol^{-1} when the acid is buffered in the cytosol. The plasma membrane is very permeable to lactate (and pyruvate) and then the enthalpy change depends on the nature of the buffer in the medium [4]. It is –80 kJ mol^{-1} when excreted into a bicarbonate buffer, –59 kJ mol^{-1} into a phosphate buffer and –77 kJ mol^{-1} into 20 mM HEPES buffer. The molar amount of lactate produced per unit amount of oxygen consumed (Lac/O_2) indicates the relative extent of aerobic glycolysis. The catabolic (k) heat change per mol O_2, $\Delta_k H_{(ox+anox)}$ (CR ratio), is then calculated as,

$$\Delta_k H_{(ox+anox)} = \Delta_k H_{O_2} + Lac/O_2 \times \Delta_k H_{Lac} \qquad (26)$$

Similar equations can be constructed for other anaerobic products (p); in a generalised equation, p can be substituted for Lac and, if there is more than one such product, the heat effect is additive, $\sum_p / O_2 \times \Delta_k H_p$.

As shown previously [4,11,22,44,59,64], in many cases of highly exothermic CR ratios the enthalpy balance approach in Equation (26) proved that aerobic glycolysis to produce lactate was the cause. The situation is not simple for many of the cell types in culture, however, because the various different growth media almost always contain glutamine. This is present primarily for purine and pyrimidine synthesis in the anabolism of nucleic acids. In many cases, however, this amino acid is completely oxidised to provide energy. More commonly and highly relevant to the present discussion, it also can be partially oxidised by a process called gluaminolysis to lactate [49,54], with a ATP stoichiometric coefficient for glutaminolysis of $6ATP/O_2$ – see Reference [22]). This pathway causes an overestimate of aerobic glycolysis because the oxycaloric equivalent for glutamine is within the normal range. For the HEPES-buffered medium used for 2C11-12 mouse macrophage hybridoma cells [121], the metabolic reaction and corresponding enthalpy change is [127],

$$\begin{aligned} &{}^{+}H_3N(CHCH_2CH_2CONH_2)COO^{-1}(aq) + 1\tfrac{1}{2}O_2(g) \\ &+ 3H_2O(l) + HEPES(aq) \rightarrow CH_3CH(OH)COO^{-}(aq) + 2HCO_3^{-}(aq) \\ &+ 2NH_4^{+}(aq) + HEPES - H^{+}(aq) \qquad - 695\ kJ \end{aligned} \qquad (27)$$

The overestimate can only be redressed by radioisotopic experiments of the type undertaken with the 2C11-12 cells [121]. As will be seen in Table 6, the oxidation of the glutamine is considerable and results in the production of significant amounts of lactate.

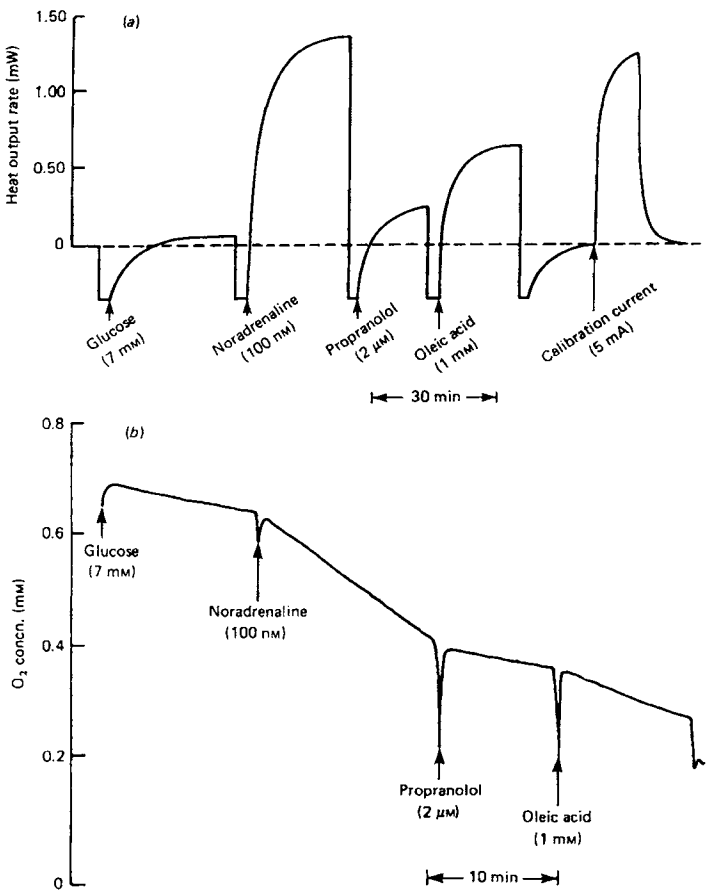

Figure 51. Representative traces of heat output (*a*) and O_2 consumption (*b*) rates by isolated brown adipocytes from cafeteria-fed rats after the sequential addition of glucose, noradrenaline, propranolol and oleic acid. Isolated brown adipocytes (2.65×10^5 cells/cm^3) were prepared from two cafeteria-fed rats. Noradrenaline, propranolol and oleic acid were prepared in Krebs-Henseleit bicarbonate-buffered saline, equilibrated at 37 °C for 3.0 min, and added in a concentrated form at the times indicated (Reproduced from Reference [146] with permission).

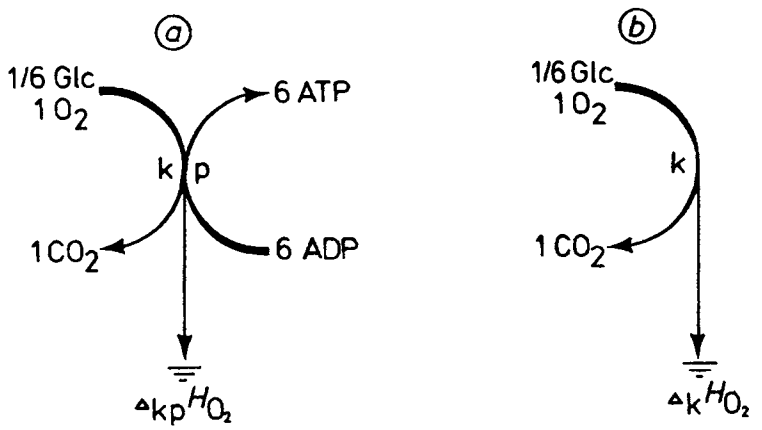

Figure 52. Energy transformation half cycles in (*a*) fully coupled conservative metabolism, and (*b*) uncoupled catabolism. *a*: Net synthesis of ATP in fully coupled metabolism. The enthalpy change per mol O_2 is the sum of the catabolic (k, exothermic) and phosphorylation (p, endothermic) half cycle. *b*: The dissipative catabolic half cycle provides the stoichiometric basis for calculating the oxycaloric equivalent, $\Delta_k H_{O_2}$ (Reproduced from Reference [25] with permission).

Table 6

Metabolic flux of [U-^{14}C] glucose, J_{Glc} in pmol s^{-1} per 10^6 cells (%) and [U-^{14}C] glutamine, J_{Gln} in pmol s^{-1} per 10^6 cells (%)[a] by 2C11-12 mouse macrophage hybridoma cells in standard incubation medium (average of 4 experiments).

	Activated cells				Triggered cells			
	J_{Glc}		J_{Gln}		J_{Glc}		J_{Gln}	
Lactate	55±5	(73)	9±1	(38)	30±2	(30)	4±0.5	(21)
Pyruvate	0.5±0.1	(0.7)	1±0.1	(5)	6±0.5	(6)	0.2±0.1	(0.9)
Carbon dioxide	23±2	(10)	10±1	(9)	90±7	(29)	7±1	(7)
Glutamine	–		7±0.5	(29)	–		5±0.5	(26)
Total		(83.7)		(81)		(65)		(54.9)

[a] Calculated from the specific activity of the relevant substrate.
Reproduced from Reference [121] with permission.

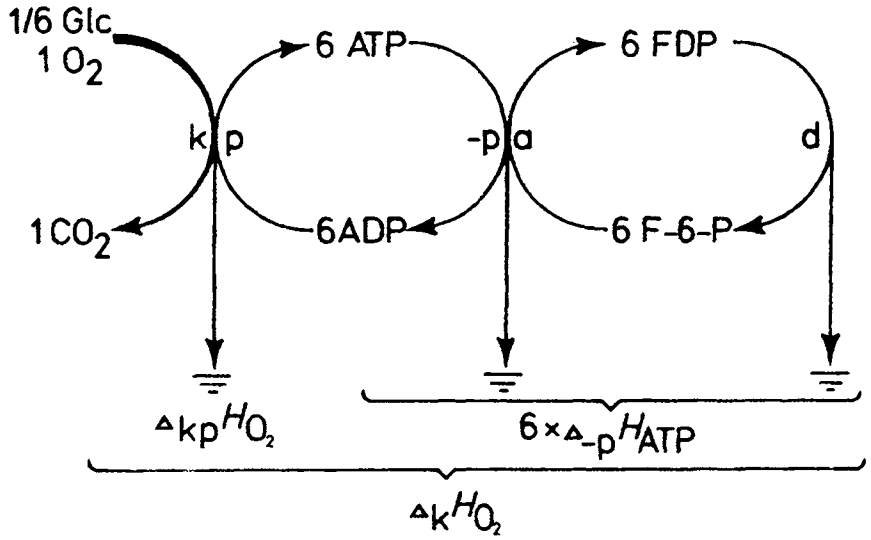

Figure 53. Half cycles in dissipative maintenance metabolism with steady state ATP turnover, decoupled by futile cycling. The fructose 6-phosphate/fructose 1,6-bisphosphate cycle is shown as an example. The net enthalpy change is calculated from the net biochemical change which, at steady state levels of ATP and all anabolic intermediates, is exclusively due to the catabolic half cycle reaction, equivalent to uncoupled catabolism (oxycaloric equivalent). Enthalpy is intermittently conserved in endothermic half cycles (p, phosphorylation; a, anabolic), but an equivalent amount of enthalpy is exothermic in the reversed exergonic half cycles (–p, dephosphorylation; d, dissipative). Therefore, ATP turnover and futile cycling raise the heat flux strictly proportional to the catabolic flux which, however, can be augmented by anaerobic catabolism with a corresponding anaerobic contribution to total heat flux (Reproduced from Reference [25] with permission).

If the enthalpy recovery is not achieved for lactate, then it is important to look for possible methodological deficiencies before resorting to further metabolic analyses. Or, better still, try to avoid them in the first place. The use of ratios considerably increases experimental error, so it is vital to set the conditions for both measurements to be as similar as possible. All polarographic measurements of OUR are done for stirred cell suspensions whereas there is only a limited availability of stirred calorimetric vessels. Not only does this lead to the so-called "crowding" effect (see Section 3.1.1) with increased glycolysis due to the

Pasteur effect, but the respirometer gives an incorrect reflection of OUR in the unstirred vessel. In many cases, the calorimetric vessel has a gaseous headspace that allows recruitment of oxygen, whereas OUR is measured without one.

It should be remembered that microcalorimeters have extremely low detection limits that can only be matched by some of the better respirometers, for instance the high resolution Oroboros Oxygraph with large diameter Orbisphere electrodes (see Reference [128]). For this reason, the small oxygen electrode used in the Thermometric TAM insertion vessel [123] may only be suitable for OUR measurements at relatively high cell densities. Nevertheless, if both measurements are made, then the experimenters should attempt an enthalpy balance to detect possible systematic errors that could invalidate the results. For instance, it has been shown that the basic fibroblast growth factor (bFGF) appeared to depress the heat flux and OUR (see Figure 54) of dissociated foetal rat mesencephalic cell suspensions normally used to compensate for neurological deficiencies by implantation into the striatum [148]. This was the opposite of the predicted result of stimulating metabolism as a cell signal (see Section 5.4.3) for a neurotrophic effect. From the results, the CR ratio can be calculated to be an inexplicably low –103 kJ mol^{-1} O_2.

The reason that normal mammalian cells in culture produce lactate in many cases may be poor medium design [51]. The classical cell culture medium was formulated on the basis of a buffered physiological saline with glucose, the essential amino acids and serum. It was not designed for the actual needs of the cells. Thus, glucose and glutamine are used by cells as biosynthetic precursors for compounds not available, or not in the correct quantities, in the medium [44]. In the glycolytic pathway, amino sugars arise from fructose 6-phosphate and the amino donor, glutamine; the amino acids serine (for fatty acids) and alanine from 3-phosphoglycerate; the heterocyclic acids, phenylalanine, tyrosine and tryptophan from phosphoenolpyruvate; and oxaloacetate from pyruvate and carbon dioxide (the anaplerotic reaction). It will be noted that these reactions mostly require three-carbon units to be produced at a rapid rate. As a result, a large quantity of pyruvate is available that is surplus to energy requirements and is reduced to lactate to pay back NAD^+. As stated earlier, the partial oxidation of glutamine to lactate catalysed by some of the enzymes of the Krebs' cycle and followed by transamination, enables other amino acids to be formed from α-ketoglutarate and oxaloacetate.

In order to optimise cell growth and minimise the production of toxic lactate (and ammonia), Xie and Wang [114] undertook an exhaustive (and exhausting!) stoichiometric analysis of all the metabolic requirements for growth of a

particular hybridoma cell and this reduced their lactate production by 90%. A more empirical approach monitored by the heat flux probe [51] was taken to improve the culture medium of recombinant CHO 320 cells. The redesigned medium (see Table 7) improved the specific growth rate and the flux of IFN-γ (Figure 55) while decreasing the catabolic flux, especially of glucose and lactate (Table 8).

An illustration of the relationship between highly negative CR ratios and growth can be seen in Figure 56 from a study of the growth of recombinant CHO 320 cells [103]. It will be seen that the oxygen flux of the viable cells remained constant over the whole culture period even when there was no net cell growth. On the other hand, the CR ratio was highly exothermic (~ –700 kJ mol^{-1} O_2) during growth, only reducing to a level (–443 kJ mol^{-1} O_2) indicative of oxidative metabolism when there was a decline in cell numbers (see Figure 56). Guan et al. [103] stated that there was some evidence that the amount of

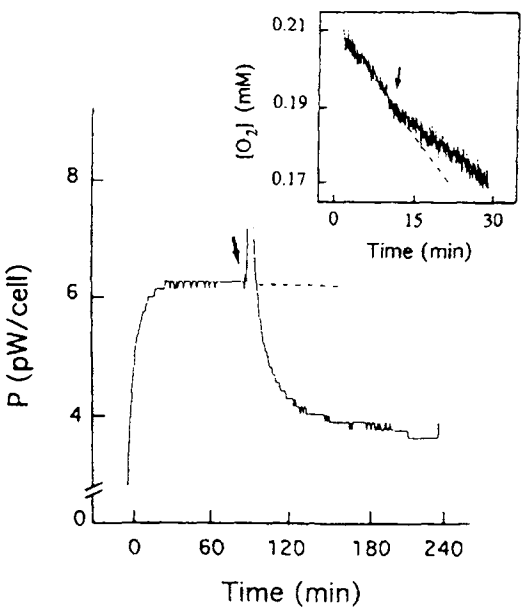

Figure 54. Heat dissipation, *P*, and oxygen consumption of foetal mesencephalic cell suspensions. The arrows show the addition of the basic fibroblast growth factor (bFGF) to a final concentration of 50 ng/cm^3. The discontinuous lines indicate the effect of the addition of medium without the bFGF (Reproduced from Reference [148] with permission).

Table 7
Comparison of the compositions of the improved and the original media for growing CHO 320 cells in suspension.

Medium components	Original	Improved
Glucose	10.5 mM	10.5 mM
BSA	5.0 g dm^{-3}	7.5 g dm^{-3}
Insulin	5 mg dm^{-3}	5 mg dm^{-3}
Human transferrin	5 mg dm^{-3}	5 mg dm^{-3}
Gentamycin	50 mg dm^{-3}	50 mg dm^{-3}
Putresine	1 μM	1 μM
$FeSO_4$	10 nM	10 nM
Na_2SeO_4	10 nM	10 nM
$CuSO_4$	10 nM	10 nM
$ZnSO_4$	3.0 μM	3.0 μM
Methotrexate	0.1 μM	0.1 μM
Pentex ExCyte	No	5 (v/v) %
Sodium pyruvate	1 mM	2.5 mM
Glutamine	2 mM	3.3 mM
Alanine	0.1 mM	0.2 mM
Asparagine	0.38 mM	0.5 mM
Arginine	1.15 mM	1.15 mM
Aspartate	0.15 mM	0.5 mM
Cystine	0.21 mM	0.5 mM
Glutamate	0.14 mM	0.5 mM
Histidine	0.1 mM	0.5 mM
4-Hydroxy Proline	0.15 mM	0.5 mM
Proline	0.17 mM	0.5 mM
Glycine	0.13 mM	0.5 mM
Isoleucine	0.38 mM	0.5 mM
Leucine	0.38 mM	0.5 mM
Lysine	0.22 mM	0.5 mM
Methionine	0.10 mM	0.5 mM
Phenyl alanine	0.09 mM	0.5 mM
Proline	0.17 mM	0.5 mM
Serine	0.29 mM	0.5 mM
Threonine	0.17 mM	0.5 mM
Tryptophan	0.024 mM	0.5 mM
Tyrosine	0.11 mM	0.5 mM
Valine	0.17 mM	0.5 mM

Table 8
Representative fluxes of the major metabolites for CHO 320 cells growing in the original medium and the improved version of it at 48 h during batch culture in a bioreactor.

Medium	Fluxes			
	μ (h^{-1})	Glucose (mol s^{-1} per cell)	glutamine (mol s^{-1} per cell)	lactate (mol s^{-1} per cell)
Improved	0.049	4.11×10^{-17}	1.67×10^{-17}	5.28×10^{-17}
Original	0.028	5.81×10^{-17}	1.78×10^{-17}	1.08×10^{-16}

Reproduced from Reference [51] with permission.

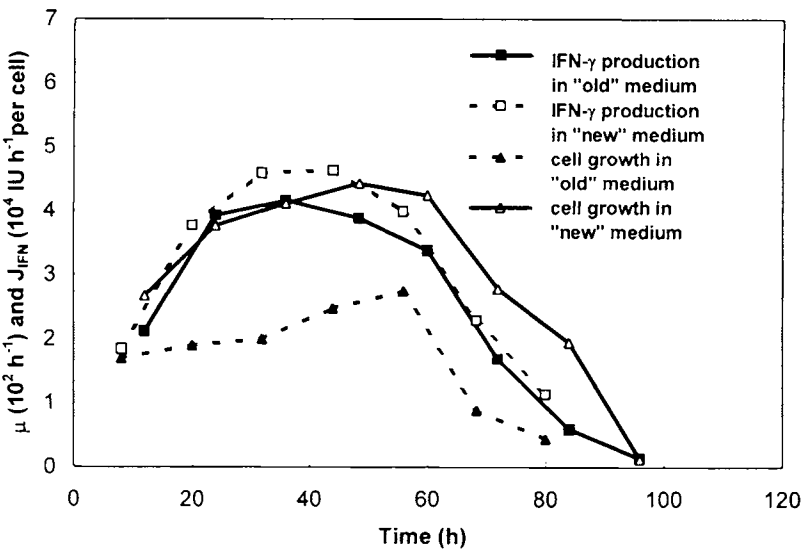

Figure 55. The effects of the semi-empirically improved growth medium that is based on RPMI 1640 on both the specific cell growth rate and the production flux of interferon-γ during a batch culture of CHO320 cells in a controlled bioreactor.

excreted lactate decreased after glucose and glutamine were fully exhausted in the medium (Figure 57). Since there was still an oxygen flux (see Figure 56), it

is possible that the lactate was oxidised as a source of energy. The mechanism for the oxidation of the lactate to pyruvate requires the isozyme H_4 of the lactate dehydrogenase complex and there must be a low NADH/NAD^+ ratio. These conditions occur in liver cells for the operation of the Cori cycle to convert lactate to glucose but it is not clear that "ordinary" cells can operate in this way. It seems probable that pyruvate carboxylase (PYC) is more important to the continuation of this oxidative pathway than the dehydrogenase and there is evidence that transfection of BHK cells with a *PYC* construct dramatically decreased lactate production and improved growth [149]. In any case, it would seem advantageous to the control of cells in bioreactors to combine the on-line measurement of OUR with the heat flux probe developed by us [103]. It is likely that the former would be most sensitively measured for the typically dilute cell suspensions in batch cultures by the method of the stationary liquid phase balance [150].

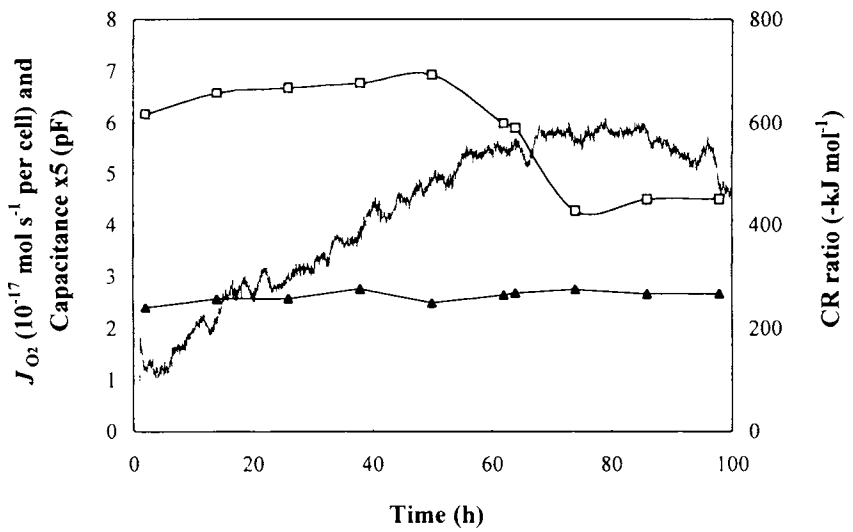

Figure 56. Comparison of the viable cell concentration measured by the on-line capacitance signal with oxygen flux and the calorimetric-respirometric (CR) ratio in a batch culture of growing CHO320 cells. The medium was buffered by 20 mM HEPES and 4 mM sodium bicarbonate. The curves are □——□ for the averaged oxygen flux in terms of an individual viable cell on average, and ▲——▲ for CR ratio. The trace —— stands for the smoothed capacitance signal in which the value for the cell-free medium is deducted by the Applikon BioXpert software.

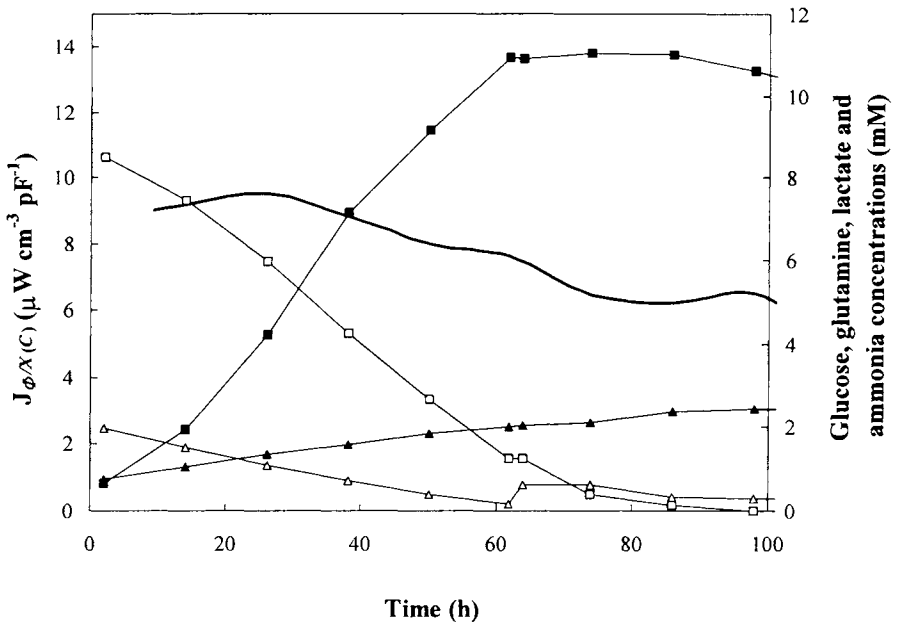

Figure 57. Heat flux ($J_{\Phi/X(C)}$) compared with the changes in concentrations of glucose, lactate, ammonia, glutamine for a typical batch culture of CHO 320 cells. Symbols are —— for specific heat flow rate, □——□ for glucose, ■——■ for lactate, ▲——▲ for ammonia, and Δ——Δ for glutamine (Reproduced from Reference [103] with permission).

6. CONCLUSIONS

Wadsö [129] was recently pessimistic about the impact that calorimetric measurements have had in animal cell biology. While it is certainly true that few Cell Biology laboratories have a calorimeter, it is also undeniable that thermobiochemistry already has had a significant impact in several areas associated with the subject and particularly in the applied fields of biotechnology and pharmacology. Its importance will multiply in the coming age of post-genomics, when all of us will be wishing to know the functions of every one of those expression systems and how they interact to give life. Calorimetry has the advantage of a rigorous theoretical foundation in thermodynamics and this will ensure its precise contribution to cell biology and physiology.

REFERENCES

1. A.V. Hill, J. Physiol., 44 (1912) 466.
2. I. Wadsö, Acta Chem. Scand., 22 (1968) 927.
3. R.B Kemp, in M.E. Brown (Ed.), Handbook of Thermal Analysis and Calorimetry, Vol. 1, Principles and Practice, Ch. 14, Elsevier, Amsterdam, 1998, p. 577.
4. R.B. Kemp, Thermochim. Acta, 219 (1993) 17.
5. D.R. Wilkie, Prog. Biophys. Biophys. Chem., 10 (1960) 259.
6. R.C. Woledge, in A.E. Beezer (Ed.), Biological Microcalorimetry, Academic Press, London, 1980, p.145.
7. R.C. Woledge, N.A. Curtin, E. Homsher, Energetic Aspects of Muscle Contraction, Academic Press, London, 1985.
8. J.M. Ritchie, Prog. Biophys. Mol. Biol., 26 (1973) 147.
9. R.B.Kemp, in A.E. Beezer (Ed.), Biological Microcalorimetry, Academic Press, London, 1980, p. 113.
10. R.B. Kemp, in A.M. James, Thermal and Energetic Studies of Cellular Biological Systems, Wright, Bristol, 1987, p. 147.
11. R.B. Kemp, Thermochim. Acta, 193 (1991) 253.
12. V.B. Pizziconi, D.L. Page, Biosensors Bioelectronics, 12 (1997) 287.
13. R.B. Kemp, in T. Letcher (Ed.), Chemical Thermodynamics: A 'Chemistry for the 21st Century' monograph, Ch. 22, Blackwell Sci.Publ., Oxford, 1999, p. 277.
14. M.A. Paulik, R.G. Buckholtz, M.E. Lancaster, W.S. Dallas, E.A. Hull-Ryde, J.E. Weiel, J.M. Lenhard, Pharm. Res., 15 (1998) 944.
15. P.J. van Ekeren, in M.E. Brown (Ed.), Handbook of Thermal Analysis and Calorimetry, Vol. 1, Principles and Practice, Ch. 2, Elsevier, Amsterdam, 1998, p. 75.
16. R.B. Kemp, in E.E. Bittar, N. Bittar (Eds.), Principles of Medical Biology, Vol. 4, Cell Chemistry and Physiology, Part III, JAI Press, Greenwich, Connecticut, 1996, p. 303.
17. H.V. Westerhoff, K. van Dam, Thermodynamics and Control of Biological Free-Energy Transduction, Elsevier, Amsterdam, 1987, p. 65.
18. E.H. Battley, Energetics of Microbial Growth, Wiley-Interscience, New York, 1987, p. 360.
19. E. H. Battley, Thermochim. Acta, 309 (1998) 17.
20. U. von Stockar, L. Gustafsson, C. Larsson, I. Marison, P. Tissot, E. Gnaiger, Biochim. Biophys. Acta, 1183 (1993) 221.
21. L. Garby, P.S. Larsen, Bioenergetics: Its Thermodynamic Foundations, Cambridge University Press, Cambridge, 1995, p. 75.

22.R.B. Kemp, Y. Guan, Thermochim. Acta, 309 (1998) 63.
23.J.A. Roels, Energetics and Kinetics in Biotechnology, Elsevier, Amsterdam, The Netherlands, 1983.
24.I. Prigogine, Introduction to the Thermodynamics of Irreversible Processes, Wiley, New York, 3rd Edit., 1967, p. 147.
25.E. Gnaiger, Thermochim. Acta, 172 (1990) 31.
26.E. Gnaiger, Pure Appl. Chem., 65 (1993) 1983.
27.E.H. Battley, Can. J. Microbiol., 41 (1995) 388.
28.C. Spink, I. Wadsö, in D. Glick (Ed.), Methods of Biochemical Analysis, Vol. 23, Academic Press, New York, 1976, p.1.
29.I.Wadsö, in K.N. Marsh, P.A.G. O'Hare (Eds.), Experimental Thermodynamics, Vol. IV, Blackwell Sci. Publ., Oxford, 1994, p. 267.
30.R.J. Miles, A.E. Beezer, B.F. Perry, in A.M. James, Thermal and Energetic Studies of Cellular Biological Systems, Wright, Bristol, 1987, p. 106.
31.C. Larsson, A. Blomberg, L. Gustafsson, Biotechnol. Bioeng., 38 (1991) 447.
32.Y. Guan, P.C. Lloyd, P.M. Evans, R.B. Kemp, J. Thermal Anal., 49 (1997) 785.
33.Y.H. Guan, P.C. Lloyd, R.B. Kemp, Thermochim. Acta, 332 (1999) 211.
34.J.D. Loike, S.L. Silverstein, J.M. Sturtevant, Proc. Natn. Acad. Sci., USA, 78 (1981) 5958.
35.M. Pätel, B. Schaarschmidt, I. Lamprecht, in B. Miller (Ed.), Vol. II, Wiley, Chichester, 1982, p. 857.
36. S. Thorén, J. Suurkuusk, B. Holma, J. Biochem. Biophys. Meth., 18 (1989) 149.
37.A. Schön, E. Walum, in Abstracts, 37th American Society for Cell Biology Meeting, Washington, DC, 13-17 December, 1997, A3479.
38.A. Schön, I. Wadsö, J. Biochem. Biophys. Meth., 13 (1986) 135.
39.A.-T. Chen, I. Wadsö, J. Biochem. Biophys. Meth., 6 (1982) 297.
40.R.J. Willson, A.E. Beezer, J.C. Mitchell, W. Loh, J. Phys. Chem., 99 (1995) 7108.
41.Y.H. Guan, R.B. Kemp, "Chemical calibration of both flow and insertion calorimetric vessels for biological applications: limitations and solutions", Thermochim. Acta (submitted).
42.H. Forstner, E. Gnaiger, in E. Gnaiger, H. Forstner, (Eds.), Polarographic Oxygen Sensors, Springer-Verlag, Berlin, 1983, Appendix A, p.330.
43.D. Singer, O. Schunck, F. Bach, H.-J. Kuhn, Thermochim. Acta, 251 (1995) 227.
44.R.B. Kemp, Y. Guan, Thermochim. Acta, 300 (1997) 199.
45.A. Schön, I. Wadsö, Cytobios, 48 (1986) 195.
46.P. Bäckman, Thermochim. Acta, 172 (1990) 123.

47.P. Lönnbro, A. Schon, Thermochim. Acta, 172 (1990) 75.
48.W.F. Boron, Ann. Rev. Physiol., 48 (1986) 377.
49.M.S.M. Ardawi, E.A. Newsholme, Essays Biochem., 21 (1985) 1.
50.E.A. Newsholme, B. Crabtree, M.S.M. Ardawi, Q. J. Exp. Physiol. 70 (1985) 473.
51.Y.H. Guan, R.B. Kemp, Cytotechnol., 30 (1999) 107.
52.M.C. Borys, D.I.H. Linzer, E.T. Papoutsakis, Biotechnol. Bioeng., 43 (1994) 505.
53.T. Omasa, K.-I. Higaskiyama, S. Shloya, K.-I. Suga, Biotechnol. Bioeng., 39 (1992) 556.
54.W.L. McKeehan, in M.J. Morgan (ed.), Carbohydrate Metabolism in Cultured Cells, Plenum Press, New York, 1986, p.111.
55.W. Zhou, A. Mulchandani, ACS Symp. Ser., 613 (1995) 88.
56.C.M. Harris, R.W. Todd, S.J. Bungard, R.W. Lovitt, J.G. Morris, D.B. Kell, Enzyme Microb. Technol., 9 (1987) 181.
57.H.M. Davey, D.B. Kell, Microbiol. Revs., 60 (1996) 641.
58.M. Kleiber, The Fire of Life: An Introduction to Animal Energetics. Wiley, New York, 1961, p.54.
59.R.B.Kemp, E. Gnaiger, in W.Weiser, E. Gnaiger (Eds.), Energy Transformations in Cells and Organisms, Georg Thieme, Stuttgart, 1989, p. 91.
60.L. Nässburger, L. Truettson, M. Monti, Biol. Cell, 62 (1988) 33.
61.C. Hinkle, M.A. Kumar, A. Resetar and D.L. Harris, Biochemistry, 30 (1991) 3576.
62.A.D. Beavis, J. Biol. Chem., 262 (1987) 6165.
63.R.C. Wilhoit, in H.D. Brown (Ed.), Biochemical Microcalorimetry, Academic Press, New York, 1969, p. 305.
64.E. Gnaiger, R.B. Kemp, Biochim. Biophys. Acta, 1016 (1990) 328.
65.A.V. Hill, Trails and Trials in Physiology, Arnold, London, 1965.
66.F. Bach, D. Singer, M. Bauer, H.J. Bretschneider, R. Larsen, Thermochim. Acta, 251 (1995) 161.
67.R.C. Woledge, in W.Weiser, E. Gnaiger (Eds.), Energy Transformations in Cells and Organisms, Georg Thieme, Stuttgart, 1989, p.36.
68.N.A. Curtin, R.C. Woledge, J. Physiol., 288 (1979) 353.
69.A. Chinet, T. Clausen, L. Girardier, J.Physiol., 265 (1977) 43.
70.A. Decrouy, P.C. Even, A. Chinet, Experientia, 49 (1993) 843.
71.P.C. Even, A. Decrouy, A. Chinet, Biochem. J., 304 (1994) 649.
72.J. Suurkuusk, I. Wadsö, Chem. Scr., 20 (1982) 155.
73.B. Fagher, M. Monti, I. Wadsö, Clinical Sci., 70 (1986) 63.
74.B. Fagher, H. Liedholm, M. Monti, U. Moritz, Clinical Sci., 70 (1986) 435.

75.J.S. Walker, I.R. Wendt, C.L. Gibbs, Amer. J. Physiol., 252 (1988) C88.
76.P. Lönnbro, P. Hellstrand, J. Physiol., 440 (1991) 385.
77.A. Mokhtarian, A. Decrouy, A Chinet, P.C. Even, Pflügers Arch., 431 (1996) 527.
78.D.G. Allen, D.A. Eisner, C.H. Orchard, J. Physiol., 350 (1984) 615.
79.Ch. Holubarsch, Pflügers Arch., 396 (1983) 277.
80.D.S. Loiselle, Pflügers Arch., 405 (1985) 155.
81.A. Chinet, R. Venturaclapier, G. Vassort, J. Mol. Cell. Cardiol., 25 (1993) 145.
82.B.C. Abbot, A.V. Hill, J.W. Howarth, Proc. Roy. Soc., Ser. B, 148 (1958) 149.
83.J.V. Howarth, R.D. Keynes, J.M. Ritchie, J. Physiol., 194 (1968) 745.
84.M. Kallerhoff, M. Karnebogen, D. Singer, A. Dettenbach, U. Gralher, R.H. Ringert, Urological Res., 24 (1996) 83
85.G. Müller, K.-J.Wolf, F. Fubbe, J. Boese-Landgraf, C. Germer, J. Beuthen, in P.Spinelli (Ed.), Photodynamic Therapy and Biomedical Lasers, Elsevier, Amsterdam, 1992.
86.K. Giering, I. Lamprecht, O. Minet, A. Handke, Thermochim. Acta, 251 (1995) 199
87.P.J. Haines, M. Reading, F.W. Wilburn, in M.E. Brown (Ed.), Handbook of Thermal Analysis and Calorimetry, Vol. 1, Principles and Practice, Ch. 5, Elsevier, Amsterdam, 1998, p. 279.
88.F.Bach, D. Singer, H.J. Bretschneider, R. Larsen, Thermochim. Acta, 251 (1995) 161.
89.U. Bandmann, M. Monti, I. Wadsö, Scand. J. Clin. Lab. Invest., 35 (1975) 121.
90.M. Monti, R. Fäldt, J. Ankerst, I. Wadsö, J. Immunol. Meth., 37 (1980) 29.
91.R.I. Freshney, Culture of Animal Cells and Manual of Basic Techniques, A.R. Liss, New York, 3rd Edit., 1994.
92.R.B. Kemp, Pestic. Sci., 6 (1975) 311.
93.M. Pätel, U. Reichert, B. Schaarschmidt, I. Lamprecht, in W. Hemminger (Ed.), Thermal Analysis, Vol. II, Birkhäuser, Basel, 1980, p.559.
94.M. Wallén-Öhman, P. Lönnbro, A. Schön, C.A.K. Borrebaeck, Cancer Lett., 75 (1993) 103.
95.M.G. Nordmark, J. Laynez, A. Schön, J. Suurkuusk, I. Wadsö, J. Biochem. Biophys. Meth., 10 (1984) 187.
96.U. Reichert, B. Schaarschmidt, Experientia, 42 (1986) 173.
97.Y. Guan, R.B. Kemp, in O.-W. Merten, P. Perrin, B. Griffiths (Eds.), New Developments and New Applications in Animal Cell Technology:

Proceedings of the 15th ESACT Meeting, Kluwer, Dordrecht, The Netherlands, 1998, p. 321.
98. A.J. Fontana, L.D. Hansen, R.W. Breidenbach, R.S. Criddle, Thermochim. Acta, 172 (1990) 105.
99. T.W. Randolph, I.W. Marison, C. Berney, U. von Stockar, Biotechnol. Techniques, 3 (1989) 369.
100. I. Marison, J.S. Liu, S. Ampuero, U. von Stockar, Thermochim. Acta, 309 (1998) 157.
101. I. Marison, M. Linder, B. Schenker, Thermochim. Acta, 310 (1998) 43.
102. R. B. Kemp, P.M. Evans, Y. Guan, J. Thermal Anal., 49 (1997) 755.
103. Y. Guan, P.M. Evans, R.B. Kemp, Biotechnol. Bioeng., 58 (1998) 464.
104. A.N. Tikhonov, V.Y. Arsenin, Solutions of Ill-posed Problems, V.H. Winston and Sons, Washington, 1977.
105. Y.H. Guan, R.B. Kemp, J. Biotechnol., 69 (1999) 95.
106. T. Gurakan, I.W. Marison, U. von Stockar, L. Gustafsson, E. Gnaiger, Thermochim. Acta, 172 (1990) 251.
107. W.M. Thornton, Phil. Mag., Sixth Series, 33 (1917) 196.
108. U. von Stockar, I.W. Marison, Thermochim. Acta, 193 (1991) 215.
109. L.E. Erickson, in A.M. James (Ed.), Thermal and Energetic Studies of Cellular Biological Systems, Wright, Bristol, 1987, p. 12.
110. M.E. Bushell, S.L. Bell, M.F. Scott, R.E. Spier, J.N. Wardell, P.G. Sanders, Biotechnol. Bioeng., 44 (1994) 1099.
111. N. Vriezen, J.P. van Dijken, Biotechnol. Bioeng., 59 (1998) 28.
112. Ruffieux, P-A., Determination of Metabolic Fluxes for Animal Cells in Continuous Culture, Ph.D. Thesis, EPFL, Lausanne, 1998.
113. H.P.J. Bonarius, C.D. de Gooijer, J. Tramper, G. Schmid, Biotechnol. Bioeng., 45 (1995) 524.
114. L. Xie, D.I.C. Wang, Biotechnol. Bioeng., 43 (1994) 1175.
115. L. Xie, D.I.C. Wang, Biotechnol. Bioeng., 51 (1996) 725.
116. J.J. Heijnen, J.P. van Dijken, Biotechnol. Bioeng., 39 (1992) 833.
117. P.M.L. Castro, P.M. Hayter, A.P. Ison, A.T. Bull, Appl. Microbiol. Biotechnol., 38 (1992) 84.
118. S.J. Pirt, Principles of Microbe and Cell Cultivation, Blackwell Scientific Publ., Oxford, 1975, p. 31.
119. Y.H. Guan, R.B. Kemp, in F. Wurm, A. Bernard (Eds.), Products from Cells; Cells from Products: Proceedings of the 16th ESACT Meeting, Kluwer, Dordrecht, The Netherlands, in press.
120. C. Eftimiadi, G. Rialdi, Cell Biophys., 4 (1982) 231.
121. R.B. Kemp, A. Belicic-Kolsek, S. Hoare, C. Schmalfeldt, C. Townsend, P.M. Evans, Thermochim. Acta, 250 (1995) 259.

122. P. Bäckman, Heat Production in Cellular Systems, Ph.D. Thesis, University of Lund, Sweden, 1991, Appendix IV, p.9.
123. P. Bäckman, I. Wadsö, J. Biochem. Biophys. Meth., 23 (1991) 283.
124. P. Bäckman, T. Kimura, A. Schön, I. Wadsö, J. Cell Physiol., 150 (1992) 99.
125. E. Gnaiger, in E. Gnaiger, H. Forstner (Eds.), Polarographic Oxygen Sensors, Aquatic and Physiological Applications, Springer-Verlag, Berlin, 1983, p.337.
126. L.-E. Briggner, X.-R. Ni, F. Tempesti, I. Wadsö, Thermochim. Acta, 109 (1986) 139.
127. L.T. Buck, P.W. Hochachka, A. Schön, E. Gnaiger, Am. J. Physiol., 265 (1993) R1014.
128. T. Haller, M. Ortner, E. Gnaiger, Anal. Biochem., 218 (1994) 338.
129. I. Wadsö, Chem. Soc. Revs., (1997) 79.
130. B. Schaarschmidt, I. Lamprecht, Experientia, 25 (1973) 505.
131. R.H. Hammerstedt, R.E. Lovrien, J. Exp. Zool., 228 (1983) 459.
132. P.B. Inskeep, S.F. Magargee, R.H. Hammerstedt, Arch. Biochem. Biophys., 241 (1985) 1.
133. A. Schön, I. Wadsö, Cytobios, 55 (1988) 33.
134. J. Bermudez, P. Bäckman, A. Schön, Cell Biophys., 20 (1993) 111.
135. T. Roig, J. Bermúdez, Biochim. Biophys. Acta, 1244 (1995) 283
136. S. Haldar, J. Chintapalli, C.M. Croce, Cancer Res., 52 (1996) 1253.
137. A. Manzano, T. Roig, J. Bermudez, R. Bartrons, Amer. J. Physiol., 40 (1996) C1957.
138. X. Liu, C.N. Kim, J. Yang, R. Jemmerson, X. Wang, Cell, 86 (1996) 147.
139. O.-A. Antoce, V. Antoce, K. Takahashi, N. Pomohaci, I. Namolosanu, Thermochim. Acta, 233 (1995) 297.
140. D.L. Page, V.B. Pizziconi, Biosensors Bioelectronics, 12 (1997) 559
141. R. Sörbris, P. Nilsson-Ehle, M. Monti, I. Wadsö, FEBS Lett., 101 (1979) 411.
142. B. Fagher, M. Monti, P. Nilsson-Ehle, B. Åkesson, Clin. Sci., 81 (1991) 793.
143. M.J. Dauncey, Themochim. Acta, 250 (1995) 305.
144. J. Nedergaard, B. Cannon, O. Lindberg, Nature, 267 (1977) 518.
145. A. Palou, C. Pico, M.L. Bonet, P. Oliver, Int. J. Biochem. Cell Biol., 30 (1998) 7.
146. D.G. Clark, M. Brinkman, S.D. Neville, Biochem. J., 235 (1986) 337.
147. I.G. Jarrett, D.G. Clark, O.H. Filsell, J.W. Harvey, M.G. Clark, Biochem. J., 180 (1979) 631.

148. M. Espejo, T. Roig, B. Cutillas, J. Bermúdez, R. Bartrons, S. Ambrosio, Neurosci. Lett., 221 (1996) 5.
149. C. Schulz, N. Irani, M. Wirth, J. van den Heuvel, R.Wagner, in F. Wurm, A. Bernard (Eds.), Products from Cells; Cells from Products: Proceedings of the 16th ESACT Meeting, Kluwer, Dordrecht, The Netherlands, in press.
150. P.-A. Ruffieux, U. von Stockar, I.W. Marison, J. Biotechnol., 63 (1998) 89.

Handbook of Thermal Analysis and Calorimetry. Vol. 4: From Macromolecules to Man.
R.B. Kemp, editor.

Chapter 12

CALORIMETRIC STUDIES IN MEDICINE

M. Monti

Department of Cell Biology 1, University Hospital of Lund, 221 85 Lund, Sweden

1. HEMATOLOGY

1.1 Anaemia, obesity

All biochemical processes are accompanied by either the production or absorption of heat. Measurement of heat effects by calorimetry is thus a general method to monitor such processes. Cell metabolism is usually measured by estimation of substrate or oxygen consumption and products of metabolism, usually lactate and/or carbon dioxide. In the last three decades the development in the field of calorimetry has been extensive and has resulted in the construction of very sensitive microcalorimeters, suitable for measurements on small biological samples. Calorimetric methods are not specific, therefore estimation of heat should often be combined with biochemical measurements. However, although non-specificity is a limitation, it can also be advantageous since general and non-specific methods are suitable for detection of unknown phenomena. Calorimetry thus provides a means for measuring total cell metabolism, which is of clinical interest in many pathological conditions, e.g. blood and nutritional/metabolic disorders.

Microcalorimetry has been used for investigations of blood cells metabolism as one of the first applications of this methodology in the medical field. Preliminary studies have been carried out to develop suitable methods that could be applied in clinical investigations.

The heat production rate (P) produced by erythrocytes was found to be dependent on the experimental conditions. Venous blood from healthy volunteers was collected into 10 cm^3 Vacutainer tubes containing 143 USP units of sodium heparin. The preparation work, which was performed at room temperature, was started within 10 min after the blood sample was collected. Unless otherwise stated, the erythrocyte suspensions were prepared by the column adsorption method described by Nakao et al. [1]. In one series of experiments cells prepared by a centrifugation method were used. This latter

method was identical to one of the preparation methods used in a previous work on erythrocytes [2], method c. Preparation by Nakao's method took 1.5 h, whereas the centrifugation method required about 2.5 h. The purified cells were suspended either in autologous plasma, which had been made cell-free by centrifugation at 3000 g for 15 min, or in glucose-phosphate buffer (108 mmol NaCl, 3.9 mmol KCl, 5.0 mmol MgCl, 4 mmol glucose, and 20 mmol Na_2HPO_4 per litre, respectively: the pH was adjusted to 7.40 with phosphoric acid). In some experiments with plasma suspension the pH was adjusted to high or low values, and in some experiments with buffer suspensions decreased or increased glucose concentrations were used. The erythrocyte suspensions were normally stored for 0.5 h at about 4°C before the calorimetric experiments were started. When other conditions were used, these were indicated in the text. The hematocrit range in the erythrocyte suspensions was 34.8-45.2. By Nakao's preparation method the range of leukocytes in the first 16 experiments was 0-175/mm^3, and the range of platelets 0-6750/mm^3. For the succeeding experiments with the same cell preparation technique the mean values from the first 16 experiments were used: ca. 50/mm^3 for leukocytes and 2000/mm^3 for platelets. Preparations by the centrifugation method gave a leukocyte range of 0-950 (mean, 330)/mm^3) and a platelet range of 1500-4000 (mean, 2060)/mm^3. Three different types of microcalorimeters were used [2]: a static ampoule calorimeter, an air perfusion calorimeter, and a flow calorimeter. They were all of the heat conduction type. P value increased linearly in the physiological pH range [3]. A rapid increase of P values was found when temperature was increased [3]. Using glucose as substrate, no dependence was found of heat production on glucose concentration, at normal or higher levels, in the cell suspension [3]. When erythrocytes were stored at 4°C, an increase of P was found by 6% per h during the first hours; after 24 h storage, the value was about 50% higher than the initial one [3]. P values were the same when simultaneous measurements were made on the same erythrocyte samples using different types of calorimeters: static ampoule, air perfusion and flow calorimeter [2]. P values were found to be significantly higher for erythrocytes in phosphate buffer than for cells suspended in autologous plasma [2]. Isolation of erythrocytes by the column adsorption technique resulted in P values higher than those obtained by a centrifugation procedure [2].

Calorimetric studies were also performed on platelets [4]: heat production rate was measured under different conditions of pH, temperature, cell concentration, preparation and storage time. Blood samples were collected from healthy volunteers into 10 cm^3 Vacutainer tubes containing heparin and dextrane. After centrifugation, the supernatant, free of leukocytes and erythrocytes but containing the platelet fraction, was used for the calorimetric measurement. Duplicate platelet counts were made by phase microscopy, the range was 160-350x10^6/cm^3 (mean 250). There was a slight degree of contamination with other blood cells. The mean value of leukocytes present

was $170x10^3/cm^3$ and the corresponding value for erythrocytes was $300 x10^3/cm^3$. Two identical microcalorimeters of the heat conduction type were used. The samples were enclosed in stainless steel ampoules, volume 1 cm^3. Measurements were made under static conditions. P values increased linearly in the pH range 7.00-7.95, by 20% per pH unit. The temperature coefficient for the heat effect was found to be $Q_{10} = 2.0$ for the temperature interval 32-42°C. Heat production rate per cell was not significantly affected by variations in cell concentration, or by storage for several hours at room temperature. When citrate replaced heparin as anticoagulant significantly higher heat effect values were found.

Heat production rates in lymphocytes were determined under some defined experimental conditions [5]. About 40-60 cm^3 of blood was obtained from healthy volunteers. One set of blood was collected into Vacutainer tubes containg heparin, while the other was defibrinated by gently shaking with glass beads. Lymphocytes were isolated from each set by density gradient centrifugation in Ficoll-Paque medium (Pharmacia, Uppsala, Sweden). The phagocytic cells present, granulocytes and monocytes, were removed by two different methods. In one method the impure lymphocytes were suspended in Hanks' balanced salt solution (Flow Labotatories) containing 20% autologous plasma mixed with iron powder (Merck) and incubated at 37°C under gentle rotation. After 40 min the phagocytic cells, which had ingested the iron particles, were removed with a magnet. In the second method lymphocytes were suspended in Hanks' balanced salt solution containing 20% plasma and applied to a Sephadex column at 37°C. The phagocytic cells adhered to the column while the lymphocytes were eluted from the column with the suspension medium. The lymphocytes were then resuspended in cell-free plasma at concentrations between 0.5 and $6.0x10^6/cm^3$. There was a low degree of contamination of other blood cells, less than $0.02x10^6$ erythrocytes per cm^3 and less than $0.3x10^6$ platelets per cm^3. One cm^3 of the cell suspension was enclosed in 1.1 cm^3 stainless steel ampoule just before calorimetre measurements. Recording were made under static conditions in two identical microcalorimetrs of the heat conduction type. As for erythrocytes and platelets also for lymphocytes was found a dependence of P values on pH in the lymphocyte suspensions in the pH range investigated, 7.00-8.20. The effect of temperature was investigated in the interval 25-42°C. P values of lymphocytes obtained from heparinized blood were found to be lower than P values of lymphocytes from defibrinated blood. Heparinized blood was found to be more convenient to handle and gave higher yields of lymphocytes. In contrast to lymphocytes from defibrinated blood, lymphocytes from heparinized blood also often gave steady-state calorimetric curves at higher cell concentrations. When lymphocytes suspended in plasma were stored unstirred in a test tube for 4 hours at 25°C, P values were found to decrease 5% per hour.

Using P values determined for the different cell fractions of blood, it was found that there is a considerable difference, being the lowest for erythrocytes and the highest for granulocytes and lymphocytes (see Table 1); however, due to the larger number of erythrocytes compared to other cells, they account for about 50% of the heat production in whole blood [6] (see Table 1).

Table 1
Heat production rate (P) for whole human blood and different cell fractions and plasma, presented as means ± SD. Source: reference 6.

Cell type	P	
	mW dm^3 blood mean ± SD	per cell
Whole blood	62 ± 7	------ ----
Erythrocytes	34 ± 2	10 fW
Granulocytes	13 ± 6	3.5 pW
Lymphocytes	12 ± 3	2.2 pW
Platelets	12 ± 2	59 fW
Plasma	0.5 ± 0	----------

Several groups of investigators have applied microcalorimetry to the study of erythrocyte metabolism in different types of anaemia and found increased metabolic rate [7,8,9] (see Table 2).

Table 2
Heat production rate in erythrocytes from anaemic patients and normal subjects.

Source	Calorimeter	Anaemic patients	Normal subjects
Levin [9]	flow, mW dm^3	116 - 232	116 ± 18 (SD)
Monti and Wadsö [8]	static, mW dm^3	126 ± 29 (SD)	79 ± 11 (SD)
Boyo and Ikomi-Kumm [7] (calculated values from mcal cm^3)	flow, mW dm^3	149 - 232	86 ± 11 (SD)

Using microcalorimetry, a group of researchers have studied in sickle cell anaemia the blood viscosity alterations secondary to erythrocyte shape changes; the authors suggest that measurement of heat production could be used for the evaluation of results during therapy in sickle cell anaemia [10]. The understanding of the mechanisms behind the development of anaemias could be increased by a more complete knowledge of the erythrocyte metabolism in such pathological conditions. Examples of this are the studies carried out in renal insufficiency [11] and liver diseases [12] (see Table 3).

Table 3
Erythrocyte heat production rate (P) without and with stimulation of the pentose phosphate shunt by methylene blue (MB).

		P, mW dm^3 erythrocytes, mean ± SD	
	Source	Without	With
Renal insufficiency	Monti [11]	92 ± 12	672 ± 94
Controls	Monti [13]	76 ± 12	571 ± 22
Liver diseases	Monti [12]	101 ± 16	644 ± 54
Controls	Monti [13]	82 ± 7	619 ± 78

Previous reports had suggested that erythrocytes of these patients have decreased metabolic activity in the pentose phosphate shunt leading to cell fragility and therefore to hemolytic anaemia. The calorimetric investigations did not support this hypothesis when the erythrocyte pentose pathway activity was stimulated with MB [11,12,13].

Calorimetric estimation of erythrocyte metabolism has been found to give useful information not only concerning overall cell metabolism but also in relation to specific metabolic processes. By simultaneous measurement of cellular heat production rate with and without specific inhibition with ouabain of the sodium-potassium-adenosine triphosphatase, an estimation can be made of the energy consumed by the Na^+-K^+ pump. There is no agreement about the energy requirements of the Na^+-K^+ pump. Microcalorimetric determinations due to the active sodium potassium transport have been made in the muscles and brown adipose tissue of the rat and found to account for about 5% to 6% of the total energy flux [14]. In erythrocytes from healthy subjects, the corresponding value was 13% [15]. This principle was applied in a study of human obesity. In the last few years, the hypothesis has been advanced that a disturbance in cellular thermogenesis might lead to obesity. The Na^+-K^+ pump

has been suggested as the site of such a cellular defect. In a microcalorimetric investigation [15] no difference was found between obese and healthy subjects (see Table 4), thus speaking against the hypothesis that a cellular metabolic derangement is of importance in the pathogenesis of human obesity.

Table 4
Erythrocyte heat production rate (P) without and with inhibition of the Na^+-K^+ pump in the presence of ouabain. Obese patients and healthy subjects. Source: reference 15.

	P, mW dm^3, mean ± SD		
	- ouabain	+ ouabain	Na^+-K^+pump
Obese patients	118 ± 17	108 ± 15	13 ± 5
Controls	107 ± 13	94 ± 11	14 ± 5

1.2 Trace elements, drugs

The effect on cell metabolism of trace elements considered to be a serious environmental hazard has been tested in vitro by microcalorimetry, on human erythrocytes (lead), lymphocytes (cadmium), and granulocytes (lead, cadmium) [16]. Erythrocyte suspensions were prepared as previously described. Suspensions of lymphocytes were prepared from a 30 cm^3 venous blood sample, collected into Vacutainer tubes containing heparin. The lymphocytes were separated by gradient centrifugation in Ficoll Isopaque. Contaminant phagocytizing cells, granulocytes and monocytes, were removed by incubating the lymphocyte suspension with iron filings at 37°C under rotation 30 min and removing the iron and adherent phagocytic cells with a magnet. The lymphocytes were washed twice in buffer, pH 7.40. The separation process was completed within 3 h. Suspensions of granulocytes were prepared from a 20 cm^3 venous blood sample, collected into Vacutainer tubes containing heparin. Granulocytes were isolated from the blood by centrifugation on a density gradient in a one-step procedure using Mono-Poly Resolving Medium (Flow Laboratories, USA). On this gradient granulocytes and mononuclear cells are separated in two distinct bands with retained functional properties. Contaminating erythrocytes were removed by hypotonic lysis at 0°C using 0.3% sodium chloride for 20 s, then made isotonic with 4.5% sodium chloride and centrifuged. Estimation of the Na^+-K^+ pump activity was done by calculating the difference between two simultaneous measurements of heat production, one without and one with ouabain

octahydrate, specific ATPase inhibitor, added to the cell suspensions. Both overall cell metabolism and Na^+-K^+ pump activity were measured. Cadmium was found to decrease granulocyte overall metabolism, otherwise no other effects on cell metabolism were observed in the other calorimetric tests.

Substances of interest in human medicine also have been investigated by calorimetry measuring their effect on blood cell metabolism. It is well known that several antibiotics have potentially the capacity to cause toxic effects in blood cells, particularly leukocytes: e.g. chloramphenicol has been found to affect oxidative metabolism and phagocytic activity of human granulocytes. Especially one group of antibiotics, aminoglycosides, has been reported to cause side effects on blood cells: i.e. inhibition of the candidacidal activity of human granulocytes. However, previous studies on aminoglycoside antibiotics are controversial. Gentamicin, belonging to this group of antibiotics, is used extensively in the treatment of gram-negative infections; patients are often treated with a higher dosage of the drug and for long periods of time. Toxic side effects have been reported, the most common being nephrotoxicity and ototoxicity. The mechanism behind these complications is unknown. Reduced Na^+-K^+ ATPase has been found in experimental animals and this finding has led to the hypothesis that disturbances of the electrolyte balance might play a role in the development of nephrotoxicity.

A calorimetric study was done to investigate whether gentamicin affects the metabolism of human blood cells [17]. Venous blood was collected from healthy persons and isolation was carried out for erythrocytes, granulocytes and lymphocytes; the cells were then suspended in autologous plasma. Cell suspensions were introduced in the calorimetric vessels for measurement of heat production. Gentamicin was added to the cell suspensions at different concentrations.

Increased erythrocyte heat production rate was recorded at gentamicin concentrations above the therapeutic level, whereas no effect was found at lower concentrations. The Na^+-K^+ pump was unaffected at any concentration. Granulocytes showed a slight increase of heat production rate when gentamicin was above therapeutic level, and no effect was noted at lower concentrations. Lymphocytes were found to have normal heat production rate at any concentration.

In conclusion, the metabolism of blood cells was found to be affected by gentamicin only at concentrations above therapeutic level. Na^+-K^+ pump was unaffected at any concentration.

Two commonly used drugs in human medicine, terbutaline and propranolol, have been tested concerning their effect on erythrocyte metabolism. Terbutaline is a beta-2-adrenoceptor agonist and propranolol is a beta-1-beta-2-adrenoceptor antagonist. Both drugs are taken up into the erythrocytes.

Previous studies have shown that incubation of erythrocytes with high doses of propranolol reduces glucose catabolism, whereas other investigators have found enhanced generation and utilization of ATP; thus controversial results have been obtained.

A calorimetric study [18] was done to estimate whether propranolol and terbutaline affected human erythrocyte metabolism after short treatment with therapeutic doses of the drugs. The study had a double blind, cross-over design. Propranolol and terbutaline slow-release 7.5 mg were randomly administered twice daily for 1 week to 15 healthy non-smoking males. Placebo tablets of similar shape and colour were employed. Blood samples were taken after seven days on each drug. A "wash-out" period of at least two weeks separated each study period. Neither of the drugs was found to influence overall erythrocyte metabolism or the energy expenditure connected with the Na^+-K^+ pump.

The mechanism of action of different calcium antagonists varies, although their final effect is inhibition of the influx of extracellular calcium through channels in vascular smooth cell membranes, resulting in peripheral vasodilation. These drugs are widely used in the treatment of hypertension and ischemic heart disease. Their effect on platelet metabolism was tested by calorimetry [19]. Platelet rich plasma (PRP) suspensions were prepared from a 10 cm^3 venous blood sample collected into Vacutainer tubes containing heparin and 2 cm^3 of a 5% Dextrane solution. Thereafter the erythrocytes sedimented during 1 h at the bottom of the tubes. By centrifugation for 10 min at 100 g the lymphocytes sedimented whereas the platelets were collected in the supernatant. For two of the drugs, flunarizine and verapamil, significantly reduced platelet heat production was recorded when their concentration was above therapeutic level, whereas no effect was observed at lower concentrations. The other two calcium antagonists tested, diltiazem and nifedipine, were without effect on platelet metabolism.

Coffee is one of the most consumed beverages and caffeine is used commonly as a drug in human medicine. In a calorimetric study the influence of caffeine on cell metabolism was tested [20]. Heat production rate was measured in platelets from healthy subjects after administration of 100 or 200 mg of caffeine, corresponding to 1 or 2 cups of coffee. Increased values were recorded and return to normal levels was noted 1 h later. It is presumed that the effect of caffeine on platelet metabolism is due to increased concentrations of catecholamines. It is in fact known from previous investigations that caffeine stimulates production of adrenaline and noradrenaline. Another effect of caffeine observed in the calorimetric study was a temporary, but significant, increase of blood pressure. It is possible that the described effect on cell metabolism is not limited to platelets, as indicated by previous studies showing increased basal metabolism after administration of caffeine. It cannot

therefore be ruled out that in some diseases, e.g. heart diseases, the ingestion of coffee repeatedly might be harmful.

Further calorimetric studies [21] have been carried out on the direct effect on platelet metabolism of caffeine and two other substances, enprofylline and theophylline, belonging to the same group of drugs, the methilxanthines. The latter drugs are used in the treatment of asthma. Heat production was measured after addition of the drugs to the platelet suspensions. Caffeine in therapeutic concentrations was found to reduce platelet metabolism, thus indicating that previous studies in vivo showing increased platelet metabolism after administration of the drug [20] could not be due to a direct effect of caffeine on cell metabolism. Enprofylline and theophylline reduced platelet metabolic rate when their dosage was higher than the therapeutic level.

Other calorimetric studies [22] on human blood platelets were performed in order to clarify the mechanism of action of xanthine derivatives in relation to adenosine receptor. In addition, there were investigations on the effect of adenosine and adenosine agonists on platelet metabolism. The results showed that the two xanthine derivatives tested, enprofylline and theophylline, at therapeutic concentrations, did not modify the heat production induced by adenosine. Both adenosine and one adenosine agonist, NECA (5-N-ethyl carboxamide adenosine) increased platelet metabolism. The other adenosine agonist tested, PIA (L-N^6-phenylisopropyl-adenosine) induced a reduction of heat production. The adenosine uptake inhibitor, dipyridamol, was without effect. Thus, by microcalorimetry, useful information could be obtained concerning the complex mechanisms behind the effects on human cell metabolism of adenosine and adenosine agonists. The same applies to substances used in the treatment of asthma, xanthine derivatives; they are thought to act by inhibition of adenosine receptors.

The most important function of platelets is to arrest bleeding from damaged vessels, by adhering to the surface of the vessels and aggregating with each other, thus forming a hemostatic plug. The platelet metabolism changes during this coagulation process are not so well known. A group of investigators [23] has studied the problem by microcalorimetry using a number of substances known to induce platelet aggregation Significant increase of platelet heat production was recorded when the aggregating agents thrombin, ADP, collagen, Mn^{2+} and Cd^{2+} were added to platelet suspensions. The qualitative change of cell metabolism induced by aggregating agents was studied by using specific metabolic inhibitors. Thus, it was observed that most of the increased platelet heat production rate appears to be due to activation of the two main metabolic pathways, oxydative phosphorilation and glycolysis. The heat produced by the process of aggregation per se seems to be relatively small. These results have given further information on the mechanism of action of commonly used drugs on platelet metabolism and function, thus showing that microcalorimetry has a potential as a new methodology to uncover unknown

drug effects on cell metabolism. Further hematological studies are described in Sections 2,3,4,5.

2. MALIGNANCY

2.1 Lymphoma, cancer

A calorimetric study [24] of metabolism in cultured human T-lymphoma cells has been carried out using a new microcalorimetric vessel; the instrument was equipped with small electrodes for simultaneous measurements of heat production and oxygen consumption as well as pH. The cell suspension was stirred by means of a new type of turbine stirrer. It was found that aerobic processes accounted for 60% of the total cell heat production rate. In a further study [25], the calorimetric recording was extended over a period of 12-28 h and it was found that cell metabolism and cell growth decreased with time, concurrently with a decrease in the pH of the medium. The same group of investigators has studied the effects of experimental factors on the recording of heat production in T-lymphoma cells [26]. Temperature and pH changes were found to influence calorimetric results, whereas variations of cell concentration and stirring rate in the suspension did not affect heat production.

Microcalorimetry has been applied successfully to the study of cell metabolism in tumour cells and blood lymphocytes from patients with non-Hodgkin lymphoma (NHL) [27]. This is a disease with a great deal of variation in the clinical course due to different degrees of malignancy. A correct prognostic evaluation in each individual case is very important in order to choose the most suitable therapy. Classification of the disease into different groups is traditionally based on the morphology of the tumour cells, although this is considered not to be optimal as a prognostic parameter. From the clinical point of view, there is therefore a need for other variables in order to improve prognostic estimation.

The metabolic activity of malignant cells from a group of patients with NHL was monitored by microcalorimetry. Heat production was measured in cells aspirated from tumours and blood lymphocytes [27,28,29]. Lymphoid cells from tumour masses were obtained by repeated (3 - 6 times) fine needle punctures and the aspirated material was suspended in autologous plasma. Phagocytizing cells were removed by incubating the cell suspensions in a phosphate buffer containing iron filings and 10% autologous plasma at 37°C under rotation for 30 min and removing adherent phagocytic cells with a magnet. The cells were washed twice in a 50 cm^3 phosphate buffer, pH 7.40, and resuspended in autologous cell-free plasma which had been recentrifuged at 8000 g. This was diluted with an equal volume of saline, layered on 2 cm^3 of lymphoprep TM (sodium metrizoate/Ficoll solution) from Nyregaard & Co, Oslo and centrifuged at 500 g (MSE centrifuge with Swing-out rotor) for 20

min at 20°C to sediment contaminating erythrocytes and granulocytes. Cell count in each cell suspension was made in duplicate in a Bürker chamber just before the calorimetric measurements. Viability of the tumour cells was determined by trypan blue exclusion test. In the prepared cell suspensions, a few platelets and erythrocytes were sometimes found. The pH of the cell suspension taken directly from the calorimeter ampoule at the end of 1 h incubation at 37°C was determined using a capillary electrode pH meter (Radiometer), type G279/G7. Calorimetric measurements were also made on cell-free plasma samples and buffer medium.

P values of malignant cells from patients with non-Hodgkin lymphoma were higher in the group who did not respond to treatment compared to patients showing improvement during therapy [27] (see Table 5). Also heat production of blood lymphocytes was found to be higher in the group of patients with progressive disease as compared to the group of patients who responded to therapy. The difference between groups was significant for both tumour cells and blood lymphocytes. The results suggested that a high metabolic activity in lymphoma cells is associated with an aggressive growth of the tumour tissue. The period of observation was however short and the number of patients too small to allow conclusions about the survival rate. Further studies were later carried out in lymphocytes from NHL patients [28]: a large group was followed for a long period of time after the initiation of treatment and P values were related to the length of survival. The results showed that assessment of the heat production in peripheral blood lymphocytes has a prognostic impact in NHL. A multivariate analysis regarding prognosis showed that heat production rate was superior to age, histological classification and clinical staging, parameters traditionally used for a prognostic evaluation of the clinical course of NHL. Because cellular heat production rates are considered to reflect overall cell metabolism these results suggest that circulating lymphoid cells with high metabolic activity are especially common in patients with advanced and aggressive NHL.

Table 5
Heat production rate (P) of tumour cells and lymphocytes from non-Hodgkin lymphoma (NHL) patients and of lymphocytes from normal subjects. Source: reference 27.

	P, pW/cell, mean ± SD	
	Tumour cells	Lymphocytes
NHL without remission	5.5 ± 3.3	3.1 ± 0.8
NHL with remission	3.7 ± 1.1	2.4 ± 0.5
Controls	———	2.7 ± 0.6

The correlation between metabolism of lymphoma cells and the clinical course of the disease was confirmed in another investigation [29], where a larger group of NHL patients was studied and their survival for more or less than 2 years was evaluated. A high correlation was found between the length of patient survival and P values in tumour cells: the heat production rate before therapy was significantly lower in the patients surviving more than 2 years than in those who died within that period (see Table 6).

Table 6
Heat production rate (P) of tumour cells from 36 untreated patients with high and low grade non-Hodgkin lymphoma (NHL), and with survival for more or less than 2 years. Source: reference 28.

	P, pW/cell, median values	
NHL high grade	3.9	
		p=0.05
NHL low grade	2.8	
NHL with survival for less than 2 years	4.0	
		p=0.02
NHL with survival for more than 2 years	2.5	

For the study of tumour cells in vitro, some substances are often added to the cell suspensions: antibiotics to prevent bacterial growth, dimethyl sulphoxide (DMSO) to dissolve anticancer drugs. It is important to know whether such substances affect cell metabolism and cause artefacts that might create difficulties in the interpretation of the results obtained. Some investigators have therefore studied by the use of microcalorimetry the metabolic effects of these substances on human lymphoma cells [30]. DMSO was found to cause a dose-dependent decrease of heat production after 24 h of incubation. Penicillin, streptomycin, gentamicin and amphotericin B did not affect significantly cell metabolism.

Hyperthermia is used in the treatment of cancer. It is unclear however what metabolic changes are present in tumour cells as compared to normal cells by increasing temperature. In normal cells it has been found [1,3,4] a rapid increase of heat production with increasing temperature from 25 to 42°C. Cell

metabolism was thus still functioning normally although at an activated state, whereas tumour cells were unable ta maintain a normal metabolism when the temperature was increased above 41°C [31].

In treatment of malignant tumours there is need of a predictive test in order to measure, in vitro, the sensitivity of individual tumours to different neoplastic drugs. In fact resistancy to therapy is not uncommon and leads to delayed regression of the tumours, which is very deleterious taking into account the importance of the time-factor in this type of disease. Moreover, the drugs used might be not only inefficient but also harmful to the patients by causing serious side effects, as often is the case with anti-cancer drugs.

Since the growth of a tumour depends on cell metabolism, measurement of heat production was considered a reliable way to follow the effect of drugs presumed to inhibit such growth. A clear correlation was found between calorimetric values and cytotoxicity when methotrexate, a common antineoplastic drug, was tested on cultured lymphoma cells [32]. These results show that microcalorimetry offers the possibility to develop a quick method for testing antineoplastic drugs in vitro.

2.2 Leukaemia

Symptoms of hypermetabolism, such as sweating and loss of weight, are common in chronic lymphocytic leukaemia (CLL). Increased basal metabolism has been measured in these patients. The mechanism causing hypermetabolism is not known. A calorimetric study [32] was carried out to investigate to what extent the increased lymphocyte mass accounted for the high metabolism. The heat production rate per CCL lymphocyte was found to be lower than normal, in agreement with previous investigations showing decreased pentose phosphate shunt and glycolytic activity in CLL lymphocytes. Using the mean calorimetric value obtained, calculations of the heat production of the blood circulating lymphocytes in a healthy subject with a blood lymphocyte count of $2x10^9/dm^3$, gave a value of 0.03 W. It is not unusual that CLL patients have a lymphocyte count of $200x10^9/dm^3$ or more. It has to be taken into account that blood lymphocytes represent only a minute fraction of the total lymphocyte population, much of it accumulating in storage organs. Therefore it was calculated that in CLL the heat production of the whole lymphocyte population can account for 5-6 W or more. Relating this figure to the amount of heat produced by the normal human body, about 100 W [34], it seems that the increase of lymphocytes in CLL might play a significant role in the development of hypermetabolism. This is supported by the fact that the extirpation of the spleen, containing a large amount of lymphocytes, in CLL patients is followed by a decrease of the basal metabolism.

Heat production rate has been measured in polymorphonuclear granulocytes (PMN) from patients with acute myelogenous leukaemia and compared to the corresponding results obtained in a group of healthy individuals [35]. Patients

with acute myelogenous leukaemia (AML) were given cyclic chemotherapy. Blood specimens were taken immediately before a course of chemotherapy exclusively from patients without clinical and laboratory signs of infections. Granulocytes were prepared by layering leukocyte-rich plasma onto Ficoll-Isopaque (Lymphoprep, Nyegaard, Oslo, Norway). After centrifugation for 10 min at 70 g followed by 15 min at 700 g the sedimented granulocytes in the bottom of the tubes were washed twice in saline. The suspensions contained approximately 90-95% mature granulocytes with a normal appearance in Giemsa staining. The cells were suspended in autochtonous plasma, serum or RPMI tissue culture medium containing 10% heat inactivated calf serum and 2% Hepes. Cells were also suspended in allogenic heat inactivated sera (56°C, 30 min) diluted 1 : 2 in fresh serum from the cell donor. The heat production rates in granulocytes from AML patients and from healthy donors were determined in autochtonous plasma suspensions. A group of patients was studied in the acute stage or in remission within 6 months after diagnosis. Another group of patients was studied during remission after 6 months duration of the disease.

Increased values were found in the patients at diagnosis and during the first 6 months of remission (see Table 7), whereas during sequential analysis heat production decreased gradually. Also PMN from healthy persons show increased heat production when mixed with sera from patients with leukaemia, thus indicating that the increased cell metabolism is serum (leukaemic) dependent.

Table 7
Heat production rate (P) of polymorphonuclear granulocytes from normal subjects and patients with acute myelogenous leukaemia (AML) in the acute stage and during emission. Source: reference 35.

	P, pW/cell, mean ± SD
AML patients, acute stage	11.3 ± 3.2
AML patients, remission	9.0 ± 3.8
Controls	8.4 ± 1.7

Infections are common in patients with acute leukaemia and PMN function in general exerts an important defense against microbial organisms. There is therefore a decreased defense in leukaemic patients due to granulocytopenia but also defects in PMN function have been reported. PMN function, phagocytosis, has been studied by microcalorimetry [36]. The increase of heat

production, equivalent to phagocytosis, was measured after stimulation of the cells with immune complexes. In previous studies (see Section 3) it had been found that preformed immune complexes led to increase of PMN heat production, thus reflecting PMN phagocytic response to particles.

In a group of leukaemic patients decreased PMN responsiveness was found in the acute stage of the disease (see Table 8).

Table 8
PMN responsiveness to immune complexes in patients with acute myelogenous leukaemia (AML) and normal subjects. Source: reference 36.

	% increase of heat production, mean ± SD
AML, remission less than 6 months	27.8 ± 8.9
AML, remission more than 6 months	37.7 ± 10.8
Controls	40.2 ± 7.3

Microcalorimetry was also used for functional studies of leukaemic cells surface receptors by measurement of heat production changes following the binding of IgG to Fc receptors [37].

In a human leukaemia cell line it was found by use of microcalorimetry that antibody-induced death, apoptosis, as shown by DNA fragmentation, was energy-dependent [38].

3. IMMUNOLOGY

Microcalorimetry has been applied in a few studies to investigate metabolism, in the resting or stimulated state, of those cells who play an important role in the field of immunology: lymphocytes, macrophages and granulocytes.

3.1 Lymphocytes

Lymphocytes have the ability to recognize foreign particles (antigens) capable of causing immunoreactions, due to the presence of specific antigen receptors (antibodies) in the cell membrane. Antigen stimulation induces lymphocyte proliferation that is dependent on cell metabolism.

When horse lymphocytes were stimulated with mitogenic agents [39] significant heat production, that preceded DNA synthesis, was recorded after 2 days of incubation, reaching a maximum at 4-5 days. A similar response was observed in human lymphocytes [40] reaching a maximum of heat production

after 1-3 days and showing a great variability of individual response in the different cell preparations.

An attempt has been made to characterize lymphocytes simultaneously with biochemical measurements during stimulation with mitogens. Ross and Loos [41] have found that the energy required is provided by either glycolysis or the Krebs cycle.

In a recent investigation [42], basal lymphocyte metabolism and metabolic changes were analysed in the non-activated and activated state respectively, using phytohaemagglutinin (PHA) for antigenic stimulation. Conversion of glucose to lactate accounted for 25% of the total heat production, whereas the rest of the heat produced was due to glucose oxidation. The calorimetric values were in full agreement with the expected values, based on calculated heat flow from the rate of lactate formation and oxygen consumption due to glucose catabolism.

3.2 Macrophages

Macrophages play an important role in the field of immunology. These cells participate in the defense process by phagocytyzing foreign particles (antigens). Moreover, they activate T-lymphocytes when antigens are present in their cell membrane. The alveolar macrophages (AM) in the lungs, living on surfaces exposed to inhaled polluted air, act as scavengers, protecting the pulmonary tissue from invading microorganisms and inhaled particles. In addition to being responsible for the sterility of the lung, the AM takes part in the cell- and humoral-mediated processes in cooperation with other cells.

The interest to study macrophage metabolism by calorimetry was motivated by the need for new short-term tests for characterization of toxic effects of environmental pollutants without use of expensive and time-consuming animal experiments. The aim was to correlate toxic effects and macrophage heat production and this required development of a method [43].

AM were collected from rabbits by bronchopulmonary lavage. The animals were killed by a blow to the neck. The throat was opened under sterile conditions and the upper part of the trachea was klamped and cannulated under this point by a sterile plastic tube with a three-way valve. The lungs were washed in situ with a 0.9% physiological sodium chloride solution in 20 cm^3 portions during gentle massage of the thorax, yielding 80-100 cm^3 of cell suspension. This was centrifuged at 300 g for 10 min and decanted. The cells were resuspended in Hanks' balanced salt solution (HBSS) followed by another centrifugation and decantation. Finally, for experiments with cells in suspension, minimum essential medium (MEM) with or without serum was added to give the cell concentration desidered. HBSS was added for experiments with cells in monolayers. Contaminating erythrocytes were removed using a lysing buffer without the addition of EDTA at 37°C for 10 min followed by centrifugation and resuspension. Circular polystyrene plates

with a diameter of 10 mm were punched out of commercially available cell culture dishes. The plates were sterilized and their negative charge was increased by overnight exposure to concentrated sulfuric acid at room temperature. The acid was poured off and 10% sodium carbonate was added for 15 min to neutralize the residual acid. The dishes were finally washed with HBSS. The cells were left in HBSS to sediment and adhere to the plates for 1 h at 37°C. Non-adherent cells were rinsed out with HBSS. MEM was supplemented to give a final concentration of 20% homologous serum. The cells, in suspension and in monolayers, were stained with May-Grünwald -Giemsa for identification. Samples were taken from the cell suspensions and the proportion of viable cells was counted manually using fluorescence microscopy. At the end of the calorimetric experiments viability was assessed by measuring the extracellular activity of lactate dehydrogenase (LDH). At the start of each calorimetric experiment two supplementary calorimetric ampoules charged with cell-free medium with or without the addition of serum were placed in a thermostated oven at 37°C for 20 h. The increase in LDH activity during the calorimetric measurements was calculated as the difference between the values for the cell-charged ampules and the mean of the values for the two supplementary ampoules. For monolayers, two polystyrene tubes with cells and culture medium (pH 7.40) were placed into 5.0 cm^3 stainless steel ampoules. After the calorimetric measurements, the number of cells on the plates was determined by use of an Image Analysing Unit (Mikro Measurement III) connected to an invert microscope (Olympus IMT/LWD) and a microcomputer (Apple II) with a printer (Epson MX 80 II). By an automatic step table mounted to the microscope the monolayers were scanned. From the viability index the number of viable cells of each plate was calculated and the heat flow per living cell could be estimated.

The system was tested with AM from rabbits and heat production rate could be monitored from a low number of cells that could be easily collected. No contaminating cells were observed. The calorimetric values were found to be unchanged or to decrease very slowly over a period of about 20 h. The cells should be used only in monolayers and suspensions should be avoided since heat production rate per cell in macrophage suspensions was found to be dependent on cell concentration. There are several important advantages with the monolayer technique. The measurements can be made with a small number of cells and the washing procedure removing non-adherent cells and non-bound particles can be performed easily and rapidly. Furthermore, the monolayers can easily and repeatedly be examined microscopically.

The method was later tested with three different substances known to be potentially toxic as air pollutants [43]. In preliminary experiments it was found that non-viable macrophages did not have any heat production. This was assumed to be the case in all experiments. It was considered that exposure to toxic substances always causes a change of cell metabolism. Manganese dioxide

and quartz particles were found to be cytotoxic, unlike titanium dioxide. The results were in agreement with cell survival data found by the use of a fluorescein-ester staining method and measured by an image autoanalyser. By a combination of a calorimetric technique and a very reliable cell counting technique with a semi-automatic autoanalyser, it was found that measurement of macrophage heat production rate is possible using a small number of cells; thus making the methodology suitable for short-term screening tests in toxicology. In case toxic effects would be found, the test should be completed with biochemical measurements for more specific informations about the metabolic disturbance present in the cells. With the gradually increasing number of toxic substances in the environment there is a growing need for fast screening tests to evaluate the toxic effects on the human organism.

Peritoneal macrophages become active phagocytic cells in immunological conditions. A group of investigators has studied these cells in rats by combining a calorimetry with a luminometric method to measure the release of oxygen radicals [44]. Ten cm^3 of RPMI 1640 without bicarbonate but supplemented with 10% heat inactivated calf serum, gentamicin 72 μM, L-glutamine 2 mM, and buffer with 20 mM Hepes was injected intraperitoneally under aseptic conditions. The abdomen was massaged for 3 min. Animals were then sacrificed by inhalation of ether, and the peritoneal fluid was recollected and placed in a 15 cm^3 cell culture tube by a large bore needle. The fluid was centrifuged for 15 min at 500 g, supernatant was discarded and 2 cm^3 of the same RPMI 1640 was added and mixed gently. The cell suspension was placed in a 60 mm cell culture dish and incubated at 37°C and 5% CO_2 for 1 h. The upper medium layer was discarded and the cell layer attached to the dish was washed three times with 0.02 mM phosphate buffered saline. The remaining cells were scraped and resuspended in 2 cm^3 of the same culture medium. More than 90% of the harvested cells were identified as macrophages under light microscopy, and the cell viability was found to be above 95% using trypan blue exclusion staining test. Measurements were performed on resting cells and during phagocytic stimulation with phorbol 12-myristate 13-acetate (PMA). The cell samples obtained from rats with liver or kidney injury showed differences when compared to healthy rats.

3.3 Immune complexes

Some substances, antigens, have the ability to induce an immune response which consists of stimulating the immune system to produce antibodies. These combined with antigens form antigen-antibody complexes, also called immune complexes. It is unclear what role blood immune complexes play in the etiology and pathogenesis of some diseases, particularly rheumatic and in human neoplasms. There are several methods to detect blood immune complexes; however, the results of these measurements do not correlate well with the degree of activity of the diseases investigated, and this rather limits

their use from a clinical point of view. Due to the growing interest in blood immune complexes, an attempt was made to develop a calorimetric method for their detection. Earlier studies have shown that in the presence of immune complexes there is an increase of blood oxygen uptake [45], leading to the expectation of an increased heat production in granulocytes.

Previous calorimetric investigations have shown large increases in heat production when aerobic metabolism was stimulated in erythrocytes [13,46] and leukocytes [47].

During defined experimental conditions, antigens and their corresponding specific rabbit antisera, were found to activate the metabolism of human blood cells, when heat production was measured [48]. In this study no attempt was made to identify the blood cells responsible for heat production. An increase was observed from the normal basal heat production of blood of about 60 μW to about 200 μW cm^3. Sensitivity, specificity and reproducibility of the measurements were very good.

In further investigations, simultaneous measurements of heat production were carried out in whole blood and isolated populations of blood cells and plasma, mixed with immune complexes [49]. Granulocytes were found to be the main source of heat production. Also mononuclear cells were activated when exposed to immune complexes, but their activation level was significantly lower than for granulocytes. No increase of heat production was observed when the other blood cells and plasma were mixed with immune complexes. Binding of antigen-antibody complexes to granulocytes and subsequent activation of cell metabolism appears to be mediated by Fc and C3b receptors on the cell surface.

Granulocyte activation has also been studied by microcalorimetry, stimulating cell phagocytosis with bacteria and latex particles [47] and yeast [50]. Other investigators have stimulated granulocytes with phorbol-12-myristate-13-acetate [51,52,53].

An elaborate study [51] was carried out where calorimetric values were correlated to the enthalpy change of aerobic and anaerobic metabolism during phagocytosis; heat production was measured simultaneously with oxygen and glucose consumption as well as carbon dioxide, lactic acid and ATP production.

The capability of microcalorimetry to signal presence of immune complexes has been used in a clinical study of patients with acute leukaemia [36], (see Section 2). Another clinical application was carried out by other investigators [54] in patients with Systemic Lupus Erythematosus. It was found that leukocyte heat production increased in the presence of homogenates prepared from autochthonous leukocytes, thus suggesting the presence of antigen-antibody complexes. According to the investigators the method could be useful to estimate the degree of activity in immunological diseases.

In other investigations microcalorimetry has been used to follow in vitro

antigen-antibody reactions [55,56] and to detect complement-dependent immune reactions [57]. The results obtained indicate that microcalorimetry can be a useful tool for studying the mechanism of cellular immunological reactions.

4. ENDOCRINOLOGY

4.1 Hyperthyroidism, hypothyroidism

Thyroid dysfunction is a fairly common disorder to be found in clinical practice. The thyroid synthesizes two hormones, triiodothyronine (T_3) and thyroxine (T_4), dipeptides containing 3 and 4 atoms of iodine respectively in each molecule. The thyroid stimulates cell metabolism of most tissues, might cause hypermetabolism symptoms: loss of weight in spite of increased appetite, palpitations, tremor of the fingers, anxiety, heat intolerance. The hormone activity is mainly carried out by T_3. Most of it derives by monodeiodination from T_4 that is secreted directly by the thyroid. Both hormones in the blood are bound to plasma proteins. In the development of medical applications of microcalorimetry, among the first pathological conditions to be studied were thyroid dysfunctions.

Although it is well known that thyroid hormones stimulate metabolism, the mechanism of action is still unclear at the cellular level. The whole body basal metabolic rate (BMR) has been previously used for clinical evaluation of thyroid dysfunction but for many years largely has been abandoned because of high inaccuracy of the method. The diagnosis of thyroid dysfunction is based on the clinical features (signs and symptoms of the disease) and thyroid hormones concentrations. However, the clinical features of the disease might vary considerably between different patients with the same concentration of hormones, depending on the variability of cellular response to thyroid hormones stimulation. Old patients, for example, have often less pronounced symptoms compared to younger subjects. Thus, there is not at present a parameter reflecting the degree of metabolic disturbance at the cellular level. Microcalorimetry was then introduced in medicine about two decades ago with the purpose of providing a method to measure cellular metabolic rate in physiological conditions as well as in pathological states.

Studies in different laboratories have shown increased heat production in leukocytes [58,59] from hyperthyroid patients. In the former study [58] heat production was measured with a flow microcalorimeter in the whole leukocyte population In the latter investigation [59] microcalorimetric measurements were carried out in the lymphocyte population using a static ampoule calorimeter. The results showed a qualitative agreement between the two studies, although the two investigations are not comparable since the former

study was done on a heterogenous cell mixture comprising different sub-populations of leukocytes with variable heat production rate. A good correlation was noted between erythrocyte heat production rate and the clinical condition of the patients [60]. The increased values of heat production were found to return to normal levels after treatment [60, 61] (see Table 9).

Table 9
Heat production rate (P) of erythrocytes and lymphocytes from hyperthyroid patients before and after treatment. The variation of values is dependent of different experimental conditions.

Source	Cell samples	P		
		Before treatment	After treatment	Controls
Monti and Wadsö [60]	erythrocytes mW dm^3 ± SD	102 ± 15	85 ± 14	78 ± 5
Monti et al. [61]	"	120 ± 2	99 ± 2	108 ± 2
Valdemarsson et al. [59]	lymphocytes pW/cell ± SEM	3.43 ± 0.25		2.31 ± 0.12
Valdemarsson et al. [62]	"	3.19 ± 21		2.26 ± 0.11
Valdemarsson and and Monti [68]	"	3.37 ± 0.25	2.50 ± 0.11	2.32 ± 0.10

The action of thyroid hormones at the cellular level is expected to be carried out by attachment of the hormones at the nuclear receptors in the target cells. The increased heat production in erythrocytes, cells without a nucleus, indicates that thyroid hormones have the capability to stimulate cell metabolism also by other mechanisms than through nuclear receptors

It is well established that thyroid hormones stimulate oxygen consumption, whereas their effect on anaerobic metabolism is unclear. Calorimetric studies on erythrocytes were therefore performed to clarify the influence of thyroid hormones on anaerobic metabolism. After initial calorimetric recording of erythrocyte total metabolism, sodium fluoride was added to the cell suspension to inhibit enolase and thus stop substrate utilization through the anaerobic pathway [62]. The decrease of heat production rate in samples with sodium fluoride corresponds to the anaerobic contribution, whereas the values from samples with sodium fluoride reflect aerobic metabolism. The value from samples without sodium fluoride reflects total cell metabolism. The results of

a study in a group of hyperthyroid patients [62] show that both the aerobic and anaerobic pathways were stimulated and not less than 60% of the total erythrocyte heat production was derived from the anaerobic activity. The relative contributions of aerobic and anaerobic metabolism were found to be the same in the hyperhyroid and euthyroid state. Thus, only quantitative and no qualitative changes of erythrocyte metabolism were observed in hyperthyroidism.

Further studies in hyperthyroidism were done with nucleated cells by simultaneous measurements of heat production and oxygen consumption rates in lymphocytes from patients before and after treatment [63]. The contribution from aerobic metabolism was calculated from the product of the lymphocyte oxygen consumption rate and the enthalpy change for glucose combustion. The anaerobic contribution was calculated as the difference between heat production (total cell metabolism) and oxygen consumption. The results show that during thyroid hormone excess, adenosine triphosphate (ATP) generation has to be supplied mainly through an increased activity in the anaerobic pathway. These data support the results obtained in erythrocytes indicating a gross underestimation in the importance of anaerobic metabolism in hyperthyroidism.

The activity of the Na^+-K^+ pump has been proposed to be regulated by thyroid hormones and to account for a large contribution of the increased energy expenditure in hyperthyroidism. Microcalorimetry was used to measure erythrocyte [64] and lymphocyte [62] heat production rate during ouabain-induced inhibition of ATPase, thus estimating the importance of the sodium-potassium pump in hyperthyroidism. The results of these studies show that the raised heat production rate in this condition was not due to increased energy expenditure by the pump. This was confirmed in microcalorimetric studies with mammalian skeletal muscle [65,66] and hepatocytes [66,67].

Subclinical thyroid dysfunctions, hyper- or hypothyroidism, are frequently encountered in clinical practice, accompanied by slight changes, increase or decrease, of thyroid hormone levels. Since it is difficult to evaluate the clinical significance of these moderate alterations of hormone production, it is therefore also difficult to take decisions about the treatment of these patients. In order to clarify the effect of low degrees of thyroid dysfunction on cellular energy expenditure, an investigation was carried out where heat production was measured in lymphocytes from patients with different degrees of thyroid dysfunction [59]. The lymphocyte heat production rate was found to be significantly correlated to the thyroid hormone levels over the range from clearly hyperthyroid patients to those with subclinical hypothyroidism. In patients with subclinical dysfunction the change of cell metabolism was found to be not significant, thus supporting the conclusion that microcalorimetry is suitable for studying the effect of thyroid hormones on cells, and thereby

obtaining useful information in order to reach a decision about the choice of therapy.

Beta-adrenoceptor antagonists are used in the treatment of hyperthyroidism to alleviate symptoms but are not considered to influence thyroid hormone production nor the effect of the hormone on cell function. A study of the effect of beta-blockers on lymphocyte metabolism was done with the purpose to clarify their mechanism of action in hyperthyroidism [68]. When hyperthyroid subjects were treated with beta-blockers, lymphocyte heat production was found to be within normal limits, thus showing that beta-blockers prevent the expected increased of cell metabolism under stimulation of thyroid hormone. These results seem to indicate that increased thermogenesis in hyperthyroidism is mediated via adrenergic receptors, rather than via nuclear thyroid hormone receptors.

In a recent study [69] myocardial tissue metabolism has been measured by calorimetry in experimental hyperthyroidism in rats. It is known that hyperthyroidism is associated with increased myocardial aerobic metabolism and accelerated heart function, but it is unknown whether there is also an increase of anaerobic metabolism. Myocardial heat production, oxygen consumption and ATP content have been measured in a group of rats treated for 2 weeks with triiodothyronine. The results were compared with the corresponding values obtained from control rats who were administered saline. Tissue slices, about 5 mg, from the apical region of the heart were prepared immediately for measurement of heat production and oxygen consumption, whereas separate specimen were frozen in liquid nitrogen for ATP analysis.

The results (see Table 10) showed significantly increased heat production and oxygen consumption and decreased ATP content.

Table 10
Heat production rate (P), oxygen consumption rate (PO_2) and ATP content in heart muscle from rats treated with T_3 or saline for 2 weeks. Data are expressed as mean ± S.E. Source: reference 69.

	P, mW g^{-1}	PO_2, nmol $s^{-1}g^{-1}$	ATP, μmol g^{-1}
Hyperthyroid rats	153 ± 0.09	2.75 ± 0.16	2.82 ± 0.53
Controls	0.94 ± 0.05	1.55 ± 0.14	7.91 ± 0.44

There was a significant correlation between heat production and oxygen consumption. Aerobic metabolism accounted for about 80% of the myocardial heat production in the controls and for about 87% in the hyperthyroid rats,

thus indicating that the anaerobic metabolism was not influenced by the excess of thyroid hormone. Apparently the response is not the same in different tissues, in fact in previous studies it was found that in human lymphocytes from hyperthyroid subjects, hypermetabolism was accounted for by the anaerobic activity. The decreased ATP content in the hyperthyroid group of rats is apparently due to increased ATP expenditure and insufficient ATP generation, as indicated by the inverse relationship between heat production and ATP content of myocardial tissue.

A decrease of thyroid hormone production has been found to be accompanied by a decrease of heat production in several types of cells and tissues examined: platelets [70], adipocytes [70] and skeletal muscle [71]. The change of energy expenditure in platelets, non-nucleated cells, was found to be relatively small, although significant, and has not been recorded with less sensitive microcalorimetric technique [58]. These results supports previous findings in erythrocytes that thyroid hormones influence cell metabolism also in cells not carrying nucleus, thus indicating other mechanisms of action than only through nuclear receptors.

Administration of thyroid hormone to hypothyroid, thyroidectomized rats was found to increase heat production in liver, heart, kidney tissue as well as in skeletal muscle [66].

4.2 Acromegaly

Increased production of growth hormone in adult life causes acromegaly. The diagnosis of this condition is based on the clinical signs of the disease (large extremities) and increased levels of growth hormone and insulin-like growth factor I. However, it is not unusual to find a discrepancy between the clinical state and the level of growth hormone. This causes unsecurity in the judgement of the gravity of the disease and therefore doubt about the choice of treatment. Some of the clinical signs, feeling warm and increased perspiration, seem to indicate increased metabolism and in fact slightly elevated basal metabolic rate has been found. An attempt was made to clarify the effect of growth hormone on cell metabolism and to relate it to the degree of activity of the disease.

Heat production rate (P) was measured in lymphocytes in a group of patients with acromegaly [72]. The values obtained were compared with data from a group of healthy subjects. P value was significantly higher in samples from patients, 2.90 ± 0.15 pW/cell (mean $\pm$ SEM), than in samples from the control group, 2.31 ± 0.12 pW/cell. Heat production rates did not correlate with growth hormone levels, whereas a significant correlation was found with the clinical activity of the disease, as expressed by a score index based on symptoms often known to be present in patients with acromegaly.

5. CARDIOVASCULAR SYSTEM

5.1 Cardiovascular drugs and cell metabolism

Beta-adrenoceptor blockers represent a very important group of drugs used in the treatment of several cardiovascular diseases and hyperthyroidism. Sometimes their use is limited by the occurrence of side effects, such as fatigue in the lower extremities, general tiredness; the pathogenesis of these symptoms is unclear.

Skeletal muscle has been found to be a suitable tissue for calorimetric studies of the metabolic and thermogenetic effects of these drugs. Basal studies were first carried out to develop a microcalorimetric method that would be simple but sensitive enough for studies in vitro on small samples of muscle in physiological and pathological conditions. In order to be able to apply the method to clinical situations it was important that the quantity of material required for the measurements should be of such a magnitude that could be obtained by needle biopsy [73]. Previous studies had indicated that isolated skeletal muscle fibre bundles maintained viability in vitro which reflected fairly well the metabolic situation in vivo [74].

Muscle samples were taken during operations from patients referred to the hospital for surgery because of inguinal hernia, varicose veins, uncomplicated gallstone disease and uterine myoma. Apart from the current surgical disease, all patients were healthy and in good condition. Different microcalorimetric techniques were compared, and significantly higher values were found with perfusion calorimeters (see Table 11).

Table 11
Duplicate measurements of heat production rate (P) on human obliquus internus muscle using two different calorimeters: static and perfusion instrument. Source: reference 75.

Calorimeter	P, mW g^{-1}	
	Mean	SD
Static	0.19	0.05
Perfusion	0.50	0.14

A simple perfusion method was found to be the most suitable, reaching usually steady state heat production values within 1 h of the start of the calorimetric experiment [75]. No difference was found between intact whole length muscle

fibres and teased samples from rat quadriceps muscle; small variations in fibre length of human muscles did not affect the results. An inverse correlation was observed between P values and the age of the subjects. For some muscles significantly lower values were found for human males compared to females. Significant differences were found for samples from different human muscles (see Table 12), presumably due to the variability of fibre composition, taking into account that different types of fibres, type I and type II according to the histochemical characterization, have different metabolism, more aerobic in the former and more anaerobic in the latter fibres.

Table 12
Heat production rate (P) of different muscles from healthy human subjects, obtained with a perfusion calorimeter without stirring. Source: reference 75.

Muscle	P, mW g^{-1} Mean	SD
Obliquus internus	0.44	0.13
Vastus lateralis	0.55	0.11
Vastus medialis	0.66	0.20
Rectus abdominis	0.73	0.23

Heat production rate in human resting muscle was measured in a perfusion microcalorimeter during 2 h, then ouabain octahydrate was introduced into the calorimetric ampoule at an optimal concentration to obtain maximal inhibition of the Na^+-K^+ pump. The decrease of heat production reflected the amount of energy consumed by the pump. From the same muscle specimen, samples were taken for determination of potassium and magnesium concentration. The energy expenditure of the pump was found to correlate positively with muscle potassium and magnesium [76].

The influence of beta-adrenoceptor blockade was studied in a group of healthy subjects after performance of light physical work [77]. Three beta-blockers with different pharmacodynamic profile were used: a non-selective drug (propranolol), a beta-1-selective (atenolol) and a non-selective with partial beta-2-agonist activity (pindolol). The three drugs were given as specially prepared identical capsules which were counted for assessment of compliance. Each subject received all three drugs subsequently with at least 1 week intervening between the study periods. Muscle function was tested after 7 days in each period. Muscle biopsies and blood for analysis were taken after 8 days on each drug. Muscle heat production was found to be significantly

decreased by non-selective beta-blocker but not by beta-1-selective blockade, thus indicating that beta-2- receptors seem to account for the effect of beta-blockers on muscle metabolism (see Table 13).

Table 13
Heat production rate (P) in muscle from healthy subjects treated with 3 different beta - adrenoceptor blockers. Measurements were performed with a perfusion calorimeter. Source: reference 77.

Drug	P, mW g^{-1} Median	Interquartile range
Before treatment	0.67	0.53 - 0.75
Propranolol	0.46	0.28 - 0.68
Atenolol	0.62	0.53 - 0.72
Pindolol	0.53	0.40 - 0.63

The investigation was extended to a group of hypertensive subjects undergoing surgical operations, in order to find out whether a beta-1-selective drug, metoprolol, would affect muscle thermogenesis during stress [78]. Muscle heat production rate was found to be significantly lower in the metoprolol group compared with a hypertensive group given placebo, and a normotensive group without treatment (see Table 14).

Table 14
Muscle heat production rate (P) from hypertensive subjects treated with placebo or metoprolol, compared with normotensive subjects. Measurements were performed with a perfusion calorimeter. Source: reference 78.

Subjects	P, mW g^{-1} Median	Interquartile range
Placebo	0.71	0.56 - 0.79
Metoprolol	0.41	0.30 - 0.68
Controls	0.74	0.65 - 0.89

The metabolic effect of the drug on muscle metabolism was interpreted as being due to the blockade of beta-1-receptors in adipose tissue, resulting in diminished availability of fatty acids and reduced rate of oxidation in muscles. It is known that during stress, such as caused by surgical operations, there is normally increased sympathetic nervous system activity and stimulation of lipolysis.

The thermogenetic effect of beta-adrenergic blockade was also studied after treatment for two weeks with the selective beta-blocker metoprolol in hypertensive patients during general anaesthesia: pulmonary arterial blood temperature was measured by means of a thermistor in a indwelling pulmonary arterial catheter, simultaneously with measurements of heat production rate in skeletal muscle [79]. A significant fall of temperature and muscle heat productio rate was observed in the group of subjects treated with metoprolol compared to the placebo group.

In order further to understand the metabolic effects of beta-adrenoceptor agonist/antagonist drugs, a comparative study was carried out where skeletal mucle heat production rate was measured in healthy subjects after administration of a beta-adrenoceptor agonist, terbutaline, or a beta-adrenoceptor antagonist, propranolol [80]. Moreover, due to the insufficient understanding of the mechanisms behind potassium concentration changes during treatment with beta agonists and antagonists, a calorimetric evaluation was made of the activity of the Na^+-K^+ pump; the results were related to serum drug levels and electrolyte concentrations in the intracellular and extracellular space. Unexpectedly, a decrease of muscle heat production rate was found after administration of a beta agonist, interpreted as possibly due to desensitization of beta-2-receptors. Unchanged P values for the Na^+-K^+ pump were found after treatment with the drugs.

A double blind placebo-controlled study [81] was conducted of the effects of oral propranolol and terbutaline on erythrocyte heat production rate. Propranolol 80 mg and terbutaline slow-release 7.5 mg were randomly administered twice daily for one week to 15 healthy males, using a cross-over design. After an overnight fast of 12 h, blood samples were taken 09.00, 2.5 h after drug intake and after the subjects had rested for at least 45 min. Venous blood was collected from an antecubital vein into 10 cm^3 Vacutainer tubes containing sodium heparin 143 USP. Erythrocytes were separated from other blood cells by Nakao gel adsorption technique [1] A lack of influence of both drugs on erythrocyte heat production rate was noted, implying that drugs acting through beta-adrenoceptors have clinically no relevant effect on erythrocytes. Also incubation of terbutaline with platelets in vitro shows no effect on these cells [81].

In another study [82] the thermogenetic effect of a new drug, carvedilol, with combined beta- and alfa-1-blocking activity was investigated in skeletal muscle of rats. A comparison was made with the effect of a well known non-

selective beta-adrenoceptor drug, propranolol. Whereas the latter drug caused decreased heat production, carvedilol had no influence, presumably due to its combined beta- and alfa-blocking activity (see Table 15).

As previously mentioned (see Section 4), non-selective (propranolol) and selective (metoprolol) beta-adrenoceptor antagonists could preclude an increase of lymphocyte metabolism, otherwise present in hyperthyroid patients.

Table 15
Muscle heat production rate (P) from rats treated with propranolol or carvedilol, compared with controls. Measurements were performed with a perfusion calorimeter. Source: reference 82.

Drugs	P, mW g^{-1} Mean	Confidence interval
Propranolol	0.45	0.36 - 0.55
Carvedilol	0.63	0.55 - 0.72
Controls	0.62	0.52 - 0.73

5.2 Arterial insufficiency

Diminished blood flow in the lower limbs is in most cases due to arteriosclerosis, that causes atheromatous plaques containing cholesterol and other lipids, gradually becoming calcified with development of vascular stenosis and eventually occlusion. Less common causes of changes in the arteries, that might lead to impairment of blood supply, are inflammatory diseases and spasm of the vessels. Common symptoms of arterial insufficiency, due to diminished oxygen supply, are pain and coldness in the lower extremities, often site of arteriosclerotic changes, that in untreated cases may develop to ulcers and gangrene. There is however no reliable correlation between the magnitude of symptoms and the degree of ischemia. Also radiography and ultrasound do not give sufficient information about the degree of impairment of blood flow. The presence of collateral circulation may compensate for the stenosis or obliteration in the vessels. There are no available methods to evaluate muscle metabolic changes secondary to ischemia.

A calorimetric study was carried out with the purpose to measure heat production rate in skeletal muscle of patients with different degrees of peripheral arterial insufficiency, defined by blood flow measurements [84]. A linear positive relationship was found between heat production, reflecting overall muscle metabolism, and degree of diminished blood flow. Calorimetric

values were significantly lower in the group of patients with severe arterial insufficiency, compared to healthy subjects.

5.3 Prosthetic heart valves

Thrombo-embolism is a well known complication in patients with prosthetic heart valves. The pathogenesis of thrombo-embolic incidents is unclear but it seems that platelets play a significant role, due to the interaction between these cells and the artificial surfaces of the prosthetic valve. In an attempt to detect possible metabolic abnormalities, heat production rate was measured in platelets from patients with prosthetic cardiac valves [84]. Significantly decreased calorimetric values were observed, indicating that the metabolic activity of platelets in these patients is abnormally low (see Table 16).

Table 16
Heat production rate (P) of platelets from patients with valvular heart diseases, operated and not operated with prosthetic heart valves, compared to healthy subjects. Source: reference 84.

Subjects	P, fW/cell	
	Mean	SD
Operated	49	9
Not operated	65	11
Controls	61	10

These results are in agreement with the observations of other investigators who had previously found decreased platelet ADP and ATP as well as shortened platelet survival, that correlated with thrombo-embolic manifestations in patients with prosthetic heart valves. No conclusive explanation can be offered for the observation of decreased heat production rate in the platelets of patients with prosthetic heart valves. Previous investigators have advanced the hypothesis that mechanical, chemical or immunological factors may cause alterations of blood cell function by interaction of the cells with the prosthetic valves. It is interesting to note that in the calorimetric study, the two patients who had double prosthetic valves were found to have P values below the mean value of the whole patient group. Moreover, the only patient who exibited thrombo-embolic manifestations, had the lowest value of platelet heat production rate.

In a prospective study, a larger group of patients with severe aortic or mitral rheumatic heart disease were followed before and after prosthetic valve replacement. Platelet heat production rate did not correlate with either type of valvular disease, valvular calcification or atrial fibrillation. Before the operation a significantly elevated platelet heat productio rate was found compared to normal subjects [85] (see Table 17), probably due to the presence of a younger and metabolically more active platelet population. Platelet number before the operation was significantly lower than normal, most likely due to shortened platelet survival. The presence of larger platelets may be due to bone marrow activation and increased platelet production rate, stimulated by increased cell destruction. Previous studies have shown that young and hyperactive platelets are larger than older cells. After cardiac valve replacement the platelet heat production rate decreased significantly as compared to the pre-operative values (see Table 17). The greatest reductions were observed in two patients with thrombo-embolic complications, suggesting a relationship between platelet metabolism and thrombo-embolism.

Table 17
Heat production rate (P) of platelets from patients with valvular heart diseases, before (pre-op) and after (post-op) prosthetic heart valve replacement, compared with healthy subjects. Source: reference 85.

Subjects	P, fW/cell	
	Mean	SD
Pre-op	63	5
Post-op	58	5
Controls	59	4

These studies seem to indicate that microcalorimetry is a suitable method for the quantitative measurement of overall metabolism in platelets from patients with prosthetic heart valves. It might be of help for identification of patients with high risk to develop thrombo-embolic complications after replacement of heart valves.

5.4 Myocardial metabolism, cardiomyopathy, myocardial infarction

Very limited experience is available concerning microcalorimetric measurements in heart muscle within the frame of medical problems. Extensive information is however available concerning heat production and cardiac energetics [86,87].

For many years cardiac involvement in patients wih diabetes mellitus was thought to be due to coronary atherosclerosis, known to occur with higher frequency in diabetic than non-diabetic subjects. From medical reports in the last decade there is increasing evidence that diabetic cardiomyopathy, as applied to the cardiac disease of diabetes mellitus, is not necessarily a consequence of coronary disease. In fact, cases of diabetic cardiomyopathy have been increasingly reported, where coronary disease was not present.

A large amount of information has been provided in recent years by reports from animal studies. Defective oxydative metabolism and decreased pyruvate dehydrogenase activity have been found in heart mitochondria from genetically diabetic mice. A reduced myocardial metabolism has been reported in rats with streptozotocin-induced diabetes. Diabetic hamsters have been found to show reduced activity of several enzymes and ATP content in the myocardium.

The hypothesis that a negative energy balance in the myocardial tissue might be the cause of the heart dysfunction in diabetes was tested in a calorimetric study [88], where heat production rate was measured in myocardial tissue of rats with streptozotocin-induced diabetes. Lower P values were found in heart muscle of diabetic rats as compared to the corresponding values in healthy rats (see Table 18). These results give support to the hypothesis that a derangement of myocardial metabolism is present in diabetes mellitus, independent of coronary disease.

Table 18
Heat production rate (P) in myocardial tissue of diabetic rats, compared to controls. Source: reference 88.

Rats	P, $\mu W\ mg^{-1}$	
	Mean	SD
Diabetic	0.79	0.23
Controls	0.96	0.13

Congestive heart failure (CHF) due to ischemic heart disease is a very common clinical situation, particularly in the elderly group of patients. It is however unclear how the myocardial cells behave metabolically when decreased blood flow in the myocardial tissue develops as a result of stenosis, or obstruction of coronary vessels, eventually leading to myocardial infarction. Myocardial metabolism was studied by microcalorimetry and oxygen consumption measurement in tissue from rats with CHF after a myocardial infarction, induced by ligation of the left coronary artery [89].

The results show that the consequences of the vessel occlusion are not limited to the damaged tissue, but will also affect the metabolism of myocardial cells in other parts of the left ventricle. It seems that the myocardial cells have lost the ability to increase their metabolic activity, as a necessary compensatory mechanism, in CHF due to the myocardial infarction. The results are unexpected, in fact previous studies have shown increased activity of myocardial oxidative enzymes, stimulated by enhanced sympathetic nervous system activity in CHF. Heat production rate in the ischemic myocardium indicated a persistent metabolic activity with continuous demand of oxygen and fuel supply. This finding is of interest with regard to the possibility to use drugs that may improve the metabolic condition and survival of the damaged myocardium.

5.5 Hybernation and myocardial metabolism

It is well known that hypothermia can induce ventricular fibrillation and circulatory arrest in humans. Enlargement of the heart increases the susceptibility to fibrillation. The pathogenesis of hypothermia-induced fibrillation is unclear. Some investigators suggest that difficulty of coordination of the myocardial cells might lead to electrophysiological disturbances. There is evidence that hypothermia induces abnormal cation fluxes and changes in cellular energetics via the activity of membrane ATPase. Hedgehogs and other hibernators develop apparently a biochemical adaptation to cold during hibernation that makes them resistant to heart fibrillation. In a previous study however no significant difference was found in the lactate content of myocardium between hibernating and non hibernating hedgehogs; similar values were also found in guinea pigs. Thus the mechanism behind the resistance of hedgehogs to fibrillation remains obscure.

Microcalorimetry has been used in an attempt to detect metabolic differences in myocardial tissue by comparing a hibernator and two non-hibernators [90]. Twenty-four animals consisting of 12 hibernators (6 summer hedgehogs and six winter hedgehogs), and 12 non-hibernators (6 rats and 6 guinea pigs) were studied. The hedgehogs were trapped in late August and were all in the non-hibernating state during the period of study. All the animals were kept in the experimental house at room temperature between 18 and 20°C. The hearts of the animals were removed on different days under ether anesthesia and immediately stored in ice-cold Na-Krebs bicarbonate buffer containing glucose at 5 mM as substrate and saturated with carbogen (a mixture of gases, composed of 95% oxygen and 5% carbon dioxide). From each animal, slices of cardiac tissue were removed under the cold buffer and stored in the same for determination of the rates of heat production and oxygen consumption rates about 40 min later. Measurements of heat production and oxygen consumption in heart tissue were carried out at 20°C and 37°C. A quantitative evaluation of cell metabolic energy linked to the transport of sodium and potassium was also

done by determination of the changes of metabolic rate induced by specifc inhibition of the Na^+-K^+ pump. A higher rate of energy production and utilization was observed in the cardiac tissue of the hedgehog than in that of the non-hibernators, rat and guinea pig, at both temperatures (see Table 19).

Table 19
Mean values(± SEM) of heat production rate (P) and oxygen consumption rate (PO_2) in myocardial tissue from the guinea pig (GP), the rat (RT), the non-hibernating summer and winter hedgehog (SH and WH), at 20°C and 37°C. P values are expressed as mW g^{-1} tissue. PO_2 values are expressed as mW g^{-1} tissue, recalculated from the recorded values in units mol $s^{-1}g^{-1}$ tissue. Source: reference 90.

Samples	20°C		37°C	
	P	PO_2	P	PO_2
GP	0.56 ± 0.22	0.38 ± 0.17	0.80 ± 0.19	0.78 ± 0.24
RT	0.60 ± 0.13	1.13 ± 0.27	1.09 ± 0.10	1.34 ± 0.52
SH	1.04 ± 0.41	0.85 ± 0.15	1.79 ± 0.43	1.49 ± 1.06
WH	1.22 ± 0.39	1.68 ± 0.54	2.00 ± 0.74	4.57 ± 1.23

The temperature coefficients of total heat production and of the amount of heat connected with the Na^+-K^+ pump were significantly higher in the hibernator. These results indicate that microcalorimetry is a suitable tool to detect metabolic differences between hibernators and non-hibernators

6. NUTRITIONAL AND METABOLIC DISORDERS

6.1 Obesity

Obesity, excessive amount of body fat, is a very common nutritional disorder in the developed countries. Excessive fat accumulates because there is an imbalance between energy intake and expenditure. It increases mortality in all age groups and it affects the quality of life. There are conditions where the cause of excessive adiposity is well identified, as is the case in endocrinological disturbances and excessive caloric intake or physical inactivity. In many cases however the etiology of the disease is unclear.

Several studies indicate variations in the cell metabolic efficiency that might play an important role in the pathogenesis of obesity. In some of these studies it was observed that there were subjects who in spite of excessive caloric intake did not show any increase in weight; on the other hand, some subjects did not reduce their weight in spite of a strict diet.

Several hypothesis have been advanced concerning the development of increased metabolic efficiency, such as altered specific dynamic action of food, alterations of metabolism of brown fat or variations of ATP breakedown. It seems that genetic factors as well as diet in early life might play an important role for the development of obesity.

Alterations of glucose and lipid metabolism have been observed in obese subjects. In fat cells have been found changes of enzyme activities, substrate utilization, receptor functions and responsiveness to hormones.

The characterization of energy balance in cells and tissues relies upon the measurement of several variables: oxygen and substrate consumption, lactate and carbon dioxide production. These measurements however give only indirectly and partly quantitative information about the energy balance in obesity. Whole body calorimetry and direct measurement of cell heat production have been introduced as a complement to the assessment of energy balance in the whole organism and energy expenditure on the cellular level.

A method was developed for the quantitative measurement of heat production in human adipocytes [91]. Fat cells were isolated by collagenase treatment of biopsy specimens of adipose tissue; there was no evidence of significant cell breakage during the preparation procedure. Plots of heat production against time were stable for at least 4 h.

The presence of substrate (glucose) and insulin was necessary in the cell suspension, otherwise much lower values were recorded (see Table 20). As with other cells (see Section 1), a pH and temperature dependence of the heat production was observed. Adipocyte metabolic activity was found to be high, the heat production per cell was about 15 times greater than the corresponding value for leukocytes, but lower than that reported for brown rat fat cells.

Table 20
Effect of substrate (glucose) and insulin on adipocyte heat production rate (P)
Source: reference 91.

	P, $\mu W\ g^{-1}$ adipocyte
Glucose and insulin present	82
in the cell suspension	88
Glucose and insulin absent	20
	20

Further methodological development in recent years has made it possible to measure heat production during several days by maintaining adipocytes from rats [92,93] and humans [94] in gel cultures, thus allowing it to be easier to study how adipocytes respond to the influence of substrate and hormones. After excision of fat tissue, samples were minced with scissors and incubated in culture medium containing 2 mg/cm^3 collagenase in a shaking water bath for 60 min at 37°C. Isolated fat cells were filtered through a 1000 μ nylon mash and subsequently washed three times with culture medium. Cell number was determined microscopically with a hemocytometer. Gel cultures were prepared in glass ampoules. 150 mm^3 of packed adipocytes were embedded in a 3D-matrix of agar gel. Then the ampoules were filled up to 1.5 or 2.25 cm^3 with agar-free medium. The gas phase was 1.5 or 0.75 air with 5% CO_2.

Some investigators have applied microcalorimetry to thermogenetic studies in brown adipose tissue [95] and brown adipocytes [96] from rats. The major conclusion drawn from these studies was that only about 5% of the total cell heat production is associated with the function of the Na^+-K^+ pump.

In a preliminary study [97] one group of 14 obese patients and one group of 12 matched healthy controls, were studied. Open biopsies from the gluteal region were taken in the morning after 10 h fasting. Local anaesthesia with 1% Carbocain was given intradermally. The obese patients had been on a standardized weight-maintaining diet for 5 days and the controls had been on their own regular diet. Adipocytes were isolated from the biopsy material by collagenase treatment. The fat cell suspension was washed by repeated centrifugations, and 0.9 cm^3 samples, corresponding to 0.45 cm^3 packed cells, were taken for microcalorimetric measurements. The microcalorimetric measurements were performed with the cells suspended in 0.05 M Krebs-Ringer bicarbonate buffer (pH 7.4) containing 0.1 U/cm^3 insulin and 11 mmol/dm^3 glucose. Adipocyte heat production rate was found to be lower in the obese group than in the lean control group; it was however unclear whether the decrease in heat production was a cause or a consequence of obesity.

A further study [98] was carried out where heat production was measured in adipocytes from obese subjects before and after weight reduction and compared with lean individuals. In order to minimize possible differences in caloric intake and diet composition between the two occasions, when percutaneous fat tissue biopsies were taken, the patients were hospitalized for 1 week before and after weight reduction. They were given a balanced diet (6.7 MJ per day) with 20% of the calories derived from protein, 30% from fat and 50% from carbohydrates. The fasting period was spent in a health center. After 5 weeks fasting the patients were instructed to break gradually the fast, aiming at obtaining their usual food intake after about 2 weeks. After another 1-2 weeks they were again admitted to the ward and subjected to the same diet

and regimen as before the fasting period. Samples were taken from the patients after about 1 week on the standard diet and after weight reduction. Biopsies were taken in the gluteal region and adipocyte heat production rate measured as described earlier. A weight loss of about 13 kg (mean) was noted during the fasting period. The heat production rate per adipocyte was significantly lower in the obese group compared to lean subjects. After weight reduction, calorimetric values were found to increase by about 40%, but were still significantly lower than in the control group (see Table 21).

Table 21
Adipocyte heat production rate (P) in lean subjects and obese patients before and after weight reduction by fasting. Source: reference 98.

Groups	P, $\mu W\ g^{-1}$ tissue Mean	SD
Lean subjects	133.4	48.1
Obese patients, before treatment	39.7	23.9
Obese patients, after treatment	64.6	28.2

The same investigators found in a later study [99] that also after pronounced weight reduction by surgical treatment, gastroplasty, adipocyte P values were found to increase compared to values before the operation (see Table 22).

Table 22
Adipocyte heat production rate (P) in obese patients before and after weight reduction by gastroplasty. Source: reference 99.

Groups	P, $\mu W\ g^{-1}$ tissue Mean	SD
Before gastroplasty	66	9
After gastroplasty	115	7

The results of these studies give support to the hypothesis that there is an altered metabolic efficiency in obesity. However, the change of adipocyte

metabolism towards normality after weight reduction suggests that the initially reduced adipocyte heat production rate is a consequence rather than a cause of obesity. In any case, whatever is the primary cause of obesity, reduced cell heat production rate indicates lower metabolism that may contribute to the accentuation and perpetuation of the obese state.

Many metabolic abnormalities previously observed in obese subjects have been suggested to play an important role in the pathogenesis of obesity. Among them that has attracted particular attention is the finding of decreased activity of Na^+-K^+ ATPase, which is the enzyme expression of the Na^+-K^+ pump, in erythrocytes from obese subjects. The hypothesis was then presented that a defect in the Na^+-K^+ pump function may lead to decreased energy expenditure and accumulation of fat tissue. The issue has however been controversial in view of the fact that other investigators have found normal or increased Na^+-K^+ ATPase activity in erythrocytes and increased values in liver homogenate from obese subjects.

In order to obtain further information that might help to clarify the existing controversy, a calorimetric study was carried out [100]. By measurement of heat production, the changes in overall metabolism induced by specific inhibition of the Na^+-K^+ pump were quantified in erythrocytes from normal and obese subjects. A group of obese patients with stable weight and without signs of endocrine disease was investigated and compared to a group of lean subjects. Heat production rate was measured in erythrocytes suspended in plasma with and without the cardioactive glycoside ouabain, specific inhibitor of the Na^+-K^+ ATPase. Emphasis was put on the response of cellular metabolism to inhibition of the Na^+-K^+ ATPase activity and not on quantitative values of Na^+-K^+ ATPase activity per se. No difference was found between obese and lean subjects. The results were thus speaking against the hypothesis that a metabolic derangement connected with a defective Na^+-K^+ pump could be of importance in the development of obesity.

6.2 Adiposis dolorosa

Adiposis dolorosa is a clinical condition characterized by tenderness of the adipose tissue. The cause of pain is obscure. In order to estimate whether a metabolic derangement is present, microcalorimetry was used to measure overall adipocyte metabolism in a group of patients with adiposis dolorosa [101]. For many years they had been suffering of the generalized type of this disease with a constant burning pain in their subcutaneous adipose tissue in all areas of the body, gradually increasing during the course of the disease. They were about 50% overweight.

Adipose tissue specimens were obtained by open surgery from the upper lateral gluteal region, where all patients had moderate pain at palpation. Heat

production was measured as previously described [91] after isolation of adipocytes by collagenase treatment of adipose tissue.

Fat cells were larger than those of weight-matched subjects and similar in size to those of a grossly obese group. The mean heat production rate of adipose lipid weight was significantly lower than the corresponding value of both lean healthy subjects and weight-matched obese control subjects. However, the decrease was not found when heat production was calculated per cell. When compared with the group of grossly obese subjects, the patients with adiposis dolorosa had almost twice as high heat production rate per cell. These results indicate that the cell metabolic derangement in adiposis dolorosa is different than that in ordinary non-painful obesity.

6.3 Anorexia nervosa

Anorexia nervosa is a disease affecting mainly young girls, characterized by the patients' lack of appetite and preoccupation with food that makes them lose weight by minimizing their caloric intake and by excessive physical activity. Sometimes it is associated with bulimia, characterized by overeating followed by self-induced vomiting.

The pathophysiology of starvation in anorexia nervosa is obscure. Basal metabolism has been found to be reduced, probably due to the decrease in cell mass of the body. Atrofic changes in skeletal muscle and adipose tissue have been observed, otherwise no information is available about the metabolic state of different tissues.

In order to further elucidate the metabolism at the tissue level in anorexia nervosa, a calorimetric investigation was carried out. The purpose of this study was to evaluate cellular metabolism in skeletal muscle and platelets by measurement of heat production [102]. A group of patients was recruited after the diagnosis of anorexia nervosa had been establishd at the Department of Psychiatry. Some of the patients had symptoms of bulimia. They were in malnourished state, although not critically ill, due to their self-imposed state of starvation. Their average weight deficit was 35% compared with the healthy control group. Biopsies were taken from the middle portion of the vastus lateralis muscle by needle technique. Visible fat and connective tissue were removed and the fibre bundles of muscle with a diameter of about 1 mm were teased away and the samples introduced into the calorimeter. The weight of the specimens, about 50 mg, was the same in both patient and control groups. Blood samples were taken at the same time for preparation of platelet-rich plasma suspensions.

The heat production rate in skeletal muscle was found to be about 50% lower in the group of anorexia nervosa patients in comparison with the control group. The patients' platelet heat production also was significantly lowered, although to a lesser extent than muscle. There was no difference between patients with and without bulimia. The reduced cellular heat production,

indicating hypometabolism, is presumably due to decreased substrate availability caused by the low caloric intake.

6.4 Malignant hyperpyrexia

Patients with this disorder develop very rapidly a rise of body temperature when exposed to some inhalation anesthetics e.g. halothane. The pathogenesis of the disease is a release of calcium from the sarcoplasmic reticulum into the muscle intracellular space, leading to increased glycolysis, ATP consumption and uncoupling of oxidative phosphorylation with high production of heat, lactate and carbon dioxide. In spite of progress of treatment of this condition in recent years, the mortality remains high. It is therefore of paramount importance to identify the subjects with inheritance for this disorder among the relatives of every patient with the clinical diagnosis of malignant hyperpyrexia (MH).

The susceptibility to MH can be identified with in vitro testing of muscle exposed to halothane and caffeine. It is a time-consuming technique, requiring an open muscle biopsy. It would therefore be desirable to develop a simpler method. The main disturbance of MH is hypermetabolism of muscle, however platelets also contain contractile elements and there have been descriptions of abnormalities of platelet metabolism and aggregation [103,104].

In an attempt to develop a diagnostic test for MH without the need for open muscle biopsy, measurements were carried out of the changes in heat production brought about when muscle and platelets were exposed to halothane and caffeine [105]. The study was done in a group of subjects previously identified as MH-susceptible and a group of persons with a negative test. Muscle samples were obtained by needle biopsy. No difference of heat production was found between the two groups. Thus the conclusion was drawn that the microcalorimetric method, as used in the present investigation, could not distinguish between tissues from susceptible and non-susceptible subjects to MH.

6.5 Liver

The liver plays a central role in the nutritional and metabolic state of the body. In carbohydrate metabolism this organ regulates blood glucose concentration by supplying carbohydrates, either glucose derived from glycogen breakdown or synthesized in the hepatocytes. Dietary aminoacids are taken up by the liver and released into the blood for transport to other tissues; moreover, hepatocytes use aminoacids for protein synthesis. The main function of the liver in lipid metabolism is by taking up dietary fat, mostly triglycerides, and breaking it down to small particles for use in several metabolic processes; hepatocytes have also the capability to synthesize lipid molecules. From a clinical viewpoint, the metabolism of drugs and alcohol is another very important function of the liver.

In medical practice several function tests are used for evaluation of the extent of liver damage. However the liver has the capability to compensate in the healthy hepatocytes if only part of the organ is diseased. Moreover, these function tests have insufficient sensitivity and specificity and therefore give an indication of the presence and extent of a pathological condition only in pronounced derangement of liver function/metabolism. It would therefore be useful to have a test that could record metabolic changes of low degree at an early stage of liver diseases.

With this purpose in mind, a microcalorimetric method was developed for measurement of heat production rate in hepatocytes cultured on microplates [106] and in cell suspensions [106,107]. The measurements in cell suspensions were suitable only for short-term experiments, whereas hepatocytes cultured on microplates were found to be viable and with a stable metabolism for several days, thus allowing long-term experiments and repeated measurements on the same cell population. Hepatocytes were prepared by the collagenase procedure. The use of different calorimeters, rotating batch-type and static ampoule instruments, gave results that were in good agreement.

Evaluation of the aerobic respectively anaerobic component of hepatocyte metabolism was done by measurement of oxygen consumption [107] or by inhibition of the aerobic pathway with sodium azide [106], and inhibition of the anaerobic pathway with sodium fluoride [106]. Oxygen consumption was found to be constant in experimental conditions that enhanced substrate cycling [107]: different dietary regimen, age and genetic profile.

A method has been developed for measurement of heat production rate on pieces of liver tissue with the aim to avoid eventual alterations of cellular metabolic processes during the cell preparation procedure [108]. Samples, 5-8 mg, were taken from rats by aspiration needle biopsy. Oxygen consumption was measured at the same time. Sodium fluoride was used for inhibition of the anaerobic pathway. The metabolic aerobic/anaerobic profile showed a good qualitative agreement with the earlier studies on isolated hepatocytes. The results indicated that the technique used, with small liver samples, was suitable for studying overall metabolism of human hepatic tissue in different liver diseases.

The developed calorimetric technique was applied to the study of liver tissue injury caused by ischemia [109]. Organs can be damaged by decreased blood flow during surgical procedures. The liver is exposed to this danger in connection with organ transplantation, and also when ischemia is caused with the purpose of obtaining tumor regression. It is therefore important to know what is the time-limit of tolerability of the organ to ischemia, in order to avoid serious irreversible changes of liver function.

Liver biopsies were taken from rats after variable periods of ischemia by occlusion of the blood vessels, between 30 and 300 min. Heat production rate was measured applying the technique previously described [108]. A gradual

decrease was observed reaching a maximum of 25% of the initial value after 1 h, thereafter heat production level remained constant for several hours. When reperfusion of the liver was carried out, there was complete reversibility of the metabolic change when ischemia had lasted no longer than 90 min. Longer periods than 90 min caused irreversible damage.

The present study shows that microcalorimetry offers a suitable methodology for evaluation of liver metabolism during ischemia, that can be applied to different clinical studies when surgical procedures are expected to cause a decrease of blood flow in the hepatic tissue.

7. KIDNEY

7.1 Renal insufficiency

Patients with renal insufficiency are often found to be affected by multiple metabolic problems. Anaemia is often present and some of its causes are well identified, but can only partly explain the anaemia of such a severe degree as found in uremia. It is known that a certain degree of decreased erythropoiesis is present. Often occurs blood loss due to bleeding tendency. A third mechanism by which anaemia might develop is hemolysis, in fact the life-span of erythrocytes from uremic patients is shortened, but normal survival is noted when erythrocytes are injected into healthy persons. Erythrocytes from healthy subjects have a shortened survival time when injected into uremic patients. Thus, it seems that extracorpuscular factors account for the development of hemolysis.

According to some investigators, uremic toxins affect erythrocytes [110]; several groups of investigators have described abnormalities of cell metabolism in uremic erythrocytes. However, the results are very controversial. Both increased and decreased erythrocyte glycolysis have been found and an increase of reduced-glutathione concentration and G-6-PD activity have been noted in erythrocytes from uremic subjects.

In a group of uremic patients with anaemia, erythrocyte total heat production (see Table 3) and glucose consumption rates were found to be increased when compared to a group of healthy subjects [11]. When the pentose phosphate pathway activity of erythrocytes was stimulated with methylene blue, significantly higher levels of heat production rate were found in the group of uremic patients than in a group of healthy subjects (see Table 3) [11]. These results do not give support to the hypothesis previously advanced that anaemia among uremic patients is due to decreased erythrocyte aerobic metabolism.

Patients on regular haemodialysis treatment lose considerable quantities of carnitine in the dialysate. Depletion of carnitine during haemodialysis has therefore been implicated as a possible cause of disturbances of metabolism and

function in cardiac and skeletal muscle, frequently occurring in these patients. However, the issue is controversial since pre-dialysis plasma carnitine levels are re-established between treatments. Conflicting results have been presented concerning muscle carnitine concentration, showing decreased levels and reduced fat utilization in some studies. The hypothesis has been presented that acute removal of carnitine during dialysis might cause metabolic disturbances, that could be prevented by carnitine administration. Improvement of muscular strength after carnitine treatment has been noted.

A microcalorimetric study [111] was carried out with the purpose of collecting more information about muscle metabolism and function, that might help to clarify the controversy about possible beneficial effects of carnitine administration during regular haemodialysis. Total metabolism in resting muscle was monitored in vitro by measurement of heat production in a perfusion calorimeter of the thermopile heat conduction type, using the technique previously described [75]. Muscle biopsies were taken from the vastus lateralis. For each patient, the same amount of muscle was introduced into the calorimetric vessel, about 40 mg. Muscle strength, as maximum dynamic strength, was measured in the knee extensor using an isokinetic dynamometer.

Twenty-eight haemodialysis patients were randomized to L-carnitine, 2 g i.v. three times a week, and saline over a 6-week period. After carnitine administration the muscle carnitine level increased about 60% (see Table 23).

Table 23
Concentration of total carnitine in muscle of haemodialysis patients, before and after administration of carnitine. Control subjects received placebo. Median values. Source: reference 111.

Groups	mmol kg^{-1} tissue
Carnitine	14.6
Placebo	11.6
After 6 weeks	
Carnitine	23.7
Placebo	11.9

Maximum dynamic muscular strength was reduced in the patient group with a mean value of 44% compared with healthy controls. Total metabolic activity

of isolated skeletal muscle fibres, measured as heat production, showed a value that was 25% lower than normal. Carnitine administration had no effect on muscular metabolism and function. Thus, the present data do not support the hypothesis that carnitine deficiency contributes to muscle dysfunction in patients on chronic haemodialysis.

Total plasma carnitine increased level more than tenfold (see Table 24). No relationship was found between muscle and plasma carnitine level.

Table 24
Concentration of total carnitine in plasma from haemodialysis patients before and after administration of carnitine or placebo. Median values and total range (within parentheses). Source: reference 111.

Groups	μmol dm^3
Carnitine	39.2 (18.6-156)
Placebo	42.9 (28.3-80.4)
Controls	49.9 (34.0-82.0)
After 3 weeks	
Carnitine	496 (75 - 1359)
Placebo	47.7 (17.1 - 89.8)
After 6 weeks	
Carnitine	639 (320 - 1000)
Placebo	47.1 (29.5 - 98.7)

It has been previously discussed whether muscular dysfunction in uremia might be related to decreased thyroid hormone production. Earlier studies have often shown decreased thyroid hormone concentration in uremic patients. However, the clinical feature of these patients was euthyroid and no adequate studies have been carried out to establish whether tissue hypometabolism was present.

In a group of haemodialysis patients, muscle thermogenesis was evaluated by measurement of heat production in skeletal muscle samples [112]. Biopsies were taken from the vastus lateralis muscle by needle technique, using the same amount of muscle for each patient, about 45 mg. Microcalorimetric measurements were made in a perfusion calorimeter of the thermopile heat conduction type, as previously described. Blood samples for measurement of thyroid hormone concentration were collected the morning before dialysis after the patients had been fasting for 12 h. About 40% of the group of haemodialysis patient were found to have decreased muscle heat production

rate, and this was associated with decreased thyroid hormone concentration (see Table 25).

In conclusion, the present results indicate that decreased thyroid function plays a role in the development of muscle dysfunction in patients with renal insufficiency.

Table 25
Muscle heat production rate (P) and thyroid hormones concentrations in haemodialysis patients. TT4 = total thyroxine, TT3 = total triiodothyronine. Source: reference 112.

	Patients		Controls	
	Mean	SD	Mean	SD
P, mW g^{-1}	0.42	0.18	0.58	0.13
TT4 (nmol dm^3)	65	21	91	15
TT3 (nmol dm^3)	1.3	0.4	1.9	0.4

In skeletal muscle, as in other tissues, aerobic metabolism is dependent of oxygen supply. Due to anaemia there is a clear risk for insufficient oxygenation which might contribute to cause skeletal muscle dysfunction. In earlier calorimetric studies [113] of muscle metabolism a positive correlation was found between resting muscle metabolism and haemoglobin concentration. It is therefore possible that treatment with erythropoietin could influence positively muscle metabolism and function, by causing a rise of haemoglobin concentration; several studies have in fact shown improved ergometric exercise capacity and also improved isokinetic strength of quadriceps muscle.

A calorimetric study was carried out to evaluate whether treatment of anaemia with erythropoietin would increase the overall metabolism of skeletal muscle in haemodialysis patients [114]. Ten patients on dialysis treatment for a long time were selected; all of them had severe anaemia since at least 3 months. Muscle samples, about 35 mg, were taken from vastus lateralis with a needle biopsy in the morning just before dialysis was started. The perfusion microcalorimeter used was of the thermopile heat conduction type. Measurements were performed again after erythropoietin treatment for a period of 6-14 months.

The effect of therapy was a significant increase in haemoglobin level of 42% (mean), rising from the very low value of 76 to 102 g dm^3. Pre-treatment skeletal muscle heat production rate was lower than normal, 0.36 mW g^{-1}

muscle, rising after treatment to 0.47 mW g^{-1}, 42% (median) (see Table 26). The value after treatment was not significantly different from that of normal controls.

Table 26
Muscle heat production rate (P) and haemoglobin level (Hb) in haemodialysis patients before and after treatment with erythropoietin. Source: reference 114.

	P, mW g^{-1}		Hb g dm^3	
	Mean	Interquartile range	Mean	SD
Before treatment	0.36	0.29 - 0.52	76	13
After treatment	0.47	0.41 - 0.88	102	16

The conclusion of this study is that erythropoietin administration leads to increased skeletal muscle metabolism, and that the anaemia per se accounts partly for the deranged muscle dysfunction, which seems to have a multifactorial background.

7.2 Biocompatibility

It is known that the introduction of foreign substances into the body results in an inflammatory process with mobilization of granulocytes to the site of inflammation. In the last decades, several medical devises have been developed for introduction into the body, with the purpose of substituting organs or parts of organs (e.g. heart valves) damaged by diseases, or as complement because of decreased function of some organ (e.g. artificial kidney). These foreign materials can induce adverse reactions of various degrees depending on their body compatibility.

Membranes used in artificial kidneys are of particular interest for studying such reactions, owing to the relatively large surface area exposed to the blood in combination with the regularity and duration of exposition. It has been found that when blood is exposed to foreign substances, adsorption of plasma components occurs, mainly proteins. The adsorbed protein layer on the foreign surface can then interact with other plasma proteins and activate the complement, coagulation, fibrinolytic and kinin system. Leukocytes and platelets also can participate in the interaction between blood and foreign substances, leading eventually to blood coagulation on the foreign surfaces.By using microcalorimetry, the interaction between granulocytes and biomaterials was studied [115]. Three polymers commonly used as membranes in artificial kidneys were tested. One of them, cuprophan (Cu), is a natural

polymer originating from cotton. Two others were membranes manufactured from synthetic polymers: polyetherpolycarbonate (PC) and polyacrylnitrile (AN).

Stainless steel (SS) has generally been accepted as a suitable material for calorimetric vessels when performing studies on biological samples. The choice of SS was justified by qualities like high heat conductivity, tensile strength and apparent biocompatibility. Using SS vessels and standardized procedures, the metabolism of erythrocytes, platelets and lymphocytes has earlier been evaluated with good precision and reproducibility. However, a similar application has been unsuccessful with respect to granulocytes, due to unreproducibility of heat production values, apparently due to reactions between granulocytes and steel surface of the vessels. In fact, internal surface imperfections have been shown to be present in SS material [116]. By lining the SS vessels with fluorinated ethylene-propylene polymer (FEP), the interaction between granulocytes and SS vessels can be avoided [117].

Venous blood was collected from each of ten healthy donors. Granulocytes were resuspended in autologous plasma. The inside of each vessel was lined with one of three different polymers to be tested: Cu, PC and AN. FEP lined vessels were used as controls. The basal rate of heat production was recorded, and the values obtained were used to characterize the metabolic state of the granulocytes in contact with the artificial surfaces. Thereafter, the residual activity of the granulocytes was evaluated by calorimetric measurement after stimulation of granulocytes with zymosan, a substance capable of stimulating phagocytosis. The results show an initial activation of granulocyte basal metabolism due to the interaction with each of the three polymers lining the calorimetric vessels. The phagocytic response was quantified according to the increase of heat production after addition of zymosan.

Granulocyte degree of activation was found to be inversely correlated to the degree of previous stimulation in the resting state (see Table 27).

Table 27
Granulocyte heat production rate in the presence of different polymers. Values are expressed as pW/cell, mean ± SD. The percentage increase after zymosan stimulation is given in parentheses. Source: reference 115.

FEP	AN	PC	Cu
1.47 ± 0.31 (1237 ± 471)	3.15 ± 0.63 (586 ± 155)	5.48 ± 2.05 (304 ± 82)	8.87 ± 6.09 (130 - 188)

The polymers with the lowest degree of blood compatibility caused the highest stimulation of granulocyte basal metabolism thus achieving the highest degree of energy depletion in the cells. Taking into account that granulocyte phagocytosis plays an important role in the defense mechanism against infections, it is obvious that reduced phagocytic capability has practical implications, and therefore it is of clinical importance to have available a calorimetric method that can quantify phagocytosis.

The calorimetric results, obtained in experiments in vitro with activation of granulocytes, do not take into account eventual interactions between blood cells when the same process occurs in vivo. Therefore, a calorimetric study [53] was carried out in order to clarify the physiology of granulocyte activation in their normal environment. Heat production was measured in granulocytes activated with phorbol-12-myristate-13-acetate, in the absence and presence of erythrocytes. Following granulocyte activation, methaemoglobin formation occurs as a result of the oxidative influence of granulocytes on erythrocytes. In the presence of CO, methaemoglobin formation is prevented.

Thus, it appears that the interaction between granulocytes and erythrocytes during granulocyte activation occurs at haeme group of the erythrocytes, leading to metabolic stimulation of the erythrocytes with heat production.

7.3 Uremic plasma

Plasma is the physiological milieu for blood cells. It is therefore to be expected that changes of plasma composition might affect the metabolism and function of circulating cells. Previously it has been found that several substances are present in uremic plasma, which have not been found in plasma from healthy subjects. It has also been shown that some of these substances disturb the functions of phagocytic cells.

In a group of uremic patients, plasma heat production (see Table 28) and oxygen consumption rates were found to be significantly increased compared to controls [118].

Table 28
Heat production rate (P) of uremic plasma, compared to plasma from healthy subjects. Source: reference118.

	P, $\mu W\ cm^3$	
	Mean	SD
Uremic	2.31	0.92
Controls	1.31	0.31

A significant correlation was found between rates of heat production and rates of oxygen consumption. In uremia there is apparently an activation of oxidative heat-producing processes, which nature is unknown. Heat production was significantly correlated to the plasma concentration of creatinine, whereas no such correlation was found with urea.

In further metabolic studies [119], heat production and oxygen consumption rates were measured in plasma from uremic patients on chronic haemodialysis treatment. Both were found to be significantly increased compared to healthy subjects, and also when compared to patients on continuous ambulatory peritoneal dialysis (see Table 29).

Table 29
Heat production rate (P) of uremic plasma from patients before (Pre-HD) and after haemodialysis (Post-HD), and from patients on continuous peritoneal dialysis (CAPD) treatment. Source: reference 119.

	P, $\mu W\ cm^3$	
	Mean	SD
Pre-HD	5.7	2.7
Post-HD	9.0	3.7
CAPD	2.8	1.5

After haemodialysis, heat production showed a further increase (Table 29), presumably due to heparinization. Heparin is used as an anticoagulant to inhibit blood clotting during extracorporeal circulation of blood in the artificial kidney. Heparin is known to release enzymes, such as lipases and diamino oxidases, into the circulation. Thereby exothermic chemical reactions are expected to be induced in the plasma. On the other hand, oxygen consumption decreased significantly after haemodialysis, probably due to removal of oxygen-consuming substances.

REFERENCES

[1] M. Nakao, T. Nakayama and T. Kankura, Nature New Biology, 264 (1973) 94.
[2] M. Monti and I. Wadsö, Scand. J. Clin. Lab. Invest., 36 (1976) 573.
[3] M. Monti and I. Wadsö, Scand. J. Clin. Lab. Invest., 36 (1976) 565.
[4] M. Monti and I. Wadsö, Scand. J. Haematol., 19 (1977) 111.

[5] J. Ikomi-Kumm, M. Monti and I. Wadsö, Scand. J. Clin. Lab. Invest., 44 (1984) 745.
[6] U. Bandmann, M. Monti and I. Wadsö, Scand. J. Clin. Lab. Invest., 35 (1975) 121.
[7] A. E. Boyo and J. Ikomi-Kumm, Lancet, 1 (1972) 1215.
[8] M. Monti and I. Wadsö, Scand. J. Clin. Lab. Invest., 32 (1973) 47.
[9] K. Levin, Scand. J. Clin. Lab. Invest., 32 (1973) 55.
[10] L. C. Cerny, F. B. Cook and D. M. Stasiw, Biorheology, 2 (1974) 235.
[11] M. Monti, Scand. J. Haematol., 18 (1977)154.
[12] M. Monti, Scand. J. Haematol., 19 (1977) 313.
[13] M. Monti and I. Wadsö, Scand. J. Clin. Lab. Invest., 36 (1976) 431.
[14] A. Chinet, T. Clausen and T. Girardier, J. Physiol., 265 (1977) 43.
[15] M. Monti and J. Ikomi-Kumm, Metabolism, 34 (1985) 183.
[16] M. Monti and L. Nässberger, International Symposium on Metabolism of Minerals and Trace Elements in Human Discases. New Delhi, Sept. 1987.
[17] L. Nässberger and M. Monti, Human Toxicol., 6 (1987) 223.
[18] B. Fagher, H. Liedholm and M. Monti, Eur. J. Pharmacol., 45 (1993) 571.
[19] L. Edvinsson, J. Ikomi-Kumm and M. Monti, Human Toxicol., 8 (1989) 131.
[20] V. Ammaturo and M. Monti, Acta Med. Scand., 220 (1986) 181.
[21] M. Monti, L. Edvinsson, E. Ranklev and R. Fletcher, Acta Med. Scand., 220 (1986) 185.
[22] L. Edvinsson, J. Ikomi-Kumm and M. Monti, Br. J. Clin. Pharmacol., 22 (1986) 685.
[23] P. D. Ross, A. P. Fletcher and G. A. Jamieson, Biochim. Biophys. Acta, 313 (1973) 106.
[24] P. Bäckman and I. Wadsö, J. Biochem. Biophys. Methods, 23 (1991) 283.
[25] P. Bäckman, Heat production in cellular systems. A thermochemical and methodological study. Thesis, Lund, Sweden, 1991.
[26] P. Bäckman, Thermochim. Acta, 172 (1990) 123.
[27] M. Monti, L. Brandt, J. Ikomi-Kumm, H. Olsson and I. Wadsö, Scand. J. Haematol., 27 (1981) 305.
[28] M. Monti, L. Brandt, J. Ikomi-Kumm and H. Olsson, Eur. J. Haematol., 45 (1990) 250.
[29] M. Monti, L. Brandt, J. Ikomi-Kumm, and H. Olsson, Scand. J. Haematol., 36 (1986) 353.
[30] P. Lönnbro and I. Wadsö, J. Biochem. Biophys. Methods, 22 (1991) 331.
[31] P. Lönnbro and A. Schön, Thermochim. Acta, 172 (1990) 75.
[32] A. Schön, Microcalorimetric studies of the energetics of mammalian

cells. Thesis, Lund, Sweden, 1987.
[33] L. Brandt, J. Ikomi-Kumm, M. Monti and I. Wadsö, Scand. J. Haematol., 22 (1979) 141.
[34] M. Kleiber, The Fire of Life, John Wiley & Sons, Inc., New York, 1961.
[35] R. Fäldt, J. Ankerst and M. Monti, Br. J. Haematol., 58 (1984) 671.
[36] J. Ankerst, R. Fäldt and M. Monti, Leukemia Res., 8 (1984) 997.
[37] R. Fäldt and J. Ankerst, Leukemia Res., 10 (1986) 1147.
[38] P. Lönnbro, Some applications in biocalorimetry. Thesis, Lund, Sweden, 1987.
[39] T. Krakauer and H. Krakauer, Cell. Immunol., 26 (1976) 242.
[40] A. Gorski and K. Levin, Science Tools, 24 (1977) 27.
[41] D. Ross and J. A. Loos, Exp. Cell Res., 77 (1973) 127.
[42] D. Gebrelassie, L. Ljunggren and M. Monti, Thermochim. Acta, 251 (1994) 177.
[43] S. A. Thorén, Microcalorimetry and image analysing developed for short-term tests in toxicology using alveolar macrophages as target cells. Thesis, Lund, Sweden, 1991.
[44] D. Gebrelassie, A microcalorimetric study of resting and activated cellular systems. Thesis, Lund, Sweden, 1996.
[45] B. S. Trauss and C. A. Stetson, J. Exp. Med., 112 (1960) 653.
[46] K. Levin, Scand. J. Clin. Lab. Invest., 36 (1976) 431.
[47] K. Levin, Scand. J. Clin. Lab. Invest., 32 (1973) 67.
[48] M. Monti, R. Fäldt, J. Ankerst and I. Wadsö, J. Immunol. Methods, 37 (1980) 29.
[49] R. Fäldt, J. Ankerst, M. Monti and I. Wadsö, Immunology, 46 (1982) 189.
[50] H. Hayatsu, T. Miyamae and M. Yamamura, J. Immunol. Methods, 109 (1988) 157.
[51] C. Eftimiadi and G. Rialdi, Cell. Biophys., 4 (1982) 231.
[52] L. Ljunggren, M. Monti and G. Rialdi, Thermochim. Acta, 207 (1982) 23.
[53] L. Ljunggren, M. Monti, C. Eftimiadi and G. Rialdi, Thermochim. Acta, 217 (1993) 49.
[54] K. Levin and B. Thomasson, Acta Med.Scand., 195 (1974) 191.
[55] D.R. Stanworth, P. Johns and B. Jasani, Science Tools, 19 (1972) 6.
[56] G. Rialdi and S. Raffanti, Immunol. Letters, 7 (1984) 335.
[57] J. Ankerst, R. Fäldt and H. D. Sjögren, J. Immunol. Methods, 77 (1985) 267.
[58] K. Levin, Clin. Chim. Acta, 32 (1971) 87.
[59] S. Valdemarsson, J. Ikomi-Kumm and M. Monti, Acta Endocrinol., 123 (1990) 155.
[60] M. Monti and I. Wadsö, Acta Med. Scand., 200 (1976) 301.

[61] M. Monti, P. Hedner, J. Ikomi-Kumm and S. Valdemarsson, Acta Endocrinol., 115 (1987) 87.
[62] S. Valdemarsson, J. Ikomi-Kumm and M. Monti, Acta Endocrinol., 126 (1992) 291.
[63] S. Valdemarsson and M. Monti, Eur. J. Endocrinol., 130 (1994) 276.
[64] M. Monti, P. Hedner, J. Ikomi-Kumm and S. Valdemarsson, Metabolism, 36 (1987) 155.
[65] R. Biron, A. Burger, A. Chinet, T. Clausen and R. Dubois-Ferrier, J. Physiol., (London) 297 (1979) 47.
[66] K. Bachmann, A. Arieli, A. G. Burger and A. E. Chinet, Endocrinol., 117 (1985) 1084.
[67] D. G. Clark, M. Brinkman, O. H. Filsell, S. J. Lewis and M. N. Berry, Biochem. J., 202 (1982) 661.
[68] S. Valdemarsson and M. Monti, Thermochim. Acta, 251 (1995) 191.
[69] S. Valdemarsson and M. Monti, Thermochim. Acta, 279 (1996) 83.
[70] S. Valdemarsson, B. Fagher, P. Hedner, M. Monti and P. Nilsson-Ehle, Acta Endocrinol., 108 (1985) 361.
[71] B. Fagher, M. Monti, P. Nilsson-Ehle and H. Thysell, Scand. J. Clin. Lab. Invest., 47 (1987) 91.
[72] S. Valdemarsson, J. Ikomi-Kumm and M. Monti, Acta Endocrinol., 122 (1990) 422.
[73] J. Bergström, J. Clin. Lab. Invest., 35 (1975) 609.
[74] A-C. Bylund, J. Holm, K. Lundholm and T. Schersten, Enzyme, 21 (1976) 39.
[75] B. Fagher, M. Monti and I. Wadsö, Clin. Sci., 70 (1986) 63.
[76] B. Fagher, A. Sjögren and M. Monti, Acta Physiol. Scand., 131 (1987) 355.
[77] B. Fagher, H. Liedholm and M. Monti, Clin. Sci., 70 (1986) 435.
[78] B. Fagher, M. Monti and T. Thulin, Acta Med. Scand., 223 (1988) 139.
[79] B. Fagher, J. Magnusson, M. Monti and O. Werner, Acta Anesthesiol., Scand., 32 (1988) 117.
[80] B. Fagher, H. Liedholm, A. Sjögren and M. Monti, Br. J. Clin. Pharmacol., 35 (1993) 629.
[81] B. Fagher, H. Liedholm and M. Monti, Eur. J. Clin. Pharmacol., 45 (1993) 571.
[82] B. Fagher and M. Monti, Thermochim. Acta, 251 (1995) 183.
[83] B. Fagher and M. Monti in I. Okyayuz-Baklouti and O. Hudlicka (Eds.), Muscle Ischemia and Functional and Metabolic Aspects, Wolf und Sohn, Munchen, 1987, p. 145.
[84] M. Monti and B. Fagher, Clin. Chim. Acta, 102 (1980) 83.
[85] B. Fagher and M. Monti, Eur. Heart J., 5 (1984) 55.
[86] C. L. Gibbs, Physiol. Rev., 58 (1978) 174.
[87] D. S. Loiselle, Pflugers Arch., 405 (1985) 155.

[88] M. Monti and J. Ikomi-Kumm, Eur. Heart J., 10 (Suppl.) (1989) 326.
[89] S. Valdemarsson, A. Bergdahl, X. Y. Sun, T. Hedner. M. Monti and L. Edvinsson, Thermochim. Acta, 286 (1996) 131.
[90] J. Ikomi-Kumm, M. Monti, A. Hanson and B. W. Johansson, Cryobiology, 31 (1994) 133.
[91] M. Monti, P. Nilsson-Ehle, R. Sörbris and I. Wadsö, Scand. J. Clin. Lab. Invest., 40 (1980) 581.
[92] H. Böttcher, J. Nittinger, S. Engel and P. Furst, J. Biochem. Biophys. Methods, 23 (1991) 181.
[93] H. Böttcher, S. Engel and P. Furst, Thermochim. Acta, 187 (1991) 27.
[94] H. Böttcher, S. Engel and P. Furst, Clin. Nutr., 11 (1992) 53.
[95] A. Chinet, T. Clausen and L. Girardier, J. Physiol., 265 (1977) 43.
[96] G. Clark, M. Brinkman and S. N. Neville, Biochem. J., 81 (1991) 793.
[97] R. Sörbris, P. Nilsson-Ehle, M. Monti and I. Wadsö, FEBS Lett., 101 (1979) 411.
[98] R. Sörbris, M. Monti, P. Nilsson-Ehle and I. Wadsö, Metabolism, 31 (1982) 973.
[99] S-Å. Olsson, M. Monti, R. Sörbris and P. Nilsson-Ehle, Int. J. Obesity, 10 (1986) 99.
[100] M. Monti and J. Ikomi-Kumm, Metabolism, 34 (1985) 183.
[101] B. Fagher, M. Monti, P. Nilsson-Ehle and B. Åkesson, Clin. Sci., 1 (1991) 793.
[102] B. Fagher, M. Monti and S. Theander, Am. J. Clin. Nutr., 49 (1989) 476.
[103] C. C. Salomons, S. Tan and J. A. Aldrete, in J. A. Aldrete and B. A. Britt (eds.), Second International Symposium in Malignant Hyperthermia, Grune and Stratton, New York, 1978, p. 221.
[104] E. K. Zsimond, J. Penner and S. P. Kothary in J. A. Aldrete and B. A. Britt (eds.), Second International Symposium in Malignant Hyperthermia, Grune and Stratton, New York, 1978, p. 213.
[105] E. Ranklev, M. Monti and R. Fletcher, Br. J. Anaesth., 57 (1985) 991.
[106] L. Nässberger, E. Jensen, M. Monti and C-H. Floren, Biochim. Biophys. Acta, 882 (1986) 353.
[107] I. G. Garrett, D. G. Clark, O. H. Filsell, J. W. Harvey and M. G. Clark, Biochem. J., 180 (1979) 631.
[108] H. Asakawa, L. Nässberger and M. Monti, Res. Exp. Med., 190 (1990) 25.
[109] H. Asakawa and L. Nässberger, Res. Exp. Med., 190 (1990)33.
[110] S. Giovannetti, L. Cioni, P. L. Balestri and M. Biagini, Clin. Sci., 34 (1968) 141.
[111] B. Fagher, G. Cederblad, M. Eriksson, M. Monti, U. Moritz, P. Nilsson- Ehle and H. Thysell, Scand. J. Clin. Lab. Invest., 45 (1985) 169.

[112] B. Fagher, M. Monti, P. Nilsson-Ehle and H. Thysell, Scand. J. Clin. Lab. Invest., 47 (1987) 91.
[113] B. Fagher, Thesis, Lund, Sweden,1988.
[114] B. Fagher, H. Thysell and M. Monti, Nephron, 67 (1994) 167.
[115] J. Ikomi-Kumm, L. Ljunggren, U. Lund, M. Monti and H. Thysell, Blood Purif., 9 (1991) 177.
[116] L. Carlsson, Kemisk Tidskrift, 4 (1990) 26.
[117] J. Ikomi-Kumm, L. Ljunggren and M. Monti, J. Material Science: Materials in Medicine, 3 (1992) 151.
[118] L. Ljunggren, M. Monti, H. Thysell and A. Grubb, Scand. J. Clin. Lab. Invest., 52 (1992) 813.
[119] L. Ljunggren, M. Monti, H. Thysell and A. Grubb, Thermochim. Acta, 251 (1995) 173.

Handbook of Thermal Analysis and Calorimetry. Vol. 4: From Macromolecules to Man.
R.B. Kemp, editor.

Chapter 13

CALORIMETRIC METHODS FOR ANALYSIS OF PLANT METABOLISM

R. S. Criddle[a] and L. D. Hansen[b]

[a]Section of Molecular and Cellular Biology, University of California, Davis, CA 95616, USA. [b]Department of Chemistry and Biochemistry, Brigham Young University, Provo, UT 84602, USA

1. BACKGROUND AND GENERAL METHODS

1.1. Introduction.

Calorimetry plays a unique role in measurement of plant metabolic properties. Calorimetry provides more than just another means for measuring metabolic rate because it measures a fundamentally different property (energy) while other methods measure mass. Combination of calorimetry with mass-based methods of measuring metabolic rate allows determination of the rate and efficiency of energy storage within the plant, growth rate properties, and the effects of environmental conditions on growth.

Most calorimetric studies of plant tissues, until recently, have been either combustion analyses measuring tissue energy contents, differential thermal analysis, or temperature scanning analyses of lignin and cellulose [1-5], of phase transitions in plant lipids [6, 7], or of the freezing of water in plant tissues [8]. Methods employed in combustion analyses [9] and studies of plant products [10] have been reviewed elsewhere. This discussion focuses on methods for measurement and interpretation of rates of heat production from plant metabolic processes. while it has long been recognized that plants produce heat during metabolism and that measurements of metabolic heat of plants could guide understanding of plant physiology, only recently has metabolic heat in plants become a rapidly expanding area of study.

As early as 1908 Pierce used differential calorimetry of plants to establish that energy was released by plants during respiration [11]. Recognizing that "heat is liberated in great quantity whenever germination or fermentation takes place under such conditions that only a small portion of the heat liberated is lost by radiation", he used two silvered Dewar flasks to follow temperature increase

during germination. One Dewar was filled with live, and the other with dead, pea seeds. Cotton plugs in the tops of the Dewars allowed diffusion of respiration gases. Mercury thermometers were used to monitor the difference in temperature rise between the two flasks as a function of time. A time dependent temperature rise of about 20 °C was observed for the live seed sample, maximizing at 9 days.

Prior to Pierce's studies, measurements of temperature increase during germination were marginal, "for example, one obtains, with good luck, a difference of 0.5 °C, between live and dead peas in the course of twenty-four hours, or perhaps a whole degree, or, best of all, 1.5 °C!" Pierce concluded that the small temperature increases reported previously resulted from "trouble with insulation of the vessels in which the respiring and dead plants or parts are contained; for if radiation and absorption were reduced to a minimum, the live and respiring peas would certainly grow warmer." These experiments allowed Pierce to conclude that the increases in "temperatures are given as the evidence that energy (heat) is liberated in respiration."

A new aspect of plant calorimetry was developed in 1939 when a photocalorimeter was used to measure the quantum efficiency of photosynthesis in algae [12]. Further improvements in photocalorimetry have occurred only recently and application to plants has been limited [13, 14].

Plant metabolic calorimetry received its next major boost from the work of Henri Prat in the 1940s [15, 16]. Prat defined many characteristics of plant metabolism that could be studied by calorimetric techniques. Specifically, he pointed out that "in plants as in microorganisms, the thermic flux is mostly a function of cell multiplication." This was a key consideration suggesting use of calorimetric measurements to monitor growth-related processes. "Specific features of thermograms can be used to help define stress responses and, under appropriate conditions, calorimetry can be used to monitor plant growth rates and thus rapidly examine the effects of factors that modify growth rate." Prat's early experiments demonstrated the feasibility of plant calorimetry in answering many questions in plant physiology. His successes prompted him to write in 1969 that "we have been able to give only a short account of the innumerable applications of microcalorimetry in the physiological study of higher organisms" [16].

In spite of this early promise, calorimetry was largely ignored as a tool for studying plant physiology. Achieving the potential outlined so long ago by Pierce and Prat was delayed until improved instrumentation and development of paradigms relating measured heat rate to plant properties became available. Use of plant calorimetry to measure physiological properties was reborn in 1988 [17] in a series of studies directed primarily by Hansen and Criddle [18], and finally

begins to realize its potential to guide thinking and studies on the energetics of plant growth.

1.2. Quantities measured during plant calorimetry

The major challenge in plant calorimetry is to use the heat production rate to infer meaningful conclusions about plant growth and biochemical responses to changes in the environment. Metabolic heat rate in the dark, i.e. respiration, is the usual quantity measured during plant calorimetry. Heat rates, as opposed to integrated total heat, are proportional to reaction rates, which in turn are related to growth rates and rates of biochemical reactions in the tissues. These heat rate-metabolic rate-growth rate relations allow calorimetric measurements to aid in defining energetic and physiological processes that limit growth rate. Understanding growth and stress responses of plants further requires the ability to measure heat rates by a series of isothermal measurements [17] or by temperature scanning calorimetry [19] over the range of temperatures encountered by plants during growth. Measurements of heat rates over a range of temperatures on tissues exposed to a variety of environmental conditions can be used to monitor plant responses to multivariate changes in temperature and such factors as water supply or availability of nutrients.

To obtain sufficient information to estimate energy use efficiency for calculation of plant growth properties, it is necessary to combine heat rate (Φ) measurements with additional measures of respiration rate, commonly the rate of CO_2 production (R_{CO2}) or O_2 consumption (R_{O2}) [20]. Measurement of both R_{CO2} and R_{O2} would be better. Combination of calorimetry with measurement of CO_2 and/or O_2 flux is commonly referred to as calorespirometry. CO_2 production rates of plant tissues can be measured in parallel with heat rates using matched plant samples and standard CO_2 analyzers or manometric techniques, but it is better to measure R_{CO2} directly in the calorimeter ampule on the same tissue sample used for heat rate determination. Existing methods employ a CO_2 trapping process [21]. Similarly, O_2 determinations can be made in parallel on separate tissue aliquots or simultaneously on a single sample. O_2 fluxes have been determined in solution by oxygen electrode measurements or in the gas phase by gas chromatography and by pressure changes in the presence of a CO_2 trap [22].

Calorespirometry measurements of animal tissues, cell cultures, and microbial populations have typically been made in perfusion calorimeters or flow calorimeters [23-25]. Flow methods allow continuous monitoring of input and output materials as well as heat and gas fluxes. However, flow systems often do not work well with most plant samples. Plant cell cultures commonly clump badly, interfering with the mechanics of the perfusion process. Marine plants,

such as algae, are well suited to study using liquid flow calorimeters, but plant tissues in general do not respond well to being immersed in liquids. A further major disadvantage of flow calorimeters for many applications is limited throughput (possibly one sample per day), restricting the number of variables and reaction conditions that can be studied. Consequently, short-term batch studies are more commonly employed with plant tissues enclosed in a calorimeter ampule with adequate nutrient and O_2 supply. Monitoring O_2 and CO_2 in the gaseous head space of a sealed calorimeter ampule may be accomplished by chromatographic, mass spectrometric, thermal, or pressure analysis. To date, electrochemical and spectral methods for gas phase analysis in calorimeter ampules have not proven effective but may in the future.

The final required measurement for most plant calorimetry is tissue mass. Commonly both sample fresh weight (g FW) and dry weight (g DW) are determined. Dry weights are obtained after drying in a vacuum or convection oven at 75 to 85 °C for at least 24 hr.

R_{CO2}, R_{O2}, Φ, and tissue mass measurements are the readily obtained data. Producing meaningful conclusions regarding plant growth rates and physiology from the limited and nonspecific data requires well designed experiments, carefully designed controls, and an appropriate paradigm for relating the measures of mass and energy fluxes to plant properties.

1.3. Tissues used for calorimetry studies

Many types of tissues and plant species have been studied by calorimetry. Some will be described later as specific examples of calorimetric studies. Selection of tissue for study depends on the questions being asked. For example, meristematic tissue or rapidly expanding, whole young shoots are often used to study growth rates. Studies of the effects of salinity on plant growth may employ root tips to examine effects on the cells interacting directly with the salt, or meristematic tissue to determine metabolic and growth rate consequences of salt in the root zone. Cold tolerance may be studied on germinating seeds to investigate emergence during cold spring weather, or on growing branch tips to examine freeze tolerance. Other tissues that have been successfully studied by calorespirometry include expanding leaves, cotyledons, buds, stem tissue, flowers and cultured cells [18, 20, 26].

1.4. Amounts of tissue required

Tissue sample size for calorimetric or calorespirometric measurements is set by the interdependent variables: calorimeter detection limit, specific heat rate, ampule volume, temperature, and time required for measurement. Assuming a

required experimental accuracy of 2% and the use of a calorimeter with baseline stability and reproducibility of ± 2 μW, then it is necessary to have sufficient sample to produce at least 100 μW. Plant tissue activities vary widely, but rapidly expanding tissues commonly produce 5 to 15 μW mg^{-1} dry weight at 20 °C. With such tissues, 10 to 50 mg dry weight (or 100 to 500 mg fresh weight) are required.

As one method of obtaining R_{CO2} data, measurement of heat rates from trapping CO_2 in NaOH solutions is employed. Sorption heat rates measured for CO_2 are typically about 20% of the metabolic heat rate. Thus, tissue samples producing metabolic heat rates of 100 μW will produce only 20 μW from reaction of CO_2 to form carbonate. Thus the ± 2 μW baseline error becomes a ±10% error in CO_2 rate measurements. To maintain a 2% maximum error in R_{CO2}, sufficient plant tissue must be used to produce Φ values above 500 μW.

There is an upper limit on heat rates, however, because plants require an adequate supply of oxygen to maintain aerobic metabolism. The minimum time required for calorimeter equilibration before heat rate measurements are made in isothermal studies is typically 0.5 h and commonly a measurement takes close to one hour to allow observation of the stability of isothermal heat rates over time. Maintaining a heat rate of 500 μW (μJ sec^{-1}) for 3600 s requires nearly 4 μmol of O_2. This follows from Thornton's rule that combustion of carbon compounds produces (455 ± 15) x 10^3 μJ per μmol O_2 [27]. The sample head space in the calorimeter ampule therefore must contain at least 4 μmol O_2 (a volume of air of approximately 0.5 cm^3) to support respiration. If experiments must run longer, less tissue or larger head space volume is required. Alternatively, tissue samples may in some cases be flushed with O_2 instead of air to extend measurement times.

Because many plant calorimetry experiments run for several hours and/or at temperatures higher than 20 °C where metabolic rates are higher, larger ampules, providing larger head space volume, are desirable. However, a large volume calorimeter has a longer equilibration time, resulting in decreased sample throughput, and greater O_2 requirement.

Tissue sample size requirements are thus defined by the balance between increased sample size for greater accuracy of measurements and minimized sample size so that sufficient O_2 is present for aerobic metabolism. This balance must be considered for each calorimeter and tissue used. Plant tissue producing 100 to 400 μW in an ampule volume of 1 cm^3 and with a 0.5 h thermal equilibration time yields acceptable results for many experiments. This commonly requires 10 to 50 mg dry weight, but there are many exceptions to this generalization. One mg fresh weight voodoo lily appendix tissue at anthesis in an

enriched O_2 atmosphere produces heat rates approaching one mW [28], while a gram of dry seeds may only produce one μW.

1.5. Tissue preparation

Plant tissue preparation procedures for calorimetric analyses are often very simple: excise a section of plant tissue and place it in the calorimeter ampule. However, some standard precautions must be observed and some tissues require special handling or treatment to ensure meaningful measurements.

Microbial contamination is a universal concern. In most studies, microbial metabolic activity on plant tissue surfaces contributes negligibly to overall metabolic activity and can be ignored. Contamination in plant cell cultures and plant tissues that have been severely damaged may be significant, however, and should be carefully considered. Microbial infection within tissue sections may have a significant effect on measured heat rate, but this has only been studied in a few tissues [29, 30]. Usually, the presence of microbial contamination can be detected by the characteristic exponential increase in heat rates with time characteristic of microbial growth.

Plant tissue wound responses must also be considered. When injured by excision, a tissue section may show a wound healing response, i.e. increased metabolic rates and altered metabolic pathways. The wound response may also affect sections cut sequentially from the same plant because the entire plant may respond to the injury. Minimizing the area of cut surfaces and cutting with a sharp tool to avoid tearing offer the best means for minimizing wound responses. Care must be taken to evaluate wound responses and enhanced microbial activity associated with damaged tissue in each test. Fortunately, in most cases the size of the thermal signal due to wound responses is negligible. Notable exceptions are the metabolic wound responses in potato tuber slices [31] and rapid oxidation of phenolic compounds in sections from banana stem tissues [32]. A rapid assay of wound healing contributions to metabolic heat rates can be obtained by sectioning the tissue into multiple smaller pieces and determining if the heat rate changes [33].

Addition of buffer or nutrient solution to plant tissue samples in the calorimeter ampule are generally not needed. In closed ampules, the vapor phase is rapidly saturated with water in the presence or absence of added buffers. Water loss from the tissues to the head space is small and insignificant with larger tissue samples. With very small samples compared to ampule volume, the water loss from the tissue to achieve saturation may cause significant tissue dehydration so water should be added to the ampule, but preferably not in contact with the sample. Dipping leaf or meristem tissue in water just prior to calorimetric measurement or

leaving tissue samples in contact with water generally causes decreased heat rates. Oxygen diffusion through aqueous solutions is slow and may be rate determining, making meaningful measurements of plant properties impossible. Obviously, addition of alkaline buffer to counteract water loss must be avoided when CO_2 determinations are desired.

Exceptions to the practice of not adding buffer to plant tissue samples are numerous. Root tissues must be maintained moist and consequently are examined while in close contact with buffer-saturated filter paper disks [34, 35]. Immersing root tissue in water does not yield satisfactory data. Callus tissue cells and cell cultures are commonly measured while being maintained on agar or in liquid media. Marine tissues may be examined in water suspension by flow calorimetry, but unstirred samples rapidly settle to the bottom of the ampule and become O_2 limited during batch calorimetry.

Pretreatment of plant tissue samples is sometimes necessary to achieve stable, reproducible signals. An obvious example is the calorimetric study of seed germination. Seeds are commonly soaked in water until the initial hydration steps are complete, then transferred to calorimeter ampules. Thermal signals related to the germination process can then be followed for several hours by isothermal calorimetry. Anekonda et al. [36] found that coast redwood samples are stabilized by exposure of the tissue to 5 °C for at least 30 min prior to measurement. Following this pretreatment, subsequent storage of detached tissue for up to three days at 5 °C had no apparent further effects on measured heat rates. Detached tissues of many other plant species do not require cold treatment for stabilizing the heat rate signal, but can be transported and stored at 5 °C for several days without degradation of the thermal signal.

1.6. Plant sources

Calorespirometric methods for predictions of plant growth rate characteristics or sensitivities of plants to environmental conditions are currently reliable only in relative terms. Interspecies comparisons of growth properties based on respiratory measurements are difficult. While it is often possible to use calorespirometric methods to rapidly identify which genotype of a particular species may grow best or which may be most cold tolerant, it is not yet possible to predict absolute growth rate or temperature tolerance. Even relative measurements have major limitations if the plants to be compared are grown in greatly different environments. Best results are obtained when all plants are grown in identical conditions such as controlled environment chambers with identical light, nutrients, etc. Increasing uncertainty enters in attempts to rank performance of

plants grown outdoors in common garden plots, in broad regions across climate zones, or in randomly selected sites across a species growth range.

Prediction from calorespirometry studies of the plant growth properties of progeny is most successful for those derived by clonal propagation. Predictions for growth properties of full-sib based on parental characteristics are good; half-sib performance is less predictable. The parameters measured by calorespirometry are heritable, but complex, so that much more information than currently available will be required to precisely predict the distribution of growth rate performances of progeny from any specific cross.

Because plant calorespirometry measurements reflect the rate of energy conservation into structural biomass of plants, it is expected that this value will change with factors such as season, plant age and stress. Acclimation causes changes in metabolic heat rates and substrate carbon conversion efficiency. Both rate and efficiency of accumulation of carbon into biomass follow a continuously changing but definable pattern through the growth season. Thus, comparisons among plants should be made on plants at similar growth stages.

1.7. Calorimeter requirements

Plant calorimetric studies do not, in general, require a very low detection limit for heat rates. Baseline detection limits of 2-3 μW are adequate for nearly any study since single, small seedlings generally weigh tens of mgs and generate >100 μW. Lower detection limits are not generally useful because of the long equilibration time. The limiting factors for calorimeter design for plant studies are the heat rate, head space gas availability, and the measurement-time relations described above in section 1.4. Sample size is usually not limiting, so increased signal to noise can be obtained by larger sample sizes. Larger samples are often preferable so that tissue integrity and measured activity approximate activities in intact plants.

Among the most important features of a calorimeter for plant studies are:

1. Multiple sample capabilities. Plant studies routinely require examination of many samples, particularly when the objectives of the study include identification of phenotypes with desired growth, stability, or yield characteristics. Screening large populations for individuals with desired metabolic characteristics is impossible in single-sample calorimeters. Current commercial multiwell calorimeters allow up to three samples to be run simultaneously. A calorimeter with as many as 100 sample wells could be effectively employed for plant studies.
2. Ampules that allow ready, repeated access to samples. During the course of plant measurements, the calorimeter must be opened and ampules must be

accessed to allow insertion or removal of aqueous and gas phase reagents. Removable ampules are preferred so they can be sterilized when necessary. Readily resealable ampules are required. Ampules do not have to be made of expensive alloys or be gold plated to render them resistant to corrosion at extreme conditions. Plant tissues themselves are not resistant to harsh conditions. Hastelloy works well, but stainless steel is corroded by halides and is not useable. Glass is useable, but gives slow responses due to poor thermal conductivity.

3. Ampules sufficiently large to contain adequate tissue and headspace gases for supporting respiration throughout the time required for measurements.

4. Ampules must be readily accessible and such that tubes exiting the calorimeter can be attached. In many experiments it is advantageous to sample headspace gas. The ability to withdraw samples for chromatography or mass spectrometry is a major advantage for plant calorimetry studies. In addition, gas flux determinations by pressure change during calorimetry measurements is important. Again this requires penetration of the ampules with a tube connected to a pressure sensor. New methods are needed for determination of changes in O_2 and CO_2 in headspace gases. Current methods have limited sensitivities, are slow, are not compatible with scanning studies, and often require precise determination of sample volume. Incorporation of new methods for gas analysis again requires ready accessibility of ampules within the calorimeter.

5. Rapid equilibration time. Minimizing sample equilibration time is important to obtaining the high throughput required for most plant calorimetry studies.

6. Rapid adjustment of temperature for isothermal studies. Stepwise adjustment of temperature during isothermal determination of plant metabolic heat rates on the same tissue sample is essential for interpretation of metabolic properties. This generally requires a calorimeter with both rapid scanning and isothermal capabilities.

7. Temperature scanning capabilities. While many of the measurements required for plant calorimetry studies are best done in an isothermal mode, measurements of metabolic heat rates while scanning over the viable range of plant growth adds an important dimension for interpretation of plant properties. Studies are facilitated by the ability to scan temperature both up and down.

8. Photocalorimetric capabilities. An effective photocalorimeter may answer key questions regarding energetics of photosynthesis and rates of respiration in the light [26]. Initial work on construction of photocalorimeters has been reported [13, 14] but requires further refinement.

No existing calorimeter has all of the above desirable features for plant calorimetry. Most of the commercial calorimeters suitable for plant studies and some characteristics related to their function in plant calorimetry studies are listed

in Table 1. The choice of which calorimeter is best is answerable only in terms of specific experiments. Calorimeters number 1 through number 3 have scanning capabilities. Of these only number 2 has multiple sample wells. This makes the CSC 4100 the best choice for practical applications that require a large sample throughput. Calorimeter number 1, with 10 times the potential sample size of number 2 while differing by only a factor of 5 in minimum long-term detectable heat rate, offers a better signal to noise ratio than number 2. If this Setaram calorimeter was constructed using the detector present in the MS80, greatly enhanced accuracy of heat rates would be obtained and it would be a superior instrument for some plant calorimetry applications. The Thermometric TAM 2277 (number 5) has a superior detection limit and adequate ampule volume, but is not designed with scanning capabilities and is slow to shift temperature for successive isothermal studies. Likewise, number 4, number 6 and number 7 may each be useful for a limited number of specialized applications in plant calorimetry, but thermal equilibration is very slow during sample measurement and following adjustment to new temperatures. This makes them unsatisfactory for most studies. Calorimeter number 2 has multiple samples, easy ampule accessibility, scan-up and down capability, removable ampules and adequate (but not the best) detection limit and sample volume. This makes it the best choice among currently available calorimeters for many plant calorimetry studies. Other instruments excel in specific applications.

Table 1
Characteristics of calorimeters suitable for plant calorimetry studies, from [37].

Calorimeter Model	minimum detectable heat rate/μW	number samples	scanning capability	volume /cm^3
1. Setaram C80	20	1	yes	10
2. CSC 4100	4	3	yes	1
3. Setaram Micro-DSC	0.4	1	yes	1
4. Setaram MS80	0.4	3	no	100
5. Thermometric AB TAM2277	0.2	3	no	5
6. CSC 4400	0.2	3	no	100
7. CSC 4200 & 4500	0.006	1	no	1

1.8. Isothermal calorimetry methods

Experimental methods for measuring plant respiratory heat rates, gas exchange rates, and relating these to growth rates and stress responses have been much refined over the past decade. Examples of experimental methods currently in use for specific applications are outlined here.

1.8.1. Isothermal heat rate measurements

The studies of Criddle et al. [17] on carrot and tomato cell cultures outlined basic procedures for isothermal heat rate measurements of plant tissues. Samples are placed in an ampule, sealed to prevent any water vapor loss, placed in the calorimeter at the desired temperature and the heat rates recorded directly. Figure 1a shows the type of thermogram obtained. There is an initial rapid change in recorded heat rate while sample and ampules are thermally equilibrated. Following equilibration, (about 45 min in this example) the amplitude of the thermal signal is corrected for baseline values obtained with empty ampules to yield the sample metabolic heat rate. Temperature may then be adjusted to new values to establish temperature coefficients of heat rate or the ampules may be opened and the sample environment modified before the ampule is resealed and re-equilibrated for evaluation of effects of the modification on plant activities. Because plants are ectotherms that live in a variable temperature environment, temperature dependence studies using sequential isothermal measurements are essential for characterization of plant physiological properties.

1.8.2. Isothermal measurements of time dependent activity loss

When the metabolic heat rate is not constant, curves similar to that in Figure 1b are obtained. The initial thermal equilibration is followed by a decreasing metabolic heat rate. The rate of decrease (slope of the curve) measures the rate of activity loss by the sample. For many plant tissues in favorable environmental and temperature conditions, heat rates remain nearly constant until ampule oxygen is depleted. However, high and sometimes low temperatures (or other conditions that cause activity loss) give rise to curves of the type shown in Figure 1b. Comparison of the thermogram of treated samples with untreated control samples allows definition of the time course of treatment effects on plant metabolic activity. For example, it is often possible to examine the rate of inactivation of tissue by high temperature or by exposure to inhibitors.

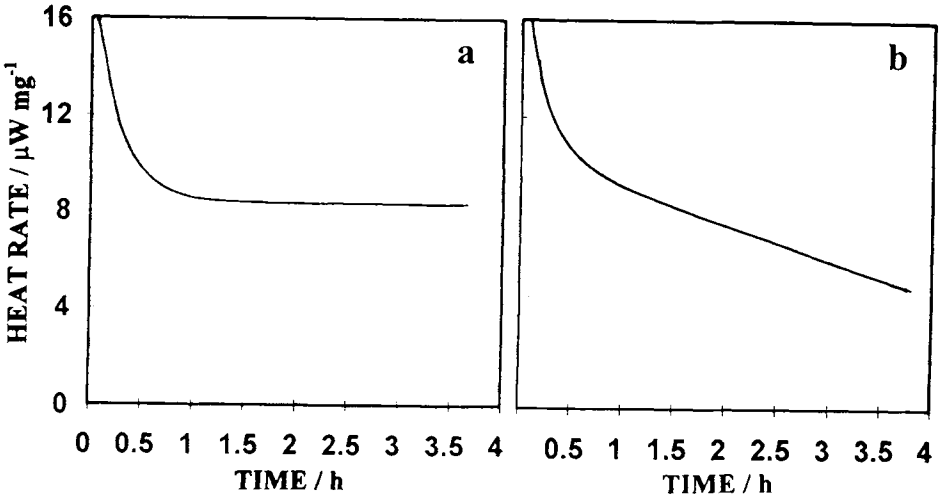

Figure 1. Isothermal measurement of plant metabolic heat rates. Plant tissue samples are placed in the calorimeter ampules, sealed, and heat rates are followed over time. The initial rapid changes in heat rates observed in this figure illustrate thermal equilibration of ampules and samples. This is followed by heat rate values that, when adjusted for any baseline corrections, represent the metabolic heat rate of the tissue preparation. When tissue metabolic rates are stable over the time course of the experiment, constant heat rates are obtained (a). When tissues are unstable or are stressed so that metabolic activity decreases during the calorimetric measurement, a decreasing heat rate is observed (b).

1.8.3. Temperature cycling

The capability of calorimeters to cycle between temperatures for isothermal measurements can be used to examine the time course of plant metabolic responses to high and low temperatures. Studies by Rank et al. [38] illustrated the usefulness of this method. They showed that there is no critical temperature for either high or low temperature inactivation of tomato cells grown in culture. Rather, a time-temperature function is required to describe rates of inactivation.

Cycling experiments are performed by first measuring the heat rates at some reference temperature at which the tissue is stable, then exposing the sample to a temperature near the high or low limit for viability for various time intervals. The samples are returned to the reference temperature to compare initial heat rate values with values after exposure to the temperature extreme. When inactivation occurs at the temperature extreme, heat rate values measured at the reference

temperature are reduced. This cycle is repeated until much of the metabolic activity is lost. Then the stress temperature is altered and the cycling repeated with a new tissue sample. A series of measurements generated using a range of extreme temperatures produces data for a three dimensional surface response plot (Figure 2) and development of equations relating time of exposure, exposure temperature, and activity loss. Any other selected stress condition could be substituted for temperature in this type of experiment. Thus, cycling methods offer general procedures to monitor time and magnitude of stress effects on metabolic activity.

1.8.4. Calorespirometry

Batch studies. Methods and equipment have been described for isothermal measurement of metabolic heat rates and determination of the flux rates of both O_2 and CO_2 [21, 22, 39]. Isothermal heat rates are determined as in section 1.8.1. O_2 rates are determined by pressure change. CO_2 rates are determined by two methods, one measuring heat rate increases in the presence of a CO_2 trap and the other by measuring pressure change.

R_{O2} determinations are made using modified calorimeter ampules connected via capillaries to pressure sensors. During respiration, O_2 is consumed by the tissue and CO_2 is produced. In the presence of 0.4 M NaOH, the CO_2 is trapped and changes in pressure within the ampule reflect O_2 uptake. Pressure changes (ΔP) are related to mol O_2 (n) uptake by careful measurement of headspace volume (V), temperature (T), and the relation $n = \Delta P\ (V/T)$. O_2 depletion rates ranging from several hundred to as low as 0.5 nmol sec^{-1} can be measured with an accuracy of about $\pm$ 0.9% in 1 cm^3 ampules [23].

One method of CO_2 determination measures isothermal heat rate of a tissue sample first in the presence of a small container of water, then in the presence of the container with 0.4 M NaOH. With NaOH present, CO_2 is trapped as carbonate with concomitant production of heat. The increased heat rate in the presence of base can be related to R_{CO2} through the known enthalpy change for carbonate formation, -108.5 kJ mol^{-1} CO_2 [40] Thus, the difference in heat rates measured for tissue in the presence and absence of NaOH divided by 108.5 yields R_{CO2}[23].

The second method of R_{CO2} determination is based on pressure measurements. With no NaOH present in the calorimeter ampule, the pressure change during metabolism depends on R_{CO2} minus R_{O2}. With NaOH present, pressure change depends only on R_{O2} and gas volume. The combination of pressure changes in the presence and absence of NaOH thus yields values for R_{O2}.

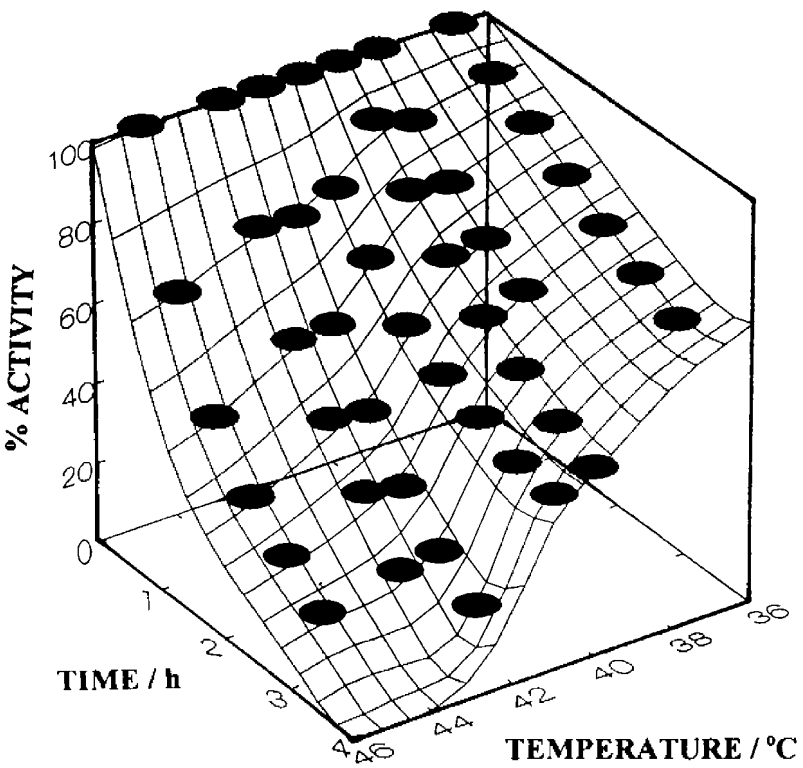

Figure 2. Isothermal measurement of tomato cell metabolic heat rates over a range of temperatures near the high temperature tolerance limits. Data were obtained by cycling isothermal measurements of a single tissue sample between a reference temperature in the mid range for normal plant growth and a high temperature that causes inactivation. The data are plotted as metabolic heat rate remaining at the reference temperature vs. cumulative time of exposure of the plant tissue at the high temperature. The experiment is then repeated with additional tissue samples and cycling to successively higher temperatures. The family of activity vs. time at high temperature curves thereby generated are then combined to yield a response surface indicating activity loss following exposure to combinations of time and temperature.

Flow and perfusion studies. Flow of liquid media through calorimeter sample vessels to ensure nutrient and oxygen supply is a standard practice in animal and microbial calorimetry [41-43]. These methods are less extensively employed for plant studies but have been used for addition of plant growth effectors to monitor tissue response. Studies of plant cells using flow calorimetry are hampered by the tendency for plant cells to clump, become inhomogeneous in the cultures, and to clog flow lines. However, Anderson and Lovrien [44] and Anderson et al. [45] successfully examined the effects of indole-3-acetic acid on metabolism of corn with flow apparatus. Flow calorimeters offer distinct advantages for long term studies requiring constant addition of test substances to the plant materials.

Backman et al. [46] developed a gas perfusion microcalorimeter for studies of metabolic rates of plant tissue. Two, twin-heat conduction calorimeters were connected by gas-tight tubing. During measurement, a flow of humidified air scrubbed of CO_2 enters the main calorimeter containing the plant tissue for metabolic heat rate measurement. The outgoing gas is passed through a second calorimeter where CO_2 is trapped in alkaline solution and the resulting heat of carbonate formation serves as an online CO_2 analyzer. A constant input of gas guarantees constant headspace gas composition, an improvement over the batch calorimetry methods. Also, the input gas composition and humidity can be varied, allowing this calorimeter to be used in examination of effects of O_2, NO_x, or gas phase effectors on activity.

1.8.5. Batch studies of samples requiring contact with liquid media

Ensuring that tissues have adequate access to the oxygen that is available is sometimes a problem in batch calorimetry. Diffusion of oxygen to the plant materials can become limiting with tightly packed tissues, or tissues such as roots or cell cultures that may be submerged in unstirred liquids,. This is sometimes avoidable by using less tissue, and providing soluble nutrients to tissue sections via wetted fiber filters upon which the samples rest so that samples are not submerged.

A means of measuring plant cell culture activities in liquid media by unstirred batch calorimetry was demonstrated by Fontana et al. [47]. Cells were floated on liquid media supplemented with an inert, high density preparation of Percoll™. Other additives could also be used to increase media density. Cells at the air-media interface were able to obtain adequate supplies of both O_2 and nutrients for rapid metabolism without diffusion rate limitations.

1.8.6. Studies above ambient pressure

Pressurization of specially constructed calorimetry ampules using common bottled gases is relatively simple [39]. Pressurizable ampules can be constructed that are suitable for both scanning and isothermal determinations with selected gases or gas mixtures. This allows direct determination of pressure effects on metabolic rates as a function of temperature. However, few high pressure calorimetry studies have been done on plants.

Non-calorimetric studies of effects of hydrostatic high pressure on plant sources are more common. In general, pressure effects on plant metabolic rates are small, but some distinct changes have been noted in growth, photosynthesis, temperature responses, and plant structure [48]. Interpretation of the role of pressure on plant metabolism remains uncertain. Hypotheses that have been framed to explain pressure effects are generally written in terms of volume changes and structural transitions in chloroplasts and in lipid membranes, but there are equally tenable alternative explanations such as pressure effects on equilibria.

A scanning calorimetry study of tomato cells at elevated pressures by Criddle et al. [39] was able to identify important elements related to high temperature inactivation. Metabolic heat rate measurements were conducted at temperatures from 25 to 60 °C and at pressures from ambient to 12 MPa. Elevated pressure increased the inactivation temperature for the tomato cells. The combined calorimetry and pressure results thus show that a reaction with a positive volume change is associated with high-temperature inactivation of tomato cells.

1.9. Temperature scans of plant metabolic rates

1.9.1. Heat rate measurements by temperature scanning calorimetry

Heat conduction differential scanning calorimetry methods for the measurement of metabolic heat rates of plant tissues as a continuous function of temperature were developed by Hansen and Criddle [19]. Thermally induced transitions and heat rates can be determined simultaneously.

Loike et al. [49] showed previously that temperature scanning calorimetry could be used to rapidly obtain data on the metabolic rate of mammalian cell cultures as a function of temperature. These workers identified an ambiguity present in their studies, i.e. the data provided no general basis for deciding whether a change in the calorimeter output was due to variation in the metabolic heat rate or to the apparent specific heat of the sample. This calorimeter had a limited range of scan rates only available in an upward direction, so, it was not possible to overcome the ambiguity. However, temperature scanning calorimeters with a wider range of scan rates and the ability to scan down as well as up have been used to

eliminate this ambiguity. Hansen and Criddle [19] described a method for measuring metabolic heat as a continuous function of temperature and developed this for estimation of the errors involved in, and thus the optimization of, the application of scanning calorimetry to measurement of metabolic rates in plants. They also established conditions under which the thermal effects of physical changes can be distinguished from metabolic effects. Starting with the recognition that overall metabolic heat is always exothermic irrespective of scan direction, while phase changes must be endothermic on upward scans and, if reversible, exothermic on downward scans, methods and rationale were developed for examining both metabolic heat and phase changes.

One important finding from the initial scanning calorimetry studies on plants was that high temperature inactivation as a direct consequence of lipid phase transitions in plant tissues is unlikely. Such transitions, if they exist, can not involve more than 6% of the total lipids. These findings support the conclusions of Rank et al.[38] obtained by temperature cycling methods that inactivation is a function of time and temperature, but it is unknown what physical event or events, or even if there is such an event, that initiates plant stress at temperatures causing chilling or heat shock.

1.9.2. Temperature scanning methods

A typical experimental protocol for a temperature scanning experiment with chilling tolerant tissues might involve isothermal determination of metabolic heat rate at 20 °C and at 5 °C, followed by an up-scan from 5 to about 65 °C at a rate of 10 °C h^{-1} followed by another isothermal measurement at 65 °C. At the end of each experiment, samples are dried and weighed. A temperature scan on a tropical plant that would suffer chilling injury would start at a higher temperature. The high temperature may be selected to be sufficiently high to inactivate normal metabolic activity of the tissue, as in the example, or may be below temperatures that cause heat shock. Or, an experiment might be started at a temperature near room temperature and the temperature scanned down to determine the response of the tissue to chilling or freezing temperatures. Quantitative interpretation of the scanning results requires isothermal measurements as part of the protocol [19].

A determination of sample heat rate requires a minimum of two sets of temperature scans: a baseline scan with both ampules empty and a scan with sample present in one ampule. Because reference ampules and contents cannot be exactly matched to the mass and heat capacity of the sample, baseline corrections for precise determination of sample metabolic heat rates are complex. The absolute determination by DSC of both the metabolic heat rate

and heat capacity of the sample is inaccurate. Curves of apparent sample heat capacity vs. temperature have the correct shape, but the absolute positions of the curves can be in error by large factors. However, if the endpoints of the curves are accurately established by an independent method, the entire curve is accurately established. Measurement of isothermal heat rates of the sample at both ends of a thermogram proved to be the most practical method for establishing values for the ends of the curve. With these points established, the curve can be mathematically adjusted with a linear correction to link the initial and final isothermal values and give an accurate description of heat rate vs. temperature values [19].

Sample selection and preparation for scanning studies are similar to those for isothermal measurements, but ensuring an adequate supply of O_2 during scanning runs is more difficult because sufficient O_2 is required for several hours of measurement. The oxygen requirement may be met in some cases by increasing the partial pressure of O_2 above the normal 20% or by reducing the sample size. The total amount of O_2 required for an experiment may be estimated from the total heat production, approximated as the summation of the heat rate during each data interval multiplied by the time interval. Heat rate may be assumed to double every ten degrees for this purpose. Division of the estimated total heat by 455 ± 15 kJ mol^{-1} then gives an estimate of the required moles of O_2 [27]. The number of moles of O_2 available at the start of the assay may be estimated from the volume of the calorimeter ampule headspace, the temperature at which the ampule is sealed and the partial pressure of O_2 by use of the ideal gas law $n = PV/RT$. The amount of O_2 in a 1 cm^3 ampule filled with air at 1 atm and 25 °C is 8.2 μmoles. If O_2 consumed during an experiment exceeds 90% of the O_2 available, the data should be discarded. As a simple first approximation of sample size for upward scans, samples in a 1 cm^3 ampule filled with air should have a heat rate less than 100 μW at 20 °C.

1.9.3. Interpretation of scanning thermograms

Scanning calorimetry allows rapid assessment of metabolic heat rates as a continuous function of temperature. This is a significant improvement over traditional methods of determining metabolic and growth rate responses to temperature that are often slow, allow measurements at only a few temperatures, and require interpolation to predict rates at other temperatures. The thermograms often show fine structure that would not be identified by the traditional methods.

Figure 3 illustrates the major features of typical metabolic heat rate vs. temperature curves from a scanning analysis [50]. The shapes of the

thermograms and key temperatures are species dependent, allowing comparisons among species and defining the response of plant tissue to temperature increase. The dashed curve in Figure 3 was obtained from data collected on the smallest bracts on the "brush" branch of *Callistemon* during mid May and is an example of metabolic thermograms obtained on plant tissues. The segment of the curve from approximately 15 to 30 °C (A-B) shows an approximately exponential increase in metabolic rate as temperature is increased, in accordance with predictions from the Arrhenius relation.

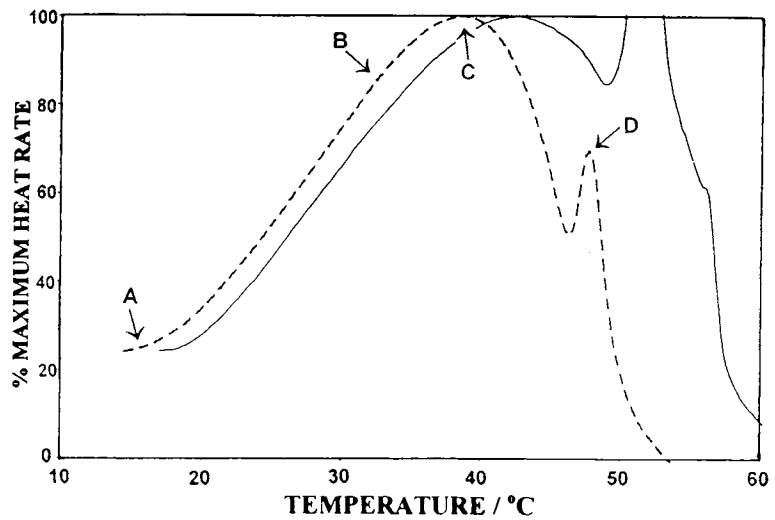

Figure 3. Metabolic heat rate vs. temperature curves and features that may be used for species comparisons. The dashed curve in Figure 1 was obtained from data collected on *Callistemon* during mid May. The segment of the curve from 15 to 30 °C (A-B) shows an approximately exponential increase in metabolic rate as temperature is increased. B is an inflection point termed the low shoulder temperature (T_{ls}) above which metabolic rates no longer increase exponentially and the slope decreases with temperature increase. C indicates T_{max}, the temperature at which maximum rate is achieved. The exothermic peak at D depends on the amount of O_2 remaining in the calorimeter ampule when this temperature is reached. A second scan of *Callistemon* tissue examining a tissue sample collected from the same plant two months later in the season is also shown (solid line).

At temperatures above B, metabolic rates no longer increase exponentially, instead the slope decreases with temperature. Thus, B is an inflection point we have named the low shoulder temperature (T_{ls}).

A second point of significance is T_{max}, the temperature at which maximum rate is achieved (indicated by C in Figure 3). The decrease in metabolic activity with increasing temperature above T_{max} is largely irreversible on the time scale of these studies. Most plant tissues exhibit an exothermic reaction (probably oxidation of polyunsaturated lipids) at a higher temperature (D). The size of the peak at D depends on the amount of O_2 remaining in the cell when this temperature is reached. When all the O_2 in the ampule is consumed prior to reaching the temperature at point D, no exothermic peak is observed. While not an important event in relating the thermogram profile to physiologically important activities, the exothermic peak at D provides a useful indicator of the quality of scanning measurements. Good measurements require that oxygen be present in adequate supply throughout the study. Appearance of an exothermic peak at the high temperature end of the scan confirms that this condition is met.

A second scan of *Callistemon* tissue examining a sample collected from the same plant two months later in the season is shown in Figure 3 (solid line). This curve has the same overall shape as the earlier scan, but metabolic rates are somewhat lower and T_{max} is shifted to a higher temperature. Similar shifts in properties with plant age, nutrient stress, or other environmental factors affecting plant yields can equally well be studied with these methods.

1.9.4. Results obtained from scanning studies

The results of scanning studies clearly show that no "typical" curve describes the effects of temperature on plant metabolism and growth rates. Plant metabolic rates are not simple, smooth functions of temperature and rates show a wide range of species and cultivar specific, season specific and development stage specific responses to changes in temperature. Thermograms are highly reproducible for repeat measurements on individual plants when ample O_2 is present and the scanning conditions, the tissue sampled, and the tissue age are carefully controlled. Differences between curves for different plants are related to plant thermal stability differences, which in turn may be related to different rationales for growth, survival, and reproduction among the species [51].

For example, thermograms of soybean cultivars show that plants from the northern end of the growth range in southern Canada and northern USA differ from those from the southern end of the range [33]. Northern cultivars have T_{ls} near 25 °C, i.e. these plants do not continue to increase metabolic rates rapidly when temperature exceeds 25 °C. Plants adapted to more southern climates do

not exhibit this shoulder in the thermograms. Cultivars commonly grown at the southern end of the commercial range maintain a near exponential increase in metabolic rates to near 35 °C.

Also, Anekonda et al. [51] showed that redwood (*Sequoia sempervirens*) ecotypes originating from sites across the entire range of native redwood growth, but grown at a single location, had metabolic temperature responses that varied systematically with climate of origin. The latitudes of origin of each ecotype (as a surrogate for climate) were matched to patterns of the metabolic heat rate as a function of temperature. Similar studies on species as varied as bitterbrush [52] and lettuce [53] also confirm that metabolic heat rate vs. temperature curves are significant indicators of plant growth as a function of temperature. Figure 4 illustrates this relation for bitterbrush plants originating from across the entire Great Basin region of the USA, but grown for four years in a common garden near Provo, Utah. The temperature coefficient of $\Phi(\mu_\Phi)$ is plotted against a function of latitude and elevation of origin of these plants. Plants from high latitude and high elevation, at the right side of the figure, have low values of μ_Φ Plants from low latitude and elevations have high values of μ_Φ. A similar relation appears to hold for other plant species. Plants from tropical zones tend to have higher μ_Φ than plants from more temperate zones. Metabolic

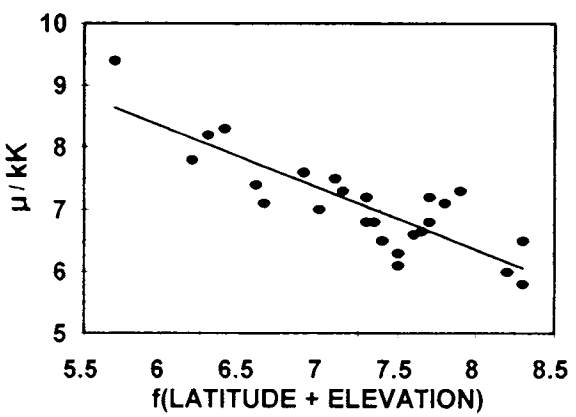

Figure 4. Variation in μ_Φ with latitude and elevation of origin of bitterbrush (*Chrysothamnus nauseosus*) plants from the Great Basin region of the USA. The function of latitude and elevation obtained from this plot, i.e. f(latitude + elevation), is (1.43kK km^{-1})(elevation km) + (0.122kK $deg.^{-1}$.of latitude) (deg. of latitude), where kK is kilokelvins. Low latitude and elevation plants are at the left side of the plot and high latitude, high elevation plants are at the right side of the plot.

rate responses, therefore, appear to be accurate indicators of plant growth response to temperature and can be used as a guide to optimal growth climates for species and ecotypes.

Scanning calorimetry measurements yield strong indications of relative reaction rates or relative stabilities of plants, but do not give absolute measurement of key thermal temperatures. Both the peak temperatures observed in the thermograms and curve shapes vary with temperature scan rates. Inactivation of metabolism at high temperature is a function of both time and temperature [38] so that increasing scan rates result in higher values of T_{max}. Therefore, precise comparison of thermograms among plants requires that all experiments be done under identical conditions.

1.10. Limitations in plant calorimetry measurements and interpretations.

This discussion so far has discussed limitations to plant calorimetry based only on calorimeter sensitivity, sample size, and O_2 depletion. Additional sample-specific problems are encountered, however, and incautious consideration of data can lead to errors in interpretation.

In some cases, plant tissues are sensitive to gas phase inhibitors or activators. The most evident of these is CO_2 produced via metabolism so that concentration is increased in the sample ampule. Respiration in some plants appears very sensitive to CO_2. For example, isothermal values of soybean leaf tissue metabolic rates are not constant, but rapidly decrease with time [33]. Opening the ampule, flushing with air, and resealing restores the initial heat rate and initiates the process of decline once more. When a CO_2 trap is included in the ampule to maintain CO_2 at near zero pressure, stable heat rates are obtained. Thus, the buildup of CO_2 appears to be responsible for the declining rate. Cauliflower tissue also shows decreased metabolic rate in sealed ampules [54], but for different reasons. Emission of a metabolic modifier from the cauliflower flowerets appears responsible for the decline in this case.

Other tissues fail to give stable, reproducible heat rate values because of tissue sensitivity to handling and/or calorimeter conditions. It has not been possible to study leaf samples of water fern, *Lemna minor*, or of arabadopsis in spite of extensive efforts. Tree meristematic tissue measurements in early spring shortly after breaking dormancy are also highly variable. No evidence has been obtained to explain this behavior, but rapid changes in plant growth hormones in the tissue during this developmental stage may be responsible.

Problems have also occurred from over-interpretation of the consequences of metabolic heat production in plants. In a series of papers, Raskin and coworkers [55-57] postulated that a temperature increase from metabolic heating protects

certain plants from chilling injury. The alternative respiratory pathway was proposed to have an important role in the heat production providing this protection. However, calculation of the potential temperature increase due to metabolic heating shows at most an increase of 0.05 °C, hardly enough to offer significant protection to the plant tissues [58]. Raskin and coworkers failed to account for the rapid dissemination of heat in uninsulated conditions, a problem thoroughly discussed by Pierce in 1908 [11].

Many workers over the years have implied that switching from the normal cytochrome mediated pathway to the alternative pathway causes large increases in metabolic heat rates. However, the change to alternative pathway has only a small effect (about 10%) on the enthalpy change. A heat rate increase is indeed observed, but from an increase in reaction rate rather than the energetic differences between the pathways, ie. $\Phi = (dn/dt)\Delta H$ and (dn/dt) changes greatly but ΔH is approximately constant. Uncoupling of oxidative phosphorylation leads to large increases in heat production rate, but again through increasing (dn/dt) and not through large changes in ΔH.

Studies by Skubatz and Meeuse [59]and Skubatz et al. [60] illustrate another problem with interpretation of calorimeter data. These workers presented data that were interpreted to indicate temperature cycling in the reproductive tissues of cycads. They failed to balance masses in sample and reference ampules. This resulted in a cyclic overshoot during equilibration with a periodicity equal to the instrument time constant. Interpretation of the cycles in terms of a periodicity in tissue metabolism is obviously incorrect. Also, in some of their work, samples were not left in the ampules long enough to reach steady-states of heat evolution.

These errors in interpretation illustrate a general concern with any calorimetry study. Heat production occurs from nearly all chemical and physical events. Thus, careful interpretation, proper controls, and theoretical evaluation of results is essential for all studies.

2. PLANT GROWTH MODEL

2.1. Introduction

The potential contributions of plant calorimetry to understanding plant physiology that were postulated years ago by Pierce, Prat, and others were not realizable prior to development of an appropriate model relating plant metabolism, i.e. Φ, R_{CO2} and R_{O2} values to growth and substrate carbon conversion efficiency [20].

Initial insight into necessary components of a growth model that includes both energy and mass, came from recognition that dark respiration rate has

frequently been found to correlate with plant growth rates [61, 62]. Such correlations indicate that respiration rate is, or is covariant with, the rate limiting process controlling growth. However, simple, empirical correlations have not proven to be robust enough for applications such as use of respiration measurements for selection of individual genotypes within a species. Several respiration-based growth models have been developed in attempts to describe the basis for this correlation, but they too lack selective capabilities [61].

The metabolic rate, substrate carbon conversion efficiency, and availability of inputs such as nutrients and light all play a role in determining growth rate (Figure 5). When all inputs are present in optimum concentrations, the rate and efficiency of respiratory and biosynthetic processing become the determinant of the maximum rate of production of structural biomass, R_{SG}. However, because both the rate and efficiency of respiration are temperature dependent, growth rate is also determined by climatic temperature and genetically determined plant responses to temperature even when all the inputs listed in Figure 5 are optimal.

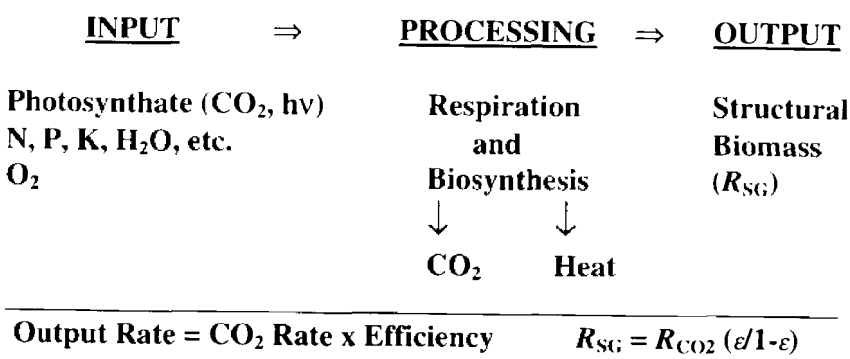

Figure 5. Conceptual model for plant growth indicating inputs to plant growth, processing steps, and output biomass. CO_2 and heat are products of the processing reactions. Growth rate (output, R_{SG}) is given by the product of rate (R_{CO2}) and efficiency function ($\varepsilon/1\text{-}\varepsilon$), whether limited by availability of an input or by the rate of respiration and/or biosynthesis.

If one or more of the inputs is present in less than optimum amount, then the respiratory rate and efficiency, and hence the formation of structural biomass (growth rate), will be reduced to the rate determined by the rate of acquisition of

the limiting resource. But, note that measurements of respiration rate and efficiency still accurately reflect growth rate under these stressed conditions [20, 26]. If inputs are present in greater than optimum amounts and reach toxic levels, or if other toxins such as aluminum or heavy metals are present, by definition the rate of growth is reduced. Again, growth reduction is reflected by a decrease in the product of respiration rate and efficiency. Thus, effects of toxins or stress can result in either a decrease or increase in respiration rate and efficiency, but the product of rate and efficiency must decrease with increasing stress and concentration of toxin. The responses of plants to nutrient deficiency and toxic conditions constitute further links between the environment and metabolism.

2.2. Development of plant growth model

Plant respiration rate has commonly been measured as R_{CO2} or R_{O2}, and less commonly as metabolic heat rate, Φ. Combining R_{CO2} and R_{O2} measurements with data on Φ provides the ratios Φ/R_{CO2} and Φ/R_{O2} which are related to the substrate carbon conversion efficiency, i.e. the fraction of the photosynthate carbon that is conserved in the biomass produced by growth. The ratio Φ/R_{O2} has a value of -455±15 kJ/mole O_2 for direct combustion of nearly all organic compounds (Thornton's rule) [27], equal to the expected value of Φ/R_{O2} for fully aerobic respiration unaccompanied by growth. The ratio Φ/R_{CO2} is proportional to Thornton's constant, with the proportionality dependent on the oxidation state of the substrate carbon, i.e. γ_p. (Degree of reduction, γ_p - 4, is used by some authors instead of oxidation number.) The third ratio of respiratory rates, i.e. R_{CO2}/R_{O2} depends on the oxidation states of the substrate consumed and the biomass produced. Thornton's rule makes energy use efficiency equivalent to substrate carbon conversion efficiency and makes it possible to relate energy use efficiency to growth rate. When a plant is more efficient in using energy, less photosynthate is required to provide the necessary energy to drive biosynthesis and more of the photosynthate can be used to produce biomass.

The relations among Φ, R_{CO2}, and R_{O2} have been derived by Hansen et al. [20]. The specific growth rate R_{SG} depends on the metabolic rate and efficiency of respiratory metabolism as shown by equations 1 and 2,

$$R_{SG} = -[\ \Phi + R_{CO2}(1-\gamma_P/4)\Delta H_{O2}]/\Delta H_B = R_{CO2}(\varepsilon/1-\varepsilon) \quad (1)$$

$$(\varepsilon/1-\varepsilon) = [-(1-\gamma_P/4)\Delta H_{O2} - \Phi/R_{CO2}]/\Delta H_B \quad (2)$$

where ε is the substrate (photosynthate) carbon conversion efficiency, γ_P is the mean chemical oxidation state of substrate carbon, ΔH_{O2} is the constant from Thornton's rule, and ΔH_B is the enthalpy change for conversion of one mole of substrate carbon into one mole of non-photosynthate biomass carbon. (Note, R_{SG}, specific growth rate in moles time^{-1} mass^{-1}, is equivalent to RGR in plant physiology and μ in microbiology.) These equations, with measurement of only Φ and R_{CO2} and assumptions about γ_P and ΔH_B, allow determination of relative specific growth rates and substrate carbon conversion efficiencies of individual plants. The $R_{CO2}(1-\gamma_p/4)\Delta H_{O2}$ term represents the total rate of energy made available to the tissue by respiration. The heat rate, Φ, represents the rate of loss of respiratory energy to the surroundings. The difference is the rate of energy retained in the tissue in the form of new biomass, i.e. growth. Growth rate is thus proportional to the **difference** between two measures of respiratory rate. Only if ε and ΔH_B are relatively constant or covariant with R_{SG} across genotypes will R_{SG} be correlated with a single respiratory measure. Variability in ε and ΔH_B probably accounts for much of the scatter in published growth-respiration correlations.

In addition to defining the relation between growth rate and respiration rate, Equations 1 and 2 also allow prediction of growth rate and substrate carbon conversion efficiency as functions of temperature from measurements of Φ and R_{CO2} as functions of temperature. The temperature dependence of both Φ and R_{CO2} at "nonstressful" temperatures is closely approximated by the Arrhenius function. (Nonstressful in this context means the general range of temperature in which the plant grows well and tissues are not damaged by thermal effects. In reality the equations demonstrate continuous variation in efficiency with changing temperature except for unique values of the parameters. Thus, the term "nonstressful temperature" is misleading, although commonly used to mean the range between cold damage and heat damage.) Substitution of the Arrhenius functions into equation 1 gives equation 3,

$$R_{SG} = [A_\Phi e^{-\mu\Phi/T} - \Delta H_{CO2} A_{CO2} e^{-\mu CO2/T}]/\Delta H_B \qquad (3)$$

where A_Φ and A_{CO2} are constants, μ_Φ and μ_{CO2} are the respective temperature coefficients for Φ and R_{CO2}, and T is the absolute temperature. ΔH_{CO2} is the enthalpy change for one mole substrate carbon conversion to CO_2. Equation 3 assumes that neither γ_P nor ΔH_B are temperature dependent. Growth rate as a function of temperature is thus the difference between two Arrhenius functions,

and the shape of the curve depends on the relative values of μ_Φ and μ_{CO2}. Equation 2 shows that the temperature dependence of ε is related to the temperature dependence of the ratio Φ/R_{CO2}. Approximating Φ and R_{CO2} with Arrhenius functions gives their ratio as

$$\Phi/R_{CO2} = A_\Phi e^{-\mu\Phi/T}/A_{CO2}e^{-\mu CO2/T} \quad (4)$$

If $\mu_\Phi \neq \mu_{CO2}$, the ratio Φ/R_{CO2} varies with temperature, and consequently so must ε (Eq. 2). In general $\mu_\Phi \neq \mu_{CO2}$. The consequences of this lack of equality are highly important to plant growth in different and highly variable climates. The strong dependence of metabolic rate on temperature along with different temperature dependencies of Φ and R_{CO2} within a plant mandate continuously changing values of substrate carbon conversion efficiency and growth rates as temperature changes. Equations 1-4 show that growth rate responses to temperature can be predicted from simple physiological measurements, i.e. from Φ and R_{CO2}.

2.3. Test of temperature dependence predictions

The accuracy of respiration-based predictions are confirmed by comparison of predicted growth rates with measured growth rate data on tomato and cabbage

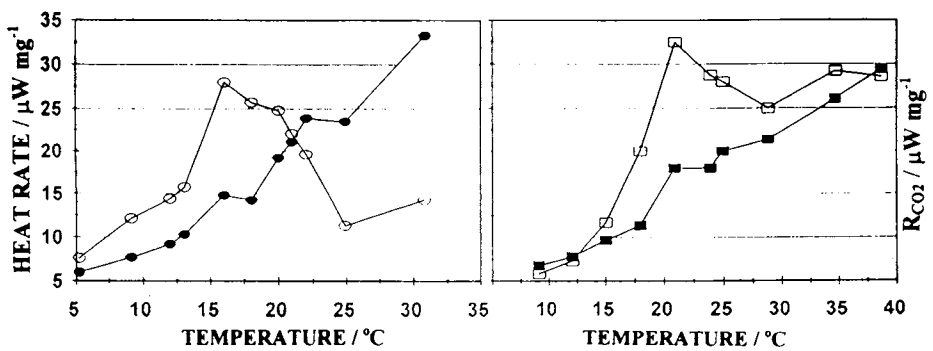

Figure 6. Variation of Φ and 455 R_{CO2} with temperature for cultivars of (a) cabbage, a cool-climate plant, and (b) tomato, a warm-climate plant. Differences in the temperature dependences of the heat and CO_2 rates lead to constantly changing substrate carbon conversion efficiencies of these plants as temperature changes. Specific growth rate is proportional to the difference between the curves for Φ and 455 R_{CO2}. At temperatures where $\Phi > 455\ R_{CO2}$, growth stops.

(Figure 6) [63]. Tomato and cabbage were selected to illustrate broad differences in the growth and respiration responses that occur among warm and cool climate species respectively. Strong agreement was obtained between measured growth rate for these species at different temperatures and growth rate predictions as a function of temperature based on measurement of the respiration parameters.

The ability to link measured physiological parameters and growth rate follows from a non-conventional, but precise definition of growth rate as the rate at which plants store chemical energy in structural biomass (i.e. $R_{SG}\Delta H_B$), the information obtained from calorimetry studies of plant metabolism. Such a definition conveys no information about plant growth habit, partitioning, etc., but is the best indication of total energetic costs for biosynthesis. This definition incorporates both rate and efficiency data into the model for describing plant response to temperature change.

A respiration-based description of temperature dependence demonstrates a novel rationale for the existence of a growth rate maximum in the mid-range of growth temperatures and growth rate changes observed at temperature extremes. Because the temperature responses of Φ and R_{CO2} are different, the substrate carbon conversion efficiency (ε, see equations 2 and 4) must change continuously with temperature and can exhibit either an increase or decrease with increasing temperature. Growth rates increase with temperature only as long as the product $R_{CO2}(\varepsilon/1\text{-}\varepsilon)$ increases as temperature increases. Growth rate decreases with increasing temperature when the efficiency function decreases faster than R_{CO2} increases. Thus, growth behavior can be explained without postulating reversible or irreversible inactivation of enzyme activities or membrane phase changes.

The study of cabbage and tomato [63] shows that in the range of temperature where $\Phi < 455R_{CO2}$, relative specific growth rates can be estimated from the difference between measured values of Φ and R_{CO2}. However, near both the lower and upper temperature limits for growth, curves of Φ vs. temperature and $455R_{CO2}$ vs. temperature cross, Φ becomes $>455R_{CO2}$, R_{SG} becomes negative and the rate of heat loss is greater than the available rate of energy production calculated for respiration of photosynthate with $\gamma_p = 0$. Figures 6a and 6b and Equations 1 and 2 show that inability of respiration to supply needed energy can be the primary cause of cessation of growth beyond these limits.

Unique conclusions arising from this study [63] include: (a) Respiration measurements, together with a physiological plant growth model, provide a non-empirical means for quantitative predictions of plant growth rate responses to temperature change; (b) demonstration that energy use efficiency changes continuously with temperature requires that growth rates depend not only on the

temperature dependence of metabolic rates but also of efficiencies, (c) variation of growth rates with temperature can be explained without invoking activation and inactivation of enzymes or changes in cellular structures, (d) the physiological basis for high- and low-temperature limits to plant growth is described, (e) physiological differences that define adaptability of plants to climatic temperature are described, (f) a re-evaluation of what can be implied by the term "plant temperature stress" is provided, and (g) respiration measurements can be used to identify plants suited to growth in selected environments.

3. APPLICATIONS

3.1. Introduction

In a 1994 lecture at a symposium on thermal analysis and calorimetry, Wadsö raised the question: "Microcalorimetric techniques for characterization of living cellular systems. Will there be any important practical applications?" [64] He concluded that microcalorimetric work in cell systems has resulted in important fundamental knowledge, but that there had not yet been any significant breakthrough from a practical application point of view. It was noted that potential applications had been illustrated by a large number of model experiments and that instruments and working procedures have been much improved; but realization of the apparent potential remains unmet. Wadsö suggested that multifunctional instruments combining calorimetry with specific sensors may provide the most probable route to specific practical applications.

Since this conclusion by Wadsö, developments of plant applications of calorimetry have moved forward significantly. Plant and agricultural sciences may be the first areas to fully implement important practical applications. However, as suggested by Wadsö, these applications will in most cases require combination of calorimetric and respirometric sensors. Currently, calorimetry in plant science remains poised between model applications and full practical application. Consideration of the examples discussed below shows that plant applications are expanding rapidly and are moving from the research laboratory scale to larger field applications. The major barrier to immediate implementation of some practical applications in agriculture is the current lack of calorimeters with large numbers of ampules capable of high sample throughput. The following survey is not intended to be a complete review, but rather to illustrate the many potential applications of calorimetry to plant physiology, ecology, and agriculture.

3.2. Growth rates and production

All agricultural crops have as an ultimate goal the harvest of biomass. In some cases, total plant biomass or total, above-ground biomass is desired, in others more specific fractions are harvested. Whether total plant or some partitioned fraction is the desired product, better growth rates generally correlate with better yield. For example, the measurable parameter best correlated with maize yields is the total growth of the plants [65, 66]. Partitioning of biomass is important to yield, but poor growing plants have little to partition. This observation encourages continued development of calorimetric measurements, as these specifically measure properties related to plant growth. There have been no reports, to date, of calorimetric measurements of metabolic parameters related specifically to partitioning of biomass or to developmental processes such as fruit formation. It should be possible, however, to identify and study tissues involved in such processes. For example the metabolic properties of oil forming tissue must reflect the rate and chemical characteristics of the oil products. Plants that differ in oil production capabilities should be discernible by comparative calorimetric analysis of the tissues, offering an opportunity to use metabolic analysis to quantify production potential.

Results of calorimetric analyses of plant growth have emphasized the important roles of temperature on metabolic rates and efficiencies of plants. Selection of the correct match between plant and growth climate appears as important as all other physiological factors in determining plant growth properties. Identification of a plant with superior growth characteristics must always be framed in terms of growth climate. Anekonda et al. [67] showed that the fastest growing family of *Eucalyptus camadulensis* in plantings at Anderson CA is the slowest growing family in the plantings at Concord CA only 250 km away and with nearly identical average, but not the same fluctuations in, temperature. Normally, such conclusions can only be reached by long-term growth studies done at every planting location. Calorespirometry studies can be completed within a season on plants grown at a single location to allow identification and selection of plants matched to climate.

3.3. Taxonomy

Plant respiratory properties are stable genetic traits that differ among species and to a lesser extent within species. Measurements of properties such as metabolic heat rates, CO_2 rates, and energy efficiencies produce particular combinations of respiratory properties sufficiently unique to separate *Eucalyptus* species by canonical analysis of the respiratory variables [68-70]. Canonical discriminant analysis using the measured respiratory properties Φ, R_{CO2} , Φ/R_{CO2} , and μ_{Φ} and

the calculated properties R_{SG} (specific growth rate) and ε (carbon use efficiency) for 17 *Eucalyptus* species, shows distinct separation of species. Each of the species has a characteristic distribution of growth rates and range of temperatures in which it can grow. These are successfully predicted by the respiratory parameters.

The two largest subgenera of *Eucalyptus*, *Symphyomyrtus* and *Monocalyptus* are also well separated by canonical analysis of respiration properties (Figure 7) [70]. Species within the two subgenera differ significantly in their specific patterns of metabolic parameters and also differ in their responses to growth in exotic climates. This led Anekonda et al. [70] to speculate that the major differences in survival of the two subgenera are determined by the differences to metabolic rate responses to climate. Thus, metabolic properties may not only assist in taxonomic separation of the subgenera, but also help to account for differences in growth

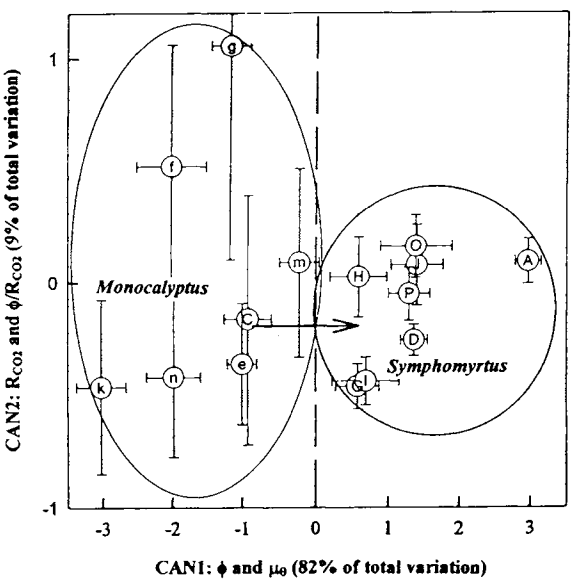

Figure 7. First and second canonical variables, CAN1 and CAN2, for respiration traits from 15 *Eucalyptus* species examined by canonical discriminant analysis. CAN1 is dominated by Φ and μ_Φ while CAN2 is influenced more by R_{CO2} and Φ/R_{CO2}. Each species has a distinct combination of respiratory parameters that gives rise to the separations shown. The dashed vertical line emphasizes the general separation of species in the two major *Eucalyptus* subgenera on the basis of the respiratory traits. Capital letters in this plot refer to *Symphomyrtus* species; small letters refer to *Monocalyptus* species.

properties. Further identification of *Eucalyptus* species by morphological differences is difficult in many instances and could be aided by calorespirometry.

3.4. Dormant or near dormant tissues, germination, and vernalization.

Studies of seed germination were the earliest focus of plant calorimetry. It is particularly simple to add water to seeds in a calorimeter ampule and measure the rate of heat production as a function of time to reflect germination and early growth processes. As noted earlier, Pierce [11] used pea seeds to demonstrate heat production during germination. Prat then demonstrated distinct patterns of thermogenesis in germinating seeds and examined the influence of physical, chemical, and biotic factors on the germination process [15, 16, 71]. He was the first to show that the measured heat rates could be correlated with rates of germination and vigor and, thus, defined plant properties of physiological significance.

With the increased sensitivity of calorimeters since Prat's early studies it has become possible to examine metabolic rates of "dry" (not hydrated) seeds. Though heat rates are low (a few μW per g), they are significant. Heat rates of non-hydrated seeds may be used as a measure of metabolic rates under storage conditions and has been used as an index of storage life of impatiens seeds and predictor of seedling vigor [72]. Isothermal studies on dry seeds may become a useful tool for monitoring seed storage.

The temperature dependence of germination has been used to study germinating soybean seeds [73] and to identify seeds from tomato plants that are capable of early spring germination [74]. Tomato cultivars that can be directly seeded into the field to initiate growth during cool spring temperatures are desired to extend the harvest and processing seasons for tomatoes. Comparisons of cold temperature germination of cultivars can be done by simply imbibing the seeds with water at a selected temperature (5 to 10 °C for tomato) and following the time course of heat rate increase thereafter. The correlation of heat production and germination allows putative identification of cultivars for early sowing. Combining seed studies with studies of the tomato seedlings allows further identification of cultivars that are early germinating and have good growth rates at the low temperatures of early spring.

Water plays a fundamental role in the storage longevity of seeds. Vertucci and coworkers [8, 75] used differential scanning calorimetry to examine the state of water in seeds and then to investigate glass transition behavior in bean seeds. Bean axes glass transition temperatures were dependent on water content. Correspondence of data from bean to models suggested that the intracellular glasses are composed of a complex sugar and water matrix. The data obtained so

far are not able to relate the implications of a glassy state to storage stability of seeds.

Many temperate zone plants require winter chilling for sufficient time and at low enough temperatures to fulfil the chilling requirements to break dormancy (vernalization) and achieve good production. For example, grape vines generally must be exposed to a period of winter chilling below about 7 °C to produce good yields the following season [76]. Lack of chilling results in low percent budbreak, lack of uniform shoot growth, and few clusters. Quantification of dormancy has been difficult. Isothermal calorimetric measurement of respiration appears to offer one means of monitoring the dormancy state of tissues and predicting when bud break and growth will occur. The methods allow direct measurements on the tissues to be used in judging dormancy states rather than relying on calculated models of time-temperature relations. This has several commercial applications in guiding addition of effectors such as hormones to prevent early budbreak or prepare growers to force dormancy breaking when necessary.

Gardea and coworkers [77] have shown that the pattern of respiratory changes during dormancy and development of Pinot Noir primary grape buds could be followed by calorimetry. Respiration decreased during endodormancy and increased during ecodormancy and as bud development progressed. Definition of the pattern of metabolic change was used to identify stages of budbreak and the progress of this process. Clark et al. [78] approached examination of dormant grape buds by thermal analysis to examine supercooling and seasonal cold hardiness. The results were suggestive of a relation between thermal analysis predicted hardiness and actual field hardiness, but more careful studies are needed to establish such a relation.

Both scanning and isothermal calorimetry have been used to examine vernalization of peach seeds [79]. A quantitative relation was established between vernalization time and seedling vigor measured as metabolic heat rates by isothermal calorimetry. In addition, scanning calorimetry showed a relation between vernalization time and high temperature sensitivity. Longer vernalization treatments gave greatly enhanced seedling vigor and lowered the maximum for high temperature stability.

3.5. Temperature dependence of plant growth

The spatial distribution of a plant species is limited by the adaptive range of climatic conditions of the species. Temperature is one of the most significant determinants of plant distribution, but except for lethal limits, little is known about physiological changes in response to differences in environmental temperature. Microcalorimetry has been used to examine temperature dependence

of plant metabolic rates over the normal environmental temperature range for selected annual and perennial plants [52]. Distinct differences were found in the metabolism of woody perennial plants from high latitudes and high elevations and closely related low-latitude and low-elevation plants [52]. Low-latitude and low-elevation woody perennials have Arrhenius temperature coefficients for metabolism that are larger than those for congeneric high-latitude and high-elevation plants. A simple function was developed relating Arrhenius temperature coefficients to latitude and elevation for accessions of three, woody perennial species complexes of plants collected from a wide geographic range. The difference in Arrhenius coefficients is maintained when plants are grown for years in a common garden, indicating that this is a genetically defined trait, rather than a difference due to acclimation to different climates. In general, plants that are adapted to growth in climates with large diurnal and seasonal temperature variation have temperature coefficients of metabolism that are smaller than those of plants native to climates with small temperature fluctuations. The temperature dependence of metabolism can thus serve as an indication of the range of climatic temperatures suitable for growth of a given plant.

A second important finding from these studies [52] was that Arrhenius plots of log metabolic heat rate vs. reciprocal absolute temperature for many plants within a species produces a family of lines with different slopes, but a common intersection temperature, i.e. all the genotypes measured have the same metabolic rate at a temperature (or narrow range of temperatures) referred to as the isokinetic temperature. The isokinetic temperatures measured so far all fall within the normal range of growth temperatures. The ranking of metabolic rates for the genotypes is reversed in going from one side to the other of the isokinetic temperature. To the extent that growth rate is proportional to metabolic rate, this also indicates a change in ranking of growth rates for plants grown at temperatures on either side of the isokinetic temperature. These findings offered the first insight into physiological properties measurable by calorimetry that could be used to provide information on optimum temperatures for growth of individual plants.

The relation between climate and temperature coefficients has been used as one criterion to guide planting of crops or selection of plants suitable for growth at select locations [52]. For example, studies of western yarrow have been carried out to help in range management [80]. western yarrow (Achillea millefolium) is widely distributed throughout many semiarid communities in the Intermountain Region of the USA and is currently used to restore disturbed sites, replace annual weeds, and reduce site degradation. Individual populations differ in adaptability, persistence and establishment. Studies were conducted to determine if respiratory

metabolism could be used to predict growth and survival among populations grown within a common garden. Growth performance and respiratory metabolism of eight populations were measured through two growing seasons. Relative specific growth rates and substrate carbon conversion efficiencies as functions of temperature were calculated from calorimetric measurement of heat rates and respiration rates. These calculations allow identification of optimal temperature conditions for growth of each of the western yarrow populations. This information is of potential value for selecting among western yarrow populations for revegetation projects.

3.6. Low and high temperature hardiness

The ability to rapidly measure high and low temperature tolerance limits for survival of plants has been a major objective for range extension of crop and ornamental plants. Non-calorimetric methods, mostly based on analysis of cell damage after a temperature stress event, are currently used for most estimates of small differences in survival at temperature extremes [81]. Among the early applications of calorimetry in examining plant temperature hardiness were DSC analyses of phase transitions. Chang et al. [82] studied thermotrophic properties of thermophilic, mesophilic and psychrophilic blue-green algae grown at high, room and low temperatures. Stability of these algae correlated with temperature of the endothermic denaturation peak related to biliprotein denaturation. Intact tissues of most plants do not show phase transitions in scanning calorimetry [83], but phase transitions in lipid preparations from plants are readily observed [84]. Lipids from cool climate crops are generally less saturated than those from warm climate crops and have correspondingly higher "melting temperatures". While this correlation holds well, differences among melting temperatures do not allow sufficiently fine discrimination among plants for selection of cold tolerant genotypes.

The procedures of Rank et al. [38] using a temperature cycling method based on isothermal measurements (outlined in 1.8.3 above) describes the time and temperature dependence of damage to the plant tissues at both high and low temperatures. The procedures, while producing a thorough description of plant inactivation and insight into inactivation processes, are slow and not suited to comparative analysis of large numbers of plants. Another calorimetric-based rationale has been developed for selection of low temperature tolerance. For many plants, stability at low temperature can be related to the ability to maintain a sufficient level of respiration at low temperature to overcome effects of degradative reactions such as photooxidation that damage plants at low temperatures. Plants that can maintain respiration at a low temperature are able to

repair such damage. With this rationale, metabolic heat rates at 3 to 5 °C have been used to rank cold tolerance of 16 species of *Eucalyptus*. The ranking obtained correlates well with the accepted cold stability rankings based on years of studies on these species. The calorimetic studies are relatively rapid, allowing calorimetry to be used to examine intra-species cold tolerance [85].

3.7. Stresses other than temperature

3.7.1. Salt

The effect of salinity stress on metabolic heat output of barley (*Hordeum vulgare*) root tip was measured by isothermal calorimetry [34]. Root tips were placed on moistened filter paper in a calorimeter ampule and isothermal heat rates measured. The roots were then flushed with salt solution in increasing increments and metabolic heat rates remeasured at each concentration. Barley root metabolism remained relatively constant as salt concentration was increased to a critical level at which heat rates dropped precipitously. Three barley varieties differing in tolerance to salinity were compared and differences quantified. Two levels of inhibition by increasing salt were found. Following the transition from the initial rate to the first level, inhibition remained at about 50% with further increases in salt concentration up to 150 mM. The concentration of salt required to inhibit to this level was cultivar dependent. At higher concentrations (>150mM) of salt, metabolism was further decreased. This decrease was not cultivar dependent. The decreased rate of metabolic heat output at the first transition could be correlated with decreases in uptake of NO_3^-, NH_4^+ and inorganic phosphate that occurred as the salt concentration was increased. The high degree of dependence of the inhibition of metabolic heat output on NaCl concentration points to a highly cooperative reaction responsible for the general inhibition of metabolism and nutrient uptake. Inhibition of root tip metabolism was not reversed by washing with salt free solutions.

Studies of salt inhibition of the halophilic shrub Kochia gave a different pattern of salt inhibition of metabolic rates [86]. Metabolic rates decreased nearly linearly with increased salt concentration. Possibly this response by the halophile reflects a continuous use of metabolic energy to pump out salt, as opposed to barley which may exclude salt until it is no longer successful and is injured.

Salt inhibition of *Chlorella* has also been studied by calorimetric methods by Loseva et al. [87]. Addition of low salt concentrations causes an increase in metabolic rate. The increased metabolic rate is not sufficient to offset energetic losses and growth rate of the *Chlorella* is reduced.

3.7.2. Methanol

Methanol at high application rates severely stresses plants and results in decreased growth rates or mortality. However, some reports suggest that at low concentrations, methanol may stimulate growth and enhance yields of many commercial crops by as much as 50 to 100% [88]. The initial reports of stimulation of yield by methanol have been difficult to duplicate. Many authors have discounted the initial results. Others have achieved small increases in yields under field conditions. No one has been able to repeat the initially reported large yield increases, identify why the results are not reproducible, or satisfactorily explain how methanol could act to cause increases. One problem with most studies to date is an inability to address the multiple variables that can influence response to methanol. It is virtually impossible to control and alter sufficient numbers of variables in field studies. Evaluation of the effects of changing variables in long term growth studies in controlled environments is possible, but analysis requires growth seasons to complete so that the large number of possible variables makes analysis difficult by growth yield procedures. Hemming et al. [89] developed calorimetric methods to examine short-term effects of methanol on metabolic heat rates and efficiencies. Metabolic rate measurements were used to calculate growth rates following exposure of plants to methanol under an array of conditions. Because these experiments required only a few hours rather than growth seasons to complete, a wide range of treatment and plant growth variables could be examined to determine whether appropriate conditions for methanol stimulation could be developed. This study showed that methanol at low concentration generally increases metabolic rate but decreases substrate carbon conversion of bell pepper. Only under very limited conditions was an increase in both metabolic rate and efficiency of methanol treated tissues noted.

3.8. Nutrient limitations

Nutrient limitations or imbalances stressing plant growth are reflected in metabolic rates and efficiencies. A multifactorial study by Hilt et al. [90] showed that radish seedling growth and respiration are extremely sensitive to both the absolute and relative concentrations of N, P, and K in environments with multiple nutrient limitations. Resource limitations on growth were reflected as changes in respiration measured as both metabolic heat rate and CO_2 rate. Limiting concentrations of the macronutrients N, P, and K cause increased CO_2 and metabolic heat rates, decreased efficiency, and a corresponding decrease in growth rates of the radish seedlings. The model of Hansen et al. [20] relating plant growth rates to respiration parameters was used to describe resource-limited growth rate.

3.9. Herbicide effects on plant metabolic properties

Suwanagul [91] developed microcalorimetric methods for early detection of weed resistance to herbicides by measurement of differences in metabolic responses between herbicide resistant and susceptible biotopes. Herbicides were applied to young weeds and, after appropriate times, metabolic heat rates of meristematic tissue was measured. Three weed species and three herbicides with different modes of action were examined: atrazine, metsulfuron-methyl and diclofop-methyl. Susceptible weed metabolic rates were inhibited at lower concentration of herbicides than the resistant biotopes. Calorimetry offered a rapid way to screen for resistant weed populations. Suwanagul concluded that early detection of weed resistance via calorimetry is an important tool for assisting farmers in dynamic managing of weed resistance.

3.10. Pathogens on plants

Lawrence and Yuen [92] developed isothermal microcalorimetric techniques to rapidly assess fungicide activity with a goal of screening for the presence of antifungal metabolites in plant extracts and microbial fermentation broths. Although not strictly plant calorimetric measurements, since the heat measured is generated by the fungi, this study is cited here to illustrate a promising method for examining properties of plant products by their effects on the metabolic heat rates of other organisms. Lawrence and Yuen used decreased metabolic heat rates in the presence of plant extracts and other substances as a measure of antifungal activity. The were able to measure fungicidal activities against the filamentous fungi *Pythium aphanidermatum* and *Pyricularia oryzae* in as little as 4 to 8 h with only nanogram quantities of inhibitors. These studies are analogous to the many studies published investigating antibiotic activities on microbial cultures [93, 94].

Cofie-Agblor et al. [29] have recently examined insect activity in stored wheat by isothermal calorimetry. They measured isothermal heat of respiration of *Cryptolestes ferrungineus* (Stephens) adults and larvae and interpreted the enhanced heat rates in insect contaminated wheat as an indication of insect levels. It appears that calorimetric assay of insects during feeding on plant materials may become a convenient means for identifying levels of activity and for studying effects of insecticide treatments on viability. Once again the major barrier to practical application of these methods appears to be the limited sample throughput with current calorimeters.

3.11. Forestry Applications

Forest products are important economic commodities. Demand for these products is increasing while availability is decreasing. Calorimetric methods have

the potential to identify trees capable of rapid biomass formation and therefore appear to be of use in restoring availability of wood and wood products. The studies reviewed here are aimed at this goal.

3.11.1. Larch

The first calorimetric studies of tree metabolic heat rates simply examined possible correlations between metabolic heat rate and growth rate of Larch (Larix larcina, Koch) [95]. Using small meristematic tissue sections from the growing branch tips, the results showed that (a) there is a wide variation of metabolic heat rates among larch clones, even among populations that have been selected for growth rate by traditional methods, (b) for some of the populations a correlation exists between measured metabolic rates and growth rate of trees in field test plots, and (c) in these populations, the metabolic rates could probably be used to select trees with potentially fast growth rates.

3.11.2. Redwood

The next calorimetric study of trees also searched for correlations between growth rate and metabolic heat rates, but began to address additional questions of tree age effects on measured metabolic rates [96]. Coast redwood (*Sequoia sempervirens*) was examined both as 60-day-old unrooted clones and as 25-year-old trees. Metabolic heat rates were linearly related to integrated growth rates of both the unrooted clones and the 25-year-old trees, though the proportionality coefficient differed for the different age classes of trees. It was proposed that dark metabolic heat rate is directly proportional to growth rate of redwoods under optimum conditions if the efficiency with which the photosynthate is converted into biomass is constant. If the efficiency is not constant, heat rate measurements are not a sufficient measure of growth rates, and measurements of both efficiency and metabolic rate are required to predict plant growth rate [96].

Redwood studies were extended to examine growth of trees collected from across the entire natural range for coast redwoods and growth in a single plantation [97]. This study initiated analysis of both heat rates and R_{CO2} as a first attempt to include efficiency determinations in the growth-metabolic rate relations. The relation between growth rate traits (height, basal diameter, stem volume, and branch diameter) and respiratory traits (Φ, R_{CO2} and Φ/R_{CO2}) was examined on a collection of 192 genotypes of coast redwoods. Height, basal diameter, and stem volume gave highly significant ($p< 0.001$) positive correlations with calorespirometrically measured metabolic traits. Combining the four growth traits and the three respiratory variables to give two canonical variates, one representing growth and one representing respiration, gives a strong

linear correlation (r = 0.85). These data suggest that simultaneous assay of multiple respiratory measures on juvenile trees can be used to predict their longer-term growth rates.

Respiratory rate properties of coast redwood were shown to differ systematically with the native growth site of individual clones. Redwoods collected from different parts of the native range and grown in a common garden-plantation differed in their responses to temperature. Scanning calorimetric analysis of metabolic activity from 10 to 55 °C showed the overall patterns of changing metabolism with temperature of 16 representative clones were generally similar for all the coast redwood tested. However, high temperature stability, as measured by the temperature of peak activity and the peak metabolic heat rate, differed substantially for samples from the five regions. This is shown in Figure 8 with the high temperature regions of Arrhenius plots of representative clones from each region. Plants from the warmer southern and inland portions of the range had higher temperatures for peak activity. Those from the northern portion of the range were more sensitive to the high temperatures. The high temperature at which activity began to decline was directly related to the native extreme high temperature. The practical value of these results is demonstration of the possibilities of scanning calorimetry for selection of clones likely to adapt to particular sites or defined ranges of sites. In a broader sense these results show the match between respiration properties and native growth climate and support a conclusion that this match is critical in determining growth range and survival.

Further analysis of adaptability of redwood to the range of natural habitat was performed by comparing heat rate and efficiency changes of coast redwood and giant sequoia (*Sequoiadendron giganteum*) as temperature is changed [98]. Coast redwood and giant sequoia currently have separate, relatively narrow native geographic distributions. Distinct differences exist in the climates to which these two species are adapted, i.e. coast redwood is native to a narrow range of coastal or near coastal locations with near uniform, moderate temperatures in northern California while giant sequoia survive in a similarly narrow range of Sierra mountain sites but with wide temperature variations. Measurement of the temperature dependencies of respiratory properties of plants from the two species allows description of the differences in temperature dependence of growth and thereby an insight into physiological features governing their differences in climatic adaptation. Simultaneous respiration rate measurements of Φ and R_{CO2} followed by calculation of efficiency and specific growth rates indicated that coast redwood do not grow at temperatures below about 10 °C. Both metabolic rate and efficiencies increase with increasing temperature above 10 °C and growth rate reaches a maximum near 25 °C. Near 35 °C, efficiency

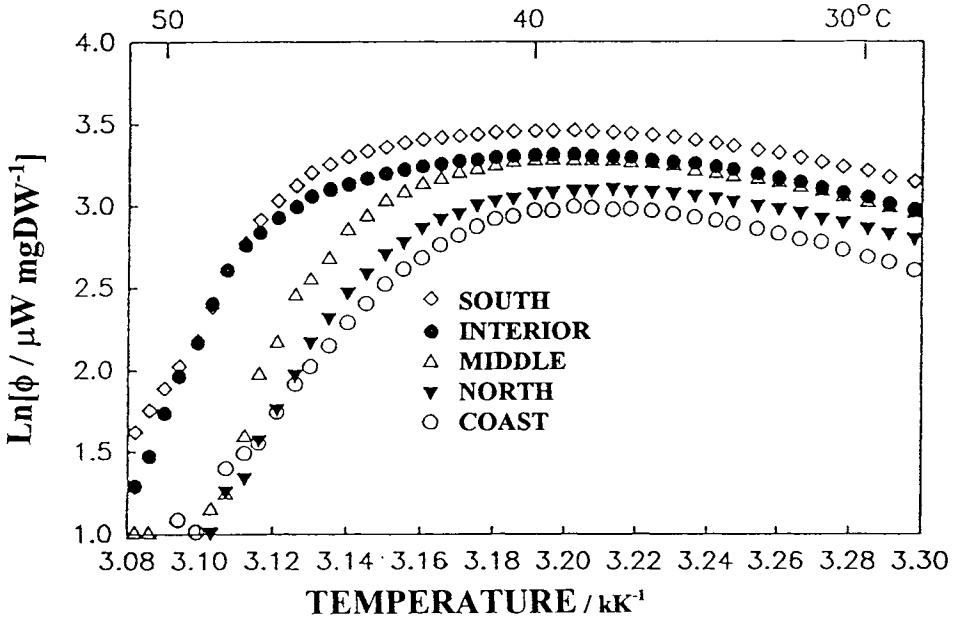

Figure 8. Scanning calorimetric analysis of tissue from coast redwood clones native to different regions of the redwood growth range, but grown in a common garden. An Arrhenius plot of metabolic heat rate vs. reciprocal temperature shows differences in sensitivity to high temperature parallel high temperatures in the native growth sites. South indicates plants from the southern end of the native growth range. Extreme high temperatures of native locations decrease systematically in the order south, interior, middle, north, and coast.

becomes zero and growth stops. Thus, respiration measurements and growth rate calculations indicate a range of growth between 10 and 35 °C for coast redwood.

In contrast, based on respiration measurements, giant sequoia is predicted to grow efficiently, albeit slowly, near 0 °C, increase rate and efficiency up to about 15 °C, decline in growth rate with higher temperatures, and stop growth above 21 °C. The growth rate vs. temperature patterns predicted from calorespirometry measurements indicate the distinct temperature responses of the two redwoods that are evident in their native growth environments.

Because the responses of metabolic properties to changing temperature reflect the differences in native growth climates of the coast and giant redwood, it is possible to measure metabolic properties of additional coast redwood and giant

sequoia ecotypes, identify intra-species variation in response to temperature, and infer climatic conditions most favorable for growth of each ecotype.

3.11.3. Eucalyptus

Many of the experiments on redwood have been repeated and extended in studies of *Eucalyptus*. The relation between respiratory physiology and growth rate of *Eucalyptus* and the effects of environment on this relation were studied by Criddle et al. [99, 100] for the purpose of developing means for accelerating and improving selection of trees for biomass production. The relations among biomass production, respiratory metabolism and growth temperature were determined in controlled environments. Three *Eucalyptus* clones were selected for this study because of known qualitative differences in their growth responses to temperature. These genotypes (clones) were grown in controlled environments at three temperatures. Measurements were made of growth rate, metabolic heat rate, and dark CO_2 production rate for plants grown at each of the three temperatures. This allowed determination of respiration rates of plants adapted during growth at three different temperatures and also determination of respiration changes resulting from rapid changes in temperature during short-term measurements of respiration rates. Metabolic heat rates and the temperature dependence of metabolic rate differed for plants adapted to growth at different temperatures, but relative order of clones remained the same. The metabolic rates measured for all three genotypes at three growth temperatures are linearly and positively correlated with measured biomass growth rates. Thus, relative growth rate performance in any environment can be predicted from a knowledge of respiratory parameters measured as a function of temperature for plants grown in a common environment.

Calorespirometry has also been used to examine relationships among measured plant growth and respiratory parameters, geographical origins, and growth climate [101, 102]. Twenty *Eucalyptus* species and 33 rapid-growing *E. camaldulensis* trees growing in common gardens were examined. Metabolic heat rate measurements were made at different temperatures by isothermal calorimetry and as a continuous function of temperature by differential scanning calorimetry in the range from 10 to 40 °C. The values of respiratory and growth variables of *Eucalyptus* species are significantly correlated with latitude and altitude of origin of their seed sources. The results show the maximum metabolic heat rate, the temperature of the maximum heat rate, the temperature coefficients of metabolic rate, and the temperatures at which the slopes of Arrhenius plots change are all genetically determined parameters that vary both within and among species. Since the mechanistic relation between respiration

and growth rates is known, determination of the growth rate - respiration rate - temperature relations guide understanding of differences in relative growth rates of *Eucalyptus* species and individual genotypes in different climates. The temperature dependence of respiration rates is a dominant factor determining relative growth rates of eucalypts in different climates. To achieve optimum biomass production, the values of temperature dependence of individual plants must be matched to growth climate.

Calorespirometry studies have also examined the use of respiration parameters in selection strategies for obtaining superior trees for breeding programs [102]. Respiratory and specific growth rate parameters of *Eucalyptus* were measured on poor and superior trees from 17 *Eucalyptus* species, all growing in a common garden. The results show the respiratory traits predict the known growth rates with a high degree of reliability. High heritability of the respiratory traits makes it possible to use these traits to select superior trees for breeding programs. Respiratory properties are useful for selection of superior taxonomic groups such as superior subgenera or superior species within subgenera or superior provenances within a species, or superior individuals within open-pollinated half-sib progenies to use in genetic improvement programs.

Respiratory parameters in species of eucalypts change with maturation state of the trees. Metabolic heat rates, CO_2 production rates, and temperature coefficient of heat rate all showed systematic changes with tree age. Therefore, maximizing economic returns also depends on understanding and quantifying the growth rate as a function of tree age.

3.11.4 Other trees

Poplars. Hybrid poplar clone growth rates have been correlated with tissue metabolic heat rates and CO_2 rates measured through an entire growing season. A general correlation was shown between increased Φ and R_{CO2} and increased growth rates of the clones. Also, plants with high Φ/R_{CO2} generally were poorer growers than those with low Φ/R_{CO2}. In spite of these general correlations, the data scatter was large and respiratory values were not highly useful for identifying clones with superior growth capabilities [103]. A major problem appears to be the marked differences in temperature responses among the clones. Calculated R_{SG} values for some clones indicated greatly enhanced growth rates at high temperatures while others became inefficient and slowed growth as temperature increased above about 20 °C. Since growth temperature fluctuated both diurnally and with season, there was a change in the relative growth rates of the clones. Identification of the best clones for growth will

require accurate analysis of metabolic properties and average kinetic temperatures for growth at each planting location.

Pines. Calorimetric studies of growth rates and temperature responses have not been employed to examine pine trees. Two studies were conducted to analyze effects of air pollutants on the respiration properties of Ponderosa and Jeffrey pine needles. Bower [104] used one-cm needle segments and demonstrated a correlation between the extent of ozone damage, measured as the number of lesions on the needles, and isothermal metabolic heat rates. He also measured increases in metabolic heat rates resulting from acid and nitrate deposition on the needles. Momen et al. [105] conducted a more controlled study of acid rain and ozone effects on Ponderosa pine with defined applications to plantation grown plants. In seedlings, metabolic heat rates increased in response to ozone and combinations of ozone and acid rain. Mature tree metabolic activities showed no response to ozone, acid, or combinations of the two. No studies were made to determine whether metabolic efficiencies were altered by these treatments. Thus the results show that calorimetry can be used to monitor pollutant effects on trees, but more definitive experiments must be done to identify how the observed responses relate to growth and survival of the trees.

3.12. Annual crops

Calorimetric studies are beginning to be used to evaluate growth properties of annual crop plants. Celery metabolic rates following cold treatment can be used as an index for bolting. Tomato metabolic rates at high temperature may be used as an indication of fruit production as high values of R_{SG} at elevated temperatures, determined from calorespirometric measurements, are commonly associated with poor fruit production. Tomato plants that are stressed and have poorer R_{SG} at high temperature shut down vine growth and have larger fruit yield [74]. This inverse relation between fruit production and vigorous vine growth at high temperature is well known from other observations. The advantage of calorimetry is in using young plants to rapidly identify the growth-temperature characteristics.

Lettuce has been studied in detail and will be used here to demonstrate the capabilities of calorimetry in helping to guide production of annual crops. To maintain a steady supply of commercial lettuce, plants are grown throughout the year at locations with different climates. For maximum yield, it is important to plant varieties with growth properties matched to the climates. This has been largely an empirical procedure. Fontana et al. [106] describe rapid metabolic rate measurements to identify suitable growth climates. Commercial lettuce

varieties were raised under common conditions in a greenhouse to allow comparison of their metabolic properties. Metabolic heat rates were examined over a wide range of temperatures. Each variety, although grown under common conditions, has distinct values of metabolic heat rate per mg tissue, distinct temperature dependence of metabolism, and cultivar specific maximum activity temperatures. Values of the metabolic parameters readily separate coastal from desert, winter from summer, and Romaine from iceberg varieties. Growth rate predictions based on metabolic parameters for individual varieties agree with available information on commercial yields and growth temperatures. A combination of metabolic rate measurements that define growth rate differences, and differences in the effects of temperature on growth rate can be used to rapidly identify and select lettuce varieties most suited to growth within a given climate. These methods provide opportunities for enhancing breeding programs for development of additional varieties for increased production.

3.13. Ecology and climate change

Widdows [107] and Reh [2] have reviewed plant calorimetry applications related to ecology. Most thermal studies related to ecology have measured heats of combustion of trees, pollen, stem, bark, etc., or have employed TGA to examine characteristics of plant constituents or isolated products [108]. DSC studies of plant properties have focused largely on physical properties of plant products, such as studies of lipid transitions [6] or of wood properties before and after fungal degradation [3-5]. Isothermal calorimetry studies in plant ecology have been largely directed at determination of microbial activities using various plant tissue sources as substrates.

Measurement of plant metabolic properties has the potential to contribute strongly to ecological studies in the future. It is hypothesized that inferences about species distributions and changes in species distributions can be drawn from knowledge of the effects of temperature on respiratory parameters. The hypothesis suggests calorespirometry can be used to study plant distribution and temperature linked responses of plants in the wild.

Little information is currently available on the physiological parameters that control plant distribution changes in response to temperature changes. Most studies of the effects of temperature on species distribution have focused on plant survival and reproductive ability when confronted with climatic temperature extremes and on the biochemistry of responses to extreme temperature events [109]. However, temperature affects plants in two ways. Extremes of temperature, either high or low, can kill or prevent reproduction.

This is well known and the process is well characterized, i.e. the effects of an extreme temperature event are reasonably predictable. What is much less appreciated and poorly characterized in ecology is the effect of small changes in temperature regimen on growth (competitive success) and reproduction (reproductive success) of plants even when extreme limits are not exceeded [110, 111].

Some studies [51-53, 102] strongly suggest that respiratory metabolism and climatic temperature regimen must be closely matched if a plant is to thrive. Other recent work leads to the postulate that there are "respiration ecotypes" with respiratory metabolism related to certain environmental variables just as there are often morphological ecotypes of a species in different environments. The observation that respiration rates of different ecotypes of a species are all approximately equal when measured at the mean growth temperature in the climate of origin [112] is evidence in support of this hypothesis. The correlations found between extreme temperatures and indications of changes in respiratory metabolism [47] are further support for this hypothesis. Also, the temperature dependence of metabolic heat rates measured in the dark is a physiological characteristic correlated with climatic temperature[50]. Fitness for growth in an environment requires an appropriate μ_{Φ} and μ_{CO2} for metabolism. Inappropriate temperature dependence is a major reason why plants adapted to geographic regions with narrow ranges of temperature fluctuation do not grow well in regions where larger fluctuations are experienced, even when temperature stability limits are not exceeded and average temperatures are the same [51].

μ_{Φ} and μ_{CO2} values for different ecotypes are often not the same nor are they necessarily equal to the nominal value of about 8 kK. Values differ widely within and among species. Some plants more than double their metabolic and growth rates with a ten degree change in temperature while others of the same species do not closely approach a doubling of rate. Thus, increasing average temperatures will have greater effects on some species and some ecotypes of each species than on others. Also, plants growing in most temperate climates are repeatedly exposed to high temperatures that stress growth, even when other environmental factors are near optimum [26]. Plant growth rates within and among species differ markedly in tolerance to high temperatures, and further differ in survivability following high temperature stresses. This again emphasizes that high temperatures and increasing average temperatures will affect ecotypes within a species differently. Metabolic ecotypes optimize growth within different temperature ranges within the species range of adaptation.

3.15. Molecular Biology

Seven calorespirometrically measurable respiratory traits and three calculated traits that define plant growth rates and adaptation to a given environment have been defined, Φ, R_{CO2}, Φ/R_{CO2} , R_{O2} , μ_{ϕ}, μ_{CO2}, the temperature of maximum metabolic rate, the temperature at which activity increase with temperature deviates from Arrhenius behavior and ε and R_{SG}. These are genetically controlled, heritable traits that can be selected in genetic crosses for growth improvement. The ten respiratory characteristics occur in specific, distinct combinations among different species and among different genotypes within a species. Since each respiratory parameter contributes uniquely to growth rate and temperature adaptation, a rationale for breeding programs to develop rapidly growing genotypes can be based on combination of appropriate respiratory characters. This provides a new rationale for rapid improvement of biomass production.

Much discussion has occurred regarding genetic engineering of plants for more rapid biomass production. However, there have been few candidate genes (quite possibly no viable proposals) suggested as targets for increased growth rates. The recent calorespirometric studies have made a start in narrowing the field in a search for possible gene sites that may be altered to increase rates by identification of distinct metabolic processes defining growth rate. Much remains to be done to further define reactions that are rate or energy use efficiency limiting within the ten identified metabolic processes defining growth rates before rational attempts at genetic engineering are possible. However with distinct, readily measurable, quantifiable traits related to growth rate in a given environment, it is now possible to initiate genetic analyses by RAPDS or similar techniques to begin molecular investigation of means for preparing truly superior plants.

References

[1] H. Lieth, Measurement of caloric values, In H. Lieth and R. Whittaker (Eds.) Primary productivity of the Biosphere, Springer-Verlag New York, 1975, p 119.

[2] U. Reh, Thermochim. Acta, 193 (1991) 107.

[3] U. Reh, G. Kraepelin and I. Lamprecht, Appl. Environ. Microbiol., 52 (1986) 1101.

[4] U. Reh, G. Kraepelin and U. Schulze, Differential scanning calorimetry in wood biodegradation studies. Sequence of white-rot and brown-rot decay. Int. Symp. Lignin Enzymic and Microbial Degradation. Paris, France Apr 23-24. Ed. INRA No.40, Paris, 1987.

[5] U. Reh, G. Kraepelin and I. Lamprecht, Thermochim. Acta, 119 (1987) 143.
[6] J.M. Lyons, J.K. Raison and P.L Steponkus,. The plant membrane in response to low temperature: an overview, in J.M. Lyons, D. Graham, and J.R. Raisons (Eds.) Low Temperature Stress in Crop Plants: The Role of the Membrane, Academic Press, New York, 1979, pp. 1.
[7] J.K. Raisons and G.R. Orr, Plant Physiology 81 (1986) 807.
[8] C.W. Vertucci, Biophys. J., 58 (1990) 1463.
[9] N.R. Chiariello, H.A. Mooney and K. Williams, Growth, carbon allocation and cost of plant tissues, in R.W. Pearcy, J.R. Ehleringer, H.A. Mooney and P.W. Rundel (Eds.) Plant Physiological Ecology, Chapman and Hall, London, (1989) p. 327.
[10] A. Raemy and P. Lambelet, Thermochim. Acta, 193 (1991) 417.
[11] G.J. Pierce, Botanical Gazette, 46 (1908) 193.
[12] J.L. Magee, T.W. Dewitt, , E.C. Smith, and G.J. Daniels, J. Am. Chem. Soc., 61 (1939) 3529.
[13] V. Ye. Petrov, A. Ju. Alyabyev, N.L. Loseva, G.S. Klementyeva and V.I. Tribunskih, Thermochim. Acta, 251 (1995) 351.
[14] P. Johansson, Microcalorimetric Methhods for Studies of Photosynthesis, Abstracts 51st Calorimetry Conference, University of British Columbia, Vancouver, British Columbia, Canada, Aug 4-9, 1996.
[15] H. Prat. Bot. Rev., 14 (1948) 603.
[16] H. Prat, Calorimetry of higher organisms. In H.D. Brown (Ed.) Biochemical Calorimetry, Academic Press, New York, 1969, p. 181.
[17] R.S. Criddle, R.W. Breidenbach, E.A. Lewis, D.J. Eatough, and L.D. Hansen, Plant, Cell and Environ., 11 (1988) 695.
[18] R.S. Criddle, R.W. Breidenbach and L.D. Hansen, Thermochim. Acta, 193 (1991) 67.
[19] L.D. Hansen and R.S. Criddle, Thermochim. Acta, 160 (1990) 173.
[20] L.D. Hansen, M.S. Hopkin, D.R. Rank,. T.S. Anekonda, R.W. Breidenbach and R.S. Criddle, Planta, 194 (1994) 77.
[21] R.S. Criddle, A.J. Fontana, D.R. Rank, D. Paige, L.D. Hansen and R.W. Breidenbach, Anal. Biochem., 194 (1991) 413.
[22] A.J. Fontana, K.L. Hilt, D. Paige, L.D. Hansen and R.S. Criddle, Thermochim. Acta, 258 (1995) 1.
[23] A.E. Beezer, Biological Microcalorimetry, Academic Press, London, 1980, pp. 483.
[24] C. Spink and I. Wadso, Calorimetry as an Analytical Tool, in D. Glick (ed.) Methods of Biochemical Analysis. 23, 1976, p. 1.
[25] U. von Stockar and I.W. Marison, Thermochim. Acta, 229 (1993) 157.

[26] L.D. Hansen, M.S. Hopkin, D.K. Taylor, T.S. Anekonda, D.R. Rank, R.W. Breidenbach, and R.S. Criddle Thermochim. Acta, 250 (1994) 215.
[27] L.E. Erickson in Thermal and Energetic Studies of Cellular Biological Systems, Wright, Bristol 1987 p14.
[28] B.N. Smith, C.M. Lytle, L.D. Hansen and R.S Criddle, Am. J. Botany, 79 (1992) 107.
[29] W.E. Cofie-Agblor, Q. Muir, Q. Zhang, and R. N. Sinha, Can. Agricultural Engineering, 38 (1996) 37.
[30] E. Iversen, E. Wilhelmsen and R.S. Criddle, J. Food Sci., 54 (1989) 1246.
[31] B.N. Smith, R.S. Criddle and L.D. Hansen, Metabolic heat and respiratory substrate changes in aging potato slices, in A.H.C. Huan and L. Tiaz (Eds) Molecular Approaches to Compartmentalization and Metabolic Regulation, Proc. 14th Annual Riverside Symposium in Plant Physiology. Jan 10-13, 1991.
[32] R.S. Criddle and L.D. Hansen, Unpublished observations.
[33] D.J.B. Hemming, Calorimetric studies of plant respiration: Three applications of a thermodynamic model. M.S. Thesis Brigham Young University, Provo UT (1995).
[34] R.S. Criddle, L.D. Hansen, R.W. Breidenbach, M.R. Ward and R.C. Huffaker, Plant Physiology, 90 (1989) 53.
[35] R.S. Criddle and L.D. Hansen, J. Plant Physiology, 138 (1991) 376.
[36] T.S. Anekonda, R.S. Criddle, R.W. Breidenbach, W.J. Libby and L.D. Hansen, Plant, Cell and Environment, 17 (1994) 97.
[37] L.D. Hansen, Pharmaceutical Tech., 20 (1996) 64.
[38] D.R. Rank, R.W. Breidenbach, A.J. Fontana, L.D. Hansen and R.S. Criddle, Planta, 185 (1991) 576.
[39] R.S. Criddle, R.W. Breidenbach, A.J. Fontana and L.D. Hansen, Thermochimica Acta, 226 (1993) 147.
[40] D.D.Wagman, W.H. Evans, V.B. Parker, R.H. Schumm, I. Halow, S.M. Churney and R.L. Nuttall, The NBS tables of chemical thermodynamic properties. J.Phys. Chem. Ref. Data, 11, Suppl. 2, (1982) pp 392.
[41] E. Gnaiger, The twin-flow microrespirometer and simultaneous calorimetry, in E. Gnaiger and H. Forstner (Eds.) Polarographic Oxygen Sensors: Aquatic and Physiological Applications, Springer, Berlin (1983) 134.
[42] U. von Stockar and B. Birou, Biotechnol. Bioeng., 34 (1989) 86.
[43] E. Gnaiger, J.M. Shick and J. Widdows, Metabolic microcalorimetry and respirometry of aquatic animals, in, C.R. Butler and P.J. Bridges (Eds.), Techniques in comparative Respiratory Physiology: An Experimental

Approach, Society for Experimental Biology Seminar Series, Cambridge University Press Cambridge, MA, (1988) p. 113.
[44] P.C. Anderson and R.E. Lovrien, Anal. Biochem., 100 (1979) 77.
[45] P.C. Anderson, R.E. Lovrien and M.L. Brenner, Planta, 151 (1981) 499.
[46] P. Backman, R.W. Breidenbach, P. Johansson, and I. Wadso, Thermochim. Acta, 251 (1995) 323.
[47] A.J. Fontana, L.D. Hansen, R.W. Breidenbach and R.S. Criddle, Thermochim. Acta, 172 (1990) 105.
[48] Vidaver, W. Symp. Soc. Exp. Biol., 26 (1972) 159.
[49] J.D. Loike, S.C. Silverstein and J.M. Sturtevant, Proc. N. Acad. Sci. U.S.A., 78 (1981) 5958.
[50] S.A. Douglass, K.A. Hilt, L.D. Hansen, D.B.J. Hemming, A. Gardea, and R.S. Criddle, Unpublished observations.
[51] T.S. Anekonda, R.S. Criddle, W.J. Libby and L.D. Hansen, Can. J. For. Res., 23 (1994) 1793.
[52] R.S. Criddle, M.S. Hopkin, E.D. McArthur and L. D. Hansen, Plant, Cell & Environment, 17 (1994) 233.
[53] A.J. Fontana, J.M. Lyons, L.D. Hansen, E. Wilhelmsen, M. Mulanax, A. Louie and R.S. Criddle, Submitted..
[54] L.D. Hansen and R.S. Criddle, Thermochim. Acta 154 (1989) 81.
[55] E. Nevo, A. Ordentlich, A. Beiles and I. Raskin, Theroetical and Appl. Genet., 84 (1992) 958.
[56] A. Ordentlich, R.S. Linzer and I. Raskin, Plant Physiol., 97 (1991) 1545.
[57] M. R. Moynihan, A. Ordentlich and I. Raskin, Plant Physiol., 108 (1995) 995.
[58] M.Saxon, W.R. Breidenbach, L.D. Hansen, and R.S. Criddle, The role of heat generated by the alternative pathway in non-thermogenic plants. Submitted.
[59] H. Skubatz and B.J.D. Meeuse, J. Exp. Botany, 44 (1993) 493.
[60] H. Skubatz, W. Tang and B.J.D. Meeuse, J. Exp. Botany, 44 (1993) 489.
[61] J.S. Amthor, Respiration and Crop Productivity, Springer-Verlag, New York (1989) pp. 216.
[62] J.H.M. Thornley and I.R. Johnson, Plant and crop Modeling: A Mathematical Approach to Plant and Crop Physiology, Oxford University Press, Oxford, 1990 pp. 669.
[63] R. S. Criddle, B.N. Smith and L.D. Hansen, Planta, (1997) in press.
[64] Wadso, I, Thermochim. Acta, 269 (1995) 337.
[65] M. Tollenaar and A. Aquilera, Agron. J., 84 (1992) 536.
[66] M. Tollenaar, Crop Science , 29 (1989) 1365.

[67] T.S. Anekonda, , L. D. Hansen, H. Tong, J.F. Church, F.T. Ledig and R.S. Criddle, Respiration parameters determine growth traits in Eucalyptus: Effects of growth climate. Submitted.
[68] T.S. Anekonda, R.S. Criddle, M. Bacca and L.D. Hansen, Respiration-based selection strategies for breeding superior eucalypts and prediction of biomass quality using microcalorimetry. in Eucalypt Plantations: Improving Fiber Yield and Quality. CRC-IUFRO Conference, Hobart Australia, 1995.
[69] R.S. Criddle, A.J. Anekonda, R.W. Breidenbach and L.D. Hansen, Thermochimica Acta, 251 (1995) 335.
[70] T.S. Anekonda, R.S. Criddle, M. Bacca and L.D. Hansen, Experimental Evidence for contrasting adaptation of two *Eucalyptus* subgenera and their association with respiratory differencese. Submitted.
[71] H. Prat, Microcalorimetric studies of germinations of cereals, Can. J. Bot., 30 (1952) 379.
[72] A.J. Fontana, L.D. Hansen, and R.S. Criddle, Unpublished observations.
[73] B. Wade, R. Mullen, and P. Ackerman, Iowa Seed Science II, (1989) 2-4.
[74] A.J. Fontana and R.S. Criddle, Unpublished observations (1996).
[75] O. Leprince and C. Walters-Vertucci, Plant Physiol., 109 (1995) 1471.
[76] M.N. Westwood, Temperate-Zone Pomology. Revised edition, Timber Press. Portland OR, 1988, 428 pp.
[77] A.A. Gardea, Y.M. Moreno, A.N. Azarenko, L.D. Daley and R.S. Criddle, J. Am. Soc. Hort. Sci., 119 (1994) 756.
[78] H.R., Clark, T.K. Wolf and M.K. Warren, Hort. Science, 31 (1996) 79.
[79] A.N. Azarenko, personal communication.
[80] T. A. Monaco, S.B. Monsen, B.N. Smith, L.D. Hansen and L. Cluff, Dark respiration-growth-temperature relations among eight populations of western Yarrow (Achillea millefolium) growing in a common garden. Submitted.
[81] S.T. Dexter, Adv. Agron. 8 (1956) 203.
[82] C.H. Chang and D.S. Berns, Plant Physiol., 66 (1980) 59.
[83] L.D. Hansen, M. Afzal, R.W. Breidenbach, and R.S. Criddle, Planta, 195 (1994) 1.
[84] J.M. Lyons, D. Graham and J.K. Raisons, Low Temperature Stress in Crop Plants: The Role of the Membrane, Academic Press. New York, 1979 pp. 565.
[85] T.S. Anekonda, unpublished observations.

[86] A.H. Belal, A.M. Rammah, M.S. Hopkin and L.D. Hansen, in H. Lieth and A. Al Masoon (Eds.), Towards the Rational Use of High Salinity Tolerant Plants, Vol. 2, Dortrecht, Holland 1993, p. 213.
[87] N.L. Loseva, A.J. Alyabyev, G.C. Rachimova and R.I. Estrina, Thermochim. Acta 251 (1995) 357.
[88] A.M. Nonomura and A.A. Benson, Proc. N. Acad. Sci. USA, 87 (1992) 9794.
[89] D.J.B Hemming, R.S. Criddle and L.D. Hansen, J. Plant Physiol., 146 (1995) 193.
[90] K.L. Hilt, D.R. Rank, M.A. Cheney, A.J. Fontana, L.D. Hansen and R.S.Criddle, Effects of limiting N, P, and K on the relation between growth and respiration of radish seedlings. Submitted.
[91] D. Suwanagul, Early Detection of weed resistance: Pattern-thinking and rapid microcalorimetric analysis. PhD. Thesis, Oregon State University, Corvallis OR, 1995.
[92] E.B. Lawrence and H.K. Yuen, Plant Dis., 79 (1995) 605.
[93] B.Z. Chowdhry, A.E. Beezer and E.J. Greenhow, Talanta, 30 (1983) 209.
[94] A.E. Beezer, J.C. Mitchell, R.M. Colegate, D.J. Scally, L.J. Twyman and R.J. Willson, Thermochim. Acta, 250 (1995) 277.
[95] L.D. Hansen, E.A. Lewis, D.J. Eatough, D.P. Fowler and R.S. Criddle, Can. J. Forest Res., 19 (1989) 606.
[96] L.D. Hansen, R.A. Woodward, R.W. Breidenbach and R.S. Criddle. Thermochim. Acta, 211 (1993) 21.
[97] T.S. Anekonda, R.S. Criddle, W.J. Libby, R.W. Breidenbach, and L.D. Hansen, Plant, Cell and Environment, 17 (1994) 197.
[98] Criddle, R.S., Church, J.N., Anekonda, T.S. and Hansen, L.D. Influence of temperature on the growth rates of *Sequoia sempervirens* and *Sequoiadendron giganteum*. Submitted.
[99] R.S. Criddle, R.W. Breidenbach, A.J. Fontana, J-M. Henry, B.N. Smith and L.D. Hansen, Russian J. Plant Physiology, 43 (1996) 698.
[100] R.S. Criddle, T.S. Anekonda, L.D. Hansen, R.M. Sachs, R.W. Breidenbach, and L.D. Hansen, Can. J. For.Res., 26 (1996) 1569.
[101] T.S. Anekonda, L.D. Hansen, M. Bacca and R.S. Criddle, Can. J. For Res. 26 (1996) 1556.
[102] Anekonda, T.S., Criddle, R.S. and Hansen, L.D. New methods for early selection and development of plant genotypes for rapid biomass

production. Bioenergy 94, Using Biofuels for a Better Environment. Western Regional Biomass Energy Program, Reno NV, 1995.
[103] R.W. Breidenbach, personal communication.
[104] K. Bower, Calorimetric determination of the impact of air pollution on pine trees. Ph.D. Dissertation, University of California, Davis CA. (1990).
[105] B. Momen, J.A. Helms, and R.S. Criddle, Plant Cell and Environment, 19 (1996) 47.
[106] A.J. Fontana, J.M. Lyons, L.D. Hansen, E. Wilhelmsen, M. Mulanax, A. Louie, and R.S. Criddle. Submitted.
[107] J. Widdows, Applications of calorimetric methods in ecological studies, in A.M. James (Ed.) Thermal and energetic studies of cellular biological systems. Wright, Bristol, 1987, 182.
[108] J.A. Caballero, R. Font, and A. Marcilla, Thermochimica Acta, 276 (1996) 57-77.
[109] N. Smirnoff, Metabolic Flexibility in Relation to the Environment, (in) Environment and Plant Metabolism, Flexibility and Acclimation, N. Smirnoff (ed.) Bios Scientific Publishers, Oxford, 1995, p. 1.
[110] R.C. Leegood, Effects of Temperature on Photosynthesis and Photorespiration, (in) Environment and Plant Metabolism, Flexibility and Acclimation, N. Smirnoff (ed.) Bios Scientific Publishers, Oxford, 1995, p. 45.
[111] J.J. Burke, Enzyme Adaptation to Temperature, (in) Environment and Plant Metabolism, Flexibility and Acclimation, N. Smirnoff (ed.) Bios Scientific Publishers, Oxford (1995), p. 63.
[112] D.E. Collier, Can. J. Botany, 74 (1996) 317.

This Page Intentionally Left Blank

Handbook of Thermal Analysis and Calorimetry. Vol. 4: From Macromolecules to Man.
R.B. Kemp, editor.

Chapter 14

WOOD

H. G. Wiedemann[a] and I. Lamprecht[b]

[a]Mettler-Toledo GmbH, Sonnenbergstrasse 74, CH-8603 Schwerzenbach, Switzerland
[b]Institut für Biophysik, Freie Universität Berlin, Thielallee 63, D-14195 Berlin, Germany

1. INTRODUCTION

Since the awakening of mankind wood has played an ever increasing role in daily life. With the "taming and domestication" of fire at the very beginning of the energetic evolution and civilization of man the first direct heat source besides the sun was adapted for human life giving chance to conquer otherwise not habitable regions of the Earth. Wood to construct shelters for the night and fences against wild animals supported this development. Wooden tools and weapons facilitated hunting and harvesting, simple furniture made life easier. Drugs from plants, shrubs and trees cured diseases or transposed into magic states during shamanic activities and tied connections to demons or gods. Trees became animate beings and homes of divine creatures as shown in many of the botanical names. Bark, bast and other parts of the tree served as sources of early paper production enabling the written tradition of history or connection between different people. Well sounding pieces of beaten wood or flutes made from whole branches were the first music instruments used by our ancestors long ago. In the romantic periods of previous centuries deep sentiments towards trees and forests developed, from anxiety in the gloomy pine and spruce preserves to religious admiration in the light-flooded assembles of beeches and oaks. In modern times of increasing influence of plastic material wood experiences a special esteem in house construction, inside decoration and furniture or accessories. The present chapter deals with some of the thermoanalytical aspects of wood application in our daily life.

2. CHARACTERISTICS OF WOOD

Wood is a strongly anisotropic, multicomponent, molecularly non-homogeneous material whose components exist in continuous separate intermingling structures [1]. Its main entities are three polymers: (i) 40 to 50 % cellulose exclusively constructed of glucose units; (ii) 20 to 30 % hemicellulose with xylose, mannose, glucose, galactose and arabinose as sugar subunits; and (iii) 20 to 30 % resin like lignin. To present one example more precisely, the data for the balsam fir (*Abies balsamea*) are the following: 49.4 % alpha-cellulose, 15.4 % hemicellulose, 27.7 % lignin, 1.5 % acetyl, 0.5 % ash and 4.6 % extractives [1]. Moreover, wood contains an extraordinary diversity of substances such as fats, fatty acids, resin acids, waxes, tannins, phlobaphenes, colouring matters, gums and others in changing quantities. The general elementary composition is: 52 % carbon, 41 % oxygen, 6 % hydrogen and 1 % ashes [2].

Wood has a triple function in the life of a tree. It serves (i) as a structural element to guarantee stability and rigidity; (ii) as a hydrosystem to transport water and essential elements from roots to branches and leaves; and (iii) as a storage tissue for reserve substances, surplus elements like calcium and silicon, or for special heartwood compounds such as colour molecules, resins or tannins with pest control abilities. The heartwood centre of a tree is characterized by dead cells, while the sapwood of the outer parts of a trunk contains the "living" parenchymal wood of the tree. This is the region of the secondary growth in thickness with its typical seasonal fluctuations leading to the well-known annual rings of early and late wood. The transition from the inner, dead heartwood to the outer, living sapwood is not a process of slow dying, but an active process with mobilization of reserve substances in the heartwood and deposition of tannins and the mentioned surplus elements instead of them.

The dead tertiary outward tissue of the tree is formed by the bark. Its thickness together with incorporated tannins and phlobaphenes - responsible for the darker colour of this part - offer an effective protection against fungi and parasitic insects. Moreover, bark increases the survival chances of trees in wildland fires since it is hardly flammable and almost not combustible.

The interest in wood as fuel is small in industrial communities, while in poor or developing countries no real alternatives for wood exist [3]. A first worldwide investigation of energy consumption led to the great surprise that families relying exclusively on wood for all needs of daily life use as much as 3 to 4 t annually. In their global statistics about woodfuel consumption, the Food and Agricultural Organization (FAO) determined that the demand for wood as an energy source is at least as high as that for all other purposes together: about 10^9 t per year [4]. Thus, wood is a very important source of energy exceeding that of nuclear and hydro

plants [3]. Although wood contributes only 1 % to the fuel consumption of industrial countries, there it plays an important role as the source for the production of paper, furniture, cellulose and other products. About one ton of dry wood is used per capita and year.

More detailed information about wood may be found in specialised monographs [5-8] or textbooks of plant biology [9,10].

3. INVESTIGATIONS ON WOOD

Due to its importance in many fields of engineering and industry, wood is investigated by a broad spectrum of different methods, including all kinds of chemical analysis and chemical decomposition into its main components hemicellulose, cellulose and lignin, many physical procedures and some microbiological tests. They will be cited - if necessary - in connection with the presentation of thermoanalytical results.

Although wood in general is a dead and living tissue at the same time with active metabolism in the parenchymal region of bast between sapwood and bark and although isothermal microcalorimetric experiments are possible on such specimens (see below), we will concentrate on thermoanalytical investigations under a programmed temperature control in this chapter. Experiments to "quantitatively compare apples and oranges" [11] or to determine the growth abilities of clones of larch [12] or coast redwood [13,14] are left for Chapter 10 "Calorimetric Methods for Studies of Plant Energetics" in this Handbook.

Differential Thermal Analysis (DTA), Differential Scanning Calorimetry (DSC), Thermomechanical Analysis (TMA) and Thermogravimetry (TG; including Derivative Thermogravimetry DTG) - sometimes coupled with Mass Spectrometry (MS) or Fourier Transform Infrared Spectrometry (FTIR) - were introduced into this field of research mainly after the Second World War (see Volume I for technical details). The literature from these early days was compiled in some reviews [15-17]. In the well-known monographs "Differential Thermal Analysis" of Mackenzie [18,19], two chapters are connected with wood: That of Mitchell's and Birnie's [20] broad survey of "Biological Materials" with investigations on roots and leaves and thermal analyses of pine needles (*Pinus contorta*), and Tang's [21] contribution to "Forest Products" with historical data and own experiments. He states that "...published work has not as yet fully explored the capability of thermoanalytical techniques in forest-product research". Although the number of papers dealing with all the different questions of wood properties and reactions has increased considerably we do believe that his statement is still correct, perhaps not as severe as twenty five years ago. Tang points

to the fact that thermoanalytical methods could be used to investigate processes in forestry connected with (i) formation and decomposition reactions; (ii) growth and decay of wood; (iii) gain or loss of moisture, gases or volatiles during pyrolysis; and (iv) absorption or evolution of heat, all these processes as function of the experimental temperature (programme) [21].

4. PYROLYSIS OF WOOD

Pyrolysis - the thermal decomposition of a chosen substance - is essential in most wood analyses. Combustion of wood and of its components, cellulose and lignin, begins with pyrolysis which creates gases and vapours (volatiles) and a solid residue called char, especially charcoal. These volatiles burn with a flame when oxygen is present, while char burns by glowing without a flame. Therefore, cellulose and hemicellulose stimulate a flaming combustion as they are mainly decomposed to volatiles, while char originates from lignin [2]. The volatile compounds in wood, often called extractives, are chemical substances formed during a tree's metabolism. They include sugars, fats, amino acids and a myriad of aromatic compounds [22]. In an early paper Domanský and Rendos investigated the pyrolysis of different kinds of woods under nitrogen by means of DTA and compared the thermograms with those of the components cellulose, hemicellulose and lignin [23]. Wood exhibited a small endothermic effect between 100 and 170°C with a peak at 119°C and a more pronounced exothermic one above 215°C with a maximum around 270°C.

A combination of TG and FTIR was applied during oxidative pyrolysis with and without catalytic potassium to investigate the volatile products of cottonwood (*Populus trichocarpa*) heated up to around 480°C [24,25]. Main volatile products included water, formic and acetic acid and methanol. Further TG and TG/FTIR experiments of Richards and coworkers - mainly with cottonwood - concerned the influence of iron on the gasification of chars [26], of other metal ions on ignition and combustion of sapwood [27], on the pyrolysis of newsprint and biomass [28] and on gasification of cellulosic chars [29,30]. A similar technique was applied on aspen poplar wood (*Populus tremuloides*) to determine the dehydration and condensation reactions under nitrogen during pyrolysis of hemicellulose (near 230°C) and of cellulose and lignin (between 350 and 420°C) [31]. The obtained recondensed material showed a polyaromatic nature and was not volatile below 420°C and only partly up to 700°C.

Arima [32-34] performed simultaneous TG and DSC investigations on the thermal decomposition of various tropical soft- and hardwoods in air and in nitrogen. Under air, two main exothermic peaks and an exothermic shoulder were ob-

served while nitrogen exposure caused two endothermic peaks [32]. Holocellulose showed similar thermograms to those of wood while lintercellulose, some other types of cellulose, hemicellulose and lignin exhibited specific endothermic and exothermic peaks depending upon preparation and experimental conditions [33,34].

Decomposition of Western Larch (*Larix occidentalis*), Douglas-Fir (*Pseudotsuga menziesii*), Ponderosa Pine needles (*Pinus ponderosa*) and foliage from gallbery (*Ilex glabra*) was investigated by TG and DTG [35]. All four samples showed unusual, strong peaks from unknown combustible volatiles. In the first one arabinogalactan could be determined as the source of a peak between 325 and 350°C, while suberin became active in fir bark above 400°C and cutin in the same temperature range in pine and gallbery. The water-soluble hemicellulose arabinogalactan is associated with cell walls and forms an abundant component in larch. It totals up to 35 % in the heartwood of some species. Suberin is found in large quantities in the cork of Douglas-fir bark. It is a complex polymer of hydroxy fatty acids esterified to phenolic acids. Cutin - an almost exclusive polymer of hydroxy fatty acids - is the main compound in cuticular membranes of pine and gallbery. As the authors point out, it is essential to have a sound knowledge about such compounds because they are important for the prediction and control of wildland fires which are an integral part in the life of native ecosystems [35].

Stems and leaves of the Chilean *Euphorbia copiapina* were analyzed by means of TG, DSC and combustion calorimetry to evaluate their quality as a source of botanochemical compounds and fuels, using various zeolitic catalysts [36]. The applied catalysts shifted the pyrolysis to mixtures with interest as fuels and industrial chemicals.

Cozzani and coworkers published a series of papers concerning the pyrolysis of refuse-derived fuel (RDF) by means of TG, DSC and a laboratory-scale fixed bed reactor [37-39]. The commercial pelletized RDF had a portion of 65 to 70 % paper and board, 14 to 16 % plastic film and 4 to 6 % wood, rubber and leather and could be characterized by the following primary reacting species: cellulose (53%), lignin (14 %), hemicellulose (1 %), polyethylene (20 %) and inerts (20 %). Thus, three "key components" had a crucial influence on pyrolysis behaviour: paper and cardboard, plastics and wood-like materials. The authors found that the interactions between the key components of RDF are negligible, results similar to those of Arseneau [1] published earlier. Some limitations to these ideas are given by Back and Johanson [40,41] who point out that interactions between the lignin and hemicellulose/cellulose components may be possible since at the same time radical initiated and inhibiting reactions take place upon heating. In this way lignin could act as a radical scavenger for cellulose and hemicellulose radicals. Nevertheless, in a first approximation the overall behaviour of pyrolysis can be

considered as the sum of the individual contributions and these may enter a kinetic model of pyrolysis in a weighted portion [37]. In an additional paper a direct TG analysis was presented to determine the content of cellulose and lignin in biomass [42]. It could be shown that larger errors might be introduced into the results if xylans are used as substitute materials for hemicellulose in pyrolysis calculations.

5. PYROLYSIS OF WOOD COMPONENTS

As lignin and especially cellulose are used in different industrial applications, many investigations on these wood components are performed by means of thermal analysis. Only a few examples can be cited here, some more are found in the following sections, mainly in connection with fire retardments.

Lignins as byproducts in the paper industry are mainly used for heating due to their combustibility but there is intensive research for other, ecologically more sensible applications [43]. The molecular structure of lignins is very complex and until now not fully resolved. This lack originates from the effect that lignins can be neither isolated completely from the other components, nor the structure be reserved when it is split into the monomeric parts (for a review of literature see [43]).

DTA analyses proved that the size and the position of endo- and exothermic peaks in the thermograms of lignin depended on the way lignin was prepared [44]. Sulphuric acid derived lignin exhibited the highest stability. In addition, it was shown that lignin from coniferous wood (spruce) was more stable than that of deciduous one (aspen, birch, oak). The authors stated that larger differences in DTA thermograms are found between different preparations of the same wood than between similar preparations of different woods.

Jakab and coworkers [45] found that a combination of TG and mass spectrometry (MS) is a means suitable for the evaluation of the thermal behaviour of technical lignins. They investigated the thermal decomposition of Kraft lignin, acetosolv lignin and various lignosulfonates, all prepared from coniferous wood, mainly spruce in an inert gas atmosphere between 30 and 950°C. The results showed that lignin decomposition under the chosen conditions is a relatively slow charring process connected with the production of considerable amounts of volatiles. The organically bonded cations (mainly sodium) in lignosulfonates facilitated dehydration and decarboxylation and led to chars with high yields, while the formation of organic gases with low molecular masses was suppressed [45]. TG/DTG together with IR analysis was applied for the isothermal pyrolysis of Klason lignins from some Argentinian hardwoods in the temperature region

from 226 to 435°C under nitrogen atmosphere [43]. The thermogravimetric results were used for kinetics of decomposition reactions, the change of the IR spectra with temperature identifying modifications in the functional groups of the different lignins.

Pyrolysis of cellulose proceeds in two competitive pathways, one leading to monomeric levoglucosan which might be further decomposed to volatiles like aldehydes, ketones, furans, and pyrans [46], the other in an initial dehydration step to the formation of gases and char. TG/DTG analysis was applied to microcrystalline cellulose known as Avicel cellulose in a temperature range up to 600°C [47]. The onset temperature of the characteristic weight loss was near 290°C, and the process was complete at 400°C. An activation energy of 188 kJ/mol was determined via Friedman signatures in good agreement with data from the literature.

Pappa and coworkers [46] investigated commercial cellulose and Kraft lignin derived from needles of the Mediterranean pine *Pinus halepensis* with DSC and TG under inert conditions, partly in connection with fire retarding compounds (see below). Thermal degradation of lignin becomes visible as weight loss in TG at about 220°C. The lignin DSC exotherm observed around 400°C is due to the recombination of degradation products like phenols and phenolic derivatives which leads to the formation of char. The registered DSC thermograms of intact pine needles are rather complex with endothermic peaks at 88, 171, 242 and 302°C and one exothermic peak around 348°C connected with char formation from lignin. The endothermic peaks are explained by the authors as results of moisture, softening and melting of resinous acids, evaporation of volatiles and perhaps pyrolysis of cellulose at 302°C.

Wiedemann [48,49] looked for changes of cellulose and lignin concentrations with age in the wood of Big-tree (*Sequoia giganteum*) for a period of more than 2000 years and found that the ratio of these two components shifted with time. Twenty one air dried, carbon-14 dated wood samples taken from different growth rings of the "General Sherman tree" from the Sierra Nevada, were analyzed with TG and DSC in air. They showed pyrolysis between 200 and 350°C for cellulose and between 350 and 450°C for lignin, rendering enthalpy changes of -4.81 and -4.91 MJ/kg, respectively. The DSC thermograms of sequoia wood altered over long periods from 700 B.C. to 1988 A.D. (Figure 1). For a shorter period of time changes were analyzed in a 100 years old branch of the same tree with samples taken from annual rings with 20 years distance. A shift to lower temperatures in the cellulose and lignin peaks were obvious. Further investigations on wood age and caloricity and/or annual rings for spruce (*Picea abies*) are given by Ivask [50] and Reh and Kraepelin [51].

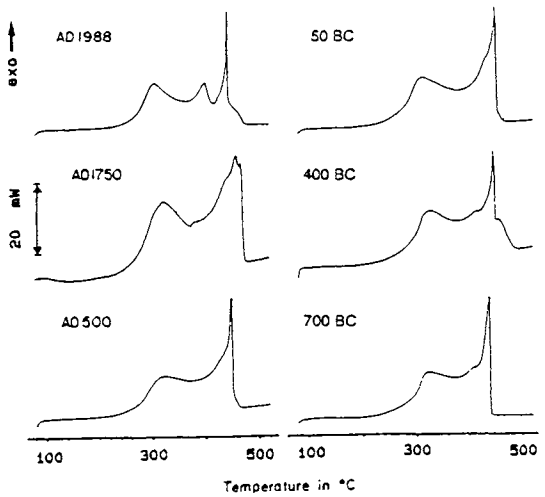

Figure 1. DSC thermograms of samples taken from growth rings of *Sequoia giganteum* [48].

In TG, DTG and DSC measurements of plant material on its course "From Wood to Coal", air-dried samples of birch (*Betula* spec.), beech (*Fagus* spec.) and redwood (*Sequoia sempervirens*; of different age) were used in order to simulate charcoal-burning [49]. After 14 h lignin was completely changed to charcoal. Tempering decreased the amount of cellulose, producing more and more charcoal from lignin and underlining that the amount of fixed carbon depends only on the lignin content of the sample. The following conclusions can be cited from this paper: (i) Wood and plants undergo constitutional changes under ambient conditions, leading to altered content and composition of lignin, while cellulose is not affected; (ii) cellulose is easily decomposed between 200 and 340°C in charring wood and some of its carbonous degradation products combine with lignin; (iii) the formation of coal is only dependent on lignin, with no contribution from cellulose as a non-aromatic carbohydrate.

Thermal analytic questions connected with coal (see also below) are by far too numerous to be treated here. But as coal is intimately coupled to wood just one example of coal combustion shall be given in this chapter. TG proved to be a convenient and quick means for a proximate analysis of coal to determine the moisture content, the volatiles, fixed carbon and the amount of ash. Figure 2 shows the burning profile of different coal samples heated slowly from 50 to 800°C in an oxidative atmosphere. Steps in the TG curve are due to a small loss

of moisture, a weight increase due to oxidation processes without loss of gaseous products and the combustion of carbon at high temperatures [49].

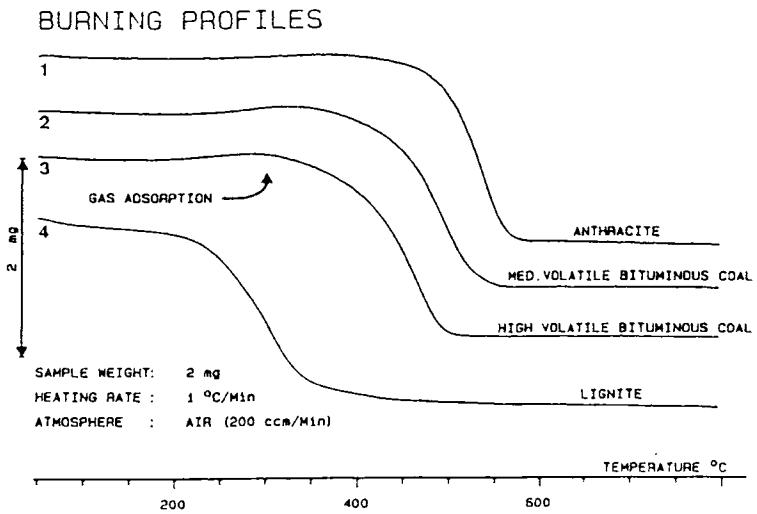

Figure 2. Burning profiles of different coal samples obtained by TG measurements in air Start of weight loss, temperature range and temperature of maximum decomposition rate characterize the coal qualities [49].

6. WOOD AND FIRE RETARDANTS

Every year large areas of natural forests are destroyed by wildland fires due to self-ignition or arson. One of the different techniques against such fires is the application of special chemicals in aqueous solutions which serve as fire retardant. Most common substances are ammonium phosphate or sulphate. On the other hand, woods used for construction purposes should be protected to some degree against fire, and modern building codes require wood to be treated with fire retardants for many applications [52,53]. Besides the mentioned ammonium compounds borax, boric acid, phosphoric acid and zinc chloride are applied in this field [52]. These retardants change the decomposition profile of wood, promote the formation of char and reduce the evolution of combustible gases. Moreover, char itself is hard to burn and acts as a thermal insulation layer [52].

These great advantages of fire retarding agents are coupled to several drawbacks: due to the incorporation of hydrated salt molecules into the wood cell walls the treated wood looses mechanical strength and increases hygroscopicity,

acidity and corrosivity [52]. These effects may be due to a degeneration of cell wall structures, comparable with effects seen in wood at increased moisture contents [53]. Thus, it is desirable to develop quick and simple test methods to evaluate the loss of stability in wood treated with fire-retarding agents.

Several authors investigated the influence of such additives on wood and wood component pyrolysis by thermal analysis. TG was applied on birchwood and marine plywood impregnated with phosphate. Its presence led to the primar formation of phosphorous acid followed by a cycle of dehydration, esterification, ester cleavage and polymerisation and thus to a lowering of the decomposition temperature of cellulose between 200 and 250°C, and to a higher char yield [54]. Glucose, glucovanillin and phenylpropane monomers were used as model compounds for wood degradation in the presence of phosphoric acid [55]. TA and IR spectrometry indicated a lowered initial dehydration temperature at 15 % mercury phosphate and no formation of levoglucosan. Ammonium phosphate and sulfamate, sodium borate, boric acid and guanidine sulfamate were applied to cellulose and studied under nitrogen atmosphere by means of DSC, supplemented by some DTA and TG experiments under vacuum [56]. Two endotherms were found by DSC and DTA which changed their position and size by treatment. The results were correlated with pyrolysis mechanisms and Arrhenius parameters.

Woo and Schniewind [52] used DSC to study the influence of moisture content and several fire retardants on specimens of sugar pine (*Pinus lambertiana*), Douglas-fir (*Pseudotsuga menziesii*) and Californian black oak (*Quercus kelloggii*). They concentrated their work on the first of the three distinctive peaks usually seen in the thermal degradation of wood (see above), since the two later ones required higher temperatures or longer treatment periods to become significant in the present respect. They determined activation energies between 71 and 151 kJ/mol depending upon the moisture content and the chemical treatment. The tendency of decreasing activation energies with increasing moisture content indicated that water enhanced the thermal degradation of wood. In a second paper of the authors a strong correlation was found between the loss of mechanical strength and the size of the first peak of DSC [53]. This observation held good for untreated wood of sugar pine and such treated with boric acid or zinc chloride. Mechanical strength was characterized by the modulus of rupture (MOR, given as MPa of static bending of the specimens) and the toughness (given as work consumed per specimen) following the prescriptions of ASTM D143 (American Society for Testing and Materials 1979). The authors concluded from their results that "it is therefore possible to compare the potential detrimental effects of fire retardant chemicals on wood strength simply by conducting DSC experiments, rather than thermal exposure followed by mechanical tests... " [53].

As shown above, flame retardants change the thermal decomposition of cellulose (fibres) to a more intensive char-formation which may be further increased by addition of intumescents [57]. These substances not only lead to a thicker char barrier which is well-known as fire protection but also to "char-bonded" structures. They are resistant to air oxidation at elevated temperatures and thus form a second flame and heat barrier. As the thickness of the char layer has a strong influence on the thermal gradient between the surface and the fibre it improves the thermal protection of the material. TG, TMA and DSC were applied to four samples of cotton fabrics treated with different commercial flame retardants and two commercially available intumescents. The results show the interaction between flame-retardant cotton fibres and the intumescents, an enhanced char formation and the expected char-bonded structures [57].

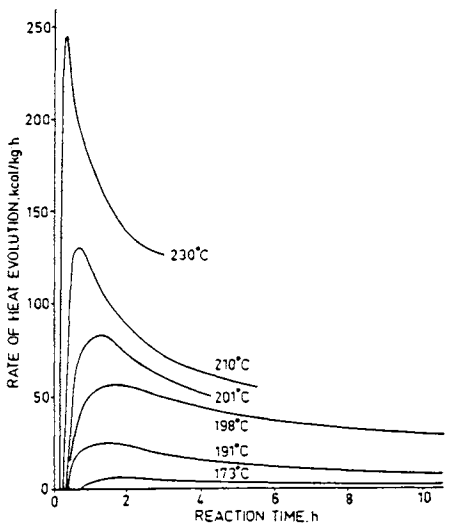

Figure 3. Rates of isothermal heat release as function of time and temperature for a hardboard made of groundwood [41]

Back and Johanson [40,41] applied an isothermal labyrinth air flow calorimeter to investigate the heat dissipation occuring during tempering ("curing") wet produced hardboards and semihardboards. Curing at temperatures around 165°C for several hours is necessary to increase water resistance, dimensional stability, strength and stiffness of the boards. Oxidative auto-crosslinking of wood polymers and degradations take place leading to exothermic reactions of considerable heat release. There may be the danger of self-heating and auto-ignition. Speci-

mens made from *Picea abies* and *Pinus silvestris* were chosen, in some cases with and without fire retardants. Figure 3 shows the rate of isothermal heat release as a function of time for hardboard at different temperatures above that used for curing, with a dramatic short time increase at higher temperatures. The initial rate of heat dissipation at 200°C was significantly higher for lignocellulosic samples than for delignified ones. Application of fire retardants to pyrolysis of these lignocellulosic materials resulted in an relative increase in char yield and thus led to a reduction of heat dissipation [41].

Finally, the already mentioned investigations on the Mediterranean pine *Pinus halepensis* shall be cited again in which commercial cellulose as a model compound for studies of forest fuel pyrolysis, pine needles, pine needle lignin and extractives were analyzed with and without two ammonium salts as fire retardants [46]. Both salts provoked a lowered pyrolysis temperature of cellulose and a significant increase in char formation for cellulose (up to 2.4 times) and intact needles (up to 1.7 times), but they had negligible effects on lignin and extractives.

7. WOOD AND SYNTHETIC POLYMERS

Wood fibres and wood flour are frequently used in combination with synthetic polymers, both as general fillers or together with adhesives. TG and DSC were applied to study the thermal behaviour and crystallinity of the new blends and various other physical methods for stiffness, brittleness, moisture content and further characteristics.

The addition of boric acid to wood fibres in a polystyrene matrix led to an increased stiffness when blended at 350°C. The boric acid had no influence on polystyrene but reacted with the wood fibres while the addition of plasticizer decreased the glass transition temperature of the polystyrene [58]. Similar results were obtained by Simonsen and Rials [59] for wood flour and polyethylene/polystyrene polymers with improved stiffness but also increased brittleness. DSC showed no interaction between the polyethylene and the other phases in the composite, but between polystyrene and the wood filler. Wood fibre-reinforced composites made from thermomechanical pulp, Kraft lignin, and microcrystalline cellulose filler were investigated by means of modulated DSC [60] to determine the effects of fibres on polymer crystallization. Wood adhesives originating from softwood Kraft lignin exhibited three exothermic peaks between 79 and 145°C depending upon the way of preparation and providing high quality bonds [61]. Larch (*Larix gmelini*) derived tannins were mixed with phenol-formaldehyde adhesive and studied for their utilization as (TPF) adhesives in plywood and hardboard [62]. Tannins could replace phenol up to 60 % of weight in the mixture.

Under TG and DSC, TPF resin showed good thermal stability together with curing characteristics similar to those of the original PF adhesive. Similar DSC experiments were performed on a commercial phenol-formaldehyde adhesive plus Southern pine (*Pinus* sp.) sapwood treated with a chromated copper arsenate (CCA) preservative [63]. The thermograms indicated that curing can be accelerated at lower temperatures than normal depending upon the state of CCA in the wood.

Heat capacities of a new porous carbon material called "Woodceramics" were investigated by means of DSC. Fibreboards made from pine wood (*Pinus radiata*) were impregnated with phenol resin, dried, harden-treated at 135°C and then burnt at 800 or 2800°C. These new ceramics exhibited special characteristics like high heat and corrosion resistance, heat and electrical conductivity, impermeability to gas and hardness. The observed heat capacities between ambient and 250°C with 0.5 to 0.94 J/(g K) for the 2800°C sample and even 1.0 to 5.5 J/(g K) for the 800°C sample are relatively large compared with those of metals and alloys and rather close to those of rubber, porcelain or concrete [64].

8. WOOD AND WATER

DSC is frequently applied to determine the different properties of water in cells and tissues. Simpson and Barton [65] used this technique to estimate for the first time the fibre saturation point (FSP) of wood which is defined as the maximum possible amount of water that the composite polymers of the cell wall can hold and that does not freeze in contrast to the "free water". FSP is important in wood technology since physical characteristics - especially shrinkage - change significantly at moisture contents above this point. Experiments were performed on heart- and sapwood of two West Australian eucalypt species, *Eucalyptus marginata* and *E. diversicolor*, and a plantation softwood, *Pinus radiata*. The observed endothermic peak around 8°C is due to melting of frozen water in the larger voids of the cell lumen (Figure 4). From the obtained melting enthalpies and the total moisture content of the wood, FTP was calculated as 32.8 to 37.9 % in eucalypt samples and as 27.9 to 32.9 % for pine depending upon sap- and heartwood and experimental conditions. A second small additional peak below the main transition is seen in Figure 4 which might be connected with a sandwiched layer of water between non-freezing and free water.

Freezing of deeply undercooled water in cold-hardened stems of 16 woody taxa was determined in DTA experiments on nonthawed, thawed and freeze-killed specimens [66]. Freezing exotherms were observed down to onset temperatures of -53°C and appeared in size and position in dependence of the wood pre-

paration. The authors concluded that the effects are due to (i) the cell wall which does not allow external ice to propagate through to nucleate intracellular water and (ii) to the plasma membrane which protects the solute in the cell against being diluted to the extracellular water. Thus, cellular water migrates from the cell during periods of prolonged cold and freezes outside. At the same time the concentration of the cell solutes increases and lowers the nucleation temperature of the cell sap [66].

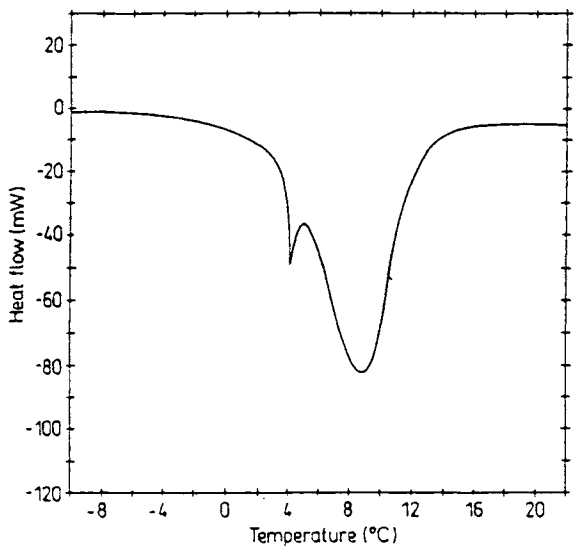

Figure 4. Low-temperature DSC thermogram under nitrogen of Jarrah sapwood (*Eucalyptus marginata*) with a water content of 52.8 %. The main endothermic peak is due to melting of the frozen free water in the cell lumen, the small peak around 4 °C to sandwiched water (see text) [65].

The connection of water and fire retardents was already mentioned above [52,53]. But as wood is used in many processes at varying moisture contents, it is necessary to know the influence of water on other parameters as well, e.g. its softening temperature. DSC was applied to birch (*Betula verrucosa*) and Norwegian spruce (*Picea abies*) samples and to spruce specimens treated in two ways to obtain different degrees of lignin crosslinking [67]. After conditioning to specified relative humidities, DSC runs were performed between -20 and +150°C leading to a small, but pronounced endothermic peak around 60°C with an enthalpy change comparable to that of synthetic polymers. It was not at all de-

tectable at low moisture contents. As water acts as a plasticizer in wood, the authors concluded that water and lignin form a relatively stable network breaking down at the softening of lignin and that the endothermic peak is only connected with the physical change of lignin.

Moisture sorption of ligno-cellulosic material was investigated by DSC and TG since it has the mentioned effects on swelling and softening of wood and on some other physical characteristics. The experiments showed that the main contributions to adsorption originate from hydroxyl groups of cellulose and lignin. Calculations of bindings for model substances and experimental results are in a good agreement [68].

The surface energy of wood shows a transition around 60°C as determined by the dynamic contact angle (DCA) technique and confirmed by a glass transition of lignin observed by DSC [22]. The obtained values correspond to those for synthetic polymers so that - in spite of the complex composition and structure of wood - it can be investigated and understood like such polymers. The experiments were performed on the diffuse-porous hardwood of the yellow poplar (*Liriodendron tulipifera*) and the ring-porous hardwood of the red oak (*Quercus rubra*) at 12 and 31 % moisture content. Clear glass transitions were observed in the poplar sample at 75°C (12 %) and 63°C (31 %) and at 68°C (12 %) and 66°C (31 %) for oak in significant dependence upon the moisture content.

Cork is a special secondary plant tissue covering stems and roots, well-known for its low specific weight and bad thermal, electric and acoustic conductivity. DSC experiments were applied among others to determine the amount of absorbed water in cork structures which modify the dielectric properties of this material [69]. Changes occurred after heating above 60°C or evacuation for several days and were reversible in room air after a few weeks. It was concluded that the observed modifications were due to a desorption and re-absorption of water molecules in the cork structure.

9. ENERGY CONTENT OF WOOD

Part of the chemical energy bound in wood (and other plant systems) can be liberated by microbial degradation under the naturally occuring environmental conditions [70]. Piles of organic material may be used as a continuous source of low temperature energy for household heating or warm water supply. Composting of household litter rendered total heats of −34 to −42 MJ/kg carbon [71]. Larger heaps of brushwood prepared after the method of Jean Pain may produce about 14 kW over periods of half a year, equal to a permanent flow of water of 4 L/min heated from 10 to 60°C [72]. This idea is not new at all but used since thousands

of years by the Australian brush-turkey *Alectura lathami* to bread its eggs just by metabolic heat in large piles of branches and undergrowth in local forests [73]. Although the various methods to gain energy from the microbial decomposition of wood and other organic substances may have some future in private or medium-scaled systems, they shall not be discussed here in detail. More information can be found in the review "Calorimetry in ecology" by U. Reh [74]. This paragraph concentrates only on determining the energy content of wood by means of TA and combustion calorimetry (see also Chapter 7 "Bomb Calorimetry in Biology" in this Handbook).

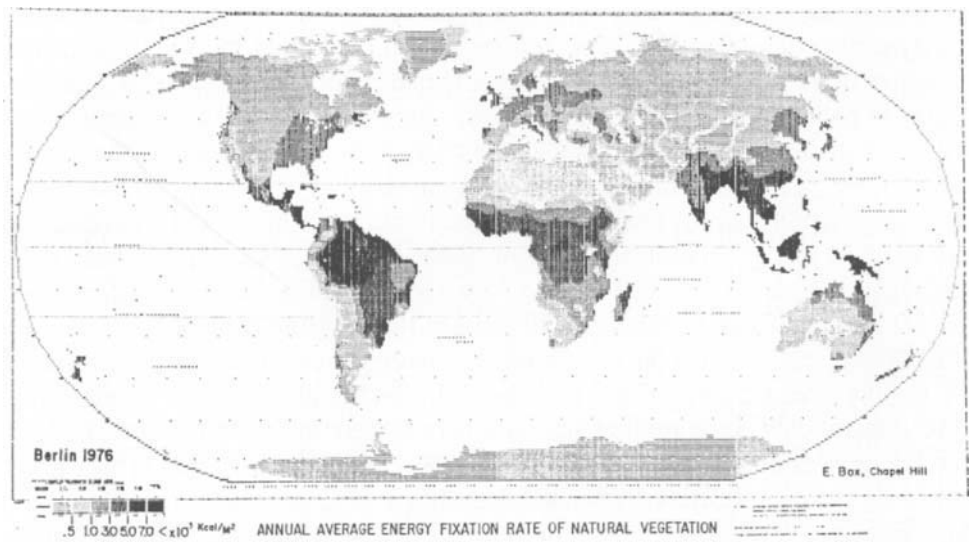

Figure 5. Berlin map of the energy fixation rate in different parts of the Earth derived from an earlier global vegetation map and energy fixation rates of various ecosystems [77].

In a series of papers, Lieth [75-77] used published data on growth productivity, evapotranspiration, temperature and precipitation to construct global maps of productivity zones and belts on the Earth. These local values were combined with combustion heats of typical plants to design the "Berlin" map of the global energy density in MJ/m^2 (Figure 5). Highest values above 30 MJ/m^2 are found around the equator and between the tropics in some parts of the Earth [77].

As was pointed out in the Introduction there is no real alternative to wood as an energy source in poor and developing countries [3]. One and a half billion people in these countries are entirely depending on wood and charcoal for their energy requirements, and a further billion to at least 50 % [78]. Thus, well-handled fuelwood plantations are of increasing importance in such regions and supported by several international programmes [4,78] since they can increase the energy yield up to tenfold compared with the usual local results. The typical 1 to 5 t/ha of a natural tropic forest may be amplified to 10 to 50 t/ha leading to much smaller amounts of ground used for the energy supply in rural areas [3].

Tuskan and De la Cruz [79] investigated the solar input and the energy storage in a five-year-old plantation of the American sycamore (*Platanus occidentalis)* by means of bomb calorimetry. The obtained caloric values ranged from −18.8 MJ/kg for stem wood to −19.9 MJ/kg for stem bark. The mass yield amounted to −20.3 t/ha above-ground biomass or a total energy yield of -38.6×10^{10} J, corresponding to a storage efficiency of 0.55 % [79].

A tree is mainly composed of wood (65 to 90 % dry weight) but contains about 50 % water which must be evaporated when fresh samples are burnt. In general, the combustion heat of bone-dry wood amounts to about −19 MJ/kg but may increase to −25 MJ/kg when resins or other high energy compounds are present in the specimen. The combustion heat decreases to only −10 to −12 MJ/kg for wet wood since a high portion of energy is consumed for evaporation. Air dried wood keeps approximately 20 % water so that −16 MJ/kg may be expected [3,80,81].

Pipp and Larcher [82,83] presented a truly comprehensive literature review about 7583 combustion heats and 2792 ash contents of more than 1500 plant species, among them around 200 trees and shrubs. Data were differentiated for various plant tissues. The authors came to the resumé that (i) woody plants have higher energy contents than herbaceous ones; that (ii) the same is true for coniferes compared with dicotyledonous woody plants; while (iii) dicotyledons show larger combustion heats than monocotyledons; and that (iv) generative tissues are above vegetative ones. The data material is by far too comprehensive and detailed to give mean values for trees or special tissues of them.

Bomb calorimetry was applied to determine the energy contents of different species of undergrowth and their seasonal changes in Spain [84]. Forest residues from afforestation, forest clearing and firebreaks showed mean combustion heats near −19 MJ/kg similar to the value for solid municipal waste. The authors state that forest residues may be thus added to such wastes as further fuel in energy-recovery plants and - if continuously harvested - decrease the risk of forest fires. In two further publications different woodland species from the humid Atlantic zone and the dry continental hillside, plateau and high mountain zones were in-

vestigated for their chemical composition, moisture content, flammability and calorific values as function of the season [85,86].

A further combustion calorimetric investigation was carried out on wood of the balsam fir (*Abies balsamea*) which was either healthy or killed by the spruce budworm (*Choristoneura fumiferana*). Four classes of samples were distinguished: (i) living material as control; (ii) wood 6 months; (iii) 12 months; and (iv) 22 months dead. Oven-dried material of all four classes showed the same gross combustion heat of −20 MJ/kg without any significant differences. The moisture content dropped from 56.8 % for class 1 to 38.8 % for class 4. As the usuable heat in MJ/kg decreases with growing amounts of moisture, the energy value of dead wood is considerably higher than that of the living one [87].

Specimens of young sprouts of nine hardwood species were separated into wood, bark, twigs and leaves and investigated for dry matter, specific gravity, ash content and caloric values. They showed a mean combustion heat of −20.1 MJ/kg with intraspecies differences between tissues larger than the relatively small deviations between species [88]. The highest caloric values were found in leaves (-21.1 MJ/kg), lowest in bark (−19.4 MJ/kg). To demonstrate these differences between tree tissues, caloric values for wood, bark and leaves of hornbeam, maple and oak are shown in Table 1 obtained by Phillipson bomb calorimetry [89]. In a further paper Oszlányi [90] reported about the combustion heats of leaves (needles), wood, bark and roots of the Scotch pine (*Pinus silvestris* L.), the Norway spruce (*Picea excelsea* Link.) and the European beech (*Fagus silvatica* L.) and found significant differences between these tree species as well as their tissues. Abe [91] studied forest biomass and determined a mean heat content of −19.7 MJ/kg for 40 fast-growing trees. Perennial plants from deserts and arid woodlands were investigated for their caloric content, among them several trees, differentiated into wood, bark, twigs and leaves [92]. Combustion heats varied from −13.4 to −22.5 MJ/kg oven-dry mass. Oxalate salts had a strong influence on these figures. When such data are used for ecological studies the author recommends to look for (i) the significance of caloric values in plant energetics; (ii) the functions of compounds which are responsible for high or low values of the combustion heat; and (iii) for the relative rates of metabolism and dry matter production for those plants [92]. Siafaca and coworkers [93] determined the caloric and ash content of 15 evergreen sclerophyllous (ES) and 8 deciduous (D) plants which are important in the Greek maquis ecosytem. Ash content varied from 0.5 to 18.9 % with a mean of 3.2 % for ES and 3.8 % for D plants. Caloric values were presented for leaves, bark and wood. With three exceptions leaves showed the highest combustion heats of the tissues. Because these tissues contributed to the above ground woody mass of the maquis with 20, 7 and 73 %, respectively, it was possible to calculate the mean ash-free figures of −18.7 (ES) and −18.6

MJ/kg (D). The fraction of D plants in the maquis is seldom higher than 20 %, so that the caloric content of this ecosystem can be assumed as −18.7 MJ/kg ash-free d.w.

Table 1
Energy content (and 99 % reliability interval) for four tree species and three different tissues [89].

		Wood	Bark	Leaves
		MJ/kg	MJ/kg	MJ/kg
Hornbeam	*Carpinus betulus*	19.10 ± 0.46	19.11 ± 0.82	19.77 ± 1.30
Maple	*Acer campestre*	18.19 ± 0.46	18.70 ± 0.81	19.64 ± 1.50
Oak	*Quercus cerris*	19.01 ± 0.58	19.56 ± 0.64	20.65 ± 0.66
Oak	*Quercus petraea*	18.12 ± 0.37	18.25 ± 0.85	19.09 ± 1.26

Tan and Stott performed a comparative study on rubberwood (*Hevea brasiliensis*) and some Malaysian wood species by means of DTA and TG to evaluate the combustion characteristics rather than the energy content [2]. Although energetic values could have been given, the authors show thermograms of all the woods and determine DTA peak temperatures and heights, densities, extra burning time or char yield but no combustion heats [2].

Table 2
Heat of combustion of *Sequoia* samples of different ages [48].

No	Year	ΔH (cellulose)	Peak temperature	ΔH (lignin)	Peak temperature
		J/g	°C	J/g	°C
1	AD 1988	−3834	305	−4294	400/440/460
2	AD 1750	−3756	320	−4563	460
3	AD 500	−4406	320	−5127	455
4	50 BC	−5048	310	−4662	450
5	400 BC	−4320	325	−4636	440
6	700 BC	−4807	320	−4911	440

Test conditions: 4°C/min, aluminum crucible, still air.

Reh and Kraepelin [51] investigated the wood of spruce (*Picea abies*) and birch (*Betula* sp.) by DSC and chemical analysis in connection with the influence

of rafting and water storing on the quality of wood for music instruments (see below). They found an increase in energy content (i) from −8.2 to −9.7 MJ/kg when the density of annual rings increased from 5.5 to 22 rings/cm; (ii) from −9.1 to −9.3 MJ/kg when wood was soaked for one month; and (iii) to −10.2 MJ/kg in artificially aged wood. This energy increase was accompanied by a corresponding rise in the energy of the lignin fraction [51].

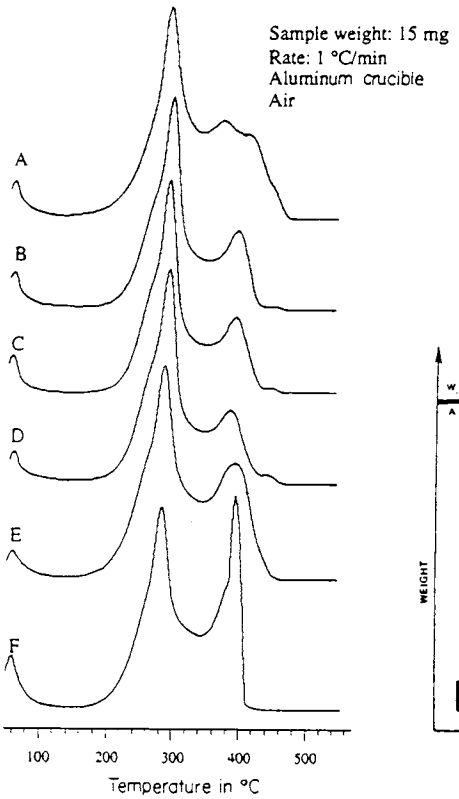

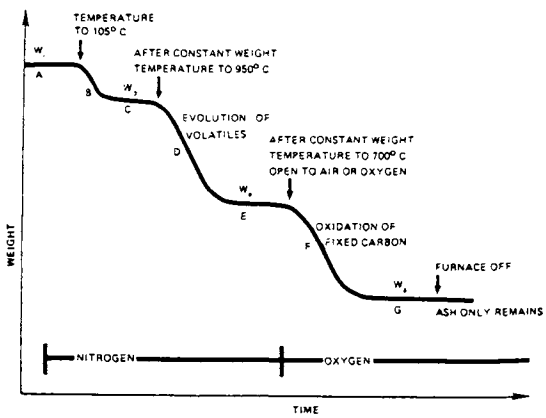

Figure 6. DTG curves (in inverted direction) of annual growth rings of different age. A is nearest to the bark, B to F taken in twenty years intervals, F one hundred years old. Observe the nearly constant temperatures of the cellulose (left) and lignin (right) peaks [48].

Figure 7. Schematic thermogram with the different steps during the determination of the proximate analysis of coal or lignite [95].

Wiedemann [48,49] determined the heat release from sequoia wood (*Sequoia giganteum*) of different age by integration of the cellulose and the lignin peak in DSC thermograms. Table 2 shows the peak temperatures and enthalpies of C-14-dated samples and Figure 6 the thermograms from different annual rings of a 100-year-old branch of a Big-tree (see above). Numerical integration rendered −4.81 MJ/kg for cellulose and −4.91 MJ/kg for lignin. Highest values are always found in the oldest rings, in contrast to observations of Ivask who saw no differences between old and new rings but between those with low and high ring density [50]. The combustion heats found in these investigations of together about −10 MJ/kg are rather small compared with the data given above. But one has to bear in mind that the additional energy release from char is missing in this balance.

Back and Johanson studied the isothermal heat evolution of different kinds of lignocellulosic sheet material in a labyrinth air flow calorimeter between 150 and 230°C [40,41]. Groundwood-based boards were impregnated with fire retardents (ammonium phosphate, borax/boric acid, see above), dried and press-dried before combustion. The energetic data were analyzed as function of weight loss due to vaporization of oxidised and unoxidised degradation products of hemicellulose, cellulose and lignin or due to loss of extractives. For commercial hardboards, -18.4 MJ/kg was found, a value similar to that for softwood, while groundwood showed a smaller heat release.

A glimpse to studies of the combustion of coal reveals methods applied in that field that might easily be adapted to wood research. The industrial analysis of coal proceeds in three steps in accordance with the ASTM Standards [94]: (i) proximate analysis for moisture, volatile matter, fixed carbon and ash content; (ii) ultimate analysis for elemental content (carbon, hydrogen, sulfur, nitrogen, phosphorous and oxygen) plus ash; (iii) calorific value by combustion. Proximate analysis may be carried out by TG with changing gas flows of at first nitrogen and then oxygen and with different temperature programmes as shown in Figure 7 [95,96]. An indirect calculation of the energy content can be performed by the Goutal equation for coal from known amounts of volatiles and of fixed carbon [96,97]. Although this equation could be modified in its coefficients to fit to wood combustion, it has - to our knowledge - never been applied in this field. The Goutal equation reads

$$P\ (\mathrm{cal/g}) = 82\ C + a\ V$$

where P is the caloric value of the coal, C the percentage of fixed carbon on a moisture free basis and V the corresponding percentage of volatiles. a given in cal/(% volatiles) is a coefficient varying with V that has to be determined empirically. It decreases from a = 145 cal/% at V = 5 % to a = 80 cal/% at V = 40 %.

Experiments on more than 100 bituminous coals revealed differences between calculations and bomb calorimetric determinations that were seldom larger than 2 %. A modified Dulong equation with the elemental composition of wood was used by Abe in his investigations of 40 fast-growing tree species [91]. The Dulong equation together with some other models to calculate combustion heats from chemical compositions of wood is discussed in Chapter 7 "Bomb Calorimetry in Biology" in this Handbook.

10. AGING AND FOSSILIZATION OF WOOD

Aging and fossilization of wood are the exceptions in nature since the bulk of the organic matter is destroyed by microbial decomposition in the course of time. The biochemical subunits of plants are "recycled" and incorporated into new life in an eternal succession. Sometimes wood contains some antimicrobial compounds which prevent the usual destruction. The oldest samples of air-kept wood are dated to 290000 years while water-logged specimens from ship wrecks, bulwarks and posts are supposed to be as old as 8500 years [98]. Different physical and chemical techniques were applied to the analysis of "archaeological" wood and to the estimation of appropriate conservation means for the future [99], but TA is rare.

Tomassetti and colleagues performed thermogravimetric studies on archaeological waterlogged wood of a Roman vessel from the first century A.D. [100-102]. Earlier microscopic investigations on these samples had identified the coniferous and broadleaf origin of the wood. Therefore, the authors compared their results with fresh heartwood specimens of red fir, larch, elm and beech since they were the most probable trees to be used during construction. Both, old and fresh wood had water saturation contents above 50 % , while the amount of ash varied considerably between archaeological coniferous and broadleaf samples and between them and fresh wood. All samples rendered nearly identical thermograms so that it was not possible to distinguish between the different origines in ancient wood. TG/DTG curves of fresh wood showed decomposition effects at 300 and 400°C, the ancient specimens rendered a pronounced step between 350 and 450°C, a series of little steps between 200 and 350°C and a very small peak between 450 and 650°C. Thus, decomposition of cellulose (around 300°C) is scarcely detected in archaeological wood while that of lignin is clearly evident in all thermograms - as to be expected in agreement with data from microbial degradation of wood (see below) [100].

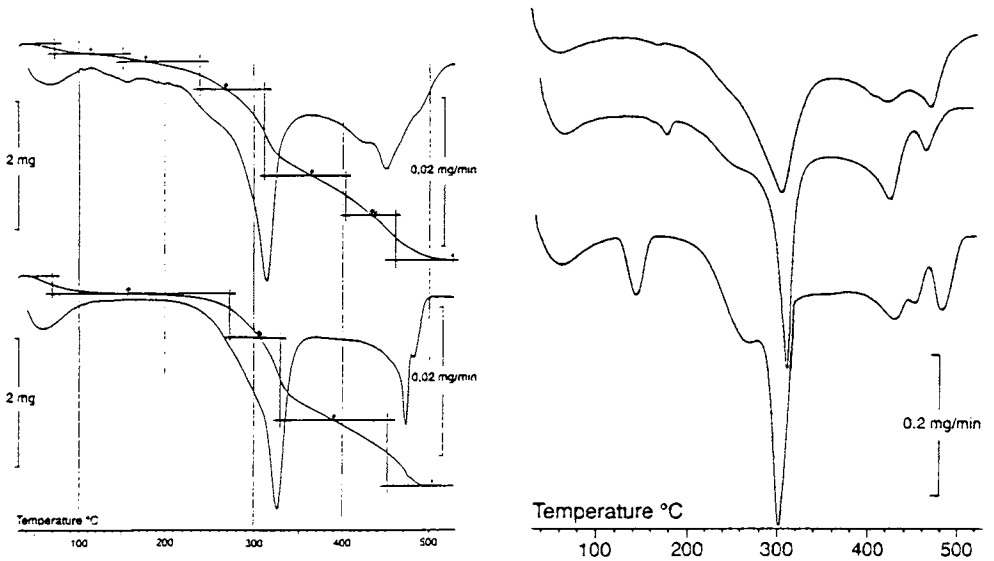

Figure 8. TG/DTG comparison of a wood sample (3.5615 mg) of a cedar coffin fragment from Luxor/Egypt (top) with a recent sample (3.3258 mg) from a living cedar growing in Switzerland. Scanning rate: 10 °C/min, air flow: 5 ml/min [103].
Figure 9. TG/DTG comparison of three tamarisc samples from an ancient Egyptian coffin and a living tree. Top: sample from the coffin vat (3.4303 mg); center: sample from the coffin cover (2.9957 mg); bottom: sample from a living tree (4.4435 mg; *Tamarix africana*, growing in Elba/Italy) [103].

In two further publications [101,102] the authors extended their investigations to ancient wood samples (fir, larch, spruce) from portals of churches from the 13th to the 18th century and to 2 million years old fossil wood. The latter showed a similar behaviour to that of waterlogged specimens. The ancient samples exhibited the expected high content of carbon due to the relative decrease of cellulose as a consequence of microbial degradation and the corresponding relative increase of lignin.

In a recent line of thermoanalytical experiments Wiedemann [103] investigated wood samples taken from ancient Egyptian coffins and compared them with corresponding samples of modern origin. Looking at these results one has to keep in mind that a severe scarceness of useful wood was typical for all periods of Egypt, that trees like sycamore, date and dum palm, tamarisc and acacia posses only poor quality for board production and that good material like cedars had to be imported. Only wealthy people could effort such coffins, the others had to be

content with sycamore and tamarisc boards. Thus, it became habit that coffins were covered with a layer of Nile mud and recarbonated calcium oxide painted in a way to immitate wood of foreign origin.

Figure 8 shows a comparison of TG/DTG curves of an ancient coffin fragment from Luxor/Egypt made from cedar with those of a living, seven year old cedar grown in Switzerland. The fragment was dated to a period between 606 and 406 BC by means of the ^{14}C radio carbon method. As was mentioned above wood changes its composition with age so that differences in the traces are easily explainable. The DTG curves render the following composition for the samples from coffin/tree: water 8.1/8.4; hemicellulose 12.4/20.8; cellulose 38.6/38.8; lignin 37.5/31.0; ash 3.4/1.0 %. A similar comparison of an ancient sycamore coffin (Egypt) with a 20 years old tree from Elba/Italy brought the following results: water 12.0/6.3; hemicellulose -/17.3; cellulose 68.1/38.3; lignin 13.7/31.0; ash 6.2/7.1. A final example for such TG/DTG investigations is shown in Figure 9 for an at least 2700 years old coffin (Egypt) made from tamarisc with a tree growing in Elba. Again an astonishing congruence of the main peaks was observed indicating that characterization and identification of wood may be performed by such an approach.

Besides these papers and the investigations of Wiedemann on 2000 year old sequoia wood [48] or ancient paper and its plant origin [104] (see below) no further publications were found in the literature. The present authors are sure that an interesting and stimulating field of research is waiting here for DSC and TG/DTG.

11. WOOD FOR MUSIC INSTRUMENTS

Wood plays an important role in the construction of different body parts of musical instruments and several physical characteristics have to be met by wood to be chosen as high quality. These factors comprise Young's modulus, bulk density, damping factor, critical frequency, stiffness, hardness, flexural rigidity and movement (shrinkage) [105,106]. Transposed to the characteristics of wood, they translate to a not too high content of resin, the absence of branches, and a constant or steadily de- or increasing density of annual rings. However, the breadth of rings below 3 mm (4 mm) has no influence [107]. Nevertheless, narrow rings are preferred for the resonant wood of violins [51].

Only very few investigations by means of thermal analysis are found in the literature. Reh and Kraepelin [51] applied DSC and chemical analyses to spruce samples of two ring densities and observed thermograms with different peak heights for holocellulose (around 350°C) and lignin (around 490°C), respectively

(Figure 10). A sample with 5.5 rings per cm showed a total heat release of 8.22 MJ/kg d.w., a holocellulose peak of 51.6 % and a lignin peak of 32.0 % of the total energy. In contrast, 22 rings per cm wood had the following values: 9.74 MJ/kg, 53.7 % and 33.7 %, respectively A higher content of lignin is thus visible in the preferred type of wood.

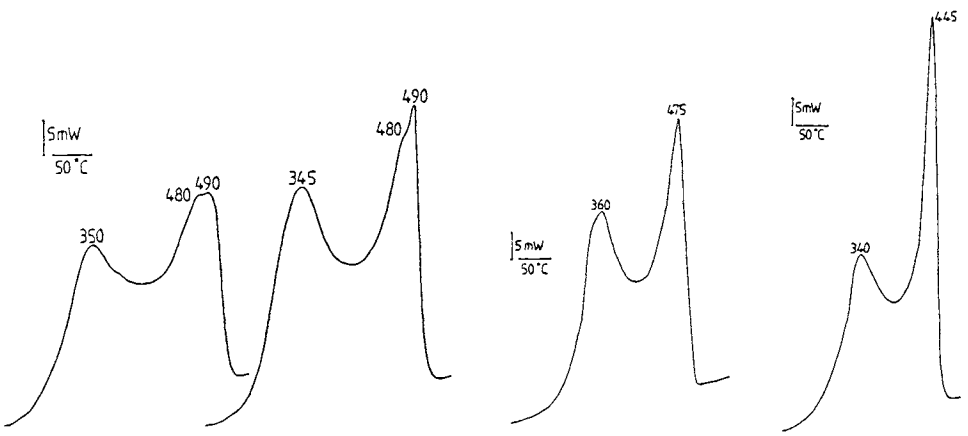

Figure 10. DSC thermograms of untreated spruce wood with 5.5 (left) and 22 rings per cm (right) [51].
Figure 11. DSC thermograms of artificially aged (left) and autoclaved and one month soaked spruce wood (right) [51].

Table 3
Distribution of different kinds of wood in a classical violin [109]

Spruce	Maple	Ebony
top plate	bottom plate	peg
rib	neck	fingerboard
bassbar	scroll	tailpiece
soundpost	bridge	endbuttom
corner blocks		
upper blocks		

Because it is often assumed that rafting and storing of wood in water accompanied by a microbial decay of hemicellulose has a positive influence on the sound of the later music instruments [108], Reh and Kraepelin [51] investigated

sound and water soaked wood of spruce (*Picea abies*) and birch (*Betula* sp.). The samples were stored in tap water for up to four months. In the corresponding thermograms the peak temperature of lignin shifted down to 475 and 445°C (Figure 11) in soaked and artificially aged wood with low content of hemicellulose. The energy content per g total mass increased from 46 to 54 % for lignin by rinsing, that of holocellulose decreased correspondingly. Microorganisms had some influences on the peaks, but they were negligible compared with the physical effects of soaking or autoclaving [51].

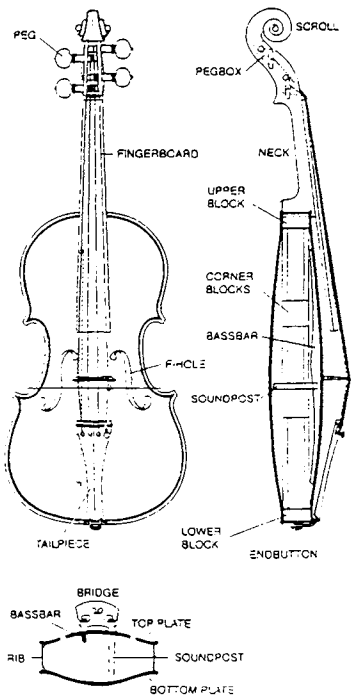

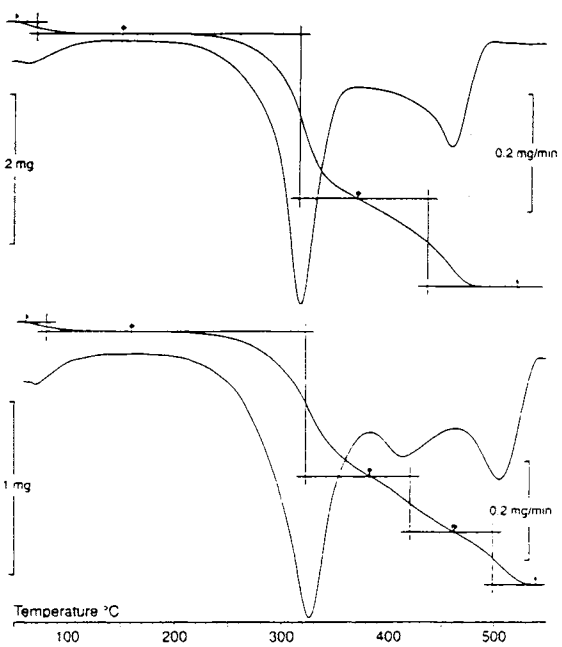

Figure 12. Design of a violine and indication of its different parts [109].
Figure 13. TG/DTG comparison of a sample taken from a Stradivari violin with one from the corresponding tree. Top: Specimen (3.7546 mg) from a Swiss spruce tree of 250 years cut in 1984 and still used for instrument construction; bottom: specimen (1.7551 mg) from the (spruce) top plate of the violin. Scanning rate: 10 °C/min; air flow: 5 ml/min [109].

In recent TG/DTG experiments combined with MS, Wiedemann [109] analysed wood specimens from violins and compared the results with those of samples from old trees cut a few years ago and used for modern music instruments. These

trees grown in Switzerland were hewn in 1984 and had an age of 250 years corresponding to the golden age of violin production by Antonio Stradivari and Giuseppe Guaneri in Cremona/Italy. Seven violins were investigated when opened for restoration and samples taken from inside for a general analysis and from outside to study the varnish/wood composition. For a better understanding Figure 12 presents a sketch of a violin and Table 3 details the distribution of the different kinds of wood in the instrument. Clear differences, but also similarities are seen in the TG/DTG curves (with step analysis) of Swiss spruce (top) and the top plate of a Stradivari violin (bottom; Figure 13). The water content is approximately the same, the ash content of the violin sample nearly doubled with a high contribution of silicon, its cellulose peak reduced and its slightly higher lignin component split into two peaks. This double peak might be due to a waterglass treatment of the instrument for wood conservation, as it was detected earlier in papyrus prepared with $CaCl_2$ [104]. A bar diagram comparison between a sample from the maple bottom plate of the same instrument and from the old Swiss maple tree is shown in Figure 14. Most striking is the large difference in the hemicellulose content between the maple sample and the violin, partly compensated by the cellulose. Again a doubling of the ash content becomes manifest and a split of the lignin component in two peaks as in Figure 13.

12. WOOD AND PAPER

Paper has played an important role in the development of social cultures all around the Earth. Depending upon the local vegetation, different raw materials were connected with the discovery and evolution of papermaking techniques. Plants and bark or bast of certain trees were taken as writing and painting support, and they are still in use in some aboriginal tribes [110]. Papyrus sheets served for writing in the ancient Egypt, while the *real* paper was invented 2000 years later in China around 105 A.D. Our modern words *paper* (papyrus) and *library* (the Latin "liber" means wood bast) signalize the plant origin of the material.

In spite of the high importance of paper in daily life, only a few TA investigations have been performed, mainly in connection with historical and archaeological interests. In an early contribution of Wiedemann and Bayer on papyrus paper from ancient Egypt, DTA, TG and DTG thermograms were shown for different parts of the papyrus plant and for old and modern papyri [111,112]. Again hemicellulose, cellulose and lignin were present and additionally starch as glue for multiple layers in historical papyri. Figure 15 exhibits TG/DTG curves of such a papyrus sheet with oxidative degradation of cellulose between 250 and 350°C and of lignin at 380 to 450°C [112]. Pyrolysis in nitrogen rendered a very uncha-

racteristic DTG graph. The investigation made clear that the height and position of the lignin peak was very sensitive to age, preservation and preparation/processing of the material [48,112].

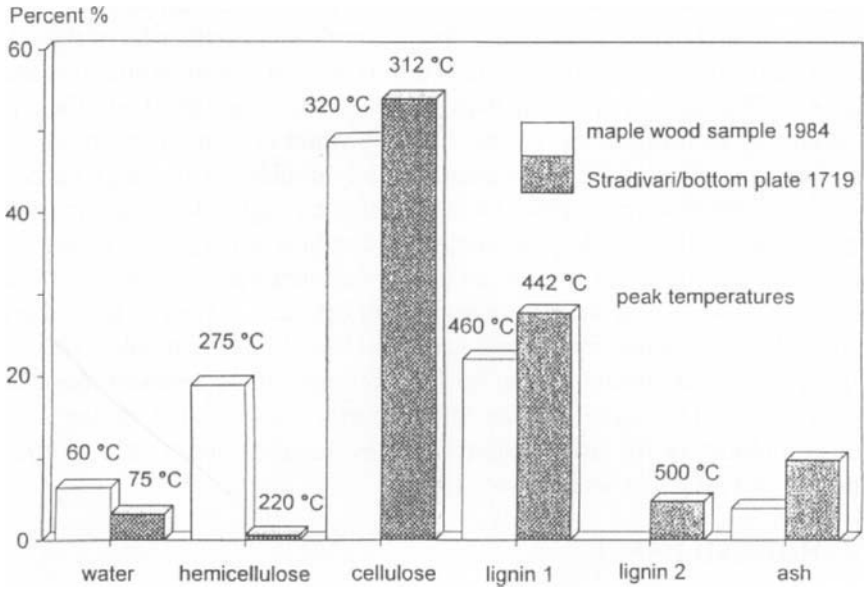

Figure 14. Results of a TG/DTG comparison of samples from the (maple) bottom plate of a Stradivari violin and a Swiss maple tree of the same age [109].

The composition of papyri of four millenia (1900 B.C. to 1977 A.D.) showed some variations with no visible trend: water (4.93 to 7.47 %), cellulose (53.12 to 68.96%), lignin (22.42 to 32.77 %) and ash (2.04 to 14.78 %). Recent papyri from Egypt and Sicily exhibited large differences with almost no lignin peak in the latter one. This peak decreased with age in the old papyri while the cellulose remained more stable during time [112].

To study the two ancient papyri producing techniques of (i) pressing and (ii) beating, the same authors prepared their own papyri in the two ways. Pressing intensified the physical contact between different layers of papyrus stripes and strengthened the chemical adhesions by gumlike substances from cell sap. The mechanical destruction of the material by beating lowered the heat of combustion and the height of the lignin peak significantly compared with those of pressed samples (Figure 16). The small endothermic peak at 140°C is due to a dehydra-

tion of calcium oxalate monohydrate, a typical component of fast growing plants like papyrus and additionally formed during beating. The exotherm effect between 320 and 390°C reflects the decomposition of calcium oxalate [112]. It can be concluded from these early experiments that DTA like investigations are useful (i) for the determination of a rough age of papyri by their lignin content; (ii) to distinguish between unbeaten and beaten material; (iii) to estimate the treatment with different chemicals (e.g. calcium chloride); and (iv) to evaluate microbial destructions of papyri by fungi seen as additional peaks in the thermograms (e.g. of chitin) [113].

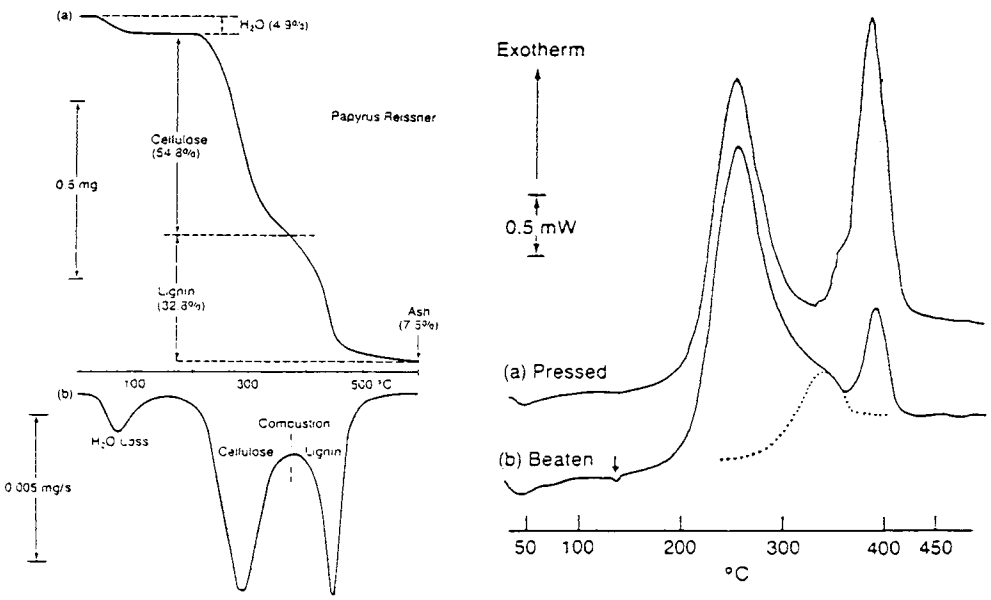

Figure 15. TG (a) and DTG (b) curves of an ancient papyrus sheet (1900 B.C.) [112].

Figure 16. DTA thermograms of (a) pressed and (b) beaten papyrus sheets (see text) [112].

The technology of modern paper originated from China and spread to the West and to Japan. Ancient Japanese papers were prepared from bast of the mulberry tree "Kozo" (*Morus alba*), later ones up to now from bast of the trees "Mitsumata" (*Edgeworthia papyrifera*) and "Gampi" (*Diplomorpha sikokiana*). DTA thermograms of these two papers and corresponding basts are presented in

Figure 17 [104]. The broad cellulose peaks in the basts point to hemicellulose which is absent after preparation to paper. In the Gampi sample the temperature stable parts diminished, while in Mitsumata the lignin part was altered. Three exothermic peaks are detectable which reflect the different degrees of polycondensation of the substituted coniferyl alcohols [114]. The differences in DSC curves of Mitsumata, Gampi and Kozo samples are so significant that it is possible to decide which fibres are present in the various papers [110].

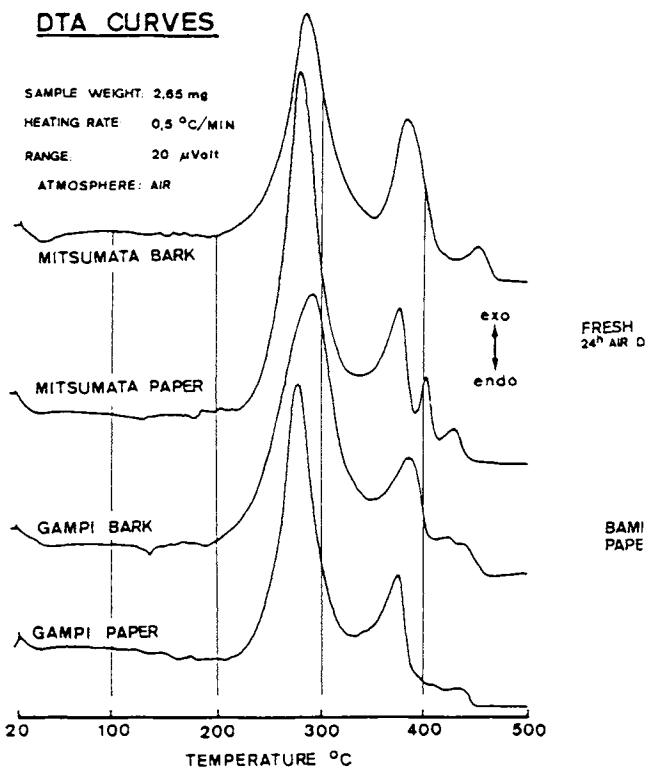

Figure 17. DTA thermograms of Mitsumata and Gampi bark and paper [104].

Quite another kind of "paper" was used in Middle America in the Maya and Aztec cultures. Barkcloth tunics evolved into a writing material named "huum", a paper far superior to the Egyptian papyrus both in texture and durability [104]. The Aztecs produced their paper from bast fibres of the amtal-tree (*Ficus* sp.). The authors had the chance to investigate samples from the Codex Huamantla by

means of DSC and TG-MS and to compare them with recent papers of the Mexican Otomi Indians. Figure 18 presents DSC curves of the ancient Codex and of new papers of different botanical origin. The white Otomi paper is most similar to the Codex specimen so that it might also be produced from wild fig trees (*Ficus padafolia*). The small endothermic peak around 150°C was already discussed above as due to oxalic acid and to the technique of beating the wood during paper production [114].

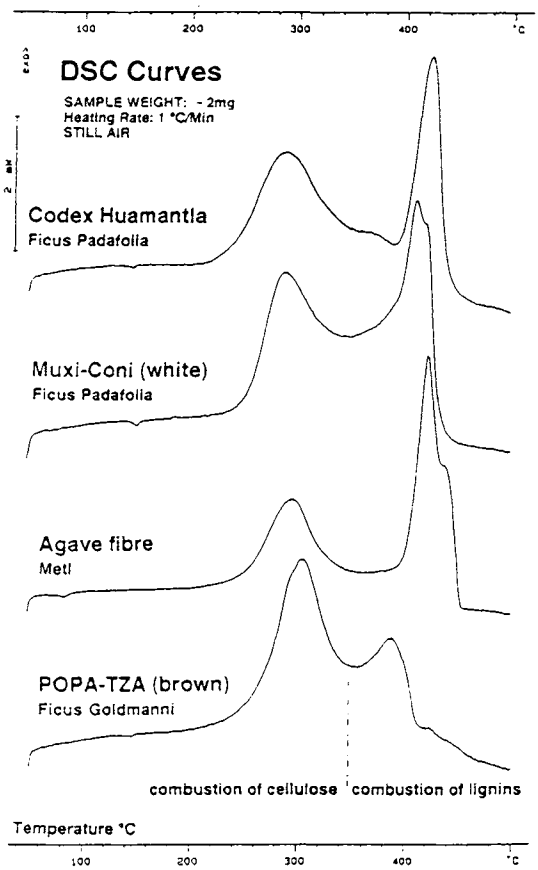

Figure 18. DSC thermograms of the Codex Huamantla and recently produced Mexican bast papers [114].

Even more exotic are the "pseudo" papers of Polynesia known as Tapa which are not produced in the usual way [113]. They consist of a single layer of beaten bast of the paper mulberry tree (*Broussonetia papyrifera*), the bread-fruit tree (*Artocarpus altilis*) and fig trees (*Ficus* sp.). The paper has textile structure and characteristics. Again the small endothermic peak is observed around 150°C in DTA thermograms besides a dominant cellulose peak (180 to 350°C) and a sometimes split lignin peak between 350 and 450°C (Figure 19).

Since newsprint contributes about 30 % to the municipal waste of industrial countries and only parts of it can be recycled into paper, Richards and Zheng [28] studied the possibilities to increase the pyrolysis yields of this matter by addition of ferrous sulfate (see also the section 20.4 about Pyrolysis). The production of levoglucosan was stimulated fivefold and that of levoglucosenone also. The authors point to the fact that - instead of enlarging the waste mountains of modern society - pyrolysis of newsprint generates a chemical feedstock (of these two compounds) and forms char at the same time which already contains ferrous ions as an efficient catalyst [28].

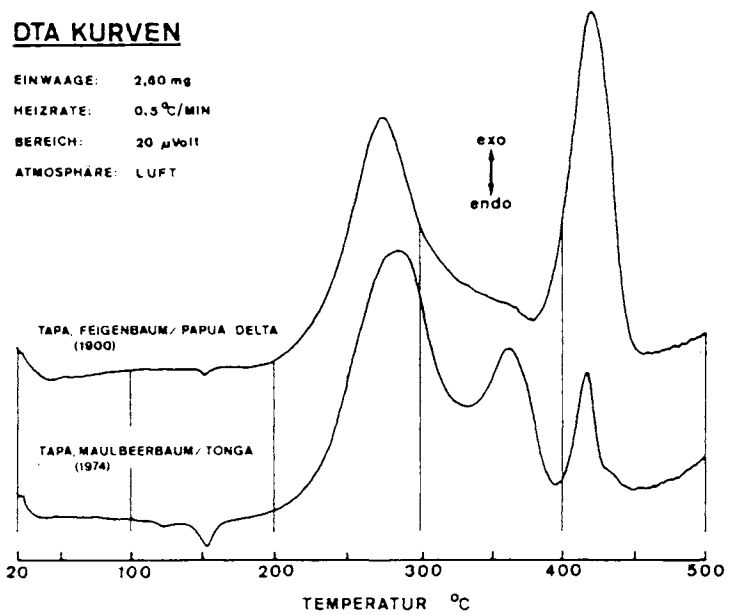

Figure 19. DTA thermograms of Tapa papers. Top: Fig-tree tapa from the Papua Delta (1900), bottom: Mulberry tree tapa from Tonga (1974) [113].

To finish this section, investigations with TG, DSC and thermal volatilization analysis shall be mentioned applied to the thermal decomposition of pure cellulose and pulp paper [115]. High heating rates led to a depolymerisation of cellulose to levoglucosan, low rates to an autocatalytic dehydration and formation of char. Kraft paper was decomposed by both mechanisms simultaneously with a larger release of volatile carbonylic compounds.

13. WOOD AND WASP NESTS

Some insect species - among them mainly paper wasps (*Polistinae*) and other social wasps or hornets (*Vespidae*), some termites and ants - construct paper covers for their nests to improve the thermoregulatory behaviour. They use slightly rotten, intensively chewed, wood as the basic material and the chitin-containing spittle secretion of their saliva glands as cement. This hardens within seconds [116] and produces a water repellent outer layer [117]. The multi-layered envelope contains the combs which are constructed from nearly the same material. Although such nests were investigated with different chemical and physical techniques [116,118,119], no TA measurements have been found in the literature.

Recently experiments were performed on nests of the hornet *Vespa crabro* and of several wasps by means of combustion calorimetry and DSC, TG/DTG and MS. The ash content of most nests is small (about 3 %) comparable to that of wood (see above) with the exception of nests of the wasp *Dolichovespula* (7.4 %). In contrast to wood with more than 50 % (fresh) and about 20 % (dry) the water content of wasp nests is extremely low with only 3.6 %. This is of special importance for the insulating properties of the envelope. The combustion energy with values between −16 and −18 MJ/kg corresponds to that of wood [120].

Figure 20 shows the thermogram of a nest envelope of the wasp *Vespula vulgaris*. An endothermic peak due to water loss is observed at about 75°C, a transition from endothermic to exothermic effects around 252°C and three exothermic peaks around 335°C (cellulose), 435°C (lignin) and 510°C (supposedly components formed during pyrolysis) [120]. As the nests are constructed from several thousand small wood particles of a few milligrams and of different origins, wasp nests are not at all identical in their chemical composition between one another and in themselves. Thus, larger variations in the height, the shape and the temperature of peaks may occur. Differences are also seen between the envelope, the combs and the pedicels of a single nest.

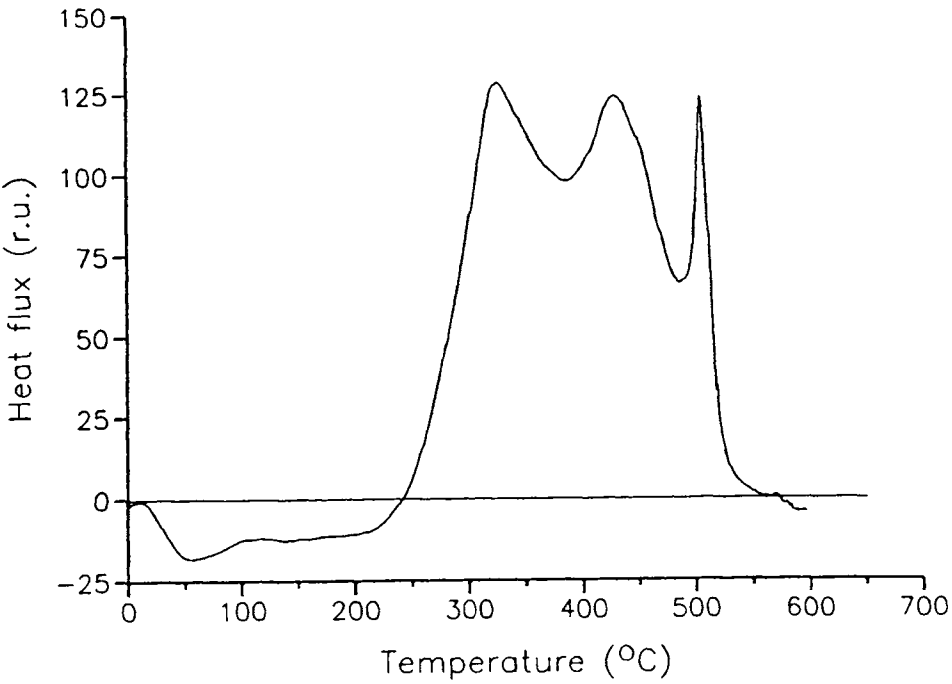

Figure 20. Thermogram of the nest envelope of the wasp *Vespula vulgaris*. All three exothermic peaks are typical for envelopes but vary in their relative height and temperature within a nest and between nests of different origins and years [120].

14. MICROBIAL DEGRADATION OF WOOD

A manyfold of biological agents decompose wood, among them fungi and bacteria. They may attack different components, e.g. the brown-rot fungi mainly the polysaccharides, white-rot fungi all cell walls, and this at changing rates depending upon the active species [121]. Such decay by progressive fungal degradation is connected with a loss of strength. Even at slight weight losses of less than 10 % significant reductions of important wood characteristics can occur so that a rapid means to determine the "incipient decay" is of interest beside the usual weight loss evaluation [122]. TA could be such an approach but only few papers are published on microbial deterioration of wood. White- and brown-rotting of birchwood was followed over 12 weeks by means of TG but significant

results could only be obtained after a weight loss of more than 50 % [123]. Effects earlier than the readily-obtainable weight losses could be detected from DSC on white- and brown-rotten aspenwood during a seven-week period by evaluating the endothermic peak areas [124]. Both papers assumed that there is a strong correlation between the thermal instabilities and the changes induced by microbial degradation on the degree of polymerization of cellulose [122]

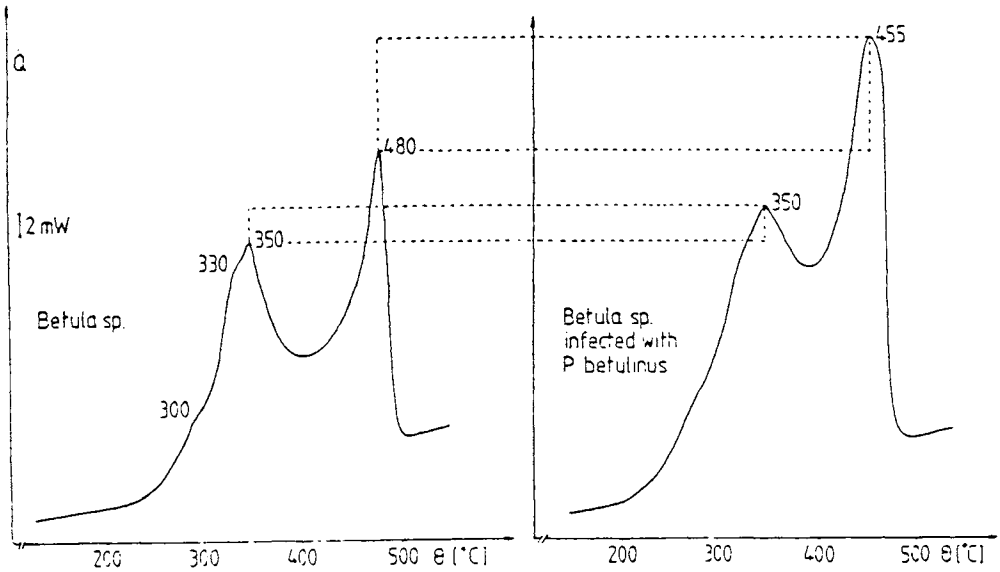

Figure 21. Thermograms of sound birchwood (left) and outdoor birchwood (right) infected with *P. betulinus* [127].

Baldwin and Streisel [122] investigated poplar sapwood samples (*Populus maximowiczii* × *trichocarpa*) taken from the same growth ring. After surface sterilization, small specimens were incubated in petri dishes with the brown-rot fungus *Lenzites trabea* for 3 to 15 days. Every third day samples were analyzed by DSC under nitrogen between 227 and 427°C and by chemical means. Above a weight loss of 4.7 %, DSC was a useful tool to ascertain the extent of decay in agreement with the earlier observations [123,124]. The highly crystalline alpha-cellulose was the most stable wood component and did not change much during this initial degradation state, while extractive-free wood showed a clear relationship between the size of the endothermic peak and the weight loss [122].

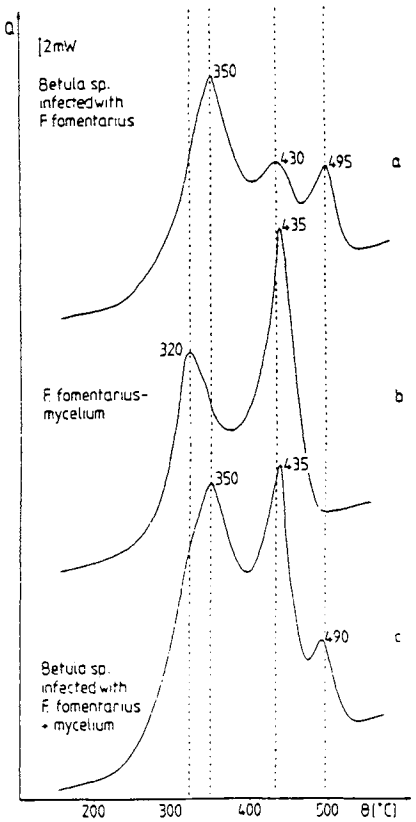

Figure 22. Thermograms of (a) birchwood sample infected with *F. fomentarius*, (b) pure mycelium of *F. fomentarius*, (c) mixed sample of (a) and (b) showing the superposition of the presumed mycelium peaks [127].

Each year, considerable amounts of useful wood are lost due to fungal degradation activities. On the other hand, there is an intensive screening for white-rot fungi which could be suitable for biotechnological purposes [125,126]. With this background, Reh and coworkers made DSC and isothermal calorimetric investigations on sound and microbially degraded wood [127-129]. Two Basidiomycetes, *Fomes fomentarius* and *Piptoporus betulinus*, were used in the form of pure aerial mycelia collected from field samples of birchwood (*Betula* sp.). Besides some combustion profiles of sound wood from spruce (*Picea abies*), beech

(*Fagus sylvatica*) and eucryphia (*Eucryphia cordifolia*) the experiments concentrated on sound and degraded birchwood and some wood reference compounds.

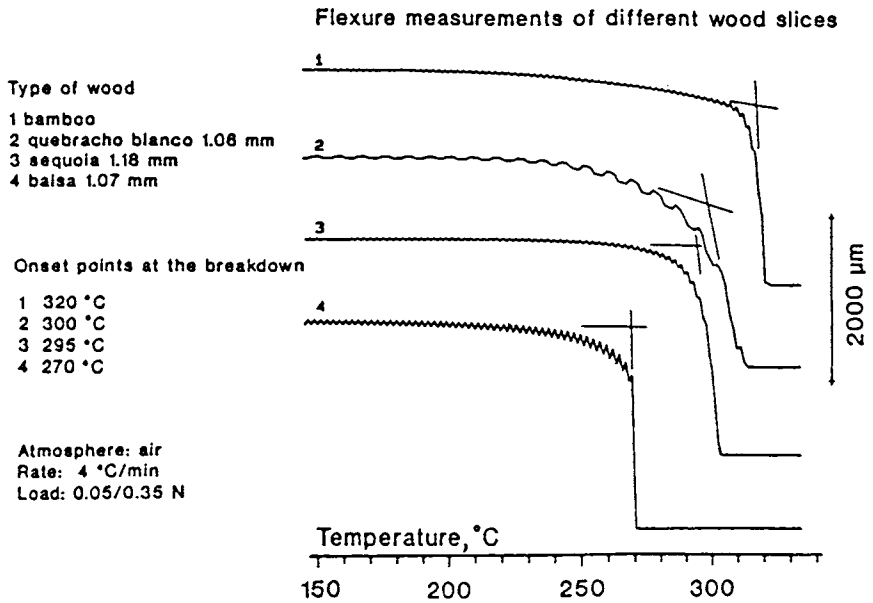

Figure 23. Thermal stability of different kind of woods determined by flexure measurements (DLTMA) [130].

All wood thermograms showed the two well-known peaks of cellulose (345 to 360°C) and lignin (470 to 480°C) and two more or less distinct shoulders around 300 and 330 to 335°C. The first shoulder may be traced to xylan, but the reason for the second one is unclear, although it is similar in position to Björkman lignin. Figure 21 exhibits the graphs of a sound (left) and degraded birchwood (right) with a clear increase of the (relative) lignin content and a shift of its main peak from 480 to 455°C. While the brown-rot fungus *P. betulinus* selectively removes cellulose from wood and accumulates modified lignin, the white-rot fungus *F. fomentarius* preferentially degrades lignin and induces the appearance of several small peaks between 400 and 510°C [128]. Figure 22 indicates that even the mycelium of the Basidiomycetes can be detected as an additional peak around 430°C and as a shoulder at 320°C in white-rotted wood, but never in brown-rotted specimens [127].

15. OTHER OBSERVATIONS ON WOOD

Wiedemann [130] used samples of redwood (*Sequoia sempervirens*), balsa (*Ochroma pyramidale/lagopus*), quebracho blanco (*Aspidosperma quebracho-blanco*) and beech wood (*Fagus* spec.) to determine the mechanical properties of wood by means of TMA and DSC. Flexure measurements as depicted in Figure 23 show different, highly reproducible onset temperatures for breakdown in the chosen samples from the very light balsa wood to the very hard South American quebracho blanco and - for comparison - bamboo. TMA together with DSC results indicates that such breakdowns take place only after the complete decomposition of cellulose.

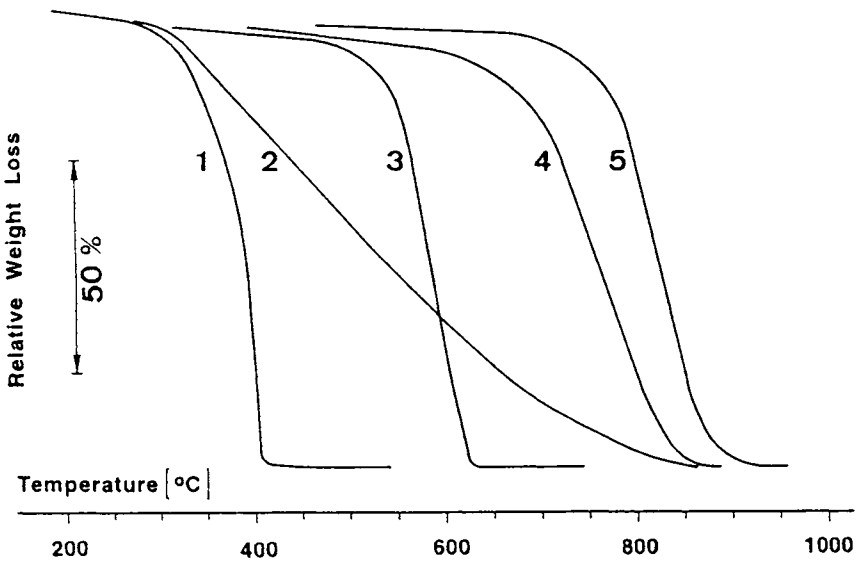

Figure 24. TG burning profiles of different carbon compounds in air. 1,3: charcoal of beechwood, 2: carbonaceous matter from the Allende meteorite, 4: highly crystalline graphite flakes, 5: diamond sugar [131].

The following TA investigation by Wiedemann and Reller [131] is in a loose connection with wood or wood components. They isolated carbonaceous matter from the Allende and the Murchison meteorite by wet chemistry and analyzed its degradation in an oxidizing atmosphere by means of TG. Figure 24 compares the degradation of the extraterrestrial material of the Allende meteorite (2) with that of Earth-bound samples of beech charcoal (1,3), crystalline graphite flakes (4)

and diamond sugar (5). It may be concluded from slope (2) that different forms of carbon compounds were present in the meteorite ranging from hydrocarbons to graphite. High-resolution electron microscopy revealed the presence of poorly ordered graphite. Graphite is one of the degradation products of the natural carbonization besides lignin, bituminous coal and anthracite and can be formed from charcoal at high temperatures. As the meteorite material underwent a complicated temperature programme when plunging into the Earth atmosphere different transitions of carbonaceous samples were possible. Thus, the investigations gave evidence for the presence of organic carbon compounds in the bulk of the Murchison meteorite and made macromolecular carbon compounds probable [131].

16. CONCLUSION

Wood plays an important role in all aspects of the daily life, as timber for housing, as fuel for warming, as ornamentally structured specimens for furniture or decoration, as substrate for sculptures, as source of natural drugs for our health and welfare, as basis of paper for communication: a role in the fullest sense of the word "from the cradle to the grave". Correspondingly broad is the field of application of thermoanalytical methods in wood research. Although Westeners feel that it is a pity just to burn wood and prefer to reserve it to relax by open fireplaces or barbeques, it should be kept in mind that wood is the essential (or only) fuel for the majority of mankind. We have to use our natural resources with providence, replant the cuts where it is possible and create new plantations to fulfill the elementary needs of population. Nature has to be handled with care to survive together with man.

Civilisation started with cutting the first tree -
and it ends with cutting the last!

REFERENCES

1. D.F. Arseneau, Can. J. Chem., 39 (1961) 1915.
2. A.G. Tan and J.B. Stott, J. Nat. Rubb. Res., 2(1) (1987) 27.
3. A.I. Fraser, Endeavour, New Series, 17(4) (1993) 168.
4. FAO, Woodfuel Surveys. FAO, Rome 1983.

5. H.H. Bossard, Holzkunde, Band 2, Zur Biologie, Physik und Chemie des Holzes. Birkhäuser Verlag, Basel 1975, p. 261.
6. D. Fengel and G. Wegener, Wood - Chemistry, Ultrastructure, Reactions. De Gruyter, Berlin 1989, pp.613
7. K. Freudenberg and A.C. Neish, Constitution and Biosynthesis of Lignin. Springer Verlag, Berlin 1968, p. 129.
8. B.M. Hausen, Woods Injurious to Human Health. A Manual. de Gruyter, Berlin 1981, p. 189.
9. P.H. Raven, R.F. Evert and S.E. Eichhorn, Biology of Plants, 5th ed., Worth Publishers, New York, 1992
10. E. Treiber, Die Chemie der Zellwand, Springer Verlag, Berlin 1957.
11. R.S. Criddle, R.W. Breidenbach and L.D. Hansen, Thermochim. Acta, 193 (1991) 67.
12. L.D. Hansen, E.A. Lewis, D.J. Eatough, D.P. Fowler and R.S. Criddle, Can. J. For. Res., 19 (1989) 606.
13. L.D. Hansen, R. Woodward, R.W. Breidenbach and R.S. Criddle, Thermochim. Acta, 211 (1992) 21.
14. T.S. Anekonda, R.S. Criddle, W. J. Libby and L.D. Hansen, Can. J. For. Res., 23 (1993) 1793.
15. E.L. Schaffer, USDA, USFS Forest Products Laboratory, Research Note FPL-0145, Madison, WI (1966) pp.55.
16. F.C. Beall and H.W. Eickner, USDA, USFS Forest Products Laboratory, Research Paper, FPL-130, Madison, WI, (1970) pp26.
17. F.C. Beall, Wood Sci., 5(2) (1972) 102.
18. R.C. Mackenzie (ed.), Differential Thermal Analysis. vol. 1 Fundamental Aspects. Academic Press, London 1970, pp. 775.
19. R.C. Mackenzie (ed.), Differential Thermal Analysis. vol. 2, Applications. Academic Press, London 1970, pp. 607.
20. B.D. Mitchell and A.C. Birnie, Biological materials. in R.C. Mackenzie (ed.), Differential Thermal Analysis. vol. 1 Fundamental Aspects. Academic Press, London 1970, p-673-703.
21. K.W. Tang, Forest products, in R.C. Mackenzie (Ed.) Differential Thermal Analysis, vol. 2, Applications. Academic Press, London, 1972, pp. 523-553.
22. D.W. Gunnels, D.J. Gardner and M.P. Wolcott, Wood Fiber Science, 26(4) (1994) 447.
23. R. Domanský and F. Rendos, HOLZ als Rohstoff und Werkstoff, 20 (1962) 473.
24. W.-P. Pan and G.N. Richards, J. Anal. Appl. Pyrol., 16 (1989) 117.
25. W.-P. Pan and G.N. Richards, J. Anal. Appl. Pyrol., 17 (1990) 261.
26. G.R. Ponder and G.N. Richards, Energy & Fuels 8 (1994) 705.

27. G.N. Richards and F.-Y. Hshieh, in: G.L. Nelson (ed.), Fire and Polymers: Hazards Identification and Prevention. ACS Symposium Series No. 425, American Chemical Society, Washington DC, 1990, 361.
28. G.N. Richards and G. Zheng, J. Anal. Appl. Pyrol., 21 (1991) 133.
29. M.P. Kannan and G.N. Richards, Fuel, 69 (1990) 999.
30. T.G. Devi, M.P. Kannan and G.N. Richards, Fuel, 69 (1990) 1440.
31. J.L. Grandmaison, J. Thibault and S. Kaliaguine, Anal. Chem., 59 (1987) 2153.
32. T. Arima, J. Japan. Wood Res. Soc. (Nihon-mokuzai-gakkai), 19(9) (1973) 435.
33. T. Arima, J. Japan. Wood Res. Soc. (Nihon-mokuzai-gakkai), 19(9) (1973) 443.
34. T. Arima, J. Japan. Wood Res. Soc. (Nihon-mokuzai-gakkai), 19(10) (1973) 475.
35. J.M. Rogers, R.A. Susott and R.G. Kelsey, Can. J. For. Res., 16 (1986) 721.
36. S. Gnecco, M. Montecinos, R. Cid, A. Pavlath, K. Gregorski and S. Tillin, Bol. Soc. Chil. Quim., 40(1) (1995) 49.
37. V. Cozzani,L. Petarca and L. Tognotti, Fuel 74(6) (1995) 903.
38. V. Cozzani, C. Nicolella, L. Petarca, M. Rovatti and L. Tognotti, Ind. Eng. Chem. Res., 34 (1995) 2006.
39. V. Cozzani, C. Nicolella, M. Rovatti and L. Tognotti, Ind. Eng. Chem. Res., 35 (1996) 90.
40. E.L. Back and F. Johanson, Holzforsch., 44 (1990) 21.
41. E.L. Back and F. Johanson, Holzforsch., 44 (1990) 177.
42. V. Cozzani, A. Lucchesi and G. Stoppato, Can. J. Chem. Eng., 75 (1997) 127.
43. C.E. López Pasquali and H. Herrera, Thermochim. Acta, 293 (1997) 39.
44. G.E. Domburg, V.N. Sergeeva and A.I. Kalninsh, in H.G. Wiedemann (Ed.) Thermal Analysis, Birkhäuser Verlag, 1972, 327.
45. E. Jakab, O. Faix, F. Till and T. Székely, Holzforsch., 45 (1991) 355.
46. A.A. Pappa, N.E. Tzamtzis, M.K. Statheropoulos and G.K. Parissakis, Thermochim. Acta, 261 (1995) 165.
47. S. Cooley and M.J. Antal, J. Anal. Appl. Pyrol., 14 (1988) 149.
48. H.G. Wiedemann, Thermochim. Acta, 229 (1993) 215.
49. H.G. Wiedemann, R. Riesen, A. Boller and G. Bayer, in: C.M. Earnest (Ed.) Compositional Analysis by Thermogravimetry. ASTM, Philadelphia, 1988, pp.227.
50. M.M. Ivask, Lesovedenie, (3) (1984) 49.
51. U. Reh and G. Kraepelin, Thermochim. Acta, 151 (1989) 91.

52. J.K. Woo and A.P. Schniewind, Holzforsch., 41 (1987) 305.
53. H. Berndt, A.P. Schniewind and J.K. Woo, Holzforsch., 44 (1990) 439.
54. T.P. Brady and H.G. Langer, in W. Hemminger (Ed.) Thermal Analysis, vol. 2, Birkhäuser Verlag, Basel, 1980,pp.443.
55. C. Domburg, G. Rossinskaya and G. Dobele, in W. Hemminger (Ed.) Thermal Analysis, vol. 2, Birkhäuser Verlag, Basel, 1980, pp.449.
56. T. Hirata and T. Nishimoto, Thermochim. Acta, 193 (1991) 99.
57. B.K. Kandola, S. Horrocks and A.R. Horrocks, Thermochim. Acta, 294 (1997) 113.
58. Y.X. Wang, J. Simonsen, C.P. Neto, J. Rocha, T.G. Rials and E. Hart, J. Appl. Polym. Sci., 62(3) (1996) 501.
59. J. Simonsen and T.G. Rials, J. Thermoplast. Comp. Mat., 9(3) (1996) 292.
60. V.E. Reinsch and S.S. Kelley, J. Appl Polym. Sci., 64(9) (1997) 1785.
61. K. Shimatani and Y. Sano, Holzforsch., 49(4) (1995) 351.
62. Y. Lu, Q. Shi and Z. Gao, Holz als Roh- und Werkstoff, 53(3) (1995) 205.
63. C.B. Vick and A.W. Christiansen, Wood and Fiber Science, 25 (1993) 77.
64. M. Kano, M. Momota, T. Okabe and K. Saito, Thermochim. Acta, 292 (1997) 175.
65. L.A. Simpson and A.F.M. Barton, Wood Sci. Technol., 25 (1991) 301.
66. L. V. Gusta, N.J. Tyler and T.H.-H. Chen, Plant Physiol., 72 (1983) 122.
67. G. Östberg, L. Salmén and J. Terlecki, Holzforsch., 44 (1990) 223.
68. J. Berthold, M. Rinaudo and L. Salmen, Physicochem. Engin. Asp. 112 (1996) 117.
69. M.S.C. Dionisio, N.T. Correia, J.F. Mano, J.J.M. Ramos, A.C. Fernandes and B. Saramago, J. Mater. Sci., 30 (1995) 4394.
70. I. Lamprecht, Thermochim. Acta, 40 (1980) 157.
71. F. Pöpel, Stuttgarter Bericht zur Siedlungswasserwirtschaft, 41 (1968) 5.
72. E. Svikovsky, In: Bio-Energie. Duttweiler, Rüschlikon 1978, p.127.
73. R.S. Seymour and D.F. Bradford, The Condor, 94 (1992) 134.
74. U. Reh, Thermochim. Acta, 193 (1991) 107.
75. H. Lieth, in H. Lieth and R. Whittacker (eds.) Primary Productivity of the Biosphere. Springer-Verlag, Berlin 1975, 119.
76. H. Lieth, in: O.L. Lange, L. Kappen and E.-D. Schulze (eds.), Water and Plant Life. Ecological Studies. Analysis and Synthesis. vol 19, Springer-Verlag, Berlin 1976, 392.
77. H. Lieth, in: I. Lamprecht and B. Schaarschmidt (eds.), Application of Calorimetry in Life Sciences. de Gruyter, Berlin 1977, 325.
78. National Academy of Sciences, Firewood Crops. Shrub and Tree Species for Energy Production. National Academy of Sciences, Washington D.C., 1980, pp. 236.

79. G.A. Tuskan and A.A. De La Cruz, For. Ecol. Manage., 4(2) (1982) 191.
80. D.A. Tilman, Wood as an Energy Resource. Academic Press, New York 1978.
81. F. Shafizadeh and W.F. Degroot, in: Fuels and Energy from Renewable Resources (D.A. Tilman, K.V. Sarkanen and L.L. Anderson eds.) Academic Press, New York 1977.
82. E. Pipp and W. Larcher, Sitzungsber. Österr. Akad. Wiss. Math.-Naturw. Kl. Abt. I, 196. Bd. 4. H. (Smn 196-4), Wien 1987, 37.
83. E. Pipp and W. Larcher, Sitzungsber. Österr. Akad. Wiss. Math.-Naturw. Kl. Abt. I, 196. Bd. 13. H. (Smn 196-13), Wien 1987, 249.
84. J.A.R. Anon, F.F. Lopez, J.P. Castineiras, J.P. Ledo, L.Nunez-Regueira, Biores. Techn., 52 (1995) 269.
85. L. Nunez-Regueira, J.A.R. Anon and J.P. Castineiras, Biores. Techn., 57 (1996) 283.
86. L. Nunez-Regueira, J.A.R. Anon and J.P. Castineiras, Biores. Techn., 61(2) (1997) 111.
87. D.P. Barnes and S.A. Sinclair, Wood Fiber Sci., 16(4) (1984) 518.
88. M. Neenan and K. Steinbeck, For. Sci., 25(3) (1979) 455.
89. J. Oszlányi, Biologia, 34(4) (1979) 775.
90. J. Oszlányi, Ekológia (CSSR), 1(3) (1982) 289.
91. F. Abe, Bull. For. For. Prod. Res. Inst., (352) (1988) 1.
92. M.S. Darling, Oecologia (Berl.), 23 (1976) 127-139.
93. L. Siafaca, S. Adamandiadou and N.S. Margaris, Oecologia (Berl.), 44 (1980) 276.
94. ASTM Standards, Gaseous Fuels, Coal, and Coke, Part 26, Methods D3172-75, 1973.
95. D. Aylmer and M.W. Rowe, in: B. Miller (Ed.) Thermal Analysis, vol. II, John Wiley & Sons; Chichester 1982, pp.1270.
96. C.M. Earnest and R.L. Fyans, in: B. Miller (Ed.) Thermal Analysis, vol. II, John Wiley & Sons; Chichester 1982, pp.1260.
97. M. Goutal, Compt. Rend., 135 (1902) 477.
98. D. Fengel, Wood Sci. Technol., 25 (1991) 153.
99. R.M. Rowell and R.J. Barbour (eds.), Archaeological wood. Properties, chemistry and preservation. Advances in Chemistry Series No. 225, American Chemical Society, Washington DC, 1989, pp. 472.
100. M. Tomassetti, L. Campanella, R. Tomellini and C. Meucci, Thermochim. Acta , 117 (1987) 297.
101. M. Tomassetti, L. Campanella and R. Tomellini, Thermochim. Acta, 170 (1990) 51.

102. L. Campanella, M. Tomassetti and R. Tomellini, J. Therm. Anal., 37 (1991) 1923.
103. H.G. Wiedemann, J. Therm. Anal., 52 (1998) 93-107.
104. H.G. Wiedemann, Natl. Bur. Stand. Special Publication, 580 (1979) 201.
105. D. Holz, J. Acoust. Soc. Am., 99(3) (1996) 1795.
106. D. Holz, Holzforschg., 50 (1996) 121.
107. D. Holz, Holztechnol., (1984) 31.
108. J. Nagyvary, Chem. Eng. News, May 23 (1988) 24.
109. H.G. Wiedemann, Chem. Unserer Zeit, submitted.
110. H.G. Wiedemann, J.R. Günter and H.R. Oswald, Thermochim. Acta, 282/283 (1996) 453.
111. G. Bayer and H.G. Wiedemann, in: B. Miller (Ed.) Thermal Analysis, vol. II, John Wiley & Sons; Chichester 1982, pp.1470.
112. H.G. Wiedemann and G. Bayer, Anal. Chem., 55 (1983) 1220A.
113. H.G. Wiedemann, in E. Marti, H.R. Oswald and H.G. Wiedemann (Eds.) Angewandte Chemische Thermodynamik und Thermoanalytik. Birkhäuser Verlag, Basel, 1979, pp. 242.
114. H.G. Wiedemann and A. Boller, J. Therm. Anal., 46 (1996) 1033-1045.
115. S. Soares, G. Camino and S. Levchik, Polym. Degrad. Stab., 49 (1995) 275.
116. J.S. Ishay, and E. Ganor, J. Morphol., 203 (1990) 11.
117. F. Schremmer, L. März and P. Simonsberger, Mikroskopie, 42 (1985) 52.
118. K.E. Espelie and H.R. Hermann, J. Chem. Ecol., 16 (1990) 1841.
119. K.E. Espelie and D.S.Himmelsbach, J. Chem. Ecol., 16 (1990) 3467.
120. E. Schmolz, B. Schricker and I. Lamprecht, Thermochim. Acta, submitted.
121. R.A. Blanchette, T. Nilsson, G. Daniel and A. Abad, in: R.M. Rowell and R.J. Barbour, Archaeological Wood. Properties, Chemistry, and Preservation. Advances in Chemistry Series 225, American Chemical Society, Washington DC, 1990, p.141.
122. R.C. Baldwin and R.C. Streisel, Wood Fiber Sci., 17(3) (1985) 315.
123. F.C. Beall, W. Merrill, R.C. Baldwin and J.-H. Wang, Wood Fiber, 8(3) (1976) 159.
124. P.R. Blankenhorn, R.C. Baldwin, W. Merrill and S. Ottone, Wood Sci., 13(1) (1980) 26.
125. K.-E.L. Eriksson, R.A. Blanchette and P. Ander, Microbial and Enzymatic Degradation of Wood and Wood Components. Springer Series in Wood Science IX. Springer-Verlag, Berlin, 1990, pp.407.
126. A. Ginterova and A. Lazarova, Folia Microbiol., 34(2) (1989) 141.
127. U. Reh, G. Kraepelin and I. Lamprecht, Appl. Environm. Microbiol., 52 (1986) 1101.

128. U. Reh, G. Kraepelin and U. Schulze, in INRA (Ed.) Lignin Enzymic and Microbial Degradation. Les Colloques de l'INRA, no 40. Paris, 1987, 291.
129. M. Becker, G. Kraepelin and I. Lamprecht, Thermochim. Acta, 187 (1991) 15.
130. H.G. Wiedemann, J. Therm. Anal., 37 (1991) 1557.
131. H.G. Wiedemann and A. Reller, Naturwiss., 79 (1992) 172.

This Page Intentionally Left Blank

Handbook of Thermal Analysis and Calorimetry, Vol. 4: From Macromolecules to Man.
R.B. Kemp, editor.

Chapter 15

DYNAMIC MECHANICAL ANALYSIS OF ELASTOMERS

C.M. Roland

Naval Research Laboratory
Chemistry Division, Code 6120
Washington, DC 20375-5342
USA

1. VISCOELASTICITY

1.1 Modes of Motion in Polymers

An understanding of the physical and mechanical behavior of materials requires consideration of two fundamental dependencies - of time and of temperature. This is especially true for polymers due to their viscoelasticity. While many materials exhibit viscoelasticity (e.g., concrete, biological materials, and metals at elevated temperature) [1], polymers are invariably viscoelastic. Their large molecular size gives rise to a broad range of relaxation length-scales. This means that for any perturbation, there are some relaxation mechanisms transpiring at short times, hence contributing a viscous response, and other relaxation modes, involving larger portions of the chain molecule, which are slow compared to the experimental time scale, thus responding elastically. The combination of both viscous and elastic contributions gives rise to a time dependence of the mechanical response; that is, viscoelasticity.

The range of motions available to a polymer spans the high-frequency secondary relaxations, involving motion of pendant groups, to the slow so-called chain modes, which reflect motion over large (>10 nm) distances. The slowest relaxation process is the terminal mode, corresponding to motion of the entire molecule. These dynamics can be illustrated with an example, poly(vinylethylene) (PVE), an elastomer also known as 1 ,2-polybutadiene.

The pendant vinyl group in PVE undergoes a waggling motion which has minimal effect on the stress, but can be detected by dielectric spectroscopy. This

secondary relaxation, which has an Arrhenius temperature dependence, occurs at higher frequencies and/or lower temperatures than the glass transition region of the viscoelastic spectrum. At room temperature the time scale of the secondary relaxation in PVE is 10^{-6} s (i.e., MHZ frequencies) [2].

The next fastest relaxation corresponds to the local segmental motion associated with the glass transition, which has a length equal to a few backbone bonds. This relaxation appears as a peak in the loss modulus spectrum, situated at end of the glassy plateau. While measurements of local segmental relaxation are usually done near T_g, the glass transition temperature, in order to bring the dynamics into the range of typical instrumentation (e.g., 10^{-3} to 10^{+2} Hz), the "T_g-relaxation" can in principle be measured at any temperature. For PVE, whose glass transition temperature is 0 °C, the segmental relaxation time at room temperature is about 10^{-3} s (kHz frequencies) [3]. The VFTH equation (see below) is commonly used to describe the temperature dependence of segmental relaxation in polymers, as well as the glass transition relaxation in small molecule, glass-forming liquids. The latter, which have no chain segments, undergo reorientational motions at T_g, rather than the segmental relaxation of polymers.

Relaxation slower than segmental relaxation involves longer portions of the chain molecule, and are responsible for the glass transition ("softening") region of the viscoelastic spectrum. Such motions are quite complicated. Bead-spring analogs, and in particular the Rouse model modified for neat polymers [4], are used to model the dynamics. The Rouse model describes the motion of chain segments which are long and flexible enough to exhibit Gaussian behavior; that is, the end-to-end distribution function of the segments is Gaussian. The distance for Rouse motion extends from roughly 50 Å up through the length scale associated with the molecular weight between entanglements. This entanglement molecular weight varies with chemical structure; for PVE, M_e = 4900 [5]. This equates to a distance of about 200 Å, which defines the upper limit of applicability for the Rouse model for PVE.

For polymeric liquids having molecular weights large enough for entanglement coupling, the motion of increasingly larger sections of the chain gives rise to the rubbery plateau region of the viscoelastic spectrum. The slowest dynamics comprise the terminal relaxation, which marks the end of this plateau. The terminal dynamics involve motion of the entire chain molecule. A measure of the terminal relaxation time is the time required for the chain to diffuse a distance equal to its coil size. This relaxation time is thus strongly molecular weight

dependent, typically varying with roughly the 3.4 power of molecular weight. For PVE having a molecular weight equal to 400,000, for example, the terminal relaxation time at room temperature is about 10,000 s. This is 10 orders of magnitude longer than the secondary motions, and 7 decades slower than the segmental relaxation, illustrating the enormous time scale of polymer dynamics. The temperature dependence of both the Rouse modes and the terminal relaxation are usually described using the WLF equation (see below). At high temperature, the temperature dependence for the terminal relaxation may obey an Arrhenius law, although only unsaturated polymers have sufficient thermal stability for this to be observable.

The various motions of a polymer molecule not only occur at different rates, but they are also affected differently by temperature changes. These two aspects are considered in detail below.

1.2 Time Dependence of Relaxation

Relaxation functions, describing the time dependence of the modulus, are either derived from a model or simply an empirically-adopted fitting function. Only the former are amenable to interpretation. However, an empirical function with some theoretical basis is the Kohlrausch-Williams-Watts equation [6], which describes a variety of relaxations observed in many different materials [7]

$$G(t) = G_0 \exp -\left(\frac{t}{\tau_{KWW}}\right)^{\beta} \qquad (1)$$

In this equation, G_0 is the high frequency limiting value of the modulus (the "unrelaxed" modulus), τ_{KWW} is the relaxation time, and β a shape parameter. The KWW function has been found to describe various processes. Most importantly for polymers, the local segmental relaxation dynamics conform closely to form of equation 1.

A number of models, especially for relaxation in the vicinity of the T_g, yield the KWW function. These are variously based on constraint dynamics [8,9], free volume [10,11], defect diffusion [12], or relaxation time distributions [13,14].

The most useful theoretical approach is the coupling model, because it provides verifiable predictions concerning the relationships between chemical structure, and the time and temperature dependencies. The coupling model, when applied to local segmental motion, is a homogeneous relaxation theory (i.e., all basic units are relaxing in the same manner at the same time). Of course, a

distribution of relaxation times exists on a molecular level [15]. In a densely packed system such as a polymer melt, the relaxing units mutually interact, and all cannot move in the same manner at the same time; this is either impossible or very inefficient. Intermolecular constraints thwart some of the attempted conformation transitions, giving rise to random variations in the success rate for transitions by individual segments. The interaction and correlation among the relaxing units slow down the individual relaxation rates. The coupling model addresses relaxation of *macroscopic* variables (e.g., stress, dielectric polarization, density fluctuation, mean-square-displacement, enthalpy, etc.) [16], which represent such an average over the basic relaxing units.

According to the coupling model, for neat polymers at the times appropriate for most experimental measurements, the slowing down of segmental relaxation gives rise to a correlation function having the form of equation (1). The stretch exponent is a measure of the strength of the intermolecular constraints on the relaxation. These constraints depend on molecular structure because the chemical structure determines the intermolecular interactions. However, the complexity of cooperative dynamics in dense liquids and polymers precludes direct calculation of β; it is invariably deduced from experiment. An assumption fundamental to the model is that the time at which intermolecular cooperativity effects become manifest is independent of temperature.

Smaller β implies stronger cooperativity and a broader spectral dispersion. Non-cooperative relaxation (β=1) yields exponential relaxation, which is only seen for polymers in high-frequency, low temperature relaxations or in their terminal relaxation at very high temperature. Exponential decay, or a Lorentzian frequency response, is often associated with an Arrhenius temperature dependence. In fact, a barrier model for relaxation leads directly to both an Arrhenius temperature dependence and exponential decay [17,18].

2. TEMPERATURE DEPENDENCE OF RELAXATION

Increasing temperature invariably reduces the magnitude of the relaxation time, by as much as a factor of 10^{10}. Despite this enormous effect on the time of relaxation, for a thermorheologically simple material, temperature has no effect on the rate at which the stress decays (i.e., the shape of the relaxation function). At least for linear polymers, the terminal relaxation function and height of the rubbery plateau are minimally affected by temperature. Segmental

relaxation behavior is more often sensitive to temperature and, when the relaxation function does change, it invariably narrows (faster relaxation rate) with increasing temperature.

The functional form of the temperature dependence can vary. For a thermally activated process, wherein the relaxation mechanism is governed by the microscopic success rate in transitioning an energy barrier, Arrhenius behavior obtains

$$\tau = \tau_0 \exp(-E_A/RT) \tag{2}$$

where E_a is the activation energy, τ_0 the pre-exponential factor, and RT has its usual significance.

Very often relaxation data is interpreted in terms of free volume, for example, using the theories of Bueche [19] and Fujita [20]. The idea that free volume governs molecular mobility gives rise to the two most common forms for the temperature dependence of polymer viscoelasticity. If the free volume goes to zero at absolute zero temperature, the equation of Williams-Landel-Ferry (WLF) can be derived [4,17]

$$\log \tau = \frac{-c_1(T-T_0)}{c_2+T-T_0} \tag{3}$$

where c_1 and c_2 are constants and T_0 is a reference temperature.

As an alternative, the assumption can be made that the unoccupied volume is not all "free", or accessible for the relaxing species. This approach leads to the prediction that the free volume equals zero at some temperature T_∞, which is above zero Kelvin. The resulting expression for the temperature dependence of the relaxation times is the Vogel-Fulcher-Teymann-Hess (VFTH] equation [4,17]

$$\tau = A\exp\left(\frac{B}{T-T_\infty}\right) \tag{4}$$

in which A and B are constants. Although the use of equations (3) or (4) implies different assumptions about free volume, the two functions are mathematically equivalent [21]. As suggested by the form of these relations, relaxation data are often expressed as a function of the difference between the measurement temperature and a reference temperature, in an attempt to "normalize" for the effect of temperature changes on free volume. While free volume no doubt exerts an influence on relaxation, there is a good deal of evidence [22-25] that

it does not actually govern molecular mobility. Consideration must be given to the inherent cooperativity of the molecular motions in condensed matter in order to achieve a quantitative description of the relaxation dynamics.

Since relaxation times must be measured at temperatures wherein their magnitudes fall within the experimental window of the available instrumentation, they are rarely measured for different materials at the same temperature. This introduces uncertainty into any attempt to compare the temperature dependence of different materials. Recently a normalization scheme has been widely adopted for the comparison of data obtained on different polymers, and even on small molecule, glass-forming liquids. In this method, shift factors are plotted as a function of inverse temperature normalized by T_g, or by a "dynamic" glass transition temperature, defined as one at which the relaxation time assumes some arbitrary value (e.g., 100 s).

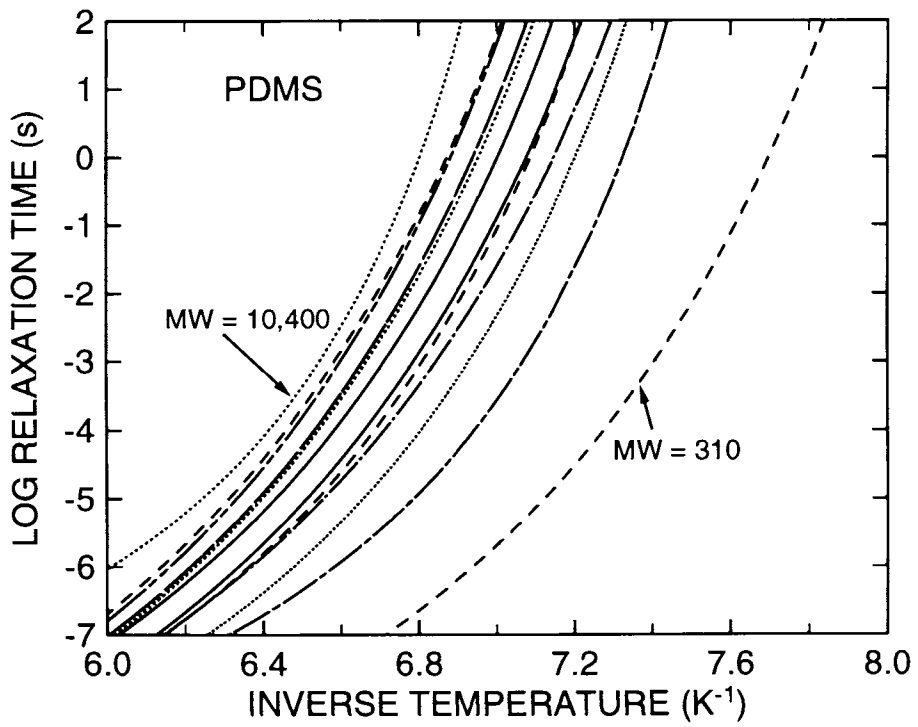

Figure 1. The segmental relaxation times for PDMS varying in molecular weight from 310 to 10,370 g mol^{-1}, which yields glass transition temperatures from 129K to 150K.

Angell [26,27] provided a theoretical basis for the T_g-normalized Arrhenius plot. If a liquid gains access to a high density of energetically-preferred configurational states when the temperature is raised through T_g, the glass transition will be accompanied by a large entropy increase; consequently, the heat capacity and relaxation times will change markedly with temperature changes near T_g. Such a liquid is classified as "fragile", a reference to the loss of short range order accompanying the transition from the glassy state. "Strong" liquids, on the other hand, have fewer potential energy minima, lose less of their local "structure", and thus exhibit smaller heat capacity increments at T_g. This thermally induced degradation of structure refers only to the loss of local order, not to chemical stability. There is no marked change in the structure factor for a polymer glass-forming small liquid as T_g is traversed, only a falling out of equilibrium (non-ergodicity). Hence, the terms strong and fragile are probably inappropriate; nevertheless, the term "fragility plot" is often used to refer to plots of $\log(\tau(T))$ versus T_g/T.

This approach has been applied extensively in recent years to polymers [16,27-31]. From comparisons of segmental relaxation times for various polymers made on the basis of T_g-scaled Arrhenius plots, correlations between the shape of the relaxation function and chemical structure have been demonstrated [3,16,32,33]. Fragility plots are also useful in interpreting the relaxation behavior of polymer blends, since the relaxation function itself is complicated due to inhomogeneous broadening [34-37].

The validity of the fragility plot approach can be demonstrated by comparing such plots for liquids differing in their glass transition temperatures, but not in their dynamics [38]. The obvious way to do this is to compare polymers differing only in molecular weight. Below some high polymer limit, the glass transition temperature is a function of molecular weight, whereby segmental relaxation times, and hence T_g, become molecular-weight-dependent. Since the segments themselves are identical, however, the relaxation behavior, and thus the fragility plots, should be the same. This can be illustrated with an example.

Dielectric relaxation measurements have been reported [39] for 13 different poly(dimethylsiloxanes), ranging in degree of polymerization from 8 to 139 (MW = 310 to 10370 g mol^{-1}). The chains were trimethyl-terminated, whereby the nonpolar end groups do not contribute to the dielectric response. In Figure 1, the segmental relaxation times, defined as the inverse of the frequency of the maximum in the dielectric loss, are shown as a function of temperature. As the molecular weight decreases, there is a decrease in the glass transition

temperature. This effect is well known, and reflects the additional configurational entropy (or "free volume") conferred on the melt by the presence of a higher concentration of chain ends in lower molecular weight samples. At sufficiently high molecular weight, T_g becomes invariant.

The lower MW PDMS have shorter relaxation times at every temperature. Defining a reference temperature as the temperature at which the relaxation time equals 1 s (this value is arbitrary, and chosen to be appropriate for the frequency range of the experimental technique employed), fragility plots can be constructed from the data. As seen in Figure 2, this causes the curves, which differed by as much as 9 orders of magnitude in Figure 1, to collapse into a single curve. Such results corroborate the fragility plot approach as a self consistent means to classify the segmental relaxation behavior.

2.1. Thermorheological Simplicity and Complexity

It is not a trivial problem to obtain a complete characterization of a material responding over many decades of time. The brute force method would be to carry out experiments over many decades of time. More efficient is to employ more than one instrument, and cover a time span that includes high frequencies. This is now possible with broad dielectric spectroscopy, with which the frequency range from 10^{-3} to 10^{9} can be attained by using different techniques – time domain spectroscopy, frequency response analysis using AC-bridges, and coaxial line reflectrometry. Of course, each isothermal experiment has to be repeated at various temperatures in order to determine the temperature dependence.

It is common to measure some viscoelastic quantity at constant frequency (or isochronally) over a series of temperatures, thus efficiently gaining a view of all viscoelastic mechanisms. However, since the relaxation function is temperature dependent, employing temperature as the independent variable convolutes the time and temperature dependencies, yielding data that are not amenable to theoretical analysis. The convenience of sweeping temperature at fixed test frequency comes at the expense of rigor.

Often the assumption is made that a material is thermorheologically simple, meaning all mechanisms contributing to the response have the same temperature dependence. In this situation, temperature only changes the relaxation time, not the shape of the relaxation function. Accordingly, the principle of time-temperature superpositioning can be applied. The measured quantities are shifted

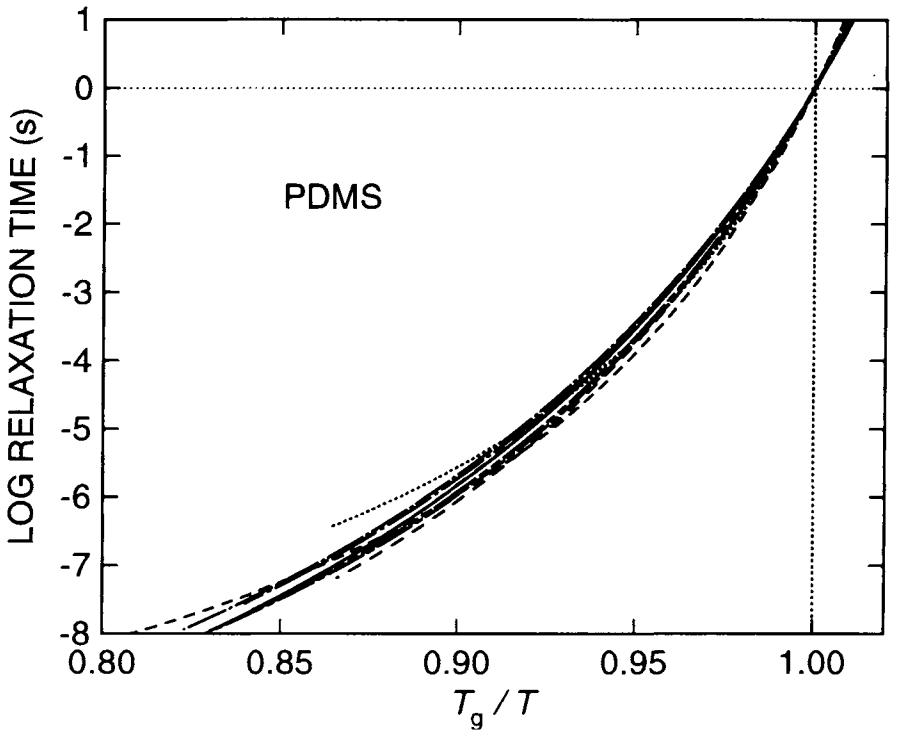

Figure 2. T_g-normalized Arrhenius plots of the PDMS data in Figure 1.

along the logarithmic time or frequency axis to produce "mastercurves". The reduced frequency range is many times greater than that of the actually measured frequencies.

Notwithstanding the fact that the polymer literature is replete with examples of the application of the time-temperature superposition principle, its underlying premise cannot be easily verified. Successfully superimposing data obtained with a conventional instrument, covering only 3 or 4 decades of time, does not prove the correctness of the procedure. A more stringent test is to obtain shift factors for both the segmental and the terminal relaxations *at the same temperatures*. To bring the response of these disparate mechanisms into the available frequency range usually requires that the high frequency dynamics be probed at low temperatures, while the slow frequency modes are measured at high temperatures. The mere demonstration that both sets of time-temperature shift factors can be interpolated by the same equation is only consistent with, but does not establish, thermorheological simplicity.

It is now generally accepted that neat polymers exhibit thermorheological complexity in their viscoelastic spectra [40], as most clearly observed when measurements are made in the glass transition (softening) zone. In this region of the viscoelastic spectrum, both segmental and terminal modes contribute to the measured response; hence, their differing temperature dependencies are manifested as a change in the spectrum with change in temperature. A breakdown of the time-temperature superposition principle has been reported for polystyrene [41], poly(vinyl acetate) [42], poly(phenylmethylsiloxane) [43], polypropylene glycol [44], atactic polypropylene [45] and polyisobutylene [46]. The thermorheological complexity of the latter is ironic (Figure 3), since experiments on polyisobutylene were so instrumental in the acceptance of the time-temperature superpositioning principle [4].

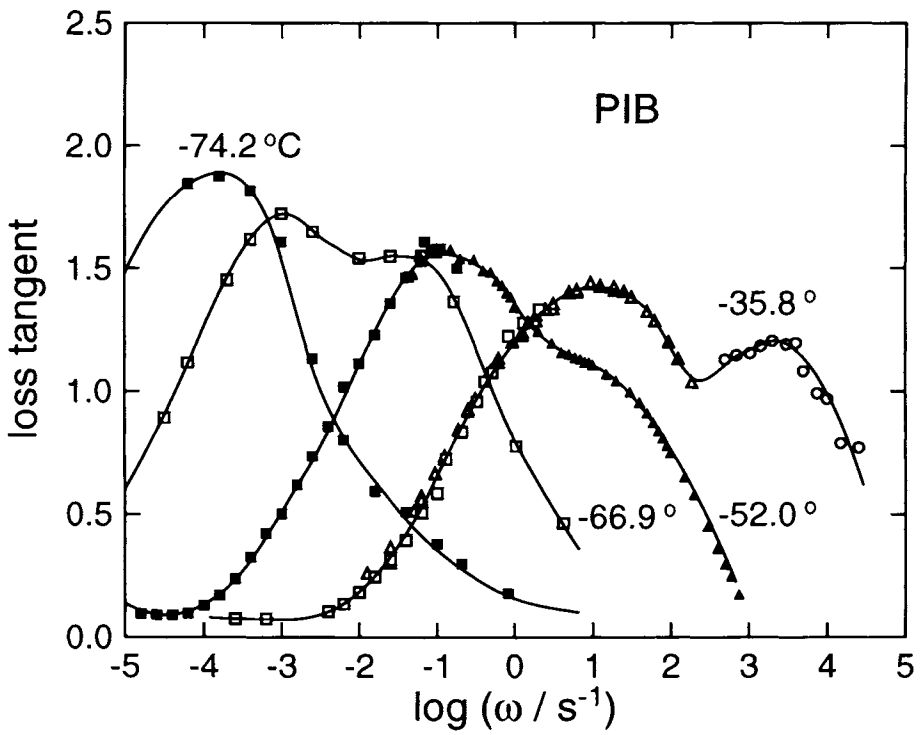

Figure 3. The loss tangent of polyisobutylene measured by dynamic mechanical spectroscopy (circles and triangles) and by creep (squares).

Of course, thermorheological complexity does not necessarily mean that

superpositioning is not useful. It does mean, however, that one must be sure that different modes of motion (e.g., the chain modes and segmental relaxation) do not contribute to a measured viscoelastic property. When only one mode is being observed, any spectral changes with temperature are usually subtle. However, if the measured response is due to more than one mechanism, the resulting mastercurves are not reliable. At best they are only semi-quantitative.

3. COMPOUNDING VARIABLES

3.1. Crosslink Density

According to classical rubber elasticity theory, intermolecular forces have no effect on the equilibrium chain configurations, and thus no effect on the stress. The relaxation of rubber toward mechanical equilibrium, however, is governed by the interactions among neighboring segments. This relationship has led to various attempts to interpret the elastic properties of rubber in terms of the network dynamics [47-52].

Recent experimental advances reinforce the idea that the microscopic motions and the elastic properties can be usefully interrelated. For example, quasielastic neutron scattering measurements probe the motions of the network junctions [53,54]. Molecular dynamics simulations have also added new insight, for example, by demonstrating the existence of local constraints on the network chains at strand lengths less than the molecular weight necessary for chain entanglements [55]. Recently ^{31}P NMR spin-lattice relaxation experiments on crosslinked rubber have been used to monitor specifically the dynamics of the network junctions [52,56].

The effect of crosslink density on the segmental relaxation behavior was determined by experiments carried out on a series of PVE networks [3]. Higher crosslink density causes increases in the glass transition temperatures, as well as broader segmental relaxation functions (Figure 4). T_g-scaled Arrhenius plots of the segmental relaxation times (once again defining a "dynamic" T_g as the temperature at which the relaxation time assumes an arbitrary value) reveal that enhanced intermolecular cooperativity is the primary mechanism for the broadening. This demonstrates the approach of using temperature dependencies to analyze inhomogenously broadened relaxations, whose relaxation function can not be directly interpretted.

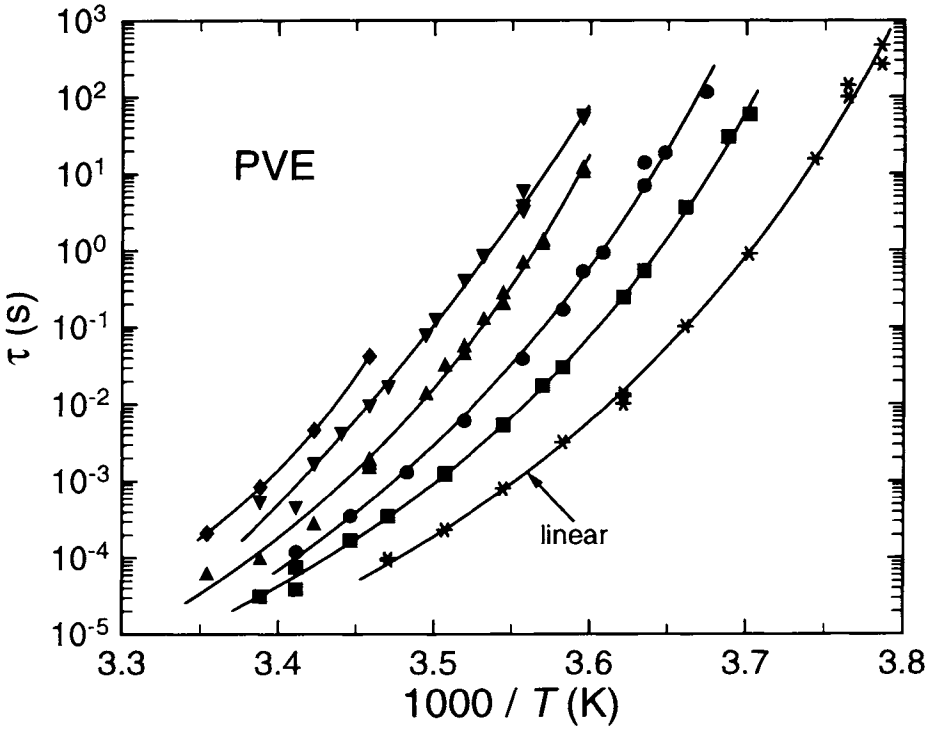

Figure 4. The segmental relaxation time of poly(vinylethylene) elastomers having crosslink densities increasing from 0 (far right) to $>10^{-3}$ moles per cm^3 (far left).

3.2. Diluent and Blending

The use of diluents ("plasticizers") to reduce the relaxation times of polymers is a well established method for altering their physical properties. Often the desired result of incorporating some small molecule liquid is a reduction in the viscosity of the polymer melt, which facilitates processing. The reduction is caused by two effects - the dilution of the chain entanglements and the decrease of the local friction. The latter is the case, at least if the friction coefficient of the diluent is less than that of the polymer, which is the expectation if the former has a lower glass transition temperature.

The detailed consequences of mixing on polymer dynamics are not fully understood [57]. Segmental relaxation times of the diluent and the polymer are expected to be closer in magnitude when mixed, than when in their respective pure states. Free-volume concepts would suggest that a polymer mixed with a

lower T_g diluent will exhibit a smaller relaxation time than when neat (i.e. plasticization); that is, if the diluent dynamics are faster than the polymer dynamics, the segmental relaxation of the polymer will become faster. In the less frequent situation, in which the diluent has a higher T_g than the polymer, the segmental relaxation times of the polymer should increase upon addition of the diluent (i.e. anti-plasticization).

A number of recent studies have shown deviations from this simple behavior when the components have nearly equal T_g's. For mixtures of polymers with diluent [35,58-61], as well as for polymer blends [62-64], measured relaxation times are not always found to be intermediate between those of the pure components. Specifically, addition of a higher T_g component often increases the relaxation rate.

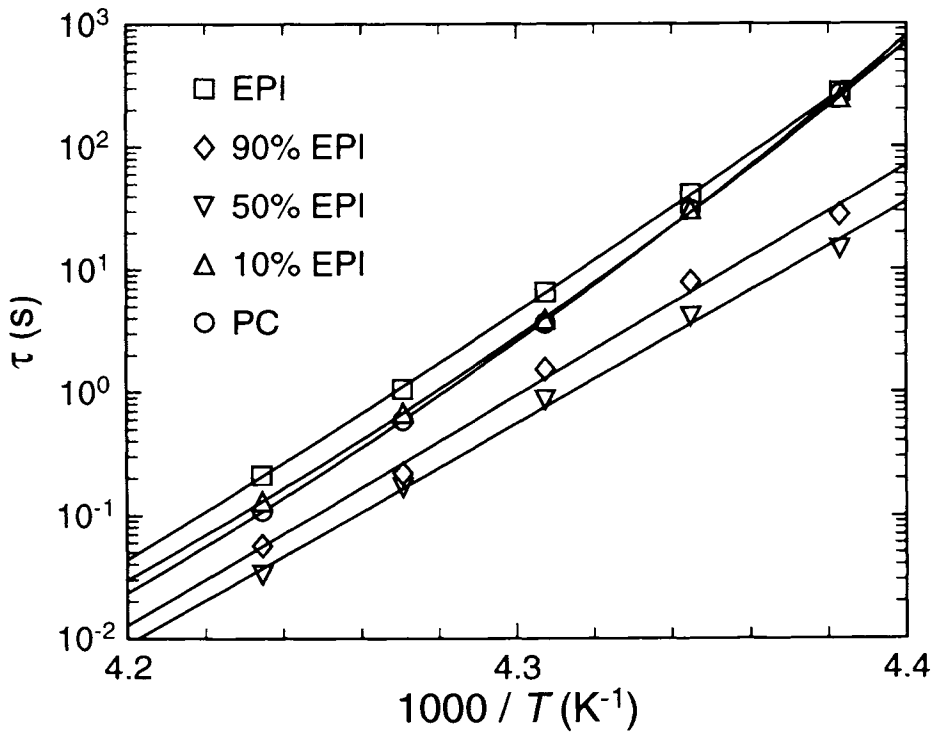

Figure 5. Segmental relaxation times for epoxidized polyisoprene and polychloroprene, and two of their blends. The latter exhibit faster relaxation than the either neat components.

An example of this unexpected result in a rubber blend is shown in Figure 5. At 25 mole % epoxidation, polyisoprene has a T_g very nearly equal to that of polychloroprene. Mixtures of the two polymers, however, exhibit shorter relaxation times than either neat component. The origin of such anomalous behavior is unclear, but it appears to arise from two factors [59,61]. In miscible mixtures, the pure component volumes are not necessarily additive. There can be an excess volume, which is either negative or positive. Such non-zero mixing volumes can be quite large for macromolecules mixed with small molecule diluents. Additionally, the intermolecular cooperativity which governs the segmental dynamics can change drastically, and in unanticipated ways, upon mixing two pure species.

3.3. Filler Reinforcement (Carbon Black)

The most widely used polymeric composite is rubber reinforced with carbon black. The use of carbon black not only lowers the cost of the material, but also improves the properties. The mechanical properties of filled rubber are very strain dependent, particularly for strains exceeding about 0.1%. In combination with the viscoelasticity of the material, this non-linearity makes the finite-element modeling of elastomers very complex. Filled rubbers exhibit the highest modulus at low strains, due to the presence of a three-dimension network of agglomerated filler particles. The presence of a filler particle network contributes to the temperature dependence of the mechanical properties of filled rubber [65]. As the strain increases, high hysteresis (heat buildup) occurs, associated with the breakup of the agglomerates [65,66]. This is an important practical problem, contributing, for example, to the rolling resistance of automobile tires. Mechanical energy dissipation in the tires accounts for about 10% of the fuel consumption in a typical automobile.

Much effort has been expended in reducing the hysteresis of filled rubber by minimizing the agglomeration of carbon black. One approach is to intensify the mixing procedure. This causes more extensive coating of the carbon black particles with the polymer, which reduces subsequent particle-particle bonding. This effect is illustrated in Table 1 [67,68], in which the loss modulus, which is proportional to the amount of heat generation, is seen to decline in proportion to the extent of mixing. Another approach to reducing filler agglomeration through enhanced bonding with the polymer chains is the use of adhesion promoters [69].

It is difficult to characterize the mechanical properties of elastomers at strains

below about 10^{-4}. Nevertheless, it had long been reported [70-72] that the modulus of filled rubber exhibited a maximum in the vicinity of strains of this magnitude. Such results imply that the carbon black agglomeration is induced by the deformation, with implications concerning the behavior of filled rubber in the unstrained condition. This is of some import, for example, concerning the use of carbon black to impart electrical conductivity to elastomers.

Acoustic measurements enable strains as low as 10^{-9} to be achieved. The response of unfilled rubber to acoustic perturbations is virtually identical to that for low strain mechanical deformation. As shown by the data in Table 1, obtained on a styrene-butadiene copolymer (SBR) [68], this is also the case for filled elastomers. The putative maxima [70-72] in the storage and loss moduli are nonexistent. The high stiffness associated with the presence of a filler network is maintained down through the lowest strains.

Table 1
Acoustic and mechanical results for SBR with 45% (by wgt.) carbon black

	storage modulus		loss modulus	
mill passes	acoustic[1]	mechanical[2]	acoustic[1]	mechanical[2]
0	35.5	26.7	6.7	3.7
5	32.6	22.1	6.8	3.3
20	30.6	15.0	5.2	2.7

[1] frequency = 1 kHz; $T = 30°C$; $10^{-6} \leq$ strain amplitude $\leq 10^{-9}$
[2] frequency = 40 Hz, $T = 26°C$; strain amplitude = 10^{-3}

Less mixing results in compounds having a higher low strain modulus, reflecting more extensive carbon black agglomeration. Mixing promotes interaction between polymer and filler, suppressing subsequent particle agglomeration.

At moderate strains, sufficient for disruption of the filler network, some modulus enhancement is still observed, due to strain amplification of polymer chains near the carbon black [73-75]. This hydrodynamic effect is analogous to the viscosity increase of liquids upon addition of solid particles. The effect in carbon black can be described using the Einstein equation; however, quantitative agreement with experimental results requires that a higher than actual volume fraction of filler be used in the calculation, presumably to account for occluded rubber [66,75]. Such

occluded material is made inextensible through its confinement in the interstices of the filler particles; thus, occluded rubber contributes to the filler reinforcement.

ACKNOWLEDGEMENTS

This work was supported by the Office of Naval Research.

REFERENCES

1 H. Markovitz, Linear Viscoelasticity, Carnegie-Mellon, Pittsburgh, 1980.
2 X. Quan, G.E. Johnson, E.W. Anderson and F.S. Bates, Macromolecules, 22 (1989) 2451.
3 C.M. Roland, Macromolecules, 27, (1994) 4242.
4 J.D. Ferry, Viscoelastic Properties of Polymers, Wiley, New York, 1980.
5 C.M. Roland, J. Poly. Sci. Poly. Phys. Ed., 26 (1988) 839.
6 G. Williams and D.C. Watts, Trans. Faraday Soc., 66 (1970) 80.
7 H. Scher, M. F. Shlesinger, J. T. Bendler, Physics Today, (January 1991) 26.
8 K.L. Ngai, R.W. Rendell, A.K. Rajagopal, S. Teitler, Ann. N.Y. Acad. Sci., 484 (1986) 150.
9 C.M. Roland and K.L. Ngai, J. Chem. Phys., 103 (1995) 1152.
10 M.H. Cohen and G.S. Grest, Phys. Rev., B 24 (1981) 4091.
11 M.H. Cohen and G.S. Grest, Phys. Rev., B 26 (1982) 2664.
12 M.F. Schlesinger and E.W. Montroll, Proc. Natl. Acad. Sci. USA, 81 (1984) 1280.
13 R.B. Palmer, D.L. Stein, E. Abrahams and P.W. Anderson, Phys. Rev. Lett., 53 (1984) 958.
14 A.T. Ogielski and K.L. Stein, Phys. Rev. Lett., 55 (1985) 1634.
15 K. Schmidt-Rohr and H.W. Spiess, Phys. Rev. Lett., 66 (1991) 3020.
16 C.M. Roland and K.L. Ngai, Macromolecules, 24 (1991) 5315; 25 (1992) 1844.
17 E.-J. Donth, Relaxation and Thermodynamics in Polymers, Akademie Verlag, Berlin, 1992.
18 N.G. McCrum, B.E. Read and G. Williams, Anelastic and Dielectric Effects in Polymeric Solids, Dover, New York, 1967.
19 F. Bueche, Physical Properties of Polymers, Interscience: New York, 1962.
20 H. Fujita, Macromolecules, 26 (1993), 643; 26 (1993) 4720.
21 M.L. Williams, R.F. Landel and J.D. Ferry, J. Amer. Chem. Soc., 77 (1955) 3701.
22 K.L. Ngai, R.W. Rendell and A.F. Yee, Macromolecules, 21 (1988) 3396.

23 B.D. Malhotra and R.A. Pethrick, Eur. Poly. J., 18 (1983) 457; Poly. Comm., 24 (1983) 165.
24 J.J. Curro and R.-J. Roe, Polymer, 25 (1984) 1424.
25 J.G. Victor and J.M. Torkelson, Macromolecules, 20 (1987) 2241.
26 C.A. Angell, in Relaxations in Complex Systems, K.L. Ngai and G.B. Wright (Eds.), Government Printing Office, Washington, D.C., 1985.
27 C.A. Angell, J. Non-Cryst. Solids, 131-133, (1991) 13.
28 L.M. Torell and M. Grimsditch, Proc. Phys. 37 (1989) 196.
29 D.J. Plazek and K.L. Ngai, Macromolecules, 24 (1991) 1222.
30 R. Bohmer, K.L. Ngai, C.A. Angell and D.J. Plazek, J. Chem. Phys., 99 (1993) 4201.
31 P.G. Santangelo, K.L. Ngai and C.M. Roland, Macromolecules, 26 (1993) 2682.
32 K.L. Ngai and C.M. Roland, Macromolecules, 26 (1993) 6824.
33 K.L. Ngai and C.M. Roland, Macromolecules, 26 (1993) 2688.
34 C.M. Roland and K.L. Ngai, Macromolecules, 24 (1991) 2261.
35 K.L. Ngai and C.M. Roland, Macromolecules, 28 (1995) 4033.
36 K.L. Ngai, C.M. Roland, J.M. O'Reilly and J.S. Sedita, Macromolecules, 25 (1992) 3906.
37 C.M. Roland and K.L. Ngai, Macromolecules, 25 (1992) 363.
38 C.M. Roland and K.L. Ngai, Macromolecules, 25 (1992) 5765.
39 K.U. Kirst, F. Kremer, T. Pakula and J. Hollingshurst, Colloid Poly. Sci., 272 (1994) 1420.
40 K.L. Ngai and D.J. Plazek, Rub. Chem. Technol., 68 (1995) 376.
41 D.J. Plazek, J. Phys. Chem., 6 (1965) 612.
42 D.J. Plazek, J. Poly. Sci. Poly. Phys. Ed., 20 (1982) 729.
43 D.J. Plazek, C. Bero, S. Neumeister, G. Floudas, G. Fytas and K.L.Ngai, Colloid. Poly. Sci., 272 (1994) 1430.
44 K.L. Ngai, A. Schonhals and E. Schlosser, Macromolecules, 25 (1992) 4915.
45 D.L. Plazek and D.J. Plazek, Macromolecules, 16 (1983) 1469.
46 D.J. Plazek, I.-C. Chay, K.L. Ngai and C.M. Roland, Macromolecules, 28 (1995) 6432.
47 M.H. Wagner and J. Schaeffer, J. Rheology 37 (1993) 643.
48 S.F. Edwards, Polymer J. 17 (1985) 271.
49 M. Warner, J. Phys. C, 14 (1981) 4990.
50 T.A. Vilgis and F. Boue, J. Poly. Sci., 26 (1988) 2291.

51 C.M. Roland and K.L. Ngai, J. Non-Crystalline Solids, 172-174, (1994) 868.
52 K.L. Ngai and C.M. Roland, Macromolecules, 27 (1994) 2454.
53 J.S. Higgins, K. Ma and R.H. Hall, J. Phys. C, 14 (1981) 4995.
54 R. Oeser, B. Ewen, D. Richter and B. Farago, Phys. Rev. Lett., 60 (1988) 1041.
55 E.R. Duering, K. Kremer and G.S. Grest, Phys. Rev. Lett., 67 (1991) 3531; Macromolecules, 26 (1993) 3241.
56 J.-F. Shi, L.C. Dickinson, W.J. MacKnight and J.C.W. Chien, Macromolecules, 26 (1993) 5908.
57 T.P. Lodge, J. Phys. Chem., 97 (1993) 1480.
58 A. Rizos and K.L. Ngai, Phys. Rev., B 46 (1992) 8126.
59 P.G. Santangelo, K.L. Ngai and C.M. Roland, Macromolecules, 27 (1994) 3859.
60 K.J. McGrath and C.M. Roland, Macromolecules, 28 (1995) 2982.
61 C.M. Roland, P.G. Santangelo, K.L. Ngai and G. Meier, Macromolecules, 26 (1993) 6164.
62 C.M. Roland, P.G. Santangelo, Z. Baram and J. Runt, Macromolecules, 27 (1994) 5382.
63 K.J. McGrath and C.M. Roland, Rub. Chem. Technol., 67 (1994) 629.
64 A. Alegria, I. Telleria and J. Colmenero, J. Non-Cryst. Solids, 172-174, (1994) 961.
65 A.R. Payne and R.F. Whittaker, Rub. Chem. Technol., 44 (1971) 440.
66 A.I. Medalia, Rub. Chem. Technol., 51 (1978) 437.
67 C.M. Roland, J. Rheology, 34 (1990) 25.
68 C.M. Roland and G.F. Lee, Rub. Chem. Technol., 63 (1990) 554.
69 D. Graves, Rub. Chem. Technol., 66 (1993) 61.
70 A.Voet and F.R. Cook, Rub. Chem. Technol., 40 (1967) 1364.
71 A.K. Sircar and T.G. Lamond, Rub. Chem. Technol., 48 (1975) 79.
72 J.-B. Donnet and A. Voet, Carbon Black - Physics, Chemistry, and Elastomer Reinforcement, Marcel Dekker, New York, 1976.
73 H.M. Smallwood, J. Appl. Phys., 15 (1944) 758.
74 E. Guth, Rub. Chem. Technol., 18 (1945) 596.
75 A. Medalia, Rub. Chem. Technol., 47 (1974) 411.

Handbook of Thermal Analysis and Calorimetry. Vol. 4: From Macromolecules to Man.
R.B. Kemp, editor.

Chapter 16

THERMAL ANALYSES IN FOODS AND FOOD PROCESSES

A. Schiraldi, L. Piazza, D. Fessas and M. Riva

Dipartimento Scienze e Tecnologie Alimentari e Microbiologiche,
University of Milan, via Celoria 2, 20133 Milano, Italy

1. INTRODUCTION

Every kind of thermal analysis so far known has found applications in the study of foods and food processes. Traditional calorimetry was employed some decades ago to determine heat capacities of many food materials [1-3] and describe the behaviour of frozen ice-forming foods [4]. These pioneering studies were followed by the worldwide development of DSC applications [5], sustained by the availability of easy-to-use commercial instruments. In more recent years other thermal analysis techniques, like TGA, TMA and DTMA, have been used for specific applications in the realm of food science and technology.

Because of the intrinsic heterogeneity of many food materials, the reproducibility of a given thermal analysis trace is usually poorer than those obtained from purified chemicals, and, when extended throughout a wide temperature range, shows a large number of humps and bumps (Figure 1) that make the interpretation rather difficult. In the case of DSC, base line shifts due to glass transitions often partially overlap to peak signals of first order transitions and chemical, biochemical and microbe-sustained reactions. This explains why for many years DSC has been considered and referred to as mere analytical tool by food scientists and technologists.

Many papers indeed appeared where DSC traces were reported in figures devised to allow just a qualitative comparison [6-7] between samples of foods or food ingredients modified by some treatment (Figure 2). In some cases tentative evaluations of the relevant enthalpy changes were reported, although based on a rather arbitrary choice of the base line trend across the signals. As a consequence, wide discrepancies can be found in the literature among enthalpy values related for instance to starch gelatinization and retro gradation [8-10].

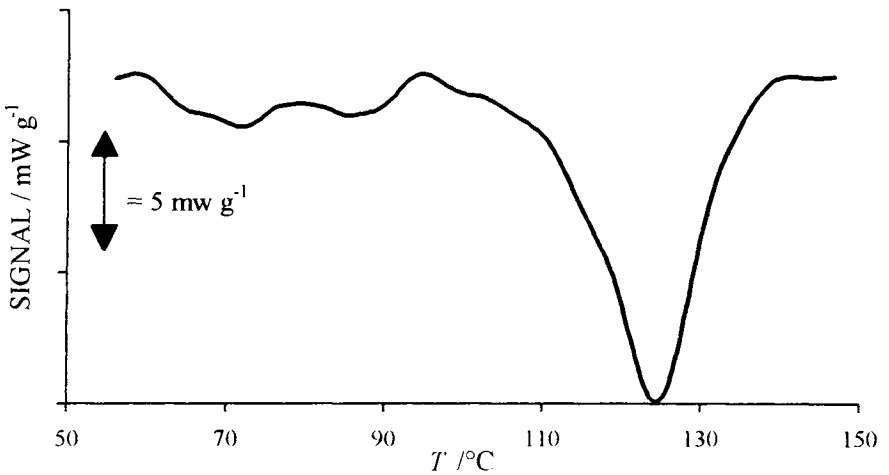

Figure 1. DSC trace from a fresh cheese sample. The series of endotherms is related to the unfolding of fragments of partially proteolysed casein [M. Riva, unpublished data].

A worthwhile improvement to the results from DSC investigations of foods and food processes came from the large body of data published since the seventies about protein unfolding and denaturation [11,12]: the careful choice of the base line trend and the deconvolution of the traces into single-transition components became more diffused among food scientists and the first examples of what should be done appeared in the relevant literature [13].

Two simple elements accordingly became basic to the interpretation of a calorimetric signal: namely, the thermal effect (endo- or exothermic peak), and a base line shift due to the heat capacity drop across the peak. The single contribution (peak and base line shift) can be described according to either a thermodynamic or kinetic approach (see Appendix A1), with the former being more adequate for traces obtained at low heating rates, and the latter at high rates.

When more signals appear in a given temperature range, the relevant deconvolution of the trace must be carried out by assigning to each of them the above two basic elements. In the case of food samples, which can contain a large number of compounds undergoing transitions and/or chemical reactions, the DSC traces show trends that cannot be treated by mathematics. Nonetheless some assumptions can simplify the approach without significant loss of reliability [14].

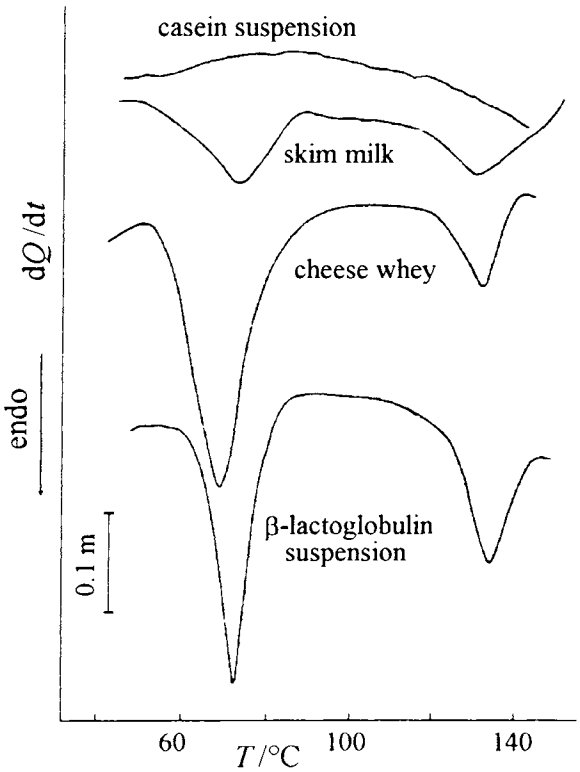

Figure 2. Qualitative comparison between DSC traces of casein, skim milk, cheese whey, β-Lgb (modified from ref [6]).

For example the base line trend can be tentatively defined with a SP-line (or even a straight line) across peak shaped signals, or with a sigmoidal function when a second-order like transition is supposed to take place. Once the trace is accordingly scaled, it can be deconvolved into the minimum number of gaussian functions to attain an acceptable correlation ($P < 0.05$). This treatment allows a tentative estimation of the enthalpy associated to each peak and the progress across the respective temperature span. Related kinetic parameters, like kinetic order and kinetic constant are accordingly assessed [14]. Comparison with signals in DSC traces obtained from pure compounds can be of help to improve the analysis of each gaussian peak.

Simulation of heat treatment is among the aims of DSC investigations of foods. Concerning this, it must be emphasized that no water escapes from the

sealed pans in the course of the temperature scan: the consequent pressure increase does not significantly affect the transitions occurring below or just above 100 °C, but the constant moisture level kept within the sample does not correspond to the real conditions of many heat treatments in the industrial practice. On the other hand, if one uses open pans, the large endothermic effect accompanying water vaporization will conceal any other transition signal.

Since most of these treatments, like cooking and baking, are carried out, or practically occur, in isothermal conditions, DSC investigations aimed to simulate the process should be carried out at constant temperature: in other words, one should drop the sample to be investigated into an empty calorimetric vessel previously heated up to the desired temperature. Unfortunately commercial DSC instruments do not allow an easy access to the sample in the course of the run; their use to investigate chemical reactions in isothermal conditions is therefore severely reduced. This explains why no isothermal DSC investigations were reported in food-science literature until recent years [15-17].

In the case of isothermal traces, the instrumental time lag is to be accounted in order to recognize the kinetic law underlying the observed signal. A simple procedure [14] allows one immediately to determine whether a signal corresponds to a simple or a multistep process (starch glass transition preceding gelatinization) and to assess kinetic order and kinetic constant of simple transformations (see Appendix A1). These procedures were employed to characterize several food systems and processes, like gelatinization and staling of cereal products, milk pasteurization, egg white denaturation, pasta and rice isothermal cooking, etc.

Food spoilage and preparation of particular dairy foods, like cheeses, yogurt, kyr, etc., are sustained by specific microbial activity. In these cases prediction of the effects is of paramount importance to assess the shelf-life and the best operating conditions. To this aim thermal analysis - above all isothermal calorimetry - can be of some help and integrate with the traditional techniques of microbiology. Cultures of living organisms, like yeast and fermenting bacteria, can be indeed characterized with isothermal calorimetry, since, under strictly defined conditions, the recorded signal is directly related [18-20] to growth and metabolic rate. It was found [21] that the same logistic equations used to fit plate count data, like the Gompertz function, can be of help to describe the calorimetric traces obtained from microbial cultures and facilitate the deconvolution of the signal into "growth" and "metabolic" contributions.

Thermogravimetric analysis (TGA) is the thermal analysis related to the weight loss occurring in the course of a temperature scan at given heating rate. The released compounds are conveyed to the exterior by a gentle nitrogen stream

and can be analytically determined if the out-flow is connected to a gas chromatographer or an IR spectrophotometer. With these optional facilities one is able to realize whether more volatiles leave the heated sample. When so, the weight loss trend shows several, more or less separate steps, each related to a single compound.

The output of modern instruments usually includes the DTG, namely the trace of weight loss rate, dm/dt, *vs* T (where T is the thermodynamic temperature), or *vs* t (t stands for time). When several compounds are released within the same T (or t) range, DTG trace allows the relevant T_m , T_o, and T_e (mean, onset and end temperature, respectively) to be more easily determined for each of them. In this case the DTG trace appears as a multi-peak trend. It can be easily shown that the DTG trace can be deconvolved into a sum of gaussian or gaussian-like peaks, each related to a single compound. This is the start point to make a kinetic parameter of the weight loss (see Appendix A2).

Food dehydration processes are easily simulated with a TGA experiment, although it can be difficult to use these data to describe even phenomenologically the underlying diffusion mechanism. Significant improvements of this technique come from the simultaneous record of a DSC trace, since it allows evaluation of the enthalpy associated to the weight loss (Figure 3). In the case of food samples, most of the weight loss corresponds to water released, and the vaporization enthalpy usually ranges about 2.2 kJ/g [22].

Pyrolysis of many compounds can be studied by means of TGA [23]. Among others, carbohydrates and naturally occurring polysaccharides, like Guar gums and Xanthan gum, decompose above 250°C with formation of carbonyl compounds [23]. TGA when run under various different atmospheres (air, nitrogen, CO_2, etc.) allows studies of the caramelization process of sugars, and, in the presence of proteins, evaluations of the Maillard reaction [23]: this can be true for the case of honey. Mass spectrometry gives specific patterns of the volatiles produced. Analogous investigations can be extended to the decomposition of amino acids [23]. These mainly produce CO, CO_2, alkylamines and HCN.

TGA can be used to study thermal degradation of lipids [20]. Since oxygen is captured by the unsaturated bonds, a mass gain is observed. The onset takes place, at a given temperature, after an induction period (IP), the length of which is a measure of the oil's resistance to oxidation. An autocatalytic oxidation follows when the mass gain reaches its maximum rate. The subsequent phase deals with the decomposition of the product and is accompanied by a mass loss, mainly due to the release of aldehydes, ketones, alcohols and esters.

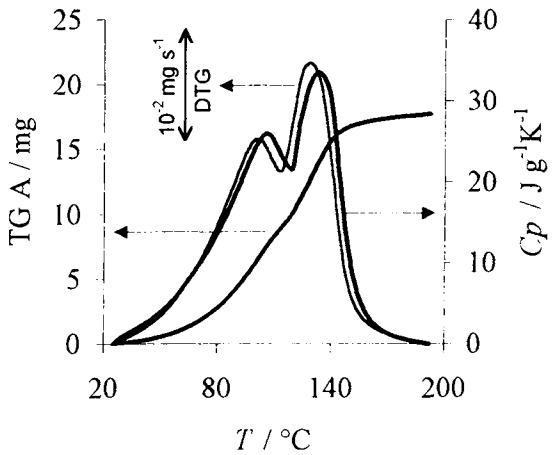

Figure 3. TGA-DSC trace of wheat dough dehydration at 2 K min^{-1} heating rate (modified from [22]).

Since the mass uptake corresponds to the oxygen bound to form peroxide rings, it is a direct measure of the chemical stability to the oxidation; the maximum oxidation rate depends on the exposed surface area, which supports the conclusion that oxygen diffusion determines the reaction rate [23].

Mechanical and rheological properties are of fundamental importance to predict and design processing, storage and consumption of foods. They change with temperature, water content and water activity, and can be related to phase transitions occurring in the nonequilibrium state [24]. The system which behaves like a rigid brittle solid at low temperatures becomes rubbery at intermediate temperatures, and finally melts at high temperatures, where it can flow, as a result of the increased polymer segmental mobility [25].

Five regions in the dependence of viscoelastic behaviour of temperature for high-molecular-weight poymer are generally distinguished (Figure 4): glassy, glass transition, rubbery plateau, rubbery flow and liquid flow.

The rheological properties of the material are connected with these physico-chemical states. In recent years significant advances have been made in both the theory of viscoelasticity and the related instrumentation. In particular dynamic, mechanical and thermal testing have become quite popular after successful applications to the analysis of polymer systems [26], some elements of which are given in the Appendix A3.

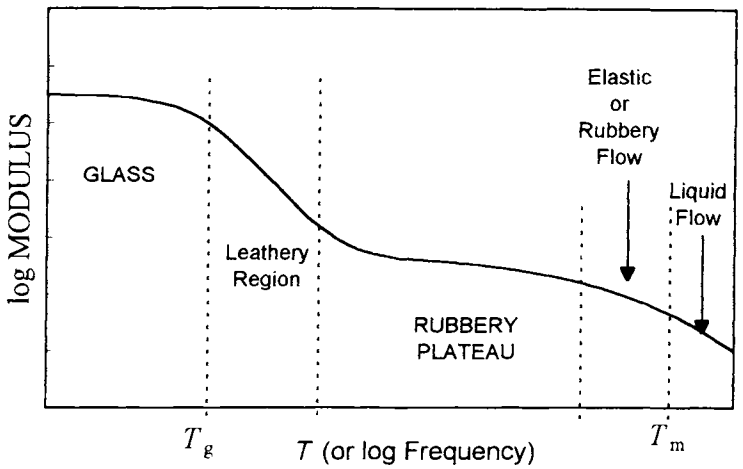

Figure 4. Five typical regions of viscoelastic behaviour of a synthetic partially crystalline polymer: T_g and T_m stand for glass transition and melting temperature, respectively (modified from [27])

DMA, DMTA, TMA, and mechanical spectrometry can be combined with thermodielectric analysis, electron spin and nuclear magnetic resonance, and other methods [27] to investigate glass transitions and their effect on mechanical properties [28], as well as molecular mobility and diffusivities in food ingredients and products. Unfortunately, since the glass transition is kinetically controlled and cannot be referred to as an equilibrium phase transition [26], T_g values obtained by different methods from the same sample, or even by the same method using different experimental conditions, show significant discrepancies. T_g depends, in fact, on temperature-time or frequency conditions of measurement [29-31]. In real food products, where water-binding macromolecules are heterogeneously distributed, thermomechanical analyses are recommended in addition to DSC, because of their greater sensitivity [27].

Cereal products are multi-component mixtures. They are the subject of a number of studies designed to define the viscoelastic behaviour as functions of temperature and water content. The viscoelastic behaviour of dough is non linear at all except for small deformations. However, the traditional equipment to examine dough behaviour provide data only in the non-linearity region, which cannot be used to assess the basic rheological relationships. Therefore dynamic rheological testing is of extreme interest because it allows an approach to the fundamental properties of doughs.

Detailed descriptions of the methods employed to study dough rheology may be found in several exhaustive works [32-40]. Linear and non linear models have been proposed to predict flow behaviour of dough in shear and extension, in order to optimize process design [41,42] and formulation [43,44]. Most rheological measurements on wheat flour dough have been carried out at ambient or proofing temperatures, whereas only minor attention has been paid to studies of rheological properties at higher temperatures. Thermomechanical analyses, which determine the dynamic moduli of samples of regular geometry over a wide temperature range, have proved a valuable experimental tool to characterize objectively doughs and baked products.

These general considerations aim to stress that a thermal analysis approach to the study of foods and food processes requires specific skills and experience, as well as instruments of very good quality. Any blind use of a TA device to acquaint some generic reference should therefore be discouraged at all times.

In the following some applications of thermal analyses are reported in connection with the characterization of the most important foods and food ingredients, as well as with the simulation of some heat treatment, like cooking, baking, pasteurizing, etc.

2. PHASE DIAGRAMS

A fundamental improvement in the interpretation of DSC and Thermomechanical Analysis traces relevant to foods and food ingredients came from the recognition that compounds with a small molecular mass can directly affect the molecular mobility of larger molecules and therefore modify the overall viscosity of the system [45], as revealed by changes of the glass transition temperature. The ubiquitous compound responsible for such effects in foods is water. For a number of compounds became therefore of great interest the study of the respective binary with water by defining the relevant *phase diagram* in the plane T - *vs* - c(w), where c(w) is the water content. The curve that fits the T_g - *vs* -c(w) trend separates the underlying glassy region, where because of the low molecular mobility and high viscosity no transition or reaction can take place, from the upper region of the diagram where these changes can occur [24, 46-49].

A scheme of the various regions of the diagram can be summarized as follows (Figure 5). A liquidus curve fits the freezing points of water-rich compositions: it starts from T = 273 K for pure water and bends down with increasing solute content until it intecepts the T_g curve in the point [T_g', c'(w)], that is the lowest temperature at which a liquid phase can be observed in the

presence of ice crystals: at higher solute contents the viscosity of the solution would be too high for any further ice nucleation and the expected eutectic point cannot be attained. T_g' accordingly is the T_g of maximally freeze-concentrated solutes.

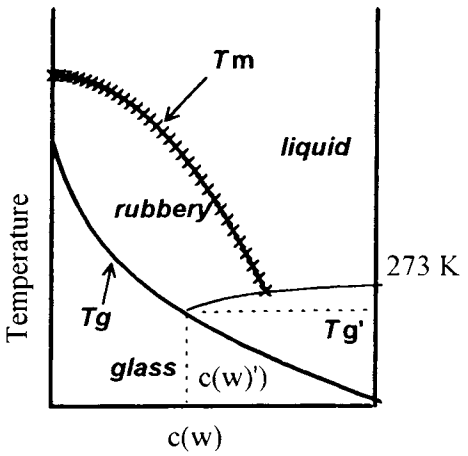

Figure 5. Phase diagram of a hypothetical aqueous binary. The T_g' -vs-c(w) curve represents the boundary between low and high molecular mobility regions; lettering is specified in the text.

For c(w) < c'(w) and $T \leq T_g'$ the system is an amorphous glass-like system. For c(w) > c'(w) and $T < T_g'$ ice can still nucleate and grow although at much lower rate. Therefore when a sample with c(w) > c'(w) is thawed (at a given rate) from $T < T_g'$, the DSC trace shows a first endothermic shift of the base-line at $T = T_g'$, which can be immediately followed by an exothermic wave that corresponds to ice crystallization. When T_g' is attained some ice melting takes place as revealed by an endothermic peak: the larger the c(w) the broader the endotherm. An example of such a behaviour is given in Figure 6.

The DSC trace for samples with c(w) < c'(w) shows an endothermic shift of the base-line at $T = T_g'$ which can be followed by other signals according to the nature of the solute. In the case of simple compounds, like sugars and pure polysaccharides, a broad endotherm peak is observed which corresponds to the solubilization into the liquid phase. The solubility curve bends down from the fusion point of the pure solute (when it actually exists) and crosses the freezing curve of primary ice separation in the vicinity of the point [T_g', c'(w)], although the intersection usually occurs at a slightly higher temperature. When the solute is

a biopolymer, several conformational changes can take place above T_g, like formation of entangled chain gel, gel-sol transition, thermosetting, etc., according to the chemical nature of the compound [45].

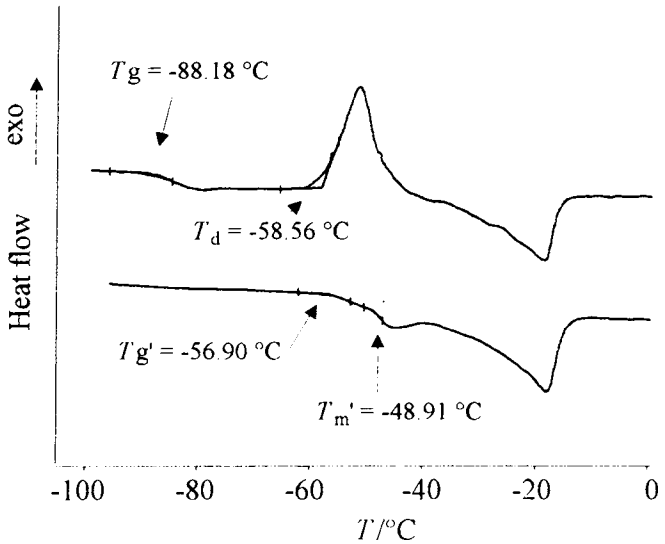

Figure 6. DSC trace from a vegetal: the base-line shift at T_g is followed by an exotherm related to a partial ice formation at T_g' and, an endotherm, at higher temperature, related to ice melting (modified from ref. [50]).

A particular emphasis has been recently given to the application of the Modulated DSC (MDSC) to separate reversing from non-reversing heat-flow signals obtained from food systems [51]. The main application concerns the heat capacity drop observed at T_g from the the stress-relaxation endotherm (non-reversing signal) that is often observed on heating samples previously cooled at subzero temperatures, like frozen doughs. The changes of the relaxation enthalpy are worth determining since they are related to the residual molecular mobility in quenched products and therefore with their stability and shelf-life.

A number of applications and/or phenomena of technological interest, like freeze-drying, caking of powders, cryopreservation, etc., have been described on the basis of the relevant phase diagrams [45], as well as an application to extrusion processing of flour [52]. A number of papers [53-60] therefore appeared where various experimental approaches to T_g, like DSC, TMA, DTMA, NMR, ESR, fluorescence and phosphorescence decay, etc., were reported and sometimes compared to each other. It however should be emphasized that some

spectroscopic techniques, like NMR and ESR, reveal changes of short range molecular mobility within a 10^{-6} - 10^{-8} s time scale, being practically blind for the macroscopic modifications of viscosity and specific heat at the operator's time scale which can be detected through other approaches, like thermal analyses.

3. CEREAL PRODUCTS

3.1.Starch

A huge literature is available about starch transitions in cereal products. To summarize some basic points, one has first to emphasize that starch is not a chemical compound, but rather a naturally-built structure with a grossly spherical shape, named the starch granule, mainly formed by amylose and amylopectin. Some crystal order can be recognized in superficial layers of starch granules [61-64] where the side chains of amylopectic molecules form radially directed arrays. This crystal region rests upon an amorphous core formed by randomly arranged amylose and amylopectin chains. The crystal phase is responsible of the birefringency of the granules when suspended in water at ambient temperature. Some water (10 - 14% w/w) is trapped within the granule being mainly bound to the tertiary helical structure of the polysaccharides.

Most, if not all, transformations of starch require a previous degradation of the granule. This takes place when the amorphous core softens and consequently is no longer able to act as a firm basement for the external crystal regions. This transition, namely the starch glass transition, occurs at a temperature, T_g, that depends on the endogenous water content of the granule, ranging from 323 to 338 K, according to the vegetal origin of the starch. The core of the starch granule is practically inaccessible to external water while the absolute temperature remains below T_g; once this threshold is attained, the external water can diffuse through the superficial layers, which miss their crystal character, and migrate toward the core. The granule swells (although keeping a spheroidal shape) and its birefringence disappears at the same time.

The diffusing water enhances the molecular mobility of the polysaccharide chains and sustain the irreversible transition to a gel state. The plasticizing role of water can promote nucleation and growth of some amylose crystal embrios and/or the enlargement of amylose crystals already present in the core [45].

The whole process, named *starch gelatinization*, produces a broad DSC signal which can be described in the following way. The onset corresponds to an endothermic shift of the base line related to the heat capacity increase at the starch T_g; this is followed by an endothermic peak related to the break of the

crystal regions, and a final exothermic effect accompanying the partial crystallization of amylose (Figure 7).

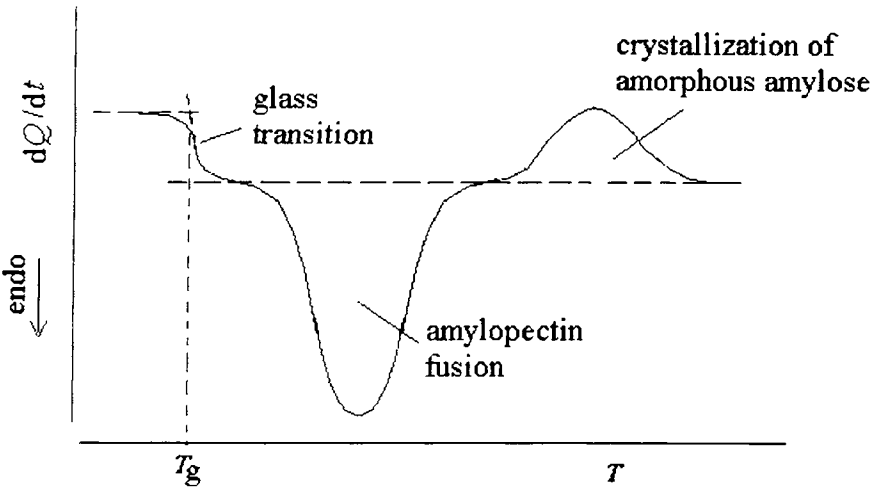

Figure 7. Idealized DSC signal of the starch gelatinization in excess water.

The first papers dealing with DSC studies of starch gelatinization showed that the water content did significantly affect the shape of the trace. The early base line shift of the glass transition is crucial to define the rest of the signal, since both amylopectin "fusion" and amylose partial crystallization do not imply significant heat capacity changes: in other words, the base line trend does not change above T_g. It can however happen that some starch granules have crystal regions more resistant to the dismantling action of water and undergo fusion at higher temperatures. This produces a double endothermic peak in the DSC trace [60].

Aqueous suspensions of starch granules (Figure 8) with a water content larger than 70% (w/w) produced a "single-peak" signal; when compositions poor in water were considered, the trace changed into a "double-peak" signal with onset at the same temperature as the "single-peak" observed for water richer samples; when the water content was less than 20%, the DSC trace again showed a "single peak" signal, although at much higher temperature [60].

At higher temperature (383-393 K) some samples show a further endotherm that is related to the fusion of amylose-lipid complexes, the presence of which depends on the vegetal source of the starch [60]. A clear interpretation comes from inspection of the diagram where the T_g is plotted vs water content.

Bearing in mind that any transition can occur only above the starch T_g, which depends on the endogenous moisture of the granules, the onset of the DSC signal has to be matched with this temperature, no matter the overall water content of the sample.

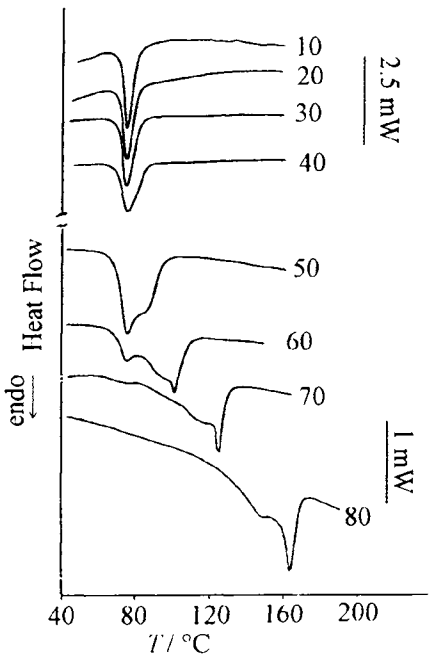

Figure 8. DSC signal of starch gelatinization: effect of the moisture (modified from [9])

Once starch T_g is surpassed, the system becomes homogeneous, since all the available water can be uniformly distributed throughout the sample. The T_g of this homogeneous starch-water system is much lower than the starch T_g. Inspection of the state diagrams shows that the larger the water content the closer is the system to the solubility curve. This means that water rich systems undergo amylopectin solubilization just above the threshold of starch T_g: the T_g base line shift in the DSC trace is therefore immediately followed by the endothermic peak of amylopectin solubilization, so as to give the appearance of a neat "single-peak" signal. For water-poor systems the solubilization of amylopectin crystals takes place at significantly higher temperatures: the T_g shift is well distinguished from the subsequent solubilization endotherm, although still rather close to it, so as to give the impression of a "double-peak" signal with respect to the starting trend of

the base line. If the water available were not enough to sustain the gelatinization of all the starch granules (*e.g.*, it is less than 60% w/w), the relevant endotherm would be smaller than for water-rich samples. Finally when the water content of the sample is very low, the endotherm occurs much above the starch T_g and therefore can give the misleading appearence of a "single-peak" DSC trace.

TMA (Thermomechanical Analyser) was used in dilatometry mode by Biliaderis [53] and coworkers to investigate the effects of water on glass transition and fusion of crystallites of rice starches. TMA measures the change in dimension of a sample as a function of temperature. The dimensional change causes displacement of a counter-balanced probe touching the top surface of the sample. A change in voltage is recorded and converted into displacement units.

A thermomechanical analyzer equipped with a volume dilatometer probe was used to examine the volume expansion changes in 50% starch/water mixtures at 2 K/min in the temperature range 298 - 370 K. Weight loss due to water evaporation during experiments was taken into account to evaluate the actual volume expansion (Figure 9).

Four regions of volume espansion changes were in principle expected: 1) reversible thermal expansion from room temperature up to T_g; 2) irreversible granule swelling at T_g due to the relaxation of amorphous amylose (mainly) not bound or loosely connected to crystallites; 3) above T_g (plateau region) no change of the swollen granules; 4) sharp volume change due to melting. When TMA and DSC traces were reported together, it was seen that both endothermic and dilatometric events occurred in the same temperature region (Figure 10).

This was indicative of the changes in specific heat and expansion coefficient when passing through the glass transition. Furthermore, the sharp volume changes seen at the end of the TMA traces corresponded to the melting endotherm of the starch crystallites. In non-waxy samples the expansion behaviour was strongly affected by the presence of the linear starch component, as revealed by the rather extended plateau beyond the glass transition region. In TMA traces of the waxy rice starch (Figure 10) the glass transition region was followed by first-order phenomena and no plateau was evident.

In contrast, hydrated starch showed a two-stage swelling pattern, the components of which were attributed to the glass transition of the amorphous phase and the melting of crystallites, respectively.

All these phenomena should be taken into account when starch-rich products, like flours, dough, potatoes, rices, etc. are studied by thermal analysis. Here non-starch compounds, like soluble and insoluble proteins, soluble and insoluble pentosans, oligosaccharides, etc. can compete for the available water and therefore produce a shift of the amylopectin solubilization to higher

temperatures [60, 65-77]. In the case of flour doughs, added ingredients, like fats, sugars, hydrocolloids, salt and leavening (chemical and/or cellular yeast), can have important effects, and some of them (e.g., sugars and hydrocolloids) can even affect starch gelatinization at all [73,78].

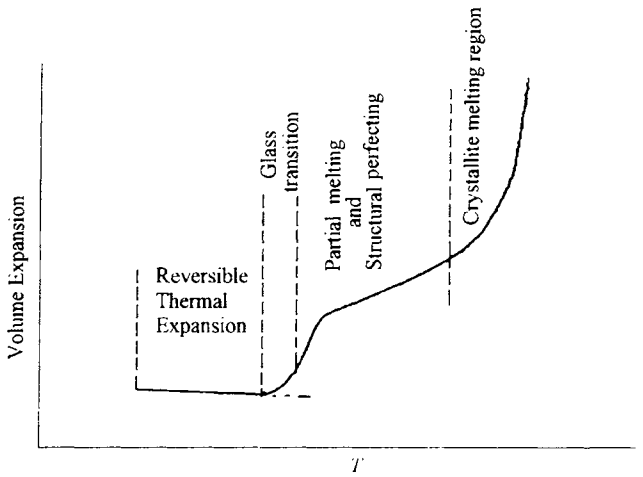

Figure 9. Generalized swelling behaviour , as revealed by a typical TMA curve, for non-waxy rice starch (modified from [53]).

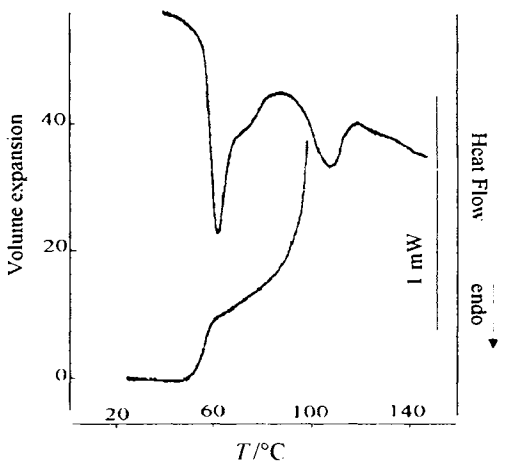

Figure 10. DSC and TMA traces, obtained at 10 and 2 °C min^{-1} heating rate, respectively, from rice starch with 50% w/w moisture (modified from [53]).

The only part of the DSC trace that is not affected by the presence of these compounds is the base line shift at the starch T_g, although it can be concealed by signals related to sugar solubilization, fat fusion, gel-sol transition of hydrocolloids, etc., all occurring in the same temperature range [79].

The effects produced by added fats are simpler to check, since most of them do not interact with starch and therefore produce a reversible endotherm of fusion in the 30-50 °C range, while a small fraction is involved in the formation of amylose-lipid complexes throughout the temperature range of starch gelatinization and therefore enhances the signal at 110 °C: a semiquantitative evaluation of both effects is indeed possible [78].

Starch gelatinization in doughs was investigated with DSC and referred to as a reliable measure of the baking progress, in spite of the naive model used to describe the overall process [80,81].

3.2. Doughs

Dough is a dynamic system undergoing a continuous change under the action of physical and chemical driving forces. It is a mixture of flour, water, salts, yeast or chemical leavening agents and, sometimes, other ingredients. The properties and the behaviour of high molecular weight polymer components of doughs, like other crosslinked systems, mainly depend on temperature. Understanding the thermal behaviour of dough is very important to tailor the quality of the final bakery product, which results from two very important thermally induced phenomena: starch gelatinization and protein denaturation [57,82,83]. In principle, one can assume that dough constituents react on heating and give rise to intermolecular and intramolecular cleavages which produce a highly crosslinked macromolecular structure. These phenomena modify the rheological properties of doughs and are responsible for the solid-like properties of baked products.

Many of the viscoelastic properties of the dough are the result of the properties of gluten [84] which is in an amorphous metastable state, sensitive to moisture and temperature [29,57,85]. This polymer is the result of the interaction between native gliadins and glutenins with formation of intramolecular disulphide cross-links in the course of flour dough preparation and kneading in the presence of water and oxygen. The role of gluten in the mechanism of toughening (and, in general, of staling) of high moisture baked goods during post-bake storage and post-bake heat treatments (reheating) and the possible entanglements between gluten and starch during aging are the major subjects of thermomechanical characterization of the baked product.

Slade and Levine [86] describe wheat gluten as an amorphous, water- and lipid-compatible polymer which behaves like either a thermoplastic or a thermosetting polymer in response to heat-moisture treatment of baking. When the system reaches the glass transition temperature T_g, gluten undergoes an irreversible structural transformation from viscous liquid polymer system with transient crosslinks to elastic, permanently crosslinked gel with a higher network T_g. The thermosetting behaviour is considered to be a consequence of irreversible protein denaturation and "heat-set" gelation which involves formation of permanent rubber-like elastic networks. Crosslinks are permanent covalent bonds, like those in vulcanized rubber. According to Bagley [25] labile crosslinks (hydrogen bonding, ionic interactions) may serve as crosslinks sites and, because of their nature, can cause irreversible deformation. These labile crosslinks are responsible for the flow of a solid under the action of applied forces. Thermosetting of gluten proteins occurs with essentially no change in the total free -SH groups. Thus progressive thiol-disulfide exchange reactions account for the changes in both mechanical and thermodynamic properties [87,88]. The thermoset gluten network is incompletely cured during baking [86], but its cure can be extended by further heat treatments (e.g., microwaves), where superheated steam could provide internal temperatures greater than those attained in baking. Consequently, the gluten network T_g would increase up to $T_{g\infty}$ (the network T_g of the fully cured system). It can be verified that thermal effects related to specific transitions of gluten, like glass transition and reticulation, are negligible when compared with those of starch and therefore cannot be recognized in the DSC trace of a flour dough (Figure 11). The progress of gluten reticulation within a dough can be reliably monitored with rheological investigations.

TMA studies of gluten at low moisture content [89] provided information about the dependence of T_g on time: the increase of gluten T_g in the course of heat treatment at temperatures slightly above the starting T_g was explained as a consequence of thermosetting via intermolecular disulphide crosslinks. Dimensional changes occurring during glass transition of cookie doughs have been investigated by Miller et al. [90].

Hard-wheat flour cookie doughs underwent an apparent glass transition at a lower temperature than did soft wheat flour cookie doughs. Decreasing the sugar level in the dough, T_g decreased.

These experiments confirmed the better sensitivity of TMA with respect to DSC to rheological changes occurring at and below the gel point of a thermosetting polymer. According to Slade and Levine [91], it is possible that the thermal energy that enhances molecular mobility can cause interchange in disulfide linkages with significant entropy reduction and negligible enthalpy drop:

very weak signal, or even no signal at all, therefore would be the result in DSC thermograms.

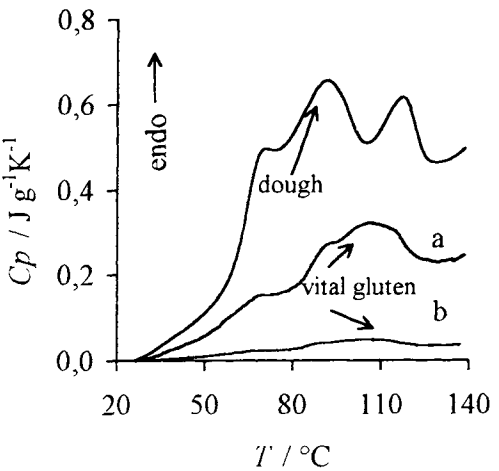

Figure 11. DSC traces from flour dough (upper curve) and gluten-water mixture [lower curves: (a) pure gluten, (b) scaled to the actual content of the dough] obtained at 5 K min^{-1} heating rate (modified from [22]).

The mobility of the matrix and the transitions during baking are greatly affected by the presence of water which acts as a solvent and plasticizes the hydrophilic components. The extent of water sustained plasticization of gluten has been discussed by Hoseney [85] who showed (Figure 12) that the trend of gluten T_g determined from DSC measurements is a function of water content.

Moisture depressed T_g by about 10 degrees per water % weight, ranging from 433 K for the glassy polymer containing less than 1 moisture % to 288 K for the rubbery polymer at 16 moisture %. When non-aqueous plasticizers were used, gluten remained thermoplastic [92-94]. A DSC study by Lawton and Wu [95] confirmed the findings of earlier works on the behaviour of gluten as a water plasticizable polymer similar to many synthetic amorphous polymers. Other water binding components naturally present in flour, like pentosans, or added during processing, like hydrocolloids, compete for the available water so modifying the glass transition temperature and, therefore, the mobility of gluten. This mobility, in turn, affects the physico-chemical and the physical properties of the bakery product [96].

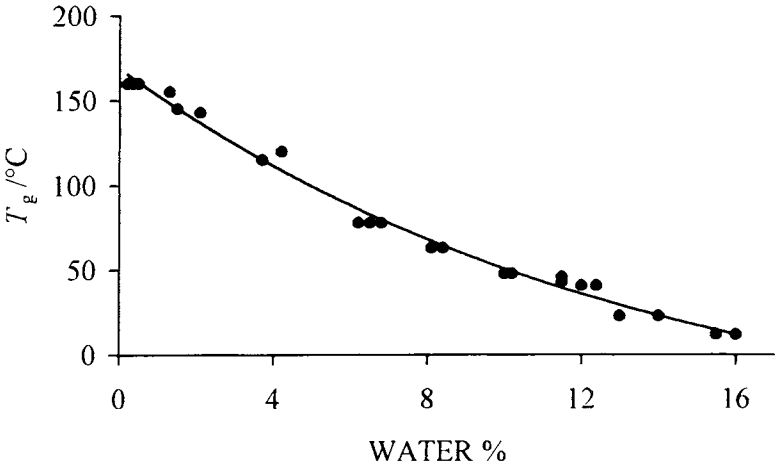

Figure 12. T_g versus water content (w%) for hand-washed and lyophilized gluten (modified from [85]).

For synthetic amorphous polymers the thermosetting process can be described by a time-temperature-transformation (TTT) diagram [97-100] where the cure and the glass transition properties of the thermosetting system are presented as a function of the heat treatment conditions. In general terms dough behaves like a composite material hosting two main components, gluten and starch, with different T_g. The dynamic map of its transformation during baking can therefore be represented through the TTT diagram (see section 2).

The starch in dough acts as a filler for the gluten polymer. At room temperature starch plays a less important role than gluten in the formation of dough structure, acting as an inert filler. Above the glass transition temperature starch gelatinizes forming a continuous structure , thereby increasing the overall strength of the dough. [101]. According to Hoseney and coworkers [102], the increase in the rheological properties with temperature indicates that gelatinization can extend hydrogen bonding between gluten polypeptides and starch molecules.

The effects of starch and gluten on dough viscoelastic properties were investigated by Abdelrahman and Spies [34,103]. On addition of starch to flour there was an increase of either modulus (Figure 13).

The relationship between amount of starch added and increase of the elastic modulus, G', was not linear and the rate of G' increase was larger than that of the loss modulus, G''. When the flour was added with either gluten or starch both

elastic and viscous responses were larger. According to the authors this behaviour could depend on the amount of free water which remained at the disposal of the matrix in the "solution" phase. Specific studies were however devoted to investigate possible starch/gluten interactions (see below).

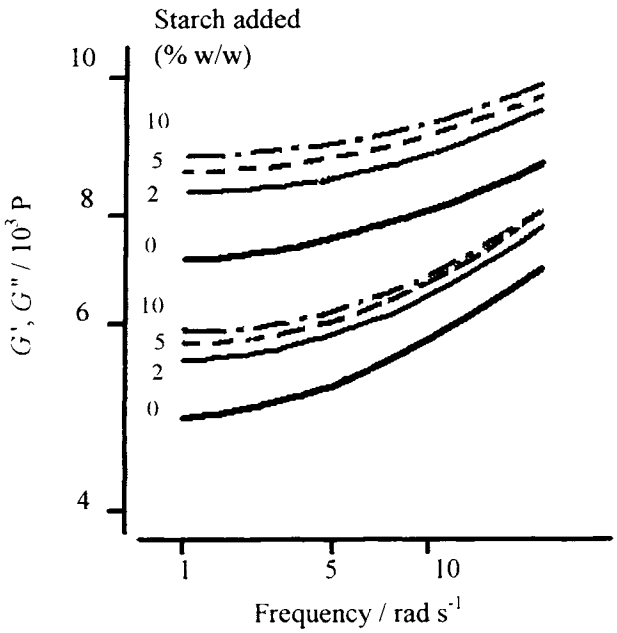

Figure 13. Effect of added starch on storage (G') and loss (G'') moduli of flour-water doughs (modified from [103])

Because of their water avidity, soluble proteins, hydrocolloids and pentosans reduce the water available to sustain starch gelatinization. As a consequence, this takes place at higher temperature (above 70 °C) and can be incomplete. These compounds can form reversible gels in the presence of water and therefore increase the rheological properties (G' and G'') of the dough and hinder the molecular mobility of other polymers, like gluten and starch polysaccharides [76]. The network formed within the kneaded dough is less tight and allows a larger leavening-sustained volume increase of the loaves [79]. Just as in the case of gluten reticulation, these effects do not imply specific DSC signals and should therefore be studied with other techniques, like dilatometry, thermomechanical analysis, image analysis, etc..

3.3 Viscoelastic Properties of Doughs

Comprehensive reviews on theory and application of rheology to dough changes from mixing to the final baking process and the effect of dough components on dough rheological behaviour are reported in the above quoted literature. The effect of the modified concentration of the major dough macromolecules has been widely examined and several authors have shown that the values drawn for the dynamic components of viscoelasticity depend on the testing conditions [33,34,101,103-115].

3.3.1. Testing conditions.

In performing dynamical measurements, many experimental parameters, which include heating rate, strain amplitude, oscillation frequency, and rest time before test, may affect the rheological response of viscoelastic materials [26]. The appropriate rheological techniques must avoid any effect of the experimental procedure on the forming structure and provide information about the intrinsic rheological properties of the system. These can be related, via existing theories, to structural changes and network formation.

Strain Amplitude. One of the principles of the theory of viscoelasticity is that in a stress-strain test the material response must be independent of strain amplitude. Figure 14 shows the influence of strain amplitude (given by the percent of angular deformation with respect to height) on the gluten-water mixture at 22 and 43°C.

The strain sweep test was performed [101] by means of a dynamic mechanical spectrometer (Rheometrics RDS 2) equipped with parallel plates. To avoid rapid drying during the test, the exposed edges of the specimen were covered with a thin layer of vaseline. It was noticed (Figure 14) that if the deformation was kept below 10%, both moduli remained relatively constant.

Above 10% strain amplitude, both G' and G'' decreased with the increase in strain. By means of the strain sweep test, therefore, a strain threshold was identified, above which the structure progressively changed, thereby inducing nonlinearity. The linear behaviour observed for small strains implies no "breaking" of the dough structure under these conditions. An additional information (Figure 14) was that the extent of linearity range was substantially independent of temperature. This was in agreement with the data by Smith [108] and Weipert [36].

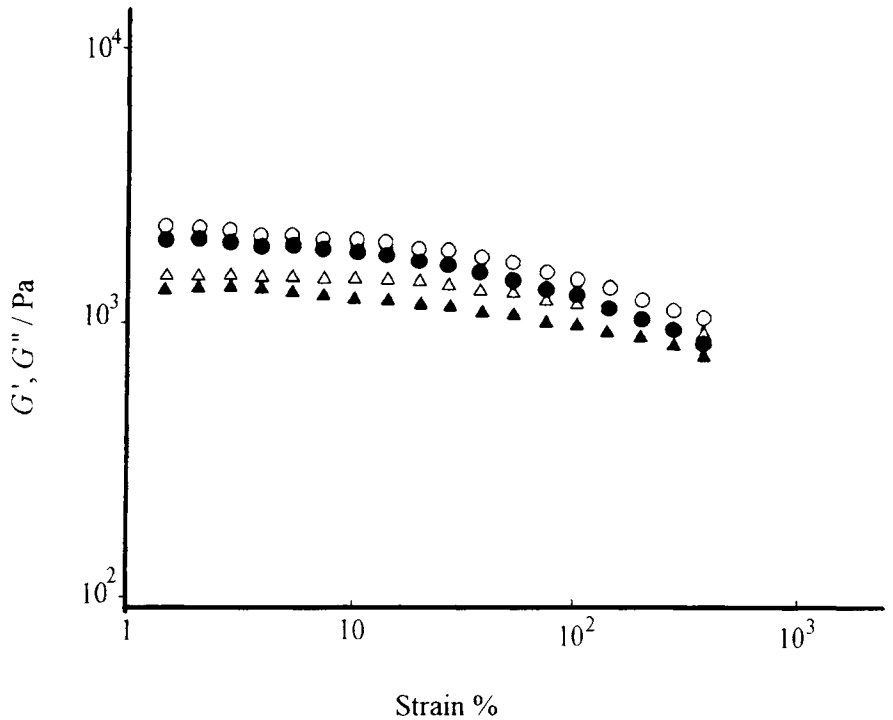

Figure 14. Storage (G', circles) and loss (G'', triangles) moduluses of a gluten - water mixture from a strain sweep test carried out at 28 (open symbols) and 43 °C (full symbols), and 1 rad s-1 frequency (modified from [101]).

Oscillation Frequency. Since the dynamic moduli of viscoelastic materials vary with the experimental time scale, G' and G'' were expected to change with frequency. Figure 15 shows the elastic and the loss moduli of gluten-water mixtures as a function of the frequency, ω [108]. Both elastic and viscous moduli increased with increasing frequency. These data confirmed the observations by Cumming and Tung [109] and Smith [108].

On increasing the testing frequency, at either small or large strain, viscosity significantly decreased, while the storage and loss moduli increased, due to shear thinning behaviour of wheat dough (Figure 16).

The increase of moduli with frequency is typical of entangled polymeric networks [116] where breaking and deformation of labile physical bonds allow relaxation of part of the applied stress. The testing frequency, i.e. the

experimental time scale, must therefore be selected depending on the network being tested: the faster the applied deformation, the smaller the observed breaking and deformation.

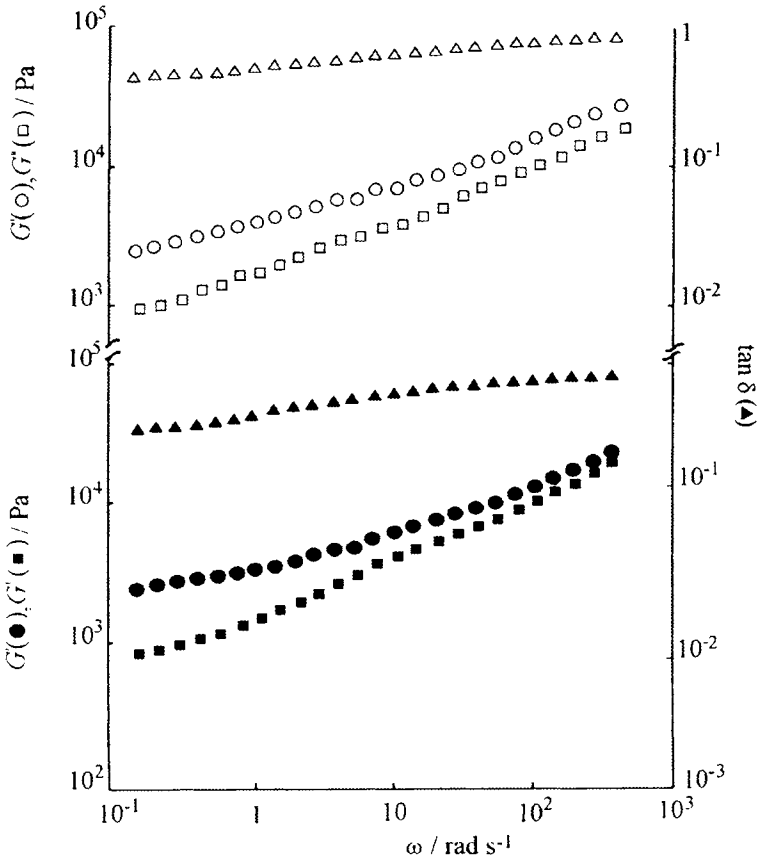

Figure 15. Storage and loss (G' and G'') moduluses of a gluten - water mixture from frequency sweep tests at 28 and 43 °C (open and full symbols) and 10% strain (modified from [101]).

At small strains G' was much higher than G'', just as expected for an elasto-viscous, solid-like body. However, at large strains, the G'/G'' ratio decreased until, in the 10% strain range, G'' became predominant: this means that at large strains the dough behaves like a viscous liquid with poor elasticity [36].

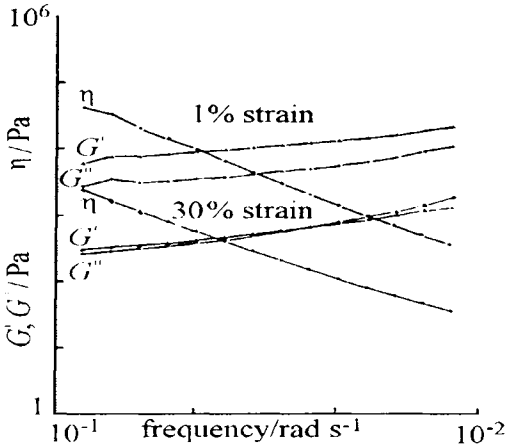

Figure 16. Frequency sweep of wheat dough at low and high strains at ambient temperature (modified from [36])

Rest Time before test. When a gluten-water mixture was examined in a 40 minute sweep test at 10% strain amplitude and 1 Hz frequency, no significant difference in the rheological response was noticed, whether the text was carried out just after mixing or after 60 minute rest [101]. This suggested that relaxation phenomena, which took place in gluten network as a consequence of manual mixing, could evolve too rapidly or too slowly with respect to the experimental time scale.

Heating Rate. As for the dependence of rheological behaviour on temperature, experimental tests carried out at different heating rates (from 0.1 to 5°C/min) showed curves with a similar dependence on temperature (Figure 17), although the slower the heating rate, the larger the G' variation with temperature [101]. This was a consequence of time rather than temperature dependence of the structure formation.

3.4 Baked and Cooked Products

3.4.1. TA Investigations.

Water release from the sample must be allowed to actually simulate a real baking process of a given dough. In these conditions most of the peculiarities of the DSC trace related with starch gelatinization and competition for the available water are largely concealed by the overwhelming effect of water vaporization.

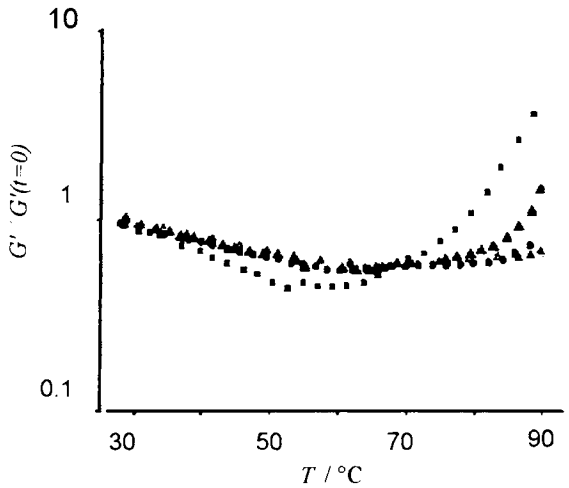

Figure 17. Effects of the heating rate [0.1(■), 0.5(▲), 1.0(•), 5.0 (Δ) °C min^{-1}] on G' in a temperature sweep test [1 rad s^{-1} frequency, 10% strain] (from [101]).

The process can be studied by means of TGA and/or TGA-DSC combinations [22]. The weight loss recorded shows a broad sigmoidal trend, although the process can involve separate steps: the DTG trace (viz., the time derivative of the TGA trace) actually shows a neat double peak, which can be directly matched with the analogous signal in the relevant DSC trace (see Figures 3 and 18).

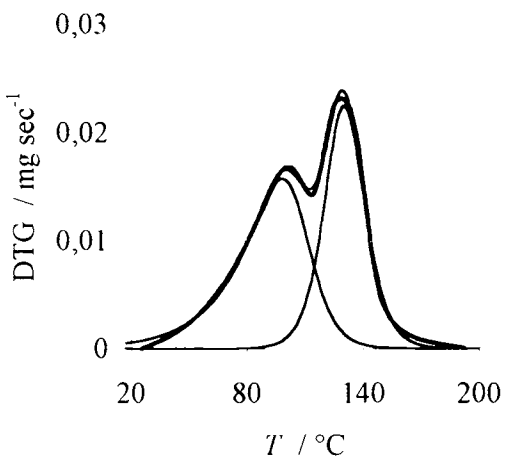

Fig.18 TGA, DTG and DSC traces from a flour dough (A. Schiraldi and D. Fessas, unpublished data)

The area underlying each DTG peak gives the mass of the water released in that step, while the ratio between the areas underlying DSC and DTG related peaks gives the corresponding vaporization enthalpy, $\Delta_{vap}H$. A couple of significantly different $\Delta_{vap}H$ values can be therefore estimated for a given dough. The first is rather close to the vaporization enthalpy of pure water and is related to a water loss that encompasses a large temperature range, namely from 298 to 433 K, and accounts for almost 65% of the overall mass loss; the second $\Delta_{vap}H$ value is about 10% smaller and deals with water released at higher temperature, namely from 373 to 433 K [22].

In the presence of hydrophilic ingredients, like hydrocolloids and/or pentosans, the enthalpy related to the first DTG peak is larger although the corresponding water loss is smaller [22]. This simply means that, as expected, water is more tightly bound by these compounds. The large width of this peak can be explained by taking into account the dishomogeneity of the temperature within the sample and the diffusion limited process of water release from the free surface of the dough sample.

A much better approach to this quantity is possible if special Knudsen cells are used: the cover of these has an orifice (10-100 μm) whose size is comparable with the mean free path of a gas molecule. When the system is maintained under high vacuum ($p < 10^{-4}$ mm Hg) and constant T, the release of the volatiles occurs at a constant rate and the relevant heat flux attains a constant level. Thus both DSC and DTG traces are horizontal straight lines: the DSC/DTG ratio gives therefore the vaporization enthalpy at any moment of the weight-loss process [117]:

$$\frac{dQ/dt}{dm/dt} = \frac{dQ}{dm} = \Delta_{vap} H \tag{1}$$

It can be demonstrated [118] that the weight loss rate occurring in a Knudsen experiment is directly related to the pressure drop across the hole.

$$\Delta p = k \frac{dm}{dt} \tag{2}$$

Since the release of volatile is severely limited by the hole size, the pressure within the cell is very close to the vapour pressure at the temperature considered, i.e. that of the saturated vapour. The pressure drop across the hole is therefore

$$\Delta p = (p_{sat} - p_{ext}). \tag{3}$$

If $p_{ext} << p_{sat}$, $\Delta p \sim p_{sat}$ and one obtains that

$$\frac{dm}{dt} \propto p_{sat} \tag{4}$$

Taking into account the definition of water *activity*, namely,

$$a_w = \frac{p_{sat}}{p^*_{sat}} \tag{5}$$

a_w can be accordingly evaluated as

$$a_w = \frac{(dm/dt)}{(dm/dt)^*} \tag{6}$$

where the terms at the numerator and denominator are the DTG signals obtained from the food sample under consideration and pure water, respectively, at the same temperature [118]. Because of the evaporation, the water content of the sample changes and the relevant DTG trace slants up (Figure 19).

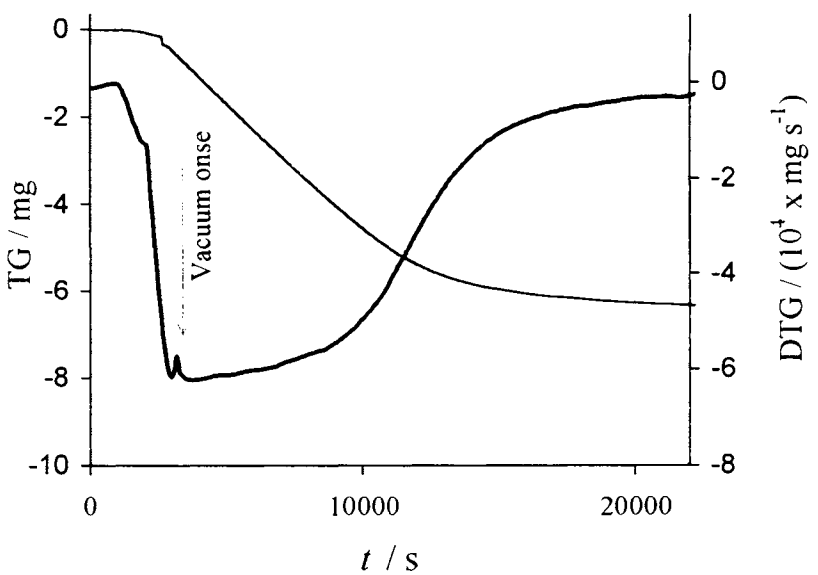

Figure 19. Isothermal dehydration (25 °C) of soft wheat dough: TGA and DTG trace from Knudsen cells (D.Fessas and A.Schiraldi, unpublished data).

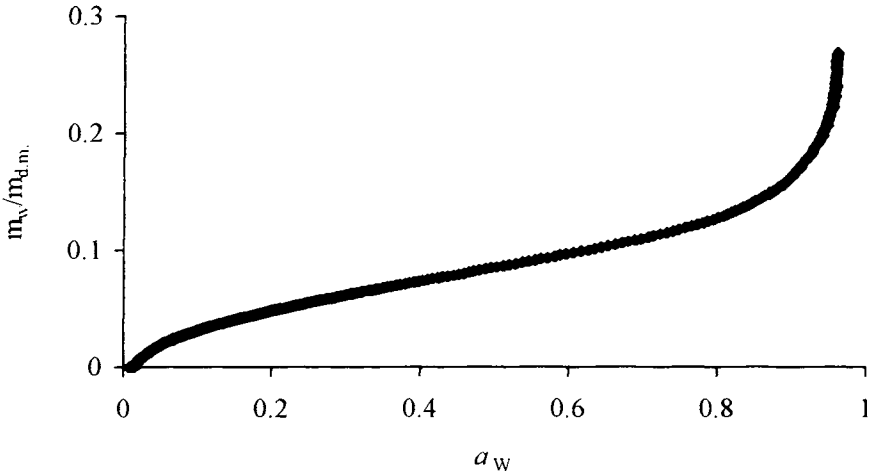

Figure 20. Isothermal desorption curve of soft wheat dough as a result of a TGA investigation with Knudsen cells (A. Schiraldi and D. Fessas, unpublished data).

The TGA trace obtained from the samples is directly related to the residual water content of the sample. If this is plotted versus the a_w obtained from the ratio of the DTG signal, the whole desorption isotherm is obtained (Figure 20) which nicely obeys either the BET(Benauer - Emmet - Teller) or GAB (Guggenheim - Anderson- de Boers) equation [118].

Simulation of cooking cereal products, like pasta and rice, requires isothermal investigations [16,17] with use of *ad hoc* vessels that allow the sample to be poured into the adequate amount of preheated water (Figure 21).

The calorimetric signal recorded (Figure 22) can be easily described (see Appendix A1) if one assumes first order kinetics for starch gelatinization, as largely supported by the experimental evidence and easily verified by use of a proper elaboration of experimental data.

Most of cereal products where starch gelatinization has been previously induced undergo a significant hardening in the course of the shelf-life. In the case of a bakery product the changes observed contribute to an overall process, named *staling*, where the increase of firmness is the main macroscopic effect, although it is accompanied by subtle and equally important phenomena, like starch retrogradation, water migration toward the surface, loss of crispiness of the crust, moderate but nonetheless significant overall moisture decrease, loss of aroma compounds, etc. [119-129]. Starch retrogradation corresponds to the partial recrystallization of the amylopectin which can be easily revealed as an endotherm in the DSC trace of stale bread samples.

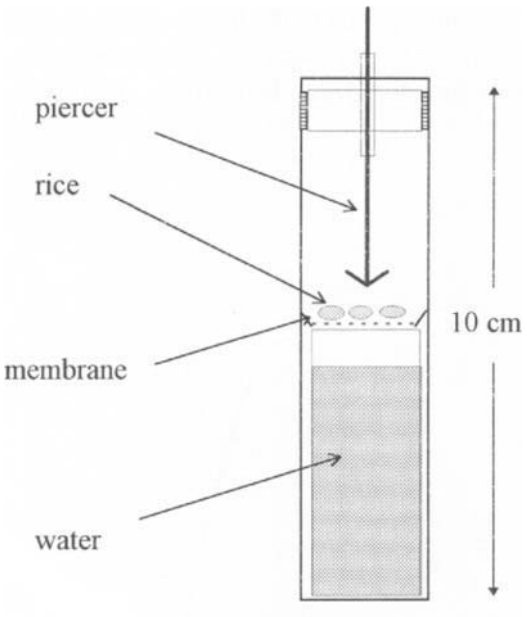

Figure 21. Schematic view of the cells used to study the isothermal gelatinization of cereal products, like pasta and rice.

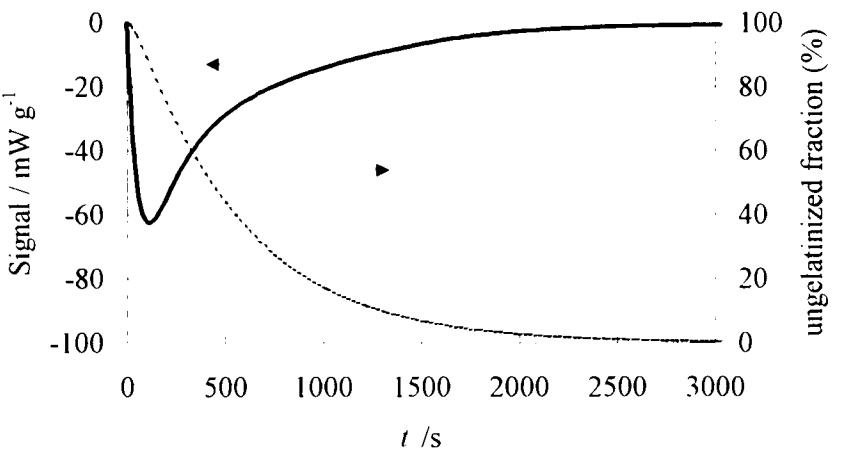

Figure 22. Isothermal DSC trace related to starch gelatinization in rice.

The signal (Figure 23) corresponds to the fusion of the crystals formed in the course of the shelf-life and its intensity, viz., the underlying area, increases with bread aging. Some authors found that this behaviour can be described with the Avrami equation, namely

$$Q(t) = A \exp(k\, t^n) \tag{7}$$

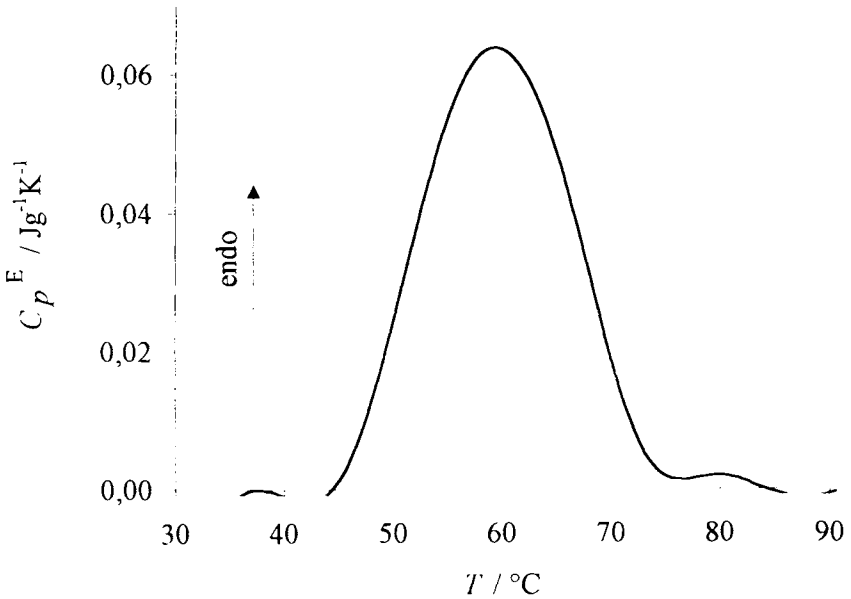

Figure 23. DSC trace from staled bread: fusion of amylopectin crystals formed in 24-hour ageing (D. Fessas and A. Schiraldi unpublished data).

It should be noticed that Avrami parameters, viz., k and n, relevant to retrogradation do not always coincide [130] with those drawn from the analysis of other physical properties, like the Young modulus, that is used to describe the increase of firmness: the correlation between starch retrogradation and increase of firmness is indeed dubious, since it significantly depends of the bread type considered (Figure 24). Starch retrogradation therefore does not seem sufficient to exhaustively justify the overall staling process [126].

Water loss occurring in ageing bread crumb can be reliably detected by means of TGA. Stale bread samples that undergo a TGA run at a given heating rate show a weight loss rate which can be related with ageing. The corresponding

DTG traces show a shouldered peak that can be resolved into a couple of gaussian signals, with maximum at about 50 and 95 °C, respectively. Again water seems to exist in at least two binding conditions [126]. Investigations of different nature, like EPR, NMR, Near IR, etc., could provide in the future further reliable evidences and support some interpretation at the molecular level [130].

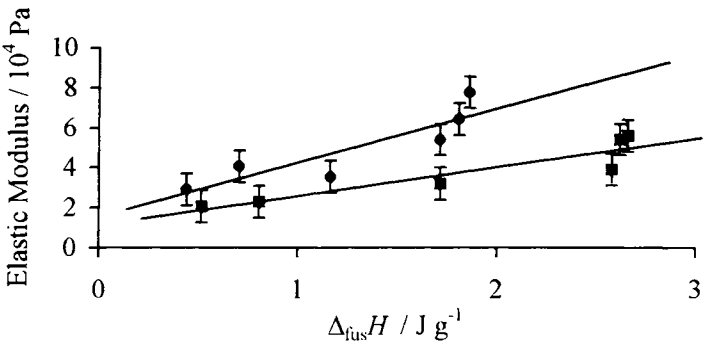

Figure 24. Fits of the elastic modulus versus $\Delta_{fus}H$ of amylopectin crystals of standard (lower curve) and gluten enriched bread crumb.

3.4.2. Thermomechanical Analysis of Baked Products.

Dynamic mechanical thermal analysis (DMTA or DMA) has been used to analyze glass transitions in foods (cheese, casein, gluten, soy isolates, starches and chocolate) [131,132]. T_g is measured as the middlepoint of the change in elastic (E') or loss (E") moduluses, as well as the loss peak in *tan* δ , as a function of temperature. The modulus drop at T_g encompasses two or three orders of magnitude; the DTMA determination of T_g is therefore much easier than by DSC, since the relevant heat capacity change at T_g can be very small [132].

Dynamic mechanical thermal analysis can be used to produce a state diagram, which can be useful to evaluating textural changes in food processes and during the shelf life. It is commonly accepted [125,133-137] that the texture and the shelf life of the product are determined by the water content.

Bread crumb texture during ageing and shelf-life is one of the most investigated phenomena in rheological analysis of food products. Many studies are based on steady measurements, mostly in steady compression mode. Some approached the dynamic measurements, both in shear, and in compressive oscillatory mode. As

for this last operative mode, strain sweep tests are published for fresh and aged bread crumb [138], but no thermomechanical analyses are presented.

TMA has been used to study glass transition and the viscoelastic properties of gluten and white pan bread [139-142] (Figure 25).

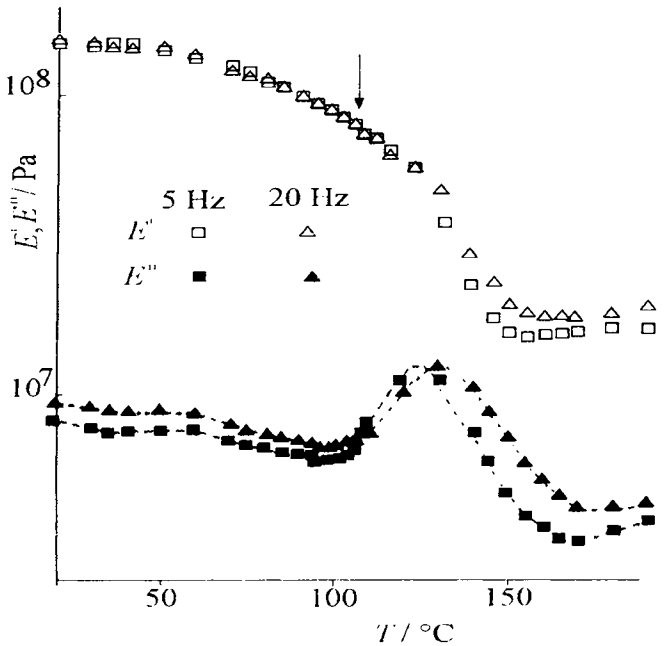

Figure 25. Effects of temperature on storage and loss moduluses (E' and E'') of white pan bread determined with a viscoanalyser at 1 °C min^{-1} heating rate (modified from [142]).

By applying a sinusoidal oscillator to a traditional TMA instrument, changes in size and softness can be determined on heating the sample. T_g cannot be reliably singled out as a change in the thermal expansion coefficient, since volume changes in bread can come from a number of causes (thermal expansion of gas and melting of retrograded starch). Conversely, softening can be referred to as a more satisfactory indicator of glass transition than are volume changes. Specific studies on gluten have been proposed by Kalichevsky et al. [140]: T_g dependence from moisture content and from added humectants concentrations was investigated.

Gluten, starch and ground bread pallets were equilibrated at the same relative humidity and analyzed to determine the respective T_g. According to Le Meste's results, gluten and bread have very close T_g values, and gluten T_g can be considered the onset point for bread softening. The same author proposed another instrument to study the effects of temperature, moisture content and frequency on the viscoelastic properties of white pan bread and extruded flat bread [141,142]: compression and tensile tests can be carried out by means of a viscoanalyzer operating in dynamic conditions at 1°C/min heating rate, and 5 to 50 Hz frequency.

DMA has been used by Hallberg and Chinachoti [143] to determine the glass transitions responsible for the mechanical firmness of bread, namely the "effective" network T_g, at various moisture content and storage time in a shelf-stable bread for 3 years (see Figure 26).

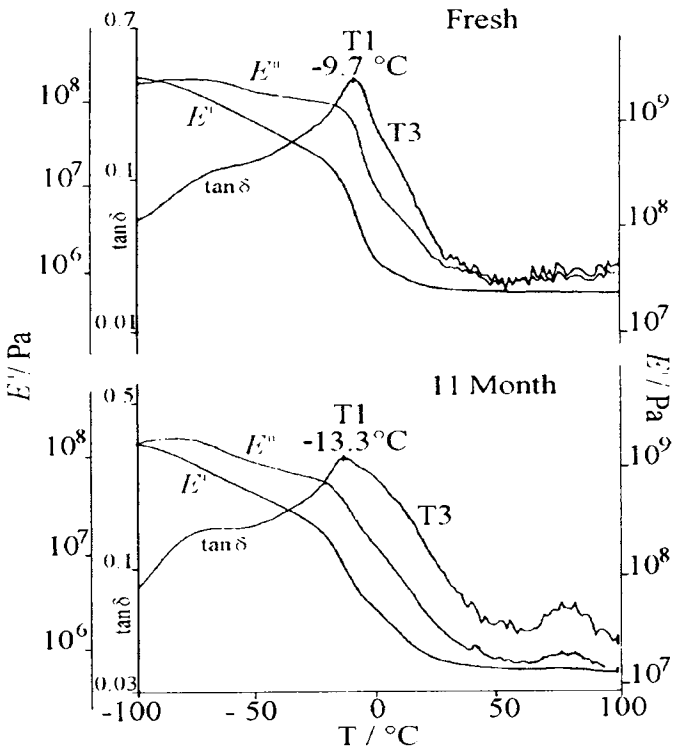

Figure 26. Evolution of dynamic rheological parameters in DMA traces obtained for breads of different age. (modified from [143]).

In DMA experiments, a sinusoidal stress is applied to the sample on increasing temperature.The response strain frequency is either in phase or out of phase with the stress depending on the viscoelastic properties of the system considered. These authors pre-cooled the sample down to –90 °C and then heated it up to 200 °C at 2 °C/min; stress was applied at various frequencies (up to 20 Hz) in a three point bending test. As for the fresh sample, the trace presents a sharp drop of E' and E" and a peak of *tan* δ . This main transition is attributable to a first order transition (ice melt) that occurred simultaneously with a change in heat capacity (a second order transition, glass transition).

A second minor glass transition T2 is due to the presence of glycerol in bread formulation. Another strong shoulder in tan δ to the right of the main transition peak T3 is due to water-unmiscible components (i.e. shortenings). By varying the moisture content in fresh bread from 2.6 to 28.8 % it was demonstrated that T1 and T2 were moisture-dependent transitions, while T3 was a moisture-independent. In particular, T1 was more significantly affected in the 2% - 20% moisture range, the transition temperature decreasing from about 160 °C at 2.6% moisture to about –11 °C at 28.8% moisture. Since all the three transition temperatures (T1, T2 and T3) remained relatively unchanged throughout a 3 year storage period, there should have been no network improvement. Due to hermetical sealing, any moisture loss was avoided during storage and the effective T_g did not change.

In a more recent publication the same authors [144] characterized the thermal transitions occurring in dried or stored bread by applying deconvolution techniques to tan delta curves obtained in DMA temperature sweep tests. Mechanical data were coupled with the analysis of "freezable" water content conducted with differential scanning calorimetry. A typical DMA thermogram of high moisture bread resulted in a broad transition region, as evidenced by the tan delta curve and E' drop spanning a temperature range of 50°C in the ice melting region. Ice melting seemed to dominate the thermomechanical events in crumb at higher moisture content, i. e. when freezable water was present.

Moisture loss below "freezable" water range was mainly responsible, according to Vittadini et al. [145], for the thermomechanical behaviour of pre-baked pizza dough reheated with a microwave oven as detected with DMA in three-point bending mode. Thermal transitions were associated to pizza texture characteristics : thermograms presented two transitions : a transition was detected at 60±40°C and was found responsible for the leathery texture in microwaved pizza, while the one detected at 0±30 °C was the dominating transition in the soft pizza reheated by conventional oven.

Nikolaidis and Labuza [132] used DTMA for measuring (deformation by single cantilever clamped-bending) the T_g of crakers in order to relate crispness changes to water activity (Figure 27).

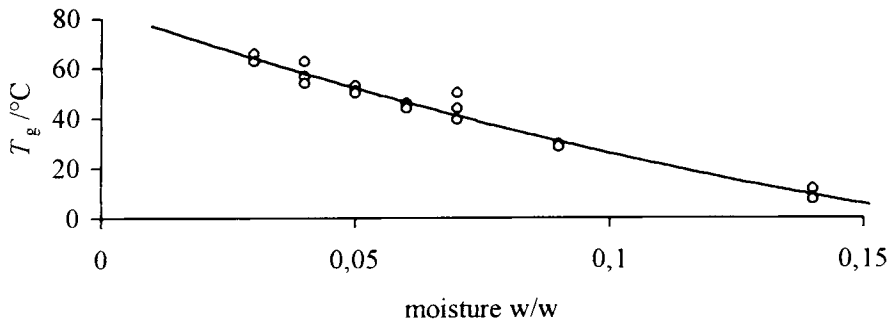

Figure 27. Glass transition temperature of commercial crackers determined by means of DTMA (Modified from [132]).

4. PROTEINS

Proteins are practically ubiquitous in foods where their functional and chemical properties are responsible for a number of physicochemical effects, like foaming, gel formation, water uptake, the Maillard reaction, release of amines, etc., which largely depend on interactions with other food components.

Heat treatment significantly affects their behaviour, but large differences in effect are observed according to whether they are globular or chain-forming molecules in the native conformation. It is therefore necessary to be aware of their structure and factors that can affect it fully to understand the behaviour of food proteins, from both nutritional and functional points of view.

The conformation of a protein molecule is thought to be dictated first by the genetic code that determines the primary structure (amino acid sequence) and then by parameters that produce the transition from a linear polypeptide to a three-dimensional folded structure. Proteins in their folded state usually are sufficiently stable against small changes of external conditions. But if the deviation exceeds some critical values the protein denatures within a relatively narrow range of temperature, pressure, pH, denaturant concentration, etc. [146-148]. Denaturation produces changes in many properties of the protein molecule that are sensitive to its three-dimensional structure, suggesting that this process

involves a breakdown of the entire native protein structure. In the case of small globular proteins, all these properties change simultaneously, suggesting an " all-or-none " process. Thermodynamically, this means that the denaturation process can be tentativelly regarded as a simple reversible transition between the two macroscopic states, namely the native (N) and denatured (D).

Food scientists now realize that the simplistic view of such a mechanism is untenable to describe the behaviour of proteins in mixtures of components like foods. Furthermore, previous studies by protein chemists concerned isolated proteins, usually in aqueous solution at low concentrations and at pH values so far away from the isoelectric point as to discourage protein interactions and aggregation. For this reason, scanning microcalorimeters have been developed that have a detection limit low enough to study 1% w/w protein solutions [149]. This, of course, up raises the question of the influence of concentration on DSC data and, therefore, the applicability of results obtained from one system to the other. It has been proved that water concentration plays an important role in the DSC response. Thus, it seems unlikely that conclusions based on dilute protein solutions examined by microcalorimetry can be directly transferable to much of the work done on food proteins at higher concentrations.

At high protein concentrations, additional events occur and the corresponding DSC trace is the sum of partially overlapped endothermic and exothermic effects. Thus, the overall endotherm seen during denaturation is a combination of truly endothermic reactions, such as the leakage of hydrogen bonds, and exothermic reactions, like the ordering of water molecules around apolar groups (which come to the exterior surface when hydrophobic interactions weaken) and thermal effects of protein aggregation [150,151]. In addition, it must be noticed that foods, like meat, milk and eggs, contain several proteins, the transitions of which can be largely overlapped. A tentative deconvolution of the DSC traces obtained from food specimens is possible only when each single protein of the "mixture" is studied as a pure solute in a series of separate investigations. Here the effects of environmental changes can be tested, including those of protein concentration. This information is necessary to assist in identifying the relevant signal from the DSC trace of a food specimen. Only then can DSC become a reliable tool to assess food quality parameters. As an example, this technique can be used to check the quality of stored eggs and processed egg white [152,153]. When eggs are aging, ovalbumin is converted, through an intermediate conformation, into a stable form called s-ovalbumin. At some storage time, egg white contains ovalbumin, s-ovalbumin and intermediate species, the amounts of which can be evaluated from the areas of the corresponding endothermic DSC peaks of unfolding.

Although a throrough understanding of the protein conformational transitions during a food process is not available at present, it is of practical importance to be aware of the experimental approaches, as well as the fundamental thermodynamic and kinetic laws that can be applied to understand how the protein structure depends on the environmental parameters.

4.1. Thermodynamic Approach to Protein Denaturation

DSC allows direct measurement of the enthalpy change related to the denaturation process; this property can be referred to as the "excess average enthaly" $< \Delta H(T) >$, referred to a particular thermodynamic state (the "native" state) and averaged on all the accessible macroscopic states at a given temperature T. This definition does not imply any particular model or mechanism for the specific process considered. A general relationship of statistical thermodynamics states that:

$$<\Delta H(T)> = \mathrm{R}T^2 [\, \partial \ln Q(T)/\partial T] \tag{8}$$

where $Q = \sum_i F_i$ is the partition function over all the states i of given probability F_i. This function can allows evaluation of the number of the discrete and stable macroscopic states and the changes of every thermodynamic parameter, across a transition and the relative populations as a function of temperature (see Appendix A4.1) [154]. The quantity $<\Delta H(T)>$ can be experimentally approached since [155],

$$< \Delta H(T) > = \int_{T_o}^{T} [C_p(T) - C_p^{N}(T)]\, \mathrm{d}T = \int_{T_o}^{T} C_p^{E}(T)\, \mathrm{d}T \tag{9}$$

where T_o is the onset temperature of the DSC signal, $C_p^{E}(T)$, the excess molar heat capacity of the protein, relative to the "native" state, is the difference between the apparent heat capacity of the solution per mole of protein (i.e. the observable quantity $C_p(T)$) and the apparent molar heat capacity of the solution containing the protein in its native state, $C_p^{N}(T)$, at any temperature T. The detailed and accurate knowledge of this function is the basis to evaluate thermodynamic parameters or test statistical mechanical models. Thermal denaturation of globular proteins proceeds with extensive heat absorption and, what is more, a significant increase in heat capacity $\Delta_d C_p$. Generally in the case of

small globular proteins with a small molecular mass (less than 20 kDa), thermal denaturation of proteins produces a sharp endothermic peak in the DSC trace.

Figure. 28 shows the DSC trace from the denaturation of RNase A which is a useful example of the thermodynamic relevance of calorimetric data [156-164] and can serve as a good "control" case. The same considerations hold for lysozyme which is reported to be 40% homologous with lactalbumin [165], a protein of great interest in foods. Heat capacity studies of the lysozyme - water system [166,167] are also relevant to hydrophilic/hydrophobic effects in food aqueous systems.

When a thermodynamic analysis can be applied (proteins in dilute solutions), the DSC trace allows an assessment (see Appendix A4.1) of if the denaturation process can be referred to as a one step reversible process [168-170], namely:

$$N \underset{}{\overset{K}{\longleftrightarrow}} D \tag{10}$$

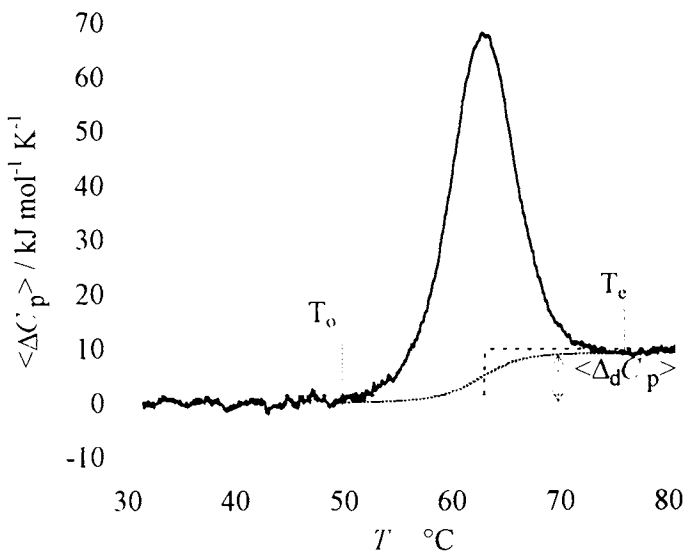

Figure 28. Excess molar heat capacity of RNase A versus T (pH 5, acetate buffer, protein concentration 1.810^{-4} M, ionic strength 0.1 M)

The following quantities can be thence evaluated across the N → D transition:

- Gibbs function,

$$\Delta_d G = G^D - G^N = -RT \ln K \tag{11}$$

- enthalpy,

$$\Delta_d H = H^D - H^N = R \frac{\partial \ln K}{\partial 1/T} \tag{12}$$

- volume,

$$\Delta_d V = V^D - V^N = -RT \frac{\partial \ln K}{\partial p} \tag{13}$$

- number of bound ligands,

$$\Delta_d n = n^D - n^N = \frac{\partial \ln K}{\partial \ln a} \tag{14}$$

where a is the relevant thermodynamic activity. Since

$$\Delta_d Cp = \left(\frac{\partial \Delta_d H}{\partial T} \right)_p \tag{15}$$

the increase in heat capacity of a protein upon denaturation means that the related enthalpy change is temperature-dependent and should increase with increasing T. Integration of equation (15) gives the enthalpy difference between the native and denatured states over the considered temperature range:

$$\Delta_d H(T) = \Delta_d H(T_d) + \int_{T_d}^{T} \Delta_d C_p(T)\, dT \tag{16}$$

If $\Delta_d C_p$ is constant, the function corresponds to a straight line,

$$\Delta_d H(T) = \Delta_d H(T_d) + (T - T_d)\Delta_d C_p \tag{17}$$

$\Delta_d H(T)$ of many globular proteins was found to have this behaviour, although with a slope that depends on the specific protein [171]. If the specific enthalpy values (i.e., the values calculated per gram of protein) are plotted versus T, the various straight line $\Delta_d H(T)$ trends converge toward a single point at about T_H^* = 383 K [172,173]. A similar situation was found with the entropy functions, $\Delta_d S(T)$, which are not straight lines but converge at about the same temperature as the specific enthalpies, T_S^* =385 K,

$$\Delta_d S(T) = \frac{\Delta_d H(T_d)}{T_d} + \Delta_d C_p \ln\left(T/T_d\right) \tag{18}$$

where T_d is the midpoint temperature of the transition and $\Delta_d C_p$ is again considered constant. Since $\Delta_d H(T)$ contains contributions primarily arising from the exposure of buried apolar groups to the solvent and from the cleavage of hydrogen bonds within secondary and tertiary structure [171], it has been argued that at the convergence temperature (T_H^* =383 K, T_S^* =385 K), the hydrophobic contribution to the enthalpy and entropy should be zero [174,175].

The thermodynamic analysis allows a quantitative description of protein thermal stability, referred to as the work required for breaking the native structure. When unfolding is treated as a transition between stable macroscopic states, this work coincides with the difference of the Gibbs function.

Since $\Delta_d G(T)$ is not very sensitive to $\Delta_d C_p$ changes within a broad temperature range [171,161], $\Delta_d C_p$ can be treated as a constant in equations 17 and 18; one accordingly obtains:

$$\Delta_d G(T) = \frac{T_d - T}{T_d}\Delta_d H(T_d) - (T_d - T)\Delta_d C_p + T\Delta_d C_p \ln\left(T/T_d\right) \tag{19}$$

The most remarkable feature of $\Delta_d G(T)$ is that it goes through a maximum, at a temperature T_s where $\Delta_d S(T_s) = 0$ and the stability of the native conformation, $\Delta_d G(T)$, is therefore only enthalpic (see Figure 29).

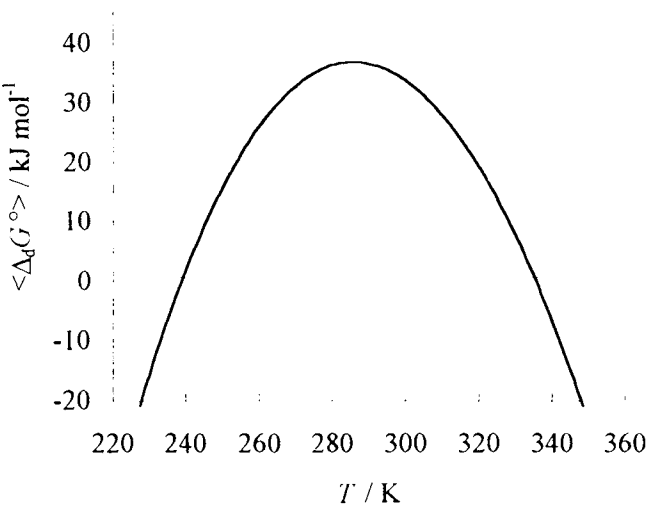

Figure 29. $\Delta_d G(T)$, for RNase A at pH 5.0 evaluated from DSC data (Figure 28).

On decreasing temperature, $\Delta_d H(T)$ goes through zero and then reverses sign, thus becoming a destabilizing factor. At a sufficiently low temperature, T'_d, where $\Delta_d G(T'_d) = 0$, the protein unfolds, undergoing a "cold denaturation" [176-182],

$$T_d' \approx \frac{1}{2} T_d^2 \left[\frac{\Delta_d H(T_d)}{\Delta_d C_p} + T_d \right] \tag{20}$$

Protein cold denaturation was DSC investigated and found to be a highly reversible process: on cooling across T'_d heat is released, while on reheating heat is adsorbed (see Figures 30 and 31).

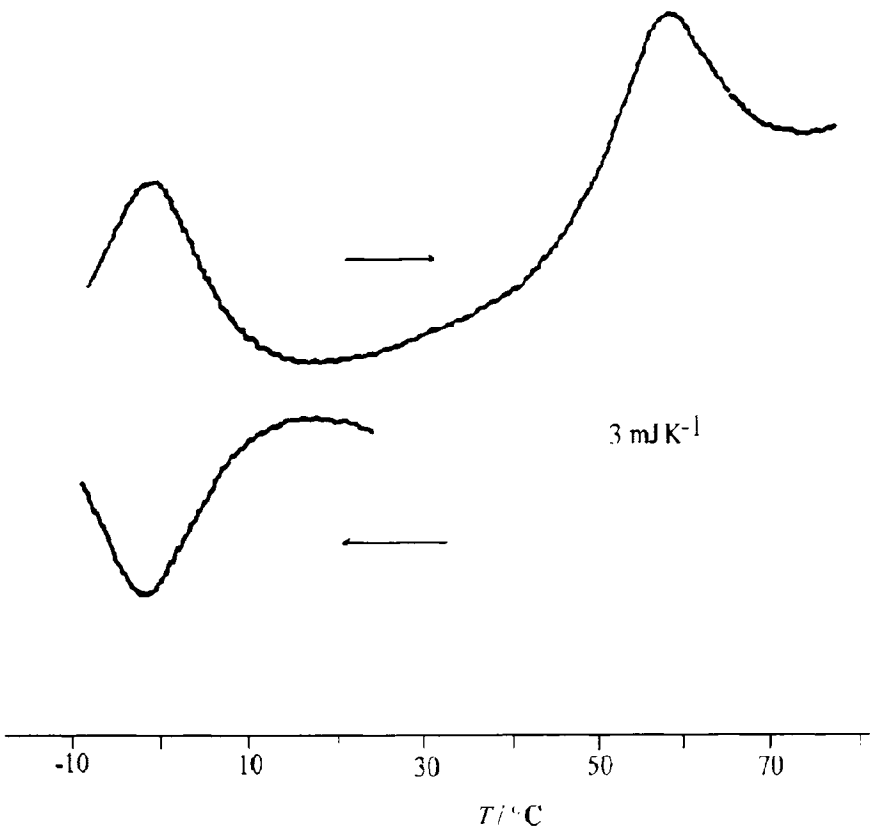

Figure 30. The heat effect observed on cooling and subsequent heating of apomyoglobin (modified from [183]).

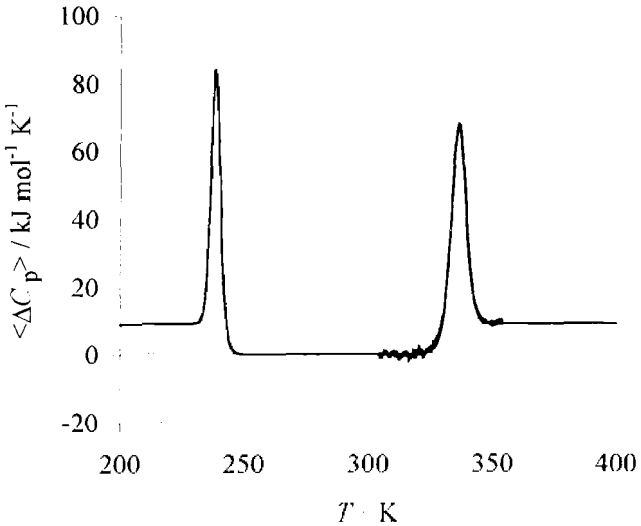

Figure 31. Simulated and experimental (heavy line) excess heat capacity function for RNase A. The peak on the left hand side corresponds to the "cold denaturation" which is undetectable because of water freezing.

At T_d the protein again undergoes unfolding with heat adsorption ("heat denaturation"). Cold and heat denaturation therefore occur with opposite heat effects and define the thermal stability range (T_d -T'_d) of the native conformation.

The equilibrium constant K for the process $N \overset{K}{\longleftrightarrow} D$ is expressed as function of temperature by:

$$K(T) = \exp\left\{-\frac{\Delta_d H}{R}\left(\frac{1}{T}-\frac{1}{T_d}\right) + \Delta_d C_p\left[1-\left(T_d/T\right)+\ln\left(T_d/T\right)\right]\right\} \qquad (21)$$

where $\Delta_d H$, $\Delta_d C_p$, and T_d are the thermodynamic parameters of the denaturation process which can be directly determined from the experimental DSC trace. In this case an analytical expression can be obtained [184] which allows simulation of the DSC trace for heat and cold denaturation, which are both referred to as two-state transitions,

$$C_p^E(T) = \frac{\Delta_d H^2}{RT^2}\frac{K(T)}{[Q(T)]^2} + \Delta_d C_p \frac{K(T)}{Q(T)} \qquad (22)$$

where the canonical partition function $Q(T)$ for a two-state system (the native state being the reference) is (see Appendix A4.1),

$$Q(T) = 1+K(T) \tag{23}$$

Small globular proteins show DSC traces which can be satisfactorily justified with the two-state transition model. An increasing number of experimental studies, however, have shown that many food proteins give calorimetric traces which significantly differ from those expected for a simple two-state process [185,186]. To give these DSC traces a physical meaning and obtain the desired thermodynamic parameters dealing with the stability of the native conformation, "deconvolution" of the thermal profiles is necessary. This means singling out the transitions which form the overall denaturation process. Basically, two models have been developed for the analysis of complex calorimetric curves.

As a simple approach the denaturation process can be referred to as a sum of independent two-state transitions [184, 187-189]: though this hypothesis can seem unrealistic in view of the complexity of the denaturation process of food macromolecules, the well-established existence of more or less independent domains in protein structures significantly support such an assumption. When this is so, the overall excess heat capacity function is given by:

$$C_p^E(T) = \sum_{i=1}^{n} C_{p_i}^E(T) \tag{24}$$

where every $C_{p_i}^E(T)$ obeys equation (22). The deconvolution of the calorimetric trace of RNase BS at pH 5.0 [189] required two independent two-state transitions (see Figure 32).

In another approach the denaturation process is referred to as a sequential progress through intermediate states:

$$N \xleftrightarrow{K_1} I_1 \xleftrightarrow{K_2} I_2 \xleftrightarrow{K_3} \cdots\cdots \xleftrightarrow{K_m} D \tag{25}$$

The thermodynamic analysis is the starting point to predict the behaviour of the thermal stability of the food proteins in such environmental conditions as changes in pH, presence of strong ligands, denaturants, salts, sugars, etc.

4.2. pH Effects

The effects of pH changes on the thermal properties of a protein have been very well assessed. For small globular proteins, at extreme pH conditions, in either acid or alkaline region, lower values of both T_d and $\Delta_d H$ were found [190-195]: for a series of small globular proteins, $\Delta_d H$ and T_d determined at various pH values could be correlated to each other with a straight line [190]. The $\Delta_d H$ changes therefore would not be a direct pH effect, as they simply follow the changes of T_d according to equation (17). This is instead the case for $\Delta_d S(T_d)$. Since $\Delta_d S(T_d)$ is intrinsically related to T_d, the latter would change with pH because of the $\Delta_d S(T_d)$ variation. It can be finally stated that the pH effects on the protein stability are mainly of an entropic nature.

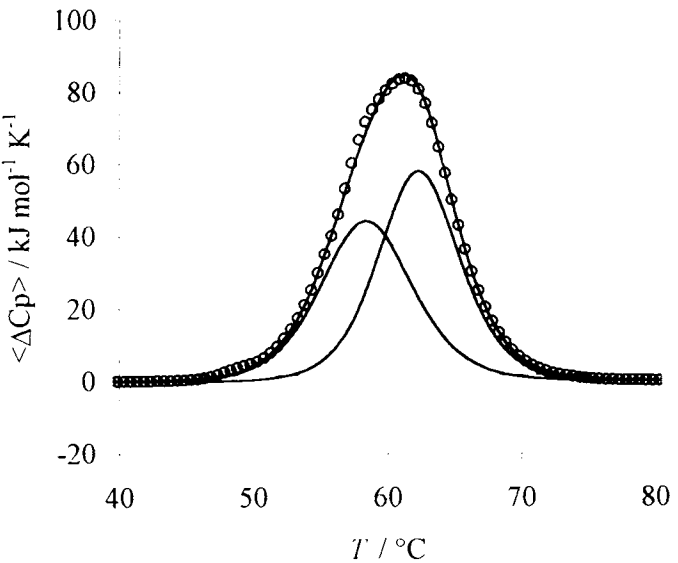

Figure 32. Model of the independent transitions of domains for RNase BS. Dots and continuous line represent the experimental and simulated trends of the excess heat capacity.

Some stability curves ($\Delta_d G$ *-vs* $-T$) drawn according to equation (19) are reported in Figure 33. It should be noticed that the thermodynamic stability, referred to as the value of $\Delta_d G$ at $T_{max}=T_S$, decreases on decreasing pH. The effect of pH on $\Delta_d G(T)$ was theoretically analyzed by Hermans and Scheraga [196] who suggested that hydrogen ions would preferentially bind to the unfolded

conformation. On this basis these authors drew an analytical expression for $C_p^E(T)$, which explicitly accounted for the hydrogen ion concentration $[H^+]$ (see Appendix A4.2).

4.3. Effect of ligands and other protein modifiers.

Co-solutes like metal ions that have specific binding properties, anionic detergents, like succinic or maleic anhydride, SDS, denaturants, like GuHCl, urea etc., significantly affect the thermal stability of proteins. Protein unfolding and ligand binding (when the ligand concentration is below the saturation level) are related to each other with significant deviations from a two-state transition mechanism. This behaviour was explained [197,198] through a thermodynamic analysis which allowed simulation of calorimetric traces and evaluation of association constants and binding enthalpy (see Appendix A4.2).

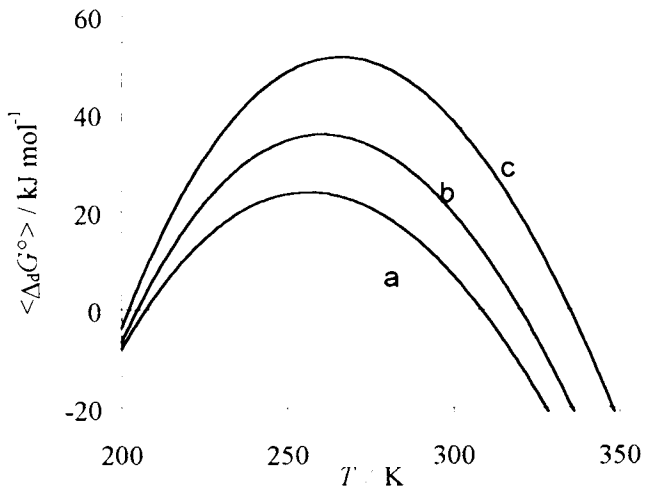

Figure 33. A series of stability curves $\Delta_d G(T)$ for a model globular protein at different pH values: 2 (a), 3.5 (b), 5.5 (c).

In the presence of ligands (below saturation level), the experimental DSC traces show a broad and complex signal (often reversible on cooling), that is rather different from a two-state transition peak. One could say that the transition is nearly biphasic, since a partial resolution of the signal in two peaks is apparent. Figure 34 reports experimental and simulated DSC traces for RNase A in the presence of 2'CMP [162].

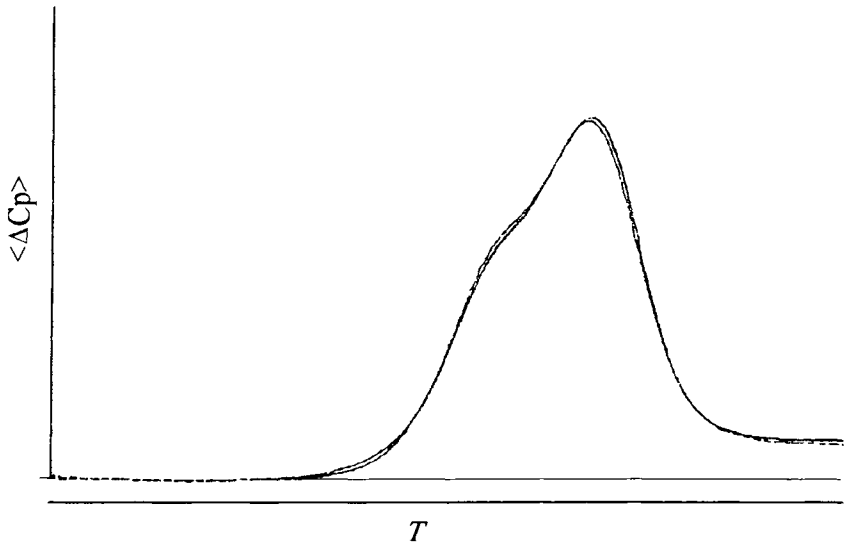

Figure 34. Experimental and simulated DSC traces for RNase A in the presence of 2'CMP (pH = 5.5, acetate buffer, 0.1 M KCl solution) [162].

A similar behaviour is reported (see Figure 35) for the more complex case of BSA - SDS interaction [199]. Ionic surfactants have the peculiarity to denature proteins at millimolar concentrations (molar concentrations are necessary for other denaturants, like urea and guanidinium chloride), provided that the surfactant/protein molar ratio can be higher than the number of the strongly binding sites.

In the presence of sodium dodecyl sulphate, the BSA (which has about 70 binding sites for SDS, 10-11 of which showing larger affinity than the others) undergoes a biphasic denaturation: two endotherms appear in the DSC trace which are related to protein denaturation and binding equilibrium, respectively, (rather than to denaturation of different protein domains) [199].

Urea and guanidinium hydrochloride are commonly used as protein denaturants, but the mechanism of their action is not yet fully understood. It is indeed matter of discussion whether the action of these agents is direct, i.e., related to the binding of denaturant molecules onto the protein surface, or indirect, i.e., mediated by a change in the properties of the solvent [200-204].

The effect of a ligand on thermal stability of protein can be explicitly accounted for by relating the binding equilibrium to the thermal denaturation process [205].

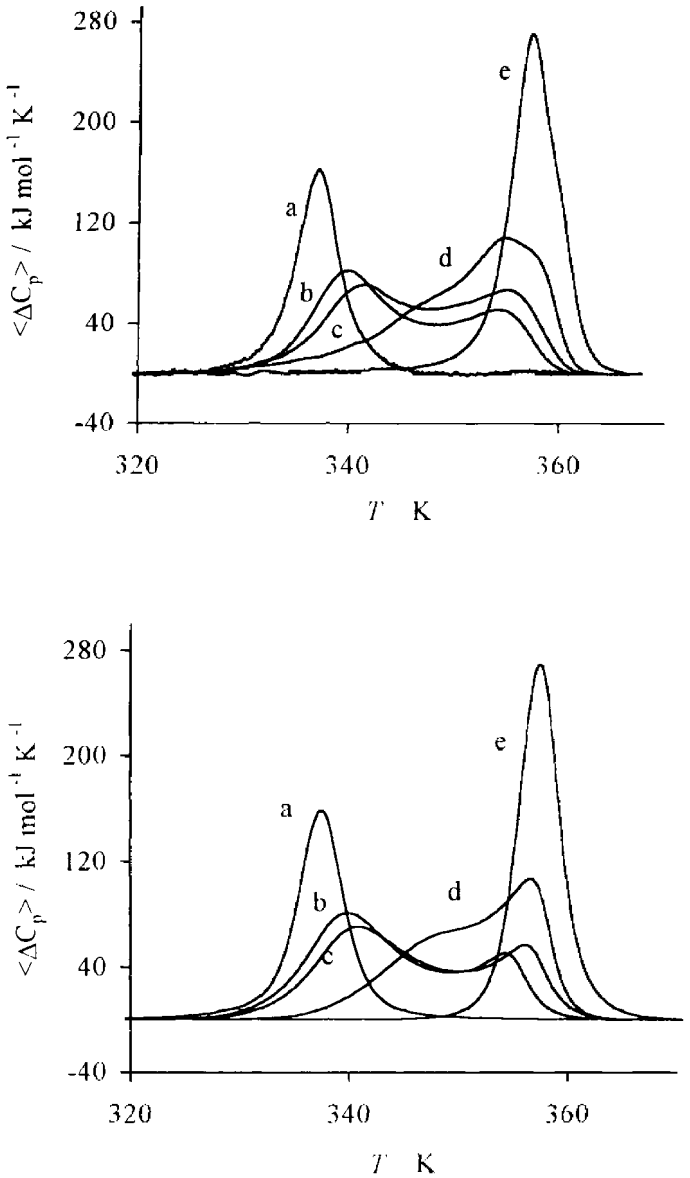

Figure 35.Experimental (upper) and simulated (lower) DSC traces of BSA (pH 7.0 phospate buffer and 0.15M NaCl) for various SDS/BSA ratios, r, [199]. a) BSA alone b) r=2; c) r=3; d) r=5; e) r=10.

This analysis can be tentatively based on the "denaturant binding model" by Aune and Tanford [206]. The model assumes that urea or GuHCl can bind to different independent sites of native and denatured conformations of the protein. Following this line, the DSC trace obtained in the presence of these denaturants can be simulated (see Appendix A4.2) according to the canonical partition function formalism [162,197].

The simulated DSC traces of RNase A according to the best fit of the experimental data at different GuHCl molar concentrations at pH 6.00 are shown in Figure 36.

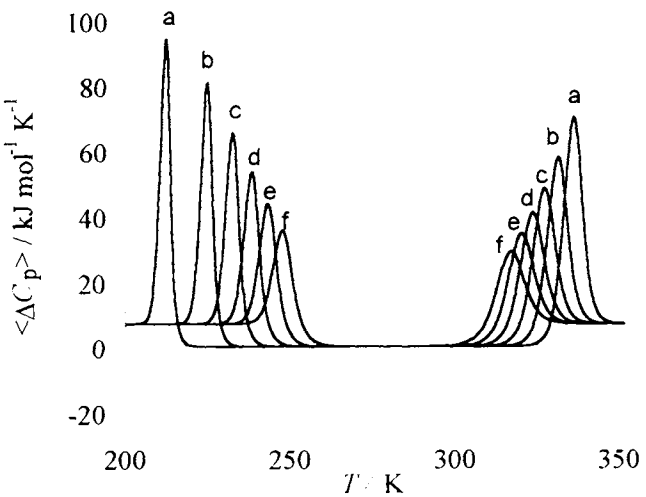

Figure 36. Simulated (see Appendix A4.2) excess heat capacity of RNAase A from the best fit of experimental traces [163] obtained at increasing [GuHCl]: 0 (a), 0.5 (b), 1 (c), 1.5 (d), 2 (e), 2.5 (f). The predicted cold denaturation curves (experimentally undetectable) have been included.

It is crucial to realize that in the course of calorimetric investigations the denaturation process is induced both physically, by rising T, and chemically, by action of a denaturing agent, like GuHCl and urea. The simultaneous action of these two factors can lead to an unexpected behaviour.Finkelstein and Shakhnovich [207,208] have shown, with general theoretical arguments, that the denaturation process for small globular proteins can be described as the sum of two phenomena: a first-order phase transition from the native to a compact denatured state, and a second-order phase transition from the compact denatured

state to a random coil conformation. These denatured states strongly depend on solvent features, since solvent and co-solvent molecules can penetrate into the macromolecule core [209-211].

In these conditions the basic principles of the theory of macromolecules apply: when the solvent is "poor", the denatured protein is stable in the globular native conformation; when the solvent is "good" (theta conditions), the protein conformation is a random coil. These authors [206,207] have also defined phase diagrams which show the stability regions for the protein conformations at various temperatures and concentrations of denaturant. The diagram emphasizes the presence of regions where the stable states are the so-called "wet molten globule" and "swollen globule". This theoretical analysis indicates that the two-state model may be incorrect and misleading [209,212,213]. However the necessity of treating the experimental data makes this oversimplified model of more practical use.

The binding of GuH^+ ion is an exothermic process with a negative entropy change. The exothermic effect demonstrates that the interaction of GuH^+ ion is more favourable with polar groups of a polypeptide chain than with water molecules. Instead the entropy decrease associated with the binding is due to a loss of the translational degree of freedom of GuH^+ ions. However it has been also suggested that, if the denaturant binding model is a realistic representation of the GuHCl action, the entropy decrease can be partially ascribed to the stiffening of the denatured conformation, which would be predominant in the presence of bound GuH^+ ions. Makhatadze and Privalov [214] were able to characterize the binding sites of GuH^+ ions on RNAase A and assess the type of interaction. The sites would be unspecific and correspond to some next neighbouring polar groups where GuH^+ ions bind forming four or five hydrogen bonds.

4.4. Protein aggregation

The above analyses are based on equilibrium thermodynamics and require the experimental heat capacity data to accurately reflect the equilibrium protein unfolding [154]. It must be nevertheless recognized that, in many cases, the overall process that takes place during the DSC run is irreversible, as shown by the lack of thermal effect on reheating.

Irreversible denaturation of simple proteins is often thought to involve at least two steps: (i) reversible unfolding of the native protein (N), (ii) irreversible alteration of the unfolding protein (U) to yield a final state (F) that is unable to fold back to the native conformation [215, 216]

The two- step nature of the irreversible denaturation can be schematically described by the Lumry and Euring model [217]: $N \longleftrightarrow U \longrightarrow F$.

This model implies different situations depending on the rate of the irreversible step [218-221]: if it is fast enough, the transition is entirely determined by the kinetics of formation of the final state and no equilibrium thermodynamics can be applied. However, even in the case of strongly rate-limited denaturation, the effects of ligand and protein concentration on the transitions can be observed by DSC if the release of ligand and the protein dissociation into monomers take place before the rate-determining step [222]. These appear as non-saturating effects, like those predicted by equilibrium thermodynamics for reversible unfolding transitions. Some simple cases are illustrated in the Appendix A4.3.

Aggregation is generally an exothermic reaction that lowers the overall enthalpy value [149], although the energy involved is quite small. However, [195,223-226] by adjusting the experimental conditions of pH, ionic strength, and protein concentration it is possible to separate the denaturation endotherm from the aggregation exotherm of the DSC thermal curve [195] (Figure 37).

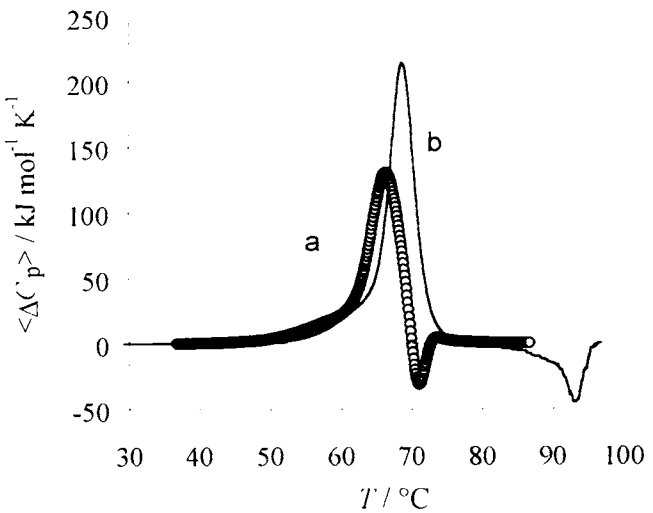

Figure 37. Experimental DSC trace of BSA (0.01 M phoshate buffer and 0.15M NaCl) at pH 6.0 and 8.0, respectively: shift of the exothermic peak is related to aggregation of denatured molecules.

The importance of knowledge of these pH effects is particularly relevant in terms of food processing. For example a food area for which pH changes many impact food protein processing is the dairy industry. Although k-casein does not denature or show a DSC transition when heated up to 120 °C, other milk proteins

(principally β-lactoglobulin and α-lactalbumin) do give typical protein denaturation curves strong depending on pH .

Alkaline conditions destabilize the β–lactoglobulin protein. This was first observed using differential thermal analysis (DTA) where transition temperatures dropped from 81.5 to 66.5 °C as the pH was increased from 5.0 to 9.0 [227].

As for α–lactalbumin, the T_d value remains fairly constant in the alkaline region [228]. However, at acid pH values (pH 3.5 and lower) there is a sharp decrease in both T_d and $\Delta_{den}H$, while no endoterm is observed at pH 2.5. This has been related to a conformational transition at pH 3.3 [229].

The pH dependence of protein aggregation is also very important for the food technology. Overall, DSC provides a valuable tool for quality control purposes, and problems associated with poor pH control can be readily detected.

Disulphide bond formation and intermolecular peptide bonds (isopeptides) are crosslinking mechanism frequently investigated in food systems. Little agreement exists in the literature about which reaction will occur in a particular protein under a given set of conditions. One major factor that is often discounted in such systems is the protein/water ratio. This parameter would seem to dictate the nature of the protein-protein interactions occurring, much as the starch/water ratio determines the events during heating of the starch-containing systems [62].

That water content can influence reaction mechanism in protein systems is shown from the work of Sheard et al. [230] in which heat treatment of soy protein at high water contents led to aggregation by hydrophobic interactions while decreasing water levels changed this mechanism to favour covalent disulphide bonding. In general, it would appear that lowered water contents and higher processing temperatures promote covalent bonding forces at the expense of noncovalent ones. Specific aggregation of whey proteins are mainly determined by ionic bonding under enthalpic control, while non-specific aggregation of whey proteins are mainly determined by hydrophobic interactions, under entropic control.

4.5. Effects of salts and sugars

Even when present as a low fraction of the total mass, salts can have a considerable impact on the functionality of food proteins. According to their specific effect, salts have been classified so as to form the so-called Hofmeister or lyotropic series [231].

At $\mu \geq 0.5$ ionic strengh, anions can be chaotropic (e.g., thiocyanide. iodide), namely with a destabilizing effect, or non chaotropic (e.g., acetate, chloride, sulphate, citrate), if their action is opposite. For example, the T_d of vinicilin [232] and oat globulin [233] decrease in the presence of SCN^- and I^-

ions, whereas in either case T_d increases when Br^-,or Cl^- are present. Changes in $\Delta_{den}H$ can however be observed only at concentrations of 1M; under these conditions, $\Delta_{den}H$ is larger in the presence of Cl^-. The stabilizing effect is the result of a reduced electrostatic repulsion.

For a given anion, different effects on T_d have been observed depending on the specific cation considered. For example both vinicilin and legumins are stabilized in the presence of K^+, Na^+, and Li^+ at $\mu \geq 0.5$, whereas Ca^{2+} ions have an opposite effect [234]. Although similar findings concern oat globulin, milk and many other proteins, they cannot be referred to as a general salt effect, since they rather seem to directly depend on the specific protein structure and salt concentration. For example, low concentration (<0.3 M) KCl makes collagen T_d to decrease [235]. Thus use of salt reduce the thermal stability of the muscle protein but has the opposite effect on plant proteins.

Sugars too can affect protein stability. It is well known that sugars have a stabilizing effect on the globular protein structure, which is related to hydrophobic interactions. Low levels of sugars increase the number of hydrophobic associations as evidenced by the decrease of surface hydrophobicity [236]; these interactions are strengthened [237] with increasing sugar content, although to a different extent according to the specific protein considered. Therefore structure is an important factor in protein-sugar interactions.

As an example of practical use of the sugar stabilizing effect is given by the recipe of the angel cake, where the sucrose content is "tuned" so as to make the denaturation temperature of ovalbumin (the main protein of egg albumen) to coincide with the gelatinization temperature of the wheat starch, since these conditions allow the characteristic angel-cake structure to be built up on baking [238].

4.6.Protein gels

Protein aggregation during food preparation plays a significant role in structure formation of many gel-type or emulsion-type products [239]. Ferry [240] described protein gelation as the result of structure unfolding that exposes reactive sites, intermolecular aggregation, and eventual formation of infinite, crosslinked gel networks. As the conformation of proteins is modified under the influence of heat, protein-protein interactions become more prevalent with formation of covalent and non covalent bonds. Covalently bonded proteins may be considered crosslinked: different protein molecules can stick together or protein molecules can bind non protein components [241].

As for large oligomeric proteins like those found in vegetal tissues, an early effect produced by heats is dissociation into subunits [242,243]. Because of the

consequent exposure of previously buried apolar groups, the surface hydrophobicity of the protein can be therefore expected to increase [244,245]. The subunits separated on heating can then form crosslinks of various kinds, like normal peptide bonds, intermolecular crosslinks (LAT = lathonine type, LAL = lysinoalanine type), Maillard products, isopeptide bonds, etc.. Intermolecular peptide bonds, because of the larger energy of formation, are expected to occur under more severe conditions, like those found during thermal extrusion [244,245], although this type of covalent bonding can be produced in milder environments [246]. Non covalent bonds are mainly involved in hydrophobic interactions that often sustain structure formation.

Protein unfolding implies increased hydrophobicity and partial loss of tertiary and quaternary structure with major effects on functional properties [247]; other factors, like chain flexibility, could justify [248-250] the differences between various protein species.

Food scientists working with biologic tissues usually encounter mixed proteins in the concentration range of 5-20%. The use of concentrated protein solutions maximizes protein-protein interactions and results in calorimetric data with a marked dependence on water content.

Whey proteins show excellent physicochemical, gelation, and binding properties and, therefore, are widely used as functional ingredients in many formulated bakery, dairy, and sausage products [239]. Furthermore, a number of environmental factors (e.g. pH, ionic strength, protein concentration, and time and temperature of heating) influence whey protein gelation and other functional characteristics [251-257]. β–Lactoglobulin, β-LG, the most abundant whey protein in milk (up to 50% of the total whey protein), is largely responsible for whey protein functionality [253-255]. Although the gelation mechanism of β-LG has not yet been studied systematically, it is well acknowledged that gelation properties of β-LG are affected by extrinsic factors [253-255].

There is some evidence that protein molecules in high concentrations do not unfold totally, since the protein-protein interactions overwhelm the ability of the protein to compete for water hydrogen bonds. We can say that proteins in food are water -plasticizable amorphous polymers. In fact a number of proteins are not water soluble, but they become plasticized by water in the amorphous state.

Glass transitions and water plasticization have been found to occur in systems rich in milk proteins, like casein and sodium caseinate, as well as in concentrated solutions of enzymes, elastin, and cereal proteins.

These physical properties are however better approached through rheological investigations. Cereal proteins have been chosen to give some details of these studies.

4.7. Cereal Proteins

4.7.1. State diagrams of Cereal Proteins.

Cereal proteins exist in an amorphous, metastable state that is sensitive to changes in moisture, temperature and shear which occur during mixing and baking [29,57,85,258]. In the glassy state, the "free volume", which is the volume not occupied by the macromolecules, is at its lowest thermodinamically possible value. On heating above T_g , the amorphous matrix undergoes a physical change from a viscous "glass" to a less viscous "rubber", as the "free volume" increases and the chain segments of the polymer have sufficient room to complete their movements within the time scale of the experiment. The temperature and the moisture content at which these changes and the related rheological properties occur depend on the particular protein studied, i.e. on its molecular weight and its molecular weight distribution.

In the research by Kokini and coworkers [57,258-260] the temperature and the frequency dependence of storage and loss moduluses were obtained for the most important cereal proteins.

The physical states that gliadin, glutenin and zein (corn protein) encounter during processing, have been visualized in state diagrams, summarizing the information collected on protein phase transitions observed by means of DSC and mechanical spectrometry (small-amplitude oscillatory measurements at atmospheric pressure and under high pressure).

The RMS-800 mechanical pressure spectrometer (Rheometrics, Piscataway, N.J.) was used to determine dynamic properties. Freeze-dried samples were brought to the appropriate moisture content with distilled water, equilibrated to different relative humidities and then tested. Frequency and temperature sweeps provide information about the structure of the biopolymer and supply parameters to define the state diagram.

Figure 38 shows the temperature sweep of gliadin with 25% moisture obtained in 1Hz tests at 5 °C and fixed 0.5% strain.

Three steps can be identified in the structure formation of gliadin: the entangled polymer flow region (up to 70 °C) is characterized by equal values of G' and G'' . Then a large increase of G' follows, which is attributed to cross-linking/aggregation reactions among gliadin molecules: because of disulphide linkages the resulting network structure is similar to that of vulcanized rubber. At 120 °C G' reaches a peak and G'' goes through a minimum. This temperature, that was found to be independent of moisture content in the moisture range of 20-40%, corresponds to the maximum of structure formation. A further temperature increase (up to 130 °C) causes reduction of G' coupled with a positive G'' peak

which corresponds to the softening of the cross-linked gliadin. The temperature at which this softening occurs does not significantly vary with the moisture content.

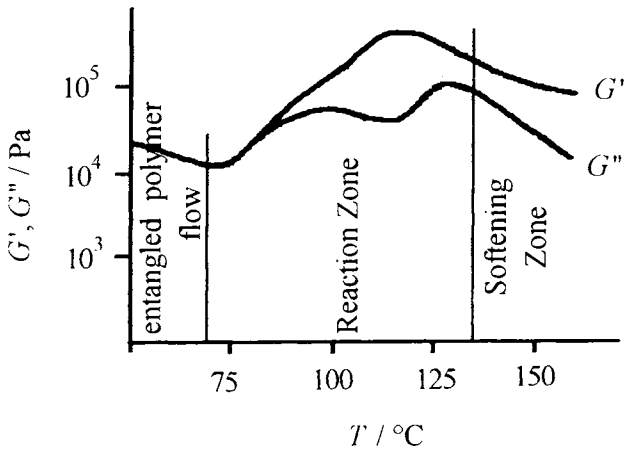

Figure 38. Temperature sweep (% K min^{-1})of gliadin (25% moisture) at 0.5% strain and 1 Hz frequency (modified from [258]).

Further information were collected through frequency sweep experiments conducted at 0.5% strain in the frequency range 0.01-100 rad sec^{-1} at different temperatures (50, 70, 100, 140 °C).

In the entangled polymer flow state, the magnitude of G' and G'' are expected to be relatively close and, in the case of a three-dimensional network, the slope of log G' *vs* log ω is expected to practically naught, whereas for a liquid flow material the expected slope value is about 2 [26]. Therefore small slope values indicate that the polymer system is largely crosslinked.

As an example, Figure 39 shows a frequency sweep of gliadin at 70°C. Both elastic and loss moduluses increase linearly with frequency, whereas they become less dependent on frequency with increasing temperature, just as expected for highly crosslinked rubbery polymers. The beginnning of cross-linking reactions is evident at 70 °C, as G' and G'' at 0.1 rad sec^{-1} attain100-fold larger values than those at 50 °C.

The reduction of G' and G'' at 140 °C suggests softening of the cross-linked/aggregated gliadin. Figure 40 shows, as an example, the effect of moisture on T_g for glutenin.

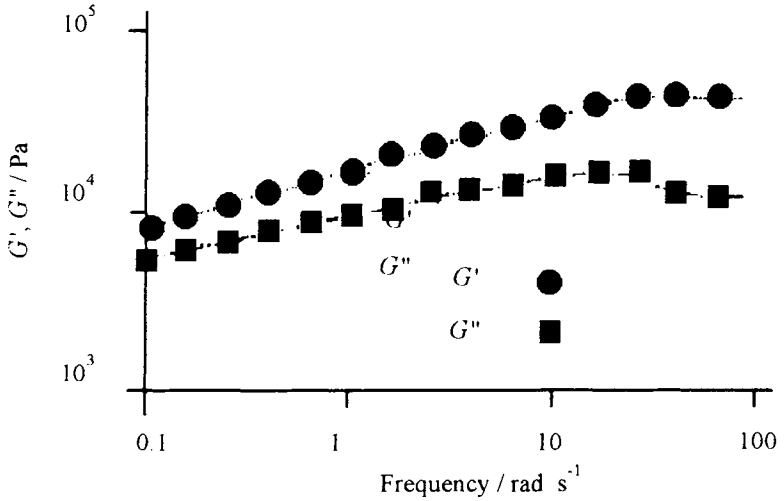

Figure 39. Frequency sweep of gliadin (25% moisture) at 70 °C and 0.5% strain (modified from [258]).

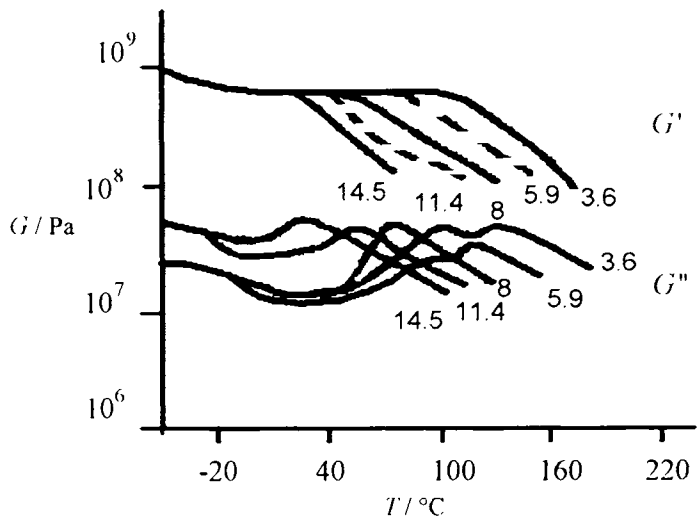

Figure 40. Storage and loss moduluses (G' and G'') of glutenin at different water content in a temperature sweep test (5 K min^{-1} heating rate; 0.5% strain; 1 Hz frequency). For each data series, moisture content (%) decreases from the left to the right hand side (modified from [258], where further details are given).

The glass transition locus separates the region of the phase diagram where the system is glassy (below) from the rubbery region (above) where the system shows a smaller viscosity which corresponds to a larger molecular mobility. A further temperature increase makes the rubbery soft material to change into a high-viscosity liquid, referred to as the "entangled polymer flow" state.

The temperature of the G'' maximum corresponds to T_g. The inflection of the G' curve and the characteristic maxima in G'' are shifted at lower temperatures for larger moisture contents: the decrease of T_g with increasing moisture is a consequence of the plasticizing effect of water. T_g exhibits a nonlinear dependence on moisture content. Approximately a decrease of 6 °C per weight percent of water can be observed (see Figure 41).

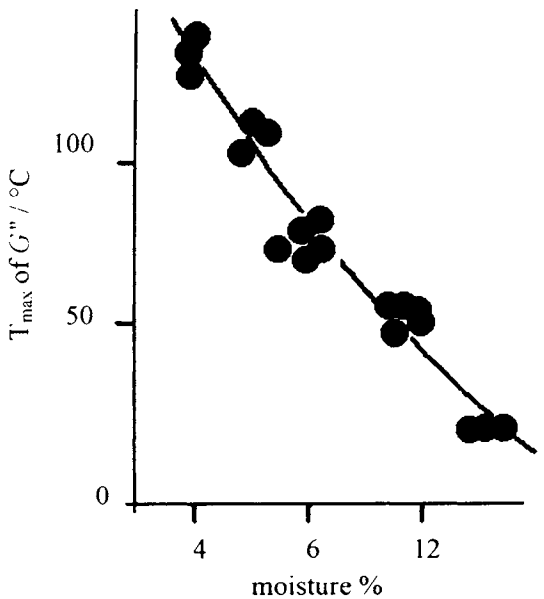

Figure 41. The glass transition temperature of glutenin as a function of moisture content (modified from [258]).

By applying this technique, the concentration-independent glass transition, T_g', can be also determined. Gliadin, zein and glutenin show differences in rheological properties, as for the effects of water content and onset temperatures of networking and softening reactions. In the case of zein, these effects (including the higher softening temperature) are attributed to the higher hydrophobicity of this protein with respect to gliadin. As for glutenin, the glass transition occurs at a higher temperature: the reaction zone starts at 90 °C, the maximum structure

extension is reached at 135 °C and the softening of the crosslinked network starts at 150 °C (Figure 42).

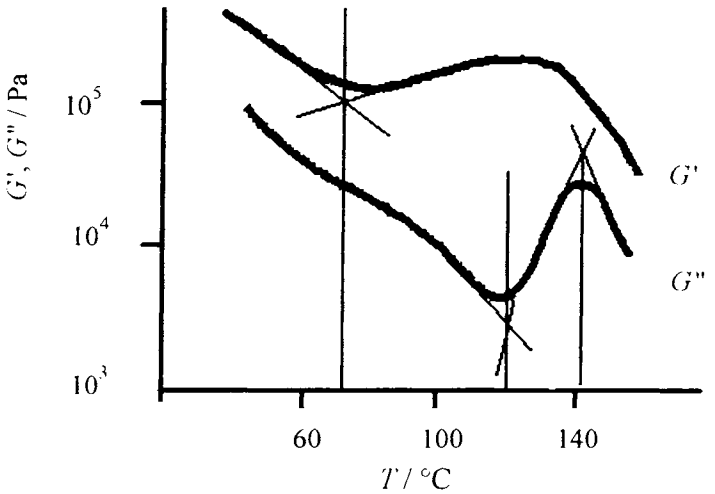

Figure 42. Storage and loss moduluses (G' and G'') of glutenin (30% moisture content) in a temperature weep test (0.5 K min^{-1} heating rate; 0.5% strain; 1 Hz frequency) carried out with a pressure rheometer (modified from [258]).

State diagrams can be therefore drawn from T_g -*vs*-moisture data and G' and G'' trends in temperature and frequency sweep tests. Figure 43 shows the state diagram for gliadin.

A dashed line in the state diagrams represents the locus of the transition from rubber to entangled polymer flow. When the protein has enough mobility, it undergoes a networking reaction (reaction zone in the phase diagram) which produces softening of the system. The onset temperature of softening is not significantly affected by moisture content.

State diagram therefore account for all the physical states a polymer system will encounter during processing and storage. As an example, Figure 44 summarizes, in a hypothetical phase diagram, the transformations of cereal proteins during the wetting, heating and cooling/drying stages of extrusion cooking. Khatkat et al. [261] evaluated dynamic rheological properties of glutens and gluten fractions of two wheat cultivars with a controlled stress rheometer (Reo-Tech International) and found that the gliadin/glutenin ratio causes differences in the viscoelastic behaviour of gluten. Gliadin was found to express a plasticizing effect and an interference role in glutenin-glutenin interaction.

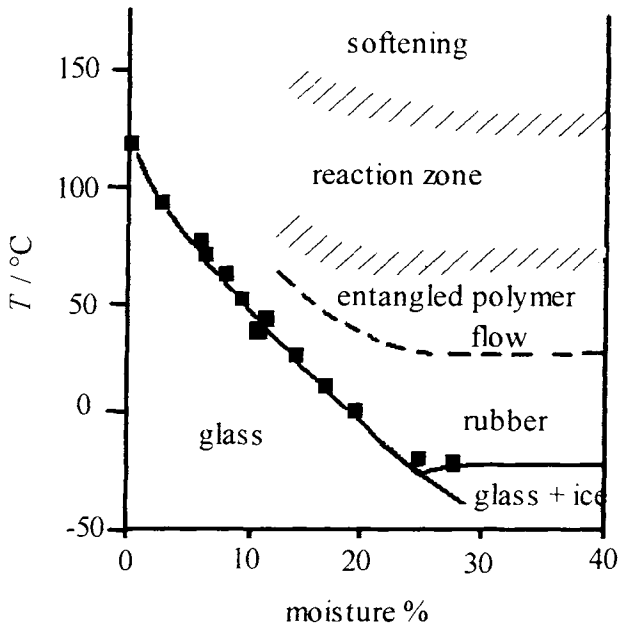

Figure 43. State diagram of gliadin (modified from [258]).

4.7.2.Gluten thermoset and gluten-starch interactions.

Attenburrow et al. [262] performed temperature sweep tests on gluten balls from different wheat varieties by means of a mechanical spectrometer, using parallel plates geometry. The operating conditions were: 1 °C min^{-1} heating rate, 5% strain, and 25-100 °C temperature range (Figure 45). Their results can be summarized as follows. G' and G'' decrease until about 60 °C; where both of them go through a relative and absolute minimum, respectively. Beyond that G'' reattains a decreasing trend, while G' (which becomes larger than G'') increases with a small slope until 90 °C and much more steeply above. The same results were obtained by Masi et al. [263]) and He and Hoseney [102].

Since new disulphide bonds are formed when glutenins or gluten are heated above 60 °C, Attenburrow concluded that gluten thermosetting could be the result of crosslink formation probably via disulphide bonds, since in the presence of oxidizing agents the dynamic storage modulus increased, whereas reducing agents had the opposite effect.

In order to complete these observations on protein structurization, Masi et al. [263] collected further information by means of two-heating-run sweep tests carried out at 2 K min^{-1} on gluten-water mixtures.

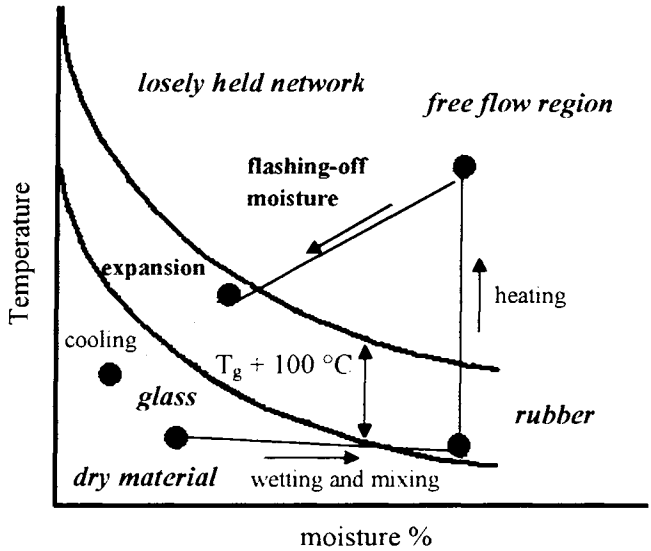

Figure 44. Transformations of cereal proteins during wetting, heating and cooling/drying steps of extrusion cooking, in the framework of a hypothetical state diagram (modified from [259]).

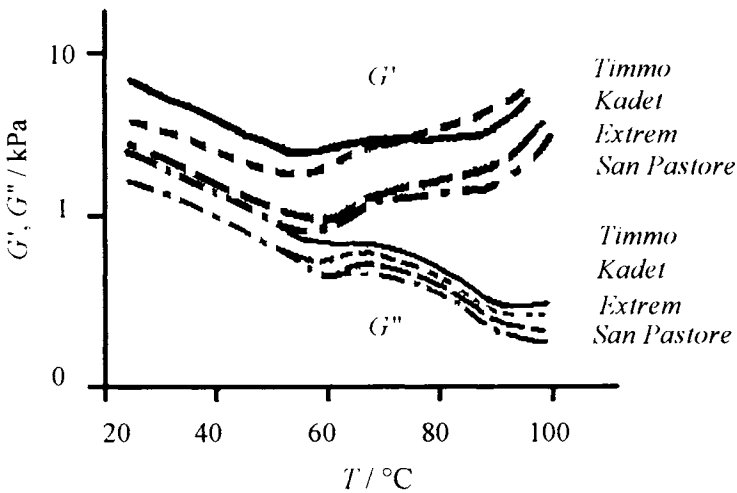

Figure 45. Storage and loss moduluses (G' and G'') of different varieties of wheat gluten observed in a temperature sweep test at 1 K min $^{-1}$ heating rate, and 5% strain (modified from [262]).

The instrument used was a Reometrics RDS2 rheometer. In the first run the temperature was increased up to a selected level (46, 66 and 90 °C), then the oscillatory motion was stopped, the sample was rapidly cooled to ambient temperature, and then reheated in a new sweep test. Large differences were observed between the first and the second run for gluten samples heated up to 90 °C, since in the second run G' was almost independent on temperature.

The results supported the conclusion that below a critical temperature (about 60 °C) rheological changes are not caused by permanent modifications of the structure and therefore are fully reversible. By contrast, the structure formed above this temperature is responsible for permanent changes of the system and its rheological behaviour. The onset of this process is indeed close to 60°C, as revealed by solubility into SDS [262], although its rate becomes significant temperatures above 80 °C.

Were the development of mechanical strength associated to a single reaction mechanism, the only effect of temperature would be an acceleration of the process rate and the time-temperature superposition principle (see appendix) would imply a single master curve to represent of the progress of structure formation. However, when single G'-vs-time curves were obtained keeping gluten at different constant temperatures (time sweep test) and were shifted with respect to that at 30 °C, no superposition was observed just as expected for a process actually sustained by more mechanisms with different rates (Figure 46).

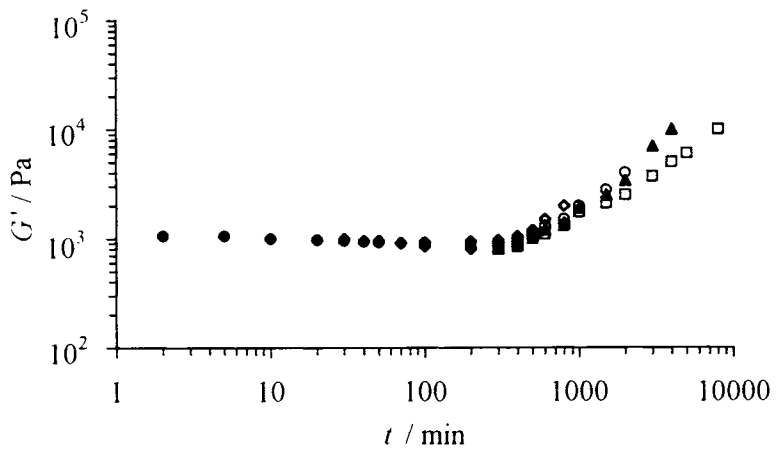

Figure 46. Storage modulus, G', of gluten - water mixtures in a time sweep test 10% strain, 1 Hz frequency). The master curve has been obtained by applying the time-temperature superposition principle. Temperatures considered: 40 (●), 50 (◆), 60 (◊), 70 (○), 80 (▲), and 90 (□) °C (modified from [263]).

Since residual starch is present in the gluten separated from flour, starch gelatinization is the other phenomenon appearing and is overlapped to protein crosslinking. The rheometric analysis of water-starch-gluten mixtures containing starch and gluten in different poportions (liquid to solid ratio 1:1 , range of starch content from 10 to 75% w/w) confirms these observations (Figure 47).

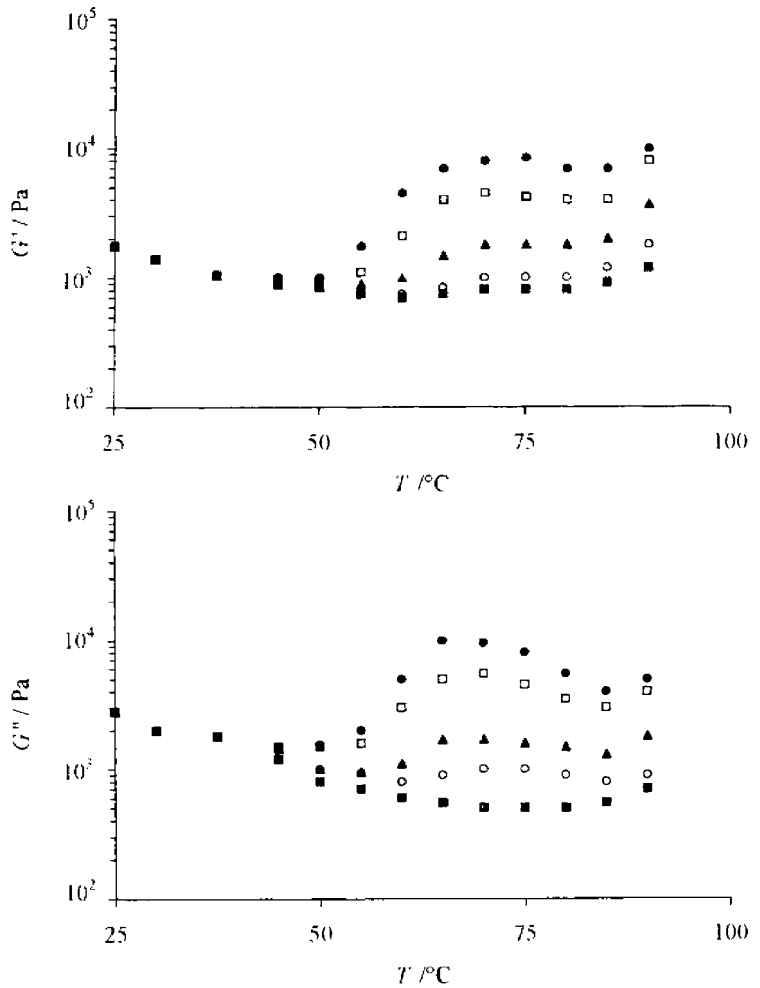

Figure 47. Storage and loss moduluses (G', upper, and G'', lower) of different gluten - starch - water mixtures with a starch content (w/w dry basis) of: 75 (●), 50 ( ), 25 (▲), 10 (○), and 0 %(■), in a temperature sweep test (2 K min^{-1} heating rate, 10% strain, and 1 Hz frequency). (modified from [263]).

Gelatinization and crosslinking seem to be independent to each other and differently affected by temperature. Frequency sweep tests show that the dough elasticity decreases and the viscous dissipation increases on increasing starch content. This can be explained by taking into account that a larger starch content implies a proportional reduction of the volume concentration of proteins and, consequently, a looser and less elastic network when the system is hydrated. On the other hand, starch granules do not take part in the network formation, acting as filling material: the viscous dissipation is therefore enhanced with increasing starch content.

Heat induced modifications of gluten were also monitored as changes of T_g by Attenburrow [264] by means of a Dynamic Mechanical Thermal Analyser (DTMA). Samples were examined by Attenburrow in the double-cantilever-bending mode at 1Hz frequency of and 2% strain. The temperature was scanned from -90 to +40 °C at 2 K min^{-1} rate. The glass transition region, characterized by a sharp drop of the storage modulus, is shown in Figure 48 which reports the (*log E'*) -*vs*- *T* plots (*E'* stands for storage modulus) for gluten samples previously set at 90 and 150 °C, respectively.

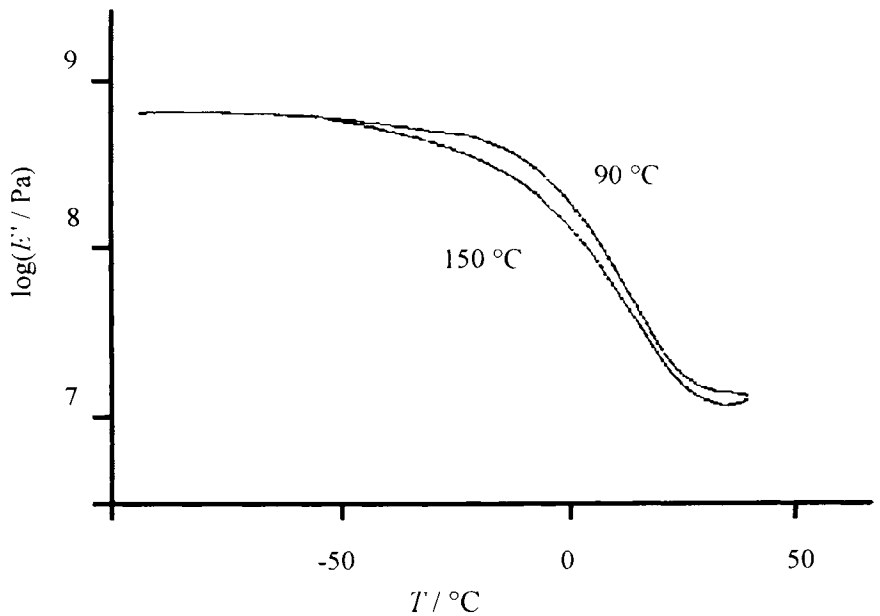

Figure 48. DTMA trace of gluten heat-set at 90 and 150 °C (modified from [264]).

Unexpectedly the gluten thermoset at 150 °C (characterized by a higher molecular crosslinking) showed a lower T_g. According to Attenburrow, this finding can be explained by guessing that, besides the heat-sustained cross-linking of gluten, other changes, like unfolding of the gluten molecules deamination, reduction in polymer chain length, etc., would take place and counterbalance the effect of increasing cross-linking on the T_g value.

4.7.3. Thermomechanical Evaluation of Dough.

Sinusoidal stress/strain testing have also been used to examine the temperature dependent changes in rheological properties that occur in the real complex system: the dough. Dreese, Faubion, and Hoseney [113,114,102] used a homemade apparatus, assembled from commercially available transducers and related electronics (Figure 49).

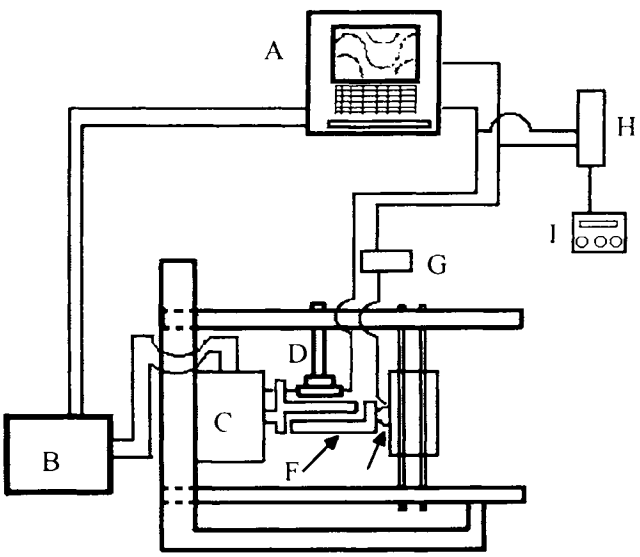

Figure 49. Apparatus used by Dreese, Faubion and Hoseney (modified from [32]). (A) microcomputer; (B) power amplifier; (C) vibration exciter; (D) deformation transducer; (E) force transducer; (F) rigid test stand; (G) transducer coupler; (H) amplifier; (I) phase to voltage converter.

In order to measure the rheological changes occurring during heating, the top and the bottom plates of the rheometer were attached to a variable transformer, so as to heat the sample by the Joule effect of the resulting electric current. According

to the authors, the use of electric heating reduced temperature gradients within the dough mass. The heating rate was tuned at 2.5 K min^{-1}; the samples were heated up to 90 °C, thence cooled and reheated. The exposed dough surfaces at the edges of the plates were coated with a lubricating grease to prevent drying and the dough was allowed to rest in the rheometer for 5 minutes before the tests. These were carried out at 2% strain and 5 Hz frequency and the rheological parameters were calculated according to Faubion et al. [32]. The experimental findings reported can be summarized in the following way. During the initial heating, the G' values slightly increased with temperature. At approximately 55 °C, the trend of the elastic modulus bent upward and attained a maximum at about 75 °C, while the tan δ accordingly decreased (Figure 50)

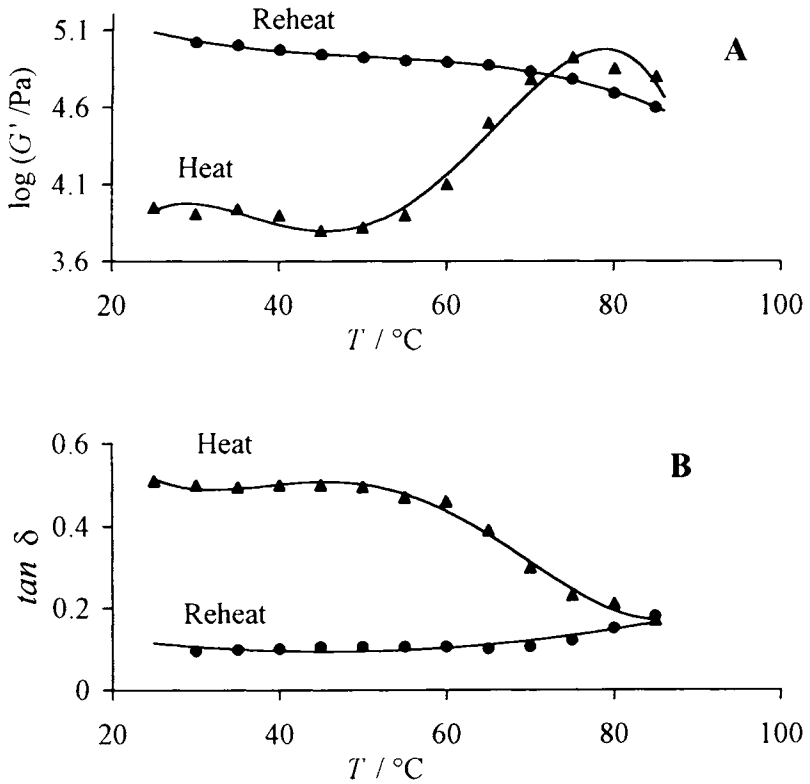

Figure 50. Effect of heating on the storage modulus, G', and *tan* δ of flour-water doughs. A reheating run was carried out after a previous heating up to 90 °C (modified from [113]).

The decreasing trend of G' in the 75 - 90 °C range could be tentatively attributed to weakening of noncovalent bonds, whereas its increasing trend above 90 °C could be a consequence of the cross-linking of the gluten proteins.

These observations agreed with experimental data reported by Weipert [36]. The results obtained by modifying the gluten/starch ratio suggested that the rheological changes observed in the 55 - 75 °C range could be attributed to starch gelatinization (Figure 51).

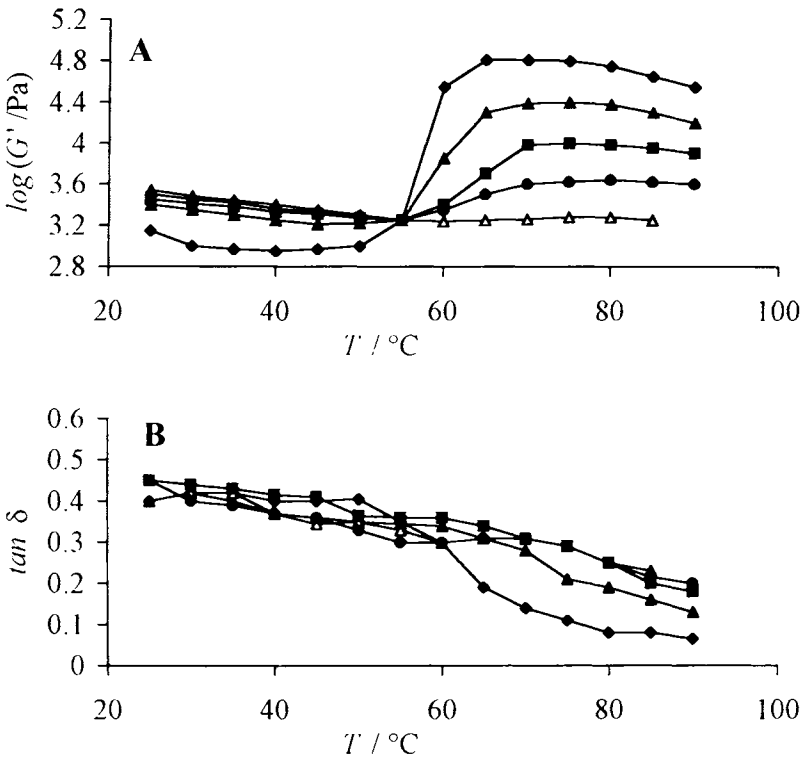

Figure 51. Effect of heating on the storage modulus, G', and *tan* δ of doughs prepared from blends of commercial starches. The gluten fraction in the blend is reported close to the relevant curve (modified from [113]).

It is noteworthy that such a behaviour was similar to that of gluten-starch-water mixtures which showed, above 55 °C, a change of G' proportional to the amount of the starch present. After cooling, the G' value remained close to that reached at 90 °C and did not change on reheating: it could be therefore concluded that the rheological changes produced by heating were irreversible. The

behaviour was confirmed by testing doughs containing pregelatinized starch. According to these authors, the phenomena described for the single biopolymers of dough would be the same as those observed on heating the whole dough.

Nonetheless Hoseney and coworkers [113] came to different conclusions about starch/gluten interactions. They suggested indeed that the increase of G' above T_g would indicate that starch gelatinization can sustain a more extended hydrogen bonding between gluten polypeptides and starch polysaccharides.

If the difference $\Delta G'$ between the readings at 30 °C, before and after heating at 90 °C, were plotted versus the % fraction of starch (Figure 52) a nearly straight line trend was obtained with an intercept at 0% starch very close to zero. Data by He and Hoseney [102] showed that the elastic modulus of gluten increased as starch was added: then an interaction between the gluten and the starch could be responsible for the rheological behaviour of doughs.

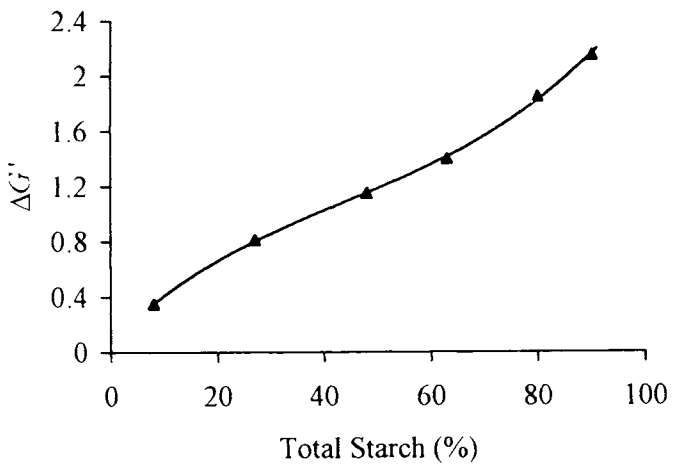

Figure 52. $\Delta G'$ (difference in G' at 30 °C before and after heating up to 90 °C) for a gluten - starch dough versus the fraction of starch (modified from [113]).

Gluten proteins should not be affected by heating to 90 °C, or more correctly, effects of heating were not detectable with a dynamic rheometer. Conversely, when gluten:water doughs were steamed (100 °C) for 15 minutes before the test, a large increase in the storage modulus was observed due to the formation of disulphide cross-linking in gluten protein. Accordingly the starch would act as a non-inert filler within the gluten meshes [113].

APPENDIX

A.1. Treatment of DSC signals

A.1.1. Thermodynamic approach

This is adequate for signals related to a two-state transition and obtained at a heating rate as low as to practically achieve thermodynamic equilibrium in any point of the temperature range across the DSC peak, viz.,

$$K = \frac{\alpha}{1-\alpha} = \exp(-\Delta G / RT) \tag{A1}$$

where α is the extent of the transition. One can easily get the expression for the peak signal, $s_{peak} = dQ/dt$, with $Q = -\alpha\ \Delta H$ (downward shifts of the trace correspond to endothermic effects):

$$s_{peak} = v\ \Delta H = K(1-\alpha)^n \tag{A2}$$

where β is the heating rate and ΔH is the enthalpy change. In a similar way one gets the expression for the ΔC_p base line shift across the peak:

$$s_{base} = v\ \Delta H = K(1-\alpha)^n \tag{A3}$$

where k is a constant term that can be dropped in the subsequent elaboration. Accordingly the overall signal becomes:

$$s = -\frac{\beta}{R}\left(\frac{\Delta H}{T}\right)^2 \alpha(1-\alpha) - \beta\Delta C_p\alpha \tag{A4}$$

This expression corresponds to a skewed peak, the first term of which can be often replaced with a gaussian function across the respective temperature range; the second term can be reliably reproduced with a sigmoidal function centred on the same gaussian mean.

A.1.2. Kinetic approach

The kinetic model predicts a peak function that accounts for the change of the transition rate with the temperature; one must also account for the time-lag of the instrument to reproduce the smooth onset of the signal at a given temperature. In this case the parameters to be assessed are the kinetic order, n, and the kinetic constant, K, and its dependence on T.

$$s_{peak} = v\,\Delta H = K(1-\alpha)^n \tag{A5}$$

where v is the reaction rate. The same kinetic law that underlies the peak has to be used to describe the ΔC_p base line shift. The resulting peak is significantly skewed and cannot be replaced with a gaussian function.

$$s_{base} = \Delta C_p\,\alpha[T(t)] \tag{A6}$$

Isothermal DSC traces can be easily interpreted, provided that the lag-time of instrument is accounted for. For first order kinetics, the calorimetric signal, s, can be described as:

$$s = \left(\frac{dQ}{dt}\right) = (K \times Q_\infty)(1-\alpha) = s_{max}(1-\alpha) \tag{A7}$$

where α and Q_∞ stand for the extent and the overall heat of reaction, respectively. For $\alpha = 0$, the expected signal is $s_{max} = (K \times Q_\infty)$. To acccount for the time-lag of the instrument, τ, the term on the right hand side has to be multiplied by the damping term $exp\,(-\tau / t)$:

$$s = s_{max}(1-\alpha) \times \exp(-\tau / t). \tag{A8}$$

The order of the kinetic law for a given process can be drawn from a data treatment based on the following self-explaining expressions, where lettering has the same meaning as above:

$$\frac{d\alpha}{dt} = K\,(1-\alpha)^n = K\frac{s}{s_{max}} \tag{A9}$$

and therefore,

$$(1-\alpha)^n = \frac{s}{s_{max}} \tag{A10}$$

The simple case of $n = 0$ can be easily recognized, since the relevant signal tends to a constant value throughout the trace, namely, $s \quad s_{max}$. In all the other cases ($n \neq 0$), one can write:

$$\alpha = 1 - \left(\frac{s}{s_{max}} \right)^{1/n} \tag{A11}$$

and therefore,

$$d\alpha = -\frac{1}{n}\left(\frac{s}{s_{max}} \right)^{N} \frac{ds}{s_{max}} = K \frac{s}{s_{max}} dt \tag{A12}$$

where $N = (1 - n)/n$. By rearranging the last two terms one obtains:

$$s^{(N-1)} ds = -n K s_{max}^{N} dt \tag{A13}$$

and by integration,

$$s^{N} = s_{max}^{N} \left[1 - (1-n) K t \right] \tag{A14}$$

By changing into the logarithmic form and deriving, one finally obtains

$$\frac{s}{D} = \frac{1-n}{n} t - \frac{1}{k n} \tag{A15}$$

where $D = ds / dt$. This expression, that holds for any $n \neq 0$, does not account for the damping function, but is nonetheless of practical use for a preliminary approach, since it allows the values of n and K to be tentatively drawn from the s/D - vs - t straight line plot: an improved K value can be easily attained in a further step of the elaboration based on equation (A8).

A2. Treatment of TGA signals

In most cases an Arrhenius behaviour is assumed and the mass loss is described according to a first order kinetics:

$$-\frac{dm}{dt} = -\frac{d\,[m - m(\infty)]}{dt} = K \left[m - m(\infty) \right]^{n} \tag{A16}$$

$$\left\{ \log\left[-\frac{dm}{dt} \right] \right\} = \log K + n \log[m - m(\infty)] = A - \frac{E_{att}}{RT} + n \log[m - m(\infty)] \tag{A17}$$

$$\Delta\left\{\log\left[-\frac{dm}{dt}\right]\right\} = -\frac{E_{att}}{R}\Delta\left\{\frac{1}{T}\right\} + n\,\Delta\left\{\log[m - m(\infty)]\right\} \qquad \text{(A18)}$$

where $m(\infty)$,K and n are the final sample mass, the kinetic constant and the kinetic order, respectively.

If equal $\Delta\left\{\frac{1}{T}\right\}$ spans are considered, then $\Delta\left\{\log\left[-\frac{dm}{dt}\right]\right\}$ and $\Delta\left\{\log[m - m(\infty)]\right\}$ are correlated with each other according to straight line. One can therefore draw the values of E_{att} and n.

In the case of a dehydration process, one can describe the signal as the result of the combined effect of two driving forces, namely temperature increase and gradient of the chemical potential across the core-to-surface span, since the evaporation rate becomes significant at the surface, but is indeed limited by the supply of further molecules that diffuse from the internal regions toward the surface, because of temperature and concentration gradients.

$$J = \frac{1}{A}\frac{dm}{dt} = -D\nabla\mu(H_2O) =$$
$$= -D_0 \exp\left(\frac{-E_{att}}{RT}\right)\times\left[\nabla\mu(H_2O) - \int_{T_0}^{T}\nabla\bar{S}(H_2O)\,dT\right] \qquad \text{(A19)}$$

where D, A and $\mu(H_2O)$ are the diffusion coefficient, the free surface area and the chemical potential of water, respectively, and T_0 is the starting temperature of the TGA run..

A3 Elements of thermomechanical analysis in polymer science

Thermal scanning rheology is the measure of the dynamic mechanical deformation of a material undergoing a given temperature-time program. Thermomechanical analysis is the measure of the dynamic moduluses of a sample of regular geometry over a temperature range. When small amplitude strains are applied to the sample, the material structure is preserved from any mechanical breaking. Linear time-dependent shear experiments can be performed in transient (i.e. non-periodic) mode or, when information about shorter relaxation times is required, by applying a sinusoidal stress of given frequency [26]. Samples undergo small oscillating sinusoidal deformations of amplitude γ_0 and frequency ν:

$$\gamma(t) = \gamma_0 \sin \omega t \qquad \text{(A20)}$$

where t is time and $\omega = 2\pi\nu$. For an ideal solid, the Hooke law applies, i.e., stress and strain are directly proportional. In a dynamic test strain is in phase with deformation and varies periodically (Figure A1):

$$\tau(t) = G^*\gamma = G^*\gamma_0 \sin \omega t \tag{A21}$$

where τ and G^* stand for stress and dynamic modulus, respectively.

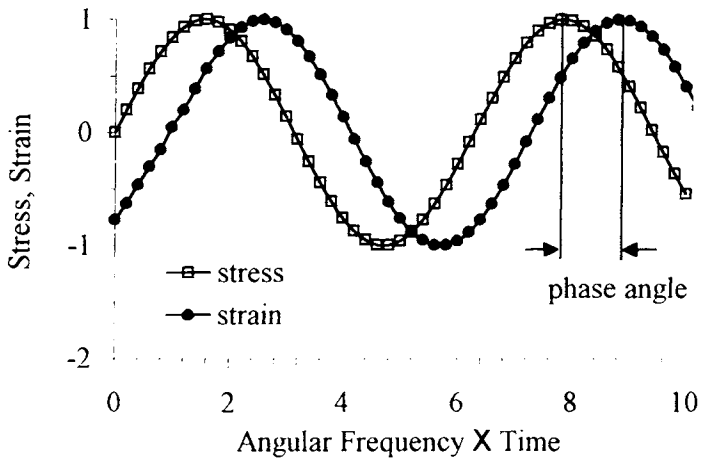

Figure A1. Synusoidally imposed stress and accompanying strain.

If the sample is a perfectly viscous liquid, the Newton law applies, i.e. stress is proportional to the strain rate. In a dynamic test stress and strain rate show a $\pi/2$ phase shift:

$$\tau(t) = \eta\dot{\gamma} = \eta\omega\gamma_0 \cos \omega t \tag{A22}$$

where η is the viscosity.

Viscoelastic materials show an intermediate behaviour with the angle phase shift, δ, in the range 0 - $\pi/2$. In this case it is expedient the use of complex number notation for G*:

$$G^* = G' + j\,G''. \tag{A23}$$

G^* is therefore referred to as the vectorial sum of two orthogonal components, namely, the storage modulus G' (the elastic component), and the loss modulus G''

(the viscous component). In a dynamic test G' and G'' are related to stress and strain:

$$\tau(t) = \gamma_0 (G' \sin \omega t + G'' \cos \omega t) \qquad \text{(A24)}$$

and $\tan \delta = G''/G'$ is a measure of the relative contribute of the viscous and elastic component to the rheological characteristics of the sample. In compression or flexure mode tests (TMA, DTMA) G' and G'' are often denoted by E' and E'', respectively.

Measurements of viscoelastic properties of polymers supply information about the nature and the rates of short- and long-range configurational rearrangements and the mutual position and interaction of the macromolecules. Below T_g polymer chain backbones are largely immobilized and viscoelastic properties do not change with time or frequency. This conversely occur in the intermediate region between glass-like and rubber-like states, where relaxation times steeply decrease with increasing T [26]. When the cooperative motions of individual chains can be supposed to depend on a single average friction coefficient, ξ_0, use of "reduced variables" (or "viscoelastic corresponding states") allows to superpose the effect of increasing temperature to that of increasing frequency in experiments where a sinusoidal stress is applied to the system.

The trend of the moduluses G' and G'', determined at the constant temperature T on varying the frequency, ν, can be "super-posed" to that expected at a reference temperature, T_0, by plotting the reduced moduluses, namely, $G'_p = G'(T_0 \times \rho_0/T \times \rho)$ and $G''_p = G'' (T_0 \times \rho_0/T \times \rho)$, versus the variable $(\nu \times a_T)$, where ρ and ρ_0 stand for the density at T and T_0, respectively, and a_T is the ratio of the corresponding relaxation times. As a result of this change of variables, the relaxation spectrum (in a logarithmic plot) is shifted upward by $log(\rho T/\rho_0 T_0)$ and to left by $log(a_T)$, while its shape remains unaltered (Figure A2), thus allowing "superposition" of the behaviours observed at different temperatures.

In some experimental methods, like DTMA, where temperature can be varied more easily than frequency; the traces observed are plots of isochrone data, obtained at a given frequency, ν, versus T. Traces obtained at different frequencies are not "super-posable" to one another by shifting along the temperature axis, since a_T does not depend linearly on T (see below). However an isochrone trace can be transformed into an effective isotherm, at $T = T_0$, simply by replotting the data versus $(\nu \times a_T)$.

When the experimental trends do not allow such matching, it can be argued that a single friction coefficient cannot describe all the motions within the system under consideration.

The principle of using reduced variables and the relevant reduced-variable curve are commonly referred to as *time-temperature superposition principle* and *master curve*, respectively.

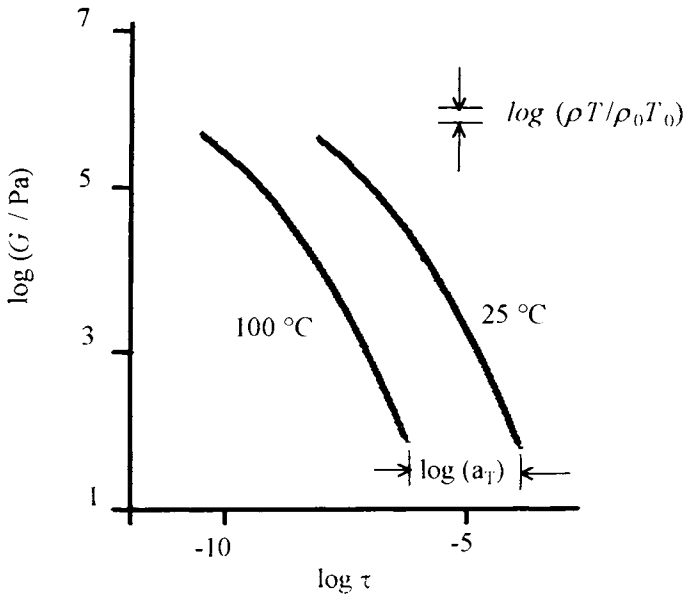

Figure A2. Effect of temperature change (from T_0 to T) on the relaxation spectrum (τ stands for relaxation time). (modified from [26]).

The a_T (T) function may be fitted as

$$\log a_{Tg} = - c_1^g (T-T_g) / (c_2^g + T - T_g), \qquad \text{(A25)}$$

known as the William-Landolt-Ferry (WLF) equation, where T_g stands for the reference temperature. This equation fits data of many different systems over the [T_g - (T_g +100 K)] temperature range when c_1^g and c_2^g are given the constant values of 17.44 and 51.6, respectively.

Many of the properties of liquids, whether polymeric or not, depend on the presence of significant fraction of free volume in the form of holes of molecular size or smaller voids. When a polymeric liquid or soft solid is cooled, the free

volume collapses because of the molecular adjustments that take place within the time scale of the experiment. The lower the temperature, the slower the relaxation. If crystallization does not occur first, at $T = T_g$ the free volume relaxation becomes much slower than the cooling run: the systems vitrifies, i.e., it assumes a solid-like character. The glass transition is therefore the result of a reduction of molecular mobility.

Below T_g the WLF equation cannot be applied, since the temperature dependence of a_T obeys a simple Arrhenius law:

$$log a_T = (\Delta H_a/R)(1/T - 1/T_0) \tag{A26}$$

A4. Proteins

A4.1. Two-state equilibrium transition

Two different tests can be applied to check whether the denaturation of a given protein can be described with the two-state transition model, namely, the population test and the Vant'Hoff test. The population fractions of native and denatured state, $f_N(T)$ and $f_D(T)$, are independently evaluated [154,184] (see Figure A3):

$$f_N(T) = \frac{1}{Q(T)} \tag{A27}$$

$$f_D(T) = \frac{1}{Z(T)} \tag{A28}$$

where $Q(T)$ is the canonical partition function of the macromolecule in solution (with reference to the native state), drawn from the experimental heat capacity curve and $Z(T)$ is the canonical partition function of the macromolecule in solution (with reference to the denatured state), evaluated from the relationship:

$$Q(T) = \exp\left[\int_{T_o}^{T} \left(< \Delta H(T) >\right) / RT^2 dT\right] \tag{A29}$$

$$Z(T) = \exp\left\{\int_{T}^{T_e} \left[\left(\Delta_d H - < \Delta H(T) >\right) / RT^2\right] dT\right\} \tag{A30}$$

where T_o and T_e stand for onset and end point of the DSC signal. Since $f_N(T)$ and $f_D(T)$ are independently determined,

$$f_N(T) + f_D(T) = 1 \qquad \text{(A31)}$$

is a necessary condition for a two-state process at any temperature

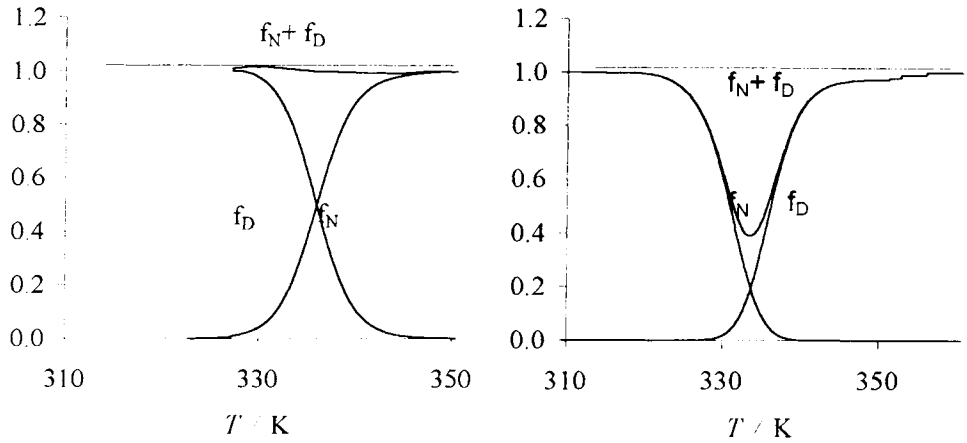

Figure A3. Population fraction test in the case of (a) RNase A (one step denaturation), and (b) RNase BS (more complex behaviour).

If the denaturation process is correctly referred to as a two-state transition, $N \Leftrightarrow D$, then:

$$\Delta_d H^{VH}(T_d) = ART_d^2 \frac{C_p^E(T_d)}{\Delta_d H(T_d)} \qquad \text{(A32)}$$

with $A = 4$. If $\Delta_d H^{VH}(T_d)$ coincides (within ± 10%) with the $\Delta_d H(T_d)$ directly measured, unfolding can be tentatively supposed to be a one-step process [12] (such a coincidence indeed represents a necessary condition).

For an actually reliability of such a conclusion, $\Delta_d H^{VH}(T)$ and $\Delta_d H(T)$ should coincide, within experimental uncertainties, in the whole temperature range where denaturation occurs and not only for $T=T_d$. A straightforward algebra [169,184] allows the van't Hoff and the calorimetric enthalpy for the unfolding transition (see Figure A4) to be expressed as

$$\Delta_d H^{V.H}(T) = RT^2 \left[\frac{C_p{}^E(T)}{<\Delta H(T)>} - \frac{C_{p,D}{}^E(T)}{<\Delta H(T)>_D} \right] \qquad \text{(A33)}$$

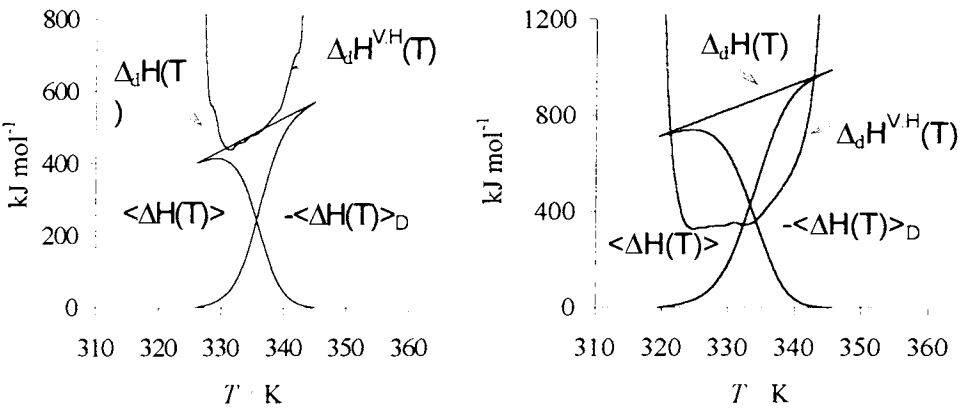

Figure A4. Application of the vant' Hoff test in the case of (a) RNase A and (b) RNase BS. The large divergences at the limits of the denaturation temperature range are artefacts due to the form of the analytical expression of equation A33.

$$\Delta_d H(T) = <\Delta H(T)> - <\Delta H(T)>_D \qquad \text{(A34)}$$

where $C_p{}^E$ and $<\Delta H(T)>$, and $C_{p,D}{}^E(T)$, $<\Delta H(T)>_D$ are the excess heat capacity and the excess enthalpy functions with respect to native and denatured state, respectively. When the two function superimpose to each other, the system can be reliably described by the two-state transition model [169,184] (such superposition is indeed a necessary and sufficient condition).

A4.2. The effect of pH and other co-solutes on thermal stability of globular proteins: the preferential binding model

The decrease of protein thermodynamic stability on pH decreasing suggests a preferential binding of protons to the unfolded state. The effect of pH on the standard denaturation Gibbs function, $\Delta_d G$, has been theoretically analyzed by

Hermans and Scheraga [196] and can be expressed with the following relationship:

$$\Delta_d G = \Delta_c G - RT \ln\left(\frac{\Sigma^D}{\Sigma^N}\right) \tag{A35}$$

where $\Delta_c G$ is the conformational contribution to $\Delta_d G$ when variations in the ionization state of protein are disregarded. Σ^D and Σ^N are the binding polynomials describing the denatured and native state, which, when protons bind on identical and independent sites, take the form [265]:

$$\Sigma^D = \left(1 + K_{b.D}[H^+]\right)^{n_D} \tag{A36}$$

$$\Sigma^N = \left(1 + K_{b.N}[H^+]\right)^{n_N} \tag{A37}$$

where $[H^+]$ represents the molar concentration of protons; $K_{b,D}$ and $K_{b,N}$ are the association constants of the protons, and n_D, n_N are the number of binding sites of denaturated and native state, respectively. Assuming $K_{b,D} = K_{b,N}$ as a reasonable basis, the canonical partition function of the system is

$$Q(T) = 1 + K_d(1 + K_b[H^+])^{\Delta n} \tag{A38}$$

where $\Delta n = (n^D - n^N)$ and K_d is the constant of a purely conformational equilibrium. The excess heat capacity function determined from statistical thermodynamics [160-164]:

$$C_p^E(T) = \left[\left(<\Delta H^2> - <\Delta H>^2\right) / RT^2\right] + f_D \Delta_d Cp \tag{A39}$$

where $<\Delta H^2>$ and $<\Delta H>^2$ can be calculated by means of equations (9) and (A40), and f_D is given by:

$$f_D = \frac{K_d\left(1 + K_b[H^+]\right)^{\Delta n}}{Q} \tag{A40}$$

The same principles hold for denaturants, like GuHCl and urea; equation (A38) has to be substituted by

$$Q(T) = 1 + K_d(1 + K_b a_L)^{\Delta n} \quad \text{(A41)}$$

where a_L is the activity of the ligand or, in the case of GuHCl, the mean ionic activity, given by the following polynomial expansion [266]:

$$a_L = 0.6761\text{M} - 0.1468\text{M}^2 + 0.02475\text{M}^3 - 0.00132\text{M}^4 \quad \text{(A42)}$$

The thermodynamic model which describes the effect of sub-saturating amount of a ligand follows the ideas and formalism suggested by Robert, Gill and Wyman [267]. When a protein denatures according to a one-step mechanism and has a single binding site in the native conformation,

$$\begin{array}{ccc} N + L & \xleftrightarrow{K_d} & D + L \\ & \searrow^{K_b} \quad \swarrow_{K'} & \\ & NL & \end{array} \quad \text{(A43)}$$

the canonical partition function of this system is given by:

$$Q(T) = 1 + K_b[L] + K_d \quad \text{(A44)}$$

where $[L]$ is the free ligand concentration.

The excess enthalpy function (see Figure A5) normalized with respect to the state of the total native protein (alone or bounded with the ligand) is given by:

$$< \Delta H >= RT^2 \left[\frac{\partial \ln(Q / Q_0)}{\partial T} \right]_{p,[L]} \quad \text{(A45)}$$

where $Q_0 = \{1 + K_b[L]\}$ and $[L]$ can be evaluated from the mass balance,

$$[L_{tot}] = [L] + [L][P_{tot}] \quad \text{(A46)}$$

where $[L_{tot}]$ and $[P_{tot}]$ are the total ligand and protein concentration, respectively, and $[\bar{L}]$ represents the binding isotherm calculated from the partition function:

$$[\bar{L}] = \left[\frac{\partial \ln\left(Q / Q_0\right)}{\partial \ln[L]} \right]_{T,p} = \frac{K_b[L]}{Q} \quad \text{(A47)}$$

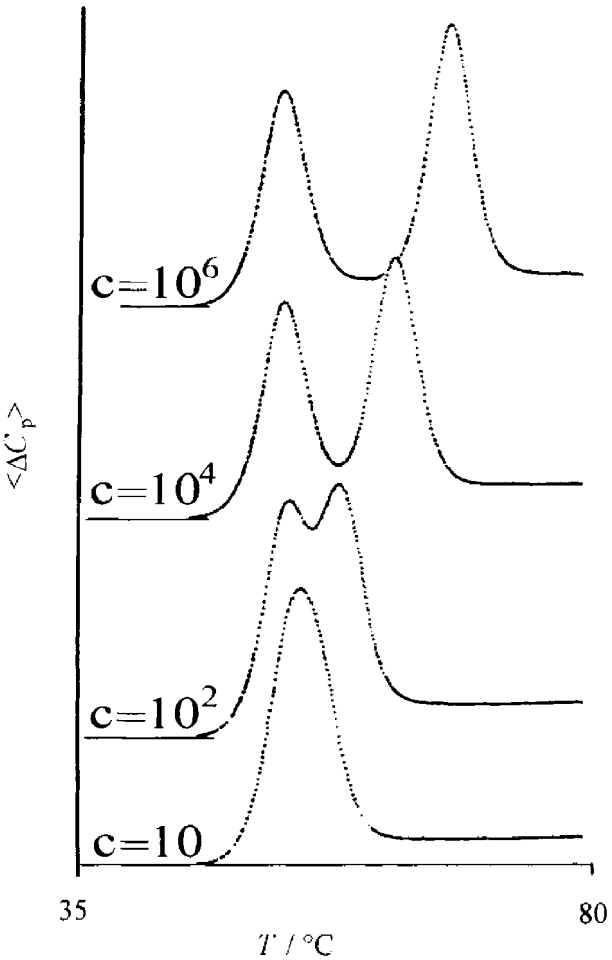

Figure A5. DSC profiles, simulated according to the described model, for different C ($C=K_b[P]_{tot}$) values. The curves have been shifted along the y axis for displaying purposes.

The excess heat capacity function is therefore given by:

$$C_p^{E}(T) = \left[\frac{\partial < \Delta H >}{\partial T}\right]_{[L]} + \left[\frac{\partial < \Delta H >}{\partial [L]}\right]_{T}\left(\frac{\mathrm{d}[L]}{\mathrm{d}T}\right) \qquad \text{(A48)}$$

where $\left(\frac{d[L]}{dT}\right)$ is numerically evaluated. If $\Delta_d Cp = \Delta_b H = 0$ can be assumed, then

$$C_p^E(T) = \left(\frac{\Delta_d H^2}{RT^2}\right)\frac{K_d Q_0}{Q^2} - \Delta_d H \frac{K_d K_b}{Q^2}\frac{d[L]}{dT} \qquad \text{(A49)}$$

Simulations have shown that the maximum distortion of the DSC peak from the two-state transition profile occurs for $[L]_{tot} / [P]_{tot} = 0.5$. Moreover, it has been observed that the complex shape of DSC profile does not depend on the value of the binding constant alone, but markedly depends on the product $K_b[P]_{tot}$ at T_d.

This approach can be generalized in cases where more independent domains are present in the protein, each of with different number of binding sites.

$$Q = \left(1 + K_1 + \sum_{i=1}^{n}\binom{n}{i} K_{b1}^i [L]^i\right)\left(1 + K_2 + \sum_{j=1}^{m}\binom{m}{j} K_{b2}^j [L]^j\right) \qquad \text{(A50)}$$

A4.3. Dissociation and aggregation

For a simple dissociation

$$N_\mu \xleftrightarrow{K} \mu U \qquad \text{(A51)}$$

where a multimeric protein undergoes two-state reversible unfolding with simultaneous dissociation into monomers, the temperature of the maximum of the DSC transitions, T_m, increases with the total protein concentration according to [268]:

$$\Delta_d H^{v.H.} / RT_d + (\mu - 1)\ln C_{tot} = \text{constant} \qquad \text{(A52)}$$

where $\Delta_d H^{v.H.}$ is the vant't Hoff enthalpy and C_{tot} is the total protein concentration. The value of A depends on μ (for example, for μ=1, 2, etc., A=2, 6, etc) [269,270].

Often aggregation follows dissociation according to the Lumry and Eyring model:

$$N_\mu \overset{K}{\longleftrightarrow} \mu U \qquad \text{(A53)}$$
$$\downarrow k$$
$$F$$

Depending on the rate of the irreversible step, this model will lead to different situations. When the equilibrium between the native and the unfolded states is always established but the irreversible step is dominant, the following expressions hold [216]:

effect of the heating rate, u, on T_d (at constant C_{tot}):

$$\ln(u / T_d^2) = cons\tan t - \frac{E_{app}}{RT_d} \qquad \text{(A54)}$$

where $E_{app} = E_a + (\Delta_d H_U/\mu)$, with E_a the Arrhenius activation energy.

shape of the excess heat capacity profile:

$$C_p^{E} = \frac{\Delta_d H E_{app}}{RT_d^2} \exp\left(\frac{E_{app}\Delta T}{RT_d^2}\right) \times \left[1 + \frac{1-\mu}{\mu} \exp\left(\frac{E_{app}\Delta T}{RT_d^2}\right)\right]^{1/(\mu-1)} \qquad \text{(A55)}$$

where $\Delta T = T - T_d$

apparent activation energy in terms of the transition parameters:

$$E_{app} = \mu^{1/(\mu-1)} RT_d^2 C_{P,d}^{E} / \Delta_d H \qquad \text{(A56)}$$

effect of the total protein concentration on T_d (at constant scanning rate):

$$\frac{E_{app}}{RT_d} - 2\ln T_d + \frac{\mu - 1}{\mu} \ln C_{tot} = cons\tan t \qquad \text{(A57)}$$

For reasonable values of E_{app}, $2 \ln T_d$ can be treated as a constant; the $\ln C_{tot}$ versus $1/T_d$ trend is therefore a straight line with slope $-\mu E_{app} / (\mu - 1)R$.

5. REFERENCES

1. L. Riedel, Fette Seifen Anstrichmittel, 57 (1955) 771.
2. L. Riedel, Chemie, Mikrobiologie und Technologie von Lebensmitteln, 5 (1977) 118.
3. L. Riedel, Chemie, Mikrobiologie und Technologie von Lebensmitteln, 5 (1978) 129.
4. H. G. Schwartzberg, J. Food Sci., 41 (1976) 152.
5. V.R. Harwalkar and C.Y. Ma (Eds.), Thermal Analysis of Foods, Elsevier Appl. Sci. Publ., Barking, England, 1990.
6. J.N. de Wit, Neth. Milk Dairy J., 35 (1981) 47.
7. J.N. de Wit and G.K. Klarenbeek, J. Dairy Sci., 67 (1984) 2701.
8. D. Lund, CRC Crit. Rev. Food Sci. Nutr., 20 (1984) 249.
9. C.B. Biliaderis, T.J. Maurice, and J.R. Vose, J. Food Sci., 45 (1980) 1669.
10. A.C. Eliasson, in R.D. Hill and L. Munk (Eds.), New Approaches to Research on Cereal Carbohydrates, Elsevier Sci. Publ. B.V. Amsterdam, 1985, p.93
11. E. Freire and R. Biltonen, Biopolymers, 17 (1978) 463
12. P.L. Privalov, Advan. Protein Chem., 33 (1979) 167.
13. J.W. Donovan, C.J. Mapes, D.J. Davis and J.A. Garibaldi, J. Sci. Fd Agric., 26 (1975) 73.
14. M. Riva and A. Schiraldi, Thermochim. Acta, 220 (1993) 117.
15. T. Shiotsubo, Carbohydr. Res., 158 (1986) 1.
16. M. Riva, L. Piazza and A. Schiraldi, Cereal Chem., 68 (1991) 622.
17. M. Riva, A. Schiraldi and L. Piazza, Thermochim. Acta, 246 (1994) 317.
18. A. Schiraldi and M. Riva, in L. Bonati, U. Cosentino, M.Lasani, G. Moro, D. Pitea, A. Schiraldi (Eds.), Trends in Ecological Physical Chemistry, Elsevier Publ., Amsterdam, 1993, 167.
19. L. Franzetti, E. Mariani, M. Riva, A. Galli, Ann. Microbiol. Enzymol., 44 (1994) 237.
20. L. Franzetti, A. Galli, A. Perazzoli, M. Riva, Ann. Microbiol. Enzymol., 45 (1995) 291.
21. A. Schiraldi, Pure Appl. Chem., 67 (1995) 1873.
22. L. Piazza, A. Schiraldi, and D. Fessas, in R. Jowitt (Ed.), Enginnering in Foods at ICEF7, Sheffield Acad. Press, Sheffield, UK, 1997, p. H5.
23. S.M. Dyszel, in V.R. Harwalkar and C.Y. Ma (Eds.), Thermal Analysis of Foods, Elsevier Appl. Sci. Publ., Barking, Essex, England, 1990, chapt. 10, p. 333.

24. Y.H. Roos, Phase transitions in foods, Academic Press Limited, London, 1995.
25. E.B. Bagley, in H.G. Schwartzberg and R.W. Hartel (Eds.), Physical Chemistry of Foods, Marcel Dekker Inc. New York, 1992, p. 573.
26. J.D. Ferry, Viscoelastic Properties, John Wiley and Sons, New York, 1980.
27. L. Slade and H. Levine, in J.M.V. Blanshard and P.J. Lillford (Eds.), The Glassy State in Foods, Nottingham University Press, Loughborough, 1993, p. 305.
28. G. Allen, in J.M.V. Blanshard and P.J. Lillford (Eds.), The Glassy State in Foods, Nottingham University Press, Loughborough, 1993, p.1.
29. H. Levine and L. Slade, in H.G. Schwartzberg and R.W. Hartel (Eds.), Physical Chemistry of Foods, Marcel Dekker Inc. New York, 1992, p. 83.
30. B. Wunderlich, in E.A. Turi (Ed.), Thermal Characterization of Polymeric Materials, Academic Press, Orlando, 1981, p.91.
31. B. Wunderlich, Thermal Analysis, Academic Press, Boston, 1990.
32. J.M. Faubion, P.C. Dreese and K.C. Diehl, in: H. Faridi (Ed), Rheology of Wheat Products, AACC, St. Paul, MN, 1985, p. 91.
33. G.E. Hibberd and N.S. Parker, Cereal Chem., 52 (1975) 1.
34. G.E. Hibberd and N.S. Parker, Rheol. Act., 14 (1975) 151.
35. A.S. Szczesniak, Cereal Foods World, 33 (1988) 841.
36. D.Weipert, Cereal Chem., 67 (1990) 311.
37. A.H. Bloksma, Cereal Foods World, 35 (1990) 228.
38. A.H. Bloksma, Cereal Foods World, 35 (1990) 237.
39. M.E. Castell-Perez and J.F. Steffe, in M.A. Rao and J.F. Steffe (Eds.), Viscoelastic Properties of Foods, Elsevier Sci. Pub., Ldt. Barking, England, 1992, p.77.
40. J.I. Amemiya and J.A. Menjivar, J. Food Eng., 16 (1992) 91.
41. J.L. Kokini, C-F. Wang, H. Huang and S. Shrimanker, J. Texture Studies, 26 (1995) 421.
42. S. J. Dusand J.L. Kokini, J. Rheol. 34 (7) (1990) 1069.
43. D.H.S. Ramkumar, M. Bhattacharya, J.A. Menjivar and T.A. Huang, J. Texture Studies, 27 (1996) 517.
44. E.B. Bagley and D.D. Christianson , J. Rheol., 31 (1987) 405.
45. L. Slade and H. Levine, Crit. Rev. Food Sci. Nutr., 30 (1991) 115.
46. L. Slade and H. Levine, J. Food Eng., 22 (1994) 143.
47. Y. Roos and M. Karel, J. Food Sci., 56 (1991) 38.
48. Y. Roos and M. Karel, J. Food Sci., 1676.

49. Y. Roos and M. Karel, in J.M.V. Blanshard and P.J. Lillford (Eds.), The Glassy State In Foods, Nottingham Univ. Press, Loughborough, England, 1993, p.207.
50. M.M.Sá and A.M. Sereno, Thermochim. Acta, 246 (1994) 285.
51. M.J. Izzard, S. Ablett, P.J. Lillford, V.L. Hill and, and I.F. Groves, J. Therm. Anal., 47 (1996) 1407.
52. G. Kalentunç and K.J. Breslauer, J. Therm. Anal., 47 (1996) 1267.
53. C.G. Biliaderis, C. M. Page, T.J. Maurice, B.O. Juliano, J. Agric. Fd Chem., 34 (1986) 6.
54. K.J. Zeleznak and R.C. Hoseney, Cereal Chem. 63 (1987) 121.
55. P. Chinachoti, M.Kim-shin, F. Mari abd L. Lo, Cereal Chem., 68 (1991) 245.
56. M. Peleg, Rheol. Acta, 34 (1995) 215.
57. A.M. Cocero and J.L. Kokini, J. Rheol., 35 (1991) 257.
58. J.M. Johnson, E.A. Davis and J. Gordon, Cereal Chem., 67 (1990) 286.
59. N.K. Shah and R.D. Ludescher, Biotechnol. Prog., 11 (1995) 540.
60. P.L. Russel, J. Cereal Sci., 6 (1987) 133
61. D.B. Lund and M. Wirakartakusumah, in B.M. McKenna (Ed.), Engineering Sciences in the Food Industry: Engineering and Food, Elsevier Appl. Sci. Publ., London, 1984, vol. I, p.42.
62. C.G. Biliaderis, Food Chem., 10 (1983) 239.
63. R.C. Hoseney, K.J. Zeleznak and D.A. Yost, Starch/Stärke, 38 (1986) 407.
64. H.F. Zobel, Starch/Stärke, 40 (1988) 1.
65. J.W. Donovan, J. Sci. Food.Agric., 28 (1977) 571.
66. M.J. Miles, V.J. Morris and S.G. Ring, Carbohydr. Res., 135 (1985) 271.
67. V.J. Morris, Trends in Food Sci., July (1990) 2.
68. S.G. Ring, Starch/Stärke, 37 (1985) 80.
69. H.Liu and J.Lelièvre, Carbohydr. Polymers, 19 (1992) 179.
70. M. Michniewicz, C.G. Biliaderis and W. Bushuk, Cereal Chem., 68 (1991) 252.
71. D.E. Rogers, K.J. Zeleznak and R.C. Hoseney, Cereal Chem., 65 (1988) 398.
72. M. Gudmundsson and A.C. Eliasson, Starch, 43 (1991) 5.
73. C.S. Kim and C.E. Walker, Cereal Chem., 69 (1992) 212.
74. K. Ghiasi, R.C. Hoseney, E. Varriano-Marston, Cereal Chem., 60(1982) 58.
75. A. M. Abboud and R.C. Hoseney, Cereal Chem., 61 (1984) 34.
76. C. Ferrero, M.N. Martino, N.E. Zaritzky, J. Therm. Anal., 47 (1996) 1247
77. D.C.White and G.N. Lauer, Cereal Foods World, 35 (1990) 728.
78. S.D. Horton, G.N. Lauer, J.S. White, Cereal Foods World, 35 (1990) 734.
79. L. Piazza, A. Schiraldi, O. Brenna and E. Vittadini, J. Therm. Anal., 47 (1996) 1339.

80. B. Zanoni, D. Smaldone and A. Schiraldi, J. Food Sci., 56 (1991) 1702.
81. B. Zanoni, A. Schiraldi and R. Simonetta, J. Food Eng., 24 (1995)25.
82. J.M.V. Blanshard, P.J. Frazier and T. Galliard, Chemistry and Physics of Baking, Royal Society of Chemistry, London, 1986.
83. W. Bushuk , in H. Faridi (Ed.), Rheology of Wheat Products, AACC, St. Paul, MN, 1985, p. 1.
84. R.C. Hoseney, in H.G. Schwartzberg and R.W. Hartel (Eds.), Physical Chemistry of Foods, Marcel Dekker Inc. New York, 1992, p.443.
85. R.C. Hoseney, K. Zeleznak and C.S. Lai, Cereal Chem., 63 (1986) 285.
86. L. Slade and H. Levine, in H. Faridi (Ed.), The Science of Cookie and Craker Production, Chapman & Hall, London, 1994, p.23.
87. J.D. Schofield, R.C. Bottomley, G.A. LeGrys, M.F. Timms and M.R. Booth, in A. Graveland and J.H.E. Moonen (Eds.), Gluten Proteins, TNO Wageningen, 1984, p.81.
88. H. Levine and L. Slade, in H. Faridi and J.M. Faubion (Eds.), Dough Rhelogy and Baked Product Texture: Theory and Practice, Van Nostrand Reinhold, New York, 1989.
89. W. Dong, Measurements of Certain Rheological Properties and Transformations in Wheat Flour, M.S. thesis, Kansas State University, Manhattan, 1992.
90. Miller, R. Mathew and R.C. Hoseney, J. Thermal Anal., 47 (1996) 1329.
91. Slade, H. Levine and J.W. Finley, in R.D. Phillips and J. W. Finley (Eds.), Protein Quality and the Effects of Processing, Marcel Dekker, New York, 1989, p.9.
92. Levine and L. Slade, in F. Franks (Ed.),. Water Science Reviews", Cambridge University Press, Cambridge, 1988, vol 3, p.79.
93. G. Kalichevsky, E.M. Jaroszkiewicz and J.M.V. Blanshard, Int. J. Biol. Macromol., 14 (1992) 257.
94. G. Kalichevsky, E.M. Jaroszkiewicz and J.M.V. Blanshard, Int. J. Biol. Macromol., 14 (1992) 267.
95. Lawton and Y.V. Wu, Cereal Chem, 70 (1993) 471.
96. Karel, in D. Simatos and J.L. Multon (Eds.), Properties of Water in Foods, Martinus Nijhoff, Dordrecht, 1985, p.153.
97. R.B. Prime, in E.A. Turi (Ed.), Thermal Characterization of Polymeric Materials", Academic Press, Orlando, 1981, p.435.
98. J.K. Gilham, in J.C. Seferis and L Nicolais (Eds.), The Role of Polymeric Matrix in the Processing and Structural Properties of Composite Materials, Plenum, New York, 1983, p.127.
99. A. Schiraldi, Thermochim. Acta, 162 (1990) 253.

100. L.H. Sperling, Introduction to Physical Polymer Science, Wiley-Intersci., N.Y., 1986.
101. S. Cavella, L.Piazza and P. Masi, Ital. J. Food Sci., 4 (1990) 235.
102. H. He and C. Hoseney, Cereal Chem., 68 (1991) 526.
103. A. Abdelrahman and R. Spiess, in H.Faridi and J. Faubion (Eds.), Rheology of Wheat Products, AACC, St. Paul, MN, 1985, p. 87.
104. H. Faridi and J.M. Faubion, Dough Rheology and Baked Product Texture, Van Nostrand Reinhold, New York, 1990.
105. G.E. Hibberd and W. J. Wallance, Rheol. Acta, 5 (1966) 193.
106. G.E. Hibberd, Rheol. Acta, 9 (1970) 497.
107. Hibberd, Rheol. Acta, 9, (1970), 501.
108. J.R. Smith, T.L. Smith, N.W. Tschoegl, Rheol. Acta, 9 (1970) 239.
109. D.B. Cuming and M.A. Tung, Can. Inst. Food Sci. Tech. J., 10 (1977) 109.
110. L. Bohlin and T.L.G. Carlson, Cereal Chem., 57 (1980) 175.
111. G.A. Legrys, M.R. Booth and S.M. Baghdadi, in Y. Pomeranz and L. Munch (Eds.), Cereals: a Renewable Resource, AACC, St. Paul, MN, 1981.
112. L.L.Navickis, R.A. Anderson, E.B. Bagley and B.K. Jasberg, J. Texture Studies, 13 (1982) 249.
113. P.C. Dreese, J.M. Faubion and R.C. Hoseney, Cereal Chem, 65 (1988) 348.
114. P.C. Dreese, J.M. Faubion and R.C. Hoseney, Cereal Foods World, 33 (2) (1988) 225.
115. P. Masi, in R.P. Singh and A.G. Medina (Eds.), Food Properties and Computer - Aided Engineering of Food Processing Systems, Kluwer, Dordrecht, 1989, p.357.
116. A. Tobolsky, Properties and Structure of Polymers", John Wiley & Sons, New York,(1967).
117. B. Palecz, L. Benosist, A. Schiraldi and G. Della Gatta, Proc. 6th ESTAC (Grado, Italy, 1994) p.224.
118. A. Schiraldi, A.Stassi and B. Palecz, in R. Jowitt (Ed.), Enginnering in Foods at ICEF7, Sheffield Acad. Press, Sheffield, UK, 1997, p. H9.
119. G. Attenburrow and A.P. Davies, in J.M.V. Blanshard and P.J. Lillford (Eds.), The Glassy State in Foods, Nottingham Univ. Press, Loughborough, England, 1993, p.317.
120. M. Gudmundsson, A.C. Eliasson, S. Bengtsson, and P. Åman, Starch, 43 (1991) 5.
121. M.T. Kalichevski, J.M.V. Blanshard and R.D.L. Marsh, in J.M.V. Blanshard and P.J. Lillford (Eds.), The Glassy State in Foods, Nottingham Univ. Press, Loughborough, England, 1993, p.133.
122. P.L. Russel, J. Cereal Sci., 6 (1987) 147.

123. H. He and R.C. Hoseney, Cereal Chem. 67 (1990) 603.
124. J. Longton and G.A. Le Grys, Starch, 33 (1981) 410.
125. R.D.L. Marsh and J.M. Blanshard, Carbohydr. Polymers, 9 (1988) 301.
126. A. Schiraldi, L. Piazza, M. Riva, Cereal Chem., 73 (1996) 32.
127. G. A. Reineccius, Cereal Foods Worls, 37 (1992) 272.
128. J. Silverio, E. Svensson, A.C. Eliasson and G. Olofsson, J. Therm. Anal., 47 (1996) 1179.
129. F. Nakazawa, S. Noguchi, J. Takahashi and M. Takada, Agric. Biol. Chem., 48 (1984) 201.
130. M. Kim-Shin, F. Mari, P.A. Rao, T.R. Stengle and P. Chinachoti, J. Agric. Food Chem., 39 (1991) 1915.
131. R.E. Wetton and R.D.L. Marsh, DTMA in Food Materials, British Society of Rheology, University of Warwick, UK, 1989.
132. A.Nikolaidis and T.P. Labuza, J. Thermal Anal., 47 (1996) 1315.
133. K. Kulp and J. Ponte, CRC Crit. Revs. Food Sci. Nutr., 15 (1981) 1.
134. K. J. Zeleznak and R.C. Hoseney, Cereal Chem., 63 (1986) 407.
135. Z. Czuchajowska and Y. Pomeranz, Cereal Chem., 66 (1989) 305.
136. L. Piazza and P. Masi, Cereal Chem., 72 (1995) 320.
137. M. Le Meste, G. Roudaut and S. Davidou, J. Thermal Anal., 47 (1996) 1361.
138. D. Weipert, Cereal Foods World, 42(3) (1997) 132.
139. M. LeMeste, V.T. Huang, J. Panama, G.Anderson and R. Lentz, Cereal Foods World, 37(3) (1992) 264.
140. M.T. Kalichevsky, E. M. Jaroszkiewicz and J.M.V. Blanshard, Int. J. Biol. Macromol., 14 (1992), 257.
141. M. LeMeste, S. Aynié and B.Colas, IAA, 109(11) (1992) 862.
142. M. LeMeste, S. Davidou and I. Fontanet, IAA, 110(1-2) (1994) 11.
143. L.M. Hallberg and P. Chinachoti, J. Food Sci., 57 (5) (1992) 1201.
144. Y. Vodovotz, L. Hallberg and P. Chinachoti, Cereal Chem., 73(2) (1996) 264.
145. E. Vittadini, X.J. Chen and P. Chinachoti, J. Food Sci., 61(5) (1996) 990.
146. C. Tanford, Adv. Protein. Chem, 23 (1968) 121.
147. E.Freire and K.P.Murphy. J. Mol. Biol. 222 (1991) 687.
148. P.L. Privalov, E.I. Tiktopulo, S.Yu. Venyaminov, Yu.V. Griko, G.I. Makhatadze and N.N.Khechinashvili. J. Mol. Biol., 205 (1989) 737.
149. W. M. Jackson and J.F. Brandts, Biochemistry, 9 (1970) 2294.
150. M. A. H. Ismond, E. D. Murray, and S. D. Arntfield, Food Chem., 21 (1986) 27.

151. S.D. Arntfield, E. D. Murray, and M. A. H. Ismond, J. Food Sci., 51 (1986) 371.
152. C.D. Myers, in V.R. Harwalkar and C.-Y. Ma (Eds.), Thermal Analysis of Foods, Elsevier Applied Science, London, 1990, p.16;
153. S. Barbut and C.J. Findlay, in V.R. Harwalker and C.-Y. Ma (Eds.), Thermal Analysis of Foods, Elsevier Applied Science, London, 1990, p. 126.
154. E. Freire and R. Biltonen, Biopolymers, 17 (1978) 481 (see also [11]).
155. G.Barone, P.Del Vecchio, D. Fessas, C.Giancola, and G.Graziano, J.Therm. Anal., 38 (1992) 2779.
156. E. I. Tiktopulo, and P.L. Privalov, Biophys. Chem., 1 (1974) 349.
157. M. Flogel, and R. L. Biltonen, Biochemistry, 14 (1975) 2603.
158. A. L. Jacobson and C. L. Turner, Biochemistry, 19 (1980) 4534.
159. T.Y. Tsong, R.P. Hearn, D.P. Wrathall, J.M. Sturtevant, Biochemistry, 9 (1970) 2666.
160. G.Barone, P. Del Vecchio, D. Fessas, C. Giancola, G. Graziano, and A. Riccio, in W.J.J. van den Tweel et al. (Eds.), Stability and Stabilization of Enzymes, Elsevier, The Netherlands, 1993, p. 198.
161. G. Barone, P. Del Vecchio, D. Fessas, C. Giancola, G. Graziano, and A.Riccio, in N.Russo, J. Anastasso-poulou and G.Barone (Eds.), Chemistry and Properties of Biomolecular Systems, Kluwer Ac. Publ., 1994, vol. 2, p. 49.
162. G. Barone, P. Del Vecchio, D. Fessas, C. Giancola, G. Graziano, and A. Riccio, J.Therm. Anal., 41 (1994) 1263.
163. G. Barone, P. Del Vecchio, D. Fessas, C. Giancola, G. Graziano, and A. Riccio, J.Therm. Anal., 41 (1994) 1357.
164. G. Barone, F. Catanzano, P. Del Vecchio, D. Fessas, C. Giancola, G. Graziano, and A. Riccio, J.C.A.T., 95 (1995) 21.
165. R. N. Sharma and C. C. Bigelow, J. Mol. Biol., 88 (1974) 247.
166. J. Suurkuusk, Acta. Chem. Scand., Ser. B, 28 (1974) 409.
167. P.-H Yang, and J. A. Rupley, Biochemistry, 18 (1979) 2654.
168. P.L. Privalov, and S.A. Potekhin, Methods Enzymol., 131 (1986) 4.
169. S-I. Kidokoro and A. Wada. Biopolymers, 26 (1987) 213.
170. J. Wyman and S.J. Gill, Functional Chemistry of Biological Macromolecules, University Science, Mill Valley, CA, 1990.
171. P.L. Privalov and S.J. Gill, Adv. Protein Chem., 39 (1988) 191.
172. P.L. Privalov and N.N. Khechinashvili, J. Mol. Biol., 86 (1974) 665.
173. P.L. Privalov, Adv. Protein Chem., 33 (1979) 167.
174. K.P. Murphy and S.J. Gill, Thermochim. Acta, 172 (1990) 11.
175. K.P. Murphy and S.J. Gill, J. Mol. Biol. 222 (1991) 699.

176. J.F. Brandts, in S.N. Timasheff and G.D. Fasman (Eds.), Structure and Stability of Biological Macromolecules, Marcel Dekker, New York, 1969, p. 213.
177. W. Becktel, and S.A. Schellman, Biopolymers, 26 (1987) 1859.
178. P.L. Privalov, CRC Crit. Rev Biochem. Mol. Biol., 25 (1990) 281.
179. A.Schiraldi.and E. Pezzati, Thermochim. Acta, 199 (1992) 105.
180. Y.V. Griko and P.L. Privalov. Biochemistry, 31 (1992) 8810.
181. A.I. Azuaga. M.L. Galisteo, O.L. Mayorga, M.Cortijo and P.L. Mateo, Febs Letters, 309 (1992) 258.
182. A. Schiraldi, in C. Rossi and E. Tiezzi (Eds.), Ecological Physical Chemistry, Elsevier Science Publishers B. V., Amsterdam, 1991, p.73.
183. P.L. Privalov in E. Creighton (Ed.), Protein Folding, W.H. Freeman Company Publ., 1992, p. 83.
184. G. Barone, P.Del Vecchio, D. Fessas, C.Giancola, and G.Graziano, in N.Russo, J.Anastas-sopoulou and G. Barone (Eds.), Chemistry and Properties of Biomolecular Systems, Kluwer Ac. Publ., 1994, vol. 2, p. 67.
185. A. Ginsburg and M. Zolkiewski. Biochemistry, 30 (1991) 9421.
186. J.F. Brandts, C.Q. Hu, and Lung-Nan Lin, Biochemistry, 28 (1989) 8588.
187. P. L. Privalov and V. V. Filimonov, J. Mol. Biol., 122 (1978) 447.
188. L. H. Chang, S. J. Li, T. L. Ricca, A.G. Marshall, Anal. Chem., 56 (1984) 1502.
189. G. Barone, P. Del Vecchio, D. Fessas, C. Giancola, and G. Graziano, Thermochim. Acta, 227 (1993) 185.
190. P.L. Privalov and N.N. Khechinashvili, J. Mol. Biol., 86 (1974) 665.
191. Y. Kuroda, Shun-ichi Kidokoro and A. Wada. J. Mol. Biol., 223 (1992) 1139.
192. J.H. Carra, E.A. Anderson, and P.L. Privalov. Protein Science, 3 (1994) 944.
193. A. Laligant, E. Dumay, C.C. Valencia, J.L. Cuq, and J.C. Cheftel, J. Agric. Food Chem., 39 (1991) 2147.
194. M.T.A. Evans, M.C. Phillips, and M.N. Jones, Biopolymers, 18 (1979) 1123.
195. G. Barone, S. Capasso, P. Del Vecchio, C. De Sena, D. Fessas, C. Giancola, G. Graziano, and P. Tramonti, J.Therm. Anal., 45 (1995) 1255.
196. J. Jr. Hermans and H. A. Scheraga, J. Am. Chem. Soc., 83 (1961) 3283.
197. J.F. Brandts and Lung-Nan Lin. Biochemistry, 29 (1990) 6927.
198. G. Barone, S. Capasso, P. Del Vecchio, C. De Sena, D. Fessas, C. Giancola, and G. Graziano, J.C.A.T., 95 (1995) 173.

199. Giancola, C. De Sena, D. Fessas, G. Graziano, G. Barone, Int. J. Biol. Macromol. 20 (1997) 193
200. J. A. Schellman, Biopolymers, 17 (1978) 1305.
201. J. A. Schellman, Biopolymers,17 (1987) 549.
202. J. A. Schellman, Biophys. Chem., 37 (1990) 121.
203. S. N. Timasheff, Biochemistry, 31 (1992) 9857.
204. G.Barone, P.Del Vecchio, D. Fessas, C.Giancola, and G.Graziano, in W.J.J. van den Tweel et al. (Eds.), Stability and Stabilization of Enzymes, Elsevier, The Netherlands, 1993, p. 37.
205. J. Wyman, Adv. Protein Chem., 19 (1964) 223.
206. K. C. Aune and C. Tanford, Biochemistry, 8 (1969) 4579 and 4586.
207. A. V. Finkelstein and E. I. Shakhnovich, Biopolymers, 18 (1979) 288.
208. E. I. Shakhnovich and A. V. Finkelstein, Biopolymers, 28 (1989) 1667.
209. P.L.Privalov and G.I. Makhatadze, J. Mol. Biol. 232 (1993) 660.
210. Y.V. Griko, G.I.Makhatadze, P.L. Privalov, and R. W. Hartley, Protein Science, 3 (1994) 669.
211. E. Freire and K P. Murphy. J.Mol. Biol., 222 (1991) 687.
212. G. Barone, P. Del Vecchio, D. Fessas, C. Giancola, G. Graziano, P. Pucci, A. Riccio, and M. Ruoppolo, J.Therm. Anal., 38 (1992) 2791.
213. D. Xie, V. Bhakuni, and E. Freire, Biochemistry, 30 (1991)10673.
214. G. I. Makhatadze and P. L. Privalov, J. Mol. Biol., 226 (1992) 491.
215. A. M. Klibanov and T. J. Ahern, in D. L. Oxender and C. F. Fox Eds.) Protein Engineering, Alan R. Liss, New York, 1987, p. 213.
216. J. M. Sanchez-Ruiz, Biophys. J., 61 (1992) 921.
217. R. Lumry and H Eyring, J. Phys. Chem.., 58 (1954) 110.
218. J.R. Lepock, K.P. Ritchie, M. C. Kolios, A. M. Rodahl, K.A. Heinz, and J. Kruuv, Biochemistry 31 (1992) 12706.
219. M.L. Galisteo, P.L. Mateo, and J.M. Sanchez-Ruitz, Biochemistry, 30 (1991) 2061.
220. J.M. Sanchez-Ruitz, J.L.Lopez-Lacomba, P.L. Mateo, M.Vilanova, and M.A. Serra, Eur. J. Biochem., 176 (1988) 225.
221. M.L. Galisteo, F.Conejero-Lara, J. Nunez, J.M.Sanchez-Riutz and P.L. Mateo, Thermochim. Acta, 199 (1992) 147.
222. S. D'Auria, R. Barone, M. Rossi, R. Nucci, G. Barone, D. Fessas, E. Bertoli, and F. Tamfani, Biochem. J., 323 (1997) 833.
223. J.R. Bacon, T.R. Noel, and D.J. Wright, J. Sci. Food Agric., 49 (1989) 335.
224. A. Kato, Y.Nagase, N. Matsudomi and K Kobayashi, Agric. Biol. Chem., 47 (1983) 1829.
225. C. -Y. Ma and V.R. Harwalkar. J. Food Sci., 53 (1988) 531.

226. J.W. Donovan and C.J. Mapes, J. Sci. Food Agric., 27 (1976) 197.
227. T. Itoh, Y. Wada, and T. Nakanishi, Agric. Biol. Chem., 40 (1976) 1083.
228. A.M. Hermansson, in J. Adler Nissen (Ed.), Proc. 11th Meeting FEBS Symp. A3, 1978, p. 99.
229. V. Bernal and P.J. Jelen, Dairy Sci., 67 (1984) 2452.
230. P.R. Sheard, A. Fellows, D.A. Ledward, and J.R. Mitchell, Food Technol., 21 (1986) 55.
231. W. Melander and C. Horvath, Arch. Biochem. Biophys., 183 (1977) 200.
232. M.A.H. Ismond, E.D. Murray, S.D. Arntfield, Food Chem., 21 (1986) 27.
233. V.R. Harwalkar and C.-Y. Ma, J.Food Sci., 52 (1987) 396.
234. S.D. Arntfield, E.D. Murray, M.A.H. Ismond, J. Food Sci., 51 (1986) 371.
235. A. Finch and D.A. Ledward, Biochim. Biophys. Acta, 295 (1973) 296.
236. M.A.H. Ismond, E.D. Murray, S.D. Arntfield, Food Chem., 29 (1988) 189.
237. J.F. Back, D. Oakenfull, and M.B. Smith, Biochemistry, 18 (1979) 5191.
238. P.O. Hegg and B. Löfqvist, J. Food Sci., 39 (1974) 1231.
239. J.E. Kinsella and D.M. Whitehead, Adv. Food Nutr. Res., 33 (1989) 343.
240. J.D. Ferry, Adv. Protein Chem., 4 (1948) 1.
241. M. Friedman, in M Friedman (Ed.), Protein Crosslinking. Nutritional and Medical Consequences, Plenum Press, New York, 1977.
242. N. Catsimpoolas and E. W. Meyer, Cereal Chem., 47 (1970) 559.
243. D. W. Stanley,. in C. Mercier, P. Linko, and J.M. Harper (Eds.), Extrusion Cooking, AACC, Inc., St. Paul, MN, 1989, p.325.
244. L.P. Voutsinas, E. Cheung and S. Nakai, J. Food Sci. 48 (1983) 26.
245. S.S. Deshpande, S. Damodaran, Biochim. Biophys. Acta, 998 (1989) 179.
246. M. Otterburn, M. Healy, and W. Sinclair, in M. Friedman (Ed.), Protein Crosslinking. Nutritional and Medical Consequences, Plenum Press, New York, 1977, p.239.
247. A. Kato, and S. Nakai, Biochim. Biophys. Acta, 624 (1980) 13.
248. N. Matsudomi, H. Mori, A. Kato, and K. Kobayashi, Agric. Biol. Chem., 49 (1985) 915.
249. M. Hirotsuka, H. Taniguchi, H. Narita, and M. Kito, J. Food Sci., 49 (1984) 1105.
250. Y.L. Hsien and J. M. Regenstein. J.Food Sci., 57 (1992) 856.
251. P.R. Kuhn and E.A. Foegeding, J. Food Chem., 39 (1991) 1013.
252. C.V. Morr and E.A. Foegeding, Food Technol., 44 (1990) 100.
253. D.M. Mulvihill and M. Donovan, Food Sci. Technol., 11 (1987) 43.
254. D.M. Mulvihill and J.E. Kinsella, Food Technol. 41 (1987) 102.
255. D.M. Mulvihill and J.E. Kinsella, J. Food Sci. 53 (1988) 231.

256. R.H Schmidt, in J.P. Cherry, (Ed.), Protein Functionality in Foods, Am. Chem. Soc., Washington, DC, 1981, p.131.
257. R.H Schmidt, V.S. Packard, and H.A. Morris, J. Dairy Sci., 67 (1984) 2723.
258. J.L. Kokini, A.M. Cocero and H. Madeka, Food Technol., 49 (1995) 74.
259. J.L. Kokini, A.M. Cocero, H. Madeka and E. de Graaf, Trends in Food Sci. and Technol., 5 (1994) 281.
260. Madeka and J.L. Kokini, J. Food Eng., 22 (1994) 241.
261. Khatkar, A.E. Bell and J.D. Schofield, J. Cereal Sci., 22, (1995), 29.
262. Attenburrow, D.J. Barnes, A.P. Davies and S.J. Ingman, J. Cereal Sci., 12 (1990) 1.
263. Masi, S. Cavella and L. Piazza, in: W.E.L. Spiess and H. Shubert (Eds.), Engineering and Food.: Physical properties and Process Control, Elsevier Sci. Pub., Ldt. Barking, England, 1990, vol.1, p. 122.
264. E. Attenburrow, A.P. Davies, R.M. Goodband and, and S.J. Ingman, J. Cereal Sci., 16 (1992) 1.
265. J.A. Schellman, Biopolymers, 14 (1975) 999.
266. C.N. Pace and K.E. Vanderburg, Biochemistry, 18 (1979) 288.
267. C.H. Robert, S.J. Gill and J. Wyman, Biochemistry, 27 (1988) 6829
268. .K. Takahashi and J.M. Sturtevant, Biochemistry, 20 (1981) 6185.
269. S.P. Manly, K.S. Mathews and J.M. Sturtevant. Biochemistry 24 (1985) 3842.
270. H.H. Klump, in M.M. Jones (Ed.), Biochemical Thermodynamics, Elsevier, 1988, 100.

This Page Intentionally Left Blank

Handbook of Thermal Analysis and Calorimetry. Vol. 4: From Macromolecules to Man.
R.B. Kemp, editor.

Chapter 17

THERMAL ANALYSIS AND CALORIMETRY OF PHARMACEUTICALS

James L. Ford[a] and Richard Willson[b]

[a]School of Pharmacy and Chemistry, Liverpool John Moores University, Byrom Street, Liverpool, L3 3AF, United Kingdom

[b]SmithKline Beecham Pharmaceuticals, New Frontiers Science Park (South), Third Avenue, Harlow, Essex,CM19 5AW, United Kingdom

1. INTRODUCTION

Thermal analysis and calorimetry have many applications within the Pharmaceutical disciplines. It is the intention of this chapter to review the current applications of thermal and calorimetric techniques to the development of pharmaceutical products. To prevent the chapter from becoming overlong, it focuses on the specific techniques that are an established part of the research and development armoury within pharmaceutics. Clearly, such applications include the study of morphological form and stability, chemical stability (of solutions and of the solid state), biological studies and photo-stability. The current thermal and calorimetric techniques available for such studies, described in Volume 1, Principles and Practice of this Handbook, include: differential thermal analysis (DTA) and differential scanning calorimetry (DSC) with the recently commercialised modulated techniques [whether dynamic DSC (DDSC) or modulated DSC (MDSC)]; thermogravimetry (TG); thermo-mechanical analysis (TMA) dynamic thermal analysis (DTA) and the closely related torsional braid analysis (TBA); and the earliest technique, hot stage microscopy (HSM). Calorimetric techniques include isothermal microcalorimetry with the recent addition of nanoWatt technology, isoparobolic solution calorimetry, isothermal flow microcalorimetry, isothermal titration calorimetry, large scale batch calorimetry for studying crystallisation processes, bomb calorimetry and photo-microcalorimetry.

At present, thermal analysis and calorimetry are regarded as two separate disciplines. Thermal analysis would normally make measurements as a function of temperature whereas calorimetry would normally make isothermal measurements as a function of time. However with the advent of micro-scanning calorimeters, where operation under pseudo-isothermal conditions can give sensitivity approaching that of microcalorimeters, the distinction is becoming less defined. Also, specific calorimetric and thermo-analytical instruments are often ubiquitous and can be used in several different modes of operation.

2. CHARACTERISATION OF PHARMACEUTICAL SOLIDS

The criteria for novel drug molecule selection are naturally focused on pharmacological activity, safety and potential clinical and commercial value. However, the progression of a drug to the market place depends on issues such as stability, bioavailability, toxicology and ease of manufacture. These issues are invariably encountered during the development of a drug and may cause a candidate to be considered unsuitable or slow its rate of progression to a commercial product. Thermal analysis and calorimetric techniques are mostly assigned to the study of aspects of stability.

Ideally, only one set of stability measurements would be required to define the stability of a given product. These results could then be applied to all subsequent batches of the product. This could only be the case if all batches were manufactured identically. However, many of the processes that constitute the manufacturing chain cannot be completely controlled. There is, therefore, the possibility that batch to batch variation may lead to unpredictable stability and changes in the physical properties of the product. Many examples illustrate that dramatic changes in stability may be caused by minor changes in the input materials [1].

There is often insufficient understanding of how key production parameters and the manufacturing environment may affect the morphology and physical properties of a drug. A manufacturer needs to ascertain, for example, how concentration, stir rate and reaction temperature affect crystal habit and morphology of material during primary manufacture; how pressure, temperature and relative humidity affect crystallinity during particle size reduction in secondary manufacture; and how purity and crystallinity affect stability in the final product. An inadequate understanding of these and other key parameters makes defining the specifications for conditions and tolerances of each stage of

the manufacturing process a precarious responsibility. As an example, bought in excipients normally have general guidelines on purity content. The primary manufacturing company may not be required to inform about process changes providing that the purity profile remains within the original specification. It is therefore possible for the quality of a product to be compromised even though there is no apparent change in the materials or the manufacturing procedure [2].

Thermal analysis and calorimetry provide the opportunity for detailed analysis during each step of the manufacturing process. The isothermal microcalorimeter, with high sensitivity to measure very small changes, and rapid thermal analytical techniques which characterise materials, are powerful tools for such analyses.

Within routine studies of new chemical entities, the initial focus is to explicate a comprehensive description of the drug. The aim is to provide specific information on its physical aspects such as morphological form, polymorphism, crystal habit and solvate state. This information is combined with data from other techniques such as dynamic vapour sorption (DVS), particle size analysis, XRPD (x-ray powder diffraction), solid state NMR, IR spectrophotometry and Raman spectroscopy.

The second stage is to investigate the ability of the drug to resist change when subjected to stressful conditions within the manufacturing environment, for example changes in temperature, pressure, relative humidity, pH and drying times. The investigation into morphological stability should also define the environmental boundary conditions beyond which the morphological stability of the compound may be compromised. This should then allow greater control during each stage in production where specific tolerances can be tailored for each drug to yield a more predictable end-product.

As a cautionary note, other morphological forms may be identified as a potential patent risk since the final product is normally patented as a specific morphological form. It is possible to loose exclusive market rights if another, more appropriate, form is subsequently discovered by a competitor.

Changes in the morphological structure caused by the manufacturing processes may only affect a small proportion of the overall material. However, this damaged material is often in an unstable state and may have a disproportionate effect on the overall performance of the product. Excipients should similarly be treated with care. Recently, there has been realisation that the morphology of excipients also plays an important role in the stability of the final product.

The third stage is to determine the chemical stability of the drug. This includes a study of the chemical stability alone, and a study of the compatibility of the drug with each excipient.

Chemical instability is defined as a chemical interaction that causes a detrimental change to the material and can lead to a loss of potency. This may also result in the formation of potentially harmful degradation of products. Chemical degradation can be environmentally initiated (e.g., photo-degradation, oxidation from atmospheric oxidants, hydrolysis) or by a host of other reactive species external to the drug formulation [3]. Additionally, chemical degradation can be initiated from within the drug formulation such as by autocatalysis and interactions with other excipients [4] or impurities associated with the excipients. Chemical stability studies are mainly concerned with the stability of the drug and the compatibility of the drug with excipients which were initially developed with good stability characteristics in mind.

The evaluation of the chemical stability of new drug molecules primarily focuses on the kinetics of degradation or interaction. The aim is to establish rates of degradation leading to predictions about the shelf life of the active ingredient. The characterisation of drug degradation is required by licensing law and is also valuable information to formulators who can then develop an appropriate formulation with a predictable shelf life.

There are many different techniques available for the study of chemical and morphological stability [5,6]. Chemical degradation is traditionally studied using HPLC in combination with long term "accelerated" temperature storage. This type of long-term storage at elevated temperatures is expensive and time-consuming. Considerable resources are required to set up and store samples over long time periods under controlled environmental conditions. Furthermore, it is generally accepted that "accelerated" stability studies are a notoriously unreliable way for prediction of reaction rates under normal environmental conditions. The reaction mechanism at the elevated temperatures of accelerated storage may not confidently be attributed to the same degradation pathway at lower temperatures. Therefore there is a possibility of considerable error when extrapolation of reaction rates for accelerated degradation is made to ambient temperature [7]. Thermal analysis, particularly DSC, has been used extensively for chemical stability and compatibility studies [8]. However, its use remains to be established in mainstream stability programs. Calorimetric analysis of chemical stability perhaps offers a more reliable method for such studies. The technological advances made in increasing the sensitivity of micro-calorimeters and the

advances in data interpretation now provide an opportunity for such techniques to be routinely used.

Techniques traditionally used to study morphological stability include XRPD, NMR, IR, Raman spectroscopy and Electron microscopy. These techniques are very useful in identifying general physical attributes at the molecular level and so allow the categorisation of specific morphologies. However, they do not possess the flexibility and, in some cases, the sensitivity to identify small differences in crystal structure, for example, different hydrate states where there is small interaction with the hydrate water and to quantify amorphous material or small amounts of impurity [9].

2.1. Morphological stability

Until recently, the propensity of a material to be morphologically changed when in a stressful environment was not always appreciated. This was partly due to a lack of sensitivity of the available analytical techniques to study the often small differences associated with morphological change. This is especially true when small amounts of the overall material are affected. For example, XRPD can detect amorphous material in a crystalline sample if it is present in significant quantities (empirically 15% or above is a detectable level although often sample dependent). In contrast studies using calorimetry, such as isothermal microcalorimetry coupled with RH perfusion, solution calorimetry and related techniques such as Dynamic Vapour Sorption (DVS) are now established. These techniques can give detailed information about the morphology and morphological stability of a compound, and can often differentiate modest quantities of changed material.

Experience with new chemical entities indicates that many have the propensity to be morphologically altered (to differing degrees of severity) during the rigours of normal manufacturing processes. The morphological diversity of compounds *per se* is clearly recognised [10]. However the consequences of morphological change, especially if only a small proportion of the overall material is affected, are often overlooked. Not all morphological issues present a serious stability problem but the findings clearly illustrate the polymorphic diversity that can be exhibited by relatively simple low molecular weight chemical entities. Interestingly, conventional analytical techniques, i.e. FTIR, XRPD, NMR and Raman spectroscopy, may not demonstrate potential morphological problems often revealed by thermal and calorimetric techniques. The main criteria for a morphological stability study are:

(a) assessment of polymorphic purity

(b) identification of a morphological form (polymorphs and hydrates included) and an assessment of their stability in different environments
(c) determination of hygroscopicity and critical RH of the solid, and
(d) quantification of crystal damage during various stages in production, and the impact that they may have on product quality and processability

The routine often employed to progress such investigations is to make measurements of morphology before and after the material has been subjected to a defined level of stress. Additionally, the analytical device itself may provide degrees of stress during the observation period, such as RH perfusion and multi-ramp DSC. In either case, the main criterion is to observe a morphological change when a quantifiable amount of stress has been applied.

2.1.1. Polymorphism

Polymorphism is the ability of a molecule to crystallise in more than one form of molecular orientation. Crystal habit is the ability of molecules to crystallise at different rates in different directions along the forming crystal giving different shapes of crystals whilst maintaining the same molecular unit structure. Pseudopolymorphism [8] or solvate formation are an ability to incorporate water or other solvent in the forming crystals. Thermal analysis and calorimetry are able to differentiate many of these states; however other techniques must be used to substantiate and validate the DSC/DTA findings. For instance, IR spectra and XR-diffraction patterns confirm differences in crystal structure, although these changes may be very subtle, especially when differentiating habits. Finally, it should be remembered that certain materials might not crystallise but pass into an amorphous or glassy state. Thermal analysis and calorimetry of hydrates, solvates and the glassy state is found in later sections. Thorough reviews of the thermal analysis of these systems have been produced [8,11].

DSC of polymorphs provides valuable information on the melting point, the enthalpy of fusion and the transition temperature, whether in the solid or liquid state, of one polymorphic form to another. Various types of polymorphism exist, depending on the inter-changability of the morphological forms or their thermal stability. Thus, enantiotropic polymorphism or monotropic polymorphism may be described. Enantiotropic forms may be encountered below the melting point of either polymorph. Storage, therefore, of these less stable forms will result in conversion to a more stable polymorph when the temperature is below the melting point of either form. This, therefore represents a solid-solid transformation. In monotropy, one polymorph is stable throughout

the temperature range up to the melting point of the highest polymorph which is difficult to reconvert to the lower melting point polymorph.

Knowledge of which form of polymorphism is evident is derived from the solid I to solid II equilibrium curves [11]. In enantiotropy, there is a reversible transition temperature between the two forms [12]. The lower melting point form is stable below the transition point but at higher temperatures the polymorph with the higher melting point is the stable form. This transition temperature can be measured by thermal analysis. The value of this temperature varies to residual solvent, the presence of impurity and particle size. By convention, the highest melting pint form is designated as Form I. Burger [12] suggested rules for determining the type of polymorphism present. For enantiotropy, the transition temperature is below the melting point of this form. Form I is stable above this transition temperature but Form II is stable below this transition and the transition is reversible. The solubility of Form I is higher below the transition temperature but the solubility of Form II is higher at temperatures greater than the transition [12]. Additionally, the transition of Form II to Form I is endothermic. The heat of fusion of Form I is lower than that of Form II.

Knowledge of enantiotropy may be derived from DSC curves. A check may be made on the solid-solid transformation temperature. Thermogravimetric analysis should be undertaken so that mass loss can be eliminated as being a cause for the transition [11]. Examples include tolbutamide for which the transition temperature is less than 50°C but the melting point is in excess of 125°C [11]. The transition is below the melting point, for example with penicillamine, acetazolamide, indalpin or metoclopramide [11]. Using the technique of melting, followed by recrystallisation (cooling) and secondary melting either enantiotropic form may be formed. However, materials may melt with decomposition producing an impurity that recrystallizes. Such an example is phthalysulphathiazole but thermogravimetry may again be used to detect decomposition [13]. Giron [14] also pointed out that during DSC either form may melt with no subsequent conversion, an example being butylhydroxanisole. Thus, the use of thermomicroscopy must not be underestimated in confirming changes during heating. Additionally, several events described above, may be apparent in the DSC of monotropic forms.

Monotropy represents irreversible transition between polymorphs. The higher melting point form is always the thermodynamically stable form. Additionally, if the melting points of two monotropic forms differ by 25-50°C, it is very difficult to crystallise the lower melting point form [11]. In effect, the transition

temperature between the two forms is always greater than the melting point of Form I which is always the stable form. The transition is irreversible [12]. The solubility of Form I is always less than that of Form II, the transition from Form II to Form I is always exothermic and the heat of fusion of Form I is always greater than the heat of fusion of Form II [12]. In DSC or DTA curves, the solid to solid transition occurs before the melting point of the higher melting point form and is exothermic.

A melt to recrystallisation to melt phenomenon on a DSC curve may represent either monotropic or enantiotropic conversion. Small amounts of decomposition may favour transitions or the apparent production of a polymorph. Frequently thermogravimetry will detect this decomposition. An example of monotropic polymorphism is displayed by temazepam [11].

Every polymorph formed by a given material will have a different lattice energy. The most stable morphological form is that with the largest free energy change (ΔG) from the amorphous form for a given set of conditions. In time, each unstable polymorph will change to the most stable form. A correlation between rates of dissolution and free energy change for a series of polymorphs can also be shown [12], i.e. amorphous materials (with the largest potential for change) have the greatest dissolution rates. However, one should not, of course, describe kinetic events from thermodynamic terms. Incidentally, given sufficient time, all polymorphs of a given drug substance, including hydrates, solvates or amorphous material, will reach the same equilibrium concentration in a given solvent. However that time required to reach the equilibrium concentration for each polymorph can differ considerably.

In some cases the difference in crystal lattice energy between two polymorphs is relatively small reflecting only a small difference between the unit structure. Hakanen and Laine [15] illustrated the use of thermal analysis to the determination of polymorphs. Using terfenadine, two polymorphs and a solvate were identified using x-ray diffraction (XRD), DSC and TG to determine kinetic parameters for the structural change of the methanol solvate by desolvation on heating. Laine et al [16] examined the polymorphic structures within ibopamin which exists in two monotropic forms. The melting points of Form I and II were $134.8 \pm 0.4°$ and $130.2 \pm 0.5°$ respectively.

As a cautionary note, Cartensen and Franchini [17] also showed that some polymorphs are indistinguishable except by XRD. Failing to show significant differences in solubility and observing only slight differences in melting point, which indeed could be due to impurities does not, therefore, eliminate polymorphism.

Other changes may occur on preparation [18]. Modification I of nimodipine melted at 124°C but crystallised as the racemic compound. DSC, IR, Raman, C-13-NMR, XRD, pycnometry and solubility determinations were needed to confirm that it recrystallised as a racemic compound. Form II, melting point 116°C, was a conglomerate [18]. Thermodynamic relationships were illustrated as a schematic energy-temperature diagram (Figure 1). Form II was stable in the range up to 90°C. The melting characteristics of the two forms are illustrated by Figure 2.

The complications of solid-solid characterisation may be illustrated using dehydroepiandrosterone [19]. Three polymorphs (Form I, Form II and Form III) were isolated and four solvates, a 4:1 hydrate (Form SI), a monohydrate (Form SII), a further monohydrate (Form SIII) and a methanol half-solvate (Form SIV). A new polymorph, Form V was isolated using hot stage microscopy. Only Form I and Form SIV exhibited reproducible DSC scans. Five of the isolated forms underwent phase transformation on heating and gave poorly reproducible scans. HSM was used to interpret the DSC scans. According to the suggestions of Burger [12], Forms I, II and III were monotropic polymorphs with decreasing stability in the order Form I > Form II > Form III. The melting onsets and heats of fusion were 149.1°C, 25.5 kJ mol^{-1}, 140.8°C, 24.6 kJ mol^{-1} and 137.8°C, 24.0 kJ mol^{-1} respectively. Heat of solution and DSC data were used to show a melting point of SI at 127.2°C. During dissolution all modifications were converted into the stable monohydrate, Form SII. An example of enantiotropy is provided by the lukotrience D-4 antagonist RG12525 [20].

Three crystalline modifications of fluocinolone acetonide (Forms A, B and C) were characterised by FTIR, DSC, TG - FTIR, micro-FTIR and XRD [21]. On heating Form A and Form C were converted into Form B. Polymorph A was enantiotropically related to Form B while Form C was monotropically related to B [21]. Giron et al [22] examined tetracaine hydrochloride. Ten different forms were identified: six anhydrous crystalline forms, an amorphous form, a hemihydrate, a monohydrate and a tetrahydrate. The anhydrous Form I is the stable thermodynamic modification at ambient temperature. Form 2 was reversibly enantiotropic to Form I. The other four modifications (3, 4, 5 and 6) were monotropic polymorphs of Form I. Only Form 1 and Form 5 were stable at room temperature [22].

Isoparobolic solution calorimetry is a good technique to measure both enthalpy change and rate of dissolution of polymorphs. The high sensitivity of this technique allows the study of polymorphism even when differences in crystal lattice energy are relatively small and hence difficult to study by other

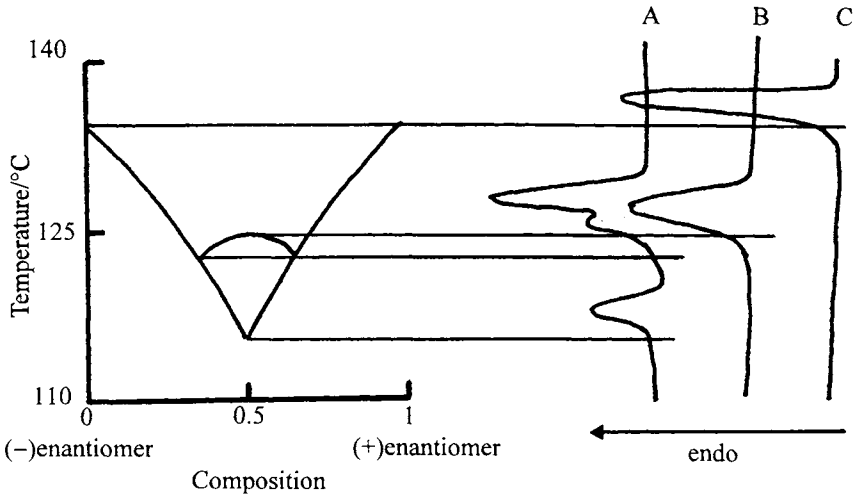

Figure 1. Phase diagram and DSC scans of nimodipine: (A) conglomerate, (B) racemic compound and (C) (−)enantiomer. Reprinted from reference [18] with permission from Elsevier Science.

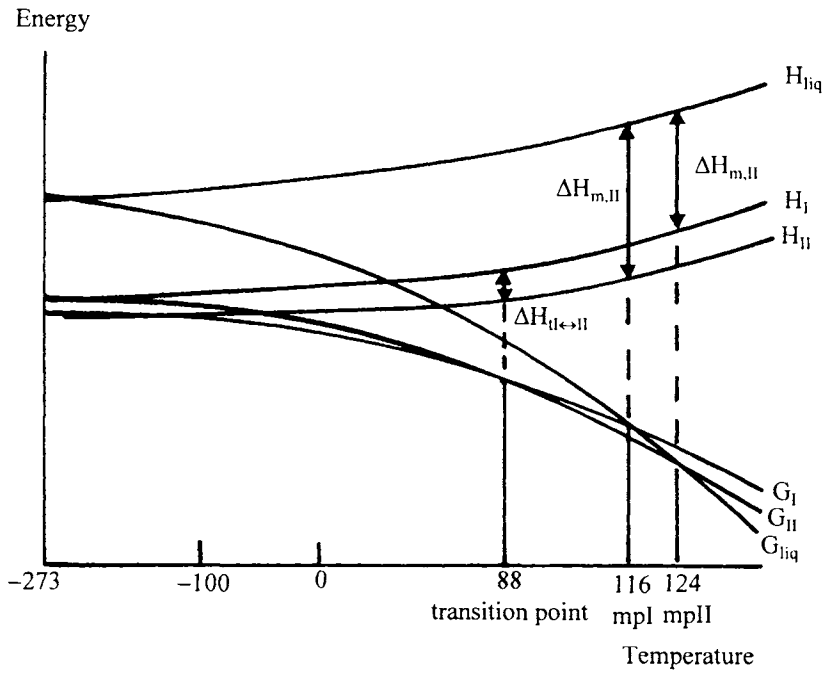

Figure 2. Energy/temperature diagram for nimodipine. Form I has a melting point of 124°C, with heat of fusion of $\Delta H_{m,I}$. Form II has a melting point of 116°C and a heat of fusion of $\Delta H_{m,II}$. The transition of Form I to Form II occurs at 88°C with a heat of transition of $\Delta H_{tI\leftrightarrow II}$. The enthalpies are given by H_{liq}, H_I and H_{II} and the free energies by G_{liq}, G_I and G_{II} for the liquid and Forms I and II respectively. Reprinted from reference [18] with permission from Elsevier Science.

techniques. The procedure to adopt for such studies has similarities to the procedures for studying amorphous materials. Therefore a detailed account is given in section 2.1.4.

2.1.2. Solvates and hydrates

DSC and DTA each display transitions with loss of water or solvent of crystallisation. Figure 3 shows the DSC of a sample of I-lactose monohydrate in both open and closed pans. The problem is that desolvation leads to a build up of vapour pressure inside the sample pans. This will reduce the rate of and increase the temperature at which desolvation occurs. The results are very much related to the integrity of the pans. The rate of loss can be classified on the bases of pan integrity as open pans > pin-holed lid pans > normal pans > hermetically sealed pans. Clearly solvent loss would be controlled by the size of the pin hole, and for rupturing pans, the temperature at which the seal integrity is lost. Thus, although energies can be derived for desolvation, the shape of the curve is very much sample pan dependent. A further problem, seen for example with some hydrochloride salts which are hydrates, is that the trapped moisture and the acidity of the counter ions, may lead to degradation of the sample.

Solvent loss needs to be verified by alternative techniques. The suspension of powders in a liquid, typically liquid paraffin, can lead to the visualisation of solvent release via gas formation during hot stage microscopy. The stoichiometric amount of water (or solvent) included in the crystal structure can be determined from thermogravimetic analysis. Figure 4 shows an example. Clearly, however, loss of weight may be due to decomposition and evolved or effluent gas analysis, through for instance mass spectroscopy, will confirm the nature of the volatile materials.

It should be remembered that loss of solvent may not occur as a discrete event prior to melting of the parent drug [11] or even after melting. Solvates or hydrates themselves may be polymorphic in nature. Examples include the dioxane solvate of oxazepam [23] and hydrates of nitrofurantoin [24].

Finally, although not hydrates themselves, many polymers are capable of adsorbing moisture into their chemical structure. These includes cellulose ethers [25], starches [26], and polyvinylpyrrolidone [27]. Quantification of this water can also be achieved from thermogravimetric analysis.

Isothermal microcalorimetry in conjunction with an RH perfusion cell may be used to study hydrates and solvates under isothermal conditions. The RH perfusion device manufactured by Thermometric AB [28] allows the humidifying chamber to be filled with different solvents. The interaction

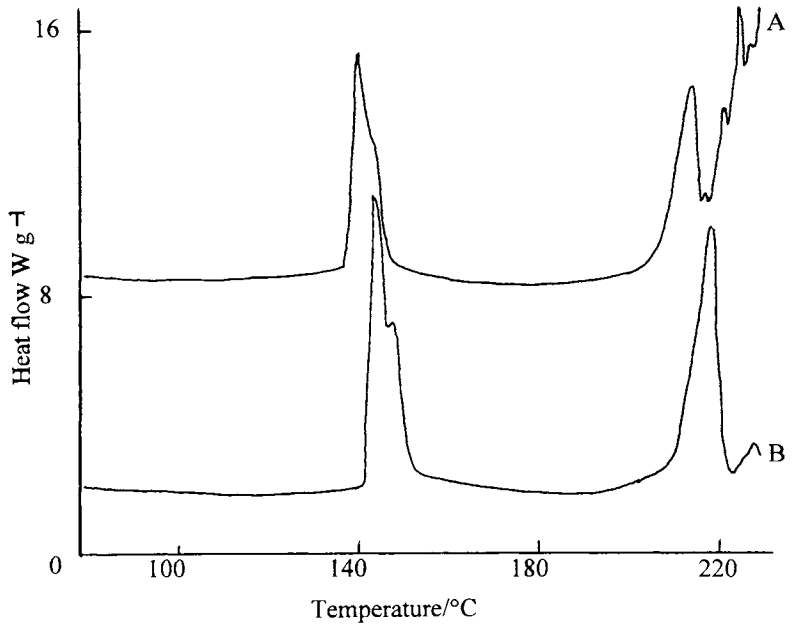

Figure 3. DSC scans of α–lactose monohydrate obtained at 10°C min^{-1} Sample A was in a pin-holed pan. Sample B was in a sealed pan.

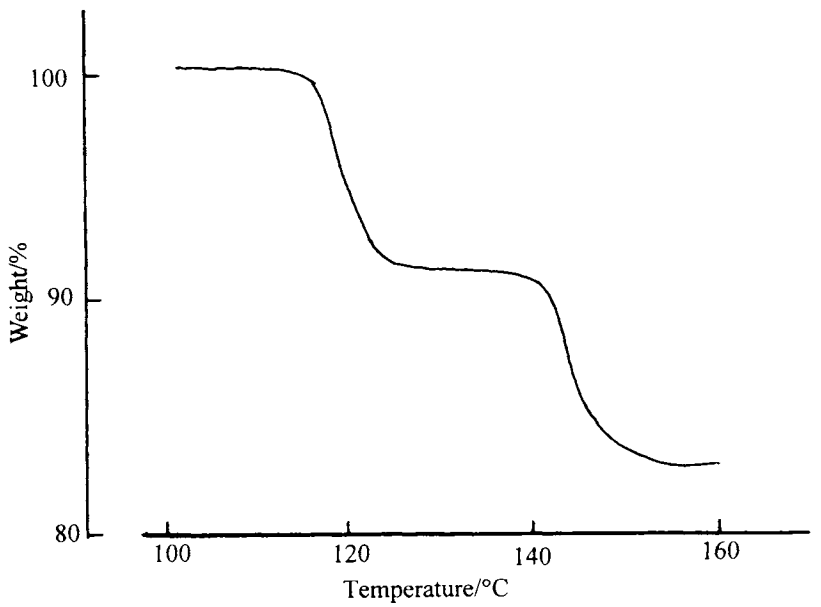

Figure 4. Schematic TG scan of a dihydrate drug losing its water of hydration in two states, via the monohydrate, to form the anhydrous drug.

between a solvent and crystal lattice may be investigated by perfusing different solvents over the crystalline material, for example to evaluate the interaction of various solvents with a drug for recrystallisation purposes. It is a simple task to measure the enthalpy change as a function of the partial pressure for different

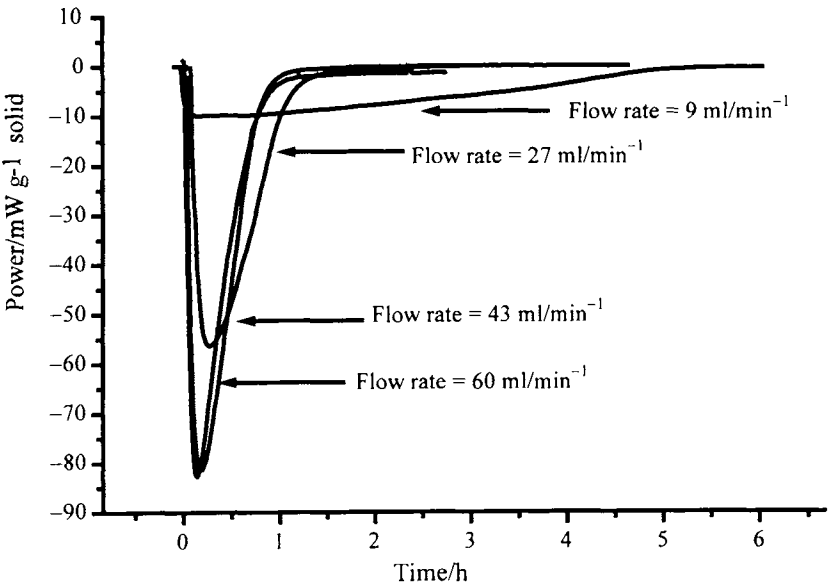

Figure 5. An isothermal microcalorimeter RH perfusion experiment showing the relationship between the rate of dehydration of a hydrate drug and air flow rate. Dehydration was achieved by taking the RH from 10 to 0% RH in a single step. At all flow rates the enthalpy change for the dehydration event was found to be 134.5 ± 2.5 J g^{-1} solid. The theoretical water content for this antibiotic is 3.6%. The enthalpy change for the vapourisation of this quantity of water is 87.84 J g^{-1}. Therefore, the excess 46 J g^{-1} can be ascribed to a morphology change associated with the removal of water from the crystal lattice. The rate of dehydration in this experiment is dependent on the air flow rate below 43 ml min^{-1}.

solvent vapours perfused over the material. The solvent with the smallest interaction (sorption enthalpy change) will have the least tendency to form a solvate with the drug.

The RH perfusion device is extremely useful in the study of water sorption behaviour of powders. Many pharmaceutical drugs and excipients are low molecular weight organic crystalline materials. It has been found that the majority of hydrate drug substances will lose their water of hydration when the environmental RH is taken close to 0% RH [29]. Figure 5 provides an example.

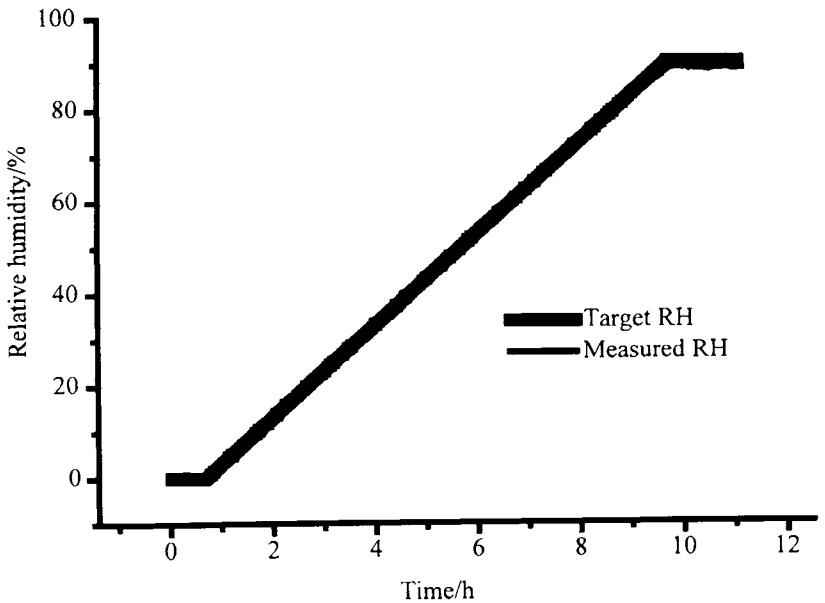

Figure 6. The RH generated in the Thermometric RH perfusion chamber was measured using a Vaisala HMP233 humidity meter customised to fit the outlet tube of the RH perfusion device. The generated RH shows good correlation with the target RH.

The RH perfusion device lends itself to such studies and the performance of the Thermometric RH perfusion device has been found to be ±1% RH from 0.5 to 95% RH (see Figure 6). The removal of the hydrate water has a corresponding enthalpy change that is proportional to the hydration state of the molecule. For this calculation, the enthalpy of vaporisation for water of 2.44kJ g^{-1} [30] can be used.

This type of analysis should be used in conjunction with other techniques that quantify the loss of mass associated with dehydration. For example, a DVS experiment can be made directly comparable with a RH perfusion experiment. DVS provides information about the mass change of a sample as a function of the RH change, whereas, the RH perfusion experiment provides information about the enthalpy change as a function of RH change, both under isothermal conditions. By interlinking the two sets of data, the equivalent mass change determined by DVS can be subtracted from the RH perfusion data leaving information about the morphological change associated with the dehydration, (see Figure 7). Many of the processing conditions during manufacture are desiccating. It is therefore useful to know the magnitude of the morphological change during dehydration so that its impact can be assessed.

Additionally, as the study is performed under isothermal conditions, it is possible to obtain kinetic information about the dehydration and subsequent re-hydration step. This, in turn, may provide mechanistic information about how the water is structured within a crystal lattice [31]. For example, it is possible to observe two kinetic regions associated with the re-sorption of a di-hydrate drug substance.

Some crystalline solids can accommodate significant amounts of water at high RH values that is not as highly structured as in conventional hydrates. This water still forms an integral part of the crystal lattice structure of the solid and so, strictly, is crystal hydrate water. Such materials are termed channel hydrates and can be thought of as being extended micro-structures within the crystal lattice that are available for hydration at high partial pressures of water vapour. For example, Figure 8 shows an antibiotic that exhibits channel hydrate behaviour. The DVS graph exemplifies typical channel hydrate behaviour where, at a critical partial pressure of water, the channels are accessible for hydration.

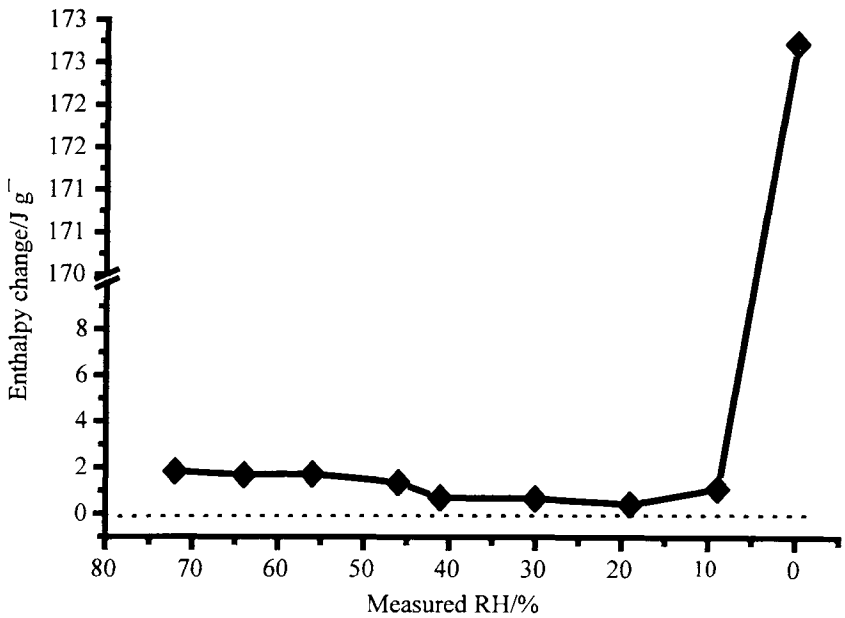

Figure 7. Desorption of a hydrate drug from 70 to 0% RH, studied using a RH perfusion chamber coupled with an isothermal microcalorimeter. This revealed a morphology change at 0% RH. Here the enthalpy change for water vapourisation was subtracted from the overall enthalpy change determined by calorimetry. The resulting graph shows the enthalpy change associated solely with drug – water interaction and morphology change. The enthalpy change for water vapourisation was determined from the mass change at each RH step measured by dynamic vapor sorption (DVS).

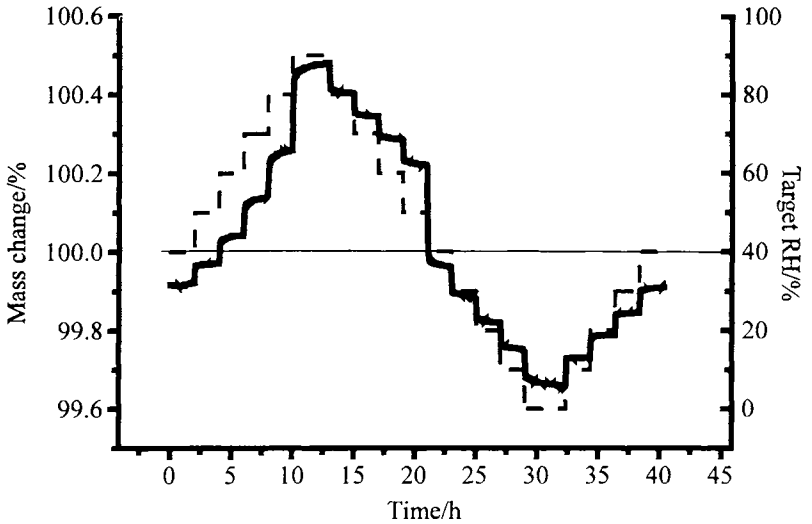

Figure 8. DVS graph for a typical channel hydrate. These are typified by a greater mass increase during the hydration step than the mass decrease during the dehydration step. The corresponding isotherm plot would show significant hysteresis. The solid line indicates the mass change.

Adsorption isotherms. Isothermal microcalorimetry, in conjunction with an RH perfusion device, is a powerful method for mapping surface properties of solids and especially drugs [32]. The principle of the study is to adsorb and desorb water vapour onto and off the surface of a solid in small steps and measure the associated enthalpy change. At low RH values, monolayer water sorption conforms to a BET (Brunauer, Emmett and Teller) model and can therefore be used to determine surface properties. The analysis of the data can be achieved by plotting the water sorption isotherm as a function of RH and fitting to a modified BET type equation [33]. This can provide information about the surface affinity for water and the hydrophilic surface area, parameters

likely to be altered by aggressive processing of the crystalline material during manufacture.

2.1.3. Hygroscopicity

Hygroscopicity is a general term used to describe materials that readily take up water in a non-structured way. Thus, the adsorbed water is not structured within a crystal lattice and is reversible. The term hygroscopicity is not a quantitative definition and so should be qualified. It is, therefore, up to each individual to define the boundary conditions that lead to the categorisation of hygroscopic and non-hygroscopic materials. As an approximation, pharmaceuticals that pick up more than 5% by mass, between 40 and 90% RH at 25°C, are described as hygroscopic. Materials that pick up less than 1%, under the same conditions are regarded as non-hygroscopic [34].

A hygroscopic material may deliquesce (where adsorbed water starts to solvate molecules of the solid) if the critical RH of the solid is lower than that of the surrounding atmosphere (Figure 9).

The calorimetric RH perfusion cell can be used to characterise the hygroscopic nature of a compound. A useful complementary technique for studying hygroscopicity is DVS [35]. The principle of operation is similar to the calorimetric RH perfusion technique except that it measures mass change as a function of RH whereas the calorimetric RH perfusion device measures enthalpy change as a function of RH. The application of both techniques to the study of hygroscopicity is sufficiently similar so that the methods of operation are described together.

A typical experimental procedure would commence at 40% RH and progress to 90% RH in small increments. At each step, sufficient time is allowed so that the sample reaches equilibrium with the environmental RH. The start point of 40% RH has been found to give the minimum amount of morphological stress to the initial material and therefore does not cause damage to the material. As the RH is progressively increased the calorimetric response will show characteristic adsorption peaks and the DVS response will show characteristic mass change steps. The quantity of water adsorbed at each step can be found directly from the mass change determined by DVS or calculated from the enthalpy change determined by calorimetry. It must be noted that the calorimetric response is the sum of all events that occur during the adsorption process. Other processes that may accompany the water sorption step, for example a morphological change, can be deduced from the difference between the calculated enthalpy change for each sorption step and the theoretical

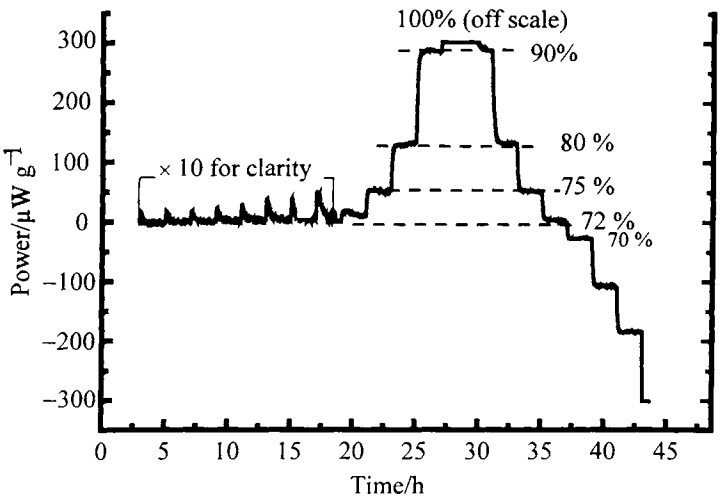

Figure 9. A RH perfusion study for crystalline sodium chloride. From 0 to 72% RH, typical water sorption exotherms are produced. Above 72% RH the water sorption no longer reaches an equilibrium, hence, the power does not return to the baseline. The sodium chloride crystal lattice begins to dissolve at 75% RH. In time all the solid will be solvated and the calorimetric signal will return to zero.

enthalpy change for the movement of water at each RH. Figure 10 gives an example of hygroscopicity.

Using these techniques hygroscopic materials can be characterised by increased water sorption at high RH values. The experimental method can be extended to examine the mechanism of the water sorption process. At 90% RH, the target RH is then taken down to 0% RH so that each equilibrium desorption step mirrors the adsorption steps. The mass change associated with water sorption onto hygroscopic materials should be equal for the adsorption and desorption at any given RH. The quantity of water taken up by each step is

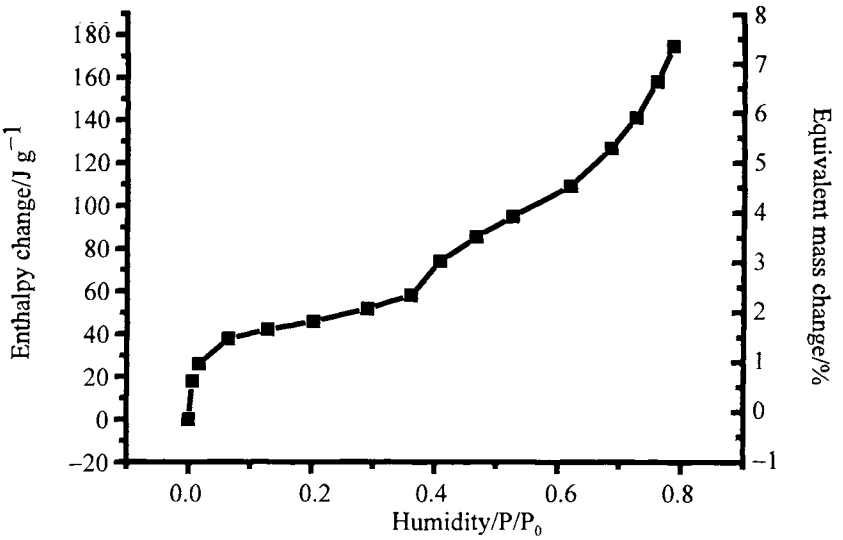

Figure 10. The enthalpy change for water vapor sorption determined as a function of RH using a RH perfusion device coupled with an isothermal microcalorimeter. Assuming a second order BET model, the enthalpy of moisture sorption was found to be 53.33 kJ mol^{-1} of water from 0 to 40% RH and 43.77 kJ mol^{-1} of water from 40 to 80% RH (close to the enthalpy change of vaporisation). The available surface area changed from 0.68 mg m^{-2} to 0.72 mg m^{-2}. The data suggest binding to the drug surface up to 40% RH then formation of multiple hydrate spheres above 40% RH.

proportional to the surface interaction between the drug substance and water. However, if water is structured into the crystal lattice the water will be retained so that the equivalent absorption masses will be different to the corresponding desorption steps.

2.1.4. Amorphousness and the glassy state

DSC and DTA allow the determination of glass transitions, the glass transition temperature T_g and at temperatures above the T_g, of any crystallisation

or subsequent melting. The techniques do not, *per se*, assess the influence of moisture on these events, although a lowering (plasticization) or increase in T_g may be seen. It must be remembered that on increasing the temperature, moisture may be lost from a sample bulk. Thus any glass transition determined may not be that of the sample prior to treatment. A glass transition can be observed for glassy drugs or amorphous polymers.

Ford [36] examined the glassy nature of several drugs. These studies were reviewed and extended by Craig and co-workers [37]. It must be emphasised that the glass transition should be checked for loss of mass by TGA. The presence of impurity, induced by previous heating, increases the tendency of drugs not to crystallise but to remain in the glassy state on cooling.

DSC or DTA might not necessarily detect changes in a material. Decomposition may lead to a false glass transition temperature and a fast heating rate may be too quick to detect changes by actually preventing recrystallisation. Slow scanning may result in an increase in decomposition; repetitive scans may depress the melting point by an accumulation of degradates. The sample pan design may also influence the quality of the DSC or DTA trace. Indeed, the shapes of the DSC scans can be modified by impurity, heating rate and particle size.

For materials in which a large proportion of glassiness is formed, DSC can lead to an estimate of the crystalline or amorphous (by subtraction) content provided the heat of fusion of the fully crystalline material is known. The heat of fusion of a sample can be percentified as a function of the heat of fusion of a standard giving the crystalline content. Clearly, the same polymorphic form should be present in both sample and standard. The technique has errors and can not be used to estimate the amorphous content when this is low, perhaps less than 5%. Re-scanning a glassy material may determine if it is subject to polymorphic modifications.

The glass transition of many drugs is readily apparent from DSC once the glass has been formed, if on heating this transition is well separated from any recrystallisation events that follow. Since the glass transition is not a kinetic event but a change in heat capacity of the material, the size of the transition is heating rate dependent. Thus the transition is larger at faster heating rates. These faster heating rates may prevent recrystallisation of the material. The transition may be obscured, for instance, by recrystallisation or endotherms due to solvent loss. This is alleviated by modulated methods of DSC. The glass transition is shown in the MDSC reversing or DDSC storage curves. Thus the transition can be seen in samples of spray-dried lactose where the glass

transition of the small portion of the sample that is in the glassy state is masked by the dehydration of the lactose [38]. Analogous separation from dehydration events can be seen in polymers such as HPMC [39] and cross linked starch products [40]. The glass transition may also be resolved from the recrystallisation events as with a novel drug candidate, Saquinvir [41].

The glass transition can also be derived from DVS studies on polymers by noting how the moisture sorption is modified as the polymer passes through the glass transition. Amorphous materials, when compared to the corresponding crystalline forms, have a greater tendency for change, i.e., the free energy ΔG is larger for the transformation. This (although as noted previously, one should not describe dissolution rates from thermodynamic terms) imparts some interesting properties such as more rapid dissolution rates and increased bio-availability. Consequently, amorphous materials tend to be hygroscopic as well as morphologically and chemically unstable. Amorphous materials are prone to recrystallise to a more stable form (with lower ΔG) if given sufficient molecular mobility through events such as raised temperature or high relative humidity. Drug products such as intravenous formulations that incorporate amorphous materials for their rapid dissolution must, therefore, be protected from both temperature and moisture during storage.

In some cases, where a drug substance is highly insoluble, associated amorphous material may be reasonably morphologically stable. In these cases it may be advantageous to include some associated amorphous material to enhance the bioavailability of the product. For both hydrophobic and hydrophilic materials, the amorphous component associated with a crystalline substance can have a profound effect on the overall performance of the product. Extreme care should be taken to understand and quantify the amorphous material. Reduction of amorphous material in poorly soluble/hydrophobic materials may drastically reduce bioavailability. An increase in amorphous content in a hydrophilic material may cause reduction in chemical stability and transformation to an inappropriate form.

Calorimetric techniques can be used to quantify accurately the amorphous content of a sample even when the sample is predominantly crystalline. Experience has shown that for a crystalline sample an amorphous content in the order of 0.5% can be routinely detected [42,43]. It is evident that rough treatment of crystalline material, such as grinding, drying or compaction, can cause damage to the crystallinity of the material and hence increase the amorphous nature [44]. As an illustration, Figure 11 shows the relationship

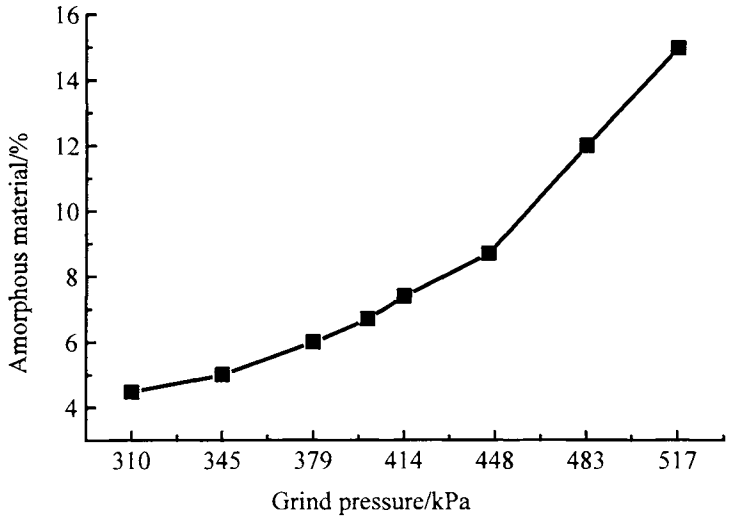

Figure 11. A solution calorimetric investigation to correlate the effect of attrition during micronisation on crystal damage. The experiment was set up to favour the dissolution of the amorphous component. Quantification of amorphous material, from the micronisation study, was made by comparison of the enthalpy change on dissolution to that of 100% amorphous material. Normal grinding pressure (feed pressure) for this material would be in the order of 448 kPa.

between the quantity of amorphous material and grind pressure when a crystalline material is passed through a micronising mill.

In addition to conventional techniques used to observe amorphous material, such as DVS and XPRD, isothermal microcalorimetry and solution calorimetry can be used to observe and accurately quantify amorphous materials.

Isothermal microcalorimetry. The study of amorphous materials using microcalorimetry relies on the physical properties of the amorphous fraction being significantly different to the crystalline form. In general, amorphous materials tend to be hydrophilic and thermodynamically unstable. If maintained in a high RH environment, the amorphous material would eventually

recrystallise. The thesis is that the environment provides sufficient "plasticity" to the material so that molecular re-orientation can occur (the same principle applies to recrystallisation of amorphous materials using thermal analysis, although here increased temperature provides the extra mobility to the solid). Organic solvents can be used to encourage recrystallisation where a drug is excessively hydrophobic.

The crystallisation of amorphous material has an associated enthalpy change that can be measured using isothermal microcalorimetry. Providing the observed calorimetric signal can be calibrated using 100% amorphous material, the measured enthalpy change is directly proportional to the quantity of amorphous material present.

The crystallisation of an amorphous material tends to be a co-operative event, that is, all the amorphous material tends to crystallise together when sufficient water has been adsorbed. The time taken for the recrystallisation event to occur can be regulated by the quantity of amorphous material present, the RH to which the material is subjected, and the temperature of the study. Figure 12 shows a typical calorimetric signal for the recrystallisation of an oral antibiotic. Here the reaction chamber was regulated at 80% RH and 40°C. For a good analysis of the data there should be sufficient separation of the water adsorption peak and the recrystallisation peak. This can be achieved by trial and error selecting different reaction conditions (temperature, relative humidity and quantity of material) to optimise the peak separation. Further information may be found in reference [45].

Solution calorimetry. There are two methods that can be used to quantify amorphous material based on solution calorimetry. The first method exploits differences in the rate of dissolution of the amorphous material compared to the crystalline form. The second method exploits the difference in enthalpy change of dissolution for the amorphous content compared to the crystalline form.

In general, the amorphous form of a crystalline drug substance will dissolve more rapidly and initially, to a higher concentration [46]. A quantitative analysis of amorphous material in an essentially crystalline sample can be made if the rate of dissolution of the amorphous form is significantly different to the corresponding crystalline form. The technique is to disperse the sample into a discriminating solvent e.g. water within the solution calorimeter, and measure the enthalpy change for essentially the most rapidly dissolving material. Where the rate of dissolution of the amorphous form is significantly faster than that of

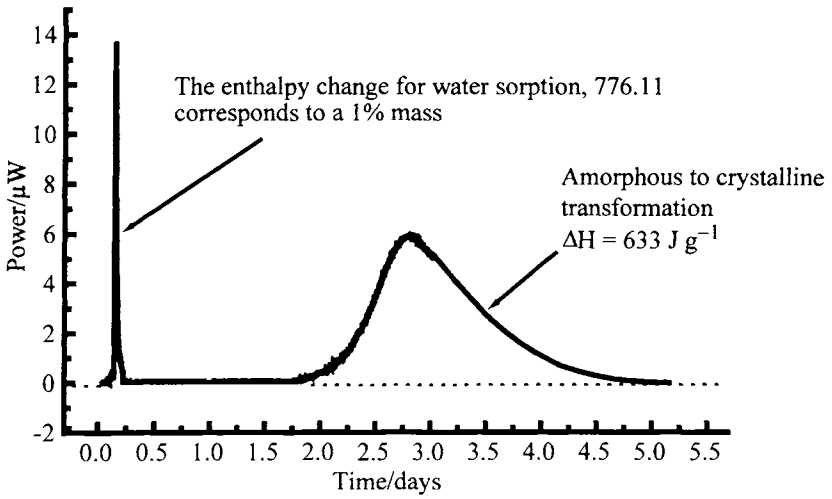

Figure 12. An RH perfusion device, coupled to an isothermal microcalorimeter was used to study an amorphous to crystalline transformation of a lyophilised drug. The calorimetric signal shows an initial water sorption exotherm as the RH within the perfusion device is changed from 40% RH to 80% RH. There is then a delay followed by recrystallisation of the material. The interval between adsorption and crystallisation is, presumably, related to random nucleation. However there is probably a dependency on hydrophobicity, sample mass, the relative humidity of the chamber and temperature. As a comparison, amorphous β-lactose monohydrate, under the same conditions as above, would take about 30 minutes to recrystallise.

the crystalline form the observed signal can be used to quantify the amorphous content.

Differences in the thermodynamics of dissolution can also be exploited for a quantification of amorphous component. Here a solvent is chosen that will allow rapid and total dissolution for both the crystalline and amorphous

components. The solvent can be conveniently chosen using solubility parameters [47], where the solubility parameter for the solid is determined and compared with the solubility parameters of various solvents. The solvents with a solubility parameter close to that for the solid is likely to give the best dissolution.

The choice between the kinetic or the thermodynamic method of analysis of amorphous materials depends on the dissolution rate and the enthalpy of dissolution of the solid. If the crystalline material is very water-soluble or the amorphous component is very hydrophobic then the thermodynamic method for analysis should be used. However if the crystal lattice energy is small and, therefore, the enthalpy of dissolution of the crystalline material is similar to that of the amorphous material, the kinetic method for analysis should be used.

2.1.5. Purity

Purity determination by DSC is based on the depression of melting point by an impurity and its relationship with the van't Hoff equation. The method suffers from a major disadvantage that the composition of the impurity(s) is NOT known.

DSC (and to a lesser extent DTA) gives valuable information on the melting of drugs and excipients. Easily determined are extrapolated onset temperatures, peak temperatures and true onset temperatures. Coupled with the derived knowledge of the heat of fusion and how melting changes may occur on reheating, and indeed changes on recrystallisation on cooling, the polymorphic modifications of the material can be easily characterised. (See Section 2.1.1). It must always be emphasised that ancillary techniques should be used to confirm these suspected changes. Hot stage microscopy (and associated video replaying facilities) enable the changes to be interpreted. Infra-red spectra and X-ray diffraction patterns further give information on the polymorphic form. However, a simple observation of the width of the melting endotherm, and the depression of melting point are indicative of the purity of a material. The inclusion of an impurity will lead to a depression of melting point, provided the impurity is miscible in the liquid melt. The relationship between impurities and melting point depression is well established from the van't Hoff equation (Equation 1):

$$T_m = T_o - \frac{R\,T_o^2\,X_2}{\Delta H_o} \cdot \frac{1}{F} \qquad (1)$$

where T_m is the sample at equilibrium (K), T_0 is the melting point (K) of the pure component, R is the gas constant, X_2 is the concentration of impurity (mole fraction) and F is the fraction molten at T_m. This equation gives a straight line when T_m is plotted against $1/F$. The slope is equal to the term $(RT_o^2 / \Delta H_o)X_2$ and when $F = 1$, i.e. all the sample is melted, the difference between T_0 and T_m corresponds to the melting point depression brought about by the impurity. Clearly, an estimate of purity may be derived from a single DSC scan. The fraction melted in a melting endotherm can be determined by the fraction of the area under the curve to a certain temperature divided by the total melting area. The true melting point of the pure material T_0 can be derived from the slope of the van't Hoff plot. One problem is that the van't Hoff equation is based on the sample being in equilibrium. This is not true since the sample is being heated. This is compensated by, but not entirely corrected for, by scanning at slow speeds, preferably less than 1°C min^{-1}.

Figure 13 demonstrates the technique for estimating the purity of indomethacin. Pharmaceutically, however the method has a large number of limitations. The pre-requisite is that the impurity should be known: it itself may possess pharmacological or toxicological side effects. The thermal method of purity determination does not identify the impurity. Since the method relies on depression of melting point via eutectic formation, materials that form solid solutions do not obey the van't Hoff predictions and corrections are needed that are only partly quantitative. It is axiomatic that many impurities will have similar chemical structures to the drug molecule and are therefore likely to form solid solutions. Additionally, materials that do not form eutectics are not detected by the method. Glass particles or fumed silica are examples of materials that, in the normal scanning ranges for a drug, do not melt, and if present as impurities, would not cause a change in endotherm shape. Thus their presence will go undetected, apart from when the heats of fusion of the drug are known. Values for this enthalpy will be reduced by the impurity, but at low contaminating levels, not by a level sufficient to produce an enthalpy significantly different to that of the drug.

The slow scanning rates required for establishment of quasi-equilibrium may also cause decomposition during the scanning process, thus lowering the apparent purity of the drug. Since such decomposition may be particle size dependent, further complications to purity determination are obvious. It is probable that although DSC can lead to a rapidly determined estimate of impurity, it should only be used as an impromptu estimate during stages of chemical synthesis. Reliance on the method for a final quality measurement is

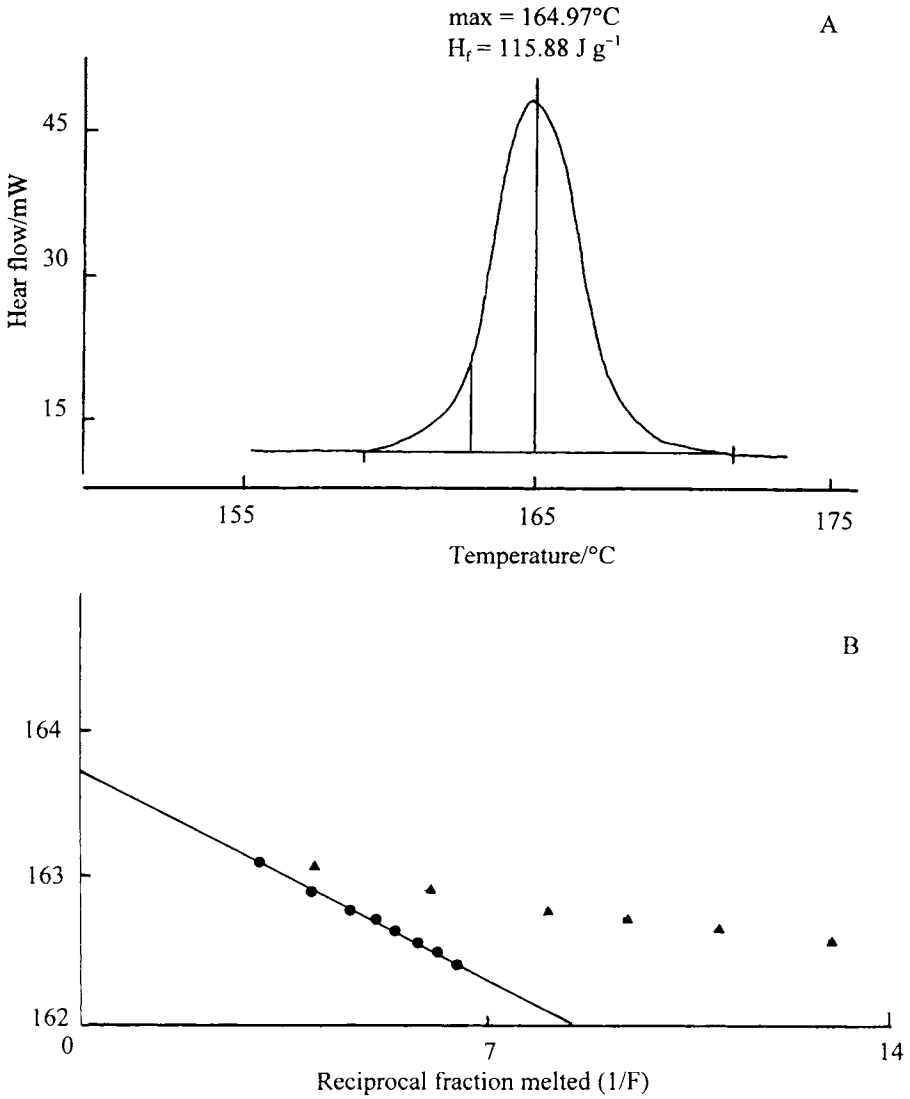

Figure 13. DSC plot of indomethacin (A), obtained at 1°C min^{-1} showing the melting transition and representative areas. The peak was from 158.72° to 170.81°C and the peak area from 162.76° to 164.92°C was used to produce the van't Hoff plot (B) which gave a heat of fusion of 46216.87 J mol^{-1}. The T_m and T_0 values were 163.51 and 163.7°C respectively. An x-correction of 11.77% gave a purity value of 99.44%. The van't Hoff plot of temperature against reciprocal of the fraction melted (1/F) shows corrected (•) and uncorrected (♉) data.

uncertain. Giron and Goldbron [48] highlighted the uses of DSC purity determinations and suggested that:

1. The method was attractive because the low sample size meant the technique could be used when small amounts of material were available, as in early development.
2. A very fast analysis time could be used.
3. The method should not replace chromatographic methods that determined levels of specific impurities.

Attempts have regularly been described that are developed on standards. For instance, Yamamoto et al [49] used a test material based on ethyl-ρ-aminobenzoate and n-butyl-ρ-hydroxybenzoate. The authors derived the solubility curve and showed that the phenomenon in which ρ-aminobenzoate dissolved in the melted eutectic mixture was close to ideal solutions based on Raoult's law. The heat of mixing, at infinite dilution was given a value of $-1.9\ J\ g^{-1}$. Therefore, the heat of dissolution and heat of fusion coincided within the allowable error.

Yamamoto et al [50] also considered that the stepwise method was more accurate than the dynamic method. Yoshii [51] noted a number of problems including lack of reproducibility between instruments. Additionally:

(a) the analytical region in the linearisation of the van't Hoff plot influenced the purity result,
(b) calibration of heat resistance with indium had little effect, and
(c) a calculation without a eutectic peak area overestimated the purity.

Yoshii [51] considered that appropriate conditions for purity determinations were 1 ± 0.1 mg sample size, $2°C/min^{-1}$ as heating rate and linearisation of the van't Hoff plot in the 10-50% peak height. Paracetamol was considered to be an unsuitable drug for purity analysis because of other phase transitions [51]. The technique has been extended to examine the enantiomeric purity of chiral drugs [52,53].

3. CHEMICAL STABILITY STUDIES

3.1. Chemical stability studies of solutions

Traditionally chemical stability studies are performed using relatively long term studies that involve artificially stressing the material at elevated temperature and RH conditions. The degradation products formed are then measured using photospectroscopic techniques. These methods of analysis are very costly and time consuming and provide little information about the long-

term stability of the sample under ambient conditions. Isothermal microcalorimeters with nanoWatt technology provide the opportunity to measure extremely small enthalpy changes. The stability of the instrument allows such studies to be made over relatively long time periods with confidence that the drift in the signal is negligible [54]. The advent of nanoWatt technology (and picoWatt technology to be soon developed) allows a signal of about 10 nW to be measured [55]. If the instrument is carefully set-up and located, it is possible to observe a calorimetric response in the order of 5 nW, see Figure 14. In terms of a chemical degradation study, a 3 g sample with a reaction enthalpy change of 95 kJ mol^{-1}, a molecular weight of 500 and a degradation rate of 0.08% per year (2207 year life time assuming first order kinetics) will produce a signal of 14 nW. This is well within the specified detection limit of the instrument.

This capability for measuring chemical degradation over relatively short observation periods may prove to be an extremely powerful analytical technique that could greatly support conventional chemical stability studies or in some cases replace them altogether. The use of isothermal microcalorimetry in the study of chemical stability in the solution phase is relatively straightforward. The sample is placed in the reaction ampoule and measurements are made. However the difficulty arises in interpretation of the data and, in particular, with reaction kinetics. This is reflected in the literature where attempts to analyse reaction kinetics are normally reserved for first order reactions that are relatively easy to solve. However, there are some promising methods for data analysis which may be divided into three categories. The choice of method depends on the information required from the study.

The first method is a simple approach where an observation of a calorimetric signal that is not at the baseline is indicative of a chemical reaction. Reactions in the solution phase are not complicated by morphological changes. However, care should be taken that the observed calorimetric signal is for a chemical reaction and not a physical change, such as precipitation. This non-quantitative method of analysis is useful as a screen for potentially unstable compounds.

The second approach is slightly more useful in that a quantitative analysis can be made if the reaction rate is sufficiently fast so that the observation period captures a significant proportion of the overall reaction. The progress of a reaction can be determined by the ratio of area under the calorimetric curve at any time to the area at infinite time.

The final method is a sophisticated analysis of the data that allows the calculation of the kinetic, thermodynamic and mechanistic parameters to

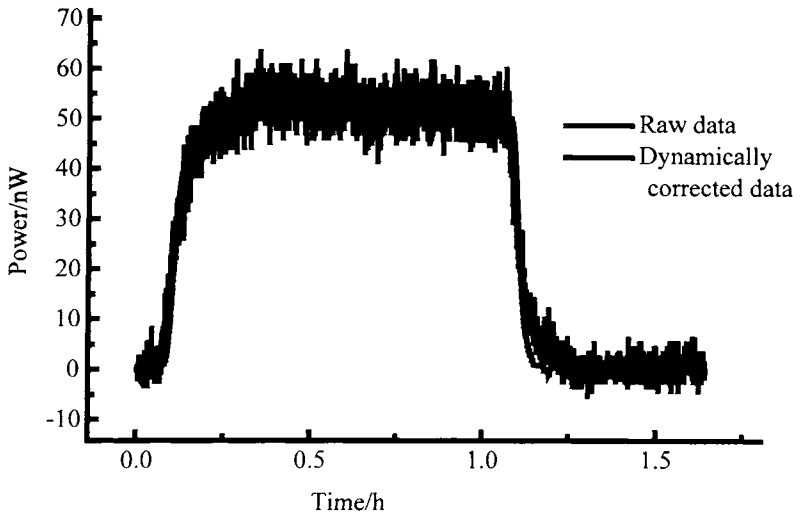

Figure 14. The response for an electrical impulse into the reaction chamber of an isothermal microcalorimeter of 50 nW. The analysis of this result provides a basis for a performance certification of the instrument. In this case for an instrument set up at 25°C, fitted with a nano Watt detector, the overall noise level for raw data is 3.17 nW, and 12.2 nW over 24 h. The time response of the reaction chamber was found to be 97 sec.

describe the chemical reaction. Having calculated these parameters accurate predictions on the reaction rate can be determined. Full details of this method of analysis are given by Willson and co-workers [54, 56]. The advantage of this method of analysis is that the calculated reaction parameters are "real" kinetic, thermodynamic and mechanistic parameters. These give specific information about the chemical reaction. Secondly, only a small fraction of the total reaction need be observed. From this observation period, the reaction parameters

calculated apply for the whole of the reaction and accurate predictions about the total reaction time can be made. Examples of application include:

3.1.1. Simple observation of the calorimetric signal

This is a non quantitative method of analysis. The method of analysis is to place a compound into the calorimeter and observe the resulting signal. A signal that remains at the baseline is indicative of a non reacting system. For example see Figure 15.

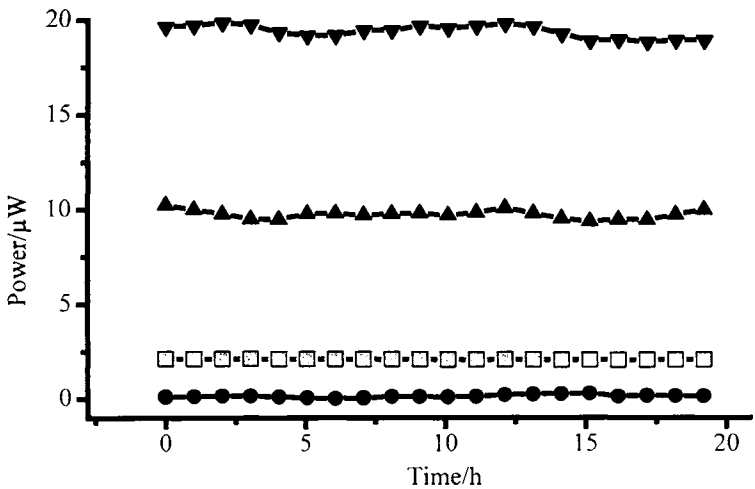

Figure 15. The gas perfusion device coupled with an isothermal microcalorimeter provides an opportunity to assess chemical interactions with reactive gases. Here an antibiotic drug was perfused with nitrogen (-●-), air (-■-), ammonia (-▲-) or oxygen (-▼-). A calorimetric response displaced from the baseline can be ascribed to a reaction between the gas and the drug.

3.1.2. The determination of reaction extent using fractions

This method of analysis only gives reasonable results if the observation period forms a significant percentage of the total reaction time. The analysis requires a polynomial-type fit to the data that can be extrapolated to infinite time, i.e. when the reaction has gone to completion. The extent of reaction at any time can then be found by integration of the curve to that time and proportioning the area to the total area at infinite time, an example being Figure 16.

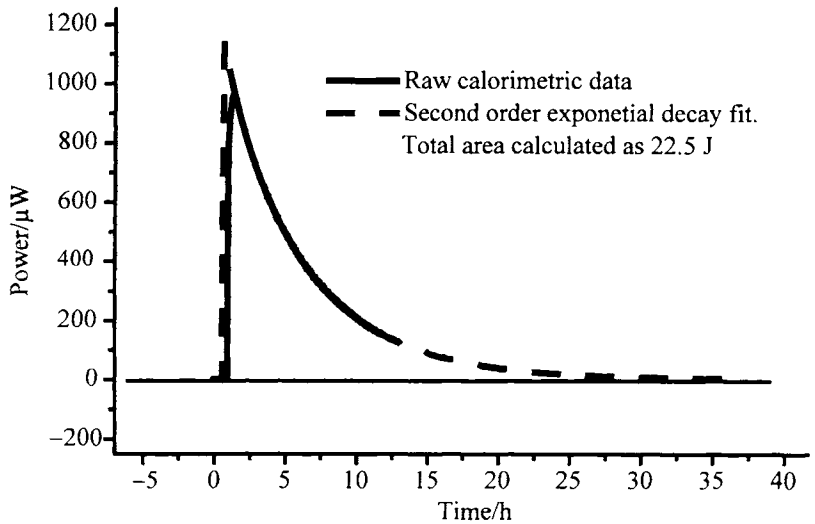

Figure 16. A isothermal microcalorimetric study for the degradation of Cimetidine at 40°C and in 1M HCl. The analysis of the data was made by fitting a second order exponential decay curve (Chi^2 = 0.09869). The resulting curve can then be extrapolated from t = 0 to t = ∞. The integration of this curve provides the enthalpy change for the reaction (Q). The percentage reacted at any time can then be expressed by integrating to a defined time point (q) and calculating q/Q × 100 to give the percentage of reaction at any time.

3.1.3. The calculation of the kinetic and thermodynamic parameters that specifically describe the reaction

This method of analysis can be applied to reactions of any order. The theory for the analysis is to calculate the kinetic, thermodynamic and mechanistic parameters that will describe the reaction. For example a mono molecular reaction (for simplicity) can be described by Equation (2).

$$-\frac{dx}{dt} = k.(A - x)^n \tag{2}$$

where A is the initial quantity of reactant, x is the quantity reacted at time t, k is the rate constant and n is the reaction order. Equation (2) can be transformed to describe calorimetric data by substitution because:

$$q = x \times \Delta H \tag{3}$$

The enthalpy change at time t, (q) is equal to the quantity reacted at time t multiplied by the total enthalpy change for the reaction. Substitution for (x) in equation (2) gives Equation (4):

$$-\frac{dq}{dt} = k.\Delta H^{1-n}.(Q - q)^n \tag{4}$$

The rate constant in Equation (4) is, in fact, dependent on volume. In the majority of publications concerning solution phase reactions, the rate constant is not corrected for volume and different results for different concentrations are obtained. A volume term can be added to Equation (4) to give Equation (5):

$$-\frac{dq}{dt} = k \times \Delta H^{1-n}(\frac{Q - q}{V})^n \tag{5}$$

In Equation (5), Q is the enthalpy change for the reaction and V is the volume of the solution. Integration of Equation (5) gives Equation (6) and shows the relationship between the calorimetric signal and time, for solution phase reactions.

$$-\frac{dq}{dt} = k \times \Delta H \left[\frac{V}{k \times t \times n - k \times t + \left(\frac{V}{A}\right)^{n} \times A} \right]^{\frac{n}{n-1}} \quad (6)$$

The strategy for the analysis of the data is calculation of the reaction order (n), calculation of the enthalpy change (ΔH) and calculation of the rate constant (k).

3.1.4. Calculation of the reaction order (n)

The order of a reaction can be determined from the ratio of two time points corresponding to two values of dq/dt selected from the power-time calorimetric data [54]. It has been found that for two values of dq/dt that are a given percentage of the initial calorimetric signal (ie dq/dt when time = 0), the ratio of the corresponding times t_1 and t_2 is a constant. This constant is dependent only on the reaction order [54]. There is no dependency on rate constant, enthalpy change or quantity of material involved in the reaction. There is also no constraint on where the initial calorimetric signal is taken. In practice, a point near the start of the observation period is selected as the initial signal. The principle of the analysis is to simulate calorimetric data as a function of reaction order. The t_2/t_1 constant from the simulated data can then be compared to the t_2/t_1 constant derived from the experimental data and the reaction order determined (Table 1).

The values for t_1 and t_2 can then be normalised to t = 0 by subtraction of the time value that corresponds to this initial power value. For example, if dq/dt_1 is 94% of the initial calorimetric signal and dq/dt_2 is 4% of the initial calorimetric signal then the t_2/t_1 constant will be about 52 for a first order reaction, 127 for a second order reaction and 156 for a 2.5 order reaction, etc. In practice, the analysis should be performed using a mathematical algorithm in a spread sheet, such as Mathcad™[57]. The analysis can be set up to perform a calculation for every data point in the data set and the statistical evaluation made.

3.1.5. The calculation of the enthalpy change and rate constant

From Equation 6, the initial quantity of material (A) loaded into the calorimeter, the sample volume (V) and the reaction order (n) are known. k and ΔH can be solved by a simultaneous equation using different values of dq/dt

Table 1.
The reaction order can be determined directly from the data by choosing two data points from separate regions of the reaction signal. Here, for example, data points were chosen at 94% and 4% of the initial signal. The corresponding t_2t_1 are 52 for a first order reaction, 127 for a second order reaction and 156 for a 2.5 order reaction, etc.

Reaction order (n)	t_2/t_1
0.8	36
0.9	44
1.0	52
1.1	60
1.2	68
1.3	76
1.4	84
1.5	92
1.6	100
1.7	107
1.8	114
1.9	121
2.0	127
2.1	133
2.2	139
2.3	145
2.4	150
2.5	156

with the associated time values. This can be accomplished using a suitable graphic-fitting program such as Origin™ [58] or a mathematical type spread sheet such as Mathcad™ [57].

Having found the values for k, ΔH and n, a simulated calorimetric signal can be constructed for the reaction over any time interval and the extent of reaction determined. The reaction half life ($t_{1/2}$) can be found from Equation (7):

$$t_{\frac{1}{2}} = \frac{2^{n-1} - 1}{(n-1) \cdot k \cdot A^{n-1}} \tag{7}$$

A standard test reaction can be performed in the calorimeter and analysed using the above method. This should provide confidence for the application of the method. The imidazole catalysed hydrolysis of triacetin [54,59] may be used as such a standard reaction because of the extensive characterisation it has received. Not only would this provide an opportunity to test the ability to recover the reaction parameters from the data but also to provide information about the performance of the calorimeter being used. Using the reaction conditions of 0.18 g triacetin mixed with 3 ml imidazole buffer (the imidazole buffer consists of 1.6 g ethanoic acid plus 2.72 g imidazole in 10 ml water), the solutions were thoroughly mixed in 3 ml glass ampoules and loaded into the calorimeter at 25°C [59]. This reaction can be studied over long time periods (weeks) so that the long-term performance of the calorimeter can be determined. An observation period at about 120 h is recommended for an initial study where confidence may be gained in the experimental results for a good separation on the y axis of the initial and final data points. The analysis of the data yields the reaction parameters; reaction order (n) of 2, an enthalpy change of 95.2 kJ mol^{-1} and a rate constant of 4.73 x10^{-5} dm^3 mol^{-1} s^{-1}. Willson et al [54] gave the rate constant is given as 8.64x10^{-4} dm^3 mol^{-1} s^{-1}. This is a rate constant that is dependent on concentration. For solution phase reactions, in general, the concentration dependent rate constant (the rate constant that is normally erroneously stated) can be converted to the concentration independent rate constant by use of Equation (8):

$$k = k_{obs} V^{n-1} \tag{8}$$

In equation (8), V is the volume of reaction sample and (n) is the reaction order. Figure 17 shows an observation period of 50 days for the hydrolysis of triacetin. Fifty days represent 70% of reaction completion (~8% in time). The analysis of this data shows that the isothermal microcalorimeter has sufficiently long term baseline stability to allow observations over this time period. This is

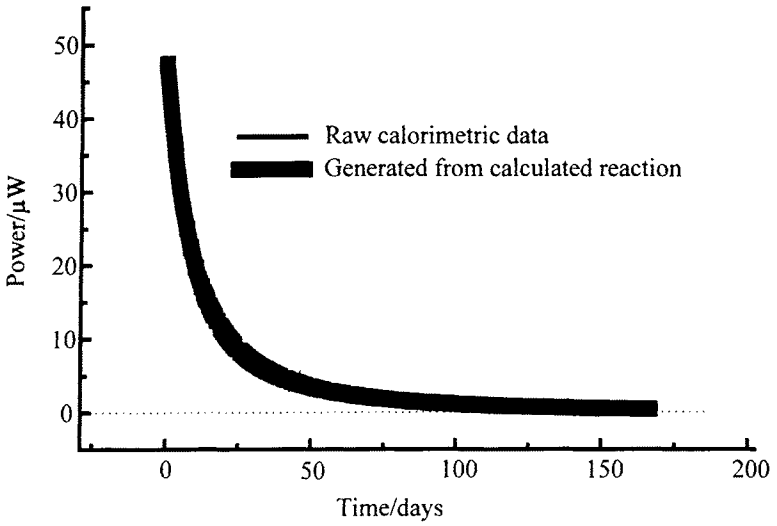

Figure 17. The imidizole catalysed hydrolysis of triacetin as followed in an isothermal microcalorimeter at 25°C. The study was performed over a 50 day period to assess the performance of the instrument over long time periods of continuous use. The analysis of the calorimetric data gives values for the rate constant of $8.64 \times 10^{-4} \pm 1.5 \times 10^{-5}$ dm^3 mol^{-1} s^{-1}, enthalpy change of 95.2 ± 1.6 kJ mol^{-1} and a reaction order of 2. Using these parameters the reaction signal from time = 0 to time = ∞ can be simulated.

essential for studying slow reactions (Table 2) where baseline noise increasingly contributes to the error associated with the calculation of the reaction parameters.

Other examples for the application of this analytical method to other types of solution phase reactions can be found elsewhere [60,61].

As a purely academic exercise, calorimetric data can be simulated using Equation (6). To this, different degrees of error can be added representing noise in the calorimetric signal. An investigation can then be made as to the degree of

Table 2.
A rational nomenclature suggested for the classification of reaction rates.

First Order Rate Constant	Half life	Percent reaction completed	
1×10^{-2}	69 s	<1% s^{-1}	Fast reaction
1×10^{-3}	693 s	1% s^{-1}	
1×10^{-4}	1.9 h	30% h^{-1}	
1×10^{-5}	19.25 h	3.5% h^{-1}	Medium reaction
1×10^{-6}	8 days	8% day^{-1}	
1×10^{-7}	11.5 weeks	5.8% $week^{-1}$	
1×10^{-8}	2.2 years	2.4% $month^{-1}$	
1×10^{-9}	22 years	3% $year^{-1}$	Slow reactions
1×10^{-10}	222 years	0.3% $year^{-1}$	
1×10^{-11}	2207 years	0.03% $year^{-1}$	

error in the simulated calorimetric signal that will still allow the correct reaction parameters to be recovered. This provides the basis of a validation for the data analysis where the lowest quality of the calorimetric data acceptable for analysis can be defined. Figure 18 shows simulated data for a reaction with a rate constant of 3.7×10^{-4}, an enthalpy change of 33.3 kJ mol^{-1}, a reaction quantity of 0.00116 mol and a reaction order (n) of 1.6. To this simulated data, a random error of between 1 and 6 TW was added.

The analysis of the data for a 48 h observation time period returned a reaction order of 1.6. Figure 19 shows the distribution of the calculated reaction order for each data point in the analysis. The calculation of reaction rate constant and enthalpy change gave good agreement with the initial values chosen. By progressively adding different degrees of error to the simulated data, it was found that there is a relationship between the signal to noise ratio and the required duration of the observation period. Although purely empirical, Equation (9) predicts this relationship.

$$Ln\left(\frac{NSR}{0.00016}\right) \times 0.0735 = \%\ signal\ change \qquad (9)$$

where NSR is the error amplitude divided by the initial calorimetric signal. The % signal change is the difference between the signal at time = 0 and the signal at the end of the observation period. The results become more accurate with increase in this separation.

An equation such as Equation (9) may be useful in determining quickly how long a reaction should be left to run to ensure the successful calculation of the reaction parameters. Because the noise to signal ratio is determined at the start

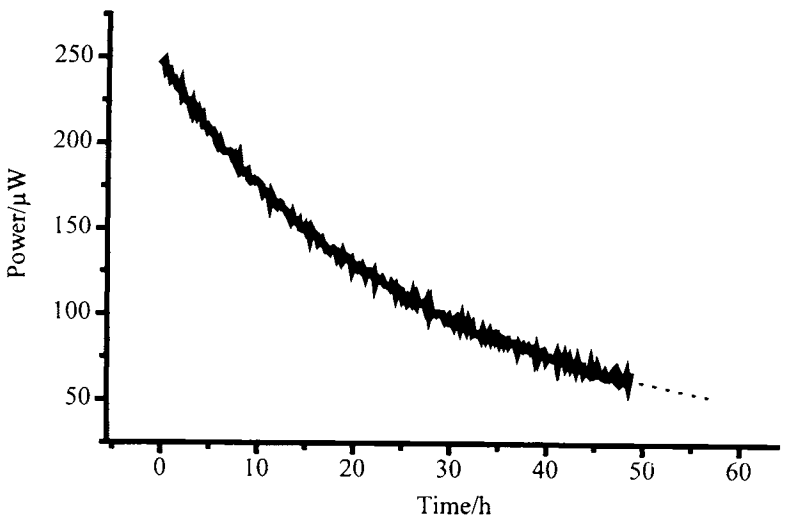

Figure 18. A simulated calorimetric signal was constructed using the reaction parameters of; k=3.7 × 10^{-4}, ΔH=33.3 kJ mol^{-1}, A = 0.00116 mols and n=1.6. To this a random error of between 1 and 6 μW was added. The resulting data was analysed to determine if the original reaction parameters could be recovered. The results shown in the above graph are reassuringly close to the initial reaction parameters.

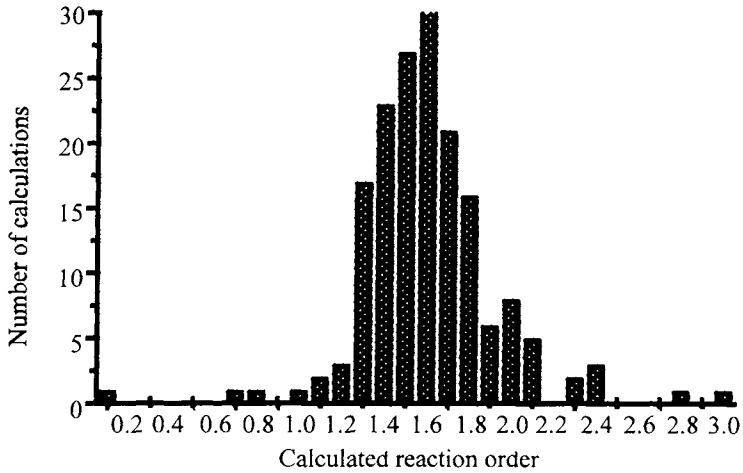

Figure 19. A distribution plot for the calculation of reaction order. The number of calculations made relate to pairs of data points from the simulated data set, with added error as seen in Figure 18. The initial reaction order of 1.6, used to simulate the data set, is confidently recovered in the analysis.

of the reaction, the % signal change that is required for an accurate analysis of the data, may be calculated at the onset of the experiment. The experiment can then be run until this point is reached.

3.2. Chemical stability study of the solid state

There have been many attempts to derive a comprehensive model for solid state reactions, however, no completely satisfactory method has been applied universally. This probably reflects the complex nature of a solid state reaction. This problem must be addressed if general predictions are to be made about the long-term stability of drugs in the solid state.

Solid state reactions have, in the main, been modelled on the bases of areas of stress or points of damage to the crystal lattice that propagate solid state degradation. Mathematical models describing such mechanisms of solid state degradation have been suggested [62,63,64] where the fraction of reacted material in three dimensional space is calculated as a function of time. These models are based on thermal decomposition where at least one product is a gas. Such reactions give sigmoidal curves when the fraction of material that has reacted is plotted against time (Figure 20). The shape of the sigmoidal-type

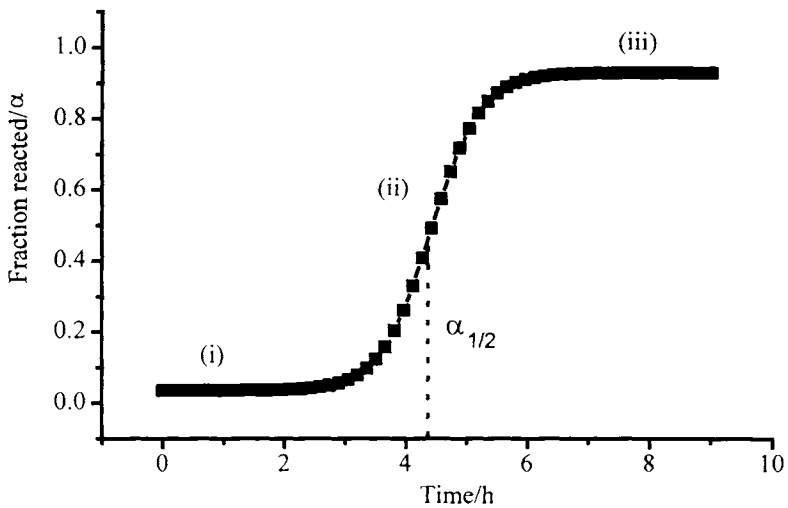

Figure 20. A typical solid state fractional degradation curve. The curve is characterised by three areas; (I) the induction phase, where there is growth of reactive sites; (ii) the acceleration phase where the rate of reaction reaches a maximum; (iii) the lag phase where the reaction finally terminates. $\alpha_{1/2}$ corresponds to the reaction half life.

curve is dependent on three phases of the reaction; induction, acceleration and decline. The relationship between the three phases can provide information about the mechanism of the solid state reaction. Table 3 shows the derived mathematical models for various combinations of the three phases.

Table 3.
The equations for various solid state degradation models. (p) and (q) are fitting parameters related to the mechanism of reaction. $\alpha_{1/2}$ is the half life of the reaction.

p	q	$\alpha_{1/2}$		
1	1	-	$d\alpha/dt = k$	Linear
0	1	1	$d\alpha/dt = k.\alpha$	Exponential
1/2	1	1	$d\alpha/dt\ k.\alpha^{1/2}$	Square
1	0	0	$d\alpha/dt = k\,(1-\alpha)$	Unimolecular decay
1	1/*n*	0	$d\alpha/dt = k(1-\alpha)^{1-1/n}$	Contracting envelope
1	1/2	0	$d\alpha/dt = k.(1-\alpha)^{1/2}$	Contracting surface
1	1/3	0	$d\alpha/dt = k.(1-\alpha)^{2/3}$	Contracting sphere
0	0	0.5	$d\alpha/dt = k.\alpha.(1-\alpha)$	Prout-Tompkins
1/3	1/3	0.5	$d\alpha/dt = k.\alpha^{2/3}\,(1-\alpha)^{2/3}$	Roginskii-Shultz
0.2	0.36	0.56	$d\alpha/dt = k.\alpha^{0.8}\,(1-\alpha)^{0.64}$	Erofeev

Equations such as the general Ng equation (Equation (10)) are commonly used to model solid state reactions, where the rate of reaction is plotted against the fraction of degradation.

$$\frac{d\alpha}{dt} = k \times \alpha^{p} \times (1-\alpha)^{r} \tag{10}$$

where k is the solid state rate constant, α is the fraction reacted and p, r are reaction parameters relating to the reaction model. Equation (10) can be applied to calorimetric data by substitution for α to give Equation (11):

$$q = \alpha \times Q \tag{11}$$

which gives Equation (12):

$$\frac{dq}{dt} = k.Q.\left(\frac{q}{Q}\right)^{p}.\left(1-\frac{q}{Q}\right)^{r} \tag{12}$$

In equation (12), dq/dt is the calorimetric signal, q is the enthalpy change at time t and Q is the total enthalpy for the reaction. At present p and r can not be determined independently of the other reaction parameters. Therefore this method of analysis is restricted to reactions where (Q) can be found experimentally. The observation period must therefore be sufficiently long so that (Q) can be determined directly. This is a severe limitation for the analysis of solid state reactions that must be resolved. Progress is, however, being made. Having found (Q) by integration of the calorimetric data, the other reaction parameters, k, p and r can be determined by iteration. A plot of dq/dt vs. q is made using a graphics fitting computer program such as Origin™ [58]. Equation (12) is then applied in the iterative procedure to solve for k, p and r.

Isothermal microcalorimetry has proved useful for the study of solid state reactions giving rise to information about the reaction model and hence the reaction mechanism [65,66]. Additional studies have been performed where a satisfactory outcome of the data analysis was achieved [67-71].

Reaction kinetics from DSC, DTA or TGA, have been used to examine the stability of a limited number of pharmaceutical materials. Various models have been used including the Power Law, Avarami-Erofeev and Prout-Tomkins models [72]. These methods are also based on the Kissinger [73], ASTME 698 [74] or Ozawa [75] methods [8]. Most frequently, they have been applied to the dehydration of various materials such as theophylline monohydrate [76], phenobarbitone monohydrate or hemihydrate [77], phenylbutazone [78], oxazepam [23] and trazodone tetrahydrate [79]. The uses are limited for pharmaceutical systems, not least because dehydration is particle size dependent. Thermal analysis, especially DSC, DTA and TG, has been used outside the pharmaceutical area in the prediction of reaction kinetics as described elsewhere in this handbook. Methods used include those by Borchart and Daniels [80], Kissinger [73], Freeman and Carroll [81] and Flynn and Wall [82]. Although these techniques are well established and, if used properly, can give pertinent information, their use in pharmaceutical arenas is restricted to dehydration and decomposition.

3.3. Compatibility studies

Since the 1969, when Jacobson and Rieir [83] demonstrated that the stability of penicillins with various tablet lubricants could be predicted from thermal analysis, many attempts have been made to use both DSC and DTA as the basis of compatibility prediction. The basis of the method is to blend the drug under investigation and the excipient at the 1:1 level and to scan through major

transitions such as melting, dehydration and re-crystallisation. The scans are compared with the scans of the individual components. In an ideal world, compatibility would be demonstrated by the appearance of a scan whose transitions would correspond to those of the two pure components overlapped onto each other. Incompatibility would be shown by different scans. This presupposes that the two materials are not miscible in each other's melt which would give scans that correspond to the simple eutectic or other phase interactions. When one considers that the DSC scans are also particle size dependent, the reader should realise that accurate interpretation is not easily achieved.

3.3.1. Compatibility studies using thermal analytical techniques

The use of DSC or DTA in compatibility testing is, or should be, falling out of favour. The concept of any stress test is that a formulation may be stored in conditions that stress the sample and subject it to a likelihood of accelerated decomposition. DSC or DTA have been used, occasionally to examine the final formulation but more usually to examine incompatibility between any two ingredients in a formulation. Thus, in its simplest terms the drug and a chosen excipient are scanned individually from ambient through their dehydration, melting or decomposition events. Then the materials are scanned as their 1:1 physical mix. The stress is thus provided by an increase in scanning temperature and no contribution of, for instance, humidity to instability can be assessed.

The assessment of compatibility in such systems is very much an art rather than a science. It is axiomatic that the mixing of two materials will lead to a melting point depression unless the materials are so immiscible in both the liquid and solid states that neither can depress each other's melting point. However most materials, when mixed, will demonstrate a partial miscibility, if only in the liquid state leading to a depression of melting/freezing points. This automatically leads to consideration of phase equilibria and the experienced formulator must consider if complex formation, eutectic formation, solid solution formation etc. are a true incompatibility or acceptable or a problem. The researcher is thus directed to establish a phase diagram for the system, and assess its implications to the final formulation. This is in direct opposition to the original reason proposed for the technique, of a rapid prediction of incompatibility.

The choice of a 1:1 mixture is dubious. Originally intended to maximise the detection of incompatibility between two ingredients, it does not represent the compositions or ratios found in the final formulation. A particular example of

this problem is the use of 1:1 blends with drug-lubricant mixtures. The ratio in the formulation of drug:lubricant could be, for a 100 mg dose, in the order of 200:1. Such low levels of lubricant are unlikely to cause major decomposition. However, the use of the 1:1 blend for DSC or DTA studies produces problems such as loss of moisture, melting of different fatty acid fractions in magnesium stearate since it is not a single chemical entity, and dissolution of the drug in the melt as the temperature is increased. Again, a full analysis across the whole composition range is desirable, for instance ibuprofen-magnesium stearate [84]. By using a 1:1 blend with lubricants, an erroneous impression of incompatibility can be created because the ratios found in the final formulation do not lead to significant incompatibility. Therefore a broad statement may be that DSC and DTA lead to, on the one hand, an over-exaggeration of the problem because incompatibility is artificially induced, and secondly do not provide a realistic impression because hydrolysis is a major determinant of stability.

The criterion for accepting reasonable compatibility or stability is very much an educated guess. Several factors should be considered including that already suggested concerning a realistic drug-excipient, or indeed excipient-excipient ratio. Firstly the melting depression may indeed be due to eutectic formation, or similar physico-chemical phenomena, which may not be deemed incompatibility. However it may also represent instability. A rule of thumb might suggest that a decrease in peak temperature of more than 10°C may be important. If this were due to degradation during the heating scan, a slower heating rate might result in more degradation and therefore a greater lowering of melting point. For expediency and speed, a standard heating rate of 10°C min^{-1} is usually recommended. Clearly degradation will be more easily detected at slower heating rates, although adding time to the experimental procedure.

Dehydration, especially of hydrates like α-lactose monohydrate or calcium phosphate dihydrate, leads to spurious data because of the experimental set up. Lactose would lose its water at ~145°C leading to possible warping of the sample pan if hermetically sealed pans are used. This moisture accelerates the degradation of materials, especially where hydrochloride salts are concerned. It should be remembered that lactose melts with decomposition at ~220°C. Slowing the scan speed decreases the temperature at which this decomposition occurs. Where hydrochloride salts are present, this decomposition is accelerated lowering the apparent melting points. Additionally, trituration during mixing will lead to particle size changes in the drug and lactose, further accelerating the

decomposition during scanning and lowering the temperature at which dehydration occurs, probably because of crack propagation within the lactose crystals. The question that a formulator should ask is if degradation occurs at elevated temperatures (>190°C) and if the temperature at which dehydration occurs is reduced by, for example, 5°C, is this indicative of significant incompatibility? The probable answer is no. This brings into question the whole technique because if degradation/decomposition/physical changes occur at temperatures considerably in excess of ambient temperature, are they relevant to normal storage conditions?

Given these criticisms of the technique, it is pertinent to ask when does that technique give reliable usable data? The answer would seem to be when one of the components does not melt in the temperature range of the scan. Then changes due to the second material are almost certainly due to incompatibility between the two materials. Thus materials such as talc and silicon dioxide are easily assessed with drugs. Changes in melting point are easily detected; the heat of fusion (or indeed dehydration) also gives a quantitative assessment of change. Examples in the literature of interactions between materials are numerous. Although many papers describing the compatibility or stability by DSC or DTA were reported in the 1970's and 1980's, their frequency has decreased. Examples of recent publications are the studies on ketoprofen [85] carteolol hydrochloride where DSC was complemented by hot stage microscopy [86], nefazodone where DSC studies were complemented by UV, IR and HPLC analysis [87], Ibuprofen [88] and albendazole [89].

In conclusion the technique gives ambiguous data that may indicate that interactions and or incompatibility occur. The techniques over-estimate the risk of this incompatibility.

3.3.2. Compatibility studies using isothermal calorimetry

More recently isothermal microcalorimetry has proved a valuable asset for compatibility studies where an observation of a chemical reaction between two or more materials can be rapidly recorded. The principle of a calorimetric investigation for the compatibility of a drug substance and associated excipients is to make 1:1 mixtures of the drug substance and each of the other components that make up the final formulation, in turn. If a chemical reaction occurs between two materials, the observed calorimetric signal will be displaced from the baseline. If there is no interaction between the two materials the calorimetric signal will remain at the base line. The magnitude of displacement from the baseline for two reacting materials is proportional to the rate, enthalpy change

and the quantity of material involved in the reaction. In the solid state, the quantity of material involved in the reaction is determined by the reactive surface area of the two materials. The chemistry at the interface of the reactive surface is complex [90] and is related to particle size and solvent quantity. A solvent, often water, is required at the interface to facilitate the reaction. To optimise the calorimetric signal the experiment can be performed using 1:1 binary mixtures of the active drug substance and excipient in an aqueous slurry. This will give the maximum reactive surface contact in an environment favourable for a reaction. Care should be taken to ensure that the solute, e.g., water, is not itself a cause of a chemical reaction with the drug or excipient.

Compatibility testing using isothermal microcalorimetry is used mainly as a screen for drug/excipient chemical interactions and not as a quantitative means of analysis. This is because, at present, it is not possible to obtain information about the quantity of material at the active surface in the solid state (see chemical stability in the solid state section 3.2).

Compatibility testing using this method has a drawback in that the formation of 1:1 aqueous slurries may not be a good representation of the real system. For example a potential compatibility problem between a drug substance and a lubricant such as magnesium stearate may not materialise into a problem in the real system where the proportion of magnesium stearate is relatively small. It may be difficult, therefore, to assess the impact of a positive result between two materials on the stability of the final product. However, the choice of an excipient can at least be made with knowledge about the possibility of stability problems in mind. As an example, Figure 21 shows an investigation of compatibility for an antibiotic with various lubricants. The aim of the study was to rapidly determine a chemically compatible lubricant for a tablet formulation. The study was performed by mixing dry powders of drug substance and each excipient in turn in a 1:1 blend. This was then loaded into the calorimeter at 75% RH and 50°C. During this study, an interaction was found between the sterol based lubricant in the formulation and the drug substance. Figure 21 shows that a rapid screen of the drug with various lubricants provides the opportunity to select other lubricants that may be more appropriate for the final product.

Compatibility studies for drug and gas phase components can also be studied using a perfusion type device in the isothermal microcalorimeter. For example, gases that the drug substance may come into contact with during processing or storage through packaging, etc., can be perfused over the drug substance in the

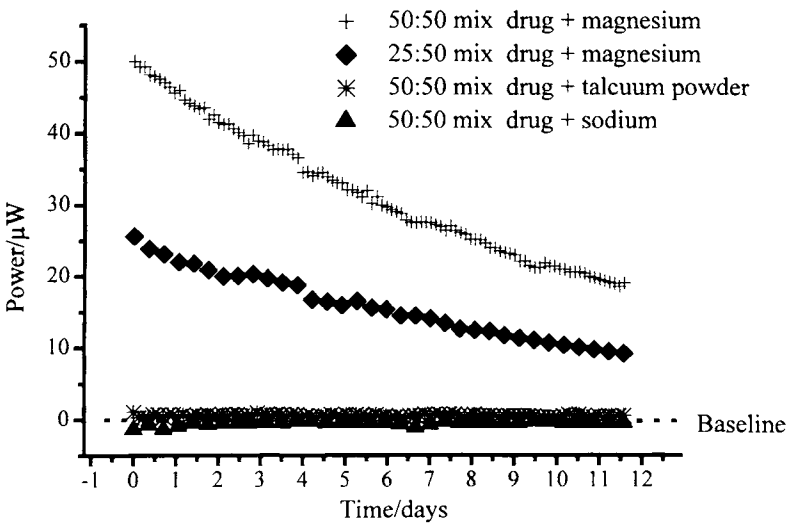

Figure 21. A isothermal calorimetric study for the compatibility of an antibiotic drug with a stearol excipient used as a lubricant during tabletting. The study shows that there is an interaction when stearol type lubricants are used, but not with other lubricant types.

perfusion chamber and any interaction recorded. For example, compatibility studies using gases such as formaldehyde, ammonia and oxygen can be made.

3.4. Bomb calorimetry

Bomb calorimetry is generally used to measure the heat of combustion for organic materials. The principle of operation is to saturate the material with oxygen, within a sealed container (the bomb) and ignite using a hot wire. During the rapid combustion carbon molecules are converted to carbon dioxide, hydrogen to water and nitrogen to gaseous nitrogen. The recorded enthalpy change is thus a sum of all bonds broken and bonds made converting the organic solid into simple gaseous molecules. The measured enthalpy change for this type of analysis is often referred to as the enthalpy of formation. Note that,

in fact, this type of calorimeter operates at constant volume. As such, the energy measured is internal energy change (ΔU) and not enthalpy change (ΔH).

Within the pharmaceutical industry, bomb calorimetry is used mainly for safety testing of materials. From a calculation of ΔU an assessment can be made for the explosive force that could be produced if the material was to detonate during rough treatment. During a safety test, the material is shocked under varying conditions of temperature and relative humidity to determine if detonation would take place. During one such study a compound was found to be about 5 times more explosive than nitro-glycerine ($\Delta H = 1809$ kJ / mol).

3.5. Heat capacity

Heat capacity studies are important for safety reasons where bulk storage of products, especially liquids, is necessary. The main concern is thermal run-away reactions. A small degradation reaction of the drug in a container may cause an accelerating heating rate if the rate of heating is greater than the dissipation of the heat from the container. A violent outcome is inevitable under these conditions. As a preventative measure, the reaction rate and associated enthalpy change for a material under storage is determined as well as the heat capacity. From Equation (13), where C_p is the heat capacity and has the units kJ mol^{-1} K^{-1}, the net temperature change of the material can be determined for a given time period. This is then related to the rate of heat efflux from the container.

$$C_p = \frac{\Delta H}{T} \tag{13}$$

Differences between the heating rate from the drug material and the cooling rate from the container will then allow predictions about the heat build up over time. A thermal run-away reaction can then be avoided. The heat capacity of a material is defined as the energy required to raise 1g of the material by 1 K.

In practice the heat capacity of a material can be found by DSC either by reference to known calibrants as sapphire or by the use of modulated methods of thermal analysis [91]. It should be remembered that the best results are for non–reacting systems where the observed calorimetric signal is not complicated by the enthalpy change associated with a chemical reaction.

3.6. Biological stability studies

Protein-based drugs are increasingly being considered as medicinal agents. Such products will present an interesting challenge to the pharmaceutical industry where conventional stability studies using elevated temperatures may not be possible because of protein denaturation. There are several techniques available for structural and general characterisation of protein based drugs. However, techniques for functional analysis and stability studies remain limited. The technological advances made in isothermal microcalorimetry and isothermal titration calorimetry now provide a powerful technique for such studies [92]. A concise publication detailing applications of calorimetric techniques and thermal analysis to the study of biological systems is given in Reference [93].

Isothermal titration calorimetry provides the ability to make direct measurements of the enthalpy change for interactions such as protein–ligand binding. The sensitivity of the technique allows such measurements to be made under ambient conditions and for relatively dilute solutions, representing real systems. From a single titration experiment it is possible to determine the enthalpy change for a protein ligand interaction, the equilibrium constant, the Gibbs free energy and the entropy change. In addition it is possible to determine the stoichiometry of the ligand–protein interaction. It is also possible, by performing additional experiments using different buffer systems, to determine the number of protons lost from the protein when it interacts with the ligand. This gives an indication of the reaction mechanism [94].

Conventional methods for data analysis are to plot the change in macromolecule–ligand concentration as a function of free ligand concentration. Examples of data analysis using conventional methods have been developed [95]. The analysis of calorimetric data using these conventional methods has significant limitations. The equations are structured so that a measurement of the complex quantity formed is determined as a function of free ligand added to the system. This is not a convenient manipulation, especially as the quantity of free ligand may not be easily determined. However it is possible to re-arrange these equations to the total quantity of ligand added to the system so avoiding this potential problem. Given the reaction scheme, Equation (14):

$$[M]+[L] \Leftrightarrow [ML] \tag{14}$$

where [*M*] is the quantity of free macromolecule, [*L*] the quantity of free ligand and [*ML*] is the quantity of macromolecule bound to ligand, the equilibrium constant (*K*) is defined as in Equation (15):

$$K = \frac{[ML]}{[M] \times [L]} \tag{15}$$

The total quantity of ligand and macromolecule [*Lo*] and [*Mo*] is the sum of the free and bound ligand and macromolecule, respectively. Therefore Equation (15) can be re-written in terms of [*ML*], [*Mo*] and [*Lo*], as Equation (16).

$$(ML) = K \cdot (Mo - ML) \cdot (Lo - ML) \tag{16}$$

Both [*Mo*] and [*Lo*] are known as [*Mo*] is the start concentration of the macromolecule and [*Lo*] is the sum of ligand added at each aliquot. It is possible, therefore, to plot [*ML*] as a function of [*Lo*], the total concentration of ligand, using Equation (7):

$$[ML] = \frac{1}{2} \times \frac{\left[1 + B + C - \sqrt{\left(1 + 2 \times B + 2 \times C + B^2 - 2 \times K^2 \times Mo \times Lo + C^2\right)}\right]}{K} \tag{17}$$

where $B = K.[Mo]$ and $C = K.[Lo]$.

From Equation (17) an analysis can be made if the quantity of *ML* can be determined as a function of ligand added at each aliquot. However considerable errors may arise as this quantity must be assayed, after each aliquot of ligand is added. However non-invasive techniques such as isothermal microcalorimetry calorimetry can be used to directly determine the quantity of *ML* without disturbing the system. For a calorimetric analysis an estimation of the enthalpy change for the macromolecule–ligand interaction must be made. An assumption can be made that at the start of the study, the initial aliquot of ligand added to the system, if sufficiently small, will completely bind to the macromolecule (as initially the macromolecule will be in excess). The enthalpy change associated with this interaction can then be used to calculate the ΔH for the interaction (Equation (3)).

Knowing ΔH, Equation (17) can be modified to Equation (18) so that the calorimetric response (*q*) can be plotted as a function of ligand concentration (*Lo*):

$$q = \left[\frac{1}{2} \times \frac{\left[1 + B + C - \sqrt{\left(1 + 2 \times B + 2 \times C + B^2 - 2 \times K^2 \times Mo \times Lo + C^2 \right)} \right]}{K} \right] \times \Delta H \tag{18}$$

A typical titration experiment is performed by titrating small quantities of ligand into a solution of the macro-molecule. The data can then be interrogated by plotting q, the calorimetric signal against the total ligand concentration (*Lo*) at each aliquot, using a suitable graphic software program [58]. By iteration, the equilibrium constant (*K*) can be found. Specific equations such as the single site binding, Equation (17), as well as multiple site binding models can be applied. From the equilibrium constant, the Gibbs free energy (ΔG) can be determined from Equation (19):

$$\Delta G = -R \times T \times Ln(K) \tag{19}$$

Knowing the value of ΔG, and ΔH, the entropy change (ΔS) can be found, as in Equation (20):

$$\Delta G = \Delta H - T \times \Delta S \tag{20}$$

Another important application of isothermal titration calorimetry includes the study of the activity coefficient of a drug in aqueous solutions. The solute–solute interaction is an important parameter to measure as it has implications to solubility parameters [47]. In practice, the activity coefficient can be conveniently measured by isothermal titration calorimetry by simply titrating aliquots of drug solute in solvent into the pure solvent. If the activity coefficient of a drug is one (that is, there is no molecular interaction between solute particles in the solvent) then the resulting calorimetric signal will record a ΔH of zero. If, however there is a deviation from ideality, the calorimetric signal would record an endothermic or exothermic signal depending on a positive or negative deviation form ideality [96,97].

3.7. Photo-stability

The application of isothermal microcalorimetry to photo-degradation studies, especially in relation to chemical stability, is gaining considerable interest

within the pharmaceutical industry. Guidelines governing the stability testing of materials (The International Conference on Harmonisation Tripartite Guideline, 1996) suggest that photo-stability testing of drugs and compounds should be an integral part of stability-testing. At present, conventional methods for the study of photo-stability can be difficult to implement and may be of limited usefulness for a proper understanding of photo-stability issues. The difficulty arises because of uncertainties about how to generate "normal daylight" conditions and the validation of actinometers for the interpretation of the results. Isothermal microcalorimetry offers an advantage for photo-stability testing over conventional techniques; the calorimeter has such high sensitivity for monitoring change that the input light source can be of relatively low energy. Technology now provides the ability to feed light of specific wavelengths and defined intensity through fibre optics. This can be focused on the material within the calorimeter so that photo-degradation can be studied.

There have been several successful attempts to construct photo-calorimeters, mainly to study rapid photo reactions, for example the rearrangement of rhodopsin [98]. The development of photo-calorimetry is progressing towards a differential instrument capable of studying relatively slow degradation reactions [99,100].

4. MISCELLANEOUS USES

A number of miscellaneous uses for thermal analysis within the pharmaceutical sciences exist. The following sub-sections illustrate examples of such uses. By their nature, only selected examples are given.

4.1. Phase diagrams

The interactions between drugs and excipients or polymers or between excipients are of vital importance to formulation. Under the assessment of compatibility by DSC or DTA it was suggested that 1:1 blends may be used to maximise any interaction between two materials. This is one of the major limitations of the technique. It does not seek to establish true equlibrium between the materials. A combination of DSC or DTA with HSM provides the best way of establishing the phase diagram.

On first sight it might seem sensible to scan, by whichever method, physical mixes of the two materials. The initial melt on a DSC or DTA scan represents the solidus temperature of the phase diagram. The initial melt should be taken, not as the extrapolated onset temperature, but as the true onset. This creates

problems because this may be very subjective. The liquidus temperature can be taken as the peak temperature of the melting endotherm. Generally, two melting endotherms will be seen for the melting of a physical mixture corresponding to the melting of, in its simplest terms, the eutectic component, and the second to the component in excess. It is the peak temperature of the second melting endotherm that is used for the liquidus temperature. Hot stage microscopy may be used to follow the melting events. However, the use of physical mixes may lead to misinterpretations of the phase diagrams, especially when complex formation occurs giving rise to peritectics or discrete complexes. Therefore the experiments should be repeated on pre-heated materials to confirm the changes. The classic example of complex formation is probably the paracetamol-phenazone system [101]. The most used examples of phase equilibrium are in the field of solid dispersions, either in polyvinylpyrrolidone (PVP) or polyethylene glycol (PEG) [102].

The technique of determining phase equilibria is to carefully prepare physical mixes at different ratios by trituration and scan, by DSC or DTA, at moderate heating rates, say 5°C min^{-1}. Poor mixing of the samples may result in poor estimates of solidus and liquidus temperatures. Consequently, the sample should then be rescanned. The advantage of this is that the second scan will produce more reproducible scans. However, decomposition may be induced in the sample AND a tendency of polymers to undercool without crystallisation may cause misinterpretation of the data since throughout the cooling process and subsequent reheating the drug and/or carrier may remain in the molecularly dispersed state or as a glass. This causes a problem in attributing liquidus or solid temperatures to the system [103]. Consequently, the use of hot stage microscopy to supplement the studies is highly recommended. Again care has to be taken with sample preparation since the powders on the first scan may be too finely separated giving poor reproducibility. The added advantage, however, of second scanning, whether by DSC, DTA or HSM, is that complex formation with resultant recrystallisation exotherms, can be demonstrated and the stoichiometric ratios determined for the complex or peritectic point.

The reheating method presupposes that both drug and polymer melt within the temperature of the scan. This is acceptable for polyethylene glycols whose molecular weight analogue of ~6,000 melts at ~66°C. However, for polyvinylpyrrolidone (PVP), which does not melt and decomposes at temperatures in excess of 250°C, other approaches have to be sought. One is to disperse the drug and polymer in a solvent prior to the analysis. This naturally

occurs for solid dispersions where drug and carrier are recovered frequently by evaporation from an organic solvent.

Thus for PVP dispersions, rather than both drug and PVP melting during the scan, only the drug will melt. This gives some practical importance because DSC can then be used to determine the solubility of the drug in the polymer. The study of Theeuves et al. [104] was pivotal to the development of the technique. By scanning films containing various levels of the drug, a phase diagram can be produced, not of melting temperatures against composition but of heats of fusion against composition (Figure 22). Where the drug is

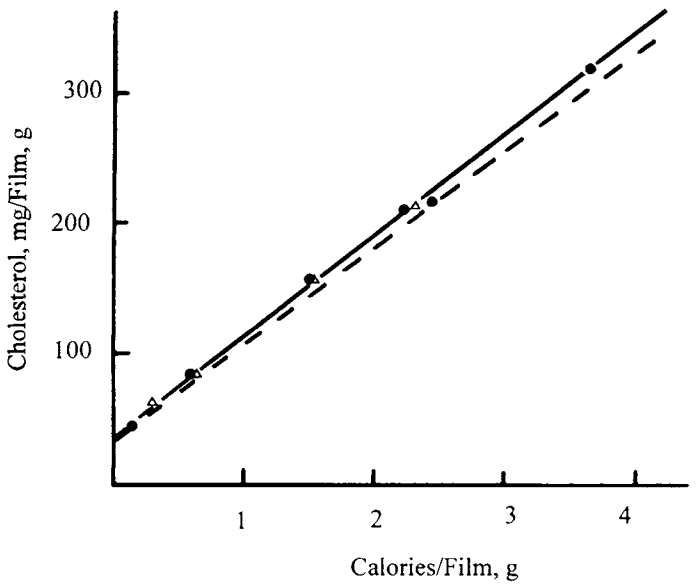

Figure 22. Cholesterol concentration of film samples as a function of the observed heat. Key: •, observed heats at first melting; Δ, observed heats at second melting; —, average line through experimental data; and – – –, calculated line from drug solubility intercept and heat of melting of the pure drug. From reference [104]; copyright permission requested.

molecularly dispersed, or present as a solid solution, no melting is observed. Once crystallites are present, they will melt during the DSC scan and display as an endotherm. By plotting this heat of fusion against composition a straight line is obtained that can be extrapolated to zero heat of fusion. This represents the solubility of the drug in this carrier. This technique needs minor correction for

heat of mixing [104] but an estimate of the solubility, at least at this melting point, can be quantified. In addition, any polymorphic transformation of the drug will also be detected.

The phase equilibria produced with polyethylene glycol may be quite complicated because of the ability of drugs to disperse molecularly within the polymer chains [105]. Thus, the systems may display solid solution and glass formation [103] due to a relatively high solubility of the drug in polymer, e.g. indomethacin, or a virtual monotectic due to a very limited solubility of the drug in the polymer, e.g. the triamterene - PEG system [106].

In a method analogous to the determination of drug solubility in a polymer, the heats of fusion may be used to further characterise a system. Again the heats of fusion of the eutectic and excess components can be plotted as a function of composition. There are straight line relationships between the heats of fusion attributable to the excess components which decrease with addition of the second component [107]. Each should intersect zero enthalpy at the eutectic composition. Concomitantly, the heats of fusion of the eutectic components increase directly from zero at the pure components to intersect at the eutectic composition. Such a technique was used to evaluate the sulphamethoxazole-mannitol system. [107]. The technique can be further extended when complexation occurs, as for example with the dapsone-dilauryldapsone system [108].

It should always be remembered that the actual heating of a sample moves the system equilibrium. What is apparently stable at room temperature ceases to be stable on heating and changes may therefore occur during scanning. DSC/DTA will detect this as fusion or recrystallisation but phase equilibria studies should always be collaborated with microscopic studies. However, Craig [105] cautioned against the prediction of simple eutectics with polymers such as PEG, since the melting behaviour of a drug in molten PEG may not be the same as that of a pure drug. Indeed, peak broadening of the endotherm corresponding to the drug was noted at low drug contents [109].

In many ways pharmaceutical dosage forms can be regarded as dispersions of drugs in carriers. Whereas this is utilised in solid dispersions, it is equally applicable to suppositories or pessaries, or indeed any system where heat (or solvent and subsequent evaporation) is used to produce a dispersion of a drug in a carrier. Thermal analysis, and especially DSC, can be used to measure the development of structure or subsequent storage. This can be reflected as an increase in fusion enthalpy on storage [110, 111] of solid dispersions, or conversion of the crystalline form, whether polyethylene glycol [110] or as a

change in the polymorphic nature of glycerides used in suppository or pessary bases [112].

4.2. Polymers of Pharmaceutical Interest

Thermal analysis of polymers is one of the broadest topics for thermal analysis. General thermal analysis of polymers has been dealt with elsewhere within this Handbook. This section restricts itself to a limited number of examples of interest to the pharmaceutical scientist. Some reference to drug-polymer systems has been made in the previous section.

4.2.1. Polyethylene glycols

Polyethylene glycols vary in molecular weight from ~200 to up to >1,000,000 Da. Their nature changes from liquids through semi-crystalline materials to resinous solids. Their general structure is $H\text{-}[\text{-}O\text{-}CH_2\text{-}CH_2]_nOH$. The structure of PEGs has been comprehensively reviewed by Craig [105] and clearly IR, Raman and NMR studies are fundamental to elucidating their structure. Thermal analysis does, however, play roles in examining the crystallinity and types of crystals present in the crystalline and semi-crystalline material. Undoubtedly, in the crystal lattice, PEGs are arranged as lamellae. The polymer chains exist as either extended or folded forms. The proportion of crystals in the folded or extended form is very much dependent on molecular weight. Buckley and Kovacs [113] showed that in PEG 6000 one- and two-folded crystals were apparent. In PEG 10000, one-, two-, three- and four-folded crystals were apparent. Thermal analysis, especially DSC may be used to resolve the structure. Scanning a sample of PEG, cooling and immediately re-scanning, results in the production of unstable forms manifesting as a number of endotherm peaks or inflections on the DSC scan. Additionally on second scanning, the heats of fusion will be lower, indicative of an introduction of amorphousness, or less crystallinity, in the sample (Figure 23). For PEG 4000, Kovacs and Buckley [113] found evidence for instability of the folded crystal form. As the scanning rate increased from 0.5°C min^{-1} to 8°C min^{-1}, the melting endotherm for the unstable form increased since the lower rates allowed unfolding to occur during the heating process.

The scans of PEG are also much dependent on prior recrystallisation. Craig and Newton [114] demonstrated that ambient cooling conditions altered both the melting point and heat of fusion. Additionally, the heat of fusion, determined as $kJmol^{-1}$ increased as the molecular weight of PEG increased.

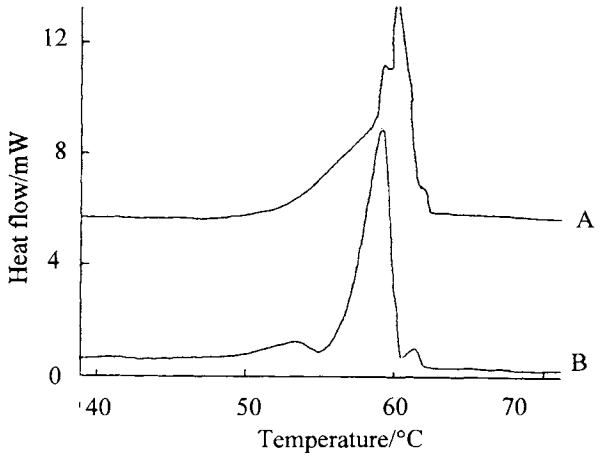

Figure 23. DSC scans of a sample of PEG 6000, each was scanned at 2°C min^{-1}. Scan A was the sample as supplied. It was subsequently cooled to 20°C to allow recrystallisation and re-scanned to give Scan B. Scans are displaced for clarity.

Both DMA [115] and dielectric spectroscopy [116] may be used as these techniques are sensitive to changes in crystal structure.

4.2.2. Poly-lactic acids

Poly-*ortho*-esters are one, among many polymer types that include biological-based polymers such as alginates, gelatin and albumin, that have been incorporated into microspheres for drug targeting. The poly-*ortho*-esters possess the advantages that they are synthesised, and therefore contain no antigenic structures, whilst retaining their biodegradability. The two commonly used poly-*ortho*-esters are poly-glycolic acid and poly-lactic acids, which apart from finding applications as surgical sutures, are used in drug delivery. Microspheres, are made by a number of processes including coacervation, spray congealing and emulsification and have provided a rich vein of pharmaceutical research, and especially thermal analysis. For the sake of brevity this section will concentrate on poly-d,l-lactic acid, known for its amorphousness and glass

transition and generally synthesised from the dimer of lactic acid, dilactide, which also gives rise to the other name for the polymer, polylactide.

Like many polymers poly-d,l-lactide is available in a great range of molecular weights. Rak et al [117] were amongst the first authors to describe the effects of molecular weight on the glass transition of poly-d,l-lactic acid. Values were found between 51.0 and 54.6°C for molecular weights between 44.7 to 68.8 $\times$ 10^3. A relaxation enthalpy was found which correspondingly varied from 5.7 to 6.4 J g^{-1}. However, the molecular weights of 2.6 and 6.4 $\times$ 10^3 had lower values of T_g, indicating a molecular weight dependence of T_g at low molecular weights. The relaxation enthalpies cause a problem in determining the precise location of the T_g, which has only been recently resolved by using modulated methods of thermal analysis.

Figure 24 shows a typical scan of poly-*d*,l-lactic acid in which the heat flow curve demonstrates a relaxation endotherm around the glass transition. The glass transition is resolved in the storage curve or reversing curve of DDSC or MDSC. The extension of TMDSC to formulated microspheres is best exemplified by the study of Hill et al [118]. Although many studies had examined the thermal analysis of microspheres using conventional DSC or DTA, this study examined microspheres containing 0-50% w/w progesterone and poly(*d*,l-lactide). The glass transition of the polymer was identified by a step change in the MTDSC-measured heat capacity. Conclusions were made that the drug plasticised the polymer at contents up to 20%. At the 30% level recrystallisation of progesterone was noted indicating that the drug was present in an amorphous state. TMDSC suggested that in samples containing 50% progesterone, the drug was mainly present in the crystalline state. As with all good thermal analytical studies, the conclusions were supported by results from other techniques, in this case SEM and PXRD data.

In many ways the analysis of polymer-based delivery systems, especially microspheres, illustrates a fundamental problem of the use of thermal analysis in pharmaceutical-based systems. In normal evaluation of polymers, prior history is removed by thermal treatment. Whereas for PEG this can be accomplished by melting giving a more amorphous, less crystalline system which gradually on storage returns to a more crystalline system, this alters the structure of the material. For amorphous materials this can be used to allow evaluation of the glass transition temperature. This has benefits for examination of the polymer alone since prior treatment will probably remove any relaxation endotherm associated with the glass transition. As seen with the work of Hill et al [118] a 'without prior knowledge' heat treatment could result in the loss of

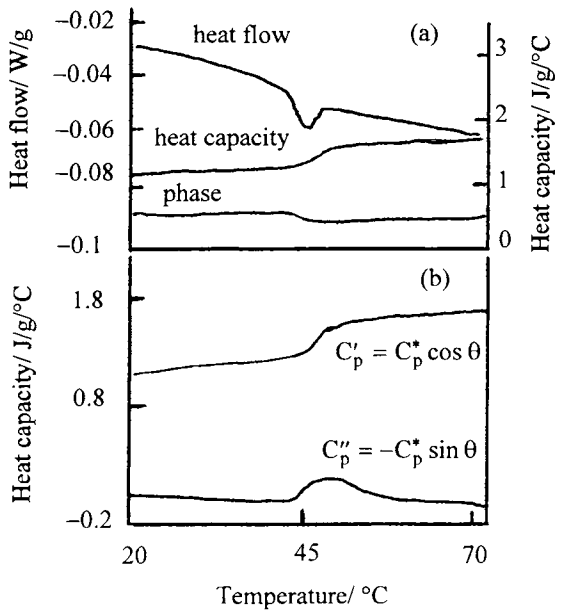

Figure 24. (a) Total heat flow, complex heat capacity and phase lag, θ, measured by TMDSC for poly(d,l-lactide) as supplied. (b) Results of phase correction of the complex heat capacity, where C^*_p = complex heat capacity, C'_p = reversing heat capacity and C''_p = kinetic heat capacity. From reference [118]; copyright permission requested.

important information. It is well known that relaxation endotherms develop on storage. Indeed many early workers, without corroboration of these scans with other observations, stated that poly-*d*,l-lactic acid melted at ~55°C, its glass transition temperature. There are, however, more important reasons why

preliminary heat treatment, known as annealing, should not be used in a formulated system. Armstrong et al [119] clearly demonstrated that there was residual solvent remaining in microspheres following their preparation. This was detected, partly, as a result of a lowering of the T_g. The lowering would not have been apparent had the microspheres been annealed prior to their DSC. Used alone, thermal analysis cannot provide unequivocal proof of residual solvent. Indeed even TGA would probably be insensitive to the amount of solvent entrapped in the microspheres. Proof of its presence would require, perhaps, head space analysis. DSC or DTA gives a clue, by lowering of the glass transition, that some residue was possibly present.

4.2.3. Cellulose Ethers

A review of the thermal analysis of cellulose ethers, especially HPMC (hydroxypropylmethylcellulose) has been published [25]. DSC of untreated samples of HPMC, and indeed many polymers based on celluloses or starch, is relatively uncomplicated in the absence of large quantities of water. The materials demonstrate a broad endotherm, corresponding to the loss of adsorbed water generally in the range 50° to 120°C. Clearly encapsulation affects this process. Open pans would lose their water quickly, moving the endotherm to lower temperatures. Hermetically-sealed pans would trap the vapour above the powder generating a partial pressure above the sample, moving the moisture loss endotherm to higher temperatures. Pans with pin-holed lids would demonstrate intermediate temperatures for the loss of water.

One danger is that the build-up of pressure would distort sample pans giving irreproducible scans that were dependent on the contact between the pan and the temperature sensor. Although TGA could be used to quantify any weight loss, the results would still depend on the moisture content of the samples prior to treatment. On an 'as is' product, this could be quite variable. At elevated temperatures the sample would start to decompose and this would inevitably be detected as a weight loss.

This moisture loss could however obscure the important glass transitions of these materials. For ethylcellulose, a hydrophobic cellulose ether, dissemination of a T_g is relatively straight forward. The general technique is to cast a film of the polymer on a flat surface (glass will suffice) and remove the residual solvent under vacuum. Velasco et al [120], casting films of ethylcellulose from dichloromethane, demonstrated the glass transition by both conventional DSC and MTDSC (Figure 25). Clearly, if the transition is evident, the latter technique is not required. Because HPMC is more hydrophilic, it has a greater

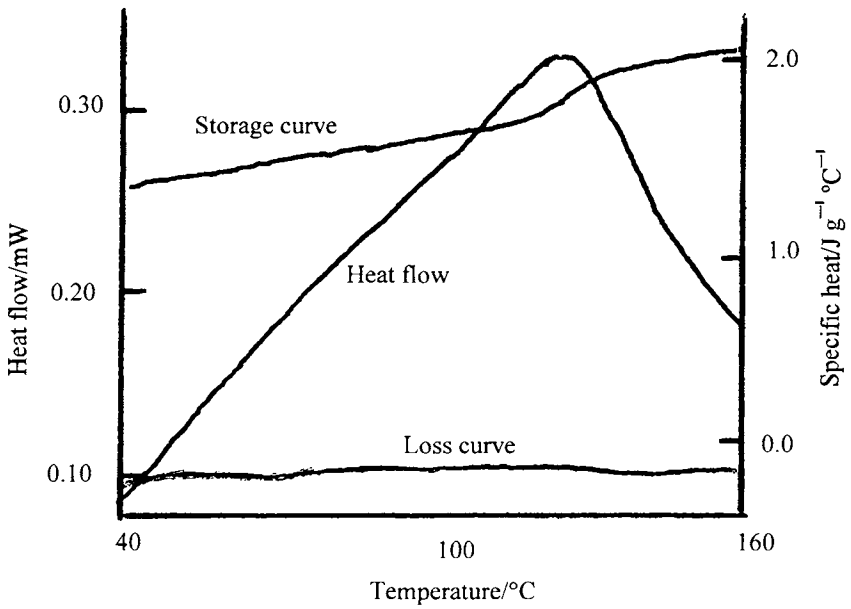

Figure 25. DDSC scan of ethylcellulose film cast at room temperature. From reference [120]; copyright permission requested.

tendency for water to adsorb to its surface. This creates major problems in assessing its T_g which is frequently overlapped by the endothermic desorption of adsorbed water. In an ideal situation, the T_g could be determined from the powder. MTDSC is capable of resolving the glass transition from the dehydration [39]. It should be remembered, however, that this gives a transition temperature that in all probability is different to that of the starting material, which contains low levels of adsorbed water. Water, because of its strong interaction with HPMC, is difficult to remove. Porter and Ridgeway [121] utilised a technique in which the polymer solution was added dropwise to the

DSC sample pan. After each drop had been added, the solvent was evaporated. Repetitive addition of 20-30 drops produced a film suitable for analysis. Other techniques, including torsional braid analysis (TBA) and DSC were used to evaluate HPMC [122]. Not surprisingly, the techniques gave a wide range of values (157° to 180°C) which represents problems in producing a dry sample and possibly problems with conductivity caused by entrapped air.

4.3. Polymer-hydration

It was outlined in the previous section that the thermal analysis of polymers is not without problems caused by moisture. Pharmaceutically, the presence of moisture may be desirable, unavoidable or part of the functional aspects of the polymer. Thus the presence of low levels of moisture improves the compaction of HPMC by plasticisation [123], increases tablet strength by hydrogen bonding, is part of the function by which hydrophilic polymers perform in matrix tablets [123], or are used as water absorbents in wound dressings [125]. Finally, gels containing water, formed at the surface of a matrix tablet, or as gels for topical delivery contain defined quantities of water. Whichever system is examined, their use is controlled by their properties, some of which can be assessed by thermal analysis.

In theory, water interacts with polymers in at least three ways. (1) Water may be tightly bound to the polymer (and is therefore incapable of freezing, certainly at temperatures > –50°C). (2) Water may be loosely bound to the polymer, but if the temperature is low enough will freeze. This loosely bound water is generally assumed to freeze in the range –50° to –20°C. (3) Thirdly water may be present that has not interacted with the polymer. This behaves and freezes as bulk water.

In many ways such a broad definition of types of water is difficult to sustain, not least because the types of polymer examined vary from water soluble (such as HPMC), virtually insoluble in water (such as ethylcellulose) or are hydrophilic polymers which are basically insoluble but are capable of sequestering water and incorporating it into side chains attached to an insoluble polymer back-bone. Given that water can penetrate pores in a polymer, the ability to freeze depends on the pore size. Since the resultant DSC/DTA scan is dependent on the particle size of the water crystals, it results in a very confusing situation regarding interpretation of DSC/DTA scans. However, this section reviews some of the existing methods of assessing water-polymer interactions. As ever, researchers are strongly advised to use adjunct techniques to confirm findings. ESR is one of those methods of choice.

In its simplest form, water-polymer samples may be allowed to equilibrate in hermetically-sealed simple pans. Following this period, the samples are examined, following cooling to sub-ambient temperatures, preferably less than –50°C, by heating back up to ambient conditions. If the cooling scan is controlled and recorded, initially the so-called bulk water will freeze, followed by water loosely bound to the polymer. The difference in enthalpies between the sum of these two events, and the theoretical value corresponding to all the water weighed into the sample, represents the moisture allegedly strongly bound to the sample, although as indicated earlier, there may be alternative interpretations of the water distribution. It is unlikely on scanning that differences in melting of these two apparently frozen types of water will be detected. However, this does not rule out the occurrence of further recrystallisation during the warming scan, as observed for HPMC-water gels [126]. Typical DSC scans are shown in Figure 26. Data treatment is by plotting

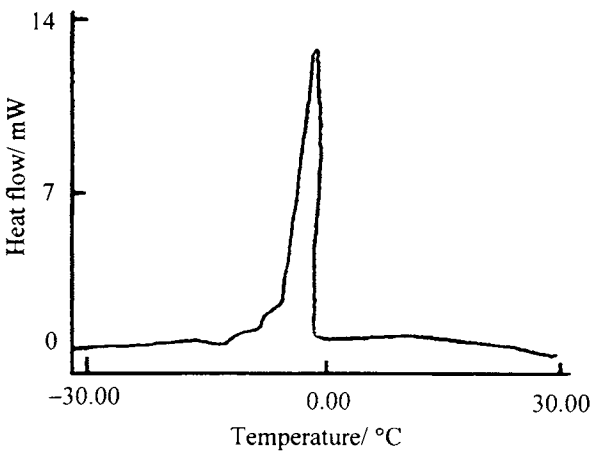

Figure 26. DSC scan of HPMC K15M gel stored for 24 h at a heating rate of +1°C min^{-1} following cooling at –10°C min^{-1}. Reprinted from reference [126] with permission from Elsevier Science.

the enthalpy of the melting endotherms as a function of water per g polymer. At low levels of water, theoretically all bound to the polymer, no melting enthalpies would be detected. At higher levels, where melting enthalpies are detected, there should be a straight line relation between the enthalpies and composition. Its intercept with the abscissas gives the maximum amount of water that can be bound to the polymer. The slope should be 334 J g^{-1} corresponding to the melting enthalpy of water. Lower values indicate a strong interaction between the polymer and water. The technique has been used for HPMC-water [127,128] and polyvinyl alcohol [129] systems.

Alternatively the polymers may be exposed to different relative humidities and the samples scanned after storage. This requires careful treatment of samples since adsorbed water may be easily lost on transfer of samples from the humidity cabinet to the encapsulation device. Weight gain may be assessed by weight loss on TG analysis or by the enthalpy of dehydration during the DSC scan [125]. The technique has been used to study water distribution for HPMC [128] and in gelatin, pectin and sodium carboxymethylcellulose samples [125].

Clearly, the techniques of thermal analysis may also be used for systems in the gel from when the polymers may be regarded as already hydrated. Since these are effectively dissolved polymers, the thermal scans will be dominated by the endotherm corresponding to the melting of free water. However, other thermal events may be detected to the low temperature side of these major endotherms. These may be due to melting of different classes of water, or even a glass transition, followed by recrystallisation of phase-concentrated water [25]. Differentiation of the events by dielectric spectroscopy has at least allowed partial confirmation of the thermal data [130].

4.4. Liposomes

Liposomes enhance drug solubility or provide a method of targeting delivery of drugs to specific organs. They enable drugs to be trapped centrally, or in their bimolecular layer [131], depending on the hydrophilicity of the drug molecules. The bilayer or multilayer of the liposomes is made of phospholipid. For homogenous phospholipid, the bilayer is relatively unstable, although concentrated dispersions of this bilayer, on thermal analysis heating, display two transitions, a smaller pre-transition followed by disaggregation of the phospholipid, a process frequently called melting and probably due to dehydration of the phospholipid. Such phospholipids include natural phospholipids such as phosphatidylcholine, phosphatidylserine or phosphatidylglycerol or synthetic phospholipids such as

distearoylphosphatidyl-choline (DSPC) and dimyristoylphosphatidylcholine. Traditionally liposomes are formed by adding an aqueous medium to a phospholipid film [131]. Agitation results in multilamellar vesicles (MLVs) that have more than one bilayer surrounding an aqueous core [131]. Generally, more stable liposomes are found when the vesicles consist of a mixture of phospholipids.

Crude DTA of 1,2-diacyl-L-phosphatidylcholines suggest that they were isolated from organic solvents as the monohydrate form [132]; the water was lost on heating in open DTA pans. This corresponded to a large endothermic transformation below the melting point. Addition of water to DSPC lowered the temperature of the gel to liquid crystalline phase transition, a limiting value was reached at approximately 20% w/w water content [133]. Ice melting was not detected until endotherms were present in samples containing ~25% w/w water. The 20% w/w concentration corresponds to a phospholipid:water ratio of 1 molecule of phospholipid to 10 molecules of water [133].

However, researchers are well advised not to rely on DSC or DTA but to use high sensitivity DSC or isoperibol calorimetry, since this will resolve the melting processes into a number of transitions. Prolonged incubation at low temperatures produces fully hydrated long chain phosphatidylcholines which exist in an ordered, condensed crystalline subgel state. On heating a transition, commonly referred to as the subtransition, demonstrates the conversion from a subgel to another state where the phospholipids have increased mobility and further penetration of water into the bilayers [134, 135]. These subtransitions may be further classified as Type I and Type II transitions, depending on the type of phospholipid [131]. Even sub-subtransitions have been described [136].

Many mixtures of phospholipids, especially phosphatidylcholines, do not demonstrate these subtransitions. The pretransition is thought to be associated with a structural change from a one dimensional lamellar to a two dimensional system [131]. The temperature of this gel to liquid-crystalline phase transition increases with molecular weight (chain length) of the fatty acid. Because naturally occurring phospholipids have a broader distribution of the fatty acids, the transition also tends to be broader.

Biological membranes and liposomes contain a mixture of phospholipids which results in a broadening of the temperature range over which they melt. When the hydrocarbon chains differ by two carbon atoms ideal mixing of phases occurs. Increasing the difference results in deviation from ideality with gel phase immiscibility and possibly peritectic behaviour [137]. Where the

hydrocarbon chains differ by six carbon atoms, monotectic behaviour is observed.

In the formulation of liposomes, cholesterol is frequently added to control the release of entrapped drug or to increase their stability. Addition of cholesterol eliminates the pretransition and decreases the mass transition temperature, with a reduction in the heat of transition until the transition apparently disappears. Raman studies demonstrate that a transition does take place but over a wide temperature range [138]. The condition of liposomes is fundamental to the release of the entrapped drugs. Greater fluidity of the liposomes should result in faster drug release. The interactions of a number of drugs with liposomes have been studied. The drugs include steroids [139] when measurement of the transition peak at half of its width was utilised as a measurement of the interaction between compounds and the phospholipid bilayers. Its evaluation allows an estimate of how much drug has been included into liposomes [140]. However, where the drug might be included in a liposome can only be proved by other methods of analysis.

Zingel et al [141] prepared iopromide-carrying liposomes by lypophilisation. DSC and resistance temperature measurements were used to determine the maximum allowable temperature during primary drying. Melting was detected at –21°C by DSC but conductivity changes down to –40°C were detected. The use of DSC and modulated methods of thermal analysis has been extended to freeze dried liposomal preparations [142,143].

Liposomes have also been used as models for the prediction of drug activity ranging from disruption of bilayers by antimicrobials [144] and the ability of anaesthetics to increase the fluidity of nerve cell membranes [145].

4.5. Thermal analysis and industrial processes

A number of pharmaceutical processes may result in a change of state of the processed material. Both spray drying and freeze-drying (lyophilisation) may result in a change in the solid state of a material, with a high possibility that amorphousness will be induced into a sample. Obviously thermal analysis is one of the fundamental techniques that may be used to characterise these products. Similarly coating by polymers, whether onto microspheres or tablets, involves solubilising the polymer and its consequent deposition may result in changes in polymer structure. This section examines the thermal analysis of spray-dried products, lyophilised products and of polymer films that might be used to coat dosage forms.

4.5.1. Spray-dried products

Spray-dried products are usually recognised for an increase in amorphousness. The technique offers a variety of operative conditions such as inlet and outlet temperatures, drug concentration and solvent, each of which may vary the crystallinity of the final product. Thermal analysis is thus used as one of the techniques to evaluate the final product, for example phenylbutazone and lactose.

Matsuda et al [146] provided evidence, via DTA, of the polymorphic transformation in spray dried phenylbutazone encouraged by varying the inlet temperature from 30° to 120°C. Importantly and indicative of its use, TGA was utilised to confirm that there was no residual solvent in the sample, in the form of a solvate. Two or three crystal forms were present. At 120°C the δ-form was produced, at 80° and 100°C, a mixture of two forms was formed and a third form was apparent at 70°C [146]. Mixtures containing two forms contained the β- and δ-form, and when three forms were present, they corresponded to the β-, δ- and ε-forms. A single DTA endotherm was found in samples prepared at 100° and 120°C with an endothermic peak at 103°C, equivalent to the δ-form. Melting endotherms at 91-92°C were found for samples obtained at 70°C and 80°C. In these samples a recrystallisation exotherm at 93°C, corresponding to the δ-form was found; again the δ-form subsequently melted as an endotherm at 103°C [146].

Therapeutically (and for reasons of stability) it is best if only one polymorph is present in the final product. Similarly, if amorphousness is produced in a sample, it should not be lost on storage, due to crystallisation. The likelihood of this transformation may be partly assessed by thermal analysis. Spray-drying caused amorphousness in spray dried hydroflumethiazide [147] which was demonstrated as an exotherm corresponding to recrystallisation of an amorphous sample (Figure 27), even when spray-dried in the presence of 1% to 20% w/w PVP. Its peak temperature increased with increasing levels of PVP, suggesting that PVP enhanced the stability of the system. The introduction of polymers, such as polyvinylpyrrolidone into the atomising solvent will favour, because of the induced high viscosity, the production of amorphousness.

The quality of a product may depend on the amorphousness within a sample. Spray-dried lactose is a term that embraces several types of products, depending on how the product was manufactured. If a suspension of α-lactose monohydrate is spray dried, the lactose in solution acts as a binder during the spraying process to bind the crystals of lactose together as aggregates. Thus, the predominant nature of α-lactose is maintained. The amorphousness of the

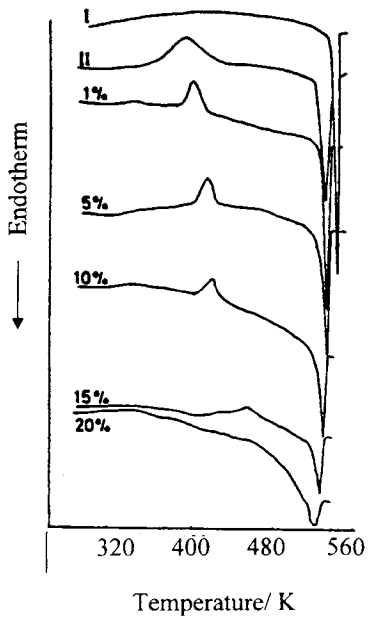

Figure 27. DSC scan of hydroflumethiazide spray-dried with PVP. I, crystalline drug; II, spray-dried drug. % values represent the per cent of PVP present in the final spray-dried material. From reference [147]; copyright permission requested.

bridges accounts for improvement of compressibility and its precise content is difficult to quantify.

Angberg [148] reviewed the manufacture of lactose products. Recrystallisation from a supersaturated lactose solution below 93.5°C yields almost exclusively α-lactose monohydrate. Crystalline lactose powders with a high content of anhydrous forms are manufactured for direct compression.

These are mixtures of anhydrous α- and β lactose, frequently containing a small amount of α-lactose monohydrate. DSC, DTA and TG have been used to characterise many of the forms of lactose. Some of these uses were reviewed previously [8]. However, isothermal microcalorimetry has the potential to quantify the amount of amorphousness in a sample. Exposure to moisture in a microcalorimeter will convert an amorphous form to a crystalline form. The energy of this transformation will be representative of the amorphous content [148]. Indeed the technique also allows the transformation of crystalline anhydrous α- and β-lactose to α-lactose monohydrate to be followed. Angberg [148] suggested that although dehydration could be followed by DSC, the equivalent process of rehydration via exposure of anhydrous materials to selected relative humidities, could be followed by microcalorimetry and the results of the two processes compared. Angberg [148] was able to demonstrate the hydration of anhydrous α-lactose in β-lactose that was roller dried. Also, β-lactose, at high humidities, could mutarotate to α-lactose which could subsequently hydrate [148]. This explanation was used to explain high heat flow signals at 94% RH. At lower humidities than 94% the hydration of α-lactose anhydrate could be followed. Following the DSC of the lactose derivatives, it was considered that α-lactose may mutarotate to β-lactose due to the increasing heat flow during a DSC measurement [149], especially in closed DSC sample pans. The β–lactose to α-lactose conversion is also possible in closed DSC sample pans [150].

Generally, DSC can be used to monitor increased hydration, by following the DSC dehydration. Angberg [148] also described a miniature humidity chamber technique at 100% RH, to monitor changes in lactose samples, since much of the heat evolution in conventional microcalorimetry took place in the early stages of the experiment and the data were therefore lost. The technique showed clearly the biphasic nature of water uptake in systems containing both anhydrous α- and β-lactose. However, again data were lost at the start of experimentation causing a problem in estimating α-lactose anhydrate content. Humidities lower than 100% RH slowed down the reaction rate [148].

However, as described earlier, amorphousness in lactose samples depends on the method of preparation. The amorphous portions are in a high energy state and should easily absorb water vapour. The amorphous portions will crystallise when the glass temperature has been decreased by the increased water content to below the experimental temperature [151]. Angberg [148] considered that in a sorption isotherm, crystallisation will be shown as a rapid drop in the curve, since the freed crystalline parts desorb the superfluous water. The amount of

water vapour absorbed before crystallisation provides an estimate of the small amounts of amorphous material [152]. When DSC is used, the amorphous material can be detected as subsequent recrystallisation. However at least a 10% amorphous content must be entrapped to produce a reliable result [152]. The miniature humidity chamber technique enables the amorphous content to be evaluated. A 100% amorphous sample, stored at 57% RH, showed three, endothermic heat flow phases, the first two phases representing the absorption of water by the amorphous content and the actual crystallisation process [152]. Integration of this second peak is a measure of the amorphous content. Microcalorimetry could probably be used down to an amorphous content of 1% [148]. Correlation with DSC and XRD data was achieved at 20% amorphous content. Below this level microcalorimetry was the more sensitive technique.

The position of the glass transition is difficult to prove by microcalorimetric techniques. Hill et al [38] specifically examined the glass transition temperature of spray-dried lactose using modulated temperature DSC. They prepared anhydrous lactose from its 10% w/v aqueous solution via spray drying with an inlet temperature of 130°C and an outlet temperature of 80°C. This produced a spray-dried material that was totally amorphous. The MTSCD raw data and converted curves were obtained at an overall heating rate of 2°C min^{-1}. Three peaks were generated with maxima at 117°, 171° and 206°C. The MTDSC deconvoluted heat flow compared well with the DSC conventional curve. Broad endotherms from 10° to 110°C corresponded to water loss, confirmed by TG analysis. A second small endotherm was apparent in both curves at 116°C. This was shown, via deconvoluted heat flow signals, to be equivalent to a glass transition temperature seen in the reversing heat flow curve [38]. The second change at 170°C was due to recrystallisation, followed by melting at >200°C. Hermetic pans, where water could not be released, did not show dehydration and the glass transition temperature was lowered to 75°C (by DSC) but 83°C for MTDSC [138].

4.5.2. Freeze-drying (lyophilisation)

The production of freeze-dried pharmaceuticals (and other products) is of paramount importance since many drugs, used in parenteral products, are freeze-dried powders intended for reconstitution in aqueous solvent prior to administration. Control of the freeze-drying conditions is important in producing a usable product and to allow drying of the sample. Residual water may result in drug degradation and conversion of a glassy state to a crystalline

state. Indeed the glassy state may be the least physico-chemically stable state and the crystalline state is the preferred status.

Thermal analysis has found a whole host of applications from determining cyclic conditions to characterisation of the final product. Ford and Timmins [8] reviewed the use of thermal analysis in lyophilisation up to 1988. Under simple conditions, freeze-drying consists of initially freezing the samples, often under rotation and/or quickly, to produce a shell of small ice crystals. A vacuum is applied to reduce the pressure to below the triple point. With the careful application of heat, large volumes of water vapour are produced, giving a porous solid. This is known as primary drying giving a solid of low moisture (~ 0.5%) that must be removed on secondary drying, often raising the temperature up to 50° to 60°C to produce a stable product [8]. Care has to be taken, however, to optimise the cycle. The heat added should not produce melting; to avoid foaming or puffing during freeze-drying the temperature should not exceed the eutectic temperature for a crystalline solute, or the collapse temperature for an amorphous state. Additionally on cooling the solute/eutectic might not recrystallise giving a glassy deposit in an ice matrix. This would give a long drying time and difficulty in removing solvent. Raising the temperature may induce crystallinity. Clearly it is not just a solution (or suspension) of the drug that is freeze dried. Buffers would also be entrapped giving a phase diagram type of eutectic reaction [153]. Once again, thermal analysis can be used to assess this phase equilibrium. Thermal analysis of a drug-sodium citrate-lactose system, in water, in the presence of 9.8% sodium chloride was undertaken to show a simple eutectic diagram [154]. In comparison, a drug-sodium citrate-lactose-sodium acetate (10.5:75:10) system did not show a melting endotherm corresponding to the eutectic, indicating that on cooling part of the system could be amorphous and difficult to freeze-dry [154]. The phase diagrams produced from thermal analysis may be used to determine the fraction melted at given temperatures. Patel and Hurwitz [154] considered that a high eutectic temperature and a low percentage melted at temperatures near the eutectic were desirable for freeze-drying vehicles.

The position of the glass transition temperature and its determination are vital to successful freeze-drying. Unfortunately, thermal analysis may not yield transitions equivalent to changes in electrical resistance. A study on nafcillin-sodium-water systems demonstrated that liquid crystal formation could take place [155]. Figure 28 shows that for a 15% drug content a small endotherm occurred at –5°C on the endotherm corresponding to water melting. On cooling, a single recrystallisation exotherm was visible but on rewarming the small

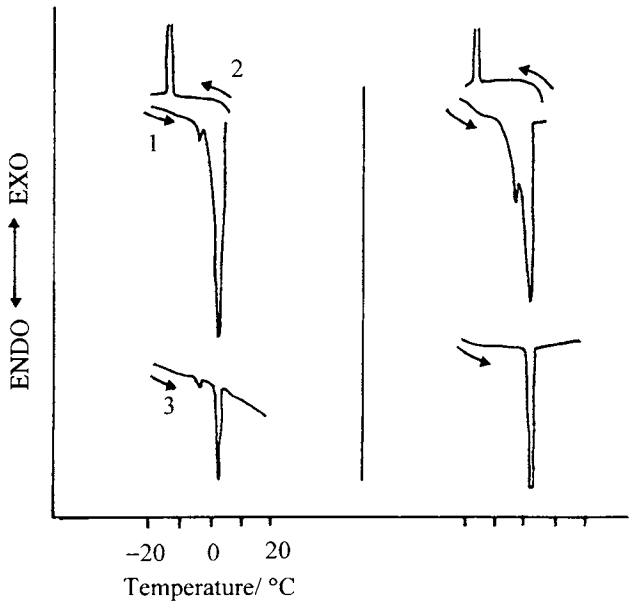

Figure 28. DSC scans for 15% nafcillin sodium-water mixtures. Scans 1 and 2 were run at 2.5°C/min while scan 3 was obtained at 0.625°C/min. Prior to scan 1 the samples were cooled from ambient temperature to −20°C at 2.5°C/min. From reference [155]; copyright permission requested.

endotherm was still apparent but the major melting endotherm was narrower. A lack of melting point depression was attributed to micelle formation. A small endotherm present in the initial run but not in the re-warming run for the 35% drug system [155] was postulated to be caused by a metastable eutectic formation. Hot stage microscopy was required to relate the transitions to the presence of three crystalline phases and a lamellar mesophase.

Thermogravimetry may be used to determine the water content of products that have been freeze-dried, ideally using a coupled method of analysis to confirm the nature of the volatile(s) associated with the loss.

The optimisation of the process is best illustrated with reference to the studies of Gatlin and De Luca [156]. Rapid cooling, prior to primary drying, may result in a glassy state being produced. Thermal analysis can predict the temperature at which the glassy transition occurs. Above this temperature, recrystallisation can be induced in a sample. The DSC scans of a typical solution of cefazolin sodium solution depicted a glass transition temperature at –20°C as an endothermic shift, a recrystallisation endotherm at –11°C and ice melting starting at –4°C. A similar composition was pre-treated following cooling by warming to –6°C. This allowed recrystallisation to occur. Re-cooling to –25°C showed only the melting of ice on the subsequent DSC scan [156]. This indicated a conversion of the amorphous form to a crystalline drug. This suggested that rewarming and cooling should be incorporated into the manufacturing cycle to produce a crystalline product.

One other point of interest of thermal analysis in freeze drying is the use in examining phase concentration. Frequently, inert sugars or polyhydric alcohols such as mannitol or sucrose are included in solutions to be freeze dried. Roos [157] reviewed the frozen state transitions in relation to freeze-drying. It is these conditions that should be used to derive a proper freeze-drying condition. Freeze-dried products should be porous and easy to hydrate. However if collapse occurs during dehydration a product may exhibit poor dehydration properties. Collapse occurs if the temperature of ice is higher than the collapse temperature, T_c, of a material.

The state diagram (Figure 29) of sucrose displays the problems to freeze-drying induced by highly viscous materials which do not readily recrystallise on cooling. DSC or DTA may be used to establish the state diagram of the system. Rapid cooling to a temperature below the T_g of the solution followed by analysis produces scans that will demonstrate the T_g of the solution, followed by recrystallisation and melting processes. Slow cooling, depending on composition, allows crystallisation of ice particles that continues initially increasingly as the temperature is lowered. However, the remaining solution will become increasingly viscous which eventually retards further recrystallisation. This solution is said to be freeze concentrated; the proportion of water decreases in the non-crystallised material [157]. This material passes through its own transition temperature T_g' which is said to be the glass transition temperature of the maximally freeze-concentrated solution. The T_g' is

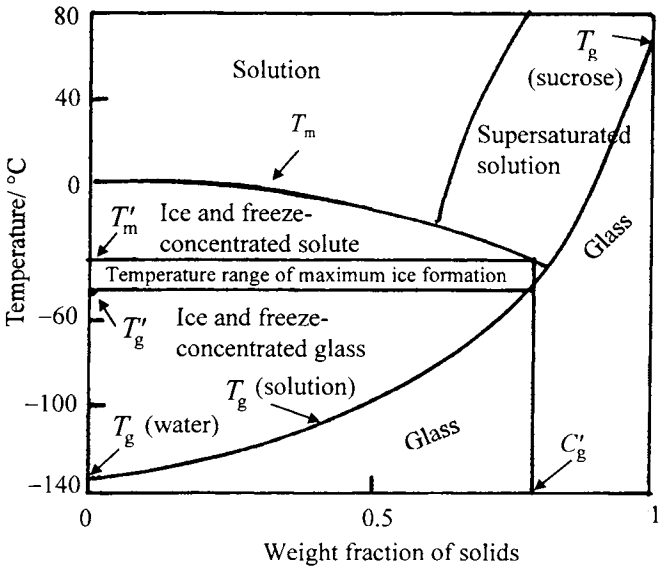

Figure 29. State diagram for sucrose showing experimental and predicted data for equilibrium ice melting temperature, T_m, onset temperature for ice melting within the maximally freeze-concentrated solute matrix, T'_m, glass transition temperature of the maximally freeze-concentrated solute matrix, T'_g, with concentration, C'_g, and glass transition temperature, T_g, as a function of solute concentration. From reference [157]; copyright permission requested.

relatively independent of the initial solute concentration (Figure 29). DSC of these treated solutions will display a T_g' followed by a T_m', which may be

defined as the onset temperature of ice melting. DSC (or DTA) of these solutions will, in the case of a rapidly cooled solution, demonstrate a T_g that can be predicted by the Gordon-Taylor equation, followed by recrystallisation of ice, known as devitrification, before final melting occurs. In the temperature range between T_g' and T_m' maximum recrystallisation can occur. Therefore annealing the sample at temperatures intermediate to T_g' and T_m' will allow recrystallisation. Subsequent DSC will show the T_g' (not the T_g) and the T_m', characteristic of the initial melting.

Figure 30 demonstrates a typical example. Knowledge of these temperatures is indispensable to optimising freeze-drying [157]. It is essential to the

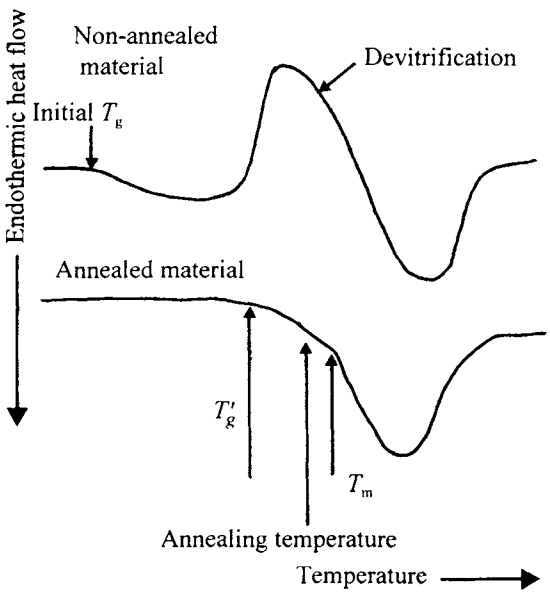

Figure 30. Schematic representation of scans of rapidly cooled, nonannealed sugar solutions and annealed sugar solutions with maximum ice formation after proper annealing at $T_g' < T < T_m'$. From reference [157]; copyright permission requested.

successful freeze drying of sugars (and proteins) that collapse does not occur (at or above the collapse temperature, T_c), and that amorphousness is maintained in the samples, at least in the freeze-concentrated portion. DSC and DTA demonstrate that annealing the sample at temperatures between T_g' and T_m' allows successful freeze-drying. Thus, according to Roos [157], temperatures below T_g' allow removal of ice from within the solid, glassy solutes with no change in volume. At temperatures above T_m' unfrozen material exists that means sublimation is not occurring. Therefore collapse can result, preventing effective water removal since the material can flow, collapse and/or foam. These events are composition dependent, hence the need to produce an accurate state diagram. Additionally, if the samples are stored above their T_g (of the solid) reabsorption of water will depress the T_g, plasticise the material and cause collapse on storage.

Incidentally, knowledge of the state diagram also explains why low molecular weight sugars are difficult to freeze-dry. The T_g' values for pentoses are –65°C to –67°C, hexoses –57°C to –62°C but disaccharides are –40°C to –46°C. Similarly the T_g' increases in the order pentoses < hexoses < disaccharides [157]. Values for high molecular weight carbohydrates of T_g' and T_g merge at around 0°C. Therefore, high molecular weight materials may be added to biological materials to prevent collapse and loss of quality on freeze-drying and subsequent storage [157].

Finally, on two points. Most maximally freeze-concentrated carbohydrates contain ~80% w/w solids and 20% w/w unfrozen water [158] and that for ionic materials, crystalline freeze-dried materials are easily obtained when the T_c is at temperatures above the eutectic melting temperature [159].

4.5.3. Polymeric films and film coating

Thermal analysis of polymeric blends has proved an indispensable method of improving the quality of films used to film coat tablets. An earlier section described how the T_g of polymers produced from films can be determined. It is appropriate to coat pharmaceuticals for taste masking, to protect against moisture-induced and light-induced degradation and to modify the release of drug from the coated dosage forms. Whichever its purpose, it is imperative that the coat be intact to avoid penetration or rapid drug release. The coat should also be capable of stretching and contracting during the coating and storage. In the broadest sense, therefore, the coat should possess a glass transition temperature that is below the coating temperature to allow stretching. Drug release, via diffusion through a coating membrane, is more rapid when the film

is in its rubbery state above the T_g. Because of the increased polymer flexibility, diffusion is facilitated. Drug release may also occur via diffusion through pores in the membrane. This may be facilitated by using polymers which are deemed to be incompatible or immiscible. Each phase will display a separate glass transition.

It should be borne in mind that to reduce the T_g of a polymer, a plasticiser may be added, for example polyethylene glycol, glycerol or triethylcitrate. No matter what the proposed function of the polymer film, thermal analyses provides an excellent means of determining phase compatibility and the glass transition temperature. It should not be forgotten that one of the best plasticisers is water and indeed the effects of water can be easily determined from a knowledge of the glass transition across the polymer:water composition range. Such studies have been performed with polyvinylpyrrolidone-water [160].

Plasticisation of a polymer results in a lowering of the glass transition temperature, with a broadening of the range over which the transition occurs [161]. The determination of the thermal properties utilises the full gambit of thermal analytic techniques.

Hydrophilic cellulose ethers, such as HPMC, are plasticized by water but also by the addition of specific plasticisers. Okamafe and York [161] demonstrated that the glass transition temperature of HPMC was reduced by the addition of triethyl citrate. This was detected by both a lowering of the glass transition temperature and a broadening and lowering of a softening point as detected by thermomechanical analysis [161]. The glass transition could be obscured because the transition broadened to a range in excess of 30°C. Such transitions may be detected by modulated methods of thermal analysis, as seen for instance in the DDSC of the films of Surelease®, a commercial latex formulation of ethylcellulose [120].

In situations where complete miscibility occurs between polymer and polymer or polymer and plasticiser throughout the composition range, only one glass transition temperature will be detected. This can be predicted from the glass transition of the individual components by use of, for instance, the Gordon-Taylor equation. Where complete miscibility does not occur, the incorporation of a plasticiser will lower the T_g to a level where the solubility of the plasticiser is exceeded. At higher plasticiser levels, transitions due to both the plasticiser and the plasticised polymer will be detected. The former, in the case of PEG as a plasticiser, will be a melting transition. In the case of the latter, the transition will be a glass transition. Such examples are the plasticisation of

HPMC by PEG which has been followed by both DSC [162] and torsional braid analysis (TBA) [163].

In polymer-polymer systems where there is limited mutual solubility, and therefore immiscibility at intermediate compositions, an even more complicated situation arises whereby the polymers are said to be incompatible. Such an example is provided by admixtures of ethylcellulose and HPMC [164]. In films containing low levels of EC, two transitions were apparent. One is equivalent to ethylcellulose-rich HPMC phase, the other is due to an HPMC-rich phase. These two phases are immiscible. Similarly to the ethylcellulose rich side of the composition, low levels of HPMC resulted in two phases. Such changes may be too subtle to be detected by DSC or DTA. They are picked up in the mechanical spectra of DMA curves or by TBA. The studies of Sakellariou and other workers [163-166] confirm these findings. Figure 31 displays a typical spectrum determined by torsional braid analysis. Clearly, TBA and DMA provide more than useful techniques in determining both glass transitions and phase miscibility. Sakellariou et al [166] also examined the interactions and partitioning of PEG 400 in HPMC and PVA blends by TBA, showing PEG 400 to be the better plasticiser for HPMC than PVA. The polymer films, by necessity, are prepared by casting from their solutions. These may be cast directly onto glass surfaces or by dipping the braid (a series of glass spindles) into the other polymeric solution. The former technique may also be used to produce films that may be cut and prepared for DSC, giving a means of providing good thermal contact with the sample pans.

The separation into two phases of aqueous mixed polymers can be detected by DMA and DSC. Sakellariou et al [167] showed that these techniques proved separation in PVA/HPMC blends where each phase excluded the other polymer. The HPMC rich phase was amorphous with a constant T_g. The PVA phase showed a limited degree of crystallinity but a constant T_g for the amorphous part.

4.6. Thermal analysis of transdermals and semi-solids

This is a broad area of thermal analysis, samples ranging from the triglycerides and polyethylene glycols that are the basis of pessaries and suppositories, through to formulated creams and ointments.

Typical studies on suppository bases were demonstrated by Liversidge et al [112]. Melting triglycerides on an initial DSC scan shows the material as supplied by the manufacturer. It would be expected that this would represent the most stable polymorphic form. The scan would show only one peak if one solid

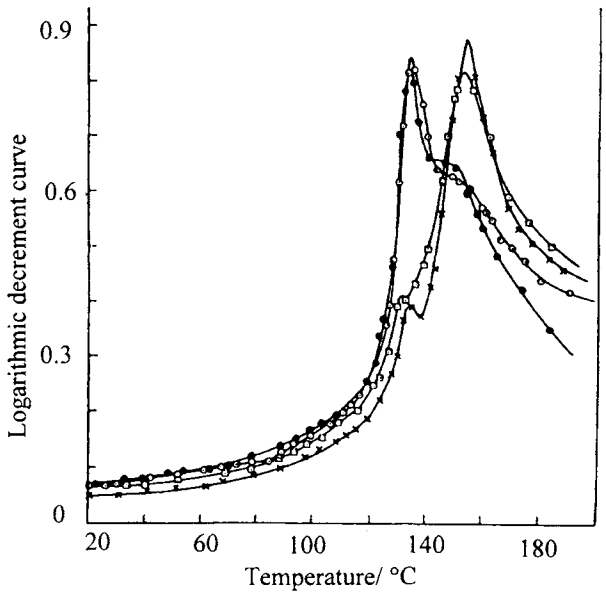

Figure 31. The thermomechanical spectra (logarithmic decrement curves) for ethylcellulose/hydroxypropylmethylcellulose blends. Percentages are of ethylcellulose by weight. Reprinted from reference [164] with permission from Elsevier Science.

state had formed and that corresponded to the stable polymorph. Obviously if more than one melting endotherm or exotherms are present the solid has more than one structural form. Indeed, recrystallisation between the melting endotherm indicates an ease of conversion [112]. However, the shape of the DSC scan is very much heating rate dependent. A faster speed may not allow solid-solid or solid-liquid-solid conversions to occur. A slow speed, if the enthalpies are low, may not allow detection of certain transitions. Figure 32 shows the effect of scanning speed on the DSC of a tristearin. DSC can be used

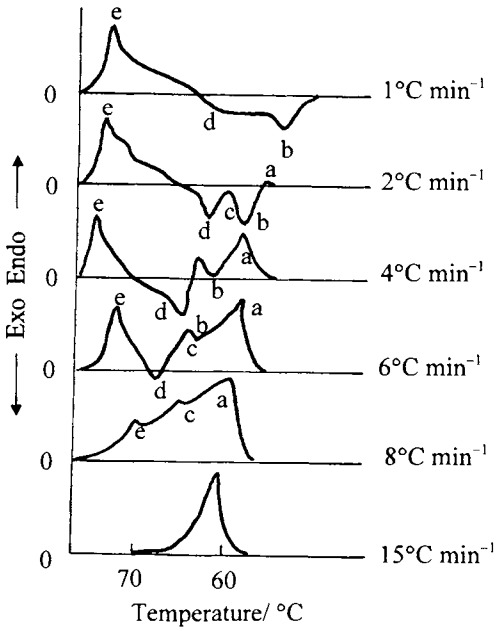

Figure 32. The effect of heating rate on the DTA curve of tristearin (6 mg). The assignment of the peaks is as follows: a, melting of α-polymorph; b, crystallisation of β′-polymorph; c, melting of β′-polymorph; d, crystallisation of β-polymorph; e, melting of β-polymorph. Reprinted from reference [112] with permission from Elsevier Science and The Royal Society of Chemistry.

to assess the form of a solidified formulation. Additionally knowledge of potential changes may also give cognisance of potential storage and formulation problems.

Similar changes may be seen for ointment bases such as polyethylene glycol (e.g. PEG 6000; Figure 23). The lower enthalpies of the second scan are due to an increased amorphousness in the samples. Certainly for PEG this suggests

that a gradual increase of structure, indeed of crystallinity, may occur on storage. Again, such knowledge can be used to optimise formulation.

Formulated creams, whether they are either oil in water (o/w) or water in oil (w/o) emulsions, provide a complicated structure [168]. An o/w cream is a mixture of a basic continuous aqueous phase, hydrated ingredients, and liquid crystals. Each of these contribute to peaks shown on a DSC scan. The proportion of each peak alters according to the formulation of the product and is altered by the manufacturing conditions. Thermal analysis provides a means of optimising formulation, manufacture and storage problems [168]. Even TGA may be used to assess the physical properties of creams. TGA showed two main peaks in the first derivative curves of Aqueous Cream BP corresponding to free and lamellar water [169]. The profiles varied to the manufacturing source of the creams although there appeared poor correlation with rheological measurements.

A typical study by Simon and Suverkrup [170] compared techniques used to characterise the crystallisation behaviour of fatty acid bases. In addition to DSC, isothermal DSC, NMR, oscillation rheometry and thermorheography were used. The crystallisation of hard fats was a biphasic process [170]. The formation of crystal nuclei was controlled by the partial glyceride content; the degree of super-cooling determined the formation of crystal nuclei; the final solidification level depended on the crystallisation temperature. Similar studies [171] showed that the recrystallisation rates and the degree of supercooling before crystallisation occurred depended on the molecular weight of PEG.

Many suppositories are composed of triglyceride bases. Thermal analysis was used [172] to determine the influence of monoglycerides, a fatty acid - fatty acid methyl ester blend, fatty acid polyethylene glycol esters and indomethacin on the melting behaviour and hardening of triglyceride suppository bases. Incorporation of indomethacin resulted in higher melting temperatures but no important influence of the additives or the drug were seen on the hardening behaviour of the suppository bases [172].

Pryce-Jones et al [173] used DSC to investigate decomposition of aminophylline suppositories as a rapid and sensitive detection method for the appearance of decomposition products. The DSC scans indicated that ethylenediamine interacted with the suppository base. The decomposition product of the aminolysis of the triglycerides were responsible for the observed changes in the DSC scans.

The thermal analysis of creams is more complicated. Pasaleevan and Nurnberg [174] examined binary macrogol stearate 400 - water systems.

Lamellar arrangements were detected by polarised light microscopy. DSC and XRD confirmed that chains of emulsifier were in the crystalline state. Ternary systems with liquid paraffin were isotropic, homogenous o/w creams for a wide composition range. Incorporation of 50 mol % cholesterol lead to the separation of a gel-liquid crystalline phase within the layer [174]. The transition energies, derived from DSC, decreased linearly with increasing cholesterol concentration. Optical microscopy should be used to confirm phase separation in creams [175].

Lashmar et al [176] examined process variables for the manufacture of a semi-solid paraffin in water emulsion. The total DSC enthalpy change was used as an important indicator of the stability of an o/w emulsion together with the appearance under polarised light. On this basis, homogenisation speed was identified as the single most important factor or the production of a stable emulsion.

4.7. Transdermal delivery of drugs

The use of penetrants to increase the passage of drugs through the skin to allow for systemic delivery has become an area of major research which is at the interface of the biological and pharmaceutical disciplines. The use of penetrants, such as azone, increases drug passage by increasing the permeability of the skin. The theory is that the penetrants actually modify the biochemical nature of the stratum corneum. Such modifications can be detected by a number of techniques including thermoelectric measurements [177], FTIR spectroscopy [178,179] and thermal methods such as DSC [180,181].

These events such as those shown in Figure 33 which displays an alleged change in skin structure can be attributed to plasticisation and a consequent change in the second-order structure of the skin. A variety of skins has been used to examine penetrants varying from human cadaver skin to porcine skin. It is well understood that the passage of drugs is modified by the hydration status of the skin.

A number of enhancers has been shown to alter skin structure. Kaplun-Frischoff and Touitou [182] used DSC to show that menthol decreased the melting point of cholesterol oleate and ceramides and modified the DSC scan of isolated stratum corneum. This partly accounted for an eight-fold enhancement of the skin flux of testosterone.

Moghimi et al [183] recognised that the principal barrier to transdermal delivery of many drugs is the lamellar intracellular lipid matrix of the stratum corneum. A model matrix was prepared containing 20% cholesterol, 25% water and 55% stratum corneum free fatty acids and their soaps. DSC of the matrix

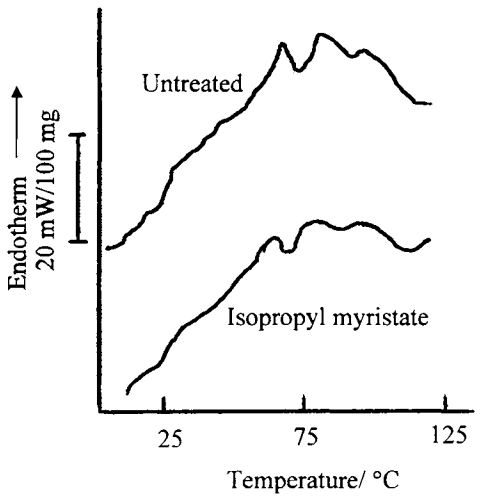

Figure 33. Typical DSC scans for human stratum corneum after pretreatment with different vehicles. From reference [185]; copyright permission requested.

showed seven endothermic peaks in the range –30°C to 120°C. These corroborated studies using hot stage polarised light microscopy that showed a lamellar mesomorphic structure from ambient to ~100°C, a hexagonal mesomorphic phase at 105°C and an isotropic liquid at 140°C [183]. DSC also showed that 20% of the water was bound in the matrix.

The destruction of the intercellular lipid lamellar structure is important to increasing the permeation of drugs such as 5-fluorouracil. DSC has been used to probe the mechanisms by which enhancers exert their effects [184]. The enhancement effects of d-limonene and oleic acid are saturable within 6 h [184].

Leopold and Lippold [185] used DSC of isolated human stratum corneum to determine which materials were penetration enhancers. The stratum corneum

was treated with isopropylmyristate, light mineral oil, caprylic/capric acid triglycerides containing phospholipids, dibutyl adipate, dimethicone 100 and triglycerides [185]. Most vehicles altered the phase transition temperatures and the enthalpies of the stratum corneum lipids. Mineral oil and isopropyl myristate reduced the enthalpy and decreased the phase transition temperatures suggesting that these vehicles fluidised the lamellar-gel phase of the stratum corneum lipids and that they partially dissolved the lipids. Dibutyl adipate and caprylic/capric acid triglycerides containing 5% phospholipids decreased the enthalpy only, possibly due to extraction or dissolution of the stratum corneum lipids [185].

Recently Al-Saiden et al [181] examined the thermal transitions in desiccated stratum corneum membranes of neonatal rats, rabbits and adult abdominal human skin. Four endothermic transitions were observed at 39-45°C, 55-58°C, 68-74°C and 77-86°C. The transitions at 39-45°, 68-74° and 77-86°C were attributed to phase charges in the intercellular lipid bilayers. A fifth transition at 48° was seen only in the neonatal rabbit stratum corneum and was attributed to lipid melting.

Numerous studies have attempted to elucidate the effect of skin penetrants by thermal analysis. Kaplun-Frischoff and Touitou [182] showed that methanol decreased the melting peaks of cholesteryl oleate and ceramides and modified the DSC of isolated stratum corneum; this alters its barrier properties. Similarly a soybean-lecithin micro-emulsion gel was shown to affect the stratum corneum lipid organisation by FTIR and DSC [186] and hydroxypropyl-β-cyclodextrin can increase the permeability of the stratum corneum, possibly as a result of lipid extraction that induced modest changes in the stratum corneum lipid transition temperature [179].

The structure of stratum corneum lipids by DSC has been described in a series of papers [178,187,188]. Cornwall et al. [189] examined the modes of action of terpene penetration enhancers. DSC identified two major lipid transitions at 72°C and 83°C in stratum corneum. d-Limonene reduced the temperatures of both transitions by ~20°C without effecting the transition enthalpies. 1-8-Cineole reduced the temperatures similarly but the enthalpy for the first transition was reduced. d-Limonene increased the combined entropy change of both transitions by 11%, whereas 1-8-cineole decreased the entropy by 32%. This suggested that 1-8-cineole is lipid disruptive at skin temperature.

REFERENCES

1. J.I. Wells, Pharmaceutical Preformulation, Ellis Horwood, Chichester, 1988.
2. R.C. Rowe, M.D. Parker, D. Bray, Pharm. Tech. Eur., 6 (2) (1994) 26.
3. L. Parnetti, Clin. Pharmacokinetics, 2 (1995) 110.
4. D.D. Wirth, S.W.Baertschi, R.A. Johnson, S.R. Maple, S.M. Gregg, J. Pharm. Sci., 87 (1998) 31.
5. A. Constantinescu, D. Han, L. Packer, J. Biol. Chem., 268 (1993) 10906.
6. H.P. Klug, L.E. Alexander, X-ray Diffraction Procedures for Procrystalline and Amorphous Materials, Wiley, New York, 1974.
7. G. Buckton, A.E. Beezer, Int. J. Pharm., 72 (1991) 181.
8. J.L. Ford, P. Timmins. Pharmaceutical Thermal Analysis, Techniques and Applications, Ellis Horwood, Chichester, 1989.
9. L.S. Taylor, G. Zografi, Pharm. Res., 15 (1998) 755.
10. A.T. Florence, D. Atwood, Physiochemical Principles of Pharmacy, MacMillan Press Ltd., London, 1998.
11. D. Giron, Thermochim. Acta, 248 (1995) 1.
12. A. Burger, Acta Pharm. Technol., 28 (1982) 1.
13. J.A. McCauley, A.I.Chem. Eng. Symp. Serv., 87 (1991) 58.
14. D. Giron, S.T.P. Pharma, 6 (1990) 87.
15. A. Hakanen, E. Laine, Thermochim. Acta., 248 (1995) 217.
16. E. Laine, J. Pirttimaki, R. Rajala, Thermochim. Acta., 248 (1995) 205.
17. J.T. Carstensen, M.K. Franchini, Drug Dev. Ind. Pharm., 21 (1995) 523.
18. A.Grunenberg, B. Keil, J.O. Henck, Int. J. Pharm., 118 (1995) 11.
19. L.C. Chang, M.R. Caira, J.K. Guillory, J. Pharm. Sci., 84 (1995) 1169.
20. R.A. Carlton, T.J. Difeo, T.H. Powner, I. Santos, M.D. Thompson, J. Pharm. Sci., 85 (1996) 461.
21. M. Bartolomei, M.C. Ramusino, P. Ghetti, J. Pharm. Biomed. Anal., 15 (1997) 1813.
22. D. Giron, M. Draghi, C. Goldbronn, S. Pfeffer, P. Piechon, J. Therm. Anal., 49 (1997) 913.
23. J. Masse. O Hourri, P. Bernier, M. Ribet, Thermochim. Acta., 216 (1993) 191.
24. M. Otsuka, Y. Matsuda, J. Pharm. Pharmacol., 45 (1993) 406.
25. J.L. Ford, Int. J. Pharm., 179 (1999) 209.
26. J.W. Donovan, K. Lorenz, K. Kulp, Cereal Chem., 60 (1983) 381.
27. L.N. Bell, Drug Dev. Ind. Pharm., 21 (1999) 164.

28. Thermometric product information. RH perfusion device. Thermometric, AB, Jafalla, Sweden.
29. Y. Takahashi, K. Nakashima, I. Sugimoto, Chem. Pharm. Bull., 32 (1984) 4963.
30. N.A. Lange, G.M. Forker (eds.), Handbook of Chemistry, Handbook Publishers, 9th. Ed., 1956.
31. J. Kiesvaara, Pharm. Tech. Int., 5 (1993) 40.
32. B. Bhatt, M.H. Rubinstein, Drug Dev. Ind. Pharm., 9 (1983) 215.
33. M. Pudipeddi, T.D. Sokoloski, S.P. Duddu, J.T. Carstensen, J. Pharm. Sci., 85 (1996) 381.
34. K. Umprayn, R.W. Mendes, Drug Dev. Ind. Pharm., 13 (1987) 653.
35. M.S. Bergren, Int. J. Pharm., 103 (1994) 103.
36. J.. Ford, Drug Dev. Ind. Pharm.,13 (1987) 1741.
37. D.M. Craig, P.G. Royall, V.L. Kett, M.L. Hopton, Int. J. Pharm., 79 (1999) 179.
38. V.L. Hill, D.Q.M. Craig, L.C. Feely, Int. J. Pharm., 161 (1998) 95.
39. H. McPhillips, D.Q.M. Craig, P.G. Royall, V.L. Hill, Int. J. Pharm., 180 (1999) 83.
40. V. Velasco, J.L. Ford, A.R. Rajabi-Siahboomi, Pharm. Res., in press.
41. P.G. Royall, D.Q.M. Craig, C. Doherty, Pharm. Res., 15 (1998) 1117.
42. L.E. Briggner, G. Buckton, K. Bystrom, P. Darcy, Int. J. Pharm., 105 (1994) 125.
43. K. Bystrom, L-E Briggner, Resp. Drug Del., 4 (1994) 297.
44. T. Sebhatu, M. Angberg, C. Ahlneck, Int. J. Pharm., 104 (1994) 135.
45. H. Ahmed, G. Buckton, A. Rawlins, Int. J. Pharm., 167 (1998) 139.
46. W. Curatolo, Pharm. Sci. Tech. Today, 1 (1998) 387.
47. A.E. Beezer, Pure Appl. Chem., 61 (1989) 153.
48. D. Giron, C. Goldbronn, J. Therm. Anal., 44 (1995) 217.
49. K. Yamamoto, H. Kitamura, M. Momota, K. Narita, Thermochim. Acta., 267 (1995) 313.
50. K. Yamamoto, M. Momota, H. Kitamura, K. Narita, Anal. Sci., 12 (1996) 893.
51. K. Yoshii, Chem. Pharm. Bull., 45 (1997) 338.
52. R.J. Prankerd, M.Z. El-Sabee, (1995) Thermochim. Acta., 248 (1995) 147.
53. T. Beyrich, J. Junghanel, G. Mietz, J. Hauschke, Pharmazie, 52 (1997) 512.

54. R.J. Willson, A.E. Beezer, A.E. Hills, J.C. Mitchell, Thermochim. Acta., 325 (1999) 125.
55. Thermometric product information. High Sensitivity titrations with the Nano-Watt amplifier, Thermometric AB, Jafalla, Sweden.
56. R.J. Willson, A. E. Beezer, J.C. Mitchell, W. Loh, J. Phys. Chem., 99 (1995) 7108.
57. Mathsoft, 101 Main Street, Cambridge, MA 02142, USA.
58. Microcal Software, One Roundhouse Plaza, Northampton, MA 01060, USA.
59. L.E. Briggner, I. Wadso, J. Biochem. Biophys. Meth., 22 (1991) 101.
60. R.J. Willson, A.E. Beezer, J.C. Mitchell, Thermochim. Acta., 264 (1995) 27.
61. M.J. Pikal, K.M. Dellerman, Int. J. Pharm., 50 (1989) 233.
62. P. Jacobs, F. Tompkins, W.E. Garner (Eds.), Chemistry of the Solid State, Butterworths, London 1955.
63. W. Ng, Aust. J. Chem., 28 (1975) 1169.
64. S.R. Bryn, Solid State Chemistry of Drugs, Academic Press, London, 1982.
65. R.J. Willson, A.E. Beezer, J.C. Mitchell, Int. J. Pharm., 132 (1996) 45.
66. S.P. Duddu, N.G. Das, T.P. Kelly, T. Sokoloski, Int. J. Pharm., 114 (1995) 247.
67. J.T. Carstensen, R.C. Kothari, J. Pharm. Sci., 72 (1983) 1149.
68. M.J. Koenigbauer, S.H. Brooks, G. Rullo, R.A. Couch, Pharm. Res., 9 (1992) 939.
69. J.T. Carstensen, R.C. Kothari, J. Pharm. Sci., 70 (1981) 1095.
70. V. Lehto, E. Laine, Thermochim. Acta., 317 (1998) 47.
71. A.L.W. Po, P. Mroso, W.J.Irwin, Int. J. Pharm., 16 (1983) 115.
72. D. Dollimore, J. Therm. Anal., 38 (1992) 111.
73. H.E. Kissinger, Anal. Chem., 29 (1957) 1702.
74. ASTME E698-79 Arrhenius kinetic constants for thermally unstable materials, 624.
75. T. Ozawa, J. Therm. Anal., 2 (1970) 301.
76. C.O. Agbada, P. York, J. Pharm. Pharmacol., 41 (1989) 65P.
77. D.E. Brown, M.T. Hardy, Thermochim. Acta., 90 (1985) 149.
78. Y. Matsuda, E. Tatsumi, E. Chiba, Y. Miwa, J. Pharm. Sci., 73 (1984) 1453.
79. K. Sasaki, H. Suzuki, H. Nakagawa, Chem. Pharm. Bull., 41 (1993) 325.
80. H.J. Borchardt, F. Daniels, Chem. Phys., 79 (1957) 41.

81. E.S. Freeman, B. Carroll, J. Phys. Chem., 62 (1958) 394.
82. J.H. Flynn, L.A. Wall, Polym. Lett., 4 (1966) 323.
83. H. Jacobson, J.H. Reier, J. Pharm. Sci., 58 (1969) 631.
84. R.E. Gordon, C.L. van Koevering, D.J. Reits, Int. J. Pharm., 21 (1984) 99.
85. P. Mura, A. Manderioli, G. Bramanti, S. Furlanetto, S. Pinzauti, Int. J. Pharm., 119 (1995) 71.
86. M.A. Holgado, M. Fernandez-Arevalo, J.M. Gines, I Caraballo, A.M. Rabasco, Pharmazie, 50 (1995) 195.
87. F. Balestrieri, A.D. Magri, A.L. Magri, D. Marini, A. Sacchini, Thermochim. Acta., 285 (1996) 337.
88. S. Aoki, A. Okamoto, K. Danjo, H. Sunada, A. Otuka, Drug Dev. Ind. Pharm., 23 (1997) 561.
89. C.E.P. Malan, M.M. deVilliers, A.P. Lotter. Drug Dev. Ind. Pharm., 23 (1997) 533.
90. M.E. Brown, A.K. Galwey, G.G.T. Guarini, J. Therm. Anal., 49 (1997) 1135.
91. N.J. Coleman, D.Q.M. Craig, Int. J. Pharm., 135 (1996) 13.
92. M.J. Koenigbauer, Pharm. Res., 11 (1994) 777.
93. J.E. Ladbury, B.Z. Chowdhry, Biocalorimetry, Applications of Calorimetry in the Biological Sciences, Wiley, Chichester, 1998.
94. A. Cooper, C.M. Johnson, Methods in Molecular Biology, Vol. 22, C. Jones, B. Mulloy and A. Thomas (Eds), Humana Press, Totowa NJ, 1994.
95. A. Fersht. Enzyme Structure and Function, W.H Freeman and Co., New York, 1977.
96. R.W. Gurney, Ionic Processes in Solution, McGraw Hill, New York, 1977.
97. M.J. Blandamer, M.D. Butt, P.M. Cullis, Thermochim. Acta., 211 (1992) 49.
98. A. Cooper, C. Converse, Biochemistry, 15 (1976) 2970.
99. C. Teixeira, I. Wadso, J. Chem. Thermodyn., 22 (1990) 703.
100. C. Teixeira, I. Wadso, Netsu Sokutei, 21 (1994) 29.
101. D.J.W. Grant, H. Jacobson, J.E. Fairbrother, C.G. Patel, Int. J. Pharm., 5 (1980) 109.
102. J.L. Ford, Pharm. Acta Helv., 61 (1985) 69.
103. J.L. Ford, M.H. Rubinstein, Pharm. Acta Helv., 53 (1978) 327.
104. F. Theeuves, A. Hussein, T. Higuchi, J. Pharm. Sci., 63 (1974) 427.
105. D.Q.M. Craig, Thermochim. Acta., 248 (1995) 189.

106. S.K. Dordunoo, J.L. Ford, M.H.Rubinstein, Drug Dev. Ind. Pharm., 17 (1991) 1685.
107. J.L. Ford, M.M. Francomb, Drug Dev. Ind. Pharm., 11 (1985) 1111.
108. T.T. Yang, J. Swarbrick, J.Pharm. Sci., 75 (1986) 53.
109. D.Q.M. Craig, J.M. Newton, Int. J. Pharm., 76 (1992) 17.
110. S.K. Dordunoo, J.L. Ford, M.H. Rubinstein, J. Pharm. Pharmacol., 49 (1997) 390.
111 E.S. Saers, C. Nystrom, M. Alden, Int. J. Pharm., 90 (1993) 103.
112. E.G. Liversidge, D.J.W. Grant, J.M. Padfield, Anal. Proc., 19 (1982) 549.
113. C.P. Buckley, A.J. Kovacs, Colloid Polym. Sci., 254 (1976) 693.
114. D.Q.M. Craig, J.M. Newton, Int. J. Pharm., 74 (1991) 33.
115. D.Q.M. Craig, F.A. Johnson. Thermochim. Acta., 248 (1995) 97.
116. D.Q.M. Craig, J.M. Newton, R.M. Hill, J. Mat. Sci., 28 (1993) 405.
117. J. Rak, J.L. Ford, C. Rostron, V. Walters, Pharm. Acta Helv., 60 (1985) 162.
118. V.L. Hill, N. Passerini, D.Q.M Craig, M. Vickers, J. Anwar, L.C. Feely, J. Therm. Anal., 54 (1998) 673.
119. D.J. Armstrong, P.N.C. Elliott, J.L. Ford, B. Guiziou, C. Rostron. Proc. 13th Pharm. Tech. Conf. (Strasbourg), 1 (1994) 57.
120. M.V. Velasco, J.L. Ford, A.R. Rajabi-Siahboomi. Pharm. Pharmacol Commun., 5 (1999) 259.
121. S.C. Porter, K. Ridgeway. J. Pharm. Pharmacol., 35 (1983) 341.
122. P. Sakellariou, R.C. Rowe, E.F.T. White, Int. J. Pharm., 22 (1985) 267.
123. A. Nokhodchi, J.L. Ford, P.H. Rowe, M.H. Rubinstein, J. Pharm. Pharmacol., 48 (1996) 116.
124. C.D. Melia, Crit. Rev. Ther. Drug Sys., 8 (1991) 395.
125. G. Bhaskar, J.L. Ford, D.A. Hollingsbee, Thermochim. Acta., 322 (1998) 153.
126. C.B. McCrystal, J.L. Ford, A.R. Rajabi-Siahboomi, Thermochim. Acta., 294 (1997) 91.
127. H.N. Joshi, T.D. Wilson, J. Pharm. Sci., 82 (1993) 1033.
128. A. Nokhodchi, J.L. Ford, M.H. Rubinstein, J. Pharm. Sci., 86 (1997) 608.
129. W-Z Zhang, M. Satoh, J. Komiyama, J. Membr. Sci., 42 (1989) 303.
130. C.B. McCrystal, J.L. Ford, R. Ho, D.Q.M. Craig, A.R. Rajabi-Siahboomi, J. Pharm. Pharmacol., 50 (1997) 153.
131. K.M.G. Taylor, R.M. Morris, Thermochim. Acta., 248 (1995) 289.
132. D. Chapman, R.M. Williams, B.D. Ladbrooke, Chem. Phys. Lipids, 1 (1967) 445.

133. B.D. Ladbrooke, D. Chapman, Chem. Phys. Lipids, 3 (1969) 304.
134. B.A. Lewis, S.K. DasGupta, R.G. Griffin, Biochemistry, 23 (1984) 1988.
135. M.J. Ruocco, G.G. Shipley, Biochim. Biophys. Acta., 684 (1982) 59.
136. J.L. Slater, C. Huang, Biophys. J, 52 (1987) 667.
137. N. Matubayasi, T. Shigematsu, T. Iehara, H. Kamaya, I. Ueda, J. Memb. Biol., 90 (1986) 37.
138. J.L. Lippert, W.L. Peticolas, Proc. Natl. Acad. U.S.A., 68 (1971) 1572.
139. F.J.J. Fildes, J.E. Oliver, J.Pharm. Pharmacol., 30 (1978) 337.
140. M. Arrowsmith, J. Hadgraft, I.W. Kellaway, Int. J. Pharm., 16 (1983) 305.
141. C. Zingel, A. Sachse, G.L. Rossling, R.H. Muller, R.D. Int. J. Pharm., 140 (1996) 13.
142. E.C.A. van Winden, H. Talsma, D.J.A. Crommelin, J. Pharm. Sci., 87 (1998) 231.
143. K. Ozaki, T. Hayashi, T. Int. J. Pharm., 160 (1998) 219.
144. P. Gilbert, G.W. Barber, J.L. Ford, in Mechanisms of Action of Chemical Biocides: Their Study and Exploitation, S.P. Denyer, W.B. Hugo (Eds.), Blackwell Scientific Publications, London, 1989.
145 A.G. Lee, Biochemistry, 15 (1976) 2948.
146. Y Matsuda, S. Kawaguchi, H. Kobayashi, J. Nishijo, J. Pharm. Sci., 73 (1984) 173.
147. I. Corrigan, E.M. Holohan, J. Pharm. Pharmacol., 36 (1984) 217.
148. M. Angberg, Thermochim. Acta., 248 (1995) 161.
149. C.F. Lerk, A.C. Andreae, A.H. de Boer, P. de Hoog, K. Kussendrager, J. Van Leverink, J. Pharm. Sci., 73 (1984) 857.
150. A. Olqano, N. Corzo, I. Martinez-Castro, Milchweissenschaft, 38 (1983) 471.
151. C. Ahlneck, G. Zografi, Int. J. Pharm., 62 (1990) 87.
152 A. Saleki-Gerhardt, C. Ahlneck, G. Zografi, Int. J. Pharm., 101 (1994) 237.
153. P.P. De Luca, P. Lachman, J. Pharm. Sci., 54 (1965) 617.
154. R.M. Patel, A. Hurwitz, J. Pharm. Sci., 61 (1972) 1806.
155. J.B. Bogardus, J. Pharm. Sci., 71 (1982) 105.
156. L. Gattin, P.P. De Luca, J. Parent. Drug Assoc., 34 (1980) 398.
157. Y.H. Roos, J. Therm. Anal., 48 (1997) 535.
158. Y.H. Roos, Carbohyd. Res., 238 (1993) 39.
159. K. Ito, Chem. Pharm. Bull., 18 (1970) 1509
160. Y.Y. Tan, G. Challa, Polymer, 17 (1976) 739.

161. A.O. Okhamafe, P. York, Pharm. Res., 2 (1985) 19.
162. P. York, A.O. Okhamafe, Anal. Proc., 22 (1985) 40.
163. P. Sakellariou, R.C. Rowe, E.F.T. White, Int. J. Pharm., 31 (1986) 55.
164. P. Sakellariou, R.C. Rowe, E.F.T. White, Int. J. Pharm., 34 (1986) 93.
165. P. Sakellariou, R.C. Rowe, E.F.T. White, J. Appl. Polym. Sci., 34 (1987) 2507.
166 P. Sakellariou, A. Hassan, R.C. Rowe, Coll. Polym. Sci., 272 (1994) 220.
167. P. Sakellariou, A. Hassan, R.C. Rowe, Polymer, 34 (1993) 1240.
168. E. Schwarz, S. Pfeffer, J. Therm. Anal., 48 (1997) 557
169. V.L. Peramal, S. Tamburic, D.Q.M. Craig, Int. J. Pharm., 155 (1997) 91.
170. K. Simon, R. Suverkrup, R. Thermochim. Acta., 248 (1995) 271.
171. S.K. Dordunoo, J.L. Ford, M.H. Rubinstein, J. Pharm. Pharmacol., 48 (1996) 782.
172. C. Demuynck, J.P. Remon, Int. J. Pharm., 85 (1992) 103.
173. R.H. Pryce-Jones, G.M. Eccleston, B.B. Abu Bakar, Int. J. Pharm., 86 (1992) 231.
174. V. Paspaleevakuhn, E. Nurnberg, Pharm. Res., 9 (1992) 1336.
175 L.E. Pena, B.L. Lee, J.F. Stearns, J. Soc. Cosmet. Chem., 44 (1993) 337.
176. U.T. Lashmar, J.P. Richardson, A. Erbod, Int. J. Pharm., 125 (1995) 315.
177. W.H.M. Crane-van Hinsberg, J.C. Verhoef, H.E. Junginger, H.E. Boddé, Thermochim. Acta., 248 (1995) 303.
178. M. Wegener, R. Neubert, W. Rettig, S. Wartewig, Int. J. Pharm., 128 (1996) 203.
179. M. Vitoria, L.B. Bentley, R.F. Vianna, S. Wilson, J.H. Collett, J. Pharm. Pharmacol., 49 (1997) 397.
180. R.O. Potts, C.M. Golden, M.L. Francoeur, V.H.M. Mak, R.H. Guy, J. Contr. Rel., 15 (1991) 249.
181. S.M. Al-Saidan, B.W. Barry, A.C. Williams, Int. J. Pharm., 168 (1998) 17.
182. Y. Kaplun-Frischoff, E. Touitou, J. Pharm. Sci., 86 (1997) 1394.
183. H.R. Moghimi, A.C. Williams, B.W. Barry, Int. J. Pharm., 131 (1996) 103.
184. M.A. Yamane, A.C. Williams, B.W. Barry, Int. J. Pharm., 116 (1995) 237.
185. C.S. Leopold, B.C. Lippold, J. Pharm. Pharmacol., 47 (1995) 276.
186. F. Dreher, P. Walde, P. Walther, E. Wehrli, J. Cont. Rel., 45 (1997) 131.
187. R. Neubert, W. Rettig, S. Wartewig, M. Wegener, A. Weinhold, Chem. Phys. Lipids, 89 (1997) 3.

188. M. Wegener, R. Neubert, W. Rettig, S. Wartewig, Chem. Phys. Lipids, 88 (1997) 73.
189 P.A. Cornwall, B.W. Barry, J.A. Boustra, G.S. Gooris, Int. J. Pharm., 127 (1996) 9.

INDEX

A

Abra tenuis 476
acid corrections 185
acoustic signals 417
acromegaly 680
activation energy 234, 569
active transport pump 578
acute myelogenous leulaemia 669
adenylate energy charge 621
adipocytes 630, 632, 680, 691
adipose tissue 694
adiposis delorosa 694
advancement 560
AE 230, 232
aerobic acidosis 491
aerobic batch culture 339
aerobic metabolism 418, 469, 697, 715
aggregation 875
aggregation enthalpy 154
aggregation process 97
aging 786
agricultural crops 740
algae 293, 306, 712
algae elemental composition 293
algae, enthalpy of combustion 306
Aliquat 336
allelic enzymes 488
alternative respiratory pathway 733
alveolar macrophages 672
amino acids 601, 644, 863
ammonia 285, 471, 492, 567, 571, 644
ammonium 355
ammonium limitation 336
ammonium phosphate 775
amorphous 947
amorphous material 945
amorphousness 942, 981, 990
amphiphilic molecules 113
ampoule 566
ampules 718
amylopectin 839
amylose 839
amylose-lipid complexes 840
anabolic equations 233
anabolic half reaction 606
anabolic pathways 472
anabolic reaction 375
anabolism 228, 231, 247, 321, 371
anaemia 660
anaerobic batch experiment 344
anaerobic conditions 573
anaerobic growth 389
anaerobic metabolism 377, 411, 472, 643, 675, 697
anaerobic pathways 617
anaerobic processes 469
anaerobic quiescence 490
anaerobic reactions 326
anaesthesia 432
anhydrobiosis 493
animal 184, 193, 511, 514, 518, 522, 523, 526, 534, 537, 539
animal cells 220, 361, 683
animal tissues 557
anionic surfactant 155
Annelida 473, 475
annelids 452
annual rings 766, 771, 785
anorexia nervosa 695
anoxia 451, 470, 475, 477, 478, 480, 491, 590, 619
anoxic 578
antibiotics 356, 446, 668
antigene technology 12, 32
antigens 674
anti-plasticisation 823
antisense sequences 54
ants 443
apnea 495
apoptosis 628, 633, 671
aquatic animals 407, 445
arabadopsis 732
ArcA-ArcB 385
Arrheius activation energy 910
Arrhenius behaviour 95, 815, 898
Arrhenius function 736
Arrhenius law 903
Arrhenius plot 569, 750, 817
Arrhenius relation 729, 736
Arrhenius temperature dependence 814
Artemia franciscana 490, 493
arterial insufficiency 685
Arthropoda 473, 475

arthropods 479
ash 287, 291, 294, 782, 791
ash content 178, 181, 184, 185, 189, 194, 197, 198, 200, 203, 205, 211, 294, 299
athermal solution 136, 161
ATP 322, 372, 394, 470, 575, 577, 587, 592, 617, 628, 686
ATP cycle 561, 570
ATP production 635
ATP stoichiometric coefficient 640
ATP turnover 470, 471, 561
ATP/ADP cycle 372
ATP/O_2 ratio 639
ATPase 678
atrazine 748
autocatalysis 926
auto-ignition 775
autotrophic growth 229
auxotrophic 379
available electrons 230, 283, 346
available energy 203
average relative rate 598
Avrami equation 858
azeotropic point 141
B
bacteria 187, 228, 293, 299, 306, 500, 798
bacteria, elemental composition 293
baked products 852, 859
baker's yeast 225
banana stem slices 716
bark 205, 755, 766, 769, 793, 793
barley 746
barstar 78
basal metabolic rate 528, 540, 541, 543
base line 831, 896
batch calorimeter 557, 725, 923
batch culture 220
batch studies 723
beads 593
bean 742
beetle 456
behaviour 534, 544, 547, 549, 550
beta blockers 663
beta-adrenergic antagonist 679
beta-adrenoceptor blockade 682
bicarbonate 471
binding constant 125, 165
binding enthalpy 150
bioadhesion 387
biocompatibility 702
biodegradability 978
bioenergetics 367
biological energy demand 228
biological membranes 109, 989
biological stability 973
biomass 181, 221, 225, 248, 285, 288, 289, 292, 304, 312, 324, 337, 343, 356, 369, 373, 560, 597, 604, 736
biomass carbon 736
biomass yield 329
biomatter 180
biopsy 568, 588
bioreactor 261
biosensor 599
biosynthetic precursors 606, 617
biotechnology 219
birds 194
blood 562, 662
blood cell metabolism 657
blue-green algae 745
Boltzman constant 262
bomb calorimeter 181, 190, 227, 230, 244, 252, 636, 781, 923, 971
bound energy 560
brain slices 483
breeding 757
brine shrimp 471
brine shrimp embryos 490
brown adipocytes 637
brown fat 637
buffering capacity 471
bulbs 191
bumblebees 439
C
cabbage 737
cadmium 455, 662
caffeine 664, 696
calcium 696
calcium antagonists 664
calcium phosphate dihydrate 968
calibration 101, 277, 369, 446, 566, 594
calibration heater 564
Callistemon 729
calorespirometry 713, 723
caloric values 782
calorimeter cells 100
calorimeter design 718
calorimetric chamber 515, 523, 543, 544, 548
calorimetric enthalpy 70, 85, 97

calorimetric measurements 367
calorimetric RH perfusion 940
calorimetric signal 966
calorimetric-respirometric ratio 469, 471, 473, 574, 635
Calvet 176
cancer 624, 666
canonical ensemble 81
canonical partition function 906
canopy 515, 523, 543
capacitance 597
Carassius auratus 480
Carassius carassius 480
carbohydrate 395, 520, 529, 530, 531, 536, 692, 1000
carbon 306, 315, 372, 600, 736, 766,
carbon balance 316
carbon black 824
carbon conservation 331
carbon dioxide 412, 414
carbon dioxide production 520, 539
carbon mol (Cmol) 226
carbon starvation 382
carbon use efficiency 741
carbonyl cyanide p-(trifluoromethoxy)phenylhydrazone 630
cardiac muscle 583
cardiac tissue 690
cardiovascular drugs 681
carnitine 699
carvedilol 685
catabolic half reaction 606
catabolism 228, 233, 252, 321, 371, 560
cauliflower 732
CD melting 9
celery 754
cell cycle 240, 317, 576
cell cycle oscillations 319, 343
cell lines 558
cell metabolism 681
cell number 597
cell signalling 633
cellular composition 224, 225
cellular entropy 226
cellular substance 219, 247
cellulose 711, 766, 771, 984
cellulose ethers 984
ceramides 1006
cereal 882
cereal protein state diagram 882, 888
chain mode 811, 821
chamber volume 515, 523
char 771
charcoal 186, 197, 768, 772, 802
cheese 830
chemical calibration 566
chemical degradation 926
chemical stability 925, 951, 963
chemostat 370
Cherax quadricarinatus 479
chiral drugs 951
chirality 27
Chlorella 746
CHN measurement 288
CHO 320 cells 594, 603
cholesterol 129, 132, 989, 1006
Chordata 474
chronic lymphocytic leukaemia 669
citrate 995
climate 737
closed system 220, 559
cmc 155
Cmol 226
C-mol 283, 337, 601
Cnidaria 473, 475
CO_2 732, 752
CO_2 production rates 713, 752
coal 772, 785
cockroach 432
coffin 787
cold denaturation 77
cold temperature unfolding 72
cold tolerance 714
collagen 880
collapse temperature 997
combustion 768, 772
combustion analysis 224
combustion calorimetry 175, 405, 407, 454, 769, 780, 797
compatibility 966, 968
condenser 585
conformational entropy 2, 11
congestive heart failure 688
conservation constraints 285
conservative process 236
contact inhibition 573
continuous culture 239, 360, 378, 608
control variable 599
co-operative unit 70, 86, 135
copepod 479

Cori cycle 637, 658
cork 779
coupled metabolism 374
coupling model 812
CR ratio 469, 474, 486, 497, 640, 645
crab 449, 585
Crassostrea virginica 472, 486, 487
crayfish 479
creams 1005
creatine phosphate 578, 581
cricket 418
critical micellar concentration, 155
crowding effect 591, 643
crucian carp 482
cryopreservation 838
crystalline material 948
crystallisation 946
crystallites 978
cubic phase 117
culture medium 220
cumulated quantities 308, 310, 311
curing 777
cyanide 384, 621
cycads 733
Cyclops abyssorum 479
cytochrome 733
Cytodex beads 593
D
dapsone979
data acquisition dilution 539, 548
Debye equation 245
decomposition 943, 964
decoupling 639
degree of reductance 178, 233, 604, 605
degree of reduction 283, 285, 300, 331, 346, 349
dehydration 937
demicellization, 155, 158
denaturant binding model 874
denaturation 69
denaturation of a dimeric protein 104
denaturation of a monmeric protein 102
denaturation temperature 50
depression of the melting point 948
developmental physiology 485
Dewer flask 428
diabetic cardiomyopathy 688
diapause 490, 497
dielectric 586, 817
dielectric constant 41
dielectric relaxation 81
dielectric spectrometer 597
dielectric spectroscopy 981, 988
differential scanning calorimetry (DSC) 63, 117
differential scanning calorimetry 767, 829, 923
differential thermal analysis 767
diluents 822
dilution rate 357, 368, 608
dipalmitoyl-phosphatidylcholine (DPPC)/water 118
dissipative process 559
dissolved oxygen 274
distearoylphosphatidylcholine (DSPC) 119
divalent cations 127
DMA 835
DMPC/DPPC mixtures 139
DMTA 835
DNA 3, 5, 8, 297, 633
DNA fragmentation 639
dormancy 490, 743
dough thermomechanical properties 892, 894
DPPC 118
drug release 1000
drugs 624, 924, 934, 978
dry-matter 182
DSC 117, 118, 134, 727, 767, 774, 802, 929, 943
DSC signals 896
DSC traces deconvolution 830
DSPC 119, 120
DTG (time-derivative of TGA) 833
Dulong equation 177, 786
duplex-to-coil 13
Durham tube 225
DVS 937, 945
dynamic experiment 311
dynamic growth conditions 272
dynamic thermal analysis 923
dynamic vapour sorption 925, 927
E
ecology 454, 755
ecosystem 390, 454
ecotoxicity 394
ecotypes 756
efficiency 253, 257, 391
efficiency of enthalpy conservation 254
effluent gas analysis 933

eggs 195, 196, 198, 201, 207, 208
Einstein equation 825
elastomers 811, 824
electrical calibration 566
electron acceptor 324, 396, 397, 469
electron conversion 254
electron conversion efficiency 258, 261
electron donor 229, 255, 323
electron equivalence 233
electrons 229, 230
electrophoretic migration 21
elemental analysis 222, 344
elemental balance 285, 361, 361
elemental composition 197, 287, 291, 298 300, 600, 604
elemental formula 288
embryo 489
empirical analysis 225
empirical formula 226
end-effects 3
endoscope 415, 450
endotherm 943, 949, 976, 1003
energy 219, 781
energy balance 276, 278, 281, 314, 371, 513, 530, 539, 542, 545, 602, 691
energy expenditure 512, 514, 520, 527, 536, 539, 542, 544, 548, 550
energy intake 513, 529, 540, 545
energy metabolism 469, 514, 537, 531, 536, 547, 549
energy recovery 369
energy regulation 391
energy use efficiency 713
enprofylline 665
entantiotropic polymorphism 928
entantiotropy 928
enthalpy 179, 220, 240, 242, 247, 259, 320, 814, 868
enthalpy balance 371, 560, 571, 596, 601, 603
enthalpy change 268, 558, 640, 896, 937, 946, 956, 966, 971, 1006
enthalpy change of reaction 268
enthalpy conservation efficiency 260
enthalpy difference 67
enthalpy dissipation 327
enthalpy flux 603
enthalpy of anabolism 602, 606
enthalpy of combustion 282, 304, 307, 314, 604
enthalpy of combustion of biomass 304
enthalpy of formation 603
enthalpy of hydration 281
enthalpy of hypothetical combustion 284
enthalpy of neutralization 471
enthalpy of the protein 82
enthalpy of vaporisation 854, 937
enthalpy recovery 603
enthalpy-entropy compensation 2, 3, 10
entropic heat 262
entropy 180, 261, 262, 330, 605, 868, 1008
entropy change 220, 253, 558, 560, 587, 973
entropy change of reaction 268
entropy difference 67
entropy of formation 240, 242, 247
entropy production 332
epinephrine 487
equilibration time 719
equilibrium constant 68
equilibrium curve 96
equilibrium thermodynamics 238
equivalents 230
ergodicity 82
error 514, 524, 527
erythrocyte 657, 663, 677, 698
erythromycin production 351, 356
erythropoietin 701
Escherichia coli 385
Escherichia coli K12 225
estivation 495
ethanol 308, 336, 341, 361, 373
ethylcellulose 984, 1002
Eucalyptus 740, 746, 752
Eucryphia cordifolia 801
Eunapius fragilis 497
eutectic 995
eutectic melting reaction 118
eutectic mixture 951
eutrophication 445
evaporation 426
excipient 925, 966
exergonic reaction 321
exonucleases 54
exothermic gap 479
extent of reaction 959
extrinsic membrane proteins 109, 110

F

fat 520, 529, 530, 536, 633, 690, 766
fatty acid 1005

FCCP 630, 634
fed-batch 347, 351, 356, 378
fed-batch culture 607
fermentation 378
fermentative assimilation 222
fermentative pathways 469
fibroblast growth factor 644
filamentous fungi 293, 306
filamentous fungi elemental composition 293
filamentous fungi, enthalpy of combustion 306
final state 220, 222
fire retardants 770, 776
first order kinetics 94, 96
first order transition 65
fish 388, 423, 446, 488
fish eggs 446
fit macros 101
fit strategy 92
fixation 183
flammability 190
flight 434
flight calorimeter 434
flip-flop 115
flour 838
flow calorimeter 557, 563, 658, 713
flow calorimetry 596, 923
flow microcalorimetry 676
fluid L_{α}-phase 142
fluid-mosaic membrane model 109
fluocinolone acetonide 931
flux of electrons 322
fluxmeter 383
FMR1 21
food composition 522, 539, 536
food intake 522, 526, 540
foods 829
forestry 748, 768
formalin 183
fossilization 786
fourier transform infrared spectroscopy 767
four-way junctions 28
fragile 817
fragile x syndrome, 22
fragility plot 817
free energy 257, 259, 944
free energy change 256, 284
free energy change of hypothetical combustion 284
free energy conversion efficiency 255
free energy of formation 245, 248
free volume 812, 818
free-energy 220, 240, 241, 247
freeze drying 999
freeze-drying 994
frog 423
fructose 622, 643
fruit fly 427
fuel 210
fuelwood 207, 210, 781
Fulton's cube law condition factor index 201
Fundulus heteroclitus 488
fungi 187, 748, 798
fungicide 748
futile cycles 375

G

ganglioside 112, 143
gas analysis 523, 526
gas flow 525, 548
gas perfusion calorimeter 725
gaseous exchange 512, 520, 527, 548
gastroplasty 632, 693
Gaussian behaviour 812
gel electrophoresis 14, 31
gel phase 115
gel phase immiscibility, 140
gel-gel phase transition 122
gel-liquid-crystalline phase transition 121
gels 987
gemmules 497
gene control 8
generalised degree of reduction 284, 292, 295
genetic engineering 757
gentamycin 663, 668
giant sequoia 750, 771
Gibbs energy 320, 560, 582, 585, 944
Gibbs energy change 558
Gibbs energy dissipation 327, 329, 333
Gibbs energy flow rate 579
Gibbs energy of reaction 268
Gibbs free energy 14, 15, 36, 39, 66, 179, 237, 238, 252, 973
Gibbs free energy equation 238, 241, 252, 263

Gibbs function 868
Gibbs-Donnan effect 222
Gibbs-Helmholtz equation 31
Giese equation 177
gills 483, 500
glass transition 812, 820, 835, 837, 885, 942, 981, 994, 1001
glass transition temperature 816
glassy state 994
gliadin 844, 883, 887
globular protains 48
glucocerebrosides 112
gluconeogenesis 472
glucose 279, 282, 312, 332, 334, 336, 355, 368, 381, 381, 384, 570, 598, 605, 610, 621, 622, 644, 692
glucose oxidation 576
glucose pulse 341, 349, 357
glucose-limited continuous culture 301
glutamine 570, 575, 598, 605, 610, 614, 640
glutaminolysis 571, 605, 640
gluten 845, 848, 891
gluten DTMA trace 891
gluten storage and loss modulus 888, 890
glutenin 844, 884
gluten-starch interaction 887, 895
glyceride 1005
glycerol 369, 1001
glycogen 488, 618
glycolysis 381, 574, 615, 643
glycolytic flux 383, 470
glycolytic oscillations 385
glycyl group 78
GM2 activator protein 143
Gnuplot 101
goldfish 480
Gordon-Taylor equation 999
Goutal equation 785
Gouy-Chapman theory 126
G-quartets 12, 33
granulocyte 663, 670, 703
granulocyte activation 675
grape 743
graphite 803
grasshoppers 428
groove binder 16
group effects 427
growth 712
growth limitation 379
growth process 220, 257
growth process equation 223, 228, 234
growth rate 717, 730, 734, 752
growth reaction 283, 600
growth stoichiometry 347
guanine quarter structures 32
gum 833
gut fermentation 525, 547

H

haemodialysis 698
hairpin structures 22, 33, 41, 49, 51, 53
halothane 696
Hamiltonian 82
hammerhead ribozymes 29
hamster 688
H-bonds 4, 39, 40
headgroup 111, 123, 127, 143
heart rate 414, 514, 537
heat 371
heat accumulation calorimeter 270, 594
heat capacity 64, 65, 76, 79, 84, 86, 92, 100, 102, 156, 516, 728, 865, 906, 972
heat capacity change 10, 15, 64, 67
heat capacity of protein 64
heat capacity of the native state 76
heat capacity of the unfolded state 73, 74
heat compensation calorimeters 270
heat conduction calorimeter 269, 557
heat conduction differential calorimetry 726
heat content 514, 516, 548
heat dissipation 495, 469
heat dissipation rate 469, 477
heat exchange 518, 547
heat flow rate 597
heat flux 399, 476, 488, 571, 579, 589, 598, 599, 608, 635
heat loss, 512, 518, 523, 531, 540, 548
heat of anabolism 373
heat of combustion 242, 244, 247, 248, 755, 792
heat of dilution 30
heat of dissociation 147, 149
heat of fusion 978
heat of ion binding 150
heat of reaction 146, 149, 279
heat production 514, 520, 531, 536, 548, 575, 667
heat production rate 659, 682
heat rate 721, 728, 749, 754

heat storage 514, 529, 548
heat transfer 512, 531
heat yield 375, 376, 594
heating rate 64, 67, 95, 98, 830, 972
hedgehog 689
hemicellulose 766, 788
Henry's Law 240
hepatocytes 697
herbicide 748
Hess's Law 576, 603
heterotrophic growth 228
hexose monophosphate shunt 612
hexoses 1000
Hirudo medicinalis 479
homeothermic 409
honey 833
honeybee 417, 437, 457
hoogsteen 6, 7, 19, 20
Hopkins optic 415
hormones 571
hornets 440, 797
host-parasite system 200
hot stage microscopy 969
hot-stage microscopy 930
HPMC 944, 984, 1001
HPMC-water gels 987
human calorimetry 406
human growth hormone 634
humans 511, 518, 522, 534, 539
humidity 427
hybernation 689
hybridoma 595, 614, 571, 593
hydrates 928
hydrocolloids 848
hydroflumethiazide 991
hydrophobic drugs 166
hydrophobic effect 163
hydrophobicity 24
hydroxypropylmethylcellulose 984
hygroscopic materials 941
hygroscopicity 940
hyperchromicity 44
hypertensive patients 683
hyperthermia 668
hyperthyroidism 676
hypometabolic state 485
hypothermia 689
hypothyroidism 678
hypoxia 423, 430, 451, 452, 457, 485, 567
hypoxia tolerance 480
hypoxic 445

I

ibuprofen 969
ICCmol 226, 228
ice 837, 1000
illumination 415, 434
imidazole 471
imidazole buffer 959
immune complexes 674
immunoglobulin E 629
immunology 671
indirect balancing 316
indirect calorimetry 405, 406, 410
indium 951
indole 152
indomethacin 949, 1005
initial state 220, 221
inosine 7
insects 184, 196, 206, 426, 797
instantaneous rate 598
integral membrane proteins 109
intercalators, 20
interdigitated phases 117
interferon-γ 594, 647
intestinal mucus 389
intrinsic membrane proteins 109, 110, 143
intumescents 775
invertebrate larvae 585
ion binding 123
ion containing carbon mol (ICCmol) 226
ion content 290
ion leakage 482
ion pump 661, 684
ion transport 580
ion-containing unit-carbon formula (ICUCF) 226
ionic strength 125
ions 150, 287, 289
iopromide 990
irreversible growth 559
irreversible kinetics 66
irreversible thermodynamics 219
irreversible transitions 94
ischaemia 590, 685, 697
isolated tissues 481
isoperibol calorimetry 989
isothermal calorimetry 469, 721, 767, 832, 857, 923, 933, 945
isothermal titration calorimetry (ITC) 146
isothermal titration calorimetry 973

isotope dilution 514, 537
isotopes 414
ITC 146
K
ketoprofen 969
Kharasch degree of reduction 284
kidney 702
kinetic approach 830
kinetic parameters 953
Kleiber's Rule 573
Knudsen TGA 854
Kohlrausch-Williams-Watts equation 812
Kraft lignin 776
kyr 832
L
lactate 488, 571, 575, 610, 617, 633, 640, 644, 673
lactic acid 981
lactose 968, 990, 991
lactose monohydrate 968
Langmuir adsorption isotherm 165
Laplace transforms 99
larch 749, 769, 776
larvae 435
Law of the Conservation of Mass 223
Ldh-B locus 488
lead 662
leaves 715, 782
lecithin 1008
leech 450, 479
lettuce 754
leukocytes 658, 702
lichens 192
ligation effects 73
light guide 620
lignin 711, 766, 770, 779, 786, 790, 801
limiting substrate 370
lipid 471, 745, 755, 833, 988, 1008
lipid bilayers 109
lipid degradation 833
lipid immiscibility 129
lipid mixtures 129
lipid-peptide interactions 164
lipid-protein interactions 143, 164
lipids 113, 395, 711
lipid-surfactant mixtures 144
liposomes 110, 988
liquid crystal 995
liquid paraffin 1005
liquid-crystalline phase 114
liquidus temperature 076
liver 590, 696
liver diseases 661
lizard 408, 424
l-lactose monohydrate 933
local segmental motion 812
locomotor activity 513, 526, 532, 540, 548
Locusta migratoria 480
locusts 480
Lucinoma aequizonata 500
Lumbriculus variegatus 478
Lumry-Eyring model 94, 877, 909
lymphocytes 659, 663, 667, 672
lymphoma 666
lyophilisation 994
lyophilization 182, 183, 223, 287
lyophobic mesomorphism 114
lyotropic behavior 113
lyotropic lamellar and hexagonal phases 116
lyotropic phases 114
lyotropic series 879
lyzozyme 444
M
macromolecule 974
macronutrients 222
macrophage 673
magnesium stearate 970
Maillard reaction 833
maintenance energy 374, 386
maize 740
malignant hyperpyrexia 696
mammalian brain 481
mammalian cells 589
manganese dioxide 673
manometric determination 412, 413
manometry 225, 226
mass 572
mass balance 235, 605
mass fractions 291
mass spectrometer 525, 537, 548
mass spectroscopy 767
MDSC 838
melting temperatures, 35
membrane reconstitution 144
metabolic activity 386, 388, 561, 608, 667
metabolic body mass 523
metabolic control analysis 382
metabolic flux 380, 598, 602
metabolic inhibitors 381

metabolic rate 470, 592, 660, 734
metabolic uncoupling 374
metabolic weight 408
metabolism 511, 529, 536, 767, 832
metabolites 511, 538, 548
metamorphosis 428, 434, 487
meteorite 802
Methanobacterium thermoautotrophicum 289, 291
methanol 747
methotrexate 624
methylated cytosine 19
methylcytosine 19
Mettler RC-1 calorimeter 594
mice 413
micelle 114, 144, 156, 157, 161
microbial degradation 779, 787, 798
microbial ecology 219
microbial growth 219, 832
microbial metabolism 832
microbial processes 367
microbomb 176
microcalorimeter 368
microcalorimetry 657
microcarriers 593
micronutrients 222, 571, 603
microorganism 184, 187, 219, 267, 279, 297, 319, 387, 672
microphone 416, 434, 441
microtitre plates 558
milk 831
minerals 224
mismatched complex 14
mitochondria 484
mixed micelles 144, 145
model compound 72, 77, 109
modified enthalpy of combustion 305
modulated differential scanning calorimetry 829, 923
modulated DSC 943
moisture 180, 186, 209, 287, 774, 777
molar balance 280
molar enthalpy 560
molar enthalpy of glucose oxidation 576
molar mass 288
molar reaction enthalpy 561, 603, 615
molar yield coefficient (MYC) 228
mole balance 278, 312
Mollusca 473
molten globular state 17
monoclonal antibodies 593
monolayers 673
monotropy 929
monovalent cations 125
morphological stability 926
mosses 192
moth 429, 433
motion detectors 513, 534, 544
mRNA 35
mucus 199, 390
mulberry 793
Mulinia lateralis 477
multilamellar vesicles 989
multiple limited growth 333
multistem DNA structures 27
muscle 559, 577, 578, 699
muscle thermogenesis 700
music instruments 784
musical instruments 765, 788
mussels 448
MYC 228, 231, 235
myocardial infarction 687
myocardial tissue 688
myocardial tissue metabolism 679
myoglobin 72, 73, 77
Mytilus edule 472, 476, 487
N
Na^+-K^+ pump, 694
NAD(P)H 394
NADH 376, 637
NADPH 575, 612
nafcillin 995
nanoWatt technology 952
negentropy 329
neoplastic drugs 669
nerve 584
nests 439, 441, 797
neutrophils 612
newsprint 768, 796
Ng equation 965
nimodipine 930
nitrate 397
nitrate respiration 500
nitrite 397, 501
nitrofurantoin 933
nitrogen excretion 512, 520, 527
nitrogen starved 382
NMR 2, 862, 926
non-conservative process 236
non-equilibrium thermodynamics 238, 559

non-growing state 380
non-Hodgkin lymphoma 666
non-ideality parameter 142, 161
non-linear structures 1
noradrenaline 640
normoxia 477, 480, 483, 578
nucleic acids 570
nutrient 713, 747
nutrient feeding 610
nutrition 511, 539, 545
nystatin, 153
O
O_2 732
oak 770, 774
obesity 511, 536, 539, 545, 550, 633 690
ointment 1004
oleic acid 1007
oligochaete 446, 451
oligomeric proteins 85, 92
oligopeptide 165
oligosaccharide 78
open system 220, 559, 596
optical fluorescence microsensing 504
order of reaction 957
order-disorder transitions 13
Oreohelix 496
organic cations 127
organic product 232
oscillations 383
osmotic pressure 569, 607
osmotic regulatory events 478
Otala lactea 496
ouabain 578
OUR 578, 583, 617, 635, 643
oxazepam 933
oxidation 511, 519, 526,540, 570, 926
oxidation-reduction process 229
oxidative assimilation 222
oxidative phosphorylation 575, 617, 637, 733
oxidized donor 322
oxido-reductive metabolism 334, 339
oxycaloric equivalent 305, 306, 393, 407, 411, 437, 472, 635, 639
oxycaloric quotient 307
oxygen 334, 407, 413, 471, 491, 501, 567, 607, 766, 833, 971
oxygen consumption 360, 391, 411, 414, 425, 469, 477, 520, 522, 537, 575, 617, 645, 657, 672, 689, 697, 713
oxygen debt 425
oxygen diffusion 717
oxygen electrode 228, 418, 419, 420, 504, 713
oxygen flux 573, 635, 648
oxygen limitation 476, 481
oxygen metabolites 612
oxygen sensors 419
oxygen tension 566, 567
oxygen uptake rate 578
oxygen-limited continuous cultures 334
Oxygraph 644
oyster 485
P
P/O ratio 326, 372
P:O ratios 484
paper 765, 788, 791
papyri 792
papyrus 793
paracetamol 951, 977
Parr 185
partial molar heat capacity 79
particle collision 98
partition coefficient 145, 158, 159, 161
partition function 63, 83, 84, 86, 865, 871
Pasteur effect 644
peach 743
pediveligers 486
PEG 979, 1002
Peltier 176
Peltier battery 423
Peltier elements 563
Peltier sensors 446
penetrants 1006
penicillin 966
pentachlorophenol 455
pentosans 848
pentose phosphate shunt 661
pentoses 1000
Percoll 593, 620, 725
perfusion calorimeter 713
perfusion vessel 567, 700
peripheral membrane proteins 109
peritoneal macrophages 674
permittivity 586
peroxide 834
pessary 979
pH 491, 567
pH electrodes 504
phagocytic cells 659

phagocytosis 671
pharmaceuticals 924
phase changes 727
phase diagram 139, 163, 836
phase transitions 133, 137, 711
phenol resin 777
phenylbutazone 990
pheromones 433, 437
Phillipson 176, 201, 782
phorbol 612, 614, 674
phosphagen 471, 578, 581
phosphatidic acids (PA) 123
phosphatidylcholine 989
phosphatiylserine 988
phospholipid-cholesterol mixtures 129, 132
phospholipids 110, 111, 164, 988, 1007
phosphorus 289
phosphorylation 578, 643
phosphorylation efficiency 484
photo calorimeter 976
photocalorimetry 712
photo-degradation 926, 975
photosynthate 735
photosynthesis 712
piglet ileal mucus 390
pine 754, 769, 771
pK 127
plant 184, 188
plant calorimetry 720
plant growth model 733
plant growth rate 717
plant tissue preparation 716
plasma heat production 704
plasma membrane 778
plasmalogens 111
plasticisers 822, 984
platelet 658, 665, 680, 686, 695
platelet aggregation 665
p-loop 26
PNA 16, 24
poikilothermic 409
pollen 189, 190, 755
pollution 445, 458
poly(dimethylsiloxanes) 817
poly(vinylethylene) 811
polybutadiene 811
polyene antibiotics 153
polyethylene glycol 977, 980, 1001
polyisoprene 824
poly-lactic acid 981
polymer 811, 822, 1000
polymer thermomechanical properties 901
polymer-hydration 986
polymorph 930
polymorphism 925, 928
polynucleotides 151
polysaccharides 833, 839
polyvinylpyrrolidone 977, 991, 1001
Pompeii worm 458
poplars 753, 768
Porifera 473, 475
postprandial thermogenesis 528, 540, 543
potato 842
potato tuber slices 716
potential energy 399
pressure 420, 458, 726
pressure transducer 418, 448
progesterone 982
propranolol 663., 684
prosthetic heart valves 686
protein 63, 471, 520, 527, 540, 588, 692, 858, 861, 865, 869, 875, 880, 901 863, 973
protein aggregation 875, 909,
protein cold denaturation 869
protein degradation 491
protein denaturation 861, 863, 865, 879,
protein denaturation, effects of salts and sugars 879
protein denaturation, ligand effect 873
protein denaturation, pH effect 871
protein energetics 63
protein folding 81
protein gels 880
protein macrosystem 82
protein microsystem 82
protein population fraction test 904
protein stability 66
protein stability 858, 863
protein synthesis 482
proton leakage 484
protozoan 444
pseudo-binary phospholipid mixtures 133
pseudoknots 2, 42, 45
Pseudomonas fluorescens 396
Pseudomonas putrefaciens 396
pseudopolymorphism 928
pulse 272
purine 640
PVP 977

pyrimidine 640
pyrolysis 768, 774, 797
pyruvate 617
pyruvate carboxylase 648

Q
quail 422
quartz 674
quasi-crystalline lamellar phases 124
quiescence 490
R
radish 747
rafting 789
Raman spectroscopy 927
random coil 77
Raoult's law 951
rat 682, 689, 1008
rate constant 94, 95, 956, 965
rate of dissolution 946
RC-1 calorimeter 273
reaction enthalpy 10, 147
reaction extent 955
reaction flux 561, 603
reaction half life 959
reaction kinetics 966
reaction molar flux 561
reaction order 957
reaction rate 961
redox process of growth 560
reduced donor 322
reductance degree 233
redwood 749
reference state 282, 305
regulation 511, 531, 540, 549
relative humidity 927
relative partition model 90
relaxation 811, 826
relaxation time 98
renal insufficiency 661, 698
reptiles 195, 423
resin 190, 205
respiration 496, 583, 711, 748
respiration ecotypes 756
respiratory burst 612
respiratory capacity 628
respiratory exchange ratio 496
respiratory quotient 347, 413, 420, 437
response time 515, 524
resting potential 578
restriction enzymes 39
retained energy 513, 545
reversible unfolding 67
RH 941, 970, 994
RH perfusion 927, 934
RH value 939
rhodopsin 976
rhythms 428
ribozymes 38, 40
rice 843
RNA 34, 53, 297
RNA polymerase 35
RNA world 38
RNase 876
rotenone 630
Rouse model 812
RQ 350, 520, 526, 538
rubber 777, 824, 826
rubbery plateau 834
rubbery plateau region 812
rubbery state 1000
S
S. cerevisiae 274, 302, 317, 338, 375
Saccharomyces cerevisiae 224, 235, 246, 251, 256, 289, 291, 343, 368, 606
salinity 198, 714
salt 714, 746
saquinvir 944
sarcolemma 578, 579
sarcoplasmic reticulum 696
scalar flux 572
scanning calorimetry 713, 728, 743
Schistocerca gregaria 480
Scophthalamus maximus 488
second law of thermodynamics 71
secondary relaxation 811, 819, 822
secondary structure 42
sediments 393
Seebeck 176
Seebeck effect 421
Seebeck thermopiles 623
seed germination 742
seed storage 742
seeds 189, 191, 202, 203, 714
segmental relaxation time 816
sensors 517, 524
serotonin 483
serum 601, 670
shell 199
shift-up in dilution rate 341

shrimp 449
Sigmaplot 101
signal to noise ratio 64
silica 949
simulation (of baking, cooking, etc) 832
Singer-Nicolson model 109
Sipunculida 473, 475
Sipunculus nudus 479
skeletal muscle 580, 680, 695
skin 1006, 1008
skinned muscle 582
skins 195, 196
smooth muscle 581
snail 415, 420, 448, 449, 455, 495
snake 423
social insects 422
social life 406
sodium fluoride 677, 697
sodium pump 684
soil 205, 391
solid state degradation model 965
solid state reactions 963
solidus and liquidus curves 136
solidus temperature 976
solution calorimetry 946
sorption isotherms 856
sound 417, 440
soybean 730
specific growth rate 572, 599, 735
specific heat capacity 590
specific volume 65
spectroscopic techniques 839
spermatozoan 620
sphingolipids 112
sponge 497, 770, 790
spray-dried products 990
squid giant axon 587
stability curve 68
stability of the protein 68
stacking 37, 44, 50, 52
staling 856
standard enthalpy 70
standard entropy 245
standard Gibbs energy 72
standard Gibbs energy difference 68
standard state 240
staphylococcal nuclease 72
starch 839, 858, 944
starch gelatinization 840
starch retrogradation 858
starvation 386, 390
starved 380
state 4 respiration 484
state diagram 997
state of substrates for energy balance 282
statistical physics 81
statistical thermodynamical analysis 65
steroids 232
sterol 970
stoichiometric coefficients 560, 602, 610
stoichiometric equation 602
stoichiometry 71, 76, 87, 88, 89, 91, 283, 512, 520, 578
storage 531, 541
Stradivari 790
strand invasion 26
stratum corneum 1006
stress 713
striated muscle 577
structural biomass 738
substrate 219, 220, 272, 512, 520, 529, 539, 546, 578
substrate carbon conversion efficiency 718, 733
substrate oxidation 512, 518, 527, 542
substrate phosphorylation 617, 628
succinate 471
sugar 837
sugar pucker 36
sugar-phosphate backbone 34
sulfur 288
sulphide 452
suppository 1002
symbiosis 500
system boundary 278
systemic lupus erythematosis 675
T
tannins 776
taxol 626
Taylor series 75
telomeric DNA 22
telomeric sequences 32
temperature cycling 722, 745
temperature tolerance 745
terbutaline 664, 684
terfenadine 930
terminal mode 811
terminal relaxation 812, 814, 819
tertiary structures 42, 44, 46,
tetraloops, 47, 49, 51

TGA 832,898
TGA signal 898
TGA-DSC combination 853
Thais haemastoma 478
theophylline 665
theophylline monohydrate 966
thermal advancement 560
thermal conductivity 590
thermal decomposition 964
thermal imaging 630
thermal melting 4
thermal volume 566
thermodielectric analysis 835
thermodynamic approach 830
thermodynamic boundary 279, 559, 596
thermodynamic efficiency 639
thermodynamic equilibrium constant 238
thermodynamic properties 243, 246, 249
thermodynamic stability 34, 49, 50, 52, 54
thermodynamic system 220
thermodynamics 558
thermoelectric device 628
thermogenesis 427, 440
thermogram 409, 799
thermo-gravimetric analysis 829, 832
thermogravimetry 767, 793, 923, 996
thermomechanical analysis 899, 923
thermomechanical properties 892, 894, 901
thermomicroscopy 929
thermophiles 45
thermopile 577, 629
thermoregulation 540, 547
thermorheological complexity 820
thermorheological simplicity 818
thermotropic behavior 113
thermotropic mesomorphism 114
third strand binding code 6
Thornton regularity 604
Thornton's Rule 250, 251, 636, 715, 735
three way junctions 27, 28, 29, 31
three-state model 88, 90
thrombo-embolism 686
thyroid 700
thyroid hormones 676
thyroxine 701
Tian equation 409
Tikhonov functional 598
time constant 274, 275, 408
time resolution 523, 527, 534, 548
time-temperature superposition 902
time-temperature superposition principle 820, 902
tissue/cell damage 562
tissues 714
titanium dioxide 674
titration calorimetry 975
titration pump 557
T-lymphoma cells 567, 615, 624, 666
TMA 835, 842
tomato 724, 737, 742, 754
torsional braid analysis 986, 1002
total heat 372, 728
toxicity 455
toxicology 924
tracer techniques 413
trans-gauche isomerization 115
transition enthalpy 121
transition temperature 65, 93, 118, 121
trees 766
trehalose 495
triacetin 595, 959
triglyceride 1002, 1007
triglycine 79
trinucleotide expansion 21
tripeptides 78
triple helices 5
triplet-to-duplex transition 13
triplex formation 7, 9, 11, 12, 20, 26
tristerin 1003
TTT diagram 847
Tubifex tubifex 478
tumour 576, 588, 669
tumour cells 666
turbot 488
turtle 480
turtle brain 481
two-state model 87, 88
two-state transition 69, 75, 83, 135
U
uncoupled metabolism 374
uncoupling 374, 637
unfolding 88
unstirred layers 484
urea 496, 520, 527, 533, 876, 906
uremic plasma 704
UV hypochromicity 22
UV melting 21, 31
V
valvular heart disease 687

van't Hoff enthalpy 17, 31, 70, 82, 96, 97, 909
van't Hoff equation 948
van't Hoff plot 3, 31, 951
van't Hoff test 903
varnish 791
ventilation 435, 452, 495
vernalization 743
Vero cells 573
vesicles 110, 161
VFTH equation 812
video 415, 447
viroids 45
visco-elastic properties 834, 849
viscoelasticity 811
Vogel-Fulcher-Teymann-Hess equation 815
voodoo lily 715
W
warm-blooded animals 568
wasps 797
water 181, 194, 516, 536, 711, 742, 766, 792
water 855, 927, 946, 987
water activity 855
water fern 732
water vapour 939
Watson-Crick double helix 5, 46
weeds 748
white adipocytes 632
Williams-Landel-Ferry equation 815, 902
WLF equation 812, 902
wood 749, 755, 765, 777
woodfuel 766
work 577, 579
worm 450, 453
X
X-ray crystallography 6
X-ray diffraction 930, 948
X-ray powder diffraction 925
XRD 1005
XRPD 925, 945
xylans 770
Y
yeast 187, 223, 228, 293, 306, 388, 562
yeast elemental composition 293
yeast, enthalpy of combustion 306
yolk 198